molecules

Special Issue Reprint

Recent Developments in the Synthesis and Functionalization of Nitrogen Heterocycles

Volume I

Edited by
Alexey M. Starosotnikov, Maxim A. Bastrakov and Igor L. Dalinger

mdpi.com/journal/molecules

MDPI

Recent Developments in the Synthesis and Functionalization of Nitrogen Heterocycles—Volume I

Recent Developments in the Synthesis and Functionalization of Nitrogen Heterocycles—Volume I

Editors

Alexey M. Starosotnikov
Maxim A. Bastrakov
Igor L. Dalinger

MDPI

Basel • Beijing • Wuhan • Barcelona • Belgrade • Novi Sad • Cluj • Manchester

Editors

Alexey M. Starosotnikov
N.D. Zelinsky Institute of Organic Chemistry RAS
Moscow
Russia

Maxim A. Bastrakov
N.D. Zelinsky Institute of Organic Chemistry RAS
Moscow
Russia

Igor L. Dalinger
N.D. Zelinsky Institute of Organic Chemistry RAS
Moscow
Russia

Editorial Office
MDPI AG
Grosspeteranlage 5
4052 Basel, Switzerland

This is a reprint of articles from the Special Issue published online in the open access journal *Molecules* (ISSN 1420-3049) (available at: https://www.mdpi.com/journal/molecules/special_issues/Synthesis_Nitrogen_Heterocycles).

For citation purposes, cite each article independently as indicated on the article page online and as indicated below:

Lastname, A.A.; Lastname, B.B. Article Title. *Journal Name* **Year**, *Volume Number*, Page Range.

Volume I
ISBN 978-3-7258-2079-5 (Hbk)
ISBN 978-3-7258-2080-1 (PDF)
doi.org/10.3390/books978-3-7258-2080-1

Set
ISBN 978-3-7258-2077-1 (Hbk)
ISBN 978-3-7258-2078-8 (PDF)

Contents

About the Editors

Alexey M. Starosotnikov

Alexey M. Starosotnikov was born in 1978 in Moscow, Russia. He graduated from the Higher Chemical College of the Russian Academy of Sciences in 2000. He obtained his Ph.D. (2003) and Doctor of Science (2016) degrees at the N.D. Zelinsky Institute of Organic Chemistry of the Russian Academy of Sciences. At present, he serves as a Research Group Leader within this institute. His research interests include the chemistry of nitrogen heterocycles and aromatic nitro-compounds, as well as the pericyclic reactivity of aromatic systems.

Maxim A. Bastrakov

Maxim A. Bastrakov was born in Yoshkar-Ola, Russia, in 1982. He graduated from Mary State University in 2005. In 2008, he defended his Ph.D. theses under the supervision of Professor Svyatoslav A. Shevelev. Currently, Dr. Bastrakov is a Senior Scientist of the Laboratory of Aromatic Nitrogen Compounds at the N.D. Zelinsky Institute of Organic Chemistry. In 2014, he was awarded a Gold Medal of the Russian Science Academy for his work as a young scientist. His research interests cover the chemistry of heterocyclic compounds and nitroarenes and the synthesis of multi-purpose compounds on this basis.

Igor L. Dalinger

Igor L. Dalinger was born in 1961 in Moscow, Russia. He graduated from the Lomonosov Moscow State University (Department of Chemistry) in 1983. He received his Ph.D. (1988) and Doctor of Chemical Science (2013) degrees from the N.D. Zelinsky Institute of Organic Chemistry. At present he serves as Head of the Laboratory of Aromatic Nitrogen Compounds at the same institute. His research interests include the molecular design, synthesis, and characterization of nitrogen-rich heterocycles and their use as energetic materials.

Preface

Nitrogen heterocycles constitute a broad class of organic compounds. Many of their representatives have found applications in pharmaceuticals, high-energy substances, dyes, and non-linear optical materials, among many others. The rapid development of the pharmaceutical industry and material science has stimulated the search for new synthetic approaches and new methods for the functionalization of N-heterocycles; these are some of the key objectives of modern organic chemistry. As a result of such research, in addition to achieving these objectives, new and sometimes unexpected applications of N-heterocycles may arise. This reprint brings together recent original research papers and high-quality reviews on the synthesis, reactivity, and applications of aromatic and saturated nitrogen heterocyclic compounds, contributed by an international team of leading experts in this field. This reprint offers useful information for a wide range of synthetic chemists.

Alexey M. Starosotnikov, Maxim A. Bastrakov, and Igor L. Dalinger
Editors

molecules

MDPI

Article

Rapid Assembly of Pyrrole-Ligated 1,3,4-Oxadiazoles and Excellent Antibacterial Activity of Iodophenol Substituents

Hyein Kim [1,†], Lina Gu [1,2,†], Huisu Yeo [1], Umji Choi [3], Chang-Ro Lee [3,*], Haiyang Yu [4] and Sangho Koo [1,2,*]

[1] Department of Chemistry, Myongji University, Myongji-Ro 116, Cheoin-Gu, Yongin 17058, Gyeonggi-Do, Republic of Korea
[2] School of Pharmacy, East China University of Science and Technology, Meilong Road 130, Shanghai 200237, China
[3] Department of Biological Sciences and Bioinformatics, Myongji University, Myongji-Ro 116, Cheoin-Gu, Yongin 17058, Gyeonggi-Do, Republic of Korea
[4] Tianjin State Key Laboratory of Modern Chinese Medicine, Tianjin University of Traditional Chinese Medicine, Tianjin 300193, China
* Correspondence: crlee@mju.ac.kr (C.-R.L.); sangkoo@mju.ac.kr (S.K.)
† These authors contributed equally to this work.

Abstract: Pyrrole-ligated 1,3,4-oxadiazole is a very important pharmacophore which exhibits broad therapeutic effects such as anti-tuberculosis, anti-epileptic, anti-HIV, anti-cancer, anti-inflammatory, antioxidant, and antibacterial activities. A one-pot Maillard reaction between D-Ribose and an L-amino methyl ester in DMSO with oxalic acid at 2.5 atm and 80 °C expeditiously produced pyrrole-2-carbaldehyde platform chemicals in reasonable yields, which were utilized for the synthesis of pyrrole-ligated 1,3,4-oxadiazoles. Benzohydrazide reacted with the formyl group of the pyrrole platforms to provide the corresponding imine intermediates, which underwent I_2-mediated oxidative cyclization to the pyrrole-ligated 1,3,4-oxadiazole skeleton. The structure and activity relationship (SAR) of the target compounds with varying alkyl or aryl substituents of the amino acids and electron-withdrawing or electron-donating substituents on the phenyl ring of benzohydrazide were evaluated for antibacterial activity against *Escherichia coli*, *Staphylococcus aureus*, and *Acinetobacter baumannii* as representative Gram(–) and Gram(+) bacteria. Branched alkyl groups from the amino acid showed better antibacterial activities. Absolutely superior activities were observed for **5f-1** with an iodophenol substituent against *A. baumannii* (MIC < 2 μg/mL), a bacterial pathogen that displays a high resistance to commonly used antibiotics.

Keywords: pyrrole; 1,3,4-oxadiazole; Maillard reaction; D-ribose; L-amino acid; pyrrole-2-carbaldehyde; iodine effect; antibacterial activity

Citation: Kim, H.; Gu, L.; Yeo, H.; Choi, U.; Lee, C.-R.; Yu, H.; Koo, S. Rapid Assembly of Pyrrole-Ligated 1,3,4-Oxadiazoles and Excellent Antibacterial Activity of Iodophenol Substituents. *Molecules* **2023**, *28*, 3638. https://doi.org/10.3390/molecules28083638

Academic Editors: Alexey M. Starosotnikov, Maxim A. Bastrakov and Igor L. Dalinger

Received: 30 March 2023
Revised: 17 April 2023
Accepted: 18 April 2023
Published: 21 April 2023

1. Introduction

Oxadiazole is a five-membered heterocyclic aromatic compound composed of four structural isomers depending on the positions of two nitrogen atoms relative to an oxygen atom [1]. Among them, 1,3,4-oxadiazole has received intensive attention in the field of medicinal chemistry due to its broad metabolic profile [2–4] and in the field of material science for its excellent optoelectronic properties [5–8]. As an isostere of an amide and an ester, 1,3,4-oxadiazole serves as a promising pharmacophore for the discovery of new drugs exhibiting antimicrobial, anticonvulsant, anti-inflammatory, analgesic, antitumor, antiviral, antihypertensive, and enzyme inhibitory activities [9]. There have been extensive literature reviews on the specific synthetic methods and diverse biological activities of 1,3,4-oxadiazole derivatives [10–12].

Motivated by Raltegravir [13,14], an antiretroviral drug used to treat HIV/AIDS, and Zibotentan [15,16], an anti-cancer drug candidate, a number of poly heterocyclic

compounds containing a 1,3,4-oxadiazole pharmacophore were constructed, and their biological activities were investigated. Indole-ligated 1,3,4-oxadiazoles [A] were synthesized and evaluated to show antimicrobial, anti-inflammatory, and antiproliferative activities (Figure 1) [17,18]. Their biological importance was also identified by their antioxidants and acetylcholinesterase inhibition properties [19]. Likewise, various 2-benzofuranyl-1,3,4-oxadiazoles [B] were synthesized [20,21], demonstrating their biological activities in α-Glucosidase inhibition as well as the inhibition of glycogen synthase kinase 3β for treating diabetes and Alzheimer's disease, respectively [22–24].

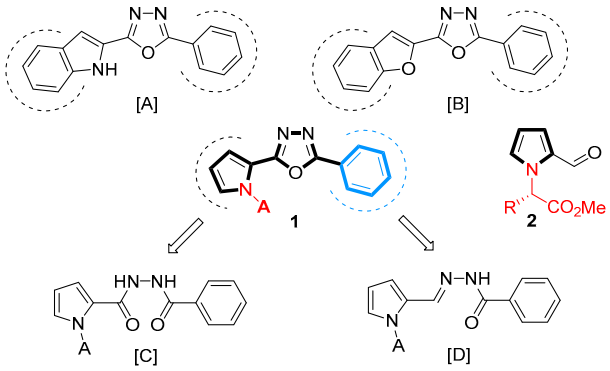

Figure 1. Heterocycle-ligated 1,3,4-oxadiazoles [A] and [B], and retrosynthesis of **1** from pyrrole **2** through the cyclization using key precursors [C] and [D].

Pyrrole is a very important structural motif in drug discovery projects because of the wide presence of natural, biologically active pyrrole alkaloid products [25,26]; thus, pyrrole-ligated 1,3,4-oxadiazole would be a perfect base structure for the development of potential lead compounds [27]. Considering the efficacy of the procedures of constructing a 1,3,4-oxadiazole ring, 2-pyrrolyl-5-phenyl-1,3,4-oxadizole **1** would be an ideal core structure, achieved either through dehydration from aroylhydrazide [C] or by cyclization from aroylhydrazone [D]. In the benzene ring, the substituent effects of the core structure **1** on antibacterial activity have been reported for the cases of 4,5-dibromopyrrole [28,29] and 4-nitropyrrole [30], respectively.

Pyrrole-2-carbaldehydes **2**, derived from the conversion of D-ribose with L-amino acids [31], were demonstrated to be useful, sustainable platform chemicals for the construction of highly functionalized poly heterocyclic compounds [32]. Since natural amino acids themselves demonstrate specific biological activities [33–35], it was envisioned that 1,3,4-oxadiazoles **1** from pyrrole-2-carbaldehydes **2** with the *N*-amino acid moiety would be very interesting core structures for the investigation of their biological activities. The effect of the amino acid moiety of **1** on antimicrobial activities was screened first, and the substituent effects on the benzene ring were then investigated for **5** and **6** with some selected amino acid moieties. We found a marginal size effect of the alkyl groups from amino acids (Val and Ile, etc.) and superior antibacterial activity of the iodophenol substituents of pyrrole-ligated 1,3,4-oxadiazoles **5** and **6** against *S. aureus* and *A. baumannii*. All the syntheses of pyrrole-ligated 1,3,4-oxadiazoles **1**, **5**, and **6** and their antibacterial activities are closely described herein.

2. Results and Discussion

Structure and activity relationships (SARs) for pyrrole-ligated 1,3,4-oxadiazoles **1** were generally studied by changing substituent groups in the aromatic rings [28–30]. We were interested in the SAR of **1** by *N*-alkyl substituents because pyrrole-2-carbaldehydes **2**, the starting materials for 1,3,4-oxadiazoles **1**, are easily prepared from L-amino acids, and each amino acid has its own biological activity. Ten L-amino acids with hydrogen, alkyl, aralkyl, ester, and sulfide substituents R were selected to assess the size effect (linear or branched) or potential electronic effect. Pyrrole-2-carbaldehydes **2** were efficiently prepared by a one-pot ribose conversion with an L-amino methyl ester in the presence of oxalic acid in DMSO,

following an improved procedure under 2.5 atm argon at 80 °C [32]. The corresponding pyrrole platform chemicals **2a**–**2j** with the *N*-amino acid moiety were prepared in yields of 32~63% (Scheme 1 and Table 1).

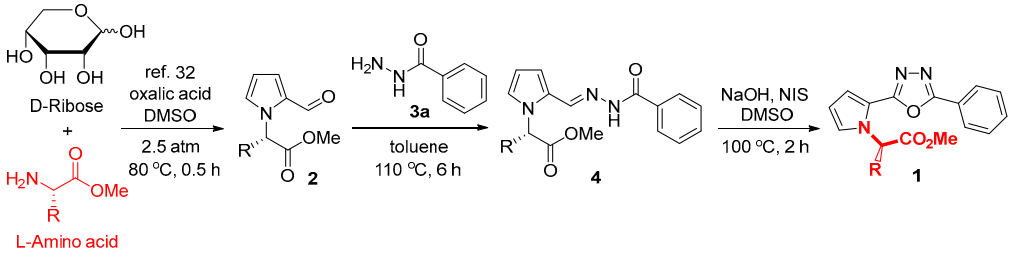

Scheme 1. Preparations of pyrrole-2-carbaldehydes **2**, *N*-benzoylhydrazones **4**, and 1,3,4-oxadiazoles **1** from D-ribose conversion with L-amino acids.

Table 1. Yields of pyrrole-2-carbaldehydes **2**, *N*-benzoylhydrazones **4**, and 1,3,4-oxadiazoles **1** from D-ribose conversion with L-amino acids in Scheme 1. 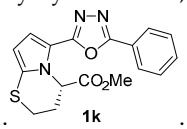 **1k** .

Entry	Amino Acid (R)	Yield 2 (%) [1]	Yield 4 (%) [2]	Yield 1 (%) [2]
a	Gly (H)	32	96	80
b	Ala (Me)	38	88	91
c	Val (*i*-Pr)	42	83	98
d	Leu (*i*-Bu)	63	77	87
e	Ile (*s*-Bu)	40	86	90
f	Phe ($PhCH_2$)	54	83	86
g	Bn ($PhCH_2CH_2$)	53	79	86
h	AsP (MeO_2CCH_2)	47	70	88
i	Glu ($MeO_2CCH_2CH_2$)	37	81	95
j	Met ($MeSCH_2CH_2$)	46	82	50 [3]

[1] Yields from one-pot reaction [32]. [2] Isolated yields after SiO_2 flash column chromatography. [3] Cyclized product **1k** was also obtained in 49% yield.

Two representative procedures are generally utilized for the construction of the 1,3,4-oxadizole core, as depicted in Figure 1 [12]. The cyclodehydration route from diacylhydrazine [C] is suitable for pyrrole-2-carboxylic acids [36], whereas the oxidative cyclization route from *N*-acylhydrazone [D] is widely used for pyrrole-2-carbaldehydes as starting materials [37]. There were various cyclization conditions for 1,3,4-oxadiazoles reported for each conversion [12]. We adopted the oxidative cyclization route of *N*-acylhydrazones **4**, which can be obtained from pyrrole-2-carbaldehydes **2** by condensation with benzohydrazide **3a**. The corresponding *N*-benzoylhydrazones **4a**–**4j** were obtained in decent yields (70~96%) at the reflux temperature of toluene. Oxidative cyclization conditions were then screened using NBS, NIS, and I_2 under K_2CO_3, DBU, Et_3N, and NaOH as a base. The condition using NIS/NaOH in DMSO at 100 °C was optimal for providing pyrrole-ligated 1,3,4-oxadiazoles **1** in yields of 80~98%. It is noteworthy that the NIS-mediated further cyclization of the methylsulfide chain on the pyrrole ring occurred partly for **1j** derived from methionine to produce **1k** (at a yield of 49%), which explains the lower yield of **1j** (50%). All eleven pyrrole-ligated oxadiazoles **1a**–**1j** were rapidly assembled from pyrrole platform chemicals **2** with different amino acid residues and ready for antibacterial assays against *Escherichia coli* and *Staphylococcus aureus* as two representative Gram(–) and Gram(+) bacteria (Table 2).

Table 2. Minimum inhibition activity (MIC) of 2-pyrrolyl-5-phenyl-1,3,4-oxadiazoles **1** against *E. coli* and *S. aureus*.

Entry	Compound	Amino Acid (R)	MIC/*E. coli* (μg/mL)	MIC/*S. aureus* (μg/mL)
1	**1a**	Gly (H)	>2048	2048
2	**1b**	Ala (Me)	512	512
3	**1c**	Val (*i*-Pr)	256	128
4	**1d**	Leu (*i*-Bu)	512	128
5	**1e**	Ile (*s*-Bu)	256	64
6	**1f**	Phe ($PhCH_2$)	1024	512
7	**1g**	Bn ($PhCH_2CH_2$)	1024	512
8	**1h**	Asp (MeO_2CCH_2)	2048	1024
9	**1i**	Glu ($MeO_2CCH_2CH_2$)	2048	2048
10	**1j**	Met ($MeSCH_2CH_2$)	>2048	2048
11	**2k**	*c*-Met (SCH_2CH_2)	256	256

There was a definite size effect of the alkyl substituent R on antibacterial activity in 1,3,4-oxadiazoles **1**. The highest MIC value was required for **1a** from glycine (R = H), and it decreased as the size (branch) of the alkyl group increased from alanine (R = Me) to isoleucine (R = *s*-Bu) (entries 1–5, Table 2). A benzene ring seemed be unimportant, judging from the cases of the benzyl and homobenzyl substituents (entries 6–7). There was no functional group effect for the ester and sulfide, reflecting a lack of electronic interactions between the substituent R and the bacterial enzymes. A comparison of the MIC values for **1j** and its cyclized derivative **1k** confirmed the importance of the size (or rigidity) effect of R on antibacterial activity (entries 10 and 11). An additional point to mention is that the MIC values for **1** were not much different between Gram(–) and Gram(+) bacteria, indicating that there would be no transport barriers through membranes for these small molecules.

The electronic effects of the substituents on the phenyl ring against antibacterial activities were then investigated for 2-pyrrolyl-5-phenyl-1,3,4-oxadiazoles **5** and **6** with the maximum size effect in the series, derived from valine (R = isopropyl) and isoleucine (R = *sec*-butyl), respectively. Commercial benzohydrazides **3** with a substituent X of a different electronic nature (e.g., F, Cl, OH, and OMe) were utilized in the synthesis of **5** and **6** (Scheme 2 and Table 3). The condensation reaction of pyrrole-2-carbaldehyde **2c** (R = *i*-Pr) and **2e** (R = *s*-Bu) with various benzohydrazides **3** produced the corresponding *N*-benzoylhydrazone intermediates in refluxing toluene, which underwent an oxidative cyclization reaction (without purification) to afford 2-pyrrolyl-5-phenyl-1,3,4-oxadiazoles **5** (R = *i*-Pr) and **6** (R = *s*-Bu) with various electronic substituents X on the phenyl ring.

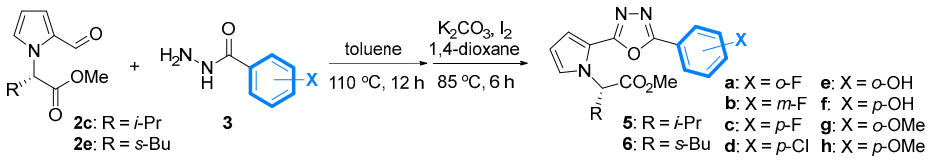

Scheme 2. Two-step preparation of various 1,3,4-oxadiazoles **5** and **6** with various electronic substituents X, derived from valine and isoleucine.

A milder oxidative cyclization condition was required in these cases, for which I_2/K_2CO_3 in 1,4-dioxane at 85 °C was optimal for the production of **5** in yields of 40~85% and **6** in yields of 62~89% in two steps [38]. Serendipitously, we found extra iodination reactions under the oxidative cyclization conditions for 1,3,4-oxadiazoles **5e**, **5f**, **6e**, and **6f** with phenol substituents, obtaining the corresponding di-iodination or tetra-iodination products **5e-1**, **5f-1**, **6e-1**, and **6f-1**, respectively in yields of 32~45% (Figure 2). It was very fortunate to achieve further iodination on the phenol rings so that we were able to find the superior Iodophenol antibacterial effects for these oxadiazole derivatives (vide infra). The corresponding deiodination (originally intended) products were prepared by reduction

using Zn dust in AcOH to produce **5f** (X = *p*-OH) in a yield of 97%, **6e** (X = *o*-OH) in a yield of 50%, and **6f** (X = *p*-OH) in a yield of 42%.

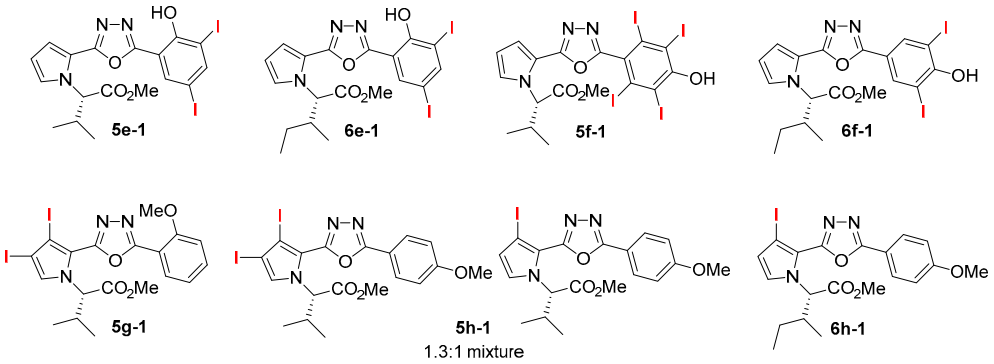

Figure 2. Extra iodination products from 2-pyrrolyl-5-phenyl-1,3,4-oxadiazoles **5** and **6**.

Table 3. Yields of various 1,3,4-oxadiazoles **5** and **6** with various electronic substituents X, derived from valine and isoleucine in Scheme 2.

Entry	X	Yield 5 (%)	Yield 6 (%)
a	*o*-F	40	89
b	*m*-F	70	88
c	*p*-F	54	62
d	*p*-Cl	62	79
e-1	*o*-OH (I)	33 [1]	45 [2]
e	*o*-OH	-	50 [3]
f-1	*p*-OH (I)	32 [4]	43 [5]
f	*p*-OH	97 [6]	42 [7]
g	*o*-OMe	85	80
g-1	*o*-OMe	61 [8]	-
h	*p*-OMe	70	79
h-1	*p*-OMe	69 [9]	83 [10]

The structures of [1] **5e-1**, [2] **6e-1**, [4] **5f-1**, [5] **6f-1**. [8] **5g-1**, [9] **5h-1**, and [10] **6h-1** are depicted in Figure 2, which were produced by extra iodination reactions. The compounds [3] **6e**, [6] **5f**, and [7] **6f** were prepared by deiodination using Zn in AcOH at 25 °C from **6e-1**, **5f-1**, and **6f-1**, respectively. The compounds [8] **5g-1**, [9] **5h-1**, and [10] **6h-1** were prepared by separate iodination reaction (I_2 in DMSO) at 85 °C for 6 h from **5g**, **5h**, and **6h**, respectively.

To assess the "iodine effect" on antibacterial activity, separate iodination reactions (I_2 in DMSO at 85 °C) were intentionally carried out for the 1,3,4-oxadiazoles **5g**, **5h**, and **6h** with the electron-rich anisole substituent in which 3-mono-iodination or 3,4-di-iodination reactions proceeded on the pyrrole ring (not on the anisole ring) to provide the corresponding **5g-1** (X = *o*-OMe) in a yield of 61%, **5h-1** (X = *p*-OMe) in a yield of 69% as a 1.3:1 mixture of di- and 3′-mono-iodination products, and **6h-1** (X = *p*-OMe) in a yield of 83%, respectively. All twenty-two pyrrole-ligated oxadiazoles **5** and **6** were rapidly assembled from pyrrole-2-carbaldehydes **2c** (R = *i*-Pr) and **2e** (R = *s*-Bu) with diversely X-substituted benzohydrazide **3** and ready for antibacterial assays against *Escherichia coli*, *Staphylococcus aureus*, and *Acinetobacter baumannii* together with Vancomycin and Erythromycin as positive controls (Table 4).

SARs of the phenyl substituent X of 2-pyrrolyl-5-phenyl-1,3,4-oxadiazoles **5** and **6** can be deduced from the MIC (μg/mL) in Table 4. *ortho*-F substitutions provided generally better antibacterial activities than the *meta*- and *para*-F counterparts (entries 1–3 and 12–14), and chloride was better than fluoride (entries 4 and 15 versus 3 and 14). Iodophenol substituents exhibited superior antibacterial activities against *A. baumannii* and *S. aureus* regardless of the position of the hydroxyl substituent (entries 5, 6, 16, and 18). The MIC values of <2 μg/mL for **5f-1** and 8 μg/mL for **6f-1** against *A. baumannii* were much lower than those of the positive controls (>1024 μg/mL for vancomycin and 128 μg/mL for erythromycin). The "iodophenol effect" on antibacterial activity is obvious when compared with the cases

of deiodination products **5f** and **6f**, the MIC values for which were significantly increased to 128 μg/mL and 512 μg/mL, respectively (entries 7 and 19). The mechanism of the "iodophenol effect" is not clear at present, but it is reasonable to explain that iodide or molecular I_2 may be liberated by the neighboring OH group [39]. No effects or only slight improvements in antibacterial activities were observed for the pyrrole iodination products **5g-1** and **5h-1** from **5g** and **5h** (entries 8–11), whereas the reverse effect was clear for the pyrrole iodination product **6h-1** from **6h** (entries 21 and 22).

Table 4. Minimum inhibition concentration (MIC) of 1,3,4-oxadiazoles **5** and **6** against *E. coli*, *S. aureus*, and *A. baumannii*.

Entry	Comp'd	X	*E. coli* (μg/mL)	*S. aureus* (μg/mL)	*A. baumannii* (μg/mL)
1	**5a**	*o*-F	512	256	128
2	**5b**	*m*-F	>1024	>1024	512
3	**5c**	*p*-F	>1024	>1024	256
4	**5d**	*p*-Cl	512	256	512
5	**5e-1**	*o*-OH (I) [1]	1024	4	64
6	**5f-1**	*p*-OH (I) [1]	1024	4	<2
7	**5f**	*p*-OH	>1024	128	128
8	**5g**	*o*-OMe	>1024	512	256
9	**5g-1**	*o*-OMe (I) [2]	512	512	256
10	**5h**	*p*-OMe	>1024	512	256
11	**5h-1**	*p*-OMe (I) [2]	512	256	128
12	**6a**	*o*-F	512	256	256
13	**6b**	*m*-F	1024	256	256
14	**6c**	*p*-F	>1024	512	512
15	**6d**	*p*-Cl	512	512	256
16	**6e-1**	*o*-OH (I) [1]	1024	<2	512
17	**6e**	*o*-OH	256	64	64
18	**6f-1**	*p*-OH (I) [1]	1024	<2	8
19	**6f**	*p*-OH	1024	8	512
20	**6g**	*o*-OMe	>1024	512	256
21	**6h**	*p*-OMe	>1024	256	256
22	**6h-1**	*p*-OMe (I) [2]	1024	512	512
23	Vancomycin	-	>1024	4	>1024
24	Erythromycin	-	1024	4	128

[1] Extra iodination product on the phenol ring. [2] Extra iodination product on the pyrrole ring. The structures of extra iodination products are depicted in Figure 2.

3. Materials and Methods

3.1. Experimental

3.1.1. General Chemical Syntheses

^{1}H- and ^{13}C-NMR spectra were recorded on 400 MHz and 100 MHz NMR spectrometers, respectively, in a deuterated solvent (notified in parenthesis) with tetramethylsilane (TMS) as an internal reference. The column chromatography was performed using the method of Still with silica gel 60 and a 70–230 mesh ASTM, using a gradient mixture of EtOAc/hexanes. Reactions were performed in a well-dried flask under an argon atmosphere unless mentioned otherwise.

3.1.2. General Procedure for the Preparation of 1

Formation of Hydrazone 4 from pyrrole-2-carbaldehyde (Step-1): The solution of pyrraline **2** (~1.00 g, 1 equiv.) and benzohydrazide **3a** (1 equiv.) in toluene (10 mL) was heated at 110 °C for 6 h. The reaction mixture was cooled to room temperature, diluted with EtOAc, washed with brine and H_2O, dried over anhydrous Na_2SO_4, filtered, and concentrated under reduced pressure. The crude product was purified by SiO_2 flash column chromatography to obtain the corresponding benzohydrazone **4**.

2-pyrrolyl-5-phenyl-1,3,4-oxadiazole 1 from hydrazone 4 (Step-2): The mixture of benzohydrazone **4** (1 equiv.), NaOH (2 equiv.), and *N*-iodosuccinimide (1 equiv.) in DMSO (10 mL) was heated at 110 °C for 2 h. The reaction mixture was cooled to room temperature, diluted with EtOAc, washed with brine and H_2O, dried over anhydrous Na_2SO_4, filtered, and concentrated under reduced pressure. The crude product was purified by SiO_2 flash column chromatography to obtain the corresponding 2-pyrrolyl-5-phenyl-1,3,4-oxadiazole **1**.

Methyl 2-(2-(5-phenyl-1,3,4-oxadiazol-2-yl)-1H-pyrrol-1-yl)acetate (**1a**). Data for **4a**: white solid in a yield of 96% (1.64 g, 5.76 mmol); ^{1}H-NMR (DMSO-d_6) δ = 3.69 (s, 3H), 5.21 (s, 2H), 6.16 (dd, *J* = 3.6, 2.8 Hz, 1H), 6.53 (dd, *J* = 3.6, 1.6 Hz, 1H), 7.02 (dd, *J* = 2.8, 1.6 Hz, 1H), 7.48–7.54 (m, 2H), 7.54–7.60 (m, 1H), 7.86–7.90 (m, 2H), 8.28 (s, 1H), 11.49 (s, 1H) ppm; ^{13}C-NMR (DMSO-d_6) δ = 51.1, 53.1, 109.9, 117.2, 128.4, 128.7, 129.7, 129.9, 132.7, 134.9, 142.0, 163.7, 170.7 ppm; IR (CH_2Cl_2) ν = 3237, 3063, 3006, 2954, 2848, 1750, 1649, 1616, 1552, 1494, 1468, 1433, 1345, 1322, 1279, 1216, 1188, 1140, 1086, 1031, 1001, 914, 801, 754, 690 cm^{-1}.

Data for **1a**: light-yellow solid in a yield of 80% (0.60 g, 2.13 mmol); ^{1}H-NMR (acetone-d_6) δ = 3.73 (s, 3H), 5.39 (s, 2H), 6.32 (dd, *J* = 4.0, 2.4 Hz, 1H), 7.06 (dd, *J* = 4.0, 1.6 Hz, 1H), 7.18 (dd, *J* = 2.4, 1.6 Hz, 1H), 7.57–7.65 (m, 3H), 8.08–8.14 (m, 2H) ppm; ^{13}C-NMR (acetone-d_6) δ = 50.1, 51.6, 109.2, 114.3, 117.5, 124.0, 126.5, 129.1, 129.2, 131.6, 159.1, 162.4, 168.9 ppm; IR ν = 3119, 3069, 2957, 2927, 2857, 1752, 1713, 1614, 1556, 1501, 1490, 1455, 1424, 1401, 1376, 1328, 1304, 1297, 1264, 1213, 1106, 1081, 995, 956, 787, 773, 760, 725, 693, 583 cm^{-1}; HRMS (ESI) calcd for $C_{15}H_{13}N_3O_3$+Na, 306.0849: found 306.0851.

Methyl (S)-2-(2-(5-phenyl-1,3,4-oxadiazol-2-yl)-1H-pyrrol-1-yl)propanoate (**1b**). Data for **4b**: white solid in a yield of 88% (1.45 g, 4.85 mmol); ^{1}H-NMR (DMSO-d_6) δ = 1.70 (d, *J* = 7.2 Hz, 3H), 3.67 (s, 3H), 6.02 (q, *J* = 7.2 Hz, 1H), 6.20 (dd, *J* = 3.6, 2.8 Hz, 1H), 6.54 (dd, *J* = 3.6, 1.6 Hz, 1H), 7.17 (dd, *J* = 2.8, 1.6 Hz, 1H), 7.48–7.61 (m, 3H), 7.86–7.92 (m, 2H), 8.32 (s, 1H), 11.51 (s, 1H) ppm; ^{13}C-NMR (DMSO-d_6) δ = 19.1, 53.4, 56.1, 110.2, 117.5, 126.6, 128.2, 128.7, 129.6, 132.7, 134.9, 142.4, 163.7, 172.8 ppm; IR ν = 3232, 3065, 2954, 1748, 1716, 1644, 1612, 1556, 1494, 1461, 1426, 1359, 1286, 1225, 1146, 1091, 1063, 1031, 962, 910, 887, 857, 802, 714, 695 cm^{-1}; HRMS (ESI) calcd for $C_{16}H_{17}N_3O_3$+Na, 322.1162: found 322.1164.

Data for **1b**: light-yellow solid in a yield of 91% (0.70 g, 2.35 mmol); ^{1}H-NMR (CD_3OD) δ = 1.82 (d, *J* = 7.2 Hz, 3H), 3.71 (s, 3H), 6.00 (q, *J* = 7.2 Hz, 1H), 6.33 (dd, *J* = 4.0, 2.8 Hz, 1H), 7.02 (dd, *J* = 4.0, 1.6 Hz, 1H), 7.23 (dd, *J* = 2.8, 1.6 Hz, 1H), 7.50–7.59 (m, 3H), 8.00–8.04 (m, 2H) ppm; ^{13}C-NMR (CD_3OD) δ = 19.5, 54.5, 58.5, 112.2, 117.6, 119.7, 126.0, 128.1, 129.1, 131.7, 134.4, 162.1, 165.5, 174.7 ppm; IR ν = 3129, 3003, 2955, 2848, 1751, 1663, 1608, 1553, 1505, 1450, 1384, 1336, 1289, 1224, 1203, 1110, 1091, 1062, 1015, 981, 962, 853, 813, 776, 729, 691, 610 cm^{-1}; HRMS (ESI) calcd for $C_{16}H_{15}N_3O_3$+Na, 320.1006: found 320.1007.

Methyl (S)-3-methyl-2-(2-(5-phenyl-1,3,4-oxadiazol-2-yl)-1H-pyrrol-1-yl)butanoate (**1c**). Data for **4c**: white solid in a yield of 83% (1.30 g, 3.98 mmol); ^{1}H-NMR (DMSO-d_6) δ = 1.03 (d, *J* = 6.8 Hz, 3H), 1.35 (d, *J* = 6.8 Hz, 3H), 2.76 (m, 1H), 4.04 (s, 3H), 6.35 (d, *J* = 8.8 Hz, 1H), 6.57 (dd, *J* = 3.6, 2.8 Hz, 1H), 6.87 (dd, *J* = 3.6, 1.6 Hz, 1H), 7.51 (dd, *J* = 2.8, 1.6 Hz, 1H), 7.82–7.97 (m, 3H), 8.21–8.30 (m, 2H), 8.73 (s, 1H), 11.90 (s, 1H) ppm; ^{13}C-NMR (DMSO-d_6) δ = 17.6, 18.4, 31.3, 51.4, 62.8, 108.8, 114.6, 124.7, 126.6, 126.7, 127.6, 130.7, 132.8, 140.3, 161.7, 169.9 ppm; IR ν = 3241, 3071, 2975, 2878, 1750, 1644, 1615, 1557, 1495, 1459, 1433, 1392, 1356, 1286, 1211, 1160, 1133, 1083, 1057, 1023, 1005, 952, 915, 890, 835, 800, 755, 715, 695, 617 cm^{-1}.

Data for **1c**: light-yellow solid in a yield of 98% (0.15 g, 0.46 mmol); ^{1}H-NMR (CD_3OD) δ = 0.81 (d, *J* = 7.2 Hz, 3H), 1.08 (d, *J* = 7.2 Hz, 3H), 2.53 (m, 1H), 3.76 (s, 3H), 5.99 (d, *J* = 10.0 Hz, 1H), 6.38 (dd, *J* = 4.0, 2.8 Hz, 1H), 7.03 (dd, *J* = 4.0, 1.6 Hz, 1H), 7.36 (dd, *J* = 2.8, 1.6 Hz, 1H), 7.54–7.64 (m, 3H), 8.06–8.12 (m, 2H) ppm; ^{13}C-NMR (CD_3OD) δ = 20.4, 21.1, 35.2, 54.1, 67.1, 112.3, 119.0, 128.5, 130.0, 130.5, 131.1, 134.4, 136.0, 145.0, 167.8, 174.2 ppm; IR ν = 2958, 2927, 2851, 1744, 1669, 1609, 1560, 1500, 1454, 1376, 1260, 1221, 1105, 1076, 1013, 775, 727, 691 cm^{-1}; HRMS (ESI) calcd for $C_{18}H_{19}N_3O_3$+Na, 348.1319: found 348.1319.

Methyl (S)-4-methyl-2-(2-(5-phenyl-1,3,4-oxadiazol-2-yl)-1H-pyrrol-1-yl)pentanoate (**1d**). Data for **4d**: white solid in a yield of 77% (1.18 g, 3.46 mmol); ^{1}H-NMR (DMSO-d_6) δ = 0.86 (d, *J* = 6.4 Hz, 3H), 0.92 (d, *J* = 6.4 Hz, 3H), 1.92 (dd of A of ABq, J_{AB} = 14.0, J_d = 9.2, 4.8 Hz, 1H), 2.12 (dd of B of ABq, J_{AB} = 14.0, J_d = 11.6, 4.4 Hz, 1H), 3.67 (s, 3H), 6.21 (dd, *J* = 3.6,

2.8 Hz, 1H), 6.30 (dd, *J* = 9.2, 4.4 Hz, 1H), 6.52 (dd, *J* = 3.6, 1.6 Hz, 1H), 7.19 (dd, *J* = 2.8, 1.6 Hz, 1H), 7.48–7.62 (m, 3H), 7.86–7.92 (m, 2H), 8.34 (s, 1H), 11.52 (s, 1H) ppm; ^{13}C-NMR (DMSO-d_6) δ = 22.6, 24.1, 25.7, 42.1, 53.5, 58.5, 110.6, 117.6, 127.2, 128.4, 128.7, 129.6, 132.7, 134.8, 142.5, 163.6, 172.8 ppm; IR ν = 3234, 3065, 2956, 2874, 1743, 1646, 1614, 1556, 1495, 1459, 1427, 1348, 1278, 1240, 1203, 1174, 1086, 1034, 998, 953, 928, 903, 795, 754 cm^{-1}.

Data for **1d**: light-yellow solid in 87% yield (1.35g, 4.01 mmol); ^{1}H-NMR (acetone-d_6) δ = 0.94 (d, *J* = 6.4 Hz, 3H), 0.95 (d, *J* = 6.4 Hz, 3H), 1.49 (m, 1H), 2.02–2.16 (m, 1H), 2.16–2.30 (m, 1H), 3.71 (s, 3H), 6.38 (dd, *J* = 3.6, 2.8 Hz, 1H), 7.06 (dd, *J* = 3.6, 1.6 Hz, 1H), 7.34 (dd, *J* = 2.8, 1.6 Hz, 1H), 7.56–7.65 (m, 3H), 8.08–8.16 (m, 2H) ppm; ^{13}C-NMR (acetone-d_6) δ = 20.9, 22.3, 24.7, 41.0, 51.9, 58.0, 109.8, 114.4, 117.6, 123.9, 126.1, 126.6, 129.2, 131.6, 159.3, 162.3, 171.2 ppm; IR ν = 3119, 3069, 2957, 2867, 1750, 1704, 1664, 1609, 1557, 1504, 1454, 1412, 1369, 1333, 1273, 1240, 1197, 1176, 1133, 1106, 1080, 1021, 1000, 964, 925, 880, 836, 811, 730, 690, 613 cm^{-1}; HRMS (ESI) calcd for $C_{19}H_{21}N_3O_3$+Na, 362.1475: found 362.1474.

Methyl (2S,3S)-3-methyl-2-(2-(5-phenyl-1,3,4-oxadiazol-2-yl)-1H-pyrrol-1-yl)pentanoate (**1e**). Data for **4e**: white solid in a yield of 86% (0.91 g, 2.67 mmol); ^{1}H-NMR (DMSO-d_6) δ = 0.79 (t, J = 7.2 Hz, 3H), 0.96 (d, *J* = 6.4 Hz, 3H), 1.01–1.20 (m 2H), 2.15–2.26 (m 2H), 3.69 (s, 3H), 6.03 (d, J = 6.8 Hz, 1H), 6.22 (dd, *J* = 3.6, 2.8 Hz, 1H), 6.52 (dd, *J* = 3.6, 1.6 Hz, 1H), 7.18 (dd, *J* = 2.8, 1.6 Hz, 1H), 7.49–7.62 (m, 3H), 7.88–7.95 (m, 2H), 8.39 (s, 1H), 11.55 (s, 1H) ppm; ^{13}C-NMR (DMSO-d_6) δ = 10.7, 15.5, 24.3, 38.1, 52.2, 62.8, 109.7, 115.5, 125.4, 127.5, 127.6, 128.4, 131.6, 133.6, 141.1, 162.5, 170.9 ppm.

Data for **1e**: light-yellow solid in 90% yield (0.42 g, 1.23 mmol, a 2:1 mixture of stereoisomers); ^{1}H-NMR (major isomer, $CDCl_3$) δ = 0.84 (t, *J* = 7.2 Hz, 3H), 1.05 (d, *J* = 6.4 Hz, 3H), 1.06–1.28 (m, 2H), 2.27–2.40 (m, 1H), 3.75 (s, 3H), 6.18 (d, *J* = 10.4 Hz, 1H), 6.39 (dd, *J* = 4.0, 2.8 Hz, 1H), 7.04 (dd, *J* = 4.0, 2.0 Hz, 1H), 7.40 (dd, *J* = 2.8, 2.0 Hz, 1H), 7.58–7.66 (m, 3H), 8.10–8.16 (m, 2H) ppm; ^{13}C-NMR (major isomer, $CDCl_3$) δ = 10.1, 15.0, 24.7, 38.8, 51.7, 63.7, 110.1, 114.0, 114.1, 123.9, 126.0, 126.6, 129.2, 131.6, 159.3, 162.4, 170.7 ppm; IR ν = 3144, 3124, 3066, 2970, 2932, 2879, 1747, 1704, 1606, 1552, 1501, 1492, 1449, 1414, 1387, 1334, 1284, 1236, 1196, 1178, 1100, 1077, 1020, 964, 926, 883, 727, 694, 618 cm^{-1}; HRMS (ESI) calcd for $C_{19}H_{21}N_3O_3$+Na, 362.1475: found 362.1475.

Methyl (S)-3-phenyl-2-(2-(5-phenyl-1,3,4-oxadiazol-2-yl)-1H-pyrrol-1-yl)propanoate (**1f**). Data for **4f**: white solid in a yield of 83% (0.94 g, 2.51 mmol); ^{1}H-NMR (DMSO-d_6) δ = 3.42 (d of A of ABq, J_{AB} = 14.4, J_d = 10.0 Hz, 1H), 3.49 (d of B of ABq, J_{AB} = 14.4, J_d = 6.4 Hz, 1H), 3.67 (s, 3H), 6.11 (dd, *J* = 3.6, 2.8 Hz, 1H), 6.43 (dd, *J* = 3.6, 1.6 Hz, 1H), 6.49 (dd, *J* = 10.0, 6.4 Hz, 1H), 7.10–7.25 (m, 6H), 7.50–7.62 (m, 3H), 7.88–7.93 (m, 2H), 8.23 (s, 1H), 11.50 (s, 1H) ppm; ^{13}C-NMR (DMSO-d_6) δ = 39.1, 53.6, 61.1, 110.4, 117.6, 127.5, 127.7, 128.2, 128.7, 129.3, 129.7, 130.4, 132.8, 134.9, 137.9, 142.2, 163.8, 171.7 ppm; IR ν = 3236, 3064, 3033, 2957, 2843, 1743, 1645, 1613, 1555, 1497, 1455, 1436, 1348, 1280, 1220, 1185, 1164, 1076, 1032, 1008, 904, 843, 802, 753, 699 cm^{-1}.

Data for **1f**: light-yellow solid in a yield of 86% (2.31 g, 6.19 mmol); ^{1}H-NMR (CD_3OD) δ = 3.38 (d of A of ABq, J_{AB} = 14.0, J_d = 10.0 Hz, 1H), 3.59 (d of B of ABq, J_{AB} = 14.0, J_d = 5.2 Hz, 1H), 3.75 (s, 3H), 6.29 (dd, *J* = 4.0, 2.8 Hz, 1H), 6.39 (dd, *J* = 10.0, 5.2 Hz, 1H), 6.90 (dd, *J* = 4.0, 1.6 Hz, 1H), 7.02–7.14 (m, 5H), 7.24 (dd, *J* = 2.8, 1.6 Hz, 1H), 7.54–7.62 (m, 3H), 8.01–8.05 (m, 2H) ppm; ^{13}C-NMR (CD_3OD) δ = 41.4, 54.6, 63.9, 112.5, 117.3, 119.8, 126.0, 129.2, 129.2, 129.4, 130.7, 131.5, 131.8, 134.5, 139.0, 162.1, 165.5, 173.4 ppm; IR ν = 3068, 3033, 3004, 2956, 2848, 1747, 1703, 1665, 1606, 1559, 1505, 1449, 1412, 1372, 1337, 1274, 1230, 1201, 1174, 1107, 1083, 1012, 982, 926, 884, 778, 728, 699, 615 cm^{-1}; HRMS (ESI) calcd for $C_{22}H_{19}N_3O_3$+Na 396.1319, found 396.1321.

Methyl (S)-4-phenyl-2-(2-(5-phenyl-1,3,4-oxadiazol-2-yl)-1H-pyrrol-1-yl)butanoate (**1g**). Data for **4g**: white solid in a yield of 79% (1.31 g, 3.48 mmol); ^{1}H-NMR (DMSO-d_6) δ = 2.36–2.60 (m, 4H), 3.68 (s, 3H), 6.00–6.07 (m, 1H), 6.26 (dd, *J* = 3.6, 2.8 Hz, 1H), 6.58 (dd, *J* = 3.6, 1.2 Hz, 1H), 7.11–7.28 (m, 6H), 7.50–7.61 (m, 3H), 7.87–7.92 (m, 2H), 8.34 (s, 1H), 11.52 (s, 1H) ppm; ^{13}C-NMR (DMSO-d_6) δ = 32.8, 35.1, 53.5, 60.1, 110.6, 117.2, 127.2, 128.5, 128.7, 129.5, 129.6, 129.6, 129.6, 132.7, 134.8, 141.8, 142.3, 163.7, 172.1 ppm; IR ν = 3227, 3063, 3030, 2951, 2866,

1744, 1646, 1610, 1558, 1494, 1457, 1431, 1325, 1287, 1217, 1164, 1079, 1055, 1037, 1029, 1004, 952, 913, 755, 698 cm^{-1}.

Data for **1g**: light-yellow solid in 86% yield (0.42 g, 1.13 mmol); ^{1}H-NMR (CD_3OD) δ = 2.40–2.67 (m, 4H), 3.71 (s, 3H), 5.92 (dd, *J* = 10.4, 4.0 Hz, 1H), 6.43 (dd, *J* = 4.0, 2.8 Hz, 1H), 6.99–7.05 (m, 3H), 7.06 (dd, *J* = 4.0, 1.6 Hz, 1H), 7.08–7.16 (m, 2H), 7.31 (dd, *J* = 2.8, 1.6 Hz, 1H), 7.53–7.62 (m, 3H), 8.00–8.06 (m, 2H) ppm; ^{13}C-NMR (CD_3OD) δ = 31.4, 33.3, 51.7, 58.9, 110.0, 114.5, 117.3, 123.2, 125.8, 126.0, 126.4, 128.0, 128.0, 129.0, 131.7, 139.8, 159.2, 162.7, 171.3 ppm; IR ν = 3064, 3026, 2956, 2931, 2854, 1745, 1662, 1606, 1557, 1504, 1450, 1415, 1254, 1233, 1198, 1177, 1082, 1012, 979, 814, 772, 725, 698, 605 cm^{-1}; HRMS (ESI) calcd for $C_{23}H_{21}N_3O_3$+Na, 410.1475: found 410.1477.

Dimethyl (S)-2-(2-(5-phenyl-1,3,4-oxadiazol-2-yl)-1H-pyrrol-1-yl)succinate (**1h**). Data for **4h**: white solid in a yield of 81% (1.01g, 2.84 mmol); ^{1}H-NMR (CD_3OD) δ = 3.27 (d of A of ABq, J_{AB} = 16.8, J_d = 8.0 Hz, 1H), 3.37 (d of B of ABq, J_{AB} = 16.8, J_d = 6.0 Hz, 1H), 3.63 (s, 3H), 3.73 (s, 3H), 6.20 (dd, *J* = 3.6, 2.8 Hz, 1H), 6.32 (dd, *J* = 8.0, 6.0 Hz, 1H), 6.58 (dd, *J* = 3.6, 1.6 Hz, 1H), 7.02 (dd, *J* = 2.8, 1.6 Hz, 1H), 7.46–7.60 (m, 3H), 7.86–7.91 (m, 2H), 8.24 (s, 1H) ppm; ^{13}C-NMR (CD_3OD) δ = 39.4, 53.8, 54.6, 59.5, 112.0, 120.3, 129.4, 129.9, 130.0, 131.1, 134.4, 136.0, 144.6, 167.8, 173.2, 173.8 ppm; IR ν = 3411, 2958, 1737, 1644, 1613, 1581, 1554, 1495, 1444, 1414, 1348, 1285, 1238, 1177, 1123, 1084, 1008, 979, 908, 803, 786, 712 cm^{-1}.

Data for **1h**: light-yellow solid in 88% yield (0.79 g, 2.22 mmol); ^{1}H-NMR (CD_3OD) δ = 3.25 (d of A of ABq, J_{AB} = 16.8, J_d = 8.0 Hz, 1H), 3.41 (d of B of ABq, J_{AB} = 16.8, J_d = 6.0 Hz, 1H), 3.63 (s, 3H), 3.72 (s, 3H), 6.32 (dd, *J* = 3.6, 2.8 Hz, 1H), 6.39 (dd, *J* = 8.0, 6.0 Hz, 1H), 7.03 (dd, *J* = 3.6, 1.6 Hz, 1H), 7.17 (dd, *J* = 2.8, 1.6 Hz, 1H), 7.50–7.60 (m, 3H), 8.00–8.07 (m, 2H) ppm; ^{13}C-NMR (CD_3OD) δ = 36.4, 51.2, 52.0, 56.8, 109.8, 115.0, 117.0, 123.2, 126.4, 126.7, 129.0, 131.7, 159.1, 162.8, 169.9, 170.5 ppm; IR ν = 3123, 3006, 2958, 2854, 1741, 1662, 1605, 1553, 1505, 1485, 1439, 1417, 1371, 1271, 1224, 1173, 1083, 1010, 985, 860, 819, 781, 726, 692, 672, 611 cm^{-1}; HRMS (ESI) calcd for $C_{18}H_{17}N_3O_5$+Na, 378.1060: found 378.1062.

Dimethyl (S)-2-(2-(5-phenyl-1,3,4-oxadiazol-2-yl)-1H-pyrrol-1-yl)pentanedioate (**1i**). Data for **4i**: white solid in a yield of 70% (1.52 g, 4.08 mmol), ^{1}H-NMR (DMSO-d_6) δ = 2.10–2.21 (m, 1H), 2.24–2.42 (m, 2H), 2.44–2.53 (m, 1H), 3.55 (s, 3H), 3.70 (s, 3H), 6.01–6.09 (m, 1H), 6.22 (dd, *J* = 3.6, 2.8 Hz, 1H), 6.55 (dd, *J* = 3.6, 1.6 Hz, 1H), 7.12 (dd, *J* = 2.8, 1.6 Hz, 1H), 7.49–7.61 (m, 3H), 7.87–7.92 (m, 2H), 8.32 (s, 1H) ppm; ^{13}C-NMR (DMSO-d_6) δ = 28.7, 31.3, 52.7, 53.6, 59.7, 110.7, 117.5, 127.6, 128.5, 128.7, 129.7, 132.8, 134.8, 142.2, 163.7, 171.7, 173.5 ppm; IR ν = 3234, 3020, 2954, 1738, 1650, 1615, 1558, 1458, 1437, 1346, 1280, 1218, 1177, 1075, 1029, 913, 888, 801, 753 cm^{-1}.

Data for **1i**: light-yellow solid in a yield of 95% (1.04 g, 2.82 mmol); ^{1}H-NMR (acetone-d6) δ = 2.24–2.39 (m, 2H), 2.44–2.54 (m, 1H), 2.63–2.73 (m, 1H), 3.57 (s, 3H), 3.73 (s, 3H), 6.24 (dd, *J* = 10.8, 5.2 Hz, 1H), 6.39 (dd, *J* = 3.6, 2.8 Hz, 1H), 7.06 (dd, *J* = 3.6, 1.6 Hz, 1H), 7.30 (dd, *J* = 2.8, 1.6 Hz, 1H), 7.58–7.65 (m, 3H), 8.10–8.16 (m, 2H) ppm; ^{13}C-NMR (acetone-d6) δ = 29.4, 31.4, 52.6, 53.7, 60.7, 111.8, 116.2, 119.4, 125.6, 128.0, 128.3, 130.9, 133.3, 160.9, 164.1, 172.0, 173.7 ppm; IR ν = 3120, 3005, 2956, 2923, 2853, 1741, 1664, 1607, 1552, 1504, 1490, 1450, 1371, 1240, 1202, 1174, 1106, 1078, 1012, 989, 964, 930, 882, 847, 821, 727, 694, 612 cm^{-1}; HRMS (ESI) calcd for $C_{19}H_{19}N_3O_5$+Na, 392.1217: found 392.1220.

Methyl (S)-4-(methylthio)-2-(2-(5-phenyl-1,3,4-oxadiazol-2-yl)-1H-pyrrol-1-yl)butanoate (**1j**) and methyl (S)-6-(5-phenyl-1,3,4-oxadiazol-2-yl)-3,4-dihydro-2H-pyrrolo[2,1-b][1,3]thiazine-4-carboxylate (**1k**). Data for **4j**: white solid in a yield of 82% (0.77 g, 2.14 mmol); ^{1}H-NMR (DMSO-d_6) δ = 2.02 (s, 3H), 2.24–2.46 (m, 4H), 3.69 (s, 3H), 5.97–6.05 (m, 1H), 6.22 (dd, *J* = 3.6, 2.8 Hz, 1H), 6.55 (dd, *J* = 3.6, 1.2 Hz, 1H), 7.15 (dd, *J* = 2.8, 1.2 Hz, 1H), 7.48–7.61 (m, 3H), 7.86–8.02 (m, 2H), 8.33 (s, 1H) ppm; ^{13}C-NMR (DMSO-d_6) δ = 15.8, 30.8, 32.9, 53.6, 59.7, 110.6, 117.3, 127.4, 128.5, 128.7, 129.7, 132.8, 134.8, 142.1, 163.7, 171.8 ppm; IR ν = 3230, 3006, 2957, 12918, 2849, 1743, 1649, 1614, 1556, 1491, 1459, 1431, 1350, 1288, 1230, 1209, 1144, 1091, 1033, 1001, 955, 909, 888, 798, 756, 613 cm^{-1}.

Data for **1j**: light-yellow solid in a yield of 50% (0.31 g, 0.86 mmol); ^{1}H-NMR (CD_3OD) δ = 2.03 (s, 3H), 2.28–2.36 (m, 1H), 2.43–2.63 (m, 3H), 3.74 (s, 3H), 6.18 (dd, *J* = 10.0, 4.8 Hz, 1H), 6.39 (dd, *J* = 4.0, 2.8 Hz, 1H), 7.07 (dd, *J* = 4.0, 2.0 Hz, 1H), 7.25 (dd, *J* = 2.8, 2.0 Hz, 1H),

7.55–7.63 (m, 3H), 8.06–8.10 (m, 2H) ppm; ^{13}C-NMR (CD_3OD) δ = 13.7, 29.6, 31.1, 51.8, 58.7, 109.8, 114.8, 117.2, 123.2, 126.4, 129.0, 131.7, 159.2, 162.8, 171.0, 179.6 ppm; IR ν = 2956, 2925, 2857, 1750, 1667, 1603, 1554, 1505, 1452, 1381, 1274, 1243, 1090, 1016, 961, 883, 817, 774, 732, 691 cm^{-1}; HRMS (ESI) calcd for $C_{18}H_{19}N_3O_3S$+Na, 380.1039: found 380.1040.

Data for **1k**: light-yellow solid in 49% yield (0.31g, 0.72 mmol); ^{1}H-NMR (CD_3OD) δ = 2.39–2.49 (m, 1H), 2.86–3.02 (m, 3H), 3.73 (s, 3H), 5.94 (dd, *J* = 5.2, 3.2 Hz, 1H), 6.06 (d, *J* = 4.0 Hz, 1H), 7.01 (d, *J* = 4.0 Hz, 1H), 7.49–7.57 (m, 3H), 7.97–8.01 (m, 2H) ppm; ^{13}C-NMR (CD_3OD) δ = 22.0, 28.0, 53.3, 58.2, 108.5, 116.1, 119.0, 124.7, 127.7, 128.7, 130.3, 132.9, 160.2, 163.6, 172.5 ppm; IR ν = 3008, 2948, 2852, 1751, 1648, 1604, 1552, 1497, 1439, 1401, 1355, 1292, 1257, 1214, 1176, 1145, 1125, 1085, 1070, 1023, 974, 929, 898, 854, 758, 727, 696 cm^{-1}; HRMS (ESI) calcd for $C_{17}H_{15}N_3O_3S$+Na, 364.0726: found 364.0729.

3.1.3. General Procedure for the Preparation of **5** (R = i-Pr) and **6** (R = s-Bu)

Step-1: At 25 °C, under an argon atmosphere, benzohydrazide **3** (1.1 equiv.) was added to a stirred solution of pyrrole-2-carbaldehyde **2** (~1.0 g, 1 equiv.) in toluene/DMSO (*v*:*v* = 15:1). The mixture was heated at 110 °C for 12 h and cooled to room temperature. The solvent was removed under reduced pressure in a rotary evaporator, and the crude product was filtered through a short pad of SiO_2 (EtOAc eluent) and concentrated under reduced pressure.

Step-2: I_2 (1.2 equiv.) and K_2CO_3 (3 equiv.) were added to a stirred solution of the above imine in 1,4-dioxane (20 mL). The mixture was heated at 85 °C for 6h under an argon atmosphere and cooled to room temperature. The mixture was diluted with CH_2Cl_2, washed with a 10% $Na_2S_2O_3$ solution, dried over anhydrous Na_2SO_4, filtered, and concentrated under reduced pressure. The product was purified by SiO_2 flash column chromatography to obtain pyrrole-fused 1,3,4-oxadiazole **5** or **6**.

Methyl (S)-2-(2-(5-(2-fluorophenyl)-1,3,4-oxadiazol-2-yl)-1H-pyrrol-1-yl)-3-methylbutanoate (**5a**). Orange oil, 40% yield (663 mg, 1.93 mmol); R_f = 0.45 (4:1 hexane/EtOAc); Data for **5a**: ^{1}H-NMR ($CDCl_3$) δ = 0.83 (d, *J* = 6.4 Hz, 3H), 1.08 (d, *J* = 6.4 Hz, 3H), 2.48 (m, 1H), 3.75 (s, 3H), 6.15 (d, *J* = 10.0 Hz, 1H), 6.36 (dd, *J* = 4.0, 3.2 Hz, 1H), 6.98 (dd, *J* = 4.0, 2.0 Hz, 1H), 7.23–7.28 (m, 1H), 7.28–7.34 (m, 1H), 7.31 (dd, *J* = 3.2, 2.0 Hz, 1H), 7.50–7.57 (m, 1H), 8.08–8.13 (m, 1H) ppm; ^{13}C-NMR ($CDCl_3$) δ = 18.5, 19.3, 33.2, 52.3, 64.6, 110.4, 114.5, 117.0 (d, *J* = 20.5 Hz), 117.8, 124.6 (d, *J* = 3.1 Hz), 126.0, 129.6 (d, *J* = 1.5 Hz), 133.3 (d, *J* = 8.4 Hz), 158.8, 159.4, (d, *J* = 5.4 Hz), 159.7 (d, *J* = 1.5 Hz), 161.3, 171.3 ppm; IR ν = 2970, 2880, 1748, 1605, 1500, 1475, 1450, 1273, 1239, 1219, 1200, 1185, 1170, 1102, 1078, 1009, 827, 742, 669, 617 cm^{-1}; HRMS (ESI) calcd for $C_{18}H_{18}FN_3O_3$+Na 366.1224: found 366.1225.

Methyl (S)-2-(2-(5-(3-fluorophenyl)-1,3,4-oxadiazol-2-yl)-1H-pyrrol-1-yl)-3-methylbutanoate (**5b**). Orange oil, 70% yield (759 mg, 2.21 mmol); R_f = 0.59 (4:1 hexane/EtOAc); Data for **5b**: ^{1}H-NMR ($CDCl_3$) δ = 0.83 (d, *J* = 6.4 Hz, 3H), 1.08 (d, *J* = 6.4 Hz, 3H), 2.49 (m, 1H), 3.75 (s, 3H), 6.14 (d, *J* = 10.0 Hz, 1H), 6.37 (dd, *J* = 4.0, 2.8 Hz, 1H), 6.97 (dd, *J* = 4.0, 2.0 Hz, 1H), 7.20–7.27 (m, 1H), 7.32 (dd, *J* = 2.8, 2.0 Hz, 1H), 7.47–7.54 (m, 1H), 7.76–7.81 (m, 1H), 7.87–7.91 (m, 1H) ppm; ^{13}C-NMR ($CDCl_3$) δ = 18.5, 19.3, 33.1, 52.3, 64.6, 110.4, 113.8 (d, *J* = 24.2 Hz), 114.4 117.7, 118.6 (d, *J* = 21.2 Hz), 122.5 (d, *J* = 3.0 Hz), 125.7 (d, *J* = 9.1 Hz), 126.1, 130.9 (d, *J* = 8.3 Hz), 159.7, 161.6, (d, *J* = 2.3 Hz), 164.0, 171.2 ppm; IR ν = 2970, 2880, 1750, 1600, 1565, 1500, 1495, 1450, 1410, 1375, 1307, 1275, 1240, 1205, 1181, 1105, 1080, 1010, 995, 870, 800, 735, 680, 615 cm^{-1}; HRMS (ESI) calcd for $C_{18}H_{18}FN_3O_3$+Na 366.1224: found 366.1226.

Methyl (S)-2-(2-(5-(4-fluorophenyl)-1,3,4-oxadiazol-2-yl)-1H-pyrrol-1-yl)-3-methylbutanoate (**5c**). Yellow oil, 54% yield (721 mg, 2.10 mmol); R_f = 0.65 (4:1 hexane/EtOAc); Data for **5c**: ^{1}H-NMR ($CDCl_3$) δ = 0.83 (d, *J* = 6.4 Hz, 3H), 1.08 (d, *J* = 6.4 Hz, 3H), 2.48 (m, 1H), 3.75 (s, 3H), 6.14 (d, *J* = 10.0 Hz, 1H), 6.36 (dd, *J* = 4.0, 2.8 Hz, 1H), 6.94 (dd, *J* = 4.0, 2.0 Hz, 1H), 7.18–7.25 (m, 2H), 7.31 (dd, *J* = 2.8, 2.0 Hz, 1H), 8.07–8.13 (m, 2H) ppm; ^{13}C-NMR ($CDCl_3$) δ = 18.5, 19.3, 33.1, 52.3, 64.6, 110.3, 114.1, 116.4 (d, *J* = 22.0 Hz), 120.2 (d, *J* = 3.0 Hz), 125.9, 129.0 (d, *J* = 9.1 Hz), 159.4, 161.8, 163.4, 165.9, 171.2 ppm; IR ν = 2970, 2880, 1750, 1605, 1500,

1470, 1455, 1435, 1415, 1270, 1235, 1215, 1200, 1160, 1100, 1075, 1015, 965, 845, 740, 625 cm^{-1}; HRMS (ESI) calcd for $C_{18}H_{18}FN_3O_3$+Na 366.1224, found 366.1228.

Methyl (S)-2-(2-(5-(4-chlorophenyl)-1,3,4-oxadiazol-2-yl)-1H-pyrrol-1-yl)-3-methylbutanoate (**5d**). Brown solid, 62% yield (533 mg, 1.48 mmol); R_f = 0.61 (4:1 hexane/EtOAc); Data for **5d**: ^{1}H-NMR ($CDCl_3$) δ = 0.82 (d, *J* = 6.4 Hz, 3H), 1.08 (d, *J* = 6.4 Hz, 3H), 2.48 (m, 1H), 3.75 (s, 3H), 6.14 (d, *J* = 10.0 Hz, 1H), 6.36 (dd, *J* = 4.0, 2.8 Hz, 1H), 6.95 (dd, *J* = 4.0, 2.0 Hz, 1H), 7.31 (dd, *J* = 2.8, 2.0 Hz, 1H), 7.48–7.53 (m, 2H), 8.01–8.06 (m, 2H) ppm; ^{13}C-NMR ($CDCl_3$) δ = 18.5, 19.3, 33.2, 52.3, 64.6, 110.3, 114.3, 117.8, 122.3, 126.0, 128.1, 129.5, 137.8, 159.6, 161.8, 171.2 ppm; IR ν = 2970, 2880, 1750, 1605, 1500, 1485, 1455, 1410, 1270, 1237, 1200, 1180, 1100, 1080, 1015, 970, 840, 740 cm^{-1}; HRMS (ESI) calcd for $C_{18}H_{18}ClN_3O_3$+Na 382.0929, found 382.0933.

Methyl (S)-2-(2-(5-(2-hydroxy-3,5-diiodophenyl)-1,3,4-oxadiazol-2-yl)-1H-pyrrol-1-yl)-3-methylbutanoate (**5e-1**). White solid, 33% yield (748 mg, 1.26 mmol); R_f = 0.54 (4:1 hexane/EtOAc); Data for **5e-1**: ^{1}H-NMR ($CDCl_3$) δ = 0.82 (d, *J* = 6.4 Hz, 3H), 1.09 (d, *J* = 6.4 Hz, 3H), 2.49 (m, 1H), 3.77 (s, 3H), 5.99 (d, *J* = 9.6 Hz, 1H), 6.40 (dd, *J* = 4.0, 2.8 Hz, 1H), 7.05 (dd, *J* = 4.0, 2.0 Hz, 1H), 7.36 (dd, *J* = 2.8, 2.0 Hz, 1H), 8.06 (d, *J* = 2.0 Hz, 1H), 8.18 (d, *J* = 2.0 Hz, 1H) 11.02 (s, 1H) ppm; ^{13}C-NMR ($CDCl_3$) δ = 18.6, 19.3, 33.2, 52.4, 64.9, 81.3, 86.7, 109.8, 110.8, 115.7, 116.9, 127.0, 134.7, 149.8, 156.2, 158.7, 160.1, 171.0 ppm; IR ν = 2970, 2890, 1750, 1600, 1565, 1535, 1500, 1445, 1415, 1380, 1255, 1240, 1220, 1185, 1105, 1080, 1015, 1000, 915, 870, 740, 660, 615, 600 cm^{-1}; HRMS (ESI) calcd for $C_{18}H_{17}I_2N_3O_4$+Na 615.9201: found 615.9203.

Methyl (S)-2-(2-(5-(4-hydroxy-2,3,5,6-tetraiodophenyl)-1,3,4-oxadiazol-2-yl)-1H-pyrrol-1-yl)-3-methylbutanoate (**5f-1**): Yellow solid, 32% yield (1.33 g, 1.57 mmol); R_f = 0.55 (4:1 hexane/EtOAc); Data for **5f-1**. ^{1}H-NMR ($CDCl_3$) δ = 0.81 (d, *J* = 6.4 Hz, 3H), 1.07 (d, *J* = 6.4 Hz, 3H), 2.41–2.53 (m, 1H), 3.75 (s, 3H), 6.09 (d, *J* = 10.0 Hz, 1H), 6.36 (dd, *J* = 4.0, 2.8 Hz, 1H), 6.96 (dd, *J* = 4.0, 1.6 Hz, 1H), 7.31 (dd, *J* = 2.8, 1.6 Hz, 1H), 8.40 (s, 1H) ppm; ^{13}C-NMR ($CDCl_3$) δ = 18.5, 19.3, 33.1, 52.3, 64.6, 82.4, 110.4, 114.5, 117.7, 119.9, 126.1, 137.6, 156.2, 159.5, 159.6, 171.2 ppm; IR ν = 3450, 3145, 3125, 2970, 2875, 1745, 1610, 1595, 1500, 1450, 1395, 1300, 1270, 1235, 1220, 1200, 1180, 1160, 1135, 1105, 1075, 1010, 995, 965, 910, 890, 810, 735, 710, 685, 650, 615 cm^{-1}; HRMS (ESI) calcd for $[C_{18}H_{15}I_4N_3O_4–I_2+H_2]$+Na 615.9201: found 615.9213.

Methyl (S)-2-(2-(5-(2-methoxyphenyl)-1,3,4-oxadiazol-2-yl)-1H-pyrrol-1-yl)-3-methylbutanoate (**5g**). Red oil, 85% yield (1.03 g, 2.89 mmol); R_f = 0.66 (3:2 hexane/EtOAc); Data for **5g**: ^{1}H-NMR ($CDCl_3$) δ = 0.83 (d, *J* = 6.4 Hz, 3H), 1.07 (d, *J* = 6.4 Hz, 3H), 2.48 (m, 1H), 3.74 (s, 3H), 4.00 (s, 3H), 6.19 (d, *J* = 10.0 Hz, 1H), 6.35 (dd, *J* = 4.0, 2.8 Hz, 1H), 6.94 (dd, *J* = 4.0, 2.0 Hz, 1H), 7.06–7.12 (m, 2H), 7.29 (dd, *J* = 2.8, 2.0 Hz, 1H), 7.48–7.53 (m, 1H), 7.99 (dd, *J* = 7.6, 2.0 Hz, 1H) ppm; ^{13}C-NMR ($CDCl_3$) δ = 18.5, 19.3, 33.2, 52.2, 56.0, 64.5, 110.1, 112.0, 112.9, 113.9, 118.2, 120.7, 125.5, 130.2, 132.8, 158.0, 159.0, 161.3, 171.4 ppm; IR ν = 2970, 2875, 2840, 1750, 1600, 1545, 1500, 1470, 1455, 1440, 1270, 1260, 1235, 1215, 1185, 1170, 1130, 1100, 1075, 1025, 750, 735, 675, 616 cm^{-1}; HRMS (ESI) calcd for $C_{19}H_{21}N_3O_4$+Na 378.1424, found 378.1428.

Methyl (S)-2-(2-(5-(4-methoxyphenyl)-1,3,4-oxadiazol-2-yl)-1H-pyrrol-1-yl)-3-methylbutanoate (**5h**). Ivory solid, 70% yield (1.12 g, 3.15 mmol); R_f = 0.70 (3:2 hexane/EtOAc); Data for **5h**: ^{1}H-NMR ($CDCl_3$) δ = 0.82 (d, *J* = 6.4 Hz, 3H), 1.07 (d, *J* = 6.4 Hz, 3H), 2.48 (m, 1H), 3.74 (s, 3H), 3.89 (s, 3H), 6.15 (d, *J* = 10.0 Hz, 1H), 6.35 (dd, *J* = 4.0, 2.8 Hz, 1H), 6.92 (dd, *J* = 4.0, 2.0 Hz, 1H), 7.00–7.05 (m, 2H), 7.29 (dd, *J* = 2.8, 2.0 Hz, 1H), 8.01–8.05 (m, 2H), 7.99 (dd, *J* = 7.6, 2.0 Hz, 1H) ppm; ^{13}C-NMR ($CDCl_3$) δ = 18.5, 19.3, 33.1, 52.3, 55.5, 64.5, 110.1, 113.8, 114.5, 116.4, 118.2, 125.6, 128.6, 159.0, 162.2, 162.6, 171.3 ppm; IR ν = 2970, 2875, 1745, 1610, 1600, 1505, 1450, 1395, 1300, 1270, 1240, 1220, 1200, 1180, 1160, 1135, 1100, 1080, 1015, 995, 910, 890, 735, 715, 685, 650, 615 cm^{-1}; HRMS (ESI) calcd for $C_{19}H_{21}N_3O_4$+Na 378.1424: found 378.1426.

Methyl (2S,3S)-2-(2-(5-(2-fluorophenyl)-1,3,4-oxadiazol-2-yl)-1H-pyrrol-1-yl)-3-methylpentanoate (**6a**). Orange-red oil, 89% yield (1.03 g, 2.89 mmol); R_f = 0.47 (4:1 hexane/EtOAc); Data for **6a**: ^{1}H-NMR ($CDCl_3$) δ = 0.84 (t, *J* = 7.2 Hz, 3H), 1.05 (d, *J* = 6.4 Hz, 3H), 1.06–1.27 (m,

2H), 2.21–2.32 (m, 1H), 3.74 (s, 3H), 6.20 (d, *J* = 9.6 Hz, 1H), 6.36 (dd, *J* = 4.0, 2.8 Hz, 1H), 6.98 (dd, *J* = 4.0, 2.0 Hz, 1H), 7.23–7.29 (m, 1H), 7.30–7.34 (m, 1H), 7.31 (dd, *J* = 2.8, 2.0 Hz, 1H), 7.50–7.57 (m, 1H), 8.08–8.13 (m, 1H) ppm; ^{13}C-NMR ($CDCl_3$) δ = 11.0, 15.6, 24.8, 39.2, 52.3, 63.8, 110.3, 114.6, 117.0 (d, *J* = 21.3 Hz), 117.9, 124.6 (d, *J* = 3.8 Hz), 126.0, 129.6 (d, *J* = 0.5 Hz), 133.3 (d, *J* = 8.4 Hz), 158.8, 159.4, (d, *J* = 5.4 Hz), 159.6 (d, *J* = 1.5 Hz), 161.3, 171.4 ppm; IR ν = 2970, 2937, 2880, 1750, 1600, 1500, 1475, 1450, 1400, 1260, 1235, 1198, 1180, 1100, 1080, 1026, 1000, 910, 825, 767, 735, 698, 670, 615 cm^{-1}; HRMS (ESI) calcd for $C_{19}H_{20}FN_3O_3$+Na 380.1381:found 380.1386.

Methyl (2S,3S)-2-(2-(5-(3-fluorophenyl)-1,3,4-oxadiazol-2-yl)-1H-pyrrol-1-yl)-3-methylpentanoate (**6b**). Orange-red oil, 88% yield (0.99 g, 2.77 mmol); R_f = 0.47 (4:1 hexane/EtOAc); Data for **6b**: ^{1}H-NMR ($CDCl_3$) δ = 0.84 (t, *J* = 7.2 Hz, 3H), 1.05 (d, *J* = 6.4 Hz, 3H), 1.06–1.28 (m, 2H), 2.20–2.32 (m, 1H), 3.75 (s, 3H), 6.19 (d, *J* = 10.0 Hz, 1H), 6.36 (dd, *J* = 3.6, 2.8 Hz, 1H), 6.97 (dd, *J* = 3.6, 2.0 Hz, 1H), 7.20–7.27 (m, 1H), 7.33 (dd, *J* = 2.8, 2.0 Hz, 1H), 7.47–7.53 (m, 1H), 7.76–7.81 (m, 1H), 7.87–7.91 (m, 1H) ppm; ^{13}C-NMR ($CDCl_3$) δ = 10.9, 15.5, 24.8, 39.1, 52.3, 63.8, 110.4, 113.8 (d, *J* = 24.2 Hz), 114.5, 117.7, 118.6 (d, *J* = 21.3 Hz), 122.5 (d, *J* = 3.0 Hz), 125.7 (d, *J* = 8.3 Hz), 126.1, 130.9 (d, *J* = 8.4 Hz), 159.6, 161.6 (d, *J* = 3.1 Hz), 164.0, 171.3 ppm; IR ν = 2970, 2940, 2880, 1750, 1595, 1560, 1505, 1490, 1454, 1415, 1245, 1205, 1178, 1105, 1080, 995, 915, 870, 795, 735, 680, 615 cm^{-1}; HRMS (ESI) calcd for $C_{19}H_{20}FN_3O_3$+Na 380.1381, found 380.1384.

Methyl (2S,3S)-2-(2-(5-(4-fluorophenyl)-1,3,4-oxadiazol-2-yl)-1H-pyrrol-1-yl)-3-methylpentanoate (**6c**). Yellow oil, 62% yield (768 mg, 2.15 mmol); R_f = 0.58 (4:1 hexane/EtOAc); Data for **6c**: ^{1}H-NMR ($CDCl_3$) δ = 0.83 (t, *J* = 7.2 Hz, 3H), 1.04 (d, *J* = 6.4 Hz, 3H), 1.05–1.27 (m, 2H), 2.22–2.32 (m, 1H), 3.74 (s, 3H), 6.19 (d, *J* = 10.4 Hz, 1H), 6.36 (dd, *J* = 3.6, 2.8 Hz, 1H), 6.94 (dd, *J* = 3.6, 2.0 Hz, 1H), 7.18–7.25 (m, 2H), 7.31 (dd, *J* = 2.8, 2.0 Hz, 1H), 8.07–8.13 (m, 2H) ppm; ^{13}C-NMR ($CDCl_3$) δ = 10.9, 15.5, 24.8, 39.1, 52.3, 63.7, 110.3, 114.2, 116.4 (d, *J* = 22.8 Hz), 117.9, 126.0, 129.1 (d, *J* = 8.3 Hz), 159.4, 161.8, 163.4, 165.9, 171.4 ppm; IR ν = 2970, 2940, 2880, 1750, 1670, 1605, 1500, 1455, 1415, 1240, 1200, 1180, 1160, 1080, 1015, 1000, 850, 740, 620 cm^{-1}; HRMS (ESI) calcd for $C_{19}H_{20}FN_3O_3$+Na 380.1381: found 380.1387.

Methyl (2S,3S)-2-(2-(5-(4-chlorophenyl)-1,3,4-oxadiazol-2-yl)-1H-pyrrol-1-yl)-3-methylpentanoate (**6d**). Orange oil, 79% yield (254 mg, 0.68 mmol); R_f = 0.65 (4:1 hexane/EtOAc); Data for **6d**: ^{1}H-NMR ($CDCl_3$) δ = 0.83 (t, *J* = 7.2 Hz, 3H), 1.04 (d, *J* = 6.4 Hz, 3H), 1.06–1.27 (m, 2H), 2.20–2.32 (m, 1H), 3.74 (s, 3H), 6.19 (d, *J* = 10.4 Hz, 1H), 6.36 (dd, *J* = 4.0, 2.8 Hz, 1H), 6.95 (dd, *J* = 4.0, 1.6 Hz, 1H), 7.32 (dd, *J* = 2.8, 1.6 Hz, 1H), 7.48–7.52 (m, 2H), 8.01–8.05 (m, 2H) ppm; ^{13}C-NMR ($CDCl_3$) δ = 10.9, 15.5, 24.8, 39.1, 52.3, 63.8, 110.3, 114.4, 117.8, 122.3, 126.1, 128.1, 129.4, 137.8, 159.5, 161.8, 171.3 ppm; IR ν = 2970, 2935, 2880, 1750, 1605, 1505, 1485, 1455, 1410, 1255, 1235, 1200, 1178, 1095, 1080, 1015, 840, 735 cm^{-1}; HRMS (ESI) calcd for $C_{19}H_{20}ClN_3O_3$+Na 396.1085: found 396.1089.

Methyl (2S,3S)-2-(2-(5-(2-hydroxy-3,5-diiodophenyl)-1,3,4-oxadiazol-2-yl)-1H-pyrrol-1-yl)-3-methylpentanoate (**6e-1**). Green solid, 45% yield (893 mg, 1.47 mmol); R_f = 0.50 (4:1 hexane/EtOAc); Data for **6e-1**: ^{1}H-NMR ($CDCl_3$) δ = 0.83 (t, *J* = 7.2 Hz, 3H), 1.05 (d, *J* = 6.4 Hz, 3H), 1.02–1.22 (m, 2H), 2.20–2.33 (m, 1H), 3.77 (s, 3H), 6.04 (d, *J* = 9.6 Hz, 1H), 6.39 (dd, *J* = 4.0, 2.8 Hz, 1H), 7.04 (dd, *J* = 4.0, 1.6 Hz, 1H), 7.37 (dd, *J* = 2.8, 1.6 Hz, 1H), 8.06 (d, *J* = 2.0 Hz, 1H), 8.17 (d, *J* = 2.0 Hz, 1H), 11.02 (s, 1H) ppm; ^{13}C-NMR ($CDCl_3$) δ = 10.9, 15.5, 24.8, 38.1, 52.4, 64.0, 81.3, 86.7, 109.8, 110.8, 115.7, 116.9, 127.0, 134.7, 149.8, 156.2, 158.7, 160.1, 171.1 ppm; IR ν = 3415, 2970, 2880, 1750, 1605, 1565, 1530, 1500, 1455, 1415, 1380, 1255, 1235, 1190, 1180, 1100, 1080, 990, 915, 875, 758, 740, 665, 598 cm^{-1}; HRMS (ESI) calcd for $C_{19}H_{19}I_2N_3O_4$+Na 629.9357: found 629.9358.

Methyl (2S,3S)-2-(2-(5-(4-hydroxy-3,5-diiodophenyl)-1,3,4-oxadiazol-2-yl)-1H-pyrrol-1-yl)-3-methylpentanoate (**6f-1**). Yellow oil, 43% yield (935 mg, 1.54 mmol); R_f = 0.45 (4:1 hexane/EtOAc); Data for **6f-1**: ^{1}H-NMR ($CDCl_3$) δ = 0.83 (t, *J* = 7.2 Hz, 3H), 1.04 (d, *J* = 6.4 Hz, 3H), 1.05–1.24 (m, 2H), 2.20–2.32 (m, 1H), 3.75 (s, 3H), 6.14 (d, *J* = 10.0 Hz, 1H), 6.21 (br s, 1H), 6.36 (dd, *J* = 4.0, 2.8 Hz, 1H), 6.96 (dd, *J* = 4.0, 2.0 Hz, 1H), 7.32 (dd, *J* = 2.8, 2.0 Hz, 1H), 8.40 (s, 2H), 8.17 (d, *J* = 2.0 Hz, 1H), 11.02 (s, 1H) ppm; ^{13}C-NMR ($CDCl_3$) δ = 10.9, 15.5, 24.8, 39.1, 52.3, 63.8, 82.5, 110.4, 114.5, 117.7, 119.9, 126.1, 137.6, 156.2, 159.4, 159.6, 171.3

ppm; IR ν = 3450, 3145, 3125, 3070, 2970, 2880, 1745, 1608, 1595, 1500, 1450, 1395, 1300, 1235, 1195, 1178, 1155, 1105, 1075, 990, 890, 775, 736, 710, 685, 615 cm^{-1}; HRMS (ESI) calcd for $C_{19}H_{19}I_2N_3O_4$+Na 629.9357: found 629.9360.

Methyl (2S,3S)-2-(2-(5-(2-methoxyphenyl)-1,3,4-oxadiazol-2-yl)-1H-pyrrol-1-yl)-3-methylpentanoate (**6g**). Orange-red oil, 80% yield (768 mg, 2.08 mmol); R_f = 0.19 (4:1 hexane/EtOAc); Data for **6g**: ^{1}H-NMR ($CDCl_3$) δ = 0.83 (t, *J* = 7.2 Hz, 3H), 1.04 (d, *J* = 6.4 Hz, 3H), 1.05–1.27 (m, 2H), 2.20–2.32 (m, 1H), 3.73 (s, 3H), 3.99 (s, 3H), 6.24 (d, *J* = 9.6 Hz, 1H), 6.34 (dd, *J* = 3.6, 2.8 Hz, 1H), 6.94 (dd, *J* = 3.6, 1.6 Hz, 1H), 7.05–7.11 (m, 2H), 7.30 (dd, *J* = 2.8, 1.6 Hz, 1H), 7.47–7.53 (m, 1H), 7.98 (dd, *J* = 7.6, 2.0 Hz, 1H) ppm; ^{13}C-NMR ($CDCl_3$) δ = 11.0, 15.5, 24.8, 39.2, 52.2, 56.0, 63.7, 110.1, 112.0, 112.9, 114.0, 118.3, 120.7, 125.6, 130.2, 132.8, 157.9, 159.0, 161.3, 171.5 ppm; IR ν = 2970, 2942, 2882, 2845, 1750, 1605, 1550, 1500, 1485, 1455, 1440, 1415, 1255, 1240, 1200, 1180, 1100, 1080, 1050, 1025, 915, 730, 678, 650, 620 cm^{-1}; HRMS (ESI) calcd for $C_{20}H_{23}N_3O_4$+Na 392.1581: found 392.1585.

Methyl (2S,3S)-2-(2-(5-(4-methoxyphenyl)-1,3,4-oxadiazol-2-yl)-1H-pyrrol-1-yl)-3-methylpentanoate (**6h**). Orange oil; 79% yield (739 mg, 2.00 mmol); R_f = 0.24 (4:1 hexane/EtOAc); Data for **6h**: ^{1}H-NMR ($CDCl_3$) δ = 0.83 (t, *J* = 7.2 Hz, 3H), 1.03 (d, *J* = 6.4 Hz, 3H), 1.05–1.23 (m, 2H), 2.20–2.30 (m, 1H), 3.74 (s, 3H), 3.88 (s, 3H), 6.20 (d, *J* = 9.6 Hz, 1H), 6.34 (dd, *J* = 3.6, 2.8 Hz, 1H), 6.92 (dd, *J* = 3.6, 1.6 Hz, 1H), 6.99–7.03 (m, 2H), 7.29 (dd, *J* = 2.8, 1.6 Hz, 1H), 8.00–8.04 (m, 2H) ppm; ^{13}C-NMR ($CDCl_3$) δ = 11.0, 15.5, 24.8, 39.1, 52.2, 55.4, 63.7, 110.1, 113.8, 114.5, 116.4, 118.2, 125.6, 128.6, 158.9, 162.2, 162.6, 171.4 ppm; IR ν = 2970, 2940, 2880, 2840, 1750, 1610, 1500, 1460, 1445, 1310, 1255, 1180, 1100, 1080, 1030, 1000, 915, 840, 730, 700, 625, 610 cm^{-1}; HRMS (ESI) calcd for $C_{20}H_{23}N_3O_4$+Na 392.1581: found 392.1584.

3.2. General Procedure for Deiodination Reaction on the Phenol Ring

Zn dust (2~5 equiv.) and acetic acid (5 equiv.) were added to a stirred solution of 2-pyrrolyl-5-(iodophenolic)-1,3,4-oxadiazole **5f-1** or **6e-1** (~0.5–1.0 g, 1 equiv.) in THF (30mL). The mixture was stirred at 25 °C for 1~6 h under an argon atmosphere. The mixture was quenched with saturated $NaHCO_3$ solution, extracted with Et_2O, dried over anhydrous Na_2SO_4, filtered, and concentrated under reduced pressure. The product was purified by SiO_2 flash column chromatography to produce the deiodination product.

Methyl (S)-2-(2-(5-(4-hydroxyphenyl)-1,3,4-oxadiazol-2-yl)-1H-pyrrol-1-yl)-3-methylbutanoate (**5f**). White solid, 97% yield (270 mg, 0.79 mmol); R_f = 0.58 (3:2 hexane/EtOAc); Data for **5f**: ^{1}H-NMR ($CDCl_3$) δ = 0.83 (d, *J* = 6.4 Hz, 3H), 1.08 (d, *J* = 6.4 Hz, 3H), 2.43–2.54 (m, 1H), 3.75 (s, 3H), 6.13 (d, *J* = 9.6 Hz, 1H), 6.36 (dd, *J* = 4.0, 2.8 Hz, 1H), 6.93 (dd, *J* = 4.0, 1.6 Hz, 1H), 7.01 (d, *J* = 8.4 Hz, 2H), 7.30 (dd, *J* = 2.8, 1.6 Hz, 1H), 7.99 (d, J = 8.4 Hz, 2H) ppm; ^{13}C-NMR ($CDCl_3$) δ = 18.5, 19.3, 33.1, 52.3, 64.6, 110.2, 114.0, 116.0, 116.2, 118.0, 125.7, 128.8, 159.0, 159.1, 162.7, 171.3 ppm; IR ν = 3120, 2970, 2940, 2880, 1750, 1610, 1595, 1500, 1440, 1394, 1375, 1335, 1285, 1270, 1240, 1200, 1105, 1090, 1075, 1010, 995, 915, 840, 775, 735, 719, 635 cm^{-1}; HRMS (ESI) calcd for $C_{18}H_{19}N_3O_4$+Na 364.1268: found 365.1271.

Methyl (2S,3S)-2-(2-(5-(2-hydroxyphenyl)-1,3,4-oxadiazol-2-yl)-1H-pyrrol-1-yl)-3-methylpentanoate (**6e**). White solid, 50% yield (210 mg, 0.59 mmol); R_f = 0.54 (3:2 hexane/EtOAc); Data for **6e**: ^{1}H-NMR (DMSO-d_6) δ = 0.79 (t, *J* = 7.2 Hz, 3H), 0.96 (d, *J* = 6.4 Hz, 3H), 0.98–1.19 (m, 2H), 2.16–2.26 (m, 1H), 3.69 (s, 3H), 6.02 (d, *J* = 9.6 Hz, 1H), 6.24 (dd, *J* = 3.6, 2.8 Hz, 1H), 6.56 (dd, *J* = 3.6, 1.6 Hz, 1H), 6.92–6.99 (m, 2H), 7.20 (dd, *J* = 2.8, 1.6 Hz, 1H), 7.41–7.46 (m, 1H), 7.86–7.90 (m, 1H) 8.39 (s, 1H) ppm; ^{13}C-NMR (DMSO-d_6) δ = 11.1, 16.0, 24.8, 38.5, 52.7, 63.3, 110.3, 115.9, 116.5, 117.8, 119.3, 126.2, 127.8, 128.6, 134.2, 142.5, 159.8, 164.9, 171.3 ppm; IR ν = 3240, 3080, 2970, 2935, 2880, 1750, 1640, 1600, 1570, 1540, 1495, 1465, 1425, 1360, 1335, 1315, 1258, 1230, 1200, 1175, 1155, 1105, 1075, 1060, 1040, 995, 950, 895, 825, 757, 740, 670, 618 cm^{-1}; HRMS (ESI) calcd for $C_{19}H_{23}N_3O_4$+Na 380.1581: found 380.1586.

Methyl (2S,3S)-2-(2-(5-(4-hydroxyphenyl)-1,3,4-oxadiazol-2-yl)-1H-pyrrol-1-yl)-3-methylpentanoate (**6f**). White solid, 42% yield (98 mg, 0.28 mmol); R_f = 0.67 (3:2 hexane/EtOAc); Data for **6f**: ^{1}H-NMR ($CDCl_3$) δ = 0.77 (t, *J* = 7.2 Hz, 3H), 0.98 (d, *J* = 6.8 Hz, 3H), 0.98–1.18 (m, 2H), 2.26–2.35 (m, 1H), 3.70 (s, 3H), 5.96 (d, *J* = 10.0 Hz, 1H), 6.38 (dd, *J* = 3.6, 2.8 Hz, 1H), 6.97 (d, *J* = 8.4 Hz, 2H), 6.98 (dd, *J* = 3.6, 1.6 Hz, 1H), 7.40 (dd, *J* = 2.8, 1.6 Hz, 1H), 7.90 (d,

J = 8.4 Hz, 2H), 10.34 (s, 1H) ppm; ^{13}C-NMR ($CDCl_3$) δ = 10.9, 15.5, 24.8, 39.1, 52.3, 63.7, 110.3, 114.2, 115.5, 117.9, 125.9, 129.0, 136.9, 157.7, 159.2, 161.1, 171.4 ppm; IR ν = 3137, 2965, 2875, 2838, 1742, 1610, 1579, 1558, 1497, 1464, 1466, 1438, 1338, 1307, 1287, 1254, 1224, 1202, 1173, 1092, 1060, 1027, 961, 938, 911, 837, 810, 798, 731, 696 cm^{-1}; HRMS (ESI) calcd for $C_{19}H_{21}N_3O_4$+Na 378.1424: found 378.1427.

3.3. General Procedure for Iodination Reaction on the Pyrrole Ring

I_2 (4 equiv.). was added to a stirred solution of 2-pyrrolyl-5-(anisyl)-1,3,4-oxadiazoles **5g**, **5h**, or **6h** (~1.0 g, 1 equiv.) in DMSO (10 mL). The mixture was heated at 90 °C for 3~5 h under an argon atmosphere. After cooling to room temperature, the mixture was diluted with Et_2O, washed with 10% $Na_2S_2O_3$ solution, dried over anhydrous Na_2SO_4, filtered, and concentrated under reduced pressure. The product was purified by SiO_2 flash column chromatography to produce iodination products **5g-1**, **5h-1**, or **6h-1** on the pyrrole ring.

Methyl (S)-2-(3,4-diiodo-2-(5-(2-methoxyphenyl)-1,3,4-oxadiazol-2-yl)-1H-pyrrol-1-yl)-3-methylbutanoate (**5g-1**). Orange oil, 61% yield (923 mg, 1.52 mmol); R_f = 0.60 (3:2 hexane/EtOAc); Data for **5g-1**: ^{1}H-NMR ($CDCl_3$) δ = 0.86 (d, *J* = 6.4 Hz, 3H), 1.04 (d, *J* = 6.4 Hz, 3H), 2.42 (m, 1H), 3.73 (s, 3H), 4.03 (s, 3H), 6.12 (d, *J* = 10.0 Hz, 1H), 7.08–7.14 (m, 2H), 7.45 (s, 1H), 7.51–7.56 (m, 1H), 8.12 (dd, *J* = 7.6, 1.6 Hz, 1H) ppm; ^{13}C-NMR ($CDCl_3$) δ = 18.6, 19.2, 33.1, 52.5, 56.0, 65.6, 78.0, 80.4, 112.0, 112.3, 120.8, 121.4, 130.4, 130.5, 133.2, 156.7, 158.1, 162.1, 170.6 ppm; IR ν = 2970, 2937, 2880, 2840, 1750, 1665, 1605, 1590, 1545, 1500, 1475, 1470, 1435, 1390, 1285, 1265, 1220, 1205, 1185, 1165, 1130, 1060, 1050, 1025, 943, 915, 768, 755, 735, 677, 650 cm^{-1}; HRMS (ESI) calcd for $C_{19}H_{19}I_2N_3O_4$+Na 629.9357: found 629.9363.

Methyl (S)-2-(3,4-diiodo-2-(5-(4-methoxyphenyl)-1,3,4-oxadiazol-2-yl)-1H-pyrrol-1-yl)-3-methylbutanoate (**5h-1**). Yellow oil (a 1.3:1 mixture of di- and mono-iodide products); di-iodide, 39% yield (199 mg, 0.33 mmol, calcd), mono-iodide, 30% yield (121 mg, 0.25 mmol, calcd); R_f = 0.60 (3:2 hexane/EtOAc); Data for di-iodide at pyrrole: ^{1}H-NMR ($CDCl_3$) δ = 0.86 (d, *J* = 6.4 Hz, 3H), 1.05 (d, *J* = 6.4 Hz, 3H), 2.43 (m, 1H), 3.74 (s, 3H), 3.89 (s, 3H), 6.09 (d, *J* = 10.0 Hz, 1H), 7.05 (d, *J* = 8.8 Hz, 2H), 7.44 (s, 1H), 8.11 (d, *J* = 8.8 Hz, 2H) ppm; ^{13}C-NMR ($CDCl_3$) δ = 18.6, 19.1, 33.0, 52.5, 55.5, 65.7, 78.0, 80.4, 114.6, 116.0, 120.3, 128.9, 130.6, 156.7, 162.5, 163.4, 170.5 ppm; IR ν = 2970, 1750, 1615, 1590, 1560, 1500, 1485, 1460, 1440, 1390, 1335, 1255, 1205, 1175, 1160, 1065, 1030, 945, 840, 755, 745, 625 cm^{-1}; HRMS (ESI) calcd for $C_{19}H_{19}I_2N_3O_4$+Na 629.9357, found 629.9358. Data for mono-iodide at pyrrole (C-3): ^{1}H-NMR ($CDCl_3$) δ = 0.61 (d, *J* = 6.4 Hz, 3H), 1.06 (d, *J* = 6.4 Hz, 3H), 2.43 (m, 1H), 3.76 (s, 3H), 3.89 (s, 3H), 6.13 (d, *J* = 9.6 Hz, 1H), 7.01 (d, *J* = 2.0 Hz, 1H), 7.02 (d, *J* = 8.4 Hz, 2H), 7.35 (d, *J* = 2.0 Hz, 1H), 8.02 (d, *J* = 8.4 Hz, 2H) ppm; ^{13}C-NMR ($CDCl_3$) δ = 18.5, 19.2, 33.3, 52.4, 61.3, 64.9, 77.2, 114.5, 116.0, 120.1, 121.5, 128.6, 130.1, 157.7, 162.4, 162.8, 170.8 ppm; HRMS (ESI) calcd for $C_{19}H_{20}IN_3O_4$+Na 504.0396: found 504.0387.

Methyl (2S,3S)-2-(3-iodo-2-(5-(4-methoxyphenyl)-1,3,4-oxadiazol-2-yl)-1H-pyrrol-1-yl)-3-methylpentanoate (**6h-1**). Yellow oil, 83% yield (308 mg, 0.67 mmol); R_f = 0.40 (4:1 hexane/EtOAc); Data for **6h-1**: ^{1}H-NMR ($CDCl_3$) δ = 0.84 (t, *J* = 7.2 Hz, 3H), 1.02 (d, *J* = 6.4 Hz, 3H), 1.06–1.26 (m, 2H), 2.16–2.28 (m, 1H), 3.75 (s, 3H), 3.89 (s, 3H), 6.18 (d, *J* = 10.0 Hz, 1H), 6.99–7.04 (m, 2H), 7.01 (d, *J* = 1.6 Hz, 1H), 7.35 (d, *J* = 1.6 Hz, 1H), 7.99–8.03 (m, 2H) ppm; ^{13}C-NMR ($CDCl_3$) δ = 10.9, 15.4, 24.8, 39.2, 52.4, 55.5, 64.1, 77.2, 114.6, 116.0, 120.1, 120.3, 128.7, 130.1, 157.6, 162.4, 162.9, 171.0 ppm; IR ν = 2970, 2935, 2880, 2840, 1750, 1607, 1498, 1464, 1440, 1310, 1260, 1176, 1100, 1065, 1030, 1000, 915, 840, 815, 745, 640, 625, 607 cm^{-1}; HRMS (ESI) calcd for $C_{20}H_{22}IN_3O_4$+Na 518.0547: found 518.0548.

3.4. Biological Evaluation

The minimum inhibitory concentrations (MICs) were determined using the broth microdilution method in a 96-well plate [40,41]. The 96-well plates containing chemicals in two-fold serial dilutions (4 μg/mL to 2048 μg/mL for series **1**; 2 μg/mL to 1024 μg/mL for series **5** and **6**) were prepared in Luria–Bertani (LB) medium. *E. coli*, *S. aureus*, and *A. baumannii* cells were grown in LB broth to the exponential phase. A 10 μL volume of cells diluted with LB broth to a concentration of 10^8 cells/mL was inoculated on the plates. The

MIC was determined after incubation at 37 °C for 16 h under aerobic conditions. The optical density was measured in triple at 600 nm (OD_{600}) using a microplate reader (Bio-Rad, USA) at 20 h after treatment of the chemicals in concentrations of 2, 4, 8, 16, 32, 64, 128, 256, 512, and 1024 μg/mL. The average and standard deviation values of OD_{600} are reported in Table S1 and Table S2 of the Supporting Information. Vancomycin and Erythromycin were used as positive controls (see Table S2 for the average and standard deviation values of OD_{600}). As the chemicals were dissolved in 100% DMSO, 100% DMSO and triple-distilled water were used as negative controls. The minimum inhibitory concentration (MIC) in Tables 2 and 4 is defined as the lowest concentration of chemicals which provides an average OD_{600} value of less than 0.100.

4. Conclusions

We extended the synthetic utility of pyrrole platform chemicals **2**, which can be readily prepared from the sustainable ribose conversion with amino acids, to the pyrrole-ligated 1,3,4-oxadiazole core structure **1** through the reaction with benzohydrazide **3a**. The size effect of the R group from the amino acids clearly offered better antibacterial activities for 1,3,4-oxadiazoles **1c** and **1e**, which were derived from valine and isoleucine, respectively. Benzohydrazides **3** with various electronic X-substituents were utilized for the construction of 2-pyrrolyl-5-phenyl-1,3,4-oxadiazoles **5** and **6** with *N*-valine and *N*-isoleucine residues, respectively. Relationships of structure and antibacterial activity were deduced from MIC values for 1,3,4-oxadiazoles **5** and **6** against *E. coli*, *S. aureus* and *A. baumannii*. A positive *ortho* effect was marginally observed for fluoride substituents. Most importantly, a superior iodophenol effect was evident in the antibacterial activities of 1,3,4-oxadiazoles **5f-1** and **6f-1**, which provided much lower MIC values against *A. baumannii* than those of the vancomycin and erythromycin as positive controls. These findings provide a guiding principle for the design of superior future antimicrobial agents.

Supplementary Materials: The following supporting information can be downloaded at: https://www.mdpi.com/article/10.3390/molecules28083638/s1, (1) $^{1}H/^{13}C$-NMR spectra; (2) MIC data against *E. coli*, *S. aureus*, and *A. baumannii*; (3) High-Resolution Mass Spectra for the entire 1,3,4-oxadiazoles synthesized in this paper. Table S1. Determination of MIC for **1** for *E. coli* and *S. aureus* by OD600 (20 h). Each value was obtained as an average of at least triple measurements. Table S2. Determination of MIC for **5** and **6** for *E. coli*, *S. aureus,* and *A. baumannii* by OD600 (20 h). Each value was obtained as an average of at least triple measurements (vancomycin and erythromycin as positive controls).

Author Contributions: Conceptualization, S.K.; methodology, S.K., H.Y. (Haiyang Yu), and C.-R.L.; validation, S.K., H.Y. (Haiyang Yu), and C.-R.L.; formal analysis, H.K., L.G., and H.Y. (Huisu Yeo); investigation, H.K., L.G., H.Y. (Huisu Yeo), and U.C.; resources, S.K. and C.-R.L.; data curation, S.K. and C.-R.L.; writing—original draft preparation, S.K.; writing—review and editing, S.K. and C.-R.L.; visualization, S.K.; supervision, S.K.; project administration, S.K.; funding acquisition, S.K. All authors have read and agreed to the published version of the manuscript.

Funding: This work was supported under the framework of international cooperation program managed by the National Research Foundation of Korea (2021K2A9A1A01101863 and 2022K2A9A1A01097910) and partly by Basic Science Research Program funded by the Ministry of Education (2020R1A6A1A03038817).

Institutional Review Board Statement: Not applicable.

Informed Consent Statement: Not applicable.

Data Availability Statement: Data are contained within the article.

Conflicts of Interest: The authors declare no conflict of interest.

References

1. Romeo, G.; Chiacchio, U. Oxadiazoles. *Mod. Heterocycle. Chem.* **2011**, *2*, 1047–1252. [CrossRef]
2. Bajaj, S.; Asati, V.; Singh, J.; Roy, P.P. 1,3,4-Oxadiazoles: An emerging scaffold to target growth factors, enzymes and kinases as anticancer agents. *Eur. J. Med. Chem.* **2015**, *97*, 124–141. [CrossRef] [PubMed]

3. Vaidya, A.; Pathak, D.; Shah, K. 1,3,4-Oxadiazole and its derivatives: A review on recent progress in anticancer activities. *Chem. Biol. Drug Des.* **2021**, *97*, 572–591. [CrossRef] [PubMed]
4. Glomb, T.; Świątek, P. Antimicrobial activity of 1,3,4-oxadiazole derivatives. *Int. J. Mol. Sci.* **2021**, *22*, 6979. [CrossRef] [PubMed]
5. Schulz, B.; Bruma, M.; Brehmer, L. Aromatic poly (1,3,4-oxadiazole)s as advanced materials. *Adv. Mater.* **1997**, *9*, 601–613. [CrossRef]
6. Bruma, M.; Köpnik, T. Silicon-containing polyoxadiazoles—Synthesis and perspectives. *Adv. Colloid Interface Sci.* **2005**, *116*, 277–290. [CrossRef]
7. Kuznetsova, A.; Matveevskaya, V.; Pavlov, D.; Yakunenkov, A.; Potapov, A. Coordination polymers based on highly emissive ligands: Synthesis and functional properties. *Materials* **2020**, *13*, 2699. [CrossRef]
8. Du, M.; Bu, X.-H. Angular Dipyridyl Ligands 2,5-Bis(4-pyridyl)-1,3,4-oxadiazole and Its 3-Pyridyl Analogue as Building Blocks for Coordination. *Bull. Chem. Soc. Jpn.* **2009**, *82*, 539–554. [CrossRef]
9. de Oliveira, C.S.; Lira, B.F.; Barbosa-Filho, J.M.; Lorenzo, J.G.F.; de Athayde-Filho, P.F. Synthetic approaches and pharmacological activity of 1,3,4-oxadaizoles: A review of the literature from 2000–2012. *Molecules* **2012**, *17*, 10192–10231. [CrossRef]
10. Salahuddin; Mazumder, A.; Yar, M.S.; Mazumder, R.; Chakraborthy, G.S.; Ahsan, M.J.; Rahman, M.U. Updates on synthesis and biological activities of 1,3,4-oxadiazole: A review. *Synth. Commun.* **2017**, *47*, 1805–1847. [CrossRef]
11. Nayak, S.G.; Poojary, B. A Review on the preparation of 1,3,4-oxadiazoles from the dehydration of hydrazines and study of their biological roles. *Chem. Afr.* **2019**, *2*, 551–571. [CrossRef]
12. Patel, K.D.; Prajapati, S.M.; Panchal, S.N.; Patel, H.D. Review of synthesis of 1,3,4-oxadiazole derivatives. *Synth. Commun.* **2014**, *44*, 1859–1875. [CrossRef]
13. Deeks, S.G.; Kar, S.; Gubernick, S.I.; Kirkpatrick, P. Raltegravir. *Nat. Rev. Drug Discov.* **2008**, *7*, 117–118. [CrossRef]
14. Croxtall, J.D.; Lyseng-Williamson, K.A.; Perry, C.M. Raltegravir. *Drugs* **2008**, *68*, 131–138. [CrossRef] [PubMed]
15. Nelson, J.B.; Fizazi, K.; Miller, K.; Higano, C.; Moul, J.W.; Akaza, H.; Morris, T.; McIntosh, S.; Pemberton, K.; Gleave, M. Phase 3, randomized, placebo-controlled study of Zibotentan (ZD4054) in patients with castration-resistant prostate cancer metastatic to bone. *Cancer* **2012**, *118*, 5709–5718. [CrossRef]
16. Miller, K.; Moul, J.W.; Gleave, M.; Fizazi, K.; Nelson, J.B.; Morris, T.; Nathan, F.E.; McIntosh, S.; Pemberton, K.; Higano, C.S. Phase III, randomized, placebo-controlled study of once-daily oral zibotentan (ZD4054) in patients with non-metastatic castration-resistant prostate cancer. *Prostate Cancer Prostatic Dis.* **2013**, *16*, 187–192. [CrossRef]
17. Narayana, B.; Ashalatha, B.V.; Raj, K.K.V.; Fernandes, J.; Sarojini, B.K. Synthesis of some new biologically active 1,3,4-oxadiazolyl nitroindoles and a modified Fischer indole synthesis of ethyl nitro indole-2-carboxylates. *Bioorg. Med. Chem.* **2005**, *13*, 4638–4644. [CrossRef]
18. Narayana, B.; Ashalatha, B.V.; Raj, K.K.V.; Sarojni, B.K. Synthesis and studies on antimicrobial, anti-inflammatory and antiproliferative activities of heterocycles derived from 4-/5-/6-/7-nitro/5-fluoro/chloro/bromoindole-2-carbohydrazides. *Indian J. Chem.* **2009**, *48B*, 1794–1805.
19. Bingul, M.; Saglam, M.F.; Kandemir, H.; Boga, M.; Sengul, I.F. Synthesis of indole-2-carbohydrazides and 2-(indol-2-yl)-1,3,4-oxadiazoles as antioxidants and their acetylcholinesterase inhibition properties. *Monatsh. Chem.* **2019**, *150*, 1553–1560. [CrossRef]
20. Shekarchi, M.; Ellahiyan, F.; Akbarzadeh, T.; Shafiee, A. Syntheses of [1,2,3]Selenadiazolo[4,5-*e*]benzofuran or benzothiophene, [1,2,3]thiadiazolo[4,5-*e*]benzofuran or benzothiophene, and 2-benzofuranyl-1,3,4-oxodiazole derivatives. *J. Heterocycl. Chem.* **2003**, *40*, 427–433. [CrossRef]
21. Chen, W.; Wang, M.; Li, P.; Wang, L. Highly efficient copper/palladium-catalyzed tandem Ullman reaction/arylation of azoles via C–H activation: Synthesis of benzofuranyl and indolyl azoles from 2-(*gem*-dibromovinyl)phenols(anilines) with azoles. *Tetrahedron* **2011**, *67*, 5913–5919. [CrossRef]
22. Abedinifar, F.; Mohammadi-Khanaposhtani, M.; Asemanipoor, N.; Mojtabavi, S.; Faramarzi, M.A.; Mahdavi, M.; Biglar, M.; Larijani, B.; Hamedifar, H.; Hajimiri, M.H. Synthesis and biological evaluation of a new series of benzofuran-1,3,4-oxadiazole containing 1,2,3-triazoleacetamides as potential α-glucosidase inhibitors. *J. Biochem. Mol. Toxicol.* **2021**, *35*, e22688. [CrossRef] [PubMed]
23. Onishi, T.; Iwashita, H.; Uno, Y.; Kunitomo, J.; Saitoh, M.; Kimura, E.; Fujita, H.; Uchiyama, N.; Kori, M.; Takizawa, M. A novel glycogen synthase kinase-3 inhibitor 2-methyl-5-(3-{4-[(*S*)-methylsulfinyl]phenyl}-1-benzofuran-5-yl)-1,3,4-oxadiazole decreases tau phosphorylation and ameliorates cognitive deficits in a transgenic model of Alzheimer's disease. *J. Neurochem.* **2011**, *119*, 1330–1340. [CrossRef] [PubMed]
24. Saitoh, M.; Jun Kunitomo, J.; Kimura, E.; Iwashita, H.; Uno, Y.; Onishi, T.; Uchiyama, N.; Kawamoto, T.; Tanaka, T.; Mol, C.D.; et al. 2-{3-[4-(Alkylsulfinyl)phenyl]-1-benzofuran-5-yl}-5-methyl-1,3,4-oxadiazole derivatives as novel inhibitors of glycogen synthase kinase-3β with good brain permeability. *J. Med. Chem.* **2009**, *52*, 6270–6286. [CrossRef]
25. Kim, S.B.; Chang, B.Y.; Hwang, B.Y.; Kim, S.Y.; Lee, M.K. Pyrrole alkaloids from the fruits of Morus alba. *Bioorg. Med. Chem. Lett.* **2014**, *24*, 5656–5659. [CrossRef] [PubMed]
26. Pinder, A.R. Azetidine, pyrrole, pyrrolidine, piperidine, and pyridine alkaloids. *Nat. Prod. Rep.* **1992**, *9*, 491–504. [CrossRef]
27. Asgaonkar, K.D.; Mote, G.D.; Chitre, T.S. QSAR and molecular docking studies of oxadiazole-ligated pyrrole derivatives as enoyl-ACP (CoA) reductase inhibitors. *Sci. Pharm.* **2014**, *82*, 71–86. [CrossRef]
28. Rane, R.A.; Karpoormath, R.; Naphade, S.S.; Bangalore, P.; Shaikh, M.; Hampannavar, G. Novel synthetic organic compounds inspired from antifeedant marine alkaloids as potent bacterial biofilm inhibitors. *Bioorg. Chem.* **2015**, *61*, 66–73. [CrossRef]

29. Rane, R.A.; Gutte, S.D.; Sahu, N.U. Synthesis and evaluation of novel 1,3,4-oxadiazole derivatives of marine bromopyrrole alkaloids as antimicrobial agent. *Bioorg. Med. Chem. Lett.* **2012**, *22*, 6429–6432. [CrossRef]
30. Rane, R.A.; Bangalore, P.; Borhade, S.D.; Khandare, P.K. Synthesis and evaluation of novel 4-nitropyrrole-based 1,3,4-oxadiazole derivatives as antimicrobial and anti-tubercular agents. *Eur. J. Med. Chem.* **2013**, *70*, 49–58. [CrossRef]
31. Das Adhikary, N.; Kwon, S.; Chung, W.-J.; Koo, S. One-pot conversion of carbohydrates into pyrrole-2-carbaldehydes as sustainable platform chemicals. *J. Org. Chem.* **2015**, *80*, 7693–7701. [CrossRef] [PubMed]
32. Cho, S.; Gu, L.; In, I.J.; Wu, B.; Lee, T.; Kim, H.; Koo, S. Ribose conversion with amino acids into pyrraline platform chemicals—Expeditious synthesis of diverse pyrrole-fused alkaloid compounds. *RSC Adv.* **2021**, *11*, 31511–31525. [CrossRef] [PubMed]
33. Jones, L.H.; Narayanan, A.; Hett, E.C. Understanding and applying tyrosine biochemical diversity. *Mol. BioSyst.* **2014**, *10*, 952–969. [CrossRef] [PubMed]
34. Yin, J.; Ren, W.; Yang, G.; Duan, J.; Huang, X.; Fang, R.; Li, C.; Li, T.; Yin, Y.; Hou, Y.; et al. L-Cysteine metabolism and its nutritional implications. *Mol. Nutr. Food Res.* **2015**, *60*, 134–146. [CrossRef]
35. Elshorbagy, A.K.; Smith, A.D.; Kozich, V.; Refsum, H. Cysteine and obesity. *Obesity* **2012**, *20*, 473–481. [CrossRef] [PubMed]
36. Jha, K.K.; Samad, A.; Kumar, Y.; Shaharyar, M.; Khosa, R.L.; Jain, J.; Kumar, V.; Singh, P. Design, synthesis and biological evaluation of 1,3,4-oxadiazole derivatives. *Eur. J. Med. Chem.* **2010**, *45*, 4963–4967. [CrossRef]
37. Yu, W.; Huang, G.; Zhang, Y.; Liu, H.; Dong, L.; Yu, X.; Li, Y.; Chang, J. I_2-Mediated oxidative C−O bond formation for the synthesis of 1,3,4-oxadiazoles from aldehydes and hydrazides. *J. Org. Chem.* **2013**, *78*, 10337–10343. [CrossRef]
38. Niu, P.; Kang, J.; Tian, X.; Song, L.; Liu, H.; Wu, J.; Yu, W.; Chang, J. Synthesis of 2-amino-1,3,4-oxadiazoles and 2-amino-1,3,4-thiadiazoles via sequential condensation and I_2-mediated oxidative C−O/C−S bond formation. *J. Org. Chem.* **2015**, *80*, 1018–1024. [CrossRef]
39. Kubát, P.; Henke, P.; Mosinger, J. The effect of iodide and temperature on enhancing antibacterial properties of nanoparticles with an encapsulated photosensitizer. *Colloids Surf. B* **2019**, *176*, 334–340. [CrossRef]
40. Rodriguez-Tudela, J.L.; Barchiesi, F.; Bille, J.; Chryssanthou, E.; Cuenca-Estrella, M.; Denning, D.; Donnelly, J.P.; Dupont, B.; Fegeler, W.; Moore, C.; et al. Method for the determination of minimum inhibitory concentration (MIC) by broth dilution of fermentative yeasts. *Clin. Microbiol. Infect.* **2003**, *9*, 1–8. [CrossRef]
41. Jin, H.; Jiang, X.; Yoo, H.; Wang, T.; Sung, C.G.; Choi, U.; Lee, C.-R.; Yu, H.; Koo, S. Synthesis of Chalcone-derived heteroaromatics with antibacterial activities. *ChemistrySelect* **2020**, *5*, 12421–12424. [CrossRef]

molecules

MDPI

Article

Simple Synthetic Approach to *N*-(Pyridin-2-yl)imidates from Nitrostyrenes and 2-Aminopyridines via the *N*-(Pyridin-2-yl)iminonitriles as Intermediates

Andriani G. Chaidali and Ioannis N. Lykakis *

Department of Chemistry, Aristotle University of Thessaloniki, University Campus, 54124 Thessaloniki, Greece; chaidali.and@gmail.com

* Correspondence: lykakis@chem.auth.gr

Abstract: A facile, green, synthetic protocol of several substituted *N*-(pyridin-2-yl)imidates from nitrostyrenes and 2-aminopyridines via the corresponding *N*-(pyridin-2-yl)iminonitriles as intermediates is reported. The reaction process involved the in situ formation of the corresponding α-iminontriles under heterogeneous Lewis acid catalysis in the presence of Al_2O_3. Subsequently, α-iminonitriles were selectively transformed into the desired *N*-(pyridin-2-yl)imidates under ambient conditions and in the presence of Cs_2CO_3 in alcoholic media. Under these conditions, 1,2- and 1,3-propanediols also led to the corresponding mono-substituted imidates at room temperature. The present synthetic protocol was also developed on one mmol scale, providing access to this important scaffold. A preliminary synthetic application of the present *N*-(pyridin-2-yl)imidates was carried out for their facile conversion into the *N*-heterocycles 2-(4-chlorophenyl)-4,5-dihydro-1*H*-imidazole and 2-(4-chlorophenyl)-1,4,5,6-tetrahydropyrimidine in the presence of the corresponding ethylenediamine and 1,3-diaminopropane.

Keywords: imidates; iminonitriles; nitrostyrenes; 2-aminopyridine; *N*-heterocycles

Citation: Chaidali, A.G.; Lykakis, I.N. Simple Synthetic Approach to *N*-(Pyridin-2-yl)imidates from Nitrostyrenes and 2-Aminopyridines via the *N*-(Pyridin-2-yl)iminonitriles as Intermediates. *Molecules* **2023**, *28*, 3321. https://doi.org/10.3390/molecules28083321

Academic Editors: Alexey M. Starosotnikov, Maxim A. Bastrakov and Igor L. Dalinger

Received: 13 March 2023
Revised: 6 April 2023
Accepted: 7 April 2023
Published: 9 April 2023

1. Introduction

Imidates are considered to be one of the most important organic patterns due to their varied electronic nature [1,2]. In general, imidates serve as powerful molecules of electrophiles and nucleophiles in reactions (Figure 1) with several applications not only in structure functionalization, e.g., the synthesis of esters, amides, and amidines, but also in the synthesis of heterocyclic molecules [3]. For example, reported studies [4] on the successful transformation of imidates into a series of *N*-heterocycles, such as imidazolines, (benz)imidazoles, (benz)oxazoles, oxazolines, thiazolines, and azines, were summarized recently (Figure S1) [5]. Thus, it is interesting to note here that the last decade has witnessed the development of versatile synthetic methodologies towards their one-step synthesis using suitable imidate precursors. This synthetic strategy is still interesting and attractive, because it enables the formation of C-C and C-N bonds in one step with the nitrogen atom that comes from the imidates present in the final *N*-heterocyclic structure. Imidates have been applied in the synthesis of oxazoline-fused sugars from corresponding glycosyl-imidates [6,7] and a new C-C bond between sugars and aromatic compounds can be formed using glycosyl-trichloroacetimidates [8].

The most common synthetic process of the imidate moiety is the transformation of nitriles under acidic (a Pinner reaction) or basic conditions in alcoholic media (Figure 1A,B) [9–14]. For Pinner reactions, several methodologies have been reported, including the reactions of imidoyl halides with alkoxides and phenoxides or transesterification of imidates (Figure 1C) [2,15]; the conversion of amides to imidates in the presence of Meerwein reagents or diazo-compounds (Figure 1D) [2,16–18]; reactions of amino compounds with ortho-esters under acidic conditions (Figure 1E) [2]; the direct *N*-alkylation of imidates, using amino acid

derivatives (Figure 1F) [2]; pericyclic reactions of unsaturated *N*-allyl ynamides, triynes, tetraynes, or ring openings of *N*,*N*- and *N*,*O*- heterocyclic compounds (Figure 1G) [19–22]; and syntheses from metal complexes and organometallic compounds [2].

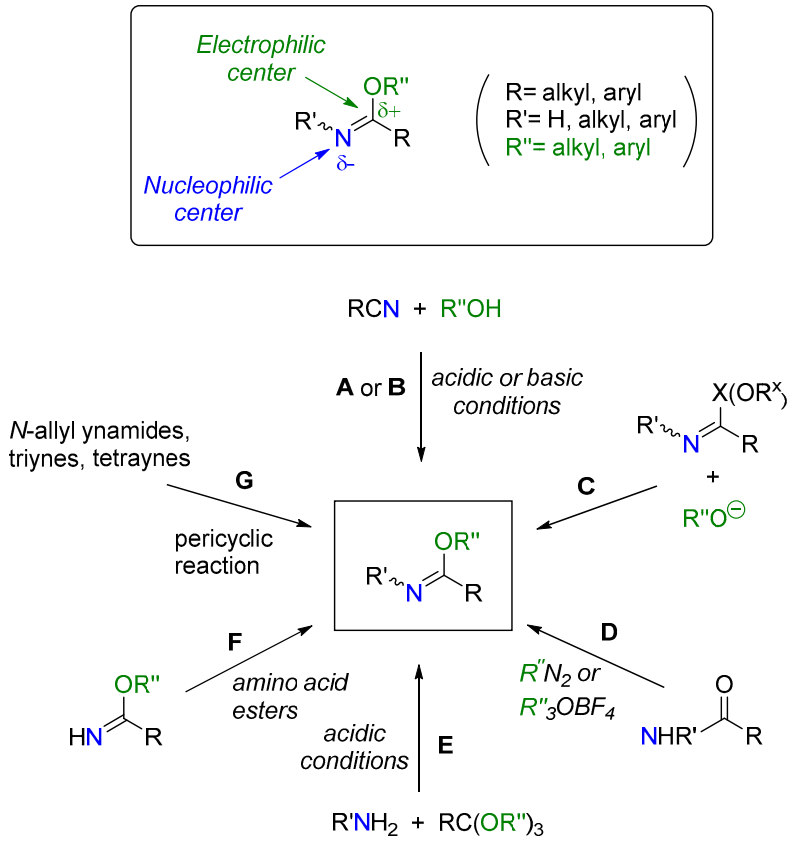

Figure 1. Synthetic methodologies (**A**–**G**) of imidates.

To date, the emphasis in research has been on developing new, efficient, and "green" methods for the conversion of α-iminonitriles to valuable imidates. To the best of our knowledge, only specific examples with limited applicability on the synthesis of *N*-(pyridin-2-yl)imidates have been reported (Scheme 1). In the literature, methyl (*Z*)-*N*-(pyridin-2-yl)benzimidate was the only example observed in an equimolar ratio with the corresponding amide under basic conditions in aqueous media (NaOH, MeOH/H_2O=1/1), initially starting from α-iminonitrile [23]. Recently, *N*-benzothiazolo-imines have been transformed into the corresponding methoxy imidates catalyzed by carbenes in the presence of sodium pyruvate, under oxidative conditions. Via this synthetic approach, only one example of *N*-(pyridin-2-yl)imidate has been presented [24]. Given the importance of this type of transformation and in terms of sustainability, the use of ambient and more eco-friendly heterogeneous conditions for the synthesis of substituted imidates continues to be a long-standing goal of chemical research. In light of our ongoing research directions for developing sustainable processes to construct *N*-heterocyclic organic molecules of high biological interest [25–30], herein we report the synthesis of a library of substituted *N*-(pyridin-2-yl)imidates from the corresponding *N*-(pyridin-2-yl)iminonitriles in the presence of Cs_2CO_3 and alcoholic media at ambient conditions (Scheme 1). Subsequently, the starting *N*-(pyridin-2-yl)iminonitriles were synthesized via a new heterogeneous catalytic process using Al_2O_3 in 1,2-dichloroethane (DCE) (Scheme 1). Thus, the present protocol is timely and of high interest, as it has a selective and sustainable synthetic character permitting the further diversification of the initial synthesized *N*-(pyridin-2-yl)iminonitriles libraries and giving us access to the synthetic, valuable substituted *N*-(pyridin-2-yl)imidates.

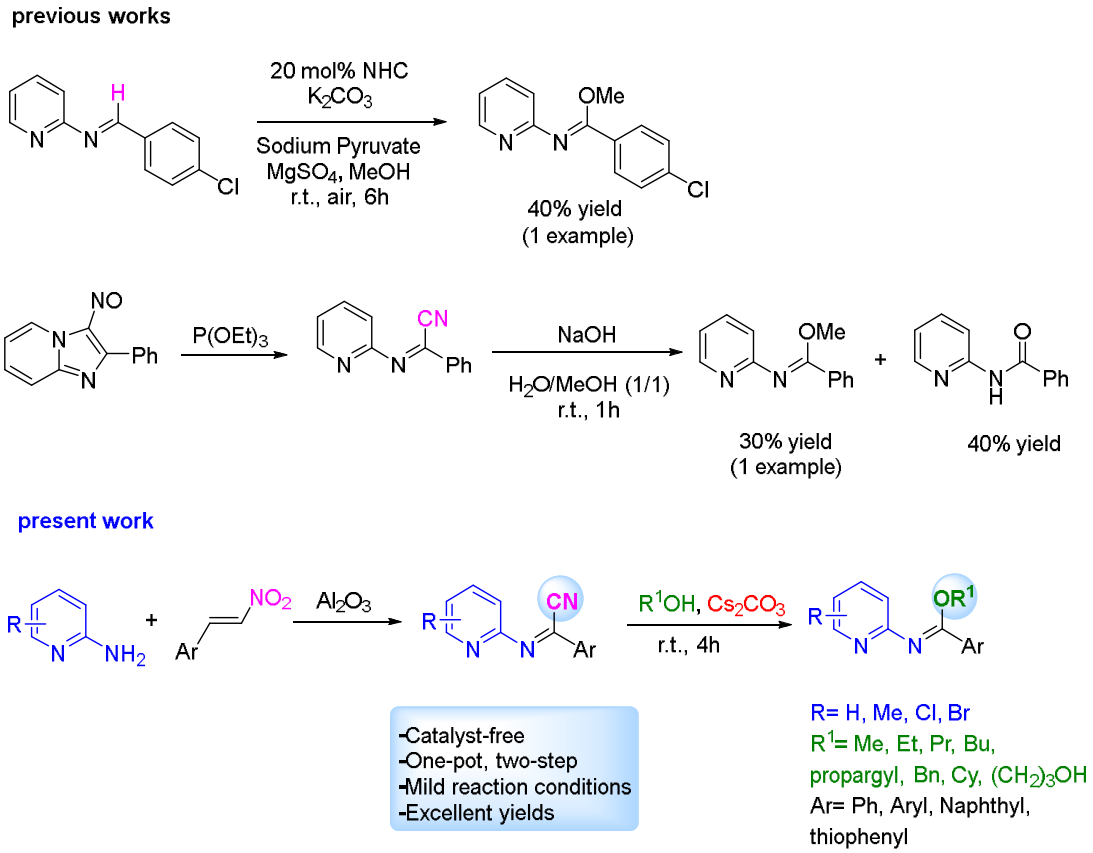

Scheme 1. Synthetic approaches to *N*-(pyridin-2-yl)imidates [23,24].

2. Results and Discussion

2.1. Evaluation of the Reaction Conditions

To optimize the reaction conditions, (*Z*)-4-methyl-*N*-(pyridin-2-yl)benzimidoyl cyanide (**1a**) was synthesized and selected as the model substrate. So far, the synthesis of *N*-(pyridin-2-yl)benzimidoyl cyanides from nitrostyrenes and 2-aminopyridine, using $Ce(OTf)_3$ as catalyst in toluene and at 120 °C, has been reported [31]. Herein, we developed a facile and green procedure for the selective synthesis of the desired α-iminonitriles by the reaction of 2-aminopyridine and nitrostyrene in the presence of Al_2O_3 and DCE as solvents (see Materials and Methods part for details). According to the literature previous work [31], herein, alumina is initially catalyzing the Michael addition of 2-aminopyridine to nitrostyrene [32–34], leading to an intermediate enamine that further undergoes a proton transfer, dehydration, and [1.5]-H sigmatropic rearrangement to produce the final α-iminonitrile product. Thus, using the present procedure, the synthesized **1a** was determined and characterized by an HRMS analysis and IR spectroscopy, as described in Figure S2, with the characteristic absorbance of the nitrile group at ca. 2200 nm. All the spectroscopic data are in agreement with those reported in the literature [31]. After that, control experiments using **1a** (0.1 mmol) in MeOH (1 mL) in the presence of different bases were performed and the results are summarized in Table 1. Among the used bases, Cs_2CO_3 and DBU were found to promote the studied transformation within 4 h and with the quantitative transformation of **1a** to the desired methyl (*Z*)-4-methyl-*N*-(pyridin-2-yl)benzimidate **2aa** (Table 1, entries 7 and 10). Byproducts such as amide **3a**, ester **4a** and **5a**, and the starting amine **4** were observed in significant amounts in the case of ^tBuOK or K_2CO_3 (Table 1, entries 3, 4, and 13). Similar results were observed when there was a lower amount of DBU (one equiv.) in the presence of molecular sieves or under an O_2 atmosphere (Table 1, entries 11 and 12). NaOH was found to promote the developed transformation; however, the corresponding amide **3a** was detected in a 6% yield (Table 1, entry 14). It is worth noting that in the absence

of a base, only a 18% yield was measured (Table 1, entry 15). Further increases in the temperature (50 °C) did not lead to significant increases in the desired product **2aa**'s yield (Table 1, entry 16); however, at 80 °C, **5a** and **6a** were formed as major products (Table 1, entry 17). All reactions were monitored by TLC and the products were characterized by ^{1}H NMR spectroscopy.

Table 1. Conditions and different bases evaluation for the transformation of **1a** to **2aa** in the presence of MeOH.

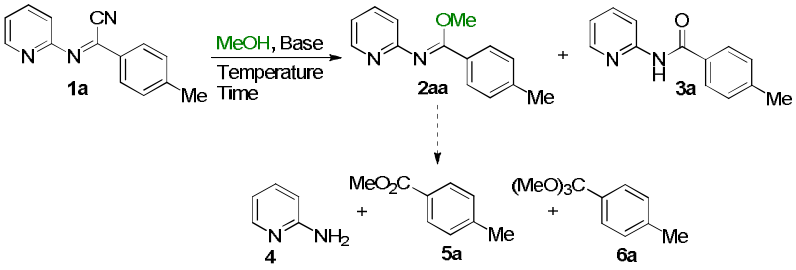

Entry	Base (eq.) [a]	Time (h)	Products (%) [b]					
			1a	2aa	3a	4	5a	6a
1	Et_3N (1.5)	4	50	50	-	-	-	-
2	Imidazole (1.5)	4	87	13	-	-	-	-
3	^{t}BuOK (1.5)	4	-	70	10	10	3	7
4	^{t}BuOK (2)	4	-	90	4	3	2	1
5	AcONa (1.5)	4	62	38	-	-	-	-
6	AcONa (2)	4	58	42	-	-	-	-
7	DBU (1.5)	4	-	100	-	-	-	-
8	DBU (2)	4	-	100	-	-	-	-
9	$NaHCO_3$ (1.5)	4	36	56	8	-	-	-
10	Cs_2CO_3 (1.5)	4	-	100	-	-	-	-
11 [c]	Cs_2CO_3 (1)	4	-	92	2	3	2	1
12 [d]	Cs_2CO_3 (1)	4	-	91	3	3	1	2
13	K_2CO_3 (1.5)	4	-	91	3	3	1	2
14	NaOH (1)	4	-	94	6	-	-	-
15	-	4	82	18	-	-	-	-
16 [e]	-	24	51	49	-	-	-	-
17 [f]	-	24	-	10	-	45	10	35

[a] Conditions: **1a** (0,1 mmol), MeOH (1 mL), room temperature. [b] Yields measured by ^{1}H NMR based on the addition of specific amount of 1,3-dimethoxybenzene as internal standard. [c] Molecular Sieves. [d] O_2 atmosphere. [e] Temperature = 50 °C. [f] Temperature = 80 °C.

To study further the present transformation, 0.1 mmol of **1a** were added into different alcoholic solvents, such as ethanol (EtOH), 1-propanol (PrOH), and 1-butanol (BuOH), and the reactions were performed in the presence of different equiv. of the Cs_2CO_3 and DBU (Tables S1–S3). In all cases, the corresponding imidates **2ab**, **2ac**, **2ad,** and **2ae** were formed in high yields. The optimum amount of Cs_2CO_3 was found to be between one and two equiv. based on the amount of **1a**. Under a lower amount of the base, no reaction completion was observed, and significant amounts of the amide **3a** were measured (Tables S1–S3). In the case of BuOH, a higher temperature was required (50 °C) for reaction completion and for better solubility of the base Cs_2CO_3 (see Table S3). The results under optimum conditions, two equiv. of Cs_2CO_3 and 24 h, from the experiments in alcoholic solvents are presented in Figure S3. It can be concluded that bulkier alcohols could lead to a decrease in the yield of the desired imidates, because the nucleophilic attack of the alcohol to the electrophilic carbon of the α-iminonitrile is more difficult due to steric effects.

To increase the synthetic value of the present protocol, we studied the selective transformation of α-iminonitrile **1a** to imidate **2aa** in the presence of two equiv. of Cs_2CO_3, using different solvent mixtures with MeOH in ratios of 1/1 and 1/4. As shown in Table 2,

in all cases, the quantitative consumption of the initial **1a** was observed and the desired **2aa** was formed in a high yield (95–99%), except in the presence of water, in which a significant amount of amide was observed (Table 2, Entry 8). These encouraging results support the plausible general application of the present facile protocol in synthetic chemistry.

Table 2. Reaction evaluation using different co-solvents for the transformation of **1a** to **2aa** in the presence of MeOH.

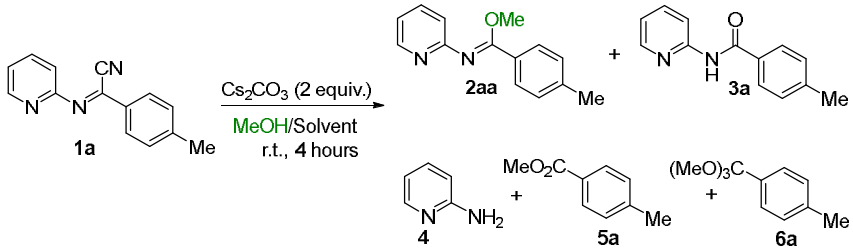

Entry	Solvent [a]	MeOH/Solvent	Products (%) [b]				
			2aa	3a	4	5a	6a
1	THF	1/1	98	2	-	-	-
2	THF	1/4	98	2	-	-	-
3	DCE	1/4	95	5	-	-	-
4	Acetone	1/4	97	3	-	-	-
5	CH_3CN	1/4	99	1	-	-	-
6	DMSO	1/1	99	1	-	-	-
7	EtOAc	1/1	95	5	-	-	-
8 [c,d]	H_2O	1/1	44	43	-	-	-

[a] Conditions: **1a** (0,1 mmol), MeOH/Solvent (1/1 or 1/4) in total volume of 1 mL, room temperature. [b] Relative yields and conversion measured by ^{1}H NMR of the crude reaction mixture based on the addition of specific amount of 1,3-dimethoxybenzene as internal standard. [c] Reaction time 24 h. [d] A total of 13% of starting material **1a** was observed.

2.2. Application of the Synthetic Transformation of N-(Pyridin-2-yl)benzimidoyl Cyanides to the N-(Pyridine-2-yl)imidates

To explore the substrate broadness of the described synthetic protocol, initially, a series of multifunctional *N*-(pyridin-2-yl)benzimidoyl cyanides were synthesized according to the above reported reaction of nitrostyrenes with 2-aminopyridine in the presence of Al_2O_3 and DCE as solvents (Scheme 2). The corresponding α-iminonitriles **1a**–**1h** and **1j**–**1s** were isolated in moderate to high yields (50–88%) after the simple filtration of the catalyst and chromatographic purification using silica gel and Hexane/EtOAc as the solvent mixture eluent (for details, see the Section 3 and the Supplementary Materials). The α-iminonitriles were characterized by ^{1}H NMR and compared with those of reported examples in the literature [31].

Having in our hands the above optimal conditions, the selective transformation of the synthesized α-iminonitriles to the corresponding imidates (**2aa**–**2hc** and **2ja**–**2sa**) was studied at ambient conditions. The observed products were summarized in Scheme 3 and the values in parentheses correspond to the isolated yields after purification by column chromatography on a silica gel using a gradient mixture of EtOAc−hexane (see Supplementary Materials). To our delight, in most cases, the desired imidates (**2aa**–**2hc** and **2ja**–**2sa**) were formed in good to high yields (56–98%). In particular, when MeOH was used, clean and quantitative transformations of the α-iminonitriles to the corresponding imidates (**2aa**–**2ha** and **2ja**–**2la**) were observed. Similarly high yields were also observed in the case of ethanolic (**2ab**–**2hb** and **2jb**–**2lb**) and propanolic (**2ac**–**2hc** and **2jc**–**2lc**) solutions (Scheme 2). Only when butanol was used as the reaction solvent was a higher temperature required (50 °C) for reaction completion, and the corresponding imidate (**2ad**) was isolated with a 77% yield within 24 h (Scheme 2). Importantly, in the reaction of **1j** (substrate bearing a -COOMe moiety in the *para*-position of the phenyl ring), an in situ transesterification was observed

in the presence of EtOH and PrOH. Thus, the isolated imidates **2jb** and **2jc** contained in their structures the -COOEt and -COOPr moieties, respectively (Scheme 3). Subsequently, a series of methyl-, chloro-, and bromo-substituted 2-aminopyridino-iminonitriles (**1m**–**1s**, Scheme 2) were successfully transformed into the corresponding imidates (**2ma**–**2sa**) using methanol and isolated in moderate to high yields, from 33% to 98% (Scheme 3). It is worth noting that the *o*-Me-substituted pyridine derivative led to the corresponding imidate (**2ma**) in a low yield (33%), even after a prolonged reaction time (4 days), probably for steric reasons.

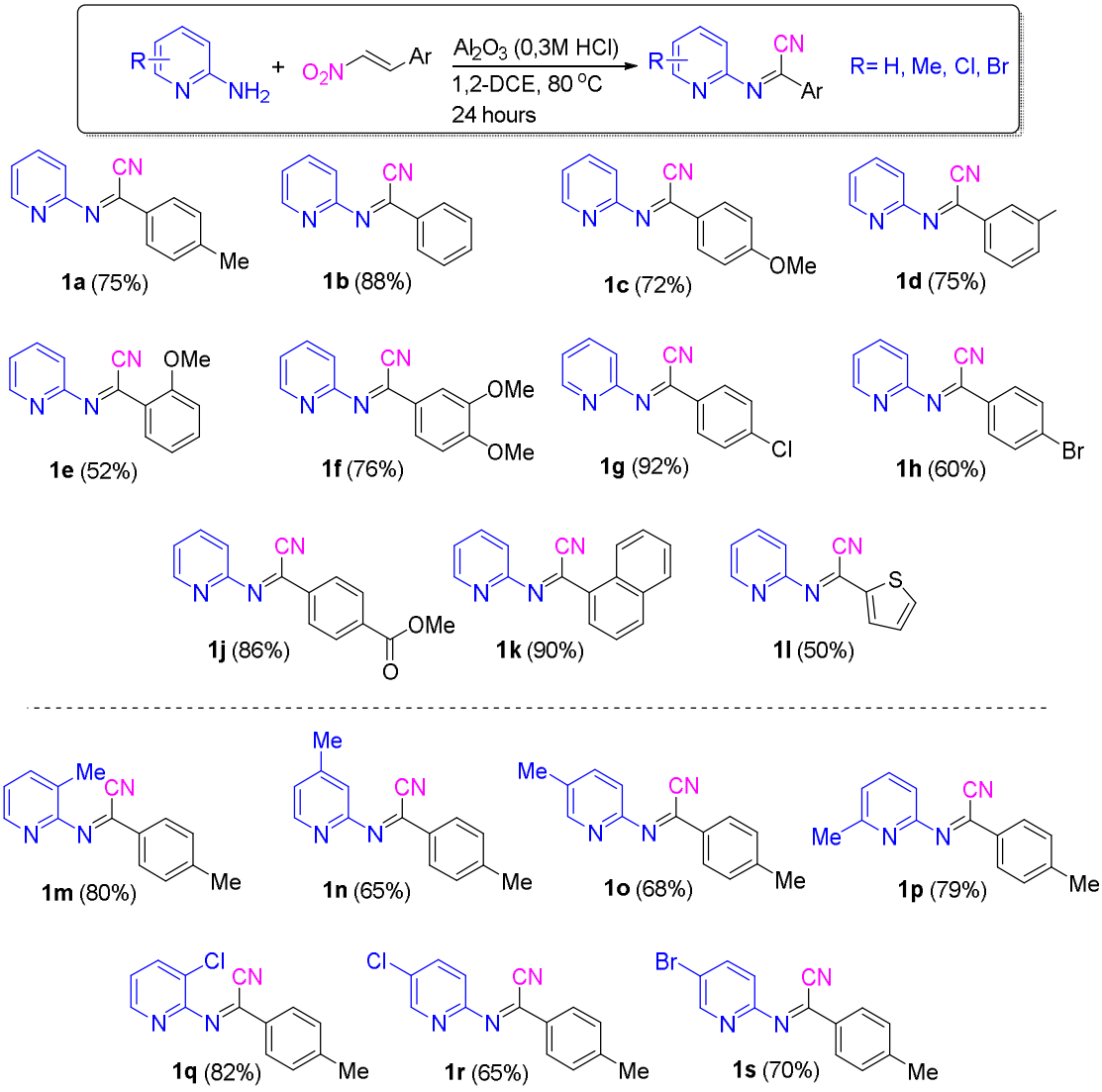

Scheme 2. Multifunctional *N*-pyridinyl substituted iminonitriles synthesized by the Al_2O_3-mediated reaction of nitrostyrenes with aminopyridines.

The synthesized imidates were characterized by NMR and HRMS spectroscopies. During HRMS operation, two fragments, $[M-31]^+$ and $[M+15]^+$, were observed with the use of a higher fragmentor voltage (200 V). The $[M-31]^+$ fragment presumably resulted from the elimination of the methoxy group (−31) to form the corresponding stable cationic intermediate, and then the addition of a formic acid molecule (+46), which was present in the eluent solvent, resulted in the $[M+15]^+$ fragment. For example, during the HRMS analysis of imidate **2ca**, except for the main fragment $[M+H]^+ = 243$ observed at 50 V, two new fragments appeared at 200 V $[M-31]^+ = 211$ and $[M+15]^+ = 257$, which corresponded to the intermediates derived by a methoxy moiety elimination and further trapping by

the formic acid (Figure S4). These observations also support the structure of the present desired imidates.

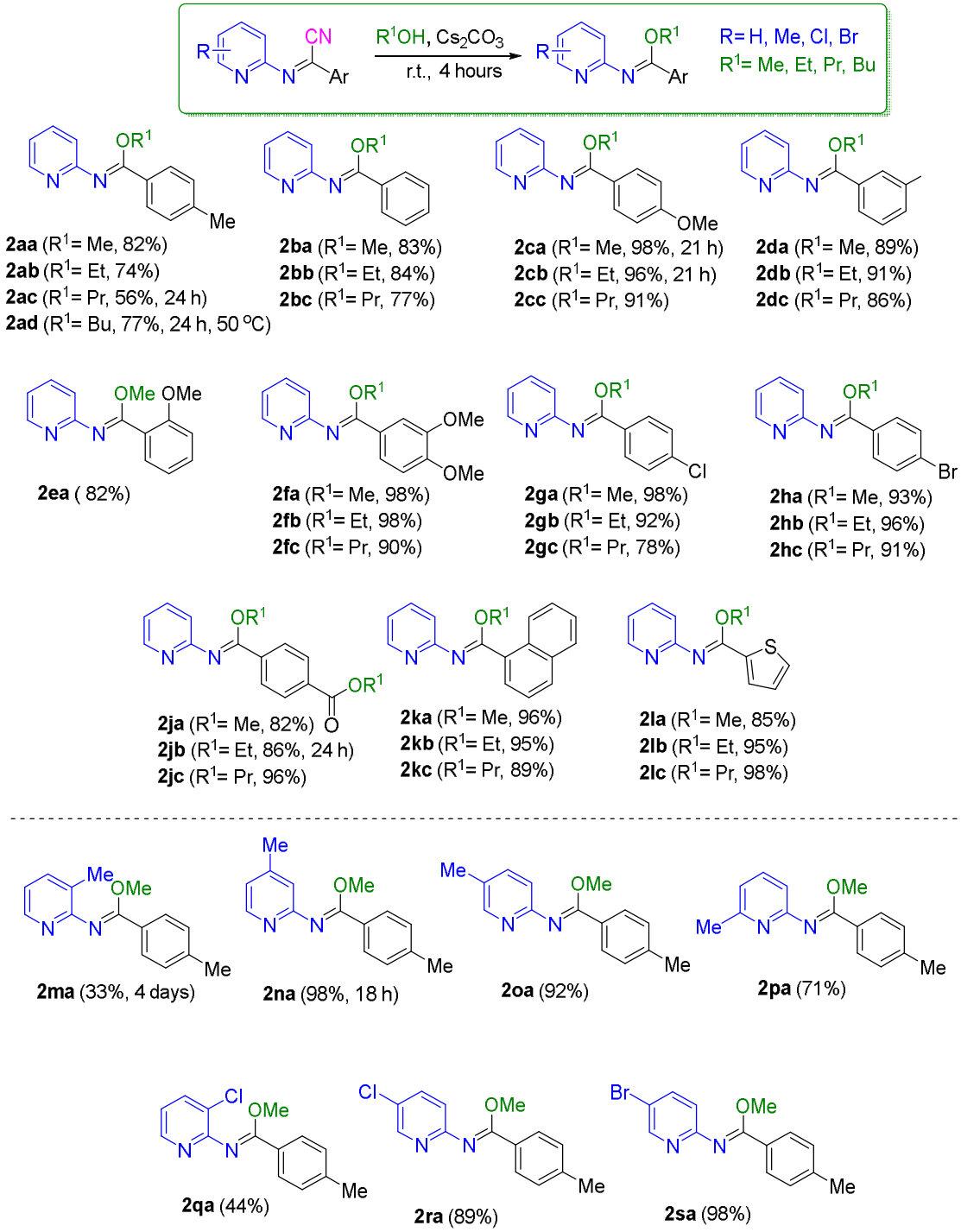

Scheme 3. Synthetic protocol of *N*-(pyridine-2-yl)imidates from *N*-(pyridin-2-yl)benzimidoyl cyanides.

To extend the substrate broadness, alcohols with a high molecular weight, such as benzyl alcohol (BnOH) and cyclohexyl alcohol (CyOH), were used in the presence of acetone as co-solvents in a ratio of 1/4 (Scheme 4). The corresponding imidates **2ag** and **2ah** were formed in good yields (90% and 43%). In addition, propargyl alcohol was found to be active under the present conditions and led to the desired imidate **2af** in a 55% yield (Scheme 4). Biobased products 1,2-propanediol and 1,3-propanediol were also tested under the present proposed conditions, with 0.1 mmol of **1a** and in the presence of different

co-solvents (DCE, acetone, and DMSO), as shown in Tables S4 and S5. To our surprise, the corresponding imidates, **2ai** and **2aj**, were formed as the major products (36% and 83%, Scheme 4), accompanied with significant amount of the amide **3a** and the esters **5i** and **5j** (Tables S4 and S5). It is worth mentioning that the imidate **2aj** was purified by column chromatography in a 30% yield; however, the yields of **2af**, **2ag,** **2ah,** and **2ai** were calculated by the ^{1}H NMR of the crude reaction mixture, with the use of 1,3-dimethoxybenzene as the internal standard.

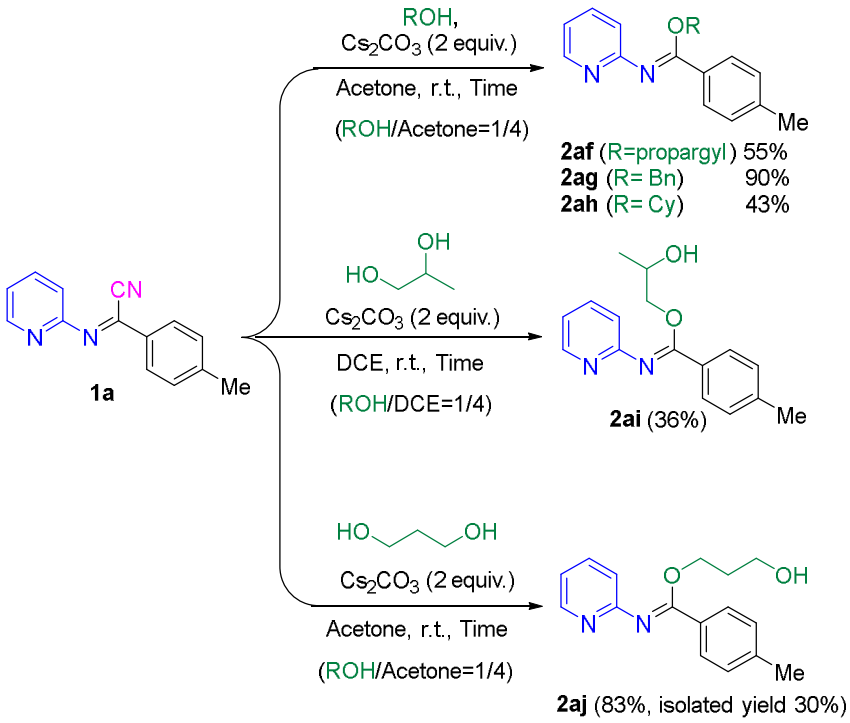

Scheme 4. Application using alcohols with higher molecular weight and diols, and synthesis of the corresponding imidates.

These results indicate the broad generality of the present protocol toward the synthesis of substituted *N*-(pyridin-2-yl)imidates in the presence of alcoholic media. Based on these encouraging results, the synthesis of the imidates **2aa**, **2ga**, **2ca,** and **2la** was further tested at the lab scale of one mmol. Thus, the corresponding amount of each iminonitrile, **1a**, **1g**, **1c,** and **1l,** was diluted in 2 mL of MeOH in the presence of two equiv. of Cs_2CO_3 at ambient temperature and stirred for an appropriate time. After reaction completion (ca. 1–4 h, based on TLC), the reaction mixture was filtered with the use of a short pad of silica gel and washed with ca. 10 mL of EtOAc. The corresponding imidates were isolated after chromatographic purification (see Materials and Methods) in 90%, 93%, 91%, and 85% yields, respectively (Scheme 5).

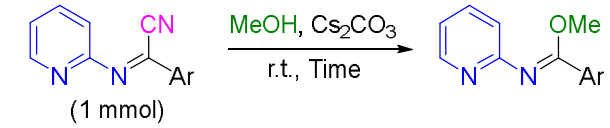

1a (Ar= *p*-Me-C_6H_4)
1g (Ar= *p*-Cl-C_6H_4)
1c (Ar= *p*-MeO-C_6H_4)
1l (Ar= thiophene)

2aa (3 h, 90%, 203 mg)
2ga (1 h, 93%, 230 mg)
2ca (4 h, 91%, 220 mg)
2la (4 h, 85%, 185 mg)

Scheme 5. One-mmol-scale process for the selective transformation of α-iminonitriles into imidates in MeOH.

Furthermore, an attempt was made to synthesize the skeleton of *N*,*N*-six- and *N*,*N*-five-membered ring heterocycles, such as 2-substituted tetrahydropyrimidines and dihydroimidazoles. These heterocycles constitute an important core of many natural products and exhibit a variety of biological effects, including antimicrobial and anti-inflammatory effects. They can even be used as therapeutic agents for the treatment of Alzheimer's disease [35–38]. Herein, we succeed in applying the present simple and mild protocol to the synthesis of 2-(4-chlorophenyl)-1,4,5,6-tetrahydropyrimidine **7g** and 2-(4-chlorophenyl)-4,5-dihydro-1*H*-imidazole **8g** via a reaction between **2ga** and 1,3-diaminopropane and ethylenediamine, respectively. The corresponding heterocycles were isolated in moderate yields, 40% and 55%, as shown in Scheme 6. These are the preliminarily results for the synthesis of *N*,*N*-heterocycles from imidates; however, further studies evaluating the reaction conditions are in progress.

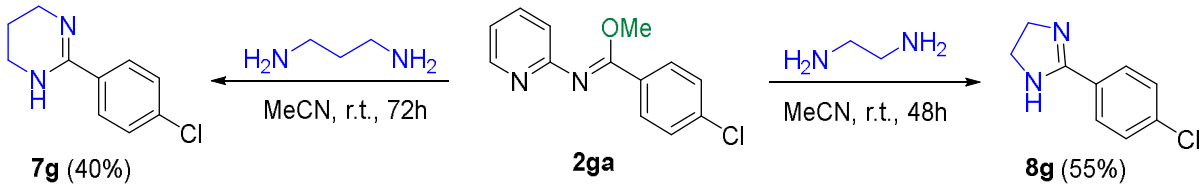

Scheme 6. Preliminary application of imidate **2ga** transformation into *N*,*N*-six- and *N*,*N*-five-membered ring heterocycles **7g** and **8g**.

3. Materials and Methods

3.1. General and Aparatus

All the reagents and solvents were purchased from Sigma-Aldrich, TCI Chemicals, AK Scientific, Fluorochem, and were used without further purification. Thin-layer chromatography was performed on Millipore precoated silica gel plates (0.20 mm thick, particle size of 25 μm). Nuclear magnetic resonance spectra were recorded on Bruker Avance 500 or 600 spectrometers and on Agilent 500 (^{1}H NMR (500 MHz), ^{13}C{H} NMR (126 MHz)). Chemical shifts for ^{1}H NMR were reported as δ values and coupling constants were measured in hertz (Hz). The following abbreviations were used for spin multiplicity: s = singlet, br s = broad singlet, d = doublet, t = triplet, q = quartet, quin = quintet, dd = double of doublets, ddd = double doublet of doublets, and m = multiplet. Chemical shifts for ^{13}C{H} NMR were reported in ppm relative to the solvent peak. Mass spectra were measured on a Waters Investigator Supercritical Fluid Chromatograph with a 3100 MS Detector (ESI) using a solvent system of methanol and CO_2 on a Viridis silica gel column (4.6 × 250 mm, 5 μm particle size) or Viridis 2-ethyl pyridine column (4.6 × 250 mm, 5 μm particle size). Mass spectra (HRMS) were carried out on an Agilent Q-TOF Mass Spectrometer, G6540B model with a Dual AJS ESI-MS source. All of the compounds (dissolved in LC-MS-grade acetonitrile containing 0.05% formic acid) were introduced into the ESI source of the mass spectrometer with a single injection of 15 μL of the sample and a flow rate of 300 μL/min of 100% methanol as the solvent in the binary pump. The experiments were run using a Dual AJS ESI source, operating in the positive ionization mode. Source operating conditions were as follows: gas temperature of 330 °C, gas flow of 8 L/min, sheath gas temperature of 250 °C, sheath gas flow of 10 L/min, and fragmentor voltage of 50–200 V. Data-dependent MS/MS analysis was performed in parallel with MS analysis in the centroid mode, using different collision energies (10, 20, 30, 40 V). All accurate mass measurements of the $[M+H]^+$ ions were performed by scanning from 100 to 800 m/z. The Q-TOF was calibrated 1 h prior to the infusion experiments by a calibration mixture. Data were acquired in an external calibration mode.

3.2. Synthesis of Aromatic β-Nitrostyrenes

Aromatic β-nitrostyrenes were synthesized according to the literature procedure [39]. In a solution of ammonium acetate (12.5 mmol) in acetic acid (10 mL), aromatic aldehyde

(5 mmol) and nitromethane (15.5 mmol) in one portion were added. The mixture was heated at reflux for 24 h. The reaction mixture was cooled at room temperature and then poured into ice water to precipitate the corresponding nitrostyrene. After extraction with organic solvent (EtOAc), the organic layer was evaporated under vacuum, and the residue was purified by column chromatography using silica gel to give final the corresponding products in good yields. In alternative, the precipitated solid was collected in pure form by filtration under vacuum in a Buchner funnel and washed with distilled water.

3.3. Synthesis of N-(Pyridin-2-yl)iminonitriles from Nitrostyrenes and 2-Aminopyridine

In a sealed tube of 1 mmol of nitrostyrene and 1.2 mmol of 2-aminopyridine, 10 mL of DCE as a solvent and 300 mg Al_2O_3 (0.3 M HCl) as a catalyst were added. The reaction mixture was stirred at 80 °C for 24 h. The reaction was monitored by thin-layer chromatography (TLC) and the slurry was filtered under pressure through a short pad of silica to withhold the catalyst with the aid of dichloromethane (DCM) and ethyl acetate (EtOAc). The filtrate was evaporated under vacuum and purified by column chromatography on a silica gel using a gradient mixture of EtOAc−hexane to afford the corresponding products in good yields.

The Al_2O_3 (0.3 M HCl) was prepared by the addition of 1 g of Al_2O_3 in 10 mL of a 0.3 M HCl aqueous medium and stirred for 2 h at room temperature. After filtration, the solid catalyst was dried in an oven at 100 °C for 24 h and was used for the present transformation.

3.4. Synthesis of N-(Pyridin-2-yl)imidates from N-(Pyridin-2-yl)iminonitriles

In a 4 mL vial, 2 equivalents of Cs_2CO_3 (0.4 mmol, 130.4 mg) and 1 mL of the corresponding alcohol were added. After stirring for a few minutes, 0.2 mmol of α-iminonitrile was added until the amount of Cs_2CO_3 was fully dissolved. The reaction mixture was stirred at room temperature for 4 h. The reaction was monitored by thin-layer chromatography (TLC) and after completion, the reaction mixture was filtered under pressure through a short pad of silica and celite to withhold the salt. The vial and the silica layer were washed with ca. 5 mL of dichloromethane (DCM) and ca. 5 mL of ethyl acetate. The organic solvents were evaporated under vacuum and the product was determined by ^{1}H NMR spectroscopy. In most cases, the imidate was formed in pure form; however, when a mixture of compounds was obtained, the desired imidate was purified by column chromatography on a silica gel using a gradient mixture of EtOAc−hexane and obtained in good to high isolated yields.

3.5. 1 mmol Scale Synthesis of N-(Pyridin-2-yl)imidates **2aa**, **2ca**, **2ga**, *and* **2la**

In a 15 mL vial, 2 mmol of Cs_2CO_3 and 2 mL of the methanol were added. After stirring for a few minutes, 1 mmol of α-iminonitrile was added until the amount of Cs_2CO_3 was fully dissolved. The reaction mixture was stirred at room temperature for 1–4 h, based on iminonitrile's conversion, which was monitored by thin-layer chromatography (TLC). After completion, the reaction mixture was filtered under pressure through a short pad of silica and celite to withhold the salt. The vial and the silica layer were washed with ca. 5 mL dichloromethane (DCM) and ca. 5 mL ethyl acetate. The organic solvents were evaporated under vacuum and the product was determined by ^{1}H NMR spectroscopy.

3.6. Synthesis of N,N-Heterocyclic Compounds from N-(Pyridin-2-yl)imidates

To a 4 mL vial containing 0.2 mmol of *N*-(pyridin-2-yl)imidate, 0.5 mL of acetonitrile and 0.4 mmol of diamine were added. The reaction mixture was stirred at room temperature for a few hours or days, depending on the progress of the reaction, monitored by thin-layer chromatography (TLC). After completion of the reaction, the solution was evaporated and then left under vacuum for 2–3 h. The mixture was then rinsed to remove the 2-aminopyridine resulting from the starting material, with simultaneous crystallization of the product using hexane.

4. Conclusions

In conclusion, we showed that a series of multi-functional *N*-(pyridin-2-yl)iminonitriles were selectively transformed into the desired *N*-(pyridin-2-yl)imidates under a simple and mild synthetic protocol. For the present study, a series of substituted *N*-(pyridin-2-yl)imidates were synthesized with the Al_2O_3-mediated reaction of the corresponding nitrostyrenes with 2-aminopyridines. The α-iminonitriles were efficiently transformed into the desired *N*-(pyridin-2-yl)imidates in the presence of Cs_2CO_3 in alcoholic media and under ambient conditions. In addition to the commonly studied methanol, ethanol, propanol, and butanol, 1,2- and 1,3-propanediols were also studied under the present conditions, leading to the corresponding imidates. The present synthetic protocol can easily be applied to at a one mmol scale, resulting an important synthetic access to this interesting scaffold. A preliminary synthetic application to the *N*,*N*-heterocycles 2-(4-chlorophenyl)-4,5-dihydro-1*H*-imidazole and 2-(4-chlorophenyl)-1,4,5,6-tetrahydropyrimidine was also presented, using the corresponding 1,2- and 1,3-diamines.

Supplementary Materials: The following supporting information can be downloaded at https://www.mdpi.com/article/10.3390/molecules28083321/s1: Figures S1–S4; Tables S1–S5; and the NMR data and spectra of compounds.

Author Contributions: A.G.C. conducted the experiments, collected the literature, conducted the NMR study, analyzed the data, and helped with the manuscript correction. I.N.L. came up with the idea, supervised the study, and wrote and corrected the manuscript. All authors have read and agreed to the published version of the manuscript.

Funding: This research received no external funding.

Institutional Review Board Statement: Not applicable.

Informed Consent Statement: Not applicable.

Data Availability Statement: Not applicable.

Acknowledgments: We would like to thank C. Gabriel and D. A. Sarigiannis of the HERACLES Research Center, KEDEK, Laboratory of Environmental Engineering (EnvE-Lab), Department of Chemical Engineering, AUTH, Greece for allowing us to use the LC-TOF apparatus and helping us perform the HRMS experiments. The authors would like to acknowledge the Center of Interdisciplinary Research and Innovation of Aristotle University of Thessaloniki, Greece, for access to the Large Research Infrastructure and Instrumentation of the Nuclear Magnetic Resonance Laboratory AUTH, for performing the NMR experiments.

Conflicts of Interest: The authors declare no conflict of interest.

Sample Availability: Not available.

References

1. Neilson, D.G. *The Chemistry of Amidines and Imidates*; Patai, S., Ed.; Wiley: New York, NY, USA, 1975; pp. 385–489.
2. Neilson, D.G. Chapter 9: Imidates Including Cyclic Imidates. In *Amidines and Imidates*; Patai, S., Rappoport, Z., Eds.; Wiley: New York, NY, USA, 1991; Volume 2, pp. 425–483.
3. Joule, J.A.; Mills, K. *Heterocyclic Chemistry*, 5th ed.; Wiley: New York, NY, USA, 2010.
4. Roger, R.; Neilson, D.G. The Chemistry of Imidates. *Chem. Rev.* **1961**, *61*, 179–211. [CrossRef]
5. Thakur, R.; Jaiswal, Y.; Kumar, A. Imidates: An Emerging Synthon for *N*-Heterocycles. *Org. Biomol. Chem.* **2019**, *17*, 9829–9843. [CrossRef] [PubMed]
6. Shaw, M.; Kumar, A. Visible-Light-Mediated β-C(Sp^3)-H Amination of Glycosylimidates: En Route to Oxazoline-Fused/Spiro Nonclassical Bicyclic Sugars. *Org. Lett.* **2019**, *21*, 3108–3113. [CrossRef]
7. Shi, W.Z.; Li, H.; Mu, G.C.; Lu, J.L.; Tu, Y.H.; Hu, X.G. 1,2-*trans*-Stereoselective Synthesis of *C*-Glycosides of 2-Deoxy-2-amino-sugars Involving Glycosyl Radicals. *Org. Lett.* **2021**, *23*, 2659–2663. [CrossRef]
8. Yang, Y.; Yu, B. Recent Advances in the Chemical Synthesis of *C*-Glycosides. *Chem. Rev.* **2017**, *117*, 12281–12356. [CrossRef]
9. Pinner, A. *Die Imidöather and Ihre Derivate*; Oppenheim: Berlin, Germany, 1892.
10. Watanabe, K.; Kogoshi, N.; Miki, H.; Torisawa, Y. Improved Pinner Reaction with CPME as a Solvent. *Synth. Commun.* **2009**, *39*, 2008–2013. [CrossRef]

11. Ptiček, L.; Hok, L.; Grbčić, P.; Topić, F.; Cetina, M.; Rissanen, K.; Pavelić, S.K.; Vianello, R.; Racané, L. Amidino Substituted 2-Aminophenols: Biologically Important Building Blocks for the Amidino-Functionalization of 2-Substituted Benzoxazoles. *Org. Biomol. Chem.* **2021**, *19*, 2784–2793. [CrossRef]
12. Caron, S.; Wei, L.; Douville, J.; Ghosh, A. Preparation and Utility of Trihaloethyl Imidates: Useful Reagents for the Synthesis of Amidines. *J. Org. Chem.* **2010**, *75*, 945–947. [CrossRef]
13. Marshall, E.K.; Acree, S.F. On the Reactions of Both the Ions and the Molecules of Acids Bases and Salts. *J. Phys. Chem.* **1915**, *19*, 589–608. [CrossRef]
14. Schaefer, F.C.; Peters, G.A. Base-Catalyzed Reaction of Nitriles with Alcohols. A Convenient Route to Imidates and Amidine Salts. *J. Org. Chem.* **1961**, *26*, 412–418. [CrossRef]
15. Barcock, R.A.; Chadwick, D.J.; Storr, R.C. Synthesis of Some Novel Imidate Derivatives of Thiophene and Furan: Investigations of Their Metallation Properties and Some Synthetic Applications. *Tetrahedron* **1994**, *50*, 4149–4166. [CrossRef]
16. Bartels, G.; Hinze, R.P.; Wullbrandt, D. Beiträge Zur Kenntnis Des Chromophoren Systems Der Corrine, VII. Notiz Über Die Reaktion von Diazoessigsäure-methylester Mit Lactamen; Eine Modellreaktion Zur Cyclisierung von 5,6-Dioxo-monosecocorrinen. *Liebigs Ann. Chem.* **1980**, *1980*, 168–170. [CrossRef]
17. Fuchs, J.R.; Funk, R.L. Total Synthesis of (±)-Perophoramidine. *J. Am. Chem. Soc.* **2004**, *126*, 5068–5069. [CrossRef]
18. Popov, K.; Somfai, P. Synthesis of Imidates: TFA-Mediated Regioselective Amide Alkylation Using Meerwein's Reagent. *J. Org. Chem.* **2016**, *81*, 3470–3472. [CrossRef]
19. Dekorver, K.A.; North, T.D.; Hsung, R.P. An Efficient Synthesis of de Novo Imidates via Aza-Claisen Rearrangements of *N*-Allyl Ynamides. *Synlett* **2010**, *16*, 2397–2402. [CrossRef]
20. Ghorai, S.; Lee, D. Synthesis of Imides, Imidates, Amidines, and Amides by Intercepting the Aryne-Isocyanide Adduct with Weak Nucleophiles. *Org. Lett.* **2019**, *21*, 7390–7393. [CrossRef]
21. Schmitt, G.; Ebertz, W. Neue Synthese Für *N*-Vinylamide. *Angew. Chem.* **1982**, *94*, 650–651. [CrossRef]
22. Guan, Z.; Hillrichs, K.; Ünlü, C.; Rissanen, K.; Nieger, M.; Schmidt, A. Synthesis of 2-Anilinobenzimidates, Anthranilamides, and 2,3-Dihydroquinazolin-4(1*H*)-Ones from *N*-Heterocyclic Carbenes of Indazole. *Tetrahedron* **2015**, *71*, 276–282. [CrossRef]
23. Birch, D.J.; Guildford, A.J.; Tometzki, M.A.; Turner, R.W. Reaction of 3-Nitroso-2-Phenylimidazo[1,2-a]Pyridine with Triethyl Phosphite. A Revised Structure for the Product. *J. Org. Chem.* **1982**, *47*, 3547–3548. [CrossRef]
24. Wang, G.; Wei, C.; Hong, X.; Fu, Z.; Huang, W. Sodium Pyruvate as a Peroxide Scavenger in Aerobic Oxidation under Carbene Catalysis. *Green Chem.* **2020**, *22*, 6819–6826. [CrossRef]
25. Tzani, M.A.; Fountoulaki, S.; Lykakis, I.N. Polyoxometalate-Driven Ease Conversion of Valuable Furfural to *trans*-*N*,*N*-4,5-Diaminocyclopenten-2-ones. *J. Org. Chem.* **2022**, *87*, 2601–2615. [CrossRef]
26. Tzani, M.A.; Gabriel, C.; Lykakis, I.N. Selective Synthesis of Benzimidazoles from *o*-Phenylenediamine and Aldehydes Promoted by Supported Gold Nanoparticles. *Nanomaterials* **2020**, *10*, 2405. [CrossRef]
27. Andreou, D.; Essien, N.B.; Pubill-Ulldemolins, C.; Terzidis, M.A.; Papadopoulos, A.N.; Kostakis, G.E.; Lykakis, I.N. Skeletally Tunable Seven-Membered-Ring Fused Pyrroles. *Org. Lett.* **2021**, *23*, 6685–6690. [CrossRef] [PubMed]
28. Tzani, M.A.; Kallitsakis, M.G.; Symeonidis, T.S.; Lykakis, I.N. Alumina-Supported Gold Nanoparticles as a Bifunctional Catalyst for the Synthesis of 2-Amino-3-arylimidazo[1,2-*a*]pyridines. *ACS Omega* **2018**, *3*, 17947–17956. [CrossRef]
29. Andreou, D.; Kallitsakis, M.G.; Loukopoulos, E.; Gabriel, C.; Kostakis, G.E.; Lykakis, I.N. Copper-Promoted Regioselective Synthesis of Polysubstituted Pyrroles from Aldehydes, Amines, and Nitroalkenes via 1,2-Phenyl/Alkyl Migration. *J. Org. Chem.* **2018**, *83*, 2104–2113. [CrossRef]
30. Kallitsakis, M.; Loukopoulos, E.; Abdul-Sada, A.; Tizzard, G.J.; Coles, S.J.; Kostakis, G.E.; Lykakis, I.N. A Copper-Benzotriazole-Based Coordination Polymer Catalyzes the Efficient One-Pot Synthesis of (*N*′-Substituted)-hydrazo-4-aryl-1,4-dihydropyridines from Azines. *Adv. Synth. Catal.* **2017**, *359*, 138–145. [CrossRef]
31. Chen, Z.; Liang, P.; Zheng, J.; Zhou, Z.; Wen, X.; Liu, T.; Ye, M. Cyanide-Free Ce(III)-Catalyzed Highly Efficient Synthesis of α-Iminonitriles from 2-Aminopyridines and Nitroalkenes via Intermolecular Dehydration Reaction. *ACS Omega* **2018**, *3*, 12520–12529. [CrossRef] [PubMed]
32. Jasiński, R.; Kula, K.; Kącka, A.; Mirosław, B. Unexpected course of reaction between (*E*)-2-aryl-1-cyano-1-nitroethenes and diazafluorene: Why is there no 1,3-dipolar cycloaddition? *Mon. Chem.* **2017**, *148*, 909–915. [CrossRef]
33. Woliński, P.; Kącka-Zych, A.; Mirosław, B.; Wielgus, E.; Olszewska, A.; Jasiński, R. Green, one-pot synthesis of 1,2-oxazine-type herbicides via non-catalyzed Hetero Diels-Alder reactions comprising (2E)-3-aryl-2-nitroprop-2-enenitriles. *J. Clean. Prod.* **2022**, *356*, 131878. [CrossRef]
34. Kallitsakis, M.G.; Tancini, P.D.; Dixit, M.; Mpourmpakis, G.; Lykakis, I.N. Mechanistic Studies on the Michael Addition of Amines and Hydrazines To Nitrostyrenes: Nitroalkane Elimination via a Retro-aza-Henry-Type Process. *J. Org. Chem.* **2018**, *83*, 1176–1184. [CrossRef]
35. Siwach, A.; Verma, P.K. Synthesis and therapeutic potential of imidazole containing compounds. *BMC Chem.* **2021**, *15*, 12. [CrossRef] [PubMed]
36. Szabo, B. Imidazoline antihypertensive drugs: A critical review on their mechanism of action. *Pharmacol. Ther.* **2002**, *93*, 1–35. [CrossRef]

37. Messer, W.S.; Abuh, Y.F.; Liu, Y.; Periyasamy, S.; Ngur, D.O.; Edgar, M.A.; El-Assadi, A.A.; Sbeih, S.; Dunbar, P.G.; Roknich, S.; et al. Synthesis and Biological Characterization of 1,4,5,6-Tetrahydropyrimidine and 2-Amino-3,4,5,6-Tetrahydropyridine Derivatives as Selective M1 Agonists. *J. Med. Chem.* **1997**, *40*, 1230–1246. [CrossRef] [PubMed]
38. Kopp, S.R.; Kotze, A.C.; McCarthy, J.S.; Traub, R.J.; Coleman, G.T. Pyrantel in Small Animal Medicine: 30 Years On. *Vet. J.* **2008**, *178*, 177–184. [CrossRef] [PubMed]
39. Cai, S.; Zhang, S.; Zhao, Y.; Wang, D.Z. New Approach to Oximes through Reduction of Nitro Compounds Enabled by Visible Light Photoredox Catalysis. *Org. Lett.* **2013**, *15*, 2660–2663. [CrossRef] [PubMed]

molecules

MDPI

Communication

Bathochromic Shift of Fluorescence Peak in Dipyrrolo[1,2-*a*:2′,1′-*c*]quinoxaline by Introducing Each of Electron-Donating and Electron-Withdrawing Substituent

Shoji Matsumoto *, Makoto Takamori and Motohiro Akazome

Department of Applied Chemistry and Biotechnology, Graduate School of Engineering, Chiba University, 1-33 Yayoi-cho, Inage-ku, Chiba 263-8522, Japan
* Correspondence: smatsumo@faculty.chiba-u.jp

Abstract: Development of organic fluorophore is an important theme. Especially, the fluorophores with longer fluorescence peaks are useful to biological probes. One of the methods to change the fluorescence peak is the introduction of substituents. However, opposing characteristics of the substituents lead to different changes in the fluorescence peaks. Furthermore, the introduction of the substituent also affects their electric properties. Thus, if the materials were developed with the substituent effect on the optical and electric properties separately, it will be useful to design the functional materials related to both optical and electric properties. Herein, we investigated the substituent effect of dipyrrolo[1,2-*a*:2′,1′-*c*]quinoxalines on fluorescence properties. We synthesized the compounds bearing electron-donating or electron-withdrawing substituents at the benzene ring on dipyrrolo[1,2-*a*:2′,1′-*c*]quinoxaline, which would have more direct influence on the optical properties. By introducing each substituent at the 6 position of dipyrrolo[1,2-*a*:2′,1′-*c*]quinoxaline, the bathochromic shift was observed in the fluorescence spectra. In the case of fluorine substituent, the change of the fluorescence peak reached was about 19 nm. Using a TDDFT calculation, we explained the reason for such a substituent effect that large on the increment of LUMO energy or decrement of HOMO energy occurred by introducing electron-withdrawing or electron-donating substituents at the 6 position, respectively. The substituent effect on the change of orbital energies is typical although the different characteristics of substituents resulted in the similar tendency about the change of fluorescence peak. Furthermore, with the introduction of phenyl substituents at the 3 and 10 positions, we achieved 40–50 nm longer fluorescence peaks compared with that of the original dipyrrolo[1,2-*a*:2′,1′-*c*]quinoxaline.

Keywords: dipyrroloquinoxaline; fluorescence; bathochromic shift; substituent effect; energy gap

Citation: Matsumoto, S.; Takamori, M.; Akazome, M. Bathochromic Shift of Fluorescence Peak in Dipyrrolo[1,2-*a*:2′,1′-*c*]quinoxaline by Introducing Each of Electron-Donating and Electron-Withdrawing Substituent. *Molecules* **2023**, *28*, 2896. https://doi.org/10.3390/molecules28072896

Academic Editors: Alexey M. Starosotnikov, Maxim A. Bastrakov, Igor L. Dalinger and Gianfranco Favi

Received: 9 March 2023
Revised: 16 March 2023
Accepted: 22 March 2023
Published: 23 March 2023

1. Introduction

The development of organic fluorophores is an important theme for the advancement of functional materials research. Fused aromatic rings are widely utilized to produce fluorescent materials because of their planar and large π-conjugated structures [1–9]. Recently, the fluorophores with longer fluorescence peaks are utilized in the biological probes because the fluorophores with shorter fluorescence peaks are affected by organs. To achieve a longer fluorescent peak, the introduction of substituents is one of the more efficient methods. However, the various electronic properties of substituents lead to various changes in the fluorescent peak, i.e., a bathochromic shift or a small change was obtained by introducing the electron-withdrawing substituent in the case of hypsochromic shift by the electron-donating substituent, and vice versa [10–14]. For example, Hirano et al. reported the substituent effect of 2-phenylimidazo [1,2-*a*]pyrazine-3(7*H*)-ones which showed the bathochromic shift on fluorescence spectra with an increase in the electron-withdrawing property [15]. Furthermore, the donor-acceptor structure is also the fundamental design to change the optical properties by introducing the substituents. It gives longer fluorescence

peaks based on a strong intramolecular charge-transfer (ICT) state [16,17]. Such compounds also show the larger Stokes shift. Therefore, those materials have a possibility to be utilized for bioimaging probes [18–20]. However, the opposing characteristic of the substituents leads to a different transition. We have reported the fluorescence properties of fused aromatic rings consisting of pyrrole and imidazole [21–24]. In the investigation of diimidazo [1,2-*a*:2′,1′-*c*]quinoxalines, the *p*-methoxyphenyl substituents at the 3 and 10 positions, we found that they resulted in a large bathochromic shift of a fluorescence peak of 13 nm based on the phenyl substituted compound, whereas a small change in fluorescence peak of 4 nm was obtained from the compound with *p*-trifluoromethylphenyl substituents [22].

The introduction of the electron-donating and electron-withdrawing substituents is also utilized for tuning the electric properties of the substrates. Usually, electron-donating substituents increase the orbital energies, and electron-withdrawing substituents decrease the orbital energies. Thus, by tuning the fluorescence peak with the introduction of substituents, the electric properties were also affected. When we must control both the optical and electric properties, it is a challenging problem to give consideration relating them to each other. For example, the emitting material in the organic light-emitting diode (OLED) is important to tune its luminescent peak as well as HOMO and LUMO energies because hole- and electron-injections are also affected by the HOMO and LUMO energies. Anzenbacher, Jr. et al. examined the OLED properties of substituted tris(8-hydroxyquinoline)aluminum (Alq_3) complexes [25]. The fluorescence peaks were given a bathochromic shift compared with the original Alq_3, but the change of HOMO and LUMO energies were varied; the properties of OLED were also affected by the device configurations. Thus, if the materials were developed with the substituent effect on the optical and electric properties separately, it will be useful for molecular design of functional materials that utilize both optical and electric properties.

We focused on the substituent effect on the benzene ring in diazolo [1,2-*a*:2′,1′-*c*]quinoxalines, which would be more directly influenced on the optical properties. Herein, we reported the bathochromic shift from the introduction of each electron-donating and electron-withdrawing substituent over 10 nm in dipyrrolo [1,2-*a*:2′,1′-*c*]quinoxalines (**1**) (Scheme 1). Furthermore, based on the (TD)DFT calculation, we found that the change of the orbital energies was typical with increments by the electron-donating substituent and with decrements by the electron-withdrawing substituent.

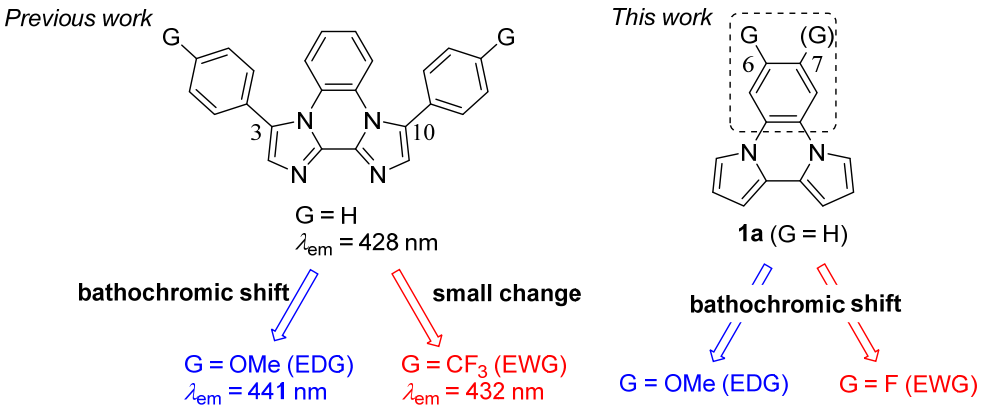

Scheme 1. Representation of the difference of fluorescence peaks of diazolo [1,2-*a*:2′,1′-*c*]quinoxalines with substituent(s) on 3,10- or 6,7-positions.

2. Results and Discussions

We chose a dipyrrolo [1,2-*a*:2′,1′-*c*]quinoxaline skeleton to examine the substituent effects because a longer fluorescent wavelength was achieved with dipyrrolo [1,2-*a*:2′,1′-*c*]quinoxaline (**1a**) (λ_{em} = 416 nm in THF) than with diimidazo [1,2-*a*:2′,1′-*c*]quinoxaline (λ_{em} = 367 nm in THF). The compounds were synthesized by the same procedure mentioned previously [22]. The coupling reaction of pyrrole and substituted dibromobenzene with a

copper catalyst produced dipyrrolylbenzenes (**2b**–**d**) by Buchwald amination [26]. After column chromatography, **2b**–**d** was treated with I_2 to give corresponding **1b**–**d** moderate yield (two steps) (Scheme 2). We also tried to synthesis the other compounds with methyl group at the 6 position or a fluorine substituent at the 5 position. However, we did not succeed in purification through recrystallization and preparative GPC purification. We could not explain the reason why such compounds were difficult to purify. But some contaminations of the positional isomers were supposed from the ^{1}H NMR spectra, whose contamination would be derived from the starting dibromobenzene derivatives. In addition, to achieve the longer fluorescence peak, we synthesized **3d** with two phenyl rings at the 3 and 10 positions by the reaction of **1d** with phenyl boric acid in 29% yield [27].

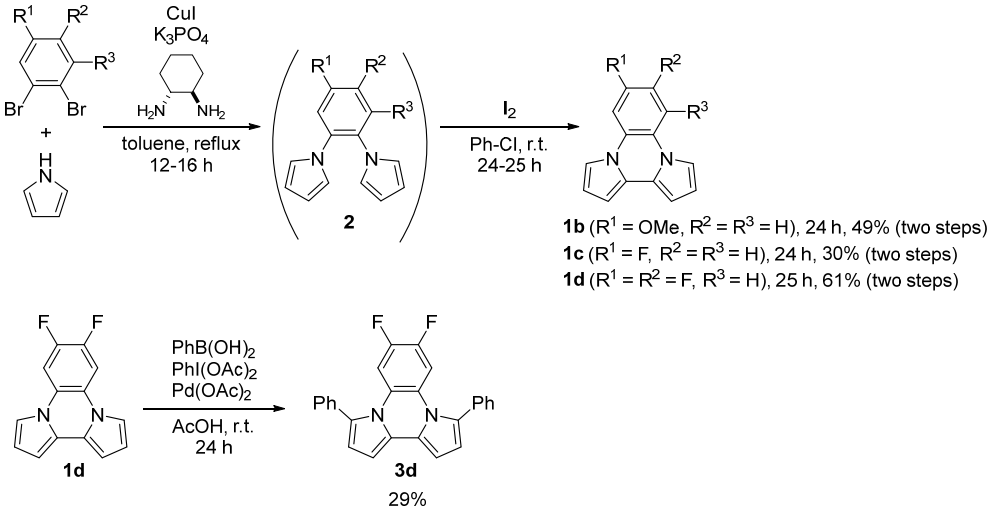

Scheme 2. Synthesis of **1** and **3d**.

Absorption and fluorescence spectra of **1** were measured in THF and CH_3CN. The results were summarized in Table 1. The absorption peak showed the bathochromic shift in the case of the compound (**1b**) bearing electron-donating group such as methoxy substituents at the 6 position against **1a** (entry 1 vs. entry 2). But a small change of absorption peak was observed in the compounds with fluorine substituent at the 6 position (**1c**) (entry 3). The solvent had little effect on the absorption spectra (Figure 1). Focused on the fluorescence peak, regardless of electron-donating or electron-withdrawing substituents, both compounds showed a bathochromic shift over 10 nm against **1a** in THF (entry 1 vs. entries 2 and 3). By changing the solvent from THF to polar CH_3CN, more bathochromic shift was obtained from **1c** whereas no solvent effect was found in **1b** (Figure 2). This solvent effect was also observed originally in **1a**. Such a solvent effect would be caused by the charge-transfer transition. Because the pyrrole ring has an electron-rich character, bipyrrole moiety would act as an electron-donating part. By introducing the electron-donating substituent on the benzene ring, charge distribution would be reduced. The Stokes shift also gives the information to their transition. The Stokes shift increases with solvent polarity when the dipole moment is higher in the excited state than in the ground state [28]. In fact, large Stokes shifts ($\Delta\lambda$ and $\Delta\nu$) in CH_3CN were obtained over 100 nm (over 8000 cm^{-1}) in the case of **1a** and **1c.** The value of Stokes shifts of **1a** and **1c** in CH_3CN were larger than those in THF. Those results also suggested that the fluorescence transition of **1a** and **1c** would be derived from ICT state. However, **1b** provided small change of the Stokes shift by the solvent polarity. Thus, the little effect of charge-transfer transition would be affected on the fluorescence of **1b**. The fluorescence quantum yields (Φ_F) were also affected by the introduction of the substituent. Especially, **1b** was strongly decreased Φ_F compared with **1a** (entry 2 vs. entry 1) although Φ_F of **1c** was kept at 0.22 in THF (entry 3). This would be caused by the increment of the vibronic part by introducing substituents such as methoxy groups. We also investigated the compound with two fluorine substituents in

the 6 and 7 positions (**1d**). As for the results, a further bathochromic shift of fluorescence peak to reach 458 nm in CH_3CN was achieved in keeping with the fluorescence quantum yield (entry 4).

Table 1. Optical Properties of **1** and **3f** in THF and CH_3CN.

Entry	Compound	λ_{abs} (nm) [ε (M^{-1} cm^{-1})] [1]		λ_{em} (nm) [2] [Φ_F] [3]		$\Delta\lambda$ (nm) [4] [$\Delta\nu$ (cm^{-1}) [5]]	
		In THF	In CH_3CN	In THF	In CH_3CN	In THF	In CH_3CN
1	**1a**	321 [10,600]	320 [10,700]	416 [0.43]	434 [0.17]	95 [7114]	114 [8209]
2	**1b**	367 [4800]	369 [4900]	435 [0.01]	434 [0.02]	68 [4259]	65 [4059]
3	**1c**	322 [11,200]	322 [15,600]	434 [0.22]	453 [0.12]	112 [8014]	131 [8981]
4	**1d**	325 [9500]	324 [8100]	449 [0.25]	458 [0.21]	124 [8498]	134 [9030]
5	**3d**	377 [10,600]	375 [8700]	466 [0.35]	473 [0.32]	89 [5066]	98 [5525]

[1] Concentration: 3.0×10^{-5} M. [2] Concentration: 3.0×10^{-7} M. Excited at λ_{abs}. [3] Determined using *p*-terphenyl (Φ_F = 0.87, 265 nm) as a standard. [4] $\Delta\lambda = \lambda_{em} - \lambda_{abs}$. [5] $\Delta\nu = 1/\lambda_{abs} - 1/\lambda_{em}$.

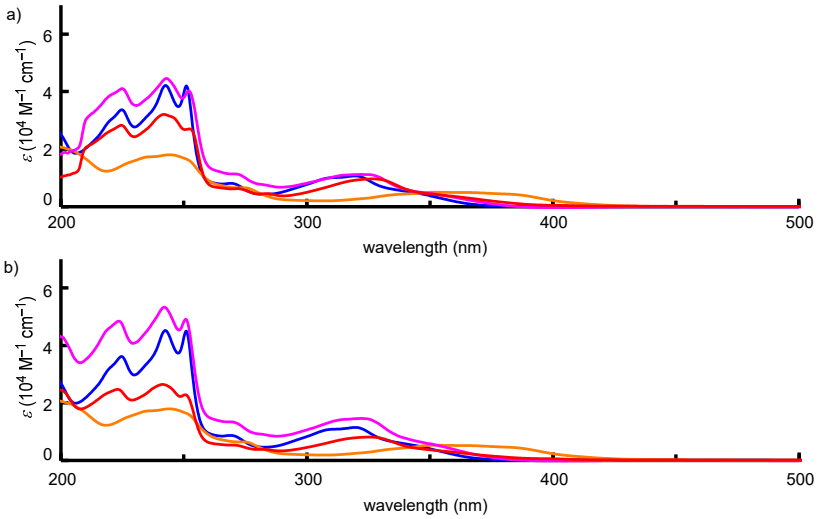

Figure 1. Absorption spectra of **1a** (blue), **1b** (orange), **1c** (purple), and **1d** (red) in (**a**) THF and (**b**) CH_3CN.

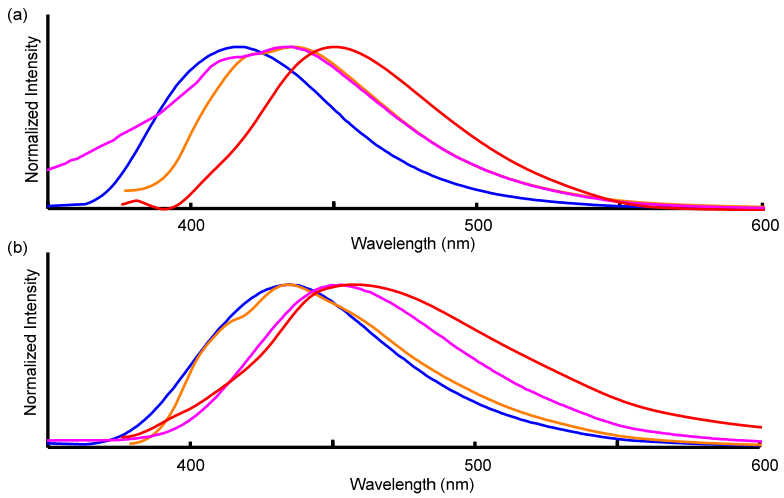

Figure 2. Fluorescence spectra of **1a** (blue), **1b** (orange), **1c** (purple), and **1d** (red) in (**a**) THF and (**b**) CH_3CN.

As mentioned in the introduction, it is rational that the compounds (**1c** and **1d**) with electron-withdrawing substituent show the longer fluorescence peak because of their ICT

character to account for the bipyrrole moiety as a donor part. However, the reason for the bathochromic shift of the compound bearing the electron-donating substituent (**1b**) is unclear. To clarify the reason for the bathochromic shift on each electronic substituent in fluorescence peak, we examined HOMO and LUMO energies by time-dependent density functional theory (TDDFT) calculation. To discuss the excited state, the optimized structure with minimum energy was estimated by TDDFT calculation. HOMO and LUMO energies, and the differences of each energy, were summarized in Table 2. The molecular orbitals were represented in Figure 3. Every HOMO was localized on bipyrrole moiety, and every LUMO was spread over the molecules. Based on the investigation concerning orbital energy, a good relationship was found between λ_{em} in THF and the energy gap between HOMO and LUMO. It is acceptable because the energy gap of HOMO and LUMO is generally attributed to the energy of the transition. In fact, all computed longest transition peaks were attributed from HOMO to LUMO (Table S1). Thus, it is rational to discuss the fluorescence peaks based on HOMO and LUMO. Focused on the energy change in HOMO and LUMO, increased energy against **1a** was obtained in **1b**, which possesses the electron-donating substituent (entry 2). The influence of HOMO energy was also larger than that of LUMO. On the contrary, reduced energy in HOMO and LUMO was obtained in **1c** and **1d** (entries 3 and 4). LUMO was observed to have efficient energy reduction. It is well known to change the orbital energies toward an increase and a decrease by introducing electron-donating and electron-withdrawing substituents, respectively. The small energy gap between HOMO and LUMO, which leads to larger λ_{em} in those compounds, would be attributed to the difference of degree of change in HOMO and LUMO energies. The electron-donating substituent increased both HOMO and LUMO energies, but more efficiently increased HOMO energy. In the case of the electron-withdrawing substituent, both energies were reduced, but LUMO energy was more efficiently decreased. As a result, the small energy gap between HOMO and LUMO energies compared with that of **1a** was obtained in all of **1b**, **1c**, and **1d**. From those findings, both electron-donating and electron-withdrawing substituents on dipyrrolo [1,2-a:2′,1′-c]quinoxalines are affected by the bathochromic shift of the fluorescence peak on the optical properties, but the different effect would occur in the case of the electric properties; i.e., the electron-donating substituent increases HOMO and LUMO energies and the electron-withdrawing substituent decreases HOMO and LUMO energies. Such changes of HOMO and LUMO energies were also obtained from the DFT calculation assigned as the ground state (Figure S1). Thus, the change of the electric properties by the introduction of a substituent would be typical both in the ground and excited states.

Table 2. HOMO and LUMO energies and the differences of each energy of **1** [1].

Entry	Compound	HOMO Energy (eV)	Difference of HOMO Energy against 1a (eV)	LUMO Energy (eV)	Difference of LUMO Energy against 1a (eV)	Energy Gap between HOMO and LUMO (eV)	λ_{em} (nm) in THF
1	**1a**	−6.5830	-	6.8151	-	6.8151	416
2	**1b**	−6.5122	0.0708	0.2653	0.0332	6.7775	435
4	**1c**	−6.7092	−0.1262	−0.0063	−0.2384	6.7029	434
6	**1d**	−6.8233	−0.2403	−0.1973	−0.4294	6.6260	449

[1] Calculated by TDDFT/ωB97XD/6-31+G(d,p) with the optimized structure.

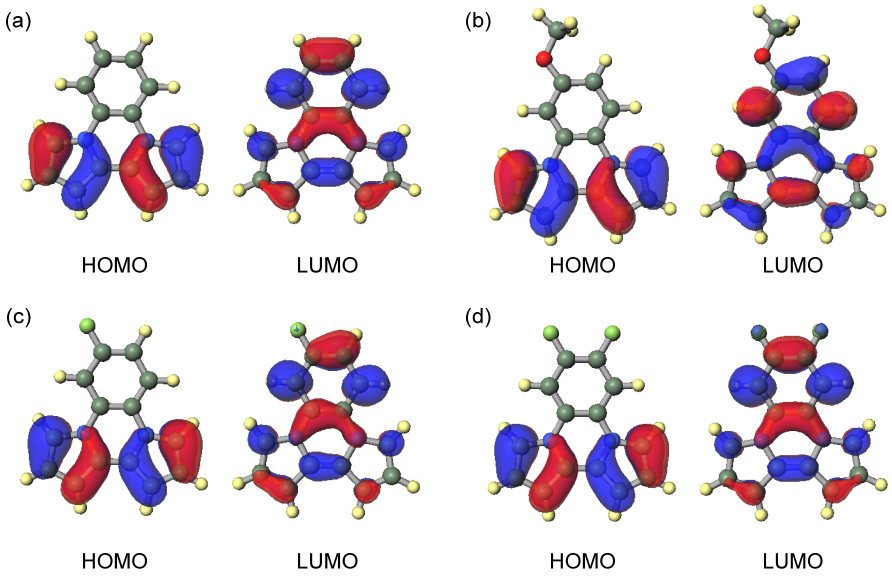

Figure 3. Shape of HOMO and LUMO of (**a**) **1a**, (**b**) **1b**, (**c**) **1c**, and (**d**) **1d** calculated by TDDFT method.

Finally, we attached phenyl rings at the 3 and 10 positions in **1d** to obtain a longer fluorescent peak. This resulted in the observed fluorescence peaks of **3d** at 466 nm and 473 nm in THF and CH_3CN, respectively (Table 1, entry 5) (Figure 4). Those values were 40–50 nm larger than the original **1a**. The influence of the introduction of phenyl rings at 3 and 10 positions on the fluorescence peak was estimated as bathochromic shift about 20 nm compared with **1d** in each solvent. In the case of the original **1a**, the compound bearing two phenyl rings at 3 and 10 positions (3,10-diphenyldipyrrolo [1,2-*a*:2′,1′-*c*]quinoxaline) showed a longer fluorescence peak of approximately 30 nm (λ_{em} = 445 nm in THF) [21]. Thus, the effect of additional phenyl rings at the 3 and 10 positions was reduce by the introduction of the fluorine substituents on benzene ring in dipyrrolo [1,2-*a*:2′,1′-*c*]quinoxaline. Interestingly, the fluorescence quantum yield was increased compared with **1d**. Such effects were also observed in diimidazo [1,2-*a*:2′,1′-*c*]quinoxalines [22]. Thus, it would stand to reason that the steric restriction of vibronic motion would occur by introducing phenyl ring.

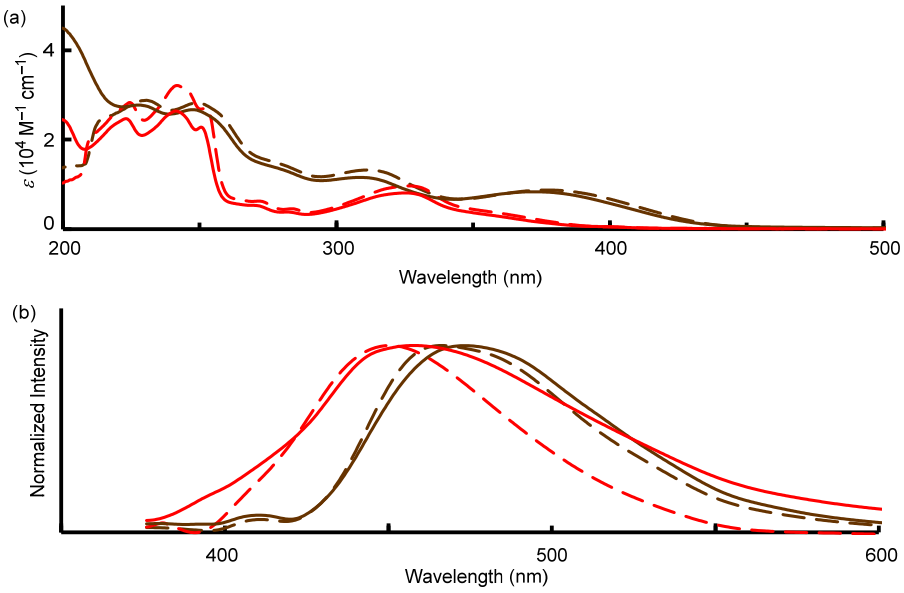

Figure 4. (**a**) Absorption and (**b**) fluorescence spectra of **1d** (red) and **3d** (brown) in THF (dashed line) and CH_3CN (plane line).

3. Materials and Methods

3.1. General Information

Melting points were determined with Yanaco MP-J3 and values were uncorrected. NMR spectra were recorded at 400 MHz (proton) (100 MHz (carbon-13)) on Bruker AVANCE III-400M. Chemical shifts (δ) of ^{1}H NMR were expressed in parts per million downfield or upfield from tetramethylsilane in $CDCl_3$ as an internal standard. Multiplicities are indicated as s (singlet), d (doublet), t (triplet), m (multiplet), and coupling constants (J) are reported in hertz units. Chemical shifts (δ) of $^{13}C\{^1H\}$ NMR are expressed in parts per million downfield or upfield from $CDCl_3$ (δ = 77.0) as an internal standard. Infrared (IR) spectra were recorded on a JASCO FT/IR-460 plus spectrometer. Mass spectra were carried out on THERMO Fisher Exactive in the Center for Analytical Instrumentation of Chiba University. Anhydrous toluene was distilled from CaH_2 and was stored with MS 4 Å. All other commercially available materials were used without further purification. The reactions were performed under nitrogen or argon atmosphere unless otherwise noted.

3.1.1. Preparation of 1,2-Dibromo-4-methoxybenzene [29]

N-bromosuccinimide (0.889 g, 4.99 mmol) and 1 *M* HCl (50 μL) was added to a solution of 3-bromoanisole (0.63 mL, 5.0 mmol) in acetone (10 mL). The mixture was stirred for 20 min at room temperature. After the disappearance of yellow color, the reaction mixture was evaporated in vacuo. The residue was extracted with $CHCl_3$ (20 mL × 3). The organic layer was dried with $MgSO_4$. After filtration and evaporation, 1,2-dibromo-4-methoxybenzene (1.171 g, 4.40 mmol) was obtained in 88% yield as colorless oil. ^{1}H NMR ($CDCl_3$, 400 MHz): δ 3.77 (s, 3H), 6.72 (dd, J = 2.9 and 8.9 Hz, 1H), 7.16 (d, J = 2.9 Hz, 1H), 7.46 (d, J = 8.9 Hz, 1H).

3.1.2. Synthesis of Substituted Dipyrrolo [1,2-*a*:2′,1′-*c*]quinoxaline (**1b**–**d**)

6-Methoxydipyrrolo [1,2-*a*:2′,1′-*c*]quinoxaline (**1b**): A mixture of 1,2-dibromo-4-methoxybenzene (1.46 g, 5.49 mmol), pyrrole (1.0 mL, 14.4 mmol), CuI (95.0 mg, 0.499 mmol), K_3PO_4 (4.22 g, 19.9 mmol), and *trans*-1,2-cyclohexanediamine (0.60 mL, 5.0 mmol) in toluene (10 mL) was stirred for 12 h under refluxing conditions. After being cooled to room temperature, the reaction mixture was filtered with a plug of Celite washing with EtOAc. After evaporation in vacuo, the residual mixture was subjected to column chromatography on silica-gel (*n*-hexane:EtOAc = 6:1) to give the product (1.507 g). The product was dissolved in chlorobenzene (4 mL). To the solution was added a solution of iodine (0.834 g, 3.29 mmol) in chlorobenzene (6 mL) in a period of 5 min. After being stirred for 24 h at room temperature, to the reaction mixture was added saturated aqueous $Na_2S_2O_3$ solution (10 mL) and acetone (10 mL) to dissolve the precipitate. The combined mixture was extracted with $CHCl_3$ (20 mL × 3). The organic layer was dried with $MgSO_4$. After filtration and evaporation, the residue was subjected to column chromatography on SiO_2 (*n*-hexane:EtOAc = 8:1) to give 6-methoxydipyrrolo [1,2-*a*:2′,1′-*c*]quinoxaline (0.638 g, 2.70 mmol, 49% (two steps)) as pale-yellow solid: m.p. = 91–92 °C (*n*-hexane/$CHCl_3$). ^{1}H NMR ($CDCl_3$, 400 MHz): δ 3.91 (s, 3H), 6.52–6.58 (m, 4H), 6.85 (dd, J = 2.7 and 9.0 Hz, 1H), 7.21 (d, J = 2.6 Hz, 1H), 7.42 (dd, J = 1.5 and 2.6 Hz, 2H), 7.64 (d, J = 8.9 Hz, 1H). $^{13}C\{^1H\}$ NMR ($CDCl_3$, 100 MHz): δ 55.7, 100.6, 100.7, 101.4, 110.2, 111.6, 111.7, 111.9, 112.4, 116.4. 119.8, 123.5, 124.4, 126.4, 156.6. IR (KBr): ν 3854, 3802, 3745, 3676, 1700, 1654, 1522, 768, 684 cm^{-1}. HRMS (ESI) *m/z*: $[M-H]^-$ calcd for $C_{15}H_{11}N_2O$ 235.0877; found 235.0884. UV-Vis absorption: λ_{abs} [ε (M^{-1} cm^{-1})] 367 [4800], 279(sh) [5307], 244.5 [18,020] nm (3.0×10^{-5} M in THF); 369 [4900], 278.5(sh) [5393], 244.5 [17,895] nm (3.0×10^{-5} M in CH_3CN).

6-Fluorodipyrrolo [1,2-*a*:2′,1′-*c*]quinoxaline (**1c**): Yield 30% (two steps) (66.5 mg) as white solid: m.p. = 107–109 °C (*n*-hexane/$CHCl_3$). ^{1}H NMR ($CDCl_3$, 400 MHz): δ 6.52–6.54 (m, 2H), 6.57 (t, J = 3.0 Hz, 1H), 6.58 (t, J = 3.6 Hz, 1H), 6.99 (ddd, J = 2.7, 7.8 Hz and $J_{H\text{-}C\text{-}C\text{-}F}$ = 9.0 Hz, 1H), 7.36 (dd, J = 1.4 and 3.0 Hz, 1H), 7.40 (dd, J = 2.7 Hz and $J_{H\text{-}C\text{-}C\text{-}F}$ = 9.5 Hz, 1H), 7.42 (m, 1H), 7.66 (dd, $J_{H\text{-}C\text{-}C\text{-}C\text{-}F}$ = 5.1 Hz and J = 9.1 Hz, 1H). $^{13}C\{^1H\}$ NMR ($CDCl_3$, 100 MHz): δ 101.3 (d, $J_{C\text{-}C\text{-}F}$ = 27.1 Hz), 102.6 (d, $J_{C\text{-}C\text{-}F}$ = 27.7 Hz), 111.1, 111.4, 111.9, 112.1, 112.3, 112.8, 116.5 (d, $J_{C\text{-}C\text{-}C\text{-}F}$ = 9.2 Hz), 122.1 (d, $J_{C\text{-}C\text{-}C\text{-}C\text{-}F}$ = 2.2 Hz), 124.2,

123.6, 126.4 (d, $J_{C\text{-}C\text{-}C\text{-}F}$ = 10.3 Hz), 159.3 (d, $J_{C\text{-}F}$ = 243.5 Hz). IR (KBr): ν 3113, 2359, 1353, 1285, 1626, 1588, 1520, 1191, 768, 682 cm^{-1}. HRMS (ESI) *m/z*: $[M+H]^+$ calcd for $C_{14}H_{10}FN_2$ 225.0823; found 225.0826. UV-Vis absorption: λ_{abs} [ε (M^{-1} cm^{-1})] 322 [11,200], 275.5(sh) [8638], 252 [40,240], 243 [44,583] nm (3.0×10^{-5} M in THF); 322 [15,600], 269(sh) [13,341], 251 [011,49], 242 [53,256] nm (3.0×10^{-5} M in CH_3CN).

6,7-Difluorodipyrrolo [1,2-*a*:2′,1′-*c*]quinoxaline (**1d**): Yield 61% (two steps) (0.566 g) as pale-green solid: m.p. = 116–117 °C (*n*-hexane/$CHCl_3$). ^{1}H NMR ($CDCl_3$, 400 MHz): δ 6.54 (dd, *J* = 1.4 and 3.7 Hz, 2H), 6.59 (dd, *J* = 3.0 and 3.6 Hz, 2H), 7.32 (dd, *J* = 1.5 and 3.0 Hz, 2H), 7.51 (t, $J_{H\text{-}C\text{-}C\text{-}F}$ = 8.5 Hz, 2H). $^{13}C\{^1H\}$ NMR ($CDCl_3$, 100 MHz): δ 101.6, 104.5 (dd, $J_{C\text{-}C\text{-}C\text{-}F}$ = 9.0 Hz and $J_{C\text{-}C\text{-}F}$ = 14.5 Hz), 112.1, 112.9, 121.78 (t, $J_{C\text{-}C\text{-}C\text{-}F}$ = 5.4 Hz), 123.8, 146.9 (dd, $J_{C\text{-}C\text{-}F}$ = 15.6 Hz and $J_{C\text{-}F}$ = 248.0 Hz). IR (KBr): ν 3744, 3675, 3412, 1685, 1598, 1340, 1265, 1227, 1083, 838 cm^{-1}. HRMS (ESI) *m/z*: $[M+H]^+$ calcd for $C_{14}H_9F_2N_2$ 243.0728; found 243.0729. UV-Vis absorption: λ_{abs} [ε (M^{-1} cm^{-1})] 325 [9500], 283.5 [4546], 272 [6252], 252 [27,013], 242 [32,073] nm (3.0×10^{-5} M in THF); 324 [8100], 282 [3810], 269.5(sh) [5297], 250.5 [22,736], 241.5 [26,341] nm (3.0×10^{-5} M in CH_3CN).

3.1.3. Synthesis of 6,7-Difluoro-3,10-diphenyldipyrrolo [1,2-*a*:2′,1′-*c*]quinoxaline (**3d**)

$PhI(OAc)_2$ (0.602 g, 1.87 mmol) and $PhB(OH)_2$ (0.230 g, 1.89 mmol) was added to acetic acid (9 mL). After being stirred for 20 min at room temperature, 1d (0.139 g, 0.574 mmol) was added to the mixture. After being stirred for 15 min, $Pd(OAc)_2$ (20 mg, 0.089 mmol) was added and then the whole was stirred for 24 h at room temperature. The reaction mixture was filtered through a plug of Celite. After evaporation in vacuo, the residue was added to water (10 mL), and was extracted with $CHCl_3$ (10 mL × 3). The organic layer was dried with $MgSO_4$. After filtration and evaporation, the residue was subjected to column chromatography on SiO_2 (*n*-hexane:EtOAc = 10:1) to give 6,7-difluoro-3,10-diphenyldipyrrolo [1,2-*a*:2′,1′-*c*]quinoxaline (65.3 mg, 0.166 mmol, 29%) as yellow solid: m.p. = 167–168 °C (*n*-hexane/$CHCl_3$). ^{1}H NMR ($CDCl_3$, 400 MHz): δ 6.56 (d, *J* = 3.7 Hz, 2H), 6.63 (d, *J* = 3.8 Hz, 2H), 7.10 (t, $J_{H\text{-}C\text{-}C\text{-}F}$ = 10.1 Hz, 2H), 7.39 (tt, *J* = 1.3 and 7.2 Hz, 2H), 7.46 (diffused t, *J* = 7.5 Hz, 4H), 7.51 (diffused d, *J* = 6.9 Hz, 4H). $^{13}C\{^1H\}$ NMR ($CDCl_3$, 100 MHz): δ 102.0, 108.5 (dd, $J_{C\text{-}C\text{-}C\text{-}F}$ = 9.5 Hz and $J_{C\text{-}C\text{-}F}$ = 15.4 Hz), 116.2, 124.0 (t, $J_{C\text{-}C\text{-}C\text{-}F}$ = 5.9 Hz), 127.4, 127.8, 128.2, 128.3, 129.0, 131.0, 133.4, 145.5 (dd, $J_{C\text{-}C\text{-}F}$ = 15.4 Hz and $J_{C\text{-}F}$ = 247.2 Hz). IR (KBr): ν 3854, 3821, 3676, 3629, 3421, 1700, 1685, 1654, 1598, 1517 cm^{-1}. HRMS (ESI) *m/z*: $[M+H]^+$ calcd for $C_{26}H_{17}F_2N_2$ 395.1354; found 395.1343. UV-Vis absorption: λ_{abs} [ε (M^{-1} cm^{-1})] 377 [10,600], 312 [13,210], 249 [28,198] nm (3.0×10^{-5} M in THF); 375 [8700], 309 [11,565], 247.5 [26,700] nm (3.0×10^{-5} M in CH_3CN).

3.2. Measurement of Absorption and Fluorescence Spectra

The materials measuring the optical properties were purified by recrystallization from $CHCl_3$ and *n*-hexane. UV-Vis spectra were measured with quartz cell (1 cm × 1 cm) on a JASCO V-570 spectrophotometer. Fluorescence spectra were measured with quartz cell (1 cm × 1 cm) on a JASCO FP-6600 spectrofluorometer.

3.3. DFT Calculation Method

Shape of orbitals, and HOMO and LUMO energies were calculated by TDDFT/ωB97XD/6-31+G(d,p) level of theory with the Gaussian 16W program version 1.1 [30]. The optimized structure was also obtained from TDDFT calculation by ωB97XD/6-31+G(d,p) level of theory.

4. Conclusions

In conclusion, the introduction of a substituent on benzene ring in dipyrrolo [1,2-*a*:2′,1′-*c*]quinoxaline was efficient to give longer fluorescence peak. Both substituents with electron-donating and electron-withdrawing character were available to make bathochromic shift. Especially, similar change was observed in THF from each compound with electron-donating methoxy group or electron-withdrawing fluorine substituent. Such substituent

effect would be unique in a dipyrrolo [1,2-*a*:2′,1′-*c*]quinoxalines skeleton. In the case of the electron-withdrawing substituent, the solvent effect was also observed, which implied that the fluorescence caused by ICT state.

The reason for the shift of fluorescence peak was explainable by change of the orbital energies. Electron-donating substituents increased both HOMO and LUMO energies, especially HOMO energy. In a complementary style, electron-withdrawing substituents decreased both HOMO and LUMO energies, especially LUMO energy. As a result, a smaller energy gap compared with the original substrate was achieved in each electron-donating and electron-withdrawing substituent. It means that the different effect against optical and electric properties was obtained by using dipyrrolo [1,2-*a*:2′,1′-*c*]quinoxaline structure.

An additional introduction of substituent such as fluorine at 7 position or phenyl ring at 3 and 10 position on dipyrrolo [1,2-*a*:2′,1′-*c*]quinoxalines is efficient to give the longer fluorescence peaks. As a result, we obtained the fluorescence peak at 473 nm from **3d**, whose value is 39 nm larger than that of non-substituted compounds (**1a**). These findings will serve as guidelines in the design of novel fluorophores with longer fluorescence.

Supplementary Materials: The following supporting information can be downloaded at: https://www.mdpi.com/article/10.3390/molecules28072896/s1, Computed three longest transition peaks of **1a–d** in the excited singlet state (Table S1), Shape and energies of HOMO and LUMO of **1a–d** calculated by DFT method (Figure S1), Energies, and Cartesian coordinates of **1a–d** by TDDFT calculation, and copies of ^{1}H and ^{13}C NMR spectra and HRMS charts for new compounds (**1b–d** and **3d**).

Author Contributions: Conceptualization, S.M.; methodology, S.M. and M.T.; software, S.M.; validation, S.M., M.T. and M.A.; formal analysis, M.T.; investigation, S.M. and M.T.; resources, S.M. and M.T.; data curation, S.M.; writing—original draft preparation, S.M.; writing—review and editing, S.M., M.T. and M.A.; supervision, S.M. and M.A. All authors have read and agreed to the published version of the manuscript.

Funding: This research received no external funding.

Institutional Review Board Statement: Not applicable.

Informed Consent Statement: Not applicable.

Data Availability Statement: Not applicable.

Conflicts of Interest: The authors declare no conflict of interest.

Sample Availability: Sample of the compounds are not available from the authors.

References

1. Wang, H.; Aydıner, B.; Seferoglu, Z.; Bureš, F.; Liu, J. Development and Application of Non-Conventional Luminophores with Aggregation Based Emission. *Dyes Pigment.* **2022**, *205*, 110354. [CrossRef]
2. Wong, M.Y.; Zysman-Colman, E. Purely Organic Thermally Activated Delayed Fluorescence Materials for Organic Light-Emitting Diodes. *Adv. Mater.* **2017**, *29*, 1605444. [CrossRef] [PubMed]
3. Yang, G.-X.; Liu, D.-H.; Jiang, S.-M.; Yang, Z.-H.; Chen, Z.-J.; Qiu, W.-D.; Gan, Y.-Y.; Liu, K.-K.; Li, D.-L.; Su, S.-J. Novel Polycyclic Fused Amide Derivatives; Properties and Application for Sky-Blue Electroluminescent Devices. *Molecules* **2022**, *27*, 5181. [CrossRef] [PubMed]
4. Yu, C.; Sun, Y.; Fang, X.; Li, J.; Wu, Q.; Bu, W.; Guo, X.; Wang, H.; Jiao, L.; Hao, E.D. Aromatic-Ring-Fused BOPPY Fluorophores: Synthesis, Spectral, Redox Properties, and Bioimaging Application. *Inorg. Chem.* **2022**, *61*, 16718–16729. [CrossRef] [PubMed]
5. Bakholdina, A.; Lukin, A.; Bakulina, O.; Guranova, N.; Krasavin, M. Dual Use of Propargylamine Building Blocks in the Construction of Polyheterocyclic Scaffolds. *Tetrahedron Lett.* **2020**, *61*, 151970. [CrossRef]
6. Yagishita, F.; Tanigawa, J.; Nii, C.; Tabata, A.; Nagamune, H.; Takanari, H.; Imada, Y.; Kawamura, Y. Fluorescent Imidazo [1,5-*a*]pyridinium Salt for a Potential Cancer Therapy Agent. *ACS Med. Chem. Lett.* **2019**, *10*, 1110–1114. [CrossRef]
7. Huang, C.-C.; Xue, M.-M.; Wu, F.-P.; Yuan, Y.; Liao, L.-S.; Fung, M.-K. Deep-Blue and Hybrid-White Organic Light Emitting Diodes Based on a Twisting Carbazole-benzofuro [2,3-*b*]pyrazine Fluorescent Emitter. *Molecules* **2019**, *24*, 353. [CrossRef]
8. Wu, D.; Chen, L.; Ma, S.; Luo, H.; Cao, J.; Chen, R.; Duan, Z.; Mathey, F. Synthesis of 1,3-Azaphospholes with Pyrrolo [1,2-*a*]quinoline Skeleton and Their Optical Applications. *Org. Lett.* **2018**, *20*, 4103–4106. [CrossRef]
9. Yagishita, F.; Nii, C.; Tezuka, Y.; Tabata, A.; Nagamune, H.; Uemura, N.; Yoshida, Y.; Mino, T.; Sakamoto, M.; Kawamura, Y. Fluorescent *N*-Heteroarenes Having Large Stokes Shift and Water Solubility Suitable for Bioimaging. *Asian J. Org. Chem.* **2018**, *7*, 1614. [CrossRef]

10. Cisse, L.; Djande, A.; Capo-Chichi, M.; Khonté, A.; Bakhoum, J.-P.; Delattre, F.; Yoda, J.; Saba, A.; Tine, A.; Aaron, J.-J. Quantitative Study of the Substituent Effects on the Electronic Absorption and Fluorescence Spectra of Coumarines. *J. Phys. Org. Chem.* **2020**, *33*, e4014. [CrossRef]
11. Chavan, S.N.; Toche, R.B.; Chavan, S.M. Substituent Effect on Absorption and Fluorescence Properties of Thieno [3,2-*c*]pyridine Derivatives. *J. Fluoresc.* **2017**, *27*, 443–450. [CrossRef]
12. Jiu, T.; Li, Y.; Liu, H.; Ye, J.; Liu, X.; Jiang, L.; Yuan, M.; Li, J.; Li, C.; Wang, S.; et al. Brightly Full-Color Emissions of Oligo(*p*-phenylenevinylene)s: Substituent Effects on Photophysical Properties. *Tetrahedron* **2007**, *63*, 3168–3172. [CrossRef]
13. Miura, Y.; Kobayashi, K.; Yoshioka, N. V-Shaped Fluorophores with a 1-Methyl-4,5-bis(arylethynyl)imidazole Skeleton Displaying Solid-State Fluorescence, Acid Responsiveness, and Remarkable Fluorescence Solvatochromism. *New J. Chem.* **2021**, *45*, 898–905. [CrossRef]
14. Vázquez, J.L.; Velazco-Cabral, I.; Flores-Álamo, M.; Turlakov, G.; Rodríguez, G.; Moggio, I.; Arias, E.; Peña-Cabrera, E.; Vázquez, M.A. Synthesis of Polysubstituted Symmetrical BODIPYs via Fischer Carbene Complexes: Theoretical, Photophysical and Electrochemical Evaluation. *Chem. Eur. J.* **2022**, *28*, e202202446. [CrossRef]
15. Takamuki, Y.; Maki, S.; Niwa, H.; Ikeda, H.; Hirano, T. Substituent Effects on the Spectroscopic Properties of Solvatochromic 2-Phenylimidazo [1,2-*a*]pyrazine-3(7*H*)-ones: An Effective Control for the Colorimetric Sensor Properties. *Tetrahedron* **2005**, *61*, 10073–10080. [CrossRef]
16. Chen, C.; Huang, R.; Batsanov, A.S.; Pander, P.; Hsu, Y.-T.; Chi, Z.; Dias, F.B.; Bryce, M.R. Temperature Phosphorescence and Thermally Activated Delayed Fluorescence. *Angew. Chem. Int. Ed.* **2018**, *57*, 16407–16411. [CrossRef]
17. Zhang, Y.; Wang, K.; Zhuang, G.; Xie, Z.; Zhang, C.; Cao, F.; Pan, G.; Chen, H.; Zou, B.; Ma, Y. Multicolored-Fluorescence Switching of ICT-Type Organic Solids with Clear Color Difference: Mechanically Controlled Excited State. *Chem. Eur. J.* **2015**, *21*, 2474–2479. [CrossRef]
18. Du, Y.; Wang, H.; Zhao, S.; Fan, J.; Huang, S.; Hao, Y. Design of an ICT-Based Fluorescent Probe with Excellent Sensitivity for Visualizing GSH Levels in Live Cells. *Chem. Pap.* **2022**, *76*, 4571–4579. [CrossRef]
19. Abeywickrama, C.S. Large Stokes Shift Benzothiazolium Cyanine Dyes with Improved Intramolecular Charge Transfer (ICT) for Cell Imaging Applications. *Chem. Commun.* **2022**, *58*, 9855–9869. [CrossRef]
20. Yu, F.; Li, P.; Song, P.; Wang, B.; Zhao, J.; Han, K. An ICT-Based Strategy to a Colorimetric and Ratiometric Fluorescence Probe for Hydrogen Sulfide in Living Cells. *Chem. Commun.* **2012**, *48*, 2852–2854. [CrossRef]
21. Matsumoto, S.; Qu, S.; Kobayashi, T.; Kanehiro, M.; Akazome, M.; Ogura, K. Novel Formation of Dipyrrolo- and Diindolo [1,2-*a*:2′,1′-*c*]quinoxaline Derivatives and Their Optical Properties. *Heterocycles* **2010**, *80*, 645–656. [CrossRef] [PubMed]
22. Matsumoto, S.; Bathmunkh, E.; Akazome, M.; Takata, Y.; Tamano, M. Novel Formation of Diimidazo [1,2-*a*:2′,1′-*c*]quinoxaline Derivatives and Their Optical Properties. *Org. Biomol. Chem.* **2011**, *9*, 5941–5944. [CrossRef] [PubMed]
23. Matsumoto, S.; Abe, H.; Akazome, M. Fluorescence of Diimidazo [1,2-*a*:2′,1′-*c*]quinoxalinium Salts under Various Conditions. *J. Org. Chem.* **2013**, *78*, 2397–2404. [CrossRef] [PubMed]
24. Matsumoto, S.; Sakamoto, K.; Akazome, M. Systematic Investigation of Fluorescence Properties of Symmetric and Asymmetric Diazolo [1,2-*a*:2′,1′-*c*]quinoxaline Derivatives. *Heterocycles* **2015**, *91*, 795–814. [CrossRef]
25. Pérez-Bolívar, C.; Takizawa, S.; Nishimura, G.; Montes, V.A.; Anzenbacher, P., Jr. High-Efficiency Tris(8-hydroxyquinoline)aluminum (Alq_3) Complexes for Organic White-Light-Emitting Diodes and Solid-State Lighting. *Chem. Eur. J.* **2011**, *17*, 9076–9082. [CrossRef]
26. Antilla, J.C.; Klapars, A.; Buchwald, S.L. The Copper-Catalyzed *N*-Arylation of Indoles. *J. Am. Chem. Soc.* **2002**, *124*, 11684–11688. [CrossRef]
27. Deprez, N.R.; Kalyani, D.; Krause, A.; Sanford, M.S. Room Temperature Palladium-Catalyzed 2-Arylation of Indoles. *J. Am. Chem. Soc.* **2006**, *128*, 4972–4973. [CrossRef]
28. Valeur, B. *Molecular Fluorescence. Principles and Applications*; Wiley-VCH: Weinheim, Germany, 2002; p. 54.
29. Andersh, B.; Murphy, D.; Olson, R. Hydrochloric Acid Catalysis of *N*-Bromosuccinimide (NBS) Mediated Nuclear Aromatic Brominations in Acetone. *Synth. Commun.* **2000**, *30*, 2091–2098. [CrossRef]
30. Frisch, M.J.; Trucks, G.W.; Schlegel, H.B.; Scuseria, G.E.; Robb, M.A.; Cheeseman, J.R.; Scalmani, G.; Barone, V.; Petersson, G.A.; Nakatsuji, H.; et al. *Gaussian 16*; Revision B.01; Gaussian, Inc.: Wallingford, CT, USA, 2016.

molecules

MDPI

Article

Mechanochemistry Frees Thiourea Dioxide (TDO) from the 'Veils' of Solvent, Exposing All Its Reactivity

Francesco Basoccu [1], Federico Cuccu [1], Pietro Caboni [1], Lidia De Luca [2] and Andrea Porcheddu [1,*]

[1] Department of Chemical and Geological Sciences, University of Cagliari, 09042 Monserrato, Italy
[2] Department of Chemical, Physical, Mathematical, and Natural Sciences, University of Sassari, Via Vienna 2, 07100 Sassari, Italy
* Correspondence: porcheddu@unica.it

Abstract: The synthesis of nitrogen-based heterocycles has always been considered essential in developing pharmaceuticals in medicine and agriculture. This explains why various synthetic approaches have been proposed in recent decades. However performing as methods, they often imply harsh conditions or the employment of toxic solvents and dangerous reagents. Mechanochemistry is undoubtedly one of the most promising technologies currently used for reducing any possible environmental impact, addressing the worldwide interest in counteracting environmental pollution. Following this line, we propose a new mechanochemical protocol for synthesizing various heterocyclic classes by exploiting thiourea dioxide (TDO)'s reducing proprieties and electrophilic nature. Simultaneously exploiting the low cost of a component of the textile industry such as TDO and all the advantages brought by a green technique such as mechanochemistry, we plot a route towards a more sustainable and eco-friendly methodology for preparing heterocyclic moieties.

Keywords: heterocycles; thiourea dioxide; TDO; mechanochemistry

Citation: Basoccu, F.; Cuccu, F.; Caboni, P.; De Luca, L.; Porcheddu, A. Mechanochemistry Frees Thiourea Dioxide (TDO) from the 'Veils' of Solvent, Exposing All Its Reactivity. *Molecules* **2023**, *28*, 2239. https://doi.org/10.3390/molecules28052239

Academic Editors: Alexey M. Starosotnikov, Maxim A. Bastrakov and Igor L. Dalinger

Received: 31 January 2023
Revised: 24 February 2023
Accepted: 25 February 2023
Published: 28 February 2023

1. Introduction

Heterocycles are ubiquitous in biologically active compounds, natural products, and common pharmaceuticals [1–9], representing a highly privileged structural motif. For example, common biocides [10], fungicides [11], antitumoral agents [12,13], and analgesics [14–16], to mention a few, contain a benzimidazole or benzothiazole moiety in their structure. Furthermore, the benzimidazole scaffold represents a benchmark for synthesizing new potential agents against various cancer or infectious diseases, even those that still cannot be effectively treated [17,18]. This is due to the benzimidazole ring's astonishing proprieties that simultaneously possess a hydrophobic unit and two hydrogen-bonding domains (Figure 1) [19].

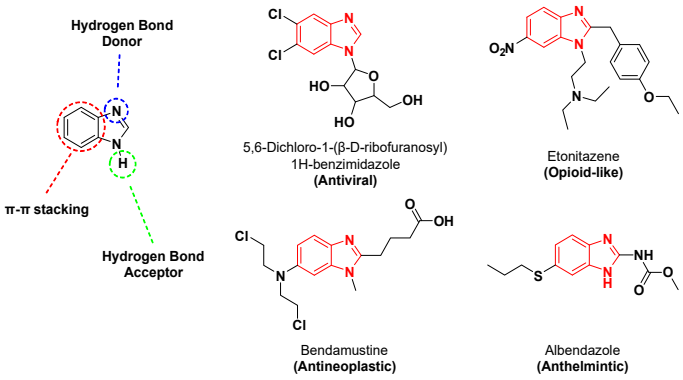

Figure 1. Benzimidazole features with common benzimidazole pharmaceutical scaffolds.

Accordingly, several endeavors have been dedicated to the synthesis of such compounds. Among all the reported methods, those using either formaldehyde or an appropriate surrogate reagent have proven to be efficient and valuable choices for preparing different heterocycles containing the benzimidazole core [20–26]. However, these strategies usually suffer from some limitations, such as employing additives, e.g., metal catalysts, harsh reaction conditions, or toxic solvents (Scheme 1).

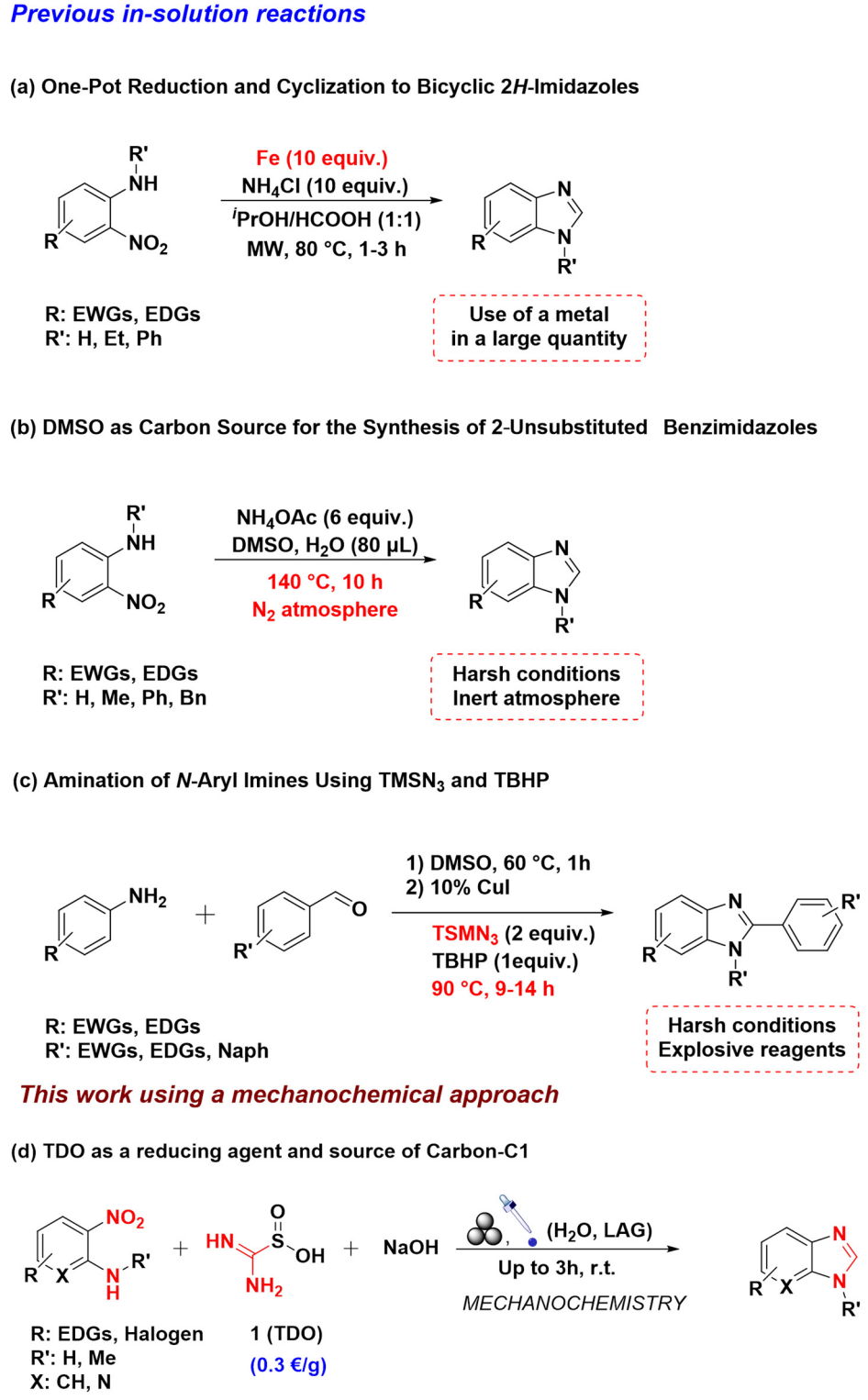

Scheme 1. A comparison between this work and previous methodologies.

In this context, thiourea dioxide (TDO), a solid surrogate for formaldehyde, could allow us to overcome many of the shortcomings mentioned above. TDO is a cheap and commercial compound commonly employed in textile industries for bleaching processes [27]. Moreover, it has also been exploited in the past for analytical measurements [28–30]. Finally, it can also be synthesized, as pioneered by Barnett (Scheme 2) [31], Lai [32], and Kluttz [33], and different studies have already been published concerning both its electrophilic and reducing nature [34–39].

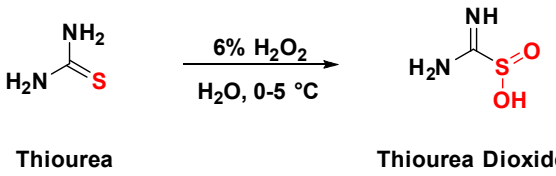

Scheme 2. TDO synthesis and structure, as reported by Barnett.

As a matter of fact, TDO is insoluble in most organic solvents as well as in water, and its reactivity can be triggered by raising the temperature. Because of this, it is typically used in mixtures of methanol and basic or heated water [40,41].

In 2021, Wu's team documented benzimidazoles' synthesis through thiourea dioxide's (TDO, **1**) electrophilic character in a solvent-based process [42]. The procedure was carried out in water at 60 °C, providing around ten benzimidazoles in satisfactory yields. A solvent screening was also made on the control reaction, proving how the insolubility of TDO in organic solvents made it unreactive compared to the employment of hot water. In addition, the use and removal of solvents during a chemical synthesis represents a significant portion of organic pollution and process energy consumption.

Benzimidazoles are generally synthesized from aniline derivatives, which in turn are often prepared from the corresponding nitrobenzenes. Furthermore, the synthetic methods to produce anilines still involve classical methodologies, and there is currently a worldwide interest in proposing new synthetic routes to improve the sustainability and applicability of such a process [43–46]. Reducing an aromatic nitro moiety usually requires an acid environment in the presence of a metal [47–50] or the employment of gaseous hydrogen [51–54]. Despite performing satisfactorily, these methodologies have concerns that must be addressed. Starting from metals, this procedure is usually run under an acidic environment [54–58], and consequently, it may not be applied to substrates sensitive to such conditions.

Furthermore, the use of metals is often associated with various risks concerning human health and the environment due to their well-established toxicity. For example, with molecular gaseous hydrogen, its use is related to an explosion hazard because of its high reactivity [55,56]. Since this procedure is exergonic ($\Delta rG^\circ < 0$), a high amount of heat is typically released during an industrial process [57]. Such heat generation can be challenging to remove and may also induce expensive cooling costs or lower the reaction yields due to reactor hot spots [58,59]. Other methods rely on electrochemistry [59,60], enzymatic processes [56], rare-earth elements [61], and hydrogen transfer reagents [61–64], all of which need specific reaction conditions and advanced equipment. Few reductions in a basic environment have been described in literature [65–67]; the most recurrent one is undoubtedly the employment of Zn powder in the presence of NaOH for synthesizing azobenzene [68]. Unfortunately, a basic environment generally implies other sub-products formed during the redox process [57,67,69]. Their presence complicates the obtention of the corresponding anilines, making the entire procedure complex and cumbersome.

On the contrary, the reducing processes of TDO are associated with the release of nontoxic side products, mainly urea and sodium sulfite [37].

The abovementioned drawbacks prompted us to assess the feasibility of grinding the reaction under solvent-free conditions. Indeed, ball-milling remains an impressive technology in this regard [69–72]. Many mechanochemical strategies described astonishing

advantages such as high reaction efficiency, the prevention of harsh reaction conditions, and the minimization of organic solvents [73–75].

As part of our ongoing interest in green synthesis via mechanochemistry [47,48], we evaluated whether heat could be easily replaced by mechanical energy, thus enabling access to higher and more sophisticated reactivities.

2. Results and Discussion

2.1. TDO as a Reducing Agent

Firstly, the reducing properties of TDO (Compound **1**) on nitrobenzenes were explored to outline and screen all the mechanochemical parameters for this step. Considering the few existing techniques for reducing nitrobenzene with TDO [76,77], we had to lay the groundwork for a methodology with a broader applicability. We set the mechanochemical procedure on a 1.0 mmol scale using nitrobenzene as a reference substrate. We milled TDO **1** (1.0 mmol), nitrobenzene **2a** (1.0 mmol), and NaOH (1.0 mmol) for 1.0 h inside a 10 mL stainless steel (SS) vessel equipped with two balls (Ø = 7 mm, 2.67 g) of the same material (Scheme 3).

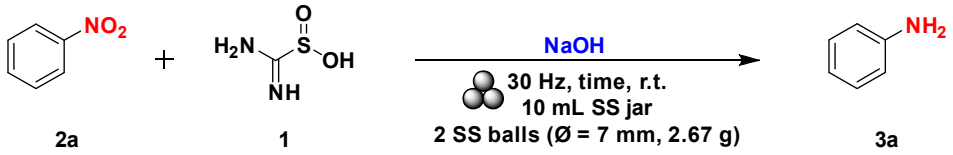

Scheme 3. General scheme of the reaction.

Unfortunately, we detected the only presence of the starting material through a GC-MS analysis (Table 1, entry 1). Several process parameters have been investigated to overcome these failures, and the whole optimization process is summarized in Table 1. To begin, we raised the ratio of **1** and NaOH (Table 1, entries 2 and 3), which allowed us to convert **2a** into aniline **3a** with a 21% yield (Table 1, entry 3). Then, prompted by these results, we tried to increase both the reaction time and the reducing mixture equivalents (TDO and NaOH). In the first case, the yield was even lower in a 2 h milling with a 5% yield (GC-analysis), probably due to the higher reactivity of the formed aniline with the redox intermediates (Table 1, entry 4). In the latter one, **2a** was consumed entirely, but the conversion to the desired product **3a** increased slightly together with other process intermediates (Table 1, entry 5). Lastly, we ran the reducing process at 70 °C to accelerate the kinetics of the reaction, but we only obtained the corresponding symmetric diazobenzene (PhN=NPh, Table 1, entry 6).

Therefore, after all these failed attempts, we considered using drops of different solvents to run a **L**iquid-**A**ssisted **G**rinding (**LAG**) [78–82] in a 90 min procedure. Consistently, less polar (decane or toluene) and polar solvents (acetone or isopropanol) did not permit a reasonable conversion rate (Table 1, entries 7–10). Lastly, methanol and water were used, as in analogous solvent-based procedures. However, in this case, the ratio of solvent/reagents was drastically cut down compared to the already reported methodologies (LAG, η = 0.44 μL/mg). In contrast to that which is usually found for solvent-based procedures, methanol used under LAG conditions produced a complex mixture of aniline and nitrobenzene reduction process intermediates (Table 1, entry 11). Water, instead, led to excellent yields of **3a** (Table 1, entry 12). Its amount, however, was found to be a critical parameter, since the conversion rate dramatically dropped when η = 0.22 μL/mg (Table 1, entry 13). Contrarily, a little increase in the reaction time of up to 2 h allowed for a quantitative conversion of **2a** to **3a** (Table 1, entry 14). Concerning the bases, weaker ones such as sodium carbonate and sodium bicarbonate did not allow for a comparable result (Table 1, entries 15 and 16), proving that NaOH plays a crucial role in the mechanochemical process—consistent with the findings of Hawkes for similar reactions in solution [83]. Lowering the NaOH amount negatively affected the reaction performance as well (Table 1, entry 17).

Table 1. Optimization process for the reduction of **2a** to **3a**.

Entry	TDO eq.	Base eq.	Reaction Time (h)	Additives [b]	Yields [a]
1	1	1	1	/	0%
2	3	6	1	/	2%
3	6	6	1	/	21%
4	6	6	2	/	5%
5	10	10	2	/	29%
6 [c]	6	6	2	/	0%
7	3	6	1.5	Decane	2%
8	3	6	1.5	Toluene	4%
9	3	6	1.5	[i] PrOH	3%
10	3	6	1.5	Acetone	5%
11 [d]	3	6	1.5	MeOH	Complex Mixture
12	3	6	1.5	H_2O	89%
13 [e]	3	6	1.5	H_2O	0%
14	**3**	**6**	**2**	**H_2O**	**97%**
15 [f]	3	6	1.5	H_2O	20%
16 [g]	3	6	1.5	H_2O	1%
17 [h]	3	3	2	H_2O	<5%

All the reactions were carried out with the same experimental parameters unless otherwise specified: nitrobenzene (1.0 mmol), compound **1** (1.0–10.0 mmol), and NaOH (1.0–10.0 mmol) in a SS jar (10.0 mL) equipped with two balls (SS, Ø = 7.0 mm, 2.67 g) at a frequency of 30 Hz. [a] The yields were calculated by GC-MS analysis. [b] The additive quantity was 250 µL. [c] The reaction was run at 70 °C; the only product obtained was the corresponding azobenzene. [d] The desired product was obtained only in traces. [e] The amount of water was reduced to 125 µL. The main product found was azoxybenzene; the remaining peaks were attributed to nitrobenzene [f] Na_2CO_3 was used instead of NaOH. [g] $NaHCO_3$ was used instead of NaOH. [h] The SM presence was not detected, and the ^1H NMR spectra presented signals that cannot be attributed to specific compounds. [i] The main spotted product was identified as hydrazobenzene; the rest of the mixture was composed of azoxybenzene, azobenzene, and *N*-phenylhydroxylamine.

With the optimized conditions in hand, we extended the entire procedure to other nitrobenzenes to validate this mechanochemical process. In the case of activated substrates **2b** and **2c**, the process smoothly proceeded to a complete conversion within 2 h, and for more complex substrates like **2s**, the process was completed in only 3 h (Scheme 4).

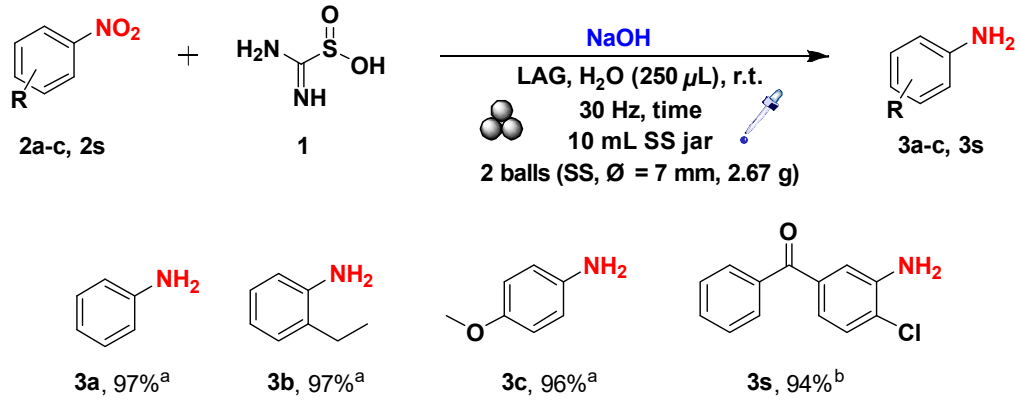

Scheme 4. Mechanochemical synthesis of anilines from the corresponding nitrobenzenes. The yields were calculated by GC-MS analysis: [a] 120 min reaction time, [b] 180 min of reaction time.

Reducing instead 2-nitroaniline **2d**, many unpredicted outcomes showed up, as summarized in Table 2. In this case, we synthesized the *o*-phenylenediamine **3d** with a 37% yield in 90 min without LAG (Table 2, entry 1). Such different behavior can be ascribed to the positive effects of an EDG. Unexpectedly, prolonging the reaction time to 2 h under neat grinding conditions resulted in the formation of the corresponding benzimidazole, albeit in low yields (Table 2, entry 2). For the sake of completeness, we also tried to reduce in neat conditions other substrates having a comparable charge distribution (Table 2, entries 3 and 4). With 2-nitro anisole, we obtained the corresponding aniline in a 54% isolated yield. At the same time, the employment of 2-nitro phenol resulted in a mixture of various unidentified products, likely generated by the high phenoxide reactivity.

Table 2. Optimization process for the reduction of **2d** to **3d**.

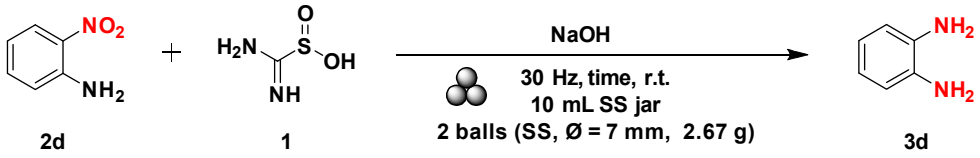

Entry	TDO eq.	Base eq.	Reaction Time (h)	Additives [b]	Yields [a]
1	3	6	1.5	/	37%
2 [c]	3	6	2	/	45%
3 [d]	3	6	2	/	54%
4 [e]	3	6	2	/	Complex mixture
5 [f]	3	6	2	MeOH	0%
6	**3**	**6**	**2**	**H_2O**	**98%**
7 [g]	3	3	2	H_2O	1%

All the reactions were carried out with the same experimental parameters unless otherwise specified: 2-nitroaniline **2d** (1.0 mmol), compound **1** (3.0 mmol), and NaOH (3.0–6.0 mmol) in a SS jar (10.0 mL) equipped with two balls (SS, Ø = 7.0 mm, 2.67 g) at a frequency of 30 Hz. [a] The yields were calculated by GC-MS analysis. [b] The additive quantity was 250 µL. [c] The *o*-phenylenediamine reacted with **1** and formed the benzimidazole **4d**, yielding 20% and other unidentified subproducts. [d] The starting material was 2-nitro anisole. [e] The starting material was 2-nitro phenol. [f] The signals in the spectra were attributed to 2-((2-nitrophenyl)diazinyl)aniline and 2,2′-(hydrazine-1,2-diyl)dianiline. [g] The 2-nitroaniline **2d** and benzimidazole **4d** were detected with a yield of 75% and 24%, respectively.

To better understand several critical details of the process, we have to better focus on several points of the process. First, under LAG conditions, the presence of methanol resulted in the concurrent formation of **3d** and various reaction intermediates. At the same time, water use was associated with the synthesis of the desired product with a nearly quantitative yield in 2 h (Table 2, entries 5 and 6). These different outcomes can be reconducted to the role covered by water as a better proton source. On the other hand, water, to some extent, also inhibits the final cyclization pathway that leads to benzimidazole formation. The reduction in the nitro group and the construction of the benzimidazole ring both consume TDO, with the latter being kinetically faster. As a result, any attempt to decrease the NaOH equivalents failed because of the high reactivity of the formed *o*-phenylenediamine towards TDO that was still present in the reaction medium (Table 2, entry 7). Once these issues are focused on, we can draw conclusions based on the above and after a long, meticulous exploratory study. Six equivalents of NaOH promote the sluggish kinetics of the reduction reaction to the detriment of the cyclization reaction, resulting in a complete reduction of the nitro group (Table 2, entry 6).

Once we understood the reactivity of 2-nitroanilines, we also extended this process to other 2-nitroaniline derivatives (Scheme 5). As a result, *o*-phenylenediamines **3e** and **3f** were successfully synthesized in a 2 h ongoing process, whereas the substrates **3g–j**

and **3o**–**p** needed a longer reaction time of 3 h. These outcomes were utterly in line with Hammett's parameters and steric hindrance on the aromatic ring of the starting materials.

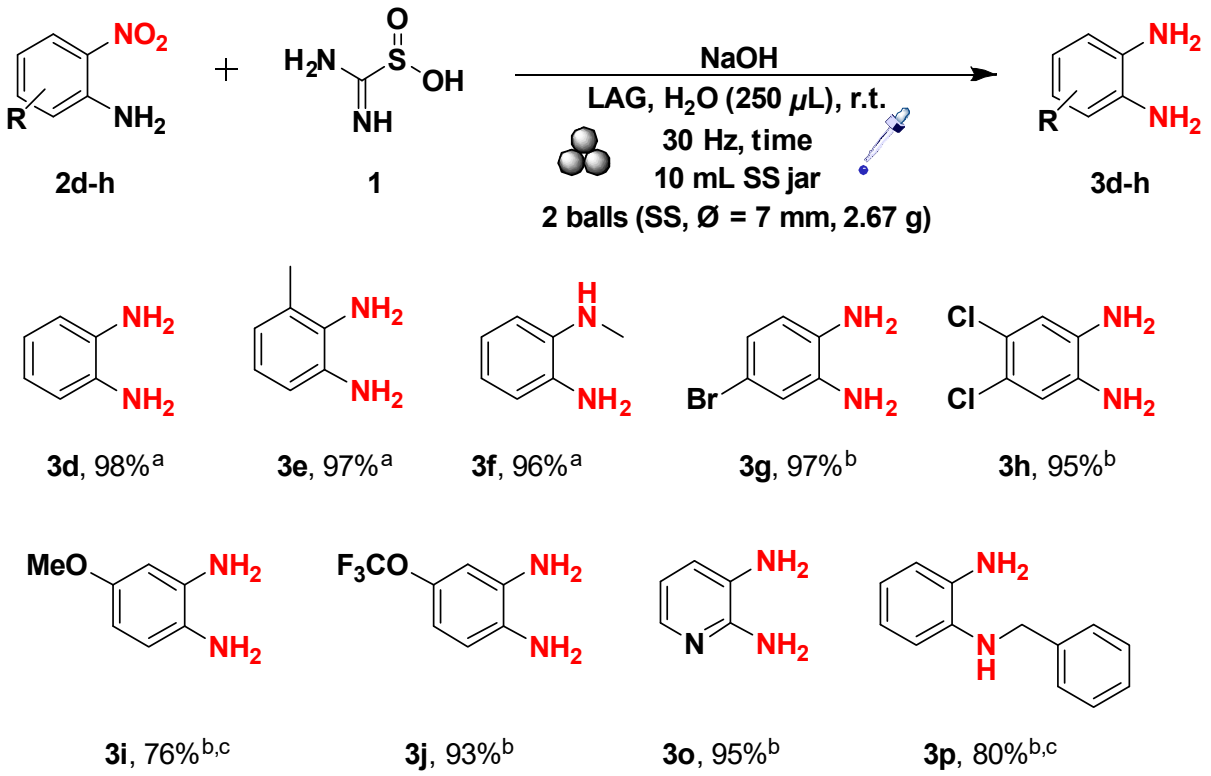

Scheme 5. Mechanochemical synthesis of *o*-phenylenediamines from the corresponding 2-nitroanilines. The yields were calculated by GC-MS analysis: [a] 120 min reaction time, [b] 180 min of reaction time. [c] The product was purified through a silica pad.

2.2. TDO as an Electrophile

Having clarified the role of TDO **1** as a reducing agent, we thoroughly analyzed its application as a "green" solid replacement for formaldehyde for synthesizing aza-heterocycles. Its electrophilicity is connected to the presence of the two nitrogen atoms depleting the central carbon atom in terms of electron density. Furthermore, an excellent leaving group such as the sulfur moiety makes the whole molecule more prone to a nucleophilic attack. We accomplished the heterocycle synthesis by establishing two separate procedures: a single-step process based on the employment of phenylenediamines (**procedure A**) and a double-step methodology starting from 2-nitroanilines (**procedure B**).

2.2.1. Procedure A

The reactivity of phenylenediamines toward compound **1** has already been reported in the literature for solvent-based processes restricted to a few very reactive substrates. [42]. We investigated the mechanosynthesis of heterocycles from less reactive substrates, in this case, the ones that possess a lower electron density in their aromatic ring (Scheme 6). All the reactions were conducted using a LAG, where water was used as the additive ($\eta = 0.44$). Starting from the *o*-phenylenediamines **3l**–**n**, we obtained the corresponding heterocycles in low yields due to the low reactivity of such compounds. Deactivating groups either on the ring or on the nitrogen atom drastically affected the ring closure process, as evidenced by the poor yields obtained for compounds **4l**–**n**. Remarkably, diamines **3q** and **3r** enabled access to molecular framework of biological interest in poor to good yields [84–86].

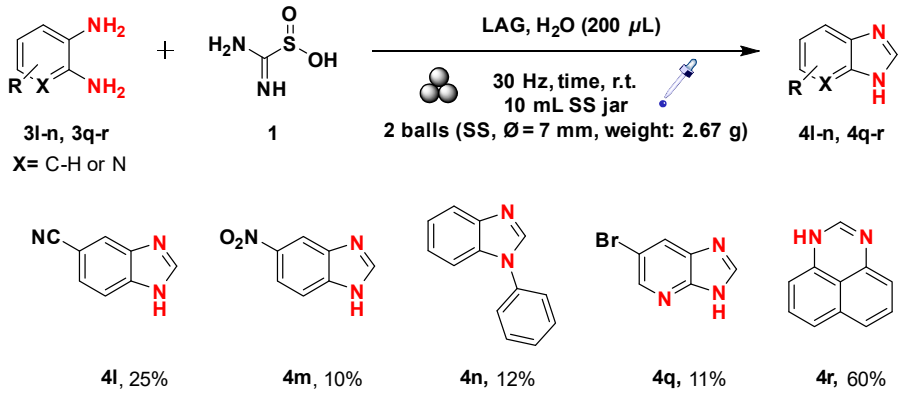

Scheme 6. Mechanochemical synthesis of aza-heterocycles from the corresponding phenylenediamines. The yields were determined by GC-MS analysis.

2.2.2. Procedure B

With the optimal conditions for reducing 2-nitroanilines in hand, we wondered whether a double-step methodology could be feasible. Bearing in mind that a basic environment consumes compound **1** for forming the reducing species, we realized that we needed to add an additional amount of it for running the second step. In addition, we added a small quantity of water, because the process was proved to perform poorly through neat grinding, as formerly stated. After these considerations, we shaped the procedure to convert 2-nitroanilines into aza-heterocycles (Scheme 7). The first step was run under fine-tuned conditions, so the newly formed *o*-phenylenediamine was ready for the forthcoming ring closure step. This last stage was successfully accomplished with a refill of **1** (3.0 mmol) and water (250 μL, η = 0.44), and it was run for further 2 h for the substrates **2d**–**f**. The 2-nitroanilines **2g**–**k** and **2o**–**p** required a longer reaction time of 3 h instead.

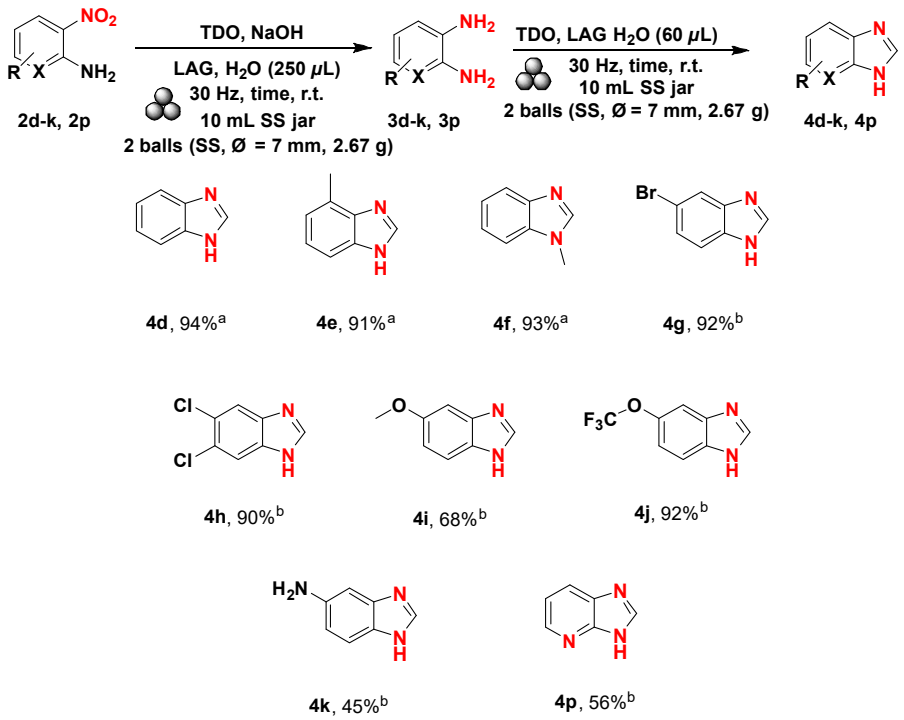

Scheme 7. Mechanochemical synthesis of aza-heterocycles from the corresponding 2-nitroanilines through a double-step procedure. Yields refer to pure isolated compounds: [a] 2 h of reaction time were required, [b] 3 h of reaction time were needed.

The reaction proceeded well in all the considered cases and provided benzimidazoles **4d**–**4j** in near-quantitative yields except for compounds **4k** and **4p** (Scheme 7).

To assess the green footprint of this mechanochemical procedure, we calculated the green metrics for our methodology and compared them with a previously reported solvent-based process. The results highlight a substantial improvement, in a green chemistry framework, of the proposed mechanochemical technique concerning the solvent-based approach (see the paragraph "Green Metrics" in the Supplementary Materials for further details).

To further demonstrate the potentialities of the developed mechanochemical protocol, various trials on a larger-scale reaction (from 2 mmol up to 5 mmol) were conducted. As illustrated in Scheme 8, the mechanochemical solvent-free reaction of **2a** (5.0 mmol) with **1** (30.0 mmol), NaOH (30.0 mmol), and water (1.5 mL) at 30 Hz for 4 h gave product **4a** in a satisfactory product yield of 91%, showing the robustness of the present method and how it could be feasibly adapted for a possible scale-up process.

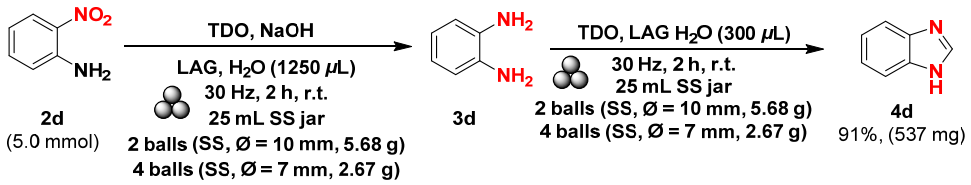

Scheme 8. Mechanochemical synthesis of benzimidazole **4a** on a 5 mmol scale. The yields were determined on the isolated product.

All the syntheses presented are easy to accomplish and proceed with a first redox process followed by a final ring closure and aromatization step (Scheme 9). The reducing ability of compound 1 has been widely described, and it exploits the formation of sulfoxylic acid [36–38,87,88]. However, such a chemical species can be formed only from the tautomer of compound 1, aminoiminomethanesulfinic acid (AIMS), usually only observed in an aqueous medium (Scheme 9, pathway 1) [89–92]. After being formed, it is converted to its more stable form, sodium hydrogen sulfoxylate, by the remaining equivalents of NaOH (Scheme 9, pathway 2). It is hard to imagine that a species such as sodium sulfoxylate could be formed due to the low acidity of sodium hydrogen sulfoxylate [87]. This last compound is then ready to participate in the redox process and will be reduced to gaseous sulfur dioxide (Scheme 9, pathway 3).

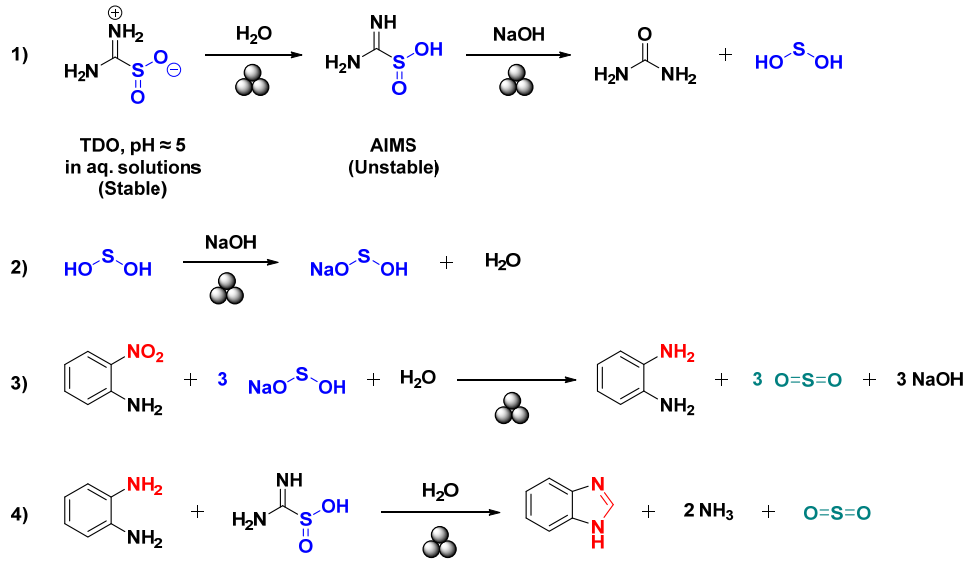

Scheme 9. Mechanochemical reaction steps under LAG condition. Water (250 μL, η = 0.44) was added in one single shot at the start of the reaction.

Nonetheless, we cannot completely rule out the presence of sodium dithionite and sodium bisulfite as reducing agents. The former can be formed by TDO degradation [39,93], and the sulfur dioxide may generate the latter in the presence of water [94]. Ultimately, adding fresh **TDO** to the reaction medium allowed the ring to be closed to the corresponding aromatic heterocycle (Scheme 9, pathway 4).

Concerning water (250 µL) used to perform the LAG process (η = 0.44), it plays three fundamental roles in the mechanochemical redox reaction. Firstly, it enables the formation of the active tautomer AIMS**,** as described by Dittmer [91] and Krug [92]. Secondly, the complete consumption of **1** to sodium sulphoxylate in a strong basic environment avoids other collateral processes such as the auto condensation of TDO to cyclic derivatives, as reported in the literature [95]. Thirdly, the presence of water might prevent the formation of other undesired redox intermediates, because it acts as a proton donor [96]. Lastly, it probably permits sodium hydroxide to participate extensively in concert with TDO due to its high solubility in water. This may also explain the poorer performance of the mechanochemical process when methanol is employed for a LAG approach.

To conclude, we also studied the reactivity of hydrazobenzene under our optimized conditions. Unfortunately, conducting the reaction with 1 mmol of hydrazobenzene with TDO (3 mmol), NaOH (6 mmol), and water (250 µL) only yielded the starting material as described by Huang [77]. Therefore, the entire redox process is wholly described in Scheme 10.

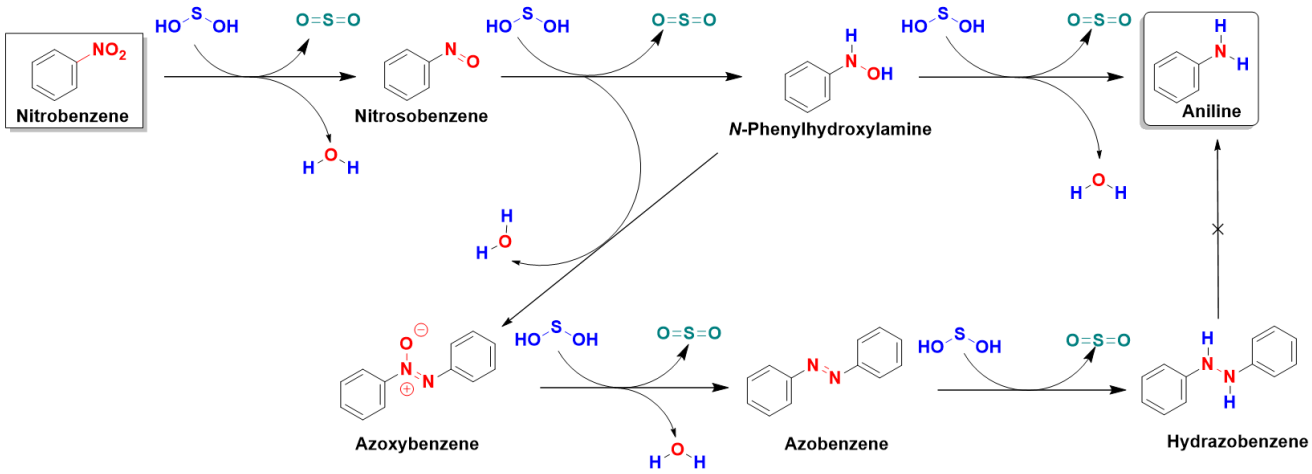

Scheme 10. The assumed redox mechanism for the mechanochemical reduction of nitrobenzene **2a** into aniline **3a**.

Considering the ring closure step, the electrophilic nature intrinsic to compound **1** makes possible the formation of a heterocycle (Scheme 11a,b). We firmly support the idea that, in the presence of NaOH, cyanimide cannot be formed by the degradation of compound **1** [97]. Therefore, the only possible pathway for heterocycle synthesis is the release of formamidine through a dismutative process (Scheme 11a pathway 1) [98,99]. After undergoing a nucleophilic attack from the *o*-phenylenediamine, formamidine allows the generation of an *N*-arylformamidine intermediate that will go through a second nucleophilic attack from the other nitrogen atom (Scheme 11a, pathway 2). The resulting 2-amino dehydrobenzimidazole then extrudes the NH_2 moiety as ammonia for forming the benzimidazole structure (Scheme 11a, pathway 3).

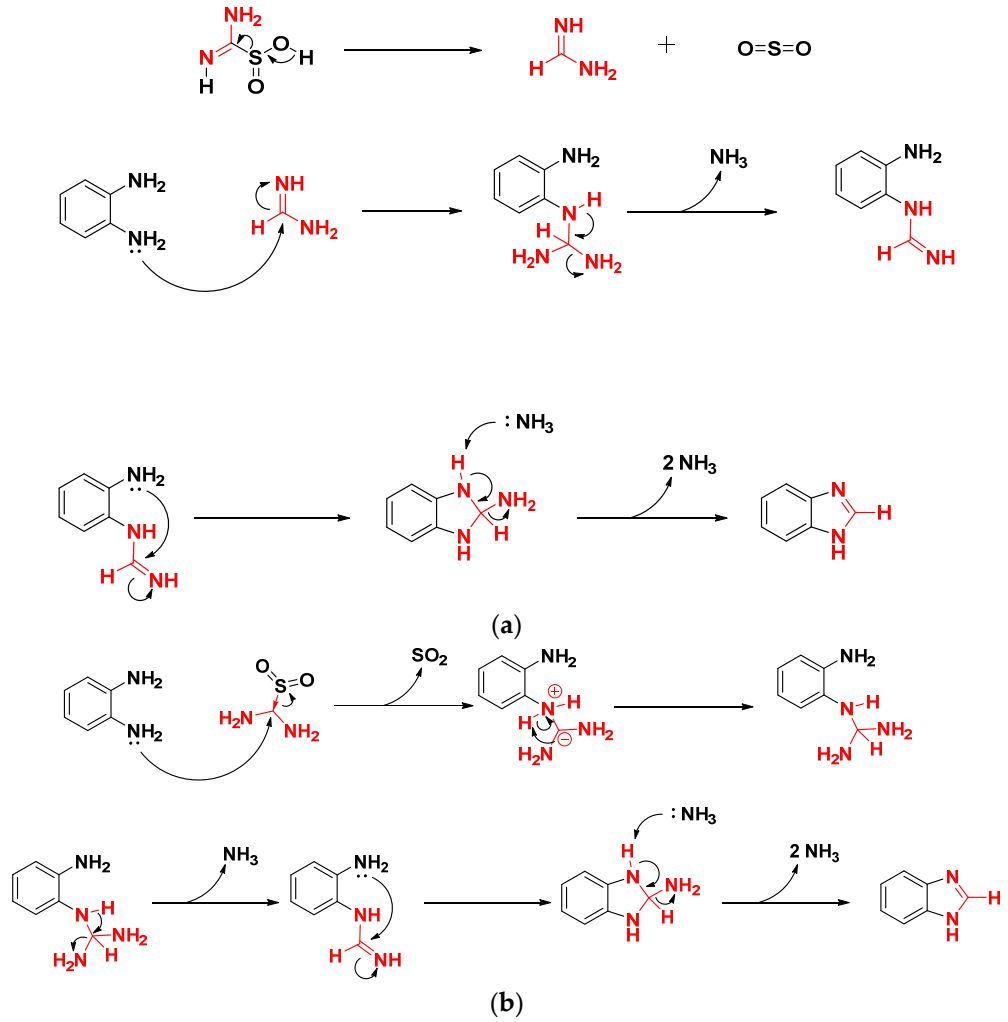

Scheme 11. (**a**) The assumed reaction mechanism for the mechanochemical synthesis of **4a** from **2a** through the release of formamidine. (**b**) The assumed reaction mechanism for the mechanochemical synthesis of **4a** from **2a** through the carbenoid pathway.

Nevertheless, we cannot rule out a reaction mechanism based on the supposed carbenoid structure of TDO as well [89,100–102] (Scheme 11b). In this case, the reaction mechanism initially follows a diverse pathway based on the minor charge separation between the two moieties of TDO (Scheme 11b, pathway 1) [90,103]. Then, after forming an *N*-arylformamidine intermediate, the process continues as mentioned above (Scheme 11b, pathway 1).

We ruled out a possible deamination approach from the corresponding 2-aminobenzimidazole for the following reasons. Firstly, when we milled commercial 2-aminobenzimidazole in the presence of NaOH, we did not see any change in the starting material's nature. Secondly, the thermodynamic stability of such a substrate prevents any structure alteration under our mild conditions [104]. Thirdly, its synthesis should be associated with an unlikely dehydrogenative process in our reaction medium. Finally, once the entire process is finished, the desired product needs to be extracted from the reaction mixture.

Along with the newly synthesized heterocycle, other subproducts were formed. We think their presence was due to the degradative processes of compound **1**, as already documented [95,105,106]. Hence, a short silica pad was made to obtain the desired product in high purity.

3. Materials and Methods

3.1. Materials

Commercially available reagents were purchased from Acros (Geel, Belgium), Aldrich (Darmstadt, Germania), Strem Chemicals (Newburyport, MA, USA), Alfa-Aesar (Haverhill, MA, USA), and TCI Europe (Zwijndrecht, Belgium) and used as received. All of the reactions were monitored by thin-layer chromatography (TLC) performed on glass-backed silica gel 60 F254, 0.2 mm plates (Merck, Darmstadt, Germania), and compounds were visualized under UV light (254 nm) or using cerium ammonium molybdate solution with subsequent heating. The eluents were technical grade. The mechanochemical reactions were performed using a Retsch Mixer Mill MM 500 VARIO apparatus (horizontal vibratory mill). The reagents were milled using a stainless steel grinding jar (10 mL) equipped with two balls (Ø = 7.00 mm, 2.67 g) of the same material. The ^{1}H- and ^{13}C-NMR spectra were recorded on a Bruker (Billerica, MA, USA) Avance III HD 600 MHz NMR spectrometer at 298 K. Proton chemical shifts are expressed in parts per million (ppm, δ scale) and are referred to as the residual hydrogen in the solvent ($CDCl_3$, 7.27 ppm or DMSO-d_6 2.54 ppm). Carbon chemical shifts are expressed in parts per million (ppm, δ scale) and are referenced to the carbon resonances of the NMR solvent ($CDCl_3$, 77.0 ppm or DMSO-d_6 39.5 ppm). GC-MS analyses were performed on an Agilent 5977B MS interfaced to the GC 7890B equipped with a DB-5ms column (J & W, New Brighton, UK). Yields refer to pure, isolated materials.

3.2. General Procedure A for Anilines and o-Phenylenediamines **3a–j**, **3o–p**, **3s** *Synthesis from 2-Nitroanilines* **2a–j**, **2o–p**, **2s**

A 10 mL stainless steel jar equipped with two stainless steel milling balls (7 mm diameter, 2.67 g) was filled with nitrobenzenes **2a–j, 2o–p, 2s** (1.0 mmol), NaOH (6.0 mmol), **1** (3.0 mmol), and 250 μL of distilled water. The vessel was then closed, and the mechanochemical reaction was conducted, ranging from 60 to 180 min at 30 Hz. Whenever necessary, further purification through flash column chromatography was performed. Lastly, the solvent was removed under reduced pressure to afford the pure anilines **3a–j, 3o–p, 3s**.

3.3. General Procedure B for Heterocycles **4l–n**, **4q–r** *Synthesis from o-Phenylenediamines* **3l–n**, **3q–r**

A 10 mL stainless steel jar equipped with two stainless steel milling balls (7 mm diameter, 2.67 g) was filled with o-phenylenediamines **3l–n**, **3q–r** (1.00 mmol), 1 (2.00 mmol), and 200 μL of distilled water. The vessel was then closed, and the mechanochemical reaction was conducted, ranging from 60 min to 180 min at a frequency of 30 Hz. At the end of the reaction, an additional silica pad (SiO_2, heptane/ethyl acetate/methanol = 1:1:0→6:3:1) was made to purify the reaction mixture. Lastly, the solvent was removed under reduced pressure to afford the pure heterocycle **4l–n**, **4q–r**.

3.4. General Procedure C for Heterocycles **4d–k**, **4p** *Synthesis from 2-nitroanilines* **2d–k**, **2p**

A 10 mL stainless steel jar equipped with two stainless steel milling balls (7 mm diameter, 2.67 g) was filled with 2-nitroanilines **2d–k**, **2p** (1.0 mmol), NaOH (6.0 mmol), 1 (3.0 mmol), and 250 μL of distilled water. The vessel was then closed, and the mechanochemical reaction was conducted, ranging from 60 to 180 min at 30 Hz. After that, an additional refill of **1** (3.0 mmol) was made, and 60 μL of distilled water and the mechanochemical reaction was made to run ranging from 60 to 180 min at a frequency of 30 Hz. At the end of the reaction, an additional silica pad (SiO2, heptane/ethyl acetate/methanol = 1:1:0→6:3:1) was made to purify the reaction mixture. Lastly, the solvent was removed under reduced pressure to afford the pure heterocycle **4d–k**, **4p**.

4. Conclusions

This work has thoroughly explained a mechanochemical protocol for synthesizing heterocycles, rediscovering a solid reagent as thiourea dioxide (TDO). Not only did the dual

nature of such a compound allow us to propose both reducing and ring closure procedures, but it also allowed us to merge these two processes in a one-pot technique starting from 2-nitroanilines. By avoiding a mixture of methanol and basic water like in the in-solution methods, we were also able to deeply analyze the already-known reducing properties of TDO, as has never been reported. The reaction is easy to perform and allows for the obtainment of the desired products with yields ranging from low to excellent. In addition, this methodology provided an alternative pathway for synthesizing scaffolds of biological and pharmaceutical interest, such as benzimidazole derivatives, and valuable building blocks with a potential application in drug design, such as perimidines and imidazopyridines.

Supplementary Materials: The following supporting information can be downloaded at: https://www.mdpi.com/article/10.3390/molecules28052239/s1, including general information, synthesis of compounds, green chemistry metrics calculations (Scheme S1: Mechanochemical preparation of **4d**, Scheme S2: Microwave preparation of benzimidazole **4d**, Scheme S3: $MgSO_4$ drying ability, Figure S1: DOZN™ score for the mechanochemical synthesis of **4d**, Figure S2: DOZN™ score for the microwave synthesis of **4d**) and spectra. References [107–124] are cited in the Supplementary Materials.

Author Contributions: Conceptualization, writing—review and editing, A.P.; validation, formal analysis, investigation, data curation, F.C., P.C. and F.B.; L.D.L. supervision; review, and editing, L.D.L.; funding acquisition, A.P. All authors have read and agreed to the published version of the manuscript.

Funding: This research was funded by MIUR Italy, PRIN 2017 project (grant number: 2017B7MMJ5_001) "MultIFunctional poLymer cOmposites based on groWn matERials" (MIFLOWER) and Fondazione di Sardegna (FdS, F72F20000230007).

Institutional Review Board Statement: Not applicable.

Informed Consent Statement: Not applicable.

Data Availability Statement: The data presented in this study are available in the Supplementary Materials.

Acknowledgments: We acknowledge the CeSAR (Centro Servizi Ricerca d'Ateneo) core facility of the University of Cagliari and Sandrina Lampis for assistance with the generation of the ^{1}H- and ^{13}C-NMR spectroscopic data. We also thank Gianluigi Corrias for the technical support in managing the ball mills and jars. Finally, we would like to dedicate our entire work to the memory of Adolfo Lai. That which he documented 50 years ago began a journey that has finally reached its end, and we are proud to have taken part in it.

Conflicts of Interest: The authors declare no conflict of interest.

Sample Availability: Samples of all the synthesized compounds are available from the authors.

References

1. Elattar, K.M.; Mert, B.D.; Monier, M.; El-Mekabaty, A. Advances in the chemical and biological diversity of heterocyclic systems incorporating pyrimido [1,6-a]pyrimidine and pyrimido[1,6-c]pyrimidine scaffolds. *RSC Adv.* **2020**, *10*, 15461–15492. [CrossRef] [PubMed]
2. Hammouda, M.M.; Gaffer, H.E.; Elattar, K.M. Insights into the medicinal chemistry of heterocycles integrated with a pyrazolo[1,5-a]pyrimidine scaffold. *RSC Med. Chem.* **2022**, *13*, 1150–1196. [CrossRef]
3. Shrivastava, N.; Naim, M.J.; Alam, M.J.; Nawaz, F.; Ahmed, S.; Alam, O. Benzimidazole Scaffold as Anticancer Agent: Synthetic Approaches and Structure-Activity Relationship. *Arch. Pharm.* **2017**, *350*, e201700040. [CrossRef]
4. Tahlan, S.; Kumar, S.; Kakkar, S.; Narasimhan, B. Benzimidazole scaffolds as promising antiproliferative agents: A review. *BMC Chem.* **2019**, *13*, 66. [CrossRef]
5. Singla, P.; Luxami, V.; Paul, K. Benzimidazole-biologically attractive scaffold for protein kinase inhibitors. *RSC Adv.* **2014**, *4*, 12422–12440. [CrossRef]
6. Mudi, P.K.; Mahanty, A.K.; Kotakonda, M.; Prasad, S.; Bhattacharyya, S.; Biswas, B. A benzimidazole scaffold as a promising inhibitor against SARS-CoV-2. *J. Biomol. Struct. Dyn.* **2022**, *41*, 1798–1810. [CrossRef] [PubMed]
7. Fuentes-Gutiérrez, A.; Curiel-Quesada, E.; Correa-Basurto, J.; Martínez-Muñoz, A.; Reyes-Arellano, A. N-Heterocycles Scaffolds as Quorum Sensing Inhibitors. Design, Synthesis, Biological and Docking Studies. *Int. J. Mol. Sci.* **2020**, *21*, 9512. [CrossRef]

8. Ramadan, S.K.; Ibrahim, N.A.; El-Kaed, S.A.; El-Helw, E.A.E. New potential fungicides pyrazole-based heterocycles derived from 2-cyano-3-(1,3-diphenyl-1H-pyrazol-4-yl) acryloyl isothiocyanate. *J. Sulfur Chem.* **2021**, *42*, 529–546. [CrossRef]
9. Verma, S.; Kumar, S.; Jain, S.L.; Sain, B. Thiourea dioxide promoted efficient organocatalytic one-pot synthesis of a library of novel heterocyclic compounds. *Org. Biomol. Chem.* **2011**, *9*, 6943–6948. [CrossRef] [PubMed]
10. Merel, S.; Benzing, S.; Gleiser, C.; Di Napoli-Davis, G.; Zwiener, C. Occurrence and overlooked sources of the biocide carbendazim in wastewater and surface water. *Environ. Pollut.* **2018**, *239*, 512–521. [CrossRef]
11. Han, P.; Rios-Miguel, A.B.; Tang, X.; Yu, Y.; Zhou, L.-J.; Hou, L.; Liu, M.; Sun, D.; Jetten, M.S.M.; Welte, C.U.; et al. Benzimidazole fungicide biotransformation by comammox Nitrospira bacteria: Transformation pathways and associated proteomic responses. *J. Hazard. Mater.* **2023**, *445*, 130558. [CrossRef] [PubMed]
12. Chu, B.; Liu, F.; Li, L.; Ding, C.; Chen, K.; Sun, Q.; Shen, Z.; Tan, Y.; Tan, C.; Jiang, Y. A benzimidazole derivative exhibiting antitumor activity blocks EGFR and HER2 activity and upregulates DR5 in breast cancer cells. *Cell Death Dis.* **2015**, *6*, e1686. [CrossRef]
13. Son, D.S.; Lee, E.S.; Adunyah, S.E. The Antitumor Potentials of Benzimidazole Anthelmintics as Repurposing Drugs. *Immune Netw.* **2020**, *20*, e29. [CrossRef]
14. Gaba, M.; Singh, S.; Mohan, C. Benzimidazole: An emerging scaffold for analgesic and anti-inflammatory agents. *Eur. J. Med. Chem.* **2014**, *76*, 494–505. [CrossRef]
15. Ersan, S.; Nacak, S.; Noyanalpan, N.; Yeşilada, E. Studies on analgesic and anti-inflammatory activities of 1-dialkylaminomethyl-2-(p-substituted phenyl)-5-substituted benzimidazole derivatives. *Arzneimittelforschung* **1997**, *47*, 834–836. [PubMed]
16. Ujváry, I.; Christie, R.; Evans-Brown, M.; Gallegos, A.; Jorge, R.; de Morais, J.; Sedefov, R. DARK Classics in Chemical Neuroscience: Etonitazene and Related Benzimidazoles. *ACS Chem. Neurosci.* **2021**, *12*, 1072–1092. [CrossRef] [PubMed]
17. Satija, G.; Sharma, B.; Madan, A.; Iqubal, A.; Shaquiquzzaman, M.; Akhter, M.; Parvez, S.; Khan, M.A.; Alam, M.M. Benzimidazole based derivatives as anticancer agents: Structure activity relationship analysis for various targets. *J. Heterocycl. Chem.* **2022**, *59*, 22–66. [CrossRef]
18. Almalki, A.S.A.; Nazreen, S.; Elbehairi, S.E.I.; Asad, M.; Shati, A.A.; Alfaifi, M.Y.; Alhadhrami, A.; Elhenawy, A.A.; Alorabi, A.Q.; Asiri, A.M.; et al. Design, synthesis, anticancer activity and molecular docking studies of new benzimidazole derivatives bearing 1,3,4-oxadiazole moieties as potential thymidylate synthase inhibitors. *New J. Chem.* **2022**, *46*, 14967–14978. [CrossRef]
19. Hosamani, K.M.; Hiremath, V.B.; Keri, R.S.; Harisha, R.S.; Halligudi, S.B. Synthesis of novel 2-alkyl substituted oleobenzimidazole derivatives using ethylene glycol as solvent. *Can. J. Chem.* **2008**, *86*, 1030–1033. [CrossRef]
20. Hanan, E.J.; Chan, B.K.; Estrada, A.A.; Shore, D.G.; Lyssikatos, J.P. Mild and General One-Pot Reduction and Cyclization of Aromatic and Heteroaromatic 2-Nitroamines to Bicyclic 2H-Imidazoles. *Synlett* **2010**, *2010*, 2759–2764. [CrossRef]
21. Nale, D.B.; Bhanage, B.M. N-Substituted Formamides as C1-Sources for the Synthesis of Benzimidazole and Benzothiazole Derivatives by Using Zinc Catalysts. *Synlett* **2015**, *26*, 2835–2842. [CrossRef]
22. Zhu, X.; Zhang, F.; Kuang, D.; Deng, G.; Yang, Y.; Yu, J.; Liang, Y. K_2S as Sulfur Source and DMSO as Carbon Source for the Synthesis of 2-Unsubstituted Benzothiazoles. *Org. Lett.* **2020**, *22*, 3789–3793. [CrossRef] [PubMed]
23. Mahesh, D.; Sadhu, P.; Punniyamurthy, T. Copper(I)-Catalyzed Regioselective Amination of N-Aryl Imines Using TMSN3 and TBHP: A Route to Substituted Benzimidazoles. *J. Org. Chem.* **2015**, *80*, 1644–1650. [CrossRef]
24. Dadwal, S.; Kumar, M.; Bhalla, V. "Metal-Free" Nanoassemblies of AIEE-ICT-Active Pyrazine Derivative: Efficient Photoredox System for the Synthesis of Benzimidazoles. *J. Org. Chem.* **2020**, *85*, 13906–13919. [CrossRef] [PubMed]
25. Das, K.; Mondal, A.; Srimani, D. Selective Synthesis of 2-Substituted and 1,2-Disubstituted Benzimidazoles Directly from Aromatic Diamines and Alcohols Catalyzed by Molecularly Defined Nonphosphine Manganese(I) Complex. *J. Org. Chem.* **2018**, *83*, 9553–9560. [CrossRef]
26. Caron, S.; Jones, B.P.; Wei, L. Preparation of Substituted Benzimidazoles and Imidazopyridines Using 2,2,2-Trichloroethyl Imidates. *Synthesis* **2012**, *44*, 3049–3054. [CrossRef]
27. Fischer, K.; Marquardt, K.; Schlüter, K.; Gebert, K.; Borschel, E.-M.; Heimann, S.; Kromm, E.; Giesen, V.; Schneider, R.; Lee Wayland, R., Jr. Textile Auxiliaries. In *Ullmann's Encyclopedia of Industrial Chemistry*; Wiley-VCH: Weinheim, Germany, 2011; p. 138.
28. Obtemper, S.I.; Zlobin, V.K. Application of Formamidinesulfinic acid for Separate Spectrophotometric Determination of para Nitrophenol, ortho Nitrophenol and meta Nitrophenol in their Mutual Presence. *Zh. Anal. Khim.* **1974**, *29*, 609–611.
29. Obtemper, S.I.; Zlobin, V.K. Use of Thiourea Dioxide in Organic-Analysis-Determination of Nitric-Acid Esters, Nitroso and Azo-Compounds. *Vestn. MGU. Khimia* **1974**, *15*, 247–249.
30. Koniecki, W.B.; Linch, A.L. Determination of Aromatic Nitro Compounds. *Anal. Chem.* **1958**, *30*, 1134–1137. [CrossRef]
31. de Barry Barnett, E. VII—The action of hydrogen dioxide on thiocarbamides. *J. Chem. Soc. Trans.* **1910**, *97*, 63–65. [CrossRef]
32. De Filippo, D.; Ponticelli, G.; Trogu, E.F.; Lai, A. Spectrochemical study of aminoiminomethanesulphinic acid and related NN′-substituted derivatives. *J. Chem. Soc. Perkin Trans. II* **1972**, *11*, 1500–1502. [CrossRef]
33. Havel, J.J.; Kluttz, R.Q. A Synthesis of Formamidinesulfinic Acids and Formamidines. *Synth. Comm.* **1974**, *4*, 389–393. [CrossRef]
34. Dictionary. In *Gardner's Commercially Important Chemicals*; Wiley-Interscience: Hoboken, NJ, USA, 2005; pp. 2–682.
35. Pu, S.; Liang, Q.; Luo, X.; Luo, J. Convenient Two-step One-pot Synthesis of Benzimidazoles Using 2-nitroanilines and Thiourea Dioxide. *J. Chem. Res.* **2014**, *38*, 118–120. [CrossRef]

36. Hamad, M.O.; Kiptoo, P.K.; Stinchcomb, A.L.; Crooks, P.A. Synthesis and hydrolytic behavior of two novel tripartate codrugs of naltrexone and 6β-naltrexol with hydroxybupropion as potential alcohol abuse and smoking cessation agents. *Bioorg. Med. Chem.* **2006**, *14*, 7051–7061. [CrossRef] [PubMed]
37. Chaudhary, P.; Gupta, S.; Sureshbabu, P.; Sabiah, S.; Kandasamy, J. A metal free reduction of aryl-N-nitrosamines to the corresponding hydrazines using a sustainable reductant thiourea dioxide. *Green Chem.* **2016**, *18*, 6215–6221. [CrossRef]
38. Chatterjie, N.; Umans, J.G.; Inturrisi, C.E. Reduction of 6-ketones of the morphine series with formamidinesulfinic acid. Stereoselectivity opposite to that of hydride reductions. *J. Org. Chem.* **1976**, *41*, 3624–3625. [CrossRef] [PubMed]
39. Svarovsky, S.A.; Simoyi, R.H.; Makarov, S.V. Reactive oxygen species in aerobic decomposition of thiourea dioxides. *J. Chem. Soc. Dalton Trans.* **2000**, 511–514. [CrossRef]
40. He, F.-S.; Yang, M.; Ye, S.; Wu, J. Sulfonylation from sodium dithionite or thiourea dioxide. *Chin. Chem. Lett.* **2021**, *32*, 461–464. [CrossRef]
41. Verma, S.; Singh, R.; Tripathi, D.; Gupta, P.; Bahuguna, G.M.; Jain, S.L. Thiourea dioxide with TBHP: A fruitful and greener recipe for the catalytic oxidation of alcohols. *RSC Adv.* **2013**, *3*, 4184–4188. [CrossRef]
42. Zhou, L.H.; Jin, Y.J.; Ma, L.F.; Huang, W.H.; Wu, Y. Highly Efficient and Catalyst-Free Synthesis of Benzimidazoles in Aqueous Media. *Russ. J. Org. Chem.* **2021**, *57*, 825–830. [CrossRef]
43. Kahl, T.; Schröder, K.-W.; Lawrence, F.R.; Marshall, W.J.; Höke, H.; Jäckh, R. Aniline. In *Ullmann's Encyclopedia of Industrial Chemistry*; Wiley-VCH: Weinheim, Germany, 2000; p. 465.
44. Available online: https://archive.vn/20020219104231/http://www.the-innovation-group.com/ChemProfiles/Aniline.htm (accessed on 30 January 2023).
45. Formenti, D.; Ferretti, F.; Scharnagl, F.K.; Beller, M. Reduction of Nitro Compounds Using 3d-Non-Noble Metal Catalysts. *Chem. Rev.* **2019**, *119*, 2611–2680. [CrossRef] [PubMed]
46. Zhang, Q.; Bu, J.; Wang, J.; Sun, C.; Zhao, D.; Sheng, G.; Xie, X.; Sun, M.; Yu, L. Highly Efficient Hydrogenation of Nitrobenzene to Aniline over Pt/CeO2 Catalysts: The Shape Effect of the Support and Key Role of Additional Ce3+ Sites. *ACS Catal.* **2020**, *10*, 10350–10363. [CrossRef]
47. Liu, Y.; Lu, Y.; Prashad, M.; Repič, O.; Blacklock, T.J. A Practical and Chemoselective Reduction of Nitroarenes to Anilines Using Activated Iron. *Adv. Synth. Catal.* **2005**, *347*, 217–219. [CrossRef]
48. Anjali, K.; Ahmed, M.; Christopher, J.; Sakthivel, A. Rhodium-calix[4]pyrrole and rhodium-tetraphenyl porphyrin: Preparation, surface grafting and their catalytic application in nitro-benzene reduction. *Dalton Trans.* **2018**, *47*, 12353–12361. [CrossRef]
49. Srilakshmi, C.; Saraf, R.; Prashanth, V.; Rao, G.M.; Shivakumara, C. Structure and Catalytic Activity of Cr-Doped BaTiO3 Nanocatalysts Synthesized by Conventional Oxalate and Microwave Assisted Hydrothermal Methods. *Inorg. Chem.* **2016**, *55*, 4795–4805. [CrossRef]
50. Mondal, P.; Purkait, M.K. Green synthesized iron nanoparticle-embedded pH-responsive PVDF-co-HFP membranes: Optimization study for NPs preparation and nitrobenzene reduction. *Sep. Sci. Technol.* **2017**, *52*, 2338–2355. [CrossRef]
51. Leng, F.; Gerber, I.C.; Lecante, P.; Moldovan, S.; Girleanu, M.; Axet, M.R.; Serp, P. Controlled and Chemoselective Hydrogenation of Nitrobenzene over Ru@C60 Catalysts. *ACS Catal.* **2016**, *6*, 6018–6024. [CrossRef]
52. Xiong, W.; Zhou, S.; Zhao, Z.; Hao, F.; Cai, Z.; Liu, P.; Zhang, H.; Luo, H. Highly uniform Ni particles with phosphorus and adjacent defects catalyze 1,5-dinitronaphthalene hydrogenation with excellent catalytic performance. *Front. Chem. Sci. Eng.* **2021**, *15*, 998–1007. [CrossRef]
53. Gong, W.; Lin, Y.; Chen, C.; Al-Mamun, M.; Lu, H.-S.; Wang, G.; Zhang, H.; Zhao, H. Nitrogen-Doped Carbon Nanotube Confined Co–Nx Sites for Selective Hydrogenation of Biomass-Derived Compounds. *Adv. Mater.* **2019**, *31*, 1808341. [CrossRef] [PubMed]
54. Lu, X.; Chen, Y.; Zhao, Z.; Deng, H.; Zhou, D.; Wei, C.; Nie, R.; Xia, Q. Highly selective one-step hydrogenation of nitrobenzene to cyclohexylamine over the supported 10% Ni/carbon catalysts doped with 3‰ Rh. *RSC Adv.* **2016**, *6*, 15354–15361. [CrossRef]
55. Diao, S.; Qian, W.; Luo, G.; Wei, F.; Wang, Y. Gaseous catalytic hydrogenation of nitrobenzene to aniline in a two-stage fluidized bed reactor. *Appl. Catal. A Gen.* **2005**, *286*, 30–35. [CrossRef]
56. Krishnan, S.; Patel, P.N.; Balasubramanian, K.K.; Chadha, A. Yeast supported gold nanoparticles: An efficient catalyst for the synthesis of commercially important aryl amines. *New J. Chem.* **2021**, *45*, 1915–1923. [CrossRef]
57. Daems, N.; Wouters, J.; Van Goethem, C.; Baert, K.; Poleunis, C.; Delcorte, A.; Hubin, A.; Vankelecom, I.F.J.; Pescarmona, P.P. Selective reduction of nitrobenzene to aniline over electrocatalysts based on nitrogen-doped carbons containing non-noble metals. *Appl. Catal. B Environ.* **2018**, *226*, 509–522. [CrossRef]
58. Niknam, T.; Bornapour, M.; Gheisari, A.; Bahmani-Firouzi, B. Impact of heat, power and hydrogen generation on optimal placement and operation of fuel cell power plants. *Int. J. Hydrogen Energy* **2013**, *38*, 1111–1127. [CrossRef]
59. Sheng, X.; Wouters, B.; Breugelmans, T.; Hubin, A.; Vankelecom, I.F.J.; Pescarmona, P.P. Cu/CuxO and Pt nanoparticles supported on multi-walled carbon nanotubes as electrocatalysts for the reduction of nitrobenzene. *Appl. Catal. B Environ.* **2014**, *147*, 330–339. [CrossRef]
60. Sheng, X.; Wouters, B.; Breugelmans, T.; Hubin, A.; Vankelecom, I.F.J.; Pescarmona, P.P. Pure and Alloyed Copper-Based Nanoparticles Supported on Activated Carbon: Synthesis and Electrocatalytic Application in the Reduction of Nitrobenzene. *ChemElectroChem* **2014**, *1*, 1198–1210. [CrossRef]

61. Zhang, T.; Xie, Z.; Jiang, L.; Zhao, W.; Cao, S.; Wang, B.; Si, R.; Zhang, R.; Liu, Y.; Zhao, Z. Selective transfer hydrogenation coupling of nitroaromatics to azoxy/azo compounds by electron-enriched single Ni-N4 sites on mesoporous N-doped carbon. *Chem. Eng. J.* **2022**, *443*, 136416. [CrossRef]
62. Zhang, M.; Liu, J.; Yang, B.; Ma, L.; Wang, N.; Wei, X. Facile Synthesis of a Novel Heterogeneous Rh/COF Catalyst and Its Application in Tandem Selective Transfer Hydrogenation and Monomethylation of Nitro Compounds with Methanol. *Ind. Eng. Chem. Res.* **2022**, *61*, 1066–1077. [CrossRef]
63. Moran, M.J.; Martina, K.; Baricco, F.; Tagliapietra, S.; Manzoli, M.; Cravotto, G. Tuneable Copper Catalysed Transfer Hydrogenation of Nitrobenzenes to Aniline or Azo Derivatives. *Adv. Synth. Catal.* **2020**, *362*, 2689–2700. [CrossRef]
64. Xu, D.; Liu, R.; Li, J.; Zhao, H.; Ma, J.; Dong, Z. Atomically dispersed Co-N4 sites anchored on N-doped carbon for aqueous phase transfer hydrogenation between nitroarenes and saturated N-heterocycles. *Appl. Catal. B Environ.* **2021**, *299*, 120681. [CrossRef]
65. Dai, X.; Cui, X.; Yuan, H.; Deng, Y.; Shi, F. Cooperative transformation of nitroarenes and biomass-based alcohols catalyzed by CuNiAlOx. *RSC Adv.* **2015**, *5*, 7970–7975. [CrossRef]
66. Liu, H.; Khuan Chuah, G.; Jaenicke, S. Alumina-entrapped Ag catalyzed nitro compounds coupled with alcohols using borrowing hydrogen methodology. *Phys. Chem. Chem. Phys.* **2015**, *17*, 15012–15018. [CrossRef] [PubMed]
67. Wei, R.P.; Shi, F. Controllable synthesis of azoxybenzenes and anilines with alcohol as the reducing agent promoted by KOH. *Synth. Commun.* **2019**, *49*, 688–696. [CrossRef]
68. Bigelow, H.E.; Robinson, D.B. AZOBENZENE. *Org. Synth.* **1942**, *22*, 28. [CrossRef]
69. Srilakshmi, C.; Vijay Kumar, H.; Praveena, K.; Shivakumara, C.; Muralidhar Nayak, M. A highly efficient iron doped BaTiO3 nanocatalyst for the catalytic reduction of nitrobenzene to azoxybenzene. *RSC Adv.* **2014**, *4*, 18881–18884. [CrossRef]
70. Mateti, S.; Mathesh, M.; Liu, Z.; Tao, T.; Ramireddy, T.; Glushenkov, A.M.; Yang, W.; Chen, Y.I. Mechanochemistry: A force in disguise and conditional effects towards chemical reactions. *Chem. Comm.* **2021**, *57*, 1080–1092. [CrossRef]
71. Cuccu, F.; De Luca, L.; Delogu, F.; Colacino, E.; Solin, N.; Mocci, R.; Porcheddu, A. Mechanochemistry: New Tools to Navigate the Uncharted Territory of "Impossible" Reactions. *ChemSusChem* **2022**, *15*, e202200362. [CrossRef]
72. Achar, T.K.; Bose, A.; Mal, P. Mechanochemical synthesis of small organic molecules. *Beilstein J. Org. Chem.* **2017**, *13*, 1907–1931. [CrossRef]
73. Bose, A.; Mal, P. Mechanochemistry of supramolecules. *Beilstein J. Org. Chem.* **2019**, *15*, 881–900. [CrossRef]
74. Shearouse, W.C.; Korte, C.M.; Mack, J. A two-step ball milling method synthesizes and purifies α,β-unsaturated esters. *Green Chem.* **2011**, *13*, 598–601. [CrossRef]
75. Do, J.-L.; Mottillo, C.; Tan, D.; Štrukil, V.; Friščić, T. Mechanochemical Ruthenium-Catalyzed Olefin Metathesis. *J. Am. Chem. Soc.* **2015**, *137*, 2476–2479. [CrossRef] [PubMed]
76. Hermann, G.N.; Bolm, C. Mechanochemical Rhodium(III)-Catalyzed C–H Bond Amidation of Arenes with Dioxazolones under Solventless Conditions in a Ball Mill. *ACS Catal.* **2017**, *7*, 4592–4596. [CrossRef]
77. Nakagawa, K.; Mineo, S.; Kawamura, S.; Minami, K. Reduction of Organic Compounds with Thiourea Dioxide. II Reduction of Aromatic Nitro Compounds and Synthesis of Hydrazo Compounds. *Yakugaku Zasshi* **1977**, *97*, 1253–1256. [CrossRef]
78. Huang, S.-L.; Chen, T.-Y. Reduction of Organic Compounds with Thiourea Dioxide II. The Reduction of Organic Nitrogen Compounds. *J. Chin. Chem. Soc.* **1975**, *22*, 91–94. [CrossRef]
79. Do, J.-L.; Friščić, T. Mechanochemistry: A Force of Synthesis. *ACS Cent. Sci.* **2017**, *3*, 13–19. [CrossRef]
80. Friščić, T.; Childs, S.L.; Rizvi, S.A.A.; Jones, W. The role of solvent in mechanochemical and sonochemical cocrystal formation: A solubility-based approach for predicting cocrystallisation outcome. *CrystEngComm* **2009**, *11*, 418–426. [CrossRef]
81. Tan, D.; García, F. Main group mechanochemistry: From curiosity to established protocols. *Chem. Soc. Rev.* **2019**, *48*, 2274–2292. [CrossRef]
82. Howard, J.L.; Cao, Q.; Browne, D.L. Mechanochemistry as an emerging tool for molecular synthesis: What can it offer? *Chem. Sci.* **2018**, *9*, 3080–3094. [CrossRef]
83. Howard, J.L.; Brand, M.C.; Browne, D.L. Switching chemoselectivity: Using mechanochemistry to alter reaction kinetics. *Ang. Chem.* **2018**, *130*, 16336–16340. [CrossRef]
84. Lewis, D.; Mama, J.; Hawkes, J. An Investigation into the Structure and Chemical Properties of Formamidine Sulfinic Acid. *Appl. Spectrosc.* **2014**, *68*, 1327–1332. [CrossRef]
85. Zhou, D.-C.; Lu, Y.-T.; Mai, Y.-W.; Zhang, C.; Xia, J.; Yao, P.-F.; Wang, H.-G.; Huang, S.-L.; Huang, Z.-S. Design, synthesis and biological evaluation of novel perimidine o-quinone derivatives as non-intercalative topoisomerase II catalytic inhibitors. *Bioorg. Chem.* **2019**, *91*, 103131. [CrossRef] [PubMed]
86. Dymińska, L. Imidazopyridines as a source of biological activity and their pharmacological potentials—Infrared and Raman spectroscopic evidence of their content in pharmaceuticals and plant materials. *Bioorg. Med. Chem.* **2015**, *23*, 6087–6099. [CrossRef]
87. Scribner, A.; Dennis, R.; Hong, J.; Lee, S.; McIntyre, D.; Perrey, D.; Feng, D.; Fisher, M.; Wyvratt, M.; Leavitt, P.; et al. Synthesis and biological activity of imidazopyridine anticoccidial agents: Part I. *Eur. J. Med. Chem.* **2007**, *42*, 1334–1357. [CrossRef]
88. Makarov, S.V.; Sal'nikov, D.S.; Pogorelova, A.S. Acid-base properties and stability of sulfoxylic acid in aqueous solutions. *Russ. J. Inorg. Chem.* **2010**, *55*, 301–304. [CrossRef]
89. Büeseken, J. Étude sur les Oxydes de Thiourée, I. Sur le dioxyde de thiourée. *Recl. Trav. Chim. Pays-Bas* **1936**, *55*, 1040–1043. [CrossRef]

90. Sullivan, R.A.L.; Hargreaves, A. The crystal and molecular structure of thiourea dioxide. *Acta Crystallogr.* **1962**, *15*, 675–682. [CrossRef]
91. Kis, Z.; Makarov, S.V.; Silaghi-Dumitrescu, R. Computational investigations on the electronic structure and reactivity of thiourea dioxide: Sulfoxylate formation, tautomerism and dioxygen liberation. *J. Sulfur Chem.* **2010**, *31*, 27–39. [CrossRef]
92. Grady, B.J.; Dittmer, D.C. Reaction of perfluoroaryl halides with reduced species of sulfur dioxide (HSO_2^-, SO_2^{2-}, $S_2O_4^{2-}$). *J. Fluor. Chem.* **1990**, *50*, 151–172. [CrossRef]
93. Krug, P. Thiourea Dioxide (Formamidinesulphinic Acid) A New Reducing Agent for Textile Printing. *J. Soc. Dye.* **1953**, *69*, 606–611. [CrossRef]
94. Makarov, S.V.; Horváth, A.K.; Silaghi-Dumitrescu, R.; Gao, Q. Recent Developments in the Chemistry of Thiourea Oxides. *Chem. Eur. J.* **2014**, *20*, 14164–14176. [CrossRef] [PubMed]
95. Johnstone, H.F.; Mattern, J.A.; Fernelius, W.C. Sulfites and Pyrosulfites of the Alkali Metals. *Inorg. Synth.* **1946**, *2*, 162–167. [CrossRef]
96. Miller, A.E.; Bischoff, J.J.; Pae, K. Chemistry of aminoiminomethanesulfinic and-sulfonic acids related to the toxicity of thioureas. *Chem. Res. Toxicol.* **1988**, *1*, 169–174. [CrossRef]
97. Surasani, S.R.; Maity, S. Deciphering Intermediates and Additives Effect on the Reduction of Nitrobenzene by SmI_2. *ChemistrySelect* **2017**, *2*, 598–603. [CrossRef]
98. Böeseken, J. Etude sur les Oxydes de Thiouree. IV. *Recl. Trav. Chim. Pays-Bas* **1948**, *67*, 603–621. [CrossRef]
99. Knopp, C. Zur verwendung von aminoiminomethanesulfinsaure ais antioxidans. *Sci. Pharm.* **1983**, *51*, 283–290.
100. Brown, D. A new synthesis of formamidine. *J. Appl. Chem.* **1952**, *2*, 202–203. [CrossRef]
101. Dunitz, J.D. The structure of sodium dithionite and the nature of the dithionite ion. *Acta Crystallogr.* **1956**, *9*, 579–586. [CrossRef]
102. Hartwig, U.; Pritzkow, H.; Rall, K.; Sundermeyer, W. Bis (trifluoromethyl) sulfene $(CF_3)_2C\ SO_2$, Isolated as Adduct. *Angew. Chem. Int. Ed. Engl.* **1989**, *28*, 221–223. [CrossRef]
103. Weber, H.P.; Craven, B.M. Structure and charge density of the 1: 1 complex of thiourea with parabanic acid at 298 K. *Acta Crystallogr. B Struct. Sci.* **1987**, *43*, 202–209. [CrossRef]
104. Wang, Y.; Chang, N.L.; Pai, C.T. Charge density study of thiourea S, S-dioxide. *Inorg. Chem.* **1990**, *29*, 3256–3259. [CrossRef]
105. Singh, P.K.; Silakari, O. Benzimidazole: Journey from Single Targeting to Multitargeting Molecule. In *Key Heterocycle Cores for Designing Multitargeting Molecules*; Elsevier: Amsterdam, The Netherlands, 2018; pp. 31–52.
106. Wang, S.; Gao, Q.; Wang, J. Thermodynamic analysis of decomposition of thiourea and thiourea oxides. *J. Phys. Chem. B* **2005**, *109*, 17281–17289. [CrossRef] [PubMed]
107. Jiang, S.; Dong, X.; Qiu, Y.; Chen, D.; Wu, X.; Jiang, S. A new ligand for copper-catalyzed amination of aryl halides to primary(hetero)aryl amines. *Tetrahedron Lett.* **2020**, *61*, 151683. [CrossRef]
108. Panja, S.; Kundu, D.; Ahammed, S.; Ranu, B.C. Highly chemoselective reduction of azides to amines by Fe(0) nanoparticles in water at room temperature. *Tetrahedron Lett.* **2017**, *58*, 3457–3460. [CrossRef]
109. Liao, B.-S.; Liu, S.-T. Diamination of Phenylene Dihalides Catalyzed by a Dicopper Complex. *J. Org. Chem.* **2012**, *77*, 6653–6656. [CrossRef]
110. Mo, C.; Zhang, Z.; Guise, C.P.; Li, X.; Luo, J.; Tu, Z.; Xu, Y.; Patterson, A.V.; Smaill, J.B.; Ren, X.; et al. 2-Aminopyrimidine Derivatives as New Selective Fibroblast Growth Factor Receptor 4 (FGFR4) Inhibitors. *ACS Med. Chem. Lett.* **2017**, *8*, 543–548. [CrossRef]
111. Sorribes, I.; Liu, L.; Corma, A. Nanolayered Co–Mo–S Catalysts for the Chemoselective Hydrogenation of Nitroarenes. *ACS Catal.* **2017**, *7*, 2698–2708. [CrossRef]
112. Romero, A.H.; Cerecetto, H.A. Common, Facile and Eco-Friendly Method for the Reduction of Nitroarenes, Selective Reduction of Poly-Nitroarenes and Deoxygenation of N-Oxide Containing Heteroarenes Using Elemental Sulfur. *Eur. J. Org. Chem.* **2020**, *2020*, 1853–1865. [CrossRef]
113. Zhang, Y.-C.; Shen, Q.; Zhu, M.-W.; Wang, J.; Du, Y.; Wu, J.; Li, J.-X. Modified Quinoxaline-Fused Oleanolic Acid Derivatives as Inhibitors of Osteoclastogenesis and Potential Agent in Anti-Osteoporosis. *ChemistrySelect* **2020**, *5*, 1526–1533. [CrossRef]
114. Ji, A.; Ren, W.; Ai, H.-w. A highly efficient oxidative condensation reaction for selective protein conjugation. *Chem. Comm.* **2014**, *50*, 7469–7472. [CrossRef]
115. Chaudhary, P.; Gupta, S.; Muniyappan, N.; Sabiah, S.; Kandasamy, J. Regioselective Nitration of N-Alkyl Anilines using tert-Butyl Nitrite under Mild Condition. *J. Org. Chem.* **2019**, *84*, 104–119. [CrossRef]
116. Penieres-Carrillo, J.-G.; Ríos-Guerra, H.; Pérez-Flores, J.; Rodríguez-Molina, B.; Torres-Reyes, Á.; Barrera-Téllez, F.; González-Carrillo, J.; Moreno-González, L.; Martínez-Zaldívar, A.; Nolasco-Fidencio, J.-J.; et al. Reevaluating the synthesis of 2,5-disubstituted-1H-benzimidazole derivatives by different green activation techniques and their biological activity as antifungal and antimicrobial inhibitor. *J. Heterocycl. Chem.* **2020**, *57*, 436–455. [CrossRef]
117. Zhang, Z.; Sun, Q.; Xia, C.; Sun, W. CO2 as a C1 Source: B(C6F5)3-Catalyzed Cyclization of o-Phenylene-diamines To Construct Benzimidazoles in the Presence of Hydrosilane. *Org. Lett.* **2016**, *18*, 6316–6319. [CrossRef] [PubMed]
118. Yu, B.; Zhang, H.; Zhao, Y.; Chen, S.; Xu, J.; Huang, C.; Liu, Z. Cyclization of o-phenylenediamines by CO_2 in the presence of H2 for the synthesis of benzimidazoles. *Green Chem.* **2013**, *15*, 95–99. [CrossRef]
119. Graham, T.H. Deprotection of N-benzylbenzimidazoles and N-benzylimidazoles with triethylsilane and Pd/C. *Tetrahedron Lett.* **2015**, *56*, 2688–2690. [CrossRef]

120. Zhu, K.; Hao, J.-H.; Zhang, C.-P.; Zhang, J.; Feng, Y.; Qin, H.-L. Diversified facile synthesis of benzimidazoles, quinazolin-4(3H)-ones and 1,4-benzodiazepine-2,5-diones via palladium-catalyzed transfer hydrogenation/condensation cascade of nitro arenes under microwave irradiation. *RSC Adv.* **2015**, *5*, 11132–11135. [CrossRef]
121. Xu, L.-L.; Zhu, J.-F.; Xu, X.-L.; Zhu, J.; Li, L.; Xi, M.-Y.; Jiang, Z.-Y.; Zhang, M.-Y.; Liu, F.; Lu, M.-c.; et al. Discovery and Modification of in Vivo Active Nrf2 Activators with 1,2,4-Oxadiazole Core: Hits Identification and Structure–Activity Relationship Study. *J. Med. Chem.* **2015**, *58*, 5419–5436. [CrossRef]
122. Aziz, J.; Baladi, T.; Piguel, S. Direct Alkynylation of 3H-Imidazo[4,5-b]pyridines Using gem-Dibromoalkenes as Alkynes Source. *J. Org. Chem.* **2016**, *81*, 4122–4133. [CrossRef]
123. Gahlon, H.L.; Schweizer, W.B.; Sturla, S.J. Tolerance of Base Pair Size and Shape in Postlesion DNA Synthesis. *J. Am. Chem. Soc.* **2013**, *135*, 6384–6387. [CrossRef]
124. Common Solvents Properties. Available online: https://macro.lsu.edu/howto/solvents/Dichloromethane.htm (accessed on 30 January 2023).

molecules

MDPI

Article

Total Synthesis of Hemerocallisamine I Paved by Gram-Scale Synthesis of (2*S*,4*S*)-4-Hydroxyglutamic Acid Lactone

Lucia Pinčeková [1], Eva Jančiová [1], Dušan Berkeš [1], Róbert Gyepes [2], Andrej Kolarovič [3] and Oľga Caletková [1,*]

[1] Institute of Organic Chemistry, Catalysis and Petrochemistry, Slovak University of Technology, Radlinského 9, 812 37 Bratislava, Slovakia
[2] Department of Inorganic Chemistry, Faculty of Science, Charles University, Hlavova 2030, 128 40 Prague, Czech Republic
[3] Department of Chemistry, Faculty of Education, Trnava University, Priemyselná 4, 918 43 Trnava, Slovakia
* Correspondence: olga.caletkova@stuba.sk

Abstract: Total synthesis of the 2-formylpyrrole alkaloid hemerocallisamine I is presented, both in racemic and enantiopure form. Our synthetic strategy involves (2*S*,4*S*)-4-hydroxyglutamic acid lactone as the key intermediate. Starting from an achiral substrate, the target stereogenic centers were introduced by means of crystallization-induced diastereomer transformation (CIDT) in a highly stereoselective fashion. A Maillard-type condensation was crucial to constructing the desired pyrrolic scaffold.

Keywords: pyrrole; alkaloid; Maillard reaction; crystallization-induced diastereomer transformation; glutamine; hydroxy amino acid; diketopiperazine

Citation: Pinčeková, L.; Jančiová, E.; Berkeš, D.; Gyepes, R.; Kolarovič, A.; Caletková, O. Total Synthesis of Hemerocallisamine I Paved by Gram-Scale Synthesis of (2*S*,4*S*)-4-Hydroxyglutamic Acid Lactone. *Molecules* **2023**, *28*, 2177. https://doi.org/10.3390/molecules28052177

Academic Editors: Alexey M. Starosotnikov, Maxim A. Bastrakov and Igor L. Dalinger

Received: 9 February 2023
Revised: 24 February 2023
Accepted: 24 February 2023
Published: 26 February 2023

1. Introduction

Daylilies (genus *Hemerocallis*) are beautiful flowering plants, now counting 16 species and over 98,000 cultivars, widely domesticated in much of the Northern Hemisphere [1,2]. Mentioned in poems compiled by Confucius more than 2500 years ago, in addition to ornamental function, they have a long history of culinary [3] and medicinal use in Eastern Asia. The flowers, buds, leaves, and roots of daylilies are edible and have been reported to be utilized, e.g., in the treatment of sleep disorders, depression, inflammation, jaundice, schistosomiasis, and chronic rheumatism [4]. In an attempt to elucidate the structures of the active ingredients, the chemical constitution of daylilies has been investigated in a number of studies. As of 31 December 2020, a total of 266 secondary metabolites have been identified in *Hemerocallis* plants, primarily focusing on species *H. citrina*, *H. fulva*, and *H. minor* [4,5].

In a search to identify sedative amino acid derivatives from *H. fulva* flower buds, in 2014, Matsuda et al. isolated hemerocallisamine I (**1**) as a novel 4-hydroxyglutamine metabolite [6] (Figure 1). The initially assigned (2*R*,4*R*)-**1** configuration, on the basis of the Flack parameter, corresponded to the unnatural D-glutamine and was puzzling. Three years later, the first total synthesis of hemerocallisamine I (**1**) was reported by Brimble et al. and resulted in a revision of the previously proposed absolute configuration from (2*R*,4*R*)-**1** to (2*S*,4*S*)-**1 [7]**. Until now, no other total synthesis of hemerocallisamine I (**1**) has been communicated.

The structure of hemerocallisamine I (**1**) features a 4-hydroxyglutamine moiety anchored in a 2-formylpyrrole ring (Figure 1). Both of these subunits are abundant in nature and of synthetic interest [8–10]. In addition to hemerocallisamine I (**1**), several other 4-hydroxyglutamine derivatives, e.g., longitubanine A, oxypinnatanine, and pinnatanine (Figure 1), as well as their *N*-glycosides, have been isolated directly from *H. fulva*

species [11–13]. Interestingly, the findings of Ogawa and coworkers indicate that oxypinnatanine might be the compound responsible for the sleep-promoting effect of *H. fulva* [14,15].

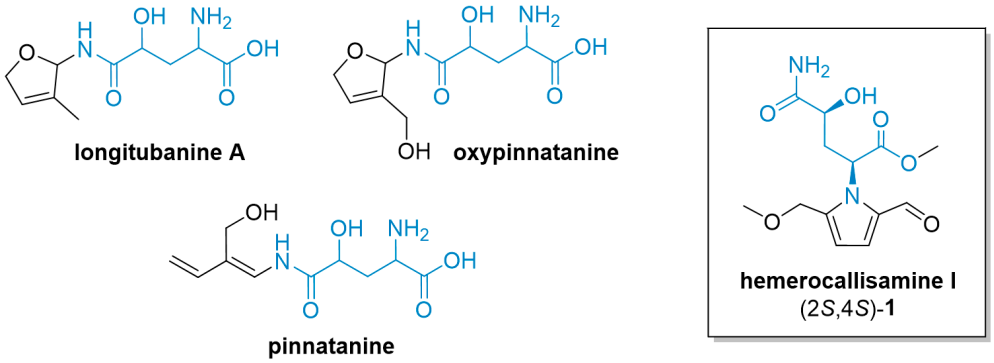

Figure 1. Structures of 4-hydroxyglutamine derivatives isolated from daylily *Hemerocallis fulva*.

With the aim of smoothly constructing the 4-hydroxyglutamine framework, the published synthesis of (2*S*,4*S*)-**1** started with commercially available *cis*-4-hydroxy-L-proline (**2**) to deliver amine **3** in 48% yield over 7 steps [7] (Scheme 1A). The critical step, Maillard-type condensation with dihydropyranone **4**, provided the functionalized pyrrole (2*S*,4*S*)-**5** only in a moderate yield of 37%. After the final deprotections and selective *O*-methylation, an 11-step synthesis of hemerocallisamine I (**1**) was successfully concluded with an 11.7% overall yield.

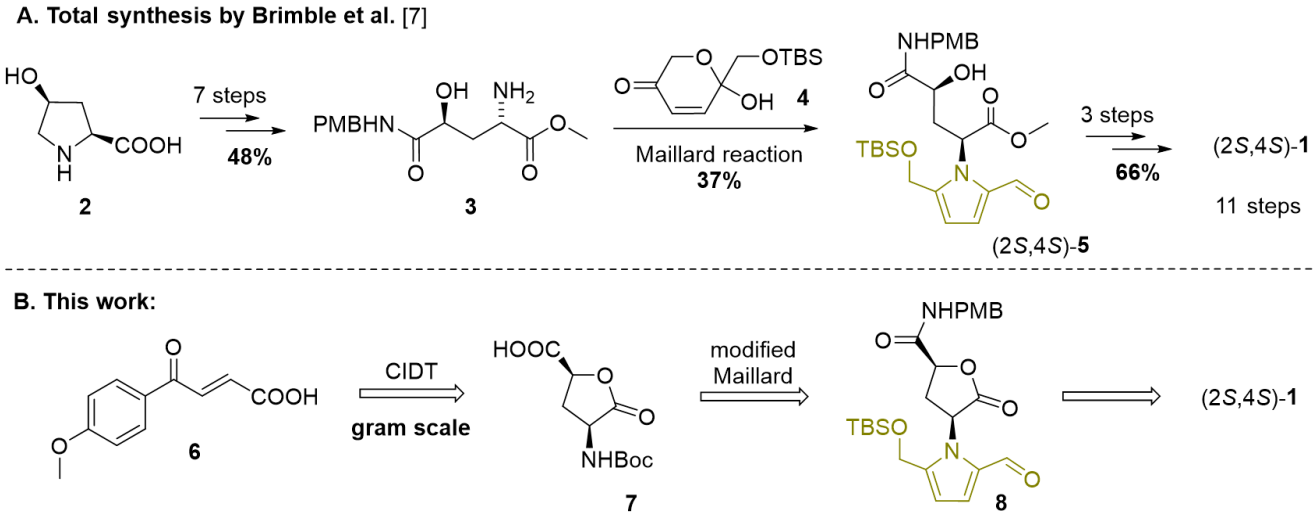

Scheme 1. (**A**) The first total synthesis of hemerocallisamine I (**1**), featuring Maillard-type condensation as the key step. (**B**) Our alternative synthetic approach to hemerocallisamine I (**1**). PMB = *p*-methoxybenzyl, TBS = *tert*-butyldimethylsilyl, Boc = *tert*-butyloxycarbonyl.

Herein we describe an alternative synthetic access to hemerocallisamine I (**1**), starting from the achiral substrate **6** (Scheme 1B). Given the importance of the 4-hydroxyglutamic motif in the chemistry of daylilies, we opted for facile stereoselective access to lactone **7** as a key intermediate.

2. Results and Discussion

Along with procedures employing *trans*- and *cis*-4-hydroxy-L-proline derivatives [16–18], utilized by Brimble et al. (Scheme 1A), synthetic strategies leading to non-racemic 4-hydroxyglutamic acids include enzymatic [19] and classic resolution [20], C4-hydroxylations of L-glutamic substrates [21–23], and cycloadditions [24,25]. Since the number of synthetic

methods available for the preparation of enantiopure 4-hydroxyglutamates is rather limited [26], we wished to develop a new, scalable, and configurationally flexible protocol based on crystallization-induced diastereomer transformations (CIDT) [27].

2.1. Synthesis of (±)-hemerocallisamine I and Optimization of the Maillard Reaction Step

Considering that the synthesis of racemic hemerocallisamine I remains undescribed and that this material might be of value, e.g., for biological activity investigation, our synthetic approach was first evaluated in its achiral variant.

The studies commenced with a routine construction of amino acid **9** by means of aza-Michael addition (Scheme 2). Shortly after mixing an excess of aq. NH_3 with aroylacrylic substrate **6** in MeOH, adduct **9** started to precipitate out of the reaction mixture and was filtered off in 77% yield. A consequent reduction step delivered a diastereomeric mixture of the corresponding γ-aryl-γ-hydroxy-α-amino acids, in a ratio *ca* 2:1. However, our one-pot CIDT protocol exploited configurational lability of the benzylic γ-hydroxy group in dilute aqueous HCl [28,29] and provided crystalline *cis*-lactone salt rac-**10**·HCl and then free amine rac-**10** in excellent diastereomeric purity (>99:1 dr). After its *N*-Boc protection, the adjacent electron-rich anisole ring was oxidatively cleaved employing a catalytic amount of in situ prepared RuO_4, with $NaIO_4$ as a reoxidant [30,31]. Our modified procedure furnished the 4-hydroxyglutamic acid lactone rac-**7** in 71% yield, over two steps. When approaching the critical Maillard reaction step, we were inspired by the studies of Brimble et al. [7] and chose to introduce the *p*-methoxybenzyl (PMB) protected amide group. The coupling with $PMBNH_2$ was mediated by ethyl chloroformate and a subsequent Boc-removal provided amine rac-**11** as a synthetic alternative to amine **3** (Scheme 1A). Pleasingly, each of the steps in the **6**–**11** sequence delivered crystalline compounds and are convenient to purify, isolate, and store.

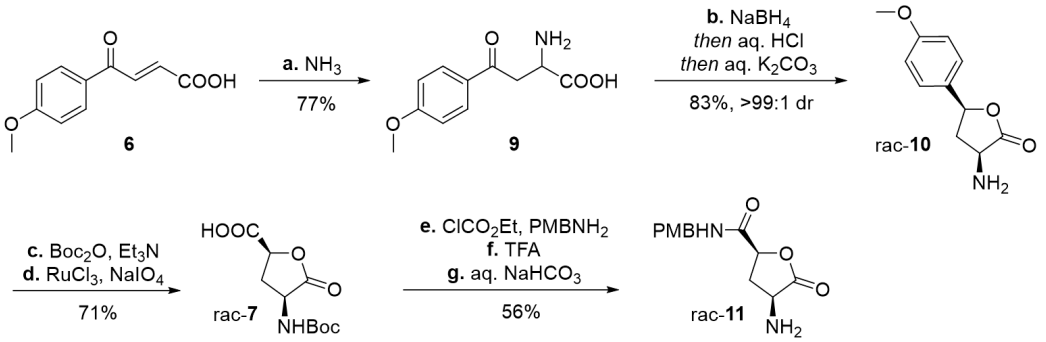

Scheme 2. Preparation of lactone rac-**11**. Reagents and conditions: (**a**) 25–27% aq. NH_3 (*ca* 4.5 equiv), MeOH, rt, 16 h; (**b**) $NaBH_4$ (3.5 equiv), MeOH/H_2O 5:1, rt, 90 min; then conc. HCl/H_2O 1:2, rt, 4 h; then 10% aq. K_2CO_3/H_2O 5:4; (**c**) Boc_2O (1.1 equiv), Et_3N (2.2 equiv), THF, rt, 4 h (94%); (**d**) 6 mol% $RuCl_3$, $NaIO_4$ (19.4 equiv), H_2O/MeCN/AcOEt 3:1:1, 10 °C → rt, 3 h (75%); (**e**) $ClCO_2Et$ (2.0 equiv), Et_3N (2.5 equiv), dry THF, 15 min, 0 °C; then $PMBNH_2$ (2.7 equiv), 0 °C, 2 h (66%); (**f**) TFA (10.6 equiv), CH_2Cl_2, 0 °C → rt, 3 h (95%); (**g**) 10% aq. $NaHCO_3$, CH_2Cl_2, (90%). Boc = *tert*-butyloxycarbonyl, PMB = *p*-methoxybenzyl, TFA = trifluoroacetic acid.

The Maillard condensations targeting the 2-formylpyrrole framework have often proved challenging [9,10]. The reported Maillard protocol towards hemerocallisamine I harnessed an open glutamine chain **3** (Scheme 1A). We hypothesized that the application of lactone **11** instead might reduce the complexity of the amine building block and provide better yields. Seeing that dihydropyranone **4** was frequently reported as a suitable sugar surrogate in Maillard reactions [7,32–37], it was picked as a reaction partner for our optimization studies (Table 1). In the published procedures, amines were usually used in 1.5- to 4-fold excess for the sake of better yields [32,33,35,36]. In our case, considering that amine **11** is not an effortless building block, it was reasonable to screen reaction conditions with equimolar amounts of rac-**11** and **4**. Somewhat confusingly, the currently recorded op-

timized protocols vary in the suggested reaction conditions from case to case. Pyridine [7], undistilled dioxane [32], THF/H_2O [33–35], and MeCN [36] were used as solvents and Et_3N [32], AcOH [35], and pyridinium *p*-toluenesulfonate [7,36] as additives, at reaction temperatures ranging from rt to 60 °C. Dihydropyranone **4** was occasionally observed to remain partially unreacted and was recovered in 8–35% yields [33,34]. Taking into account all these data, we performed a broader investigation (selected examples are in Table 1, for details, see the Supplementary Materials), screening diverse solvents and additives (entries 2–12). As found, simple heating of rac-**11** and **4** in dry toluene at 70 °C gave the best outcome, and the target 2-formylpyrrole rac-**8** was isolated in 43% yield (entry 1). Interestingly, 2,5-diketopiperazine rac-**12** was repeatedly detected as a side product in the reaction mixtures, in yields of up to 35% with respect to amine rac-**11 [38]**. These findings provide an important argument when explaining why Maillard condensations so often fail to deliver better yields and should be reflected in future synthetic strategies.

Table 1. Optimization of the Maillard reaction step.

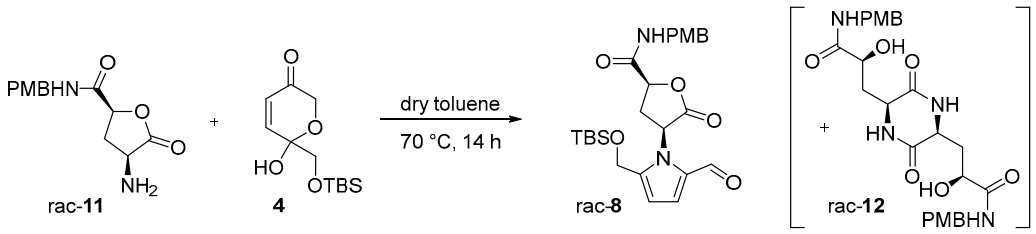

Entry	Variation from the Optimized Conditions [a,b]	Yield (%) [c]
1	none	47 (43 [d])
2	90 °C	47
3	rt	36
4	MeCN, 60 °C	30
5	THF, 60 °C	22
6	THF/H_2O 1:1, 55 °C	20
7	wet DCE, 55 °C	43
8	CH_2Cl_2, 35 °C	41
9	CH_2Cl_2, rt	33
10	+0.1 equiv rac-**11**, CH_2Cl_2, rt	37
11	AcOH (cat.), wet CH_2Cl_2, rt	32
12	TEA (1 equiv), CH_2Cl_2, rt	0

[a] Optimized reaction conditions: rac-**11** (1.0 equiv), **4** (1.0 equiv), dry toluene (0.2 M), 70 °C, under argon, 14 h. [b] The solvents used were dry unless otherwise specified. [c] Yields based on ^{1}H NMR with the internal standard are reported, unless otherwise noted. [d] Isolated yield. PMB = *p*-methoxybenzyl, TBS = *tert*-butyldimethylsilyl, DCE = 1,2-dichloroethane, PTSA = *p*-toluenesulfonic acid, TEA = triethylamine.

Having 2-formylpyrrole rac-**8** in hand, the synthesis of racemic hemerocallisamine I (**1**) could proceed to the concluding steps (Scheme 3). Under conditions developed by Okada et al. [39] and later tailored by Brimble et al. [7], rac-**8** was simultaneously desilylated and converted into a mixture of methyl ethers rac-**13** and rac-**14** in a ratio of 85:15. The crude product was directly used in a subsequent lactone opening and oxidative cleavage of the PMB group, thus providing (±)-hemerocallisamine I, (2*S**,4*S**)-**1** (Scheme 3).

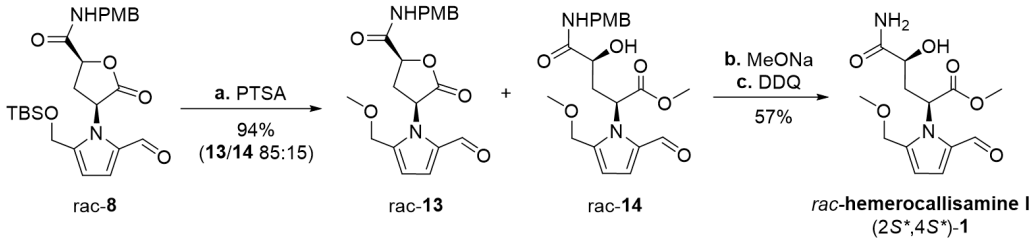

Scheme 3. Synthesis of racemic hemerocallisamine I (**1**). Reagents and conditions: (a) PTSA·H_2O (2.0 equiv), CH_2Cl_2/MeOH 3:1, rt, 4 h. (b) MeONa (0.3 equiv), dry MeOH, 0 °C, under argon, 30 min (quant); (c) DDQ (3.0 equiv), CH_2Cl_2/phosp. buffer (pH 7) 5:1, rt, 24 h (57%). PMB = *p*-methoxybenzyl, TBS = *tert*-butyldimethylsilyl, PTSA = *p*-toluenesulfonic acid, DDQ = 2,3-dichloro-5,6-dicyano-1,4-benzoquinone.

2.2. Synthesis of (–)-hemerocallisamine I

With lessons learned from successfully completing the racemic sequence, we moved towards synthesizing the natural (–)-hemerocallisamine I. The initial steps were devoted to a stereoselective assembly of 4-hydroxyglutamic acid lactone (*S*,*S*)-**7** (Scheme 4).

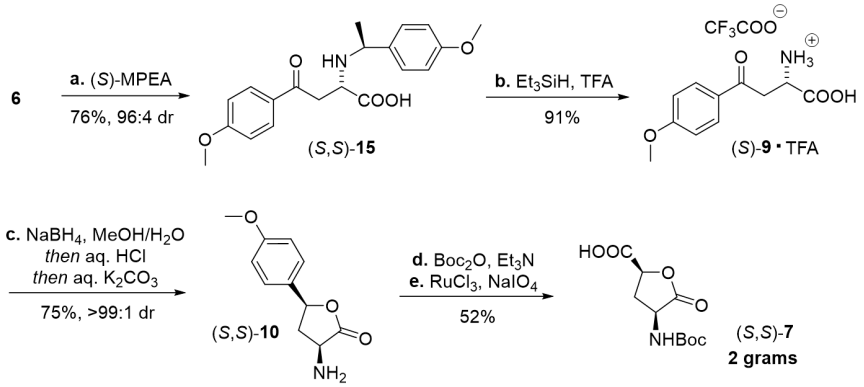

Scheme 4. Preparation of 4-hydroxyglutamic acid lactone (*S*,*S*)-**7**. Reagents and conditions: (**a**) (*S*)-MPEA (1.1 equiv), MeOH, 40 °C, 5 d; (**b**) Et_3SiH (1.0 equiv), TFA (10 equiv), 60 °C, 20 h; (**c**) $NaBH_4$ (3.5 equiv), MeOH/H_2O 5:1, rt, 90 min; then conc. HCl/H_2O 1:2, rt, 4 h; then 10% aq. K_2CO_3/H_2O 5:4; (**d**) Boc_2O (1.1 equiv), Et_3N (2.2 equiv), THF, rt, 4 h (81%); (**e**) 6 mol% $RuCl_3$, $NaIO_4$ (19.4 equiv), H_2O/MeCN/AcOEt 3:1:1, 10 °C → rt, 3 h (64%). MPEA = 1-(4-methoxyphenyl)ethan-1-amine, TFA = trifluoroacetic acid, Boc = *tert*-butyloxycarbonyl.

Crystallization-induced diastereomer transformations (CIDT) built around aza-Michael additions have been proven to provide convenient access to diversely functionalized α-amino acids in a highly stereoselective fashion [27]. (*S*)-/(*R*)-Phenylethan-1-amine has frequently been reported as a chiral auxiliary. Herein we chose to slightly alter the original procedure [40] and utilize a suitably cleavable (*S*)-1-(4-methoxyphenyl)ethan-1-amine ((*S*)-MPEA) as a chiral amine carrier. CIDT with 1.1 equiv of (*S*)-MPEA was monitored by means of HPLC, proceeded over 5 days, and crystalline amino acid (*S*,*S*)-**15** was collected in 96:4 dr. The ensuing TFA-mediated acidolytic *N*-debenzylation in the presence of a silane scavenger [41] smoothly provided crystalline salt of (*S*)-**9**. At this point, the synthetic sequence previously elaborated on the racemic substrate **9** (Scheme 2) came into play, and after the reaction steps **c.**–**e.**, the 4-hydroxyglutamic acid lactone (*S*,*S*)-**7** was obtained in gram quantities. (Scheme 4). Considering that this five-step route could be readily repurposed to deliver the unnatural (*R*,*R*)-configuration, it makes a valuable addition to the available approaches [19–26].

Continuing with (*S*,*S*)-**7** and following the verified procedures (Table 1, Scheme 3), (–)-hemerocallisamine I (*S*,*S*)-(**1**) was obtained, albeit in lower yields (Scheme 5). As confirmed both for the Maillard product (*S*,*S*)-**8** and the target (*S*,*S*)-**1** itself, the stereo-

chemical integrity of these species remained uncompromised (chiral HPLC traces of (*S*,*S*)-**8** and (*S*,*S*)-**1** are available in the Supplementary Materials). The relative configuration of (*S*,*S*)-**1** was confirmed by means of X-ray analysis[#] (#: Crystallographic data for (–)-hemerocallisamine I (2S,4S)-(1) have been deposited with the Cambridge Crystallographic Data Centre (CCDC 2236255). Copies of the data can be obtained, free of charge, via https://www.ccdc.cam.ac.uk/structures/(accessed on 31 January 2023) (Scheme 5). The specific rotation of the synthesized (–)-hemerocallisamine I ($[\alpha]^{25}_D$ -34.5 (*c* 0.12, MeOH)) matched exactly that of the natural product ($[\alpha]^{25}_D$ -34.6 (MeOH)) [6] and was lower than that reported by Brimble et al. ($[\alpha]^{21}_D$ -44.0 (*c* 0.1, MeOH)) [7]. Contrariwise, the mp value of our (*S*,*S*)-(**1**) sample (171.2–172.8 °C) was considerably higher than documented in the same paper (153.0–154.6 °C) [7].

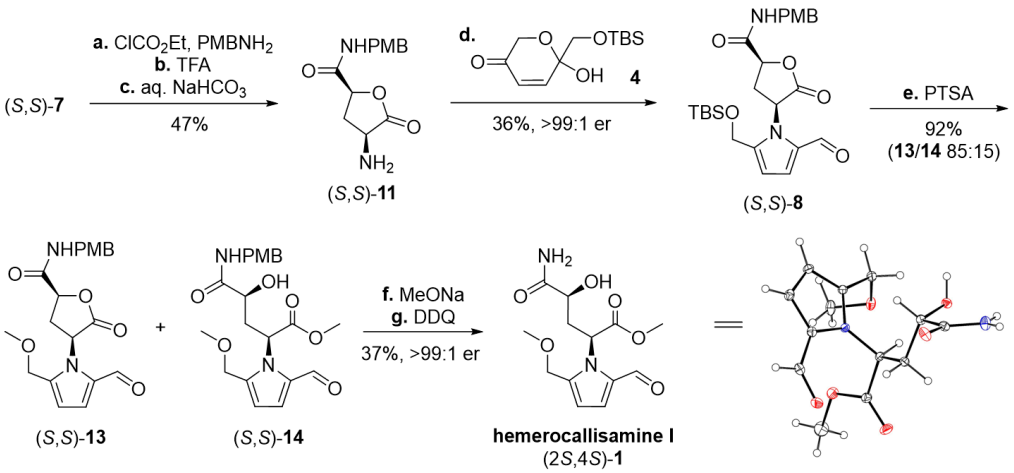

Scheme 5. Synthesis of (–)-hemerocallisamine I (2*S*,4*S*)-(**1**). Reagents and conditions: (**a**) $ClCO_2Et$ (2.0 equiv), Et_3N (2.5 equiv), dry THF, 15 min, 0 °C; then $PMBNH_2$ (2.7 equiv), 0 °C, 2 h (51%); (**b**) TFA (10.6 equiv), CH_2Cl_2, 0 °C → rt, 3 h (95%); (**c**) 10% aq. $NaHCO_3$, CH_2Cl_2, (96%); (**d**) **4** (1.0 equiv), dry toluene (0.2 M), 70 °C, under argon, 14 h; (**e**) PTSA·H_2O (2.0 equiv), CH_2Cl_2/MeOH 3:1, rt, 4 h. (**f**) MeONa (0.4 equiv), dry MeOH, 0 °C, under argon, 30 min (93%); (**g**) DDQ (3.0 equiv), CH_2Cl_2/phosp. buffer (pH 7) 6:1, rt, 24 h (40%). PMB = *p*-methoxybenzyl, TFA = trifluoroacetic acid, TBS = *tert*-butyldimethylsilyl, PTSA = *p*-toluenesulfonic acid, DDQ = 2,3-dichloro-5,6-dicyano-1,4-benzoquinone.

3. Materials and Methods

3.1. General Experimental Details

Unless otherwise noted, all chemicals were purchased from commercial sources and used without further purifications. Column chromatography was carried out using silica 60 Å, Davisil, purchased from Fisher Chemicals. Reactions were monitored by thin-layer chromatography (TLC) using Macherey-Nagel's pre-coated TLC sheets POLYGRAM SIL G/UV254, which were visualized under UV light (254 nm) or by staining with aqueous basic potassium permanganate or cerium molybdate solutions, as appropriate. HPLC analyses were performed on a Varian system using a Macherey-Nagel EC 250/4 Nucleodur Phenyl-Hexyl 5 µm, CHIRAL ART, Amylose-SA, 250 mm × 4.6 mm, 5 µm and Astec CHIROBIOTIC ®T, 250 mm × 4.6 mm, 5 µm column. All ^{1}H and ^{13}C NMR (Supplementary Materials) spectra were recorded using Bruker Avance NEO 400 MHz and/or Varian 400 MR spectrometers. Chemical shifts (δ) are given in parts per million (ppm). The ^{1}H NMR chemical shift scale is referenced to the TMS internal standard (δ = 0 ppm) or solvent residual peak (δ = 2.50 ppm for DMSO-d_6 and δ = 7.26 ppm for $CDCl_3$). The ^{13}C NMR chemical shift scale is referenced to the solvent residual peak (δ = 39.52 ppm for DMSO-d_6 and δ = 77.16 ppm for $CDCl_3$). Coupling constants (*J*) are given in hertz (Hz). The multiplicity of ^{1}H NMR signals is reported as follows: s = singlet, d = doublet, t = triplet, q = quartet, m = multiplet, bs = broad singlet, "t" for dd with two identical or

similar coupling constants, "dt" or "td" for ddd with two identical or similar coupling constants, and "q" for ddd with three identical or similar coupling constants. Optical rotations were recorded using the JASCO P-2000 polarimeter, with $[\alpha]_D$ values measured at 589 nm and the concentration (*c*) given in g/100 mL. High-resolution mass spectra were measured using a Thermo Scientific mass spectrometer with an Orbitrap analyzer and HESI ionization.

3.2. Synthesis and Characterization of Compounds

3.2.1. 2-Amino-4-(4-methoxyphenyl)-4-oxobutanoic acid (**9**)

Acid **6** (14.7 g, 71.3 mmol) was dissolved in MeOH (120 mL) and aqueous ammonia (25–27% NH_3 in H_2O, 24 mL) was added. The mixture was stirred at rt, and the reaction progress was monitored by HPLC. After 16 h, the precipitated product was collected by filtration, washed with a small amount of Et_2O, and dried in vacuo to provide amino acid **9** (12.3 g, 55.1 mmol, 77%) as a white powder. Mp 191.9–192.7 °C; ^{1}H NMR (400 MHz, DMSO-d_6): δ = 7.94 (d, *J* = 8.9 Hz, 2H), 7.60 (bs, 3H), 7.05 (d, *J* = 8.9 Hz, 2H), 3.85 (s, 3H), 3.62 (dd, *J* = 8.8, 3.4 Hz, 1H), 3.52 (dd, *J* = 18.2, 3.4 Hz, 1H), 3.27 (dd, *J* = 18.2, 8.8 Hz, 1H); ^{13}C NMR (100 MHz, DMSO-d_6 + DCl): δ = 194.64, 170.32, 163.99, 130.82, 128.59, 114.41, 55.95, 47.92, 38.10; HRMS–HESI (*m*/*z*): calcd for $C_{11}H_{14}NO_4$ $[M + H]^+$, 224.09173, found 224.09174.

3.2.2. (3*S**,5*S**)-3-Amino-5-(4-methoxyphenyl)dihydrofuran-2(3H)-one (rac-**10**)

Acid **9** (12.3 g, 55.1 mmol) was suspended in a mixture of MeOH (200 mL) and H_2O (40 mL). $NaBH_4$ (7.30 g, 0.193 mol, 3.5 equiv) was added portionwise over 30 min at rt. The reaction progress was monitored by HPLC. After 1 h, the reaction mixture was concentrated in vacuo, providing the crude hydroxy acid. The product was suspended in H_2O (120 mL), and conc. HCl (36%, 60 mL) was added. The reaction mixture was stirred at rt for 4 h. After completion of the reaction, the insoluble white precipitate was collected by filtration and washed with 1 M HCl (15 mL) and Et_2O (2 × 30 mL). The white solid was then suspended in H_2O (80 mL), and 10% aqueous K_2CO_3 solution (100 mL) was added. The resulting mixture was extracted with CH_2Cl_2 (3 × 150 mL). The combined organic layers were dried over anhydrous Na_2SO_4 and concentrated in vacuo, yielding amino lactone rac-**10** (9.5 g, 45.8 mmol, 83%, *cis*:*trans* > 99:1) as a white powder. Rf 0.36 (EtOAc:MeOH, 8:2); mp 102.4–105.4 °C; ^{1}H NMR (400 MHz, $CDCl_3$): δ = 7.31–7.27 (m, 2H), 6.94–6.90 (m, 2H), 5.30 (dd, *J* = 11.0, 5.2 Hz, 1H), 3.90 (dd, *J* = 12.1, 8.0 Hz, 1H), 3.82 (s, 3H), 2.89 (ddd, *J* = 13.0, 8.0, 5.2 Hz, 1H), 2.02 ("td", *J* = 12.4, 11.0 Hz, 1H), 1.67 (s, 2H); ^{13}C NMR (100 MHz, DMSO-d_6): δ = 178.74, 159.39, 130.85, 128.01, 113.87, 77.01, 55.12, 52.36, 39.73; HRMS–HESI (*m*/*z*): calcd for $C_{11}H_{14}NO_3$ $[M + H]^+$, 208.09682, found 208.09689.

3.2.3. (2*S**,4*S**)-4-((tert-Butoxycarbonyl)amino)-5-oxotetrahydrofuran-2-carboxylic acid (rac-**7**)

Step **c**: Lactone rac-**10** (8.4 g, 40.5 mmol) was dissolved in THF (405 mL) and Et_3N (12.4 mL, 89.2 mmol, 2.2 equiv) was added. Boc_2O (9.73 g, 44.6 mmol, 1.1 equiv) was dissolved in a small amount of THF (15 mL) and the resulting solution was added to the first one. The reaction mixture was stirred at rt and monitored by TLC. After 4 h, the reaction mixture was cooled to 0 °C and the pH was adjusted to 2–3 with 2 M HCl, followed by extraction with EtOAc (3 × 140 mL). The combined organic layers were washed with brine (200 mL), dried over anhydrous Na_2SO_4, and concentrated in vacuo. The crude product was crystallized from a mixture of EtOAc and heptane, yielding the corresponding *N*-Boc lactone (11.7 g, 38.1 mmol, 94%) as a white solid. Rf 0.69 (EtOAc); mp 175.6–176.2 °C; ^{1}H NMR (400 MHz, DMSO-d_6): δ = 7.39 (d, *J* = 8.6 Hz, 1H), 7.34 (d, *J* = 8.7 Hz, 2H), 6.98 (d, *J* = 8.7 Hz, 2H), 5.37 (dd, *J* = 11.0, 5.6 Hz, 1H), 4.56 ("dt", *J* = 11.9, 8.6 Hz, 1H), 3.76 (s, 3H), 2.70 (ddd, *J* = 11.9, 8.6, 5.6 Hz, 1H), 2.20 ("q", *J* = 11.7 Hz, 1H), 1.41 (s, 9H); ^{13}C NMR (100 MHz, DMSO-d_6): δ = 174.88, 159.53, 155.03, 130.82, 128.04, 114.00, 78.56, 77.26, 55.18, 50.90, 36.19, 28.13; HRMS–HESI (*m*/*z*): calcd for $C_{16}H_{21}NO_5Na$ $[M + Na]^+$, 330.13119, found 330.13140.

Step **d**: The *N*-Boc lactone (4.0 g, 13.0 mmol) was dissolved in a mixture of CH_3CN (65 mL) and EtOAc (65 mL). In parallel, $NaIO_4$ (54.1 g, 252.7 mmol, 19.4 equiv) was dissolved in H_2O (184 mL) and both solutions were combined. Consequently, $RuCl_3$ (162 mg, 0.782 mmol, 0.06 equiv) was added and the reaction mixture was stirred at 10 °C in a water bath. After 1 h, the bath was removed, and the reaction mixture was stirred for an additional 2 h at rt. Then the resulting thick suspension was decanted, and the white residue was washed with EtOAc (4 × 100 mL). Et_2O (50 mL) was added to the combined solutions and the resulting mixture was stirred for 30 min at rt. Afterwards, the resulting black suspension was filtered through a pad of Celite, and the pad was washed with EtOAc (3 × 50 mL). The combined filtrate was washed with 20% aqueous NaCl (3 × 100 mL) and dried over anhydrous Na_2SO_4. The filtrate volume was reduced in vacuo to *ca* 10 mL, and Et_2O (30 mL) was added. The resulting suspension was placed in a freezer for 30 min. The white precipitate was collected by filtration, washed with a small amount of Et_2O, and dried in vacuo, yielding the desired acid rac-**7** (2.4 g, 9.79 mmol, 75%) as a white solid. Rf 0.22 (EtOAc:MeOH:AcOH, 7:3:0.1); mp 166.9–169.5 °C; ^{1}H NMR (400 MHz, DMSO-d_6): δ = 13.35 (bs, 1H), 7.36 (d, *J* = 8.5 Hz, 1H), 4.89 (dd, *J* = 10.9, 6.5 Hz, 1H), 4.50 ("dt", *J* = 11.8, 8.7 Hz, 1H), 2.66 (ddd, *J* = 11.9, 8.9, 6.5 Hz, 1H), 2.12 ("q", *J* = 11.6 Hz, 1H), 1.38 (s, 9H); ^{13}C NMR (100 MHz, DMSO-d_6): δ = 174.20, 170.23, 155.00, 78.71, 72.21, 49.75, 31.21, 28.12; HRMS–HESI (*m*/*z*): calcd for $C_{10}H_{15}NO_6Na$ [M + Na]$^+$, 268.07916, found 268.07923.

3.2.4. (2*S**,4*S**)-4-Amino-N-(4-methoxybenzyl)-5-oxotetrahydrofuran-2-carboxamide (rac-**11**)

Step **e**: Acid rac-**7** (1.43 g, 5.83 mmol) was dissolved in dry THF (145 mL) at 0 °C and the solution was treated with Et_3N (1.48 g, 2.0 mL, 14.6 mmol, 2.5 equiv). Ethyl chloroformate (1.30 g, 1.1 mL, 11.7 mmol, 2.0 equiv) was added dropwise at 0 °C, under argon. After 15 min, *para*-methoxybenzyl amine (2.20 g, 2.1 mL, 15.7 mmol, 2.7 equiv) was added and the reaction mixture was stirred at 0 °C for 2 h, under argon. After completion, the reaction mixture was diluted with EtOAc (100 mL) and washed with 1M HCl (50 mL). The organic layer was dried over anhydrous Na_2SO_4 and concentrated under reduced pressure, yielding a pale-yellow solid. The crude product was treated with MeOH (5 mL), resulting in a white suspension that was cooled to 0 °C. The white precipitate was collected by filtration, washed with ice-cold MeOH, and dried in vacuo, yielding the corresponding amide (1.4 g, 3.84 mmol, 66%) as a white solid. Rf 0.48 (EtOAc); mp 192.6–194.3 °C; ^{1}H NMR (400 MHz, DMSO-d_6): δ = 8.63 ("t", *J* = 6.1 Hz, 1H), 7.38 (d, *J* = 8.5 Hz, 1H), 7.22–7.17 (m, 2H), 6.90–6.84 (m, 2H), 4.82 (dd, *J* = 10.6, 6.4 Hz, 1H), 4.51 ("dt", *J* = 11.7, 8.7 Hz, 1H), 4.28 (dd, *J* = 14.7, 6.2 Hz, 1H), 4.20 (dd, *J* = 14.7, 5.9 Hz, 1H), 3.72 (s, 3H), 2.62 (ddd, *J* = 12.0, 8.9, 6.4 Hz, 1H), 2.17–2.06 (m, 1H), 1.39 (m, 9H); ^{13}C NMR (100 MHz, DMSO-d_6): δ = 174.31, 168.04, 158.24, 155.02, 130.98, 128.59, 113.65, 78.66, 73.83, 55.04, 49.79, 41.37, 31.50, 28.10; HRMS–HESI (*m*/*z*): calcd for $C_{18}H_{24}N_2O_6Na$ [M + Na]$^+$, 387.15266, found 387.15270.

Step **f**: The amide (580 mg, 1.59 mmol) was dissolved in CH_2Cl_2 (6.4 mL), the solution was cooled to 0 °C, and trifluoroacetic acid (1.92 g, 1.3 mL, 16.8 mmol, 10.6 equiv) was added. The reaction mixture was stirred at rt for 3 h while being monitored by TLC. The mixture was concentrated in vacuo, Et_2O (10–15 mL) was added to the residue, and the mixture was kept in the ultrasonic bath for 30 min to form a white suspension. The white solid was filtered off, washed with a small amount of Et_2O (5 mL), and dried in vacuo, providing rac-**11**·TFA (574 mg, 1.52 mmol, 95%) as an off-white solid. Rf 0.26 (EtOAc:MeOH, 8:2), mp 94.0–96.2 °C; ^{1}H NMR (400 MHz, DMSO-d_6): δ = 8.84 ("t", *J* = 6.0 Hz, 1H), 8.63 (bs, 3H), 7.23–7.17 (m, 2H), 6.91–6.86 (m, 2H), 4.96 (dd, *J* = 10.3, 6.2 Hz, 1H), 4.48 (dd, *J* = 11.5, 8.9 Hz, 1H), 4.29 (dd, *J* = 14.7, 6.0 Hz, 1H), 4.22 (dd, *J* = 14.7, 5.9 Hz, 1H), 3.73 (s, 3H), 2.78 (ddd, *J* = 12.2, 9.0, 6.2 Hz, 1H), 2.22 ("td", *J* = 11.9, 10.3 Hz, 1H); ^{13}C NMR (100 MHz, DMSO-d_6): δ = 172.06, 167.04, 158.37, 130.74, 128.77, 113.75, 74.93, 55.08, 48.41, 41.62, 30.38.

Step **g**: Salt rac-**11**·TFA (570 mg, 1.51 mmol) was suspended in CH_2Cl_2 (15 mL), and the resulting suspension was washed with 10% aqueous $NaHCO_3$ (7 mL). The aqueous layer was extracted with CH_2Cl_2 (2 × 10 mL). The combined organic layers were dried

over anhydrous Na_2SO_4 and concentrated in vacuo, providing rac-**11** (360 mg, 1.36 mmol, 90%) as a white solid. Rf 0.26 (EtOAc:MeOH, 8:2); mp 105.8–107.5 °C; ^{1}H NMR (400 MHz, DMSO-d_6): δ = 8.64 (t, *J* = 6.0 Hz, 1H), 7.21–7.17 (m, 2H), 6.91–6.86 (m, 2H), 4.74 (dd, *J* = 10.1, 6.3 Hz, 1H), 4.23 (d, *J* = 6.0 Hz, 2H), 3.76–3.66 (m, 4H), 2.64 (ddd, *J* = 12.2, 8.5, 6.3 Hz, 1H), 2.01 (bs, 2H), 1.83 (ddd, *J* = 12.2, 11.0, 10.1 Hz, 1H); ^{13}C NMR (100 MHz, DMSO-d_6): δ = 178.16, 168.56, 158.28, 130.95, 128.70, 113.71, 73.95, 55.06, 50.98, 41.42, 35.12; HRMS–HESI (*m*/*z*): calcd for $C_{13}H_{17}N_2O_4$ $[M + H]^+$, 265.11828, found 265.11842.

3.2.5. (2*S**,4*S**)-4-(2-(((tert-Butyldimethylsilyl)oxy)methyl)-5-formyl-1H-pyrrol-1-yl)-N-(4-methoxybenzyl)-5-oxotetrahydrofuran-2-carboxamide (rac-**8**)

Amide rac-**11** (200 mg, 0.757 mmol) was dissolved in dry toluene (3.8 mL) and dihydropyranone **4** (196 mg, 0.757 mmol, 1.0 equiv) was added. The reaction mixture was stirred at 70 °C for 14 h, under argon. The formation of a precipitate was observed. The reaction progress was monitored by TLC. After completion, the reaction mixture was concentrated in vacuo and purified by flash column chromatography (petroleum ether:EtOAc, 1:1), providing rac-**8** (158 mg, 0.325 mmol, 43%) as a pale-yellow oil. Rf 0.42 (petroleum ether:EtOAc, 1:1); ^{1}H NMR (400 MHz, $CDCl_3$): δ = 9.34 (s, 1H), 7.40 ("t", *J* = 6.1 Hz, 1H), 7.32–7.27 (m, 2H), 7.00 (d, *J* = 4.0 Hz, 1H), 6.89–6.84 (m, 2H), 6.20 (d, *J* = 4.0 Hz, 1H), 5.45 (dd, *J* = 11.4, 9.4 Hz, 1H), 4.94 (dd, *J* = 10.3, 7.6 Hz, 1H), 4.77 (d, *J* = 13.6 Hz, 1H), 4.69 (d, *J* = 13.6 Hz, 1H), 4.57 (dd, *J* = 14.6, 6.3 Hz, 1H), 4.43 (dd, *J* = 14.7, 5.4 Hz, 1H), 3.80 (s, 3H), 3.06 (ddd, *J* = 12.4, 9.5, 7.6 Hz, 1H), 2.57 ("q", *J* = 11.4 Hz, 1H), 0.88 (s, 9H), 0.09 (s, 3H), 0.04 (s, 3H); ^{13}C NMR (100 MHz, $CDCl_3$): δ = 178.93, 171.02, 168.80, 159.15, 142.76, 131.60, 129.78, 129.29, 126.15, 114.16, 110.75, 74.72, 57.52, 55.42, 55.27, 42.94, 33.08, 25.90, 18.33, -5.08, -5.16; HRMS–HESI (*m*/*z*): calcd for $C_{25}H_{44}N_2O_6SiNa$ $[M + Na]^+$, 509.20783, found 509.20805.

3.2.6. (2*S**,4*S**)-4-(2-Formyl-5-(methoxymethyl)-1H-pyrrol-1-yl)-N-(4-methoxybenzyl)-5-oxotetrahydrofuran-2-carboxamide (rac-**13**)

2-Formylpyrrole rac-**8** (278 mg, 0.571 mmol) was dissolved in CH_2Cl_2 (8.6 mL) and a solution of *para*-toluenesulfonic acid monohydrate (217 mg, 1.14 mmol, 2.0 equiv) in MeOH (2.9 mL) was added. The resulting mixture was stirred for 4 h at rt, while being monitored by TLC. After completion, the reaction mixture was neutralized with a saturated aqueous $NaHCO_3$ (6 mL), and the aqueous layer was extracted with CH_2Cl_2 (2 × 15 mL). The combined organic layers were washed with a saturated brine solution (15 mL), dried over anhydrous Na_2SO_4, and concentrated in vacuo. The resulting crude product was purified by flash column chromatography (EtOAc:petroleum ether 3:1 → 4:1), providing a white solid (209 mg, 0.534 mmol for mole-fraction-weighted M = 391.21 g.mol^{-1}, 94%). The isolated product contained 85% of rac-**13** and 15% of rac-**14**, as confirmed by HPLC and ^{1}H NMR. This mixture was used in the next step.

Isolation of rac-**13**: The mixture of rac-**13** and rac-**14** (85:15) was treated with MeOH (3 mL), resulting in a white suspension that was placed in a freezer. The white precipitate that formed was collected by filtration, providing lactone rac-**13** (105 mg, 0.272 mmol, 47%) as a white solid. The filtrate contained a mixture of rac-**13** and rac-**14** (1:1) according to HPLC. Rf 0.39 (petroleum ether:EtOAc, 1:3); mp 131.5–133.6 °C; ^{1}H NMR (400 MHz, $CDCl_3$): δ = 9.36 (s, 1H), 7.37–7.33 (m, 1H), 7.32–7.27 (m, 2H), 7.03 (d, *J* = 4.0 Hz, 1H), 6.90–6.84 (m, 2H), 6.30 (d, *J* = 4.0 Hz, 1H), 5.39 (dd, *J* = 11.4, 9.5 Hz, 1H), 4.95 (dd, *J* = 10.4, 7.6 Hz, 1H), 4.62–4.53 (m, 2H), 4.51–4.40 (m, 2H), 3.80 (s, 3H), 3.31 (s, 3H), 3.07 (ddd, *J* = 12.4, 9.5, 7.6 Hz, 1H), 2.55 (ddd, *J* = 12.5, 11.5, 10.4 Hz, 1H); ^{13}C NMR (100 MHz, $CDCl_3$): δ = 178.88, 170.86, 168.56, 159.01, 139.60, 131.83, 129.58, 129.14, 125.75, 114.01, 112.45, 74.56, 65.69, 57.67, 55.27, 55.10, 42.77, 32.91; HRMS–HESI (*m*/*z*): calcd for $C_{20}H_{22}N_2O_6Na$ $[M + Na]^+$, 409.13701, found 409.13717.

3.2.7. (±)-Hemerocallisamine I, (2*S**,4*S**)-**1**

Step **b**: The mixture of rac-**13** and rac-**14** (85:15) (100 mg, 0.256 mmol for mole-fraction-weighted M = 391.21 g.mol^{-1}) was dissolved in dry MeOH (2.9 mL). MeONa (25w% solution in MeOH) (4.2 mg, 21 µL, 0.078 mmol, 0.3 equiv) was added to the solution at 0 °C, under an argon atmosphere. The reaction mixture was stirred at 0 °C and was monitored by TLC. After 30 min, a saturated aqueous NH_4Cl solution (2 mL) was added at 0 °C and the resulting mixture was extracted with EtOAc (3 × 10 mL). The collected organic layers were washed with brine (10 mL), dried over anhydrous Na_2SO_4, and concentrated in vacuo, yielding rac-**14** as a thick pale-yellow oil (108 mg, quantitative).

Step **c**: The crude methyl ester rac-**14** (100 mg, 0.239 mmol) was dissolved in a mixture of CH_2Cl_2 (2.3 mL) and a phosphate buffer (NaH_2PO_4, Na_2HPO_4; pH 7, *c* 1M; 0.481 mL). Subsequently, 2,3-dichloro-5,6-dicyano-1,4-benzoquinone (163 mg, 0.717 mmol, 3.0 equiv) was added to the solution. The resulting mixture was stirred at rt while the reaction progress was monitored by HPLC and TLC. After 24 h, the reaction mixture was diluted with CH_2Cl_2 (5 mL), dried with Na_2SO_4, and filtered through a Celite pad. The pad was washed first with CH_2Cl_2 (10 mL), then with dioxane (3 × 20 mL). The combined filtrates were concentrated in vacuo and purified using flash column chromatography (CH_2Cl_2:MeOH, 13:1). The desired product was isolated after trituration from MeOH–Et_2O, yielding (±)-hemerocallisamine I ((2*S**,4*S**)-**1**) (41 mg, 0.137 mmol, 57%) as a white solid. Mp 204.3–204.9 °C; ^{1}H NMR (400 MHz, DMSO-d_6): δ = 9.37 (s, 1H), 7.25 (s, 1H), 7.18–7.11 (m, 2H), 6.33 (d, *J* = 3.9 Hz, 1H), 5.74–5.66 (m, 1H), 5.27 (bs, 1H), 4.74 (d, *J* = 13.3 Hz, 1H), 4.37 (d, *J* = 13.2 Hz, 1H), 3.57 (s, 3H), 3.20 (s, 3H), 3.08–3.00 (m, 1H), 2.42–2.26 (m, 2H); ^{13}C NMR (100 MHz, DMSO-d_6): δ = 179.38, 176.32, 170.26, 141.05, 132.43, 126.44, 111.54, 69.70, 65.31, 57.50, 55.69, 52.63, 37.06; HRMS–HESI (*m*/*z*): calcd for $C_{13}H_{18}N_2O_6Na$ [M + Na]$^+$, 321.10571, found 321.10584.

3.2.8. (*S*)-4-(4-Methoxyphenyl)-2-(((*S*)-1-(4-methoxyphenyl)ethyl)amino)-4-oxobutanoic acid, (*S*,*S*)-**15**

Acid **6** (11.8 g, 57.2 mmol) was dissolved in MeOH (228 mL) and, subsequently, (*S*)-(–)-1-(4-methoxyphenyl)ethan-1-amine (9.52 g, 9.3 mL, 63.0 mmol, 1.1 equiv) was added dropwise. The reaction mixture was stirred at 40 °C while being monitored by HPLC. After 5 days, the white precipitate was collected by filtration, washed with a small amount of Et_2O, and dried in vacuo, providing (*S*,*S*)-**15** (15.6 g, 43.7 mmol, 76%, dr 96:4) as a white solid. Mp 180.3–181.1 °C; $[\alpha]^{25}_D$ +67.1 (*c* 1.00, MeOH:5% aq. HCl, 9:1); ^{1}H NMR (400 MHz, acetone + DCl): δ = 7.95–7.91 (m, 2H), 7.71–7.65 (m, 2H), 7.03–6.94 (m, 4H), 4.83 (q, *J* = 6.9 Hz, 1H), 4.12 (t, *J* = 5.3 Hz, 1H), 3.96 (d, *J* = 5.1 Hz, 2H), 3.84 (s, 3H), 3.80 (s, 3H), 1.84 (d, *J* = 6.9 Hz, 3H); ^{13}C NMR (100 MHz, acetone + DCl): δ = 194.83, 169.69, 164.91, 161.26, 131.50, 130.87, 129.40, 128.31, 115.28, 114.67, 59.19, 56.01, 55.62, 53.82, 39.17, 20.81; HRMS–HESI (*m*/*z*): calcd for $C_{20}H_{24}NO_5$ [M + H]$^+$, 358.16490, found 358.16496.

3.2.9. (*S*)-1-Carboxy-3-(4-methoxyphenyl)-3-oxopropan-1-aminium 2,2,2-trifluoroacetate, (*S*)-**9**·TFA

Amino acid (*S*,*S*)-**15** (4.37 g, 12.2 mmol) was dissolved in trifluoroacetic acid (9.4 mL, 13.9 g, 122.3 mmol, 10.0 equiv) and triethylsilane (1.9 mL, 1.42 g, 12.2 mmol, 1.0 equiv) was added. The resulting solution was stirred at 60 °C and the reaction was monitored by HPLC. After 20 h, the reaction mixture was concentrated in vacuo, and the residue was treated with Et_2O (20 mL) and placed in an ultrasonic bath for 10 min. The insoluble white solid was filtered off, washed with a small amount of Et_2O, and dried in vacuo to give (*S*)-**9**·TFA (3.75 g, 11.1 mmol, 91%) as a white solid. Mp 155.0–156.0 °C; $[\alpha]^{25}_D$ +24.3 (*c* 1.00, MeOH); ^{1}H NMR (400 MHz, DMSO-d_6): δ = 8.34 (bs, 3H), 8.00–7.95 (m, 2H), 7.12–7.03 (m, 2H), 4.31 (t, *J* = 5.1 Hz, 1H), 3.85 (s, 3H), 3.62 (d, *J* = 5.1 Hz, 2H); ^{13}C NMR (100 MHz, DMSO-d_6): δ = 194.44, 170.53, 163.75, 130.56, 128.48, 114.14, 55.68, 48.08, 38.16; HRMS–HESI (*m*/*z*): calcd for $C_{11}H_{14}NO_4$ [M + H]$^+$, 224.09173, found 224.09176.

3.2.10. (3*S*,5*S*)-3-Amino-5-(4-methoxyphenyl)dihydrofuran-2(3H)-one, (*S*,*S*)-**10**

The salt (*S*)-**9**·TFA (13.0 g, 38.5 mmol) was suspended in a mixture of MeOH (128 mL) and H_2O (28 mL). $NaBH_4$ (5.1 g, 0.135 mol, 3.5 equiv) was added portionwise over 30 min to the suspension at rt. The reaction was monitored by HPLC. After 1 h, the reaction mixture was concentrated in vacuo, providing the crude hydroxy acid. The crude product was suspended in H_2O (85 mL), and conc. HCl (36%, 45 mL) was added. The reaction mixture was stirred at room temperature for 4 h. After completion of the reaction, the insoluble white precipitate was collected by filtration and washed with 1M HCl (15 mL) and Et_2O (2 × 30 mL). The white solid was then suspended in H_2O (80 mL), and a 10% aqueous K_2CO_3 solution (100 mL) was added. The resulting mixture was extracted with CH_2Cl_2 (3 × 100 mL). The combined organic layers were dried over anhydrous Na_2SO_4 and concentrated in vacuo, providing amino lactone (*S*,*S*)-**10** (6.0 g, 29.0 mmol, 75%, *cis*:*trans* > 99:1) as a white powder. Mp 101.8–103.0 °C; $[\alpha]^{25}_D$ -1.3 (*c* 1.00, MeOH); ^{1}H NMR (400 MHz, $CDCl_3$): δ = 7.31–7.25 (m, 2H), 6.95–6.87 (m, 2H), 5.29 (dd, *J* = 11.0, 5.2 Hz, 1H), 3.89 (dd, *J* = 12.1, 8.0 Hz, 1H), 3.81 (s, 3H), 2.89 (ddd, *J* = 12.5, 8.0, 5.2 Hz, 1H), 2.02 (ddd, *J* = 12.6, 12.2, 11.0 Hz, 1H, 1H), 1.68 (bs, 2H).

3.2.11. (2*S*,4*S*)-4-((*tert*-Butoxycarbonyl)amino)-5-oxotetrahydrofuran-2-carboxylic acid, (*S*,*S*)-**7**

Step **d**: The lactone (*S*,*S*)-**10** (5.5 g, 26.5 mmol) was dissolved in THF (265 mL), and Et_3N (8.1 mL, 5.91 g, 58.4 mmol, 2.2 equiv) was added. Boc_2O (6.37 g, 29.2 mmol, 1.1 equiv) was dissolved in a small amount of THF (10 mL) and the resulting solution was added to the first one. The reaction mixture was stirred at room temperature and was monitored by TLC. After 4 h, the reaction mixture was cooled to 0 °C and the pH was adjusted to 2–3 with 2M HCl, followed by extraction with EtOAc (3 × 90 mL). The combined organic layers were washed with brine (130 mL), dried over anhydrous Na_2SO_4,, and concentrated in vacuo, yielding crude *N*-Boc lactone as a pale-yellow solid. The crude product was crystallized from EtOAc-heptane, providing the *N*-Boc lactone (6.6 g, 21.5 mmol, 81%) as white crystals. Mp 189.7–190.9 °C; $[\alpha]^{25}_D$ +9.3 (*c* 1.00, MeOH); ^{1}H NMR (400 MHz, DMSO-d_6): δ = 7.39 (d, *J* = 8.6 Hz, 1H), 7.36–7.31 (m, 2H), 7.02–6.95 (m, 2H), 5.37 (dd, *J* = 11.0, 5.6 Hz, 1H), 4.56 (dt, *J* = 11.9, 8.6 Hz, 1H), 3.76 (s, 3H), 2.70 (ddd, *J* = 12.0, 8.6, 5.6 Hz, 1H), 2.21 ("q", *J* = 11.8 Hz, 1H), 1.41 (s, 9H).

Step **e**: The *N*-Boc lactone (4.0 g, 13.0 mmol) was dissolved in a mixture of CH_3CN (65 mL) and EtOAc (65 mL). In parallel, $NaIO_4$ (54.1 g, 252.7 mmol, 19.4 equiv) was dissolved in H_2O (184 mL) and both solutions were combined. Consequently, $RuCl_3$ (162 mg, 0.782 mmol, 0.06 equiv) was added, and the reaction mixture was stirred in a water bath (10 °C). After 1 h, the bath was removed, and the reaction mixture was stirred for an additional 2 h at rt. The thick suspension was then decanted, and the white residue was washed with EtOAc (4 × 100 mL). Et_2O (70 mL) was added to the combined solutions, and the resulting mixture was stirred for 30 min at rt. Afterward, the resulting black suspension was filtered through the pad of Celite, and the pad was washed with EtOAc (3 × 50 mL). The combined filtrate was washed with a 20% aqueous NaCl solution (3 × 100 mL), dried over anhydrous Na_2SO_4, and concentrated in vacuo to provide (*S*,*S*)-**7** (2.04 g, 8.32 mmol, 64%) as a pale-yellow solid. Mp 171.7–174.6 °C; $[\alpha]^{25}_D$ -1.4 (*c* 1.00, MeOH); ^{1}H NMR (400 MHz, DMSO-d_6): δ = 7.36 (d, *J* = 8.5 Hz, 1H), 4.88 (dd, *J* = 10.9, 6.5 Hz, 1H), 4.49 ("dt", *J* = 11.7, 8.7 Hz, 1H), 2.66 (ddd, *J* = 11.8, 8.9, 6.6 Hz, 1H), 2.12 ("q", *J* = 11.6 Hz, 1H), 1.38 (s, 9H).

3.2.12. (2*S*,4*S*)-4-Amino-*N*-(4-methoxybenzyl)-5-oxotetrahydrofuran-2-carboxamide, (*S*,*S*)-**11**

Step **a**: Acid (*S*,*S*)-**7** (1.23 g, 5.02 mmol) was dissolved in dry THF (125 mL) at 0 °C and the solution was treated with Et_3N (1.27 g, 1.7 mL, 12.5 mmol, 2.5 equiv). Ethyl chloroformate (1.12 g, 1.0 mL, 10.0 mmol, 2.0 equiv) was added dropwise at 0 °C, under argon. After 15 min, *para*-methoxybenzyl amine (1.90 g, 1.8 mL, 13.5 mmol, 2.7 equiv)

was added and the reaction mixture was stirred at 0 °C for 2 h. After completion, the reaction mixture was diluted with EtOAc (85 mL) and washed with 1M HCl (1 × 40 mL). The aqueous phase was extracted with EtOAc (2 × 50 mL). The combined organic layers were dried over anhydrous Na_2SO_4 and concentrated under reduced pressure. The crude product was purified by flash column chromatography (EtOAc:Hex, 2:3 → 1:1→ 4:1), yielding the corresponding amide (930 mg, 2.55 mmol, 51%) as a pale-yellow solid. Mp 123.5–125.6 °C; $[\alpha]^{25}_D$ +1.5 (*c* 1.00, MeOH); ^{1}H NMR (400 MHz, DMSO-d_6): δ = 8.63 ("t", *J* = 6.1 Hz, 1H), 7.38 (d, *J* = 8.6 Hz, 1H), 7.22–7.17 (m, 2H), 6.90–6.85 (m, 2H), 4.82 (dd, *J* = 10.5, 6.2 Hz, 1H), 4.51 ("dt", *J* = 11.7, 8.7 Hz, 1H), 4.28 (dd, *J* = 14.8, 6.3 Hz, 1H), 4.20 (dd, *J* = 14.9, 6.0 Hz, 1H), 3.72 (s, 3H), 2.61 (ddd, *J* = 11.8, 8.7, 6.3 Hz, 1H), 2.11 ("q", *J* = 11.5 Hz, 1H), 1.39 (m, 9H).

Step **b**: The amide (650 mg, 1.78 mmol) was dissolved in CH_2Cl_2 (7.2 mL), the solution was cooled to 0 °C, and trifluoroacetic acid (2.15 g, 1.4 mL, 18.9 mmol, 10.6 equiv) was added. The reaction mixture was stirred at rt while being monitored by TLC. After 3 h, the mixture was concentrated in vacuo, Et_2O (40 mL) was added to the residue, and the mixture was kept in the ultrasonic bath for 30 min to form a white suspension. The insoluble precipitate was filtered off, washed with a small amount of Et_2O (5 mL), and dried in vacuo, yielding (*S*,*S*)-**11**·TFA (643 mg, 1.70 mmol, 95%) as an off-white solid. Mp 133.6–135.1 °C; $[\alpha]^{25}_D$ +14.6 (*c* 0.50, MeOH); ^{1}H NMR (400 MHz, DMSO-d_6): δ = 8.84 ("t", *J* = 6.0 Hz, 1H), 8.56 (bs, 3H), 7.23–7.17 (m, 2H), 6.92–6.86 (m, 2H), 4.96 (dd, *J* = 10.3, 6.2 Hz, 1H), 4.47 (dd, *J* = 11.5, 8.9 Hz, 1H), 4.29 (dd, *J* = 14.7, 6.0 Hz, 1H), 4.23 (dd, *J* = 14.6, 5.9 Hz, 1H), 3.73 (s, 3H), 2.78 (ddd, *J* = 12.2, 8.9, 6.2 Hz, 1H), 2.26–2.10 (m, 1H).

Step **c**: Salt (*S*,*S*)-**11**·TFA (643 mg, 1.70 mmol) was suspended in CH_2Cl_2 (20 mL), and the resulting suspension was washed with 10% aqueous $NaHCO_3$ (5 mL). The aqueous layer was extracted with CH_2Cl_2 (2 × 10 mL). The combined organic layers were dried over anhydrous Na_2SO_4, and concentrated in vacuo, yielding (*S*,*S*)-**11** (430 mg, 1.63 mmol, 96%) as an orange solid. $[\alpha]^{25}_D$ +14.0 (*c* 1.00, MeOH); ^{1}H NMR (400 MHz, DMSO-d_6): δ = 8.63 (t, *J* = 6.0 Hz, 1H), 7.22–7.15 (m, 2H), 6.91–6.86 (m, 2H), 4.74 (dd, *J* = 10.1, 6.3 Hz, 1H), 4.23 (d, *J* = 6.0 Hz, 2H), 3.73 (s, 3H), 3.72–3.67 (m, 1H), 2.64 (ddd, *J* = 12.2, 8.5, 6.3 Hz, 1H), 2.02 (bs, 2H), 1.83 (ddd, *J* = 12.2, 11.0, 10.1 Hz, 1H).

3.2.13. (2*S*,4*S*)-4-(2-(((*tert*-Butyldimethylsilyl)oxy)methyl)-5-formyl-1H-pyrrol-1-yl)-*N*-(4-methoxybenzyl)-5-oxotetrahydrofuran-2-carboxamide, (*S*,*S*)-**8**

Amide (*S*,*S*)-**11** (200 mg, 0.757 mmol) was dissolved in dry toluene (3.8 mL), and dihydropyranone **4** (196 mg, 0.757 mmol, 1.0 equiv) was added. The reaction mixture was stirred at 70 °C for 14 h under argon. The formation of a precipitate was observed. The reaction progress was monitored by TLC. After completion, the reaction mixture was concentrated in vacuo and purified by flash column chromatography (petroleum ether:EtOAc, 1:1), providing (*S*,*S*)-**8** (131 mg, 0.269 mmol, 36%, er > 99:1) as a pale-yellow oil. $[\alpha]^{25}_D$ +11.7 (*c* 0.70, MeOH); ^{1}H NMR (400 MHz, $CDCl_3$): δ = δ 9.34 (s, 1H), 7.40 ("t", *J* = 5.6 Hz, 1H), 7.30 (d, *J* = 8.6 Hz, 2H), 7.00 (d, *J* = 4.0 Hz, 1H), 6.89–6.40 (m, 2H), 6.20 (d, *J* = 4.0 Hz, 1H), 5.45 (dd, *J* = 11.3, 9.5 Hz, 1H), 4.94 (dd, *J* = 10.3, 7.6 Hz, 1H), 4.77 (d, *J* = 13.6 Hz, 1H), 4.69 (d, *J* = 13.7 Hz, 1H), 4.57 (dd, *J* = 14.7, 6.3 Hz, 1H), 4.43 (dd, *J* = 14.7, 5.4 Hz, 1H), 3.80 (s, 3H), 3.06 (ddd, *J* = 12.5, 9.5, 7.6 Hz, 1H), 2.57 (ddd, *J* = 12.4, 11.3, 10.3 Hz, 1H), 0.88 (s, 9H), 0.09 (s, 3H), 0.04 (s, 3H).

3.2.14. (2*S*,4*S*)-4-(2-Formyl-5-(methoxymethyl)-1H-pyrrol-1-yl)-*N*-(4-methoxybenzyl)-5-oxotetrahydrofuran-2-carboxamide, (*S*,*S*)-**13**

2-Formylpyrrole (*S*,*S*)-**8** (145 mg, 0.298 mmol) was dissolved in CH_2Cl_2 (4.5 mL), and a solution of *para*-toluenesulfonic acid monohydrate (113 mg, 0.596 mmol, 2.0 equiv) in MeOH (1.5 mL) was added. The resulting mixture was stirred for 4 h at rt while being monitored by TLC. After completion, the reaction mixture was neutralized with a saturated aqueous $NaHCO_3$ solution (3 mL), and the aqueous layer was extracted with CH_2Cl_2 (2 × 10 mL). The combined organic solutions were washed with brine (15 mL), dried

over anhydrous Na_2SO_4, and concentrated in vacuo. The resulting crude product was purified by flash column chromatography (EtOAc:petroleum ether, 3:1 → 4:1), yielding a pale-yellow oil (107 mg, 0.274 mmol for mole-fraction-weighted M = 391.21 g.mol^{-1}, 92%). The isolated product contained 85% of (*S*,*S*)-**13** and 15% of (*S*,*S*)-**14**, as confirmed by HPLC and ^{1}H NMR. This mixture was used in the next step.

3.2.15. (–)-Hemerocallisamine I, (*S*,*S*)-**1**

Step **f**: The mixture of (*S*,*S*)-**13** and (*S*,*S*)-**14** (85:15) (96 mg, 0.245 mmol for mole-fraction-weighted M = 391.21 g.mol^{-1}) was dissolved in dry MeOH (2.8 mL). MeONa (25w% solution in MeOH) (5.4 mg, 27 µL, 0.099 mmol, 0.4 equiv) was added to the solution at 0 °C, under an argon atmosphere. The reaction mixture was stirred at 0 °C. After 30 min, a saturated aqueous NH_4Cl solution (3 mL) was added at 0 °C, and the resulting mixture was extracted with EtOAc (3 × 10 mL). The combined organic layers were washed with brine (10 mL), dried over anhydrous Na_2SO_4, and concentrated in vacuo, yielding crude (*S*,*S*)-**14** as a thick pale-yellow oil (96 mg, 0.229 mmol, 93%).

Step **g**: The crude methyl ester (*S*,*S*)-**14** (96.0 mg, 0.229 mmol) was dissolved in a mixture of CH_2Cl_2 (2.8 mL) and a phosphate buffer (NaH_2PO_4, Na_2HPO_4; pH 7, *c* 1M; 0.450 mL). Subsequently, 2,3-dichloro-5,6-dicyano-1,4-benzoquinone (156 mg, 0.688 mmol, 3.0 equiv) was added to the solution. The resulting mixture was stirred at rt while the reaction progress was monitored by HPLC and TLC. After 24 h, the reaction mixture was diluted with CH_2Cl_2 (5 mL), dried with Na_2SO_4, and filtered through a Celite pad. The pad was washed first with CH_2Cl_2 (10 mL), then with dioxane (3 × 20 mL). The combined filtrates were concentrated in vacuo and purified by flash column chromatography (CH_2Cl_2:MeOH, 13:1). (–)-Hemerocallisamine I (27 mg, 0.091 mmol, 40%, er > 99:1) was isolated after trituration from MeOH:Et_2O as a white powder. Mp 171.2−172.8 °C; $[\alpha]^{25}_D$ -34.5 (*c* 0.12, MeOH); ^{1}H NMR (400 MHz, DMSO-d_6): δ = 9.37 (s, 1H), 7.24 (s, 1H), 7.20–7.07 (m, 2H), 6.33 (d, *J* = 4.0 Hz, 1H), 5.70 (bd, *J* = 5.7 Hz, 1H), 5.26 (bs, 1H), 4.73 (bd, *J* = 13.2 Hz, 1H), 4.36 (d, *J* = 13.1 Hz, 1H), 3.56 (s, 3H), 3.19 (s, 3H), 3.09–3.00 (m, 1H), 2.41–2.25 (m, 2H); ^{13}C NMR (100 MHz, DMSO-d_6): δ = 178.89, 175.83, 169.78, 140.56, 131.96, 125.96, 111.06, 67.75, 64.82, 57.02, 55.20, 52.14, 36.57.

4. Conclusions

The synthesis of the pyrrolic alkaloid (–)-hemerocallisamine I, featuring crystallization-induced diastereomer transformation (CIDT) and the Maillard reaction as the key synthetic strategies, was achieved in 12 steps and a 1.6% overall yield. The sequence involved the preparation of (2*S*,4*S*)-4-hydroxyglutamic acid lactone in gram quantities, from an achiral substrate. In parallel, the first synthesis of (±)-hemerocallisamine I was described in 11 steps and a 5.9% overall yield. A detailed inspection of the Maillard reaction conditions revealed diketopiperazine **12** as the dominant side product, arising from a cannibalistic reaction of the amine **11**. This transformation might be responsible for the often-reported depletion of the starting amino-acid-derived amines in the Maillard-type condensations.

Supplementary Materials: The following supporting information can be downloaded at: https://www.mdpi.com/article/10.3390/molecules28052177/s1, Pages S2–S4: Synthesis and characterization data of compounds **6**, **4** and rac-**12**; Pages S5–S6: HPLC data for compounds (*S*,*S*)-**8** and (*S*,*S*)-**1**; Pages S7–S8: Optimization of the Maillard reaction; Page S9: X-ray analysis of compound (*S*,*S*)-**1**; Pages S10–S27: ^{1}H and ^{13}C NMR spectra [42–46].

Author Contributions: Conceptualization, D.B., A.K. and O.C.; methodology, D.B. and O.C.; investigation, L.P. and E.J.; validation, L.P., E.J., R.G. and O.C.; formal analysis, A.K and O.C.; data curation, L.P., R.G., A.K. and O.C.; writing, A.K.; supervision, O.C.; funding acquisition, D.B. and O.C. All authors have read and agreed to the published version of the manuscript.

Funding: This research was supported by the Slovak Research and Development Agency under contract No. APVV-20-0298 and by Scientific Grant Agency of the Slovak Republic under contract No. VEGA 1/0411/22.

Institutional Review Board Statement: Not applicable.

Informed Consent Statement: Not applicable.

Data Availability Statement: Not applicable.

Conflicts of Interest: The authors declare no conflict of interest.

References

1. Plants of the World Online (POWO). Available online: https://powo.science.kew.org/taxon/urn:lsid:ipni.org:names:24324-1 (accessed on 31 January 2023).
2. American Daylily Society. Available online: https://daylilydatabase.org/ (accessed on 31 January 2023).
3. Tai, C.-Y.; Chen, B.H. Analysis and Stability of Carotenoids in the Flowers of Daylily (*Hemerocallis disticha*) as Affected by Various Treatments. *J. Agric. Food Chem.* **2000**, *48*, 5962–5968. [CrossRef] [PubMed]
4. Li, X.; Jiang, S.; Cui, J.; Qin, X.; Zhang, G. Progress of genus *Hemerocallis* in traditional uses, phytochemistry, and pharmacology. *J. Hortic. Sci. Biotechnol.* **2022**, *97*, 298–314. [CrossRef]
5. Matraszek-Gawron, R.; Chwil, M.; Terlecka, P.; Skoczylas, M.M. Recent Studies on Anti-Depressant Bioactive Substances in Selected Species from the Genera *Hemerocallis* and *Gladiolus*: A Systematic Review. *Pharmaceuticals* **2019**, *12*, 172. [CrossRef] [PubMed]
6. Matsumoto, T.; Nakamura, S.; Ohta, T.; Fujimoto, K.; Yoshikawa, M.; Ogawa, K.; Matsuda, H. A Rare Glutamine Derivative from the Flower Buds of Daylily. *Org. Lett.* **2014**, *16*, 3076–3078. [CrossRef]
7. Wood, J.M.; Furkert, D.P.; Brimble, M.A. Total Synthesis and Stereochemical Revision of the 2-Formylpyrrole Alkaloid Hemerocallisamine, I. *J. Nat. Prod.* **2017**, *80*, 1926–1929. [CrossRef]
8. Piotrowska, D.G.; Głowacka, I.E.; Wróblewski, A.E.; Lubowiecka, L. Synthesis of nonracemic hydroxyglutamic acids. *Beilstein J. Org. Chem.* **2019**, *15*, 236–255. [CrossRef] [PubMed]
9. Wood, J.M.; Furkert, D.P.; Brimble, M.A. 2-Formylpyrrole natural products: Origin, structural diversity, bioactivity and synthesis. *Nat. Prod. Rep.* **2019**, *36*, 289–306. [CrossRef]
10. Singh, N.; Singh, S.; Kohli, S.; Singh, A.; Asiki, H.; Rathee, G.; Chandra, R.; Anderson, E.A. Recent progress in the total synthesis of pyrrole-containing natural products (2011–2020). *Org. Chem. Front.* **2021**, *8*, 5550–5573. [CrossRef]
11. Ogawa, Y.; Konishi, T. *N*-Glycosides of Amino Acid Amides from *Hemerocallis fulva* var. *sempervirens*. *Chem. Pharm. Bull.* **2009**, *57*, 1110–1112. [CrossRef]
12. Zhang, Y.; Cichewicz, R.H.; Nair, M.G. Lipid peroxidation inhibitory compounds from daylily (*Hemerocallis fulva*) leaves. *Life Sci.* **2004**, *75*, 753–763. [CrossRef]
13. Inoue, T.; Iwagoe, K.; Konishi, T.; Kiyosawa, S.; Fujiwara, Y. Novel 2,5-dihydrofuryl-γ-lactam derivatives from *Hemerocallis fulva* L. var. *kwanzo regel. Chem. Pharm. Bull.* **1990**, *38*, 3187–3189. [CrossRef]
14. Ogawa, Y.; Minamizawa, A.; Tada, S.; Konishi, T. Variation of body temperature after administration of amino acid amides. *Res. J. Phytochem.* **2013**, *7*, 10–17. [CrossRef]
15. Ogawa, Y.; Uchiyama, N.; Konishi, T.; Urade, Y. Oxypinnatanine promotes non-rapid eye movement sleep in mice. *Sleep Biol. Rhythms* **2013**, *11*, 40–45. [CrossRef]
16. Zhang, X.; Schmitt, A.C.; Jiang, W. A convenient and high yield method to prepare 4-hydroxypyroglutamic acids. *Tetrahedron Lett.* **2001**, *42*, 5335–5338. [CrossRef]
17. Tamborini, L.; Conti, P.; Pinto, A.; Colleoni, S.; Gobbi, M.; De Micheli, C. Synthesis of new β- and γ-benzyloxy-*S*-glutamic acid derivatives and evaluation of their activity as inhibitors of excitatory amino acid transporters. *Tetrahedron* **2009**, *65*, 6083–6089. [CrossRef]
18. Lu, J.-Y.; Riedrich, M.; Mikyna, M.; Arndt, H.-D. Aza-Wittig-Supported Synthesis of the A Ring of Nosiheptide. *Angew. Chem. Int. Ed.* **2009**, *48*, 8137–8140. [CrossRef]
19. Benoiton, L.; Winitz, M.; Birnbaum, S.M.; Greenstein, J.P. Studies on Diastereomeric α-Amino Acids and Corresponding α-Hydroxy Acids. IX. Configuration of the Isomeric γ-Hydroxyglutamic Acids. *J. Am. Chem. Soc.* **1957**, *79*, 6192–6198. [CrossRef]
20. Lee, Y.K.; Kaneko, T. Optical Resolution and Stereochemistry of γ-Hydroxyglutamic Acid. *Bull. Chem. Soc. Jpn.* **1973**, *46*, 3494–3498. [CrossRef]
21. Krasnov, V.P.; Alekseeva, L.V.; Firsova, N.A.; Kodess, I.K.; Burde, N.L. Stereospecific synthesis of enantiomers of 4-hydroxyglutamic acid and study of their inhibiting properties with respect to glutamine synthetase. *Pharm. Chem. J.* **1984**, *18*, 369–372. [CrossRef]
22. Hanessian, S.; Vanasse, B. Novel Access to (3*R*)- and (3*S*)-3-hydroxy-L-aspartic acids, (4*S*)-4-hydroxy-L-glutamic acid, and related amino acids. *Can J. Chem.* **1993**, *71*, 1401–1406. [CrossRef]
23. Belhadj, T.; Nowicki, A.; Moody, C.J. Synthesis of the 'Northern-Hemisphere' Fragments of the Thiopeptide Antibiotic Nosiheptide. *Synlett* **2006**, 3033–3036. [CrossRef]
24. Ritter, A.R.; Miller, M.J. Asymmetric Syntheses of Novel Amino Acids and Peptides from Acylnitroso-Derived Cycloadducts. *Tetrahedron Lett.* **1994**, *35*, 9379–9382. [CrossRef]
25. Gefflaut, T.; Bauer, U.; Airola, K.; Koskinen, A.M.P. Asymmetric 1,3-Dipolar Cycloaddition: Synthesis of *N*-protected (4*S*)-4-Hydroxy L-Glutamic Acid Diester. *Tetrahedron: Asymmetry* **1996**, *7*, 3099–3102. [CrossRef]

26. Guérard-Hélaine, C.; Heuson, E.; Ndiaye, M.; Gourbeyre, L.; Lemaire, M.; Hélaine, V.; Charmantray, F.; Petit, J.-L.; Salanoubat, M.; de Berardinis, V. Stereoselective synthesis of γ-hydroxy-α-amino acids through aldolase-transaminase recycling cascades. *Chem. Commun.* **2017**, *53*, 5465–5468. [CrossRef]
27. Kolarovič, A.; Jakubec, P. State of the Art in Crystallization-Induced Diastereomer Transformations. *Adv. Synth. Catal.* **2021**, *363*, 4110–4158. [CrossRef]
28. Ďuriš, A.; Wiesenganger, T.; Moravčíková, D.; Baran, P.; Kožíšek, J.; Daïch, A.; Berkeš, D. Expedient and Practical Synthesis of CERT-Dependent Ceramide Trafficking Inhibitor HPA-12 and Its Analogues. *Org. Lett.* **2011**, *13*, 1642–1645. [CrossRef] [PubMed]
29. Berkeš, D.; Kolarovič, A.; Manduch, R.; Baran, P.; Považanec, F. Crystallization-induced asymmetric transformation (CIAT): Stereoconvergent acid-catalyzed lactonization of substituted 2-amino-4-aryl-4-hydroxybutanoic acids. *Tetrahedron: Asymmetry* **2005**, *16*, 1927–1934. [CrossRef]
30. Kasai, M.; Ziffer, H. Ruthenium Tetroxide Catalyzed Oxidations of Aromatic and Heteroaromatic Rings. *J. Org. Chem.* **1983**, *48*, 2346–2349. [CrossRef]
31. Miranda, L.S.M.; Vasconcellos, M.L.A.A. Chemoselective RuO_4 Oxidation of Phenyl or *p*-Methoxyphenyl Groups to Carboxylic Acid Functions in the Presence of a Tetrahydropyran Ring. *Synthesis* **2004**, 1767–1770. [CrossRef]
32. Geng, H.M.; Chen, J.L.-Y.; Furkert, D.P.; Jiang, S.; Brimble, M.A. A Convergent Synthesis of the 2-Formylpyrrole Spiroketal Natural Product Acortatarin, A. *Synlett* **2012**, *23*, 855–858. [CrossRef]
33. Woods, T.M.; Kamalov, M.; Harris, P.W.R.; Cooper, G.J.S.; Brimble, M. Synthesis of Monolysyl Advanced Glycation Endproducts and Their Incorporation into Collagen Model Peptides. *Org. Lett.* **2012**, *14*, 5740–5743. [CrossRef]
34. Woods, T.M.; Cooper, G.J.S.; Brimble, M. Synthesis of stable isotope-labelled monolysyl advanced glycation endproducts. *Amino Acids* **2013**, *45*, 319–325. [CrossRef]
35. Yuen, T.-Y.; Eaton, S.E.; Woods, T.M.; Furkert, D.P.; Choi, K.W.; Brimble, M.A. A Maillard Approach to 2-Formylpyrroles: Synthesis of Magnolamide, Lobechine and Funebral. *Eur. J. Org. Chem.* **2014**, 1431–1437. [CrossRef]
36. Wood, J.M.; Furkert, D.P.; Brimble, M.A. Synthesis of the 2-Formylpyrrole Spiroketal Pollenopyrroside A and Structural Elucidation of Xylapyrroside A, Shensongine A and Capparisine, B. *Org. Biomol. Chem.* **2016**, *14*, 7659–7664. [CrossRef] [PubMed]
37. Maeba, I.; Takeuchi, T.; Iijima, T.; Furukawa, H. C-Nucleosides. 7. Preparation and Utility of 6-Hydroxy-6-(2,3,5-tri-*O*-benzoyl-β-D-ribofuranosyl)-2*H*-pyran-3(6*H*)-one as a Key Intermediate of C-Nucleoside Synthesis. *J. Org. Chem.* **1988**, *53*, 1401–1405. [CrossRef]
38. Borthwick, A.D. 2,5-Diketopiperazines: Synthesis, Reactions, Medicinal Chemistry, and Bioactive Natural Products. *Chem.Rev.* **2012**, *112*, 3641–3716. [CrossRef]
39. Okada, T.; Sakaguchi, K.; Shinada, T.; Ohfune, Y. Total synthesis of (–)-funebrine via Au-catalyzed regio- and stereoselective γ-butyrolactonization of allenylsilane. *Tetrahedron Lett.* **2011**, *52*, 5744–5746. [CrossRef]
40. Yamada, M.; Nagashima, N.; Hasegawa, J.; Takahashi, S. A Highly Efficient Asymmetric Synthesis of Methoxyhomophenylalanine Using Michael Addition of Phenylethylamine. *Tetrahedron Lett.* **1998**, *39*, 9019–9022. [CrossRef]
41. Chen, C.-H.; Genapathy, S.; Fischer, P.M.; Chan, W.C. A facile approach to tryptophan derivatives for the total synthesis of argyrin analogues. *Org. Biomol. Chem.* **2014**, *12*, 9764–9768. [CrossRef]
42. Sarkar, S.K.; Upul Ranaweera, R.A.; Merugu, R.; Abdelaziz, N.M.; Robinson, J.; Day, H.A.; Krause, J.A.; Gudmundsdottir, A.D. Comparison of the Photochemistry of Acyclic and Cyclic 4-(4-Methoxy-phenyl)-4-oxo-but-2-enoate Ester Derivatives. *J. Phys. Chem. A* **2020**, *124*, 7346–7354. [CrossRef]
43. Subbiah, S.; Simeonov, S.P.; Esperança, J.M.; Rebelo, L.P.N.; Afonso, C.A. Direct transformation of 5-hydroxymethylfurfural to the building blocks 2, 5-dihydroxymethylfurfural (DHMF) and 5-hydroxymethyl furanoic acid (HMFA) via Cannizzaro reaction. *Green chemistry* **2013**, *15*, 2849–2853. [CrossRef]
44. Geng, H.M.; Stubbing, L.A.; Li-yang Chen, J.; Furkert, D.P.; Brimble, M.A. Synthesis of the revised structure of acortatarin A. *European Journal of Organic Chemistry* **2014**, *2014*, 6227–6241. [CrossRef]
45. Sheldrick, G.M. SHELXT–Integrated space-group and crystal-structure determination. *Acta Crystallogr. Sect. A Found. Adv.* **2015**, *71*, 3–8. [CrossRef] [PubMed]
46. Sheldrick, G.M. Crystal structure refinement with SHELXL. *Acta Crystallogr. Sect. C Struct. Chem.* **2015**, *71*, 3–8. [CrossRef] [PubMed]

molecules

MDPI

Article

Multicomponent Domino Cyclization of Ethyl Trifluoropyruvate with Methyl Ketones and Amino Alcohols as A New Way to γ-Lactam Annulated Oxazacycles

Marina V. Goryaeva [1], Olesya A. Fefelova [1], Yanina V. Burgart [1], Marina A. Ezhikova [1], Mikhail I. Kodess [1], Pavel A. Slepukhin [1], Vasily S. Gaviko [2] and Victor I. Saloutin [1,*]

[1] Postovsky Institute of Organic Synthesis, Ural Branch of the Russian Academy of Science (IOS UB RAS), Ekaterinburg 620108, Russia
[2] M.N. Mikheev Institute of Metal Physics, Ural Branch of the Russian Academy of Sciences (IMP UB RAS), Ekaterinburg 620108, Russia
* Correspondence: saloutin@ios.uran.ru

Abstract: A new route to bicyclic γ-lactams was found, which was proposed as a three-component cyclization of ethyl trifluoropyruvate with methyl ketones and 1,2-, 1,3-amino alcohols. As a result, a series of trifluoromethyl-substituted tetrahydropyrrolo [2,1-*b*]oxazol-5-ones and tetrahydropyrrolo[2,1-*b*][1,3]oxazine-6-ones was synthesized, in which the substituent at the nodal carbon atom was varied. The introduction of a twofold excess of ethyl trifluoropyruvate in reactions with amino alcohols and acetone made it possible to obtain the same bicycles, but functionalized with a hydroxyester fragment, which are formed due to four-component interactions of the reagents. Transformations with 2-butanone and aminoethanol lead predominantly to similar bicycles, while an analogous reaction with aminopropanol gives *N*-hydroxypropyl-2,3-dihydropyrrol-5-one. Almost all bicycles are formed as two diastereomers, the structure of which was determined using ^{1}H, ^{19}F, ^{13}C NMR spectroscopy, including two-dimensional experiments and XRD analysis. A domino mechanism for the formation of tetrahydropyrrolo[2,1-*b*]oxazacycles was proposed, which was confirmed by their stepwise synthesis through the preliminary preparation of the aldol and bis-aldol from ethyl trifluoropyruvate and methyl ketones.

Keywords: multicomponent domino cyclizations; ethyl trifluoropyruvate; methyl ketones; amino alcohols; γ-lactams; tetrahydropyrrolo[2,1-*b*]oxazolones; tetrahydropyrrolo[2,1-*b*]oxazinones

Citation: Goryaeva, M.V.; Fefelova, O.A.; Burgart, Y.V.; Ezhikova, M.A.; Kodess, M.I.; Slepukhin, P.A.; Gaviko, V.S.; Saloutin, V.I. Multicomponent Domino Cyclization of Ethyl Trifluoropyruvate with Methyl Ketones and Amino Alcohols as A New Way to γ-Lactam Annulated Oxazacycles. *Molecules* **2023**, *28*, 1983. https://doi.org/10.3390/molecules28041983

Academic Editors: Alexey M. Starosotnikov, Maxim A. Bastrakov and Igor L. Dalinger

Received: 31 January 2023
Revised: 17 February 2023
Accepted: 18 February 2023
Published: 20 February 2023

1. Introduction

The γ-lactam (2-pyrrolidone) framework is of great importance for the creation of new heterocyclic compounds, since this motif is present in many natural bioactive molecules [1], including alkaloid cotinine (I) found in tobacco [2], lactacystin (II), obtained from a Streptomyces bacterial strain [3] and clausenamide (III) extracted from Clausena lansium [4] (Figure 1). Some synthetic pharmaceuticals also have a γ-lactam moiety, for example, a respiratory stimulant doxapram (IV) [5], ethosuximide (V) used to treat absence seizures [6], and the large family of racetams that have nootropic and/or anticonvulsant effects [7]. One of the representatives of this series, dimiracetam (tetrahydropyrrolo[1,2-*a*]imidazole-2,5-dione) (VI) [8] is a bicyclic derivative of γ-lactam. Moreover, γ-lactam analogues of penem (VII) [9] and penicillin acids (VIII) [10] with antibacterial properties have been synthesized.

One of the known bicyclic γ-lactams are Meyers' lactams (tetrahydropyrrolo[2,1-*b*]oxazol-5-ones) (IX) [11] (Figure 1), which have a great synthetic potential for obtaining natural alkaloids due to the possibility of opening the oxazole ring [12]. For their preparation, a bielectrophile–binucleophile reaction of γ-keto acids with chiral amino alcohols, called Meyers' lactamization, is used [13,14]. In addition, oxazolo-annulated γ-lactams can be obtained by cyclization of levulinic acid with *R*-phenylglycinol [15] or by the reaction of

hydroxyl halogenoamides with Michael acceptors [16,17]. The latter method was also used for the synthesis of oxazine-annulated γ-lactams (tetrahydropyrrolo[2,1-*b*][1,3]oxazine-6-ones) [17]. Cyclization of ethyl 4-oxoalkanoates with amino alcohols is also a convenient protocol for the synthesis of this bicyclic system [18–20].

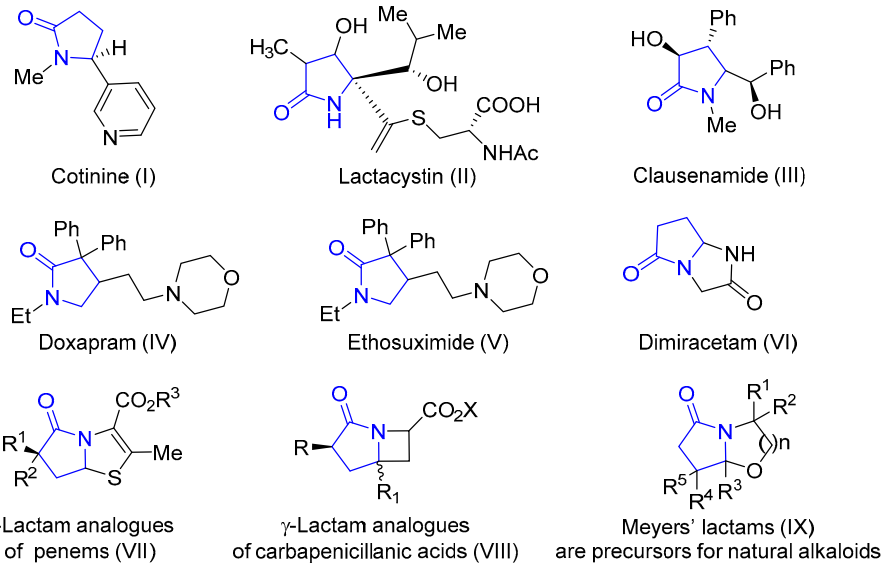

Figure 1. Examples of bioactive γ-lactams.

The preparation of fluorine-containing tetrahydropyrrolo[2,1-*b*]oxazol-5-ones is limited to a few examples. Pentafluoroethyl- and tri(di)fluoromethyl-substituted derivatives were prepared by addition of CF_3CF_2Li to the *N*-valinol imide at low temperatures [21], or acid-catalyzed cyclization of phenylalaninol with methyl 5,5,5-trifluoro-4-oxopentanoate [22] or ethyl 5,5-difluoro-4-oxopentanoate [23], respectively. Electrophilic fluorination of tetrahydropyrrolo[2,1-*b*]oxazolones via their enolation followed by the reaction with *N*-fluorobenzenesulfonimide at −70–(−78 °C) made it possible to synthesize such mono-fluorinated bicycles [24]. It is obvious that all these methods have strict restrictions on the reagents introduced, and some of them require special equipment. Information on fluorine-containing tetrahydropyrrolo[2,1-*b*][1,3]oxazine-6-ones was not found by us. Although the synthesis of fluoroorganic compounds is gaining more and more popularity [25,26], due to the unique properties [27–29] that fluorine atoms introduce to molecules [30], as a result, they have more prospects as biologically active substances.

Multicomponent synthesis is the most modern, simple and low-cost way to create new molecules from available starting reagents. Over the past 7 years, our group has been developing a new multicomponent approach that makes it possible to obtain various fluorine-containing heterocyclic compounds from commercially available polyfluoroalkyl-3-oxo esters, methyl ketones, and nucleophiles [31–34].

This protocol is based on the outstanding ability of the polyfluoracyl group of the oxoester to attach the activated methylene group of the ketone. We have recently used this method for the synthesis of pyrrolidones annulated with an imidazole or pyrimidine ring based on the three-component reaction of ethyl trifluoropyruvate and methyl ketones with ethylenediamine or 1,3-diaminopropane [35]. It was found that, in contrast to similar transformations of trifluoroacetoacetic ester, the use of an excess of ethyl trifluoropyruvate in the reaction with acetone and diamines under microwave irradiation leads to tricyclic products with two pyrrolidone fragments.

In this work, for the synthesis of γ-lactams annulated with oxazole or oxazine rings (tetrahydropyrrolo[2,1-*b*]oxazol-5-ones and tetrahydropyrrolo[2,1-*b*][1,3]oxazine-6-ones), multicomponent reactions of ethyl trifluoropyruvate **1** with methyl ketones **2** and 1,2-, 1,3-amino alcohols **3** were studied. In addition, their differences from the previously studied cyclizations with 1,2- and 1,3-diamines were found [35].

2. Results

We started our study with a three-component reaction of ethyl trifluoropyruvate **1** with acetone **2a** and 2-aminoethanol **3a** in 1,4-dioxane at an equimolar ratio of reagents at room temperature (Scheme 1), since previously such conditions were optimal in similar syntheses with diamines [35]. It turned out that the reaction in 1,4-dioxane proceeds nonselectively and, in addition to a mixture of *cis*- and *trans*-diastereomers of the expected 6-hydroxy-7a-methyl-6-(trifluoromethyl)tetrahydropyrrolo[2,1-*b*]oxazol-5-one **4a**, a small amount of ethyl 3,3,3-trifluoro-2-hydroxy-2[(6-hydroxy-5-oxo-6-(trifluoromethyl)tetrahydropyrrolo[2,1-*b*]oxazol-7a-yl)methyl]propanoate **5** is also formed as two *trans,cis*- and *cis,cis*-diastereomers (Scheme 1, Table 1, entry 1). The *cis*- and *trans*-configurations of diastereomeric bicycles **4** were determined relative to the OH-group and oxygen atom of the adjacent heterocycle. Note that the *trans,cis*- and *cis,cis*- diastereomers **5** have an additional stereocenter in the hydroxyester fragment.

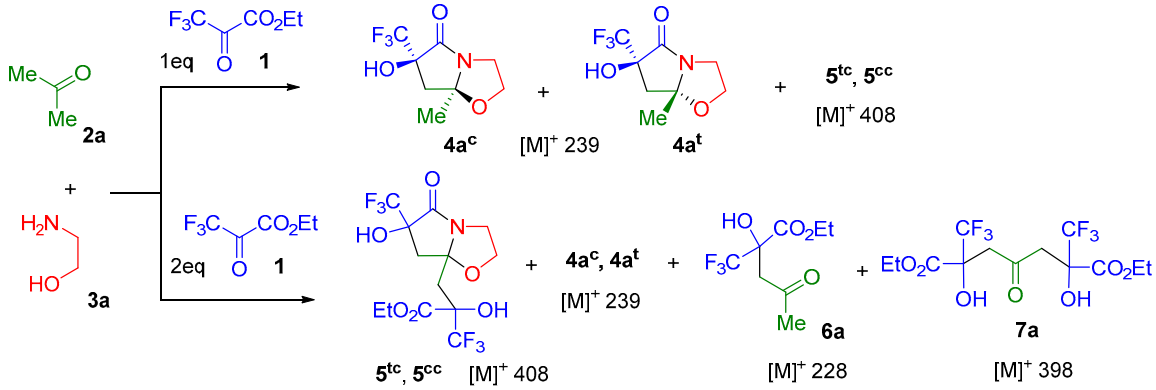

Scheme 1. Three-component reaction of ethyl trifluoropyruvate **1**, acetone **2a** and aminoethanol **3a**.

Table 1. Optimization of the reaction conditions for ethyl trifluoropyruvate **1**, acetone **2a**, and aminoethanol **3a**.

Entry	Conditions *	1 (eq)	Time, Day	T, °C	Composition of the Reaction Mixture According to ^{19}F NMR Data, δ, ppm **						
					4a^c	**4a^t**	**5^{tc}**	**5^{cc}**	**6a**	**7a**	**By-Prod.**
1	1,4-dioxane	1	7	25	26	40	11	12	-	-	11
2	Toluene	1	7	25	26	27	17	18	-	-	12
3	EtOH	1	7	25	23	26	12	16	-	-	23
4	$C_2H_4Cl_2$	1	7	25	23	25	16	15	-	-	21
5	MeCN	1	7	25	15	30	21	20	-	-	12
6	THF	1	7	25	13	29	20	22	-	-	16
7	$C_2H_4Cl_2$	2	7	25	6	5	32	30	8	4	18
8	1,4-dioxane	2	7	25	3	4	35	37	3	4	14
9	THF	2	7	25	2	3	37	40	2	10	6
10	THF	2	2	50	6	4	28	31	-	-	31

* Reactions were carried out with 170 mg (1 mmol) or 340 mg (2 mmol) of ethyl trifluoropyruvate **1**, 58 mg (1 mmol) of acetone **2a**, 61 mg (1 mmol) of aminoethanol **3a** in 2 mL of solvent. ** Determined by ^{19}F NMR spectroscopy of the reaction mixture: **4a^c** (δ_F 83.63 ppm), **4a^t** (δ_F 83.91 ppm), **5^{tc}** (δ 84.92, 83.83 ppm), **5^{cc}** (δ 84.21, 85.55 ppm), **6a** (δ 84.80 ppm) **7a** (δ 84.78, 84.79 ppm).

The formation of these products was recorded during the analysis of the reaction mixture by ^{19}F NMR spectroscopy and GC-MS. It should be noted that in the GC-MS analysis diastereomers of bicycles **4a** and **5** had the same peaks of molecular ions, but different retention times. The use of ^{19}F NMR spectroscopy is very informative in such studies, since the starting pyruvate **1** (δ_F CF_3 81.08 ppm) and products based on it have different chemical shifts of the signals of CF_3 groups.

The non-selective reaction of ethyl trifluoropyruvate **1** with acetone **2a** and aminoethanol **3a** in 1,4-dioxane prompted us to investigate this synthesis in various solvents and with different amounts of pyruvate **1**. However, varying solvents (toluene, THF, dichloroethane, ethanol, acetonitrile) at equimolar loadings of reagents invariably led to the formation of a mixture of products **4a** and **5**, while the number of heterocycles **5** in the reaction mixture even increased (Table 1, entries 1–6).

Since bicycle **5** is the result of a four-component cyclization due to the participation of two molecules of trifluoropyruvate **1**, it was logical to study these transformations with its twofold excess. Indeed, it turned out that the use of a twofold excess of pyruvate **1** increased the yield of compounds **5**, while bicycle **4a** was formed in a minimum amount of 2–6% (Table 1, entries 7–9). However, using an excess of pyruvate **1**, we detected the formation of aldol **6a** [36] and bis-aldol **7a** [35] by ^{19}F NMR spectroscopy, which were isolated and characterized earlier. The highest yield of heterocycles **5** was achieved in THF at room temperature (Table 1, entry 9). Heating the reaction mixture in THF at 50 °C to speed up the process resulted in resinification and an increase in by-products (Table 1, entry 10).

Thus, as a result of varying the conditions, it was found that 1,4-dioxane is the most optimal solvent for the preparation of heterocycle **4a**, and THF for the synthesis of product **5**.

Furthermore, we carried out three-component equimolar reactions of ethyl trifluoropyruvate **1** with methyl ketone **2a–d** and 2-aminoethanol **3a** or 3-amino-1-propanol **3b** in 1,4-dioxane at room temperature. In this case, the introduction of aminopropanol **3b** in the reaction expands the scope of these three-component transformations, allowing the synthesis of oxazine derivatives. Variation of the methyl ketone component, which used not only acetone **2a**, but also 2-butanone **2b**, 2-hexanone **2c**, and acetophenone **2d**, makes it possible to change the substituent at the nodal carbon atom of the resulting bicycles. It was found that in reactions with alkyl methyl ketones **2a–c** in each case, a mixture of *cis*- and *trans*-diastereomers of pyrrolo[2,1-*b*][1,3]oxazol-5-ones **4a–c** or pyrrolo[2,1-*b*][1,3]oxazin-6-ones **8a–c** is formed (Scheme 2). Notably, there is one more regularity: *trans*-diastereomers were prevailed in the formation of oxazole derivatives **4**, while *cis*-isomers were prevailed in the formation of oxazine bicycles **8**.

In contrast, similar cyclizations of ethyl trifluoropyruvate **1** with amino alcohols **3a,b** and acetophenone **2d** in each case, lead to one diastereomer **4d^{c}** or **8d^{t}**. The change and increase in stereoselectivity of this reaction may be due to the presence of a bulky phenyl substituent, which plays the role of a conformational anchor stabilizing the most favorable diastereomeric form.

We succeeded in isolating diastereomers **4a^{t}**, **4b^{t}**, **4c^{c}**, **4d^{c}**, **8b^{t}**, **8c^{c}**, **8d^{t}** in pure form by column chromatography. Diastereomers **4a^{c}**, **4b^{c}**, **4c^{t}**, **8a^{c}**, **8a^{t}**, **8b^{c}**, **8c^{t}**, **8d^{t}** contain from 2 to 19% impurities of the second isomer, but we were able to record ^{13}C NMR spectra for them, in which signals of only the main compound were accumulated. The isolation of bicycles **4a^{t}**, **4b^{c}** and **8a^{c}**, **8a^{t}**, **8b^{c}**, **8b^{t}** obtained from acetone **2a** and 2-butanone **2b** was complicated by side products **5**, **9**, **10**, **11**, the individual synthesis of which will be described below (Schemes 3 and 4). These compounds were formed in a small amount, but strongly interfered with the separation, while no such behavior was observed in the reactions with 2-hexanone **2c**. We were unable to isolate the bicycle **4a^{c}** in its pure form, and despite several column chromatography, it still contained impurities of by-products **4a^{t}** (2%) and **5** (20%). Difficulties in separating diastereomers are due to their similar physicochemical properties owing to structural similarity.

Further, reactions of a twofold excess of pyruvate **1** with acetone **2a** and amino alcohols **3a,b** in THF at room temperature were studied. The reaction of pyruvate **1** with acetone **2a** and aminoethanol **3a** leads to the formation of pyrrolo[2,1-*b*][1,3]oxazolone **5** functionalized with a 2-trifluoromethyl-2-hydroxypropanoate fragment (which can be called a heterocyclic aldol) as a mixture of two *trans*,*cis*- and *cis*,*cis*-diastereomers in a ratio of 60%:40% (Scheme 3), which we managed to separate. Diastereomer **5^{tc}** precipitated during the reaction, and diastereomer **5^{cc}** was isolated from the reaction mixture by column

chromatography. However, the yields of pure products are low, since fractions with an unseparated mixture of isomers remain.

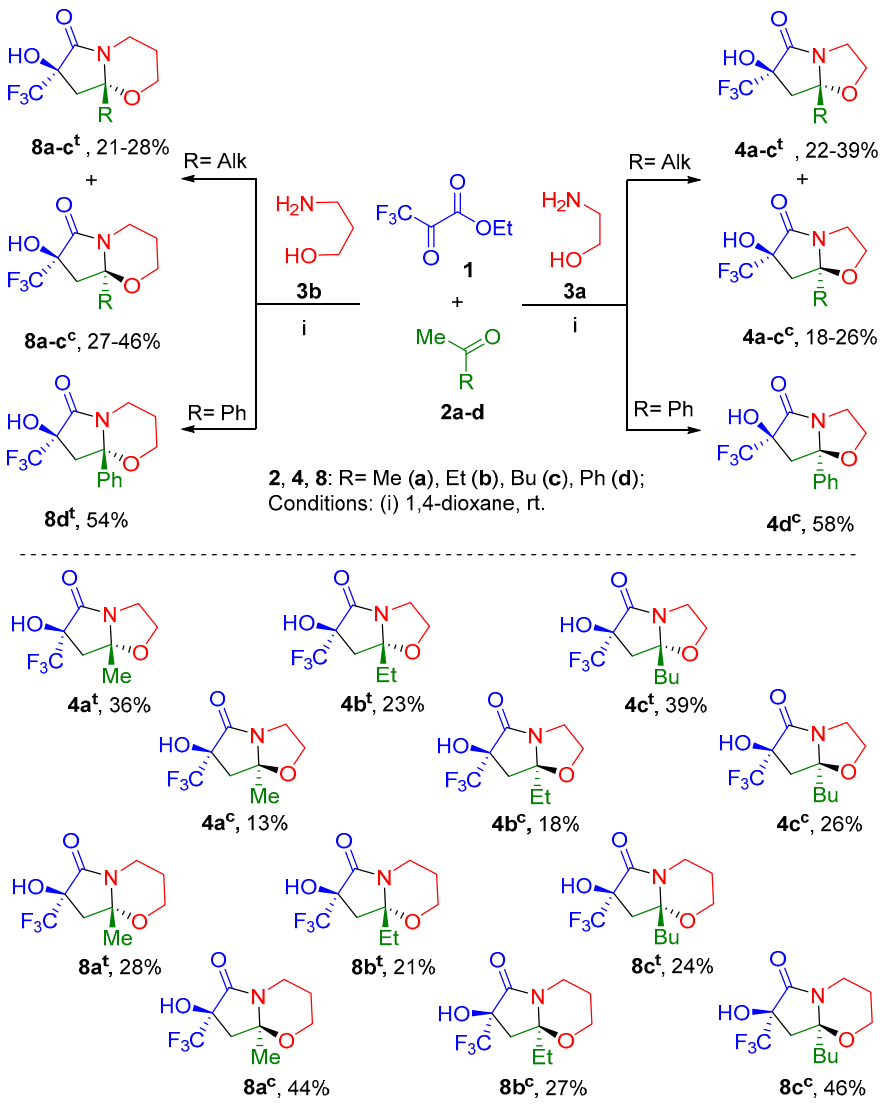

Scheme 2. Three-component equimolar reactions of ethyl trifluoropyruvate **1** and methyl ketones **2a–d** with amino alcohols **3a,b** (all yields are given for isolated products).

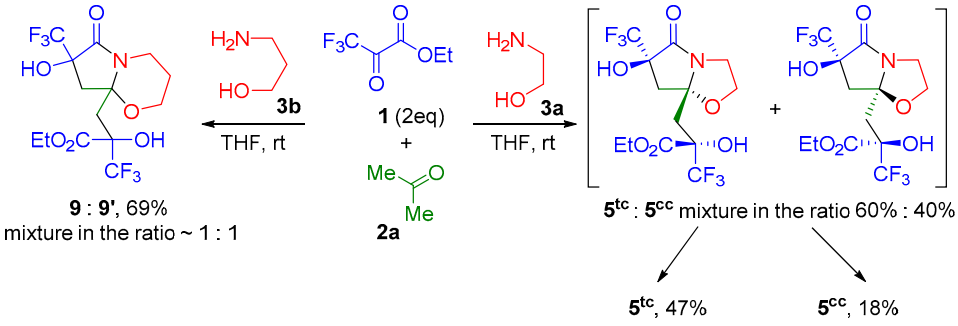

Scheme 3. Three-component reactions of a twofold excess of ethyl trifluoropyruvate **1** with acetone **2a** and amino alcohols **3a,b**.

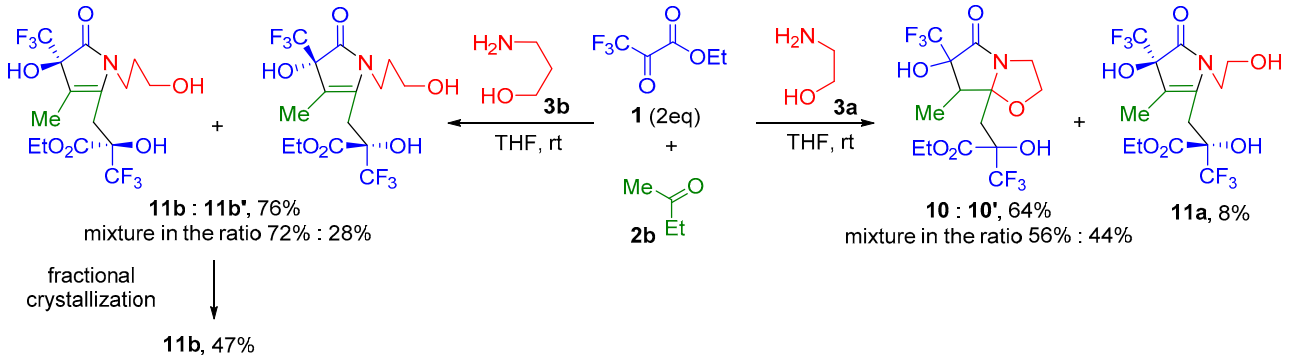

Scheme 4. Three-component reactions of a twofold excess of ethyl trifluoropyruvate **1** with 2-butanone **2b** and amino alcohols **3a,b**.

The reaction of a twofold excess of pyruvate **1** with acetone **2a** and aminopropanol **3b** proceeds similarly and leads to the formation of a mixture of diastereomers of functionalized pyrrolo[2,1-*b*][1,3]oxazinone **9** in a ratio of ~ 1:1 (Scheme 3). However, due to their very similar properties, diastereomers **9** and **9′** were not separated.

In addition, 2-butanone **2b** was introduced into interaction with a twofold excess of pyruvate **1** and amino alcohols **3a,b** (Scheme 4), and unexpected results were obtained. It turned out that the use of 2-butanone **2b** with pyruvate **1** and aminoethanol **3a** leads to the formation of 6-methyl-substituted pyrrolo[2,1-*b*][1,3]oxazolone as a mixture of diastereomers **10** and **10′** in a ratio of 56%:44% by analogy with the formation of bicycles **5** and **9** (Scheme 3). In addition, *N*-hydroxyethylpyrrol-5-one **11a** was isolated from this reaction in a small amount.

The reaction of 2-butanone **2b** with pyruvate **1** and aminopropanol **3b** leads only to *N*-hydroxypropylpyrrol-5-one **11b** as a mixture of diastereomers **11b**:**11b′** in a ratio of 72%:28% (Scheme 4). We were able to isolate diastereomer **11b** in pure form by fractional crystallization from a mixture of diethyl ether and hexane in 47% yield.

It is obvious that amino alcohols **3a,b** react as mononucleophiles during the formation of pyrrolidinones **11a,b**. Previously, we showed that amino alcohols **3a,b** in three-component reactions of polyfluoroalkyl-3-oxo esters with methyl ketones **2** or cycloketones can behave both as mono- and di-nucleophiles [32,37].

The introduction of 2-hexanone **2c** into the reaction with amino alcohols **3a,b** and a double excess of pyruvate **1** in THF led to the formation of bicycles **4c** and **8c** already obtained as a mixture of diastereomers (Scheme 5). Obviously, the nucleophilicity of a-methylene center of the butyl substituent in 2-hexanone **2c** is significantly reduced under the influence of electronic and steric factors than in 2-butanone **2b** and, therefore, does not take part in the aldol addition reaction. It can be noted that these reactions were accompanied by the formation of more by-products, compared with the reactions performed at an equimolar ratio of reagents.

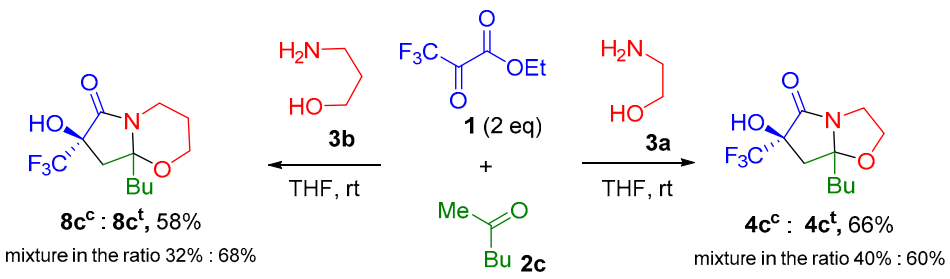

Scheme 5. Three-component reactions of a twofold excess of ethyl trifluoropyruvate **1** with 2-hexanone **2c** and amino alcohols **3a,b**.

We were unable to select conditions for the synthesis of pyrrolo[2,1-*b*]oxazolones **4a,b** or pyrrolo[2,1-*b*]oxazinones **8a,b** in good yields in three-component reactions of trifluoropyruvate **1** with methyl ketones **2a,b** and amino alcohols **3a,b** due to the formation of side bicycles **5**, **9**, **10**, **11**, formed as a result of four-component transformations. In this regard, we used a two-stage approach through the initial preparation of aldols **6a,b** from ethyl trifluoropyruvate **1** and methyl ketones **2a,b** (Scheme 6), thus, aldol **6a** was synthesized earlier [36], and the ethyl-substituted analog **6b** was obtained for the first time. Next, aldols **6a,b** were introduced into cyclization with amino alcohols **3a,b**, as a result of which bicycles **4a,b** and **8a,b** were also obtained as a mixture of *cis*- and *trans*-diastereomers.

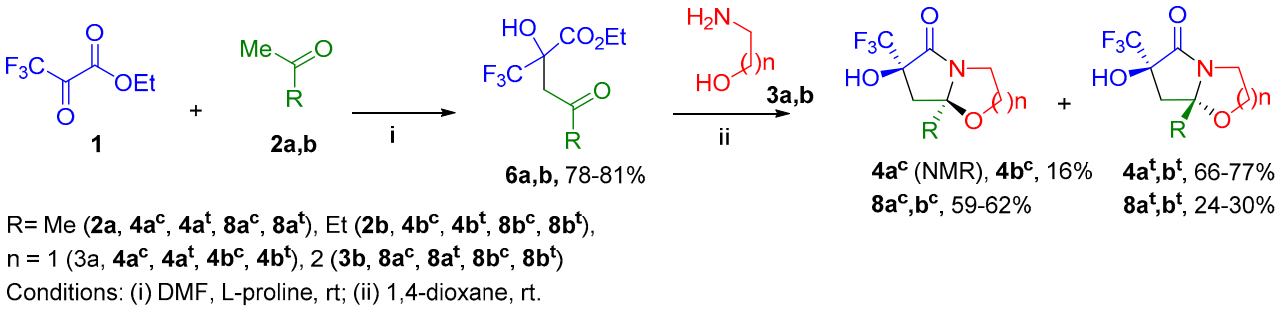

Scheme 6. Two-step approach to obtaining products **4a,b** and **8a,b**.

We analyzed the reaction mixtures obtained by two- and three-component approaches using ^{19}F NMR spectroscopy. A difference in the ratio of *cis*- and *trans*-diastereomeric products **4**, **8** (Table 2) was found, since the proportion of predominant isomers increased significantly. Thus, in the reactions of aldols **6a,b** with aminoethanol **3a**, *trans*-isomers **4a^t**, **4b^t** were formed with approximately a threefold advantage, and in reactions with aminopropanol **3b**, *cis*-diastereomers **8a^c**, **8b^c** increased by approximately two times. This made it possible to isolate diastereomers **4a,b^t** and **8a,b^c** in higher yields.

Table 2. The ratio of diastereomeric products **4** and **8** obtained by two- and three-component methods.

Products (δ_F, ppm), ^{19}F NMR Data	The Ratio of Diastereomers in the Reaction Mixture, %	
	Three-Component Method	Two-Component Method
4a^c (83.63):**4a^t** (83.91)	39:61	16:84
4b^c (83.79):**4b^t** (83.89)	44:56	22:78
8a^c (83.71):**8a^t** (84.22)	56:44	65:35
8b^c (83.85):**8b^t** (84.14)	54:46	67:33

Heterocyclic aldols **5**, **9–11**, which are products of a four-component reaction, can be assumed to form in two ways: through the cyclization of bis-aldol **7** with amino alcohol **3** or through the addition of a methyl substituent of bicycles **4** and **8** to the trifluoroacyl group of pyruvate **1**. However, an attempt to carry out the aldolization reaction of pyruvate **1** under the action of the bicycle **4a^t** was unsuccessful regardless of the conditions used (Scheme 7). While the bis-aldol **7a** easily cyclized with aminoethanol **3a**, giving a mixture of diastereomers of the expected heterocyclic aldols **5^{tc}** and **5^{cc}** with a predominance of the *trans*,*cis*-form.

The structure of the synthesized heterocycles **4**, **5**, **8–11** was confirmed by IR, ^{1}H, ^{19}F, ^{13}C NMR spectroscopy and mass spectrometry. The diastereomeric structure of bicycles **4**, **5**, **8**, **11** was established using two-dimensional experiments 2D ^{1}H-^{13}C HSQC, ^{1}H-^{13}C HMBC and X-ray diffraction analysis for **4d^c**, **5**, **8c^c**, **11b**. All diastereomers are racemates.

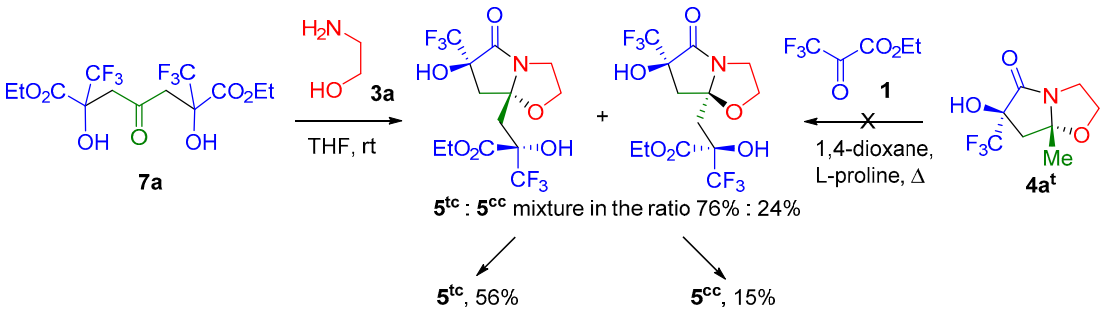

Scheme 7. Proposed pathways for the formation of heterocyclic aldols **5^{tc}**, **5^{cc}**.

The synthesized bicycles **4a–d** and **8a–d** contain two asymmetric centers C-6(7) and C-7a(8a) (Figure 2). Analyzing the chemical shifts of the diastereotopic protons H-A and H-B in the ^{1}H NMR spectra at C-7 or C-8 in heterocycles **4a–d**, **8a–d**, we found the following regularity: the values $\Delta_{AB} = \delta_A - \delta_B$ for the alkyl-substituted heterocycles **4a–c^c** and **8a–c^c**, which have the *cis*-configuration, are in the range Δ_{AB} 0.41–0.56 ppm, whereas for the trans-isomers **4a–c^t** and **8a–c^t** these values are much lower, Δ_{AB} 0.04–0.23 ppm. For diastereomers containing a phenyl substituent, the opposite pattern is observed, for example, for the *cis*-isomer **4d^c** Δ_{AB} 0.10 ppm, while for the *trans*-diastereomer **8d^t** Δ_{AB} 0.42 ppm (Table 3). It was found that the geminal spin–spin coupling constant of these protons of the *cis*-isomers **4a–d^c**, **8a–c^c** are ^2J 15.2–15.5 Hz, while for the *trans*-diastereomers **4a–c^t**, **8a–d^t** ^2J 14.2–14.9 Hz. Previously, we revealed similar features for the *trans*/*cis*-diastereomers of hexahydropyrrolo[1,2-*a*]imidazol-5-ones and hexahydropyrrolo[1,2-*a*]pyrimidin-6-ones [35].

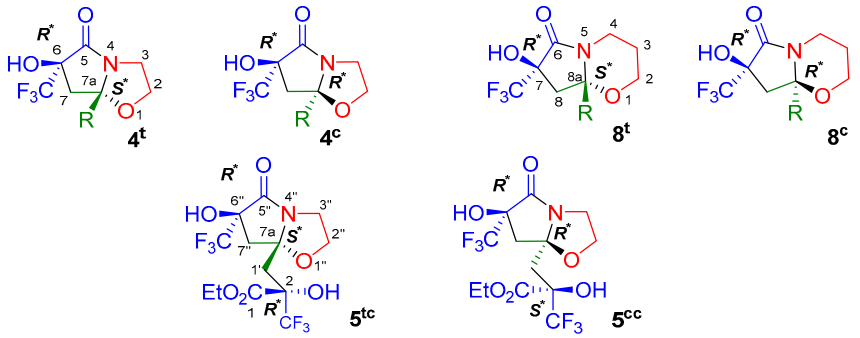

Figure 2. Diastereomeric structure of heterocycles **4**, **5** and **8**.

Table 3. Chemical shifts $\delta_{H\text{-}A}$, $\delta_{H\text{-}B}$ and spin-spin coupling constants (^2J) of diastereotopic protons at C-7(8) atoms for compounds **4a–d**, **8a–d**.

Compounds	R	$\delta_{H\text{-}A}$, ppm	$\delta_{H\text{-}B}$, ppm	Δ_{AB}, ppm	^2J, Hz
4a^c	Me	2.74	2.29	0.45	15.2
4a^t	Me	2.37	2.33	0.04	14.2
4b^c	Et	2.73	2.17	0.56	15.5
4b^t	Et	2.42	2.23	0.19	14.5
4c^c	Bu	2.73	2.19	0.54	15.4
4c^t	Bu	2.42	2.24	0.18	14.5
4d^c	Ph	2.80	2.70	0.10	15.5
8a^c	Me	2.56	2.15	0.41	15.2
8a^t	Me	2.30	2.23	0.07	14.4
8b^c	Et	2.52	2.00	0.52	15.3
8b^t	Et	2.33	2.10	0.23	14.8
8c^c	Bu	2.52	2.02	0.50	15.3
8c^t	Bu	2.33	2.12	0.21	14.7
8d^t	Ph	2.64	2.22	0.42	14.9

Some regularities were found in the shifts of the signals of trifluoromethyl group in the ^{19}F NMR spectra of pyrrolo[2,1-*b*]oxazolones **4a–d** and pyrrolo[2,1-*b*]oxazinones **8a–d**. Thus, the signals of the trifluoromethyl group of *cis*-isomers **4a–d^{c}** are observed in the range δ_F 83.63–83.79 ppm, and the *trans*-forms **4a–c^{t}** in a lower field δ_F 83.87–83.91 ppm, similarly for **8a–c^{c}** signals are recorded in the region δ_F 83.83–83.88 ppm, and for **8a–d^{t}** at δ_F 84.13–84.31 ppm.

The stereo configuration of tetrahydropyrrolo[2,1-*b*][1,3]oxazol-5-one **4** and tetrahydro-2*H*-pyrrolo[2,1-*b*][1,3]oxazine-6-one **8** was additionally confirmed by XRD analysis, which was performed for bicycles **4d^{c}** (Figure 3a) and **8c^{c}** (Figure 3b). It was found that these bicycles have the *cis*-arrangement of the OH-group in the pyrrole and the oxygen atom in the adjacent oxazacycle (Figure 3).

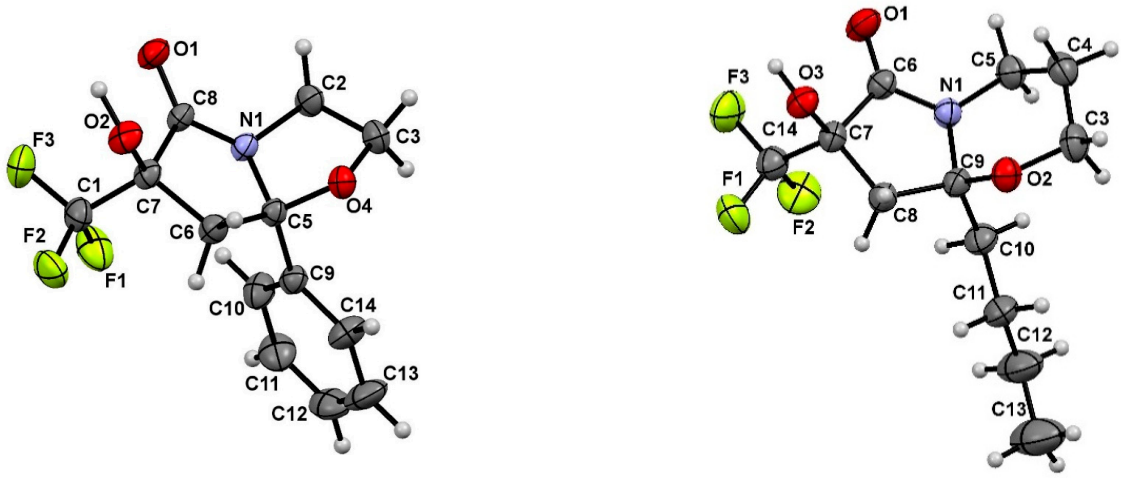

(**a**) (**b**)

Figure 3. The ORTEP view of compounds **4d^{c}** (**a**) and **8c^{c}** (**b**) according to XRD data.

A more difficult task was to determine the structure of heterocyclic aldols **5^{tc}**, **5^{cc}**, **9**, **9′** and **10**, **10′**, which have three or four asymmetric centers, respectively.

The diastereomeric structure of pyrrolo[2,1-*b*]oxazol-5-one **5^{tc}** was determined using XRD analysis (Figure 4a), conforming to which this compound is a racemic mixture of molecules having the configuration of substituents at the stereocenters C-3–*R**, C-5–*S**, C-9–*R** according to the numbering presented in Figure 4a. It was found that the hydroxyl substituent in the pyrrolidine ring and the oxygen atom of the oxazole backbone are in the *trans*-position, while this atom and the hydroxy group of the propanoate fragment are in the *cis*-position. The crystal packing of compound **5^{tc}** is formed due to intermolecular hydrogen bonds of the lactam carbonyl and hydroxyl groups of the cycle O-2–H-2 . . . O-1 1.816 Å and the ester carbonyl and hydroxyl group of the propanoate substituent O-4–H-4 . . . O-5 2.054 Å (Figure 4b).

For a pair of isolated diastereomers **5^{tc}**, **5^{cc}** (Figure 2), two-dimensional experiments 2D ^{1}H-^{13}C HSQC and HMBC were performed, on the basis of which a complete assignment of signals in the ^{1}H and ^{13}C NMR spectra was made. The ^{1}H NMR spectrum of pyrrolo[2,1-*b*]oxazol-5-one **5^{tc}** is characterized by the presence of doublet signals of the methylene protons of the pyrrolidine ring H-7″A and H-7″B at δ_H 2.99, 2.29 ppm (Δ_{AB} 0.70 ppm, ^{2}J 14.9 Hz) and propanoate substituent H-1′A and H-1′B at δ_H 2.63, 2.20 ppm (Δ_{AB} 0.43 ppm, J 14.0 Hz). The ^{13}C NMR spectrum contains characteristic signals of carbonyl atoms at C-5″ of lactam (δ_C 170.2 ppm) and at C-1 of ester (δ_C 167.8 ppm) fragments. The ^{19}F NMR spectrum contains two singlet signals of trifluoromethyl groups at δ_F 83.83 and 84.92 ppm.

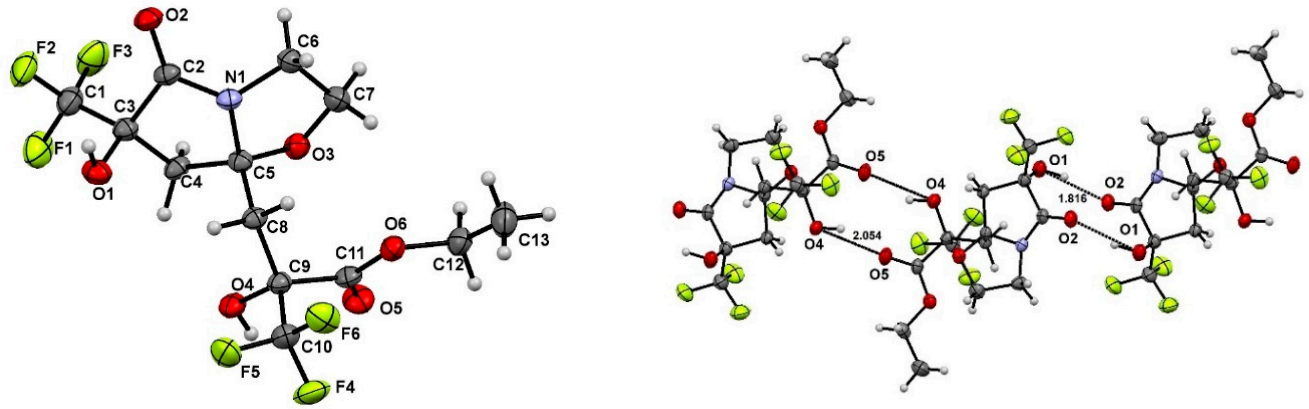

(**a**) (**b**)

Figure 4. (**a**) The ORTEP view of compounds **5**^{tc} according to XRD data; (**b**) crystal packing of compounds **5**^{tc} with indication of intermolecular hydrogen bonds.

According to ^{1}H, ^{19}F and ^{13}C NMR spectra, diastereomer **5**^{cc} has a similar set of characteristic signals. However, analyzing the ^{1}H NMR spectrum, it was found that the doublet signals of the methylene protons of the cycle at H-7″A and H-7″B (δ_H 2.61, 2.26 ppm) have a lower value Δ_{AB} 0.35 ppm and a smaller *J* constant of 14.0 Hz compared to the analogous values of the **5**^{tc} heterocycle. It is obvious that for diastereomers **5**^{tc}, **5**^{cc}, containing a hydroxypropanoate fragment, the same trend in changing Δ_{AB} and constant *J* is observed, as for bicycle **4d**^{c}, which has a bulky phenyl substituent. For the methylene protons H-1′A and H-1′B of the propanoate residue, resonating as doublet signals at δ_H 2.67, 2.50 ppm, the value of Δ_{AB} 0.17 ppm and *J* 15.0 Hz also changes. In the ^{13}C NMR spectra of the **5**^{tc} and **5**^{cc} isomers, the largest differences in shifts were recorded for the carbon atoms C-7″ (δ_C 42.1, 44.6 ppm) of the pyrrolidine ring and C-1 (δ_C 37.8, 40.8 ppm) of the propanoate substituent, which are adjacent to the C-7″ and C-2 stereocenters (Figure 2). All these data allow us to suggest that the **5**^{cc} bicycle has a *cis*,*cis*-diastereomeric structure, in which the position of the substituents at the C-7″ and C-2 stereocenters changes compared to the **5**^{tc} isomer.

The structure of pyrrolo[2,1-*b*][1,3]oxazin-6-ones **9**, **9′** and pyrrolo[2,1-*b*]oxazol-5-ones **10**, **10′** was also established using ^{1}H, ^{13}C and ^{19}F NMR spectra, which contained a double set of all signals, since we were unable to separate diastereomers of bicycles **9** and **10**. However, their spectra characteristics were similar to those of bicycles **5**^{tc} and **5**^{cc}, that allowed us to assign them a similar structure, but without determining the diastereomeric structure due to close values of the chemical shifts of protons and carbon atoms in the ^{1}H and ^{13}C NMR spectra (see the experimental part).

To establish the diastereomeric structure of dihydropyrrol-5-ones **11a,b**, which have two asymmetric centers C-2 and C-4″ (Figure 5), we used the data of ^{1}H, ^{13}C NMR spectroscopy and XRD analysis performed for **11b**. For compounds **11a** and **11b**, two-dimensional 2D ^{1}H-^{13}C HSQC and HMBC experiments were carried out, on the basis of which a complete assignment of signals in the ^{1}H and ^{13}C NMR spectra was made.

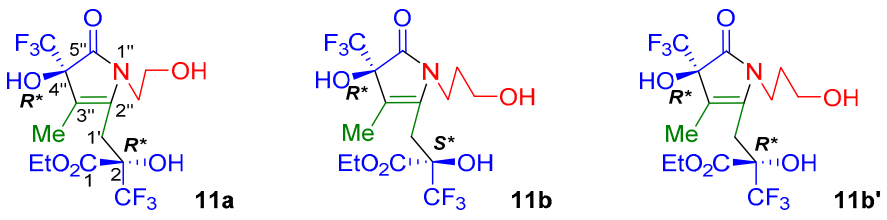

Figure 5. Diastereomeric structure of dihydropyrrol-5-ones **11**.

The diastereomeric structure of dihydropyrrol-5-one **11b** was determined by X-ray diffraction data (Figure 6a). Crystal packing is formed of a racemic mixture of molecules linked by intermolecular hydrogen bonds O-1–H-1 . . . O-2 1.882 Å, O-3–H-3 . . . O-6 2.122 Å (Figure 6b). The configuration of the substituents in the pyrrole ring at the C-1 stereocenter is *R**, and that of the propanoate substituent at C-8 is *S** (numbering is used according to X-ray diffraction data, Figure 6).

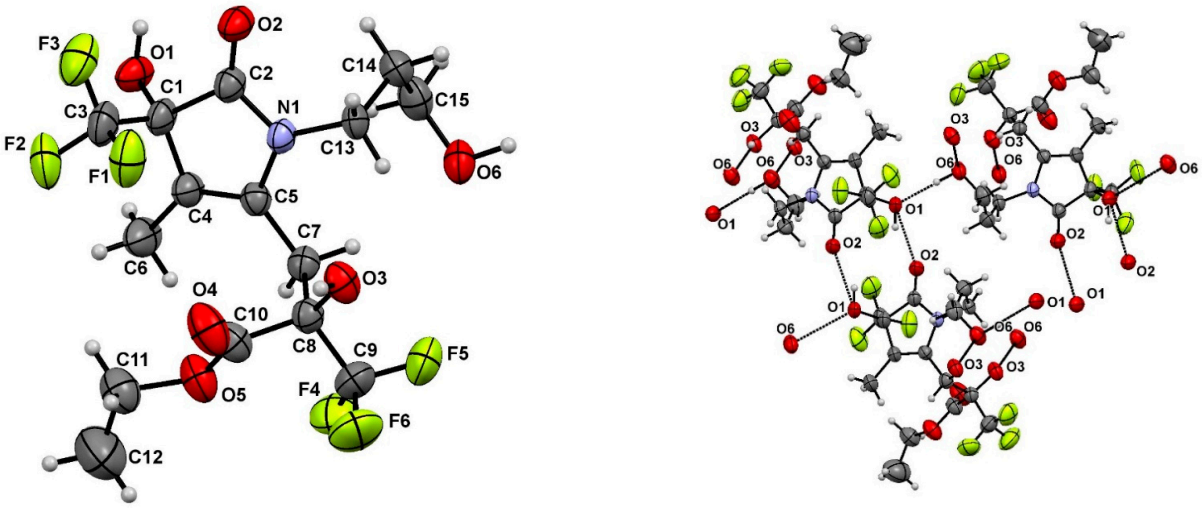

Figure 6. (**a**) The ORTEP view of compounds **11b** according to XRD data; (**b**) crystal packing of **11b** with indication of intermolecular hydrogen bonds.

The ^{13}C NMR spectra analysis of dihydropyrrol-5-ones **11b** and **11b′** revealed the presence of two downfield signals at δ_C 113.0–113.5 ppm and δ_C 137.1–138.4 ppm, which correspond to two sp^2-hybridized carbon atoms C-3″ and C-2″, respectively.

In the ^{19}F NMR spectra of diastereomers **11b** and **11b′**, the signals of the trifluoromethyl group of the pyrrole cycle (δ_F 85.74, 85.81 ppm) and the propanoate substituent (δ_F 85.81, 86.01 ppm) are observed in approximately the same range. However, according to the ^{1}H NMR spectra, the nature of the signals of the methylene protons H-1′ of the propanoate fragment of isomers **11b** and **11b′** differs, which may indicate a different configuration of substituents at the adjacent C-2 stereocenter. Thus, the protons H-1′A and H-1′B in the spectrum of isomer **11b** resonate as two doublets at δ_H 3.19 and 2.97 ppm (Δ_{AB} 0.22 ppm, *J* 14.9 Hz), while the signals of the same protons of isomer **11b′** are observed as an AB system at δ_H 3.08 ppm (J_{AB} 16.7 Hz, Δ_{AB} 0.1 ppm). Taking into account that, according to X-ray diffraction analysis (Figure 6), the substituents at the C-2 stereocenter in diastereomer **11b** have the *S**-configuration. The difference in the nature of the resonation of the protons of the neighboring methylene group C-1′ allows us to assume the opposite *R**-configuration for the **11b′** isomer (Figure 5).

The ^{13}C NMR spectrum of pyrrolone **11a** also contained characteristic low-field signals C-3″ (δ_C 113.37 ppm) and C-2″ (δ_C 137.90 ppm), confirming the presence of a double bond in the molecule. In its ^{1}H NMR spectrum, methylene protons H-1′ resonate as a singlet at δ_H 3.16 ppm, which can be a degenerate AB system with Δ_{AB} 0 ppm, which is closer in nature to the signals of similar protons of isomer **11b′** (AB-system at δ 3.08 ppm, Δ_{AB} 0.1 ppm). Based on this, we assumed that compound **11a** has the *R**-configuration of substituents at C-2 (Figure 5).

Considering the mechanism of formation of bicycles **4a–d** and **8a–d** from ethyl trifluoropyruvate **1**, methyl ketones **2a–d** and amino alcohols **3a,b**, it can be safely assumed that three-component cyclizations are a sequential domino process (Scheme 8). The first stage of which is aldolization, since by optimizing the conditions for the reaction of pyruvate **1** with acetone **2a** and aminoethanol **3a** (Scheme 1, Table 1), we detected aldol **6a**.

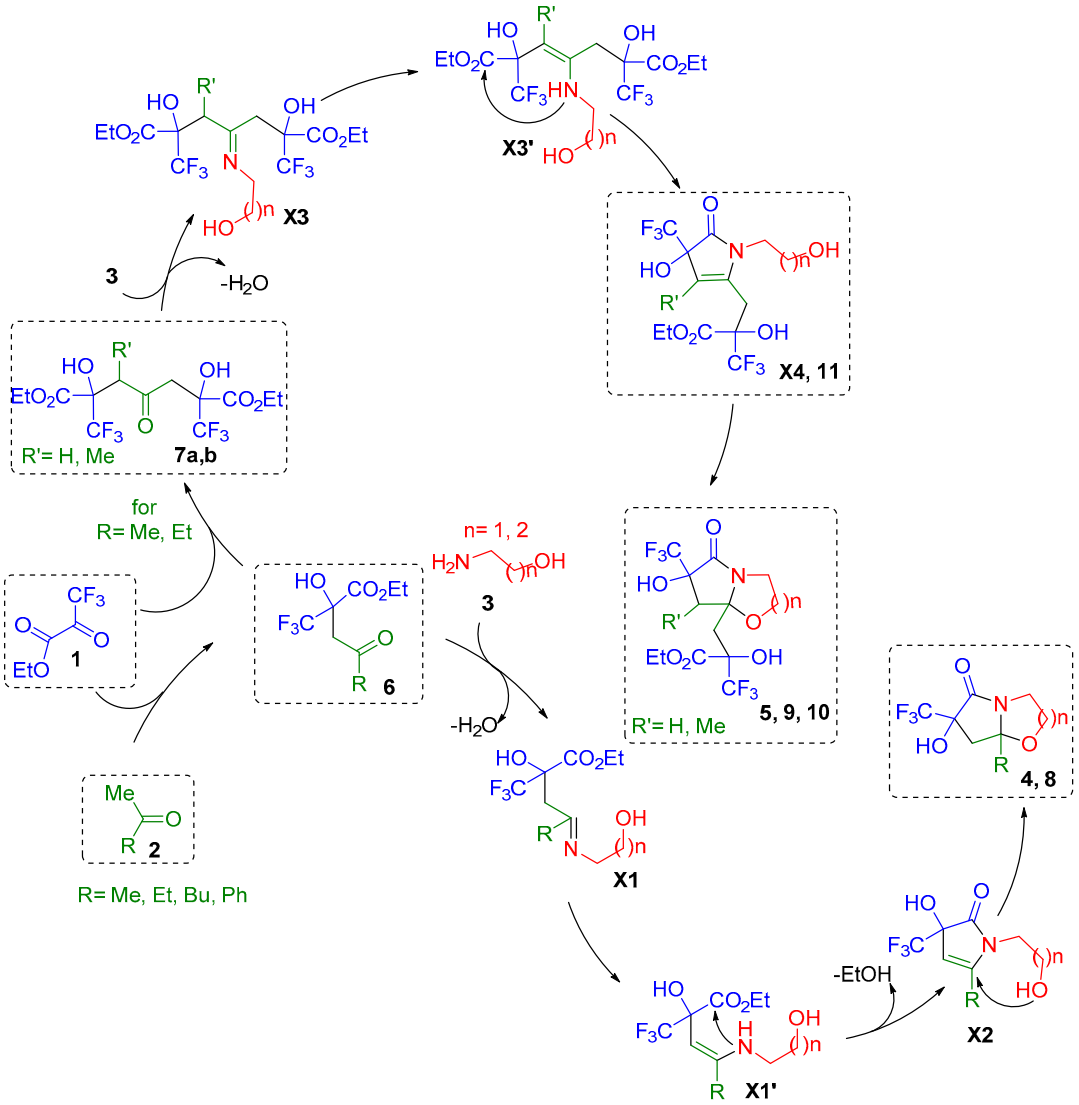

Scheme 8. Proposed mechanism of three- and four-component domino cyclization of ethyl trifluoropyruvate **1** with methyl ketones **2a–d** and amino alcohols **3a,b**.

In addition, we also experimentally demonstrated the feasibility of cyclization of aldols **6a,b** with amino alcohols **3a,b** into bicycles **4a,b** and **8a,b** (Scheme 7), presumably proceeding through the condensation of the keto group of aldol **6** with the amino group of amino alcohol **3** leading to intermediate **X1**, which after tautomerization undergoes intramolecular cyclization involving ester and amino groups, providing dihydropyrrol-5-one **X2**. At the last stage, the formation of the second cycle occurs due to the intramolecular addition of a hydroxyl group to the double bond.

Similar processes can be assumed for the four-component formation of heterocyclic aldols **5** and **9**, only the stage of formation of bis-aldol **7** is added, which then cyclizes with amino alcohol **3** (Scheme 8), forming dihydropyrrol-5-one **X4**. Such compounds were isolated and characterized in the case of Me-substituted derivatives **11a,b**. Subsequent intramolecular cyclization of pyrrolones **X4** gives bicyclic products **5**, **9**, **10**.

3. Material and Methods

3.1. Material

The solvents (acetonitrile, chloroform, hexane, diethyl ether and acetone **2a**) were obtained from AO "VEKTON" (St. Petersburg, Russia). 2-Butanone **2b**, 2-hexanone **2c**, 3-amino-1-propanol **3b** were purchased from Merck KGaA (Darmstadt, Germany). 2-

Aminoethanol **3a**, acetophenone **2d** and 1,4-dioxane were obtained from Alfa Aesar (UK). Ethyl trifluoropyruvate **1** was purchased from ABCR (GmbH, Karlsruhe, Germany). The deuterosolvent DMSO was acquired from «SOLVEX» Limited Liability Company (Skolkovo Innovation Center, Moscow, Russia).

3.2. Methods

Melting points were measured in the open capillaries with a Stuart SMP3 melting-point apparatus (Bibby Scientific Limited, Staffordshire, UK). Two FT-IR spectrometer (Perkin-Elmer, Waltham, MA, USA) using the frustrated total internal reflection accessory with a diamond crystal. The ^{1}H and ^{19}F NMR spectra were registered on a Bruker DRX-400 spectrometer (400 or 376 MHz, respectively) or a Bruker AvanceIII 500 spectrometer (500 or 470 MHz, respectively) (Bruker, Karlsruhe, Germany). The ^{13}C NMR spectra were recorded on a Bruker AvanceIII 500 spectrometer (125 MHz). The internal standard was SiMe4 (for ^{1}H and ^{13}C NMR spectra) and C_6F_6). The ^{13}C chemical shifts were calibrated using the solvent signal DMSO-d_6 (δ_C 39.5 ppm). For compounds **4a-d**, **8a-d**, **5**, **5′**, **11a**, **11b** signals in ^{1}H and ^{13}C spectra were assigned based on 2D ^{1}H-^{13}C HSQC and HMBC experiments. The high-resolution mass spectra (HRMS) were recorded on a Bruker maXis impact mass spectrometer (ESI) (Bruker, Karlsruhe, Germany). The column chromatography was performed on silica gel 60 (0.062–0.2 mm) (Macherey-Nagel GmbH & Co KG, Duren, Germany). The initial ethyl-2-hydroxy-4-methyl-4-oxo-2-(trifluoromethyl)butanoate (aldol **6a**) [35,36] and diethyl 2,6-dihydroxy-4-oxo-2,6-bis(trifluoromethyl)heptanedioate (bis aldol **7a**) [35] were synthesized by referring previously published methods.

3.3. General Procedures

*Synthesis of compounds **4** and **8** (**method A**)*: A solution of ethyl trifluoropyruvate **1** 1530 mg (9 mmol) and methyl ketone **2a–d** (9 mmol) in 1,4-dioxane (5 mL) was placed in a flat-bottomed flask. Then, amino alcohol **3a,b** (9 mmol) was added. The reaction mixture was stirred for 3–7 days at room temperature (25°C). After completion of the reaction (TLC and NMR ^{19}F monitoring), the reaction mixture was concentrated on a rotary evaporator. The residue was triturated with hexane, and the resulting precipitate was collected by filtration and purified by recrystallization from an appropriate solvent (MeCN, Et_2O), or by column chromatography (eluent: $CHCl_3$, $CHCl_3$–Et_2O/1:1).

*Synthesis of compounds **5, 9, 10** and **11** (**method B**)*: A solution of ethyl trifluoropyruvate **1** 3060 mg (18 mmol) and methyl ketone **2a,b** (9 mmol) in THF (5 mL) was placed in a flat-bottomed flask. Then amino alcohol **3a,b** (9 mmol) was added. The reaction mixture was stirred at room temperature (25°C) for 4–7 days. After completion of the reaction (TLC and ^{19}F NMR monitoring), the reaction mixture was concentrated on a rotary evaporator, the residue was purified by column chromatography (eluent: $CHCl_3$–Et_2O / 2:1, $CHCl_3$–Et_2O / 4:1). Product $\mathbf{5^{tc}}$ precipitated out during the reaction. The precipitate was filtered and purified by recrystallization from MeCN. The filtrate was evaporated, purified by column chromatography (eluent $CHCl_3$–Et_2O/2:1), product $\mathbf{5^{cc}}$ was obtained. Product **11b** was isolated from a mixture of diastereomers by fractional crystallization (hexane–diethyl ether / 1:3).

*Synthesis of products **4** and **8** (**method C**)*: A solution of aldol **6a,b** (5 mmol) in 1,4-dioxane (3 mL) was placed in a flat-bottomed flask. Then the amino alcohol **3a,b** (5 mmol) was added. The reaction mixture was stirred at room temperature (25 °C) for 4–5 days. After completion of the reaction (TLC and ^{19}F NMR monitoring), the reaction mixture was concentrated on a rotary evaporator, the residue was purified by column chromatography (eluent: $CHCl_3$–Et_2O/1:1).

*Synthesis of compounds **5** (**method D**)*: A solution of bis-aldol **7a** (1990 mg, 5 mmol) in THF (3 mL) was placed in a flat-bottomed flask. Then the amino alcohol **3a** (305 mg, 5 mmol) was added. The reaction mixture was stirred at room temperature (25 °C) for 4–5 days. After completion of the reaction (TLC and 19F NMR monitoring), the reaction mixture was concentrated on a rotary evaporator, the residue was purified by column

chromatography (eluent: $CHCl_3$–Et_2O / 1:1). Product **5^{tc}** precipitated out during the reaction. The precipitate was filtered and purified by recrystallization from MeCN. The filtrate was evaporated, purified by column chromatography (eluent $CHCl_3$–Et_2O/2:1), product **5^{cc}** was obtained.

3.4. Spectral Data

(6R,7aR*)-6-hydroxy-7a-methyl-6-(trifluoromethyl)tetrahydropyrrolo[2,1-b][1,3]oxazol-5(6H)-one (**4a^t**).* Yield 36 % (729 mg, *method A*), 77% (886 mg, *method C*); white solid; m.p. 80°C ($CHCl_3$–Et_2O / 1:1). ^{1}H NMR (500 MHz, DMSO-d_6) δ 1.48 (3H, s, Me), 2.35 (2H, AB-system, Δ_{AB} = 0.03 ppm, J_{AB} = 14.2 Hz, H-7), 3.28 (1H, ddd, *J* = 11.2, 8.1, 6.1 Hz, H-3B), 3.75 (1H, ddd, *J* = 11.2, 8.2, 5.4 Hz, H-3A), 3.96 (1H, td, *J* = 8.2, 6.1 Hz, H-2B), 4.06 (1H, td, *J* = 8.2, 5.4 Hz, H-2A), 7.51 (1H, s, OH) ppm. ^{13}C NMR (126 MHz, DMSO-d_6) δ 24.2 (Me), 40.4 (C-3), 43.0 (C-7), 65.9 (C-2), 79.6 (q, *J* = 29.8 Hz, C-6), 95.4 (C-7a), 123.9 (q, *J* = 283.8 Hz, CF_3), 169.6 (C-5) ppm. ^{19}F NMR (470 MHz, DMSO-d_6) δ 83.91 (s, CF_3) ppm. IR ν 3347 (O–H), 2997, 2919 (C–H), 1699 (C=O), 1184–1108 (C–F) cm-1. HRMS (ESI): calcd. for $C_8H_{11}F_3NO_3$ $[M + H]^+$ 226.0686; found 226.0682.

(6R,7aS*)-6-hydroxy-7a-methyl-6-(trifluoromethyl)tetrahydropyrrolo[2,1-b][1,3]oxazol-5(6H)-one (**4a^c**)* (mixed with **5^{ct}** (20%) and **4a^t** (2%)). Yield 13% (243 mg, *method A*); white solid; m.p. 156–157°C ($CHCl_3$–Et_2O/1:1). ^{1}H NMR (500 MHz, DMSO-d_6) *δ* 1.38 (3H, s, Me), 2.29 (1H, dq, $^2J_{HH}$ = 15.2, $^4J_{HF}$ = 1.3 Hz, H-7B), 2.74 (1H, d, *J* = 15.2 Hz, H-7A), 3.30 (1H, ddd, *J* = 11.2, 8.2, 6.0, H-3B, overlapped with H_2O), 3.85 (1H, ddd, *J* = 11.2, 8.2, 5.7 Hz, H-3A), 3.96 (1H, td, *J* = 8.2, 6.0 Hz, H-2B), 4.00 (1H, td, *J* = 8.2, 5.7 Hz, H-2A), 7.22 (1H, s, OH) ppm. ^{19}F NMR (470 MHz, DMSO-d_6) *δ* 83.63 (d, *J* = 1.3 Hz, CF_3) ppm. IR ν 3332 (O–H), 2993, 2912 (C–H), 1703 (C=O), 1164–1091 (C–F) cm^{-1}. HRMS (ESI): calcd. for $C_8H_{11}F_3NO_3$ $[M + H]^+$ 226.0686; found 226.0689.

(6R,7aR*)-7a-ethyl-6-hydroxy-6-(trifluoromethyl)tetrahydropyrrolo[2,1-b][1,3]oxazol-5(6H)-one (**4b^t**)* смсеь Yield 23% (495 mg, *method A*), 66% (789 mg, *method C*); white solid; m.p.134–136°C ($CHCl_3$–Et_2O / 1:1). ^{1}H NMR (500 MHz, DMSO-d_6) *δ* 0.90 (3H, t, *J* = 7.3 Hz, H-2′), 1.68 (1H, dq, *J* = 14.7, 7.3 Hz, H-1′B), 1.82 (1H, dq, *J* = 14.7, 7.3 Hz, H-1′A), 2.23 (1H, d, *J* = 14.5 Hz, H-7B), 2.42 (1H, d, *J* = 14.5 Hz, H-7A), 3.25 (1H, ddd, *J* = 11.2, 8.2, 6.4 Hz, H-3B), 3.78 (1H, ddd, *J* = 11.2, 7.9, 5.1 Hz, H-3A), 3.90–3.95 (1H, m, H-2B), 4.00 (1H, td, *J* = 8.2, 5.1 Hz, H-2A), 7.46 (1H, s, OH) ppm. ^{13}C NMR (126 MHz, DMSO-d_6) δ 7.8 (C-2′), 29.1 (C-1′), 40.1 (C-3), 41.1 (C-7), 65.6 (C-2), 79.1 (q, *J* = 29.8 Hz, C-6), 95.3 (C-7a), 123.9 (q, *J* = 284.4 Hz, CF_3), 170.3 (C-5) ppm. ^{19}F NMR (470.5 MHz, DMSO-d_6) *δ* 83.89 (s, CF_3) ppm. IR ν 3345 (O–H), 2983–2909 (C–H), 1701 (C=O), 1168–1149 (C–F) cm^{-1}. HRMS (ESI): calcd. for $C_9H_{13}F_3NO_3$ $[M + H]^+$ 240.0842; found 240.0840.

(6R,7aS*)-7a-ethyl-6-hydroxy-6-(trifluoromethyl)tetrahydropyrrolo[2,1-b][1,3]oxazol-5(6H)-one (**4b^c**).* (mixed with **4b^t** in the ratio 90:10). Yield 18 % (387 mg, *method A*), 16% (191 mg, *method C*); white solid; m.p. 110–112°C ($CHCl_3$–Et_2O / 1:1). ^{1}H NMR (500 MHz, DMSO-d_6) δ 0.88 (3H, t, J = 7.3 Hz, H-2′), 1.47 (1H, dq, *J* = 14.7, 7.3 Hz, H-1′B), 1.80 (1H, dq, *J* = 14.7, 7.3 Hz, H-1′A), 2.17 (1H, d, *J* = 15.4 Hz, H-7B), 2.73 (1H, d, *J* = 15.4 Hz, H-7A), 3.28 (1H, ddd, *J* = 11.0, 7.8, 6.4 Hz, H-3B), 3.86 (1H, ddd, *J* = 11.0, 8.1, 5.4 Hz, H-3A), 3.90–3.97 (2H, m, H-2), 7.23 (1H, s, OH) ppm. ^{13}C NMR (126 MHz, DMSO-d_6) δ 7.7 (C-2′), 27.7 (C-1′), 39.7 (C-3, overlapped with DMSO), 41.5 (C-7), 64.3 (C-2), 78.5 (q, *J* = 30.3 Hz, C-6), 96.8 (C-7a), 124.0 (q, *J* = 285.1 Hz, CF_3), 171.9 (C-5) ppm. ^{19}F NMR (376 MHz, DMSO-d_6) δ 83.79 (s, CF_3) ppm. IR ν 3398 (O–H), 3007–2883 (C–H), 1710 (C=O), 1179–1093 (C–F) cm^{-1}. HRMS (ESI): calcd. for $C_9H_{13}F_3NO_3$ $[M + Na]^+$ 262.0661; found 262.0659.

(6R,7aR*)-7a-Butyl-6-hydroxy-6-(trifluoromethyl)tetrahydropyrrolo[2,1-b][1,3]oxazol-5(6H)-one (**4c^t**) (mixed with **4c^c** in the ratio 90:10).* Yield 39 % (938 mg, *method A*); white solid; m.p. 90–94°C. ($CHCl_3$–Et_2O / 1:1). ^{1}H NMR (500 MHz, DMSO-d_6) δ 0.89 (t, *J* = 7.0 Hz, 3H, H-4′), 1.28–1.35 (4H, m, H-3′, H-2′), 1.62–1.68 (1H, m, H-1′B), 1.76–1.83 (1H, m, H-1′A), 2.24 (1H, d, *J* = 14.5 Hz, H-7B), 2.42 (1H, d, *J* = 14.5 Hz, H-7A), 3.25 (1H, ddd, *J* = 11.2, 8.0, 6.4 Hz, H-3B), 3.77 (1H, ddd, *J* = 11.2, 7.9, 5.2 Hz, H-3A), 3.91 (1H, td, *J* = 8.2, 6.4 Hz, H-2B), 4.00 (1H, td, *J* = 8.2, 5.2 Hz, H-2A), 7.46 (1H, s, OH) ppm. ^{13}C NMR (126 MHz, DMSO-d_6) δ 13.9 (C-4′),

22.2 (C-3′), 25.3 (C-2′), 35.9 (C-1′), 40.5 (C-3), 41.0 (C-7), 65.6 (C-2), 79.1 (q, *J* = 29.8 Hz, C-6), 97.5 (C-7a), 124.0 (q, *J* = 284.3 Hz, CF_3), 170.2 (C-5) ppm. ^{19}F NMR (470 MHz, DMSO-d_6) δ 83.87 (s, CF_3) ppm. IR ν 3324 (O–H), 2996–2878 (C–H), 1710 (C=O), 1179–1148 (C–F) cm^{-1}. HRMS (ESI): calcd. for $C_{11}H_{17}F_3NO_3$ $[M + H]^+$ 268.1155; found 268.1156.

(6R,7aS*)-7a-Butyl-6-hydroxy-6-(trifluoromethyl)tetrahydropyrrolo[2,1-b][1,3]oxazol-5(6H)-one (**4c**^{c}).* Yield 26 % (625 mg, *method A*); white solid; m.p. 129–130 °C (Et_2O). ^{1}H NMR (400 MHz, DMSO-d_6) δ 0.88 (3H, t, *J* = 7.0 Hz, H-4′), 1.27–1.33 (4H, m, H-3′, H-2′), 1.43 (1H, dq, *J* = 14.7, 7.0 Hz, H-1′B), 1.79 (1H, dq, *J* = 14.7, 7.0 Hz, H-1′A), 2.19 (1H, d, *J* = 15.3 Hz, H-7B), 2.73 (1H, d, *J* = 15.3 Hz, H-7A), 3.28 (1H, ddd, *J* = 11.0, 7.5, 6.9 Hz, H-3B), 3.85 (1H, ddd, *J* = 11.0, 7.9, 5.6 Hz, H-3A), 3.91–3.95 (2H, m, H-2), 7.22 (1H, s, OH) ppm. ^{13}C NMR (126 MHz, DMSO-d_6) δ 13.8 (C-4′), 22.1 (C-3′), 25.3 (C-2′), 34.5 (C-1′), 39.7 (C-3, overlapped with DMSO), 41.5 (C-7), 64.4 (C-2), 78.5 (q, *J* = 30.1 Hz, C-6), 96.5 (C-7a), 124.1 (q, *J* = 285.1 Hz, CF_3), 171.9 (C-5) ppm. ^{19}F NMR (376 MHz, DMSO-d_6) δ 83.76 (s, CF_3) ppm. IR ν 3409 (O–H), 3008–2866 (C–H), 1709 (C=O), 1178–1112 (C–F) cm^{-1}. HRMS (ESI): calcd. for $C_{11}H_{17}F_3NO_3$ $[M + H]^+$ 268.1155; found 268.1154.

(6R,7aR*)-6-Hydroxy-7a-phenyl-6-(trifluoromethyl)tetrahydropyrrolo[2,1-b][1,3]oxazol-5(6H)-one (**4d**^{c}).* Yield 58 % (1499 mg, *method A*); white solid; m.p. 155–157°C ($CHCl_3$–Et_2O / 1:1). ^{1}H NMR (500 MHz, DMSO-d_6) δ 2.70 (1H, d, J_{AB} = 15.5 Hz, H-7B), 2.75 (1H, d, J_{AB} = 15.5 Hz, H-7A), 3.16 (1H, ddd, *J* = 11.2, 8.5, 4.6 Hz, H-3B), 3.51 (1H, td, *J* = 8.5, 6.7 Hz, H-2B), 3.91 (1H, ddd, *J* = 11.2, 8.3, 6.7 Hz, H-3A), 4.10 (1H, td, *J* = 8.5, 4.6 Hz, H-2A), 7.36–7.44 (6H, m, Ph, OH) ppm. ^{13}C NMR (126 MHz, DMSO-d_6) δ 42.3 (C-3), 43.2 (C-7), 64.6 (C-2), 78.5 (q, C-6, *J* = 30.6 Hz), 96.8 (C-7a), 123.9 (q, CF_3, *J* = 284.9 Hz), 124.9 (Co), 128.5 (Cp), 128.6 (Cm), 139.8 (Ci), 172.6 (C-5) ppm. ^{19}F NMR (470 MHz, DMSO-d_6) δ 83.65 (s, CF_3). IR ν 3394 (O–H), 3076–2978 (C–H), 1713 (C=O), 1179–1149 (C–F) cm^{-1}. $C_{13}H_{12}F_3NO_3$ (287.24). Calculated: C, 54.36; H, 4.21; N, 4.88; Found: C, 54.37; H, 4.22; N, 4.89. HRMS (ESI): calcd. for $C_{13}H_{13}F_3NO_3$ $[M + H]^+$ 288.0842; found 288.0842.

Ethyl (R)-3,3,3-trifluoro-2-hydroxy-2-(((6R*,7aS*)-6-hydroxy-5-oxo-6-(trifluoromethyl)tetrahydropyrrolo[2,1-b]oxazol-7a(5H)-yl)methyl)propanoate (**5**^{tc}).* Yield 47% (1671 mg, *method B*), 56% (1106 mg, *method D*); white solid; m.p. 168–170°C. (MeCN). ^{1}H NMR (500 MHz, DMSO-d_6) *δ* 1.25 (3H, t, *J* = 7.1 Hz, $OCH_2C\underline{H}_3$), 2.20 (1H, d, *J* = 14.0 Hz, H-1′B), 2.29 (1H, d, *J* = 14.9 Hz, H-7″B), 2.63 (1H, br. d, *J* = 14.0 Hz, H-1′A), 2.99 (1H, d, *J* = 14.9 Hz, H-7″A), 3.35–3.41 (1H, m, H-3″B), 3.78–3.84 (2H, m, H-2″B, H-3″A), 3.86–3.92 (1H, m, H-2″A), 4.17 (1H, dq, *J* = 10.8, 7.1 Hz, $OC\underline{H}^BCH_3$), 4.29 (1H, dq, *J* = 10.8, 7.1 Hz, $OC\underline{H}^ACH_3$), 7.08 (1H, d, *J* = 1.6 Hz, C^2-OH), 7.56 (1H, s, $C^{6''}$-OH) ppm. ^{13}C NMR (126 MHz, DMSO-d_6) *δ* 13.7 ($OCH_2\underline{C}H_3$), 37.9 (C-1′), 40.4 (C-3″), 42.1 (C-7″), 62.3 ($O\underline{C}H_2CH_3$), 66.3 (C-2″), 76.0 (q, *J* = 27.5 Hz, C-2), 78.8 (q, *J* = 30.0 Hz, C-6″), 95.3 (C-7a″), 123.7 (q, *J* = 283.8 Hz, CF_3), 123.9 (q, *J* = 288.6 Hz, CF_3), 167.8 (C-1), 169.9 (C-5″) ppm. ^{19}F NMR (470 MHz, DMSO-d_6) *δ* 83.83 (s, 3F, CF_3), 84.92 (s, 3F, CF_3) ppm. IR ν 3456, 3284 (O–H), 2997–2924 (C–H), 1736, 1705 (C=O), 1167–1093 (C–F) cm^{-1}. HRMS (ESI): calcd. for $C_{14}H_{15}F_3NO_3$ $[M + H]^+$ 396.0876; found 396.0879.

Ethyl (S)-3,3,3-trifluoro-2-hydroxy-2-(((6R*,7aS)-6-hydroxy-5-oxo-6-(trifluoromethyl)tetrahydropyrrolo[2,1-b]oxazol-7a(5H)-yl)methyl)propanoate (**5**^{cc}).* Yield 18% (640 mg, *method B*), 15% (296 mg, *method D*); white solid; m.p. 134–136 °C. ($CHCl_3$–Et_2O/2:1). ^{1}H NMR (500 MHz, DMSO-d_6) *δ* 1.23 (3H, t, *J* = 7.1 Hz, CH_3), 2.26 (1H, d, *J* = 14.0 Hz, H-7″B), 2.50 (1H, d, *J* = 15.0 Hz, H-1′B), 2.61 (1H, d, *J* = 14.0 Hz, H-7″A), 2.67 (1H, dd, *J* = 15.0, 1.5 Hz, H-1′A), 3.40–3.46 (1H, m, H-3″B), 3.58–3.63 (m, 1H, H-2″B), 3.78–3.84 (m, 2H, H-2″A, H-3″A), 4.17 (dq, *J* =10.8, 7.1 Hz, 1H, OCH^B), 4.24 (dq, *J* =10.8, 7.1 Hz, 1H, OCH^A), 7.00 (d, *J* = 1.5 Hz, 1H, C^2-OH), 7.56 (s, 1H, $C^{6''}$-OH). ^{13}C NMR (126 MHz, DMSO-d_6) *δ* 13.6 ($OCH_2\underline{C}H_3$), 40.8 (C-1′), 42.6 (C-3″), 44.6 (C-7″), 62.1 (OCH_2), 66.7 (C-2″), 75.4 (q, *J* = 27.5 Hz, C-2), 78.6 (q, *J* = 29.8 Hz, C-6″), 95.4 (C-7a″), 123.7 (q, *J* = 284.2 Hz, CF_3), 124.1 (q, *J* = 288.4 Hz, CF_3), 167.8 (C-1), 170.2 (C-5″). ^{19}F NMR (376 MHz, DMSO-d_6) *δ* 84.23 (s, 3F, CF_3), 85.64 (s, 3F, CF_3). IR ν 3487, 3316 (O–H), 2991 (C–H), 1738, 1705 (C=O), 1169–1090 (C–F) cm^{-1}. HRMS (ESI): calcd. for $C_{14}H_{15}F_3NO_3$ $[M + H]^+$ 396.0876; found 396.0872.

*Ethyl 2-hydroxy-4-oxo-2-(trifluoromethyl)hexanoate (**6b**).* A mixture of 1530 mg (9 mmol) of ethyltrifluoropyruvate **1**, 522 mg (1.8 mmol) of 2-butanone **2b**, and 12 mg (0.1 mmol) of L-proline in 10 mL of DMF was placed in a flat-bottomed flask. The reaction mass was stirred for 2 days at a temperature (50°C). After completion of the reaction (TLC and ^{19}F NMR monitoring), the reaction mixture was poured into water (100 mL) and the organic layer was extracted with chloroform (3 × 50 mL). The solvent was concentrated on a rotary evaporator. The residue was purified by column chromatography (eluent: $CHCl_3$–hexane / 2:1). A yellow oil was isolated. Yield 1699 мг (78%). ^{1}H NMR (500 MHz, DMSO-d_6) δ 0.89 (3H, t, J = 7.1 Hz, CH_3^{Et}), 1.19 (3H, t, J = 7.1 Hz, CH_3^{OEt}), 3.07 (1H, d, J = 17.2 Hz, H-3A), 3.19 (1H, d, J = 17.2 Hz, H-3B), 2.44 (2H, dq, J = 11.0, 7.3 Hz, H-B^{Et}), 2.53 (2H, dq, J = 11.0, 7.3 Hz, H-A^{Et},), 4.13–4.23 (2H, m, CH_2^{OEt}), 6.75 (1H, d, J = 0.7 Hz, OH) ppm. ^{13}C NMR (126 MHz, DMSO-d_6) δ 7.2 (C-6), 13.67 ($OCH_2\underline{C}H_3$), 35.7 (C-5), 44.4 (C-3), 61.8 ($O\underline{C}H_2CH_3$), 74.9 (q, J = 28.1 Hz, C-2), 123.9 (q J = 287.2 Hz, CF_3), 167.7 (C-1), 205.4 (C-4) ppm. ^{19}F NMR (376 MHz, DMSO-d_6) δ 84.83 (s, CF_3) ppm. IR ν 3482 (O–H), 2987–2908 (C–H), 1747, 1626 (C=O), 1222–1097 (C–F) cm^{-1}. HRMS (ESI): calcd. for $C_9H_{14}F_3O_4$ $[M + H]^+$ 243.0839; found 243.0833.

(7R,8aR*)-7-Hydroxy-8a-methyl-7-(trifluoromethyl)tetrahydro-2H-pyrrolo[2,1-b][1,3]oxazine-6(7H)-one (**8a^t**) (mixed with **8a^c** in the ratio 84:16).* Yield 28 % (603 mg, *method A*), 30 % (358 mg, *method C*); white solid; m.p. 96–98°C ($CHCl_3$–Et_2O / 1:1). ^{1}H NMR (500 MHz, DMSO-d_6) δ 1.47–1.58 (2H, m, H-3), 1.61 (3H, c, Me), 2.27 (2H, AB-system, Δ_{AB} = 0.06 ppm, J_{AB} = 14.4 Hz, H-8), 3.21 (1H, dm, J = 13.0 Hz, H-4B), 3.75 (1H, dm, J = 11.5 Hz, H-2B), 3.86 (1H, dm, J = 13.0 Hz, H-4A), 3.98 (1H, dm, J = 11.5 Hz, H-2A), 7.21 (1H, s, OH) ppm. ^{13}C NMR (126 MHz, DMSO-d_6) δ 20.3 (Me), 24.7 (C-3), 35.2 (C-4), 43.8 (C-8), 60.6 (C-2), 74.9 (q, J = 29.9 Hz, C-7), 86.2 (C-8a), 124.4 (q, J = 285.1 Hz, CF_3), 166.2 (C-6), ppm. ^{19}F NMR (470 MHz, DMSO-d_6) δ 84.22 (s, CF_3). IR ν 3430, 3351 (O–H), 2990–2885 (C–H), 1696 (C=O), 1168–1057 (C–F) cm^{-1}. HRMS (ESI): calcd. for $C_9H_{13}F_3NO_3$ $[M + H]^+$ 240.0842; found 240.0849.

(7R,8aS*)-7-Hydroxy-8a-methyl-7-(trifluoromethyl)tetrahydro-2H-pyrrolo[2,1-b][1,3]oxazine-6(7H)-one (**8a^c**) (mixed with **8a^t** in the ratio 89:11).* Yield 44% (947 mg, *method A*), 62% (741 mg, *method C*); white solid; m.p. 76–78 °C ($CHCl_3$–Et_2O/1:1). ^{1}H NMR (500 MHz, DMSO-d_6) δ 1.49–1.64 (5H, m, Me, H-3), 2.15 (1H, br.d, J = 15.2 Hz, H-8B), 2.57 (1H, d, J = 15.2 Hz, H-8A), 3.24 (1H, td, J = 13.0, 4.0 Hz, H-4B), 3.76 (1H, dm, J = 12.2 Hz, H-2B), 3.88 (1H, dm, J = 13.0 Hz, H-4A), 4.01 (1H, td, J = 12.2, 2.9 Hz, H-2A), 7.13 (1H, s, OH) ppm. ^{13}C NMR (126 MHz, DMSO-d_6) δ 20.3 (Me), 24.7 (C-3), 35.2 (C-4), 43.8 (C-8), 60.6 (C-2), 74.9 (q, J = 29.9 Hz, C-7), 86.2 (C-8a), 124.4 (q, J = 285.1 Hz, CF_3), 166.2 (C-6) ppm. ^{19}F NMR (470 MHz, DMSO-d_6) δ 83.71 (s, CF_3). IR ν 3392, 3296 (O–H), 2997–2887 (C–H), 1702 (C=O), 1175–1058 (C–F) cm^{-1}. HRMS (ESI): calcd. for $C_9H_{13}F_3NO_3$ $[M + H]^+$ 240.0842; found 240.0850.

(7R,8aR*)-8a-Ethyl-7-hydroxy-7-(trifluoromethyl)tetrahydro-2H-pyrrolo[2,1-b][1,3]oxazine-6(7H)-one (**8b^t**).* Yield 21 % (478 mg, *method A*), 24 % (304 mg, *method C*); white solid; m.p. 68–70°C ($CHCl_3$–Et_2O / 1:1). ^{1}H NMR (500 MHz, DMSO-d_6) δ 0.84 (3H, t, J = 7.3 Hz, H-2′), 1.49–1.55 (2H, m, H-3), 1.68 (1H, dq, J = 14.5, 7.3 Hz, H-1′B), 2.10 (1H, d, J = 14.8 Hz, H-8B), 2.28–2.36 (2H, m, H-8A, H-1′A), 3.16–3.22 (1H, m, H-4B), 3.72 (1H, dm, J = 12.1 Hz, H-2B), 3.84–3.90 (2H, m, H-4A, H-2A), 7.17 (1H, s, OH) ppm. ^{13}C NMR (126 MHz, DMSO-d_6) δ 7.1 (C-2′), 24.29 and 24.30 (C-3, C-1′), 35.0 (C-4), 41.0 (C-8), 60.0 (C-2), 74.9 (q, J = 30.0 Hz, C-7), 88.5 (C-8a), 124.3 (q, J = 284.6 Hz, CF_3), 165.5 (C-6) ppm. ^{19}F NMR (376 MHz, DMSO-d_6) δ 84.14 (s, CF_3) ppm. IR (ATR) ν 3240 (O–H), 2970–2889 (C–H), 1674 (C=O), 1161–1092 (C–F) cm^{-1}. HRMS (ESI): calcd. for $C_{10}H_{15}F_3NO_3$ $[M + H]^+$ 254.0999; found 254.1006.

(7R,8aS*)-8a-Ethyl-7-hydroxy-7-(trifluoromethyl)tetrahydro-2H-pyrrolo[2,1-b][1,3]oxazine-6(7H)-one (**8b^c**) (mixed with **8b^t** in the ratio 81:19).* Yield 27 % (615 mg, *method A*), 62 % (784 mg, *method C*); white solid; m.p. 98–100°C ($CHCl_3$–Et_2O / 1:1). ^{1}H NMR (500 MHz, DMSO-d_6) δ 0.82 (3H,t, J = 7.3 Hz, H-2′), 1.47–1.71 (3H, m, H-3, H-1′B), 2.00 (1H, d, J = 15.3 Hz, H-8B), 2.38 (1H, dq, J = 14.6, 7.3 Hz, H-1′A), 2.51 (1H, d, J = 15.3 Hz, H-8A, overlapped with DMSO), 3.22 (1H, td, J = 13.0, 3.8 Hz, H-4B), 3.73 (1H, dm, J = 12.2 Hz, H-2B), 3.87 (1H, dm,

J = 13.0 Hz, H-4A), 3.92 (1H, td, *J* = 12.2, 2.7 Hz, H-2A), 7.13 (1H, s, OH) ppm. ^{13}C NMR (126 MHz, DMSO-d_6) δ 6.9 (C-2′), 23.9 and 24.3 (C-1′, C-3), 35.5 (C-4), 40.4 (C-8), 60.1 (C-2), 74.8 (q, *J* = 29.8 Hz, C-7), 88.6 (C-8a), 124.4 (q, *J* = 285.0 Hz, CF_3), 167.0 (C-6) ppm. ^{19}F NMR (470 MHz, DMSO-d_6) δ 83.85 (s, CF_3) ppm. IR (ATR) ν 3347 (O–H), 2983–2895 (C–H), 1695 (C=O), 1196–1131 (C–F) cm^{-1}. HRMS (ESI): calcd. for $C_{10}H_{15}F_3NO_3$ $[M + H]^+$ 254.0999; found 254.1019.

(7R,8aR*)-8a-Butyl-7-hydroxy-7-(trifluoromethyl)tetrahydro-2H-pyrrolo[2,1-b][1,3]oxazin-6(7H)-one (**8c^t**) (mixed with **8c^c** in the ratio 90:10).* Yield 24 % (608 mg, *method A*); white solid; m.p. 80–83°C ($CHCl_3$–Et_2O / 1:1). ^{1}H NMR (500 MHz, DMSO-d_6) δ 0.91 (3H, t, *J* = 7.3 Hz, H-4′), 1.19–1.37 (4H, m, H-2′, H-3′), 1.48–1.54 (2H, m, H-3), 1.63 (1H, ddd, *J* = 14.2, 10.8, 5.2 Hz, H-1′B), 2.12 (1H, d, *J* = 14.8 Hz, H-8B), 2.31 (1H, ddd, *J* = 14.2, 10.7, 5.7 Hz, H-1′A), 2.34 (1H, d, *J* = 14.8 Hz, H-8A), 3.18–3.24 (1H, m, H-4B), 3.72 (1H, dm, *J* = 12.0 Hz, H-2B), 3.83–3.91 (2H, m, H-2A, H-4A), 7.16 (1H, s, OH) ppm. ^{13}C NMR (126 MHz, DMSO-d_6) δ 13.9 (C-4′), 22.0 (C-3′), 24.3 (C-3), 24.6 (C-2′), 31.1 (C-1′), 35.0 (C-4), 41.5 (C-8), 60.0 (C-2), 74.9 (q, *J* = 29.9 Hz, C-7), 88.2 (C-8a), 124.3 (q, *J* = 284.5 Hz, CF_3), 165.4 (C-6) ppm.^{19}F NMR (376 MHz, DMSO-d_6) δ 84.13 (s, CF_3) ppm. IR ν 3305 (O–H), 2974–2869 (C–H), 1682 (C=O), 1174–1150 (C–F) cm^{-1}. HRMS (ESI): calcd. for $C_{12}H_{19}F_3NO_3$ $[M - H]^-$ 280.1166; found 280.1167.

(7R,8aS*)-8a-Butyl-7-hydroxy-7-(trifluoromethyl)tetrahydro-2H-pyrrolo[2,1-b][1,3]oxazin-6(7H)-one (**8c^c**).* Yield 46 % (1164 mg, *method A*); white solid; m.p. 158–160°C (MeCN). ^{1}H NMR (500 MHz, DMSO-d_6) δ 0.90 (3H, t, *J* = 7.3 Hz, H-4′), 1.18–1.26 (2H, m, H-2′), 1.29–1.38 (2H, m, H-3′), 1.41–1.51 (2H, m, H-1′B, H-3B), 1.59 (1H, qt, *J* = 12.8, 5.2 Hz, H-3A), 2.02 (1H, d, *J* = 15.5 Hz, H-8B), 2.35–2.42′ (1H, m, H-1′A), 2.51 (1H, d, *J* = 15.5 Hz, H-8A, overlapped with DMSO), 3.23 (1H, td, *J* = 13.2, 3.8 Hz, H-4B), 3.73 (1H, br. dd, *J* = 12.2, 5.2 Hz, H-2B), 3.87 (1H, br. dd, *J* = 13.2, 5.2 Hz, H-4A), 3.93 (1H, td, *J* = 12.2, 2.7 Hz, H-2A), 7.12 (1H, s, OH) ppm. ^{13}C NMR (126 MHz, DMSO-d_6) δ 13.9 (C-4′), 22.0 (C-3′), 24.3 (C-3), 24.6 (C-2′), 30.8 (C-1′), 35.5 (C-4), 41.0 (C-8), 60.2 (C-2), 74.8 (q, *J* = 29.9 Hz, C-7), 88.3 (C-8a), 124.4 (q, *J* = 284.6 Hz, CF_3), 166.9 (C-6). ^{19}F NMR (470 MHz, DMSO-d_6) δ 83.83 (CF_3) ppm. IR ν 3313 (O–H), 2961–2869 (C–H), 1686 (C=O), 1189–1116 (C–F) cm^{-1}. HRMS (ESI): calcd. for $C_{12}H_{19}F_3NO_3$ $[M + H]^+$ 282.1312; found 282.1313.

(7R,8aR*)-7-Hydroxy-8a-phenyl-7-(trifluoromethyl)tetrahydro-2H-pyrrolo[2,1-b][1,3]oxazin-6(7H)-one (**8d^t**).* Yield 58 % (1571 mg, *method A*); white solid; m.p. 143–145°C (MeCN). ^{1}H NMR (500 MHz, DMSO-d_6) δ 1.46 (1H, dm, *J* = 13.0 Hz, H-3B), 1.63 (1H, qt, *J* = 13.0, 5.1 Hz, H-3A), 2.22 (1H, d, *J* = 14.8 Hz, H-8B), 2.64 (1H, d, *J* = 14.8 Hz, H-8A), 2.97 (1H, td, *J* = 13.1, 3.8 Hz, H-4B), 3.54 (1H, td, *J* = 12.1, 2.2, H-2B), 3.83 (1H, ddm, *J* = 12.2, 4.6 Hz, H-2A), 4.02 (1H, ddm, *J* = 13.1, 5.2 Hz, H-4A), 7.23 (1H, s, OH), 7.32 (2H, dd, *J* = 8.3, 1.4 Hz, H*o*), 7.40 (1H, tt, *J* = 7.4, 1.4 Hz, H*p*), 7.49 (2H, t, *J* = 7.6 Hz, H*m*) ppm. ^{13}C NMR (126 MHz, DMSO-d_6) δ 24.2 (C-3), 36.4 (C-4), 46.2 (C-8), 61.9 (C-2), 75.0 (q, *J* = 30.0 Hz, C-7), 89.8 (C-8a), 124.1 (q *J* = 284.9 Hz, CF_3,), 125.8 (C*o*), 128.4 (C*p*), 129.2 (C*m*), 139.6 (C*i*), 167.1 (C-6) ppm. ^{19}F NMR (470 MHz, DMSO-d_6) δ 84.31 (s, CF_3) ppm. IR ν 3290 (O–H), 2968–2876 (C–H), 1695 (C=O), 1199–1121 (C–F) cm^{-1}. HRMS (ESI): calcd. for $C_{14}H_{15}F_3NO_3$ $[M + H]^+$ 302.099; found 302.0997.

*Ethyl 3,3,3-trifluoro-2-hydroxy-2-[(7-hydroxy-6-oxo-7-(trifluoromethyl)tetrahydro-2H-pyrrolo[2,1-b][1,3]oxazin-8a(6H)-yl)methyl)propanoate (mixture of **9:9′** in the ratio ≈ 1:1).* Yield 69% (2540 mg, *method B*); white solid; m.p. 135–137°C. ($CHCl_3$–Et_2O / 4:1). ^{1}H NMR (500 MHz, DMSO-d_6) δ 1.20 (1.5H, t, *J* = 7.1 Hz, CH_3^{Et}), 1.25 (1.5H, t, *J* = 7.1 Hz, CH_3^{Et}), 1.47–1.59 (2H, m, H-3″), 1.69 (0.5H, d, *J* = 14.8 Hz), 2.02 (0.5H, d, *J* = 15.3 Hz), 2.06 (d, *J* = 15.7 Hz, 0.5H), 2.57 (0.5H, d, *J* = 15.2 Hz), 2.67 (0.5H, d, *J* = 15.2 Hz), 3.15 (0.5H, d, *J* = 15.3 Hz), 3.23 (0.5H, ddd, *J* = 13.4, 12.6, 3.7 Hz), 3.29–3.37 (1H, m, overlapped with H_2O), 3.40 (d, *J* = 14.8 Hz, 0.5H), 3.65 (0.5H, dm, *J* = 12.5 Hz,), 3.73 (0.5H, dm, *J* = 12.5 Hz,), 3.80–3.90 (1.5H, m), 4.05–4.13 (1.5H, m), 4.18 (0.5H, dq, *J* = 10.8, 7.1 Hz, OCH^{Et}), 4.23 (0.5H, dq, *J* = 10.8, 7.1 Hz, OCH^{Et}), 7.10 (0.5H, s, OH), 7.12 (0.5H, s, OH), 7.16 (1H, s, OH) ppm. ^{13}C NMR (126 MHz, DMSO-d_6) δ 13.4 and 13.6 (CH_3^{Et}), 23.8 and 24.0 (C-3″), 33.3 and 33.5 (C-1′), 35.7 and 36.3 (C-8″), 39.7 and 40.7 (C-4″), 60.8 and 61.0 (C-2″), 62.2 and 62.4 (OCH_2), 74.35 (q,

J = 30.0, C-2), 74.38 (q, *J* = 30.0, C-2), 75.94 (q, *J* = 28.2, C-7″), 75.95 (q, *J* = 27.8, C-7″), 86.9 and 87.1 (C-8a ″), 123.9 (q, *J* = 288.3, CF_3), 124.0 (q, *J* = 288.3, CF_3), 124.2 (q, *J* = 284.6, CF_3), 124.3 (q, *J* = 285.0, CF_3), 167.3, 167.4, 167.5 and 168.6 (C-1, C-6″) ppm. ^{19}F NMR (470 MHz, DMSO-d_6) *δ* 83.78 (s, 3F, CF_3), 84.25 (s, 3F, CF_3), 85.23 (s, 3F, CF_3), 85.72 (s, 3F, CF_3) ppm. IR ν 3482, 3315 (O–H), 2994–2903 (C–H), 1749, 1699 (C=O), 1173–1157 (C–F) cm^{-1}. HRMS (ESI): calcd. for $C_{14}H_{16}F_6NO_6$ $[M - H]^-$ 408.0887; found 408.0890.

Ethyl 3,3,3-trifluoro-2-hydroxy-2-[(6-hydroxy-8a-methyl-5-oxo-6-(trifluoromethyl)tetrahydropyrrolo[2,1-b]oxazol-7a(5H)-yl)methyl]propanoate (mixture of ***10*:*10′*** *in the ratio 56:44).* Yield 64% (2356 mg, *method B*); white solid; m.p. 133–134°C. ($CHCl_3$–Et_2O / 2:1). ^{1}H NMR (500 MHz, DMSO-d_6) δ 0.88 (d, *J* = 6.8 Hz, 1.3H, Me), 1.08 (d, *J* = 6.9 Hz, 1.7H, Me), 1.23 (t, *J* = 7.1 Hz, 3H, CH_3^{Et}), 2.27–2.35 (m, 1H, H-1′, H-7″), 2.62–2.73 (m, 2H, H-1′, H-7″), 3.40–3.62 (m, 2H, H-2″, H-3″), 3.76–3.84 (m, 2H, H-2″, H-3″), 4.16–4.23 (m, 2H, OCH_2), 6.94, (d, *J* = 1.5 Hz, 0.44H, OH), 6.96 (d, *J* = 1.5 Hz, 0.56H, OH), 7.58 (s, 0.44H, OH), 7.66 (s, 0.56H, OH) ppm. ^{13}C NMR (126 MHz, DMSO-d_6) δ 7.7 and 8.4 (Me), 13.7 (CH_3^{Et}), 36.5 (C-1′), 41.6 and 42.9 (C-3″), 48.6 and 51.1 (C-7″), 62.0 (OCH_2), 66.9 and 68.1 (C-2″), 75.2 (q, J = 27.1, C-2), 75.3 (q, *J* = 27.2, C-2), 79.2 (q, *J* = 28.3, C-6″), 80.7 (q, *J* = 28.3, C-6″), 97.3 and 97.5 (C-7a″), 123.6 (q, *J* = 285.2, CF_3), 123.9 (q, *J* = 285.5, CF_3), 124.2 (q, *J* = 288.7, CF_3), 124.3 (q, *J* = 288.8, CF_3), 167.9 and 168.0 (C-1), 169.2 and 169.4 (C-5″) ppm. ^{19}F NMR (376 MHz, DMSO-d_6) δ 85.39 (s, 1.7F, CF_3), 85.60 (s, 1.3F, CF_3), 86.40 (s, 1.7F, CF_3), 89.73 (s, 1.3F, CF_3) ppm. IR ν 3486, 3321 (O–H), 2992–2904 (C–H), 1736, 1702 (C=O), 1194–1114 (C–F) cm^{-1}. HRMS (ESI): calcd. for $C_{14}H_{18}F_6NO_6$ $[M + H]^+$ 410.1036; found 410.1033.

Ethyl (R)-3,3,3-trifluoro-2-hydroxy-2-(((R*)-4-hydroxy-1-(2-hydroxyethyl)-3-methyl-5-oxo-4-(trifluoromethyl)-4,5-dihydro-1H-pyrrol-2-yl)methyl)propanoate (****11a****).* Yield 8% (294 mg, *method B*); white solid; m.p. 141–143 °C. ($CHCl_3$–Et_2O / 2:1). ^{1}H NMR (500 MHz, DMSO-d_6) *δ* 1.22 (3H, t, *J* = 7.1 Hz, CH_3), 1.62 (3H, s, $C^{3'}$-Me), 3.17 (2H, s, H-1′), 3.40 (1H, ddt, *J* = 10.6, 8.5 5.0 Hz, H-2‴B), 3.47 (1H, dq, *J* = 10.6, 4.7 Hz, H-2‴A), 3.57 (1H, dt, *J* = 14.6, 4.7 Hz, H-1‴B), 3.67 (1H, ddd, *J* = 14.6, 8.5, 5.0 Hz, H-1‴A), 4.12 (1H, dq, *J* = 10.8, 7.1 Hz, OC-H^B), 4.23 (1H, dq, *J* = 10.8, 7.1 Hz, OC-H^A), 4.92 (1H, t, *J* = 4.9 Hz, $C^{2'''}$-OH), 7.17 (1H, s, $C^{4''}$-OH), 7.26 (1H, s, C^2-OH). ^{13}C NMR (126 MHz, DMSO-d_6) *δ* 8.7 (Me), 13.5 (CH_3), 27.2 (CH_2), 42.6 (C-1‴), 58.8 (C-2‴), 62.5 (OCH_2), 76.2 (q, *J* = 29.4, C-4″), 77.4 (q, *J* = 27.4, C-2), 112.4 (C-3″), 123.4 (q, *J* = 286.8, CF_3), 123.9 (q, *J* = 288.1, CF_3), 137.9 (C-2″), 167.2 (C-1), 172.2 (C-5″). ^{19}F NMR (376 MHz, DMSO-d_6) *δ* 85.67 (s, 3F, CF_3), 85.69 (s, 3F, CF_3). IR ν 3494, 3302 (O–H), 2996–2903 (C–H), 1744, 1670 (C=O), 1174–1132 (C–F) cm^{-1}. HRMS (ESI): calcd. for $C_{14}H_{18}F_6NO_6$ $[M + H]^+$ 410.1033; found 410.1034.

Ethyl (S)-3,3,3-trifluoro-2-hydroxy-2-(((R*)-4-hydroxy-1-(2-hydroxyethyl)-3-methyl-5-oxo-4-(trifluoromethyl)-4,5-dihydro-1H-pyrrol-2-yl)methyl)propanoate (****11b****).* Yield 47% (1360 mg, *method B*); white solid; m.p. 120–122°C. (Et_2O–hexane / 3:1). ^{1}H NMR (500 MHz, DMSO-d_6) *δ* 1.22 (3H, t, *J* = 7.1 Hz, CH_3), 1.55–1.61 (2H, m, H-2‴), 1.63 (3H, s, $C^{3''}$-Me), 2.97 (1H, d, *J* = 15.0 Hz, H-1′B), 3.19 (1H, dd, *J* = 15.0, 1.5 Hz, H-1′A), 3.30–3.40 (2H,m, H-3‴), 3.51 (1H, ddd, *J* = 14.5, 7.5, 6.8 Hz, H-1‴B), 3.60 (1H, ddd, *J* = 14.5, 7.5, 7.0 Hz, H-1‴A), 4.12 (1H, dq, *J* = 10.8, 7.1 Hz, OC-H^B), 4.23 (1H, dq, *J* = 10.8, 7.1 Hz, OC-H^A), 4.53 (1H, t, *J* = 4.9 Hz, $C^{3'''}$-OH), 7.14 (1H, s, $C^{4''}$-OH), 7.23 (1H, d, *J* = 1.5 Hz, C^2-OH). ^{13}C NMR (126 MHz, DMSO-d_6) *δ* 8.73 (Me), 13.50 (CH_3), 26.96 (CH_2), 30.72 (C-2‴), 37.32 (C-1‴), 57.73 (C-3‴), 62.58 (OCH_2), 76.17 (q, *J* = 29.5, C-4″), 77.24 (q, *J* = 27.4, C-2), 113.03 (C-3″), 123.35 (q, *J* = 286.7, CF_3), 123.83 (q, *J* = 288.1, CF_3), 137.38 (C-2″), 167.21 (C-1), 172.12 (C-5″). ^{19}F NMR (376 MHz, DMSO-d_6) *δ* 85.64 (s, 3F, CF_3), 85.74 (s, 3F, CF_3) ppm. IR ν 3478, 3293 (O–H), 2992–2896 (C–H), 1751, 1670 (C=O), 1174–1134 (C–F) cm^{-1}. HRMS (ESI): calcd. for $C_{15}H_{20}F_6NO_6$ $[M + H]^+$ 424.1189; found 424.1186.

Ethyl (R)-3,3,3-trifluoro-2-hydroxy-2-(((R*)-4-hydroxy-1-(3-hydroxypropyl)-3-methyl-5-oxo-4-(trifluoromethyl)-4,5-dihydro-1H-pyrrol-2-yl)methyl)propanoate (****11b′****) (mixture of* ***11b*:*11b′*** *in the ratio 72:28).* Yield 76% (2893 mg, *method B*); white solid; m.p. 120–122 °C. ($CHCl_3$–Et_2O / 2:1). ^{1}H NMR (500 MHz, DMSO-d_6) *δ* 1.66 (3H, s, $C^{3''}$-Me), 3.08 (2H, AB-system, Δ_{AB} = 0.03 ppm, J_{AB} = 15.4 Hz, CH_2), 7.18 (1H, s, $C^{4''}$-OH), 7.24 (1H, s, C^2-OH) ppm; the signals of other protons coincide with the signals of the major diastereomer **11b**. ^{13}C NMR

(126 MHz, DMSO-d_6) δ 8.86 (Me), 13.54 (CH_3), 27.14 (CH_2), 30.73 (C-2‴), 37.18 (C-1‴), 57.57 (C-3‴), 62.58 (OCH_2), 76.22 (q, *J* = 29.2, C-4″), 77.02 (q, *J* = 28.0, C-2), 113.52 (C-3″), 123.52 (q, *J* = 286.2, CF_3), 123.83 (q, *J* = 288.1, CF_3), 137.12 (C-2″), 167.40 (C-1), 171.98 (C-5″) ppm. ^{19}F NMR (376 MHz, DMSO-d_6) δ 85.81 (s, 3F, CF_3), 86.01 (s, 3F, CF_3) ppm. IR ν 3475, 3292 (O–H), 2992–2896 (C–H), 1752, 1716 (C=O), 1173–1135 (C–F) cm^{-1}. HRMS (ESI): calcd. for $C_{15}H_{20}F_6NO_6$ $[M + H]^+$ 424.1189; found 424.1184

3.5. XRD Experiments

The X-ray studies for compounds **4d^c, 5^{tc}, 8c^c** were performed on an Xcalibur 3 CCD (Oxford Diffraction Ltd., Abingdon, UK) diffractometer with a graphite monochromator, λ(MoKα) 0.71073 Å radiation, T 295(2), for compound **11b** was registered on an XtaLAB Synergy (Oxford Diffraction Ltd., Abingdon, UK) diffractometer with hybrid pixel monochromator, λ(MoKα) 0.71073 Å radiation, T 295(2). An empirical absorption correction was applied. Using Olex2 [38], the structure was solved with the Superflip [39] structure solution program using charge flipping and refined with the ShelXL [40] refinement package using least squares minimization. All non-hydrogen atoms were refined in the anisotropic approximation; H-atoms at the C-H bonds were refined in the "rider" model with dependent displacement parameters. An empirical absorption correction was carried out through spherical harmonics, implemented in the SCALE3 ABSPACK scaling algorithm by a program "CrysAlisPro" (Rigaku Oxford Diffraction).

The full set of X-ray structural data for compounds **4d^c, 5^{tc}, 8c^c, 11b** was deposited at the Cambridge Crystallographic Data Center (deposits CCDC-238736 (**4d^c**), -2238737 (**5^{tc}**), -2238738 (**8c^c**), -2238739 (**11b**).

*Crystal Data for **4d^c***: $C_{13}H_{12}F_3NO_3$ (M = 287.24g/mol): triclinic, space group P-1, a = 6.0290(7) Å, b = 8.1542(10) Å, c = 13.4778(17) Å, α = 79.481(10)°, β = 86.443(10)°, γ = 75.029(10), V = 629.27(14) Å^3, Z = 2, T = 295(2) K, μ(CuKα) = 0.136 mm^{-1}, D_{calc} = 1.516 g/cm^3, 5481 reflections measured to (7.37 ° $\leq 2\Theta \leq$ 61.83°), 3339 unique (R_{int} = 0.0434, R_{sigma} = 0.0881) which were used in all calculations. The final R_1 was 0.0702 (I > 2σ(I)) and wR_2 was 0.1634 (all data) (Table S1, Supplementary Materials).

*Crystal Data for **5^{tc}**:* $C_{13}H_{15}F_6NO_6$ (M = 395.26 g/mol): monoclinic, space group $P2_1/n$, a = 10.8844(8) Å, b = 13.1919(9) Å, c = 11.3734(9) Å, $\alpha = \gamma$ =90°, β = 92.641(7)°, V = 1631.3(2) Å^3, Z = 4, T = 295(2) K, μ(CuKα) = 0.167 mm^{-1}, D_{calc} = 1.609 g/cm^3, 11283 reflections measured to (7.14° $\leq 2\Theta \leq$ 62.03°), 4404 unique (R_{int} = 0.0496, R_{sigma} = 0.0604) which were used in all calculations. The final R_1 was 0.0544 (I > 2σ(I)) and wR_2 was 0.1455 (all data) (Table S1, Supplementary Materials).

*Crystal Data for **8c^c***: $C_{12}H_{18}F_3NO_3$ (M = 281.27 g/mol): monoclinic, space group $P2_1/c$, a = 10.6332(12) Å, b = 13.8923(13) Å, c = 9.5664(15) Å, $\alpha = \gamma$ =90°, β = 102.235(13)°, V = 1381.0(3) Å^3, Z = 4, T = 295(2) K, μ(CuKα) = 0.122 mm^{-1}, D_{calc} = 1.353 g/cm^3, 10666 reflections measured to (7.06° $\leq 2\Theta \leq$ 61.72°), 3779 unique (R_{int} = 0.0582, R_{sigma} = 0.0803) which were used in all calculations. The final R_1 was 0.0611 (I > 2σ(I)) and wR_2 was 0.1539 (all data) (Table S2, Supplementary Materials).

*Crystal Data for **11b**:* $C_{15}H_{19}NO_6F_6$ (M = 423.31g/mol): monoclinic, space group P21/c, a = 19.1431(10) Å, b = 6.4882(4) Å, c = 16.4430(9) Å, $\alpha = \gamma$ =90°, β = 107.551(6)°, V = 1947.2(2) Å^3, Z = 4, T = 295(2) K, μ(CuKα) = 0.145 mm^{-1}, D_{calc} = 1.444 g/cm^3, 15118 reflections measured to (5.00° $\leq 2\Theta \leq$ 52.74°), 3972 unique (R_{int} = 0.1526, R_{sigma} = 0.0998) which were used in all calculations. The final R_1 was 0.0601 (I > 2σ(I)) and wR_2 was 0.1547 (all data) (Table S2, Supplementary Materials).

4. Conclusions

A method for the synthesis of bicyclic γ-lactam annulated oxazacycles has been developed based on the multicomponent reaction of ethyl trifluoropyruvate with methyl ketones and 1,2-, 1,3-amino alcohols. Thus, the use of aminoethanol makes it possible to obtain tetrahydropyrrolo[2,1-*b*]oxazol-5-ones, and the use of aminopropanol–tetrahydropyrrolo[2,1-*b*][1,3]oxazine-6-ones. Variation of the methyl ketone component creates opportunities for

the introduction of various substituents at the nodal carbon atom of these bicycles. The method proposed by us is distinguished by the simplicity of execution and the availability of initial reagents.

It has been shown that the structure of final γ-lactams is determined by the stoichiometric amount of ethyl trifluoropyruvate and the nature of methyl ketone. At the same time, distinctive features of the transformations of amino alcohols were found in comparison with the previously studied reactions with 1,2-, 1,3-diamines, since the use of a double excess of ethyl trifluoropyruvate results in the formation of bicyclic aldols rather than tricyclic dipyrrolooxazacycles [35]. This feature is due to the fact that the oxygen atom in the cycle does not have the opportunity for subsequent addition reactions, and, consequently, the formation of tricycles. In addition, the reaction of a double excess of pyruvate with 2-butanone and aminopropanol stops at the stage of formation of N-hydroxypropyl-2,3-dihydropyrrol-5-one, the possibility of its isolation is probably due to the lower reactivity of the hydroxyl group compared to the amino function. It can also be noted that, in contrast to the transformations of diamines, three-component cyclizations with amino alcohols are less diastereoselective, since they predominantly lead to the formation of two *cis*- and *trans*-isomers, the diastereomeric structure of which we were able to reliably establish using NMR spectroscopy and X-ray diffraction.

The mechanism of formation of bicyclic γ-lactams has been determined. It represents successive domino reactions with the initial formation of an aldol and a bis-aldol from pyruvate and methyl ketone, which becomes possible due to the increased electrophilicity of the carbonyl group at the trifluoromethyl substituent.

The synthesized tetrahydropyrrolo[2,1-*b*]oxazol-5-ones and tetrahydropyrrolo[2,1-*b*][1,3]oxazine-6-ones are of interest both for biological testing and for the following chemical transformations, for example, oxazole ring opening reactions to obtain new γ-lactams.

Supplementary Materials: The following supporting information can be downloaded at: https://www.mdpi.com/article/10.3390/molecules28041983/s1, Table S1: Crystallographic parameters and X-ray experiment details for **4d^{c}**, **5^{tc}**; Table S2: Crystallographic parameters and X-ray experiment details for **8c^{c}**, **11b**; Figure S1: ^{1}H NMR spectrum of **4a^{t}**; Figure S2: ^{13}C NMR spectrum of **4a^{t}**; Figure S3: ^{19}F NMR spectrum of **4a^{t}**; Figure S4: ^{1}H NMR spectrum of **4a^{c}** (mixed with **5^{ct}** (20%) and **4a^{t}** (2%)); Figure S5: ^{19}F NMR spectrum of **4a^{c}** (mixed with **5^{ct}** (20%) and **4a^{t}** (2%)); Figure S6: ^{1}H NMR spectrum of **4b^{t}**; Figure S7: ^{1}H NMR spectrum of **4b^{t}**; Figure S8: ^{19}F NMR spectrum of **4b^{t}**; Figure S9: ^{1}H NMR spectrum of **4b^{c}** (mixed with **4b^{t}** in the ratio 90:10); Figure S10: ^{13}C NMR spectrum of **4b^{c}** (mixed with 4bt in the ratio 90:10); Figure S11: ^{19}F NMR spectrum of **4b^{c}** (mixed with 4**b^{t}** in the ratio 90:10); Figure S12: ^{1}H NMR spectrum of **4c^{t}** (mixed with **4c^{c}** in the ratio 90:10); Figure S13: ^{13}C NMR spectrum of **4c^{t}** (mixed with **4c^{c}** in the ratio 90:10); Figure S14: ^{19}F NMR spectrum of **4c^{t}** (mixed with **4c^{c}** in the ratio 90:10); Figure S15: ^{1}H NMR spectrum of **4c^{c}**; Figure S16: ^{13}C NMR spectrum of **4c^{c}**; Figure S17: ^{19}F NMR spectrum of **4c^{c}**; Figure S18: ^{1}H NMR spectrum of **4d^{c}**; Figure S19: ^{13}C NMR spectrum of **4d^{c}**; Figure S20: ^{19}F NMR spectrum of **4d^{c}**; Figure S21: ^{1}H NMR spectrum of **5^{tc}**; Figure S22: ^{13}C NMR spectrum of **5^{tc}**; Figure S23: ^{19}F NMR spectrum of **5^{tc}**; Figure S24: ^{1}H NMR spectrum of **5^{cc}** (mixed with **5^{tc}** in the ratio 80:20); Figure S25: ^{13}C NMR spectrum of **5^{cc}** (mixed with **5^{tc}** in the ratio 80:20); Figure S26: ^{19}F NMR spectrum of **5^{cc}** (mixed with **5^{tc}** in the ratio 80:20); Figure S27: 1H NMR spectrum of **6b**; Figure S28: ^{13}C NMR spectrum of **6b**; Figure S29: ^{19}F NMR spectrum of **6b**; Figure S30: ^{1}H NMR spectrum of **8a^{t}** (mixed with **8a^{c}** in the ratio 84:16); Figure S31: ^{13}C NMR spectrum of **8a^{t}** (mixed with **8a^{c}** in the ratio 84:16); Figure S32: ^{19}F NMR spectrum of **8a^{t}** (mixed with **8a^{c}** in the ratio 84:16); Figure S33: ^{1}H NMR spectrum of **8a^{c}** (mixed with **8a^{t}** in the ratio 89:11); Figure S34: ^{19}F NMR spectrum of **8a^{c}** (mixed with **8a^{t}** in the ratio 89:11); Figure S35: ^{13}C NMR spectrum of **8a^{c}** (mixed with **8a^{t}** in the ratio 89:11); Figure S36: ^{1}H NMR spectrum of **8b^{t}**; Figure S37: ^{13}C NMR spectrum of **8b^{t}**; Figure S38: ^{19}F NMR spectrum of **8b^{t}**; Figure S39: ^{1}H NMR spectrum of **8b^{c}** (mixed with **8b^{t}** in the ratio 81:19); Figure S40: ^{13}C NMR spectrum of **8b^{c}** (mixed with **8b^{t}** in the ratio 81:19); Figure S41: ^{19}F NMR spectrum of **8b^{c}** (mixed with **8b^{t}** in the ratio 81:19); Figure S42: ^{1}H NMR spectrum of **8c^{t}**; Figure S43: ^{19}F NMR spectrum of **8c^{t}**; Figure S44: ^{13}C NMR spectrum of **8c^{t}**; Figure S45: ^{1}H NMR spectrum of **8c^{c}**; Figure S46: ^{13}C NMR spectrum of **8c^{c}**; Figure S47: ^{19}F NMR spectrum of **8c^{c}**; Figure S48: ^{1}H NMR spectrum of **8d^{t}**; Figure S49: ^{13}C NMR spectrum of **8d^{t}**; Figure S50: ^{19}F NMR spectrum of **8d^{t}**; Figure S51: ^{1}H NMR spectrum of a mixture of **9**:**9′** in the ≈ 1:1;

Figure S52: ^{13}C NMR spectrum of a mixture of **9**:**9′** in the ratio ≈ 1:1; Figure S53: ^{19}F NMR spectrum of mixture of **9**:**9′** in the ratio ≈ 1:1; Figure S54: ^{1}H NMR spectrum of mixture of **10**:**10′** in the ratio 56:44; Figure S55: ^{13}C NMR spectrum of mixture of **10**:**10′** in the ratio 56:44; Figure S56: ^{19}F NMR spectrum of mixture of **10**:**10′** in the ratio 56:44; Figure S57: ^{1}H NMR spectrum of **11a**; Figure S58: ^{13}C NMR spectrum of **11a**; Figure S59: ^{19}F NMR spectrum of **11a**; Figure S60: ^{1}H NMR spectrum of **11b**; Figure S61: ^{13}C NMR spectrum of **11b**; Figure S62: ^{19}F NMR spectrum of **11b**; Figure S63: ^{1}H NMR spectrum of mixture of **11b**:**11b′** in the ratio 72:28; Figure S64: ^{13}C NMR spectrum of mixture of **11**:**11′** in the ratio 72:28; Figure S65: ^{19}F NMR spectrum of mixture of **11**:**11′** in the ratio 72:28.

Author Contributions: Conceptualization, methodology, Y.V.B., M.V.G.; synthesis, O.A.F., M.V.G.; experimental investigation, M.A.E., M.I.K., P.A.S., V.S.G.; writing—original draft preparation, Y.V.B., M.V.G.; writing—review and editing, Y.V.B., M.V.G., O.A.F., M.I.K., M.A.E., V.I.S.; supervision, V.I.S. All authors have read and agreed to the published version of the manuscript.

Funding: This work was financially supported by the Russian Science Foundation (grant No 21-13-00390 for V.I.S.).

Institutional Review Board Statement: Not applicable.

Informed Consent Statement: Not applicable.

Data Availability Statement: Not applicable.

Acknowledgments: Analytical studies (IR and NMR spectroscopy, elemental analysis, and XRD analysis experiments) were carried out using equipment of the Center for Joint Use "Spectroscopy and Analysis of Organic Compounds" at the IOS UB RAS. The authors are grateful for Maria A. Panova for assistance in manuscript preparation.

Conflicts of Interest: The authors declare no conflict of interest.

Sample Availability: Samples of the compounds **4a–d, 5, 6a,b, 7, 8a–d, 9, 10, 11a,b** are available from the authors.

References

1. Caruano, J.; Muccioli, G.G.; Robiette, R. Biologically active γ-lactams: Synthesis and natural sources. *Org. Biomol. Chem.* **2016**, *14*, 10134–10156. [CrossRef]
2. Groaning, M.D.; Meyers, A.I. Concise synthesis of indolizidines: Total synthesis of (−)-coniceine. *Chem. Commun.* **2000**, 1027–1028. [CrossRef]
3. Fenteany, G.; Standaert, R.F.; Lane, W.S.; Choi, S.; Corey, E.J.; Schreiber, S.L. Inhibition of proteasome activities and subunit-specific amino-terminal threonine modification by Lactacystin. *Science* **1995**, *268*, 726–731. [CrossRef]
4. Chu, S.; Liu, S.; Duan, W.; Cheng, Y.; Jiang, X.; Zhu, C.; Tang, K.; Wang, R.; Xu, L.; Wang, X.; et al. The anti-dementia drug candidate, (−)-clausenamide, improves memory impairment through its multi-target effect. *Pharmacol. Ther.* **2016**, *162*, 179–187. [CrossRef]
5. Yost, C.S. A new look at the Respiratory Stimulant Doxapram. *CNS Drug Rev.* **2006**, *12*, 236–249. [CrossRef]
6. Glauser, T.A.; Cnaan, A.; Shinnar, S.; Hirtz, D.G.; Dlugos, D.; Masur, D.; Clark, P.O.; Capparelli, E.V.; Adamson, P.C. Ethosuximide, valproic acid, and lamotrigine in childhood absence epilepsy. *New Engl. J. Med.* **2010**, *362*, 790–799. [CrossRef]
7. Shorvon, S.D. Piracetam. In *the Treatment of Epilepsy*, 3rd ed.; Shorvon, S., Perucca, E., Engel, J., Eds.; Wiley-Blackwell: Oxford, UK, 2009; pp. 619–625. [CrossRef]
8. Pinza, M.; Farina, C.; Cerri, A.; Pfeiffer, U.; Riccaboni, M.T.; Banfi, S.; Biagetti, R.; Pozzi, O.; Magnani, M.; Dorigotti, L. Synthesis and pharmacological activity of a series of dihydro-1H-pyrrolo[1,2-a]imidazole-2,5(3H,6H)-diones, a novel class of potent cognition enhancers. *J. Med. Chem.* **1993**, *36*, 4214–4220. [CrossRef]
9. Boyd, D.B.; Elzey, T.K.; Hatfield, L.D.; Kinnick, M.D.; Morin, J.M. γ-Lactam analogues of the penems. *Tetrahedron Lett.* **1986**, *27*, 3453–3456. [CrossRef]
10. Baldwin, J.E.; Adlington, R.M.; Jones, R.H.; Schofield, C.J.; Zarocostas, C.; Greengrass, C.W. γ-Lactam analogues of carbapenicillanic acids. *J. Chem. Soc. Chem. Commun.* **1985**, 194–196. [CrossRef]
11. Groaning, M.D.; Meyers, A. Chiral non-racemic bicyclic lactams. Auxiliary-based asymmetric reactions. *Tetrahedron* **2000**, *56*, 9843–9873. [CrossRef]
12. Romo, D.; Meyers, A. Chiral non-racemic bicyclic lactams. Vehicles for the construction of natural and unnatural products containing quaternary carbon centers. *Tetrahedron* **1991**, *47*, 9503–9569. [CrossRef]
13. Meyers, A.I.; Harre, M.; Garland, R. Asymmetric synthesis of quaternary carbon centers. *J. Am. Chem. Soc.* **1984**, *106*, 1146–1148. [CrossRef]

14. Meyers, A.I.; Lefker, B.A. Chiral bicyclic lactams for asymmetric synthesis of quaternary carbons. The total synthesis of (-)-.alpha.-cuparenone. *J. Org. Chem.* **1986**, *51*, 1541–1544. [CrossRef]
15. Malaquin, S.; Jida, M.; Courtin, J.; Laconde, G.; Willand, N.; Deprez, B.; Deprez-Poulain, R. Water-based conditions for the microscale parallel synthesis of bicyclic lactams. *Tetrahedron Lett.* **2013**, *54*, 562–567. [CrossRef]
16. Le Goff, R.; Martel, A.; Sanselme, M.; Lawson, A.M.; Daïch, A.; Comesse, S. Simple access to highly functional bicyclic γ- and δ-lactams: Origins of chirality transfer to contiguous tertiary/quaternary stereocenters assessed by DFT. *Chem. A Eur. J.* **2014**, *21*, 2966–2979. [CrossRef]
17. Comesse, S.; Martel, A.; Daïch, A. Domino process optimized via ab initio study for an alternative access to bicyclic lactams. *Org. Lett.* **2011**, *13*, 4004–4007. [CrossRef]
18. Pilard, J.-F.; Klein, B.; Texier-Boullet, F.; Hamelin, J. Fast synthesis of heterobicycles containing a bridgehead nitrogen atom in dry media under microwave irradiation. *Synlett* **1992**, *1992*, 219–220. [CrossRef]
19. Wedler, C.; Schick, H.; Scharfenberg-Pfeiffer, D.; Reck, G. Reactions of 4-oxoalkanoic acids, 4. synthesis of (±)-6-alkyl-5-oxa-1-azabicyclo[4.3.0]nonan-9-ones, (±)-5-alkyl-4-oxa-1-azabicyclo[3.3.0]octan-8-ones, and substituted 1,6-dioxa-3,8-diazacyclodecanes by reaction of ethyl 4-oxoalkanoates with 3-aminopropanol and 2-aminoethanol. *Eur. J. Org. Chem.* **1992**, *1992*, 29–32. [CrossRef]
20. Vainiotalo, P.; Savolainen, P.-L.; Ahlgrén, M.; Mälkönen, P.J.; Vepsäläinen, J. Identification of the condensation products of 1,2- and 1,3-amino alcohols with keto esters by NMR spectroscopy, mass spectrometry and X-ray crystallography studies. Open or ring forms? *J. Chem. Soc. Perkin Trans. 2* **1991**, 735–741. [CrossRef]
21. Meyers, A.I.; Wallace, R.H. Some observations on the validity and generality of the "Cieplak stereoelectronic effect". *J. Org. Chem.* **1989**, *54*, 2509–2510. [CrossRef]
22. Hao, J.; Hou, M.; Zhuang, H.; Wang, J.; Wan, W.; Jiang, H. A Process for Preparing (3S)-3-Benzyl-7a-(Trifluoromethyl)Tetrahydropyrrolo[2,1-b]Oxazol-5(6H)-One. *Patent CN101531668 A China*, 2009.
23. Hao, J.; Hou, M.; Zhuang, H.; Wang, J.; Wan, W.; Jiang, H. Preparation of (3R)-3-Benzyl-7a-(Difluoromethyl)Tetrahydropyrrolo[2,1-b]Oxazol-5(6H)-One. *Patent CN101544658 A China*, 2009.
24. Li, B.; Guinness, S.M.; Hoagland, S.; Fichtner, M.; Kim, H.; Li, S.; Maguire, R.J.; McWilliams, J.C.; Mustakis, J.; Raggon, J.; et al. Continuous production of anhydrous *tert*-butyl hydroperoxide in nonane using membrane pervaporation and its application in flow oxidation of a γ-butyrolactam. *Org. Process Res. Dev.* **2018**, *22*, 707–720. [CrossRef]
25. Bhatt, J.D.; Patel, T.S.; Chudasama, C.J.; Patel, K.D. Microwave-assisted synthesis of novel pyrazole clubbed polyhydroquinolines in an ionic-liquid and their biological perspective. *ChemistrySelect* **2018**, *3*, 3632–3640. [CrossRef]
26. Wu, Y.; Wang, Y.; He, M.; Tao, X.; Li, J.; Shan, D.; Lv, L. Progress of trifluoroacetoacetate in the synthesis of agrochemicals and medicines with fluorine. *Mini-Rev. Org. Chem.* **2017**, *14*, 350–356. [CrossRef]
27. O'Hagan, D. Understanding organofluorine chemistry. An introduction to the C–F bond. *Chem. Soc. Rev.* **2007**, *37*, 308–319. [CrossRef]
28. Jeffries, B.; Wang, Z.; Graton, J.; Holland, S.D.; Brind, T.; Greenwood, R.D.R.; Le Questel, J.-Y.; Scott, J.S.; Chiarparin, E.; Linclau, B. Reducing the lipophilicity of perfluoroalkyl groups by CF_2–F/CF_2–Me or CF_3/CH_3 exchange. *J. Med. Chem.* **2018**, *61*, 10602–10618. [CrossRef]
29. Giornal, F.; Pazenok, S.; Rodefeld, L.; Lui, N.; Vors, J.-P.; Leroux, F.R. Synthesis of diversely fluorinated pyrazoles as novel active agrochemical ingredients. *J. Fluor. Chem.* **2013**, *152*, 2–11. [CrossRef]
30. Muller, K.; Faeh, C.; Diederich, F. Fluorine in pharmaceuticals: Looking beyond intuition. *Science* **2007**, *317*, 1881–1886. [CrossRef]
31. Goryaeva, M.V.; Burgart, Y.V.; Kudyakova, Y.S.; Ezhikova, M.A.; Kodess, M.I.; Slepukhin, P.A.; Saloutin, V.I. Three-component synthesis of 7-hydroxy-7-polyfluoroalkylhexahydroimidazo[1,2-*a*] pyridin-5(1*H*)-ones. *Eur. J. Org. Chem.* **2015**, *2015*, 6306–6314. [CrossRef]
32. Saloutin, V.I.; Goryaeva, M.V.; Kushch, S.O.; Khudina, O.G.; Ezhikova, M.A.; Kodess, M.I.; Slepukhin, P.A.; Burgart, Y.V. Competitive ways for three-component cyclization of polyfluoroalkyl-3-oxo esters, methyl ketones and amino alcohols. *Pure Appl. Chem.* **2020**, *92*, 1265–1275. [CrossRef]
33. Goryaeva, M.V.; Kushch, S.O.; Khudina, O.G.; Burgart, Y.V.; Ezhikova, M.A.; Kodess, M.I.; Slepukhin, P.A.; Volobueva, A.S.; Slita, A.V.; Esaulkova, I.L.; et al. New multicomponent approach to polyfluoroalkylated pyrido[1,2-a]pyrimidine derivatives and bis-cyclohexenones. *J. Fluor. Chem.* **2020**, *241*, 109686. [CrossRef]
34. Kushch, S.O.; Goryaeva, M.V.; Burgart, Y.V.; Triandafilova, G.A.; Malysheva, K.O.; Krasnykh, O.P.; Gerasimova, N.A.; Evstigneeva, N.P.; Saloutin, V.I. Facile synthesis of 6-organyl-4-(trifluoromethyl)pyridin-2(1H)-ones and their polyfluoroalkyl-containing analogs. *Russ. Chem. Bull.* **2022**, *71*, 1687–1700. [CrossRef] [PubMed]
35. Goryaeva, M.V.; Fefelova, O.; Burgart, Y.V.; Ezhikova, M.; Kodess, M.I.; Slepukhin, P.; Triandafilova, G.; Solodnikov, S.Y.; Krasnykh, O.P.; Saloutin, V.I. A three-component synthesis of trifluoromethylated hexahydropyrrolo[1,2-a]imidazol-5-ones and hexahydropyrrolo[1,2-a]pyrimidin-6-ones. *Chem. Heterocycl. Compd.* **2022**, *58*, 421–431. [CrossRef]
36. Landge, S.M.; Török, B. Highly enantioselective organocatalytic addition of ethyl trifluoropyruvate to ketones with subzero temperature microwave activation. *Catal. Lett.* **2009**, *131*, 432–439. [CrossRef]
37. Goryaeva, M.V.; Kushch, S.O.; Burgart, Y.V.; Ezhikova, M.A.; Kodess, M.I.; Slepukhin, P.A.; Triandafilova, G.A.; Krasnykh, O.P.; Yakovleva, E.I.; Zarubaev, V.V.; et al. New heteroanalogs of tricyclic ascidian alkaloids: Synthesis and biological activity. *Org. Biomol. Chem.* **2021**, *19*, 9925–9935. [CrossRef]

38. Dolomanov, O.V.; Bourhis, L.J.; Gildea, R.J.; Howard, J.A.K.; Puschmann, H. OLEX2: A complete structure solution, refinement and analysis program. *J. Appl. Cryst.* **2009**, *42*, 339–341. [CrossRef]
39. Palatinus, L.; Chapuis, G. SUPERFLIP—A computer program for the solution of crystal structures by charge flipping in arbitrary dimensions. *J. Appl. Crystallogr.* **2007**, *40*, 786–790. [CrossRef]
40. Sheldrick, G.M. A short history of SHELX. *Acta Crystallogr. Sect. A* **2007**, *A64*, 112–122. [CrossRef]

molecules

MDPI

Article

3-Aryl-5-aminobiphenyl Substituted [1,2,4]triazolo[4,3-*c*]quinazolines: Synthesis and Photophysical Properties

Alexandra E. Kopotilova [1], Tatyana N. Moshkina [1], Emiliya V. Nosova [1,2,*], Galina N. Lipunova [2], Ekaterina S. Starnovskaya [1,2], Dmitry S. Kopchuk [1,2], Grigory A. Kim [1,2], Vasiliy S. Gaviko [1,3], Pavel A. Slepukhin [1,2] and Valery N. Charushin [1,2]

[1] Department of Organic and Biomolecular Chemistry, Ural Federal University, 620002 Ekaterinburg, Russia
[2] I. Postovsky Institute of Organic Synthesis, Ural Branch of the Russian Academy of Sciences, 620108 Ekaterinburg, Russia
[3] M.N. Mikheev Institute of Metal Physics, Ural Branch of the Russian Academy of Sciences, 620108 Ekaterinburg, Russia
* Correspondence: emilia.nosova@yandex.ru

Abstract: Amino-[1,1′]-biphenyl-containing 3-aryl-[1,2,4]triazolo[4,3-*c*]quinazoline derivatives with fluorescent properties have been designed and synthesized. The type of annelation of the triazole ring to the pyrimidine one has been unambiguously confirmed by means of an X-ray diffraction (XRD) method; the molecules are non-planar, and the aryl substituents form the pincer-like conformation. The UV/Vis and photoluminescent properties of target compounds were investigated in two solvents of different polarities and in a solid state. The samples emit a broad range of wavelengths and display fluorescent quantum yields of up to 94% in toluene solutions. 5-(4′-Diphenylamino-[1,1′]-biphenyl-4-yl)-3-(4-(trifluoromethyl)phenyl)-[1,2,4]triazolo[4,3-*c*]quinazoline exhibits the strongest emission in toluene and a solid state. Additionally, the solvatochromic properties were studied for the substituted [1,2,4]triazolo[4,3-*c*]quinazolines. Moreover, the changes in absorption and emission spectra have been demonstrated upon the addition of water to MeCN solutions, which confirms aggregate formation, and some samples were found to exhibit aggregation-induced emission enhancement. Further, the ability of triazoloquinazolines to detect trifluoroacetic acid has been analyzed; the presence of TFA induces changes in both absorption and emission spectra, and acidochromic behavvior was observed for some triazoloquinazoline compounds. Finally, electronic-structure calculations with the use of quantum-chemistry methods were performed for synthesized compounds.

Keywords: [1,2,4]triazolo[4,3-*c*]quinazolines; cross-coupling; fluorescence; solvatochromism; pH-sensor

Citation: Kopotilova, A.E.; Moshkina, T.N.; Nosova, E.V.; Lipunova, G.N.; Starnovskaya, E.S.; Kopchuk, D.S.; Kim, G.A.; Gaviko, V.S.; Slepukhin, P.A.; Charushin, V.N. 3-Aryl-5-aminobiphenyl Substituted [1,2,4]triazolo[4,3-*c*]quinazolines: Synthesis and Photophysical Properties. *Molecules* **2023**, *28*, 1937. https://doi.org/10.3390/molecules28041937

Academic Editors: Athanassios C. Tsipis and Alexey M. Starosotnikov

Received: 24 January 2023
Revised: 9 February 2023
Accepted: 13 February 2023
Published: 17 February 2023

1. Introduction

Heterocyclic scaffolds containing the triazole rings, which are annelated with natural pyrimidine heterocycles, represent "lead compounds" for organic synthesis [1], medicinal chemistry [2] and pharmacology [3,4]. Recently, the ability of some [1,2,4]triazolo[4,3-*c*]quinazolines to act as penetrating DNA intercalators has been demonstrated [5,6]. 3,5-Diphenyl[1,2,4]triazolo[4,3-*c*]quinazoline was reported as a selective A_3A adenosine receptor antagonist [7], and 5-aryl-[1,2,4]triazolo[4,3-*c*]quinazoline-3-amine demonstrated anticonvulsant activity [8].

The main advantage of the azolodiazine domain of 1,2,4-triazole-containing hybrid molecules is associated with a planarized skeleton of aza-heterocyclic core, which has an important effect on structural modifications [9], biological interactions [10] and chromophore properties [11]. Benzoimidazo[1,2-*a*][1,2,3]triazolo[4,5-*e*]pyrimidines **A** (Figure 1) demonstrated aggregation-induced emissions (AIE) and acidochromic behaviour [12]. The emission spectra of 2*H*-[1,2,3]triazolo[4,5-e][1,2,4]triazolo[1,5-*a*]pyrimidine derivatives **B** in

acetonitrile solutions are sensitive to the presence of nitroaromatic explosives [13]. Fluorescent 2-aryl-1,2,3-triazolopyrimidine **C** was demonstrated to penetrate cells and selectively accumulate in the cell membrane, Golgi complex and endoplasmic reticulum, which opens up wide opportunities in bioimaging [11].

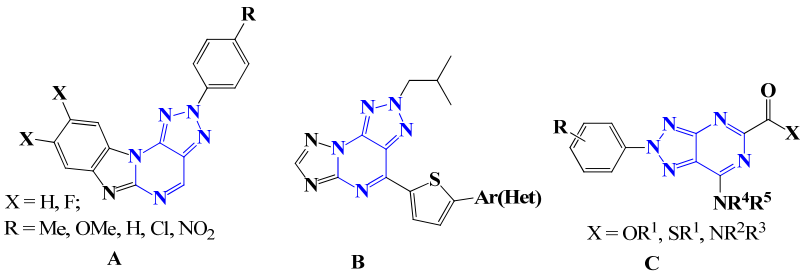

Figure 1. Representatives of triazolopyrimidine-containing chromophores (**A**–**C**).

The quinazolinyl moiety possesses a stronger electron-withdrawing ability than the pyrimidinyl core due to extra electron delocalization into the fused benzene ring. Enhanced intramolecular charge transfer (ICT) in quinazoline chromophores was illustrated by red-shifted absorption and emission with regard to their pyrimidine analogs [14]. There is limited data on the optical properties of 3,5-diarylsubstituted [1,2,4]triazolo[4,3-*c*]quinazolines. 5-Fluorenyl-, 5-spirofluorenyl and 5-(3(4)-fluorenyl)phenyl substituted 3-(4-cyanophenyl)-[1,2,4]triazolo[4,3-*c*]quinazolines (compounds **D**–**F**, Figure 2) were reported as novel electron transport heterocycles for efficient OLED materials possessing proper molecular dipole moments, which are able to be in compact contact with other organic layers in the process of forming a device [15]. Analogs of compounds **D**–**F** bearing a triphenyl-1,3,5-triazine fragment instead of a cyanophenyl one were mentioned in patent [16], and some 5-phenyl-, 5-biphenyl- and 5-napthyl- derivatives of [1,2,4]triazolo[4,3-*c*]quinazolines containing triphenyl-1,3,5-triazine residue in position C(3) have been developed [17].

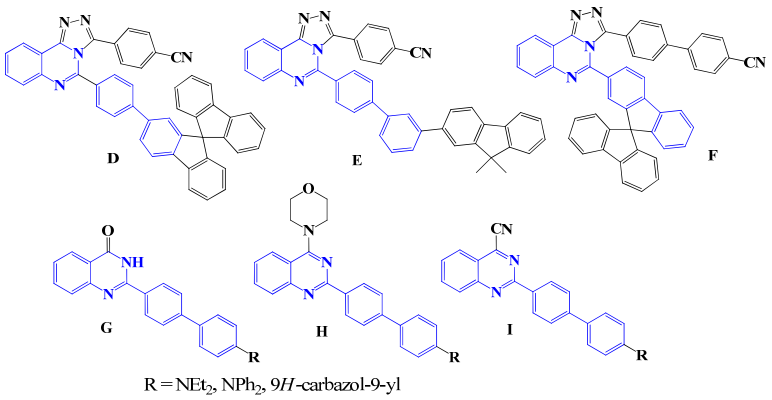

Figure 2. Representatives of biphenyl-substituted quinazoline chromophores **D**–**I**.

Our research group is working on synthetic approaches to quinazoline fluorophores and investigating the photophysical properties, as well as possible practical applications. Recently, the π-conjugated chromophores based on 2-aryl/thienyl-4-cyanoquinazolines, including 2-(4′-amino[1,1′-biphenyl]-4-yl)-containing derivatives **G**–**I** (Figure 2), have been studied [18,19]. 4-Cyanoquinazolines are shown to be less emissive in solvents and solid state than quinazolin-4-ones [19] and morpholinyl [20] counterparts; the introduction of the cyano group into position C(4) leads to orange/red coloured powder and dual emission bands [19]. Annelation of the triazole cycle can be considered another way to enhance the electron-acceptor character of the quinazoline core.

Herein, we develop the series of [1,2,4]triazolo[4,3-*c*]quinazolines bearing 3-aryl and 5-aminobiphenyl fragments to handle the detailed investigation of photophysical properties

and to discover preferable structures for practical applications. The synthetic approach involves the cross-coupling of a bromo-derivative with boronic acid under typical conditions. The target compounds appeared to exhibit fluorescent properties both in solution and solid state; the fluorophores demonstrated changes in absorption and emission spectra upon the addition of water to MeCN solutions. Moreover, triazoloquinazolines show sensing properties toward acid.

2. Results

2.1. Synthesis

Triazoloquinazoline fluorophores **2a–i** were obtained by a Suzuki–Miyaura cross-coupling reaction. The approach involves a Pd-catalyzed interaction of the corresponding 4-bromophenyl derivative **1a–c** with arylboronic acid or an arylboronic acid pinacol ester; the yields were from moderate to good (25–65%), Scheme 1. The starting 3-(*p*-tolyl), 3-(4-methoxyphenyl) or 3-(4-trifluoromethyl) substituted 5-(4-bromophenyl)-[1,2,4]triazolo[4,3-*c*]quinazolines **1a–c** were prepared from appropriate hydrazones by oxidative cyclization with bromine in glacial acetic acid at room temperature, as previously described [21].

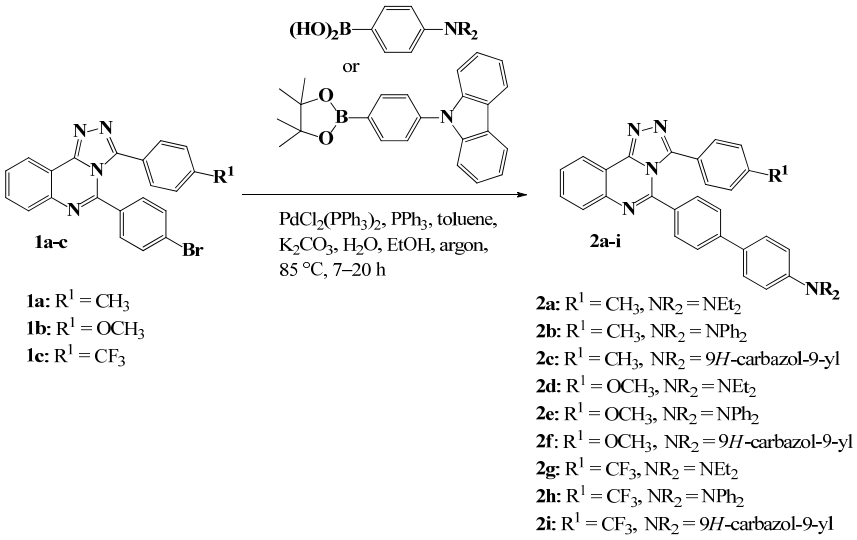

Scheme 1. Synthesis of 3-aryl-5-(4′-amino[1,1′]-biphenyl)[1,2,4]triazolo[4,3-*c*]quinazolines **2a–i**.

^{1}H NMR, ^{13}C NMR spectroscopy, mass spectrometry (Supplementary Materials—Figures S1–S9) and elemental analysis data confirmed the identity and purity of target compounds. ^{13}C NMR data for sample **2i** has not been obtained due to its poor solubility in organic solvents, including DMSO-d_6 under heating.

Single crystals of quinazolines **2a** and **2e** were obtained by a slow evaporation technique (MeCN and *n*-hexane/chloroform mixture, respectively, used as a solvent) and analyzed by an X-ray diffraction method (XRD) (Figure 3, Supplementary Materials—Tables S1–S4, Figure S10). According to XRD data, compound **2a** is crystallized in the centrosymmetric space group of the monoclinic system. The molecule is non-planar, and the aryl substituents form the pincer-like conformation (Figure 3). The mean bond lengths and angles are near expectations. The configuration of the nitrogen atom in the diethyl amino group is near to planar. The deviation of the N(34) atom from the plane C(31)C(35)C(37) is 0.099 Å. The C–N bond distances of the ethyl substituents at the amino moiety are varied within a range of 1.456–1.462 Å. The distance C(31)–N(34) of 1.387 Å is significantly shortened, and the conjugation between the N(34) atom and the aryl substituent is observed. The shortened π-π interactions between the heterocyclic part and π-donating NEt_2-phenyl substituent are observed, the distance C(5) ... C(29) [1 − x, y − 0.5, 1.5 − z] was found to be 3.274 Å, which is 0.13 Å less than sum of the V-d-W radii.

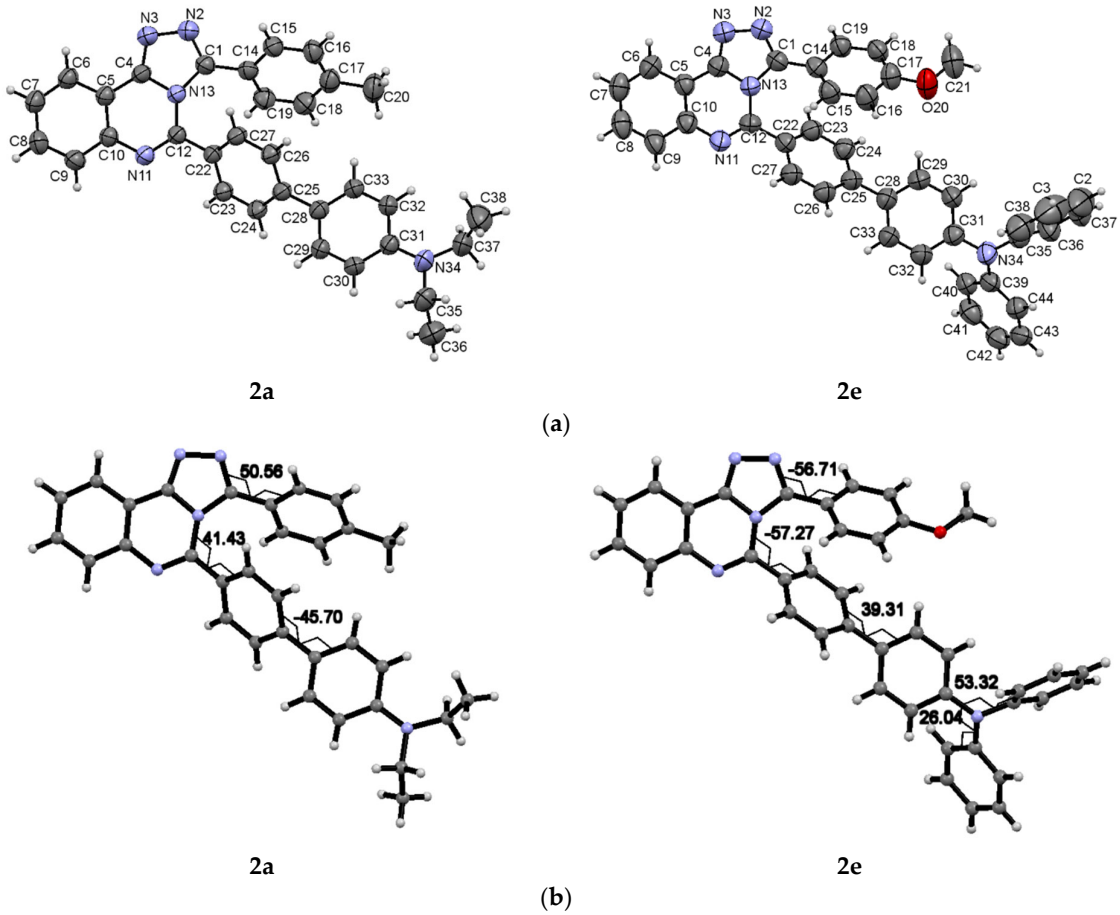

Figure 3. (**a**) Molecular structure of **2a** and **2e** in the thermal ellipsoids of 50% probability. (**b**) Selected torsion angles of compounds **2a** and **2e**.

Compound **2e** is crystallized in the non-primitive centrosymmetric space group. As well as **2a**, molecule **2e** is non-planar, and the aryl substituents form the pincer-like conformation (Figure 3). The mean bond lengths and angles were also close to expectations. The three N–C bonds at the triarylamino group are almost in the same plane. The deviation of the N(34) atom from the C(31)C(35)C(39) plane is 0.10 Å, significant torsion angles were defined between all aryl substituents and the plane of the C–N bonds. The C–N bond distances of the triarylamino moiety are varied within the range of 1.409–1.443 Å. The T-shaped Csp^2–H . . . N π-contacts take place with the participation of the nitrogen atom of the triazolo moiety. No shortened π-π interactions in the molecular packing were found.

An undoubted significance of the XRD data obtained for compounds **2a**, **e** is that the type of annelation of the triazole moiety to the quinazoline one has been unambiguously confirmed. Unfortunately, there is still conflicting information in the literature; in particular, some patents report the formation of the [4,3-*c*] isomer of triazoloquinazoline [15,17] from arylhydrazone, and others state the [1,5-*c*] isomer [16] in the presence of the same oxidant $PhI(OAc)_2$. Evidence of structure, causes of different reactions, and Dimroth rearrangement conditions were not provided.

2.2. UV/Vis and Fluorescence Spectroscopy

The UV/Vis absorption and photoluminescence (PL) spectroscopic data for toluene and MeCN solutions of [1,2,4]triazolo[4,3-*c*]quinazoline fluorophores **2a**–**i** are presented in Table 1; the corresponding spectra are shown in Supplementary Materials Figures S11–S23. The solutions of a c $\approx 10^{-5}$ M concentration were prepared for the experiments.

Table 1. Photophysical properties of [1,2,4]triazolo[4,3-*c*]quinazolines **2a–i** in toluene and MeCN solutions.

Compound	Solvent	λ_{abs}, nm (ε M, 10^4 $M^{-1}cm^{-1}$)	λ_{em}, nm	$\Delta\nu_{St}$ [a], cm^{-1}	Φ_F [c], %	Solid	
						λ_{em}, nm	Φ_F [c], %
2a	Toluene	361 (2.65)	491	7334	75	499	6
	MeCN	356 (2.79), 260 (4.31)	612	11,750	34		
2b	Toluene	361 (0.81), 301 (0.75)	474	6604	3	463	23
	MeCN	350 (4.10)	627	12,622	13		
2c	Toluene	340 (6.25), 330 (6.40), 293 (8.09)	515 *, 467	9994 [b]	<1	421	26
	MeCN	318 (2.05), 291 (2.34), 255 (3.48)	550	13,264	1		
2d	Toluene	367 (2.54)	472	6062	63	512	<1
	MeCN	371 (2.58), 264 (2.52)	592	10,062	31		
2e	Toluene	360 (5.07)	474	6680	3	447	43
	MeCN	350 (1.84)	625	12,571	18		
2f	Toluene	340 (1.53), 329 (1.59)	412	5140	36	425	20
	MeCN	320 (0.91), 292 (1.52), 260 (2.10)	530	12,382	2		
2g	Toluene	371 (2.36)	502	7034	47	501	34
	MeCN	357 (2.39)	640	12,386	24		
2h	Toluene	381 (3.33)	473	5105	94	479	>95
	MeCN	371 (3.12), 269 (4.82)	615	10,694	25		
	Toluene	340 (5.02), 328 (4.97)	517, 434 *	6370 [b]	<1	416	8
	MeCN	318 (4.55)	560	13,589	35		

[a] Stokes shifts were calculated considering the lowest energetic absorption band. [b] Relative to the major emission peak (in bold). [c] Absolute quantum yield in the solid state was measured by the integrated sphere method. * The major emission peak.

Based on the nature of substituent R^1 in the aryl fragment, we have outlined the grouping of [1,2,4]triazolo[4,3-*c*]quinazoline chromophores **2a–i** for the discussion of optical properties: Me-group (**2a–c**), MeO-group (**2d–f**) and CF_3-group (**2e–h**); in each group of compounds, the substituent NR_2 in the biphenyl fragment was NEt_2, NPh_2 or 9*H*-carbazol-9-yl.

The positions of the longest wavelength absorption bands of Et_2N and Ph_2N-containing fluorophores **2a**, **b**, **d**, **e**, **g**, **h** are observed in the UV region: 360–381 nm in toluene and 350–371 nm in MeCN (Table 1). The carbazolyl-derivatives **2c**, **2f** and **2i** are characterized by a blue-shifted (about 20–40 nm in toluene and 30–50 nm in MeCN) absorption band with respect to their diethylamino or diphenylamino counterparts, which is due to the decrease in conjugation length caused by the rigid structure of the carbazolyl unit. Notably, the profile of absorption spectra and positions of maxima in toluene are similar for compounds **2c**, **2f** and **2i** and are not influenced by the nature of substituent R^1 in the aryl fragment (Me, OMe or CF_3), whereas the absorption band of $CF_3C_6H_4$-containing triazoloquinazolines with a diethyl- or diphenyl-amino fragment (**2g** and **2h**, respectively) is bathochromically shifted with respect to the corresponding fluorophores **2a**,**d** and **2b**,**e** (Table 1).

Triazoloquinazolines **2a–i** have fluorescence emission maxima at 412–502 nm in toluene and 530–640 nm in MeCN, with quantum yields up to 94% (Table 1). We considered the influence of substituents R and R^1 on PL characteristics. For example, a red shift in emission maximum was observed in the order **2d**→**2a**→**2g** for diethylamino-containing **2a**, **2d** and **2g** both in toluene and MeCN solution (Supplementary Materials—Figures S20a and S21a), which can be explained by the decrease in electron-donating influence of the CH_3 group compared to MeO (compounds **2d** and **2a**) and by the increase in electron-withdrawing ability of the aryltriazol fragment due to the replacement of CH_3 with CF_3 (compounds **2a** and **2g**). For this set of compounds (**2a**, **2d** and **2g**), we

observed the attenuation of PL emission intensity when going from toluene to MeCN, which was probably caused by the reinforced charge transfer process in the excited state. On the contrary, the emission band of diphenylamino-containing fluorophores **2b**, **2e** and **2h** does not depend on the nature of the aryl unit at the triazole ring (Supplementary Materials–-Figures S20b and S21b). The QY of (trifluoromethyl)phenyl-[1,2,4]triazolo[4,3-*c*]quinazoline **2h** appeared to be the strongest in both solvents (Φ_F = 94% in toluene), which clearly indicates that the trifluorophenyl group plays an essential role in the intense emission for NPh_2-containing derivatives **2b**, **e**, **h**. Fluorophores **2c**, **2f** and **2i** bearing the carbazolyl unit display the emission maxima at 530, 550 and 560 nm in MeCN and show the same dependence of emission wavelength on aryl fragment nature, **2f**→**2c**→**2i** (Supplementary Materials—Figure S21c) as their diethylamino counterparts. It is worth noting that derivatives **2c** ($R^1 = CH_3$) and **2i** ($R^1 = CF_3$) display a bimodal emission band in non-polar solvent (toluene) with a peak in high energy region at 467 and 434 nm, respectively, and at low energy, wavelengths at 515 and 517 nm, whereas compound **2f** ($R^1 = OCH_3$) only shows the high energy band in toluene with a maximum at 412 nm (Supplementary Materials—Figure S20c). The bimodal emission can arise, for example, due to the existence of associates with solvents or aggregates. For the establishment of the exact reasons, additional studies will be conducted.

Along each series of quinazolines (Me-group, MeO-group, and CF_3-group), the carbazolyl-containing fluorophores **2c**, **2f** and **2i** demonstrate emissions in the highest energetic region in MeCN (λ_{max} = 550, 530 and 560 nm, Table 1, Supplementary Materials—Figure S23), which agrees with the low electron-donating ability of the carbazol-9-yl unit. The introduction of NEt_2 or NPh_2 results in the bathochromically shifted emission band (compounds **2a**, **b**, **d**, **e**, **g**, **h**, Supplementary Materials—Figure S23).

The quinazoline-based fluorophores **2a–i** display an emission in the range of 416–512 nm in the solid state (powder), as shown in Table 1. The influence of the electron-donating substituent NR_2 on the emission maximum is similar in each group of compounds; a blue shift is observed in the order NEt_2→NPh_2→carbazol-9-yl. The quantum yield increases in the order NEt_2→NPh_2, and obviously, the steric effect of a non-planar propeller-like configuration of the NPh_2 group prevents molecules from packing via π-π stacking and quenching [22–26]. (Figure 4, Supplementary Materials—Figure S24, Table 1). A very high quantum yield of the compound **2h** (>95%) should be noted.

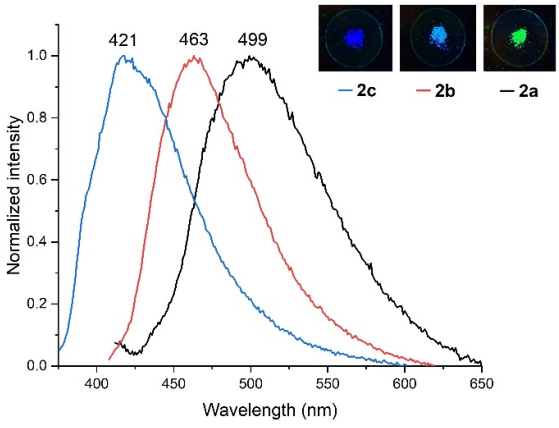

Figure 4. Normalized emission spectra of quinazolinones **2a–c** in solid state; inset: emission of compounds **2a–c** in solid state (powder). Photographs were taken in the dark upon irradiation with a hand-held UV lamp (λ_{em} = 366 nm).

It is interesting to compare the triazolo-containing fluorophores **2a–i** with their 4-morpholinylquinazoline, 4-cyanoquinazoline or quinazolin-4-one counterparts containing the same 4′-amino[1,1′-biphenyl]-4-yl substituents [19,20]. We can conclude that the absorption maximum is not significantly influenced by the nature of the quinazoline core in the set of triazoloquinazoline, 4-morpholinylquinazoline and quinazolin-4-one, whereas

emission bands of compounds **2a**–**i** undergo **a** shift to longer wavelengths in all cases compared to their analogs. For example, compound **2a** demonstrates an emission maximum at 491 nm in toluene and 612 nm in MeCN, whereas 2-(4′-N,N-diethylamino[1,1′-biphenyl]-4-yl)quinazolin-4(3*H*)-one exhibits emissions with λ_{max} = 450 nm in toluene and 535 nm in MeCN [19], and 2-(4′-N,N-diethylamino[1,1′-biphenyl]-4-yl)-4-(morpholin-4-yl)quinazoline has λ_{max} = 443 nm in toluene and 554 nm in MeCN [20]), which confirms the reinforcement of interactions between the donor and acceptor part. Moreover, photophysical characteristics of **2a**–**i** differ considerably from those of cyano derivatives (for example, the absence of a shoulder in the red region of the absorption band, a higher quantum yield both in solution and solid state, etc. [19]). Notably, in the series of triazoloquinazolines **2**, the great bathochromic shift of the emission band is observed when the electron donor NR_2 group changes from NEt_2 to NPh_2 and further to carbazolyl (78–87 nm, Table 1), while for other types of fluorophores, the position of emission maximum is less dependent on NR_2. This is probably because the presence of an aryl fragment in the triazole ring and the formation of a pincer-type structure prevents structure twisting, which leads to a more considerable and dependent correlation between the aryl donor group and emission maximum.

2.3. Effects of Solvent Polarity for **2a**, **d**, **g**, **h**

A study of luminescent properties in solvents of different polarity was performed for compounds **2a**, **2d**, **2g** and **2h** possessing high emission intensity in toluene (Φ_F 47−94%) and MeCN (Φ_F 24−34%) (Supplementary Materials—Tables S5–S8, Figure S25). The values of the emission maxima in different solvents are presented in Table 2. It has been shown that with increasing solvent polarity, the emission maximum of these chromophores underwent a red shift; the positive emission solvatochromism was observed. The most significant changes in the emission spectrum were noticed for compound **2a** (λ_{em} = 451 nm in cyclohexane and λ_{em} = 648 nm in methanol) (Figure 5a).

Table 2. Emission maxima of triazoloquinazolines **2a**, **d**, **g**, **h** in different solvents (excitation at longest wavelength absorption maximum) and parameters Z and $E_T(30)$ for the chosen solvents.

Solvent	Z, kcal/mol	$E_T(30)$, kcal/mol	λ_{em}, nm			
			2a	**2d**	**2g**	**2h**
Methanol	83.6	55.4	648	614	651	624
Acetonitrile	71.3	45.6	614	593	622	614
DMSO	71.1	45.1	632	616	643	624
DCM	64.7	40.7	555	531	565	554
THF	58.8	37.4	553	538	565	546
Toluene	-	33.9	489	478	500	482
Cyclohexane	-	30.9	451	424 *, 452	460	427, 468 *

* The major emission peak.

We observed a rather large difference in the emission maxima upon passing from the least polar to the most polar solvent for other studied compounds **2d**, **g**, **h** as well (Supplementary Materials—Figure S25).

In addition, a mathematical analysis of the solvatochromic behavior was performed for the obtained compounds according to the typical procedure based on the Lippert–Mataga equation [27–29]. The data are presented in Table 3 and Figure 5b. The linearity of the plots was found to confirm the positive solvatochromic effect in all the cases. The obtained values of the difference between the dipole moments of the ground and excited states are in the range of 17.54–22.34 D, and the maximum value of 22.34 D is observed for [1,2,4]triazolo[4,3-*c*]quinazoline **2h** bearing a triphenylamine donor moiety and *p*-(trifluoromethyl)phenyl residue. Notably, the nature of the aryl substituent at the triazole ring has a significant

impact on the Δμ value (the value increases in the order **2d**→**2a**→**2g**). Thus, a pronounced intramolecular charge transfer (ICT) process upon photoexcitation occurs in molecules **2a**, **d**, **g**, **h**.

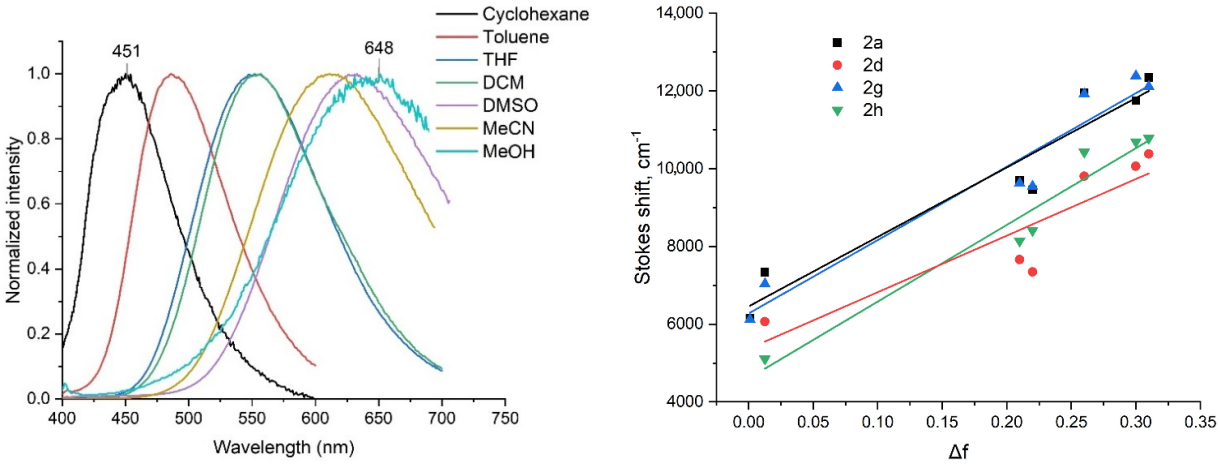

(**a**) (**b**)

Figure 5. (**a**) Fluorescence spectra of compound **2a** in different solvents; (**b**) Lippert–Mataga plot of fluorophores **2a, 2d, 2g**, **2h** in cyclohexane (for **2a**, **2g**), toluene, THF, DCM, DMSO, MeCN and MeOH.

Table 3. Data from Lippert–Mataga plot for quinazolines **2a**, **2d, 2g** and **2h**.

Comp.	Slopes	R^2	*a* [a], Å	Δμ, D
2a	17,874	0.93	4.71	19.26
2d	14,543	0.80	4.74	17.54
2g	18,893	0.94	4.78	20.24
2h	19,747	0.95	5.03	22.34

[a] *a*—Onsager radius, calculated following the literature [30].

We analyzed the dependence of the emission maxima bathochromic shift on the quantitative polarity criteria of the solvents used, in particular, according to Kosower [31,32] and Dimroth/Reichardt mathematical models [33,34]. In most cases, the longest wavelength emission maximum is observed for methanol, and the shortest value corresponds to cyclohexane. In general, the obtained values of the emission maxima correspond to the criteria for the polarity of solvents. Deviations occur for compound **2d** bearing the 4-methoxyphenyl substituent at position 3; in this case, the longest wavelength maximum is characteristic of DMSO, but a very small difference between the values of emission maxima in DMSO and methanol was noticed (2 nm). However, in all cases, the emission maximum in DMSO corresponds with the longer wavelength than in the case of acetonitrile (the difference is 3–24 nm), even though the difference between their polarity criteria is minimal.

The comparison of the obtained characteristics of **2a**, **2d**, **2g**, **2h** with the ones of some early published (hetero)aryl-substituted quinazolines allowed us to conclude that the condensation of an additional triazole ring led to a significant increase in Δμ values. Thus, in the case of 2-(hetero)aryl-4-(4-aminophenyl)quinazolines [35], the obtained Δμ values were 15.93–18.26 D. At the same time, it should be noted that the introduction of the aromatic substituent, instead of the heteroaromatic one at position C(2) of quinazoline, led to an increase in Δμ values. For the group **2** compounds bearing aromatic substituents at the analogs position C(5), developed in the current work, the larger Δμ values (up to 22.34 D) were determined.

It should be noted that the revealed positive solvatochromism phenomenon opens up a number of prospects for the application of novel group **2** compounds as potential candidates for designing fluorescent probes and as components for fluorescent and non-linear optical materials [36].

2.4. Absorption and Fluorescence Behavior of Compounds **2b**, **2e** *and* **2h** *in MeCN/water Mixture*

Frequently, triphenylamino (TPA)-containing compounds demonstrate enhancement of emission intensity (AIEE) or inducement of emission (AIE) upon aggregation [22–26]. The X-ray data (Figure 3) obtained for quinazoline derivative **2e** bearing the TPA unit confirms the non-planar structure of the studied molecules. We considered the absorption and emission behavior of the compounds **2b**, **2e** and **2h** upon the addition of water based on the above-mentioned analysis on passing from MeCN solution to solid state. For this aim, we registered absorption and emission spectra of fluorophores **2b**, **2e** and **2h** (at $c = 2 \times 10^{-6}$ M) in pure MeCN and in MeCN/water mixtures with various water fractions (f_w); see Figure 6 and Supplementary Materials Figures S26–S28. Figure 6 demonstrates changes in fluorescence spectra of **2e** in MeCN and MeCN/water mixtures (a) and a plot of relative PL intensity (I/I_0) and wavelength at emission maxima of **2e** versus the composition of the water fraction (b) at room temperature. After the first portion of H_2O, we observe a dramatic attenuation of emission intensity and red shift of the band. After 70vol% of water, the band shifts toward the blue region with the regeneration of intensity, and the strongest emission was measured at 80vol% of water. Other compounds (**2b** and **2h**) demonstrate similar changes in emission spectra. These changes are typical for luminogens with a rotatable donor–acceptor (D–A) structure, which possess two excited states: a locally excited (LE) state and a twisted intramolecular charge transfer (TICT) state. When the polarity of media increases (upon the addition of water), the TICT state becomes dominant, leading to red-shifted emission and the quenching of intensity. Further addition of water most likely led to the formation of aggregates that are less polar than initial single molecules, and this phenomenon resulted in blue-shifted emission. The intensity restores due to the restriction of rotation in the TPA group and phenylene moieties and the reducing non-radiative transitions. Thus, compounds **2b**, **2e** and **2h** exhibited aggregation-induced emission enhancement to some extent.

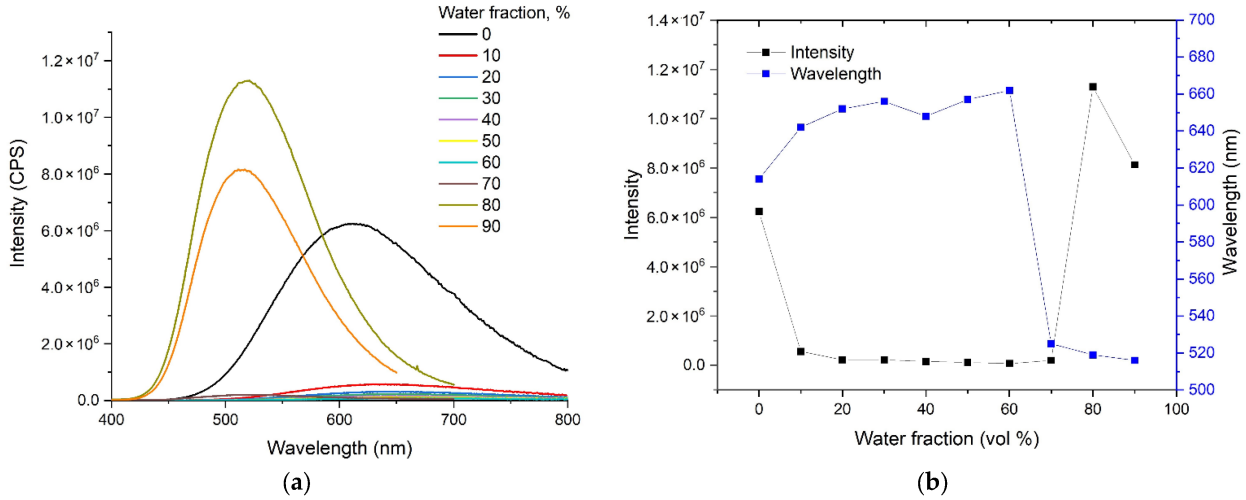

Figure 6. (**a**) The fluorescence spectra of **2e** in MeCN and MeCN/water mixtures with different water fractions (f_w); (**b**) a plot of relative PL intensity (I/I_0) and wavelength at emission maxima of **2e** versus the composition of the water fraction (vol %). T = 23 °C.

As for UV/vis spectra for quinazolines **2b**, **2e** and **2h**, we observed that the absorption band registered at 90%, 80% and 70% water fraction, respectively, was bathochromically shifted compared to pure MeCN, which can be ascribed to the formation of J-type aggre-

gates with head-to-tail arrangement (Supplementary Materials—Figures S26c, S27a and S28c) [37–39].

Additionally, we carried out a time-resolved fluorescence study of quinazolines **2b**, **2e** and **2h** in a pure MeCN and MeCN/water mixture (Supplementary Materials—Figures S26d, S27b, S28d and S29–S31); fluorescence lifetimes were estimated to complete the photophysical characterization of the fluorophores. The lifetime of compound **2b** is fitted with bi-exponential decay with an average lifetime of 2.38 ns, whereas compounds **2e** and **2h** are characterized by mono-exponential decay curves and lifetimes of 3.17 and 2.46 ns, respectively (Supplementary Materials—Table S9). Fluorescence decay profiles of aggregated quinazolines at the highest emission intensity are fitted with three-exponential decay. Notably, the highest fractional contribution is different for all three compounds. While for *p*-tolyl-containing fluorophores, the highest fractional contribution at τ_2 = 2.96 ns was detected, for their methoxy counterparts, it was observed at τ_1 = 7.76 ns. On the contrary, the introduction of an electron-withdrawing CF_3 group is reflected in the increased contribution of shorter time, τ_3 = 1.36 ns (Supplementary Materials—Table S9). Generally, the average lifetimes of compounds **2b** and **2e** increase (for **2e** more considerable) and were found to be 3.57 and 7.72 ns, respectively, while τ_{av} of **2h** decreases by 1.36 ns in the MeCN/water mixture with respect to pure MeCN.

2.5. Absorption and Fluorescence Behavior of Compounds **2e** *and* **2h** *in Acidic Media*

Because triazoloquinazolines **2a–i** bear nitrogen atoms that can bind with proton, we intend to investigate the absorption and fluorescence sensory properties of some samples toward acid. For the experiment, we have chosen quinazoline **2e**, containing an electron-donating *p*-methoxy substituent that reinforces the basicity of the triazole ring. On the contrary, the *p*-(trifluoromethyl)phenyl residue (compound **2h**) attenuates the basicity of the nitrogen atoms, and this derivative possesses the strongest fluorescence intensity in pure toluene, as was mentioned above. Nevertheless, both compounds demonstrate similar behavior upon the addition of TFA to toluene solution under UV light and daylight by the naked eye (Supplementary Materials—Figure S32). The color of the solution turns from colorless to yellow (for **2e**) or orange (for **2h**) under daylight. The emission changes from dark blue or blue to orange. Both compounds demonstrate the reversibility of absorption and emission upon the consecutive addition of TFA and TEA. The titration experiment shows that the longwave absorption peak is red-shifted (from 360 to 372 nm in the case of **2e** and from 381 to 389 nm for **2h**), forming a tail-shaped band in the region of 380–440 nm and 420–460 nm, respectively, upon the addition of an excess of TFA (Figures 7a and S33a). The emission behaviour of fluorophore **2e** is more interesting in acidic media, and the changes are observed at a lower equivalent than that of compound **2h** (Figure 7). After the first portion of acid, we observe the bathochromic shift of the emission band and gradual enhancement of emission intensity. When 200 equivalents of TFA were added, the fluorescent intensity reached the highest value, and the peak at 528 nm appeared. The subsequent addition of acid resulted in the attenuation of intensity and further red shift by 540 nm at 500 eq of acid.

The emission band of compound **2h** shifts to the red region with a gradual attenuation of intensity (Supplementary Materials—Figure S33b). The appearance of red-shifted absorption and emission bands in both cases can be associated with the reinforcement of electron-withdrawing strength of the triazoloquinazoline core due to the protonation of the nitrogen atom resulting in a stronger interaction of acceptor and donor units compared to neutral molecules. Therefore, significant acidochromic behavior was observed for compounds **2e**, **h**. We can suppose that changes in emission intensity (enhancement or quenching) of compounds **2e** and **2h** might be due to intramolecular photo-induced electron transfer (PET) or photo-induced proton transfer [40], and the elucidation of the exact interaction mechanism of the analyte with TFA is under progress.

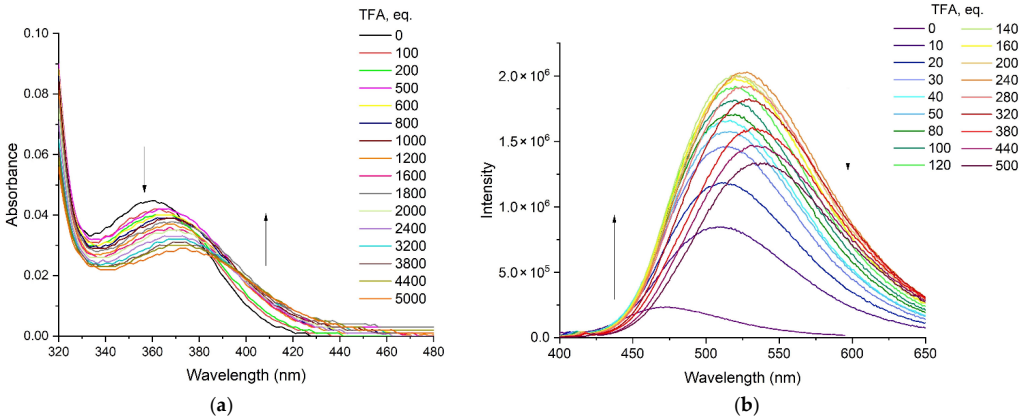

Figure 7. Changes in absorption (**a**) and emission (**b**) spectra of the toluene solution (c = 10^{-5} M) of **2e** upon gradual addition of TFA.

2.6. Quantum-Chemical Calculations

Furthermore, we performed the DFT calculations of quinazolines **2a–i** in the gas phase at the B3LYP/6–311 G* level using the Orca 4.0.1 software package [41–45] and conducted the chemical optimization on their energy levels based on DFT/B3LYP/6-31G (d,p) using Gaussian 09. The distribution plots of the HOMOs and LUMOs, as well as energy levels and energy gaps, are presented in Figure 7. Notably, the distribution plots of the HOMOs of diethylamino-containing fluorophores **2a** and **2d** are distinctly different from other counterparts. For molecules **2a** and **2d**, the HOMO electrons are mainly distributed on the 3-aryltriazolo[4,3-*c*]quinazoline fragment, which shows the considerable influence of the electronic nature of the substituent at the para-position of the phenylene ring. For compounds **2b**, **c**, **e–i,** the HOMO electrons are mainly located at the electron-donating arylamino unit, with the phenylene ring less involved in carbazolyl-derivatives **2c**, **2f** and **2i**, which confirms weaker π-conjugation of these molecules due to twisting of the rigid carbazolyl fragment and is consistent with photophysical data. The LUMOs plots are similar for all the compounds **2a–i** (Figure 8); electrons are distributed on the 5-(biphenyl-4-yl)-[1,2,4]triazolo[4,3-*c*]quinazoline framework. In general, the value of the energy gap decreases in each set of compounds bearing the same aminoaryl group with an increase in electron-withdrawing ability of the aryl substituent at position C(3). It is worth noting that energy levels of triazolo[4,3-*c*]quinazolines are closer to that of previously described 2-biphenylquinazolin-4(3*H*)-one derivatives than to ones for 4-morpholinyl or 4-cyano counterparts [19,20].

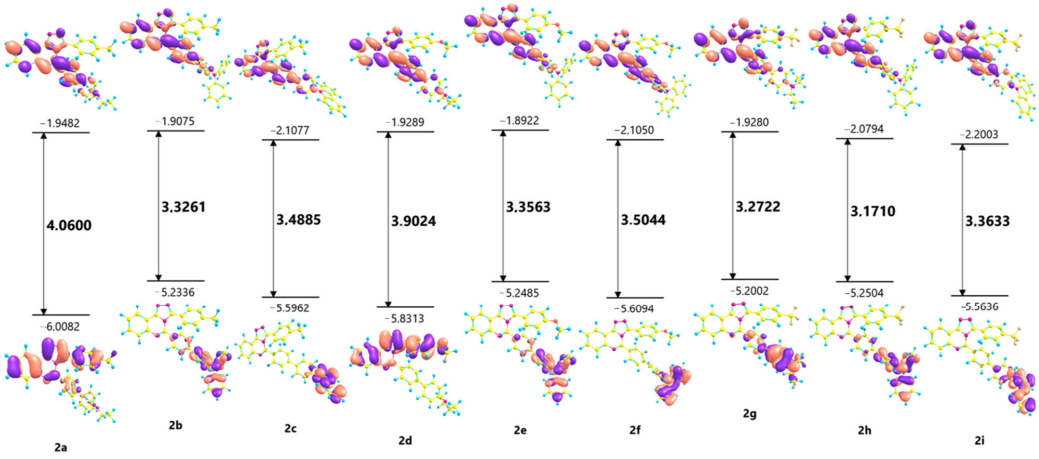

Figure 8. Optimized molecular structures and molecular orbitals of the HOMO and LUMO levels, energy gaps and electron cloud distribution of triazoloquinazolines **2a–i**.

Obviously, different electronic distributions on HOMO and LUMO levels for compounds **2a–i** confirm the intense intramolecular charge transfer (ICT) process, which is consistent with solvatochromic studies for the considered compounds.

3. Experimental Methods

3.1. General Information

Unless otherwise indicated, all common reagents and solvents were used from commercial suppliers without further purification. Melting points were determined on Boetius-combined heating stages. ^{1}H NMR and ^{13}C NMR spectra were recorded at room temperature at 400 and 100 MHz, respectively, on a Bruker DRX-400 spectrometer (Bruker, Rheinstetten, Germany). Hydrogen chemical shifts were referenced to the hydrogen resonance of the corresponding solvent (DMSO-d_6, δ = 2.50 ppm or $CDCl_3$, δ = 7.26 ppm). Carbon chemical shifts were referenced to the carbon resonances of the solvent (DMSO-d_6, δ = 39.5 ppm $CDCl_3$, δ = 77.2 ppm). Peaks are labelled as singlet (s), doublet (d), triplet (t), quartet (q) and multiplet (m). Mass spectra were recorded on the SHIMADZU GCMS-QP2010 Ultra instrument (Shimadzu, Duisburg, Germany) with the electron ionization (EI) of the sample. Microanalyses (C, H, N) were performed using the Perkin–Elmer 2400 elemental analyser (Perkin–Elmer, Waltham, MA, USA).

3.2. Photophysical Characterization

UV/vis absorption spectra were recorded on the Shimadzu UV-1800 Spectrophotometer (Shimadzu, Duisburg, Germany) using quartz cells with 1 cm path length at room temperature. Emission spectra were measured on the Horiba FluoroMax-4 (HORIBA Ltd., Kyoto, Japan) at room temperature using quartz cells with 1 cm path length. The fluorescence quantum yield of the target compounds in solution and solid state were measured by using the Integrating Sphere Quanta-φ of the Horiba-Fluoromax-4. Time-resolved fluorescence measurements were carried out using time-correlated single-photon counting (TCSPC) with a nanosecond LED (λ = 370 nm).

3.3. Crystallography

The single crystal (light yellow block of 0.38 × 0.24 × 0.20) of compound **2a** and the single crystal (yellow block of 0.43 × 0.35 × 0.28) of compound **2e** were used for X-ray analysis. Structural studies were performed using equipment available in the Collaborative Access Center "Testing Center of Nanotechnology and Advanced Materials" at the Mikheev Institute of Metal Physics, Ural Branch, Russian Academy of Sciences. The X-ray diffraction analysis was performed at room temperature on Rigaku OD XtaLAB Synergy-S diffractometer (Rigaku Oxford Diffraction, Tokyo, Japan). Using Olex2 [46], the structure was solved with the ShelXT structure solution program using Intrinsic Phasing and refined with the ShelXL [47] refinement package using full-matrix least squares minimization. All non-hydrogen atoms were refined in an anisotropic approximation; the H-atoms were placed in the calculated positions and refined isotropically in the "rider" model. Crystal data for **2a** $C_{32}H_{29}N_5$, M = 483.60, monoclinic, a = 12.64210(10) Å, b = 11.96340(10) Å, c = 17.2021(2) Å, α = 90°, β = 103.4260(10)°, γ = 90°, V = 2530.59(4) Å3, space group $P2_1/c$, Z = 4, μ(Mo Kα) = 0.077 mm^{-1}. On the angles 4.75 < 2Θ < 52.744°, 5154 reflections were measured, 3812 unique (R_{int} = 0.1062), which were used in all calculations. Goodness to fit at F^2 1.151; the final R_1 = 0.1290, wR_2 = 0.2736 (all data) and R_1 = 0.0770, wR_2 = 0.2018 (I > 2σ(I)). Largest diff. peak and hole 0.21 and –0.23 $\bar{e}Å^{-3}$.

Crystal data for **2e** $C_{40}H_{29}N_5$, M = 595.68, orthorhombic, a = 76.1636(13) Å, b = 17.3954(3) Å, c = 9.57464(12) Å, α = 90°, β = 90°, γ = 90°, V = 12685.4(4) Å3, space group Fdd2, Z = 16, μ(Mo Kα) = 0.077 mm^{-1}. On the angles 2.14 < 2Θ < 29.48°, 8203 reflections were measured, 3575 unique (R_{int} = 0.2091), which were used in all calculations. Goodness to fit at F^2 0.975; the final R_1 = 0.1695, wR_2 = 0.2165 (all data) and R_1 = 0.0605, wR_2 = 0.1491 (I > 2σ(I)). Largest diff. peak and hole 0.18 and –0.20 $\bar{e}Å^{-3}$.

The results of the X-ray diffraction analysis for compounds **2a** and **2e** were deposited with the Cambridge Crystallographic Data Centre (CCDC 2218321 for **2a** and CCDC 2217179 for **2e**). The data are free and can be accessed at www.ccdc.cam.ac.uk (accessed on 8 November 2022 for **2a** and 3 November 2022 for **2e**).

3.4. General Procedures of Suzuki Cross-Coupling

To the mixture of bromo derivative **1a–c** (0.65 mmol) in toluene (10 mL), the corresponding boronic acid or boronic acid pinacol ester (0.70 mmol), $PdCl_2(PPh_3)_2$ (46 mg, 65 mol), PPh_3 (34 mg, 130 μmol), saturated solution of K_2CO_3 (3.7 mL) and EtOH (3.7 mL) were added. The mixture was stirred at 85 °C for 7–20 h in argon atmosphere in a round-bottom pressure flask. The reaction mixture was cooled. After cooling, the organic layer was separated, washed sequentially with EtOAc (10 mL) and H_2O (10 mL), dried over Na_2SO_4, and the organic layer was evaporated at reduced pressure. The product was isolated by gradient column chromatography on silica gel, a mixture of hexane and ethyl acetate was used as an eluent.

5-(4′-Diethylamino-[1,1′]-biphenyl-4-yl)-3-(*p*-tolyl)-[1,2,4]triazolo[4,3-*c*]quinazoline (2a). Yellow powder, yield 25%; mp 195–197 °C; ^{1}H NMR ($CDCl_3$, 400 MHz) δ 1.21 (6H, t, ^3J = 7.2 Hz, $2CH_3$), 2.24 (3H, s, CH_3), 3.42 (4H, q, ^3J = 7.2 Hz, $2CH_2$), 6.74 (2H, d, ^3J = 8.3 Hz, $2CH_{phenylene}$), 6.91 (2H, d, ^3J = 7.8 Hz, $2CH_{phenylene}$), 7.08 (2H, d, ^3J = 7.8 Hz, $2CH_{phenylene}$), 7.23–7.30 (4H, m, $4CH_{phenylene}$), 7.36 (2H, d, ^3J = 8.3 Hz, $2CH_{phenylene}$), 7.73 (1H, m, CH_{quinaz}), 7.81 (1H, m, CH_{quinaz}), 8.04 (1H, d, ^3J = 8.1 Hz, m, CH_{quinaz}), 8.76 (1H, d, ^3J = 7.8 Hz, m, CH_{quinaz}); ^{13}C NMR ($CDCl_3$, 100 MHz) δ 12.7 ($2CH_3$), 21.4 (CH_3), 44.5 ($2CH_2$), 111.9, 116.5, 123.6, 125.0, 125.3, 126.7, 128.1, 128.4, 128.6, 129.1, 129.3, 129.5, 129.7, 131.8, 139.5, 141.3, 143.7, 146.1, 147.8, 149.3, 150.0; EIMS *m*/*z* 484 $[M + 1]^+$ (26), 483 $[M]^+$ (69), 469 (37), 468 (100) 234 (21); anal. C 79.47, H 14.48, N 8.94%, calcd for $C_{32}H_{29}N_5$ (483.62) C 79.40, H 6.12, N 14.11%.

5-(4′-Diphenylamino-[1,1′]-biphenyl-4-yl)-3-(*p*-tolyl)-[1,2,4]triazolo[4,3-*c*]quinazoline (2b). Beige powder, yield 48%; mp 205–207 °C; ^{1}H NMR ($CDCl_3$, 400 MHz) δ 2.24 (3H, s, CH_3), 6.93 (2H, d, ^3J = 7.7 Hz, $2CH_{phenylene}$), 7.09–7.18 (10H, m), 7.28–7.36 (10H, m), 7.76 (1H, m, CH_{quinaz}), 7.84 (1H, m, CH_{quinaz}), 8.06 (1H, d, ^3J = 8.0 Hz, CH_{quinaz}), 8.78 (1H, d, ^3J = 7.9 Hz, CH_{quinaz}); ^{13}C NMR (100 MHz, $CDCl_3$) δ 21.4 (CH_3), 116.6, 123.5, 123.6, 124.9, 125.0, 126.0, 127.9, 128.4, 128.6, 129.3, 129.4, 129.5, 129.7, 130.6, 131.9, 133.7, 139.5, 141.3, 143.1, 145.8, 147.6, 148.1, 149.2, 150.0; EIMS *m*/*z* 580 $[M + 1]^+$ (44), 579 $[M]^+$ (100), 578 (11), 289 (17); anal. C 82.88, H 5.04, N 12.08%, calcd for $C_{40}H_{29}N_5$ (579.71) C 82.88, H 5.01, N 12.00%.

5-(4′-(9*H*-Carbazol-9-yl)-[1,1′]-biphenyl-4-yl)-3-(*p*-tolyl)-[1,2,4]triazolo[4,3-*c*]quinazoline (2c). After cooling, the reaction mixture was filtered and washed with hexane. Colourless powder, yield 65%; mp 236–238 °C; ^{1}H NMR ($CDCl_3$, 400 MHz) δ 2.27 (3H, s, CH_3), 6.97 (2H, d, ^3J = 7.8 Hz, $2CH_{phenylene}$), 7.12 (2H, d, ^3J = 7.8 Hz, $2CH_{phenylene}$), 7.32 (2H, m, $2CH_{carbaz}$), 7.42–7.50 (10H, m), 7.69 (4H, m), 7.77 (1H, m, CH_{quinaz}), 7.84 (1H, m, CH_{quinaz}), 8.07 (1H, d, ^3J = 8.1 Hz, CH_{quinaz}), 8.17 (2H, d, ^3J = 7.8 Hz, $2CH_{carbaz}$), 8.80 (1H, d, ^3J = 7.8 Hz, CH_{quinaz}); ^{13}C NMR (100 MHz, $CDCl_3$) δ 21.5 (CH_3), 109.9, 116.6, 120.3, 120.6, 123.6, 123.7, 125.0, 126.2, 126.6, 127.6, 128.5, 128.6, 128.7, 129.4, 129.6, 129.8, 131.6, 132.0, 137.8, 139.2, 139.6, 140.9, 141.2, 142.6, 145.6, 149.1, 150.0; EIMS *m*/*z* 579 $[M + 2]^+$ (10), 578 $[M + 1]^+$ (45), 577 $[M]^+$ (100), 344 (11), 288 (24), 241 (11), 102 (17), 88 (12), 77 (14), 57 (10), 44 (39), 43 (28), 41 (13); anal. C 83.17, H 4.71, N 12.12%, calcd for $C_{40}H_{27}N_5$ (577.69.) C 83.12, H 4.11, N 12.15%.

5-(4′-Diethylamino-[1,1′]-biphenyl-4-yl)-3-(4-methoxyphenyl)-[1,2,4]triazolo[4,3-*c*] quinazoline (2d). After cooling, the reaction mixture was filtered and washed with hexane. The product was additionally recrystallized from CH_2Cl_2/hexane mixture. Yellow powder, yield 29%; mp 189–191 °C; ^{1}H NMR ($CDCl_3$, 400 MHz) δ 1.21 (6H, t, ^3J = 7.0 Hz, $2CH_3$), 3.41 (4H, q, ^3J = 7.0 Hz, $2CH_2$), 3.63 (3H, s, OCH_3), 6.62 (2H, d, ^3J = 8.5 Hz, $2CH_{phenylene}$), 6.74 (2H, d, ^3J = 8.5 Hz, $2CH_{phenylene}$), 7.11 (2H, d, ^3J = 8.1 Hz, $2CH_{phenylene}$), 7.8 (4H,

m, 4$CH_{phenylene}$), 7.37 (2H, d, ^3J = 8.1 Hz, 2$CH_{phenylene}$), 7.73 (1H, m, CH_{quinaz}), 7.78 (1H, m, CH_{quinaz}), 8.03 (1H, d, ^3J = 7.3, CH_{quinaz}), 8.75 (1H, d, ^3J = 7.2, CH_{quinaz}); ^{13}C NMR (100 MHz, $CDCl_3$) 12.8 (2CH_3), 44.8 (2CH_2), 55.5 (OCH_3), 112.0, 113.4, 116.6, 120.2, 123.5, 125.3, 126.7, 128.1, 128.4, 129.1, 129.4, 129.5, 131.2, 131.8, 141.3, 143.6, 146.1, 147.8, 149.1, 150.0, 160.6; EIMS *m*/*z* 500 $[M + 1]^+$ (32), 499 $[M]^+$ (85), 485 (34), 484 (100), 242 (47), 228 (11), 207 (10); anal. C 76.93, H 5.85, N 14.02%, calcd for $C_{32}H_{29}N_5O$ (499.62) C 76.90, H 5.87, N 14.10%.

5-(4′-Diphenylamino-[1,1′]-biphenyl-4-yl)-3-(4-methoxyphenyl)-[1,2,4]triazolo[4,3-*c*] quinazoline (2e). The product was additionally recrystallized from CH_2Cl_2/hexane mixture. Pale yellow powder, yield 51%; mp 242–244 °C; ^{1}H NMR ($CDCl_3$, 400 MHz) δ 3.64 (3H, s, OCH_3), 6.62 (2H, d, ^3J = 6.6 Hz, 2$CH_{phenylene}$), 7.02–7.16 (10H, m), 7.26–7.36 (10H, m), 7.74 (1H, m, CH_{quinaz}), 7.82 (1H, m, CH_{quinaz}), 8.04 (1H, d, ^3J = 8.2 Hz, CH_{quinaz}), 8.76 (1H, d, ^3J = 7.7 Hz, CH_{quinaz}); ^{13}C NMR (100 MHz, $CDCl_3$) δ 55.4 (OCH_3), 113.5, 116.6, 120.2, 123.5, 123.6, 124.8, 126.0, 127.9, 128.4, 129.3, 129.5, 129.5, 130.6, 131.2, 131.9, 133.7, 141.2, 143.0, 145.8, 147.6, 148.1, 149.0, 149.9, 160.6; EIMS *m*/*z* 597 $[M + 2]^+$ (10), 596 $[M + 1]^+$ (45), 595 $[M]^+$ (100), 298 (20); anal. C 80.65, H 4.91, N 11.76%, calcd for $C_{40}H_{29}N_5O$ (595.71) C 89.90, H 4.77, N 11.44%.

5-(4′-(9*H*-Carbazol-9-yl)-[1,1′]-biphenyl-4-yl)-3-(4-methoxyphenyl)-[1,2,4]triazolo quinazoline (2f). After cooling, the reaction mixture was filtered and washed with hexane. The product was additionally recrystallized from DMSO. Grey powder, yield 38%; mp 277−279 °C; ^{1}H NMR (DMSO-d_6, 400 MHz) δ 3.64 (3H, s, OCH_3), 6.68 (2H, d, ^3J = 8.5 Hz, 2$CH_{phenylene}$), 7.17 (2H, d, ^3J = 8.6 Hz, 2$CH_{phenylene}$), 7.31 (2H, m, 2CH_{carbaz}), 7.42 – 7.50 (m, 8H), 7.74 (2H, d, ^3J = 8.2 Hz, 2$CH_{phenylene}$), 7.80–7.86 (3H, m), 7.91 (1H, m, CH_{quinaz}), 8.04 (1H, d, ^3J = 8.0 Hz, CH_{quinaz}), 8.24 (2H, m, 2CH_{carbaz}), 8.63 (1H, d, ^3J = 7.8 Hz, CH_{quinaz}); ^{13}C NMR (100 MHz, $CDCl_3$) δ 55.4(OCH_3), 109.9, 113.5, 116.6, 120.2, 120.3, 120.6, 123.6, 123.7, 126.2, 126.6, 127.6, 128.5, 128.7, 129.4, 129.7, 131.3, 131.6, 131.9, 137.8, 139.2, 140.9, 141.2, 142.5, 145.6, 148.9, 149.9, 160.6; EIMS *m/z* 594 $[M + 1]^+$ (44), 593 $[M]^+$ (100), 344 (16), 319 (14), 296 (30), 241 (17), 223 (12), 166 (17), 140 (12), 102 (12), 88 (17), 55 (16), 44 (32), 43 (38), 42 (19), 41 (11), 39 (17); anal. C 80.68, H 4.33, N 11.97%, calcd for $C_{40}H_{29}N_5O$ (593.69) C 80.92, H 4.58, N 11.80%.

5-(4′-Diethylamino-[1,1′]-biphenyl-4-yl)-3-(4-(trifluoromethyl)phenyl)-[1,2,4]triazolo quinazoline (2g). The product was additionally recrystallized from CH_2Cl_2/hexane mixture. Yellow powder, yield 46%; mp 202–204 °C; ^{1}H NMR ($CDCl_3$, 400 MHz) δ 1.21 (6H, t, ^3J = 7.1 Hz, 2CH_3), 3.41 (4H, q, ^3J = 7.1 Hz, 2CH_2), 6.72 (2H, d, ^3J = 7.4 Hz, 2$CH_{phenylene}$), 7.30–7.42 (10H, m), 7.76 (1H, m, CH_{quinaz}), 7.84 (1H, m, CH_{quinaz}), 8.06 (1H, d, ^3J = 8.1 Hz, CH_{quinaz}), 8.77 (1H, d, ^3J = 7.9 Hz, CH_{quinaz}); ^{19}F NMR ($CDCl_3$, 376 MHz) δ – 62.73 (3F, s, CF_3); ^{13}C NMR (100 MHz, $CDCl_3$) δ 12.7 (2C, 2CH_3), 44.5 (2C, 2CH_2), 111.9, 116.3, 123.6 (1C, q, $^1J_{CF}$ = 272.5 Hz, CF_3) 123.7, 124.7 (2C, q, $^3J_{CF}$ = 3.7 Hz, $C_6H_5CF_3$), 125.6, 126.2, 128.1, 128.3, 128.5, 128.9, 129.2, 129.3, 129.4, 130.0, 130.2, 131.2, 131.5, 131.7, 132.2, 141.4, 144.5, 145.5, 147.9, 148.0, 150.6; EIMS *m*/*z* 538 $[M + 1]^+$ (30), 537 $[M]^+$ (78), 523 (36), 522 (100), 465 (12), 390 (11), 261 (25), 176 (10), 161 (12), 146 (12), 49 (12); anal. C 71.50, H 4.88, N 13.03%, calcd for $C_{32}H_{26}F_3N_5$ (537.59) C 71.40, H 4.98, N 13.00%.

5-(4′-Diphenylamino-[1,1′]-biphenyl-4-yl)-3-(4-(trifluoromethyl)phenyl)-[1,2,4]triazolo quinazoline (2h). Yellow powder, yield 64%; mp 197–199 °C; ^{1}H NMR ($CDCl_3$, 400 MHz) δ 7.08 (2H, m, 2H_{phenyl}), 7.14–7.21 (6H, m, 4H_{phenyl}, 2$H_{phenylene}$), 7.27–7.33 (4H, m, 4 CH_{phenyl}), 7.61 (2H, d, ^3J = 6.5 Hz, 2$CH_{phenylene}$), 7.76 (1H, m, CH_{quinaz}), 7.80 (2H, d, *J* = 8.1 Hz, 2$H_{phenylene}$), 7.85 (2H, d, ^3J = 8.0 Hz, 2$H_{phenylene}$), 7.90 (1H, m, CH_{quinaz}), 8.17 (1H, d, ^3J = 8.1 Hz, CH_{quinaz}), 8.56 (d, 2H, ^3J = 8.0 Hz, 2$H_{phenylene}$), 8.67 (1H, d, ^3J = 7.9 Hz, CH_{quinaz}), 8.75 (2H, d, ^3J = 8.1 Hz, 2$H_{phenylene}$); ^{19}F NMR ($CDCl_3$, 376 MHz) δ – 62.73 (3F, s, CF_3); ^{13}C NMR (100 MHz, $CDCl_3$) δ 117.4, 123.5, 123.6, 123.9, 124.3 (1C, q, $^1J_{CF}$ = 271.7 Hz, CF_3), 124.9, 125.8, 125.9, 126.6, 128.1 (2C, q, $^3J_{CF}$ = 3.7 Hz, $C_6H_5CF_3$), 128.5, 129.0, 129.5, 130.0, 131.1, 132.1, 132.4, 133.6, 133.9, 143.2, 144.0, 146.3, 147.7, 148.2, 153.3, 162.8; EIMS *m*/*z* 635 $[M + 2]^+$ (14), 634 $[M + 1]^+$ (55), 633 $[M]^+$ (100), 318 (10), 317 (34), 231 (14), 218 (13), 167

(21), 166 (15), 77 (19); anal. C 75.82, H 4.14, N 11.05%, calcd for $C_{40}H_{26}F_3N_5$ (633.68) C 75.72, H 4.18, N 10.98%.

5-(4′-(9*H*-Carbazol-9-yl)-[1,1′]-biphenyl-4-yl)-3-(4-(trifluoromethyl)phenyl)-[1,2,4]triazolo[4,3-*c*]quinazoline (2i). After cooling, the reaction mixture was filtered and washed with hexane. Grey powder, yield 50%; mp 305–307 °C; ^{1}H NMR ($CDCl_3$, 400 MHz) δ 7.32 (2H, m, $2CH_{carbaz}$), 7.39–7.49 (12H, m), 7.69 (4H, m), 7.81 (1H, m, CH_{quinaz}), 7.88 (1H, t, CH_{quinaz}), 8.10 (1H, d, ^3J = 8.2 Hz, CH_{quinaz}), 8.17 (2H, d, ^3J = 7.9 Hz, $2CH_{carbaz}$), 8.81 (1H, d, ^3J = 7.9 Hz, CH_{quinaz}); ^{19}F NMR ($CDCl_3$, 376 MHz) δ – 61.29 (3F, s, CF_3); EIMS *m*/*z* 633 $[M + 2]^+$ (10), 632 $[M + 1]^+$ (45), 631 $[M]^+$ (100), 344 (16), 342 (11), 315 (34), 264 (12), 241 (19), 230 (24), 201 (11); anal. C 76.06, H 3.83, N 11.09%, calcd for $C_{40}H_{24}F_3N_5$ (631.66) C 76.04, H 3.80, N 11.15%.

4. Conclusions

Nine push-pull molecules based on [1,2,4]triazolo[4,3-*c*]quinazolines were designed and synthesized by cross-coupling reactions. The structure of target compounds, namely the arrangement of the triazole ring, has been confirmed by means of the X-ray data method. The triazoloquinazolines **2** were shown to emit in solution and solid state. Photophysical properties (absorption, emission and QY) are influenced by the nature of arylamino residue, 3-aryltriazole fragment, as well as solvent polarity. Variations of structure and media can be used for the fine-tuning of characteristics that are necessary for practical application. Moreover, fluorophores display solvatochromic behavior and their emission maxima show bathochromic shifts with an increase in solvent polarity. Furthermore, changes in absorption and emission spectra upon the addition of water to MeCN solution, attributed to the aggregation process, have been shown. The twisted structure of fluorophores revealed by X-ray analysis can inhibit intermolecular π-π stacking interactions, thus favoring the strong solid-state emission and active aggregate forms. Additionally, triazoloquinazolines display reversible changes in color and optical properties upon the treatment with TFA and have the potential application as sensors. In general, this type of fluorophore represents a promising group of compounds for different applications and further investigation.

Supplementary Materials: The following supporting information can be downloaded at: https://www.mdpi.com/article/10.3390/molecules28041937/s1, Figures S1–S9: NMR and mass spectra of 3-aryl-5-aminobiphenyl substituted [1,2,4]triazolo[4,3-*c*]quinazolines **2a**–**i**; Tables S1–S4: Selected bond lengths and angles of compounds **2a**, **2e**; Figure S10: Planarity of compounds **2a** and **2e**; Figures S11–S23: Absorption and emission spectra of fluorophores **2a**–**i** in toluene and MeCN; Figure S24: Emission spectra of fluorophores **2a**–**i** in solid state; Tables S5–S8: Orientation polarizability for solvents (Δf), absorption and emission maxima (λ_{abs}, λ_{em}, nm) and Stokes shift (nm, cm^{-1}) of compounds **2a**, **d**, **g**, **h** in different solvents; Figure S25: Fluorescence spectra of compound **2d** (a), **2g** (b), **2h** (c) in different solvents; Figures S26–S28: Absorption and emission behavior of compounds **2b**, **e**, **h** in MeCN/water mixture; Table S9, Figures S29–S31: Detailed data of the fluorescence lifetime measurements of **2b**, **2e**, **2h**. Figures S32 and S33: Absorption and fluorescence behavior of compounds **2e** and **2h** in acidic media.

Author Contributions: Conceptualization, V.N.C.; methodology, A.E.K.; investigation, A.E.K., E.S.S., G.A.K., V.S.G. and P.A.S.; writing—original draft preparation, T.N.M., E.V.N. and D.S.K.; writing—review and editing, G.N.L.; supervision, G.N.L. and E.V.N.; project administration, E.V.N. All authors have read and agreed to the published version of the manuscript.

Funding: The research funding from the Ministry of Science and Higher Education of the Russian Federation (Ural Federal University Program of Development within the Priority-2030 Program) is gratefully acknowledged.

Institutional Review Board Statement: Not applicable.

Informed Consent Statement: Not applicable.

Data Availability Statement: The data are available on request from the corresponding authors.

Acknowledgments: Our work was performed using «Uran» supercomputer of IMM UB RAS.

Conflicts of Interest: The authors declare no conflict of interest.

Sample Availability: Samples of compounds **2a–i** are available from the authors.

References

1. Singh, P.K.; Choudhary, S.; Kashyap, A.; Verma, H.; Kapil, S.; Kumar, M.; Arora, M.; Silakari, O. An Exhaustive Compilation on Chemistry of Triazolopyrimidine: A Journey through Decades. *Bioorg. Chem.* **2019**, *88*, 102919. [CrossRef] [PubMed]
2. Zuniga, E.S.; Korkegian, A.; Mullen, S.; Hembre, E.J.; Ornstein, P.L.; Cortez, G.; Biswas, K.; Kumar, N.; Cramer, J.; Masquelin, T.; et al. The Synthesis and Evaluation of Triazolopyrimidines as Anti-Tubercular Agents. *Bioorg. Med. Chem.* **2017**, *25*, 3922–3946. [CrossRef] [PubMed]
3. Jacobson, K.A.; Boeynaems, J.-M. P2Y Nucleotide Receptors: Promise of Therapeutic Applications. *Drug Discov. Today* **2010**, *15*, 570–578. [CrossRef] [PubMed]
4. Zhang, N.; Ayral-Kaloustian, S.; Nguyen, T.; Hernandez, R.; Lucas, J.; Discafani, C.; Beyer, C. Synthesis and SAR of 6-Chloro-4-Fluoroalkylamino-2-Heteroaryl-5-(Substituted)Phenylpyrimidines as Anti-Cancer Agents. *Bioorg. Med. Chem.* **2009**, *17*, 111–118. [CrossRef] [PubMed]
5. El-Adl, K.; Ibrahim, M.-K.; Alesawy, M.S.I.; Eissa, I.H. [1,2,4]Triazolo[4,3-*c*]Quinazoline and Bis([1,2,4]Triazolo)[4,3-*a*:4′,3′-*c*]Quinazoline Derived DNA Intercalators: Design, Synthesis, in Silico ADMET Profile, Molecular Docking and Anti-Proliferative Evaluation Studies. *Bioorg. Med. Chem.* **2021**, *30*, 115958. [CrossRef]
6. El-Adl, K.; Ibrahim, M.; Alesawy, M.S.; Eissa, I.H. Triazoloquinazoline Derived Classical DNA Intercalators: Design, Synthesis, in Silico ADME Profile, Docking, and Antiproliferative Evaluations. *Arch. Pharm.* **2022**, *355*, 2100506. [CrossRef]
7. Burbiel, J.C.; Ghattas, W.; Küppers, P.; Köse, M.; Lacher, S.; Herzner, A.-M.; Kombu, R.S.; Akkinepally, R.R.; Hockemeyer, J.; Müller, C.E. 2-Amino[1,2,4]Triazolo[1,5-*c*]Quinazolines and Derived Novel Heterocycles: Syntheses and Structure-Activity Relationships of Potent Adenosine Receptor Antagonists. *ChemMedChem* **2016**, *11*, 2272–2286. [CrossRef]
8. Zheng, Y.; Bian, M.; Deng, X.-Q.; Wang, S.-B.; Quan, Z.-S. Synthesis and Anticonvulsant Activity Evaluation of 5-Phenyl-[1,2,4]Triazolo[4,3-*c*]Quinazolin-3-Amines. *Arch. Pharm.* **2013**, *346*, 119–126. [CrossRef]
9. Esteban-Parra, G.M.; Sebastián, E.S.; Cepeda, J.; Sánchez-González, C.; Rivas-García, L.; Llopis, J.; Aranda, P.; Sánchez-Moreno, M.; Quirós, M.; Rodríguez-Diéguez, A. Anti-Diabetic and Anti-Parasitic Properties of a Family of Luminescent Zinc Coordination Compounds Based on the 7-Amino-5-Methyl-1,2,4-Triazolo[1,5-*a*]Pyrimidine Ligand. *J. Inorg. Biochem.* **2020**, *212*, 111235. [CrossRef]
10. Oukoloff, K.; Kovalevich, J.; Cornec, A.S.; Yao, Y.; Owyang, Z.A.; James, M.; Trojanowski, J.Q.; Lee, V.M.Y.; Smith, A.B.; Brunden, K.R.; et al. Design, Synthesis and Evaluation of Photoactivatable Derivatives of Microtubule (MT)-Active [1,2,4]Triazolo[1,5-*a*]Pyrimidines. *Bioorg. Med. Chem. Lett.* **2018**, *28*, 2180–2183. [CrossRef]
11. Eltyshev, A.K.; Agafonova, I.A.; Minin, A.S.; Pozdina, V.A.; Shevirin, V.A.; Slepukhin, P.A.; Benassi, E.; Belskaya, N.P. Photophysics, Photochemistry and Bioimaging Application of 8-Azapurine Derivatives. *Org. Biomol. Chem.* **2021**, *19*, 9880–9896. [CrossRef]
12. Taniya, O.S.; Fedotov, V.V.; Novikov, A.S.; Sadieva, L.K.; Krinochkin, A.P.; Kovalev, I.S.; Kopchuk, D.S.; Zyryanov, G.V.; Liu, Y.; Ulomsky, E.N.; et al. Abnormal Push-Pull Benzo[4,5]Imidazo[1,2-*a*][1,2,3]Triazolo[4,5-*e*]Pyrimidine Fluorophores in Planarized Intramolecular Charge Transfer (PLICT) State: Synthesis, Photophysical Studies and Theoretical Calculations. *Dyes Pigments* **2022**, *204*, 110405. [CrossRef]
13. Verbitskiy, E.V.; Gorbunov, E.B.; Baranova, A.A.; Lugovik, K.I.; Khokhlov, K.O.; Cheprakova, E.M.; Kim, G.A.; Rusinov, G.L.; Chupakhin, O.N.; Charushin, V.N. New 2*H*-[1,2,3]Triazolo[4,5-*e*][1,2,4]Triazolo[1,5- *a*]Pyrimidine Derivatives as Luminescent Fluorophores for Detection of Nitroaromatic Explosives. *Tetrahedron* **2016**, *72*, 4954–4961. [CrossRef]
14. Achelle, S.; Rodríguez-López, J.; Guen, F.R. Photoluminescence Properties of Aryl-, Arylvinyl-, and Arylethynylpyrimidine Derivatives. *ChemistrySelect* **2018**, *3*, 1852–1886. [CrossRef]
15. Sun, E.; Fang, R.; Liu, S.; Wu, J. Compound and Application Thereof. Patent CN113527302A, 22 October 2021.
16. Sun, E.; Fang, R.; Liu, S. Organic Compound for Light-Emitting Device, Application of Organic Compound and Organic Light-Emitting Device. Patent CN112174968A, 5 January 2021.
17. Sun, E.; Liu, S.; Feng, J.; Wu, J. Organic Electroluminescent Material and Organic Electroluminescent Device. Patent CN110256439A, 20 September 2019.
18. Moshkina, T.N.; Le Poul, P.; Barsella, A.; Pytela, O.; Bureš, F.; Robin-Le Guen, F.; Achelle, S.; Nosova, E.V.; Lipunova, G.N.; Charushin, V.N. Electron-Withdrawing Substituted Quinazoline Push-Pull Chromophores: Synthesis, Electrochemical, Photophysical and Second-Order Nonlinear Optical Properties. *Eur. J. Org. Chem.* **2020**, *2020*, 5445–5454. [CrossRef]
19. Moshkina, T.N.; Nosova, E.V.; Permyakova, J.V.; Lipunova, G.N.; Zhilina, E.F.; Kim, G.A.; Slepukhin, P.A.; Charushin, V.N. Push-Pull Structures Based on 2-Aryl/Thienyl Substituted Quinazolin-4(3*H*)-Ones and 4-Cyanoquinazolines. *Molecules* **2022**, *27*, 7156. [CrossRef]
20. Moshkina, T.N.; Nosova, E.V.; Permyakova, J.V.; Lipunova, G.N.; Valova, M.S.; Slepukhin, P.A.; Sadieva, L.K.; Charushin, V.N. Synthesis and Photophysical Properties of 2-Aryl-4-(Morpholin-4-yl)Quinazoline Chromophores: The Effect of π-Linker Moiety. *Dyes Pigments* **2022**, *206*, 110592. [CrossRef]
21. Nosova, E.V.; Kopotilova, A.E.; Ivan'kina, M.A.; Moshkina, T.N.; Kopchuk, D.S. Synthesis of 5-(4-Bromophenyl)- and 5-(5-Bromothiophen-2-yl)-Substituted 3-Aryl[1,2,4]Triazolo[4,3-*c*]Quinazolines. *Russ. Chem. Bull.* **2022**, *71*, 1483–1487. [CrossRef]

22. Mei, J.; Leung, N.L.C.; Kwok, R.T.K.; Lam, J.W.Y.; Tang, B.Z. Aggregation-Induced Emission: Together We Shine, United We Soar! *Chem. Rev.* **2015**, *115*, 11718–11940. [CrossRef]
23. Du, C.; Cheng, Z.; Shang, A.; Xu, Y.; Zhao, A.; Lei, C.; Chang, Y.; Lv, Y.; Lu, P. Two Different Implementation Strategies for Highly Efficient Non-Doped Fluorescent Organic Light-Emitting Diodes Based on Benzothiadiazole Derivatives. *Chem. Eng. J.* **2022**, *435*, 135010. [CrossRef]
24. Suman, G.R.; Pandey, M.; Chakravarthy, A.S.J. Review on New Horizons of Aggregation Induced Emission: From Design to Development. *Mater. Chem. Front.* **2021**, *5*, 1541–1584. [CrossRef]
25. Wan, Q.; Zhang, B.; Tong, J.; Li, Y.; Wu, H.; Zhang, H.; Wang, Z.; Pan, Y.; Tang, B.Z. Feasible Structure-Modification Strategy for Inhibiting Aggregation-Caused Quenching Effect and Constructing Exciton Conversion Channels in Acridone-Based Emitters. *Phys. Chem. Chem. Phys.* **2019**, *21*, 9837–9844. [CrossRef] [PubMed]
26. Xu, W.; Lee, M.M.S.; Zhang, Z.; Sung, H.H.Y.; Williams, I.D.; Kwok, R.T.K.; Lam, J.W.Y.; Wang, D.; Tang, B.Z. Facile Synthesis of AIEgens with Wide Color Tunability for Cellular Imaging and Therapy. *Chem. Sci.* **2019**, *10*, 3494–3501. [CrossRef] [PubMed]
27. Lakowicz, J.R. *Principles of Fluorescence Spectroscopy*, 3rd ed.; Lakowicz, J.R., Ed.; Springer: Boston, MA, USA, 2006; ISBN 978-0-38731-278-1.
28. Lippert, E. Spektroskopische Bestimmung Des Dipolmomentes Aromatischer Verbindungen Im Ersten Angeregten Singulettzustand. *Z. Für Elektrochem. Ber. Der Bunsenges. Für Phys. Chemie* **1957**, *61*, 962–975. [CrossRef]
29. Mataga, N.; Kaifu, Y.; Koizumi, M. Solvent Effects upon Fluorescence Spectra and the Dipolemoments of Excited Molecules. *Bull. Chem. Soc. Jpn.* **1956**, *29*, 465–470. [CrossRef]
30. Mukhopadhyay, A.; Maka, V.K.; Moorthy, J.N. Remarkable Influence of 'Phane Effect' on the Excited-State Properties of Cofacially Oriented Coumarins. *Phys. Chem. Chem. Phys.* **2017**, *19*, 4758–4767. [CrossRef]
31. Kosower, E.M. *An Introduction to Physical Organic Chemistry*; Wiley: New York City, NY, USA, 1968.
32. Kosower, E.M. The Effect of Solvent on Spectra. I. A New Empirical Measure of Solvent Polarity: Z-Values. *J. Am. Chem. Soc.* **1958**, *80*, 3253–3260. [CrossRef]
33. Dimroth, K.; Reichardt, C.; Siepmann, T.; Bohlmann, F. Über Pyridinium-N-Phenol-Betaine Und Ihre Verwendung Zur Charakterisierung Der Polarität von Lösungsmitteln. *Justus Liebigs Ann. Chem.* **1963**, *661*, 1–37. [CrossRef]
34. Richard, P. 2-Aryl-4(3*H*)Quinazolinones. *J. Heterocycl. Chem.* **1971**, *8*, 699–702.
35. Moshkina, T.N.; Nosova, E.V.; Kopotilova, A.E.; Savchuk, M.I.; Nikonov, I.L.; Kopchuk, D.S.; Slepukhin, P.A.; Kim, G.A.; Lipunova, G.N.; Charushin, V.N. Synthesis and Photophysical Properties of Pyridyl- and Quinolinyl-Substituted 4-(4-Aminophenyl)Quinazolines. *J. Photochem. Photobiol. A Chem.* **2022**, *429*, 113917. [CrossRef]
36. Varghese, A.; Akshaya, K.B. Application of Fluorescence in Solvatochromic Studies of Organic Compounds. In *Reviews in Fluorescence 2017*; Geddes, C.D., Ed.; Springer International Publishing: New York, NY, USA, 2018; pp. 99–121.
37. Ilharco, L.M.; Brito de Barros, R. Aggregation of Pseudoisocyanine Iodide in Cellulose Acetate Films: Structural Characterization by FTIR. *Langmuir* **2000**, *16*, 9331–9337. [CrossRef]
38. Jia, W.B.; Wang, H.W.; Yang, L.M.; Lu, H.B.; Kong, L.; Tian, Y.P.; Tao, X.T.; Yang, J.X. Synthesis of Two Novel Indolo[3,2-*b*]Carbazole Derivatives with Aggregation-Enhanced Emission Property. *J. Mater. Chem. C* **2013**, *1*, 7092–7101. [CrossRef]
39. Das, P.; Kumar, A.; Chowdhury, A.; Mukherjee, P.S. Aggregation-Induced Emission and White Luminescence from a Combination of π-Conjugated Donor-Acceptor Organic Luminogens. *ACS Omega.* **2018**, *3*, 13757–13771. [CrossRef]
40. Valeur, B.; Berberan-Santos, M.N. *Molecular Fluorescence*; Wiley: Hoboken, NJ, USA, 2012; Volume 53, ISBN 978-3-52732-837-6.
41. Krishnan, R.; Binkley, J.S.; Seeger, R.; Pople, J.A. Self-Consistent Molecular Orbital Methods. XX. A Basis Set for Correlated Wave Functions. *J. Chem. Phys.* **1980**, *72*, 650–654. [CrossRef]
42. McLean, A.D.; Chandler, G.S. Contracted Gaussian Basis Sets for Molecular Calculations. I. Second Row Atoms, Z=11–18. *J. Chem. Phys.* **1980**, *72*, 5639–5648. [CrossRef]
43. Clark, T.; Chandrasekhar, J.; Spitznagel, G.W.; Schleyer, P.V.R. Efficient Diffuse Function-augmented Basis Sets for Anion Calculations. III. The 3-21+G Basis Set for First-row Elements, Li–F. *J. Comput. Chem.* **1983**, *4*, 294–301. [CrossRef]
44. Frisch, M.J.; Pople, J.A.; Binkley, J.S. Self-Consistent Molecular Orbital Methods 25. Supplementary Functions for Gaussian Basis Sets. *J. Chem. Phys.* **1984**, *80*, 3265–3269. [CrossRef]
45. Neese, F. The ORCA Program System. *Wiley Interdiscip. Rev. Comput. Mol. Sci.* **2012**, *2*, 73–78. [CrossRef]
46. Dolomanov, O.V.; Bourhis, L.J.; Gildea, R.J.; Howard, J.A.K.; Puschmann, H. OLEX2: A Complete Structure Solution, Refinement and Analysis Program. *J. Appl. Crystallogr.* **2009**, *42*, 339–341. [CrossRef]
47. Sheldrick, G.M. A Short History of SHELX. *Acta Crystallogr. Sect. A Found. Crystallogr.* **2008**, *64*, 112–122. [CrossRef]

molecules

MDPI

Article

ESIPT-Capable 4-(2-Hydroxyphenyl)-2-(Pyridin-2-yl)-1*H*-Imidazoles with Single and Double Proton Transfer: Synthesis, Selective Reduction of the Imidazolic OH Group and Luminescence

Nikita A. Shekhovtsov [1,*], Elena B. Nikolaenkova [2], Alexey A. Ryadun [1], Denis G. Samsonenko [1], Alexsei Ya. Tikhonov [2,*] and Mark B. Bushuev [1,*]

[1] Nikolaev Institute of Inorganic Chemistry, Siberian Branch of Russian Academy of Sciences, 3, Acad. Lavrentiev Ave., Novosibirsk 630090, Russia
[2] N. N. Vorozhtsov Novosibirsk Institute of Organic Chemistry, Siberian Branch of Russian Academy of Sciences, 9, Acad. Lavrentiev Ave., Novosibirsk 630090, Russia
* Correspondence: shekhovtsov@niic.nsc.ru (N.A.S.); alyatikh@nioch.nsc.ru (A.Y.T.); bushuev@niic.nsc.ru (M.B.B.)

Abstract: 1*H*-Imidazole derivatives establish one of the iconic classes of ESIPT-capable compounds (ESIPT = excited state intramolecular proton transfer). This work presents the synthesis of 1-hydroxy-4-(2-hydroxyphenyl)-5-methyl-2-(pyridin-2-yl)-1*H*-imidazole ($\mathbf{L^{OH,OH}}$) as the first example of ESIPT-capable imidazole derivatives wherein the imidazole moiety simultaneously acts as a proton acceptor and a proton donor. The reaction of $\mathbf{L^{OH,OH}}$ with chloroacetone leads to the selective reduction of the imidazolic OH group (whereas the phenolic OH group remains unaffected) and to the isolation of 4-(2-hydroxyphenyl)-5-methyl-2-(pyridin-2-yl)-1*H*-imidazole ($\mathbf{L^{H,OH}}$), a monohydroxy congener of $\mathbf{L^{OH,OH}}$. Both $\mathbf{L^{OH,OH}}$ and $\mathbf{L^{H,OH}}$ demonstrate luminescence in the solid state. The number of OH···N proton transfer sites in these compounds (one for $\mathbf{L^{H,OH}}$ and two for $\mathbf{L^{OH,OH}}$) strongly affects the luminescence mechanism and color of the emission: $\mathbf{L^{H,OH}}$ emits in the light green region, whereas $\mathbf{L^{OH,OH}}$ luminesces in the orange region. According to joint experimental and theoretical studies, the main emission pathway of both compounds is associated with $T_1 \rightarrow S_0$ phosphorescence and not related to ESIPT. At the same time, $\mathbf{L^{OH,OH}}$ also exhibits $S_1 \rightarrow S_0$ fluorescence associated with ESIPT with one proton transferred from the hydroxyimidazole moiety to the pyridine moiety, which is not possible for $\mathbf{L^{H,OH}}$ due to the absence of the hydroxy group in the imidazole moiety.

Keywords: imidazole; 2-hydroxyphenyl group; hydrogen bond; ESIPT; luminescence

Citation: Shekhovtsov, N.A.; Nikolaenkova, E.B.; Ryadun, A.A.; Samsonenko, D.G.; Tikhonov, A.Y.; Bushuev, M.B. ESIPT-Capable 4-(2-Hydroxyphenyl)-2-(Pyridin-2-yl)-1*H*-Imidazoles with Single and Double Proton Transfer: Synthesis, Selective Reduction of the Imidazolic OH Group and Luminescence. *Molecules* **2023**, *28*, 1793. https://doi.org/10.3390/molecules28041793

Academic Editors: Alexey M. Starosotnikov, Maxim A. Bastrakov and Igor L. Dalinger

Received: 27 January 2023
Revised: 7 February 2023
Accepted: 9 February 2023
Published: 14 February 2023

1. Introduction

Aromatic and heteroaromatic compounds featuring strong intramolecular hydrogen bonds of the O–H···Y and N–H···Y types (Y = O, NR) can manifest photoinduced intramolecular proton transfer reactions (Scheme 1) [1–14]. The photoexcitation of such molecules in their most stable, or normal (N), form leads to the electron density redistribution, followed by the excited state intramolecular proton transfer (ESIPT) reaction yielding the excited state tautomeric form (T). Radiative and non-radiative processes proceeding in the tautomeric form convert this excited state form into the ground state. The last step in this sequence of processes is the ground state intramolecular proton transfer (GSIPT) reaction, converting the tautomeric form to the normal one.

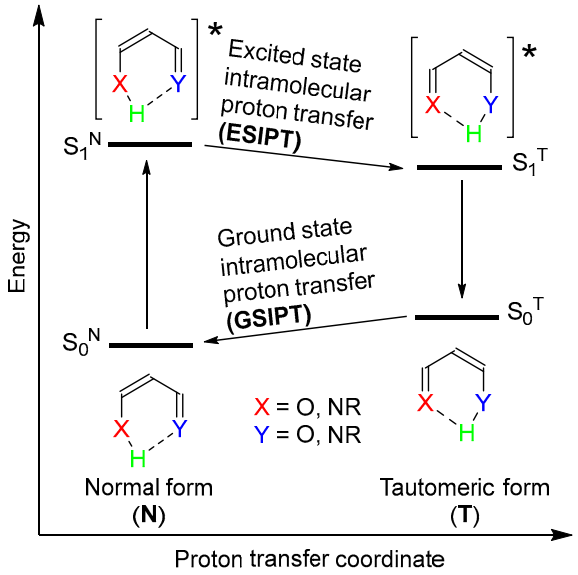

Scheme 1. The ESIPT and GSIPT processes in molecules featuring short intramolecular hydrogen bonds.

The ESIPT photoreaction (Scheme 1) is highly sensitive to substituents [15–27] and coordinated metal ions [28–33], protonation/deprotonation [34–41], the state of aggregation [42,43], the polarity of solvent [44–48] and the presence of various analytes [49–56]. If the excited state tautomerization (normal-to-tautomeric) is barrierless, the only form to emit is the tautomeric one, which typically lumineses with rather large Stokes shift [57,58]. In the case of barriers on excited state potential energy surfaces, the molecule can be trapped in a local minimum of the normal form, leading to the emission of the normal form. Modifying the barrier height in the excited state, one can achieve dual emission associated with the luminescence of both forms [59–66]. The sensitivity of ESIPT-capable compounds to various stimuli makes them an appealing platform for numerous applications [67–69].

1*H*-Imidazoles, 1,3-oxazoles, 1,3-thiazoles and their benzannulated congeners are often used in the design of ESIPT-fluorophores [70–82]. Normally, when decorated with such proton-donating groups as unsubstituted or substituted 2-hydroxyphenyl groups in the α-position to aza-atoms, their free nitrogen atoms act as proton acceptors during the ESIPT process [70–82]. Recently we proposed a new approach in the design of imidazole-based ESIPT-fluorophores in which we switched the role of the imidazole cycle to the one of a proton donor by introducing the hydroxy group in the position 1 and the pyridin-2-yl group in the position 2 of the imidazole ring [83–87]. Importantly, both roles of the imidazole ring in ESIPT-fluorophores, i.e., the proton acceptor and the proton donor ones, can be combined in a single molecule if we introduce the proton-donating 2-hydroxyphenyl group in the position 4 and the proton accepting pyridin-2-yl group in the position 2 of the 1-hydroxy-1*H*-imidazole moiety. In this case, the molecule will feature two spatially separated ESIPT-sites with two short O–H···N hydrogen bonds therein.

In this manuscript, we report the synthesis of 1-hydroxy-4-(2-hydroxyphenyl)-5-methyl-2-(pyridin-2-yl)-1*H*-imidazole ($\mathbf{L^{OH,OH}}$) as the first example of imidazole derivatives wherein the central 1-hydroxy-1*H*-imidazole moiety simultaneously acts both as a proton acceptor and a proton donor (Scheme 2). Along with the synthesis of $\mathbf{L^{OH,OH}}$, we report the reaction of $\mathbf{L^{OH,OH}}$ with chloroacetone leading to the selective formation of a corresponding 1*H*-imidazole derivative, 4-(2-hydroxyphenyl)-5-methyl-2-(pyridin-2-yl)-1*H*-imidazole ($\mathbf{L^{H,OH}}$) (Scheme 2), and proceeding without affecting the phenolic hydroxy group. Finally, we present the results of combined comparative experimental and theoretical studies of the emission of $\mathbf{L^{OH,OH}}$ and $\mathbf{L^{H,OH}}$ and the ESIPT photoreactions in both compounds.

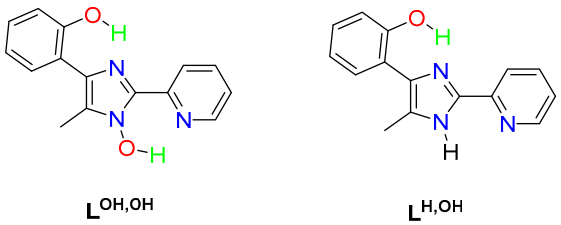

$\mathbf{L}^{\mathbf{OH,OH}}$ $\mathbf{L}^{\mathbf{H,OH}}$

Scheme 2. Structural formulae of $\mathbf{L}^{\mathbf{OH,OH}}$ and $\mathbf{L}^{\mathbf{H,OH}}$.

2. Results and Discussion

2.1. Synthesis of 1-Hydroxy-4-(2-Hydroxyphenyl)-5-Methyl-2-(Pyridin-2-yl)-1H-Imidazole ($\mathbf{L}^{\mathbf{OH,OH}}$) and 4-(2-Hydroxyphenyl)-5-Methyl-2-(Pyridin-2-yl)-1H-Imidazole ($\mathbf{L}^{\mathbf{H,OH}}$)

The ESIPT-capable imidazole-based compounds $\mathbf{L}^{\mathbf{OH,OH}}$ and $\mathbf{L}^{\mathbf{H,OH}}$ were synthesized using the following reactions (Scheme 3). The first step, i.e., the nitrosation reaction, required the protection of the hydroxy group in *ortho* hyroxypropiophenone with the benzoyl group [88]. After this, the monoxime **B** was prepared by the nitrosation of 2-benzoyloxypropiophenone (**A**) with isopropyl nitrite according to the procedure close to the one reported by Mason [88]. The second step was the construction of the 1-hydroxy-1*H*-imidazole moiety. The most convenient and widespread method for the synthesis of 1-hydroxy-1*H*-imidazoles is the condensation of monoxime diketones with aldehydes and ammonia or ammonium acetate [89]. The condensation of the monoxime **B** with pyridinecarboxaldehyde and ammonia (cf. [83]) led to the isolation of 1-hydroxy-4-(2-hydroxyphenyl)-5-methyl-2-(pyridin-2-yl)-1*H*-imidazole ($\mathbf{L}^{\mathbf{OH,OH}}$). Importantly, the benzoyl protecting group removal occurred at this step along with the simultaneous formation of the imidazole ring. The last step was the conversion of the 1-hydroxy-1*H*-imidazole derivative $\mathbf{L}^{\mathbf{OH,OH}}$ to the 1*H*-imidazole $\mathbf{L}^{\mathbf{H,OH}}$. For this conversion, along with various reducing agents (e.g., PCl_3, $(Ph)_3P$, trialkylphosphites, $TiCl_3$, etc.), halogen-substituted compounds with electron-withdrawing groups (e.g., $BrCH_2CO_2Me$ [90] and chloroacetone [91,92]) can be used. The interaction of 1-hydroxy-1*H*-imidazole with chloroacetone allows the reaction to be carried out under mild conditions through the intermediate formation of a chlorine atom substitution product, followed by its fragmentation to form reduced 1*H*-imidazole. Importantly, the reaction of $\mathbf{L}^{\mathbf{OH,OH}}$ with chloroacetone (cf. [93]) proceeded without affecting the phenolic hydroxy group, which greatly simplified the preparation of the 1*H*-imidazole $\mathbf{L}^{\mathbf{H,OH}}$ compound. Spectral and structural data for the compounds are given in Supplementary Materials.

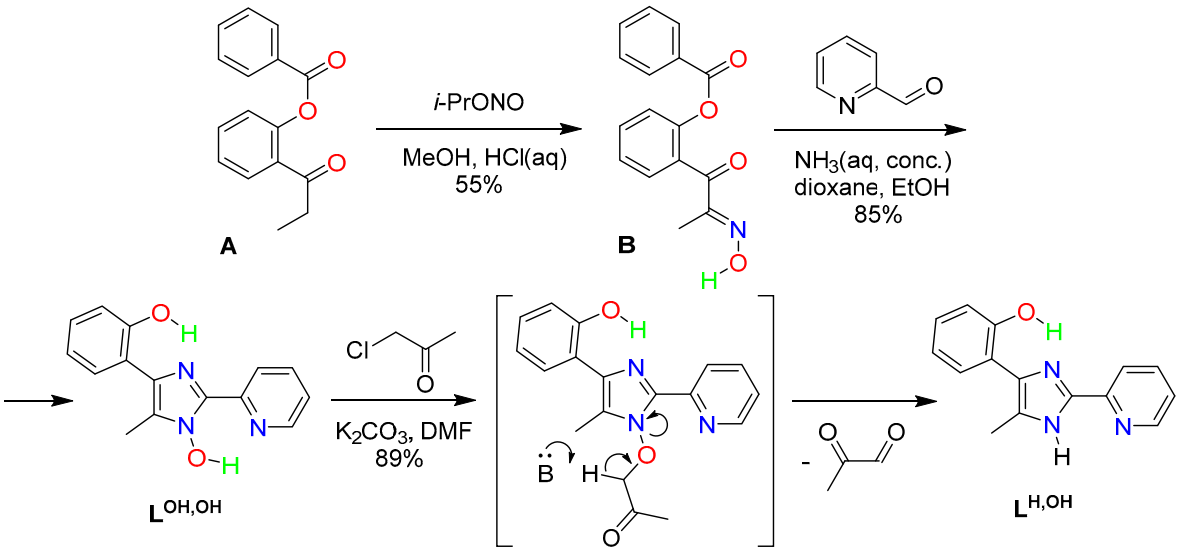

Scheme 3. Synthesis of $\mathbf{L}^{\mathbf{OH,OH}}$ and $\mathbf{L}^{\mathbf{H,OH}}$.

2.2. X-ray Single Crystal Structure of 1-Hydroxy-4-(2-Hydroxyphenyl)-5-Methyl-2-(Pyridin-2-yl)-1H-Imidazole ($\mathbf{L}^{OH,OH}$)

The dihydroxy derivative, $\mathbf{L}^{OH,OH}$, crystallizes in the monoclinic space group $P2_1/c$ (Supplementary Materials, Table S1, Figures S9–S11). There are two crystallographically independent $\mathbf{L}^{OH,OH}$ molecules in the crystal structure (Figure 1). The 2-(pyridin-2-yl)imidazole moiety in both independent molecules is practically planar with the torsions smaller than 1°. On the other hand, the 4-(2-hydroxyphenyl) group deviates from the plane of the imidazole cycle by *ca*. 7° in one and by *ca*. 12° in another $\mathbf{L}^{OH,OH}$ molecule. There are two short intramolecular O–H···N hydrogen bonds in each molecule with the O···N separations of 2.57–2.60 Å.

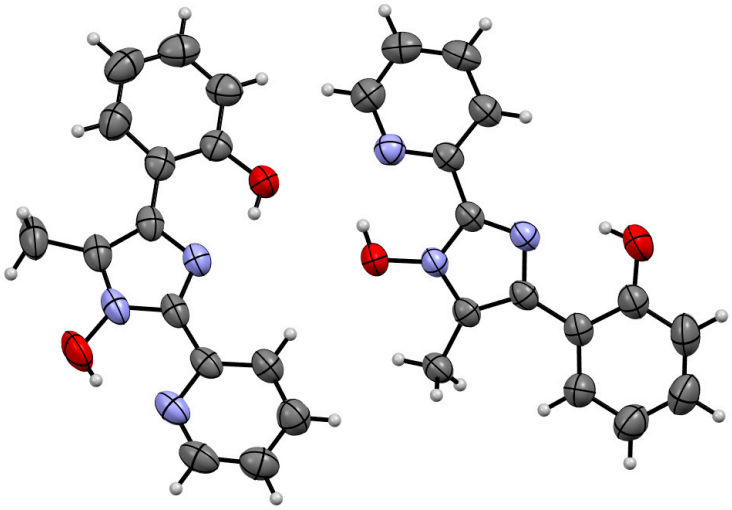

Figure 1. Two crystallographically independent molecules in the structure of $\mathbf{L}^{OH,OH}$.

The $\mathbf{L}^{OH,OH}$ molecules are assembled into corrugated ribbons running along the *c* axis through weak C–H···O hydrogen bonds (Figure 2). The ribbons are further gathered into 3D supramolecular structure via C–H···C and C–H···H–C van der Waals interactions (Supplementary Materials, Figures S9–S11).

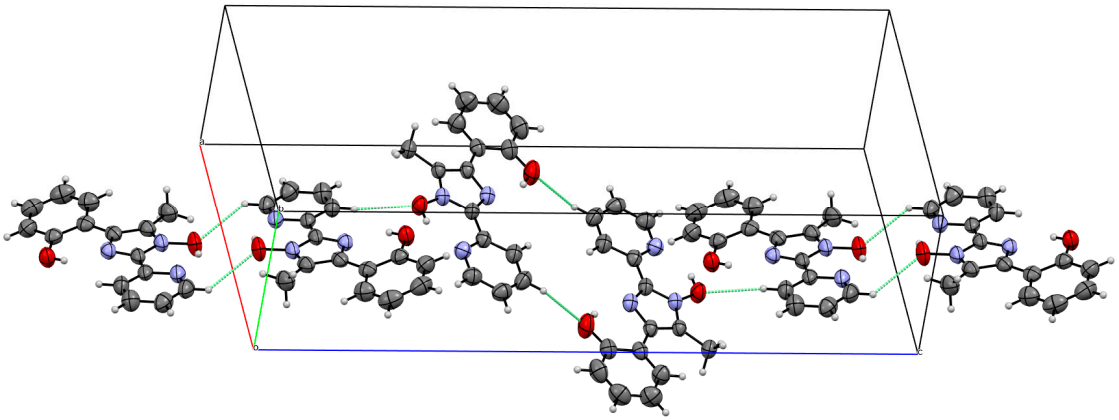

Figure 2. A supramolecular ribbon in the structure of $\mathbf{L}^{OH,OH}$.

2.3. Tautomeric Forms of $\mathbf{L}^{H,OH}$ and $\mathbf{L}^{OH,OH}$: An Introduction

$\mathbf{L}^{H,OH}$ and $\mathbf{L}^{OH,OH}$ can exist in various tautomeric forms. In this context, for the sake of clarity we introduce the following abbreviations of these forms for further discussions (Scheme 4). $\mathbf{L}^{OH,OH}$ has two proton transfer sites and therefore can exist in four tautomeric forms: i) *N,N*-$\mathbf{L}^{OH,OH}$ (no proton transferred, corresponds to the global energy minimum

and to the X-ray crystal structure), (ii) *N*,*T*-$\mathbf{L}^{\mathbf{OH,OH}}$ (one proton transferred from the hydroxyphenyl moiety to the hydroxyimidazole moiety), (iii) *T*,*N*-$\mathbf{L}^{\mathbf{OH,OH}}$ (one proton transferred from the hydroxyimidazole moiety to the pyridine moiety), (iv) *T*,*T*-$\mathbf{L}^{\mathbf{OH,OH}}$ (both protons transferred). $\mathbf{L}^{\mathbf{H,OH}}$ has only one proton transfer site and can exist in two tautomeric forms: (i) *N*-$\mathbf{L}^{\mathbf{H,OH}}$ (no proton transferred) and (ii) *T*-$\mathbf{L}^{\mathbf{H,OH}}$ (one proton transferred). The same abbreviations are used for the energy minima of ground and excited states, e.g., $S_0^{N,N}$, $S_1^{T,N}$, T_1^{T}, etc.

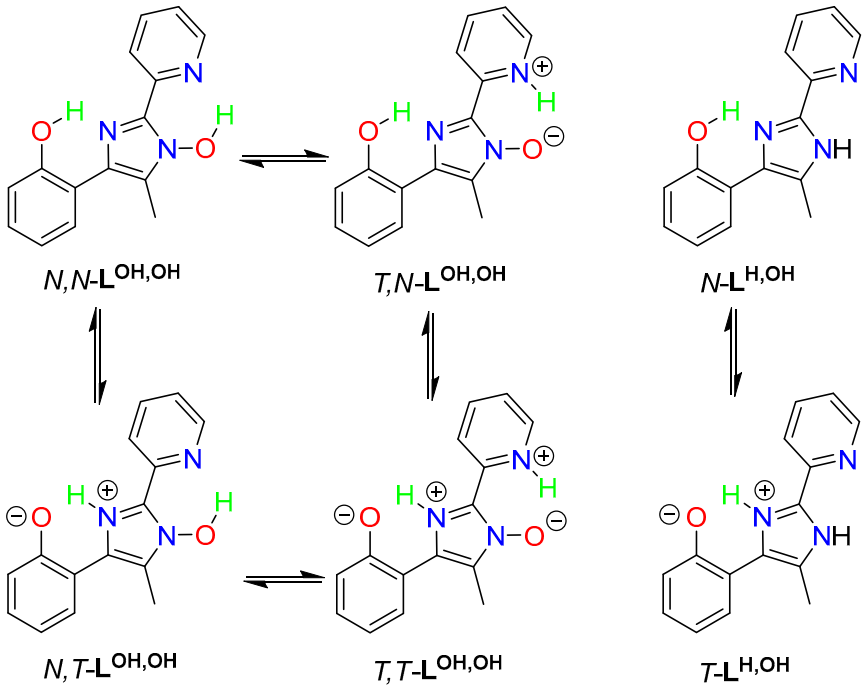

Scheme 4. Tautomeric forms of $\mathbf{L}^{\mathbf{H,OH}}$ and $\mathbf{L}^{\mathbf{OH,OH}}$.

2.4. Absorption Properties of $\mathbf{L}^{\mathbf{H,OH}}$ and $\mathbf{L}^{\mathbf{OH,OH}}$ in MeCN

In acetonitrile, both $\mathbf{L}^{\mathbf{H,OH}}$ and $\mathbf{L}^{\mathbf{OH,OH}}$ absorb in the ultraviolet domain, with the most intense peak centered at 320 and 342 nm, respectively (Figure 3). In order to test the relevance of the chosen theory level for quantum chemical computations, theoretical absorption spectra were calculated at the global energy minima of the ground state, $S_0^{N,N}$ (O^{Ph}–H 0.988 Å, O^{Imid}–H 1.010 Å, Table 1) for $\mathbf{L}^{\mathbf{OH,OH}}$ and S_0^{N} (O^{Ph}–H 0.980 Å) for $\mathbf{L}^{\mathbf{OH,OH}}$. The energies and relative intensities of the calculated vertical singlet-to-singlet absorptions are in good agreement with the experimental data (Figure 3), showing the relevance of the functional and basis set used in this study. The most intense experimental peak corresponds to the first vertical singlet-to-singlet transition ($S_0 \rightarrow S_1$), computed at 336 nm for $\mathbf{L}^{\mathbf{H,OH}}$ and 348 nm for $\mathbf{L}^{\mathbf{OH,OH}}$. In accordance with the experimental spectra, this transition indeed has the highest oscillator strength (*ca.* 0.5) among the other transitions. In terms of molecular orbitals, $S_0 \rightarrow S_1$ is a HOMO $\rightarrow$ LUMO transition. For both $\mathbf{L}^{\mathbf{H,OH}}$ and $\mathbf{L}^{\mathbf{OH,OH}}$, HOMO is distributed over hydroxyphenyl and imidazole moieties, while LUMO is located on imidazole and pyridine moieties (Figure 3). Thus, the $S_0 \rightarrow S_1$ absorption implies charge transfer from the hydroxyphenyl part of the molecule to the pyridine part. Despite there being no visual differences between the HOMO and LUMO of $\mathbf{L}^{\mathbf{H,OH}}$ and the HOMO and LUMO of $\mathbf{L}^{\mathbf{OH,OH}}$, respectively, the most intensive absorption peak of $\mathbf{L}^{\mathbf{OH,OH}}$ is slightly red-shifted compared with that of $\mathbf{L}^{\mathbf{H,OH}}$, and the computations fully reproduce this trend. A series of higher lying singlet-to-singlet transitions form the high-energy absorption band centered at *ca.* 260 nm for both ESIPT-emitters (Figure 3).

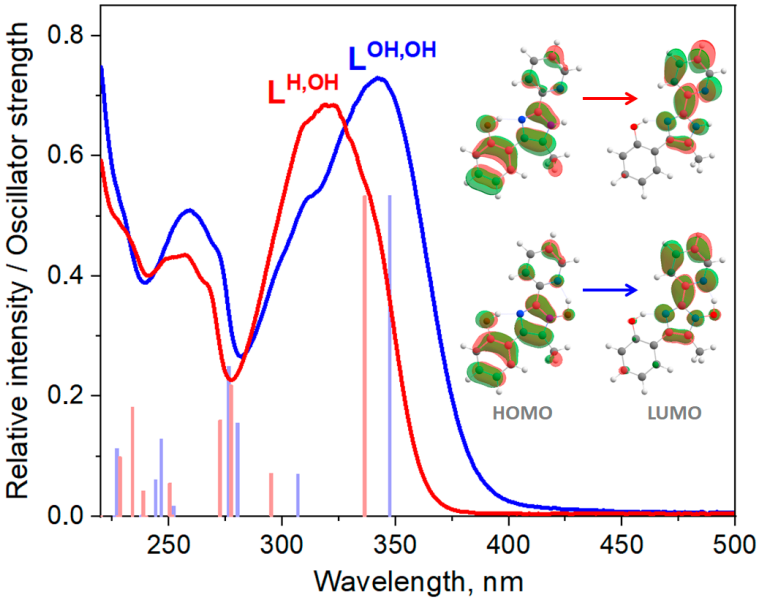

Figure 3. Absorption spectra of $\mathbf{L}^{\mathbf{H,OH}}$ (red) and $\mathbf{L}^{\mathbf{OH,OH}}$ (blue) in MeCN. Vertical bars display the positions and oscillator strengths of the singlet-to-singlet electronic transitions for $\mathbf{L}^{\mathbf{H,OH}}$ (red) and $\mathbf{L}^{\mathbf{OH,OH}}$ (blue).

Table 1. The most relevant geometric parameters for the optimized ground and excited state geometries of $\mathbf{L}^{\mathbf{H,OH}}$ and $\mathbf{L}^{\mathbf{OH,OH}}$.

Cmpd.	State	O^{Ph}–H, Å	O^{Ph}–H···N^{Imid}, Å	O^{Imid}–H, Å	O^{Imid}–H···N^{Py}, Å	θ_1, ° [a]	θ_2, ° [b]
$\mathbf{L}^{\mathbf{H,OH}}$	$S_0{}^N$	0.980	2.627	–	–	14.97	0.38
	$T_1{}^N$	1.006	2.550	–	–	5.79	0.20
	$T_1{}^T$	1.841	2.603	–	–	4.14	0.25
	near-CI [c]	3.264	3.411	–	–	84.77	1.92
$\mathbf{L}^{\mathbf{H,OH}}$	$S_0{}^{N,N}$	0.988	2.628	1.010	2.616	14.78	0.92
	$S_0{}^{T,N}$	0.992	2.592	1.595	2.542	0.79	0.04
	$S_1{}^{T,N}$	0.998	2.584	1.785	2.674	0.00	0.23
	$T_1{}^{N,N}$	1.008	2.546	1.065	2.509	−0.02	0.00
	$T_1{}^{N,T}$	1.829	2.599	1.051	2.531	−0.01	0.00
	$T_1{}^{T,N}$	0.994	2.590	1.931	2.728	−0.02	0.00
	$T_1{}^{T,T}$	1.807	2.593	1.787	2.648	−0.02	−0.01
	near-CI [c]	2.347	2.922	0.964	2.732	55.43	5.45

[a]—θ_1 is the dihedral angle between the planes of hydroxyphenyl and imidazole moieties. [b]—θ_2 is the dihedral angle between the planes of pyridine and imidazole moieties. [c]—geometries that are close to the conical intersection between the S_0 and S_1 states.

It is noteworthy that, in addition to the global energy minimum $S_0{}^{N,N}$ on the PES of the ground state, $\mathbf{L}^{\mathbf{OH,OH}}$ has a local minimum $S_0{}^{T,N}$ (O^{Ph}–H 0.992 Å, O^{Imid}–H 1.595 Å, Figure 4, Table 1), and therefore its corresponding form *T*,*N*-$\mathbf{L}^{\mathbf{OH,OH}}$ can also absorb light. $S_0{}^{T,N}$ is thermodynamically less favorable than $S_0{}^{N,N}$ by *ca.* 17 kJ/mol and is separated from $S_0{}^{N,N}$ by an energy barrier of *ca.* 20 kJ/mol. Although such a low barrier may indicate coexistence of the *N*,*N*-$\mathbf{L}^{\mathbf{OH,OH}}$ and *T*,*N*-$\mathbf{L}^{\mathbf{OH,OH}}$ tautomeric forms in solution, the fact that the experimental absorption spectrum is completely reproduced by the transitions of the *N*,*N*-$\mathbf{L}^{\mathbf{OH,OH}}$ form points to the very small contribution of the *T*,*N*-$\mathbf{L}^{\mathbf{OH,OH}}$ form to the

absorption spectrum. In the case of $\mathbf{L}^{\mathbf{H,OH}}$, there is only one minimum on the PEC of the ground state, $S_0{}^N$ (Figure 5).

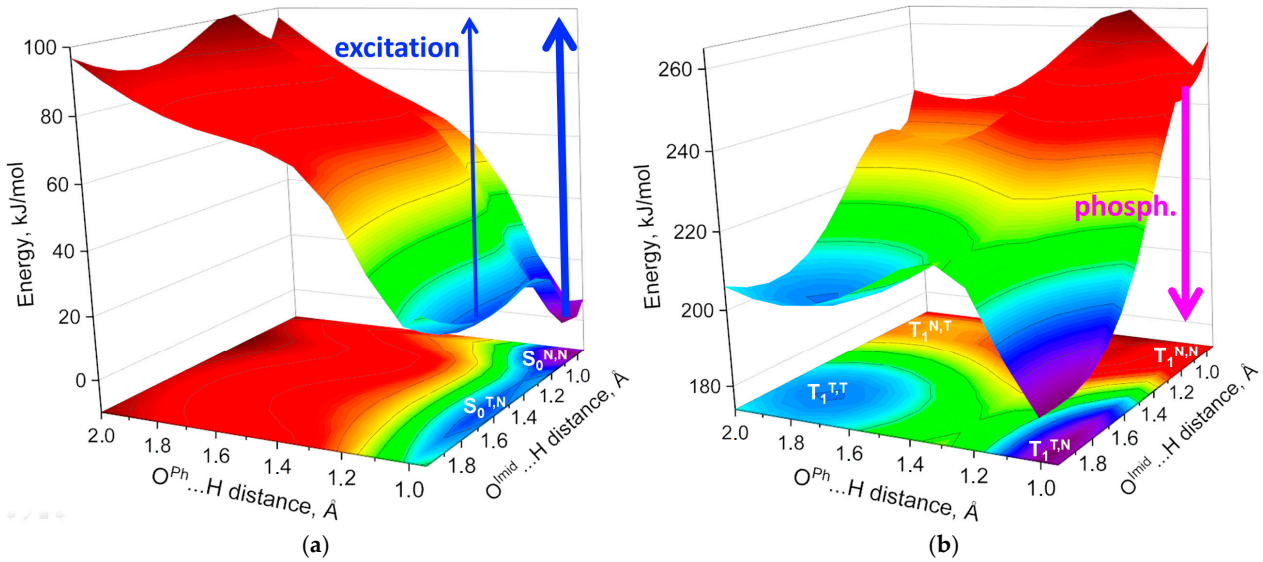

Figure 4. The potential energy surfaces (PESes) of the S_0 (**a**) and T_1 (**b**) states of $\mathbf{L}^{\mathbf{OH,OH}}$ along the proton transfer paths O^{Ph}–H···N^{Imid} and O^{Imid}–H···N^{Py} and their projections.

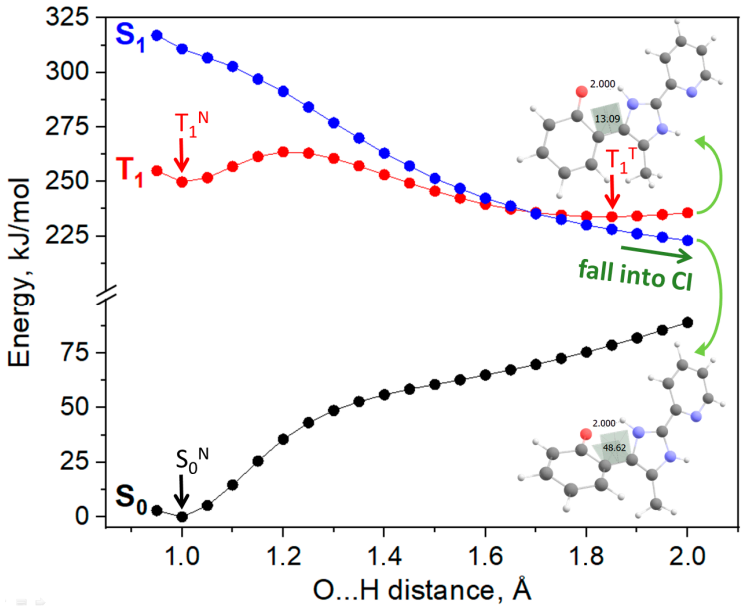

Figure 5. The potential energy curves (PECs) of the S_0, S_1 and T_1 (right) states of $\mathbf{L}^{\mathbf{H,OH}}$ along the proton transfer path O^{Ph}–H···N^{Imid}. The arrows show the energy minima on these PECs. The optimized geometries of the T_1 and S_1 states with the O^{Ph}–H distance of 2.0 Å are also depicted.

2.5. Excitation and Emission Properties of $\mathbf{L}^{H,OH}$ and $\mathbf{L}^{OH,OH}$

$\mathbf{L}^{\mathbf{H,OH}}$ and $\mathbf{L}^{\mathbf{OH,OH}}$ are non-luminescent in MeCN solution, indicating the possible predominance of various non-radiative deactivation pathways. In the solid state, $\mathbf{L}^{\mathbf{H,OH}}$ emits in the light green region (Figures 6 and 7). The broad unstructured luminescence band of $\mathbf{L}^{\mathbf{H,OH}}$ is located in the region 400–750 nm with a maximum at 546 nm. The intensity of this band depends on excitation wavelength: at λ_{ex} = 400–420 nm, it is three times more intense than at λ_{ex} = 280–360 nm. However, a change in the excitation energy does not lead to a shift of the emission maximum. $\mathbf{L}^{\mathbf{H,OH}}$ exhibits a monoexponential photoluminescence decay (Supplementary Materials, Figure S14), indicating that there

is likely only one emission mechanism. The lifetime of molecules in the excited state (τ) is 1.10 μs (λ_{ex} = 300 nm, λ_{det} = 540 nm), so the observed emission is associated with phosphorescence, i.e., with a spin-forbidden triplet-to-singlet transition. The width of the phosphorescence band is associated with the vibrational satellite structure, which involves an interplay of several transitions from the lowest vibrational level of the excited state to various vibrational levels of the ground state.

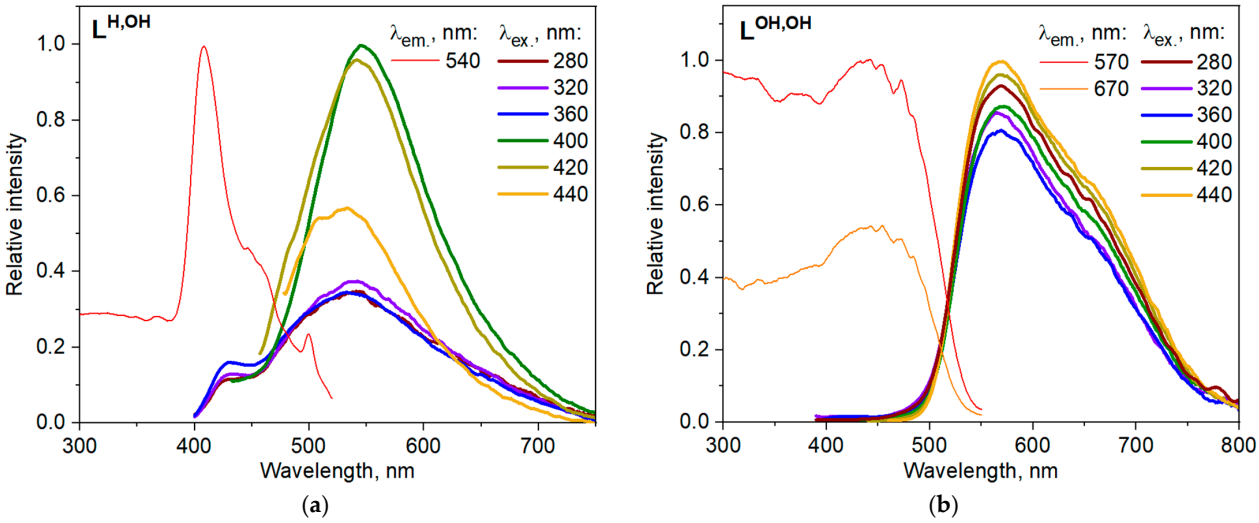

Figure 6. Excitation and emission spectra of $\mathbf{L}^{\mathbf{H,OH}}$ (**a**) and $\mathbf{L}^{\mathbf{OH,OH}}$ (**b**) in the solid state at room temperature.

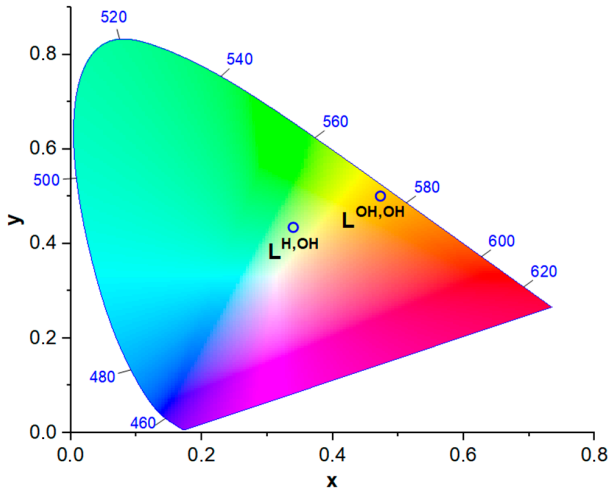

Figure 7. CIE 1931 diagram showing the chromaticity of the emission of $\mathbf{L}^{\mathbf{H,OH}}$ and $\mathbf{L}^{\mathbf{OH,OH}}$ in the solid state at λ_{ex} = 320 nm.

$\mathbf{L}^{\mathbf{OH,OH}}$ demonstrates luminescence in the orange region (Figures 6 and 7). As for $\mathbf{L}^{\mathbf{H,OH}}$, the emission spectrum is dominated by a broad band at 450–800 nm centered at 568 nm. In contrast to $\mathbf{L}^{\mathbf{H,OH}}$, an additional low-energy shoulder at *ca.* 670 nm appears in the case of $\mathbf{L}^{\mathbf{OH,OH}}$, which is responsible for the orange color of luminescence. The emission band is more or less equally intensive when excited at λ_{ex} = 280–440 nm. The luminescence decay of $\mathbf{L}^{\mathbf{OH,OH}}$ is multiexponentional and more complex than for $\mathbf{L}^{\mathbf{H,OH}}$: the long part of the photoluminescence decay reveals one lifetime in the microsecond range, τ = 1.05 μs (similar to $\mathbf{L}^{\mathbf{H,OH}}$), whereas the short part reveals two lifetimes in the nanosecond range, τ = 2 ns and τ = 21 ns (Supplementary Materials, Figure S15). Thus, $\mathbf{L}^{\mathbf{OH,OH}}$ shows two emission mechanisms, i.e., phosphorescence and fluorescence. The photoluminescence quantum yield for $\mathbf{L}^{\mathbf{H,OH}}$ and $\mathbf{L}^{\mathbf{OH,OH}}$ is less than 1% in the solid state.

Before turning to calculations that will help us identify the emission pathways, it is worthwhile to make a visual inspection of the possible number and nature of the photoluminescence mechanisms by comparing the spectra of $\mathbf{L^{H,OH}}$ and $\mathbf{L^{OH,OH}}$. As mentioned above, both compounds exhibit phosphorescence with similar lifetimes in the order of one microsecond. Owing to the close wavelength of the maxima of the most intense band (546 nm for $\mathbf{L^{H,OH}}$ and 568 nm for $\mathbf{L^{OH,OH}}$), we can assume that this band implies the same emission mechanism for both compounds. The shoulder appearing at *ca.* 670 nm in the case of $\mathbf{L^{OH,OH}}$ may be responsible for the short lifetimes and can therefore be attributed to fluorescence. The absence of this shoulder for $\mathbf{L^{H,OH}}$ may indicate that the fluorescence mechanism observed for $\mathbf{L^{OH,OH}}$ cannot be realized for $\mathbf{L^{H,OH}}$. We hypothesize that this fluorescence mechanism is somehow related to the O^{Imid}–H···N^{Py} proton transfer site, which is absent for $\mathbf{L^{H,OH}}$.

2.6. Elucidation of the Fluorescence and Phosphorescence Mechanisms for $L^{H,OH}$ and $L^{OH,OH}$

Geometry optimizations of the excited states were performed in order to establish the photoluminescence mechanisms for $\mathbf{L^{H,OH}}$ and $\mathbf{L^{OH,OH}}$ and to verify our predictions from the previous paragraph. The PEC of the first triplet excited state of $\mathbf{L^{H,OH}}$ reveals two minima, $T_1{}^N$ and $T_1{}^T$ (Figure 5). The $T_1{}^N$ optimized geometry is characterized by a slightly enlarged O^{Ph}–H distance (1.006 Å for $T_1{}^N$ vs. 0.980 Å for $S_0{}^N$) and a shortened $O^{Ph}\cdots N^{Imid}$ hydrogen bond length (2.550 Å for $T_1{}^N$ vs. 2.627 Å for $S_0{}^N$) compared with the $S_0{}^N$ relaxed geometry. The calculated $T_1{}^N \rightarrow S_0{}^N$ phosphorescence wavelength (578 nm) is in excellent agreement with the maximum of the intensive emission band (568 nm). According to the analysis of the frontier molecular orbitals, $T_1{}^N \rightarrow S_0{}^N$ is LUMO → HOMO transition (Figure 8). LUMO is a π^*-orbital that is equally located on pyridine and imidazole moieties, whereas HOMO is a π-orbital that is majorly located on hydroxyphenyl and imidazole parts of the molecule. Therefore, the observed $T_1{}^N \rightarrow S_0{}^N$ phosphorescence is associated with charge transfer from the pyridine moiety to the hydroxyphenyl moiety (this is directly opposite to the $S_0{}^N \rightarrow S_1{}^N$ absorption mechanism discussed above). Although the second minimum on the PEC of the T_1 state, $T_1{}^T$ (O^{Ph}–H 1.841 Å, Figure 5), is thermodynamically more stable than $T_1{}^N$ by *ca.* 16 kJ/mol, the energy barrier separating $T_1{}^N$ and $T_1{}^T$ is as high as *ca.* 14 kJ/mol, which impedes efficient ESIPT in the triplet manifold. Furthermore, the computed $T_1{}^T \rightarrow S_0{}^T$ phosphorescence wavelength (1095 nm) is largely overestimated compared with the position of the phosphorescence band. Thus, we attribute the observed phosphorescence of $\mathbf{L^{H,OH}}$ with τ = 1.05 μs to the $T_1{}^N \rightarrow S_0{}^N$ transition of the *N*-$\mathbf{L^{H,OH}}$ form, which is not related to the ESIPT process.

Having established the phosphorescence mechanism ($T_1{}^N \rightarrow S_0{}^N$) for $\mathbf{L^{H,OH}}$, the following question arises: how can the molecules of $\mathbf{L^{H,OH}}$ populate the T_1 state? Classically, in most compounds the triplet manifold is populated after $S_0 \rightarrow S_1$ excitation followed by $S_1 \rightarrow T_1$ intersystem crossing. Returning to our discussion of absorption properties, the $S_0{}^N \rightarrow S_1{}^N$ vertical absorption is computed at 336 nm for $\mathbf{L^{H,OH}}$ (Figure 3). At the same time, the phosphorescence band of $\mathbf{L^{H,OH}}$ in the region 450–750 nm is predominantly excited at λ_{ex} = 400–420 nm. Obviously, such low energies cannot lead to the population of the S_1 state. Therefore, we suggest that in the case of $\mathbf{L^{H,OH}}$ there is a direct population of the triplet manifold from the ground state, $S_0{}^N \rightarrow T_1{}^N$, since only triplets can be populated with λ_{ex} = 400–420 nm ($\lambda_{calc.\ S0\text{-}T1}$ = 462 nm, $\lambda_{calc.\ S0\text{-}T2}$ = 395 nm). However, the classical mechanism of populating the T_1 state ($S_0{}^N \rightarrow S_1{}^N \rightarrow T_1{}^N$) is also feasible when molecules are excited with high energy quanta (λ_{ex} < 336 nm).

In contrast to the triplet manifold, ESIPT is possible for the singlet manifold of $\mathbf{L^{H,OH}}$. After $S_0{}^N \rightarrow S_1{}^N$ excitation, the ESIPT process is barrierless in the S_1 state. There are no minima on the PEC of the first singlet excited state, as shown in Figure 5. A non-constrained geometry optimization of the S_1 state directly leads to a non-planar geometry near the conical intersection (CI) between the S_0 and S_1 states (Figure 9b). According to the literature, ESIPT is often coupled with the radiationless deactivation via twisted intramolecular charge transfer (TICT) states of a non-planar biradicaloid nature [83,85,94–99]. This non-planarity

arises from the twisting around a double-like bond between proton-donating and proton-accepting moieties (around the C^{Ph}–C^{Imid} bond in our case). Subsequent ultrafast internal conversion via S_0/S_1 CI results in the non-radiative deactivation of the excited twisted phototautomer. Since $\mathbf{L^{H,OH}}$ does not luminesce in solution and weakly luminesces in the solid state, we believe that this non-radiative deactivation is the predominant photophysical process for $\mathbf{L^{H,OH}}$, which is responsible for emission quenching. It should be noted that the precise geometry of the CI between the S_0 and S_1 states can only be optimized using ab initio methods such as CASSCF, CASPT2 or NEVPT2. However, our TDDFT optimization of the S_1 state leads to the oscillations around the CI geometry, which may serve as an indirect evidence of its existence. Figure 9b shows the geometry at the optimization step closest to the real CI geometry (with the lowest S_0-S_1 energy gap of only 2.2 kJ/mol; the dihedral angle between the proton-donating hydroxyphenyl and proton-accepting imidazole moieties reaches 85° at this geometry).

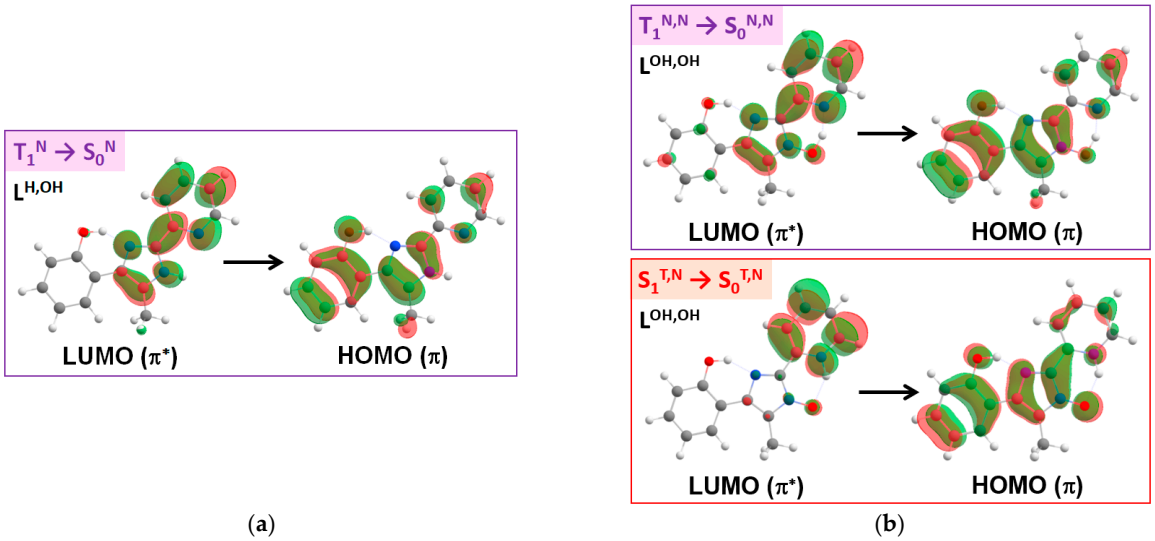

(**a**) (**b**)

Figure 8. Frontier molecular orbitals related to the emission processes observed for $\mathbf{L^{H,OH}}$ (**a**) and $\mathbf{L^{OH,OH}}$ (**b**).

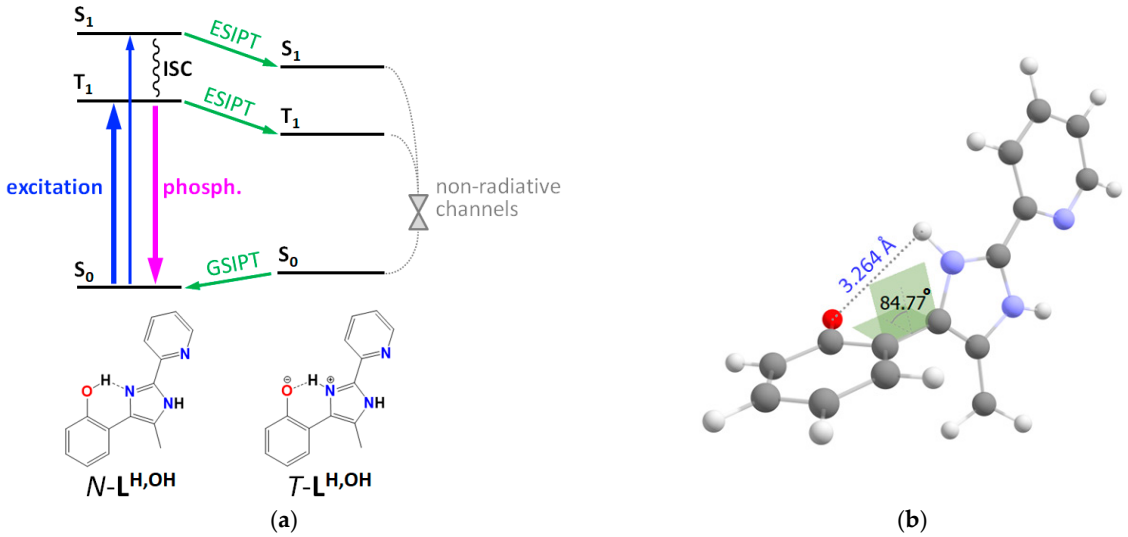

(**a**) (**b**)

Figure 9. (**a**) Photophysical and photochemical properties of $\mathbf{L^{H,OH}}$ in the solid state summarized in a simplified energy level diagram. ISC—intersystem crossing, phosph.—phosphorescence. (**b**) The geometry of $\mathbf{L^{H,OH}}$ that is close to the conical intersection between the S_0 and S_1 states.

$\mathbf{L^{OH,OH}}$ has two proton transfer sites and therefore provides more possible emission mechanisms than $\mathbf{L^{H,OH}}$. The PES of the T_1 state shows four energy minima: $T_1{}^{N,N}$ (O^{Ph}–H 1.008 Å, O^{Imid}–H 1.065 Å), $T_1{}^{T,N}$ (O^{Ph}–H 0.994 Å, O^{Imid}–H 1.931 Å), $T_1{}^{N,T}$ (O^{Ph}–H 1.829 Å, O^{Imid}–H 1.051 Å) and $T_1{}^{T,T}$ (O^{Ph}–H 1.807 Å, O^{Imid}–H 1.787 Å, Figure 4). The mechanisms of the population of the T_1 state for $\mathbf{L^{OH,OH}}$ are similar to those for $\mathbf{L^{H,OH}}$. Upon excitation with high energies ($S_0{}^{N,N} \rightarrow S_n{}^{N,N}$, where $n \geq 1$), the $S_1{}^{N,N}$ state can be reached, and the $T_1{}^{N,N}$ state can be populated from $S_1{}^{N,N}$ via $S_1{}^{N,N} \rightarrow T_1{}^{N,N}$ intersystem crossing. Upon excitation with lower energies, the $S_1{}^{N,N}$ state cannot be reached, and the $T_1{}^{N,N}$ state can be populated only via direct $S_0{}^{N,N} \rightarrow T_1{}^{N,N}$ excitation. In comparison with $S_0{}^{N,N}$, both hydrogen bonds become stronger in the $T_1{}^{N,N}$ energy minimum (O^{Ph}–H···N^{Imid}: 2.628 Å for $S_0{}^{N,N}$ vs. 2.546 Å for $T_1{}^{N,N}$; O^{Imid}–H···N^{Py}: 2.616 Å for $S_0{}^{N,N}$ vs. 2.509 Å for $T_1{}^{N,N}$). The computed $T_1{}^{N,N} \rightarrow S_0{}^{N,N}$ phosphorescence wavelength (586 nm) is in good agreement with the experimental emission maximum (546 nm). It corresponds to LUMO (π^*) → HOMO (π) transition of the *N*,*N*-$\mathbf{L^{OH,OH}}$ form, which is not related to ESIPT and has both protons at the oxygen atoms. Same as for $\mathbf{L^{H,OH}}$, this transition represents charge transfer from the pyridine heterocycle to the hydroxyphenyl moiety (Figure 8).

Three other minima on the T_1 state PES of $\mathbf{L^{OH,OH}}$, i.e., $T_1{}^{T,N}$, $T_1{}^{N,T}$ and $T_1{}^{T,T}$, are energetically more favorable than $T_1{}^{N,N}$ by *ca.* 58, 14 and 43 kJ/mol, respectively (Figure 4). However, these three minima do not lead to emission for the following reasons. Firstly, the population of the $T_1{}^{N,T}$ minimum after $S_0{}^{N,N} \rightarrow T_1{}^{N,N}$ excitation is kinetically restricted due to the high energy barrier between the $T_1{}^{N,N}$ and $T_1{}^{N,T}$ minima (*ca.* 14 kJ/mol). Secondly, although the energy barriers for the $T_1{}^{N,N} \rightarrow T_1{}^{T,N}$ and $T_1{}^{N,N} \rightarrow T_1{}^{T,T}$ ESIPT processes are significantly lower (*ca.* 1 kJ/mol), the calculated $T_1{}^{T,N} \rightarrow S_0{}^{T,N}$ and $T_1{}^{T,T} \rightarrow S_0{}^{T,T}$ phosphorescence wavelengths (959 and 1301 nm, respectively) are located in the infrared region and hugely overestimated compared with the experimental phosphorescence band. Owing to the fact that we do not observe luminescence in the infrared region, the molecules that populate the $T_1{}^{T,N}$ and $T_1{}^{T,T}$ minima most likely deactivate non-radiatively, for example via S_0/T_1 conical intersections. Thus, among four possible radiative deactivation channels in the triplet manifold associated with four energy minima, only one ($T_1{}^{N,N} \rightarrow S_0{}^{N,N}$) takes place according to the experimental data.

We did not plot the PES of the S_1 state for $\mathbf{L^{OH,OH}}$ because geometry optimizations of the S_1 state with almost all initial guess structures directly lead to the non-planar near-CI geometry and oscillate around it, proving that most of the molecules that are excited to the S_1 state deactivate non-radiatively through a conical intersection. A typical evolution of (i) the energy, (ii) dihedral angle θ between the planes of hydroxyphenyl and hydroxyimidazole parts and (iii) the S_0-S_1 energy gap during the geometry optimization is shown in Figure 10. Starting from the planar geometry with the O^{Ph}–H distance of 0.95 Å, this distance tends to increase during each optimization cycle. In parallel with the energy stabilization, the S_0-S_1 energy gap decreases during the optimization process. At the O^{Ph}–H distance of 1.75 Å, the dihedral angle θ starts to increase drastically and reaches 55° at the near-CI geometry with the S_0-S_1 energy gap of only 7.3 kJ/mol. After the 16th optimization cycle, the optimization process starts oscillating around this near-CI geometry.

However, there is one exemption to the above-mentioned trend of radiationless deactivation via CI for $\mathbf{L^{OH,OH}}$. The geometry of the *T*,*N*-$\mathbf{L^{OH,OH}}$ form can be successfully optimized in the S_1 state without falling into S_0/S_1 CI. The corresponding $S_1{}^{T,N} \rightarrow S_0{}^{T,N}$ transition ($\lambda_{calc.}$ = 731 nm, f = 0.0367) is in accordance with the position of the low-energy shoulder in the experimental luminescence spectrum of $\mathbf{L^{OH,OH}}$. This transition represents charge transfer from the π^*-orbital located on pyridine moiety (LUMO) to the π-orbital located on both hydroxyimidazole and hydroxyphenyl moieties (HOMO, Figure 8). Thus, short lifetimes of the excited states observed for $\mathbf{L^{OH,OH}}$ (τ = 2 ns and τ = 21 ns) are due to the $S_1{}^{T,N} \rightarrow S_0{}^{T,N}$ fluorescence. Now it becomes obvious that the same low-energy shoulder does not appear for $\mathbf{L^{H,OH}}$ due to the lack of the O^{Imid}–H···N^{Py} proton transfer site. Summing up, two major emission channels have been established for $\mathbf{L^{OH,OH}}$: (i) $T_1{}^{N,N} \rightarrow S_0{}^{N,N}$ phosphorescence of the *N*,*N*-$\mathbf{L^{OH,OH}}$ form related to the most intensive emission

band at 500–800 nm; and (ii) $S_1^{T,N} \rightarrow S_0^{T,N}$ fluorescence of the *T*,*N*-$\mathbf{L}^{OH,OH}$ form related to the low-energy shoulder at *ca.* 670 nm (Figure 11).

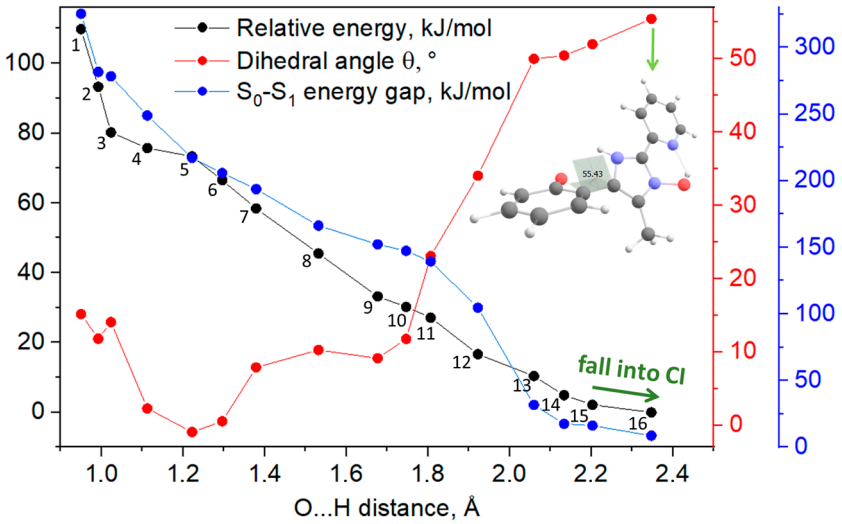

Figure 10. Evolution of energy, dihedral angle θ and the S_0-S_1 energy gap during the geometry optimization of the S_1 state for $\mathbf{L}^{OH,OH}$. The number of the optimization cycle is shown near the energy curve (black).

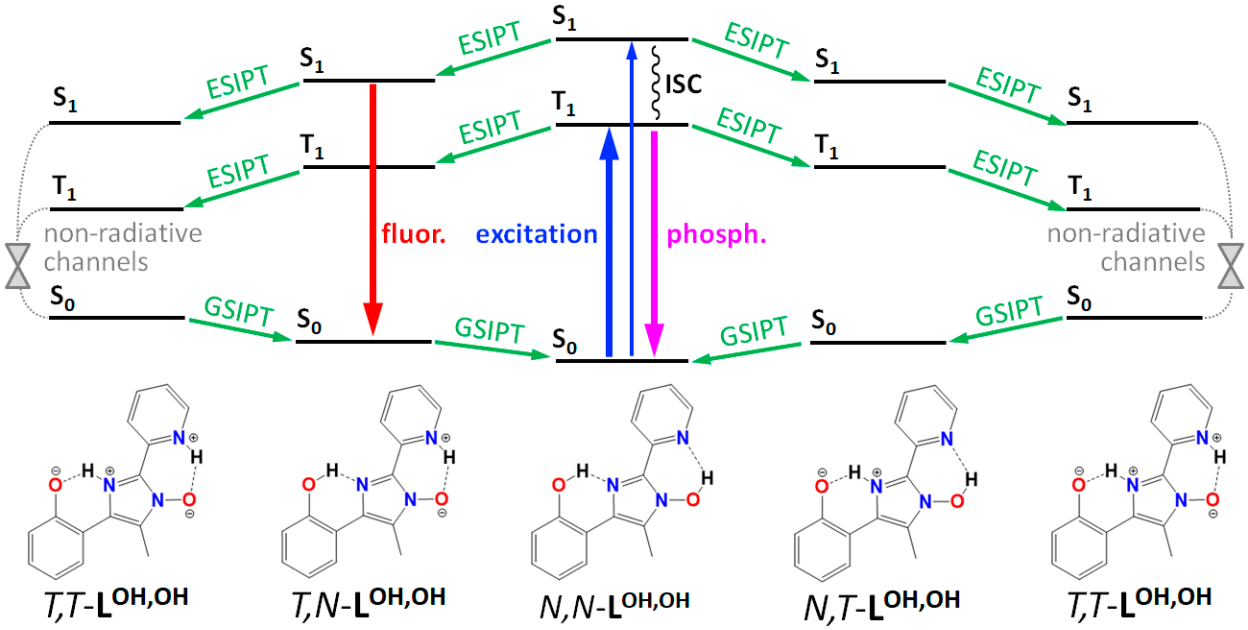

Figure 11. Photophysical and photochemical properties of $\mathbf{L}^{OH,OH}$ in the solid state summarized in a simplified energy level diagram. ISC—intersystem crossing, phosph.—phosphorescence; fluor.—fluorescence.

3. Materials and Methods

3.1. General Information

Elemental analysis was performed with a EuroEA3000 analyzer using standard technique. The IR spectra were recorded in KBr on a Bruker Vector-22 spectrometer. ^{1}H and ^{13}C NMR spectra were recorded on Bruker AV-400 (400.13 and 100.61 MHz) and Bruker DRX-500 (500.13 and 125.76 MHz) spectrometers using the residual signals of the solvent ($CDCl_3$) at 7.24 ppm for ^{1}H and 76.9 ppm for ^{13}C with respect to TMS as the internal stan-

dard. Corrected photoluminescence spectra were recorded on a Fluorolog 3 spectrometer (Horiba Jobin Yvon).

3.2. 1-(2-Benzoyloxyphenyl)-2-(Hydroxyimino)Propan-1-One (B)

A solution of isopropyl nitrite (0.74 g, 8.3 mmol) in methanol (5 mL) and then conc. HCl acid (1.4 mL) were added dropwise to a solution of 2-(benzyloxy)propiophenone (**A**) (synthesized according to the procedure reported in ref. [88]) (1.27 g, 5 mmol) in methanol (25 mL) under heating at 40 °C. The reaction mixture was stirred at 40–45 °C for 8 h, cooled and neutralized with a solution of $NaHCO_3$. After evaporation to remove methanol, the aqueous layer was extracted with $CHCl_3$ and dried over $MgSO_4$. After solvent removal under reduced pressure, the residue was purified by column chromatography (silica gel, $CHCl_3$) and then triturated with hexane to give the title product. Yield: 0.78 g (55%), m.p. 102–103 °C (100–101 °C [88]). Anal. Calc. for $C_{16}H_{13}NO_4$: C, 67.84; H, 4.62; N, 4.95. Found: C, 67.97; H, 4.62; N, 5.02%. ^{1}H NMR (400.13 MHz, $CDCl_3$) δ (ppm): 8.30 (s, 1H, OH), 8.08 (d, 2H, *J* = 7.4 Hz, H_{Ar}), 7.61 (t, 1H, *J* = 7.4 Hz, H_{Ar}), 7.57–7.52 (m, 2H, H_{Ar}), 7.47 (m, 2H, H_{Ar}), 7.33–7.27 (m, 2H, H_{Ar}), 1.97 (s, 3H, Me). ^{13}C NMR (125.76 MHz, $CDCl_3$) δ (ppm): 189.30, 164.61, 156.71, 148.41, 133.68, 132.04, 130.88, 130.05, 129.98, 128.68, 128.46, 125.53, 122.93, 8.95. IR (KBr, ν cm^{-1}): 3311, 1713 (C=O), 1670 (C=O), 1603, 1279, 1269, 1203, 1178, 1115, 1086, 1018, 906, 702, 656.

3.3. 1-Hydroxy-4-(2-Hydroxyphenyl)-5-Methyl-2-(Pyridin-2-yl)-1H-Imidazole ($\boldsymbol{L^{OH,OH}}$)

Conc. NH_4OH (19 mL) and pyridine-2-carboxaldehyde (0.44 g, 4.1 mmol) were added to a solution of 1-(2-benzoyloxyphenyl)-2-(hydroxyimino)propan-1-one (1.13 g, 4 mmol) in a mixture of 1,4-dioxane (16 mL) and EtOH (4 mL). The reaction mixture was stirred at room temperature for 3 days. After removing of the solvent, the residue was purified by column chromatography (silica gel, $CHCl_3$) and recrystallized from the hexane-ethylacetate mixture (10:1) to afford the title product. Yield: 0.91 g (85%), m.p. 121–122 °C. Anal. Calc. for $C_{15}H_{13}N_3O_2$: C, 67.40; H, 4.90; N, 15.72. Found: C, 67.45; H, 5.02; N, 15.81%. ^{1}H NMR (400.13 MHz, $CDCl_3$) δ (ppm): 13.02 (br. s, 1H, OH), 8.43 (ddd, 1H, *J* = 5.1, 1.5, 0.5 Hz, H_{Ar}), 7.99 (dt, 1H, *J* = 7.8, 1.3 Hz, H_{Ar}), 7.88 (dt, 1H, *J* = 7.8, 1.3 Hz, H_{Ar}), 7.50 (dd, 1H, *J* = 7.8, 1.3 Hz, H_{Ar}), 7.28 (ddd, 1H, *J* = 7.5, 5.1, 1.1 Hz, H_{Ar}), 7.16 (ddd, 1H, *J* = 8.1, 7.5, 1.5 Hz, H_{Ar}), 7.01 (dd, 1H, *J* = 8.1, 1.1 Hz, H_{Ar}), 6.88 (dt, 1H, *J* = 7.8, 1.3 Hz, H_{Ar}), 2.57 (s, 3H, Me). ^{13}C NMR (125.76 MHz, $CDCl_3$) δ (ppm): 156.40, 148.37, 145.61, 138.47, 132.56, 128.60, 127.77, 125.42, 122.48, 121.61, 119.42, 118.71, 117.79, 117.08, 9.19. IR (KBr, ν cm^{-1}): 1603, 1566, 1489, 1439, 1389, 1288, 1255, 1178, 1153, 1126, 1014, 773, 741, 652.

3.4. 4-(2-Hydroxyphenyl)-5-Methyl-2-(Pyridin-2-yl)-1H-Imidazole ($\boldsymbol{L^{H,OH}}$)

A mixture of 1-hydroxy-4-(2-hydroxyphenyl)-5-methyl-2-(pyridin-2-yl)-1*H*-imidazole ($\mathbf{L^{OH,OH}}$) (0.19 g, 0.71 mmol), chloroacetone (0.066 g, 0.71 mmol) and dried K_2CO_3 (0.11 g, 0.8 mmol) in dried dimethylformamide (6 mL) was stirred at room temperature for 1 h and then at 40–45 °C for 4 h. After cooling the reaction mixture was diluted with water, the residue formed was filtered, washed with water, dried and purified by column chromatography (silica gel, $CHCl_3$). The recrystallization of the residue from EtOH afforded $\mathbf{L^{H,OH}}$. Yield: 0.16 g (89%), m.p. 202–203 °C. Anal. Calc. for $C_{15}H_{13}N_3O$: C, 71.70; H, 5.21; N, 16.72. Found: C, 71.62; H, 5.34; N, 16.65%. ^{1}H NMR (400.13 MHz, $CDCl_3$) δ (ppm): 12.38 (s, 1H, NH), 11.04 (br. s, 1H, OH), 8.51 (ddd, 1H, *J* = 5.1, 1.3, 0.5 Hz, H_{Ar}), 8.07 (dt, 1H, *J* = 8.0, 1.2 Hz, H_{Ar}), 7.79 (dt, 1H, *J* = 7.8, 1.2 Hz, H_{Ar}), 7.47 (dd, 1H, *J* = 7.8, 1.2 Hz, H_{Ar}), 7.25 (ddd, 1H, *J* = 7.5, 5.1, 1.2 Hz, H_{Ar}), 7.17 (ddd, 1H, *J* = 8.0, 7.5, 1.4 Hz, H_{Ar}), 7.03 (dd, 1H, *J* = 7.8, 1.4 Hz, H_{Ar}), 6.88 (dt, 1H, *J* = 7.5, 1.3 Hz, H_{Ar}), 2.53 (s, 3H, Me). ^{13}C NMR (100.61 MHz, $CDCl_3$) δ (ppm): 156.38, 148.64, 147.49, 141.49, 137.62, 136.87, 127.97, 125.68, 124.42, 123.37, 120.15, 118.91, 118.30, 117.25, 12.47. IR (KBr, ν cm^{-1}): 3311, 1597, 1578, 1443, 1400, 1286, 1244, 1134, 999, 825, 783, 756, 742, 700.

3.5. X-ray Crystallography

Diffraction data for single-crystal $\mathbf{L^{OH,OH}}$ were obtained at 291 K on an automated four-circle Agilent Xcalibur diffractometer equipped with an area AtlasS2 detector (graphite monochromator, λ(MoKα) = 0.71073 Å, ω-scans with a step 0.25°). Integration, absorption correction, and determination of unit cell parameters were performed using the CrysAlisPro program package [100]. The structure was solved by dual space algorithm (SHELXT [101]) and refined by the full-matrix least squares technique (SHELXL [102]) in the anisotropic approximation (except hydrogen atoms). Positions of hydrogen atoms were calculated geometrically and refined in the riding model. The crystallographic data and details of the structure refinements are summarized in Supplementary Materials (Table S1). CCDC 2237906 contains the supplementary crystallographic data for this paper. These data can be obtained free of charge from The Cambridge Crystallographic Data Center at http://www.ccdc.cam.ac.uk/structures/ (accessed on 26 January 2023).

3.6. Computational Details

The quantum chemical calculations presented in this study were conducted using density functional theory (DFT), time-dependent DFT (TDDFT) and Tamm–Dancoff approximated DFT (TDADFT) methods in Gaussian 16 software package [103]. We used the hybrid exchange-correlation functional PBE0 [104] since our previous studies demonstrated its satisfying performance in modeling photophysical and photochemical properties of organic ESIPT-emitters [83,85]. Compared with probably the best known hybrid functional B3LYP, PBE0 provides absorption energies that are closer to the experimental data, while B3LYP tends to red-shift some vertical absorptions for $\mathbf{L^{H,OH}}$ and $\mathbf{L^{OH,OH}}$ (Supplementary Materials, Figures S12 and S13). The 6–31 + G(d) basis set was used for all atoms [105–109]. Absorption spectra were calculated on ground state geometries using TDDFT. Singlet excited state geometries (S_1) as well as S_1-S_0 fluorescence energies were also determined using the TDDFT approach. The optimizations of the lowest triplet excited state (T_1) geometries of $\mathbf{L^{H,OH}}$ and $\mathbf{L^{OH,OH}}$ were carried out by an unrestricted DFT (uDFT) method. Subsequent single-point TDADFT computations on T_1 optimized geometries revealed T_1-S_0 phosphorescence energies. The use of TDADFT rather than TDDFT in the latter case is justified by the fact that the Tamm–Dancoff approximation tends to strongly correct the computed triplet state energies comparatively to TDDFT. Relaxed T_1 state geometries can also be obtained using TDDFT or TDADFT approaches; however, the uDFT method is more preferable because it requires much less computational cost. In the case of absorption spectra, the solvent effects of acetonitrile molecules were considered by the polarizable continuum model (PCM), and all other computations were performed in the gas phase. The D3 version of Grimme's dispersion with Becke–Johnson damping was employed for each calculation. Potential energy curves (PECs) and surfaces (PESes) of the desired states (S_0, S_1, T_1) along the proton transfer reaction were plotted by scanning the O...H bond distance between 0.95 and 2.00 Å with a step of 0.05 Å. All frequencies in the harmonic approximation for the calculated global minimum energy geometries were positive, confirming that the optimized molecular geometries correspond to the real minima on the potential energy surfaces. The atomic coordinates of all optimized geometries are given in Supplementary Materials (Tables S3–S16). The geometries and molecular orbitals were visualized using ChemCraft software [110].

4. Conclusions

In this work we presented the synthesis of imidazole-based ESIPT-capable compounds, 1-hydroxy-4-(2-hydroxyphenyl)-5-methyl-2-(pyridin-2-yl)-1*H*-imidazole ($\mathbf{L^{OH,OH}}$) and 4-(2-hydroxyphenyl)-5-methyl-2-(pyridin-2-yl)-1*H*-imidazole ($\mathbf{L^{H,OH}}$). In the $\mathbf{L^{OH,OH}}$ trinuclear molecule, the central moiety, i.e., the 1-hydroxy-1*H*-imidazole one, is decorated with the proton-donating and proton-accepting peripheral groups and, therefore, under photoexcitation can act both as a proton acceptor and a proton donor in the ESIPT reactions. Importantly, we found a convenient synthetic pathway for the conversion of 1-hydroxy-4-

(2-hydroxyphenyl)-1*H*-imidazoles to 4-(2-hydroxyphenyl)-1*H*-imidazoles. This synthetic pathway is based on the reaction of the 1-hydroxy-4-(2-hydroxyphenyl)-1*H*-imidazole derivative with chloroacetone. Despite chloroacetone being known to interact with phenolic hydroxy groups, in our case the reaction proceeded selectively with the imidazolic hydroxy group only, leaving the phenolic hydroxy group unaffected. Thus, this reaction has high synthetic potential for selective reduction of 1-hydroxy-1*H*-imidazoles decorated with hydroxyphenyl groups to corresponding 1*H*-imidazoles.

A slight structural difference between these two compounds leads to significant changes in their photoluminescence response. $\mathbf{L^{H,OH}}$ emits in the light green region, while $\mathbf{L^{OH,OH}}$ luminesces in the orange region. According to our computations, both emitters share the same emission mechanism, i.e., phosphorescence of the normal form of the molecule (${T_1}^N \rightarrow {S_0}^N$ for the *N*-$\mathbf{L^{H,OH}}$ form and ${T_1}^{N,N} \rightarrow {S_0}^{N,N}$ for the *N*,*N*-$\mathbf{L^{OH,OH}}$ form), which is not related to ESIPT. After the ESIPT process, both compounds can decay non-radiatively through S_0/S_1 and S_0/T_1 conical intersections, which explains their low photoluminescence quantum yield. The phosphorescence band is the most intensive for both compounds. However, $\mathbf{L^{OH,OH}}$ also exhibits fluorescence of the *T*,*N*-$\mathbf{L^{OH,OH}}$ form, ${S_1}^{T,N} \rightarrow {S_0}^{T,N}$, with one proton transferred from the hydroxyimidazole moiety to the pyridine moiety. This fluorescence mechanism is responsible for the appearance of the low-energy shoulder in the emission spectrum of $\mathbf{L^{OH,OH}}$. Thus, owing to the presence of two proton transfer sites, $\mathbf{L^{OH,OH}}$ appears to be a rare example of ESIPT-emitters that exhibit fluorescence and phosphorescence simultaneously.

Supplementary Materials: The following supporting information can be downloaded at: https://www.mdpi.com/article/10.3390/molecules28041793/s1, Tables S1–S16 and Figures S1–S15: characterization data and quantum chemical calculations data.

Author Contributions: Conceptualization, A.Y.T., N.A.S. and M.B.B.; methodology, E.B.N., A.Y.T. and N.A.S.; formal analysis, E.B.N., N.A.S. and D.G.S.; investigation, E.B.N., N.A.S., D.G.S. and A.A.R.; writing—original draft preparation, N.A.S., E.B.N., A.Y.T. and M.B.B.; writing—review and editing, N.A.S., E.B.N., A.Y.T. and M.B.B.; visualization, N.A.S.; supervision, M.B.B.; project administration, M.B.B.; funding acquisition, M.B.B. All authors have read and agreed to the published version of the manuscript.

Funding: The synthesis of the ESIPT-capable compounds $\mathbf{L^{OH,OH}}$ and $\mathbf{L^{H,OH}}$, the study of the ESIPT reactions and the emission properties of $\mathbf{L^{OH,OH}}$ and $\mathbf{L^{H,OH}}$ and the interpretation of the experimental and theoretical results were funded by the Russian Science Foundation (grant № 21-13-00216, https://rscf.ru/en/project/21-13-00216/ (accessed on 26 January 2023) and performed at the Nikolaev Institute of Inorganic Chemistry.

Institutional Review Board Statement: Not applicable.

Informed Consent Statement: Not applicable.

Data Availability Statement: Data will be made available on request.

Acknowledgments: The elemental analysis data, X-ray single crystal data, the ^{1}H NMR, ^{13}C NMR, IR and UV-vis spectra were obtained using the equipment of the Multi-Access Chemical Research Centre SB RAS at the N. N. Vorozhtsov Novosibirsk Institute of Organic Chemistry and the Nikolaev Institute of Inorganic Chemistry with the financial support from the Ministry of Science and Higher Education of the Russian Federation. N.A.S. is grateful to the Foundation for the Advancement of Theoretical Physics and Mathematics "BASIS". The Siberian Branch of the Russian Academy of Sciences (SB RAS) Siberian Supercomputer Centre is gratefully acknowledged for providing supercomputer facilities. M.B.B. acknowledges the access to the Computational Centre of Novosibirsk State University.

Conflicts of Interest: The authors declare no conflict of interest.

Sample Availability: Samples of the compounds are available from the authors.

References

1. Weller, A. Über die Fluoreszenz der Salizylsäure und verwandter Verbindungen. *Naturwissenschaften* **1955**, *42*, 175–176. [CrossRef]
2. Nagaoka, S.; Nagashima, U. Intramolecular proton transfer in various electronic states of o-hydroxybenzaldehyde. *Chem. Phys.* **1989**, *136*, 153–163. [CrossRef]
3. Douhal, A.; Lahmani, F.; Zewail, A.H. Proton-transfer reaction dynamics. *Chem. Phys.* **1996**, *207*, 477–498. [CrossRef]
4. Formosinho, S.J.; Arnaut, L.G. Excited-state proton transfer reactions II. Intramolecular reactions. *J. Photochem. Photobiol. A* **1993**, *75*, 21–48. [CrossRef]
5. Chou, P.-T. The Host/Guest Type of Excited-State Proton Transfer; a General Review. *J. Chin. Chem. Soc.* **2001**, *48*, 651–682. [CrossRef]
6. Chipem, F.A.S.; Mishra, A.; Krishnamoorthy, G. The role of hydrogen bonding in excited state intramolecular charge transfer. *Phys. Chem. Chem. Phys.* **2012**, *14*, 8775–8790. [CrossRef]
7. Joshi, H.C.; Antonov, L. Excited-State Intramolecular Proton Transfer: A Short Introductory Review. *Molecules* **2021**, *26*, 1475. [CrossRef]
8. Dong, H.; Yang, H.; Zhao, J.; Liu, X.; Zheng, Y. Modulation of excited state proton transfer. *J. Lumin.* **2021**, *231*, 117840. [CrossRef]
9. Padalkar, V.S.; Seki, S. Excited-state intramolecular proton-transfer (ESIPT)-inspired solid state emitters. *Chem. Soc. Rev.* **2016**, *45*, 169–202. [CrossRef] [PubMed]
10. Zhao, J.; Ji, S.; Chen, Y.; Guo, H.; Yang, P. Excited state intramolecular proton transfer (ESIPT): From principal photophysics to the development of new chromophores and applications in fluorescent molecular probes and luminescent materials. *Phys. Chem. Chem. Phys.* **2012**, *14*, 8803–8817. [CrossRef] [PubMed]
11. Tomin, V.I.; Demchenko, A.P.; Chou, P.-T. Thermodynamic vs. kinetic control of excited-state proton transfer reactions. *J. Photochem. Photobiol. C Photochem. Rev.* **2015**, *22*, 1–18. [CrossRef]
12. Serdiuk, I.E.; Roshal, A.D. Exploring double proton transfer: A review on photochemical features of compounds with two proton-transfer sites. *Dye. Pigment.* **2017**, *138*, 223–244. [CrossRef]
13. Gayathri, P.; Pannipara, M.; Al-Sehemi, A.G.; Anthony, S.P. Recent advances in excited state intramolecular proton transfer mechanism-based solid state fluorescent materials and stimuli-responsive fluorescence switching. *CrystEngComm* **2021**, *23*, 3771–3789. [CrossRef]
14. Kwon, J.E.; Park, S.Y. Advanced Organic Optoelectronic Materials: Harnessing Excited-State Intramolecular Proton Transfer (ESIPT) Process. *Adv. Mater.* **2011**, *23*, 3615–3642. [CrossRef]
15. Liang, X.; Zhang, Z.; Fang, H. Different positions of cyano substitution controlled directionality of ESIPT processes with two asymmetric proton acceptors system: A TD-DFT study. *J. Photochem. Photobiol. A* **2023**, *436*, 114353. [CrossRef]
16. Lin, M.-Y.; Li, Y.; Fu, C.-B.; Yu, X.-F. Modulating the ESIPT dynamics of 3HF derivatives via substitution and solvent effect: A theoretical study. *J. Mol. Liq.* **2022**, *366*, 120295. [CrossRef]
17. Shang, C.; Sun, C. Substituent effects on photophysical properties of ESIPT-based fluorophores bearing the 4-diethylaminosalicylaldehyde core. *J. Mol. Liq.* **2022**, *367*, 120477. [CrossRef]
18. Chaihan, K.; Semakul, N.; Promarak, V.; Bui, T.-T.; Kungwan, N.; Goubard, F. Tunable far-red fluorescence utilizing π-extension and substitution on the excited state intramolecular proton transfer (ESIPT) of naphthalene-based Schiff bases: A combined experimental and theoretical study. *J. Photochem. Photobiol. A* **2022**, *431*, 114047. [CrossRef]
19. Su, S.; Sun, G.; Liang, X.; Fang, H. Effectively controlling the ESIPT behavior and fluorescence feature of 2-(2′-hydroxyphenyl)-4-chloromethylthiazole by changing its π-conjugation: A theoretical exploration. *J. Photochem. Photobiol. A* **2022**, *422*, 113548. [CrossRef]
20. Li, Y.; Dahal, D.; Abeywickrama, C.S.; Pang, Y. Progress in Tuning Emission of the Excited-State Intramolecular Proton Transfer (ESIPT)-Based Fluorescent Probes. *ACS Omega* **2021**, *6*, 6547–6553. [CrossRef]
21. Heyer, E.; Benelhadj, K.; Budzák, S.; Jacquemin, D.; Massue, J.; Ulrich, G. On the Fine-Tuning of the Excited-State Intramolecular Proton Transfer (ESIPT) Process in 2-(2′-Hydroxybenzofuran)benzazole (HBBX) Dyes. *Chem. Eur. J.* **2017**, *23*, 7324–7336. [CrossRef]
22. Liang, X.; Fang, H. Fine-tuning directionality of ESIPT behavior of the asymmetric two proton acceptor system via atomic electronegativity. *Spectrochim. Acta Part A Mol. Biomol. Spectrosc.* **2022**, *266*, 120406. [CrossRef] [PubMed]
23. Huang, Q.; Guo, Q.; Lan, J.; You, J. Tuning the dual emission of keto/enol forms of excited-state intramolecular proton transfer (ESIPT) emitters via intramolecular charge transfer (ICT). *Dyes Pigment.* **2021**, *193*, 109497. [CrossRef]
24. Massue, J.; Jacquemin, D.; Ulrich, G. Molecular Engineering of Excited-state Intramolecular Proton Transfer (ESIPT) Dual and Triple Emitters. *Chem. Lett.* **2018**, *47*, 1083–1089. [CrossRef]
25. Shang, C.; Wang, L.; Cao, Y.; Yu, X.; Li, Y.; Sun, C.; Cui, J. Is it possible to switch ESIPT-channel of hydroxyanthraquinones with the strategy of modifying electronic groups? *J. Mol. Liq.* **2022**, *347*, 118343. [CrossRef]
26. Pariat, T.; Munch, M.; Durko-Maciag, M.; Mysliwiec, J.; Retailleau, P.; Vérité, P.M.; Jacquemin, D.; Massue, J.; Ulrich, G. Impact of Heteroatom Substitution on Dual-State Emissive Rigidified 2-(2′-hydroxyphenyl)benzazole Dyes: Towards Ultra-Bright ESIPT Fluorophores. *Chem. Eur. J.* **2021**, *27*, 3483–3495. [CrossRef] [PubMed]
27. Khisamov, R.M.; Ryadun, A.A.; Sukhikh, T.S.; Konchenko, S.N. Excitation wavelength-dependent room-temperature phosphorescence: Unusual properties of novel phosphinoamines. *Mol. Syst. Des. Eng.* **2021**, *6*, 1056–1065. [CrossRef]

28. Kim, D.; Ahn, M.; Wee, K.-R.; Cho, D.W. Influence of picolinate ancillary ligands on unique photophysical properties of $Ir(ppz)_2(LX)$. *Phys. Chem. Chem. Phys.* **2022**, *24*, 13074–13082. [CrossRef]
29. Kim, S.; Choi, J.; Cho, D.W.; Ahn, M.; Eom, S.; Kim, J.; Wee, K.-R.; Ihee, H. Solvent-modulated proton-coupled electron transfer in an iridium complex with an ESIPT ligand. *Chem. Sci.* **2022**, *13*, 3809–3818. [CrossRef]
30. Fu, P.-Y.; Li, B.-N.; Zhang, Q.-S.; Mo, J.-T.; Wang, S.-C.; Pan, M.; Su, C.-Y. Thermally Activated Fluorescence vs Long Persistent Luminescence in ESIPT-Attributed Coordination Polymer. *J. Am. Chem. Soc.* **2022**, *144*, 2726–2734. [CrossRef]
31. Feng, W.; Fu, G.; Huang, Y.; Zhao, Y.; Yan, H.; Lü, X. ESIPT-capable Eu^{3+}-metallopolymer with colour-tunable emission for selective visual sensing of Zn^{2+} ion. *J. Mater. Chem. C* **2022**, *10*, 1090–1096. [CrossRef]
32. Huang, P.; Liu, Y.; Karmakar, A.; Yang, Q.; Li, J.; Wu, F.-Y.; Deng, K.-Y. Tuning the excited-state intramolecular proton transfer (ESIPT)-based luminescence of metal–organic frameworks by metal nodes toward versatile photoluminescent applications. *Dalton Trans.* **2021**, *50*, 6901–6912. [CrossRef] [PubMed]
33. Shekhovtsov, N.A.; Bushuev, M.B. Anomalous emission of an ESIPT-capable zinc(II) complex: An interplay of TADF, TICT and anti-Kasha behaviour. *J. Photochem. Photobiol. A* **2022**, *433*, 114195. [CrossRef]
34. Suzuki, N.; Kubota, T.; Ando, N.; Yamaguchi, S. Photobase-Driven Excited-State Intramolecular Proton Transfer (ESIPT) in a Strapped π-Electron System. *Chem. Eur. J.* **2022**, *28*, e202103584. [CrossRef]
35. Pariat, T.; Stoerkler, T.; Diguet, C.; Laurent, A.D.; Jacquemin, D.; Ulrich, G.; Massue, J. Dual Solution-/Solid-State Emissive Excited-State Intramolecular Proton Transfer (ESIPT) Dyes: A Combined Experimental and Theoretical Approach. *J. Org. Chem.* **2021**, *86*, 17606–17619. [CrossRef] [PubMed]
36. Voicescu, M. On the role of pH and temperature on ground- and excited- state proton transfer of hydroxyflavones in lipidic bilayers of lecithin. *J. Mol. Liq.* **2022**, *352*, 118696. [CrossRef]
37. Chowdhury, A.; Dasgupta, S.; Datta, A. Deprotonation-induced enhancement in fluorescence of 2-((2-hydroxybenzylidene)amino)phenol, a Schiff base. *Chem. Phys. Impact* **2021**, *3*, 100057. [CrossRef]
38. Berezin, A.S.; Selivanov, B.; Danilenko, A.; Sukhikh, A.; Komarovskikh, A. Manganese(II) Bromide Compound with Diprotonated 1-Hydroxy-2-(pyridin-2-yl)-4,5,6,7-tetrahydrobenzimidazole: Dual Emission and the Effect of Proton Transfers. *Inorganics* **2022**, *10*, 245. [CrossRef]
39. Komarovskikh, A.; Danilenko, A.; Sukhikh, A.; Syrokvashin, M.; Selivanov, B. Structure and EPR investigation of Cu(II) bifluoride complexes with zwitterionic N-hydroxyimidazole ligands. *Inorg. Chim. Acta* **2020**, *517*, 120187. [CrossRef]
40. Bushuev, M.B.; Selivanov, B.A.; Pervukhina, N.V.; Naumov, D.Y.; Rakhmanova, M.I.; Sheludyakova, L.A.; Tikhonov, A.Y.; Larionov, S.V. Luminescent zinc(II) and cadmium(II) complexes based on 2-(4,5-dimethyl-1*H*-imidazol-2-yl)pyridine and 2-(1-hydroxy-4,5-dimethyl-1*H*-imidazol-2-yl)pyridine. *Russ. J. Gen. Chem.* **2012**, *82*, 1859–1868. [CrossRef]
41. Bushuev, M.B.; Selivanov, B.A.; Pervukhina, N.V.; Naumov, D.Y.; Sheludyakova, L.A.; Rakhmanova, M.I.; Tikhonov, A.Y.; Larionov, S.V. Zinc(II) complexes with an imidazolylpyridine ligand: Luminescence and hydrogen bonding. *J. Coord. Chem.* **2014**, *67*, 611–622. [CrossRef]
42. Liang, C. Organic polymorphs based on an AEE-active tetraphenylethene salicylaldehyde Schiff-base derivative: The effect of molecular conformation on luminescence properties. *RSC Adv.* **2020**, *10*, 29043–29050. [CrossRef] [PubMed]
43. Luo, M.; Liu, Y.; Zhao, J.; Jiang, L.; Chen, X.; Li, W.; Yang, Z.; Yan, Q.; Wang, S.; Chi, Z. Magic tetraphenylethene Schiff base derivatives with AIE, liquid crystalline and photochromic properties. *Dyes Pigment.* **2022**, *202*, 110222. [CrossRef]
44. Ila; Brahma, M.; Ranjan, S.; Tripathi, P.; Krishnamoorthy, G. Modifying the proton transfer of 3,5-bis(2-hydroxyphenyl)-1*H*-1,2,4-triazole by water, confinement and confined water. *Spectrochim. Acta A Mol. Biomol. Spectrosc.* **2022**, *272*, 120911. [CrossRef]
45. Kaya, S.; Aydın, H.G.; Keskin, S.; Ekmekci, Z.; Menges, N. Exploring of indole derivatives for ESIPT emission: A new ESIPT-based fluorescence skeleton and TD-DFT calculations. *J. Photochem. Photobiol. A Chem.* **2021**, *420*, 113487. [CrossRef]
46. Zhao, G.; Shia, W.; Xin, X.; Ma, F.; Li, Y. Solvent dependence of ESIPT process in 2-(2-carbonmethoxy-3,4-dichloro-6-hydroxyphenyl) compounds. *J. Mol. Liq.* **2022**, *354*, 118807. [CrossRef]
47. Dutta, S.; Manda, D. Excited state intramolecular proton transfer of 2-phenyl,3-hydroxybenzo[g]quinolones in solution and in G4 supramolecular hydrogels. *J. Mol. Liq.* **2022**, *361*, 119651. [CrossRef]
48. Dutta, S.; Basu, N.; Mandal, D. ESIPT in a binary mixture of non-polar and protic polar solvents: Role of solvation dynamics. *J. Photochem. Photobiol. A Chem.* **2023**, *435*, 114240. [CrossRef]
49. Sedgwick, A.C.; Wu, L.; Han, H.-H.; Bull, S.D.; He, X.-P.; James, T.D.; Sessler, J.L.; Tang, B.Z.; Tian, H.; Yoon, J. Excited-state intramolecular proton-transfer (ESIPT) based fluorescence sensors and imaging agents. *Chem. Soc. Rev.* **2018**, *47*, 8842–8880. [CrossRef]
50. Zhang, Q.; Yang, Y.; Liu, Y. Recognition mechanism of imidazo[1,5-α]pyridine-based fluorescence probe towards thiophenols with multi-mechanisms of PET and ESIPT. *J. Photochem. Photobiol. A Chem.* **2023**, *437*, 114477. [CrossRef]
51. Lu, X.-L.; He, W. Research Advances in Excited State Intramolecular Proton Transfer Fluorescent Probes Based on Combined Fluorescence Mechanism. *Chin. J. Anal. Chem.* **2021**, *49*, 184–196. [CrossRef]
52. Choudhury, S.D.; Pal, H. Excited State Proton Transfer of a Versatile Fluorescent Probe in Different Reverse Micelles: An Overview. *Proc. Indian Natl. Sci. Acad.* **2019**, *85*, 507–516. [CrossRef]
53. Chen, L.; Fu, P.-Y.; Wang, H.-P.; Pan, M. Excited-State Intramolecular Proton Transfer (ESIPT) for Optical Sensing in Solid State. *Adv. Opt. Mater.* **2021**, *9*, 2001952. [CrossRef]

54. Zheng, H.-W.; Kang, Y.; Wu, M.; Liang, Q.-F.; Zheng, J.-Q.; Zheng, X.-J.; Jin, L.-P. ESIPT-AIE active Schiff base based on 2-(2′-hydroxyphenyl)benzo-thiazole applied as multi-functional fluorescent chemosensors. *Dalton Trans.* **2021**, *50*, 3916–3922. [CrossRef] [PubMed]
55. Majeed, S.; Khan, T.A.; Waseem, M.T.; Junaid, H.M.; Khan, A.M.; Shahzad, S.A. A ratiometric fluorescent, colorimetric, and paper sensor for sequential detection of Cu^{2+} and glutathione in food: AIEE and reversible piezofluorochromic activity. *J. Photochem. Photobiol. A Chem.* **2022**, *431*, 114062. [CrossRef]
56. Santhiya, K.; Mathivanan, M.; Tharmalingam, B.; Anitha, O.; Ghorai, S.; Natarajan, R.; Murugesapandian, B. A new *J*-(diethylamino)coumarin and 4-(diethylamino)phenol appended unsymmetrical thiocarbohydrazone: Detection of moisture in organic solvent and sequential fluorimetric detection of Cu^{2+} ions and cysteine. *J. Photochem. Photobiol. A Chem.* **2022**, *432*, 114105. [CrossRef]
57. Chan, N.N.M.Y.; Idris, A.; Abidin, Z.H.Z.; Tajuddin, H.A.; Abdullah, Z. White light employing luminescent engineered large (mega) Stokes shift molecules: A review. *RSC Adv.* **2021**, *11*, 13409–13445. [CrossRef]
58. Doroshenko, A.O. Physicochemical Principles of the Creation of Highly Efficient Organic Luminophores with Anomalously High Stokes' Shifts. *Theor. Exp. Chem.* **2002**, *38*, 135–155. [CrossRef]
59. Stoerkler, T.; Pariat, T.; Laurent, A.D.; Jacquemin, D.; Ulrich, G.; Massue, J. Excited-State Intramolecular Proton Transfer Dyes with Dual-State Emission Properties: Concept, Examples and Applications. *Molecules* **2022**, *27*, 2443. [CrossRef]
60. Behera, S.K.; Park, S.Y.; Gierschner, J. Dual Emission: Classes, Mechanisms, and Conditions. *Angew. Chem. Int. Ed.* **2021**, *60*, 22624–22638. [CrossRef]
61. Azarias, C.; Budzák, Š.; Laurent, A.D.; Ulrich, G.; Jacquemin, D. Tuning ESIPT fluorophores into dual emitters. *Chem. Sci.* **2016**, *7*, 3763–3774. [CrossRef] [PubMed]
62. Shekhovtsov, N.A.; Bushuev, M.B. Enol or keto? Interplay between solvents and substituents as a factor controlling ESIPT. *J. Mol. Liq.* **2022**, *361*, 119611. [CrossRef]
63. Pandey, D.; Vennapusa, S.R. ESIPT pathways and optical properties of 7-Hydroxy-1-Indanones. *J. Photochem. Photobiol. A Chem.* **2022**, *432*, 114073. [CrossRef]
64. Sathyanarayana, R.; Kumar, V.; Pujar, G.; Poojary, B.; Shankar, M.K.; Yallappa, S. Hydroxy-benzimidazoles as blue-green emitters: Synthesis, structural and DFT studies. *J. Photochem. Photobiol. A Chem.* **2020**, *401*, 112751. [CrossRef]
65. Esteves, C.I.C.; Fontes, L.F.B.; Borges, A.F.N.; Rocha, J.; Silva, A.M.S.; Guieu, S. Push-pulling induces the excited-state intramolecular proton transfer in 2′-aminochalcones. *Dyes Pigment.* **2022**, *202*, 110275. [CrossRef]
66. Tang, Z.; Han, H.; Ding, J.; Zhou, P. Dual fluorescence of 2-(2′-hydroxyphenyl) benzoxazole derivatives via the branched decays from the upper excited-state. *Phys. Chem. Chem. Phys.* **2021**, *23*, 27304–27311. [CrossRef] [PubMed]
67. Wang, D.; Shao, T.-F.; Ding, W.-H.; Li, S.-J.; Yao, Q.; Cao, W.; Wang, Z.; Ma, Y. AIE -active TPA modified Schiff base for successive sensing of Cu^{2+} and His via an on–off–on method and its application in bioimaging. *Dalton Trans.* **2023**, *52*, 434–443. [CrossRef]
68. Trannoy, V.; Léaustic, A.; Gadan, S.; Guillot, R.; Allain, C.; Clavier, G.; Mazerat, S.; Geffroy, B.; Yu, P. A highly efficient solution and solid state ESIPT fluorophore and its OLED application. *New J. Chem.* **2021**, *45*, 3014–3021. [CrossRef]
69. Singh, A.K.; Kundu, M.; Roy, S.; Roy, B.; Shah, S.S.; Nair, A.V.; Pal, B.; Mondal, M.; Singh, N.D.P. A two-photon responsive naphthyl tagged p-hydroxyphenacyl based drug delivery system: Uncaging of anti-cancer drug in the phototherapeutic window with real-time monitoring. *Chem. Commun.* **2020**, *56*, 9986–9989. [CrossRef]
70. Mishra, V.R.; Ghanavatkar, C.W.; Sekar, N. Towards NIR-Active Hydroxybenzazole (HBX)-Based ESIPT Motifs: A Recent Research Trend. *ChemistrySelect* **2020**, *5*, 2103–2113. [CrossRef]
71. Fery-Forgues, S.; Vanucci-Bacqué, C. Recent Trends in the Design, Synthesis, Spectroscopic Behavior, and Applications of Benzazole-Based Molecules with Solid-State Luminescence Enhancement Properties. *Top. Curr. Chem.* **2021**, *379*, 32. [CrossRef] [PubMed]
72. Jeżewski, A.; Hammann, T.; Cywiński, P.J.; Gryko, D.T. Optical Behavior of Substituted 4-(2′-Hydroxyphenyl)imidazoles. *J. Phys. Chem. B* **2015**, *119*, 2507–2514. [CrossRef] [PubMed]
73. Douhal, A.; Amat-Guerri, F.; Lillo, M.P.; Acuña, A.U. Proton transfer spectroscopy of 2-(2′-hydroxyphenyl)imidazole and 2-(2′-hydroxyphenyl)benzimidazole dyes. *J. Photochem. Photobiol. A* **1994**, *78*, 127–138. [CrossRef]
74. Das, K.; Sarkar, N.; Majumdar, D.; Bhattacharyya, K. Excited-state intramolecular proton transfer and rotamerism of 2-(2′-hydroxyphenyl) benzimidazole. *Chem. Phys. Lett.* **1992**, *198*, 443–448. [CrossRef]
75. Das, K.; Sarkar, N.; Ghosh, A.K.; Majumdar, D.; Nath, D.N.; Bhattacharyya, K. Excited-State Intramolecular Proton Transfer in 2-(2-Hydroxyphenyl)benzimidazole and -benzoxazole: Effect of Rotamerism and Hydrogen Bonding. *J. Phys. Chem.* **1994**, *98*, 9126–9132. [CrossRef]
76. Gutiérrez, M.; García, E.; Monterde, C.; Sánchez, F.; Douhal, A. Modulating the spectroscopy and dynamics of a proton-transfer dye by functionalizing with phenyl groups. *Phys. Chem. Chem. Phys.* **2022**, *24*, 6828–6835. [CrossRef]
77. Hurley, J.J.M.; Zhu, L. Excitation Energy-Dependent, Excited-State Intramolecular Proton Transfer-Based Dual Emission in Poor Hydrogen-Bonding Solvents. *J. Phys. Chem. A* **2022**, *126*, 5711–5720. [CrossRef]
78. Munch, M.; Colombain, E.; Stoerkler, T.; Vérité, P.M.; Jacquemin, D.; Ulrich, G.; Massue, J. Blue-Emitting 2-(2′-Hydroxyphenyl)benzazole Fluorophores by Modulation of Excited-State Intramolecular Proton Transfer: Spectroscopic Studies and Theoretical Calculations. *J. Phys. Chem. B* **2022**, *126*, 2108–2118. [CrossRef]

79. Wang, K.; Hu, R.; Wang, J.; Zhang, J.; Liu, J.; Zhou, L.; Zhou, L.; Li, B. Fine Tuning the Energetics of 2-(2′-Hydroxyphenyl)oxazoles to Obtain Highly Efficient Organic White-Light-Emitting Devices. *ACS Mater. Lett.* **2022**, *4*, 2337–2344. [CrossRef]
80. Zeng, G.; Liang, Z.; Jiang, X.; Quan, T.; Chen, T. An ESIPT-Dependent AIE Fluorophore Based on HBT Derivative: Substituent Positional Impact on Aggregated Luminescence and its Application for Hydrogen Peroxide Detection. *Chem. Eur. J.* **2022**, *28*, e202103241. [CrossRef]
81. Yang, Y.; Luo, X.; Ma, F.; Li, Y. Substituent effect on ESIPT mechanisms and photophysical properties of HBT derivatives. Spectrochim. *Acta A Mol. Biomol. Spectrosc.* **2021**, *250*, 119375. [CrossRef]
82. Georgiev, A.; Deneva, V.; Yordanov, D.; Völzer, T.; Wolter, S.; Fennel, F.; Lochbrunner, S.; Antonov, L. Benzothiazol picolin/isonicotinamides molecular switches: Expectations and reality. *J. Mol. Liq.* **2022**, *356*, 118968. [CrossRef]
83. Shekhovtsov, N.A.; Nikolaenkova, E.B.; Berezin, A.S.; Plyusnin, V.F.; Vinogradova, K.A.; Naumov, D.Y.; Pervukhina, N.V.; Tikhonov, A.Y.; Bushuev, M.B. A 1-Hydroxy-1*H*-imidazole ESIPT Emitter Demonstrating anti-Kasha Fluorescence and Direct Excitation of a Tautomeric Form. *ChemPlusChem* **2021**, *86*, 1436–1441. [CrossRef]
84. Shekhovtsov, N.A.; Ryadun, A.A.; Bushuev, M.B. Luminescence of a Zinc(II) Complex with a Protonated 1-Hydroxy-1*H*-imidazole ESIPT Ligand: Direct Excitation of a Tautomeric Form. *ChemistrySelect* **2021**, *6*, 12346–12350. [CrossRef]
85. Shekhovtsov, N.A.; Ryadun, A.A.; Plyusnin, V.F.; Nikolaenkova, E.B.; Tikhonov, A.Y.; Bushuev, M.B. First 1-hydroxy-1*H*-imidazole-based ESIPT emitter with an O–H···O intramolecular hydrogen bond: ESIPT-triggered TICT and speciation in solution. *New J. Chem.* **2022**, *46*, 22804–22817. [CrossRef]
86. Shekhovtsov, N.A.; Vinogradova, K.A.; Vorobyova, S.N.; Berezin, A.S.; Plyusnin, V.F.; Naumov, D.Y.; Pervukhina, N.V.; Nikolaenkova, E.B.; Tikhonov, A.Y.; Bushuev, M.B. *N*-Hydroxy–*N*-oxide photoinduced tautomerization and excitation wavelength dependent luminescence of ESIPT-capable zinc(II) complexes with a rationally designed 1-hydroxy-2,4-di(pyridin-2-yl)-1*H*-imidazole ESIPT-ligand. *Dalton Trans.* **2022**, *51*, 9818–9835. [CrossRef] [PubMed]
87. Shekhovtsov, N.A.; Nikolaenkova, E.B.; Berezin, A.S.; Plyusnin, V.F.; Vinogradova, K.A.; Naumov, D.Y.; Pervukhina, N.V.; Tikhonov, A.Y.; Bushuev, M.B. Tuning ESIPT-coupled luminescence by expanding π-conjugation of a proton acceptor moiety in ESIPT-capable zinc(II) complexes with 1-hydroxy-1*H*-imidazole-based ligands. *Dalton Trans.* **2022**, *51*, 15166–15188. [CrossRef] [PubMed]
88. Mason, H.L. α-Oximino and α-Amino Derivatives of o-Hydroxypropiophenone. *J. Am. Chem. Soc.* **1934**, *56*, 2499–2500. [CrossRef]
89. Nikitina, P.A.; Perevalov, V.P. Methods of synthesis and physicochemical properties of 1-hydroxyimidazoles, imidazole 3-oxides, and their benzoannulated analogs. *Chem. Heterocycl. Compd.* **2017**, *53*, 123–149. [CrossRef]
90. van Hirschheydt, T.; Voss, E. U.S. Patent 20050085473. *Chem. Abstr.* **2005**, *142*, 411373.
91. Samsonov, V.A. Synthesis of 1,5,6,7-tetrahydro-4*H*-benzimidazol-4-one derivatives from 2,6-bis(hydroxyimino)cyclohexan-1-one. *Russ. J. Org. Chem.* **2017**, *53*, 66–73. [CrossRef]
92. Nikolaenkova, E.B.; Os'kina, I.A.; Tikhonov, A.Y. Synthesis of 2-(3,4,5-trimethoxybenzoyl)-4(5)-phenyl-1*H*-imidazole. *Russ. J. Org. Chem.* **2017**, *53*, 1887–1889. [CrossRef]
93. Nikolaenkova, E.B.; Tikhonov, A.Y.; Grishchenko, S.Y. Reactivity of oximes of 1-aryl(hetaryl)-2-(hydroxyamino)propan-1-ones with ethyl glyoxylate. *Chem. Heterocycl. Compd.* **2019**, *55*, 142–146. [CrossRef]
94. Han, J.; Cao, B.; Li, Y.; Zhou, Q.; Sun, C.; Li, B.; Yin, H.; Shi, Y. The role played by solvent polarity in regulating the competitive mechanism between ESIPT and TICT of coumarin (E-8-((4-dimethylamino-phenylimino)-methyl)-7-hydroxy-4-methyl-2H-chromen-2-one). *Spectrochim. Acta A Mol. Biomol. Spectrosc.* **2020**, *231*, 118086. [CrossRef]
95. Zhao, Y.; Ding, Y.; Yang, Y.; Shi, W.; Li, Y. Fluorescence deactivation mechanism for a new probe detecting phosgene based on ESIPT and TICT. *Org. Chem. Front.* **2019**, *6*, 597–602. [CrossRef]
96. Qi, Y.; Lu, M.; Wang, Y.; Tang, Z.; Gao, Z.; Tian, J.; Fei, X.; Li, Y.; Liu, J. A theoretical study of the ESIPT mechanism of 3-hydroxyflavone derivatives: Solvation effect and the importance of TICT for its dual fluorescence properties. *Org. Chem. Front.* **2019**, *6*, 3136–3143. [CrossRef]
97. Georgiev, A.; Yordanov, D.; Ivanova, N.; Deneva, V.; Vassilev, N.; Kamounah, F.S.; Pittelkow, M.; Crochet, A.; Fromm, K.M.; Antonov, L. 7-OH quinoline Schiff bases: Are they the long awaited tautomeric bistable switches? *Dyes Pigment.* **2021**, *195*, 109739. [CrossRef]
98. Georgiev, A.; Antonov, L. 8-(Pyridin-2-yl)quinolin-7-ol as a platform for conjugated proton cranes: A DFT structural design. *Micromachines* **2020**, *11*, 901. [CrossRef] [PubMed]
99. Barboza, C.A.; Morawski, O.; Olas, J.; Gawrys, P.; Banasiewicz, M.; Suwinska, K.; Shova, S.; Kozankiewicz, B.; Sobolewski, A.L. Unravelling the ambiguity of the emission pattern of donor–acceptor salicylaldimines. *J. Mol. Liq.* **2021**, *343*, 117532. [CrossRef]
100. *CrysAlisPro Software System*, version 1.171.41.123a; Rigaku Oxford Diffraction; Rigaku Corporation: Wrocław, Poland, 2022.
101. Sheldrick, G.M. SHELXT—Integrated space-group and crystal-structure determination. *Acta Crystallogr. Sect. A* **2015**, *71*, 3–8. [CrossRef] [PubMed]
102. Sheldrick, G.M. Crystal structure refinement with SHELXL. *Acta Crystallogr. Sect. C* **2015**, *71*, 3–8. [CrossRef] [PubMed]
103. Frisch, M.J.; Trucks, G.W.; Schlegel, H.B.; Scuseria, G.E.; Robb, M.A.; Cheeseman, J.R.; Scalmani, G.; Barone, V.; Petersson, G.A.; Nakatsuji, H.; et al. *Gaussian 16*; Revision C.01; Gaussian, Inc.: Wallingford, CT, USA, 2016.
104. Adamo, C.; Barone, V. Toward reliable density functional methods without adjustable parameters: The PBE0 model. *J. Chem. Phys.* **1999**, *110*, 6158–6170. [CrossRef]

105. Ditchfield, R.; Hehre, W.J.; Pople, J.A. Self-Consistent Molecular-Orbital Methods. IX. An Extended Gaussian-Type Basis for Molecular-Orbital Studies of Organic Molecules. *J. Chem. Phys.* **1971**, *54*, 724–728. [CrossRef]
106. Hehre, W.J.; Ditchfield, R.; Pople, J.A. Self-Consistent Molecular Orbital Methods. XII. Further Extensions of Gaussian—Type Basis Sets for Use in Molecular Orbital Studies of Organic Molecules. *J. Chem. Phys.* **1972**, *56*, 2257–2261. [CrossRef]
107. Hariharan, P.C.; Pople, J.A. The influence of polarization functions on molecular orbital hydrogenation energies. *Theor. Chem. Acc.* **1973**, *28*, 213–222. [CrossRef]
108. Petersson, G.A.; Bennett, A.; Tensfeldt, T.G.; Al-Laham, M.A.; Shirley, W.A.; Mantzaris, J. A complete basis set model chemistry. I. The total energies of closed-shell atoms and hydrides of the first-row elements. *J. Chem. Phys.* **1988**, *89*, 2193–2218. [CrossRef]
109. Petersson, G.A.; Al-Laham, M.A. A complete basis set model chemistry. II. Open-shell systems and the total energies of the first-row atoms. *J. Chem. Phys.* **1991**, *94*, 6081–6090. [CrossRef]
110. Chemcraft-Graphical Software for Visualization of Quantum Chemistry Computations. Available online: https://www.chemcraftprog.com (accessed on 26 January 2023).

molecules

MDPI

Article

Heterogeneous Photocatalysis as a Potent Tool for Organic Synthesis: Cross-Dehydrogenative C–C Coupling of *N*-Heterocycles with Ethers Employing TiO_2/*N*-Hydroxyphthalimide System under Visible Light

Elena R. Lopat'eva, Igor B. Krylov *, Oleg O. Segida, Valentina M. Merkulova, Alexey I. Ilovaisky and Alexander O. Terent'ev *

N. D. Zelinsky Institute of Organic Chemistry, Russian Academy of Sciences, 47 Leninsky Prospekt, 119991 Moscow, Russia

* Correspondence: krylovigor@yandex.ru (I.B.K.); alterex@yandex.ru (A.O.T.)

Abstract: Despite the obvious advantages of heterogeneous photocatalysts (availability, stability, recyclability, the ease of separation from products and safety) their application in organic synthesis faces serious challenges: generally low efficiency and selectivity compared to homogeneous photocatalytic systems. The development of strategies for improving the catalytic properties of semiconductor materials is the key to their introduction into organic synthesis. In the present work, a hybrid photocatalytic system involving both heterogeneous catalyst (TiO_2) and homogeneous organocatalyst (*N*-hydroxyphthalimide, NHPI) was proposed for the cross-dehydrogenative C–C coupling of electron-deficient *N*-heterocycles with ethers employing *t*-BuOOH as the terminal oxidant. It should be noted that each of the catalysts is completely ineffective when used separately under visible light in this transformation. The occurrence of visible light absorption upon the interaction of NHPI with the TiO_2 surface and the generation of reactive phthalimide-*N*-oxyl (PINO) radicals upon irradiation with visible light are considered to be the main factors determining the high catalytic efficiency. The proposed method is suitable for the coupling of π-deficient pyridine, quinoline, pyrazine, and quinoxaline heteroarenes with various non-activated ethers.

Keywords: Minisci reaction; heterogeneous photocatalysis; *N*-hydroxyphthalimide; titanium dioxide; green chemistry; visible light photocatalysis

Citation: Lopat'eva, E.R.; Krylov, I.B.; Segida, O.O.; Merkulova, V.M.; Ilovaisky, A.I.; Terent'ev, A.O. Heterogeneous Photocatalysis as a Potent Tool for Organic Synthesis: Cross-Dehydrogenative C–C Coupling of *N*-Heterocycles with Ethers Employing TiO_2/*N*-Hydroxyphthalimide System under Visible Light. *Molecules* **2023**, *28*, 934. https://doi.org/10.3390/molecules28030934

Academic Editors: Alexey M. Starosotnikov, Maxim A. Bastrakov and Igor L. Dalinger

Received: 25 December 2022
Revised: 11 January 2023
Accepted: 13 January 2023
Published: 17 January 2023

1. Introduction

Heterogeneous photocatalysis in organic synthesis is a young and fast-growing area [1–5]. The semiconductor materials used in photocatalysis are inexpensive and widely available; their advantages include the ease of separation from organic products, stability and recyclability [1,5]. However, the development of this area is still hindered by several formidable obstacles, such as low catalytic efficiency due to the low degree of charge separation in photoexcited states and the fast recombination of electron–hole pairs [6,7], low visible light absorption and low selectivity due to the strong oxidation power of photogenerated valence-band (VB) holes in popular semiconductors (TiO_2, ZnO, Bi_2O_3, WO_3, etc.) [1,8]. This situation is reflected in the comparatively low number of synthetic methods in fine organic synthesis based on heterogeneous photocatalytic systems compared to the mainstream applications of heterogeneous photocatalysis: oxidative destruction of pollutants [9–11], hydrogen generation [12,13], CO_2 reduction [14–16] and water splitting [17].

Currently, the scope of synthetic transformations enabled by heterogeneous photocatalysis is much less diverse compared to the scope of homogeneous photoredox-catalyzed reactions. Heterogeneous catalysis is mainly used in comparatively simple reactions; for example, alkylarene benzylic oxidation [18–20], the oxidation of benzylamines [4,5,21,22],

alcohols [4,5] and sulfides [4,23], oxidative esterification [4], nitro-group reduction [4], thiolene reaction [24], alkene amination with aqueous ammonia [25] and the decarboxylation of carboxylic acids [26–28]. Cross-coupling reactions are much less developed and usually demand transition metal co-catalysts, such as palladium or nickel complexes [29–33].

UV irradiation, which is used frequently for the excitation of heterogeneous photocatalysts, is inconvenient due to safety issues, the comparatively high cost of UV light sources, incompatibility with common laboratory glassware (UV-transparent quartz is necessary) and possible side reactions due to the high energy of the light. The modification of heterogeneous photocatalysts, such as TiO_2, in order to shift their photoactivity spectrum from UV to visible light [10,34–37] is the key task for expanding the scope of their applications in organic synthesis, increasing selectivity and making the of use cheap and available light sources for catalyst activation possible. At present, the following modification approaches have been proposed: the immobilization of dyes (organic compounds or metal complexes) on the photocatalyst surface [34,38–41], doping with metal ions or non-metal elements [42,43], semiconductor coupling [7,44–49] and modification with organic molecules bearing hydroxyl or carboxyl groups [34,50–56], which demonstrate the occurrence of visible light absorption when adsorbed on the surface of a semiconductor.

NHPI/TiO_2 is one of the efficient catalytic systems activated by visible light based on industrially available substances (Scheme 1). The interaction of NHPI with the TiO_2 surface leads to the occurrence of visible light absorption, resulting in the photogeneration of phthalimide-*N*-oxyl radicals (PINO) [20,22]. In our previous work [20], we demonstrated that the NHPI/TiO_2 system could be successfully applied to the aerobic oxidation of alkylarenes under visible light irradiation (Scheme 1A). The conceptual novelty of this system arises from the conjunction of heterogeneous photocatalysis with homogeneous radical chain organocatalysis. A distinguishing feature of this system is the migration of PINO into the volume of solution, where the PINO/NHPI catalyzed radical chain process, once initiated on the TiO_2 surface, produces the target product without the need for additional light absorption [20]. Thus, the energy efficiency of photocatalysis is fundamentally improved by combining heterogeneous photocatalysis with homogeneous organocatalysis. In the presence of additional organocatalyst (2,2,6,6-Tetramethylpiperidin-1-yl)oxyl (TEMPO) the effective oxidative homocoupling of benzylamines [22] was achieved previously (Scheme 1B).

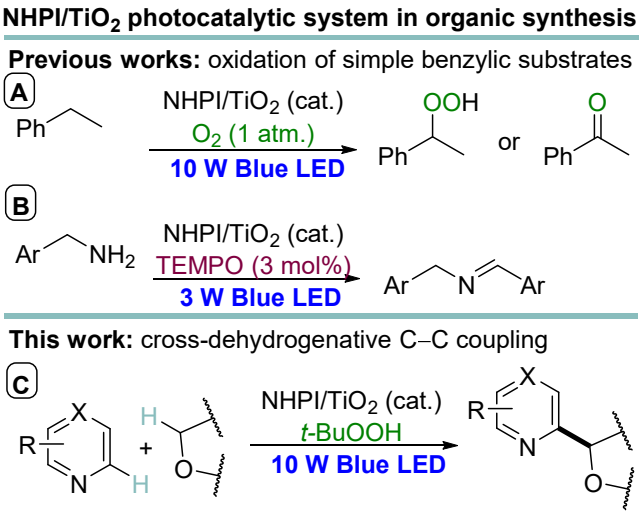

Scheme 1. Applications of NHPI/TiO_2 photocatalytic system in organic synthesis: CH-oxygenation (**A**) [20], oxidative homocoupling of benzylamines (**B**) [22], and Minisi-type corss-dehydrogenative C–C coupling reported in the present work (**C**).

In the present study, we demonstrate the successful application of the NHPI/TiO_2 system to a more challenging cross-dehydrogenative C–C coupling process (Scheme 1C).

In this case, previously reported CH-oxygenation processes [20] should be suppressed, which is a difficult task. In addition, the process of C–O coupling between NHPI-derived PINO radicals and CH-reagents [57–59] must be avoided. The oxidative coupling of ethers with π-deficient *N*-heteroaromatic compounds (a Minisci-type reaction) was chosen as a model reaction due to the practical importance for the functionalization of *N*-containing heterocycles with C–C bond formation. Minisci-type reactions [60–68] are based on the addition of nucleophilic C-centered radicals to electron-deficient arenes and represent one of the most important methods for the functionalization of such arenes, along with the nucleophilic aromatic substitution of hydrogen [69–71], and functionalization via transition-metal-catalyzed C(sp^2)–H bond activation [72–76]. The products of the Minisci reaction are of great value for medicinal chemistry [61,64]. Thus, the development of new, milder, more efficient methods tolerant to a large number of functional groups based on Minisci chemistry remains a hot research topic.

To date, many photochemical protocols have been developed for the Minisci reaction, both with the use of metal complex photocatalysts [60,77–80] and organic photocatalysts [81–83]. In some specific cases, the Minisci reaction proceeds without a photocatalyst [84–87]. At the same time, examples of the application of heterogeneous photocatalysis for the Minisci reaction that are attractive from the practical point of view remain rare [88–91]. In this work, we demonstrate the use of the developed hetero-/homogeneous NHPI/TiO_2 photocatalytic system for the Minisci reaction between π-deficient heteroarenes (pyridines, quinolines, isoquinolines, pyrazines, and quinoxaline) and non-activated ethers.

2. Results and Discussion

2.1. Optimization of Photocatalytic System Composition

Based on our previous work [20], TiO_2 with high specific surface area (anatase nanopowder, Hombikat UV100) and industrially available *N*-hydroxyphthalimide were chosen as the components of the photochemical system. Blue LEDs (455 nm) with an input power of 10 W were used as light sources. In the first step, we optimized the conditions of the photochemical cross-dehydrogenative Minisci reaction between 4-methylquinoline **1a** and tetrahydrofuran **2a** (Table 1). *Tert*-butyl hydroperoxide (TBHP) was used as an inexpensive, easily available and metal-free oxidant.

The starting conditions (10 mg of TiO_2, 20 mol.% of NHPI, 4 mmol of TBHP, 5 h, run 1) yielded 45% of the product **3aa**. The absence of either TiO_2 or NHPI resulted in the zero conversion of **1a** (runs 2, 3), proving that both components of the catalytic system are essential. Without *t*-BuOOH, the reaction proceeded with low efficiency: only trace amounts of the product were formed (run 4). As a rule, the addition of a strong Brønsted acid, such as HCl [85] or TFA [77,79,82,84,86], increases the efficiency of the Minisci reaction. Acids protonate π-deficient *N*-containing heterocycles, making them more susceptible to attack by nucleophilic C-centered radicals [67]. However, in our case, the addition of trifluoroacetic acid (TFA, run 5) had no significant effect on the yield and conversion. The addition of 0.5 mL of water resulted in a drop in **3aa** yield (run 6). Water breaks down the stable suspension of TiO_2 in THF, causing the catalyst particles to aggregate in the water droplets. Both an increase and a decrease in the amount of THF lead to a decrease in the yield of **3aa** (runs 7, 8). The dilution of the reaction mixture with such co-solvents as hexafluoroisopropanol (HFIP, run 9) and acetonitrile (MeCN, run 10) slowed down the reaction, and dilution with dichloroethane (DCE, run 11) led to the complete suppression of the target process. It is known that hydrogen peroxide can be used as the oxidant for the photocatalytic Minisci reaction [85]. However, the change of the oxidant from TBHP to aqueous H_2O_2 led to a dramatic drop in the yield (run 12). The lower efficiency of H_2O_2 compared to TBHP can be explained by the fact that H_2O_2 can not only initiate free-radical reactions but can also be an inhibitor via the formation of HOO• radicals [92–94]. The use of other organic peroxides, such as meta-chloroperoxybenzoic acid (m-CPBA, run 13), cumene hydroperoxide (run 14) and dicumyl peroxide (run 15) led to low yields or did not provide the product at all. Dibenzoylperoxide (BzOOBz, run 16) showed a yield comparable

to TBHP, but the formation of a large amount of benzoic acid, which is poorly soluble in the system, complicates the isolation of the products and limits the scalability of the procedure. Therefore, TBHP was chosen as the optimal oxidant. The standard version of the Minisci reaction often uses inorganic persulfates as oxidants. In our system, the use of persulfates was less efficient than TBHP, and led to a significant drop in yield with increasing reaction time, presumably due to the overoxidation of the product (runs 17–20). An inert atmosphere did not increase the selectivity of the process (run 21), so we decided to carry out the reaction under air.

Table 1. Influence of photocatalytic system composition, irradiation power, and nature of oxidant on the conversion of 4-methylquinoline **1a** and yield of **3aa** in photocatalytic Minisci reaction.

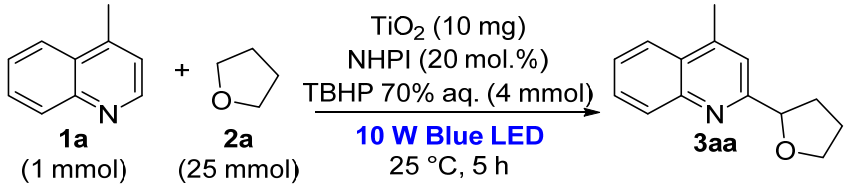

Run	Changes to the General Conditions	Conversion [a] 1a, %	Yield [a] 3aa, %
1	none	53	45
2	no TiO_2	0	0
3	no NHPI	0	0
4	no TBHP	6	4
5	TFA (1.5 mmol) added	52	45
6	H_2O (0.5 mL) added	23	9
7	THF (12.5 mmol)	38	36
8	THF (50 mmol)	32	27
9	HFIP (1 mL) added	18	16
10	MeCN (1 mL) added	17	16
11	DCE (1 mL) added	0	0
12	H_2O_2 34% aq. [b]	9	3
13	m-CPBA 75% aq. [b]	28	0
14	$PhCH(CH_3)_2OOH$ 80%	15	15
15	$PhCH(CH_3)_2OOPhCH(CH_3)_2$ 98% [b]	16	0
16	BzOOBz 75% aq. (1 mmol) [b]	59	44
17	$(NH_4)_2S_2O_8$ [b,c]	39	33
18	$Na_2S_2O_8$ [b,c]	36	22
19	$K_2S_2O_8$ [b,c]	44	39
20	$K_2S_2O_8$ [b,c], 16 h, Argon atmosphere	90	27
21	Argon atmosphere	44	39

[a] The conversion of **1a** and the yield of **3aa** were determined by ^1H NMR using $C_2H_2Cl_4$ as an internal standard. [b] instead of TBHP. [c] 1 mL of water was used as co-solvent to dissolve the persulfate.

In the next step, we optimized the NHPI/TiO_2/TBHP ratio and irradiation time to achieve the maximum yield of the coupling product **3aa** (Table 2).

Increasing the amount of TiO_2 increases the yield of **3aa** (runs 1–4). However, when switching from the TiO_2 loading of 20 mg to 40 mg, the efficiency increased only slightly. Therefore, the TiO_2 loading of 20 mg was chosen as the optimal amount. Similarly, large loadings of NHPI resulted in an increase in the **3aa** yield (runs 5–8), but the step from 20 to 40 mol.% of NHPI increased the yield of **3aa** slightly, and a slight drop in selectivity was observed. The optimum excess of THBP was 4 mmol per 1 mmol of **1a** (runs 9–11). The reaction proceeded with almost complete conversion in 8 h (run 15). It should be noted that visible-light-active heterogeneous photocatalyst g-C_3N_4 was ineffective for the model coupling reaction under the same conditions (run 16). The conditions of experiment 15 were chosen as optimal for further studies of the substrate scope for the developed method.

Table 2. Optimization of NHPI/TiO_2/TBHP ratio and reaction time for the synthesis of **3aa**.

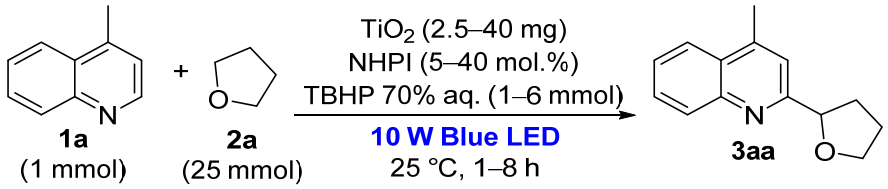

Run	TiO_2, mg	NHPI, mmol	TBHP, mmol	Time, h	Conversion [a] 1a, %	Yield [a] 3aa, %
1	2.5	0.1	2	5	5	5
2	5	0.1	2	5	12	11
3	20	0.1	2	5	44	40
4	40	0.1	2	5	55	46
5	10	0.05	2	5	0	0
6	10	0.1	2	5	39	36
7	10	0.2	2	5	44	39
8	10	0.4	2	5	52	41
9	10	0.1	1	5	31	27
10	10	0.1	4	5	49	42
11	10	0.1	6	5	38	38
12	10	0.1	2	1	5	4
13	10	0.1	2	2	20	15
14	10	0.1	2	5	34	28
15	20	0.2	4	8	96	89
16	- [b]	0.2	4	8	9	7

[a] The conversion of **1a** and the yield of **3aa** were determined by ^{1}H NMR using $C_2H_2Cl_4$ as an internal standard. [b] Bulk g-C_3N_4 (20 mg) was used instead of TiO_2 as heterogeneous photocatalyst.

2.2. Application of the Designed Photocatalytic NHPI/TiO_2 System to the Minisci Reaction

With the optimal conditions in hand (Table 2, run 15), we have synthesized a wide range of coupling products between *N*-heterocycles and ethers. The scope of ethers was explored first (Scheme 2). For substrates demonstrating lower conversions compared to **1a**, the reaction time increased in some cases up to 48 h (the reaction times and conversions are given in Scheme 2).

Among the tested ethers, we obtained the best result with THF: after 8 h of reaction, the almost complete conversion of 4-methylquinoline **1a** and a high yield of product **3aa** (89%) were observed. As a rule, the reaction proceeds more slowly and with lower selectivity for other ethers. In the reaction of 4-methylquinoline with 2-methyltetrahydrofuran **2b**, a mixture of products **3ab** (as a diastereomeric mixture, major) and **3ab'** (minor) was observed. The observed regioselectivity can be explained by the fact that although the hydrogen atom abstraction is most favored from the weakest tertiary CH-bond (position 2 of 2-methyltetrahydrofuran) [95], the resulting C-centered radical is more stable and sterically hindered than the secondary radical and reacts less efficiently with 4-methylquinoline. For 1,3-dioxolane **2c**, two isomeric products **3ac** and **3ac'** were formed, and the major product **3ac** corresponds to the breaking of the weakest C2-H bond in 1,3-dioxolane. With dioxane and tetrahydropyran, the reaction proceeded more slowly, but with a longer reaction time, its selectivity decreased simultaneously with an increase in conversion. With glyme, the dehydrogenative coupling product was not observed even after 24 h of reaction.

In the case of diethyl ether as a substrate, the reaction under the standard conditions was not effective due to the immiscibility of Et_2O and H_2O contained in TBHP (70% aq.), which led to the aggregation of TiO_2 particles in water droplets and the low conversion of **1a**. The solution to the problem was the use of anhydrous TBHP, prepared before the reaction (See experimental details for Scheme 2). The same problem limited the reaction time for the coupling of **1a** with Et_2O since the water generated during TBHP reduction accumulated in the reaction mixture and made the TiO_2 suspension unstable.

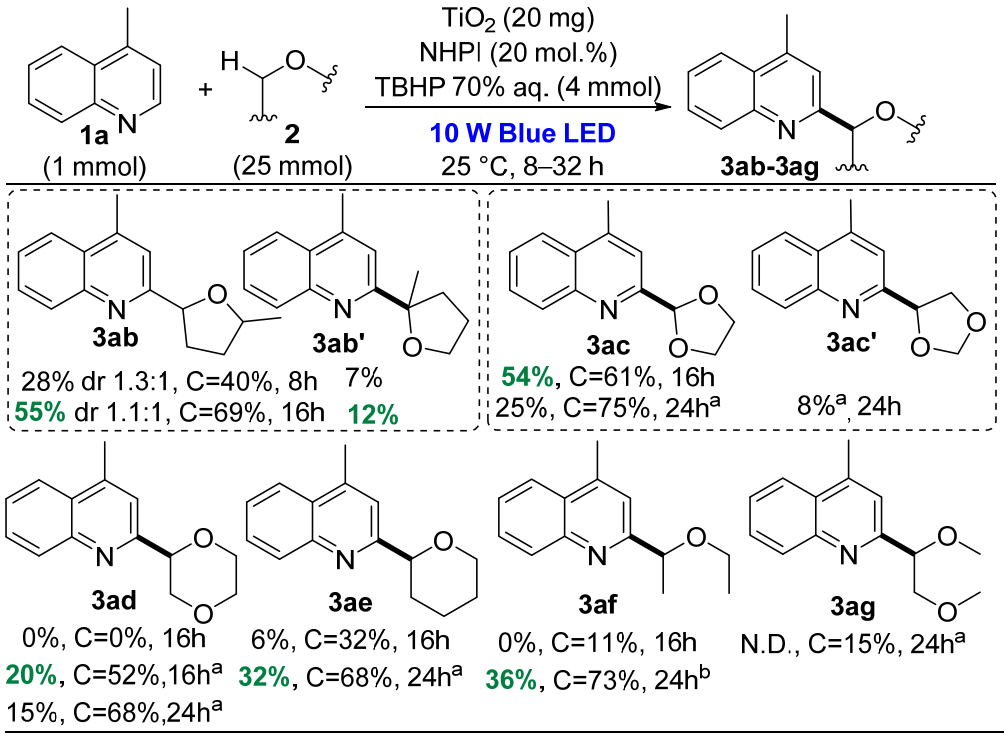

Scheme 2. Scope of ethers for the photocatalytic Minisci reaction with 4-methylquinoline **1a**.

In the next step, the scope of the electron-deficient *N*-heterocycles was tested (Scheme 3).

N-heterocycles with electron-donor groups reacted slower compared to substrates with electron-withdrawing groups, but at the same time, higher selectivity was observed (products **3ba**, **3ea** in comparison with **3ca**). The reaction is sensitive to steric hindrance: 2-chloro-5-bromoquinoline **2d** did not yield the target product of **3da**, presumably due to the presence of a bulky Br substituent near the 4th position of the quinoline. Our photochemical system is also applicable to quinoxalines and pyrazines. It is worth noting that the products of **3ga** and **3ha** have not been previously reported (See Supplementary Materials for additional information). In general, the reaction is inefficient for pyridines with no substituents or with electron-donor substituents (pyridine, picolines, lutidine), but good yields have been obtained for pyridines with electron-acceptor substituents, such as pyridine-3-carboxylic acid methyl ester (product **3ia**). 4-Methylquinoline-*N*-oxide reacted with the preservation of the *N*-oxide function (product **3ja**). Good yields have also been obtained in the reaction with isoquinoline (product **3ka**). In the reaction with imidazo [1,2-a]pyridine **2l**, it was only possible to isolate the product of deep oxidation with the destruction of the ring—**3la'**. It should also be noted that the addition of acid (TFA) afforded increased yields in some cases (products **3ba**, **3ca**, **3ea**, **3ga**, **3ha**,**3ja** and **3ka**).

It turned out that carrying out the reaction to complete the conversion of π-deficient arenes in the NHPI/TiO_2 photochemical system leads to a sharp drop in selectivity for target product **3**. We assumed that product **3** could undergo further oxidation under the reaction conditions. To find out what role the individual components of the system play in oxidation, we performed control experiments in which the pure reaction product **3aa** was placed under standard reaction conditions or irradiated in an inert atmosphere in the absence of NHPI or TBHP (Scheme 4).

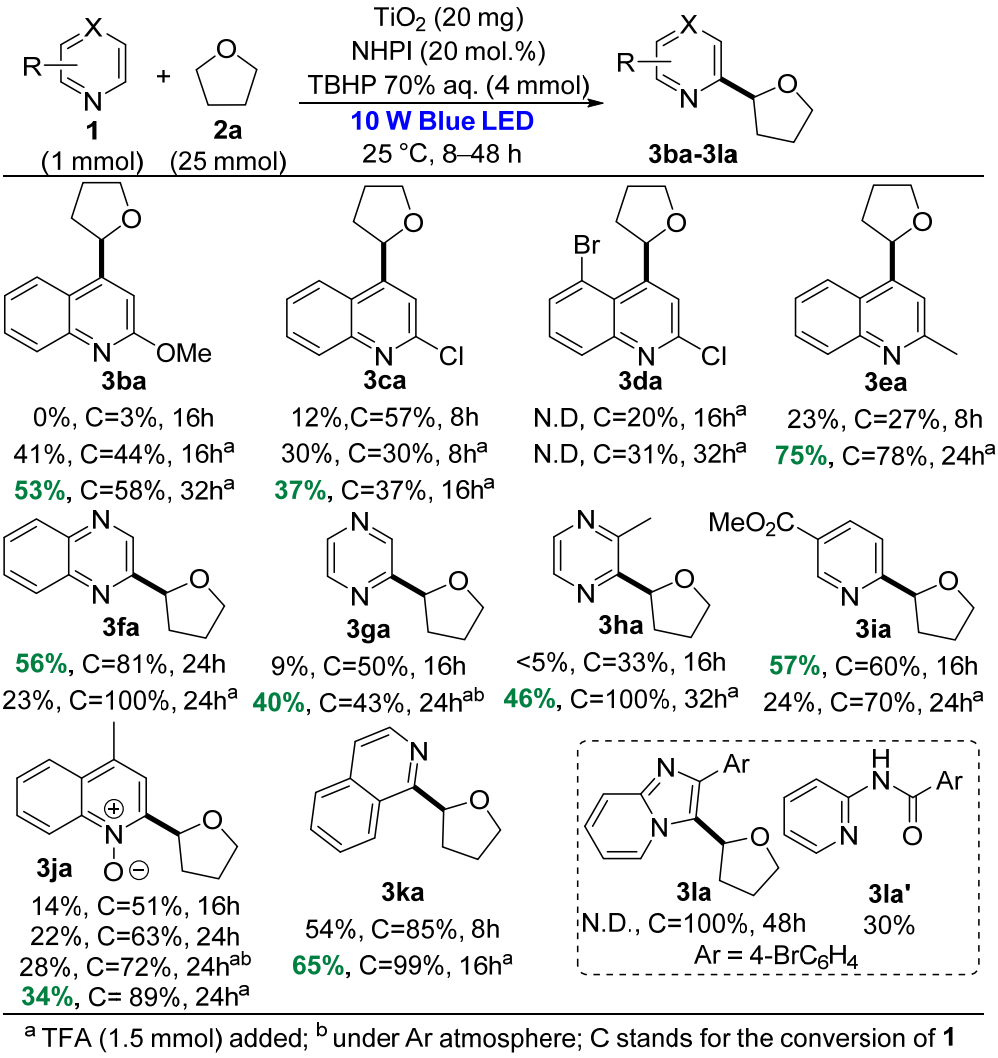

Scheme 3. Scope of π-deficient arenes for the photocatalytic Minisci reaction with tetrahydrofuran.

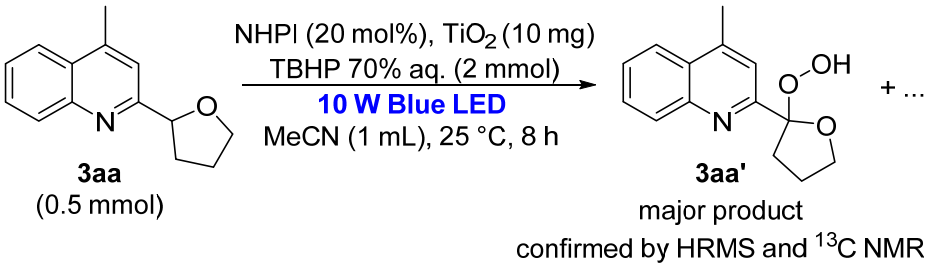

Conditions	Conversion of **3aa**, %
A. Air	86
B. Air, without TBHP	88
C. Ar	56
D. Ar, without NHPI	34

Scheme 4. Control experiments disclosing side processes of the photocatalytic Minisci reaction.

Under the standard conditions, an 86% conversion of **3aa** was observed in 8 h (Scheme 4, **A**). In the absence of TBHP under an air atmosphere, the product is also oxidized (88% conversion, Scheme 4, **B**), which suggests that a significant role in the decomposition of the product is played by air as an oxidant. The primary oxidation product was hydroperoxide **3aa'**, which was detected in a mixture of oxidation products by ^{13}C NMR

and was confirmed by HRMS (See Supplementary Materials). The ^{13}C signal with chemical shift typical for geminal alkoxyhydroperoxide fragment was observed [96]. However, carrying out the reaction under an argon atmosphere (Scheme 4, **C**) does not completely suppress the oxidation of product **3aa** since TBHP or residual amounts of oxygen can serve as oxidants. The lowest conversion of the product was observed when the reaction was carried out in an argon atmosphere without the addition of NHPI (Scheme 4, **D**), implying that NHPI-derived PINO radicals play an important role in **3aa** oxidation.

Based on the collected data, we proposed the following mechanism (Scheme 5). Upon irradiation with visible light, PINO radicals are generated from NHPI on the TiO_2 surface. Simultaneously, the *tert*-butyl hydroperoxide decomposes on the TiO_2 surface with the formation of *tert*-butoxyl radicals. *Tert*-butoxyl radicals can regenerate PINO by abstracting a hydrogen atom from the NHPI in solution [59]. *Tert*-butoxyl radicals can also generate *tert*-butylperoxy radicals from *t*-BuOOH [97,98]. Either *tert*-butoxy, *tert*-butylperoxy [99–101], or PINO radicals [59,95] can abstract a hydrogen atom from the α-CH bond in ether to form C-centered radical **A**. However, considering the fact that no cross-dehydrogenative coupling was observed without the addition of NHPI, the main role in H-atom abstraction is assumed to be played by the PINO radicals. Then, radical **A** undergoes addition to a heteroarene with the formation of the intermediate radical **B**, which is further subjected to HAT with the retrieval of aromaticity.

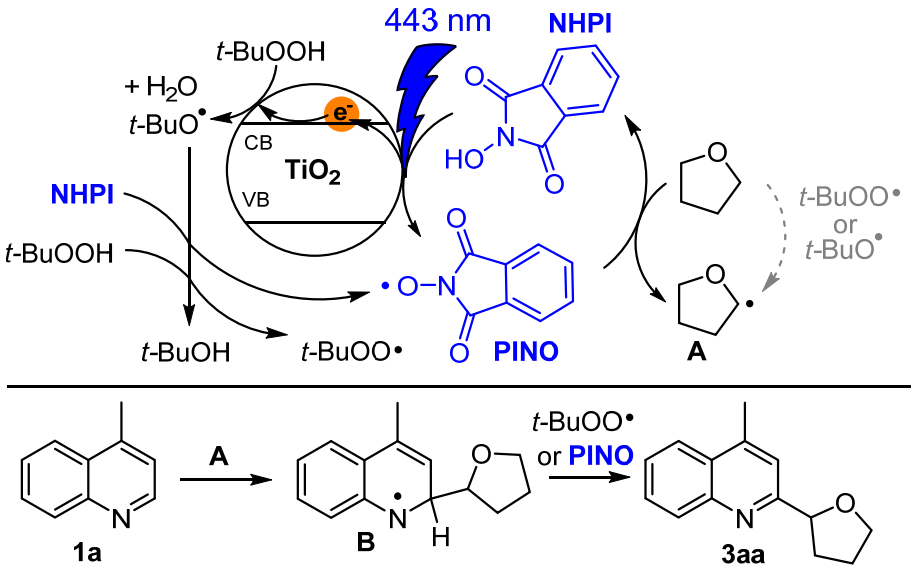

Scheme 5. Plausible mechanism of the photocatalytic Minisci reaction.

3. Materials and Methods

3.1. General

Room temperature (rt) stands for 23–25 °C.

Commercial TiO_2 Hombikat UV 100 (anatase, specific surface area, BET: 300 $m^2 \cdot g^{-1}$, primary crystal size according to Scherrer <10 nm) was used as is. *N*-hydroxyphthalimide (NHPI, 98%, Acros Organics), 4-methylquinoline (99%, Acros Organics), 2-methylquinoline (97%, Acros Organics), 2-chloroquinoline (99%, Acros Organics), isoquinoline (97%, Acros Organics), quinoxaline (99%, Acros Organics), pyrazine (99+%, Acros Organics), 2-methylpyrazine (99+%, Acros Organics), Methyl nicotinate (99%, Acros Organics), 2-methoxyquinoline, 5-bromo-2-chloroquinoline were used as is from commercial sources. 4-methylquinoline 1-oxide was synthesized according to the literature procedure [102], 2-(4-bromophenyl)imidazo [1,2-a]pyridine was synthesized according to the procedure in the literature [103]. Bulk g-C_3N_4 was prepared analogously to previously reported methods [104,105], and the urea was heated in a covered alumina crucible for 4 h at 550 °C (heating rate 5 °C·min-1). MeCN was distilled over P_2O_5, and Ethers (THF, 2-Methyltetrahydrofuran, 1,3-dioxolane,

1,4-dioxane, tetrahydropyran and diethyl ether, dimethoxyethane, bis(2-methoxyethyl) ether) were distilled over $LiAlH_4$. The reaction mixtures were sonicated in an ultrasonic bath (HF-Frequency 35 kHz, ultrasonic nominal power 80 W) before the irradiation.

Experimental details for Table 1

General reaction conditions: 4-methylquinoline **1a** (1 mmol, 143.2 mg), TiO_2 (10 mg), NHPI (0.2 mmol, 32.6 mg), *t*-BuOOH (70% aq., 4 mmol, 515 mg), THF **2a** (25 mmol, 2 mL) and a magnetic stir bar (6 × 10 mm) were placed in a 50 mL round-bottom flask. The obtained mixture was sonicated for 5 min in an ultrasonic bath, then magnetically stirred (500 rpm) in a thermostated water bath at 25 °C (±1 °C) under irradiation of 10 W blue LED for 5 h under an air atmosphere (closed flask). Then, the solvent was rotary evaporated, and $C_2H_2Cl_4$ (40–60 mg, 0.4–0.61 mmol) was added as a standard for NMR yield determination. The reaction mixture was centrifuged, and the NMR spectrum was recorded.

Experimental details for Table 2

4-methylquinoline **1a** (1 mmol, 143.2 mg), TiO_2 Hombikat UV 100 (2.5–40 mg), NHPI (0.05–0.4 mmol, 8.2–65.2 mg), *t*-BuOOH 70% aq. (1–6 mmol, 129–772 mg) and THF **2a** (25 mmol, 2 mL) and a magnetic stir bar (6 × 10 mm) were placed in a 50 mL round-bottom flask. The obtained mixture was sonicated for 5 min in an ultrasonic bath, then magnetically stirred (500 rpm) in a thermostated water bath at 25 °C (±1 °C) under irradiation of 10 W blue LED for 1–16 h under an air atmosphere (closed flask). Then, the solvent was rotary evaporated, $C_2H_2Cl_4$ (40–60 mg, 0.4–0.61 mmol) was added as a standard for NMR yield determination. The reaction mixture was filtrated through a Celite layer, and the NMR spectrum was recorded.

Experimental details for Schemes 2 and 3

Heterocycle **1** (1 mmol), TiO_2 (20 mg), NHPI (0.2 mmol, 32.6 mg), *t*-BuOOH 70% aq. (4 mmol, 515 mg), CH-reagent **2** (25 mmol) and a magnetic stir bar (6 × 10 mm) were placed in a 50 mL round-bottom flask. The obtained mixture was sonicated for 5 min in an ultrasonic bath, then magnetically stirred (500 rpm) in a thermostated water bath at 25 °C (±1 °C) under irradiation of 10 W blue LED for 8 h under an air atmosphere (closed flask). If needed, another 4 mmol of the reaction *t*-BuOOH was added, and the reaction mixture was irradiated for another 8 h. At the end of the required time, the reaction mixture was poured into 20 mL of water and extracted with 3×15 mL of CH_2Cl_2. The combined organic extracts were washed with 2 × 20 mL of $NaHCO_3$ saturated solution. The extracts were dried over $MgSO_4$, and the solvent was evaporated in a vacuum membrane pump. The residue was purified using column chromatography to afford products **3aa**–**3ka**. For the reaction of **1a** with Et_2O, anhydrous *t*-BuOOH was prepared. *t*-BuOOH 70% aq. (12 mmol, 1545 mg) was extracted with CH_2Cl_2 (10 mL). The organic layer was dried over $MgSO_4$, and the solvent was rotary evaporated. The obtained anhydrous *t*-BuOOH was used instead of *t*-BuOOH 70% aq. For the longer reaction times, the new portion of anhydrous *t*-BuOOH (4 mmol, 360 mg) was added each 8 h.

Experimental details for Scheme 4

4-methyl-2-(tetrahydrofuran-2-yl)quinoline **3aa** (0.5 mmol), TiO_2 (10 mg), NHPI (0.1 mmol, 16.3 mg), *t*-BuOOH 70% aq. (2 mmol, 257 mg) and a magnetic stir bar (6 × 10 mm) were placed in a 50 mL round-bottom flask. The obtained mixture was sonicated for 5 min in an ultrasonic bath. For the entries of C and D, the flask was vacuumed and then filled with Ar three times. The mixture was magnetically stirred (500 rpm) in a thermostated water bath at 25 °C (±1 °C) under irradiation of 10 W blue LED for 8 h. The conversion of **3aa** was determined by ^{1}H NMR in MeCN using $C_2H_2Cl_4$ as the internal standard.

3.2. Characterization Data of the Cross-Dehydrogenative C–C Coupling Products

4-Methyl-2-(tetrahydrofuran-2-yl)quinoline 3aa [91] was isolated using column chromatography (Petroleum ether/EtOAc = 2/1) as a colorless viscous liquid (190 mg, 89%).

^{1}H NMR (300.13 MHz, $CDCl_3$) δ 8.07–7.99 (m, 1H), 7.92–7.85 (m, 1H), 7.66–7.58 (m, 1H), 7.48–7.41 (m, 1H), 7.40 (s, 1H), 5.10 (t, *J* = 6.9 Hz, 1H), 4.16–4.08 (m, 1H), 4.02–3.94 (m, 1H), 2.63 (s, 3H), 2.53–2.38 (m, 1H), 2.11–1.90 (m, 3H).^{13}C{^{1}H}NMR (75.48 MHz, $CDCl_3$) δ 163.0, 147.3, 144.8, 129.5, 129.0, 127.4, 125.7, 123.6, 118.6, 82.0, 69.1, 33.2, 25.9, 18.8.

2-(2-hydroperoxytetrahydrofuran-2-yl)-4-methylquinoline 3aa'. ^{13}C{^{1}H}NMR (75.48 MHz, $CDCl_3$) δ 159.4, 146.0, 145.7, 128.8, 128.7, 127.2, 126.1, 123.4, 119.7, 113.3, 69.5, 36.8, 24.8, 19.0. HR-MS (ESI): *m*/*z* = 246.1125, calcd. for $C_{14}H_{15}NO_3$+H^+: 246.1123.

***Anti*-4-methyl-2-(5-methyltetrahydrofuran-2-yl)quinoline 3ab** was isolated using column chromatography (Petroleum ether/EtOAc = 2/1) as a colorless liquid (66 mg, 29%). ^{1}H NMR (300 MHz, Chloroform-*d*) δ 8.07–8.02 (m, 1H), 7.98–7.93 (m, 1H), 7.66 (ddd, *J* = 8.4, 6.8, 1.5 Hz, 1H), 7.50 (ddd, *J* = 8.2, 6.8, 1.3 Hz, 1H), 7.46 (s, 1H), 5.26 (t, *J* = 7.1 Hz, 1H), 4.51–4.33 (m, 1H), 2.70 (s, 3H), 2.63–2.49 (m, 1H), 2.24–2.02 (m, 2H), 1.75–1.59 (m, 1H), 1.36 (d, *J* = 6.1 Hz, 3H). ^{13}C{^{1}H}NMR (75.48 MHz, $CDCl_3$) δ 163.6, 147.3, 145.1, 129.6, 129.2, 127.5, 125.9, 123.8, 118.6, 81.8, 76.7, 34.1, 34.0, 21.5, 19.0; FTIR (KBr): ν_{max} = 2968, 2928, 2869, 1602, 1509, 1447, 1379, 1311, 1225, 1181, 1074, 910, 883, 760 cm^{-1}. HR-MS (ESI): *m*/*z* = 228.1389, calcd. for $C_{15}H_{17}NO$+H^+: 228.1383.

***Syn*-4-methyl-2-(5-methyltetrahydrofuran-2-yl)quinoline 3ab'** was isolated using column chromatography (Petroleum ether/EtOAc = 2/1) as a colorless liquid (59 mg, 26%). ^{1}H NMR (300 MHz, Chloroform-*d*) δ 8.08–8.03 (m, 1H), 7.97 (dd, *J* = 8.4, 1.5 Hz, 1H), 7.68 (ddd, *J* = 8.4, 6.9, 1.5 Hz, 1H), 7.58–7.46 (m, 2H), 5.13 (dd, *J* = 7.6, 6.5 Hz, 1H), 4.33–4.21 (m, 1H), 2.72 (d, *J* = 0.7 Hz, 3H), 2.60–2.42 (m, 1H), 2.21–1.99 (m, 2H), 1.69–1.50 (m, 1H), 1.44 (d, *J* = 6.1 Hz, 3H).^{13}C{^{1}H}NMR (75.48 MHz, $CDCl_3$) δ 163.3, 147.3, 145.2, 129.6, 129.3, 127.6, 126.0, 123.8, 118.8, 82.5, 76.9, 33.5, 33.2, 21.4, 19.1; FTIR (KBr): ν_{max} = 2970, 2928, 2870, 1736, 1602, 1563, 1509, 1447, 1380, 1090, 1032, 913, 882, 760 cm^{-1}. HR-MS (ESI): *m*/*z* = 228.1388, calcd. for $C_{15}H_{17}NO$+H^+: 228.1383.

4-methyl-2-(2-methyltetrahydrofuran-2-yl)quinoline 3ab' was isolated using column chromatography (Petroleum ether/EtOAc = 2/1) as a colorless liquid (28 mg, 12%). ^{1}H NMR (300 MHz, Chloroform-*d*) δ 8.07 (d, *J* = 8.4, 1H), 7.99–7.94 (m, 1H), 7.67 (ddd, *J* = 8.4, 6.8, 1.5 Hz, 1H), 7.62–7.60 (m, 1H), 7.51 (ddd, *J* = 8.3, 6.9, 1.3 Hz, 1H), 4.13–4.02 (m, 1H), 3.95–3.83 (m, 1H), 2.88–2.75 (m, 1H), 2.71 (d, *J* = 1.0 Hz, 3H), 2.14–1.95 (m, 2H), 1.89–1.74 (m, 1H), 1.65 (s, 3H). ^{13}C{^{1}H}NMR (75.48 MHz, $CDCl_3$) δ 166.6, 147.5, 144.6, 129.9, 129.0, 127.2, 125.8, 123.7, 118.5, 86.2, 68.1, 37.7, 28.3, 26.1, 19.1; FTIR (KBr): ν_{max} = 2977, 2931, 1600, 1447, 1383, 1363, 1196, 1101, 1033, 761 cm^{-1}. HR-MS (ESI): *m*/*z* = 228.1380, calcd. for $C_{15}H_{17}NO$+H^+: 228.1283.

2-(1,3-dioxolan-2-yl)-4-methylquinoline 3ac [65] was isolated using column chromatography (Petroleum ether/EtOAc = 2/1) as a colorless liquid (54 mg, 25%). ^{1}H NMR (500 MHz, Chloroform-*d*) δ 8.16 (d, *J* = 8.4 Hz, 1H), 7.98 (d, *J* = 8.3 Hz, 1H), 7.74–7.67 (m, 1H), 7.59–7.53 (m, 1H), 7.49 (s, 1H), 5.95 (s, 1H), 4.27–4.19 (m, 2H), 4.16–4.08 (m, 2H), 2.71 (s, 3H). ^{13}C{^{1}H}NMR (75.48 MHz, $CDCl_3$) δ 156.7, 147.2, 145.7, 130.2, 129.5, 128.4, 126.9, 123.8, 118.7, 104.3, 65.8, 19.0.

2-(1,3-dioxolan-4-yl)-4-methylquinoline 3ac' [65] was isolated using column chromatography (Petroleum ether/EtOAc = 2/1) as a colorless liquid (18 mg, 8%). ^{1}H NMR (300 MHz, Chloroform-*d*) δ 8.05 (d, *J* = 8.4 Hz, 1H), 8.00 (dd, *J* = 8.4, 1.4 Hz, 1H), 7.71 (ddd, *J* = 8.4, 6.8, 1.4 Hz, 1H), 7.60–7.52 (m, 1H), 7.48 (s, 1H), 5.34 (s, 1H), 5.33–5.26 (m, 1H), 5.15 (s, 1H), 4.47–4.36 (m, 1H), 4.08 (dd, *J* = 8.3, 5.6 Hz, 1H), 2.73 (s, 3H). ^{13}C{^{1}H}NMR (75.48 MHz, $CDCl_3$) δ 160.0, 147.1, 146.0, 129.7, 129.5, 127.8, 126.5, 123.9, 118.8, 96.4, 78.3, 71.1, 19.1. FTIR (KBr): ν_{max} = 2925, 2855, 16001, 1509, 1449, 1157, 1088, 1029, 936, 760 cm^{-1}. HR-MS (ESI): *m*/*z* = 238.0841, calcd. for $C_{13}H_{13}NO_2$+Na^+: 238.0838.

2-(1,4-dioxan-2-yl)-4-methylquinoline 3ad [85] was isolated using column chromatography (Petroleum ether/EtOAc = 2/1) as white crystals (45 mg, 20%). Mp = 81–82 °C (lit. Mp = 82–83 °C [10.1039/C9OB02653C]). ^{1}H NMR (300 MHz, Chloroform-*d*) δ 8.10 (d, *J* = 8.5 Hz, 1H), 7.98 (d, *J* = 8.7 Hz, 1H), 7.76–7.64 (m, 1H), 7.59–7.51 (m, 1H), 7.47 (s, 1H), 4.92 (dd, *J* = 10.3, 2.9 Hz, 1H), 4.25 (dd, *J* = 11.7, 2.9 Hz, 1H), 4.06–3.94 (m, 2H), 3.88–3.74 (m,

2H), 3.70–3.57 (m, 1H), 2.73 (s, 3H). $^{13}C\{^{1}H\}$NMR (75.48 MHz, $CDCl_3$) δ 157.9, 147.4, 145.3, 129.9, 129.4, 127.7, 126.3, 123.8, 119.2, 78.9, 71.2, 67.2, 66.5, 18.9.

4-methyl-2-(tetrahydro-2H-pyran-2-yl)quinoline 3ae [85] was isolated using column chromatography (Petroleum ether/EtOAc = 2/1) as a colorless liquid (73 mg, 32%). ^{1}H NMR (300 MHz, Chloroform-*d*) δ 8.06 (d, *J* = 8.4 Hz, 1H), 7.98–7.89 (m, 1H), 7.70–7.60 (m, 1H), 7.52–7.46 (m, 1H), 7.45 (s, 1H), 4.60 (dd, *J* = 11.0, 2.3 Hz, 1H), 4.25–4.15 (m, 1H), 3.75–3.60 (m, 1H), 2.68 (s, 3H), 2.16–2.04 (m, 1H), 2.03–1.88 (m, 1H), 1.83–1.66 (m, 2H), 1.66–1.51 (m, 2H). $^{13}C\{^{1}H\}$NMR (75.48 MHz, $CDCl_3$) δ 162.2, 147.2, 145.1, 129.7, 129.1, 127.6, 125.9, 123.7, 118.9, 81.6, 68.9, 32.8, 25.9, 23.8, 18.9.

2-(1-ethoxyethyl)-4-methylquinoline 3af [85] was isolated using column chromatography (CH_2Cl_2/EtOAc = 20/1) as a colorless liquid (77 mg, 36%). ^{1}H NMR (300 MHz, Chloroform-*d*) δ 8.07 (d, *J* = 8.4 Hz, 1H), 7.97 (d, *J* = 8.3 Hz, 1H), 7.68 (t, *J* = 8.4 Hz, 1H), 7.57–7.48 (m, 1H), 7.44 (s, 1H), 4.69 (q, *J* = 6.6 Hz, 1H), 3.57– 3.45 (m, 1H), 3.47–3.34 (m, 1H), 2.72 (s, 3H), 1.53 (d, *J* = 6.6 Hz, 3H), 1.22 (t, *J* = 7.1 Hz, 3H).$^{13}C\{^{1}H\}$NMR (75.48 MHz, $CDCl_3$) δ 164.1, 147.2, 145.5, 129.6, 129.3, 127.8, 126.1, 123.8, 118.4, 79.7, 64.8, 22.7, 19.1, 15.6

2-methoxy-4-(tetrahydrofuran-2-yl)quinoline 3ba was isolated using column chromatography (EtOAc/petroleum ether 1/2) as a colorless liquid (122 mg, 53%). ^{1}H NMR (300 MHz, Chloroform-*d*) δ 7.89 (d, *J* = 8.4 Hz, 1H), 7.81–7.72 (m, 1H), 7.68–7.54 (m, 1H), 7.44–7.31 (m, 1H), 7.07 (s, 1H), 5.52 (t, *J* = 6.9 Hz, 1H), 4.27–4.13 (m, 1H), 4.08 (s, 3H), 4.08–3.95 (m, 1H), 2.65–2.47 (m, 1H), 2.14–1.92 (m, 2H), 1.92–1.78 (m, 1H). $^{13}C\{^{1}H\}$NMR (75.48 MHz, $CDCl_3$) δ 162.8, 152.3, 147.1, 129.2, 128.1, 123.8, 123.3, 122.9, 108.5, 76.8, 69.1, 53.4, 33.7, 26.0. FTIR (KBr): ν_{max} = 2979, 2949, 1612, 1575, 1473, 1438, 1387, 1366, 1340, 1238, 1195, 1080, 1055, 1024, 761 cm^{-1}. HR-MS (ESI): *m*/*z* = 230.1181, calcd. for $C_{14}H_{15}NO_2$+H^+: 230.1176

2-chloro-4-(tetrahydrofuran-2-yl)quinoline 3ca was isolated using column chromatography (Petroleum ether/EtOAc = 2/1) as a slightly yellow liquid (87 mg, 37%). ^{1}H NMR (300.13 MHz, $CDCl_3$) δ 8.04 (d, *J* = 8.5 Hz, 1H), 7.85 (dd, *J* = 8.4, 1.4 Hz, 1H), 7.71 (ddd, *J* = 8.4, 6.9, 1.4 Hz, 1H), 7.60–7.49 (m, 1H), 7.54 (s, 1H), 5.55 (t, *J* = 7.1 Hz, 1H), 4.22 (m, 1H), 4.02 (m, 1H), 2.70–2.55 (m, 1H), 2.13–1.95 (m, 2H), 1.94–1.76 (m, 1H).$^{13}C\{^{1}H\}$NMR (75.48 MHz, $CDCl_3$) δ 153.1, 151.4, 148.1, 130.2, 129.5, 126.8, 124.5, 123.4, 117.9, 76.7, 69.2, 34.0, 26.1. FTIR (KBr): ν_{max} = 2965, 2928, 2871, 1586, 1560, 1506, 1292, 1264, 1145, 1099, 1081, 1041, 1021, 878, 855, 792, 763 cm^{-1}. HR-MS (ESI): *m*/*z* = 234.0688, calcd. for $C_{13}H_{12}ClNO$+H^+: 234.0680.

2-methyl-4-(tetrahydrofuran-2-yl)quinoline 3ea [91] was isolated using column chromatography (Petroleum ether/EtOAc = 2/1) as a colorless liquid (161 mg, 75%). ^{1}H NMR (300 MHz, Chloroform-*d*) δ 8.03 (d, *J* = 8.3 Hz, 1H), 7.81 (d, *J* = 8.4 Hz, 1H), 7.69–7.57 (m, 1H), 7.50–7.41 (m, 1H), 7.42 (s, 1H), 5.53 (t, *J* = 7.1 Hz, 1H), 4.24–4.14 (m, 1H), 4.00 (q, *J* = 7.1 Hz, 1H), 2.65–2.47 (m, 1H), 2.12–1.89 (m, 2H), 1.86–1.72 (m, 1H). $^{13}C\{^{1}H\}$NMR (75.48 MHz, $CDCl_3$) δ 159.1, 149.4, 147.9, 129.4, 129.0, 125.5, 123.9, 123.0, 117.2, 76.8, 69.0, 33.9, 26.0, 25.6.

2-(tetrahydrofuran-2-yl)quinoxaline 3fa [66] was isolated using column chromatography (Petroleum ether/EtOAc = 2/1) as a colorless liquid (113 mg, 56%). ^{1}H NMR (300.13 MHz, $CDCl_3$) δ 9.02 (s, 1H), 8.12–8.07 (m, 1H), 8.07–8.01 (m, 1H), 7.76–7.69 (m, 2H), 5.21 (t, *J* = 7.0 Hz, 1H), 4.17 (q, *J* = 7.0 Hz, 1H), 4.05 (dd, *J* = 7.2 Hz, 1H), 2.57–2.46 (m, 1H), 2.21–2.11 (m, 1H), 2.11–2.00 (m, 2H). $^{13}C\{^{1}H\}$NMR (75.48 MHz, $CDCl_3$) δ 157.7, 143.6, 142.0, 141.7, 130.2, 129.6, 129.3, 129.2, 80.6, 69.5, 33.0, 26.1.

2-(tetrahydrofuran-2-yl)pyrazine 3ga was isolated using column chromatography (CH_2Cl_2/MeOH = 50/1) as a colorless liquid (59 mg, 40%).^{1}H NMR (300 MHz, Chloroform-*d*) δ 8.68 (s, 1H), 8.52–8.36 (m, 2H), 5.01 (t, *J* = 6.4 Hz, 1H), 4.14–4.02 (m, 1H), 4.00–3.87 (m, 1H), 2.49–2.29 (m, 1H), 2.11–1.86 (m, 3H). $^{13}C\{^{1}H\}$NMR (75.48 MHz, $CDCl_3$) δ 158.2, 143.8, 143.5, 142.7, 79.8, 69.3, 32.9, 25.9. FTIR (KBr): ν_{max} = 3389, 2959, 2882, 1724, 1701, 1406, 1304, 1140, 1052, 1020 cm^{-1}. HR-MS (ESI): *m*/*z* = 151.0873, calcd. for $C_8H_{10}N_2O$+H^+: 151.0866.

2-methyl-3-(tetrahydrofuran-2-yl)pyrazine 3ha was isolated using column chromatography (CH_2Cl_2/MeOH = 50/1) as a slightly yellow liquid (76 mg, 46%).^{1}H NMR (300 MHz, Chloroform-*d*) δ 8.37 (d, *J* = 2.6 Hz, 1H), 8.34 (d, *J* = 2.6 Hz, 1H), 5.15 (t, *J* = 7.0 Hz, 1H), 4.13–4.04 (m, 1H), 3.99–3.89 (m, 1H), 2.63 (s, 3H), 2.31–2.19 (m, 2H), 2.17–1.96 (m, 2H).

$^{13}C\{^1H\}$NMR (75.48 MHz, $CDCl_3$) δ 154.5, 152.5, 142.6, 141.5, 78.3, 69.2, 30.4, 26.3, 21.6. FTIR (KBr): ν_{max} = 3240, 3051, 2959, 2878, 1774, 1726, 1701, 1405, 1299, 1169, 1130, 1105, 1055, 988, 923, 857, 732 cm^{-1}. HR-MS (ESI): m/z = 165.1023, calcd. for $C_9H_{10}N_2O+H^+$: 165.1022.

Methyl 6-(tetrahydrofuran-2-yl)nicotinate 3ia [91] was isolated using column chromatography (EtOAc/DCM = 1/20→1/5) as an orange liquid (119 mg, 57%). ^1H NMR (300.13 MHz, $CDCl_3$) δ 9.11 (d, *J* = 2.2 Hz, 1H), 8.25 (dd, *J* = 8.2, 2.2 Hz, 1H), 7.52 (d, *J* = 8.2 Hz, 1H), 5.11–4.95 (m, 1H), 4.32–3.74 (m, 5H), 2.57–2.33 (m, 1H), 2.09–1.81 (m, 3H). $^{13}C\{^1H\}$NMR (75.48 MHz, $CDCl_3$) δ 167.8, 165.9, 150.4, 137.9, 124.6, 119.4, 81.2, 69.3, 52.4, 33.2, 25.8.

4-methyl-2-(tetrahydrofuran-2-yl)quinoline 1-oxide 3ja [76] was isolated using column chromatography (Petroleum ether/EtOAc = 2/1) as a colorless liquid (78 mg, 34%). ^1H NMR (300 MHz, Chloroform-*d*) δ 8.81–8.74 (m, 1H), 7.99–7.92 (m, 1H), 7.80–7.71 (m, 1H), 7.67–7.59 (m, 1H), 7.44 (s, 1H), 5.58 (t, *J* = 6.7 Hz, 1H), 4.17 (q, *J* = 6.9 Hz, 1H), 4.02 (q, *J* = 7.1 Hz, 1H), 2.90–2.76 (m, 1H), 2.68 (s, 3H), 2.13–1.98 (m, 1H), 1.99–1.82 (m, 2H). $^{13}C\{^1H\}$NMR (75.48 MHz, $CDCl_3$) δ 150.8, 141.1, 135.4, 130.3, 128.8, 128.0, 124.8, 119.9, 118.9, 76.1, 69.5, 31.2, 26.0, 18.6.

1-(tetrahydrofuran-2-yl)isoquinoline 3ka [91] was isolated using column chromatography (CH_2Cl_2/EtOAc from 5/1 to 5/2) as a colorless liquid (130 mg, 65%). ^1H NMR (300.13 MHz, $CDCl_3$) δ 8.50 (d, *J* = 5.8 Hz, 1H), 8.34 (d, *J* = 8.3 Hz, 1H), 7.82 (d, *J* = 8.1 Hz, 1H), 7.75–7.52 (m, 3H), 5.72 (t, *J* = 7.1 Hz, 1H), 4.20 (q, *J* = 7.3 Hz, 1H), 4.03 (q, *J* = 7.5 Hz, 1H), 2.60–2.32 (m, 2H), 2.27–2.01 (m, 2H).$^{13}C\{^1H\}$NMR (75.48 MHz, $CDCl_3$) δ 159.7, 141.4, 136.7, 130.1, 127.5, 127.3, 126.7, 125.5, 120.7, 79.2, 69.1, 30.9, 26.3.

2-(4-bromophenyl)imidazo [1,2-a]pyridine-3-carboxylic acid 3la' [106] was isolated using column chromatography (CH_2Cl_2/EtOAc = 5/2) as slightly yellow crystals (82 mg, 30%). ^1H NMR (300 MHz, Chloroform-*d*) δ 9.27 (bs, 1H, NH), 8.41 (d, *J* = 8.4 Hz, 1H), 8.28–8.19 (m, 1H), 7.84 (d, *J* = 8.5 Hz, 2H), 7.81–7.74 (m, 1H), 7.62 (d, *J* = 8.5 Hz, 2H), 7.09 (dd, *J* = 7.3, 4.9 Hz, 1H). $^{13}C\{^1H\}$NMR (75.48 MHz, $CDCl_3$) δ 165.1, 151.5, 147.1, 139.3, 133.1, 132.2, 129.2, 127.4, 120.2, 114.8.

4. Conclusions

In this work, a new visible-light active heterogeneous photocatalyst system based on industrially available and non-toxic TiO_2 and NHPI was proposed for the cross-dehydrogenative C–C coupling of electron-deficient N-heterocycles with ethers. In this photocatalytic system, phthalimide-*N*-oxyl radicals photogenerated on the surface of titanium oxide become active mediators of the reaction, which leads to 1) an increase in efficiency due to the homogeneous organocatalytic process in solution and 2) allows the selective cleavage of the weak CH bonds. We have proposed a new mild method for the generation of C-centered radicals from non-activated esters for the Minisci reaction. Despite the fact that acidic additives are frequently used in Minisci-type reactions, the addition of acid was not necessary in our procedure in the case of several substrates. Optimal conditions were chosen for the Minisci reaction between π-deficient pyridine, quinoline, pyrazine, and quinoxaline heteroarenes with non-activated ethers.

Supplementary Materials: The following supporting information can be downloaded at: https://www.mdpi.com/article/10.3390/molecules28030934/s1, copies of NMR spectra of the synthesized products, the comparison of the developed method with the literature procedure, the determination of the side products of the studied reaction.

Author Contributions: Conceptualization, I.B.K.; methodology, I.B.K. and E.R.L.; investigation, E.R.L., O.O.S., V.M.M. and A.I.I.; writing—original draft preparation, E.R.L.; writing—review and editing, I.B.K. and A.O.T.; supervision, I.B.K. and A.O.T.; project administration, I.B.K. All authors have read and agreed to the published version of the manuscript.

Funding: This research received no external funding.

Institutional Review Board Statement: Not applicable.

Informed Consent Statement: Not applicable.

Data Availability Statement: Not applicable.

Acknowledgments: We are grateful to the Department of Structural Studies, Zelinsky Institute of Organic Chemistry for the HRMS analysis.

Conflicts of Interest: The authors declare no conflict of interest.

Sample Availability: Not applicable.

References

1. Friedmann, D.; Hakki, A.; Kim, H.; Choi, W.; Bahnemann, D. Heterogeneous Photocatalytic Organic Synthesis: State-of-the-Art and Future Perspectives. *Green Chem.* **2016**, *18*, 5391–5411. [CrossRef]
2. Xiao, J.; Liu, X.; Pan, L.; Shi, C.; Zhang, X.; Zou, J.-J. Heterogeneous Photocatalytic Organic Transformation Reactions Using Conjugated Polymers-Based Materials. *ACS Catal.* **2020**, *10*, 12256–12283. [CrossRef]
3. Kohtani, S.; Kawashima, A.; Miyabe, H. Stereoselective Organic Reactions in Heterogeneous Semiconductor Photocatalysis. *Front. Chem.* **2019**, *7*, 630. [CrossRef] [PubMed]
4. Verma, S.K.; Verma, R.; Girish, Y.R.; Xue, F.; Yan, L.; Verma, S.; Singh, M.; Vaishnav, Y.; Shaik, A.B.; Bhandare, R.R.; et al. Heterogeneous Graphitic Carbon Nitrides in Visible-Light-Initiated Organic Transformations. *Green Chem.* **2022**, *24*, 438–479. [CrossRef]
5. Chen, J.; Cen, J.; Xu, X.; Li, X. The Application of Heterogeneous Visible Light Photocatalysts in Organic Synthesis. *Catal. Sci. Technol.* **2016**, *6*, 349–362. [CrossRef]
6. Li, F.; Cheng, L.; Fan, J.; Xiang, Q. Steering the Behavior of Photogenerated Carriers in Semiconductor Photocatalysts: A New Insight and Perspective. *J. Mater. Chem. A* **2021**, *9*, 23765–23782. [CrossRef]
7. Wang, H.; Zhang, L.; Chen, Z.; Hu, J.; Li, S.; Wang, Z.; Liu, J.; Wang, X. Semiconductor Heterojunction Photocatalysts: Design, Construction, and Photocatalytic Performances. *Chem. Soc. Rev.* **2014**, *43*, 5234. [CrossRef] [PubMed]
8. Miyauchi, M.; Irie, H.; Liu, M.; Qiu, X.; Yu, H.; Sunada, K.; Hashimoto, K. Visible-Light-Sensitive Photocatalysts: Nanocluster-Grafted Titanium Dioxide for Indoor Environmental Remediation. *J. Phys. Chem. Lett.* **2016**, *7*, 75–84. [CrossRef] [PubMed]
9. Ahmed, S.N.; Haider, W. Heterogeneous Photocatalysis and Its Potential Applications in Water and Wastewater Treatment: A Review. *Nanotechnology* **2018**, *29*, 342001. [CrossRef]
10. Thambiliyagodage, C. Activity Enhanced TiO_2 Nanomaterials for Photodegradation of Dyes—A Review. *Environ. Nanotechnol. Monit. Manag.* **2021**, *16*, 100592. [CrossRef]
11. Marchuk, M.V.; Asanov, I.P.; Panafidin, M.A.; Vorotnikov, Y.A.; Shestopalov, M.A. Nano TiO_2 and Molybdenum/Tungsten Iodide Octahedral Clusters: Synergism in UV/Visible-Light Driven Degradation of Organic Pollutants. *Nanomaterials* **2022**, *12*, 4282. [CrossRef]
12. Stavitskaya, A.; Glotov, A.; Pouresmaeil, F.; Potapenko, K.; Sitmukhanova, E.; Mazurova, K.; Ivanov, E.; Kozlova, E.; Vinokurov, V.; Lvov, Y. CdS Quantum Dots in Hierarchical Mesoporous Silica Templated on Clay Nanotubes: Implications for Photocatalytic Hydrogen Production. *ACS Appl. Nano Mater.* **2022**, *5*, 605–614. [CrossRef]
13. Kurenkova, A.Y.; Medvedeva, T.B.; Gromov, N.V.; Bukhtiyarov, A.V.; Gerasimov, E.Y.; Cherepanova, S.V.; Kozlova, E.A. Sustainable Hydrogen Production from Starch Aqueous Suspensions over a $Cd_{0.7}Zn_{0.3}S$-Based Photocatalyst. *Catalysts* **2021**, *11*, 870. [CrossRef]
14. Kozlova, E.A.; Lyulyukin, M.N.; Kozlov, D.V.; Parmon, V.N. Semiconductor Photocatalysts and Mechanisms of Carbon Dioxide Reduction and Nitrogen Fixation under UV and Visible Light. *Russ. Chem. Rev.* **2021**, *90*, 1520–1543. [CrossRef]
15. Wang, J.; Guo, R.; Bi, Z.; Chen, X.; Hu, X.; Pan, W. A Review on TiO_{2-x}-Based Materials for Photocatalytic CO_2 Reduction. *Nanoscale* **2022**, *14*, 11512–11528. [CrossRef]
16. Shtyka, O.; Shatsila, V.; Ciesielski, R.; Kedziora, A.; Maniukiewicz, W.; Dubkov, S.; Gromov, D.; Tarasov, A.; Rogowski, J.; Stadnichenko, A.; et al. Adsorption and Photocatalytic Reduction of Carbon Dioxide on TiO_2. *Catalysts* **2020**, *11*, 47. [CrossRef]
17. Eidsvåg, H.; Bentouba, S.; Vajeeston, P.; Yohi, S.; Velauthapillai, D. TiO_2 as a Photocatalyst for Water Splitting—An Experimental and Theoretical Review. *Molecules* **2021**, *26*, 1687. [CrossRef]
18. Bian, Y.; Gu, Y.; Zhang, X.; Chen, H.; Li, Z. Engineering $BiOBr_xI_{1-x}$ Solid Solutions with Enhanced Singlet Oxygen Production for Photocatalytic Benzylic C-H Bond Activation Mediated by N-Hydroxyl Compounds. *Chin. Chem. Lett.* **2021**, *32*, 2837–2840. [CrossRef]
19. Shi, G.; Xu, S.; Bao, Y.; Xu, J.; Liang, Y. Selective Aerobic Oxidation of Toluene to Benzaldehyde on Immobilized CoO_x on SiO_2 Catalyst in the Presence of N-Hydroxyphthalimide and Hexafluoropropan-2-Ol. *Catal. Commun.* **2019**, *123*, 73–78. [CrossRef]
20. Krylov, I.B.; Lopat'eva, E.R.; Subbotina, I.R.; Nikishin, G.I.; Yu, B.; Terent'ev, A.O. Mixed Hetero-/Homogeneous TiO_2/N-Hydroxyimide Photocatalysis in Visible-Light-Induced Controllable Benzylic Oxidation by Molecular Oxygen. *Chin. J. Catal.* **2021**, *42*, 1700–1711. [CrossRef]
21. Wang, Y.; Wang, X.; Antonietti, M. Polymeric Graphitic Carbon Nitride as a Heterogeneous Organocatalyst: From Photochemistry to Multipurpose Catalysis to Sustainable Chemistry. *Angew. Chem. Int. Ed.* **2012**, *51*, 68–89. [CrossRef] [PubMed]

22. Hao, H.; Shi, J.-L.; Xu, H.; Li, X.; Lang, X. N-Hydroxyphthalimide-TiO_2 Complex Visible Light Photocatalysis. *Appl. Catal. B: Environ.* **2019**, *246*, 149–155. [CrossRef]
23. Li, H.; Li, X.; Lang, X. Extending the π-Conjugated Molecules on TiO_2 for the Selective Photocatalytic Aerobic Oxidation of Sulfides Triggered by Visible Light. *Sustain. Energy Fuels* **2021**, *5*, 2127–2135. [CrossRef]
24. Bhat, V.T.; Duspara, P.A.; Seo, S.; Abu Bakar, N.S.B.; Greaney, M.F. Visible Light Promoted Thiol-Ene Reactions Using Titanium Dioxide. *Chem. Commun.* **2015**, *51*, 4383–4385. [CrossRef]
25. Park, S.; Jeong, J.; Fujita, K.; Yamamoto, A.; Yoshida, H. Anti-Markovnikov Hydroamination of Alkenes with Aqueous Ammonia by Metal-Loaded Titanium Oxide Photocatalyst. *J. Am. Chem. Soc.* **2020**, *142*, 12708–12714. [CrossRef]
26. Manley, D.W.; Walton, J.C. A Clean and Selective Radical Homocoupling Employing Carboxylic Acids with Titania Photoredox Catalysis. *Org. Lett.* **2014**, *16*, 5394–5397. [CrossRef]
27. Manley, D.W.; McBurney, R.T.; Miller, P.; Walton, J.C.; Mills, A.; O'Rourke, C. Titania-Promoted Carboxylic Acid Alkylations of Alkenes and Cascade Addition–Cyclizations. *J. Org. Chem.* **2014**, *79*, 1386–1398. [CrossRef]
28. Zhu, Q.; Nocera, D.G. Photocatalytic Hydromethylation and Hydroalkylation of Olefins Enabled by Titanium Dioxide Mediated Decarboxylation. *J. Am. Chem. Soc.* **2020**, *142*, 17913–17918. [CrossRef]
29. Savateev, A.; Ghosh, I.; König, B.; Antonietti, M. Photoredox Catalytic Organic Transformations Using Heterogeneous Carbon Nitrides. *Angew. Chem. Int. Ed.* **2018**, *57*, 15936–15947. [CrossRef]
30. Bianchi, P.; Williams, J.D.; Kappe, C.O. Continuous Flow Processing of Bismuth-Photocatalyzed Atom Transfer Radical Addition Reactions Using an Oscillatory Flow Reactor. *Green Chem.* **2021**, *23*, 2685–2693. [CrossRef]
31. Ghosh, I.; Khamrai, J.; Savateev, A.; Shlapakov, N.; Antonietti, M.; König, B. Organic Semiconductor Photocatalyst Can Bifunctionalize Arenes and Heteroarenes. *Science* **2019**, *365*, 360–366. [CrossRef]
32. Wang, J.; Su, P.; Abdolmohammadi, S.; Vessally, E. A Walk around the Application of Nanocatalysts for Cross-Dehydrogenative Coupling of C–H Bonds. *RSC Adv.* **2019**, *9*, 41684–41702. [CrossRef] [PubMed]
33. Buglioni, L.; Riente, P.; Palomares, E.; Pericàs, M.A. Visible-Light-Promoted Arylation Reactions Photocatalyzed by Bismuth(III) Oxide: Visible-Light-Promoted Arylation Reactions Photocatalyzed by Bismuth(III) Oxide. *Eur. J. Org. Chem.* **2017**, *2017*, 6986–6990. [CrossRef]
34. Franchi, D.; Amara, Z. Applications of Sensitized Semiconductors as Heterogeneous Visible-Light Photocatalysts in Organic Synthesis. *ACS Sustain. Chem. Eng.* **2020**, *8*, 15405–15429. [CrossRef]
35. Peiris, S.; Silva, H.B.; Ranasinghe, K.N.; Bandara, S.V.; Perera, I.R. Recent Development and Future Prospects of TiO_2 Photocatalysis. *J. Chin. Chem. Soc.* **2021**, *68*, 738–769. [CrossRef]
36. Arora, I.; Chawla, H.; Chandra, A.; Sagadevan, S.; Garg, S. Advances in the Strategies for Enhancing the Photocatalytic Activity of TiO_2: Conversion from UV-Light Active to Visible-Light Active Photocatalyst. *Inorg. Chem. Commun.* **2022**, *143*, 109700. [CrossRef]
37. Basavarajappa, P.S.; Patil, S.B.; Ganganagappa, N.; Reddy, K.R.; Raghu, A.V.; Reddy, C.V. Recent Progress in Metal-Doped TiO_2, Non-Metal Doped/Codoped TiO_2 and TiO_2 Nanostructured Hybrids for Enhanced Photocatalysis. *Int. J. Hydrogen Energy* **2020**, *45*, 7764–7778. [CrossRef]
38. Zani, L.; Melchionna, M.; Montini, T.; Fornasiero, P. Design of Dye-Sensitized TiO_2 Materials for Photocatalytic Hydrogen Production: Light and Shadow. *J. Phys. Energy* **2021**, *3*, 031001. [CrossRef]
39. Choi, S.K.; Yang, H.S.; Kim, J.H.; Park, H. Organic Dye-Sensitized TiO_2 as a Versatile Photocatalyst for Solar Hydrogen and Environmental Remediation. *Appl. Catal. B Environ.* **2012**, *121–122*, 206–213. [CrossRef]
40. Gorduk, S.; Avciata, O.; Avciata, U. Hydrothermal in Situ Preparation of Phthalocyanine–TiO_2 Nanocomposites for Photocatalytic Activity under Visible Light Irradiation. *Res. Chem. Intermed.* **2021**, *47*, 615–635. [CrossRef]
41. Zhou, X.; Wang, X.; Li, J.; Zhang, X. Enhanced Photocatalytic Activity in Metal Phthalocyanine-Sensitized TiO_2 Nanorods. *Res. Chem. Intermed.* **2021**, *47*, 1519–1533. [CrossRef]
42. Yang, L.; Li, L.; Li, L.; Liu, C.; Li, J.; Lai, B.; Li, N. N/Fe/Zn Co-Doped TiO_2 Loaded on Basalt Fiber with Enhanced Photocatalytic Activity for Organic Pollutant Degradation. *RSC Adv.* **2021**, *11*, 4942–4951. [CrossRef] [PubMed]
43. Wafi, A.; Szabó-Bárdos, E.; Horváth, O.; Makó, É.; Jakab, M.; Zsirka, B. Coumarin-Based Quantification of Hydroxyl Radicals and Other Reactive Species Generated on Excited Nitrogen-Doped TiO_2. *J. Photochem. Photobiol. A Chem.* **2021**, *404*, 112913. [CrossRef]
44. Gui, Q.-W.; Teng, F.; Yu, P.; Wu, Y.-F.; Nong, Z.-B.; Yang, L.-X.; Chen, X.; Yang, T.-B.; He, W.-M. Visible Light-Induced Z-Scheme V_2O_5/g-C_3N_4 Heterojunction Catalyzed Cascade Reaction of Unactivated Alkenes. *Chin. J. Catal.* **2023**, *44*, 111–116. [CrossRef]
45. Khan, S.; Sadiq, M.; Kim, D.; Ullah, M.; Muhammad, N. TiO_2 and Its Binary $ZnTiO_2$ and Ternary $CdZnTiO_2$ Nanocomposites as Efficient Photocatalysts for the Organic Dyes Degradation. *Appl. Water Sci.* **2022**, *12*, 118. [CrossRef]
46. Wu, J.; Ou, P.; Lin, Y.; Tan, X.; Wei, F.; Mi, Y.; Liu, S.; Huang, K. Oxygen Vacancies and Bi_2S_3 Nanoparticles Co-Sensitized TiO_2 Nanotube Arrays for Enhanced Photoelectrochemical Sensing of Chlorpyrifos. *J. Electroanal. Chem.* **2022**, *911*, 116220. [CrossRef]
47. Liu, S.; Zou, Q.; Ma, Y.; Chi, D.; Chen, R.; Fang, H.; Hu, W.; Zhang, K.; Chen, L.-F. Metal-Organic Frameworks Derived TiO_2/Carbon Nitride Heterojunction Photocatalyst with Efficient Catalytic Performance under Visible Light. *Inorg. Chim. Acta* **2022**, *536*, 120918. [CrossRef]
48. Shawky, A.; Alahmadi, N.; Mohamed, R.M.; Zaki, Z.I. Bi_2S_3-Sensitized TiO_2 Nanostructures Prepared by Solution Process for Highly Efficient Photoreduction of Hexavalent Chromium Ions in Water under Visible Light. *Opt. Mater.* **2022**, *124*, 111964. [CrossRef]

49. Cipagauta-Díaz, S.; Estrella-González, A.; Navarrete-Magaña, M.; Gómez, R. N Doped -TiO_2 Coupled to $BiVO_4$ with High Performance in Photodegradation of Ofloxacin Antibiotic and Rhodamine B Dye under Visible Light. *Catal. Today* **2022**, *394–396*, 445–457. [CrossRef]
50. Rajh, T.; Nedeljkovic, J.M.; Chen, L.X.; Poluektov, O.; Thurnauer, M.C. Improving Optical and Charge Separation Properties of Nanocrystalline TiO_2 by Surface Modification with Vitamin C. *J. Phys. Chem. B* **1999**, *103*, 3515–3519. [CrossRef]
51. Sredojević, D.N.; Kovač, T.; Džunuzović, E.; Đorđević, V.; Grgur, B.N.; Nedeljković, J.M. Surface-Modified TiO_2 Powders with Phenol Derivatives: A Comparative DFT and Experimental Study. *Chem. Phys. Lett.* **2017**, *686*, 167–172. [CrossRef]
52. Zhang, T.; Wojtal, P.; Rubel, O.; Zhitomirsky, I. Density Functional Theory and Experimental Studies of Caffeic Acid Adsorption on Zinc Oxide and Titanium Dioxide Nanoparticles. *RSC Adv.* **2015**, *5*, 106877–106885. [CrossRef]
53. Higashimoto, S.; Nishi, T.; Yasukawa, M.; Azuma, M.; Sakata, Y.; Kobayashi, H. Photocatalysis of Titanium Dioxide Modified by Catechol-Type Interfacial Surface Complexes (ISC) with Different Substituted Groups. *J. Catal.* **2015**, *329*, 286–290. [CrossRef]
54. Moongraksathum, B.; Hsu, P.-T.; Chen, Y.-W. Photocatalytic Activity of Ascorbic Acid-Modified TiO_2 Sol Prepared by the Peroxo Sol–Gel Method. *J. Sol-Gel Sci. Technol.* **2016**, *78*, 647–659. [CrossRef]
55. Fujisawa, J.; Matsumura, S.; Hanaya, M. A Single Ti-O-C Linkage Induces Interfacial Charge-Transfer Transitions between TiO_2 and a π-Conjugated Molecule. *Chem. Phys. Lett.* **2016**, *657*, 172–176. [CrossRef]
56. Bui, H.T.; Park, H.Y.; Alvarez, P.J.J.; Lee, J.; Kim, W.; Kim, E.-J. Visible-Light Activation of a Dissolved Organic Matter–TiO_2 Complex Mediated via Ligand-to-Metal Charge Transfer. *Environ. Sci. Technol.* **2022**, *56*, 10829–10837. [CrossRef] [PubMed]
57. Terent'ev, A.O.; Krylov, I.B.; Sharipov, M.Y.; Kazanskaya, Z.M.; Nikishin, G.I. Generation and Cross-Coupling of Benzyl and Phthalimide-N-Oxyl Radicals in a Cerium(IV) Ammonium Nitrate/N-Hydroxyphthalimide/$ArCH_2R$ System. *Tetrahedron* **2012**, *68*, 10263–10271. [CrossRef]
58. Terent'ev, A.O.; Krylov, I.B.; Timofeev, V.P.; Starikova, Z.A.; Merkulova, V.M.; Ilovaisky, A.I.; Nikishin, G.I. Oxidative C-O Cross-Coupling of 1,3-Dicarbonyl Compounds and Their Heteroanalogues with *N* -Substituted Hydroxamic Acids and *N* -Hydroxyimides. *Adv. Synth. Catal.* **2013**, *355*, 2375–2390. [CrossRef]
59. Krylov, I.B.; Lopat'eva, E.R.; Budnikov, A.S.; Nikishin, G.I.; Terent'ev, A.O. Metal-Free Cross-Dehydrogenative C–O Coupling of Carbonyl Compounds with *N* -Hydroxyimides: Unexpected Selective Behavior of Highly Reactive Free Radicals at an Elevated Temperature. *J. Org. Chem.* **2020**, *85*, 1935–1947. [CrossRef] [PubMed]
60. Kammer, L.; Rahman, A.; Opatz, T. A Visible Light-Driven Minisci-Type Reaction with N-Hydroxyphthalimide Esters. *Molecules* **2018**, *23*, 764. [CrossRef]
61. Fiorati, A.; Gambarotti, C.; Melone, L.; Pastori, N.; Punta, C.; Raffaini, G.; Truscello, A. Recent Advances in Photocatalytic Minisci Reaction: An Eco-Friendly Functionalization of Biologically Relevant Heteroarenes. In *Green Synthetic Approaches for Biologically Relevant Heterocycles*; Elsevier: Amsterdam, The Netherlands, 2021; pp. 189–206, ISBN 978-0-12-820586-0.
62. Proctor, R.S.J.; Phipps, R.J. Recent Advances in Minisci-Type Reactions. *Angew. Chem. Int. Ed.* **2019**, *58*, 13666–13699. [CrossRef] [PubMed]
63. Minisci, F.; Bernardi, R.; Bertini, F.; Galli, R.; Perchinummo, M. Nucleophilic Character of Alkyl Radicals—VI. *Tetrahedron* **1971**, *27*, 3575–3579. [CrossRef]
64. Duncton, M.A.J. Minisci Reactions: Versatile CH-Functionalizations for Medicinal Chemists. *Med. Chem. Commun.* **2011**, *2*, 1135. [CrossRef]
65. Fontana, F.; Minisci, F.; Yong, M.Y.; Lihua, Z. A Novel and Mild Source of Carbon-Centered Radicals by Iodosobenzene Diacetate (IBDA) and Sodium Azide from Alcohols, Ethers, Aldehydes, Amides and Alkyl Iodides. *Tetrahedron Lett.* **1993**, *34*, 2517–2520. [CrossRef]
66. Devari, S.; Shah, B.A. Visible Light-Promoted C–H Functionalization of Ethers and Electron-Deficient Arenes. *Chem. Commun.* **2016**, *52*, 1490–1493. [CrossRef] [PubMed]
67. Tauber, J.; Imbri, D.; Opatz, T. Radical Addition to Iminium Ions and Cationic Heterocycles. *Molecules* **2014**, *19*, 16190–16222. [CrossRef]
68. McCallum, T.; Jouanno, L.-A.; Cannillo, A.; Barriault, L. Persulfate-Enabled Direct C–H Alkylation of Heteroarenes with Unactivated Ethers. *Synlett* **2016**, *27*, 1282–1286. [CrossRef]
69. Chupakhin, O.N.; Charushin, V.N. Recent Advances in the Field of Nucleophilic Aromatic Substitution of Hydrogen. *Tetrahedron Lett.* **2016**, *57*, 2665–2672. [CrossRef]
70. Charushin, V.N.; Chupakhin, O.N. Nucleophilic C—H Functionalization of Arenes: A Contribution to Green Chemistry. *Russ. Chem. Bull.* **2019**, *68*, 453–471. [CrossRef]
71. Akulov, A.A.; Varaksin, M.V.; Mampuys, P.; Charushin, V.N.; Chupakhin, O.N.; Maes, B.U.W. C(Sp^2)–H Functionalization in Non-Aromatic Azomethine-Based Heterocycles. *Org. Biomol. Chem.* **2021**, *19*, 297–312. [CrossRef]
72. Liu, X.-L.; Jiang, L.-B.; Luo, M.-P.; Ren, Z.; Wang, S.-G. Recent Advances in Catalytic Enantioselective Direct C–H Bond Functionalization of Electron-Deficient N-Containing Heteroarenes. *Org. Chem. Front.* **2022**, *9*, 265–280. [CrossRef]
73. Jeong, J.; Patel, P.; Hwang, H.; Chang, S. Rhodium(III)-Catalyzed C–C Bond Formation of Quinoline *N*-Oxides at the C-8 Position under Mild Conditions. *Org. Lett.* **2014**, *16*, 4598–4601. [CrossRef]
74. Sharma, U.; Park, Y.; Chang, S. Rh(III)-Catalyzed Traceless Coupling of Quinoline *N*-Oxides with Internal Diarylalkynes. *J. Org. Chem.* **2014**, *79*, 9899–9906. [CrossRef] [PubMed]

75. Zhang, X.; Qi, Z.; Li, X. Rhodium(III)-Catalyzed C-C and C-O Coupling of Quinoline *N*-Oxides with Alkynes: Combination of C-H Activation with O-Atom Transfer. *Angew. Chem.* **2014**, *126*, 10970–10974. [CrossRef]
76. Wu, Z.; Pi, C.; Cui, X.; Bai, J.; Wu, Y. Direct C-2 Alkylation of Quinoline *N*-Oxides with Ethers via Palladium-Catalyzed Dehydrogenative Cross-Coupling Reaction. *Adv. Synth. Catal.* **2013**, *355*, 1971–1976. [CrossRef]
77. Huang, C.; Wang, J.-H.; Qiao, J.; Fan, X.-W.; Chen, B.; Tung, C.-H.; Wu, L.-Z. Direct Arylation of Unactivated Alkanes with Heteroarenes by Visible-Light Catalysis. *J. Org. Chem.* **2019**, *84*, 12904–12912. [CrossRef] [PubMed]
78. Quattrini, M.C.; Fujii, S.; Yamada, K.; Fukuyama, T.; Ravelli, D.; Fagnoni, M.; Ryu, I. Versatile Cross-Dehydrogenative Coupling of Heteroaromatics and Hydrogen Donors via Decatungstate Photocatalysis. *Chem. Commun.* **2017**, *53*, 2335–2338. [CrossRef] [PubMed]
79. Bhakat, M.; Khatua, B.; Guin, J. Photocatalytic Aerobic Coupling of Azaarenes and Alkanes via Nontraditional Cl $^{\bullet}$ Generation. *Org. Lett.* **2022**, *24*, 5276–5280. [CrossRef]
80. Jung, S.; Lee, H.; Moon, Y.; Jung, H.-Y.; Hong, S. Site-Selective C–H Acylation of Pyridinium Derivatives by Photoredox Catalysis. *ACS Catal.* **2019**, *9*, 9891–9896. [CrossRef]
81. Tian, H.; Yang, H.; Tian, C.; An, G.; Li, G. Cross-Dehydrogenative Coupling of Strong C(Sp^3)–H with *N* -Heteroarenes through Visible-Light-Induced Energy Transfer. *Org. Lett.* **2020**, *22*, 7709–7715. [CrossRef] [PubMed]
82. Huang, C.-Y.; Li, J.; Liu, W.; Li, C.-J. Diacetyl as a "Traceless" Visible Light Photosensitizer in Metal-Free Cross-Dehydrogenative Coupling Reactions. *Chem. Sci.* **2019**, *10*, 5018–5024. [CrossRef]
83. Li, L.; Song, X.; Qi, M.-F.; Sun, B. Weak Brønsted Base-Promoted Photoredox Catalysis for C-H Alkylation of Heteroarenes Mediated by Triplet Excited Diaryl Ketone. *Tetrahedron Lett.* **2022**, *99*, 153846. [CrossRef]
84. Bhakat, M.; Biswas, P.; Dey, J.; Guin, J. Heteroarylation of Ethers, Amides, and Alcohols with Light and O_2. *Org. Lett.* **2021**, *23*, 6886–6890. [CrossRef]
85. Zhao, H.; Li, Z.; Jin, J. Green Oxidant H_2O_2 as a Hydrogen Atom Transfer Reagent for Visible Light-Mediated Minisci Reaction. *New J. Chem.* **2019**, *43*, 12533–12537. [CrossRef]
86. Zhang, L.; Zhang, G.; Li, Y.; Wang, S.; Lei, A. The Synergistic Effect of Self-Assembly and Visible-Light Induced the Oxidative C–H Acylation of N-Heterocyclic Aromatic Compounds with Aldehydes. *Chem. Commun.* **2018**, *54*, 5744–5747. [CrossRef] [PubMed]
87. Li, X.; Liu, C.; Guo, S.; Wang, W.; Zhang, Y. PIFA-Mediated Cross-Dehydrogenative Coupling of *N* -Heteroarenes with Cyclic Ethers: Ethanol as an Efficient Promoter. *Eur. J. Org. Chem.* **2021**, *2021*, 411–421. [CrossRef]
88. Utepova, I.A.; Trestsova, M.A.; Chupakhin, O.N.; Charushin, V.N.; Rempel, A.A. Aerobic Oxidative C–H/C–H Coupling of Azaaromatics with Indoles and Pyrroles in the Presence of TiO_2 as a Photocatalyst. *Green Chem.* **2015**, *17*, 4401–4410. [CrossRef]
89. Li, Z.; Wu, L.; Guo, J.; Shao, Y.; Song, Y.; Ding, Y.; Zhu, L.; Yao, X. Light-Promoted Minisci Coupling Reaction of Ethers and Aza Aromatics Catalyzed by Au/TiO_2 Heterogeneous Photocatalyst. *ChemCatChem* **2021**, *13*, 3671–3678. [CrossRef]
90. Qiao, J.; Song, Z.; Huang, C.; Ci, R.; Liu, Z.; Chen, B.; Tung, C.; Wu, L. Direct, Site-Selective and Redox-Neutral A-C−H Bond Functionalization of Tetrahydrofurans via Quantum Dots Photocatalysis. *Angew. Chem. Int. Ed.* **2021**, *60*, 27201–27205. [CrossRef] [PubMed]
91. Vijeta, A.; Reisner, E. Carbon Nitride as a Heterogeneous Visible-Light Photocatalyst for the Minisci Reaction and Coupling to H_2 Production. *Chem. Commun.* **2019**, *55*, 14007–14010. [CrossRef] [PubMed]
92. Boyd, A.A.; Flaud, P.-M.; Daugey, N.; Lesclaux, R. Rate Constants for RO_2 + HO_2 Reactions Measured under a Large Excess of HO_2. *J. Phys. Chem. A* **2003**, *107*, 818–821. [CrossRef]
93. Opeida, I.A.; Sheparovych, R.B. Inhibition by Hydrogen Peroxide in the Radical Chain Oxidation of Hydrocarbons by Molecular Oxygen. *Theor. Exp. Chem.* **2019**, *55*, 36–42. [CrossRef]
94. Opeida, I.A.; Sheparovych, R.B.; Hrynda, Y.M.; Khavunko, O.Y.; Kompanets, M.O.; Shendryk, A.N. Kinetics of Oxidation of Benzyl Alcohols with Molecular Oxygen Catalyzed by *N*-hydroxyphthalimide: Role of Hydroperoxyl Radicals. *Int. J. Chem. Kinet.* **2019**, *51*, 679–688. [CrossRef]
95. Patil, S.V.; Tanko, J.M. Radical Additions of Acyclic and Cyclic Ethers to Alkenes via an Allyl Transfer Reaction Involving Phthalimido-N-Oxyl Radical. *Tetrahedron* **2016**, *72*, 7849–7858. [CrossRef]
96. Terent'ev, A.O.; Platonov, M.M.; Krylov, I.B.; Chernyshev, V.V.; Nikishin, G.I. Synthesis of 1-Hydroperoxy-1′-Alkoxyperoxides by the Iodine-Catalyzed Reactions of Geminal Bishydroperoxides with Acetals or Enol Ethers. *Org. Biomol. Chem.* **2008**, *6*, 4435. [CrossRef] [PubMed]
97. Terent'ev, A.O.; Sharipov, M.Y.; Krylov, I.B.; Gaidarenko, D.V.; Nikishin, G.I. Manganese Triacetate as an Efficient Catalyst for Bisperoxidation of Styrenes. *Org. Biomol. Chem.* **2015**, *13*, 1439–1445. [CrossRef] [PubMed]
98. Terent'ev, A.; Borisov, D.; Semenov, V.; Chernyshev, V.; Dembitsky, V.; Nikishin, G. Selective Synthesis of Unsymmetrical Peroxides: Transition-Metal-Catalyzed Oxidation of Malononitrile and Cyanoacetic Ester Derivatives by Tert-Butyl Hydroperoxide at the α-Position. *Synthesis* **2011**, *2011*, 2091–2100. [CrossRef]
99. Pastori, N.; Gambarotti, C.; Punta, C. Recent Developments in Nucleophilic Radical Addition to Imines: The Key Role of Transition Metals and the New Porta Radical-Type Version of the Mannich and Strecker Reactions. *MROC* **2009**, *6*, 184–195. [CrossRef]
100. Vil', V.A.; Grishin, S.S.; Baberkina, E.P.; Kostyagina, V.A.; Kovalenko, A.E.; Terent'ev, A.O. Radical Addition of Tetrahydrofuran to Imines Assisted by Tert-Butyl Hydroperoxide. *Tetrahedron Lett.* **2020**, *61*, 152150. [CrossRef]

101. Clerici, A.; Cannella, R.; Pastori, N.; Panzeri, W.; Porta, O. A Free Radical Mannich Type Reaction: Selective α-CH Aminomethylation of Ethers by Ti(III)/t-BuOOH System under Aqueous Acidic Conditions. *Tetrahedron* **2006**, *62*, 5986–5994. [CrossRef]
102. Zhang, Y.; Zhang, S.; Xu, G.; Li, M.; Tang, C.; Fan, W. Cu-Catalyzed Carbamoylation *versus* Amination of Quinoline *N*-Oxide with Formamides. *Org. Biomol. Chem.* **2019**, *17*, 309–314. [CrossRef] [PubMed]
103. Godugu, K.; Nallagondu, C.G.R. Solvent and Catalyst-free Synthesis of Imidazo[1,2-a]Pyridines by Grindstone Chemistry. *J. Heterocycl. Chem.* **2021**, *58*, 250–259. [CrossRef]
104. Wen, J.; Li, X.; Li, H.; Ma, S.; He, K.; Xu, Y.; Fang, Y.; Liu, W.; Gao, Q. Enhanced Visible-Light H_2 Evolution of g-C_3N_4 Photocatalysts via the Synergetic Effect of Amorphous NiS and Cheap Metal-Free Carbon Black Nanoparticles as Co-Catalysts. *Appl. Surf. Sci.* **2015**, *358*, 204–212. [CrossRef]
105. Yao, S.; Xue, S.; Peng, S.; Jing, M.; Qian, X.; Shen, X.; Li, T.; Wang, Y. Synthesis of Graphitic Carbon Nitride at Different Thermal-Pyrolysis Temperature of Urea and It Application in Lithium–Sulfur Batteries. *J. Mater. Sci. Mater. Electron.* **2018**, *29*, 17921–17930. [CrossRef]
106. Sankari Devi, E.; Alanthadka, A.; Tamilselvi, A.; Nagarajan, S.; Sridharan, V.; Maheswari, C.U. Metal-Free Oxidative Amidation of Aldehydes with Aminopyridines Employing Aqueous Hydrogen Peroxide. *Org. Biomol. Chem.* **2016**, *14*, 8228–8231. [CrossRef]

molecules

MDPI

Article

Alkyl 4-Aryl-6-amino-7- phenyl-3-(phenylimino)-4,7-dihydro-3H-[1,2]dithiolo[3,4-b]pyridine-5-carboxylates: Synthesis and Agrochemical Studies

Victor V. Dotsenko [1,2,*], Anna E. Sinotsko [1], Vladimir D. Strelkov [1], Ekaterina A. Varzieva [1], Alena A. Russkikh [1], Arina G. Levchenko [1], Azamat Z. Temerdashev [3], Nicolai A. Aksenov [2] and Inna V. Aksenova [2]

[1] Department of Organic Chemistry and Technologies, Kuban State University, 350040 Krasnodar, Russia
[2] Department of Chemistry, North Caucasus Federal University, 355017 Stavropol, Russia
[3] Department of Analytical Chemistry, Kuban State University, 350040 Krasnodar, Russia
* Correspondence: victor_dotsenko_@mail.ru

Abstract: The reaction between dithiomalondianilide (N,N′-diphenyldithiomalondiamide) and alkyl 3-aryl-2-cyanoacrylates in the presence of morpholine in the air atmosphere leads to the formation of alkyl 6-amino-4-aryl-7-phenyl-3-(phenylimino)-4,7-dihydro-3H-[1,2]dithiolo[3,4-b]- pyridine-5-carboxylates in 37–72% yields. The same compounds were prepared in 23–65% yields by ternary condensation of aromatic aldehydes, ethyl(methyl) cyanoacetate and dithiomalondianilide. The reaction mechanism is discussed. The structure of ethyl 6-amino-4-(4-methoxyphenyl)-7-phenyl-3-(phenylimino)-4,7-dihydro-3H-[1,2]dithiolo[3,4-b]pyridine-5-carboxylate was confirmed by X-ray crystallography. Two of the prepared compounds showed a moderate growth-stimulating effect on sunflower seedlings. Three of the new compounds were recognized as strong herbicide safeners with respect to herbicide 2,4-D in the laboratory and field experiments on sunflower.

Keywords: active methylene thioamides; Michael addition; dithiomalondianilide; cyanoacetic esters; [1,2]dithiolo[3,4-b]pyridines; herbicide safeners

Citation: Dotsenko, V.V.; Sinotsko, A.E.; Strelkov, V.D.; Varzieva, E.A.; Russkikh, A.A.; Levchenko, A.G.; Temerdashev, A.Z.; Aksenov, N.A.; Aksenova, I.V. Alkyl 4-Aryl-6-amino-7-phenyl-3-(phenylimino)- 4,7-dihydro- 3H-[1,2]dithiolo[3,4-b] pyridine-5-carboxylates: Synthesis and Agrochemical Studies. *Molecules* **2023**, *28*, 609. https://doi.org/10.3390/molecules28020609

Academic Editor: Alexey M. Starosotnikov

Received: 11 December 2022
Revised: 2 January 2023
Accepted: 4 January 2023
Published: 6 January 2023

1. Introduction

[1,2]Dithiolo[3,4-b]pyridine belongs to a rather rare class of heterocyclic systems. There are only a few papers that reported the preparation of such compounds. Historically, the first example of the synthesis is probably the preparation of dithiolopyridine **1** in low yield by reaction of 2-thioxonicotinic acid with phosphorus pentasulfide [1] (Scheme 1). Later the same approach was reported in other papers [2–4]. Compound **2** can also be prepared from 2-mercaptonicotinthioamides **3** upon treatment with P_4S_{10} [4] or from 2,2′-dithionicotinic acid [5]. Dithiolopyridines **4** were synthesized in low yields by sequential treatment of 2-thioxonicotinic acid with thionyl chloride and then with ethyl glycinate [6] or from 2-bromo-N-phenylpyridine-3-thiocarboxamide and sulfur under Cu(I)-catalyzed cross-coupling conditions in 83% yield [7]. When nicotinthioamides **3** were treated with iodine or $SOCl_2$/pyridine, mixtures of isothiazolopyridines **5** with isomeric 3-(R-imino)-[1,2]dithiolo[3,4-b]pyridines **6** were isolated [8]. The formation of dithiolopyridine **7** was observed when cyclopalladated complex **8** reacted with morpholinesulphenyl chloride (MfSCl) [9] (Scheme 1). [1,2]Dithioloquinolines **9** can be prepared by reaction of *ortho*-chloroacetophenones with phenyl isothiocyanate followed by $Ce(NO_3)_3$-catalyzed oxidative cyclization of the intermediate 4-(2-chlorobenzoyl)-5-(phenylamino)-3-(phenylimino)-3H-1,2-dithiols [10]. When treated with P_4S_{10}, ketene dithioacetals **10** afforded [1,2]dithioloisoquinolines in good yields [11].

The reactions of [1,2]dithiolo[3,4-b]pyridine **2** have also been studied in a limited number of papers [3–6,8,12–14]. Information about the synthesis and properties of partially saturated [1,2]dithiolo[3,4-b]pyridines is even more scarce. Thus, the only known synthesis

of 4,5,6,7-tetrahydro[1,2]dithiolo[3,4-b]pyridine is not general and is based on the reaction of heterocyclic 1,4-dipol **11** with sulfur [15]. Finally, the reaction of dithiomalondianilide (N,N′-diphenyldithiomalondiamide) **12** with arylmethylene malononitriles yielded 4,7-dihydro[1,2]dithiolo[3,4-b]pyridines **13** [16] (Scheme 1).

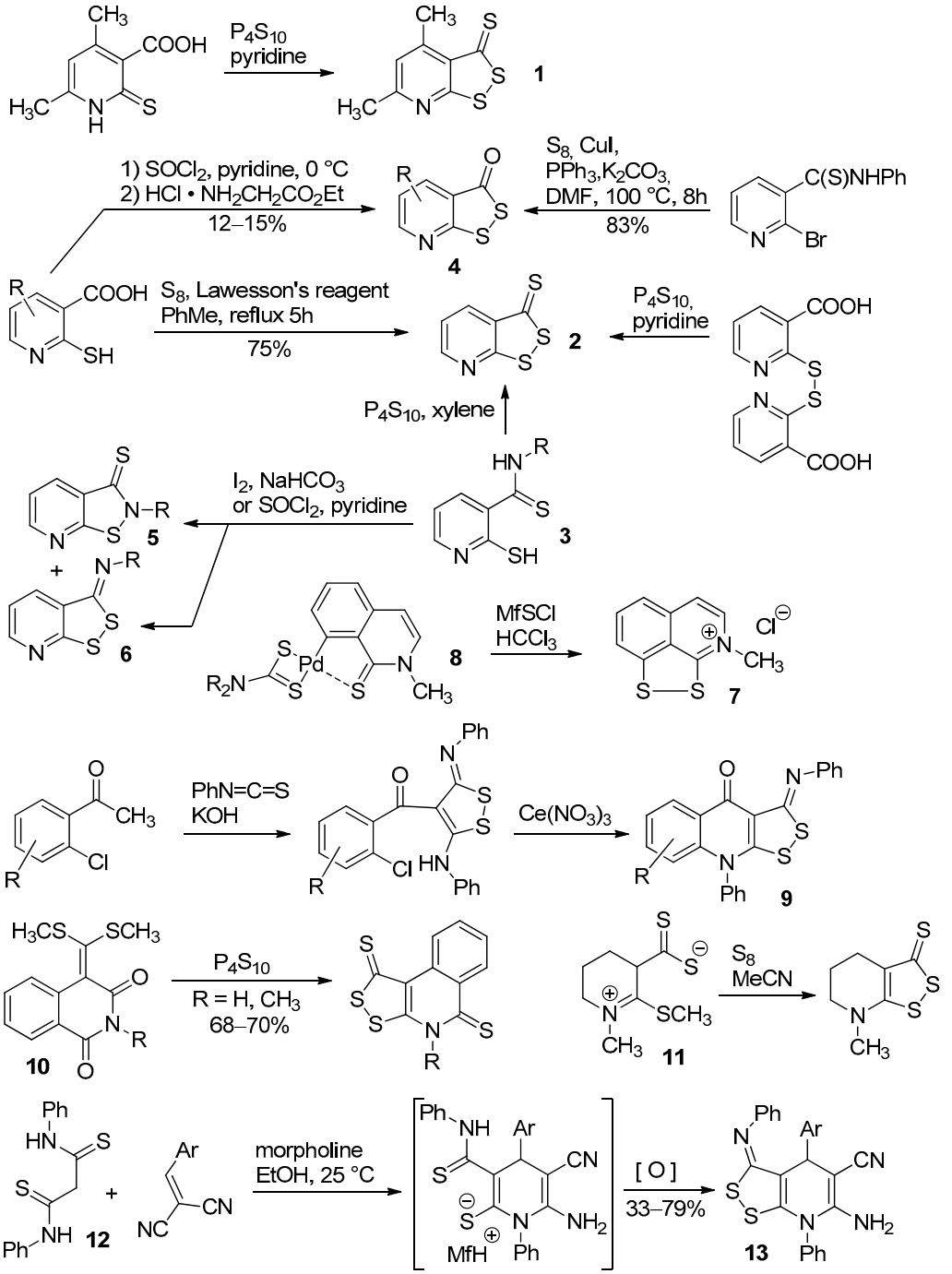

Scheme 1. The reported methods [1–16] for construction of [1,2]dithiolo[3,4-b]pyridine system.

Meanwhile, the antimicrobial, antitubercular [4] and antitumor [10] effects of [1,2]dithiolo [3,4-b]pyridines have been reported. Compounds of this type are of interest as starting reagents for the preparation of biologically active isothiazolopyridines and 2-mercaptonicotinthioamides [4,5,12,13]. As structural analogs and bioisosters of thieno[2,3-b]pyridines (for recent reviews see [17,18]), dithiolopyridines can be considered as promising molecules with still undiscovered potential.

In the context of our interest in exploring the chemistry of dithiomalondianilide **12** and its transformations leading to [1,2]dithiolo[3,4-b]pyridines [16,19–21], it seemed reasonable to study the reactions of dithiomalondianilide **12** with other Michael acceptors. It is noteworthy that despite the long-standing and active use of thioamide **12** as a bidentate S,S-chelating agent towards heavy metals (e.g., [22–25]), the heterocyclization reactions of **12** have been little studied to date [26–29].

This work presents the results of our studies of the reactions of N,N′-diphenyldithiomalondiamide **12** with 2-cyanoacrylates derived from cyanoacetic esters.

2. Results and Discussion

2.1. Synthesis

Earlier, we proposed a cascade method for the preparation of [1,2]dithiolo[3,4-b] pyridines **13** (Scheme 1) from N,N′-diphenyldithiomalondiamide **12** based on the morpholine-catalyzed Michael addition with arylmethylene malononitriles followed by heterocyclization and further air oxidation of 3-thiocarbamoylpyridine-2-thiolate intermediate [16]. As the continuation of this research, we have decided to look into the possibility to using other electron-deficient alkenes as Michael acceptors to prepare dithiolopyridines and we focused our attention on 3-aryl-2-cyanoacrylates **14**. The precursors **14** were prepared by Knoevenagel condensation of cyanoacetic esters with aromatic aldehydes in the presence of piperidine or morpholine.

Previous studies on the reactions involving cyanoacetates and active methylene thioamides and proceeding through the formation of Michael adducts **A** (Scheme 2) already showed that the further heterocyclization may follow two different reaction pathways. The first one suggests an intramolecular *6-exo-trig* process involving ester fragment COOR and leads to 3-cyanopyridin-2(1H)-ones **B** or related products (e.g., [30–33]). (pathway A, Scheme 2). An alternative path would be *6-exo-dig* heterocyclization, which leads to heterocyclic enamino esters **C** or its transformation products [34–37] (pathway B, Scheme 2).

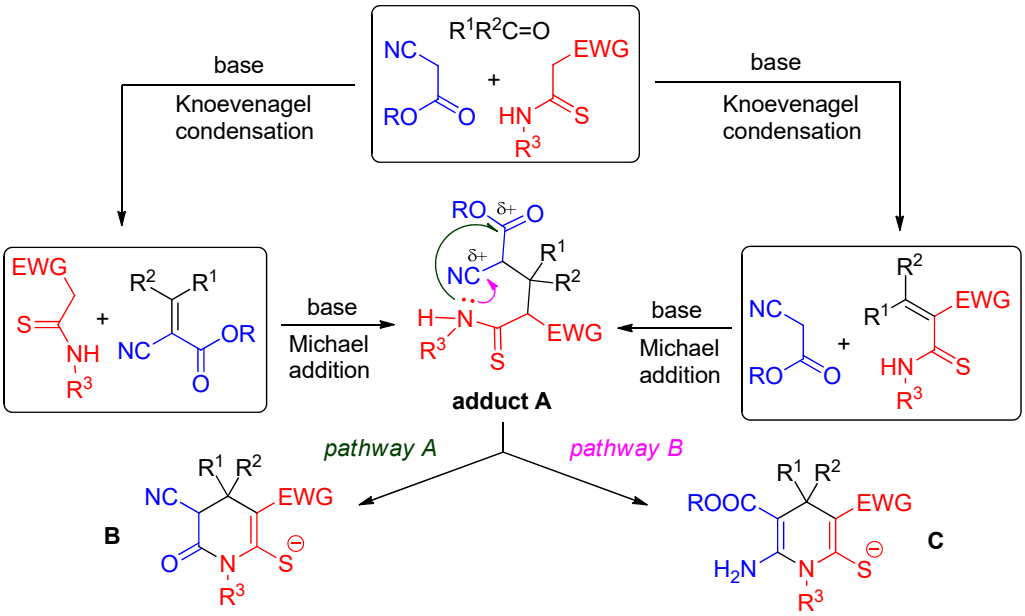

Scheme 2. Two possible directions for heterocyclization reactions of active methylene thioamides with cyanoacetic esters or 2-cyanoacrylates.

First, when a mixture of N,N′-diphenyldithiomalondiamide **12** and (*E*)-ethyl 2-cyano-3-(4-methoxyphenyl)acrylate **14a** in EtOH were treated with excessive morpholine, a yellow crystal of ethyl 6-amino-4-(4-methoxyphenyl)-7-phenyl- 3-(phenylimino)-4,7-dihydro-3H-[1,2]dithiolo[3,4-b]pyridine-5-carboxylate **15a** was isolated in 72% yield (Scheme 3). The

structure of **15a** was unambiguously confirmed by single crystal X-ray diffraction analysis (CCDC # 2219352, Figure 1).

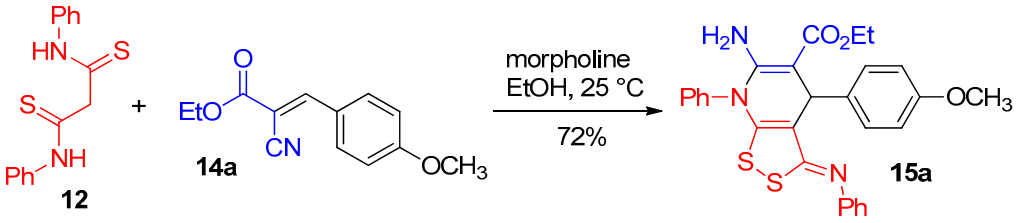

Scheme 3. Synthesis of compound **15a**.

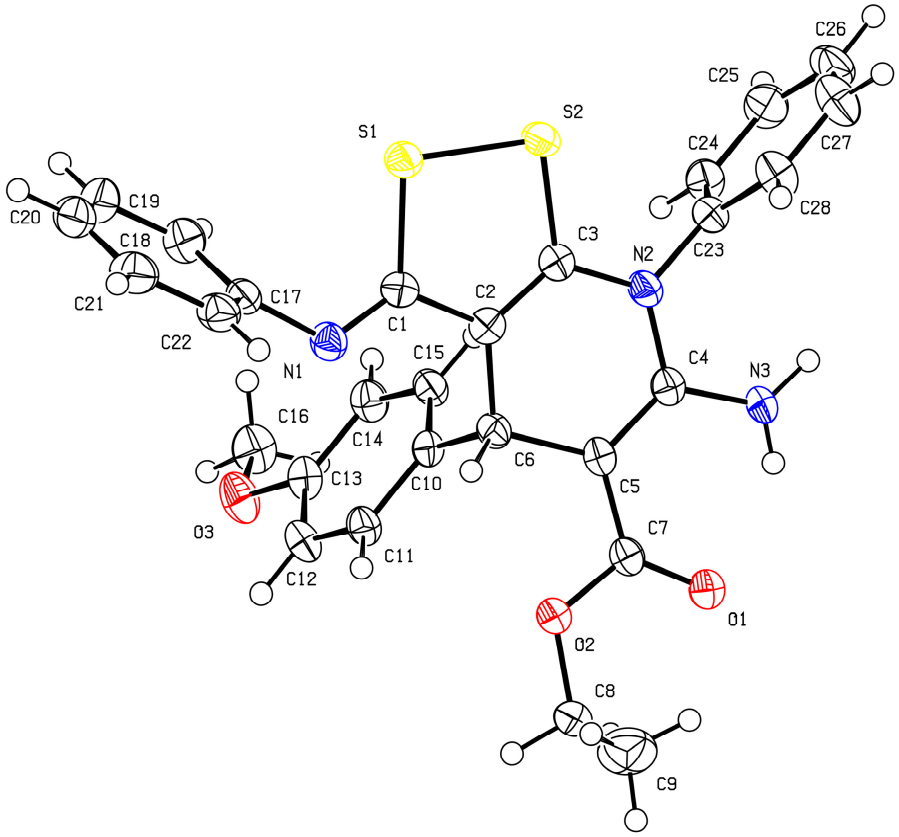

Figure 1. ORTEP drawing of the X-ray structure for ethyl 6-amino-4-(4-methoxyphenyl)-7-phenyl-3-(phenylimino)-4,7-dihydro-3H-[1,2]dithiolo[3,4-b]pyridine-5-carboxylate **15a** (CCDC deposition number 2219352). Thermal ellipsoids for non-hydrogen atoms are shown at 50% probability. Blue: nitrogen, gray: carbon atoms, red: oxygen atoms, yellow: sulfur atoms.

At this point, some efforts to optimize the reaction conditions and examine the scope and limitation of the reaction were made. The reaction proceeded smoothly in MeOH or EtOH; other tested solvents (*i*-PrOH, acetone, DMF) gave rather unsatisfactory results. The nature of amine (morpholine, piperidine, triethylamine) does not significantly affect the yields of products. Along with Michael addition of **12** to other 2-cyanoacrylates **14a–g** (Method A, Scheme 4), we also investigated the three-component reaction of dithiomalondianilide **12**, cyanoacetic esters and aldehydes in the presence of morpholine (Method B, Scheme 4). However, Method B gives somewhat lower yields of dithiolopyridines **15**.

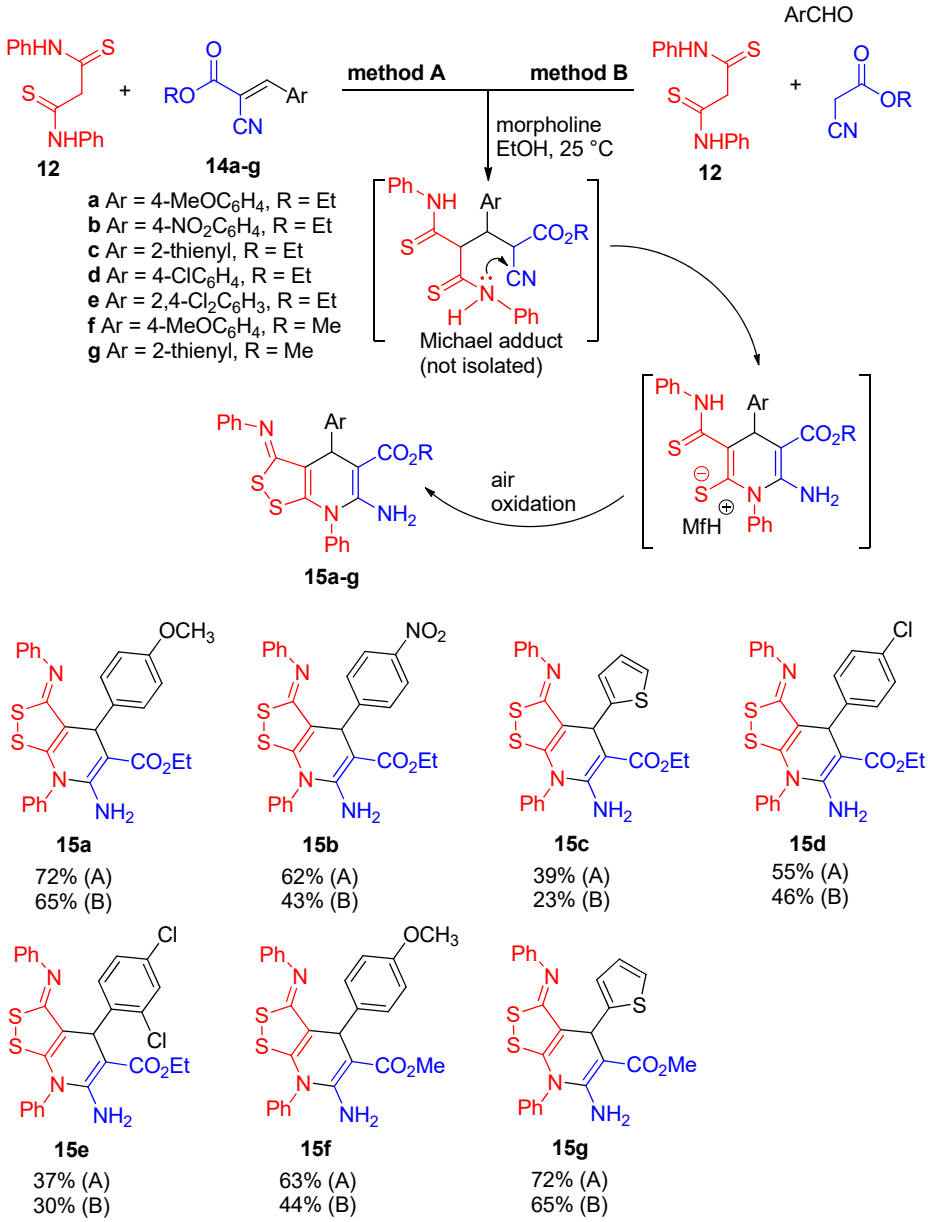

Scheme 4. Synthesis of compounds **15a–g**.

Extended refluxing of the reaction mixture does not favor the formation of dithiolopyridines **15**. Thus, when a mixture of **14a** and **12** in ethanol was heated under reflux in the presence of morpholine for as long as 15 h, a contaminated deep-brown material was obtained from which dithiolopyridine **15a** was isolated by recrystallization in only 13% yield. Less prolonged heating (1.5 h) was also accompanied by side processes and led to decreased yields; in this case, compound **15a** was obtained in 30% yield.

When the reaction of **12** with **14a** was conducted in inert atmosphere under nitrogen stream, dithiolopyridine **15a** was not isolated. This fact proves the crucial role of air oxygen for the final step of dithiolopyridine system formation. Nevertheless, the addition of oxidizing agents (hydrogen peroxide or iodine) leads to resinification of the reaction mixture. Aldehydes with both electron-donor and electron-withdrawing substituents are reacted well. However, we failed to obtain any products in the case of furfural or 2-cyano-3-(furan-2-yl)acrylates even if less nucleophilic and milder base triethylamine was taken instead of morpholine. This is probably due to the strong tendency of furan-ring-bearing electron-withdrawing substituents to undergo a nucleophilic attack at the C-5 position to form a complex mixture of furan-ring-cleavage/recyclization products.

In the IR spectra of compounds **15,** the absorption bands corresponding to NH_2 valence vibrations (ν 3371–3474 cm^{-1} and ν 3263–3290 cm^{-1}), RO(C=O) group bands (ν 1651–1661 cm^{-1}) and imino group C=N–Ph bands at ν 1622–1638 cm^{-1} were observed while the bands corresponding to C≡N groups were absent. ^{1}H NMR spectra of **15** revealed characteristic singlets attributed to H-4 protons at δ 5.02–5.94 ppm and a very broadened peak of NH_2 protons at δ 7.00–7.19 ppm. It is interesting that in some cases the signal of OCH_2 protons is detected not as a typical quartet but as a complex multiplet, probably due to the hindered rotation caused by the intramolecular hydrogen bond C=O...H-NH. Alternatively, the observed splitting of OCH_2 signal can be caused by the shielding effect of the aromatic ring at C-4, which affects one of OCH_2 protons. ^{13}C NMR spectra lacked signals attributed to C=S carbons and revealed the peaks of C=O (δ 168.7–169.1 ppm), C=N (δ 163.0–163.4 ppm), C-3a (δ 111.1–113.7 ppm), C-5 (δ 76.5–78.4 ppm) and C-4 carbons (δ 33.5–38.6 ppm). The NMR, FTIR and HRMS spectra are shown in Supplementary Materials Figures S1–S6, S8–S31 and Tables S1, S8 and S9. The crystal data is shown in Supplementary Materials Tables S2–S7.

2.2. Agrochemical Studies

The new compounds were tested as herbicide safeners with respect to 2,4-dichlorophenoxyacetic acid (2,4-D) and as plant growth regulators. 2,4-D is an herbicide that is widely used for plant protection and was reported to show no significant toxicity to humans [38]. However, the use of 2,4-D has negative side effects, including its inhibition effect on the crops themselves that gives a decrease in yield by ~15–60%. To eliminate such negative effects and to raise crop yields, herbicide safeners (also called herbicide antidotes or detoxifiers) are successfully used. Herbicide safeners [39–41] can be defined as agrochemicals that are able to neutralize phytotoxins in plants, thus protecting crop plants from herbicide injury. Safeners are harmless to crop plants (or even have a growth-stimulating effect), but do not affect the activity of herbicides against weeds.

It is known that 3-aminothieno[2,3-b]pyridines, which can be considered as structural analogs of the prepared 3-imino-3H-[1,2]dithiolo[3,4-b]pyridines **15**, are reported to be effective herbicide safeners [42,43] and plant growth regulators [44]. We studied the efficiency of new 3-imino-3H-[1,2]dithiolo[3,4-b]pyridines as 2,4-D antidotes using sunflower seedlings using the reported procedure [42] (see also Materials and Methods). The antidote effect *A* was determined as a ratio of the hypocotyl (or root) length of sunflower seedlings in the "herbicide + antidote" experiments to the length in the reference group (where the seedlings were treated with 2,4-D only) (Equation (1)):

$$A = (L_{exp}/L_{ref}) \times 100\%, \quad (1)$$

where L_{exp} is an organ length (mm) in the group of seedlings treated with herbicide and antidote, and L_{ref} is an organ length (mm) in the reference group of sunflower seedlings.

We found that three of the new compounds, dithiolopyridines **15a,c,f**, exhibited a strong 2,4-D antidote effect in the laboratory experiments (Table 1).

As we can see from the Table 1, the use of 3H-[1,2]dithiolo[3,4-b]pyridines **15a,c,f** as safeners against 2,4-D strongly reduce the toxic effects of the herbicide. Compounds **15a,c,f** reduced the negative effect of 2,4-D on sunflower seedling hypocotyls by 34–60% and by 40–55% on sunflower seedling roots.

The antidote activity of 3H-[1,2]dithiolo[3,4-b]pyridines **15a,c,f** was also studied in field experiments on sunflower in the experimental field of the Federal Scientific Center for Biological Protection of Plants (Krasnodar, Russia). Sunflower plants of cv. Master in the phase of 10–16 leaves were treated with an aqueous solution of 2,4-dichlorophenoxyacetic acid at a dose of 18 g/ha and 3 days later a safener solution was applied at a dose of 100 g/ha with the working fluid rate of 300 L/ha.

Table 1. The antidote effects of the most active compounds **15a,c,f** with respect to herbicide 2,4-D.

N	Compound	Organ	Antidote Effect *A* at Different Concentrations, % [1]			
			10^{-2}	10^{-3}	10^{-4}	10^{-5}
1	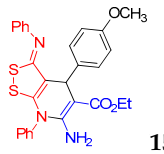 **15a**	roots	146	151	155	151
		hypocotyls	157	160	154	151
2	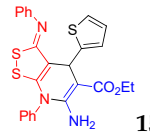 **15c**	roots	140	143	143	140
		hypocotyls	137	134	140	148
3	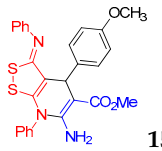 **15f**	roots	133	151	155	151
		hypocotyls	148	154	148	151

[1] The differences are reliable at $p = 0.95$.

The field tests included the following variants:

- Control group—untreated plants;
- "Herbicide" (reference) group—plants treated with herbicide 2,4-D only;
- "Herbicide + antidote" group—plants treated with herbicide 2,4-D and an antidote.

Experiments were conducted in plots of 2.8 m^2 with five-fold repetition. Sunflower harvesting was performed at the time of full seed maturity. The field antidote effect A_F was determined by the absolute value of the crop yield increase to the herbicide reference by the Equation (2):

$$A_F = \frac{Y_1 - Y_2}{Y_2} \times 100\%, \quad (2)$$

where A_F is antidote effect, %; Y_1 is crop yield in "herbicide + antidote" group; and Y_2 is crop yield in "herbicide" (reference) group.

The obtained data were statistically processed using Student's *t*-test. The field test results are presented in Table 2. As it can be seen, the use of compounds **15a,c,f** as herbicide safeners under field conditions provides an antidote effect in the range of 41.4–51.4%.

The growth-stimulating activity of compounds **15a,c,f** was evaluated in laboratory experiments using the known procedure [45] on cv. Master sunflower seedlings (Table 3). The effect was evaluated by the elongation of stems and roots of treated seedlings in comparison to control (untreated seeds) (Equation (3)):

$$E = (L_{\text{treated}}/L_{\text{control}}) \times 100\%, \quad (3)$$

where E is growth-stimulating effect, %; $L_{treated}$ is the length (mm) of stems/roots in the treated group of seedlings; and L_{control} is the length (mm) of stems/roots in the control (untreated) group of seedlings.

As we can see from the Table 3, compounds **15a** and **15f** are more active than **15c** and favored stem elongation by 12–20% relative to control and stimulated root growth by 13–22%, depending on the concentration. In general, the growth-stimulating effect of compounds **15a** and **15f** can be considered as moderate.

The study of the acute toxicity of the new compounds is in progress. According to preliminary data, the compounds do not possess obvious phytotoxicity; this is indirectly indicated by the observed plant growth-stimulating effect of the tested samples (Table 3).

Table 2. Results of field tests on the antidote activity of 3H-[1,2]dithiolo[3,4-b]pyridines **15a,c,f** against the herbicide 2,4-D on sunflower cv. Master.

N	Compound	Field Test Variants			
		"Herbicide" (Reference) Group (2,4-D Only)	"Herbicide + Antidote" Group		
				Antidote Activity	
		Crop Yield, Quintals per Hectare	Crop Yield, Quintals per Hectare	Quintals per Hectare	A_F, %
1	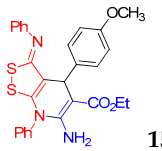 **15a**	14.0	20.8	6.8	48.6 [1]
2	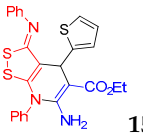 **15c**	14.0	19.8	5.8	41.4 [1]
3	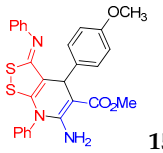 **15f**	14.0	21.2	7.2	51.4 [1]

[1] The differences are reliable at $p = 0.90$.

Table 3. The growth-stimulating effects of compounds **15a,c,f**.

N	Compound	Organ	Growth-Stimulating Effect *E* at Different Concentrations, % [1]			
			10^{-2}	10^{-3}	10^{-4}	10^{-5}
1	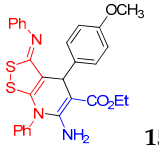 **15a**	roots	116	120	119	118
		stems	115	120	120	122
2	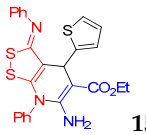 **15c**	roots	108	112	114	112
		stems	114	115	115	116
3	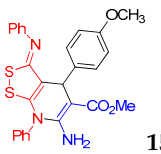 **15f**	roots	112	117	117	118
		stems	113	117	116	112

[1] The differences are reliable at $p = 0.95$.

3. Materials and Methods

^{1}H and ^{13}C DEPTQ NMR spectra and 2D NMR experiments were recorded in solutions of DMSO-d_6 on a Bruker AVANCE-III HD instrument (Bruker BioSpin AG, Fällanden, Switzerland) (at 400.40 or 100.61 MHz, respectively). Residual solvent signals were used as internal standards in DMSO-d_6–2.49 ppm for ^{1}H, and 39.50 ppm for ^{13}C nuclei. Single crystal X-ray diffraction analysis of compound **15a** was performed on an automatic four-circle diffractometer Agilent Super Nova, Dual, Cu at zero, Atlas S2. HRMS spectra were recorded using a Bruker MaXis Impact quadrupole time-of-flight mass spectrometer (Bruker

Daltonics, Bremen, Germany) equipped with an electrospray ionization source in positive ion detection mode. The voltage at the ionization source was 3.5 kV, the drying gas flow rate was 8 L/min, the spray gas pressure was 2 bar, the temperature of the ionization source was 250 °C, the mass scanning range (*m/z*) was 50–1000, the scanning speed was 3 Hz. The data were processed using Bruker Data Analysis 4.1 software. See Supplementary Materials File for NMR, FTIR and HRMS spectral charts and X-ray analysis data.

FT-IR spectra were measured on a Bruker Vertex 70 instrument equipped with an ATR sampling module (Bruker Optics GmbH & Co. KG, Ettlingen, Germany). Elemental analyses were carried out using a Carlo Erba 1106 Elemental Analyzer (Carlo Erba Strumentazione, Cornaredo, Italy) Reaction progress and purity of isolated compounds were controlled by TLC on Sorbfil-A plates (Imid Ltd, Krasnodar, Russia), eluent–acetone:hexane 1:1 or ethyl acetate:light petroleum 3:1; the spots were visualized with UV-light and iodine vapors. N,N′-Diphenyldithiomalondiamide (dithiomalondianilide) **12** was prepared from acetylacetone and phenyl isothiocyanate as described earlier [19,46]. Aldehydes, cyanoacetic esters, morpholine and solvents were purchased from commercial vendors and purified by distillation (Galachem, Moscow, Russia).

General procedure for the preparation of dithiolopyridines 15 (Method A). A vial was charged, under air, with dithiomalondianilide **12** (300 mg, 1.047 mmol), 3-aryl-2-cyanoacrylate **14** (1.1 mmol) and EtOH (6–8 mL). A mixture was treated with morpholine (0.14 mL, 1.57 mmol) at 25 °C. Complete dissolution of starting materials and formation of a deep-yellow solution occurred for a very short time (a matter of minutes). The solution was stirred for 3 h and left to stand to allow slow evaporation in air at ambient temperature. After evaporating the solvent, the resulting tarry residue was triturated with an appropriate solvent (usually acetone : EtOH (1:1) or n-BuOH were used). The yellow or light-brown crystalline solid was filtered off, washed with EtOH and hexane and recrystallized from acetone (if appropriate) to give pure dithiolopyridines **15**.

General procedure for the preparation of dithiolopyridines 15 (Method B). To a solution of ethyl(methyl) cyanoacetate (1.1 mmol) and an aromatic aldehyde (1.1 mmol) in EtOH(MeOH) (2–3 mL), morpholine (2 drops) was added. Under vigorous stirring, a mixture was warmed up to 50 °C and left to cool to generate 3-aryl-2-cyanoacrylate **14** in situ. Then, 300 mg (1.05 mmol) of dithiomalondianilide **12** and 0.13 mL of morpholine were added. The solution formed was treated as above. The crystals of dithiolopyridine were filtered off, washed with EtOH and hexane and recrystallized (if appropriate).

Ethyl 6-amino-4-(4-methoxyphenyl)-7-phenyl-3-(phenylimino)-4,7-dihydro-3H-[1,2]di- thiolo [3,4-b]pyridine-5-carboxylate (**15a**). This compound was prepared via **Method A** in a yield of 388 mg (72%). Alternatively, this compound was prepared via **Method B** employing ethyl cyanoacetate (0.12 mL), anisaldehyde (0.13 mL) and thioamide **12** (300 mg) in a yield of 351 mg (65%), bright yellow crystals. FTIR, ν_{max}, cm^{-1}: 3400, 3273 (N-H); 1651 (CO_2Et); 1628 (C=N). ^1H NMR (400 MHz, DMSO-d_6): 1.09 (t, ^3J = 7.1 Hz, 3H, $C\underline{H}_3CH_2$), 3.71 (s, 3H, MeO), 3.89–4.03 (m, 2H, $CH_3C\underline{H}_2$), 5.02 (s, 1H, H-4), 6.84–6.86 (m, 4H, H Ar), 7.00 (very br s, 2H, NH_2), 7.05–7.09 (m, 1H, H-4 Ph), 7.31–7.34 (m, 4H, H Ar), 7.60–7.66 (m, 5H, H Ar). ^{13}C DEPTQ NMR (101 MHz, DMSO-d_6): 14.4* (CH_3), 38.0* (C-4), 54.9* (OCH_3), 58.6 (OCH_2), 78.4 (C-5), 113.2* (2C, CH Ar), 113.5 (C-3a), 120.1* (2C, C2 C-6 Ph), 124.3* (C-4 Ph), 128.5* (2C, CH Ar), 129.7* (2C, C-3 C-5 Ph), 130.0* (2C, CH Ph), 130.5* (2C, CH Ph), 131.1* (C-4 Ph), 135.6 (C-1 Ph), 138.9 (C-1 Ar), 150.9 (C-1 Ph), 152.7 (C-6), 153.7 (C-8a), 157.6 (C–OMe), 163.3 (C=N), 168.7 (C=O). *Signals with a negative phase. Elemental Analysis ($C_{28}H_{25}N_3O_3S_2$, M 515,65): calculated (%): C, 65.22; H, 4.89; N, 8.15; found (%): C, 65.15; H, 5.00; N, 8.12. HRMS (ESI) m/z: calculated for $C_{28}H_{26}N_3O_3S_2$ $[M + H]^+$: 516.14156, found 516.1411 (Δ 0.89 ppm).

*3.1. X-ray Studies for Single Crystals of **15a***

Single crystals of 6-amino-4-(4-methoxyphenyl)-7-phenyl-3-(phenylimino)-4,7- dihydro-3H-[1,2]dithiolo[3,4-b]pyridine-5-carboxylate **15a** ($C_{28}H_{25}N_3O_3S_2$, M 515.63) were grown from EtOH–acetone solution. The crystal was kept at 423.15(10) K during data collection.

Using Olex2 [47], the structure was solved with the olex2.solve structure solution program using Charge Flipping and refined with the SHELXL [48] package using Gauss–Newton minimization. The crystals are orthorhombic, at 423.15(10) K: a = 10.2422(4) Å, b = 12.9088(5) Å, c = 19.2052(7) Å, α = 90°, β = 90°, γ = 90°, V = 2539.21(17) Å^3, T = 423.15(10), space group $P2_12_12_1$ (no. 19), Z = 4, μ(Cu K$_\alpha$) = 2.190 mm^{-1}, d_{calc} = 1.349 mg/mm^3, F(000) = 1080.0; a total of 21,592 reflections measured, 4994 unique (R_{int} = 0.0510), which were used in all calculations. The final wR_2 was 0.1035 (all data) and R_1 was 0.0379 (I >2σ(I)). A full set of crystallographic data has been deposited in the Cambridge Crystallographic Data Center (CCDC **2219352**).

Ethyl 6-amino-4-(4-nitrophenyl)-7-phenyl-3-(phenylimino)-4,7-dihydro-3H-[1,2]dithiolo- [3,4-b]pyridine-5-carboxylate (**15b**). This compound was prepared via **Method A** in a yield of 344 mg (62%), bright-yellow powder. Alternatively, this compound was prepared via **Method B** employing ethyl cyanoacetate (0.11 mL), 4-nitrobenzaldehyde (160 mg) and thioamide **12** (300 mg) in a yield of 240 mg (43%). FTIR, ν_{max}, cm^{-1}: 3445, 3263 (N-H); 1661 (CO_2Et); 1630 (C=N); 1524 ($NO_{2\ asym}$); 1346 ($NO_{2\ sym}$). ^{1}H NMR (400 MHz, DMSO-d_6): 0.92 (t, ^3J = 7.0 Hz, 3H, C$\underline{H_3}$CH_2), 3.81–3.95 (m, 2H, CH_3C$\underline{H_2}$), 5.94 (s, 1H, H-4), 6.72 (d, ^3J = 7.6 Hz, 2H, H-2 H-6 Ph), 7.02–7.06 (m, 1H, H-4 Ph), 7.19 (very br s, 2H, NH_2), 7.26–7.30 (m, 2H, H-3 H-5 Ph), 7.38–7.42 (m, 1H, H-4 Ph), 7.65–7.80 (m, 8H, H Ar). ^{13}C DEPTQ NMR (101 MHz, DMSO-d_6): 14.1* (CH_3), 34.6* (C-4), 58.5 (OCH_2), 76.9 (C-5), 111.7 (C-3a), 120.0* (2C, C2 C-6 Ph), 123.6* (CH Ar), 124.2* (C-4 Ar), 127.2* (CH Ar), 129.4* (2C, C-3 C-5 Ar), 130.3* (2C, CH Ph), 130.5* (2C, CH Ph), 131.3* (C-4 Ph), 133.0* (CH Ar), 135.2 (C-1 Ph), 141.1 (C-1 Ar), 148.8 (C–NO_2), 150.6 (C-1 Ph), 153.1 (C-6), 154.6 (C-8a), 163.0 (C=N), 168.7 (C=O). *Signals with a negative phase. Elemental Analysis ($C_{27}H_{22}N_4O_4S_2$, M 530,62): calculated (%): C, 61.12; H, 4.18; N, 10.56; found (%): C, 61.03; H, 4.31; N, 10.41. HRMS (ESI) m/z: calculated for $C_{27}H_{23}N_4O_4S_2$ $[M + H]^+$: 531.11607, found 531.1169 (Δ −1.56 ppm).

Ethyl 6-amino-7-phenyl-3-(phenylimino)-4-(2-thienyl)-4,7-dihydro-3H-[1,2]dithiolo[3,4-b]pyridine-5-carboxylate (**15c**). This compound was prepared via **Method A** in a yield of 201 mg (39%). Alternatively, this compound was prepared via **Method B** employing ethyl cyanoacetate (0.11 mL), thiophene-2-carbaldehyde (0.10 mL) and thioamide **12** (300 mg) in a yield of 120 mg (23%), light brown powder. FTIR, ν_{max}, cm^{-1}: 3380, 3269 (N-H); 1653 (CO_2Et); 1630 (C=N). ^{1}H NMR (400 MHz, DMSO-d_6): 1.12 (t, ^3J = 7.1 Hz, 3H, C$\underline{H_3}$CH_2), 4.05 (q, ^3J = 7.1 Hz, 2H, CH_3C$\underline{H_2}$), 5.39 (s, 1H, H-4), 6.92–6.95 (m, 4H, H-3 H-4 thienyl and H-2 H-6 Ph overlapped), 7.09–7.12 (m, 3H, H-4 Ph and NH_2 overlapped), 7.28 (dd, ^3J = 4.9 Hz, ^4J = 1.5 Hz, 1H, H-5 2-thienyl), 7.34–7.38 (m, 2H, H-3 H-5 Ph), 7.51–7.54 (m, 2H, H-3 H-5 Ph), 7.63–7.65 (m, 3H, H-2 H-6 H-4 Ph). ^{13}C DEPTQ NMR (101 MHz, DMSO-d_6): 14.5* (CH_3), 33.5* (C-4), 58.7 (OCH_2), 78.0 (C-5), 112.7 (C-3a), 120.1* (2C, C2 C-6 Ph), 122.8* (C-2 thienyl), 123.6* (C-5 thienyl), 124.4* (C-4 Ar), 126.7* (C-4 thienyl), 129.7* (2C, C-3 C-5 Ph), 129.9* (2C, C-3 C-5 Ph), 130.6* (2C, C-2 C-6 Ph), 131.1* (C-4 Ph), 135.5 (C-1 Ph), 150.9 (C-1 Ph), 151.1 (C-1 thienyl), 153.1 (C-6), 154.2 (C-8a), 163.4 (C=N), 168.5 (C=O). *Signals with a negative phase. Elemental Analysis ($C_{25}H_{21}N_3O_2S_3$, M 491,65): calculated (%): C, 61.07; H, 4.31; N, 8.55; found (%): C, 60.98; H, 4.45; N, 8.45. HRMS (ESI) m/z: calculated for $C_{25}H_{22}N_3O_2S_3$ $[M + H]^+$: 492.0874, found 492.0868 (Δ 1.22 ppm).

Ethyl 6-amino-4-(4-chlorophenyl)-7-phenyl-3-(phenylimino)-4,7-dihydro-3H-[1,2]dithiolo-[3,4-b]pyridine-5-carboxylate (**15d**). This compound was prepared via **Method A** in a yield of 300 mg (55%). Alternatively, this compound was prepared via **Method B** employing ethyl cyanoacetate (0.11 mL), 4-chlorobenzaldehyde (150 mg) and thioamide **12** (300 mg) in a yield of 240 mg (46%), yellow powder. FTIR, ν_{max}, cm^{-1}: 3371, 3271 (N-H); 1655 (CO_2Et); 1638 (C=N). ^{1}H NMR (400 MHz, DMSO-d_6): 1.07 (t, ^3J = 7.0 Hz, 3H, C$\underline{H_3}$CH_2), 3.96 (q, ^3J = 7.0 Hz, 2H, CH_3C$\underline{H_2}$), 5.04 (s, 1H, H-4), 6.83 (d, ^3J = 7.6 Hz, 2H, H-2 H-6 Ph), 7.05–7.09 (m, 3H, H-4 Ph and NH_2 overlapped), 7.30–7.35 (m, 4H, H Ar), 7.41 (d, ^3J = 8.4 Hz, 2H, H Ar), 7.50–7.55 (m, 1H, H-4 Ph), 7.64–7.67 (m, 4H, H Ar). ^{13}C DEPTQ NMR (101 MHz, DMSO-d_6): 14.3* (CH_3), 38.6* (C-4), 58.7 (OCH_2), 77.7 (C-5), 112.6 (C-3a), 120.1* (2C, C2 C-6 Ph), 124.3* (C-4 Ph), 127.8* (2C, CH Ar), 129.5* (2C, CH Ar), 129.7* (2C, C-3 C-5 Ph), 130.1* (2C, CH Ph), 130.5* (2C, CH Ph), 131.2* (C-4 Ph), 135.4 (C-1 Ph and C-Cl overlapped),

145.6 (C-1 Ar), 150.8 (C-1 Ph), 152.8 (C-6), 154.2 (C-8a), 163.2 (C=N), 168.6 (C=O). *Signals with a negative phase. Elemental Analysis ($C_{27}H_{22}ClN_3O_2S_2$ M 520,07): calculated (%): C, 62.36; H, 4.26; N, 8.08; found (%): C, 62.30; H, 4.41; N, 8.05. HRMS (ESI) m/z: calculated for $C_{27}H_{23}ClN_3O_2S_2$ $[M + H]^+$: 520.09202, found 520.0913 (Δ 1.38 ppm).

Ethyl 6-amino-4-(2,4-dichlorophenyl)-7-phenyl-3-(phenylimino)-4,7-dihydro-3H-[1,2]-dithiolo[3,4-b]pyridine-5-carboxylate (**15e**). This compound was prepared via **Method A** in a yield of 215 mg (37%). Alternatively, this compound was prepared via **Method B** employing ethyl cyanoacetate (0.11 mL), 2,4-dichlorobenzaldehyde (180 mg) and thioamide **12** (300 mg) in a yield of 175 mg (30%), brownish-yellow powder. FTIR, ν_{max}, cm^{-1}: 3474, 3290 (N-H); 1657 (CO_2Et); 1634 (C=N). ^1H NMR (400 MHz, DMSO-d_6): 1.05 (t, ^3J = 7.0 Hz, 3H, $C\underline{H}_3CH_2$), 3.87–3.99 (m, 2H, $CH_3C\underline{H}_2$), 5.36 (s, 1H, H-4), 6.79 (d, ^3J = 8.3 Hz, 2H, H-2 H-6 Ph), 7.02–7.06 (m, 1H, H-4 Ph), 7.14 (very br s, 2H, NH_2), 7.27–7.31 (m, 2H, H-3 H-5 Ph), 7.35 (dd, ^3J = 8.6 Hz, ^4J = 2.0 Hz, 1H, H-5 Ar), 7.42 (d, ^4J = 2.0 Hz, 1H, H-3 Ar), 7.52 (d, ^3J = 8.6 Hz, 1H, H-6 Ar), 7.55–7.67 (m, 5H, H Ph). ^{13}C DEPTQ NMR (101 MHz, DMSO-d_6): 14.3* (CH_3), 37.9* (C-4), 58.6 (OCH_2), 76.5 (C-5), 111.1 (C-3a), 120.1* (2C, C-2 C-6 Ph), 124.2* (C-4 Ph), 126.7* (CH Ar), 128.3* (CH Ar), 129.5* (2C, C-3 C-5 Ph), 130.4* (2C, CH Ph), 130.5* (2C, CH Ph), 130.9 (C–Cl), 131.3* (C-4 Ph), 133.7* (C-3 Ar), 133.8 (C–Cl), 135.3 (C-1 Ph), 142.7 (C-1 Ar), 150.3 (C-1 Ph), 152.9 (C-6), 154.7 (C-8a), 162.2 (C=N), 168.7 (C=O). *Signals with a negative phase. Elemental Analysis ($C_{27}H_{21}Cl_2N_3O_2S_2$ M 554,51): calculated (%):C, 58.48; H, 3.82; N, 7.58; found (%): C, 58.60; H, 3.95; N, 7.41. HRMS (ESI) m/z: calculated for $C_{27}H_{22}Cl_2N_3O_2S_2$ $[M + H]^+$: 554.05305, found 554.0532 (Δ −0.27 ppm).

Methyl 6-amino-4-(4-methoxyphenyl)-7-phenyl-3-(phenylimino)-4,7-dihydro-3H-[1,2]dithiolo[3,4-b]pyridine-5-carboxylate (**15f**). This compound was prepared via **Method A** in a yield of 330 mg (63%). Alternatively, this compound was prepared via **Method B** employing methyl cyanoacetate (0.09 mL), 4-methoxybenzaldehyde (0.13 mL) and thioamide **12** (300 mg) in MeOH in a yield of 230 mg (44%), bright-yellow powder. FTIR, ν_{max}, cm^{-1}: 3452, 3281 (N-H); 1661 (CO_2Me); 1622 (C=N). ^1H NMR (400 MHz, DMSO-d_6): 3.51 (s, 3H, COOMe), 3.71 (s, 3H, MeO–Ar), 5.04 (s, 1H, H-4), 6.84–6.88 (m, 4H, H Ar), 7.00 (very br s, 2H, NH_2), 7.06–7.10 (m, 1H, H-4 Ph), 7.30–7.35 (m, 4H, H Ar), 7.55–7.66 (m, 5H, H Ar). ^{13}C DEPTQ NMR (101 MHz, DMSO-d_6): 37.7* (C-4), 50.5* ($CO_2\underline{C}H_3$), 54.9* ($ArO\underline{C}H_3$), 78.1 (C-5), 113.4* (2C, CH Ar), 113.7 (C-3a), 120.1* (2C, C-2 C-6 Ph), 124.3* (C-4 Ph), 128.2* (2C, CH Ar), 129.7* (2C, C-3 C-5 Ph), 130.0* (2C, CH Ph), 130.5* (2C, CH Ph), 131.1* (C-4 Ph), 135.6 (C-1 Ph), 138.8 (C-1 Ar), 150.9 (C-1 Ph), 153.0 (C-6), 153.6 (C-8a), 157.6 (C–OMe), 163.2 (C=N), 169.1 (C=O). *Signals with a negative phase. Elemental Analysis ($C_{27}H_{23}N_3O_3S_2$, M 501,62): calculated (%): C, 64.65; H, 4.62; N, 8.38; found (%): C, 64.47; H, 4.70; N, 8.25. HRMS (ESI) m/z: calculated for $C_{27}H_{24}N_3O_3S_2$ $[M + H]^+$: 502.12591, found 502.1248 (Δ 2.21 ppm).

Methyl 6-amino-7-phenyl-3-(phenylimino)-4-(2-thienyl)-4,7-dihydro-3H-[1,2]dithiolo[3,4-b]pyridine-5-carboxylate (**15g**). This compound was prepared via **Method A** in a yield of 360 mg (72%). Alternatively, this compound was prepared via **Method B** employing methyl cyanoacetate (0.09 mL), thiophene-2-carbaldehyde (0.09 mL) and thioamide **12** (300 mg) in MeOH in a yield of 326 mg (65%), yellow powder. FTIR, ν_{max}, cm^{-1}: 3440, 3273 (N-H); 1660 (CO_2Me); 1627 (C=N). ^1H NMR (400 MHz, DMSO-d_6): 3.55 (s, 3H, COOMe), 5.40 (s, 1H, H-4), 6.91–6.95 (m, 4H, H-3 H-4 thienyl and H-2 H-6 Ph overlapped), 7.10–7.14 (m, 3H, H-4 Ph and NH_2 overlapped), 7.26 (dd, ^3J = 5.0 Hz, ^4J = 1.5 Hz, 1H, H-5 2-thienyl), 7.32–7.36 (m, 2H, H-3 H-5 Ph), 7.50–7.54 (m, 2H, H-3 H-5 Ph), 7.60–7.66 (m, 3H, H-2 H-6 H-4 Ph). ^{13}C DEPTQ NMR (101 MHz, DMSO-d_6): 34.0* (C-4), 51.1* ($CO_2\underline{C}H_3$), 78.1 (C-5), 112.8 (C-3a), 120.1* (2C, C2 C-6 Ph), 122.7* (C-2 thienyl), 123.7* (C-5 thienyl), 124.3* (C-4 Ar), 126.6* (C-4 thienyl), 129.7* (2C, C-3 C-5 Ph), 130.0* (2C, C-3 C-5 Ph), 130.5* (2C, C-2 C-6 Ph), 131.0* (C-4 Ph), 135.7 (C-1 Ph), 150.8 (C-1 Ph), 151.0 (C-1 thienyl), 153.3 (C-6), 154.1 (C-8a), 163.4 (C=N), 169.0 (C=O). *Signals with a negative phase. Elemental Analysis ($C_{24}H_{19}N_3O_2S_3$, M 477,62): calculated (%): C, 60.35; H, 4.01; N, 8.80; found (%): C, 60.23; H, 4.15; N, 8.75. HRMS (ESI) m/z: calculated for $C_{24}H_{20}N_3O_2S_3$ $[M + H]^+$: 478.0718, found 478.0722 (Δ −0.84 ppm).

3.2. Herbicide-Safening Effect Studies

Germinated sunflower seeds (cv. Master) with 2–4 mm long embryo roots were placed in a solution of 2,4-D (10^{-3}% by weight) for 1 h to achieve 40–60% inhibition of hypocotyl growth. After treatment, the seedlings were washed with pure water and placed into a solution of the corresponding compound **15a,c,f** (concentrations 10^{-2}, 10^{-3}, 10^{-4} or 10^{-5}% by weight, "herbicide + antidote" experiments). After 1 h the seedlings were washed with pure water and placed on paper strips (10 × 75 cm, 20 seeds per strip). The strips were rolled and placed into beakers with water (50 cm^3). The reference group of seedlings ("herbicide" experiments) was kept in 2,4-D solution (10^{-3}%) for 1 h and then in water for 1 h. The "control" seedlings were kept in water for 2 h. The temperature of all solutions was maintained at 28 °C. The seedlings were then thermostated for 3 days at 28 °C. Each experiment was performed in triplicate; 20 seeds were used in each experiment. The results are given in Table 1.

3.3. Growth-Stimulating Effect Studies

Sunflower seeds were treated with a solution of a test compound at different concentrations (10^{-2} to 10^{-5} by weight) for 1 h. After 1 h, the seeds were spread evenly on strips of filter paper, rolled up, placed in beakers with water and thermostated at 28 °C for 3 days. Then stem and root length were measured, and the data were statistically processed using Student's *t*-test, $p = 0.95$. Each experiment was carried out in triplicate with 100 seeds. The results are given in Table 3.

4. Conclusions

Generally, a new preparative method for synthesis of alkyl 6-amino-4-aryl-7-phenyl- 3-(phenylimino)-4,7-dihydro-3H-[1,2]dithiolo[3,4-b]pyridine-5-carboxylates **15** based on the base-catalyzed cascade reaction of dithiomalondianilide **12** with alkyl 3-aryl-2-cyanoacrylates was developed. Alternatively, the same compounds can also be prepared in a single step starting from aromatic aldehydes, ethyl (or methyl) cyanoacetate and dithiomalondianilide. Related reactions of dithiomalondianilide **12** with other Michael acceptors are currently underway in our laboratory. Some compounds showed a strong antidote effect with respect to herbicide 2,4-D accompanied by moderate growth-regulating activity in the experiments on sunflower seedlings. Thus, compounds **15a,c,f** reduced the negative effect of 2,4-D on sunflower seedling hypocotyls by 34–60% and by 40–55% on sunflower seedling roots in the laboratory experiments and showed an antidote effect of 41.4–51.4% in the field experiments.

Supplementary Materials: The following supporting information can be downloaded at: https://www.mdpi.com/article/10.3390/molecules28020609/s1, Figure S1. FTIR spectrum of dithiolopyridine **15a**; Figure S2. ^{1}H NMR spectrum of dithiolopyridine **15a**, DMSO-d_6 (400 MHz); Figure S3. ^{13}C DEPTQ NMR spectrum of dithiolopyridine **15a**, DMSO-d_6 (101 MHz); Figure S4. ^{1}H–^{13}C HSQC NMR spectrum of the dithiolopyridine **15**a, DMSO-d_6 (400/101 MHz); Figure S5. ^{1}H–^{13}C HMBC NMR spectrum of the dithiolopyridine **15a**, DMSO-d_6 (400/101 MHz); Figure S6. ^{1}H–^{13}C HMBC NMR spectrum of the dithiolopyridine 1**5a**, DMSO-d_6 (400/101 MHz) (fragments); Table S1. The observed correlations in the ^{1}H–^{13}C HSQC and ^{1}H–^{13}C HMBC 2D NMR spectra of dithiolopyridine **15a**; Figure S7. ORTEP drawings of the crystal structure showing 50% probability thermal ellipsoids (CCDC 2219352) of the single crystal of compound **15a**; Table S2. Crystal data and structure refinement for dithiolopyridine **15a**; Table S3. Fractional Atomic Coordinates ($\times 10^4$) and Equivalent Isotropic Displacement Parameters ($Å^2 \times 10^3$) for **15a**. U_{eq} is defined as 1/3 of of the trace of the orthogonalised UIJ tensor; Table S4. Anisotropic Displacement Parameters ($Å^2 \times 10^3$) for **15a**. The Anisotropic displacement factor exponent takes the form: $-2\pi^2[h^2a^{*2}U_{11}+...+2hka \times b \times U_{12}]$; Table S5. Bond Lengths for dithiolopyridine **15a**; Table S6. Bond Angles for dithiolopyridine **15a**; Table S7. Hydrogen Atom Coordinates ($Å \times 10^4$) and Isotropic Displacement Parameters ($Å^2 \times 10^3$) for **15a**; Figure S8. FTIR spectrum of dithiolopyridine **15b**; Figure S9. ^{1}H NMR spectrum of dithiolopyridine **15b**, DMSO-d_6 (400 MHz); Figure S10. ^{13}C DEPTQ NMR spectrum of dithiolopyridine **15b**, DMSO-d_6 (101 MHz); Figure S11. FTIR spectrum of dithiolopyridine **15c**; Figure S12. ^{1}H NMR spectrum of

dithiolopyridine **15c**, DMSO-d_6 (400 MHz); Figure S13. ^{13}C DEPTQ NMR spectrum of dithiolopyridine **15c**, DMSO-d_6 (101 MHz); Figure S14. ^{1}H–^{13}C HSQC NMR spectrum of the dithiolopyridine **15c**, DMSO-d_6 (400/101 MHz); Figure S15. ^{1}H–^{13}C HMBC NMR spectrum of the dithiolopyridine **15c**, DMSO-d_6 (400/101 MHz); Figure S16. ^{1}H–^{13}C HMBC NMR spectrum of the dithiolopyridine **15c**, DMSO-d_6 (400/101 MHz) (fragment); Table S8. The observed correlations in the ^{1}H–^{13}C HSQC and ^{1}H–^{13}C HMBC 2D NMR spectra of dithiolopyridine **15c**; Figure S17. FTIR spectrum of dithiolopyridine **15d**; Figure S18. ^{1}H NMR spectrum of dithiolopyridine **15d**, DMSO-d_6 (400 MHz); Figure S19. ^{13}C DEPTQ NMR spectrum of dithiolopyridine **15d**, DMSO-d_6 (101 MHz); Figure S20. FTIR spectrum of dithiolopyridine **15f**; Figure S21. ^{1}H NMR spectrum of dithiolopyridine **15f**, DMSO-d_6 (400 MHz); Figure S22. ^{13}C DEPTQ NMR spectrum of dithiolopyridine **15f**, DMSO-d_6 (101 MHz); Figure S23. ^{1}H–^{13}C HSQC NMR spectrum of the dithiolopyridine **15f**, DMSO-d_6 (400/101 MHz); Figure S24. ^{1}H–^{13}C HMBC NMR spectrum of the dithiolopyridine **15f**, DMSO-d_6 (400/101 MHz); Figure S25. ^{1}H–^{13}C HMBC NMR spectrum of the dithiolopyridine **15f**, DMSO-d_6 (400/101 MHz) (fragment); Table S9. The observed correlations in the ^{1}H–^{13}C HSQC and ^{1}H–^{13}C HMBC 2D NMR spectra of dithiolopyridine **15f**; Figure S26. HRMS spectrum of dithiolopyridine **15a**; Figure S27. HRMS spectrum of dithiolopyridine **15b**; Figure S28. HRMS spectrum of dithiolopyridine **15c**; Figure S29. HRMS spectrum of dithiolopyridine **15d**; Figure S30. HRMS spectrum of dithiolopyridine **15e**; Figure S31. HRMS spectrum of dithiolopyridine **15f**.

Author Contributions: V.V.D.—conceptualization, supervision, data analysis, funding acquisition, writing (original draft, review and editing); A.E.S.—investigation; V.D.S.—investigation (agrochemical studies); E.A.V.—investigation; A.A.R.—investigation; A.G.L.—investigation; A.Z.T.—data analysis; N.A.A.—data analysis; I.V.A.—supervision, data analysis. All authors have read and agreed to the published version of the manuscript.

Funding: This research was funded by the Russian Science Foundation, grant number 22-23-00458, https://rscf.ru/en/project/22-23-00458/ (accessed on 1 January 2023).

Institutional Review Board Statement: Not applicable.

Informed Consent Statement: Not applicable.

Data Availability Statement: See the file Electronic Supplementary Material.pdf containing ^{1}H and ^{13}C DEPTQ NMR, 2D NMR ^{1}H-^{13}C HSQC and ^{1}H-^{13}C HMBC, FTIR, HRMS spectral charts for dithiolopyridines (Figures S1–S6, S8–S31, Tables S1, S8 and S9) and X-ray crystallography data for dithiolopyridine **15a** (Supplementary Materials Figure S7 and Tables S2–S7).

Acknowledgments: Authors are grateful to the staff of the Federal Scientific Center for Biological Protection of Plants (Krasnodar, Russia) for help with agrochemical studies. The studies were performed using the equipment of the scientific and educational center "Diagnostics of the Structure and Properties of Nanomaterials" and the equipment of the Center for Collective Use "Ecological Analytical Center" of Kuban State University, Krasnodar.

Conflicts of Interest: The authors declare no conflict of interest.

References

1. Schmidt, U.; Kubitzek, H. Synthesen mit den Thioamiden der Malonsäure, II. Thiopyridone aus Cyan-thioacetamid. *Chem. Ber.* **1960**, *93*, 1559–1565. [CrossRef]
2. Baggaley, K.H. Isothiazolo-Pyridines. Patent GB1560726A, 6 February 1980. Available online: https://worldwide.espacenet.com/patent/search/family/010090431/publication/GB1560726A?q=pn%3DGB1560726A (accessed on 12 November 2022).
3. Baggaley, K.H.; Jennings, L.J.A.; Tyrrell, A.W.R. Synthesis of 2-substituted isothiazolopyridin-3-ones. *J. Heterocycl. Chem.* **1982**, *19*, 1393–1396. [CrossRef]
4. Pregnolato, M.; Terreni, M.; Ubiali, D.; Pagani, G.; Borgna, P.; Pastoni, F.; Zampollo, F. 3H-[1,2]Dithiolo [3,4-b]pyridine-3-thione and its derivatives. Synthesis and antimicrobial activity. *II Farm.* **2000**, *55*, 669–679. [CrossRef] [PubMed]
5. Salvetti, R.; Martinetti, G.; Ubiali, D.; Pregnolato, M.; Pagani, G. 1,2-Dithiolan-3-ones and derivatives structurally related to leinamycin. Synthesis and biological evaluation. *II Farm.* **2003**, *58*, 995–998. [CrossRef] [PubMed]
6. Martinez-Merino, V.; Gil, M.J.; Gonzalez, A.; Zabalza, J.M.; Navarro, J.; Manu, M.A. New 5-substituted derivatives of ethyl 2,3-dihydro-3-oxoisothiazolo[5,4-b]pyridine-2-acetate. *Heterocycles* **1994**, *38*, 333–344. [CrossRef]
7. Lyu, L.; Huang, M.; Liu, J.; Wang, X. Preparation Method of Benzodithiole Skeleton Compounds. Patent CN110950836A, 3 April 2020. (In Chinese). Available online: https://worldwide.espacenet.com/patent/search/family/069981368/publication/CN110950836A?q=pn%3DCN110950836A (accessed on 12 November 2022).

8. Borgna, P.; Pregnolato, M.; Invernizzi, A.G.; Mellerio, G. On the reaction between 3H-1,2-dithiolo[3,4-b]pyridine-3-thione and primary alkyl and arylalkylamines. *J. Heterocycl. Chem.* **1993**, *30*, 1079–1084. [CrossRef]
9. Davis, R.C.; Grinter, T.J.; Leaver, D.; O'Neil, R.M.; Thomson, G.A. The dithiole series. Part 8. Synthesis of ring-fused 1,2-dithiolylium and isothiazolium salts from complexes containing cyclopalladated ligands. *J. Chem. Soc. Perkin Trans. 1* **1990**, 2881–2887. [CrossRef]
10. Jian, F.; Zheng, J.; Li, Y.; Wang, J. Novel ((3Z,5Z)-3,5-bis(phenylimino)-1,2-dithiolan-4-yl) and 3H-[1,2]dithiolo[3,4-b]quinolin-4 (9H)-one heterocycles: An effective and facile green route. *Green Chem.* **2009**, *11*, 215–222. [CrossRef]
11. Kobayashi, G.; Matsuda, Y.; Natsuki, R.; Ueno, S. Studies on isoquinoline derivatives. I. Reaction of 1,3-dioxo-1,2,3,4-tetrahydroisoquinolines with carbon disulfide. *Yakugaku Zasshi: J. Pharm. Soc. Jpn.* **1973**, *93*, 322–329. [CrossRef]
12. Pagani, G.; Pregnolato, M.; Ubiali, D.; Terreni, M.; Piersimoni, C.; Scaglione, F.; Fraschini, F.; Rodríguez Gascón, A.; Pedraz Muñoz, J.L. Synthesis and in vitro anti-mycobacterium activity of N-alkyl-1,2-dihydro-2-thioxo-3-pyridinecarbothioamides. Preliminary toxicity and pharmacokinetic evaluation. *J. Med. Chem.* **2000**, *43*, 199–204. [CrossRef]
13. Ubiali, D.; Pagani, G.; Pregnolato, M.; Piersimoni, C.; Pedraz Muñoz, J.L.; Rodríguez Gascón, A.; Terreni, M. New N-Alkyl-1,2-dihydro-2-thioxo-3-pyridinecarbothioamides as antituberculous agents with improved pharmacokinetics. *Bioorganic Med. Chem. Lett.* **2002**, *12*, 2541–2544. [CrossRef] [PubMed]
14. Ogurtsov, V.A.; Karpychev, Y.V.; Rakitin, O.A. Synthesis of 1-[(1,2-dithiol-3-ylidene)methyl]pyrrolo[1,2-a]pyrazines and 2-[(1,2-dithiol-3-ylidene)methyl]pyridines from 1,2-dithiole-3-thiones. *Russ. Chem. Bull.* **2013**, *62*, 1076–1079. [CrossRef]
15. Gompper, R.; Elser, W. Stabile 1,4-Dipole aus Ketenacetalen und Schwefelkohlenstoff und ihre Verwendung zur Synthese von Heterocyclen. *Angew. Chem.* **1967**, *79*, 382–383. [CrossRef]
16. Dotsenko, V.V.; Krivokolysko, S.G.; Frolov, K.A.; Chigorina, E.A.; Polovinko, V.V.; Dmitrienko, A.O.; Bushmarinov, I.S. Synthesis of [1,2]dithiolo[3,4-*b*]pyridines via the reaction of dithiomalondianilide with arylmethylidenemalononitriles. *Chem. Heterocycl. Compd.* **2015**, *51*, 389–392. [CrossRef]
17. Dotsenko, V.V.; Buryi, D.S.; Lukina, D.Y.; Krivokolysko, S.G. Recent advances in the chemistry of thieno[2,3-*b*]pyridines 1. Methods of synthesis of thieno[2,3-*b*]pyridines. *Russ. Chem. Bull.* **2020**, *69*, 1829–1858. [CrossRef]
18. Larionova, N.A.; Shestopalov, A.M.; Rodinovskaya, L.A.; Zubarev, A.A. Synthesis of biologically active heterocycles via a domino sequence involving an S_N2/Thorpe–Ziegler Reaction Step. *Synthesis* **2022**, *54*, 217–245. [CrossRef]
19. Sinotsko, A.E.; Bespalov, A.V.; Pashchevskaya, N.V.; Dotsenko, V.V.; Aksenov, N.A.; Aksenova, I.V. N,N′-Diphenyldithiomalonodiamide: Structural Features, Acidic Properties, and In Silico Estimation of Biological Activity. *Russ. J. Gen. Chem.* **2021**, *91*, 2136–2150. [CrossRef]
20. Dotsenko, V.V.; Aksenov, A.V.; Sinotsko, A.E.; Varzieva, E.A.; Russkikh, A.A.; Levchenko, A.G.; Aksenov, N.A.; Aksenova, I.V. The reactions of N,N′-diphenyldithiomalondiamide with arylmethylidene Meldrum's acids. *Int. J. Mol. Sci.* **2022**, *23*, 15997. [CrossRef]
21. Dotsenko, V.V.; Sinotsko, A.E.; Varzieva, E.A.; Chigorina, E.A.; Aksenov, N.A.; Aksenova, I.V. N,N′-Diphenyldithiomalonamide as methylene active thioamide: A first synthesis of stable Michael adducts. *Russ. J. Gen. Chem.* **2022**, *92*, 2530–2535. [CrossRef]
22. Peyronel, G.; Pellacani, G.C.; Benetti, G.; Pollacci, G. Nickel(II) complexes with dithiomalonamide and NN′-diphenyldithiomalonamide. *J. Chem. Soc. Dalton Trans.* **1973**, 879–882. [CrossRef]
23. Pellacani, G.C. Palladium(II) complexes with dithiomalonamide and N,N′-diphenyldithiomalonamide. *Can. J. Chem.* **1974**, *52*, 3454–3458. [CrossRef]
24. Pal, T.; Ganguly, A.; Maity, D.S.; Livingstone, S.E. N,N′-diphenyldithiomalonamide as a gravimetric reagent for nickel and cobalt. *Talanta* **1986**, *33*, 973–977. [CrossRef]
25. Battaglia, L.P.; Bonamartini Corradi, A.; Marzotto, A.; Menabue, L.; Pellacani, G.C. Co-ordinative abilities of ligands which favour S,S chelation: Copper(I) halide complexes of N,N′-diphenyldithiomalonamide. The crystal and molecular structure of bis(N,N′-diphenyldithiomalonamide)copper(I) iodide–methanol (2/1). *J. Chem. Soc. Dalton Trans.* **1988**, 1713–1718. [CrossRef]
26. Nizovtseva, T.V.; Komarova, T.N.; Nakhmanovich, A.S.; Larina, L.I.; Lopyrev, V.A. Synthesis of 1,3-dithiinium salts. *Arkivoc* **2003**, *13*, 191–195. [CrossRef]
27. Elokhina, V.N.; Yaroshenko, T.I.; Nakhmanovich, A.S.; Larina, L.I.; Amosova, S.V. Reaction of dithiomalonic acid dianilide with substituted acetylenic ketones. *Russ. J. Gen. Chem.* **2006**, *76*, 1916–1918. [CrossRef]
28. Obydennov, K.L.; Golovko, N.A.; Kosterina, M.F.; Pospelova, T.A.; Slepukhin, P.A.; Morzherin, Y. Synthesis of 4-oxothiazolidine-2,5-diylidenes containing thioamide group based on dithiomalonamides. *Russ. Chem. Bull.* **2014**, *63*, 1330–1336. [CrossRef]
29. Degorce, S.; Jung, F.H.; Harris, C.S.; Koza, P.; Lecoq, J.; Stevenin, A. Diversity-orientated synthesis of 3,5-bis(arylamino)pyrazoles. *Tetrahedron Lett.* **2011**, *52*, 6719–6722. [CrossRef]
30. Dotsenko, V.V.; Frolov, K.A.; Krivokolysko, S.G.; Chigorina, E.A.; Pekhtereva, T.M.; Suykov, S.Y.; Papayanina, E.S.; Dmitrienko, A.O.; Bushmarinov, I.S. Aminomethylation of morpholinium and *N*-methylmorpholinium 3,5-dicyano-4,4-dimethyl-6-oxo-1,4,5,6-tetrahydropyridine-2-thiolates. *Chem. Heterocycl. Compd.* **2016**, *52*, 116–127. [CrossRef]
31. Dyachenko, I.V.; Dyachenko, V.D.; Dorovatovskii, P.V.; Khrustalev, V.N.; Nenaidenko, V.G. New Options of Multicomponent Condensations Leading to Functional Derivatives of 2-Pyridons. *Russ. J. Org. Chem.* **2021**, *57*, 1809–1823. [CrossRef]
32. Shestopalov, A.M.; Shestopalov, A.A.; Rodinovskaya, L.A.; Gromova, A.V. One-step synthesis of substituted 3,5-dicyanospiro-4-(piperidine-4′)-1H,4H-dihydropyridine-2-thiolates and 2,6-diamino-3,5-dicyanospiro-4-[(piperidine-4′) or (2′-oxoindole-3′)]-4H-thiopyrans. *Phosphorus Sulfur Silicon* **2009**, *184*, 1100–1114. [CrossRef]

33. Bakhite, E.A.; Abd-Ella, A.A.; El-Sayed, M.E.A.; Abdel-Raheem, S.A.A. Pyridine derivatives as insecticides. Part 1: Synthesis and toxicity of some pyridine derivatives against Cowpea Aphid, Aphis craccivora Koch (Homoptera: Aphididae). *J. Agric. Food Chem.* **2014**, *62*, 9982–9986. [CrossRef]
34. Wen, L.-R.; Sun, J.-H.; Li, M.; Sun, E.-T.; Zhang, S.-S. Application of β-(2-chloroaroyl) thioacetanilides in synthesis: An unusual and highly efficient access to thiochromeno[2,3-b]pyridine derivatives. *J. Org. Chem.* **2008**, *73*, 1852–1863. [CrossRef]
35. Li, M.; Cao, H.; Wang, Y.; Lv, X.-L.; Wen, L.-R. One-pot multicomponent cascade reaction of N,S-ketene acetal: Solvent-free synthesis of imidazo[1,2-a]thiochromeno[3,2-e]pyridines. *Org. Lett.* **2012**, *14*, 3470–3473. [CrossRef]
36. Feng, X.; Wang, J.-J.; Xun, Z.; Huang, Z.-B.; Shi, D.-Q. Multicomponent strategy to indeno[2,1-c]pyridine and hydroisoquinoline derivatives through cleavage of carbon–carbon bond. *J. Org. Chem.* **2015**, *80*, 1025–1033. [CrossRef]
37. Li, M.; Zuo, Z.; Wen, L.; Wang, S. Microwave-assisted combinatorial synthesis of hexa-substituted 1,4-dihydropyridines scaffolds using one-pot two-step multicomponent reaction followed by a S-alkylation. *J. Comb. Chem.* **2008**, *10*, 436–441. [CrossRef]
38. Peterson, M.A.; McMaster, S.A.; Riechers, D.E.; Skelton, J.; Stahlman, P.W. 2,4-D past, present, and future: A review. *Weed Technol.* **2016**, *30*, 303–345. [CrossRef]
39. Chkanikov, N.D.; Spiridonov, Y.Y.; Khalikov, S.S.; Muzafarova, A.M. Antidotes for reduction of phytotoxicity of the residues of sulfonylurea herbicides. *INEOS OPEN* **2019**, *2*, 145–152. [CrossRef]
40. Deng, X. Current advances in the action mechanisms of safeners. *Agronomy* **2022**, *12*, 2824. [CrossRef]
41. Jia, L.; Jin, X.Y.; Zhao, L.X.; Fu, Y.; Ye, F. Research progress in the design and synthesis of herbicide safeners: A review. *J. Agric. Food Chem.* **2022**, *70*, 5499–5515. [CrossRef]
42. Dotsenko, V.V.; Buryi, D.S.; Lukina, D.Y.; Stolyarova, A.N.; Aksenov, N.A.; Aksenova, I.V.; Strelkov, V.D.; Dyadyuchenko, L.V. Substituted N-(thieno[2,3-b]pyridine-3-yl)acetamides: Synthesis, reactions, and biological activity. *Mon. Für Chem. Chem. Mon.* **2019**, *150*, 1973–1985. [CrossRef]
43. Dotsenko, V.V.; Muraviev, V.S.; Lukina, D.Y.; Strelkov, V.D.; Aksenov, N.A.; Aksenova, I.V.; Krapivin, G.D.; Dyadyuchenko, L.V. Reaction of 3-Amino-4,6-diarylthieno[2,3-b]pyridine-2-carboxamides with ninhydrin. *Russ. J. Gen. Chem.* **2020**, *90*, 948–960. [CrossRef]
44. Buryi, D.S.; Dotsenko, V.V.; Aksenov, N.A.; Aksenova, I.V.; Krivokolysko, S.G.; Dyadyuchenko, L.V. Synthesis and properties of 4,6-dimethyl-5-pentyl-2-thioxo-1,2-dihydropyridine-3-carbonitrile and 3-amino-4,6-dimethyl-5-pentylthieno[2,3-b]pyridi- nes. *Russ. J. Gen. Chem.* **2019**, *89*, 1575–1585. [CrossRef]
45. Shapovalov, A.A.; Zhirmunskaya, N.M.; Zubkova, N.F.; Ovsyannikova, T.V.; Gruzinskaya, N.A. *Methodological Recommendations for Laboratory Tests of Synthetic Plant Growth Regulators*; Shapovalov, A.A., Ed.; NIITEChem: Cherkassy, Russia, 1990; p. 35. (In Russian)
46. Barnikow, G.; Kath, V.; Richter, D. Isothiocyanate. II. N,N′-Aryl-substituierte Dithiomalonsäurediamide. *J. Prakt. Chem.* **1965**, *30*, 63–66. [CrossRef]
47. Dolomanov, O.V.; Bourhis, L.J.; Gildea, R.J.; Howard, J.A.K.; Puschmann, H. OLEX2: A complete structure solution, refinementand analysis program. *J. Appl. Cryst.* **2009**, *42*, 339–341. [CrossRef]
48. Sheldrick, G.M. Crystal structure refinement with SHELXL. *Acta Crystallogr. Sect. C Struct. Chem.* **2015**, *71*, 3–8. [CrossRef] [PubMed]

molecules

MDPI

Article

Synthesis of Functionalized Isoquinolone Derivatives via Rh(III)-Catalyzed [4+2]-Annulation of Benzamides with Internal Acetylene-Containing α-CF_3-α-Amino Carboxylates

Daria V. Vorobyeva [1], Dmitry A. Petropavlovskikh [1], Ivan A. Godovikov [1], Fedor M. Dolgushin [2,3] and Sergey N. Osipov [1,*]

[1] A. N. Nesmeyanov Institute of Organoelement Compounds, Russian Academy of Sciences, 28/1 Vavilova Str., 119334 Moscow, Russia
[2] N. S. Kurnakov Institute of General and Inorganic Chemistry, Russian Academy of Sciences, Leninsky pr. 31, 119071 Moscow, Russia
[3] Plekhanov Russian University of Economics, 36, Stremyanny Per., 117997 Moscow, Russia
* Correspondence: osipov@ineos.ac.ru; Tel.: +7-499-135-1873

Abstract: A convenient pathway to a new series of α-CF_3-substituted α-amino acid derivatives bearing pharmacophore isoquinolone core in their backbone has been developed. The method is based on [4+2]-annulation of *N*-(pivaloyloxy) aryl amides with orthogonally protected internal acetylene-containing α-amino carboxylates under Rh(III)-catalysis. The target annulation products can be easily transformed into valuable isoquinoline derivatives via a successive aromatization/cross-coupling operation.

Keywords: acetylenes; amino acids; C-H activation; annulation; catalysis; isoquinolones

Citation: Vorobyeva, D.V.; Petropavlovskikh, D.A.; Godovikov, I.A.; Dolgushin, F.M.; Osipov, S.N. Synthesis of Functionalized Isoquinolone Derivatives via Rh(III)-Catalyzed [4+2]-Annulation of Benzamides with Internal Acetylene-Containing α-CF_3-α-Amino Carboxylates. *Molecules* **2022**, *27*, 8488. https://doi.org/10.3390/molecules27238488

Academic Editor: Alexey M. Starosotnikov

Received: 3 November 2022
Accepted: 24 November 2022
Published: 2 December 2022

Publisher's Note: MDPI stays neutral with regard to jurisdictional claims in published maps and institutional affiliations.

1. Introduction

Isoquinolin-1(2*H*)-ones and analogues are important nitrogen heterocycles possessing diverse bioactivities and presented in many candidates, including antitumor, anti-diabetic, anti-inflammatory and cardiovascular drugs [1–7] (Figure 1). They are also widely used as key intermediates in variety of organic transformations to access more potent bioactive molecules [8–14].

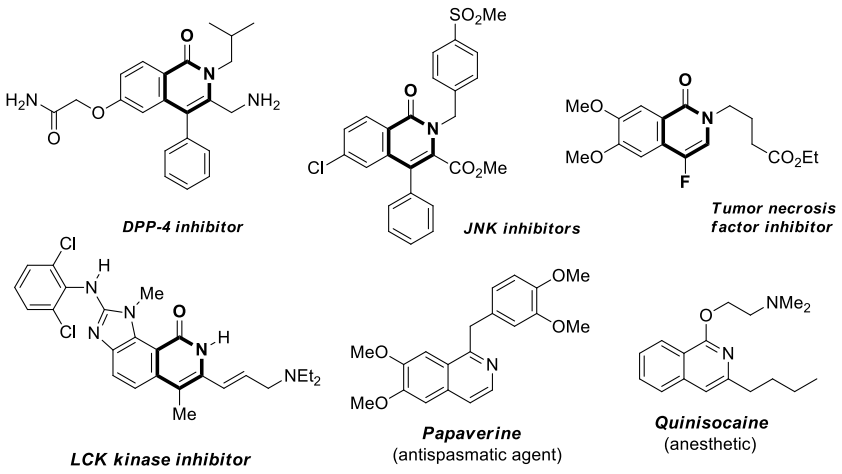

Figure 1. Selected bioactive isoquinolones and isoquinolines.

Transition-metal-catalyzed annulation reactions via C-H activation have gained great importance as a powerful step- and atom-economical strategy for the preparation of complex molecules from simple starting materials [15–18]. In particular, [Cp*Rh^{III}]-catalyzed

annulation of the akynes with (hetero)arenes bearing different directing groups has become one of the most efficient and robust synthetic methodologies for the construction of various functionalized heterocycles [19–25]. In 2010, Fagnou and co-workers discovered that the *N*-pivaloyloxy group can act both as a directing group and as an internal oxidant through N-O bond cleavage during the synthesis of isoquinolones [26,27]. Mechanistically, this redox-neutral [4+2]-annulation process between alkynes and *N*-pivaloyloxy aryl amides has shown to proceed via the formation of a seven-membered rhodacycle intermediate, which undergoes a C-N bond forming/N-O bond cleaving event to yield the free NH isoquinolones suitable for further useful transformations [28–34]. Despite significant advances made in the field, the development of effective strategies employing new coupling partners to construct functionally substituted quinolin-2(*1H*)-ones remains of great demand.

On the other hand, modern peptide-based drug design very often aims on selective derivatizing of the peptide backbone through the introduction of additional functional groups or proven heterocyclic pharmacophores in order to modulate the required properties [35–41]. In this respect, α-fluoroalkyl-containing α-amino acids are of particular interest since they find widespread bio-organic applications as biological tracers, mechanistic probes, and enzyme inhibitors as well as medical applications including blood pressure control, allergies, and tumor growth [42–46]. The incorporation of fluorinated α-amino acids into key positions of bioactive peptides is one of the most common strategies to improve their pharmacokinetic profiles, conformational and proteolytic stability, and membrane permeability [43–50]. Therefore, the development of new representatives of α-fluoromethyl-α-amino acids, including those decorated with pharmacophore heterocycle rings, is of high interest.

Recently, we have elaborated an efficient strategy for the preparation of novel α-CF_3-α-amino acid derivatives and their phosphorus counterparts with isoquinolone moiety in their backbone based on [Cp*Rh^{III}]-catalyzed [4+2]-annulation of terminal propargyl-containing α-CF_3-substituted α-amino carboxylates and α-propargyl-α-amino phosphonates with *N*-pivaloyloxy aryl amides [51] (Scheme 1).

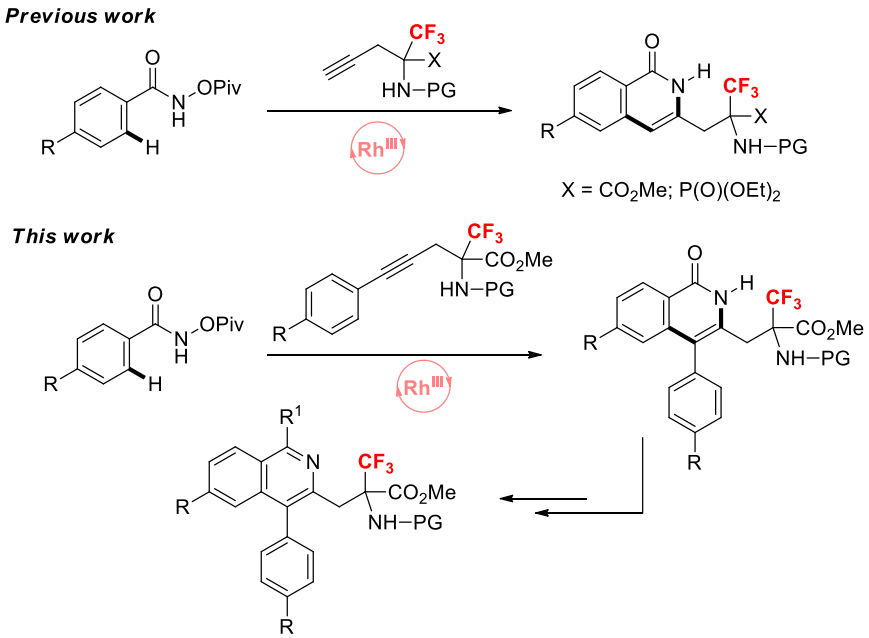

Scheme 1. Previous and present work.

In continuation of our current research on metal-catalyzed C-H bond activation [52–55], here we want to disclose a convenient regio-selective approach to new isoquinolone-containing α-amino acid derivatives derived from internal aryl acetylenes bearing protected

α-CF_3-α-amino carboxylate framework under rhodium(III)-catalysis, and their further synthetic transformations into highly functionalized isoquinolines (Scheme 1).

2. Results and Discussion

We commenced our study by examining a model reaction between phenyl hydroxamate **1a** and the readily available internal phenyl acetylene **2a** [56] bearing an *N*-Boc-protected α-CF_3-α-amino ester group for the screening of optimal conditions for the annulation. The rhodium catalytic system [Cp*$RhCl_2$]$_2$/CsOAc, as the most competent catalyst for such type of transformation, was initially tested to activate the process. As a result, the reaction was found to smoothly proceed in the presence of 5 mol% [Cp*$RhCl_2$]$_2$ and 2.0 equiv. of cesium acetate in methanol at room temperature for 4 h to give the corresponding isoquinolone derivative **3a** in 70% NMR yield (Table 1, entry 1), along with noticeable amounts of starting materials. Encouraged by this result, we screened some solvents and bases for the reaction (entries 2–5). The best conversion of the starting materials and isolated yield of **3a** (measured by ^{19}F NMR spectroscopy) were achieved by the usage of 2,2,2-trifluoroethanol (TFE) and CsOAc (entry 2). Subsequent reduction of catalyst and additive loading (entries 2–6) has revealed the optimal reaction conditions: [Cp*$RhCl_2$]$_2$ (3 mol%) and CsOAc (1 equiv.), r.t., 2 h in MeOH (entry 8). Iridium-, cobalt- and ruthenium-based complexes have proved to be absolutely inactive in the process (entries 10–12). The reaction does not take place in the absence of any catalyst or base, expectedly (entries 13, 14).

Table 1. Optimization of [4+2]-annulation of aryl hydroxamate **1a** with acetylene **2a**.

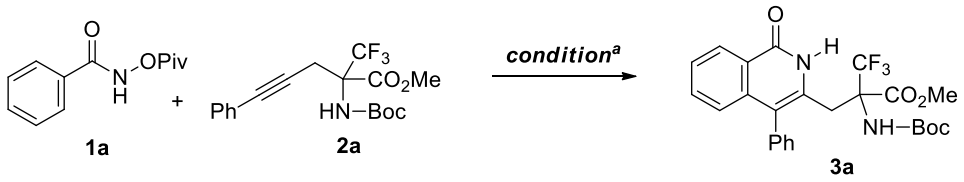

1a **2a** **3a**

Entry	Catalyst (mol. %)	Additive (equiv.)	Solvent	Yield [b] (%)
1	[Cp*$RhCl_2$]$_2$ (5)	CsOAc (2)	MeOH	70(60 [c])
2	[Cp*$RhCl_2$]$_2$ (5)	CsOAc (2)	TFE	87(72 [c])
3	[Cp*$RhCl_2$]$_2$ (5)	CsOAc (2)	toluene	65
4	[Cp*$RhCl_2$]$_2$ (5)	NaOAc (2)	MeOH	73
5	[Cp*$RhCl_2$]$_2$ (5)	KOAc (2)	MeOH	69
6	[Cp*$RhCl_2$]$_2$ (3)	CsOAc (2)	MeOH	73
7	[Cp*$RhCl_2$]$_2$ (3)	CsOAc (2)	TFE	80
8	**[Cp*$RhCl_2$]$_2$ (3)**	**CsOAc (1)**	**TFE**	**84(71 [c])**
9	[Cp*$RhCl_2$]$_2$ (3)	CsOAc (1)	MeOH	68
10	[Cp*$IrCl_2$]$_2$ (5)	CsOAc (2)	MeOH	NR
11	[Cp*CoI_2]$_2$ (5)	CsOAc (2)	MeOH	NR
12	[(*p*-cymene)$RuCl_2$]$_2$ (5)	CsOAc (2)	MeOH	NR
13	-	CsOAc (2)	MeOH	NR
14	[Cp*$RhCl_2$]$_2$ (5)	-	MeOH	NR

[a] Reagents and conditions: aryl hydroxamate **1a** (0.2 mmol), acetylene **2a** (0.2 mmol), solvent (2 mL), r.t.; [b] Determined by ^{19}F NMR spectroscopy; [c] Isolated yield.

With these found conditions in hand, different aryl hydroxamates were involved in [4+2]-annulation with different internal acetylene-containing amino ester **2a–e** (Scheme 2). The latter were easily synthesized via an addition of Grignard reagent (CH_2=C=CH-MgBr), generated from propargyl bromide, to orthogonally protected α-CF_3-α-imino carboxy-

lates followed by Sonogashira coupling with aryl halogenides according to the previously described protocol [56]. As a result, a series of the corresponding isoquinolinone-containing α-CF_3-amino carboxylates **3a–r** were obtained in good yields and high degree of regio-selectivity. The observed selectivity of the [4+2]-annulation process of **1** with α-(arylpropargyl)-α-amino esters **2a–e** bearing donor substituents in aryl group could be probably explained by alkyne insertion into initially formed 5-membered rhodacycle intermediate [26,27], according to its inherent polarity (for proposed mechanism see Supplementary Materials, Scheme S1). The nature of the substituents in hydroxamate component did not significantly affect the outcome of the reaction in all investigated cases (Scheme 2).

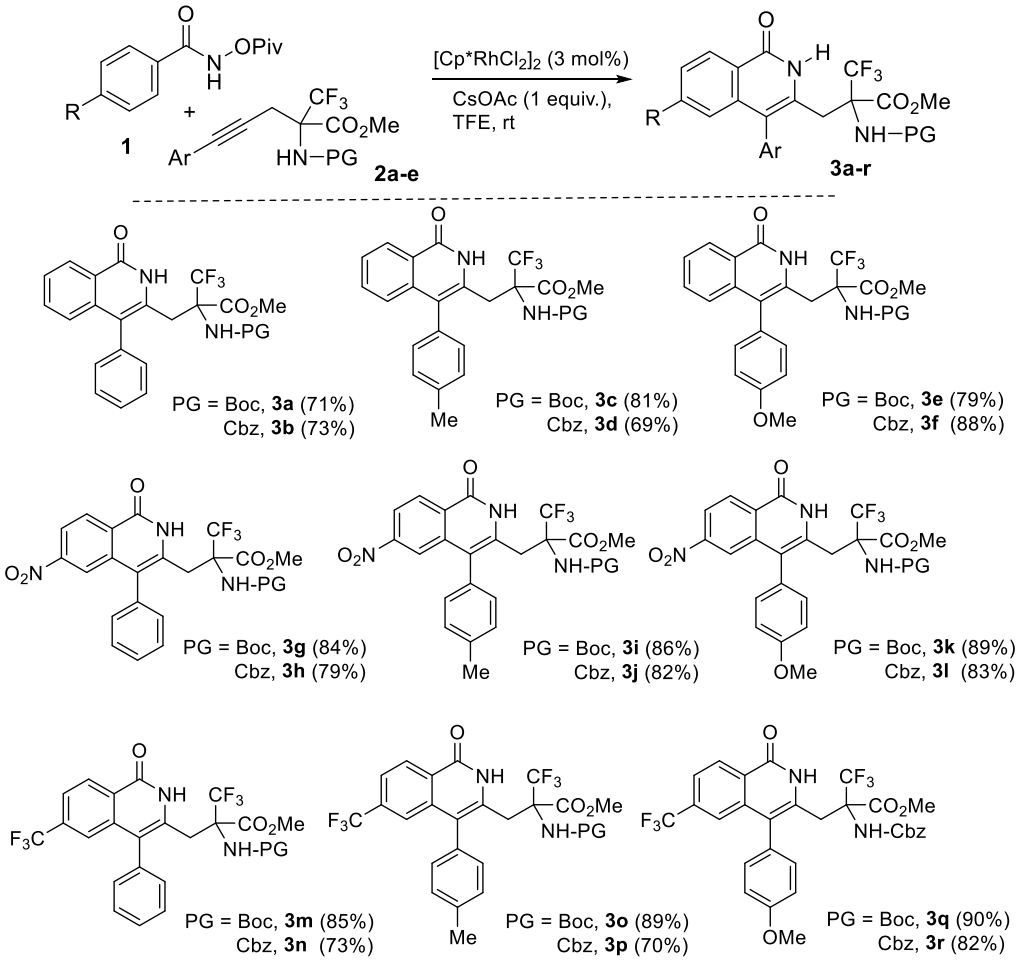

Scheme 2. Synthesis of isoquinolone-containing α-amino carboxylates **3**.

However, the presence of an electron-withdrawing nitro group in *para*-position of aryl substituent of acetylene component leads to a mixture of the corresponding regioisomers **3s** and **3t** in a ratio of 3:2 respectively, which were easily separated by column chromatography on silica gel. The absence of selectivity in this case can be likely addressed to a change in the polarity of the triple bond due to the influence of strong acceptor group. The structure of each regio-isomer was assigned by 2D NOESY experiments (see Supplementary Materials). Thus, an intensive cross peak between proton of CH_2 group of amino acid residue and ortho-proton of phenyl ring was found in the spectrum of isomer **3t** that has not been observed for compound **3s**; instead, a cross peak between the ortho-protons of close located phenyl moieties appeared (Scheme 3).

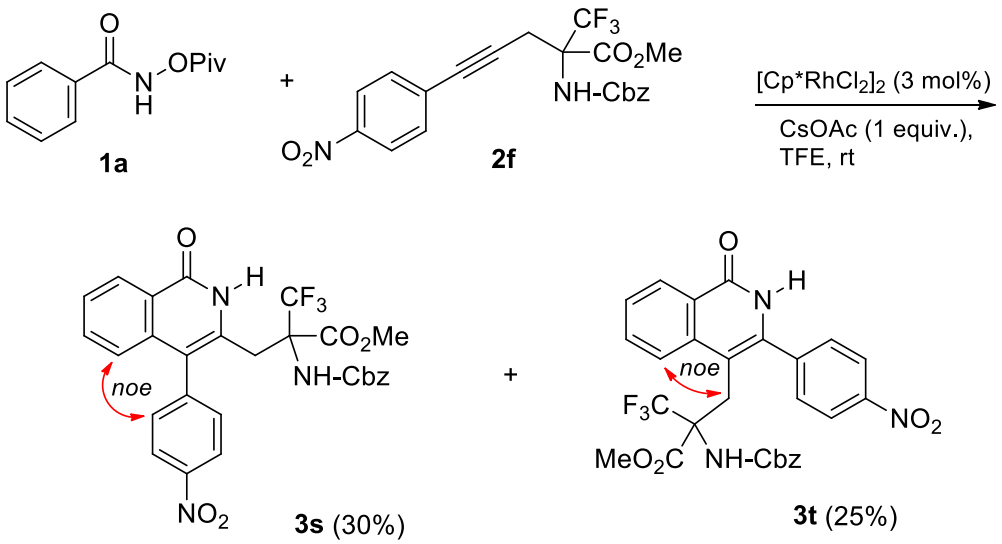

Scheme 3. Reaction of **1a** with para-nitrophenyl acetylene **2f**.

All synthesized compounds were fully characterized by physicochemical methods. In addition, the structure of isoquinolone **3a** was confirmed by X-ray crystallographic analysis (Figure 2).

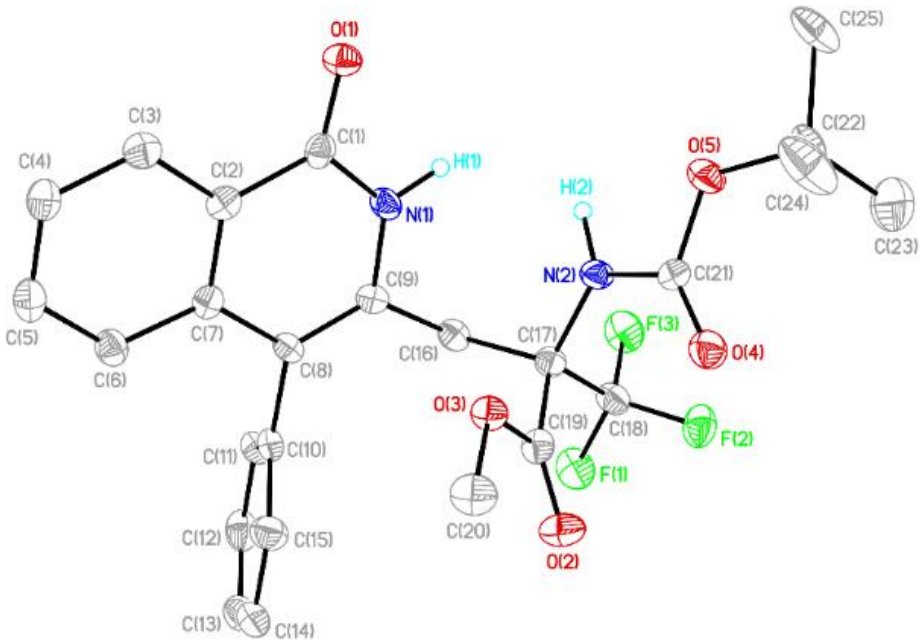

Figure 2. ORTEP representation of the molecular structure of **3a** (CCDC 2217085). Thermal ellipsoids are drawn at the 30% probability level).

Considering the fact that isoquinolines are key structural elements of many bioactive compounds including drugs [57–59] (see Figure 1), we were interested in further investigation of synthetic potential of obtained isoquinolones as universal precursors of the corresponding isoquinoline derivatives decorated with amino acid residues. Thus, we found that the isoquinolones **3** could easily undergo an aromatization into the isoquinolines under treatment with triflic anhydride in the presence of pyridine. The reactions proceed in CH_2Cl_2 under mild conditions and go to completion within 15 min at ambient temperature furnishing the corresponding 1-OTf-substituted isoquinolines **4a–o** in good to high yields (Scheme 4).

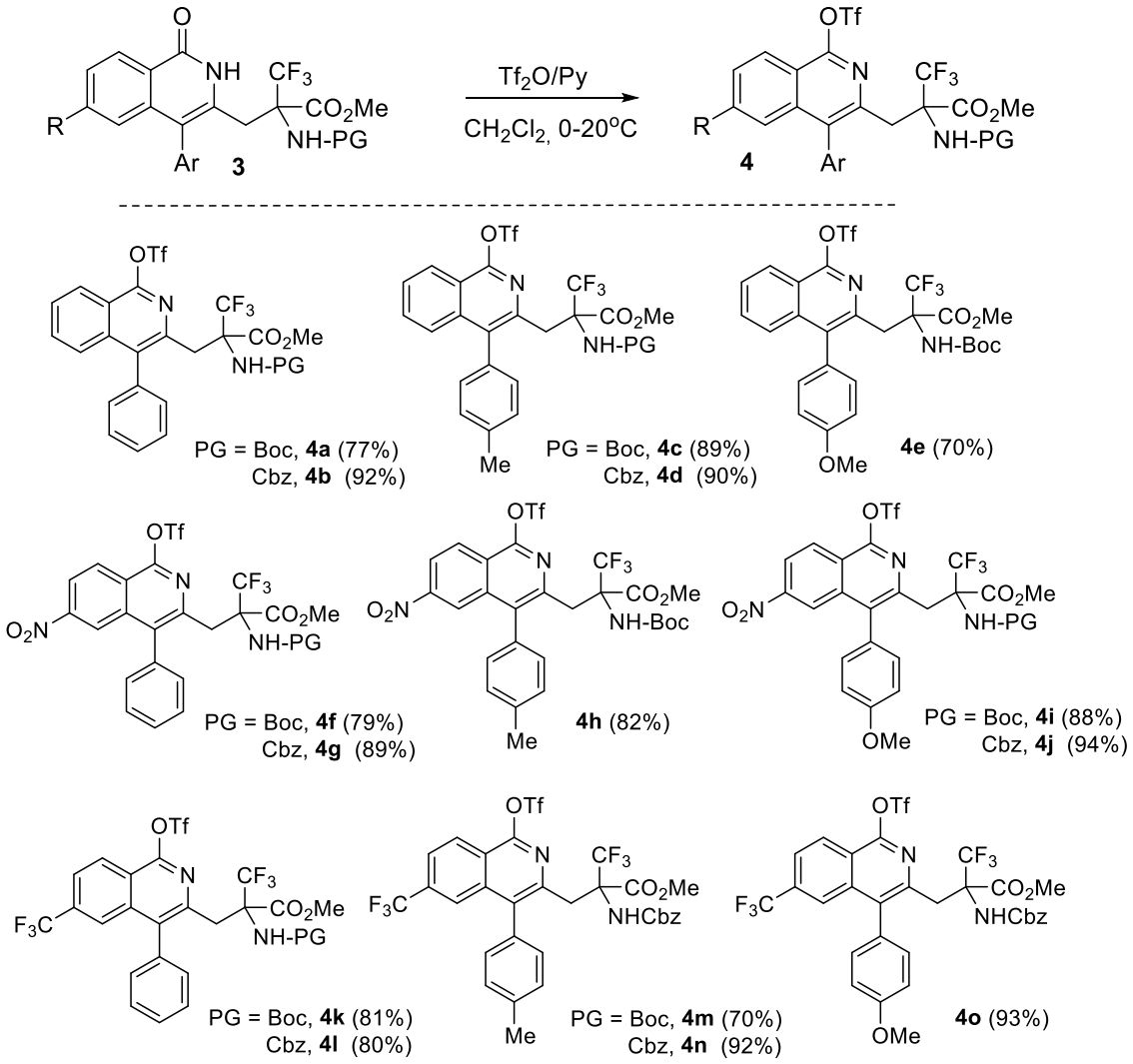

Scheme 4. Synthesis of 1-OTf-substituted isoquinolines **4**.

The well-known pseudo-halogen nature of the TfO group pushed us to explore some further useful transformations of the synthesized isoquinoline derivatives **4**, such as Pd-catalysed cross-coupling reactions. As a result, it turned out that the compounds **4** could serve as suitable cross-coupling partners in Suzuki reaction with various aryl boronic acids. It was revealed that the reactions of **4d**,**f**,**l** with 4-metoxy phenyl boronic acid readily proceeded in dioxane-water mixture under catalysis with $Pd(PPh_3)_2Cl_2/NaHCO_3$ system at 100 °C, leading to the formation of the expected cross-coupling products **5a–c** in high yields (Scheme 5a).

The same isoquinoline-containing α-amino acid derivatives **4d,f,m** were included in coupling with phenyl acetylene under the classical Sonogashira reaction conditions to afford the corresponding products **6a–c** in good yields (Scheme 5b). Finally, we found that the OTf group could be successfully removed in the presence of catalytic amounts of $PdCl_2$(dppf) complex and excess of formic acid to give isoquinolines **7a,b** in acceptable yields (Scheme 5c).

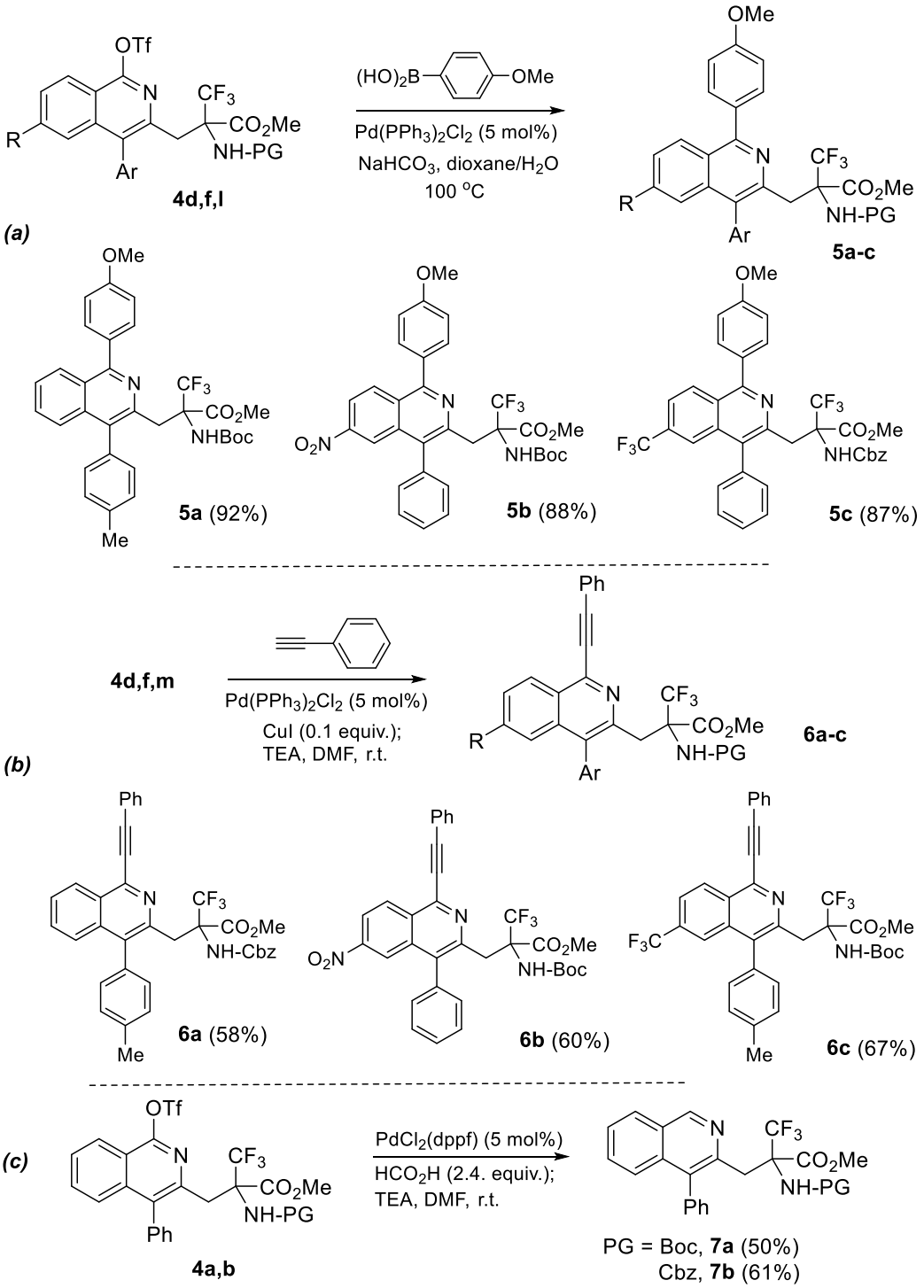

Scheme 5. Transformations of the OTf-substituted isoquinolines **4** under Pd-catalysis: (**a**) Suzuki reaction; (**b**) Sonogashira reaction; (**c**) removal of OTf group.

In addition, in order to demonstrate a feasibility for the further synthetic applications of the compounds obtained, e.g., in peptide synthesis or other useful derivatizations, we have performed selective deprotections of the *N*-PG-α-amino esters. Thus, the ester **3a** was saponified using 5% solution of potassium hydroxide in methanol to get free carboxylic acid **8** in high yield. The Boc-protective group of compound **3q** was selectively removed by the treatment of its solution in methylene chloride with excess of trifluoroacetic acid at room temperature furnishing free amino ester **9** in 85% yield (Scheme 6).

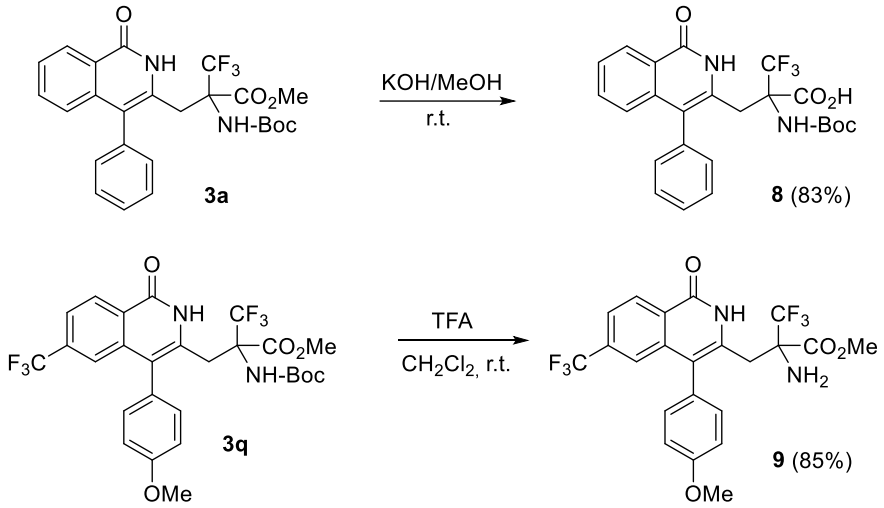

Scheme 6. Removal of protective groups.

3. Materials and Methods

3.1. General Information

All solvents used in the reactions were freshly distilled from appropriate drying agents before use. All other reagents were distilled as necessary. The corresponding starting acetylenes were easily synthesized via the previously described protocol [56]. Analytical TLC was performed with Merck silica gel 60 F_{254} plates; visualization was accomplished with UV light or spraying with $Ce(SO_4)_2$ solution in 5% H_2SO_4. Chromatography was carried out using Merck silica gel (Kieselgel 60, 0.063–0.200 mm) and petroleum ether/ethyl acetate as an eluent. The NMR spectra were obtained with Bruker AV-300, AV-400, AV-500 and Inova-400 spectrometers operating at 300, 400, and 500 MHz, respectively, for ^{1}H (TMS reference), at 101 and 126 for ^{13}C {^{1}H}, and at 282 and 376 MHz for ^{19}F (CCl_3F reference). Analytical data (C, H, N content) were obtained with a Carlo Erba model 1106 microanalyzer.

3.1.1. General Procedure for C-H Activation/Annulation of Aryl Hydroxamate with Acetylenes. Synthesis of the Compounds **3a–r**

A dried 10 mL Shlenk tube equipped with a magnetic stirring bar was subsequently charged with a corresponding acetylene (0.1 g, 0.27 mmol, 1.0 equiv.), TFE (2 mL), corresponding aryl hydroxamate (0.06 g, 0.27 mmol, 1.0 equiv.), $[Cp^*RhCl_2]_2$ (4.9 mg, 8.0 μmol, 3 mol%) and CsOAc (0.05 g, 0.27 mmol, 1.0 equiv.) under Ar. The reaction mixture was stirred at room temperature for 4 h until the completion of the reaction, monitored by TLC and ^{19}F NMR. By this time, the product precipitate had been formed and then was isolated from the reaction mixture by filtration.

3.1.2. General Procedure for the Synthesis of TfO-Derivatives **4a–o**

To a solution of the corresponding isoquinolone (0.1 g, 0.2 mmol, 1 equiv.) in dry dichloromethane (15 mL), pyridine (1.5 equiv.) and Tf_2O (1.5 equiv.) were added at 0 °C. After having been stirred at 0 °C for 30 min, the reaction mixture was treated with water and extracted with dichloromethane. The organic layer was washed with saturated $NaHCO_3$ (aq.), dried over anhydrous $MgSO_4$, filtered, and evaporated to dryness. The residue was purified by column chromatography on silica gel (eluent petroleum ether/ethyl acetate = 15/1) to give the desired product.

3.1.3. General Procedure for the Suzuki Reaction. Synthesis of the Compounds **5a–c**

A 25 mL round-bottom flask equipped with a magnetic stir bar and a reflux condenser was charged with corresponding triflate-derivative (0.1 g, 0.16 mmol, 1 equiv.),

corresponding boronic acid (0.02 g, 0.16 mmol, 1 equiv.), 1,4-dioxane—water mixture (3:1, 4 mL), $NaHCO_3$ (0.04 g, 0.5 mmol, 3 equiv.), and $Pd(PPh_3)_2Cl_2$ (1.1 mg, 1.6 μmol, 1 mol %). The resulting mixture was deaerated with argon and refluxed at 100 °C under argon for 1 h until the completion (monitored by TLC). On completion, the mixture was poured into water (7 mL) and extracted with dichloromethane (3 × 5 mL). The combined organic phases were washed with brine, dried over anhydrous $MgSO_4$, filtered, and and evaporated to dryness. The crude product was purified by column chromatography (eluent petroleum ether/ethyl acetate = 10/1) to give the desired product.

3.1.4. General Procedure for the Sonogashira Reaction. Synthesis of the Compounds **6a–c**

A dried 10 mL Shlenk tube was charged with a magnetic stir bar, DMF (5.5 mL) and corresponding triflate derivative (0.1 g, 0.15 mmol, 1.0 equiv.), and the solution was degassed three times. Then, $(Ph_3P)_2PdCl_2$ (5.2 mg, 7.5 μmol, 5 mol%) was added and the degassing procedure repeated. After that, Et_3N (0.28 mL) and phenyl acetylene (0.02 g, 0.22 mmol, 1.5 equiv.) was added and the mixture was degassed. Then, copper iodide (2.8 mg, 0.01 mmol, 10 mol%) was added and the reaction was stirred at room temperature overnight. After the completion (monitored by TLC) the reaction mixture was poured into 1M HCl (20 mL) and extracted with ethyl acetate (3 × 10 mL). The organic layers were dried over anhydrous $MgSO_4$, filtered and evaporated to dryness. The crude product was purified by column chromatography (eluent petroleum ether/ethyl acetate = 10/1) to give the desired product.

3.1.5. General Procedure for the Reduction of Triflate-Group. Synthesis of the Compounds **7a,b**

To a dried 10 mL Shlenk tube equipped with a magnetic stir bar corresponding triflate (0.1 g, 0.16 mmol, 1.0 equiv.), (dppf)$PdCl_2$ (5.8 mg, 8.0 μmol, 5 mol%), TEA (0.05 mL, 0.48 mmol, 3.0 equiv.), DMF (2.5 mL) and HCOOH (0.01 mL, 0.38 mmol, 2.4 equiv.) were added. The mixture was stirred at room temperature for 3 h. After the completion of the reaction (monitored by TLC), the solution was poured into 1M HCl (10 mL) and extracted with Et_2O (3 × 10 mL). The organic layers were washed with water and dried over anhydrous $MgSO_4$, filtered and evaporated to dryness. The crude product was purified by column chromatography (eluent petroleum ether/ethyl acetate = 8/1) to give the desired product.

3.1.6. General Procedure for Ester Hydrolysis. Synthesis of the Compound **8**

The corresponding isoquinolone 3a (0.3 g, 0.6 mmol) was dissolved in 5% KOH/MeOH-H_2O (1:1) (13 mL) and stirred at room temperature for 2 h. After evaporation of solvents under reduced pressure, water (15 mL) was added to a residue, and the suspension was washed with diethyl ester (3 × 10 mL) before being acidified with HCl conc. until pH 3–4 and extracted with ethyl acetate (3 × 7 mL). The ethyl acetate extracts were combined and dried over anhydrous $MgSO_4$, filtered, and evaporated to dryness.

3.1.7. General Procedure for the Removing of the Boc-Protecting Group. Synthesis of the Compound **9**

A solution of Boc-protected isoquinolone 3q (0.25 g, 0.42 mmol) in a biphasic mixture of trifluoroacetic acid/dichlormethane (4 mL/10 mL) was stirred at room temperature for 1.5 h. After evaporation of solvents under reduced pressure, water (15 mL) was added to the residue and the resulting water solution was neutralized with saturated solution of sodium bicarbonate until pH 7. Then the mixture was extracted with diethyl ether (3 × 10 mL). The organic layer was dried over anhydrous $MgSO_4$ and evaporated to dryness.

3.2. Characterization Data for the Products

Methyl 2-(tert-butoxycarbonylamino)-3,3,3-trifluoro-2-((1-oxo-4-phenyl-1,2-dihydroiso quinolin-3-yl)methyl)propanoate (**3a**).

Yield 71% as a white solid. M.p. 213–215 °C. ^{1}H NMR (400 MHz, DMSO-d_6): δ 10.87 (s, 1H, NH), 8.26 (d, J = 7.9 Hz, 1H, Ar), 8.15 (s, 1H, NH), 7.62 (t, J = 7.6 Hz, 1H, Ar), 7.54–7.43 (m, 4H, Ar), 7.26 (d, J = 7.3 Hz, 1H, Ar), 7.10 (d, J = 7.5 Hz, 1H, Ar), 6.97 (d, J = 8.2 Hz, 1H, Ar), 3.48 (s, 3H, OCH_3), 3.18 (d, J = 14.8 Hz, 1H, CH_2), 2.91 (d, J = 14.7 Hz, 1H, CH_2), 1.37 (s, 9H 3 CH_3). ^{13}C{^{1}H} NMR (126 MHz, DMSO-d_6): δ 164.8, 161.9, 159.2, 138.3 and 137.1, 137.1, 135.3 and 135.0, 133.5 and 133.1, 132.2 and 132.1, 131.3, 130.6 and 130.5, 129.8 and 129.5, 128.9 and 128.8, 128.4 and 128.2, 127.1 and 127.0, 125.6 and 125.5, 125.3 and 125.2, 124.6 (q, J = 285.6 Hz, CF_3), 118.9, 115.8, 81.2 and 80.7, 62.7 (q, J = 29.1 Hz, >C<), 53.0, 31.8 and 31.5, 28.3. ^{19}F NMR (376 MHz, DMSO-d_6): δ −74.13 (s, 3F, CF_3). Elemental analysis calcd (%) for $C_{25}H_{25}F_3N_2O_5$: C, 61.22; H, 5.14; N, 5.71; found: C, 61.18; H, 5.01; N, 5.65.

Methyl 2-(benzyloxycarbonylamino)-3,3,3-trifluoro-2-((1-oxo-4-phenyl-1,2-dihydroiso quinolin-3-yl)methyl)propanoate (**3b**).

Yield 73% as a white solid. M.p. 168–170 °C. ^{1}H NMR (400 MHz, acetone-d_6): δ 10.45 (s, 1H, NH), 8.37 (d, J = 7.9 Hz, 1H, Ar), 7.65–7.47 (m, 6H, Ar), 7.29–7.21 (m, 6H, Ar, 1H, NH), 7.04 (d, J = 8.1 Hz, 1H, Ar), 4.96 (s, 2H, OCH_2), 3.67 (s, 3H, OCH_3), 3.47 (d, J = 15.2 Hz, 1H, CH_2), 3.33 (d, J = 15.3 Hz, 1H, CH_2). ^{13}C{^{1}H} NMR (126 MHz, DMSO-d_6): δ 164.0, 161.4, 154.4, 137.8, 136.0, 134.5, 132.6, 131.6, 131.5, 130.8, 129.0, 128.5, 128.4, 128.2, 128.0, 127.9, 126.7, 126.6, 126.3 (q, J = 289.5 Hz, CF_3), 125.2, 124.8, 118.6, 66.5, 64.0 (q, J = 27.0 Hz, >C<), 52.7. ^{19}F NMR (376 MHz, acetone-d_6): δ −75.08 (s, 3F, CF_3). Elemental analysis calcd (%) for $C_{28}H_{23}F_3N_2O_5$: C, 64.12; H, 4.42; N, 5.34; found: C, 64.44; H, 4.66; N, 5.71.

Methyl 2-(tert-butoxycarbonylamino)-3,3,3-trifluoro-2-((1-oxo-4-p-tolyl-1,2-dihydroiso quinolin-3-yl)methyl)propanoate (**3c**).

Yield 81% as a white solid. M.p. 224–226 °C. ^{1}H NMR (500 MHz, DMSO-d_6): δ 10.83 (s, 1H, NH), 8.25 (d, J = 7.9 Hz, 1H, Ar), 8.13 (s, 1H, NH), 7.61–7.59 (m, 1H, Ar), 7.52–7.49 (m, 1H, Ar), 7.32 (d, J = 7.8 Hz, 1H, Ar), 7.29 (d, J = 7.8 Hz, 1H, Ar), 7.13 (d, J = 7.7 Hz, 1H, Ar), 6.99–6.96 (m, 2H, Ar), 3.48 (s, 3H, OCH_3), 3.20 (d, J = 15.0 Hz, 1H, CH_2), 2.92 (d, J = 15.0 Hz, 1H, CH_2), 2.38 (s, 3H, CH_3), 1.37 (s, 9H 3 CH_3). ^{13}C{^{1}H} NMR (126 MHz, DMSO-d_6): δ 164.4, 161.4, 153.9, 138.1, 137.1, 132.6, 131.6, 131.5, 131.4, 130.7, 129.6, 129.0, 126.6, 126.5, 125.2, 124.8, 124.1 (q, J = 288.0 Hz, CF_3), 118.4, 80.2, 63.9 (q, J = 23.3 Hz, >C<), 52.5, 31.1, 27.8, 20.9. ^{19}F NMR (376 MHz, $CDCl_3$): δ −75.21 (s, 3F, CF_3). Elemental analysis calcd (%) for $C_{26}H_{27}F_3N_2O_5$: C, 61.90; H, 5.39; N, 5.55; found: C, 62.04; H, 5.55; N, 5.63.

Methyl 2-(benzyloxycarbonylamino)-3,3,3-trifluoro-2-((1-oxo-4-p-tolyl-1,2-dihydroiso quinolin-3-yl)methyl)propanoate (**3d**).

Yield 69% as a white solid. M.p. 184–185 °C. ^{1}H NMR (500 MHz, $CDCl_3$): δ 12.45 (s, 1H, NH), 8.46 (d, J = 7.9 Hz, 1H, Ar), 7.57 (t, J = 7.7 Hz, 1H, Ar), 7.47 (t, J = 7.2 Hz, 2H, Ar), 7.32–7.28 (m, 2H, Ar), 7.15 (d, J = 8.0 Hz, 2H, Ar), 7.08–7.05 (m, 3H, Ar), 7.01 (d, J = 7.7 Hz, 1H, Ar), 6.93 (s, 1H, Ar, 1H, NH), 4.82 (s, 2H, OCH_2), 3.59 (s, 3H, OCH_3), 3.47 (d, J = 15.1 Hz, 1H, CH_2), 3.28 (d, J = 15.2 Hz, 1H, CH_2), 2.45 (s, 3H, CH_3). ^{13}C{^{1}H} NMR (126 MHz, $CDCl_3$): δ 165.0, 164.0, 155.1, 138.9, 138.2, 135.8, 133.0, 131.6, 131.4, 130.9, 130.8, 129.9, 129.6, 128.3, 127.9, 127.6, 127.4, 127.1, 126.0, 124.4, 124.1 (q, J = 287.5 Hz, CF_3), 121.9, 67.1, 64.9 (q, J = 27.6 Hz, >C<), 53.3, 31.9, 21.5. ^{19}F NMR (282 MHz, $CDCl_3$): δ −75.48 (s, 3F, CF_3). Elemental analysis calcd (%) for $C_{29}H_{25}F_3N_2O_5$: C, 64.68; H, 4.68; N, 5.20; found: C, 64.79; H, 4.85; N, 5.51.

Methyl 2-(tert-butoxycarbonylamino)-3,3,3-trifluoro-2-((4-(4-methoxyphenyl)-1-oxo-1,2-dihydroisoquinolin-3-yl)methyl)propanoate (**3e**).

Yield 79%. M.p. 220–221 °C. ^{1}H NMR (500 MHz, DMSO-d_6): δ 10.84 (s, 1H, NH), 8.25 (d, J = 7.9 Hz, 1H, Ar), 8.13 (s, 1H, NH), 7.61 (t, J = 7.6 Hz, 1H, Ar), 7.50 (t, J = 7.5 Hz, 1H, Ar), 7.17 (d, J = 7.8 Hz, 1H, Ar), 7.09–6.99 (m, 4H, Ar), 3.82 (s, 3H, OCH_3), 3.49 (s, 3H, OCH_3), 3.22 (d, J = 14.9 Hz, 1H, CH_2), 2.91 (d, J = 15.0 Hz, 1H, CH_2), 1.37 (s, 9H, 3 CH_3). ^{13}C{^{1}H} NMR (126 MHz, DMSO-d_6): δ 164.4, 161.4, 158.7, 153.9, 138.3, 132.8, 132.5, 132.0, 131.8, 126.6, 126.5, 126.4, 125.2, 124.8, 124.1 (q, J = 286.9 Hz, CF_3) 118.2, 114.4, 113.9, 80.2, 63.9 (q, J = 23.9 Hz, >C<), 55.1, 52.5, 31.1, 27.8. ^{19}F NMR (376 MHz, $CDCl_3$): δ −75.07 (s, 3F, CF_3). Elemental analysis calcd (%) for $C_{26}H_{27}F_3N_2O_6$: C, 60.00; H, 5.23; N, 5.38; found: C, 60.27; H, 5.55; N, 5.53.

Methyl 2-(benzyloxycarbonylamino)-3,3,3-trifluoro-2-((4-(4-methoxyphenyl)-1-oxo-1,2-dihydroisoquinolin-3-yl)methyl)propanoate (**3f**).

Yield 88% as a white solid. M.p. 200–201 °C. ^{1}H NMR (500 MHz, DMSO-d_6): δ 10.83 (s, 1H, NH), 8.61 (s, 1H, NH), 8.25 (d, J = 8.0 Hz, 1H, Ar), 7.61 (t, J = 7.6 Hz, 1H, Ar), 7.51 (t, J = 7.5 Hz, 1H, Ar), 7.37 (s, 5H, Ar), 7.17 (d, J = 8.4 Hz, 1H, Ar), 7.07 (d, J = 7.1 Hz, 1H, Ar), 7.04–6.99 (m, 3H, Ar), 5.09 (d, J = 12.2 Hz, 1H, OCH_2), 5.02 (d, J = 12.2 Hz, 1H, OCH_2), 3.82 (s, 3H, OCH_3), 3.49 (s, 3H, OCH_3), 3.25 (d, J = 15.0 Hz, 1H, CH_2), 2.95 (d, J = 14.9 Hz, 1H, CH_2). ^{13}C{^{1}H} NMR (126 MHz, DMSO-d_6): δ 164.1, 161.4, 158.7, 154.5, 138.2, 136.0, 132.7, 132.6, 132.0, 131.6, 128.5, 128.2, 128.0, 126.7, 126.5, 126.4, 125.2, 125.0 (q, J = 290.1 Hz, CF_3), 124.8, 118.3, 114.3, 113.9, 66.5, 64.0 (q, J = 25.8 Hz, >C<), 55.1, 52.7, 31.2. ^{19}F NMR (376 MHz, DMSO-d_6): δ −73.99 (s, 3F, CF_3). Elemental analysis calcd (%) for $C_{29}H_{25}F_3N_2O_6$: C, 62.81; H, 4.54; N, 5.05; found: C, 63.07; H, 4.78; N, 5.28.

Methyl 2-(tert-butoxycarbonylamino)-3,3,3-trifluoro-2-((6-nitro-1-oxo-4-phenyl-1,2-dihydroisoquinolin-3-yl)methyl)propanoate (**3g**).

Yield 84% as a white solid. M.p. 173–175 °C. ^{1}H NMR (400 MHz, DMSO-d_6): δ 11.33 (s, 1H, NH), 8.49 (d, J = 8.8 Hz, 1H, Ar), 8.24 (d, J = 9.0 Hz, 1H, Ar), 8.17 (br. s, 1H, NH), 7.75 (s, 1H, Ar), 7.60–7.50 (m, 3H, Ar), 7.33 (d, J = 7.1 Hz, 1H, Ar), 7.17 (d, J = 7.4 Hz, 1H, Ar), 3.50 (s, 3H, OCH_3), 3.21 (d, J = 14.9 Hz, 1H, CH_2), 2.96 (d, J = 14.9 Hz, 1H, CH_2), 1.37 (s, 9H, 3 CH_3). ^{13}C{^{1}H} NMR (126 MHz, DMSO-d_6): δ 164.4, 160.6, 153.9, 149.9, 138.5, 133.5, 131.6, 131.0, 130.2, 129.7, 129.4, 129.3, 128.8, 128.6, 128.3, 124.1 (q, J = 288.3 Hz, CF_3), 121.4, 120.2, 118.3, 80.4, 63.8 (q, J = 26.9 Hz, >C<), 52.7, 27.9. ^{19}F NMR (376 MHz, DMSO-d_6): δ −74.30 (s, 3F, CF_3). Elemental analysis calcd (%) for $C_{25}H_{24}F_3N_3O_7$: C, 56.08; H, 4.52; N, 7.85; found: C, 56.04; H, 4.55; N, 7.81.

Methyl 2-(benzyloxycarbonylamino)-3,3,3-trifluoro-2-((6-nitro-1-oxo-4-phenyl-1,2-dihydroisoquinolin-3-yl)methyl)propanoate (**3h**).

Yield 79% as a yellow solid. M.p. 206–208 °C. ^{1}H NMR (300 MHz, DMSO-d_6): δ 11.30 (s, 1H, NH), 8.63 (s, 1H, NH), 8.49 (d, J = 8.8 Hz, 1H, Ar), 8.25 (d, J = 8.8 Hz, 1H, Ar), 7.74 (s, 1H, Ar), 7.61–7.53 (m, 3H, Ar), 7.37 (s, 6H, Ar), 7.17 (d, J = 7.4 Hz, 1H, Ar), 5.08 (d, J = 12.2 Hz, 1H, OCH_2), 5.01 (d, J = 12.2 Hz, 1H, OCH_2), 3.50 (s, 3H, OCH_3), 3.20 (d, J = 15.9 Hz, 1H, CH_2), 3.00 (d, J = 15.2 Hz, 1H, CH_2). ^{13}C{^{1}H} NMR (126 MHz, DMSO-d_6): δ 164.4, 160.6, 153.9, 149.9, 138.5, 133.5, 131.6, 131.0, 130.2, 129.7, 129.4, 129.3, 129.1, 129.0, 128.8, 128.6, 128.3, 124.1 (q, J = 288.9 Hz, CF_3), 120.2, 118.3, 114.8, 80.4, 63.8 (q, J = 23.6 Hz, >C<), 52.7, 31.3, 27.9. ^{19}F NMR (282 MHz, DMSO-d_6): δ −74.17 (s, 3F, CF_3). Elemental analysis calcd (%) for $C_{28}H_{22}F_3N_3O_7$: C, 59.05; H, 3.89; N, 7.38; found: C, 59.31; H, 4.08; N, 7.52.

Methyl 2-(tert-butoxycarbonylamino)-3,3,3-trifluoro-2-((6-nitro-1-oxo-4-p-tolyl-1,2-dihydroisoquinolin-3-yl)methyl)propanoate (**3i**).

Yield 86% as a white solid. M.p. 211–212 °C. ^{1}H NMR (400 MHz, $CDCl_3$): δ 11.56 (s, 1H, NH), 8.60 (d, J = 8.8 Hz, 1H, Ar), 8.22 (d, J = 8.8 Hz, 1H, Ar), 7.97 (s, 1H, Ar), 7.36 (d, J = 7.7 Hz, 2H, Ar), 7.15 (d, J = 7.9 Hz, 1H, Ar), 7.09 (d, J = 7.8 Hz, 1H), 6.15 (s, 1H, NH), 3.68 (s, 3H, OCH_3), 3.49 (d, J = 14.9 Hz, 1H, CH_2), 3.33 (d, J = 15.0 Hz, 1H, CH_2), 2.47 (s, 3H, CH_3), 1.18 (s, 9H, 3 CH_3). ^{13}C{^{1}H} NMR (101 MHz, $CDCl_3$): δ 165.8, 161.9, 154.3, 150.5, 139.6, 138.9, 133.8, 131.1, 130.7, 130.5, 130.4, 130.2, 129.6, 128.6, 123.7 (q, J = 288.3 Hz, CF_3), 121.3, 120.8, 120.4, 81.8, 64.9 (q, J = 28.1 Hz, >C<), 53.8, 31.9, 27.9, 21.4. ^{19}F NMR (376 MHz, $CDCl_3$) δ −74.97 (s, 3F, CF_3). Elemental analysis calcd (%) for $C_{26}H_{26}F_3N_3O_7$: C, 56.83; H, 4.77; N, 7.65; found: C, 56.71; H, 4.57; N, 7.63.

Methyl 2-(benzyloxycarbonylamino)-3,3,3-trifluoro-2-((6-nitro-1-oxo-4-p-tolyl-1,2-dihydroisoquinolin-3-yl)methyl)propanoate (**3j**).

Yield 82% as a yellow solid. M.p. 215–216 °C. ^{1}H NMR (500 MHz, DMSO-d_6): δ 11.26 (s, 1H, NH), 8.61 (s, 1H, NH), 8.48 (d, J = 8.8 Hz, 1H, Ar), 8.24 (d, J = 8.8 Hz, 1H, Ar), 7.76 (s, 1H, Ar), 7.39 (m, 7H, Ar), 7.19 (d, J = 7.8 Hz, 1H, Ar), 7.05 (d, J = 7.7 Hz, 1H, Ar), 5.08 (d, J = 12.3 Hz, 1H, OCH_2), 5.02 (d, J = 12.3 Hz, 1H, OCH_2), 3.49 (s, 3H, OCH_3), 3.27 (d, J = 15.3 Hz, 1H, CH_2), 3.00 (d, J = 15.1 Hz, 1H, CH_2), 2.42 (s, 3H, CH_3). ^{13}C{^{1}H} NMR (126 MHz, DMSO-d_6): δ 164.1, 160.4, 154.4, 149.9, 138.6, 137.8, 135.9, 134.4, 131.3, 130.8,

130.4, 129.9, 129.3, 129.2, 128.5, 128.3, 128.2, 128.0, 123.9 (q, J = 287.4 Hz, CF_3), 120.3, 120.2, 118.3, 66.5, 64.0 (q, J = 26.7 Hz, >C<), 54.9, 52.8, 31.3. ^{19}F NMR (282 MHz, $CDCl_3$): δ −73.84 (s, 3F, CF_3). Elemental analysis calcd (%) for $C_{29}H_{24}F_3N_3O_7$: C, 59.69; H, 4.15; N, 7.20; found: C, 59.93; H, 4.43; N, 7.35.

Methyl 2-(tert-butoxycarbonylamino)-3,3,3-trifluoro-2-((4-(4-methoxyphenyl)-6-nitro-1-oxo-1,2-dihydroisoquinolin-3-yl)methyl)propanoate (**3k**).

Yield 89% as a white solid. M.p. 198–200 °C. ^{1}H NMR (500 MHz, acetone-d_6): δ 10.16 (s, 1H, NH), 8.54 (d, J = 8.7 Hz, 1H, Ar), 8.24 (d, J = 7.7 Hz, 1H, Ar), 7.92 (s, 1H, Ar), 7.38 (d, J = 7.8 Hz, 1H, Ar), 7.28 (d, J = 7.9 Hz, 1H, Ar), 7.16 (t, J = 6.7 Hz, 2H, Ar), 7.08 (s, 1H, NH), 3.91 (s, 3H, OCH_3), 3.77 (s, 3H, OCH_3), 3.50 (d, J = 14.9 Hz, 1H, CH_2), 3.37 (d, J = 14.9 Hz, 1H, CH_2), 1.27 (s, 9H, 3 CH_3). ^{13}C{^{1}H} NMR (126 MHz, acetone-d_6): δ 167.7, 161.1, 160.9, 155.4, 151.4, 140.8, 139.9, 135.9, 133.7, 133.6, 130.2, 127.0, 124.8 (q, J = 287.0 Hz, CF_3), 121.7, 120.9, 119.7, 115.8, 115.5, 114.8, 81.8, 66.2 (q, J = 27.0 Hz, >C<) 55.8, 54.2, 28.3. ^{19}F NMR (376 MHz, $CDCl_3$): δ −75.08 (s, 3F, CF_3). Elemental analysis calcd (%) for $C_{26}H_{26}F_3N_3O_8$: C, 55.22; H, 4.63; N, 7.43; found: C, 55.31; H, 4.57; N, 7.27.

Methyl 2-(benzyloxycarbonylamino)-3,3,3-trifluoro-2-((4-(4-methoxyphenyl)-6-nitro-1-oxo-1,2-dihydroisoquinolin-3-yl)methyl)propanoate (**3l**).

Yield 83% as a yellow solid. M.p.207–209 °C. ^{1}H NMR (500 MHz, DMSO-d_6): δ 11.25 (s, 1H, NH), 8.60 (s, 1H, NH), 8.48 (d, J = 8.7 Hz, 1H, Ar), 8.23 (d, J = 8.8 Hz, 1H, Ar), 7.78 (s, 1H, Ar), 7.37 (s, 5H, Ar), 7.24 (s, 1H, Ar), 7.14–7.07 (m, 3H, Ar), 5.08 (d, J = 12.2 Hz, 1H, OCH_2), 5.02 (d, J = 12.4 Hz, 1H, OCH_2), 3.84 (s, 3H, OCH_3), 3.50 (s, 3H, OCH_3), 3.28 (d, J = 15.7 Hz, 1H, CH_2), 3.00 (d, J = 15.1 Hz, 1H, CH_2). ^{13}C{^{1}H} NMR (126 MHz, DMSO-d_6): δ 164.0, 160.4, 159.1, 154.5, 149.9, 138.9, 136.0, 134.6, 132.7, 132.2, 129.2, 128.5, 128.4, 128.3, 128.1, 125.2, 123.9 (q, J = 287.9 Hz, CF_3), 120.3, 120.2, 118.1, 114.7, 114.2, 66.6, 64.0 (q, J = 26.5 Hz, >C<), 55.2, 52.9, 31.3. ^{19}F NMR (282 MHz, DMSO-d_6): δ −74.07 (s, 3F, CF_3). Elemental analysis calcd (%) for $C_{29}H_{24}F_3N_3O_8$: C, 58.10; H, 4.04; N, 7.01; found: C, 58.49; H, 4.30; N, 7.32.

Methyl 2-(tert-butoxycarbonylamino)-3,3,3-trifluoro-2-((1-oxo-4-phenyl-6-(trifluoromethyl)-1,2-dihydroisoquinolin-3-yl)methyl)propanoate (**3m**).

Yield 85% as a white solid. M.p. 181–183 °C. ^{1}H NMR (400 MHz, DMSO-d_6): δ 11.21 (s, 1H, NH), 8.47 (d, J = 8.3 Hz, 1H, Ar), 8.17 (br. s, 1H, NH), 7.84 (d, J = 8.4 Hz, 1H, Ar), 7.58–7.47 (m, 3H, Ar), 7.31 (d, J = 7.2 Hz, 1H, Ar), 7.21 (s, 1H, Ar), 7.14 (d, J = 7.4 Hz, 1H, Ar), 3.50 (s, 3H, OCH_3), 3.19 (d, J = 15.0 Hz, 1H, CH_2), 2.95 (d, J = 15.0 Hz, 1H, CH_2), 1.37 (s, 9H, 3 CH_3). ^{13}C{^{1}H} NMR (126 MHz, DMSO-d_6): δ 164.4, 160.7, 153.9, 138.1, 134.0, 133.6, 132.4 (q, J = 31.9 Hz, C_{Ar}-CF_3), 131.5, 130.9, 130.1, 129.4, 128.8, 128.6, 128.5, 127.3, 124.1 (q, J = 288.1 Hz, CF_3), 123.7 (q, J = 273.0 Hz, CF_3), 122.5, 121.8, 118.2, 80.4, 63.8 (q, J = 26.6 Hz, >C<), 52.7, 27.9. ^{19}F NMR (376 MHz, $CDCl_3$) δ −63.08 (s, 3F, CF_3), −75.05 (s, 3F, CF_3). Elemental analysis calcd (%) for $C_{26}H_{24}F_6N_2O_5$: C, 55.92; H, 4.33; N, 5.02; found: C, 55.71; H, 4.57; N, 5.27.

Methyl 2-(benzyloxycarbonylamino)-3,3,3-trifluoro-2-((1-oxo-4-phenyl-6-(trifluoromethyl)-1,2-dihydroisoquinolin-3-yl)methyl)propanoate (**3n**).

Yield 73% as a white solid. M.p. 195–196 °C. ^{1}H NMR (500 MHz, DMSO-d_6): δ 11.18 (s, 1H, NH), 8.63 (s, 1H, NH), 8.47 (d, J = 8.3 Hz, 1H, Ar), 7.84 (d, J = 8.3 Hz, 1H, Ar), 7.57–7.48 (m, 3H, Ar), 7.37–7.33 (m, 5H, Ar), 7.30 (d, J = 7.2 Hz, 1H, Ar), 7.20 (s, 1H, Ar), 7.14 (d, J = 7.6 Hz, 1H, Ar), 5.08 (d, J = 12.3 Hz, 1H, OCH_2), 5.02 (d, J = 12.2 Hz, 1H, OCH_2), 3.51 (s, 3H, OCH_3), 3.22 (d, J = 15.1 Hz, 1H, CH_2), 2.99 (d, J = 15.1 Hz, 1H, CH_2). ^{13}C{^{1}H} NMR (126 MHz, DMSO-d_6): δ 164.0, 160.6, 154.4, 138.0, 136.0, 133.8, 133.6, 132.3 (q, J = 31.8 Hz, C_{Ar}-CF_3), 131.4, 130.9, 129.3, 128.7, 128.6, 128.5, 128.2, 128.1, 127.2, 123.9 (q, J = 288.0 Hz, CF_3), 123.9 (q, J = 273.1 Hz, CF_3), 122.5, 121.8, 118.2, 66.5, 64.0 (q, J = 26.6 Hz, >C<), 52.9, 31.3. ^{19}F NMR (282 MHz, $CDCl_3$): δ −62.98 (s, 3F, CF_3), −75.16 (s, 3F, CF_3). Elemental analysis calcd (%) for $C_{29}H_{22}F_6N_2O_5$: C, 58.79; H, 3.74; N, 4.73; found: C, 59.01; H, 3.81; N, 4.95.

Methyl 2-(tert-butoxycarbonylamino)-3,3,3-trifluoro-2-((1-oxo-4-p-tolyl-6-(trifluoromethyl)-1,2-dihydroisoquinolin-3-yl)methyl)propanoate (**3o**).

Yield 89% as a white solid. M.p. 201–203 °C. ^{1}H NMR (400 MHz, $CDCl_3$) δ 11.99 (s, 1H, NH), 8.58 (d, J = 8.4 Hz, 1H, Ar), 7.70 (d, J = 8.4 Hz, 1H, Ar), 7.40–7.33 (m, 3H, Ar), 7.14–7.08 (m, 2H, Ar), 6.49 (s, 1H, NH), 3.65 (s, 3H, OCH_3), 3.49 (d, J = 15.1 Hz, 1H, CH_2), 3.32 (d, J = 15.1 Hz, 1H, CH_2), 2.46 (s, 3H, CH_3), 1.14 (s, 9H, CH_3). ^{13}C{^{1}H} NMR (101 MHz, $CDCl_3$): δ 165.6, 162.9, 154.4, 139.0, 138.7, 134.4 (q, J = 32.2 Hz, C_{Ar}-CF_3), 132.9, 131.2, 130.8, 130.7, 130.3, 130.0, 128.6, 127.1, 123.9 (q, J = 288.2 Hz, CF_3), 123.7 (q, J = 273.0 Hz, CF_3), 123.1, 122.9, 121.0, 81.5, 64.9 (q, J = 27.2 Hz, >C<), 53.5, 31.9, 27.9, 21.5. ^{19}F NMR (376 MHz, $CDCl_3$) δ −63.03 (s, 3F, CF_3), −75.05 (s, 3F, CF_3). Elemental analysis calcd (%) for $C_{27}H_{26}F_6N_2O_5$: C, 56.64; H, 4.58; N, 4.89; found: C, 56.71; H, 4.57; N, 4.77.

Methyl 2-(benzyloxycarbonylamino)-3,3,3-trifluoro-2-((1-oxo-4-p-tolyl-6-(trifluoromethyl)-1,2-dihydroisoquinolin-3-yl)methyl)propanoate (**3p**).

Yield 70% as a white solid. M.p. 213–214 °C. ^{1}H NMR (500 MHz, DMSO-d_6): δ 11.16 (s, 1H, NH), 8.62 (s, 1H, NH), 8.47 (s, 1H, Ar), 7.83 (s, 1H, Ar), 7.36–7.17 (m, 9H, Ar), 7.02 (s, 1H, Ar), 5.08 (d, J = 12.4 Hz, 1H, OCH_2), 5.02 (d, J = 12.5 Hz, 1H, OCH_2), 3.50 (s, 3H, OCH_3), 3.24 (d, J = 15.5 Hz, 1H, CH_2), 2.98 (d, J = 15.2 Hz, 1H, CH_2), 2.39 (s, 3H, CH_3). ^{13}C{^{1}H} NMR (126 MHz, DMSO-d_6): δ 164.1, 160.6, 154.5, 138.2, 137.7, 136.0, 133.8, 132.3 (q, J = 31.6 Hz, C_{Ar}-CF_3), 131.2, 130.8, 130.5, 129.9, 129.3, 128.6, 128.5, 128.2, 128.1, 127.3, 123.9 (q, J = 286.1 Hz, CF_3), 123.7 (q, J = 272.8 Hz, CF_3), 122.4, 121.8, 118.1, 66.5, 64.0 (q, J = 28.3 Hz, >C<), 52.8, 31.3, 20.9. ^{19}F NMR (376 MHz, $CDCl_3$): δ −62.98 (s, 3F, CF_3), −75.20 (s, 3F, CF_3). Elemental analysis calcd (%) for $C_{30}H_{24}F_6N_2O_5$: C, 59.41; H, 3.99; N, 4.62; found: C, 59.67; H, 4.15; N, 4.89.

Methyl 2-(tert-butoxycarbonylamino)-3,3,3-trifluoro-2-((4-(4-methoxyphenyl)-1-oxo-6-(trifluoromethyl)-1,2-dihydroisoquinolin-3-yl)methyl)propanoate (**3q**).

Yield 90% as a white solid. M.p. 206–207 °C. ^{1}H NMR (300 MHz, $CDCl_3$): δ 11.30 (s, 1H, NH), 8.57 (d, J = 8.3 Hz, 1H, Ar), 7.69 (d, J = 8.4 Hz, 1H, Ar), 7.38 (s, 1H, Ar), 7.19–7.05 (m, 4H, Ar), 6.09 (s, 1H, NH), 3.91 (s, 3H, OCH_3), 3.70 (s, 3H, OCH_3), 3.48 (d, J = 15.0 Hz, 1H, CH_2), 3.36 (d, J = 14.9 Hz, 1H, CH_2), 1.19 (s, 9H, 3 CH_3). ^{13}C{^{1}H} NMR (126 MHz, $CDCl_3$): δ 166.0, 162.3, 159.8, 154.4, 139.2, 134.3 (q, J = 32.5 Hz, C_{Ar}-CF_3), 133.1, 132.5, 132.1, 128.7, 127.3, 126.0, 123.8 (q, J = 287.8 Hz, CF_3), 123.7 (q, J = 273.3 Hz, CF_3), 123.0, 122.9, 120.4, 114.9, 114.8, 81.9, 65.1 (q, J = 27.4 Hz, >C<), 55.5, 53.9, 27.9. ^{19}F NMR (282 MHz, $CDCl_3$): δ −62.98 (s, 3F, CF_3), −75.03 (s, 3F, CF_3). Elemental analysis calcd (%) for $C_{27}H_{26}F_6N_2O_6$: C, 55.10; H, 4.45; N, 4.76; found: C, 55.21; H, 4,57; N, 4.73.

Methyl 2-(benzyloxycarbonylamino)-3,3,3-trifluoro-2-((4-(4-methoxyphenyl)-1-oxo-6-(trifluoromethyl)-1,2-dihydroisoquinolin-3-yl)methyl)propanoate (**3r**).

Yield 82% as a white solid. M.p. 199–200 °C. ^{1}H NMR (500 MHz, DMSO-d_6): δ 11.15 (s, 1H, NH), 8.61 (s, 1H, NH), 8.46 (d, J = 8.3 Hz, 1H, Ar), 7.82 (d, J = 8.4 Hz, 1H, Ar), 7.36 (s, 5H, Ar), 7.25 (s, 1H, Ar), 7.21 (d, J = 7.9 Hz, 1H, Ar), 7.11–7.04 (m, 3H, Ar), 5.08 (d, J = 12.3 Hz, 1H, OCH_2), 5.02 (d, J = 12.4 Hz, 1H, OCH_2), 3.83 (s, 3H, OCH_3), 3.51 (s, 3H, OCH_3), 3.26 (d, J = 15.5 Hz, 1H, CH_2), 2.98 (d, J = 15.1 Hz, 1H, CH_2). ^{13}C{^{1}H} NMR (126 MHz, DMSO-d_6): δ 164.1, 160.7, 159.0, 154.5, 138.4, 136.0, 133.9, 132.6, 132.5 (q, J = 31.7 Hz, C_{Ar}-CF_3), 132.2, 128.5, 128.3, 128.1, 127.3, 125.4, 124.0 (q, J = 288.5 Hz, CF_3), 123.7 (q, J = 272.8 Hz, CF_3), 122.4, 121.9, 117.9, 114.6, 114.1, 66.5, 64.0 (q, J = 27.7 Hz, >C<), 55.2, 52.9, 31.3. ^{19}F NMR (282 MHz, DMSO-d_6): δ −61.70 (s, 3F, CF_3), −74.06 (s, 3F, CF_3). Elemental analysis calcd (%) for $C_{30}H_{24}F_6N_2O_6$: C, 57.88; H, 3.89; N, 4.50; found: C, 57.79; H, 4.05; N, 4.61.

Methyl 2-(benzyloxycarbonylamino)-3,3,3-trifluoro-2-((4-(4-nitrophenyl)-1-oxo-1,2-dihydroisoquinolin-3-yl)methyl)propanoate (**3s**).

Yield 30% as a yellow solid (eluent petroleum ether/ethyl acetate = 5/1). ^{1}H NMR (500 MHz, DMSO-d_6): δ 10.98 (s, 1H, NH), 8.62 (s, 1H, NH), 8.39 (d, J = 8.6 Hz, 1H, Ar), 8.34 (d, J = 8.4 Hz, 1H, Ar), 8.29 (d, J = 8.0 Hz, 1H, Ar), 7.65–7.60 (m, 2H, Ar), 7.55 (t, J = 7.6 Hz, 1H, Ar), 7.42 (d, J = 8.5 Hz, 1H, Ar), 7.36 (s, 5H, Ar), 6.94 (d, J = 8.1 Hz, 1H, Ar), 5.07 (d, J = 12.4 Hz, 1H, OCH_2), 5.01 (d, J = 12.2 Hz, 1H, OCH_2), 3.50 (s, 3H, OCH_3), 3.19 (d, J = 15.4 Hz, 1H, CH_2), 3.03 (d, J = 15.2 Hz, 1H, CH_2). ^{13}C{^{1}H} NMR (126 MHz, DMSO-d_6): δ 164.8, 161.9, 154.9, 147.5, 142.5, 137.4, 136.4, 133.9, 133.4, 133.1, 132.5, 128.9, 128.7, 128.5, 127.5, 127.3, 125.3, 125.2, 124.5, 124.3 (q, J = 287.3, CF_3), 123.9, 117.2, 66.9, 64.5 (q, J = 26.2 Hz,

>C<), 53.4, 31.9. ^{19}F NMR (282 MHz, DMSO-d_6): δ −73.83 (s, 3F, CF_3). Elemental analysis calcd (%) for $C_{28}H_{22}F_3N_3O_7$: C, 59.05; H, 3.89; N, 7.38; found: C, 59.31; H, 4.07; N, 7.61.

Methyl 2-(benzyloxycarbonylamino)-3,3,3-trifluoro-2-((4-(4-nitrophenyl)-1-oxo-1,2-dihydroisoquinolin-3-yl)methyl)propanoate (**3t**).

Yield 25% as a yellow solid (eluent petroleum ether/ethyl acetate = 4/1). ^{1}H NMR (400 MHz, acetone-d_6): δ 10.46 (s, 1H, NH), 8.36 (d, J = 8.0 Hz, 1H, Ar), 8.31 (d, J = 8.2 Hz, 2H, Ar), 7.88 (d, J = 7.9 Hz, 3H, Ar), 7.78 (t, J = 7.8 Hz, 1H, Ar), 7.58 (t, J = 7.6 Hz, 1H, Ar), 7.41–7.30 (m, 5H, Ar), 6.49 (s, 1H, NH), 4.99 (d, J = 12.4 Hz, 1H, OCH_2), 4.91 (d, J = 12.4 Hz, 1H, OCH_2), 3.84 (d, J = 16.0 Hz, 1H, CH_2), 3.59 (d, J = 16.0 Hz, 1H, CH_2), 3.27 (s, 3H, OCH_3). ^{13}C{^{1}H} NMR (151 MHz, DMSO-d_6): δ 165.3, 161.3, 154.5, 147.6, 140.7, 139.8, 137.7, 136.3, 132.2, 132.0, 131.3, 128.4, 128.3, 128.1, 127.9, 127.5, 126.9, 126.7, 126.2 (q, J = 288.2 Hz, CF_3), 125.4, 123.3, 106.3, 66.0, 64.3 (q, J = 26.6 Hz, >C<), 52.3, 28.9. ^{19}F NMR (376 MHz, acetone-d_6): δ −73.99 (s, 3F, CF_3). Elemental analysis calcd (%) for $C_{28}H_{22}F_3N_3O_7$: C, 59.05; H, 3.89; N, 7.38; found: C, 59.27; H, 4.11; N, 7.40.

Methyl 2-(tert-butoxycarbonylamino)-3,3,3-trifluoro-2-((4-phenyl-1-(trifluoromethyl-sulfonyloxy)isoquinolin-3-yl)methyl)propanoate (**4a**).

Yield 77% as a white solid (eluent petroleum ether/ethyl acetate = 15/1). M.p. 152–154 °C. ^{1}H NMR (400 MHz, $CDCl_3$): δ 8.12 (d, J = 8.2 Hz, 1H, Ar), 7.73–7.66 (m, 2H, Ar), 7.60–7.56 (m, 1H, Ar), 7.55–7.50 (m, 2H, Ar), 7.41 (t, J = 8.8 Hz, 2H, Ar), 7.23–7.20 (m, 1H, Ar), 6.85 (s, 1H, NH), 3.87–3.84 (m, 3H, OCH_3, 1H, CH_2), 3.53 (d, J = 15.9 Hz, 1H, CH_2), 1.28 (s, 9H 3 CH_3). ^{13}C{^{1}H} NMR (101 MHz, $CDCl_3$): δ 166.9, 153.7, 150.8, 143.4, 139.9, 134.7, 134.5, 132.2, 130.3, 130.0, 129.3, 128.8, 128.7, 126.6, 126.3, 124.2 (q, J = 288.7 Hz, CF_3), 122.7, 118.7 (q, J = 320.2 Hz, CF_3), 118.5, 80.2, 64.4 (q, J = 28.2 Hz, >C<), 53.7, 33.8, 28.0. ^{19}F NMR (282 MHz, $CDCl_3$): δ −73.69 (s, 3F, CF_3), −73.95 (s, 3F, CF_3). Elemental analysis calcd (%) for $C_{26}H_{24}F_6N_2O_7S$: C, 50.16; H, 3.89; N, 4.50; found: C, 50.07; H, 4.01; N, 4.58.

Methyl 2-(benzyloxycarbonylamino)-3,3,3-trifluoro-2-((4-phenyl-1-(trifluoromethyl-sulfonyloxy)isoquinolin-3-yl)methyl)propanoate (**4b**).

Yield 92% as a white solid (eluent petroleum ether/ethyl acetate = 15/1). M.p. 140–142 °C. ^{1}H NMR (400 MHz, $CDCl_3$): δ 8.09 (d, J = 8.0 Hz, 1H, Ar), 7.74–7.67 (m, 2H, Ar), 7.57–7.51 (m, 3H, Ar), 7.38 (d, J = 8.1 Hz, 1H, Ar), 7.21–7.17 (m, 2H, Ar), 7.07–7.06 (m, 2H, Ar), 6.95–6.93 (m, 3H, Ar), 6.85 (s, 1H, NH), 5.05 (d, J = 12.3 Hz, 1H, OCH_2), 4.84 (d, J = 12.2 Hz, 1H, OCH_2), 4.08 (d, J = 16.1 Hz, 1H, CH_2), 3.92 (s, 3H, OCH_3), 3.62 (d, J = 16.4 Hz, 1H, CH_2). ^{13}C{^{1}H} NMR (101 MHz, $CDCl_3$): δ 166.6, 153.9, 150.6, 142.9, 139.9, 136.5, 134.7, 134.3, 132.0, 130.3, 129.9, 129.2, 128.7, 128.6, 127.9, 127.7, 127.4, 126.3, 124.1 (q, J = 289.0 Hz, CF_3), 122.6, 118.6 (q, J = 320.2 Hz, CF_3), 118.2, 66.7, 64.4 (q, J = 27.0 Hz, >C<), 54.2, 32.9, 29.8. ^{19}F NMR (376 MHz, $CDCl_3$): δ −74.11 (s, 3F, CF_3), −74.67 (s, 3F, CF_3). Elemental analysis calcd (%) for $C_{29}H_{22}F_6N_2O_7S$: C, 53.05; H, 3.38; N, 4.27; found: C, 53.37; H, 3.49; N, 4.52.

Methyl 2-(tert-butoxycarbonylamino)-3,3,3-trifluoro-2-((4-p-tolyl-1-(trifluoromethyl-sulfonyloxy)isoquinolin-3-yl)methyl)propanoate (**4c**).

Yield 89% as a white solid (eluent petroleum ether/ethyl acetate = 15/1). M.p. 145–146 °C. ^{1}H NMR (500 MHz, $CDCl_3$): δ 8.12 (d, J = 7.4 Hz, 1H, Ar), 7.71–7.66 (m, 2H, Ar), 7.46 (d, J = 7.6 Hz, 1H, Ar), 7.38 (d, J = 7.5 Hz, 1H, Ar), 7.33 (d, J = 7.4 Hz, 1H, Ar), 7.28 (s, 1H, Ar), 7.09 (d, J = 7.3 Hz, 1H, Ar), 6.85 (s, 1H, NH), 3.87–3.84 (s, 3H, OCH_3, 1H, CH_2), 3.52 (d, J = 15.9 Hz, 1H, CH_2), 2.48 (s, 3H, CH_3), 1.28 (s, 9H, 3 CH_3). ^{13}C{^{1}H} NMR (126 MHz, $CDCl_3$): δ 167.0, 153.7, 150.7, 143.5, 140.1, 138.6, 134.7, 132.1, 131.7, 130.2, 129.9, 129.8, 129.6, 128.8, 126.5, 124.3 (q, J = 288.4 Hz, CF_3), 122.7, 119.1 (q, J = 320.2 Hz, CF_3), 118.5, 80.2, 64.4 (q, J = 27.9 Hz, >C<), 53.7, 33.8, 28.0, 21.5. ^{19}F NMR (282 MHz, $CDCl_3$): δ −73.67 (s, 3F, CF_3), −73.83 (s, 3F, CF_3). Elemental analysis calcd (%) for $C_{27}H_{26}F_6N_2O_7S$: C, 50.94; H, 4.12; N, 4.40; found: C, 51.04; H, 4.25; N, 4.43.

Methyl 2-(benzyloxycarbonylamino)-3,3,3-trifluoro-2-((4-p-tolyl-1-(trifluoromethyl-sulfonyloxy)isoquinolin-3-yl)methyl)propanoate (**4d**).

Yield 90% as a thick oil (eluent petroleum ether/ethyl acetate = 15/1). ^{1}H NMR (500 MHz, $CDCl_3$): δ 8.07 (d, J = 8.0 Hz, 1H, Ar), 7.72–7.66 (m, 2H, Ar), 7.40 (d, J = 8.2 Hz,

1H, Ar), 7.35 (d, *J* = 7.8 Hz, 1H, Ar), 7.31 (d, *J* = 7.7 Hz, 1H, Ar), 7.08–7.03 (m, 4H, Ar), 6.98–6.92 (m, 3H, Ar), 6.83 (s, 1H, NH), 5.03 (d, *J* = 12.5 Hz, 1H, OCH_2), 4.84 (d, *J* = 12.6 Hz, 1H, OCH_2), 4.06 (d, *J* = 16.6 Hz, 1H, CH_2), 3.90 (s, 3H, OCH_3), 3.59 (d, *J* = 16.5 Hz, 1H, CH_2), 2.47 (s, 3H, CH_3). $^{13}C\{^1H\}$ NMR (126 MHz, $CDCl_3$): δ 166.7, 153.9, 150.5, 143.0, 140.1, 138.5, 136.6, 134.5, 131.9, 131.6, 130.1, 129.9, 129.8, 129.5, 128.6, 128.0, 127.7, 127.4, 126.5, 124.1 (q, *J* = 288.8 Hz, CF_3), 122.6, 118.7 (q, *J* = 320.2 Hz, CF_3), 118.3, 66.7, 64.5 (q, *J* = 28.1 Hz, >C<), 54.1, 33.0, 21.5. ^{19}F NMR (282 MHz, $CDCl_3$): δ −74.01 (s, 3F, CF_3), −74.52 (s, 3F, CF_3). Elemental analysis calcd (%) for $C_{30}H_{24}F_6N_2O_7S$: C, 53.73; H, 3.61; N, 4.18; found: C, 53.98; H, 3.90; N, 4.25.

Methyl 2-(tert-butoxycarbonylamino)-3,3,3-trifluoro-2-((4-(4-methoxyphenyl)-1-(trifluoromethylsulfonyloxy)isoquinolin-3-yl)methyl)propanoate (**4e**).

Yield 70% as a white solid (eluent petroleum ether/ethyl acetate = 15/1). M.p. 112–114 °C. ^1H NMR (300 MHz, $CDCl_3$): δ 8.11–8.09 (m, 1H, Ar), 7.71–7.68 (m, 2H, Ar), 7.48–7.47 (m, 1H, Ar), 7.32–7.29 (m, 1H, Ar), 7.11–7.03 (m, 3H, Ar), 6.84 (s, 1H, NH), 3.91 (s, 3H, OCH_3, 0.5 CH_2), 3.84 (s, 3H, OCH_3, 0.5 CH_2), 3.52 (d, *J* = 16.0 Hz, 1H, CH_2), 1.27 (s, 9H, 3 CH_3). $^{13}C\{^1H\}$ NMR (126 MHz, $CDCl_3$): δ 167.0, 159.9, 153.7, 150.7, 143.7, 140.3, 134.4, 132.1, 131.6, 131.2, 128.8, 126.7, 126.4, 124.3 (q, *J* = 288.4 Hz, CF_3), 122.7, 118.7 (q, *J* = 320.2 Hz, CF_3), 118.5, 114.6, 114.5, 80.1, 64.4 (q, *J* = 27.5 Hz, >C<), 55.5, 53.7, 33.8, 28.0. ^{19}F NMR (282 MHz, $CDCl_3$): δ −73.70 (s, 3F, CF_3), −73.89 (s, 3F, CF_3). Elemental analysis calcd (%) for $C_{27}H_{26}F_6N_2O_8S$: C, 49.69; H, 4.02; N, 4.29; found: C, 49.64; H, 4.05; N, 4.23.

Methyl 2-(tert-butoxycarbonylamino)-3,3,3-trifluoro-2-((6-nitro-4-phenyl-1-(trifluoro methylsulfonyloxy)isoquinolin-3-yl)methyl)propanoate (**4f**).

Yield 79% as a white solid (eluent petroleum ether/ethyl acetate = 15/1). M.p. 162–164 °C. ^1H NMR (400 MHz, $CDCl_3$): δ 8.49 (d, *J* = 9.2 Hz, 1H, Ar), 8.39 (s, 1H, Ar), 8.34 (d, *J* = 9.2 Hz, 1H, Ar), 7.73–7.66 (m, 3H, Ar), 7.53 (s, 1H, Ar), 7.31 (s, 1H, Ar), 6.56 (s, 1H, NH), 4.14 (d, *J* = 16.5 Hz, 1H, CH_2), 3.95 (s, 3H, OCH_3), 3.69 (d, *J* = 16.5 Hz, 1H, CH_2), 1.28 (s, 9H, 3 CH_3). $^{13}C\{^1H\}$ NMR (101 MHz, $CDCl_3$): δ 166.7, 153.4, 150.4, 149.6, 146.6, 139.5, 135.9, 133.2, 130.1, 129.9, 129.8, 129.7, 129.3, 125.2, 124.1 (q, *J* = 288.3 Hz, CF_3), 122.4, 122.2, 120.2, 118.7 (q, *J* = 320.0 Hz, S-CF_3),80.2, 64.2 (q, *J* = 26.6 Hz. >C<), 54.0, 33.5, 27.9. ^{19}F NMR (376 MHz, $CDCl_3$): δ −73.63 (s, 3F, CF_3), −74.85 (s, 3F, CF_3). Elemental analysis calcd (%) for $C_{26}H_{23}F_6N_3O_9S$: C, 46.78; H, 3.47; N, 6.29; found: C, 46.71; H, 3.49; N, 6.09.

Methyl 2-(benzyloxycarbonylamino)-3,3,3-trifluoro-2-((6-nitro-4-phenyl-1-(trifluoro methylsulfonyloxy)isoquinolin-3-yl)methyl)propanoate (**4g**).

Yield 89% as a yellow solid (eluent petroleum ether/ethyl acetate = 15/1). M.p. 123–125 °C. ^1H NMR (400 MHz, $CDCl_3$): δ 8.40 (s, 1H, Ar), 8.21 (s, 2H, Ar), 7.57 (s, 3H, Ar), 7.20 (s, 2H, Ar), 7.03 (s, 2H, Ar), 6.88 (s, 3H, Ar), 6.58 (s, 1H, NH), 4.97 (d, *J* = 12.4 Hz, 1H, OCH_2), 4.76 (d, *J* = 12.6 Hz, 1H, OCH_2), 4.18 (d, *J* = 16.9 Hz, 1H CH_2), 3.91 (s, 3H, OCH_3), 3.66 (d, *J* = 17.0 Hz, 1H, CH_2). $^{13}C\{^1H\}$ NMR (101 MHz, $CDCl_3$): δ 166.4, 153.6, 150.2, 149.5, 146.0, 139.4, 136.5, 135.7, 133.1, 130.0, 129.8, 129.7, 129.6, 129.2, 127.9, 127.7, 127.6, 125.1, 124.0 (q, *J* = 290.0 Hz, CF_3), 122.3, 121.9, 119.9, 118.6 (q, *J* = 320.0 Hz, CF_3), 66.7, 64.3 (q, *J* = 28.5 Hz, CF_3), 54.4, 32.9. ^{19}F NMR (282 MHz, $CDCl_3$): δ −73.84 (s, 3F, CF_3), −75.29 (s, 3F, CF_3). Elemental analysis calcd (%) for $C_{29}H_{21}F_6N_3O_9S$: C, 49.65; H, 3.02; N, 5.99; found: C, 49.52; H, 3.01; N, 5.87.

Methyl 2-(tert-butoxycarbonylamino)-3,3,3-trifluoro-2-((6-nitro-4-p-tolyl-1-(trifluoromethylsulfonyloxy)isoquinolin-3-yl)methyl)propanoate (**4h**).

Yield 82% as a white solid (eluent petroleum ether/ethyl acetate = 9/1). M.p. 154–155 °C. ^1H NMR (500 MHz, $CDCl_3$): δ 8.41 (d, *J* = 9.3 Hz, 1H, Ar), 8.37 (s, 1H, Ar), 8.26 (d, *J* = 9.2 Hz, 1H, Ar), 7.45 (d, *J* = 7.8 Hz, 1H, Ar), 7.38 (d, *J* = 7.8 Hz, 1H, Ar), 7.32 (d, *J* = 7.9 Hz, 1H, Ar), 7.12 (d, *J* = 6.9 Hz, 1H, Ar), 6.49 (s, 1H, NH), 4.08 (d, *J* = 16.4 Hz, 1H, CH_2), 3.88 (s, 3H, OCH_3), 3.62 (d, *J* = 16.4 Hz, 1H, CH_2), 2.51 (s, 3H, CH_3), 1.22 (s, 9H, CH_3). $^{13}C\{^1H\}$ NMR (126 MHz, $CDCl_3$): δ 166.7, 153.4, 150.3, 149.6, 146.7, 139.6, 136.2, 130.5, 130.1, 130.0, 129.9, 129.8, 125.1, 124.1 (q, *J* = 288.6 Hz, CF_3), 122.5, 122.1, 120.2, 118.7 (q, *J* = 320.3 Hz, CF_3), 114.2, 80.2, 64.2 (q, *J* = 28.1 Hz, >C<), 54.0, 33.5, 27.9, 21.6. ^{19}F NMR (282 MHz, $CDCl_3$): δ

−73.56 (s, 3F, CF_3), −74.68 (s, 3F, CF_3). Elemental analysis calcd (%) for $C_{27}H_{25}F_6N_3O_9S$: C, 47.58; H, 3.70; N, 6.17; found: C, 47.61; H, 3.77; N, 6.15.

Methyl 2-(tert-butoxycarbonylamino)-3,3,3-trifluoro-2-((4-(4-methoxyphenyl)-6-nitro-1-(trifluoromethylsulfonyloxy)isoquinolin-3-yl)methyl)propanoate (**4i**).

Yield 88% as a white solid (eluent petroleum ether/ethyl acetate = 9/1). M.p. 149–150 °C. ^{1}H NMR (500 MHz, $CDCl_3$): δ 8.41 (d, J = 9.1 Hz, 1H, Ar), 8.38 (s, 1H, Ar), 8.26 (d, J = 9.1 Hz, 1H, Ar), 7.37 (d, J = 8.4 Hz, 1H, Ar), 7.18–7.14 (m, 2H, Ar), 7.10 (d, J = 8.5 Hz, 1H, Ar), 6.48 (s, 1H, NH), 4.10 (d, J = 16.3 Hz, 1H, CH_2), 3.95 (s, 3H, OCH_3), 3.88 (s, 3H, OCH_3), 3.63 (d, J = 16.4 Hz, 1H, CH_2), 1.21 (s, 9H, 3 CH_3). ^{13}C{^{1}H} NMR (126 MHz, $CDCl_3$): δ 166.7, 160.4, 153.4, 150.2, 149.6, 146.9, 139.8, 135.9, 131.4, 131.2, 125.1, 125.0, 124.1 (q, J = 288.5 Hz, CF_3), 122.5, 122.0, 120.2, 118.7 (q, J = 320.2 Hz, CF_3) 115.1, 115.0, 80.2, 64.2 (q, J = 28.6 Hz, >C<), 55.5, 54.0, 33.5, 27.9. ^{19}F NMR (282 MHz, $CDCl_3$): δ −73.54 (s, 3F, CF_3), −74.72 (s, 3F, CF_3). Elemental analysis calcd (%) for $C_{27}H_{25}F_6N_3O_{10}S$: C, 46.49; H, 3.61; N, 6.02; found: C, 46.62; H, 3.64; N, 6.12.

Methyl 2-(benzyloxycarbonylamino)-3,3,3-trifluoro-2-((4-(4-methoxyphenyl)-6-nitro-1-(trifluoromethylsulfonyloxy)isoquinolin-3-yl)methyl)propanoate (**4j**).

Yield 94% as a yellow solid (eluent petroleum ether/ethyl acetate = 15/1). M.p. 152–154 °C. ^{1}H NMR (400 MHz, $CDCl_3$): δ 8.41 (d, J = 9.2 Hz, 1H, Ar), 8.28 (s, 1H, Ar), 8.19 (d, J = 9.1 Hz, 1H, Ar), 7.14–7.02 (m, 6H, Ar), 6.89 (s, 3H, Ar), 6.58 (s, 1H, NH), 4.97 (d, J = 12.3 Hz, 1H, OCH_2), 4.77 (d, J = 12.1 Hz, 1H, OCH_2), 4.21 (d, J = 16.4 Hz, 1H CH_2), 3.95 (s, 3H, OCH_3), 3.93 (s, 3H, OCH_3), 3.66 (d, J = 16.8 Hz, 1H, CH_2). ^{13}C{^{1}H} NMR (126 MHz, $CDCl_3$): δ 166.4, 160.4, 153.7, 150.0, 149.5, 146.4, 139.7, 136.5, 135.7, 131.4, 131.0, 127.9, 127.6, 127.5, 125.1, 124.9, 124.0 (q, J = 285.8 Hz, CF_3), 122.5, 121.8, 119.9, 118.6 (q, J = 320.4 Hz, CF_3), 115.0, 114.9, 66.7, 64.3 (q, J = 28.5 Hz, >C<), 55.5, 54.5, 32.9. ^{19}F NMR (282 MHz, $CDCl_3$): δ −73.83 (s, 3F, CF_3), −75.22 (s, 3F, CF_3). Elemental analysis calcd (%) for $C_{30}H_{23}F_6N_3O_{10}S$: C, 49.25; H, 3.17; N, 5.74; found: C, 49.29; H, 3.08; N, 5.84.

Methyl 2-(tert-butoxycarbonylamino)-3,3,3-trifluoro-2-((4-phenyl-6-(trifluoromethyl)-1-(trifluoromethylsulfonyloxy)isoquinolin-3-yl)methyl)propanoate (**4k**).

Yield 81% as a white solid (eluent petroleum ether/ethyl acetate = 15/1). M.p. 146–148 °C. ^{1}H NMR (500 MHz, $CDCl_3$): δ 8.25 (d, J = 8.8 Hz, 1H, Ar), 7.87 (d, J = 8.8 Hz, 1H, Ar), 7.72 (s, 1H, Ar), 7.63 (s, 1H, Ar), 7.57 (s, 2H, Ar), 7.44 (s, 1H, Ar), 7.24 (s, 1H, Ar), 6.59 (s, 1H, NH), 4.01 (d, J = 16.1 Hz, 1H, CH_2), 3.87 (s, 3H, OCH_3), 3.60 (d, J = 16.3 Hz, 1H, CH_2), 1.24 (s, 9H, 3 CH_3). ^{13}C{^{1}H} NMR (126 MHz, $CDCl_3$): δ 166.8, 153.5, 150.5, 145.6, 139.2, 135.1, 133.8 (q, J = 33.5 Hz, C_{Ar}-CF_3), 133.7, 130.1, 129.9, 129.6, 129.4, 129.2, 124.6, 124.2 (q, J = 288.4 Hz, CF_3), 124.2, 123.9–123.8 (m), 123.3 (q, J = 273.2 Hz, CF_3), 119.5, 118.7 (q, J = 320.2 Hz, CF_3), 80.2, 64.3 (q, J = 28.4 Hz, >C<), 53.9, 33.5, 27.9. ^{19}F NMR (282 MHz, $CDCl_3$): δ −73.69 (s, 3F, CF_3), −73.89 (s, 3F, CF_3). Elemental analysis calcd (%) for $C_{27}H_{23}F_9N_2O_7S$: C, 46.96; H, 3.36; N, 4.06; found: C, 46.87; H, 3.32; N, 4.05.

Methyl 2-(benzyloxycarbonylamino)-3,3,3-trifluoro-2-((4-phenyl-6-(trifluoromethyl)-1-(trifluoromethylsulfonyloxy)isoquinolin-3-yl)methyl)propanoate (**4l**).

Yield 80% as a white solid (eluent petroleum ether/ethyl acetate = 15/1). M.p. 109–111 °C. ^{1}H NMR (300 MHz, $CDCl_3$): δ 8.18 (d, J = 8.8 Hz, 1H, Ar), 7.87 (d, J = 8.8 Hz, 1H, Ar), 7.60–7.53 (m, 4H, Ar), 7.18–7.12 (m, 2H, Ar), 7.01 (s, 2H, Ar), 6.87 (s, 3H, Ar), 6.62 (s, 1H, NH), 4.99 (d, J = 12.5 Hz, 1H, OCH_2), 4.76 (d, J = 12.5 Hz, 1H, OCH_2), 4.12 (d, J = 16.9 Hz, 1H, CH_2), 3.92 (s, 3H, OCH_3), 3.63 (d, J = 16.8 Hz, 1H, CH_2). ^{13}C{^{1}H} NMR (101 MHz, $CDCl_3$): δ 166.5, 153.7, 150.3, 145.0, 139.1, 136.6, 134.9, 133.6 (q, J = 33.1 Hz, C_{Ar}-CF_3), 133.5, 130.1, 129.8, 129.5, 129.2, 129.0, 127.8, 127.6, 127.4, 124.3, 124.2, 124.0 (q, J = 289.1 Hz, CF_3), 123.9, 123.4 (q, J = 274.3 Hz, CF_3), 119.2, 118.6 (q, J = 320.4 Hz, CF_3), 66.7, 64.3 (q, J = 28.8 Hz, >C<), 54.4, 32.8. ^{19}F NMR (282 MHz, $CDCl_3$): δ −63.22 (s, 3F, CF_3), −73.92 (s, 3F, CF_3), −75.08 (s, 3F, CF_3). Elemental analysis calcd (%) for $C_{30}H_{21}F_9N_2O_7S$: C, 49.73; H, 2.92; N, 3.87; found: C, 49.75; H, 2.96; N, 3.83.

Methyl 2-(tert-butoxycarbonylamino)-3,3,3-trifluoro-2-((4-p-tolyl-6-(trifluoromethyl)-1-(trifluoromethylsulfonyloxy)isoquinolin-3-yl)methyl)propanoate (**4m**).

Yield 70% as a white solid (eluent petroleum ether/ethyl acetate = 15/1). M.p. 134–136 °C. ^{1}H NMR (500 MHz, $CDCl_3$): δ 8.24 (d, J = 8.8 Hz, 1H, Ar), 7.86 (d, J = 8.9 Hz, 1H, Ar), 7.77 (s, 1H, Ar), 7.42 (d, J = 7.8 Hz, 1H, Ar), 7.36 (d, J = 7.7 Hz, 1H, Ar), 7.30 (d, J = 7.8 Hz, 1H, Ar), 7.11 (d, J = 7.8 Hz, 1H, Ar), 6.61 (s, 1H, NH), 4.01 (d, J = 16.2 Hz, 1H, CH_2), 3.86 (s, 3H, OCH_3), 3.59 (d, J = 16.3 Hz, 1H, CH_2), 2.50 (s, 3H, CH_3), 1.24 (s, 9H, 3 CH_3). ^{13}C{^{1}H} NMR (126 MHz, $CDCl_3$) δ 166.8, 153.5, 150.4, 145.7, 139.3, 139.2, 135.4, 133.7 (q, J = 32.9 Hz, C_{Ar}-CF_3), 130.5, 130.3, 130.0, 129.9, 129.8, 124.5, 124.2 (q, J = 288.4 Hz, CF_3), 124.1, 123.9–123.9 (m), 123.3 (q, J = 274.2 Hz, CF_3), 120.1, 118.7 (q, J = 320.2 Hz, CF_3), 80.2, 64.3 (q, J = 28.0 Hz, >C<), 53.9, 33.6, 27.9, 21.5. ^{19}F NMR (282 MHz, $CDCl_3$) δ −63.17 (s, 3F, CF_3), −73.58 (s, 3F, CF_3), −74.38 (s, 3F, CF_3). Elemental analysis calcd (%) for $C_{28}H_{25}F_9N_2O_7S$: C, 47.73; H, 3.58; N, 3.98; found: C, 47.71; H, 3,57; N, 3.94.

Methyl 2-(benzyloxycarbonylamino)-3,3,3-trifluoro-2-((4-p-tolyl-6-(trifluoromethyl)-1-(trifluoromethylsulfonyloxy)isoquinolin-3-yl)methyl)propanoate (**4n**).

Yield 92% as a white solid (eluent petroleum ether/ethyl acetate = 15/1). M.p. 101–103 °C. ^{1}H NMR (300 MHz, $CDCl_3$): δ 8.17 (d, J = 8.8 Hz, 1H, Ar), 7.86 (d, J = 8.8 Hz, 1H, Ar), 7.65 (s, 1H, Ar), 7.38 (d, J = 7.8 Hz, 1H, Ar), 7.33 (d, J = 7.8 Hz, 1H, Ar), 7.06–6.98 (m, 4H, Ar), 6.88 (s, 3H, Ar), 6.63 (s, 1H, NH), 4.99 (d, J = 12.5 Hz, 1H, OCH_2), 4.77 (d, J = 12.5 Hz, 1H, OCH_2), 4.14 (d, J = 16.8 Hz, 1H, CH_2), 3.92 (s, 3H, OCH_3), 3.63 (d, J = 16.8 Hz, 1H, CH_2), 2.49 (s, 3H, CH_3). ^{13}C{^{1}H} NMR (126 MHz, $CDCl_3$): δ 166.6, 153.7, 150.2, 145.1, 139.3, 139.0, 136.6, 135.2, 133.5 (q, J = 32.7 Hz, C_{Ar}-CF_3), 130.4, 130.2, 129.9, 129.7, 129.6, 127.8, 127.6, 127.4, 124.2, 124.1, 124.0, 123.4 (q, J = 273.2 Hz, CF_3), 124.1 (q, J = 288.4 Hz, CF_3), 119.2, 118.6 (q, J = 319.9 Hz, CF_3), 66.7, 64.4 (q, J = 28.6 Hz, >C<), 54.4, 32.9. ^{19}F NMR (282 MHz, $CDCl_3$): δ = −63.17 (s, 3F, CF_3), −73.91 (s, 3F, CF_3), −74.98 (s, 3F, CF_3). Elemental analysis calcd (%) for $C_{31}H_{23}F_9N_2O_7S$: C, 50.41; H, 3.14; N, 3.79; found: C, 50.63; H, 3.32; N, 4.01.

Methyl 2-(benzyloxycarbonylamino)-3,3,3-trifluoro-2-((4-(4-methoxyphenyl)-6-(trifluoromethyl)-1-(trifluoromethylsulfonyloxy)isoquinolin-3-yl)methyl)propanoate (**4o**).

Yield 93% as a thick oil (eluent petroleum ether/ethyl acetate = 15/1). ^{1}H NMR (500 MHz, $CDCl_3$): δ 8.17 (d, J = 8.8 Hz, 1H, Ar), 7.86 (d, J = 8.8 Hz, 1H, Ar), 7.67 (s, 1H, Ar), 7.12–7.01 (m, 6H, Ar), 6.87 (s, 3H, Ar), 6.62 (s, 1H, NH), 4.99 (d, J = 12.5 Hz, 1H, OCH_2), 4.77 (d, J = 12.5 Hz, 1H, OCH_2), 4.16 (d, J = 16.7 Hz, 1H, CH_2), 3.93 (s, 6H, 2 CH_3), 3.64 (d, J = 16.7 Hz, 1H, CH_2). ^{13}C{^{1}H} NMR (126 MHz, $CDCl_3$): δ 166.6, 160.1, 153.7, 150.1, 145.4, 139.5, 136.6, 134.9, 133.5 (q, J = 33.0 Hz, C_{Ar}-CF_3), 131.4, 131.0, 127.9, 127.6, 127.4, 125.4, 124.2, 124.1, 124.0 (q, J = 288.7 Hz, CF_3), 124.0, 123.4 (q, J = 273.2 Hz, CF_3), 119.2, 118.6 (q, J = 320.4 Hz, S-CF_3), 114.8, 114.7, 66.7, 64.4 (q, J = 28.5 Hz, >C<), 55.5, 54.4, 32.9. ^{19}F NMR (282 MHz, $CDCl_3$): δ −63.16 (s, 3F, CF_3), −73.93 (s, 3F, CF_3), −75.01 (s, 3F, CF_3). Elemental analysis calcd (%) for $C_{31}H_{23}F_9N_2O_8S$: C, 49.34; H, 3.07; N, 3.71; found: C, 49.44; H, 3.02; N, 3.85.

Methyl 2-(tert-butoxycarbonylamino)-3,3,3-trifluoro-2-((1-(4-methoxyphenyl)-4-p-tolyl-isoquinolin-3-yl)methyl)propanoate (**5a**).

Yield 92% as a white solid (eluent petroleum ether/ethyl acetate = 10/1). M.p. 214–215 °C. ^{1}H NMR (500 MHz, $CDCl_3$): δ 8.57 (s, 1H, NH), 8.22 (d, J = 8.2 Hz, 1H, Ar), 7.77 (d, J = 8.1 Hz, 2H, Ar), 7.56–7.52 (m, 2H, Ar), 7.46 (d, J = 8.3 Hz, 1H, Ar), 7.35 (d, J = 7.7 Hz, 1H, Ar), 7.31 (d, J = 7.8 Hz, 1H, Ar), 7.24 (d, J = 7.8 Hz, 1H, Ar), 7.10 (d, J = 8.0 Hz, 3H, Ar), 3.92 (s, 3H, OCH_3), 3.71–3.67 (m, 3H, OCH_3, 1H, CH_2), 3.49 (d, J = 14.7 Hz, 1H, CH_2), 2.48 (s, 3H, CH_3), 1.37 (s, 9H, 3 CH_3). ^{13}C{^{1}H} NMR (126 MHz, $CDCl_3$): δ 167.4, 160.4, 158.2, 154.2, 144.7, 137.9, 137.7, 132.9, 131.9, 131.7, 131.6, 130.5, 130.3, 130.2, 129.7, 129.3, 127.7, 126.9, 126.4, 125.2, 124.5 (q, J = 288.0 Hz, CF_3), 115.3, 114.0, 80.0, 67.2, 64.8 (q, J = 25.4 Hz, >C<), 55.6, 53.0, 34.2, 28.3, 21.5. ^{19}F NMR (282 MHz, $CDCl_3$): δ −72.96 (s, 3F, CF_3). Elemental analysis calcd (%) for $C_{33}H_{33}F_3N_2O_5$: C, 66.66; H, 5.59; N, 4.71; found: C, 66.35; H, 5.21; N, 4.43.

Methyl 2-(tert-butoxycarbonylamino)-3,3,3-trifluoro-2-((1-(4-methoxyphenyl)-6-nitro-4-phenylisoquinolin-3-yl)methyl)propanoate (**5b**).

Yield 88% as a yellow solid (eluent petroleum ether/ethyl acetate = 10/1). M.p. 180–181 °C. ^{1}H NMR (500 MHz, $CDCl_3$): δ 8.38 (d, J = 9.2 Hz, 1H, Ar), 8.33 (d, J = 1.7 Hz, 1H, Ar), 8.23 (d_B, J = 9.2, 2.3 Hz, 1H, Ar), 7.73 (d, J = 8.3 Hz, 2H, Ar), 7.67 (br. s, 1H, NH), 7.64–7.61 (m, 1H, Ar), 7.58–7.56 (m, 2H, Ar), 7.42 (d, J = 7.0 Hz, 1H, Ar), 7.26–7.25 (m, 1H, Ar), 7.13 (d, J = 8.3 Hz, 2H, Ar), 3.94 (s, 3H, OCH_3), 3.82 (d, J = 15.3 Hz, 1H, CH_2), 3.66 (s, 3H, OCH_3), 3.59 (d, J = 15.5 Hz, 1H, CH_2), 1.29 (s, 9H, 3 CH_3). ^{13}C{^{1}H} NMR (126 MHz, $CDCl_3$): δ 167.3, 160.9, 158.6, 153.7, 148.3, 147.2, 137.1, 134.6, 132.8, 131.7, 130.5, 130.2, 130.0–129.9 (m), 129.5, 129.1, 129.0, 126.7, 124.4 (q, J = 287.3 Hz, CF_3), 122.4, 120.0, 114.2, 100.1, 80.2, 64.7 (q, J = 27.7 Hz, >C<), 55.6, 53.4, 34.1, 28.2. ^{19}F NMR (282 MHz, $CDCl_3$): δ −73.71 (s, 3F, CF_3). Elemental analysis calcd (%) for $C_{32}H_{30}F_3N_3O_7$: C, 61.44; H, 4.83; N, 6.72; found: C, 61.18; H, 4.61; N, 6.56.

Methyl 2-(benzyloxycarbonylamino)-3,3,3-trifluoro-2-((1-(4-methoxyphenyl)-4-phenyl-6-(trifluoromethyl)isoquinolin-3-yl)methyl)propanoate (**5c**).

Yield 87% as a white solid (eluent petroleum ether/ethyl acetate = 10/1). M.p. 107–108 °C. ^{1}H NMR (400 MHz, $CDCl_3$): δ 8.30 (d, J = 7.8 Hz, 1H, Ar), 7.92 (s, 1H, NH), 7.68–7.66 (m, 2H, Ar), 7.62–7.50 (m, 5H, Ar), 7.22–7.20 (m, 2H, Ar), 7.14–7.05 (m, 5H, Ar), 6.95–6.94 (m, 2H, Ar), 5.07 (d, J = 11.9 Hz, 1H, OCH_2), 4.88 (d, J = 12.0 Hz, 1H, OCH_2), 3.88 (s, 3H, OCH_3, 1H, CH_2), 3.65 (s, 3H, OCH_3), 3.59 (d, J = 16.1 Hz, 1H, CH_2). ^{13}C{^{1}H} NMR (126 MHz, $CDCl_3$): δ 167.2, 160.6, 158.5, 154.2, 145.8, 136.7, 136.5, 134.9, 132.2, 131.8 (q, J = 32.3 Hz, C_{Ar}-CF_3), 131.7, 130.6, 130.5, 130.1, 129.3, 129.1, 128.9, 128.7, 128.3, 127.9, 127.8, 126.0, 125.5, 124.3 (q, J = 287.9 Hz, CF_3), 123.9 (q, J = 273.0 Hz, CF_3), 123.8–123.7 (m), 122.4, 114.0, 66.9, 64.8 (q, J = 28.5 Hz, >C<), 55.6, 53.6, 33.8. ^{19}F NMR (376 MHz, $CDCl_3$): δ −62.99 (s, 3F, CF_3), −73.68 (s, 3F, CF_3). Elemental analysis calcd (%) for $C_{36}H_{28}F_6N_2O_5$: C, 63.34; H, 4.13; N, 4.10; found: C, 63.18; H, 4.01; N, 4.25.

Methyl 2-(benzyloxycarbonylamino)-3,3,3-trifluoro-2-((4-(phenylethynyl)-1-p-tolylnaphthalen-2-yl)methyl)propanoate (**6a**).

Yield 58% as a white solid (eluent petroleum ether/ethyl acetate = 10/1). M.p. 180–182 °C. ^{1}H NMR (400 MHz, $CDCl_3$): δ 8.52 (d, J = 8.4 Hz, 1H, Ar), 8.03 (s, 1H, NH), 7.70–7.61 (m, 4H, Ar), 7.44–7.40 (m, 4H, Ar), 7.33–7.29 (m, 2H, Ar), 7.16–7.12 (m, 2H, Ar), 7.08–7.02 (m, 5H, Ar), 5.07 (d, J = 12.5 Hz, 1H, OCH_2), 4.96 (d, J = 12.8 Hz, 1H, OCH_2), 3.85 (s, 3H, OCH_3, 1H, CH_2,), 3.56 (d, J = 15.5 Hz, 1H, CH_2), 2.47 (s, 3H, CH_3). ^{13}C{^{1}H} NMR (126 MHz, $CDCl_3$): δ 167.4, 154.3, 145.5, 141.9, 138.1, 136.6, 136.5, 133.1, 132.5, 132.3, 130.7, 130.4, 129.9, 129.6, 129.5, 129.3, 128.7, 128.3, 127.9, 127.8, 127.7, 127.4, 126.9, 126.3, 124.4 (q, J = 287.2 Hz, CF_3), 122.3, 94.0, 86.8, 66.7, 64.9 (q, J = 27.8 Hz, >C<), 53.6, 33.9, 21.5. ^{19}F NMR (282 MHz, $CDCl_3$): δ −73.59 (s, 3F, CF_3). Elemental analysis calcd (%) for $C_{37}H_{29}F_3N_2O_4$: C, 71.37; H, 4.69; N, 4.50; found: C, 71.14; H, 4.48; N, 4.27.

Methyl 2-(tert-butoxycarbonylamino)-3,3,3-trifluoro-2-((7-nitro-1-phenyl-4-(phenyl-ethynyl) naphthalen-2-yl)methyl)propanoate (**6b**).

Yield 60% as a white solid (eluent petroleum ether/ethyl acetate = 10/1). M.p. 98–99 °C. ^{1}H NMR (500 MHz, $CDCl_3$): δ 8.68 (d, J = 8.0 Hz, 1H, Ar), 8.37 (d, J = 7.8 Hz, 1H, Ar), 8.32 (s, 1H, Ar), 7.75 (s, 2H, Ar), 7.62 (s, 2H, Ar), 7.58 (s, 2H, Ar), 7.48 (s, 3H, Ar), 7.41 (s, 1H, Ar), 7.26 (br. s, 1H, NH), 3.89 (m, 3H, OCH_3, 1H, CH_2), 3.59 (d, J = 14.8 Hz, 1H, CH_2), 1.30 (s, 9H, 3 CH_3). ^{13}C{^{1}H} NMR (126 MHz, $CDCl_3$): δ 167.4, 153.6, 148.9, 148.2, 145.3, 144.9, 134.3, 134.0, 132.5, 130.5, 130.1, 129.5, 129.4, 129.3, 129.1, 128.9, 128.3, 124.4 (q, J = 290.4 Hz, CF_3), 122.6, 121.7, 121.0, 90.4, 85.9, 66.6, 64.7 (q, J = 27.2 Hz, >C<), 60.6, 53.6, 29.8, 28.2. ^{19}F NMR (282 MHz, $CDCl_3$): δ −73.71 (s, 3F, CF_3). Elemental analysis calcd (%) for $C_{33}H_{28}F_3N_3O_6$: C, 63.97; H, 4.56; N, 6.78; found: C, 63.83; H, 4.41; N, 6.54.

Methyl 2-(tert-butoxycarbonylamino)-3,3,3-trifluoro-2-((4-(phenylethynyl)-1-p-tolyl-7-(trifluoromethyl)naphthalen-2-yl)methyl)propanoate (**6c**).

Yield 67% as a white solid (eluent petroleum ether/ethyl acetate = 15/1). M.p. 198–200 °C. ^{1}H NMR (400 MHz, $CDCl_3$): δ 8.65 (d, J = 8.7 Hz, 1H, Ar), 7.82 (d, J = 8.8 Hz, 1H, Ar), 7.77–7.74 (m, 3H, Ar), 7.61 (s, 1H, NH), 7.47–7.46 (m, 3H, Ar), 7.38 (d, J = 7.7 Hz, 1H, Ar), 7.33 (d, J = 7.6 Hz, 1H, Ar), 7.23 (d, J = 8.0 Hz, 1H, Ar), 7.08 (d, J = 7.7 Hz, 1H, Ar), 3.84 (s, 3H, OCH_3, 1H, CH_2), 3.54 (d, J = 15.3 Hz, 1H, CH_2), 2.49 (s, 3H, CH_3), 1.32 (s, 9H,

3 CH_3). $^{13}C\{^1H\}$ NMR (126 MHz, $CDCl_3$): δ 167.5, 153.8, 147.6, 142.1, 138.7, 135.8, 133.7, 132.4, 132.3 (q, J = 32.3 Hz, C_{Ar}-CF_3), 131.4, 130.3, 130.0, 129.9, 129.8, 129.6, 128.8, 128.6, 128.4, 124.3 (q, J = 288.3 Hz, CF_3), 123.9–123.9 (m), 123.7 (q, J = 273.0 Hz, CF_3), 123.3, 121.9, 94.9, 86.3, 80.1, 64.7 (q, J = 27.3 Hz, >C<), 53.4, 34.2, 28.2, 21.5. ^{19}F NMR (282 MHz, $CDCl_3$): δ −62.99 (s, 3F, CF_3), −73.60 (s, 3F, CF_3). Elemental analysis calcd (%) for $C_{35}H_{30}F_6N_2O_4$: C, 64.02; H, 4.61; N, 4.27; found: C, 64.29; H, 4.41; N, 4.25.

Methyl 2-(tert-butoxycarbonylamino)-3,3,3-trifluoro-2-((4-phenylisoquinolin-3-yl)methyl)-propanoate (**7a**).

Yield 50% as a white solid (eluent petroleum ether/ethyl acetate = 5/1). M.p. 124–126 °C. ^1H NMR (400 MHz, $CDCl_3$): δ 9.19 (s, 1H, Ar), 8.01–7.99 (m, 1H, Ar), 7.94 (br. s, 1H, NH), 7.59–7.48 (m, 5H, Ar), 7.31 (s, 2H, Ar), 7.19 (m, 1H, Ar), 3.78 (s, 3H, OCH_3), 3.66 (d, J = 15.9 Hz, 1H, CH_2), 3.47 (d, J = 15.2 Hz, 1H, CH_2), 1.35 (s, 9H, 3 CH_3). $^{13}C\{^1H\}$ NMR (101 MHz, $CDCl_3$): δ 167.8, 153.9, 150.6, 145.7, 136.2, 135.9, 132.8, 130.8, 130.5, 130.1, 128.9, 128.6, 128.3, 127.6, 127.1, 125.7, 124.5 (q, J = 288.4 Hz, CF_3), 80.1, 66.5, 64.6 (q, J = 24.0 Hz, >C<), 53.2, 34.5, 28.2. ^{19}F NMR (376 MHz, $CDCl_3$): δ −72.99 (s, 3F, CF_3). Elemental analysis calcd (%) for $C_{25}H_{25}F_3N_2O_4$: C, 63.28; H, 5.31; N, 5.90; found: C, 63.08; H, 5.01; N, 5.75.

Methyl 2-(benzyloxycarbonylamino)-3,3,3-trifluoro-2-((4-phenylisoquinolin-3-yl)methyl)-propanoate (**7b**).

Yield 61% as a white solid (eluent petroleum ether/ethyl acetate = 8/1). M.p. 136–137 °C. ^1H NMR (400 MHz, $CDCl_3$): δ 9.13 (s, 1H, Ar), 7.98 (s, 1H, Ar, 1H, NH), 7.2–7.58 (m, 2H, Ar), 7.53–7.48 (m, 3H, Ar), 7.35 (d, J = 7.8 Hz, 1H, Ar), 7.23 (d, J = 7.6 Hz, 1H, Ar), 7.20–7.10 (m, 6H, Ar), 5.09 (d, J = 12.5 Hz, 1H, OCH_2), 4.94 (d, J = 12.5 Hz, 1H, OCH_2), 3.81 (s, 3H, OCH_3, 1H, CH_2), 3.55 (d, J = 15.6 Hz, 1H, CH_2). $^{13}C\{^1H\}$ NMR (126 MHz, $CDCl_3$): δ 167.6, 154.3, 150.4, 145.3, 136.6, 136.2, 135.8, 132.8, 130.7, 130.5, 130.1, 128.9, 128.6, 128.4, 128.2, 127.9, 127.7, 127.2, 127.1, 125.7, 124.4 (q, J = 286.9 Hz, CF_3), 66.7, 64.8 (q, J = 28.2 Hz, >C<), 53.5, 34.0. ^{19}F NMR (282 MHz, $CDCl_3$): δ −73.27 (s, 3F, CF_3). Elemental analysis calcd (%) for $C_{28}H_{23}F_3N_2O_4$: C, 66.14; H, 4.56; N, 5.51; found: C, 66.31; H, 4.89; N, 5.76.

2-(tert-Butoxycarbonylamino)-3,3,3-trifluoro-2-((1-oxo-4-phenyl-1,2-dihydroisoquinolin-3-yl) methyl)propanoic acid (**8**).

Yield 83% as a white solid. M.p. 176–177 °C. ^1H NMR (300 MHz, DMSO-d_6): δ 10.84 (s, 1H, NH), 8.26 (d, J = 7.7 Hz, 1H, Ar), 8.00 (s, 1H, Ar), 7.60 (t, J = 7.5 Hz, 1H, Ar), 7.51–7.42 (m, 4H, Ar), 7.25–7.23 (m, 2H, Ar), 6.92 (d, J = 8.2 Hz, 1H, Ar), 3.36 (br. s, 1H, OH), 3.10 (d, J = 14.8 Hz, 1H, CH_2), 2.87 (d, J = 14.8 Hz, 1H, CH_2), 1.37 (s, 9H, 3 CH_3). $^{13}C\{^1H\}$ NMR (126 MHz, DMSO-d_6): δ 165.3, 161.4, 153.7, 138.2, 134.6, 132.5, 132.2, 132.0, 130.8, 128.7, 128.5, 127.8, 126.6, 126.3, 125.2, 124.7, 124.4 (q, J = 287.6 Hz, CF_3), 118.6, 79.8, 64.0 (q. J = 30.8 Hz, >C<), 31.2, 27.9. ^{19}F NMR (282 MHz, acetone-d_6): δ −74.93 (s, 3F, CF_3). Elemental analysis calcd (%) for $C_{24}H_{23}F_3N_2O_5$: C, 60.50; H, 4.87; N, 5.88; found: C, 63.38; H, 5.03; N, 5.77.

2-(tert-Butoxycarbonylamino)-3,3,3-trifluoro-2-((1-oxo-4-phenyl-1,2-dihydroisoquinolin-3-yl) methyl)propanoic acid (**9**).

Yield 85% as a white solid. M.p. 184–185 °C. ^1H NMR (400 MHz, DMSO-d_6): δ 8.43 (d, J = 8.3 Hz, 1H, Ar), 7.79 (d, J = 8.4 Hz, 1H, Ar), 7.25 (s, 1H, Ar), 7.20 (d, J = 7.8 Hz, 2H, Ar), 7.16–7.09 (m, 2H, Ar, 1H, NH), 3.85 (s, 3H, OCH_3), 3.61 (s, 3H, OCH_3), 3.31 (s, 2H, NH_2), 3.06 (d, J = 15.0 Hz, 1H, CH_2), 2.93 (d, J = 14.9 Hz, 1H, CH_2). $^{13}C\{^1H\}$ NMR (126 MHz, $CDCl_3$): δ 166.6, 161.4, 159.7, 139.2, 134.3, 134.1 (q. J = 32.4 Hz, C_{Ar}-CF_3), 132.2, 131.9, 128.7, 127.5, 126.2, 124.0 (q. J = 286.9 Hz, CF_3), 123.8 (q. J = 273.0 Hz, CF_3), 122.9–122.9 (m), 122.5–122.5 (m), 118.0, 114.8, 114.6, 64.6 (q. J = 27.8 Hz, >C<), 55.5, 54.1, 31.2. ^{19}F NMR (282 MHz, $CDCl_3$): δ −62.95 (s, 3F, CF_3), −79.00 (s, 3F, CF_3). Elemental analysis calcd (%) for $C_{22}H_{18}F_6N_2O_4$: C, 54.10; H, 3.71; N, 5.74; found: C, 54.22; H, 3.99; N, 5.82.

3.3. X-ray Structure Determination of **3a**

A single-crystal X-ray diffraction experiment was carried out with a Bruker SMART APEX II diffractometer (graphite monochromated Mo-K_α radiation, λ = 0.71073 Å, ω-scan technique). The structure was solved with direct methods and refined by the full-

matrix least-squares technique against F^2,with the anisotropic thermal parameters for all non-hydrogen atoms using the SHELXL [60] program package. Hydrogen atoms of the NH groups were located in the different Fourier maps and freely refined without constraints. The remaining hydrogen atoms were placed in calculated positions and refined using a riding model with U_{iso}(H) = 1.5U_{eq}(C) for hydrogen atoms of methyl groups and U_{iso}(H) = 1.2U_{eq}(C) for other carbon atoms. The crystal data and structure refinement details are presented in Supplementary Materials (Table S1). Single-crystal X-ray diffraction analysis was performed using the equipment of the JRC PMR IGIC RAS.

4. Conclusions

In conclusion, we have elaborated a convenient pathway to a new series of α-CF_3-substituted α-amino acid derivatives bearing a pharmacophore isoquinolone core in their backbone. The method is based on [4+2]-annulation of *N*-(pivaloyloxy) aryl amides with orthogonally protected internal acetylene-containing α-amino carboxylates under Rh(III)-catalysis. The reaction smoothly proceeds at an ambient temperature in trifluoroethanol in the presence of 3 mol/% of rhodium dimer complex $(Cp^*RhCl_2)_2$ and 1 equiv. of cesium acetate to afford the target products in good yields. The latter compounds proved to be suitable substrates for further conversion to valuable isoquinoline derivatives via a subsequent aromatization/cross-coupling synthetic operation. The biological activity of the obtained compounds is currently being studied.

Supplementary Materials: The following supporting information can be downloaded at: https://www.mdpi.com/article/10.3390/molecules27238488/s1, Figures S1–S92. ^{1}H and ^{13}C NMR spectra of compounds. Figure S93. H-bonded dimer in the crystal of **3a**. Scheme S1. Proposed mechanism. Table S1. Crystal data, data collection and structure refinement parameters for **3a**.

Author Contributions: Conceptualization, S.N.O.; methodology, S.N.O.; investigation, D.V.V., D.A.P. (synthesis), I.A.G. (NMR spectra registering and characterization), F.M.D. (X-ray analysis); writing—original draft preparation, S.N.O., D.V.V.; writing—review and editing, D.V.V., S.N.O.; supervision, S.N.O.; project administration, S.N.O.; funding acquisition, S.N.O. All authors have read and agreed to the published version of the manuscript.

Funding: This work was financially supported by the Russian Science Foundation (grant RSF No. 21-13-00328).

Institutional Review Board Statement: Not applicable.

Informed Consent Statement: Not applicable.

Data Availability Statement: Data are contained within the article and Supplementary Materials.

Acknowledgments: NMR studies and spectral characterization were performed with financial support from the Ministry of Science and Higher Education of the Russian Federation using the equipment of the Center for Molecular Composition Studies of INEOS RAS.

Conflicts of Interest: The authors declare no conflict of interest.

Sample Availability: Samples of all of the compounds are available from the authors.

References

1. Chen, H.-Y.; He, L.-J.; Li, S.-Q.; Zhang, Y.-J.; Huang, J.-H.; Qin, H.-X.; Wang, J.-L.; Li, Q.-Y.; Yang, D.-L. A derivate of benzimidazole-isoquinolinone induces SKP2 transcriptional inhibition to exert anti-tumor activity in glioblastoma cells. *Molecules* **2019**, *24*, 2722. [CrossRef] [PubMed]
2. He, L.-J.; Yang, D.-L.; Li, S.-Q.; Zhang, Y.-J.; Tang, Y.; Lei, J.; Frett, B.; Lin, H.-K.; Li, H.-Y.; Chen, Z.-Z.; et al. Facile construction of fused benzimidazole-isoquinolinones that induce cell-cycle arrest and apoptosis in colorectal cancer cells. *Bioorg. Med. Chem.* **2018**, *26*, 3899. [CrossRef] [PubMed]
3. Tang, Z.; Niu, S.; Liu, F.; Lao, K.; Miao, J.; Ji, J.; Wang, X.; Yan, M.; Zhang, L.; You, Q.; et al. Synthesis and biological evaluation of 2,3-diaryl isoquinolinone derivatives as anti-breast cancer agents targeting ERα and VEGFR-2. *Bioorg. Med. Chem. Lett.* **2014**, *24*, 2129. [CrossRef] [PubMed]

4. Scalia, M.; Satriano, C.; Greca, R.; Stella, A.M.G.; Rizzarelli, E.; Spina-Purrello, V. PARP-1 inhibitors DPQ and PJ-34 negatively modulate proinflammatory commitment of human glioblastoma cells. *Neurochem. Res.* **2013**, *38*, 50. [CrossRef] [PubMed]
5. Zhang, Z.; You, Z.; Dobrowsky, R.T.; Rick, T.; Blagg, B.S.J. Synthesis and evaluation of a ring-constrained Hsp90 C-terminal inhibitor that exhibits neuroprotective activity. *Bioorg. Med. Chem. Lett.* **2018**, *28*, 2701. [CrossRef]
6. Nair, J.J.; Rarova, L.; Strnad, M.; Bastida, J.; van Staden, J. Apoptosis-inducing effects of distichamine and narciprimine, rare alkaloids of the plant family Amaryllidaceae. *Bioorg. Med. Chem. Lett.* **2012**, *22*, 6195. [CrossRef]
7. Du, J.; Xi, L.; Lei, B.; Liu, H.; Yao, X. Structural requirements of isoquinolones as novel selective c-Jun N-terminal kinase 1 inhibitors: 2D and 3D QSAR analyses. *Chem. Biol. Drug Des.* **2011**, *77*, 248. [CrossRef]
8. Guo, S.; Wang, F.; Sun, L.; Zhang, X.; Fan, X. Palladium-catalyzed oxidative cyclocarbonylation of isoquinolones with CO via C-H/N-H bond cleavage: Easy access to isoindolo[2,1-b]isoquinoline-5,7-dione derivatives. *Adv. Synth. Catal.* **2018**, *360*, 2537. [CrossRef]
9. Thirupataiah, B.; Reddy, G.S.; Ghule, S.S.; Kumar, J.S.; Mounika, G.; Hossain, K.A.; Mudgal, J.; Mathew, J.E.; Shenoy, G.G.; Parsa, K.V.L.; et al. Synthesis of 11,12-dihydro benzo[c]phenanthridines via a Pd-catalyzed unusual construction of isocoumarin ring/FeCl3-mediated intramolecular arene-allyl cyclization: First identification of a benzo[c]phenanthridine based PDE4 inhibitor. *Bioorg. Chem.* **2020**, *97*, 103691. [CrossRef]
10. Guo, S.; Sun, L.; Wang, F.; Zhang, X.; Fan, X. Rh(III)-Catalyzed oxidative annulation of isoquinolones with diazoketoesters featuring an in situ deacylation: Synthesis of isoindoloisoquinolones and their transformation to Rosettacin analogues. *J. Org. Chem.* **2018**, *83*, 12034. [CrossRef]
11. Coles-Taylor, B.L.; McCallum, S.M.; Scott Lee, J.; Michel, B.W. Accessing 4-oxy-substituted isoquinolinones via C-H activation and regioselective migratory insertion with electronically biased ynol ethers. *Org. Biomol. Chem.* **2018**, *16*, 8639. [CrossRef]
12. Wu, J.-Q.; Zhang, S.-S.; Gao, H.; Qi, Z.; Zhou, C.-J.; Ji, W.-W.; Liu, Y.; Chen, Y.; Li, Q.; Li, X.; et al. Experimental and theoretical studies on rhodium-catalyzed coupling of benzamides with 2,2-difluorovinyl tosylate: Diverse synthesis of fluorinated heterocycles. *J. Am. Chem. Soc.* **2017**, *139*, 3537. [CrossRef]
13. Salvati, E.; Botta, L.; Amato, J.; Saverio Di Leva, F.; Zizza, P.; Gioiello, A.; Pagano, B.; Graziani, G.; Tarsounas, M.; Randazzo, A.; et al. Lead discovery of dual G-quadruplex stabilizers and poly(ADP-ribose) polymerases (PARPs) inhibitors: A new avenue in anticancer treatment. *J. Med. Chem.* **2017**, *60*, 3626. [CrossRef]
14. Wu, Y.; Sun, P.; Zhang, K.; Yang, T.; Yao, H.; Lin, A. Rh(III)-Catalyzed redox-neutral annulation of primary benzamides with diazo compounds: Approach to isoquinolinones. *J. Org. Chem.* **2016**, *81*, 2166. [CrossRef]
15. Newton, C.G.; Wang, S.-G.; Oliveira, C.C.; Cramer, N. Catalytic enantioselective transformations involving C-H bond cleavage by transition-metal complexes. *Chem. Rev.* **2017**, *117*, 8908. [CrossRef]
16. Park, Y.; Kim, Y.; Chang, S. Transition metal-catalyzed C-H amination: Scope, mechanism, and applications. *Chem. Rev.* **2017**, *117*, 9247. [CrossRef]
17. Chen, J.-R.; Hu, X.-Q.; Lu, L.-Q.; Xiao, W.-J. Formal [4+1] annulation reactions in the synthesis of carbocyclic and heterocyclic systems. *Chem. Rev.* **2015**, *115*, 5301. [CrossRef]
18. Ackermann, L. Carboxylate-assisted ruthenium-catalyzed alkyne annulations by C-H/Het-H bond functionalizations. *Acc. Chem. Res.* **2014**, *47*, 281. [CrossRef]
19. Upadhyay, N.S.; Thorat, V.H.; Sato, R.; Annamalai, P.; Chuang, S.-C.; Cheng, C.-H. Synthesis of isoquinolones via Rh-catalyzed C-H activation of substituted benzamides using air as the sole oxidant in water. *Green Chem.* **2017**, *19*, 3219. [CrossRef]
20. Reddy Chidipudi, S.; Burns, D.J.; Khan, I.; Lam, H.W. Enantioselective synthesis of spiroindenes by enol-directed rhodium(III)-catalyzed C-H functionalization and spiroannulation. *Angew. Chem. Int. Ed.* **2015**, *54*, 13975. [CrossRef]
21. Zhang, X.; Si, W.; Bao, M.; Asao, N.; Yamamoto, Y.; Jin, T. Rh(III)-Catalyzed regioselective functionalization of C-H bonds of naphthylcarbamates for oxidative annulation with alkynes. *Org. Lett.* **2014**, *16*, 4830. [CrossRef] [PubMed]
22. Chuang, S.-C.; Gandeepan, P.; Cheng, C.-H. Synthesis of isoquinolines via Rh(III)-catalyzed C-H activation using hydrazone as a new oxidizing directing group. *Org. Lett.* **2013**, *15*, 5750. [CrossRef] [PubMed]
23. Pham, M.V.; Ye, B.; Cramer, N. Access to sultams by rhodium(III)-catalyzed directed C-H activation. *Angew. Chem. Int. Ed.* **2012**, *51*, 10610. [CrossRef] [PubMed]
24. Hyster, T.K.; Rovis, T. Rhodium-catalyzed oxidative cycloaddition of benzamides and alkynes via C-H/N-H Activation. *J. Am. Chem. Soc.* **2010**, *132*, 10565. [CrossRef] [PubMed]
25. Song, G.; Chen, D.; Pan, C.-L.; Crabtree, R.H.; Li, X. Rh-Catalyzed oxidative coupling between primary and secondary benzamides and alkynes: Synthesis of polycyclic amides. *J. Org. Chem.* **2010**, *75*, 7487. [CrossRef] [PubMed]
26. Guimond, N.; Gouliaras, C.; Fagnou, K. Rhodium(III)-Catalyzed isoquinolone synthesis: The N-O bond as a handle for C-N bond formation and catalyst turnover. *J. Am. Chem. Soc.* **2010**, *132*, 6908. [CrossRef]
27. Guimond, N.; Gorelsky, S.I.; Fagnou, K. Rhodium(III)-Catalyzed heterocycle synthesis using an internal oxidant: Improved reactivity and mechanistic studies. *J. Am. Chem. Soc.* **2011**, *133*, 6449. [CrossRef]
28. Mochida, S.; Umeda, N.; Hirano, K.; Satoh, T.; Miura, M. Rhodium-catalyzed oxidative coupling/cyclization of benzamides with alkynes via C-H bond cleavage. *Chem. Lett.* **2010**, *39*, 744. [CrossRef]
29. Xu, X.; Liu, Y.; Park, C.-M. Rhodium(III)-Catalyzed intramolecular annulation through C-H activation: Total synthesis of (±)-antofine, (±)-septicine, (±)-tylophorine, and rosettacin. *Angew. Chem. Int. Ed.* **2012**, *51*, 9372. [CrossRef]

30. Wang, H.; Grohmann, C.; Nimphius, C.; Glorius, F. Mild Rh(III)-Catalyzed C-H activation and annulation with alkyne MIDA Boronates: Short, efficient synthesis of heterocyclic boronic acid derivatives. *J. Am. Chem. Soc.* **2012**, *134*, 19592. [CrossRef]
31. Huckins, J.R.; Bercot, E.A.; Thiel, O.R.; Hwang, T.-L.; Bio, M.M. Rh(III)-Catalyzed C-H activation and double directing group strategy for the regioselective synthesis of naphthyridinones. *J. Am. Chem. Soc.* **2013**, *135*, 14492. [CrossRef]
32. Yu, D.-G.; de Azambuja, F.; Glorius, F. α-MsO/TsO/Cl ketones as oxidized alkyne equivalents: Redox-neutral rhodium(III)-catalyzed C-H activation for the synthesis of N-heterocycles. *Angew. Chem. Int. Ed.* **2014**, *53*, 2754. [CrossRef]
33. Wang, F.; Qi, Z.; Zhao, Y.; Zhai, S.; Zheng, G.; Mi, R.; Huang, Z.; Zhu, X.; He, X.; Li, X. Rhodium(III)-catalyzed atroposelective synthesis of biaryls by C-H activation and intermolecular coupling with sterically hindered alkynes. *Angew. Chem. Int. Ed.* **2020**, *59*, 13288.
34. Chen, J.; Zhang, L.; Zheng, X.; Zhou, J.; Zhong, T.; Yu, C. Synthesis of isoquinolinone derivatives by Rh(III)-catalyzed C-H functionalization of N-ethoxybenzamides. *Synthetic Commun.* **2020**, *50*, 1799. [CrossRef]
35. Ohata, J.; Martin, S.C.; Ball, Z.T. Metal-mediated functionalization of natural peptides and proteins: Panning for bioconjugation gold. *Angew. Chem. Int. Ed.* **2019**, *58*, 6176. [CrossRef]
36. Zhang, C.; Vinogradova, E.V.; Spokoyny, A.M.; Buchwald, S.L.; Pentelute, B.L. Arylation chemistry for bioconjugation. *Angew. Chem. Int. Ed.* **2019**, *58*, 4810. [CrossRef]
37. Rodríguez, J.; Martínez-Calvo, M. Transition-metal-mediated modification of biomolecules. *Chem. Eur. J.* **2020**, *26*, 9792. [CrossRef]
38. Haase, C.; Seitz, O. Chemical Synthesis of Glycopeptides. *Top. Curr. Chem.* **2006**, *267*, 1.
39. Wang, Y.; Cheetham, A.G.; Angacian, G.; Su, H.; Xie, L.; Cui, H. Peptide-drug conjugates as effective prodrug strategies for targeted delivery. *Adv. Drug Deliv. Rev.* **2017**, *110*, 112. [CrossRef]
40. Sunna, A.; Care, A. *Peptides and Peptide-based Biomaterials and their Biomedical Applications*; Springer Nature: Cham, Switzerland, 2017.
41. Hoppenz, P.; Els-Heindl, S.; Beck-Sickinger, A.G. Peptide-drug conjugates and their targets in advanced cancer therapies. *Front. Chem.* **2020**, *8*, 571. [CrossRef]
42. Ojima, I. *Fluorine in Medicinal Chemistry and Chemical Biology*; Wiley-Blackwell: Chichester, UK, 2009.
43. Yoder, N.C.; Kumar, K. Fluorinated amino acids in protein design and engineering. *Chem. Soc. Rev.* **2002**, *31*, 335. [CrossRef] [PubMed]
44. Jaeckel, C.; Koksch, B. Fluorine in peptide design and protein engineering. *Eur. J. Org. Chem.* **2005**, *2005*, 4483. [CrossRef]
45. Salwiczek, M.; Nyakatura, E.K.; Gerling, U.I.; Ye, S.; Koksch, B. Fluorinated amino acids: Compatibility with native protein structures and effects on protein–protein interactions. *Chem. Soc. Rev.* **2012**, *41*, 2135. [CrossRef] [PubMed]
46. Marsh, E.N.G. Fluorinated proteins: From design and synthesis to structure and stability. *Acc. Chem. Res.* **2014**, *47*, 2878. [CrossRef] [PubMed]
47. Berger, A.A.; Völler, J.; Budisa, N.; Koksch, B. Deciphering the fluorine code—The many hats fluorine wears in a protein environment. *Acc. Chem. Res.* **2017**, *50*, 2093. [CrossRef]
48. Huhmann, S.; Koksch, B. Fine-tuning the proteolytic stability of peptides with fluorinated amino acids. *Eur. J. Org. Chem.* **2018**, *2018*, 3667. [CrossRef]
49. Moschner, J.; Stulberg, V.; Fernandes, R.; Huhmann, S.; Leppkes, J.; Koksch, B. Approaches to obtaining fluorinated α-amino acids. *Chem. Rev.* **2019**, *119*, 10718. [CrossRef]
50. Smits, R.; Cadicamo, C.D.; Burger, K.; Koksch, B. Synthetic strategies to α-trifluoromethyl and α-difluoromethyl substituted α-amino acids. *Chem. Soc. Rev.* **2008**, *37*, 1727. [CrossRef]
51. Vorobyeva, D.V.; Petropavlovskikh, D.A.; Godovikov, I.A.; Nefedov, S.E.; Osipov, S.N. Rh(III)-Catalyzed C-H activation/annulation of aryl hydroxamates with CF_3-containing α-propargyl α-amino acid derivatives. *Eur. J. Org. Chem.* **2021**, *2021*, 1883. [CrossRef]
52. Iagafarova, I.E.; Vorobyeva, D.V.; Peregudov, A.S.; Osipov, S.N. CF_3-Carbenoid C-H functionalization of (hetero)arenes under chelation-controlled RhIII catalysis. *Eur. J. Org. Chem.* **2015**, *2015*, 4950. [CrossRef]
53. Iagafarova, I.E.; Vorobyeva, D.V.; Loginov, D.A.; Peregudov, A.S.; Osipov, S.N. Rh(III)-catalyzed CF3-carbenoid C-7 functionalization of indolines. *Eur. J. Org. Chem.* **2017**, *2017*, 840. [CrossRef]
54. Vorobyeva, D.V.; Vinogradov, M.M.; Nelyubina, Y.V.; Loginov, D.A.; Peregudov, A.S.; Osipov, S.N. Rhodium(III)-catalyzed CF3-carbenoid C-H functionalization of 6-arylpurines. *Org. Biomol. Chem.* **2018**, *16*, 2966. [CrossRef] [PubMed]
55. Petropavlovskikh, D.A.; Vorobyeva, D.V.; Godovikov, I.A.; Nefedov, S.E.; Filippov, O.A.; Osipov, S.N. Lossen rearrangement by Rh(III)-catalyzed C-H activation/annulation of aryl hydroxamates with alkynes: Access to quinolone-containing amino acid derivatives. *Org. Biomol. Chem.* **2021**, *19*, 9421. [CrossRef] [PubMed]
56. Shchetnikov, G.T.; Zotova, M.A.; Bruneau, C.; Dixneuf, P.H.; Osipov, S.N. Synthesis of α-Alkynyl-β,β,β-trifluoroalanine Derivatives by Sonogashira Cross-Coupling Reaction. *Eur. J. Org. Chem.* **2010**, *2010*, 1587. [CrossRef]
57. Ullyot, G.E. Basic ether-substituted isoquinolines. US Patent 2612503, 30 September 1952.
58. Merck, G. Vorläufige Notiz über eine neue organische Base im Opium. *Liebigs Ann. Chem.* **1848**, *66*, 125. [CrossRef]
59. Graulich, A.; Scuvée-Moreau, J.; Seutin, V.; Liégeois, J.-F. Orthogonal Synthesis of Indolines and Isoquinolines via Aryne Annulation. *J. Med. Chem.* **2005**, *48*, 4972.
60. Sheldrick, G.M. Crystal Structure Refinement with SHELXL. *Acta Cryst.* **2015**, *C71*, 3.

molecules

MDPI

Article

Synthesis of 1,5-Substituted Pyrrolidin-2-ones from Donor–Acceptor Cyclopropanes and Anilines/Benzylamines

Maksim A. Boichenko [1], Andrey Yu. Plodukhin [1], Vitaly V. Shorokhov [1], Danyla S. Lebedev [1], Anastasya V. Filippova [1], Sergey S. Zhokhov [1], Elena A. Tarasenko [1], Victor B. Rybakov [1], Igor V. Trushkov [2,*] and Olga A. Ivanova [1,*]

[1] Department of Chemistry, M. V. Lomonosov Moscow State University, Leninskie Gory 1-3, 119991 Moscow, Russia
[2] N. D. Zelinsky Institute of Organic Chemistry, Leninsky Pr. 47, 119334 Moscow, Russia
* Correspondence: trush@ioc.ac.ru (I.V.T.); iv@kinet.chem.msu.ru (O.A.I.); Tel.: +7-916-645-9951 (I.V.T.)

Abstract: We developed a straightforward synthetic route to pharmacologically important 1,5-substituted pyrrolidin-2-ones from donor–acceptor cyclopropanes bearing an ester group as one of the acceptor substituents. This method includes a Lewis acid-catalyzed opening of the donor–acceptor cyclopropane with primary amines (anilines, benzylamines, etc.) to γ-amino esters, followed by in situ lactamization and dealkoxycarbonylation. The reaction has a broad scope of applicability; a variety of substituted anilines, benzylamines, and other primary amines as well as a wide range of donor–acceptor cyclopropanes bearing (hetero)aromatic or alkenyl donor groups and various acceptor substituents can be involved in this transformation. In this process, donor–acceptor cyclopropanes react as 1,4-*C*,*C*-dielectrophiles, and amines react as 1,1-dinucleophiles. The resulting di- and trisubstituted pyrrolidin-2-ones can be also used in subsequent chemistry to obtain various nitrogen-containing polycyclic compounds of interest to medicinal chemistry and pharmacology, such as benz[*g*]indolizidine derivatives.

Keywords: donor–acceptor cyclopropanes; primary amines; pyrrolidin-2-ones; benz[*g*]indolizidines

Citation: Boichenko, M.A.; Plodukhin, A.Y.; Shorokhov, V.V.; Lebedev, D.S.; Filippova, A.V.; Zhokhov, S.S.; Tarasenko, E.A.; Rybakov, V.B.; Trushkov, I.V.; Ivanova, O.A. Synthesis of 1,5-Substituted Pyrrolidin-2-ones from Donor–Acceptor Cyclopropanes and Anilines/Benzylamines. *Molecules* **2022**, *27*, 8468. https://doi.org/10.3390/molecules27238468

Academic Editors: Alexey M. Starosotnikov, Maxim A. Bastrakov, Igor L. Dalinger and Jia-Rong Chen

Received: 29 October 2022
Accepted: 23 November 2022
Published: 2 December 2022

Publisher's Note: MDPI stays neutral with regard to jurisdictional claims in published maps and institutional affiliations.

1. Introduction

The γ-lactam skeleton is a component of many biologically active molecules, both natural and synthetic, including approved drugs [1,2]. In particular, 1,5-diarylpyrrolidin-2-ones or 5-aryl-1-benzylpyrrolidones have great potential in pharmacology and medicinal chemistry (Figure 1). Among 1,5-diarylpyrrolidin-2-ones, there are selective and effective inhibitors of histone deacetylases 5 and 6 [3–5], cannabinoid receptor 1 (CB1) [6,7], cyclin-dependent kinase CDK_2 [8], tankyrase [9], etc. They are also capable of inhibiting glutaminyl cyclase [10] and the glucagon receptor [11]. In addition, 5-aryl-1-benzylpyrrolidones have been shown to antagonize the dual orexin receptor at the submicromolar level [12,13] and calcitonin gene-related peptide type I receptors at the subnanomolar level [14]. Therefore, the synthesis of these promising azaheterocycles is an urgent problem in synthetic organic and pharmaceutical chemistry.

Although many methods for the γ-lactam synthesis are known [15–18], the development of new and simple strategies that also make it possible to introduce desired substituents into the resulting products remains an urgent task. Our interest in this problem is related to the possibility of solving it using the donor–acceptor (DA) cyclopropane [19–33] reactivity, which has been the subject of our studies in recent years [27,28,34–39].

In general, two types of transformations of DA cyclopropanes can be used for the synthesis of 1,5-substituted pyrrolidin-2-ones. The first one is the (3 + 2)-cycloaddition of 2-aryl- or 2-alkenylcyclopropane-1,1-diesters with the appropriate isocyanates [40,41]. This process directly afforded the corresponding pyrrolidones (Scheme 1a); however, the

resulting products contain two acceptor substituents at the C(3) atom; these groups must be removed to obtain the aforementioned bioactive compounds.

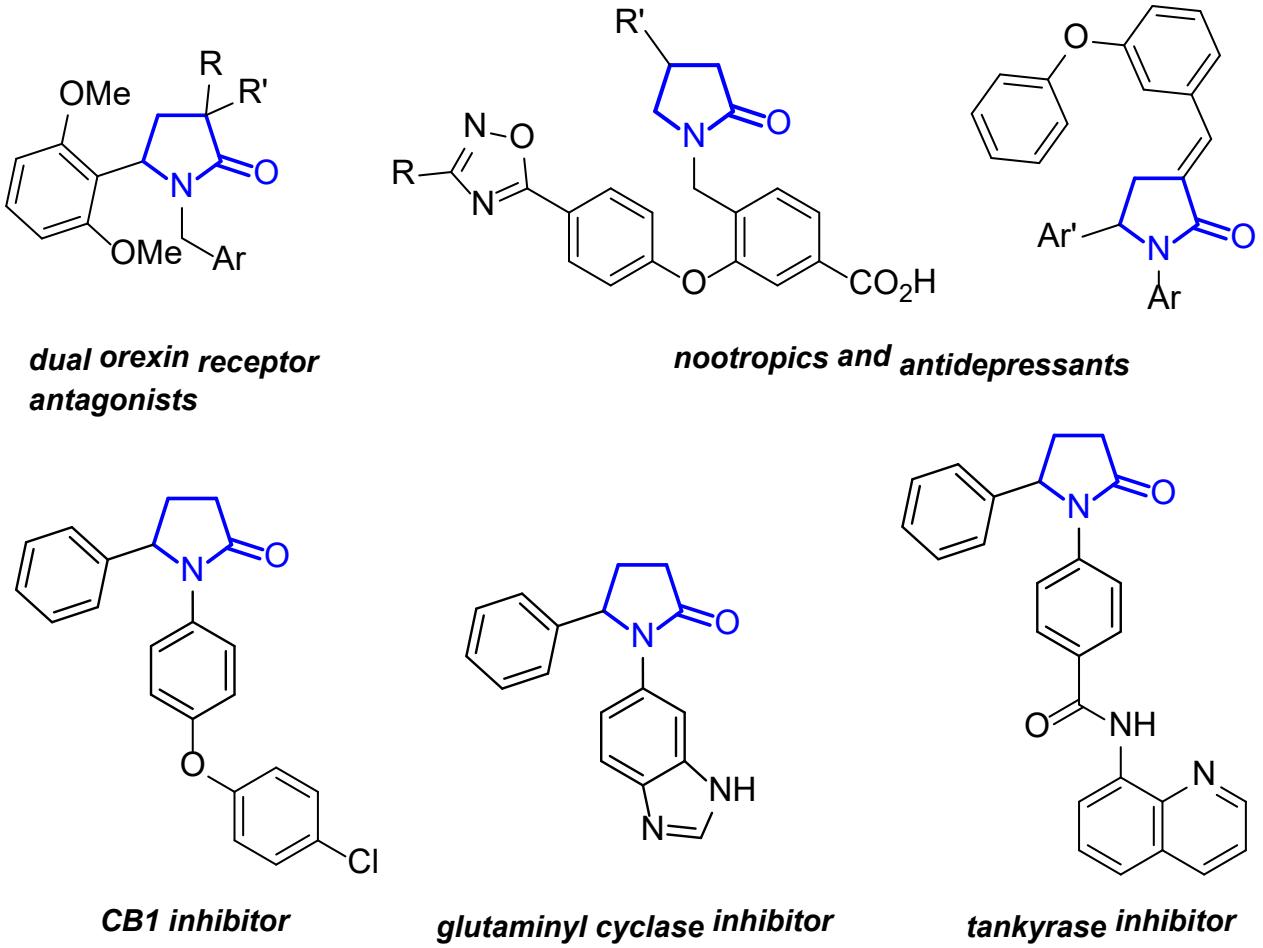

Figure 1. Bioactive molecules containing 1,5-diarylpyrrolidin-2-one or 5-aryl-1-benzylpyrrolidin-2-one frameworks.

Alternatively, these DA cyclopropanes can undergo a small ring opening with *N*-nucleophiles followed by cyclization producing the target γ-lactams. For example, we have recently developed a method for the synthesis of 1,5-substituted pyrrolidin-2-ones, the key step of which is the opening of the DA cyclopropane ring with an azide ion (Scheme 1b) [37–39]. This method includes isolation and purification of the intermediate azides; a simpler and general approach to the synthesis of 1,5-disubstituted pyrrolidin-2-ones **2**, **3** can be developed based on the reaction of DA cyclopropanes **1** with the corresponding primary amines, such as anilines, benzylamines, etc.

The reactions of DA cyclopropanes with primary amines affording both acyclic and various cyclic products, depending on the structure of the reagents and reaction conditions, have been well studied [29,42–70]. However, only a few examples of the use of this reactivity for the synthesis of 1,5-functionalized pyrrolidin-2-ones have been described [59–70]. Usually, these examples were reported as postmodifications of the primary acyclic products [59–64] that provides not the principal advantage over other stepwise transformations. The one-step formation of the requisite pyrrolidones was achieved either on specific substrates [65–70] (Scheme 1c), i.e., has limited application, or proceeded under harsh conditions, giving pyrrolidones in moderate yields [62,64].

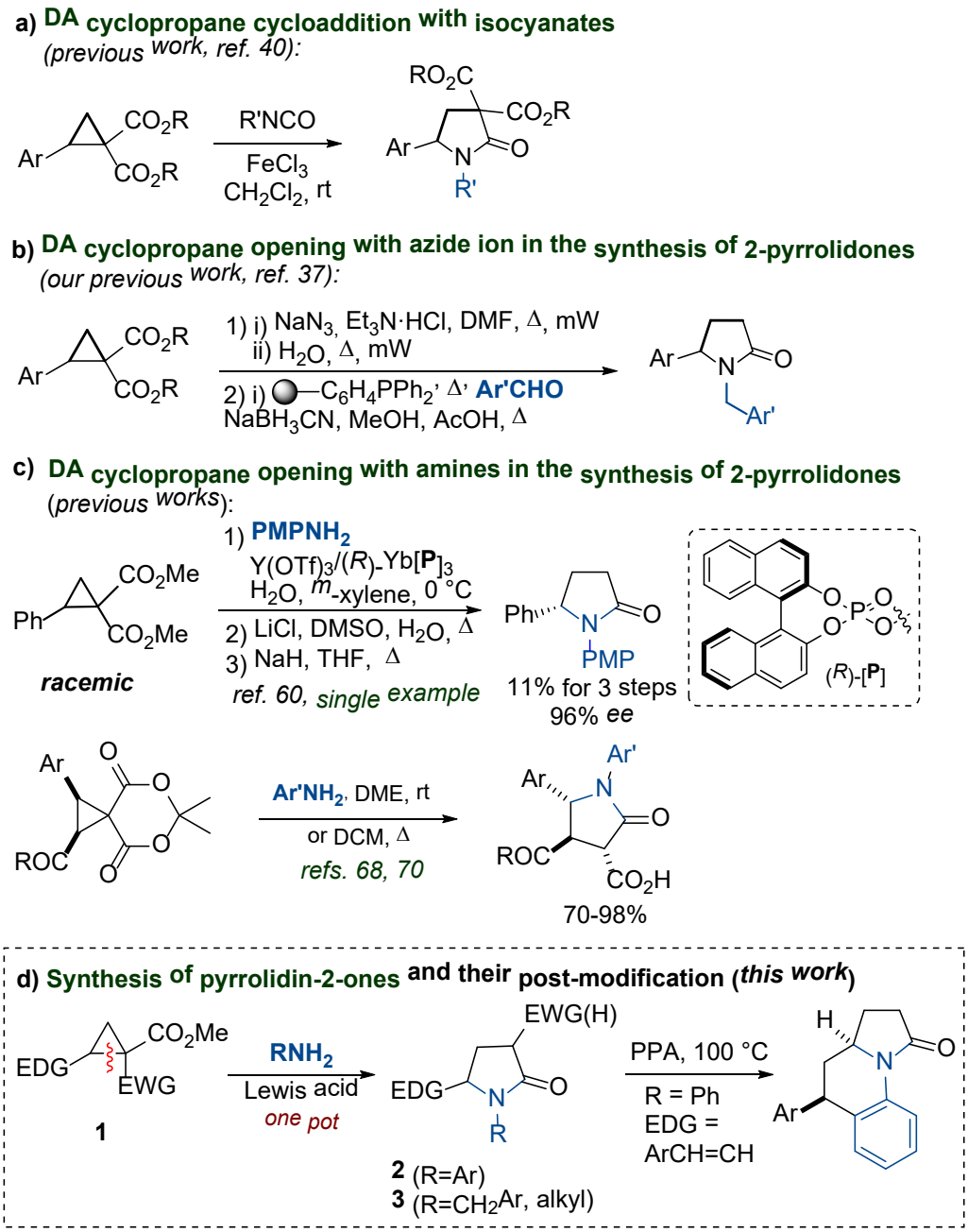

Scheme 1. Synthesis of pyrrolidin-2-ones from DA cyclopropanes. (**a**–**c**) The reported methods for the synthesis of 1,5-substitutted pyrrolidine-2-ones from DA cyclopropanes. (**d**) Transformations reported in this work.

In this paper, we demonstrate that the transformation of DA cyclopropanes to 1,5-substituted pyrrolidones can be implemented as a *one-pot* process via a Lewis acid-initiated, three-membered ring opening with anilines, benzylamines, and other primary amines, followed by lactamization, as well as further modifications of the obtained pyrrolidones to polycyclic molecules such as benz[*g*]indolizidine derivatives (Scheme 1d).

2. Results and Discussion

We started our investigation with the study of the reaction of model cyclopropane **1a** with aniline, leading to the acyclic product **4a** (Table 1). To catalyze the reaction, we tested several available Lewis acids, which are commonly used for initiating reactions of DA cyclopropanes with *N*-nucleophiles. The reaction was carried out in dichloroethane

(DCE) at room temperature for 1 h for all tested initiators. We found that $Al(OTf)_3$ did not induce the target transformation (Table 1, entry 1). Conversely, in the presence of $Fe(OTf)_3$, $Sc(OTf)_3$, or $Zn(OTf)_2$, cyclopropane **1a** reacted with aniline affording acyclic product **4a** in reasonable to good yields (Table 1, entries 2–5). The best results were achieved using 20 mol% $Ni(ClO_4)_2 \cdot 6H_2O$ or $Y(OTf)_3$; with these catalysts, compound **4a** was obtained in more than a 90% yield (Table 1, entries 6, 9). The decrease in nickel perchlorate loading led to a decrease in the product yield (Table 1, entries 7–9). The yield also decreased with increasing reaction time or when the reaction was carried out with heating; in both cases, the formation of byproducts was detected. When Brønsted acid, TfOH, was used, no reaction occurred at all presumably due to its neutralization with an excess of amine (Table 1, entry 10). With all the studied Lewis acids, only the acyclic product **4a** was formed; its cyclization to pyrrolidin-2-one did not occur at room temperature.

Table 1. Optimization of reaction conditions for the model cyclopropane **1a** opening with aniline [1].

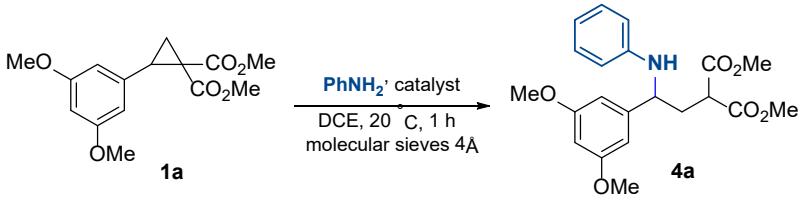

Entry	Catalyst	(mol%)	Yield of 4a, % [2]
1	$Al(OTf)_3$	20	-
2	$Fe(OTf)_3$	20	78 [3]
3	$Sc(OTf)_3$	10	60 [3,4]
4	$Sc(OTf)_3$	20	84
5	$Zn(OTf)_2$	20	80 [3]
6	$Y(OTf)_3$	20	93
7	$Ni(ClO_4)_2 \cdot 6H_2O$	5	21 [3]
8	$Ni(ClO_4)_2 \cdot 6H_2O$	10	50 [3]
9	$Ni(ClO_4)_2 \cdot 6H_2O$	20	92
10	TfOH	20	-

[1] Concentration of **1a** was 0.2 M. [2] Isolated yield. [3] NMR yields (hexamethyldisiloxane was used as internal standard). [4] Concentration of **1a** was 0.03 M.

Then, the lactamization of γ-aminoester **4a** was investigated. We found that the cyclization of compound **4a** proceeded under the reflux of its toluene solution with acetic acid. Moreover, we showed that the crude reaction mixture obtained by a nickel perchlorate-induced reaction of cyclopropane **1a** with aniline, when refluxing with 2 equiv. acetic acid in toluene efficiently produced the corresponding pyrrolidin-2-one in a one-vessel operation. This compound was obtained as a mixture of two diastereomers due to the presence of an ester group at the C(3) atom of the pyrrolidone ring. To obtain the target bioactive 1,5-diarylpyrrolidin-2-ones, this group must be removed by one of the known dealkoxycarbonylation methods. To further simplify the synthetic sequence and increase the practicality of this strategy, we realized this transformation in *one pot* using alkaline saponification of the ester group followed by thermolysis (Scheme 2). As a result, pyrrolidone **2a** was synthesized by a four-step procedure, requiring chromatographic purification only at the last stage, with an overall yield of 70%.

With the optimized conditions in hand, we investigated the reaction scope using diversly substituted DA cyclopropanes and a range of anilines (Scheme 3). We found that this *one pot* transformation was efficient for a series of DA cyclopropanes where the electron-rich het(aryl) group or styryl group was the donor substituent. A broad variety of substituents on the aromatic moiety of both DA cyclopropanes and anilines, such as halogen, alkyl, and alkoxy, were well-tolerated in these transformations. The yields of the obtained pyrrolidones **2** varied considerably from moderate to good; however, it should be taken into account that these yields were given for four-step procedures. This

is also reflected in the complex dependence of the obtained yields on the structure of the starting compounds. For example, DA cyclopropanes bearing electron-abundant aromatic substituents are typically more reactive than DA cyclopropanes with less electron-rich donors; i.e., the conversion time is shorter. However, their side reactions also proceed faster, and that can provide lower yields of the target products. For multistage processes, the overall effect of the substituent on the reaction yields is even more complex and cannot be followed by any simple model.

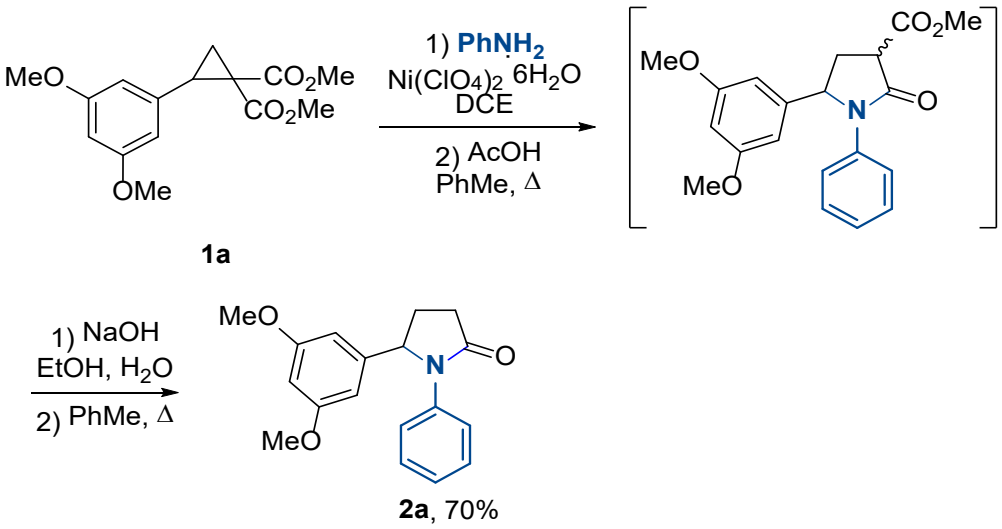

Scheme 2. One-pot synthesis of pyrrolidone **2a**.

For example, the moderate yield of pyrrolidone **2f** obtained from highly reactive furyl-substituted DA cyclopropane presumably resulted from the well-known tendency of the furan ring to undergo various acid-induced transformations [71,72]. In contrast, compound **2b** was formed in a 79% yield. Other reactive DA cyclopropanes, thienyl- and styryl-derived, produced the corresponding pyrrolidones **2g**,**h** in about a 60% yield. Less reactive 2-phenyl- and 2-(*p*-tolyl)cyclopropane-1,1-diesters produced the corresponding pyrrolidones **2c**,**d** in 47 and 45% yields. The structure of the compound **2c** was unambiguously proven by single-crystal X-ray data [73]. Cyclopropane-1,1-diesters containing the 2-nitrophenyl or 3-pyridyl groups at the C(2) atom of the small ring afforded the expected pyrrolidones **2i**,**j** in low yields. However, the yield of **2i** was improved by replacing the nickel perchlorate with 20 mol% $Y(OTf)_3$. Anilines containing both electron-withdrawing and electron-donating substituents, including fluorine or bromine in the *ortho* position, reacted well. The exceptions were 4-nitroaniline, for which the first step occurred only when the reaction mixture was refluxed, and 2-nitroaniline and 1,2-phenylenediamine, which did not afford the desired products **2k**,**l** at all. With these anilines, the process was stopped after the formation of the open-chain products **4b**,**c** (see below); cyclization products were not detected in the reaction mixtures even in trace amounts.

To demonstrate the efficiency of this *one pot* process, we scaled up the synthesis of compound **2b** using 1.00 g (3.08 mmol) of 3,4,5-trimethoxyphenyl-substituted cyclopropane **1b** and 472 mg (3.08 mmol) of 2-fluoroaniline. With this loading, the yield of compound **2b** was 841 mg (79%).

It is worth noting that, despite the potential ability of anilines to serve as ambident nucleophiles, in the studied reactions, they attacked the three-membered ring exclusively with the nitrogen atom, providing no isomeric products via the Friedel–Crafts alkylation of the electron-rich aromatic ring.

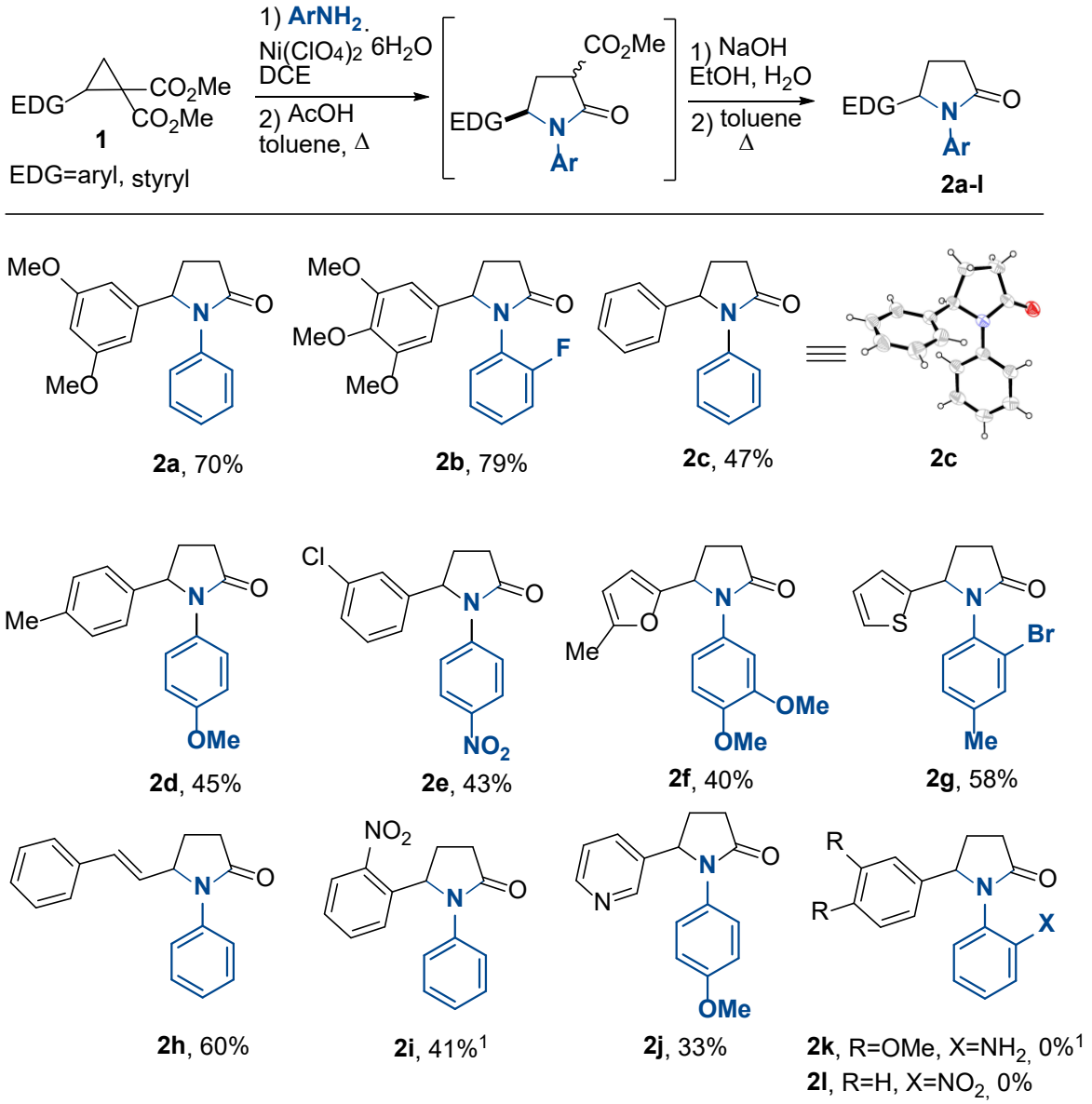

Scheme 3. Synthesis of *N*-aryl and *N*-benzyl-substituted γ-lactams **2**, **3**. [1] $Y(OTf)_3$ was used.

Benzylamines are known to be more nucleophilic than the corresponding anilines. The increased reactivity of benzylamines allowed us to synthesize pyrrolidones **3** in good yields by their direct reaction with DA cyclopropanes **1** by refluxing a dichloroethane solution in the presence of $Ni(ClO_4)_2 \cdot 6H_2O$ without an additional lactamization step. Next, we used two methods of dealkoxycarbonylation of 3-substituted pyrrolidones. The first one included alkaline hydrolysis followed by decarboxylation according to the method developed for pyrrolidones **2** (method **A**, Scheme 4). Alternatively, dealkoxycarbonylation using a NaCl-promoted Krapcho reaction in wet DMSO at 160 °C under microwave (MW) irradiation provided pyrrolidones **3** in reasonable yields (method **B**, Scheme 4). For example, benzylamine and alkoxy-substituted benzylamines produced compounds **3a**–**d** in up to 70% yields. In the reactions of DA cyclopropane with furfurylamine and (1*H*-indol-3-yl)methylamine, the corresponding pyrrolidones **3e** and **3f** were obtained in 32% and 42% yields. Given that these yields corresponded to a four-step sequence realized as a *one pot* procedure, these yields can be considered reasonable.

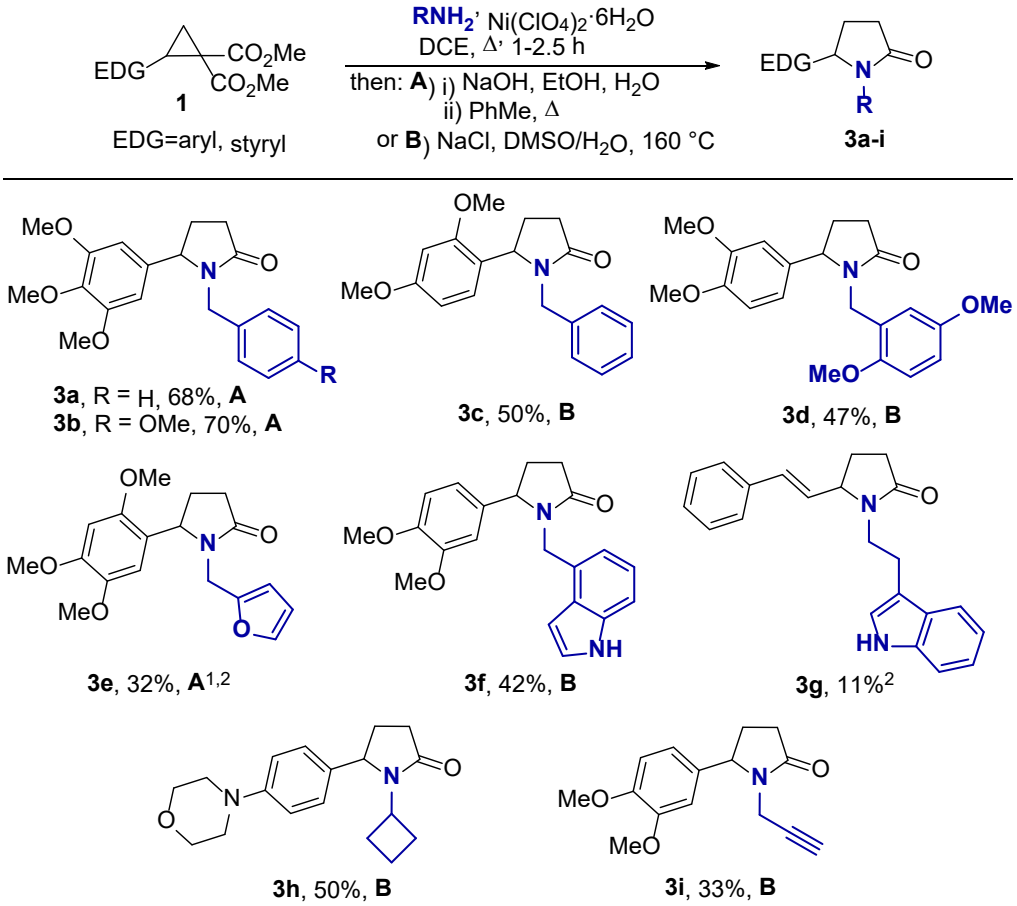

Scheme 4. Synthesis of γ-lactams **3**. [1] The reaction was performed at room temperature. [2] The reaction included a lactamization step under reflux in presence of AcOH in toluene.

Moreover, we applied the developed approach to the synthesis of 1-alkyl-5-arylpyrrolidones from DA cyclopropanes and some aliphatic amines (Scheme 4). Cyclobutylamine and propargylamine were found to participate quite efficiently in this transformation, affording the corresponding pyrrolidones **3h**,**i** in yields close to those of **3c**–**f**, although these substrates required a long reaction time (see Section 3). In contrast, tryptamine gave rise to the corresponding **3g** product in only an 11% yield. A significant tarring of the reaction mixture was detected in this reaction. When simple primary aliphatic amines, such as methylamine or ethylamine, were reacted with cyclopropane **1a** under the same reaction conditions, only unidentified byproducts were formed.

It was pointed out that above that, *o*-nitroaniline and 1,2-phenylenediamine did not produce the target products **2** under standard conditions. We tested their reactivity toward DA cyclopropanes **1** in the presence of the same catalysts in more detail (Scheme 5). We found that the full consumption of 2-phenylcyclopropane-1,1-dicarboxylate **1k** in its reaction with *o*-nitroaniline catalyzed by $Ni(ClO_4)_2 \cdot 6H_2O$ required 2 h of refluxing the solution in dichloroethane. Under these conditions, the expected acyclic product **4b** was obtained in a 71% yield. The reaction of 3,4-dimethoxyphenyl-substituted cyclopropane **1j** with 1,2-phenylenediamine under the same conditions produced the acyclic product **4c** only in a low yield. Heating this reaction mixture at 100 °C in chlorobenzene resulted in a complex mixture of unidentified products. However, the acyclic compound **4c** was obtained in a reasonable yield at room temperature using $Y(OTf)_3$ as an initiator (Scheme 5). This product was unstable, and all attempts to cyclize it were unsuccessful.

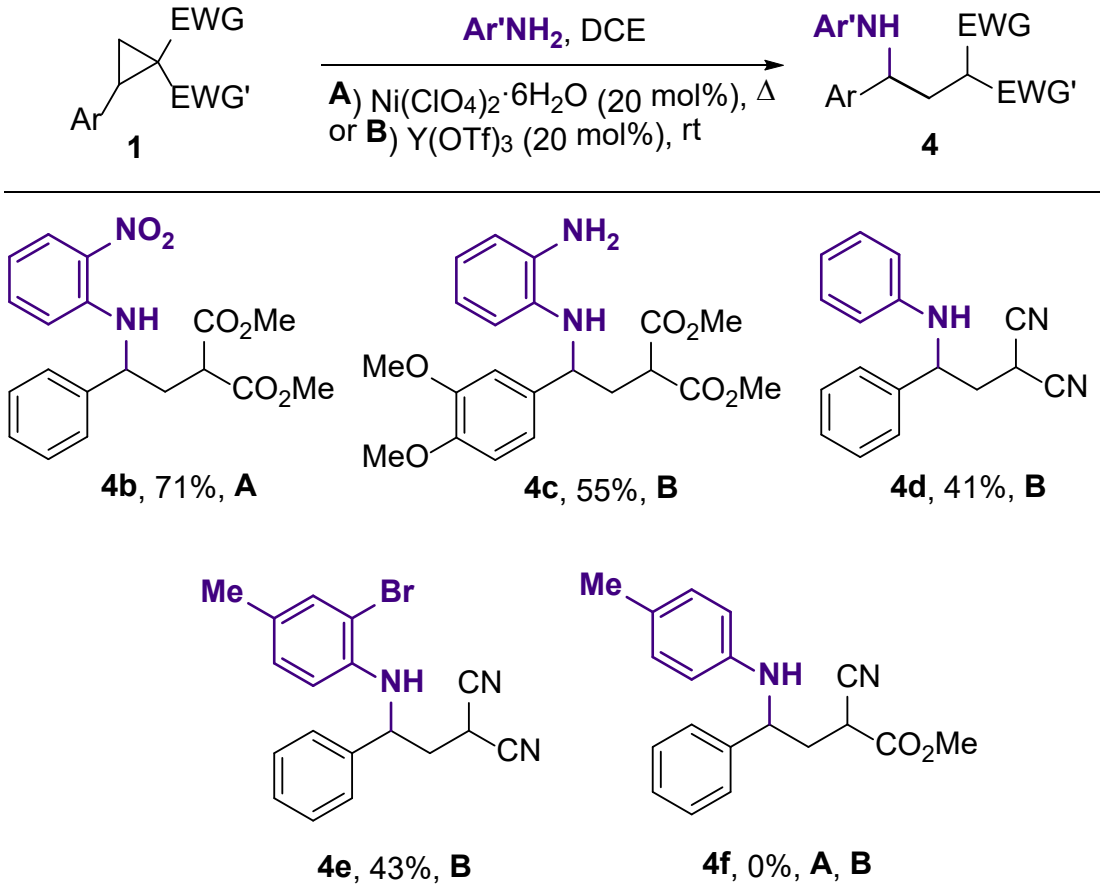

Scheme 5. Synthesis of acyclic products **4b**–**f**.

To test the generality of the DA cyclopropane ring opening with anilines, we tried to involve substrates with other acceptor groups in this reaction (Scheme 5). 2-Phenylcyclopropane-1,1-dicarbonitrile was found to undergo ring opening with aniline or 2-bromo-4-methylaniline under catalysis with 25 mol% $Y(OTf)_3$ at room temperature for 4 days. The full conversion of these substrates required a significantly longer reaction time compared to the corresponding 1,1-diesters. Despite the mild reaction conditions, **4d**,**e** were isolated only in 41% and 43% yields, presumably due to the competitive realization of the side processes resulting from the coexistence of the amino and cyano groups. 2-Phenyl-1-cyanocyclopropanecarboxylate turned out to be a less reactive substrate, which did not undergo conversion to amine **4f** even at a high temperature. Other Lewis acids, such as $Fe(OTf)_3$, $Sc(OTf)_3$, and $Ni(ClO_4)_2·6H_2O$, failed also to induce the reaction of this substrate with anilines.

Most biologically active compounds bearing chiral centers have different activities for different stereoisomers. This means that methods of their preparation in an optically pure form are highly desirable. Obviously, this also applies to bioactive-substituted pyrrolidones of types **2** and **3**, which can be considered as cyclic analogs of GABA. We tested the possibility of using the developed procedure for the synthesis of chiral pyrrolidones **2** starting from optically active DA cyclopropane **1** as a substrate. We found that dimethyl (*S*)-2-(*p*-tolyl)cyclopropane-1,1-dicarboxylate (*S*)-**1c** was converted to the corresponding γ-lactam with a full inversion of the absolute configuration of the chiral center (Scheme 6). This result is consistent with previous investigations demonstrating that the nucleophilic ring opening of DA cyclopropanes under catalysis with moderately activating Lewis acids proceeds by an S_N2-like mechanism, and subsequent stages (cyclization, saponification, and decarboxylation) do not affect the chiral center.

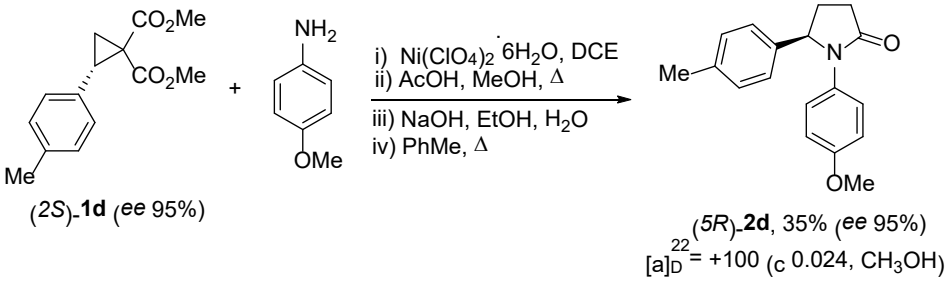

Scheme 6. Synthesis of (*R*)-γ-lactam (**2d**).

The synthetic utility of the developed transformations can be significantly extended by diverse postmodifications of their multiple functionalities of the synthesized pyrrolidones **2**,**3**, that allows for preparing complex azaheterocycles. In particular, the treatment of pyrrolidone **2h** with PPA at 100 °C produced benz[*g*]indolizidine **5** in an acceptable yield (Scheme 7). Based on NOESY spectroscopy [73] and a comparison of its spectra with spectral data for the related compounds described earlier [74], the hydrogen atoms at the stereogenic centers in compound **5** have a *cis* arrangement.

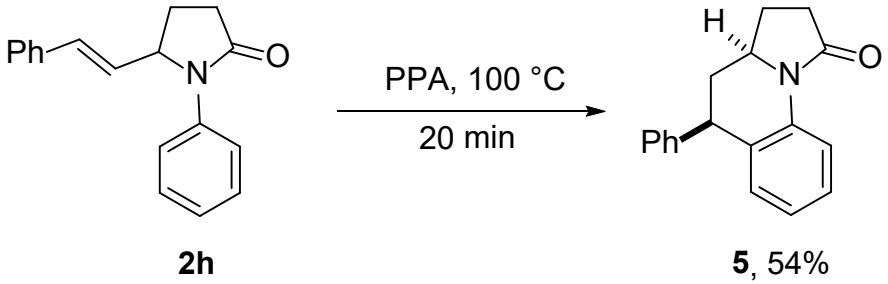

Scheme 7. Synthesis of benz[*g*]indolizidine **5**.

3. Experimental Section

3.1. General Information

The structures of synthesized compounds were elucidated with the aid of 1D NMR (^{1}H, ^{13}C) and 2D NMR (NOESY, HSQC and HMBC ^{1}H-^{13}C) spectroscopy. NMR spectra were acquired on Avance 600 and Avance 500 (Bruker, Billerica, MA, USA) and 400-MR (Agilent, Santa Clara, CA, USA) spectrometers at room temperature; the chemical shifts δ were measured in ppm with respect to solvent (1H: $CDCl_3$, δ = 7.27 ppm; CD_3OD, δ = 3.35 ppm; ^{13}C: $CDCl_3$, δ = 77.0 ppm; CD_3OD: ^{13}C: δ = 49.9 ppm). Splitting patterns were designated as s, singlet; d, doublet; m, multiplet; dd, double doublet; and br, broad. Coupling constants (J) were in Hertz. Infrared spectra were recorded on an FTIR spectrometer ALPHA II (Bruker, Billerica, MA, USA) in KBr for solid substances and as thin film for oils. High resolution and accurate mass measurements were carried out using a micrOTOF-Q^{TM} ESI-TOF (Electrospray Ionization/Time of Flight, Bruker, Billerica, MA, USA). Elemental analyses were performed with an EA-1108 CHNS elemental analyzer instrument (Fisons, Ipswich, UK). Melting points (mp) were measured using a Stuart® SMP3 melting point apparatus (Cole-Parmer, Stone, Staffordshire, UK). Microwave reactions were performed in a Monowave 200—Anton Paar microwave reactor in sealed reaction vessels. The temperature was monitored with installed IR detector. X-Ray analysis was performed on STOE STADI VARI PILATUS-100K diffractometer (Stoe & Sie, Darmstadt, Germany). Analytical thin-layer chromatography (TLC) was carried out with silica gel plates (silica gel 60, F_{254}, supported on aluminum); visualization was performed using a UV lamp (365 nm). Column chromatography was performed on silica gel 60 (230–400 mesh, Merck, Darmstadt, Germany). Enantiomeric purity of the optically active compounds was determined by chiral HPLC with a Hitachi LaChrome Elite-2000 chromatograph (Hitachi Hugh-Tech Corp, Toranomonon Minato-Ku, Japan) using a Daicel (Daicel Corp, Osaka, Japan) Chiralcel

OD-H column (0.46 × 25 cm) at room temperature. The column was eluted with heptane/*i*-PrOH = 70:30 at a flow rate of 1 mL/min, and peak detection was accomplished using a UV detector at 219 nm. Optical rotation was measured on a Krüss P8000 polarimeter (A. Krüss Optronic GmbH, Hamburg, Germany). All reactions were carried out using freshly distilled and dry solvents. Cyclopropanes **1** were prepared by Knoevenagel/Corey–Chaykovsky reaction sequences from the corresponding aldehydes [75,76]. Compounds **2c**,**j**, **3b**,**c**, and (2*S*)-**1d** were described previously [15–17,39,77,78]. Commercial reagents employed in the synthesis were analytical-grade, obtained from Sigma-Aldrich (St. Louis, MO, USA) or Alfa Aesar (Ward Hill, MA, USA). The ^{1}H NMR and ^{13}C NMR for synthesized compounds as well as 2D (HSQC and HMBC) NMR spectra for selected compounds are available in the Supplementary Materials.

3.2. Synthesis of Pyrrolidin-2-ones 2,3 from Anilines and Benzylamines

3.2.1. General Procedure 1

To a 0.2 M solution of aniline or benzylamine (1.0–1.2 equiv.) in DCE in the presence of molecular sieves, 4 Å $Ni(ClO_4)_2{\cdot}6H_2O$ or $Y(OTf)_3$ (0.2 equiv.) was added under Ar atmosphere; then, cyclopropane **1** (1–4 mmol, 1.0 equiv.) was added. The resulting mixture was stirred at room temperature for 1–3 h, diluted with dichloromethane (DCM), and filtered through a short pad of silica gel using EtOAc as the eluent. The filtrate was concentrated under vacuum; the residue was dissolved in toluene (0.13 M). Next, acetic acid (2.0 equiv.) was added, and the reaction mixture was stirred under reflux for 7 h. Then, solvent was removed under vacuum, and residue was dissolved in ethanol (0.17 M); 1M aq. solution of sodium hydroxide (2.0 equiv.) was added in one portion. The reaction mixture was stirred at room temperature for 2 h, and after that, ethanol was removed under vacuum. The residue was diluted with water, and 1M HCl was added until pH 1. The resulting mixture was extracted with ethyl acetate (3 × 10 mL). Combined organic layers were dried with Na_2SO_4 and concentrated in vacuo. The residue was dissolved in toluene (0.07 M) and was refluxed for 7 h. The solvent was removed under vacuum; the pure product was isolated by silica gel column chromatography.

3.2.2. General Procedure 2

To a 2 M solution of cyclopropane **1** (1 equiv.) and benzylamine (1.2 equiv.) in DCM or DCE in the presence of molecular sieves, 4 Å $Ni(ClO_4)_2{\cdot}6H_2O$ (0.1 equiv.) was added under Ar atmosphere The reaction mixture was placed into oil bath, which was preheated to 45 °C, and stirred at the same temperature for 1–2.5 h, and after, it was cooled to room temperature and diluted with DCM. The resulting solution was passed through a plug of silica using 1:1 petroleum ether:EtOAc system as an eluent. Concentration under reduced pressure gave a residue, which was dissolved in DMSO/H_2O mixture (3:1, 0.16 M). To this solution, NaCl (1.5 equiv.) was added; the resulting mixture was heated at 160 °C under MW irradiation for 4–6 h. Then, the reaction mixture was diluted with H_2O and extracted with EtOAc three times. Combined organic layers were washed with brine, dried with Na_2SO_4, and concentrated in vacuo. Pure product was isolated by silica gel column chromatography.

5-(3,5-Dimethoxyphenyl)-1-phenylpyrrolidin-2-one (**2a**) was obtained from dimethyl 2-(3,5-dimethoxyphenyl)cyclopropane-1,1-dicarboxylate (300 mg, 1.02 mmol), aniline (0.1 mL, 1.10 mmol), $Ni(ClO_4)_2{\cdot}6H_2O$ (75 mg, 0.2 mmol), DCE (5.1 mL), AcOH (120 μL), toluene (8.0 mL), NaOH (84 mg, 2.1 mmol), ethanol (5.9 mL), and water (2.0 mL) according to the general procedure **1**. Yield: 210 mg (69%); white solid, R_f = 0.34 (ethyl acetate:petroleum ether; 1:1). ^{1}H NMR ($CDCl_3$, 600 MHz): δ 7.44 (d, ^{3}J = 7.9 Hz, 2H, Ph), 7.27–7.25 (m, 2H, Ph), 7.08–7.06 (m, 1H, Ph), 6.37 (d, ^{4}J = 2.0 Hz, 2H, Ar), 6.33–6.32 (m, 1H, Ar), 5.17 (dd, ^{3}J = 7.2 Hz, ^{3}J = 4.2 Hz, 1H, CH), 3.73 (s, 6H, 2 × CH_3O), 2.80–2.74 (m, 1H, CH_2), 2.64–2.56 (m, 2H, CH_2), 2.03–1.97 (m, 1H, CH_2). ^{13}C{^{1}H} NMR ($CDCl_3$, 150 MHz): δ 174.8 (CO), 161.3 (2 × C), 144.0 (C), 138.3 (C), 128.7 (2 × CH), 124.9 (CH), 122.0 (2 × CH), 103.9 (2 × CH), 99.2 (CH), 63.9 (CH), 55.3 (2 × CH_3O), 31.3 (CH_2), 29.3 (CH_2). IR (KBr, cm^{-1}) 2996, 2980, 2941, 2904, 2874, 2840, 1693, 1654, 1613, 1594, 1538, 1499, 1490, 1482, 1461, 1443, 1429, 1370,

1352, 1318, 1284, 1250, 1227, 1201, 1162, 1145, 1117, 1066, 1030, 1011, 978. HRMS ESI-TOF: m/z = 298.1435 $[M + H]^+$ (298.1438 calcd. for $C_{18}H_{20}NO_3^+$).

5-(3,4,5-Trimethoxyphenyl)-1-(2-fluorophenyl)pyrrolidin-2-one (**2b**) was obtained from dimethyl 2-(3,4,5-dimethoxyphenyl)cyclopropane-1,1-dicarboxylate (1.00 g, 3.08 mmol), 2-fluoroaniline (472 mg, 3.08 mmol), $Ni(ClO_4)_2 \cdot 6H_2O$ (226 mg, 0.62 mmol), DCE (15.4 mL), AcOH (355 µL), toluene (26.7 mL), NaOH (247 mg, 6.18 mmol), ethanol (17.8 mL), and water (3.1 mL) according to the general procedure **1**. Yield: 841 mg (79%); yellowish viscous oil, R_f = 0.42 (ethyl acetate:petroleum ether; 1:2). ^{1}H NMR ($CDCl_3$, 400 MHz): δ 7.19–7.10 (m, 2H, Ar), 7.04–7.00 (m, 2H, Ar), 6.43 (s, 2H, Ar), 5.14–5.11 (m, 1H, CH), 3.75 (s, 6H, 2 × CH_3O), 3.74 (s, 3H, CH_3O), 2.78–2.58 (m, 3H), 2.09–2.00 (m, 1H). $^{13}C\{^1H\}$ NMR ($CDCl_3$, 100 MHz): δ 174.7 (CO), 157.2 (d, $^1J_{CF}$ = 250 Hz), 153.2 (2 × C), 137.1 (C), 136.3 (C), 128.4 (d, $^3J_{CF}$ = 7 Hz, CH), 127.9 (CH), 125.0 (d, $^2J_{CF}$ = 12 Hz, C), 124.1 (CH), 116.4 (d, $^2J_{CF}$ = 20 Hz, CH), 103.0 (2 × CH), 64.7 (CH), 60.5 (CH_3O), 55.8 (2 × CH_3O), 30.5 (CH_2), 29.6 (CH_2). IR (film, cm^{-1}): 2840, 2827, 1703, 1593, 1504, 1237, 1131. HRMS (ESI/TOF): m/z = 346.1449 $[M + H]^+$ (346.1449 calcd. for $C_{19}H_{21}FNO_4^+$).

1,5-Diphenylpyrrolidin-2-one (**2c**) [17] was obtained from dimethyl 2-phenylcyclopropane-1,1-dicarboxylate (100 mg, 0.4 mmol), aniline (38.6 µL, 0.4 mmol), $Ni(ClO_4)_2 \cdot 6H_2O$ (30.8 mg, 0.08 mmol), DCE (2 mL), AcOH (46 µL), toluene (2.7 mL), NaOH (35 mg, 0.8 mmol), ethanol (2.5 mL), and water (0.4 mL) according to the general procedure. Yield: 47 mg (47%); yellow crystals; mp = 109–112 °C (dec.); lit. 100 °C [17]; 106– 108 [16]; R_f = 0.25 (ethyl acetate:petroleum ether; 1:3). ^{1}H NMR ($CDCl_3$, 600 MHz): δ 7.43 (d, ^3J = 8.0 Hz, 2H, Ph), 7.32–7.30 (m, 2H, Ph), 7.26–7.22 (m, 5H, Ph), 7.07 (m, 1H, Ph), 5.27–5.25 (m, 1H), 2.80–2.74 (m, 1H), 2.67–2.59 (m, 2H), 2.04–1.98 (m, 1H). $^{13}C\{^1H\}$ NMR ($CDCl_3$, 150 MHz MHz): δ 175.0, 141.4, 138.3, 129.1 (2 × C), 128.8 (2 × C), 127.8, 126.0 (2 × C), 125.0, 122.2 (2 × C), 64.0, 31.3, 29.3. The spectral data were in accordance with the literature [17]. IR (KBr, cm^{-1}): 3379, 3107, 3095, 3083, 3042, 3028, 2992, 2969, 2952, 2895, 1709, 1596, 1497, 1480, 1456, 1415, 1367, 1356, 1324, 1308, 1281, 1238, 1224, 1194, 1179, 1194, 1114, 1077, 1052, 1031, and 1002. HRMS (ESI/TOF): m/z = 238.1226 $[M + H]^+$ (238.1228 calcd. for $C_{16}H_{16}NO^+$).

1-(4-Methoxyphenyl)-5-(p-tolyl)pyrrolidin-2-one (**2d**) was obtained from dimethyl 2-(4-methylphenyl)cyclopropane-1,1-dicarboxylate (182 mg, 0.73 mmol), *p*-anisidine (91 mg, 0.73 mmol), $Ni(ClO_4)_2 \cdot 6H_2O$ (55 mg, 0.15 mmol), DCE (5.0 mL), AcOH (90 µL), toluene (4.9 mL), NaOH (55.6 mg, 1.39 mmol), ethanol (3.9 mL), and water (1.4 mL) according to the general procedure **1**. Yield: 92 mg (45%); ivory solid; mp 112–114 °C; R_f = 0.47 (ethyl acetate:petroleum ether; 2:1). ^{1}H NMR ($CDCl_3$, 600 MHz): δ 7.28 (d, ^3J = 8.9 Hz, 2H, Ar), 7.10 (s, 4H, Ar), 6.76 (d, ^3J = 8.9 Hz, 2H, Ar), 5.14 (dd, ^3J = 7.4 Hz, ^3J = 4.6 Hz, 1H, CH), 3.63 (s, 3H, CH_3O), 2.77–2.70 (m, 1H, CH_2), 2.62–2.55 (m, 2H, CH_2), 2.29 (s, 3H, CH_3), 2.00–1.95 (m, 1H, CH_2). ^{13}C NMR ($CDCl_3$, 150 MHz): δ 174.6 (CO), 156.8 (C), 138.4 (C), 137.4 (C), 131.2 (C), 129.5 (2 × CH), 126.0 (2 × CH), 124.2 (2 × CH), 113.9 (2 × CH), 64.1 (CH), 55.2 (CH_3O), 31.1 (CH_2), 29.1 (CH_2), 21.0 (CH_3). IR (KBr, cm^{-1}): 2835, 1694, 1512, 1248, 1035. HRMS (ESI/TOF): m/z = 282.1492 $[M + H]^+$ (282.1489 calcd. for $C_{18}H_{20}NO_2^+$). Anal. calcd. for $C_{18}H_{19}NO_2$: C, 76.84; H, 6.81, N, 4.95. Found: C, 76.63; H, 6.85; N, 4.98.

(R)-1-(4-Methoxyphenyl)-5-(p-tolyl)pyrrolidin-2-one (5*R*)-**2d**) was obtained from dimethyl (*S*)-2-(*p*-tolyl)cyclopropane-1,1-dicarboxylate [79] (80 mg, 0.32 mmol, *ee* 95%, $[\alpha]_D^{20}$ –130° (c 1.0, $CHCl_3$)), 4-methoxyaniline (40 mg, 0.32 mmol), $Ni(ClO_4)_2 \cdot 6H_2O$ (24 mg, 0.066 mmol), DCE (1.6 mL), AcOH (37 µL), toluene (2.1 mL), NaOH (27 mg, 0.68 mmol), ethanol (1.9 mL), and water (0.65 mL) according to the general procedure. Yield 32 mg (35%); ivory solid; mp 112–114 °C; $[\alpha]_D^{22}$ = +100 (c 0.024, CH_3OH); R_f = 0.47 (ethyl acetate:petroleum ether; 2:1). Spectral data were identical to those of **2d**.

5-(3-Chlorophenyl)-1-(4-nitrophenyl)pyrrolidin-2-one (**2e**) was obtained from dimethyl 2-(3-chlorophenyl)cyclopropane-1,1-dicarboxylate (300 mg, 1.11 mmol), 4-nitroaniline (170 mg, 1.22 mmol), and $Ni(ClO_4)_2 \cdot 6H_2O$ (82 mg, 0.223 mmol) in DCE (5.6 mL) according to the modified general procedure **1** (2.5 h under reflux for the first step and 12 h for the second step). Yield: 151 mg (43%); yellowish solid, mp 64–66 °C, R_f = 0.56 (ethyl acetate:petroleum ether; 1:1). ^{1}H NMR ($CDCl_3$, 600 MHz): δ 8.09 (d, ^3J = 9.6 Hz, 2H, Ar),

7.66 (d, ^3J = 9.6 Hz, 2H, Ar), 7.30–7.22 (m, 2H, Ar), 7.20 (s, 1H, Ar), 7.07 (dt, ^3J = 7.2 Hz, ^4J = 1.8 Hz, 1H, Ar), 5.30 (dd, ^3J = 7.9 Hz, ^3J = 4.2 Hz, 1H, C(5)H), 2.83–2.60 (m, 3H, C(3)H_2, C(4)H_2), 2.07–1.99 (m, 1H, C(4)H_2). ^{13}C NMR ($CDCl_3$, 150 MHz): δ 175.2 (CO), 143.7 (C), 143.6 (C), 142.4 (C), 135.4 (C), 130.7 (CH), 128.5 (CH), 125.8 (CH), 124.5 (2 × CH), 123.6 (CH), 120.7 (2 × CH), 62.8 (C(5)H), 31.0 (C(3)H_2), 28.8 (C(4)H_2). IR (KBr, cm^{-1}): 1708, 1592, 1510, 1496, 1335, 1323, 1296, 1286, 1219, 1194, 112, 848. HRMS ESI-TOF: m/z = 317.0687 $[M + H]^+$ (317.0687 calcd. for $C_{16}H_{14}N_2O_3^+$).

1-(3,4-Dimethoxyphenyl)-5-(5-methylfuran-2-yl)pyrrolidin-2-one (**2f**) was obtained from dimethyl 2-(5-methylfuran-2-yl)cyclopropane-1,1-dicarboxylate (300 mg, 1.26 mmol), 3,4-dimethoxyaniline (193 mg, 1.26 mmol), $Ni(ClO_4)_2 \cdot 6H_2O$ (92.0 mg, 0.25 mmol), DCE (5.6 mL), AcOH (144 μL), toluene (8 mL), NaOH (104 mg, 2.6 mmol), ethanol (7.3 mL), and water (2.5 mL) according to the general procedure **1** (at 0 °C for the first step). Yield: 150 mg (40%); yellowish oil, R_f = 0.39 (ethyl acetate:petroleum ether; 2:1). ^{1}H NMR ($CDCl_3$, 600 MHz): δ 6.87 (d, ^4J = 2.0 Hz, 1H, Ar), 6.78 (d, ^3J = 8.6 Hz, 1H, Ar), 6.73 (dd, ^3J = 8.6 Hz, ^4J = 2.0 Hz, 1H, Ar), 6.00 (d, ^3J = 2.7 Hz, 1H, Fu), 5.83 (d, ^3J = 2.7 Hz, 1H, Fu), 5.05–5.00 (m, 1H, CH), 3.83 (s, 3H, CH_3O), 3.79 (s, 3H, CH_3O), 2.87–2.81 (m, 1H, CH_2), 2.62–2.56 (m, 1H, CH_2), 2.53–2.46 (m, 1H, CH_2), 2.33–2.28 (m, 1H, CH_2), 2.25 (s, 3H, CH_3). ^{13}C NMR ($CDCl_3$, 150 MHz): δ 174.4 (CO), 152.0 (C), 151.0 (C), 148.6 (C), 147.0 (C), 130.9 (C), 116.3 (CH), 110.8 (CH), 108.8 (CH), 108.4 (CH), 106.1 (CH), 58.7 (CH), 55.8 (CH_3O), 55.6 (CH_3O), 30.9 (CH_2), 25.2 (CH_2), 13.4 (CH_3). IR (film, cm^{-1}): 2837, 1674, 1565, 1511, 1239, 1022, 911, 538. HRMS ESI-TOF: m/z = 302.1389 $[M + H]^+$ (302.1387 calcd. for $C_{17}H_{20}NO_4^+$).

1-(2-Bromo-4-methylphenyl)-5-(thiophen-2-yl)pyrrolidin-2-one (**2g**) was obtained from dimethyl 2-(thiophen-2-yl)cyclopropane-1,1-dicarboxylate (200 mg, 0.79 mmol), 2-bromo-4-methylaniline (147 mg, 0.78 mmol), $Ni(ClO_4)_2 \cdot 6H_2O$ (61.8 mg, 0.17 mmol), DCE (4.2 mL), AcOH (96 μL), toluene (5.3 mL), NaOH (63 mg, 1.57 mmol), ethanol (4.8 mL), and water (1.7 mL) according to the general procedure **1**. Yield: 162 mg (58%); colorless solid; mp 127–129 °C; R_f = 0.54 (ethyl acetate). ^{1}H NMR ($CDCl_3$, 600 MHz): δ 7.26 (dd, ^3J = 8.2 Hz, ^4J = 2.0 Hz, 1H, Ar), 7.22 (d, ^3J = 5.0 Hz, 1H, Ar), 7.15 (br. s, 1H, Ar), 7.05 (d, ^3J = 8.2 Hz, 1H, Ar), 6.87–6.84 (m, 1H, Ar), 6.83–6.81 (m, 1H, Ar), 5.32–5.26 (m, 1H, CH), 2.87–2.81 (m, 1H, CH_2), 2.77–2.71 (m, 1H, CH_2), 2.70–2.64 (m, 1H, CH_2), 2.41–2.34 (m, 1H, CH_2), 2.11 (s, 3H, CH_3). ^{13}C NMR ($CDCl_3$, 150 MHz): δ 173.7 (CO), 143.5 (C), 137.3 (C), 135.7 (C), 132.4 (CH), 130.9 (CH), 130.0 (C), 126.9 (CH), 126.8 (CH), 125.8 (CH), 119.1 (CH), 60.7 (CH), 30.9 (CH_2), 29.6 (CH_2), 18.0 (CH_3). IR (KBr, cm^{-1}): 3100, 2853, 1694, 1528, 716, 525. HRMS ESI-TOF: m/z = 336.0052 $[M + H]^+$ (336.0052 calcd. for $C_{15}H_{15}Br^{79}NOS^+$).

(E)-1-Phenyl-5-styrylpyrrolidin-2-one (**2h**) was obtained from dimethyl 2-(*E*)-styrylcyclopropane-1,1-dicarboxylate (300 mg, 1.15 mmol), aniline (107 mg, 1.15 mmol), $Ni(ClO_4)_2 \cdot 6H_2O$ (84 mg, 0.23 mmol), DCE (5.7 mL), AcOH (140 μL), toluene (8 mL), NaOH (99 mg, 2.48 mmol), ethanol (6.9 mL), and water (2.4 mL) according to the general procedure **1**. Yield: 182 mg (60%); yellow solid; mp 71–73 °C; R_f = 0.38 (ethyl acetate:petroleum ether; 1:1). ^{1}H NMR ($CDCl_3$, 600 MHz): δ 7.50 (d, ^3J = 8.6 Hz, 2H, Ar), 7.36–7.23 (m, 7H, Ar), 7.16–7.13 (m, 1H, Ar), 6.52 (d, ^3J = 15.8 Hz, 1H, CH=), 6.14 (dd, ^3J = 15.8 Hz, ^3J = 7.4 Hz, 1H, CH=), 4.86–4.82 (m, 1H), 2.76–2.70 (m, 1H), 2.62–2.56 (m, 1H), 2.50–2.44 (m, 1H), 2.04–1.99 (m, 1H). ^{13}C NMR ($CDCl_3$, 150 MHz): δ 174.5, 138.2, 136.1, 132.2, 129.0, 128.9 (2 × C), 128.7 (2 × C), 128.1, 126.6 (2 × C), 125.4, 123.0 (2 × C), 62.4, 31.3, 26.7. IR (KBr, cm^{-1}): 3059, 3026, 2978, 2943, 2873, 1699, 1695, 1598, 1529, 1497, 1456, 1449, 1382, 1294, 1219, 1210, 1154, 1115, 1072, 1042, 1029, 968. HRMS (ESI/TOF): m/z = 286.1202 $[M+Na]^+$ (286.1202 calcd. for $C_{18}H_{17}NNaO^+$).

5-(2-Nitrophenyl)-1-phenylpyrrolidin-2-one (**2i**) was obtained from dimethyl 2-(2-nitrophenyl)cyclopropane-1,1-dicarboxylate (300 mg, 1.07 mmol), aniline (120 mg, 1.29 mmol), $Y(OTf)_3$ (118 mg, 0.22 mmol), DCE (5.4 mL), AcOH (123 μL), toluene (8 mL), NaOH (87 mg, 2.18 mmol), ethanol (6.2 mL), and water (2 mL) according to the general procedure **1**. Yield: 124 mg (41%); thick dark brown oil, R_f = 0.27 (ethyl acetate:petroleum ether; 1:3). ^{1}H NMR ($CDCl_3$, 600 MHz): δ 8.09–8.07 (m, 1H, Ar), 7.56–7.54 (m, 1H, Ar), 7.44–7.42 (m, 3H, Ar), 7.40–7.38 (m, 1H, Ar), 7.28–7.26 (m, 2H, Ar), 7.10–7.07 (m, 1H, Ar),

5.99 (dd, ^3J = 8.7 Hz, ^3J = 3.4 Hz, 1H, CH), 2.92–2.85 (m, 1H, CH_2), 2.75–2.64 (m, 2H, CH_2), 2.07–2.02 (m, 1H, CH_2). ^{13}C NMR ($CDCl_3$, 150 MHz): δ 175.1 (CO), 137.0 (C), 134.2 (CH), 129.1 (2 × CH), 128.8 (CH), 128.5 (C), 127.3 (CH), 126.8 (C), 125.8 (CH), 125.3 (CH), 121.5 (2 × CH), 59.7 (CH), 30.8 (CH_2), 28.1 (CH_2). IR (film, cm^{-1}): 3308, 3199, 3136, 3103, 3066, 3043, 2953, 2924, 2853, 1699, 1598, 1579, 1526, 1498, 1457, 1444, 1382, 1348, 1295, 1251, 1225, 1162, 1118, 1073, 1040. HRMS ESI-TOF: m/z = 283.1077 $[M + H]^+$ (283.1077 calcd. for $C_{16}H_{15}N_2O_3^+$).

1-(4-Methoxyphenyl)-5-(pyridin-3-yl)pyrrolidin-2-one (**2j**) [15] was obtained from dimethyl 2-(pyridin-3-yl)cyclopropane-1,1-dicarboxylate (250 mg, 1.06 mmol), 4-methoxyaniline (131 mg, 1.06 mmol), $Ni(ClO_4)_2 \cdot 6H_2O$ (78 mg, 0.21 mmol), DCE (5.3 mL), AcOH (122 μL), toluene (6.7 mL), NaOH (77 mg, 1.9 mmol), ethanol (5.4 mL), and water (1.9 mL) according to the general procedure **1** but the product of hydrolysis was refluxed in water (14 mL, 0.065 M) for 14 h. Yield: 95 mg (33%); brown solid; mp 72–73 °C; lit. 73–75 °C [17]; R_f = 0.14 (ethyl acetate). ^{1}H NMR ($CDCl_3$, 600 MHz): δ 8.51–8.50 (m, 1H, Ar), 8.48–8.47 (m, 1H, Ar), 7.52–7.50 (m, 1H, Ar), 7.23–7.20 (m, 3H, Ar), 6.77 (d, ^3J = 9.1 Hz, 2H, Ar), 5.22–5.20 (m, 1H, CH), 3.70 (s, 3H, CH_3O), 2.50–2.64 (m, 3H, CH_2), 2.03–1.97 (m, 1H, CH_2). ^{13}C NMR ($CDCl_3$, 150 MHz): δ 174.6 (CO), 157.2 (C), 149.4 (CH), 148.4 (CH), 136.9 (C), 133.8 (CH), 130.4 (C), 124.6 (2 × CH), 123.9 (CH), 114.2 (2 × CH), 62.0 (CH), 55.4 (CH_3O), 31.0 (CH_2), 28.9 (CH_2). IR (KBr, cm^{-1}): 3309, 3128, 3041, 3000, 2953, 2934, 2911, 2834, 1672, 1607, 1547, 1509, 1463, 1441, 1431, 1409, 1385, 1296, 1243, 1178, 1107, 1028. HRMS ESI-TOF: m/z = 269.1285 $[M + H]^+$ (269.1285 calcd. for $C_{16}H_{17}N_2O_2^+$). Spectral data are consistent with the reported ones [15].

*1-Benzyl-5-(3,4,5-trimethoxyphenyl)pyrrolidin-2-one (***3a**) To a solution of dimethyl 2-(3,4,5-trimethoxyphenyl)cyclopropane-1,1-dicarboxylate (550 mg, 1.70 mmol) in DCE (8.5 mL) in the presence of molecular sieves, 4 Å $Ni(ClO_4)_2 \cdot 6H_2O$ (63.4 mg, 0.17 mmol) was added; then, benzylamine (222 μL, 2.03 mmol) was added. The resulting mixture was refluxed for 1.5 h, diluted with DCM, and filtered through a small pad of silica gel using EtOAc as the eluent. Then, solvent was removed under vacuum; residue was dissolved in ethanol (9.8 mL), and aq. solution of NaOH (136 mg, 3.40 mmol; 3.5 mL) was added in one portion. The reaction mixture was stirred at room temperature for 2 h, and after that, ethanol was removed under vacuum. The residue was diluted with water, and 1 M HCl was added until pH 1. Then, mixture was extracted with ethyl acetate (3 × 10 mL). The combined organic layers were dried with Na_2SO_4 and concentrated in vacuo. The residue was dissolved in toluene (26.1 mL) and refluxed for 7 h. The solvent was removed under vacuum; pure product was isolated by column chromatography on silica gel. Yield: 393 mg (68%); yellowish solid; mp 99–102 °C; R_f = 0.69 (ethyl acetate). ^{1}H NMR ($CDCl_3$, 600 MHz): δ 7.27–7.21 (m, 3H, Ar), 7.08–7.07 (m, 2H, Ar), 6.29 (s, 2H, Ar), 5.01 (d, ^2J = 14.5 Hz, 1H, CH_2), 4.32 (dd, ^3J = 7.9 Hz, ^3J = 6.1 Hz, 1H, CH), 3.84 (s, 3H, CH_3O), 3.79 (s, 6H, 2 × CH_3O), 3.62 (d, ^2J = 14.5 Hz, 1H, CH_2), 2.65–2.60 (m, 1H, CH_2), 2.51–2.45 (m, 1H, CH_2), 2.41–2.35 (m, 1H, CH_2), 1.91–1.85 (m, 1H, CH_2). ^{13}C NMR ($CDCl_3$, 150 MHz): δ 175.4 (CO), 153.7 (2 × C), 137.6 (C), 136.5 (C), 136.4 (C), 128.6 (2 × CH), 128.5 (2 × CH), 127.5 (CH), 103.5 (2 × CH), 61.9 (CH), 60.9 (CH_3O), 56.2 (2 × CH_3O), 44.6 (CH_2), 30.4 (CH_2), 28.3 (CH_2). IR (KBr, cm^{-1}): 2926, 1672, 1594, 1247, 1117, 1008, 700. HRMS ESI-TOF: m/z = 342.1700 $[M + H]^+$ (342.1700 calcd. for $C_{20}H_{24}NO_4^+$).

1-(4-Methoxybenzyl)-5-(3,4,5-trimethoxyphenyl)pyrrolidin-2-one (**3b**) [39] was obtained from dimethyl 2-(3,4,5-trimethoxyphenyl)cyclopropane-1,1-dicarboxylate (550 mg, 1.70 mmol), (4-methoxyphenyl)methanamine (285 μL, 2.18 mmol), $Ni(ClO_4)_2 \cdot 6H_2O$ (63.0 mg, 0.17 mmol), DCE (8.5 mL), NaOH (128 mg, 3.20 mmol), ethanol (9.0 mL), and water (3.2 mL) according to the general procedure **2b**. Yield: 440 mg (70%); light yellow oil; R_f = 0.66 (ethyl acetate).^{1}H NMR ($CDCl_3$, 600 MHz): δ 6.96 (d, ^3J = 8.6 Hz, 2H, Ar), 6.75 (d, ^3J = 8.6 Hz, 2H, Ar), 6.27 (s, 2H, Ar), 4.92 (d, ^2J = 14.5 Hz, 1H, CH_2), 4.27 (dd, ^3J = 8.2 Hz, ^3J = 6.4 Hz, 1H, CH), 3.81 (s, 3H, CH_3O), 3.77 (s, 6H, 2 × CH_3O), 3.72 (s, 3H, CH_3O), 3.52 (d, ^2J = 14.5 Hz, 1H, CH_2), 2.60–2.55 (m, 1H, CH_2), 2.45–2.40 (m, 1H, CH_2), 2.36–2.30 (m, 1H, CH_2), 1.86–1.80 (m, 1H, CH_2). ^{13}C NMR ($CDCl_3$, 150 MHz): δ 175.3 (CO), 158.9 (C), 153.6 (2 × C), 137.5

(C), 136.4 (C), 129.8 (2 × CH), 128.4 (C), 113.7 (2 × CH), 103.5 (2 × CH), 61.8 (CH), 60.8 (CH_3O), 56.1 (2 × CH_3O), 55.2 (CH_3O), 43.9 (CH_2), 30.4 (CH_2), 28.2 (CH_2). Spectral data are consistent with the reported ones [39].

*1-Benzyl-5-(2,4-dimethoxyphenyl)pyrrolidin-2-one (***3c**) was obtained from dimethyl 2-(2,4-dimethoxyphenyl)cyclopropane-1,1-dicarboxylate (125 mg, 0.425 mmol), benzylamine (0.056 mL, 0.51 mmol), $Ni(ClO_4)_2 \cdot 6H_2O$ (16 mg, 0.044 mmol), and NaCl (37 mg, 0.64 mmol) in DCM (0.5 mL) according to the general procedure **2** (1 h for the first step and 4 h for the second step). Yield: 66 mg (50%); yellowish oil, R_f = 0.47 (ethyl acetate:petroleum ether; 2:1). ^{1}H NMR ($CDCl_3$, 400 MHz): δ 7.22–7.29 (m, 3H, Ar), 7.08–7.13 (m, 2H, Ar), 6.91–6.95 (m, 1H, Ar), 6.43–6.49 (m, 2H, Ar), 5.05 (d, ^2J = 14.7 Hz, 1H, CH_2), 4.73 (dd, ^3J = 8.5 Hz, ^3J = 4.2 Hz, 1H, CH), 3.82 (s, 3H, CH_3O), 3.71 (s, 3H, CH_3O), 3.54 (d, ^2J = 14.7 Hz, 1H, CH_2), 2.54–2.64 (m, 1H, CH_2), 2.40–2.49 (m, 1H, CH_2), 2.27–2.38 (m, 1H, CH_2), 1.83–1.94 (m, 1H, CH_2). ^{13}C NMR ($CDCl_3$, 100 MHz): δ 175.5 (CO), 160.5 (C), 158.2 (C), 136.7 (C), 128.3 (4 × CH), 128.0 (CH), 127.2 (CH), 120.6 (C), 104.0 (CH), 98.8 (CH), 56.1 (CH), 55.32 (CH_3O), 55.21 (CH_3O), 44.2 (CH_2Ph), 30.2 (C(4)H_2), 26.3 (C(3)H_2). IR (film, cm^{-1}): 3086, 3064, 3030, 3001, 2940, 2837, 1739, 1685, 1612, 1588, 1507, 1456, 1441, 1416, 1358, 1292, 1277, 1262, 1209, 1158, 1119, 1033. HRMS ESI-TOF: m/z = 312.1599 $[M + H]^+$ (312.1594 calcd. for $C_{19}H_{22}NO_3^+$). Spectral data are consistent with the reported ones [77].

1-(2,5-Dimethoxybenzyl)-5-(3,4-dimethoxyphenyl)pyrrolidin-2-on (**3d**) was obtained from dimethyl 2-(3,4-dimethoxyphenyl)cyclopropane-1,1-dicarboxylate (300 mg, 1.02 mmol), 2,5-dimethoxybenzylamine (0.184 mL, 1.22 mmol), $Ni(ClO_4)_2 \cdot 6H_2O$ (37 mg, 0.101 mmol), and NaCl (85 mg, 1.5 mmol) in DCM (0.5 mL) according to the general procedure **2** (1 h for the first step and 6 h for the second step). Yield: 178 mg (47%); yellow oil, R_f = 0.49 (ethyl acetate:petroleum ether; 3:1). ^{1}H NMR ($CDCl_3$, 500 MHz): δ 6.81 (d, ^3J = 8.2 Hz, 1H, Ar), 6.73 (dd, ^3J = 8.8 Hz, ^4J = 2.9 Hz, 1H, Ar), 6.70 (d, ^3J = 8.8 Hz, 1H, Ar), 6.66 (dd, ^3J = 8.2 Hz, ^4J = 2.0 Hz, 1H, Ar), 6.63 (d, ^4J = 2.9 Hz, 1H, Ar), 6.57 (d, ^4J = 2.0 Hz, 1H, Ar), 4.85 (d, ^2J = 14.8 Hz, 1H, CH_2), 4.42 (dd, ^3J = 8.1 Hz, ^3J = 5.8 Hz, 1H, CH), 3.86 (s, 3H, CH_3O), 3.81 (s, 3H, CH_3O), 3.78 (d, ^2J = 14.8 Hz, 1H, CH_2), 3.70 (s, 3H, CH_3O), 3.61 (s, 3H, CH_3O), 2.57–2.64 (m, 1H, CH_2), 2.42–2.50 (m, 1H, CH_2), 2.35–2.45 (m, 1H, CH_2), 1.82–1.90 (m, 1H, CH_2). ^{13}C NMR ($CDCl_3$, 125 MHz): δ 175.3 (CO), 153.3 (C), 151.6 (C), 149.2 (C), 148.5 (C), 133.7 (C), 125.5 (C), 118.8 (CH), 115.8 (CH), 112.8 (CH), 111.1 (CH), 111.0 (CH), 109.3 (CH), 61.7 (CH), 55.8 (CH_3O), 55.7 (CH_3O), 55.59 (CH_3O), 55.53 (CH_3O), 39.4 (CH_2Ar), 30.1 (C(4)H_2), 28.3 (C(3)H_2). IR (film, cm^{-1}): 3074, 2998, 2940, 2912, 2835, 2251, 2063, 1693, 1608, 1593, 1518, 1500, 1465, 1412, 1357, 1315, 1303, 1278, 1260, 1218, 1154, 1138, 1120, 1046, 1026. HRMS ESI-TOF: m/z = 372.1817 $[M + H]^+$ (372.1805 calcd. for $C_{21}H_{26}NO_5^+$).

1-(Furan-2-ylmethyl)-5-(2,4,5-trimethoxyphenyl)pyrrolidin-2-one (**3e**) was obtained from dimethyl 2-(2,4,5-trimethoxyphenyl)cyclopropane-1,1-dicarboxylate (400 mg, 1.23 mmol), furfurylamine (114 μL, 1.29 mmol), $Ni(ClO_4)_2 \cdot 6H_2O$ (90.2 mg, 0.25 mmol), DCE (6.2 mL), AcOH (140 μL), toluene (10.7 mL), NaOH (41.3 mg, 1.03 mmol), ethanol (3 mL), and water (1 mL) according to the general procedure **1**. Yield: 132 mg (32%); light yellow thick oil, R_f = 0.18 (ethyl acetate:petroleum ether; 1:1). ^{1}H NMR ($CDCl_3$, 600 MHz) δ 7.28–7.26 (m, 1H, Fu), 6.53 (s, 1H, Ar), 6.51 (s, 1H, Ar), 6.22 (dd, ^3J = 3.0 Hz, ^3J = 1.7 Hz, 1H, Fu), 6.01 (br. d, ^3J = 3.0 Hz, 1H, Fu), 4.86–4.83 (m, 2H, CH + CH_2), 3.87 (s, 3H, CH_3O), 3.77 (s, 3H, CH_3O), 3.74 (s, 3H, CH_3O), 3.69 (d, ^2J = 15.4 Hz, 1H, CH_2), 2.57–2.52 (m, 1H, CH_2), 2.44–2.32 (m, 2H, CH_2), 1.87–1.81 (m, 1H, CH_2). ^{13}C NMR ($CDCl_3$, 150 MHz): δ 175.5 (CO), 151.7 (C), 150.3 (C), 149.4 (C), 143.3 (C), 142.1 (CH), 119.9 (C), 111.2 (CH), 110.2 (CH), 108.3 (CH), 98.0 (CH), 56.7 (CH_3O), 56.4 (CH + CH_3O), 56.2 (CH_3O), 37.4 (CH_2), 30.3 (CH_2), 26.7 (CH_2). IR (film, cm^{-1}): 2992, 2935, 2836, 1687, 1684, 1611, 1513, 1463, 1456, 1440, 1411, 1399, 1348, 1317, 1276, 1208, 1163, 1116, 1079, 1032, 1012. HRMS (ESI/TOF): m/z = 331.1420 $[M]^+$ (331.1414 calcd. for $C_{18}H_{21}NO_5^+$).

1-[(1H-Indol-4-yl)methyl]-5-(3,4-dimethoxyphenyl)pyrrolidin-2-one (**3f**) was obtained from dimethyl 2-(2,4-dimethoxyphenyl)cyclopropane-1,1-dicarboxylate (100 mg, 0.34 mmol), 4-aminomethylindole (60 mg, 0.41 mmol), $Ni(ClO_4)_2 \cdot 6H_2O$ (13 mg, 0.036 mmol) in DCM (0.2 mL), and NaCl (30 mg, 0.51 mmol) according to the general procedure **2** (1 h for the

first step and 4 h for the second step). Yield: 50 mg (42%); yellow oil, R_f = 0.35 (ethyl acetate:petroleum ether; 4:1). ^{1}H NMR ($CDCl_3$, 500 MHz): δ 8.56 (br. s, 1H, NH), 7.34–7.37 (m, 1H, Ar), 7.18–7.21 (m, 1H, Ar), 7.05–7.09 (m, 1H, Ar), 6.86–6.90 (m, 1H, Ar), 6.68–6.72 (m, 2H, Ar), 6.56–6.59 (m, 2H, Ar), 5.45 (d, ^2J = 14.3 Hz, 1H, CH_2), 4.25 (dd, ^3J = 8.0 Hz, ^3J = 5.8 Hz, 1H, CH), 3.93 (s, 3H, CH_3O), 3.83 (s, 3H, CH_3O), 3.81 (d, ^2J = 14.3 Hz, 1H, CH_2), 2.68 (ddd, ^2J = 17.2 Hz, ^3J = 9.9 Hz, ^3J = 5.8 Hz, 1H, CH_2), 2.51 (ddd, ^2J = 17.2 Hz, ^3J = 9.9, ^3J = 7.2 Hz, 1H, CH_2), 2.26–2.35 (m, 1H, CH_2), 1.82–1.90 (m, 1H, CH_2). ^{13}C NMR ($CDCl_3$, 125 MHz): δ 175.0 (CO), 149.3 (C), 148.6 (C), 135.9 (C), 135.6 (C), 127.8 (C), 127.0 (C), 124.3 (CH), 121.4 (CH), 120.7 (CH), 119.1 (CH), 111.2 (CH), 110.8 (CH), 109.7 (CH), 101.3 (CH), 61.1 (CH), 55.91 (CH_3O), 55.85 (CH_3O), 42.8 (CH_2Ar), 30.5 (C(4)H_2), 28.1 (C(3)H_2). IR (film, cm^{-1}): 3465, 3396, 3371, 3308, 3293, 3272, 3118, 2998, 2932, 2875, 2836, 2384, 1730, 1665, 1611, 1595, 1516, 1462, 1443, 1415, 1347, 1317, 1305, 1259, 1236, 1173, 1151, 1137, 1086, 1025. HRMS ESI-TOF: m/z = 351.1696 $[M + H]^+$ (351.1703 calcd. for $C_{21}H_{23}N_2O_3^+$).

(E)-1-[2-(1H-Indol-3-yl)ethyl]-5-styrylpyrrolidin-2-one (**3g**) was obtained from dimethyl (*E*)-2-styrylcyclopropane-1,1-dicarboxylate (200 mg, 0.77 mmol), tryptamine (123 mg, 0.77 mmol), $Ni(ClO_4)_2 \cdot 6H_2O$ (56 mg, 0.155 mmol), DCE (3.8 mL), AcOH (90 μL), toluene (5.3 mL), NaOH (63 mg, 1.58 mmol), ethanol (4.4 mL), and water (0.8 mL) according to the general procedure **1**. Yield: 28 mg (11%); brownish thick oil, R_f = 0.31 (ethyl acetate). ^{1}H NMR ($CDCl_3$, 600 MHz): ^{1}H NMR ($CDCl_3$, 600 MHz): δ 8.23 (br. s, 1H, NH), 7.54 (d, ^3J = 7.9 Hz, 1H, Ar), 7.37–7.32 (m, 5H, Ar), 7.30–7.26 (m, 1H, Ar), 7.19–7.16 (m, 1H, Ar), 7.03–7.00 (m, 2H, Ar), 6.34 (d, ^3J = 15.6 Hz, 1H, CH=), 5.91 (dd, ^3J = 15.6 Hz, ^3J = 8.6 Hz, 1H, CH=), 4.01–3.97 (m, 1H, CH), 3.89–3.85 (m, 1H, CH_2), 3.36–3.31 (m, 1H, CH_2), 3.11–3.06 (m, 1H, CH_2), 2.99–2.94 (m, 1H, CH_2), 2.52–2.46 (m, 1H, CH_2), 2.42–2.36 (m, 1H, CH_2), 2.21–2.15 (m, 1H, CH_2), 1.80–1.74 (m, 1H, CH_2). ^{13}C NMR ($CDCl_3$, 150 MHz): δ 175.1 (CO), 136.3 (C), 135.9 (C), 133.3 (CH), 128.9 (CH), 128.7 (2 × CH), 128.2 (CH), 127.4 (C), 126.6 (2 × CH), 122.1 (CH), 122.0 (CH), 119.3 (CH), 118.8 (CH), 113.0 (C), 111.2 (CH), 61.8 (CH), 41.4 (CH_2), 30.4 (CH_2) 25.9 (CH_2), 23.5 (CH_2). IR (film, cm^{-1}): 3210, 3180, 3110, 3079, 3057, 3028, 2962, 2929, 2878, 2853, 2723, 2601, 2545, 2385, 2350, 2253, 1956, 1883, 1804, 1666, 1548, 1493, 1452, 1417, 1368, 1340, 1312, 1274, 1264, 1230, 1181, 1160, 1143, 1126, 1102, 1071, 1052, 1029, 1008, 979, 905. HRMS ESI-TOF: m/z = 331.1805 $[M + H]^+$ (331.1805 calcd. for $C_{22}H_{23}N_2O^+$).

1-Cyclobutyl-5-(4-morpholinophenyl)pyrrolidin-2-one (**3h**) was obtained from dimethyl 2-(4-morpholinophenyl)cyclopropane-1,1-dicarboxylate (300 mg, 0.94 mmol), cyclobutylamine (84 μL, 0.99 mmol) in DCE (0.5 mL), and NaCl (75 mg, 1.28 mmol) according to the general procedure **2** (2.5 h for the first step and 4 h for the second step). Yield: 142 mg (50%); yellow oil, R_f = 0.71 (chloroform:methanol, 10:1). ^{1}H NMR ($CDCl_3$, 500 MHz): δ 7.09 (d, ^3J = 8.6 Hz, 2H, Ar), 6.96–6.88 (m, 2H, Ar), 4.73 (dd, ^3J = 8.3 Hz, ^3J = 3.4 Hz, 1H, CH), 4.32–4.23 (m, 1H, CH), 3.90–3.83 (m, 4H, 2 × CH_2), 3.20–3.13 (m, 4H, 2 × CH_2), 2.58–2.59 (m, 1H, CH_2), 2.46–2.39 (m, 1H, CH_2), 2.38–2.33 (m, 1H, CH_2), 2.32–2.25 (m, 1H, CH_2), 2.15–2.07 (m, 1H, CH_2), 1.97–1.88 (m, 1H, CH_2), 1.82–1.74 (m, 2H, CH_2), 1.56–1.45 (m, 2H, CH_2). ^{13}C NMR ($CDCl_3$, 125 MHz): δ 175.3 (CO), 126.6 (2 × CH), 115.8 (2 × CH), 66.6 (2 × CH_2), 60.49 (CHAr), 49.2 (2 × CH_2), 47.7 (CHN), 30.2 (CH_2), 29.0 (CH_2), 28.18 (CH_2), 28.14 (CH_2), 15.4 (CH_2), quaternary aromatic carbons not observed. HRMS ESI-TOF: m/z = 301.1904 $[M + H]^+$ (301.1911 calcd. for $C_{18}H_{25}N_2O_2^+$).

5-(3,4-Dimethoxyphenyl)-1-(prop-2-yn-1-yl)pyrrolidin-2-one (**3i**) was obtained from dimethyl 2-(3,4-dimethoxyphenyl)cyclopropane-1,1-dicarboxylate (300 mg, 1.02 mmol), propargylamine (78 μL, 1.22 mmol) in DCE (0.5 mL), and NaCl (70 mg, 1.2 mmol) according to the general procedure **2** (2.5 h for the first step and 4 h for the second step). Yield: 86 mg (33%); yellow oil, R_f = 0.43 (ethyl acetate). ^{1}H NMR ($CDCl_3$, 400 MHz): δ 6.83 (d, ^3J = 8.3 Hz, 1H, Ar), 6.77 (dd, ^3J = 8.3 Hz, ^4J = 1.9 Hz, 1H, Ar), 6.69 (d, ^4J = 1.9 Hz, 1H, Ar), 4.73–4.69 (m, 1H, CH), 4.52 (dd, ^2J = 17.4 Hz, ^4J = 2.5 Hz, 1H, CH_2), 3.85 (s, 3H, CH_3O), 3.84 (s, 3H, CH_3O), 3.22 (dd, ^2J = 17.4 Hz, ^4J = 1.7 Hz, 1H, CH_2), 2.61–2.52 (m, 1H, CH_2), 2.50–2.42 (m, 2H, CH_2), 2.13 (dd, ^4J = 2.5 Hz, ^4J = 1.7 Hz, 1H, CH), 1.95–1.86 (m, 1H, CH_2). ^{13}C NMR ($CDCl_3$, 100 MHz): δ 174.8 (CO), 149.4 (C), 148.9 (C), 132.5 (C), 119.3 (CH), 111.2 (CH), 109.3 (CH), 77.6 (C), 71.7 (CH), 61.2 (CH), 55.84 (CH_3O), 55.80 (CH_3O), 30.3 (CH_2), 30.0 (CH_2),

28.0 (CH_2). IR (film, cm^{-1}): 3250, 3073, 2998, 2957, 2939, 2837, 2585, 2468, 2280, 2117, 2030, 2846, 1693, 1607, 1594, 1519, 1465, 1465, 1422, 1371, 1347, 1306, 1237, 1179, 1139, 1066, 1026. HRMS ESI-TOF: m/z = 260.1292 $[M + H]^+$ (260.1281 calcd. for $C_{15}H_{18}NO_3^+$).

Dimethyl 2-[2-(3,5-dimethoxyphenyl)-2-(phenylamino)ethyl]malonate (**4a**). To a solution of dimethyl 2-(3,5-dimethoxyphenyl)cyclopropane-1,1-dicarboxylate (300 mg, 1.02 mmol) in DCE (5.1 mL) in the presence of molecular sieves, 4 Å $Ni(ClO_4)_2 \cdot 6H_2O$ (75 mg, 0.206 mmol) was added under Ar atmosphere; then, aniline (0.1 mL, 1.10 mmol) was added. The resulting mixture was stirred at room temperature for 1 h, diluted with DCM, and filtered. The filtrate was concentrated under vacuum; pure product was isolated by column chromatography on silica gel. Yield: 363 mg (92%); yellow viscous oil; R_f = 0.50 (ethyl acetate:petroleum ether; 1:3). ^{1}H NMR ($CDCl_3$, 600 MHz): δ 7.13–7.10 (m, 2H, Ar), 6.69–6.67 (m, 1H, Ar), 6.56 (d, ^3J = 7.8 Hz, 2H, Ar), 6.52 (d, ^4J = 2.2 Hz, 2H, Ar), 6.36–6.35 (m, 1H, Ar), 4.40–4.37 (m, 1H, CH), 4.23 (br.s, 1H, NH), 3.77 (s, 6H, 2 × CH_3O), 3.76 (s, 3H, CH_3O), 3.73 (s, 3H, CH_3O), 3.60–3.58 (m, 1H, CH), 2.43–2.41 (m, 2H, CH_2). ^{13}C NMR ($CDCl_3$, 150 MHz): δ 170.1 (CO_2Me), 169.7 (CO_2Me), 161.2 (2 × C), 146.9 (C), 145.3 (C), 129.2 (2 × CH), 117.7 (CH), 113.5 (2 × CH), 104.4 (2 × CH), 99.1 (CH), 56.6 (CH), 55.3 (2× CH_3O), 52.8 (CH_3O), 52.8 (CH_3O), 49.3 (CH), 37.0 (CH_2). IR (film, cm^{-1}) 3386, 3088, 3051, 3003, 2953, 2839, 1748, 1732, 1602, 1506, 1460, 1433, 1347, 1313, 1290, 1277, 1260, 1234, 1205, 1156, 1120, 1064, 1020, 993. HRMS ESI-TOF: m/z = 410.1574 $[M + Na]^+$ (410.1562 calcd. for $C_{21}H_{25}NNaO_6^+$).

Dimethyl 2-{2-[(2-nitrophenyl)amino]-2-phenylethyl}malonate (**4b**). To a solution of dimethyl 2-phenylcyclopropane-1,1-dicarboxylate (200 mg, 0.85 mmol) in DCE (4.3 mL) in the presence of molecular sieves, 4 Å $Ni(ClO_4)_2 \cdot 6H_2O$ (62 mg, 0.17 mmol) was added under Ar atmosphere; then, 2-nitroaniline (118 mg, 0.85 mmol) was added. The resulting mixture was refluxed for 2 h, diluted with DCM, and filtered. The filtrate was concentrated under vacuum; the pure product was isolated by column chromatography on silica gel. Yield: 226 mg (71%); yellow oil; R_f = 0.47 (ethyl acetate:petroleum ether; 1:3). ^{1}H NMR ($CDCl_3$, 600 MHz): δ 8.45 (d, ^3J = 6.9 Hz, 1H, NH), 8.17–8.16 (m, 1H, Ar), 7.38–7.29 (m, 6H, Ar), 6.73 (d, ^3J = 8.7 Hz, 1H, Ar), 6.65–6.63 (m, 1H, Ar), 4.69–4.65 (m, 1H, CH), 3.77(s, 3H, CH_3O), 3.71 (s, 3H, CH_3O), 3.50 (t, ^3J = 7.2 Hz, 1H, CH), 2.59–2.47 (m, 2H, CH_2). ^{13}C NMR ($CDCl_3$, 150 MHz): δ 169.4 (CO_2Me), 169.3 (CO_2Me), 144.4 (C), 140.9 (C), 136.3 (CH), 132.7 (C), 129.3 (2 × CH), 128.2 (CH), 126.9 (CH), 126.4 (2 × CH), 116.2 (CH), 115.0 (CH), 55.8 (CH), 53.0 (CH_3O), 53.0 (CH_3O), 49.0 (CH), 37.0 (CH_2). IR (film, cm^{-1}): 3373, 3084, 3032, 3007, 2959, 2921, 2886, 2851, 1751, 1727, 1619, 1584, 1575, 1512, 1504, 1451, 1440, 1418, 1359, 1339, 1317, 1281, 1262, 1232, 1205, 1169, 1159, 1121, 1096, 1062, 1041, 1028, 1011, 985, 961. HRMS ESI-TOF: m/z = 373.1394 $[M + H]^+$ (373.1394 calcd. for $C_{19}H_{21}N_2O_6^+$).

Dimethyl 2-{2-[(2-aminophenyl)amino]-2-(3,4-dimethoxyphenyl)ethyl}malonate (**4c**). To a solution of dimethyl 2-(3,4-dimethoxyphenyl)cyclopropane-1,1-dicarboxylate (200 mg, 0.68 mmol) and *o*-phenylenediamine (74 mg, 0.68 mmol) in DCE (3.4 mL) in the presence of molecular sieves, 4 Å $Y(OTf)_3$ (74 mg, 0.14 mmol) was added under Ar atmosphere. The resulting mixture was stirred at room temperature for 2.25 h, diluted with DCM, and filtered. The filtrate was concentrated under vacuum; pure product was isolated by column chromatography on silica gel. Yield: 150 mg (55%); viscous yellowish oil; R_f = 0.52 (ethyl acetate:petroleum ether; 2:1). ^{1}H NMR ($CDCl_3$, 400 MHz): δ 6.87–6.83 (m, 2H, Ar), 6.80 (d, ^3J = 8.1 Hz, 1H, Ar), 6.71–6.62 (m, 3H, Ar), 6.45–6.43 (m, 1H, Ar), 3.56 (dd, ^3J = 8.0 Hz, 1H, ^3J = 6.4 Hz, 1H, 1H, CH), 3.85 (s, 3H, CH_3O), 3.84 (s, 3H, CH_3O), 3.75 (s, 3H, CH_3O), 3.71 (s, 3H, CH_3O), 3.56 (dd, ^3J = 7.4 Hz, ^3J = 6.6 Hz, 1H, CH), 2.54–2.38 (m, 2H, CH_2). Signals of NH_2 groups were not observed. ^{13}C NMR ($CDCl_3$, 100 MHz): δ 170.1 (CO_2Me), 169.7 (CO_2Me), 149.1 (C), 148.2 (C), 136.0 (C), 134.7 (C), 134.4 (C), 120.4 (CH), 119.0 (CH), 118.3 (CH), 116.5 (CH), 113.6 (CH), 111.2 (CH), 109.4 (CH), 56.3 (CH), 55.8 (2 × CH_3O), 52.7 (2 × CH_3O), 49.3 (CH), 37.1 (CH_2). IR (film, cm^{-1}): 3400, 3350, 3002, 2953, 2837, 2254, 1738, 1729, 1598, 1512, 1453, 1437, 1343, 1263, 1237, 1142, 1053, 912. HRMS ESI-TOF: m/z = 403.1855 $[M + H]^+$ (403.1864 calcd. for $C_{21}H_{27}N_2O_6^+$).

2-[2-Phenyl-2-(phenylamino)ethyl]malononitrile (**4d**) To a solution of 2-phenylcyclopropane-1,1-dicarbonitrile (417 mg, 2.48 mmol) in DCE (12 mL) and aniline (0.26 mL, 2.88 mmol)

in the presence of molecular sieves, 4Å $Y(OTf)_3$ (265 mg, 0.49 mmol, 20 mol%) was added under Ar atmosphere. The reaction mixture was stirred at room temperature for 4 days. Then, the resulting mixture was poured into saturated aq. solution of $NaHCO_3$ (12 mL) and extracted with CH_2Cl_2 (3 × 10 mL). The combined organic fractions were washed with saturated aq. solution of $NaHCO_3$ (2 × 10 mL) and water (1 × 10 mL), dried with Na_2SO_4, and concentrated in vacuo. The resulting residue was purified by column chromatography on silica gel. Yield: 266 mg (41%); white solid; m.p. 149–151 °C; R_f = 0.68 (ethyl acetate:petroleum ether; 1:3). ^{1}H NMR ($CDCl_3$, 600 MHz): δ 7.41–7.38 (m, 2H, Ph), 7.34–7.32 (m, 3H, Ph), 7.19–7.15 (m, 2H, Ph), 6.80–6.76 (m, 1H, Ph), 6.67 (d, ^3J = 8.1 Hz, 2H, Ph), 4.72–4.68 (m, 1H, CH), 3.98–3.93 (m, 2H, CH, NH), 2.51–2.47 (m, 2H, CH_2). ^{13}C NMR ($CDCl_3$, 150 MHz): δ 145.8 (C), 139.9 (C), 129.5 (2 × CH), 129.4 (2 × CH), 128.6 (CH), 126.1 (2 × CH), 119.3 (CH), 114.4 (2 × CH), 112.5 (2 × CN), 55.3 (CH), 38.4 (CH), 20.2 (CH_2). IR (KBr, cm^{-1}) 3379, 3057, 2882, 2257, 1601, 1506, 1453, 1428, 1311, 1258, 769, 754, 704. HRMS ESI-TOF: m/z = 262.1339 [M + H] (262.1339 calcd. for $C_{17}H_{16}N_3$).

2-{2-[(2-Bromo-4-methylphenyl)amino]-2-phenylethyl}malononitrile (**4e**). To a solution of 2-phenylcyclopropane-1,1-dicarbonitrile (150 mg, 0.89 mmol) and 2-bromo-4-methylaniline (200 mg, 1.07 mmol) in DCE (4.5 mL) in the presence of molecular sieves, 4 Å $Y(OTf)_3$ (96 mg, 0.18 mmol) was added under Ar atmosphere. The reaction mixture was stirred at room temperature for 3 days, poured into saturated aq. solution of $NaHCO_3$, and extracted with CH_2Cl_2 (3 × 10 mL). The combined organic fractions were washed with saturated aq. solution of $NaHCO_3$ (2 × 10 mL) and water (1 × 10 mL), dried with Na_2SO_4, and concentrated in vacuo. The resulting residue was purified by column chromatography on silica gel. Yield: 136 mg (43%); yellow viscous oil; R_f = 0.40 (ethyl acetate:petroleum ether; 1:4). ^{1}H NMR (CD_3OD, 600 MHz): δ 7.34–7.29 (m, 4H, Ar) 7.24–7.21 (m, 1H, Ar), 6.84 (d, ^3J = 7.9 Hz, 1H, Ar), 6.65 (dd, ^3J = 7.9 Hz, ^4J = 1.8 Hz, 1H, Ar), 6.59 (d, ^4J = 1.8 Hz, 1H, Ar), 4.68 (dd, ^3J = 10.6 Hz, ^3J = 4.4 Hz, 1H, CH), 2.57 (dd, ^2J = 14.2 Hz, ^3J = 10.6 Hz, 1H, CH_2), 2.45 (dd, ^2J = 14.2 Hz, ^3J = 4.4 Hz, 1H, CH_2), 2.21 (s, 3H, CH_3). Signals of CH and NH groups were not observed. ^{13}C NMR (CD_3OD, 150 MHz): δ 147.2 (CN), 142.2 (CN), 132.4 (CH), 129.9 (2 × CH), 128.9 (CH), 127.2 (2 × CH), 123.6 (C), 121.2 (CH), 121.0 (C), 115.2 (CH), 114.7 (C), 114.6 (C), 56.1 (CH), 38.5 (CH_2), 17.6 (CH_3). Signal of CH group was not observed. IR (film, cm^{-1}) 3391, 2898, 2524, 2257, 1597, 1490, 1408, 1266, 1071, 835, 701. HRMS ESI-TOF: m/z = 354.0584 [M + H^+] (354.0600 calcd. for $C_{18}H_{17}Br^{79}N_3^+$).

(*3aRS,5RS)-5-Phenyl-3,3a,4,5-tetrahydropyrrolo [1,2-a]quinolin-1(2H)-one* (**5**). (*E*)-1-Phenyl-5-styrylpyrrolidin-2-one (**2h**) (50 mg, 0.19 mmol) was dissolved in polyphosphoric acid (400 mg) in triple evacuated/N_2-filled vial. The obtained mixture was stirred at 100 °C for 20 min. Then, the reaction mixture was cooled and quenched with saturated aq. $NaHCO_3$ solution. The resulted mixture was extracted with ethyl acetate (3 × 7 mL). The combined organic phases were dried with Na_2SO_4. The solvent was removed under vacuum; the pure product was isolated by column chromatography on silica gel. Yield: 27 mg (54%); dark ivory solid; m.p. 174–176 °C; R_f = 0.69 (ethyl acetate:petroleum ether; 1:1). ^{1}H NMR ($CDCl_3$, 600 MHz): δ 8.71 (d, ^3J = 8.3 Hz, 1H, C(9)H), 7.35–7.32 (m, 2H, C(3′)H, C(5′)H), 7.28–7.26 (m, 1H, C(4′)H), 7.23–7.21 (m, 1H, C(8)H), 7.16 (br. d, ^3J = 7.2 Hz, 2H, C(2′)H, C(6′)H), 6.91–6.87 (m, 1H, C(7)H), 6.77 (d, ^3J = 7.9 Hz, 1H, C(6)H), 4.17 (dd, ^3J = 12.4 Hz, ^3J = 5.8 Hz, 1H, C(5)H), 4.14–4.10 (m, 1H, C(3a)H), 2.63 (ddd, ^2J = 17.1 Hz, ^3J = 10.8 Hz, ^3J = 9.9 Hz, 1H, C(2)H_2), 2.55 (ddd, ^2J = 17.1 Hz, ^3J = 9.7 Hz, ^3J = 2.3 Hz, 1H, C(2)H_2), 2.39 (ddd, ^2J = 13.3 Hz, ^3J = 5.8 Hz, ^3J = 2.3 Hz, 1H, C(4)H_2), 2.35–2.29 (m, 1H, C(3)H_2), 1.97–1.93 (m, 1H, C(4)H_2), 1.80–1.73 (m, 1H, C(3)H_2). ^{13}C NMR ($CDCl_3$, 150 MHz): δ 173.9 (C(1)), 145.0 (C(1′)), 136.7 (C(9a)), 130.0 (C(6)H), 129.7 (C(5a)), 128.8 (C(2′)H, C(6′)H), 128.6 (C(3′)H, C(5′)H), 127.2 (C(8)H), 126.9 (C(4′)H), 123.9 (C(7)H), 119.1 (C(9)H), 57.9 (C(3a)H), 45.0 (C(5)H), 40.2 (C(4)H_2), 32.1 (C(2)H_2), 25.0 (C(3)H_2). IR (KBr, cm^{-1}): 3080, 3064, 3021, 2985, 2934, 2916, 2849, 1682, 1645, 1598, 1580, 1487, 1449, 1439, 1385, 1372, 1320, 1307, 1294, 1271, 1240, 1227, 1202, 1184, 1166, 1147, 1124, 1116, 1066, 1042, 1032, 1024. HRMS ESI-TOF: m/z = 264.1390 $[M + H]^+$ (264.1383 calcd. for $C_{18}H_{18}NO^+$).

4. Conclusions

In summary, we developed a convenient general method for the synthesis of substituted γ-lactams based on Lewis acid-catalyzed DA cyclopropane ring opening with primary amines as the key step. Various 1,5-disubstituted γ-lactams were synthesized in moderate to good yields in three or four steps, requiring only a single purification procedure. We also demonstrated the potential of our method in the synthesis of an optically pure γ-lactam derivative from optically active DA cyclopropane. Additionally, the presence of reactive functionalities at the C(1) and C(5) atoms of γ-lactams ensured the possibility for postmodifications of the obtained products to convert them into more complex azaheterocycles, such as benz[*g*]indolizidine derivatives.

Supplementary Materials: Copies of NMR spectra for novel compounds are available online. The following supporting information can be downloaded at: https://www.mdpi.com/article/10.3390/molecules27238468/s1.

Author Contributions: Conceptualization, O.A.I. and I.V.T.; methodology, O.A.I. and M.A.B.; investigation, M.A.B., A.Y.P., V.V.S., D.S.L., A.V.F., S.S.Z., E.A.T. and V.B.R.; resources, O.A.I. and I.V.T.; formal analysis, S.S.Z. and O.A.I.; writing, S.S.Z., I.V.T. and O.A.I.; supervision, O.A.I. and I.V.T.; project administration, O.A.I.; funding acquisition, O.A.I. All authors have read and agreed to the published version of the manuscript.

Funding: This research was funded by the Russian Science Foundation (grant 21-73-20095).

Institutional Review Board Statement: Not applicable.

Informed Consent Statement: Not applicable.

Data Availability Statement: Not applicable.

Acknowledgments: The NMR measurements were carried out in the Laboratory of Magnetic Tomography and Spectroscopy, Faculty of Fundamental Medicine of Moscow State University. X-ray study was performed using a STOE STADI VARI PILATUS-100K diffractometer purchased through the MSU Development Program.

Conflicts of Interest: The authors declare no conflict of interest.

References

1. Vitaku, E.; Smith, D.T.; Njardarson, J.T. Analysis of the structural diversity, substitution patterns, and frequency of nitrogen heterocycles among U.S. FDA approved pharmaceuticals. *J. Med. Chem.* **2014**, *57*, 10257–10274. [CrossRef] [PubMed]
2. Baumann, M.; Baxendale, I.R.; Ley, S.V.; Nikbin, N. An overview of the key routes to the best selling 5-membered ring heterocyclic pharmaceuticals. *Beilstein J. Org. Chem.* **2011**, *7*, 442–495. [CrossRef] [PubMed]
3. Walji, A.; Berger, R.; Stump, C.A.; Schlegel, K.A.S.; Mulhearn, J.J.; Greshock, T.J.; Wang, D.; Fraley, M.E.; Jones, K.G. 3-Aryl and Heteroaryl Substituted 5-Trifluoromethyl Oxadiazoles as Histone Deacetylase 6 (HDAC6) Inhibitors. WO Pat. 2017222951A1, 28 December 2017.
4. Walji, A.; Berger, R.; Stump, C.A.; Schlegel, K.A.S.; Mulhearn, J.J.; Greshock, T.J.; Ginnetti, A.T.; Wang, D.; Stachel, S.J.; Fraley, M.E. 3-Heterocyclyl Substituted 5-Trifluoromethyl Oxadiazoles as Histone Deacetylase 6 (HDAC6) Inhibitors. WO Pat. 2017222950A1, 28 December 2017.
5. Mandegar, M.A.; Patel, S.; Ding, P.; Bhatt, U.; Holan, M.; Lee, J.; Li, Y.; Medina, J.; Nerurkar, A.; Seidl, F.; et al. Fluoroalkyl-Oxadiazoles and Uses Thereof. WO Pat. 2021127643A1, 24 June 2021.
6. Carpino, P.A.; Sanner, M.A. Cannabinoid Receptors and Uses Thereof. WO Pat. 2007020502A2, 19 April 2007.
7. Liu, H.; He, X.; Phillips, D.; Zhu, X.; Yang, K.; Lau, T.; Wu, B.; Xie, Y.; Nguyen, T.N.; Wang, X. Compounds and Compositions as Inhibitors of Cannabinoid Receptor 1 Activity. WO Pat. 2008076754A2, 22 December 2008.
8. Pevarello, P.; Brasca, M.G.; Orsini, P.; Traquandi, G.; Longo, A.; Nesi, M.; Orzi, F.; Piutti, C.; Sansonna, P.; Varasi, M.; et al. 3-Aminopyrazole inhibitors of CDK2/cyclin A as antitumor agents. 2. Lead optimization. *J. Med. Chem.* **2005**, *48*, 2944–2956. [CrossRef] [PubMed]
9. Bregman, H.; Chakka, N.; Guzman-Perez, A.; Gunaydin, H.; Gu, Y.; Huang, X.; Berry, V.; Liu, J.; Teffera, Y.; Huang, L.; et al. Discovery of novel, induced-pocket binding oxazolidinones as potent, selective, and orally bioavailable tankyrase inhibitors. *J. Med. Chem.* **2013**, *56*, 4320–4342. [CrossRef]
10. Heiser, U.; Ramsbeck, D.; Sommer, R.; Meyer, A.; Hoffmann, T.; Boehme, L.; Demuth, H.U. Novel Inhibitors. US Pat. 20110092501A1, 21 April 2011.

11. Lee, E.C.; Tu, M.; Stevens, B.D.; Bian, J.; Aspnes, G.; Perreault, C.; Sammons, M.F.; Wright, S.W.; Litchfield, J.; Kalgutkar, A.S.; et al. Identification of a novel conformationally constrained glucagon receptor antagonist. *Bioorg. Med. Chem. Lett.* **2014**, *24*, 839–844. [CrossRef]
12. Sifferlen, T.; Boller, A.; Chardonneau, A.; Cottreel, E.; Gatfield, J.; Treiber, A.; Roch, C.; Jenck, F.; Aissaoui, H.; Williams, J.T.; et al. Substituted pyrrolidin-2-ones: Centrally acting orexin receptor antagonists promoting sleep. Part 2. *Bioorg. Med. Chem. Lett.* **2015**, *25*, 1884–1891. [CrossRef]
13. Sifferlen, T.; Boller, A.; Chardonneau, A.; Cottreel, E.; Hoecker, J.; Aissaoui, H.; Williams, J.T.; Brotschi, C.; Heidmann, B.; Siegrist, R.; et al. Discovery of substituted lactams as novel dual orexin receptor antagonists. Synthesis, preliminary structure-activity relationship studies and efforts towards improved metabolic stability and pharmacokinetic properties. Part 1. *Bioorg. Med. Chem. Lett.* **2014**, *24*, 1201–1208. [CrossRef]
14. Crowley, B.; Fraley, M.; Potteiger, C.; Gilfillan, R.; Patel, M.; Arrington, K.; Mitchell, H.; Shirripa, K.; McWerther, M.; Biftu, T.; et al. Benzamide CGPR Receptor Antagonists. WO Pat. 2015161011A1, 22 October 2015.
15. Kise, N.; Hamada, Y.; Sakurai, T. Electroreductive coupling of aromatic ketones, aldehydes, and aldimines with α,β-unsaturated esters: Synthesis of 5-aryl substituted γ-butyrolactones and lactams. *Tetrahedron* **2017**, *73*, 1143–1156. [CrossRef]
16. Ogiwara, Y.; Uchiyama, T.; Sakai, N. Reductive amination/cyclization of keto acids using a hydrosilane for selective production of lactams versus cyclic amines by switching of the indium catalyst. *Angew. Chem. Int. Ed.* **2016**, *55*, 1864–1867. [CrossRef]
17. Yeh, C.H.; Korivi, R.P.; Cheng, C.H. Regioselective synthesis of γ-amino esters, nitriles, sulfones, and pyrrolidinones by nickel-catalyzed reductive coupling of aldimines and activated alkenes. *Angew. Chem. Int. Ed.* **2008**, *47*, 4892–4895. [CrossRef]
18. Dugar, S.; Crouse, J.R.; Das, P.R. Isolation and characterization of a unique hydrated gamma-lactam. *J. Org. Chem.* **1992**, *57*, 5766–5768. [CrossRef]
19. Xia, Y.; Liu, X.; Feng, X. Asymmetric catalytic reactions of donor–acceptor cyclopropanes. *Angew. Chem. Int. Ed.* **2021**, *60*, 9192–9204. [CrossRef] [PubMed]
20. Ghosh, A.; Dey, A.; Banerjee, P. Relieving the stress together: Annulation of two different strained rings towards the formation of biologically significant heterocyclic scaffolds. *Chem. Commun.* **2021**, *57*, 5359–5373. [CrossRef] [PubMed]
21. Augustin, A.U.; Werz, D.B. Exploiting heavier organochalcogen compounds in donor–acceptor cyclopropane chemistry. *Acc. Chem. Res.* **2021**, *54*, 1528–1541. [CrossRef] [PubMed]
22. Ghosh, K.; Das, S. Recent advances in ring-opening of donor acceptor cyclopropanes using C-nucleophiles. *Org. Biomol. Chem.* **2021**, *19*, 965–982. [CrossRef]
23. Pirenne, V.; Muriel, B.; Waser, J. Catalytic enantioselective ring-opening reactions of cyclopropanes. *Chem. Rev.* **2021**, *121*, 227–263. [CrossRef]
24. Sarkar, T.; Das, B.K.; Talukdar, K.; Shah, T.A.; Punniyamurthy, T. Recent advances in stereoselective ring expansion of spirocyclopropanes: Access to the spirocyclic compounds. *ACS Omega* **2020**, *5*, 26316–26328. [CrossRef]
25. Werz, D.B.; Biju, A.T. Uncovering the neglected similarities of arynes and donor-acceptor cyclopropanes. *Angew. Chem. Int. Ed.* **2020**, *59*, 3385–3398. [CrossRef]
26. Singh, P.; Varshnaya, R.K.; Dey, R.; Banerjee, P. Donor-acceptor cyclopropanes as an expedient building block towards the construction of nitrogen-containing molecules: An update. *Adv. Synth. Catal.* **2020**, *362*, 1447–1484. [CrossRef]
27. Ivanova, O.A.; Trushkov, I.V. Donor-acceptor cyclopropanes in the synthesis of carbocycles. *Chem. Rec.* **2019**, *19*, 2189–2208. [CrossRef]
28. Tomilov, Y.V.; Menchikov, L.G.; Novikov, R.A.; Ivanova, O.A.; Trushkov, I.V. Methods for the synthesis of donor-acceptor cyclopropanes. *Russ. Chem. Rev.* **2018**, *87*, 201–250. [CrossRef]
29. Budynina, E.M.; Ivanov, K.L.; Sorokin, I.D.; Melnikov, M.Ya. Ring opening of donor-acceptor cyclopropanes with N-nucleophiles. *Synthesis* **2017**, *49*, 3035–3068. [CrossRef]
30. Pagenkopf, B.L.; Vemula, N. Cycloadditions of Donor-Acceptor Cyclopropanes and Nitriles. *Eur. J. Org. Chem.* **2017**, *2017*, 2561–2567. [CrossRef]
31. Grover, H.K.; Emmett, M.; Kerr, M.A. Carbocycles from donor-acceptor cyclopropanes. *Org. Biomol. Chem.* **2015**, *13*, 655–671. [CrossRef] [PubMed]
32. Novikov, R.A.; Tomilov, Y.V. Dimerization of donor-acceptor cyclopropanes. *Mendeleev Commun.* **2015**, *25*, 1–10. [CrossRef]
33. Schneider, T.F.; Kaschel, J.; Werz, D.B. A new golden age for donor-acceptor cyclopropanes. *Angew. Chem. Int. Ed.* **2014**, *53*, 5504–5523. [CrossRef] [PubMed]
34. Vartanova, A.E.; Levina, I.I.; Ratmanova, N.K.; Andreev, I.A.; Ivanova, O.A.; Trushkov, I.V. Ambident reactivity of 5-aminopyrazoles towards donor-acceptor cyclopropanes. *Org. Biomol. Chem.* **2022**, *20*, 7795–7802. [CrossRef] [PubMed]
35. Vartanova, A.E.; Plodukhin, A.Y.; Ratmanova, N.K.; Andreev, I.A.; Anisimov, M.N.; Gudimchuk, N.B.; Rybakov, V.B.; Levina, I.I.; Ivanova, O.A.; Trushkov, I.V.; et al. Expanding Stereoelectronic Limits of *endo-tet* Cyclizations: Synthesis of Benz[*b*]azepines from Donor-Acceptor Cyclopropanes. *J. Am. Chem. Soc.* **2021**, *143*, 13952–13961. [CrossRef]
36. Vartanova, A.E.; Levina, I.I.; Rybakov, V.B.; Ivanova, O.A.; Trushkov, I.V. Donor-Acceptor Cyclopropane Ring Opening with 6-Amino-1,3-dimethyluracil and Its Use in Pyrimido[4,5-*b*]azepines Synthesis. *J. Org. Chem.* **2021**, *86*, 12300–12308. [CrossRef]
37. Boichenko, M.A.; Ivanova, O.V.; Andreev, I.A.; Chagarovskiy, A.O.; Levina, I.I.; Rybakov, V.B.; Skvortsov, D.A.; Trushkov, I.V. Convenient approach to polyoxygenated dibenzo[*c*,*e*]pyrrolo[1,2-*a*]azepines from donor-acceptor cyclopropanes. *Org. Chem. Front.* **2018**, *5*, 2829–2834. [CrossRef]

38. Villemson, E.V.; Budynina, E.M.; Ivanova, O.A.; Skvortsov, D.A.; Trushkov, I.V.; Melnikov, M.Ya. Concise approach to pyrrolizino[1,2-*b*]indoles from indole-derived donor-acceptor cyclopropanes. *RSC Adv.* **2016**, *6*, 62014–62018. [CrossRef]
39. Ivanov, K.L.; Villemson, E.V.; Budynina, E.M.; Ivanova, O.A.; Trushkov, I.V.; Melnikov, M.Ya. Ring opening of donor-acceptor cyclopropanes with the azide ion: A tool for construction of *N*-heterocycles. *Chem. Eur. J.* **2015**, *21*, 4975–4987. [CrossRef] [PubMed]
40. Goldberg, A.F.G.; O'Connor, N.R.; Craig, R.A.; Stoltz, B.M. Lewis Acid Mediated (3 + 2) Cycloadditions of Donor-Acceptor Cyclopropanes with Heterocumulenes. *Org. Lett.* **2012**, *14*, 5314–5317. [CrossRef]
41. Yamamoto, K.; Ishida, T.; Tsuji, J. Palladium(0)-catalyzed Cycloaddition of Activated Vinylcyclopropanes with Aryl Isocyanates. *Chem. Lett.* **1987**, *16*, 1157–1158. [CrossRef]
42. Sahu, A.K.; Biswas, S.; Bora, S.K.; Saikia, A.K. Synthesis of 3C-alkylated active methylene substituted 2*H*-indazole derivatives *via* sequential ring opening of donor-acceptor cyclopropanes and reductive cyclization reaction. *New J. Chem.* **2022**, *46*, 12456–12460. [CrossRef]
43. Unnava, R.; Chahal, K.; Reddy, K.R. Synthesis of substituted 1,2-dihydroisoquinolines via Ni(II) and Cu(I)/Ag(I) catalyzed double nucleophilic addition of arylamines to *ortho*-alkynyl donor-acceptor cyclopropanes (*o*-ADACs). *Org. Biomol. Chem.* **2021**, *19*, 6025–6029. [CrossRef]
44. Chang, F.; Shen, B.; Wang, S.; Lin, L.; Feng, X. Lewis acid catalysed asymmetric cascade reaction of cyclopropyl ketones: Concise synthesis of pyrrolobenzothiazoles. *Chem. Commun.* **2020**, *56*, 13429–13432. [CrossRef]
45. Singh, P.; Kaur, N.; Banerjee, P. Regioselective Bronsted acid-catalyzed annulation of cyclopropane aldehydes with *N*′-aryl anthranil hydrazides: Domino construction of tetrahydropyrrolo[1,2-*a*]quinazolin-5(1*H*)ones. *J. Org. Chem.* **2020**, *85*, 3393–3406. [CrossRef]
46. Augustin, A.U.; Jones, P.G.; Werz, D.B. Ring-Opening 1,3-Aminochalcogenation of Donor–Acceptor Cyclopropanes: A Three-Component Approach. *Chem. Eur. J.* **2019**, *25*, 11620–11624. [CrossRef]
47. Li, S.K.; Huang, L.L.; Lv, Y.D.; Feng, H.D. Synthesis of γ-(Arylamino)butyric Acid Derivatives via Ring-Opening Addition of Arylamines to Cyclopropane-1,1-Dicarboxylates. *Russ. J. Org. Chem.* **2019**, *55*, 1432–1438. [CrossRef]
48. Nambu, H.; Hirota, W.; Fukumoto, M.; Tamura, T.; Yakura, T. An Efficient Route to Highly Substituted Indoles via Tetrahydroindol-4(5H)-one Intermediates Produced by Ring-Opening Cyclization of Spirocyclopropanes with Amines. *Chem. Eur. J.* **2017**, *23*, 16799–16805. [CrossRef] [PubMed]
49. Garve, L.K.B.; Jones, P.G.; Werz, D.B. Ring-Opening 1-Amino-3-aminomethylation of Donor–Acceptor Cyclopropanes via 1,3-Diazepanes. *Angew. Chem. Int. Ed.* **2017**, *56*, 9226–9230. [CrossRef]
50. Xia, Y.; Lin, L.; Chang, F.; Liao, Y.; Liu, X.; Feng, X. Asymmetric ring opening/cyclization/retro-Mannich reaction of cyclopropyl ketones with aryl 1,2-diamines for the synthesis of benzimidazole derivatives. *Angew. Chem. Int. Ed.* **2016**, *55*, 12228–12232. [CrossRef] [PubMed]
51. Han, J.Q.; Zhang, H.H.; Xu, P.F.; Luo, Y.C. Lewis acid and (hypo)iodite relay catalysis allows a strategy for the synthesis of polysubstituted azetidines and tetrahydroquinolines. *Org. Lett.* **2016**, *18*, 5212–5215. [CrossRef] [PubMed]
52. Xia, Y.; Liu, X.; Zheng, H.; Lin, L.; Feng, X. Asymmetric synthesis of 2,3-dihydropyrroles by ring-opening/cyclization of cyclopropyl ketones using primary amines. *Angew. Chem. Int. Ed.* **2015**, *54*, 227–230. [CrossRef] [PubMed]
53. Nambu, H.; Fukumoto, M.; Hirota, W.; Yakura, T. Ring-opening cyclization of cyclohexane-1,3-dione-2-spirocyclopropanes with amines: Rapid access to 2-substituted 4-hydroxyindole. *Org. Lett.* **2014**, *16*, 4012–4015. [CrossRef]
54. Lebold, T.P.; Leduc, A.B.; Kerr, M.A. Zn(II)-Catalyzed Synthesis of Piperidines from Propargyl Amines and Cyclopropanes. *Org. Lett.* **2009**, *11*, 3770–3772. [CrossRef]
55. Lifchits, O.; Charette, A.B. A Mild Procedure for the Lewis Acid-Catalyzed Ring-Opening of Activated Cyclopropanes with Amine Nucleophiles. *Org. Lett.* **2008**, *10*, 2809–2812. [CrossRef]
56. Schobert, R.; Gordon, G.J.; Bieser, A.; Milius, W. 3-Functionalized Tetronic Acids from Domino Rearrangement/Cyclization/Ring-Opening Reactions of Allyl Tetronates. *Eur. J. Org. Chem.* **2003**, *2003*, 3637–3647. [CrossRef]
57. Jacoby, D.; Celerier, J.P.; Haviari, G.; Petit, H.; Lhommet, G. Regiospecific synthesis of dihydropyrroles. *Synthesis* **1992**, *1992*, 884–887. [CrossRef]
58. Blanchard, L.A.; Schneider, J.A. Diethylaluminum Chloride–Amine Complex Mediated Aminolysis of Activated Cyclopropanes. *J. Org. Chem.* **1986**, *51*, 1372–1374. [CrossRef]
59. Akaev, A.A.; Melnikov, M.Y.; Budynina, E.M. Chameleon-like Activating Nature of the Spirooxindole Group in Donor-Acceptor Cyclopropanes. *Org. Lett.* **2019**, *21*, 9795–9799. [CrossRef] [PubMed]
60. Luo, W.; Sun, Z.; Fernando, E.H.N.; Nesterov, V.N.; Cundari, T.R.; Wang, H. Asymmetric ring-opening of donor-acceptor cyclopropanes with primary arylamines catalyzed by a chiral heterobimetallic catalyst. *ACS Catal.* **2019**, *9*, 8285–8293. [CrossRef]
61. Das, S.; Daniliuc, C.G.; Studer, A. Stereospecific 1,3-aminobromination of donor-acceptor cyclopropanes. *Angew. Chem. Int. Ed.* **2017**, *56*, 11554–11558. [CrossRef] [PubMed]
62. Martin, M.C.; Patil, D.V.; France, S. Functionalized 4-carboxy- and 4-keto-2,3-dihydropyrroles via Ni(II)-catalyzed nucleophilic amine ring-opening cyclizations of cyclopropanes. *J. Org. Chem.* **2014**, *79*, 3030–3039. [CrossRef] [PubMed]
63. So, S.S.; Auvil, T.J.; Garza, V.J.; Mattson, A.E. Boronate urea activation of nitrocyclopropane carboxylates. *Org. Lett.* **2012**, *14*, 444–447. [CrossRef]
64. Stewart, J.M.; Pagenkopf, G.K. Transmission of Conjugation by the Cyclopropane Ring. *J. Org. Chem.* **1969**, *34*, 7–11. [CrossRef]

65. Badarinarayana, V.; Mahmud, H.; Lovely, C.J. An asymmetric total synthesis of martinellic acid. *Heterocycles* **2017**, *95*, 1082–1105.
66. Gratia, S.; Mosesohn, K.; Diver, S.T. Highly Selective Ring Expansion of Bicyclo[3.1.0]hexenes. *Org. Lett.* **2016**, *18*, 5320–5323. [CrossRef]
67. Chen, Y.; Cao, W.; Yuan, M.; Wang, H.; Ding, W.; Shao, M.; Xu, X. The reaction of electron-deficient cyclopropane derivatives with aromatic amines. *Synth. Commun.* **2008**, *38*, 3346–3353. [CrossRef]
68. Snider, B.B.; Ahn, Y.; O'Hare, S.M. Total Synthesis of (±)-Martinellic Acid. *Org. Lett.* **2001**, *3*, 4217–4220. [CrossRef] [PubMed]
69. Chen, Y.; Ding, W.; Cao, W.; Yu, C. The stereoselective synthesis of *N*-aryl-trans,trans-α-carboxyl-β-methoxy carbonyl-γ-aryl-γ-butyrolactams. *Synth. Commun.* **2001**, *31*, 3107–3112. [CrossRef]
70. Snider, B.B.; Ahn, Y.; Foxman, B.M. Synthesis of the Tricyclic Triamine Core of Martinelline and Martinellic Acid. *Tetrahedron Lett.* **1999**, *40*, 3339–3342. [CrossRef]
71. Abaev, V.T.; Trushkov, I.V.; Uchuskin, M.G. The Butin reaction. *Chem. Heterocycl. Compd.* **2016**, *52*, 973–995. [CrossRef]
72. Trushkov, I.V.; Uchuskin, M.G.; Butin, A.V. Furan's Gambit: Electrophile-Attack-Triggered Sacrifice of Furan Rings for the Intramolecular Construction of Azaheterocycles. *Eur. J. Org. Chem.* **2015**, *2015*, 2999–3016. [CrossRef]
73. *The Structures of* ***2c*** *was Proved by Single-Crystal X-ray Crystallography. CCDC 2180495 Contains the Supplementary Crystallographic Data for this Paper*; The Cambridge Crystallographic Data Centre: Cambridge, UK.
74. Zhang, W.; Huang, L.; Wang, J. A Concise Synthesis of Pyrrolo- and Pyrrolidino[1,2-*a*]quinolin-1-ones via Diels-Alder Reactions of Acyliminium Cations with Olefins. *Synthesis* **2006**, *2006*, 2053–2063. [CrossRef]
75. Fraser, W.; Suckling, C.J.; Wood, H.C.S. Latent inhibitors. Part 7. Inhibition of dihydro-orotate dehydrogenase by apirocyclopropanobarbiturates. *J. Chem. Soc. Perkin Trans. 1* **1990**, 3137–3144. [CrossRef]
76. Corey, E.J.; Chaykovsky, M. Dimethyloxosulfonium methylide($(CH_3)_2SOCH_2$) and dimethylsulfonium methylide ($(CH_3)_2SCH_2$). Formation and application to organic synthesis. *J. Am. Chem. Soc.* **1965**, *87*, 1353–1364. [CrossRef]
77. Maity, A.K.; Roy, S. A Multimetallic Piano-Stool Ir–Sn_3 Catalyst for Nucleophilic Substitution Reaction of γ-Hydroxy Lactams through N-Acyliminium Ions. *J. Org. Chem.* **2012**, *77*, 2935–2941. [CrossRef]
78. Meyer, W.L.; Vaughan, W.R. 1,5-Diaryl-2,3-pyrrolidinediones. VIII. Synthesis and Structure Proof. *J. Org. Chem.* **1957**, *22*, 1554–1560. [CrossRef]
79. Chagarovskiy, A.O.; Ivanov, K.L.; Budynina, E.M.; Ivanova, O.A.; Trushkov, I.V. Reaction of dimethyl (*S*)-2-(*p*-tolyl)cyclopropane-1,1-dicarboxylate with acetonitrile. *Chem. Heterocycl. Compd.* **2012**, *48*, 825–827. [CrossRef]

molecules

MDPI

Article

Regioselective Synthesis and Molecular Docking Studies of 1,5-Disubstituted 1,2,3-Triazole Derivatives of Pyrimidine Nucleobases

Vincenzo Algieri [1,*], Paola Costanzo [1,*], Matteo Antonio Tallarida [1,2], Fabrizio Olivito [1], Antonio Jiritano [1], Giulia Fiorani [3], Francesca Peccati [2], Gonzalo Jiménez-Osés [2,4], Loredana Maiuolo [1] and Antonio De Nino [1]

[1] Department of Chemistry and Chemical Technologies, University of Calabria, 87036 Rende, Italy
[2] Center for Cooperative Research in Biosciences (CIC bioGUNE), Basque Research and Technology Alliance (BRTA), Bizkaia Technology Park, 48160 Derio, Spain
[3] Department Molecular Sciences and Nanosystems, University Ca' Foscari Venezia, 30172 Mestre (VE), Italy
[4] Ikerbasque, Basque Foundation for Science, 48013 Bilbao, Spain
* Correspondence: vincenzo.algieri@unical.it (V.A.); paola.costanzo@unical.it (P.C.)

Abstract: 1,2,3-triazoles are versatile building blocks with growing interest in medicinal chemistry. For this reason, organic chemistry focuses on the development of new synthetic pathways to obtain 1,2,3-triazole derivatives, especially with pyridine moieties. In this work, a novel series of 1,5-disubstituted-1,2,3-triazoles functionalized with pyrimidine nucleobases were prepared via 1,3-dipolar cycloaddition reaction in a regioselective manner for the first time. The *N*1-propargyl nucleobases, used as an alkyne intermediate, were obtained in high yields (87–92%) with a new two-step procedure that selectively led to the monoalkylated compounds. Then, $FeCl_3$ was employed as an efficient Lewis acid catalyst for 1,3-dipolar cycloaddition between different aryl and benzyl azides and the *N*1-propargyl nucleobases previously synthesized. This new protocol allows the synthesis of a series of new 1,2,3-triazole derivatives with good to excellent yields (82–92%). The ADME (Absorption, Distribution, Metabolism, and Excretion) analysis showed good pharmacokinetic properties and no violations of Lipinsky's rules, suggesting an appropriate drug likeness for these new compounds. Molecular docking simulations, conducted on different targets, revealed that two of these new hybrids could be potential ligands for viral and bacterial protein receptors such as human norovirus capsid protein, SARS-CoV-2 NSP13 helicase, and metallo-β-lactamase.

Keywords: 1,2,3-triazoles; nucleobases; Lewis acid; click chemistry; molecular docking; ADME

Citation: Algieri, V.; Costanzo, P.; Tallarida, M.A.; Olivito, F.; Jiritano, A.; Fiorani, G.; Peccati, F.; Jiménez-Osés, G.; Maiuolo, L.; De Nino, A. Regioselective Synthesis and Molecular Docking Studies of 1,5-Disubstituted 1,2,3-Triazole Derivatives of Pyrimidine Nucleobases. *Molecules* **2022**, *27*, 8467. https://doi.org/10.3390/molecules27238467

Academic Editors: Alexey M. Starosotnikov, Maxim A. Bastrakov and Igor L. Dalinger

Received: 4 November 2022
Accepted: 29 November 2022
Published: 2 December 2022

1. Introduction

The synthesis of triazole compounds, such as 1,2,3- and 1,2,4-triazoles, is of interest due to their versatility and usefulness in several fields including agriculture [1,2], material sciences [3,4], chemistry [5–7], as well as medicine [8–10]. In particular, the use of 1,2,3-triazoles as potential pharmacophores was intensively investigated. Thanks to their ability to form various non-covalent and dipole–dipole interactions, they were tested towards different biological targets [11]. From a synthetic point of view, 1,2,3-triazoles derivatives have attracted considerable attention after the independent discoveries of Meldal and Sharpless in the early 2000s, which allowed the regiospecific synthesis of 1,4-disubstituted 1,2,3-triazoles via click chemistry [12,13]. Furthermore, in 2005, Zhang and co-workers showed that it was also possible to attain the regioselective synthesis of 1,5-disubstituted 1,2,3-triazoles by changing copper to ruthenium [14].

Other transition metal catalysts (Au, Ir, Ni, Ag) were tested [15], but despite the huge efforts, the employment of heavy metals in the synthesis restricts their application due to their hazardous nature, toxicity, and high cost. In recent years, great attention was paid to

the development of copper- and ruthenium-based alternative routes, and different protocols were developed [16]. Besides 1,2,3-triazoles, natural and modified nucleosides are another class of heterocyclic compounds with widespread applications as pharmaceutically active compounds [17,18] and diagnostic probes [19]. Considering the numerous advantages of using both triazoles and nucleosides as building blocks in drug discovery, many researchers synthesized nucleosides containing the triazole moiety [20,21]. Starting from the discovery of the broad-spectrum antiviral compound Ribavirin **I** (Figure 1), in which a 1,2,4-triazole was used as a nucleobase, different new hybrids were designed and tested, showing antiviral and/or antitumor activity. These nucleoside analogues were characterized by the introduction of a triazole group in place of the nucleobase **I** [22], or the sugar moiety **II** [23], as a linkage between them **III** [24], and as a modification group of the sugar **IV** [25] (Figure 1).

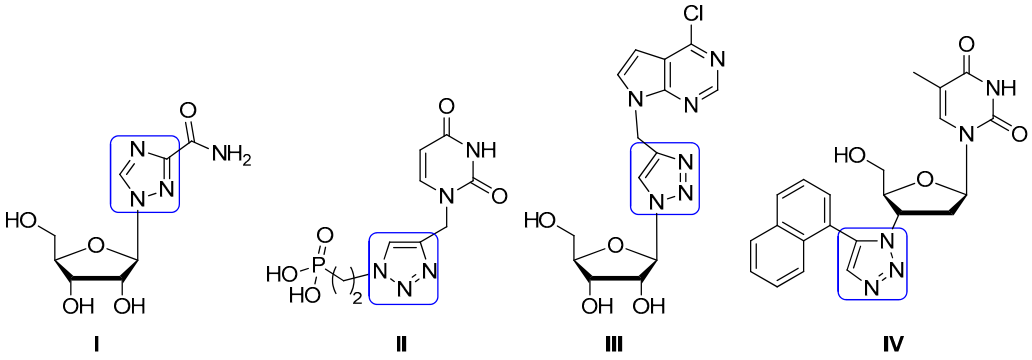

Figure 1. Some reported anticancer agents bearing triazole, nucleobase, and/or glycoside moieties.

To date, only a few examples of 1,4-disubstituted 1,2,3-triazole nucleoside derivatives were synthesized. These compounds were tested as corrosion inhibitors for steel [26], against HCV (Hepatitis C virus) [23], and against influenza virus A (H3N2) [27]. However, to the best of our knowledge, there have been no reported synthetic efforts toward 1,5-disubstituted analogues.

In this work, considering our experience in the development of alternative synthetic routes catalyzed by Lewis acids [28,29] and cycloaddition reactions [30,31], we report the synthesis of new 1,5-disubstituted 1,2,3-triazole derivatives containing pyrimidine nucleobases in high yields and a regioselective way. All of the triazole derivatives were synthesized starting from different aryl azides and non-commercial *N*1-propargyl pyrimidine nucleobases using a common Lewis acid catalyst. In detail, iron(III) chloride was selected as a suitable catalyst because of its low price, easy availability, sustainability, nontoxicity, and environmentally friendly characteristic [32,33]. Moreover, the use of *N*1-propargyl pyrimidine nucleobases allows the introduction of a methylene bridge at C-5 of the triazole, which could mimic the behavior of "fleximers", a kind of nucleoside analogue characterized by enhanced conformational freedom [34]. The pharmacokinetic properties of the synthesized derivatives were predicted through ADME (Absorption, Distribution, Metabolism, and Excretion) analysis to evaluate the medicinal chemistry friendliness. Furthermore, an in silico screening was performed towards selected receptors from the Protein Data Bank, suggesting biological potential for our products.

2. Results and Discussion

2.1. Chemistry

*N*1-propargyl nucleobases are important starting materials for the synthesis of nucleoside analogues with biological activity [35]. Usually, propargyl nucleobases are synthesized in a one-step reaction between the appropriate nucleobase and propargyl bromide under basic conditions [36] or employing an intermediate bis(trimethylsilyl)pyrimidine nucleobase using *N*,*O*-bis(trimethylsilyl)-acetamide (BSA) [37]. Unfortunately, the first methodology yields the products with low selectivity [38] because a mixture composed

of *N*1-monoalkylated and *N*1,*N*3-dialkylated pyrimidines is obtained, while the second approach results in long reaction times and low yield [26]. With this in mind, selective nucleobase propargylation is necessary, and, due to the feasibility of performing selective alkylation at the *N*-1 position of pyrimidine nucleobases, the propargylation is performed in two-reaction steps via *O*-protection by a transient group, as shown in Scheme 1.

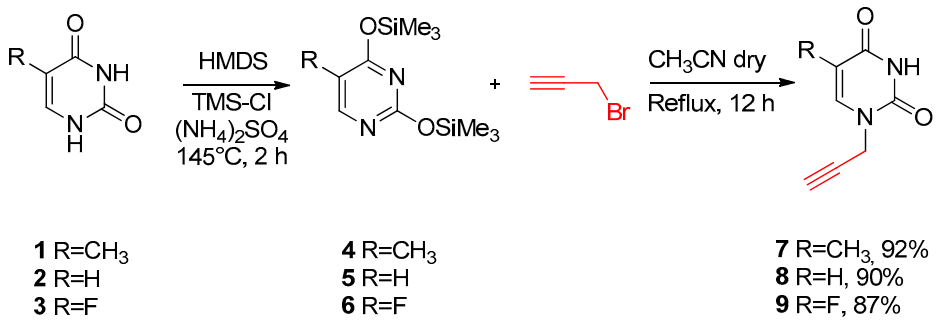

1 R=CH_3
2 R=H
3 R=F

4 R=CH_3
5 R=H
6 R=F

7 R=CH_3, 92%
8 R=H, 90%
9 R=F, 87%

Scheme 1. Synthesis of propargyl nucleobases with two reaction steps.

Here, we developed a methodology that involves the *N*1-selective propargylation of bis(trimethylsilyl)pyrimidine intermediates (**4**–**6**) to prepare compounds **7**–**9**. Thus, pyrimidine nucleobases **1**–**3** were treated under an inert atmosphere with hexamethyldisilazane (HMDS), trimethylsilyl chloride (TMS-Cl), and $(NH_4)_2SO_4$ to give the silylated nucleobases **4**–**6**, which were used without further purification and isolated by under vacuum evaporation of HMDS. In situ propargylation of **4**–**6**, conducted in dry acetonitrile at reflux under an inert atmosphere, furnished the desired products **7**–**9** with excellent reaction yields and in a regioselective way because only *N*-1 monosubstituted nucleobases were observed in all cases.

With compounds **7**–**9** in hand, we then performed a Lewis acid-catalyzed azide-alkyne 1,3-dipolar cycloaddition reaction to generate a series of 1,5-disubstituted 1,2,3-triazole derivatives of nucleobases in a regioselective way.

To begin, we chose the cycloaddition reaction between 1-propargylthymine **7** and phenyl azide **10** in the presence of Lewis acid catalysts as the model system to optimize the reaction conditions (Scheme 2). The results are reported in Table 1.

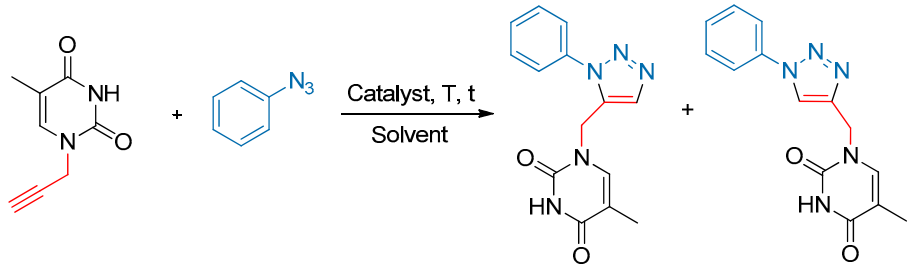

7 **10** **14a** **14b**

Scheme 2. Azide-alkyne 1,3-dipolar cycloaddition to synthesize 1,5-disubstituted-1,2,3-triazoles functionalized with pyrimidine nucleobases.

Firstly, the reaction between 1-propargylthymine **7** and phenyl azide **10**, in a 1:2 ratio, was performed with 20 mol% $Er(OTf)_3$ as the catalyst and heated at 60 °C both in CH_2Cl_2 (Table 1, entry 1) and THF (Table 1, entry 2). In both cases, no product formation was observed after 24 h of time reaction. An increase in temperature to 100 °C favored a slight formation of the product with a yield of 15% (Table 1, entry 3). Changing THF to CH_3CN allowed a small yield increase in 24 h (Table 1, entry 4). Better results were obtained by raising the temperature to 120 °C (Table 1, entry 5), and also using nitromethane as a solvent (Table 1, entry 6). However, the use of DMF as a solvent and $Er(OTf)_3$ as the catalyst at 120 °C provided good yields in only 8 h (Table 1, entry 7). At this point, a screening of

different Lewis acids was performed (Table 1, entries 8–11) and the best reaction conditions were found when $FeCl_3$ was used as the catalyst (Table 1, entry 11), leading to 88% yield in 8 h. The role of the catalyst was remarkable since it selectively led to one regioisomer, corresponding to the 1,5-disubstituted 1,2,3-triazole **14a**. However, the regioisomer **14b** was also isolated and characterized by ^{1}H NMR and ^{13}C NMR, and an 88:12 ratio was calculated by ^{1}H NMR analysis of the reaction crude (see Supplementary Materials). In fact, without any catalyst, reagents **7** and **10** under the same reaction conditions gave the 1,5-disubstituted triazoles **14** in low yield after a long reaction time (Table 1, entry 12) and a mixture of the 1,5-disubstituted/1,4-disubstituted products was observed in a 63:37 ratio. This last result suggests that the Lewis acid catalyst accelerates the reaction by increasing the electrophilicity of the alkyne group through coordination. Although the iron(III) chloride efficacy as a catalyst in an eliminative azide–olefin cycloaddition was already demonstrated for the synthesis of 1,5-disubstituted triazoles [39], we were delighted to observe such regioselectivity. Moreover, a comparison with classical cycloaddition reaction conditions was made in toluene without any catalyst. A regioisomer mixture in a 60:40 ratio was obtained in low yield after a long reaction time (Table 1, entry 13). The addition of a catalyst slightly increased the yield without significantly improving regioselectivity (Table 1, entry 14). Finally, the 1,3-dipolar cycloaddition reaction was carried out in [mPy](OTf) ionic liquid (Table 1, entry 15), prepared as reported in the literature [40], with the purpose of hypothetically recycling the solvent. Unfortunately, due to the high solubility of the pyrimidine in the ionic liquid, it was not possible to use the latter as a solvent because it was impossible to purify the product by simple liquid–liquid extraction.

Table 1. Optimization of reaction conditions of azide-alkyne 1,3-dipolar cycloaddition.

Entry [a]	Solvent	Catalyst	T (°C)	Time (h)	Yield (%) [b]	14a:14b Ratio [c]
1	CH_2Cl_2	$Er(OTf)_3$	60	24	-	-
2	THF	$Er(OTf)_3$	60	24	-	-
3	THF	$Er(OTf)_3$	100	24	15	n.c.
4	CH_3CN	$Er(OTf)_3$	100	24	30	n.c.
5	CH_3CN	$Er(OTf)_3$	120	24	53	80:20
6	CH_3NO_2	$Er(OTf)_3$	120	24	50	75:25
7	DMF	$Er(OTf)_3$	120	8	75	82:18
8	DMF	$Yb(OTf)_3$	120	24	70	85:15
9	DMF	$ZnCl_2$	120	24	71	77:23
10	DMF	$CeCl_3$	120	24	72	80:20
11	DMF	$FeCl_3$	120	8	88	88:12
12	DMF	-	120	24	56	63:37
13	Toluene	-	120	24	40	60:40
14	Toluene	$FeCl_3$	120	24	48	70:30
15	[mPy](OTf)	$FeCl_3$	120	24	-	-

[a] Reaction Conditions: **7** (1 eq), catalyst (0.2 eq), **10** (2 eq), in 8 mL of solvent for the appropriate time. [b] Isolated yield for regioisomer **14a**. [c] Regioisomeric ratio calculated from ^{1}H NMR analysis of the reaction crude on the C6H proton of the nucleobase. n.c.= not calculated.

Once the reaction conditions were optimized, we extended the protocol to various *N*1-propargyl nucleobases **7**–**9** and different azides **10**–**13** (Scheme 3, Table 2).

As shown in Table 2, the *N*1-propargyl nucleobases **7**–**9** showed a high reactivity towards the iron(III)-catalyzed 1,3-dipolar cycloaddition, and high reaction yields were obtained. Conversely, the reactivity of the azides depended on the nature of the aryl or alkyl group. In fact, benzyl azide **11** provided products **17a**–**19a** (Table 2, entries 4–6) with slightly lower yields than phenyl azide **10** (Table 2, entries 1–3).

Aromatic azides **10**, **12**, and **13** exhibited different reactivities depending on the substitution of the aromatic ring. In fact, the presence of a strong electron-withdrawing group (-NO_2) at the *para* position reduced the nucleophilicity of the azide **12** (Table 2, entries 7–9), while the presence of the electron-donor group (CH_3O^-) at the same position increased its nucleophilicity (azide **13**, Table 2, entries 10–12). Hence, the reaction yield for the re-

gioisomer **a**, as an isolated compound, was excellent in all cases. In addition, only a single regioisomer was obtained for all synthesized compounds, proving the high regioselectivity of the iron(III)-catalyzed reaction.

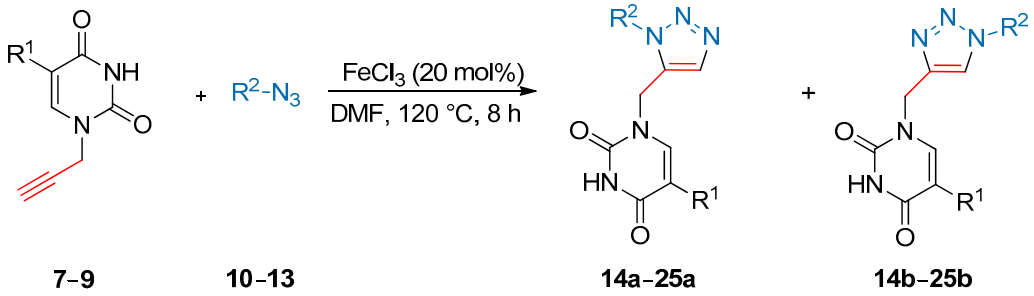

Scheme 3. 1,5-disubstituted-1,2,3-triazoles functionalized with pyrimidine nucleobases generated from various azides and propargyl nucleobases.

Table 2. Substrate scope for the synthesis of 1,5-disubstituted 1,2,3-triazoles **14**–**25**.

Entry [a]	Nucleobase	R^1	Azide	R^2	Product	Yield [b](%)	a:b Ratio [c]
1	**7**	CH_3	**10**	Ph	**14**	88	88:12
2	**8**	H	**10**	Ph	**15**	90	88:12
3	**9**	F	**10**	Ph	**16**	88	87:13
4	**7**	CH_3	**11**	Bn	**17**	85	87:13
5	**8**	H	**11**	Bn	**18**	87	88:12
6	**9**	F	**11**	Bn	**19**	84	86:14
7	**7**	CH_3	**12**	(4-NO_2)Ph	**20**	83	87:13
8	**8**	H	**12**	(4-NO_2)Ph	**21**	86	86:14
9	**9**	F	**12**	(4-NO_2)Ph	**22**	82	85:15
10	**7**	CH_3	**13**	(4-CH_3O)Ph	**23**	90	89:11
11	**8**	H	**13**	(4-CH_3O)Ph	**24**	92	89:11
12	**9**	F	**13**	(4-CH_3O)Ph	**25**	89	88:12

[a] Reaction Conditions: **7** (1 eq), catalyst (0.2 eq), **10** (2 eq), in DMF for the appropriate time. [b] Isolated yield for regioisomers 1,5-disubstituted **a**. [c] Regioisomeric ratio calculated from ^{1}H NMR analysis of the crude on the C6H proton of the nucleobases.

Finally, we proposed a possible catalytic reaction mechanism for the reaction between **7** and **10** as illustrated in Scheme 4. The first reaction step is the coordination of iron(III) chloride to the alkyne group of *N*-propargylthymine **7**, generating intermediate **a** with increased electrophilicity. Activated dipolarophile **a** reacts with phenyl azide **10** through a concerted 1,3-dipolar cycloaddition reaction to give intermediate **c**. Subsequent heterocycle aromatization of **c** gives product **14** and allows catalyst turnover.

2.2. Molecular Docking

Finally, to evaluate the potential biological activity of our products, molecular docking simulations were carried out using GOLD (CCDC Discovery) [41] and the ChemScore scoring function [42]. An in silico study was performed over 16 targets for the full set of the compounds synthesized in this work (see Supplementary Materials for further details). Compounds **20a** and **21a** were the best ranked ones (Figure 2), matching or exceeding in some cases the score of the co-crystallized ligand in the original structure, suggesting that these compounds might be able to bind the selected targets. Such targets have been at the center of great attention in the last years due to their possible implication in different pathologies. Human norovirus is one of the major causes of nonbacterial gastroenteritis in humans, and targeting the protruding P domain dimer (P-dimer) of a GII.10 Norovirus strain (Figure 2A) could be a successful strategy in drug discovery [43]. Eosinophil-derived

neurotoxin (EDN) (Figure 2B) is a member of the Ribonuclease A (RNase A) superfamily involved in inflammatory disorders and the immune response system [44]. Metallo β-lactamases (Figure 2C) are a family of enzymes employed by bacteria to hydrolyze β-lactam drugs as carbapenems, determining the resistance to antibiotics [45]. Hence, the discovery of new inhibitors capable of blocking such receptors could be of interest in combating bacterial infective diseases. As for the target reported in Figure 2D, SARS-CoV-2 NSP13 helicase was described by Newman et al. [46] in 2021 as a potential target for new antivirals due to its essential role in viral replication and its high sequence conservation.

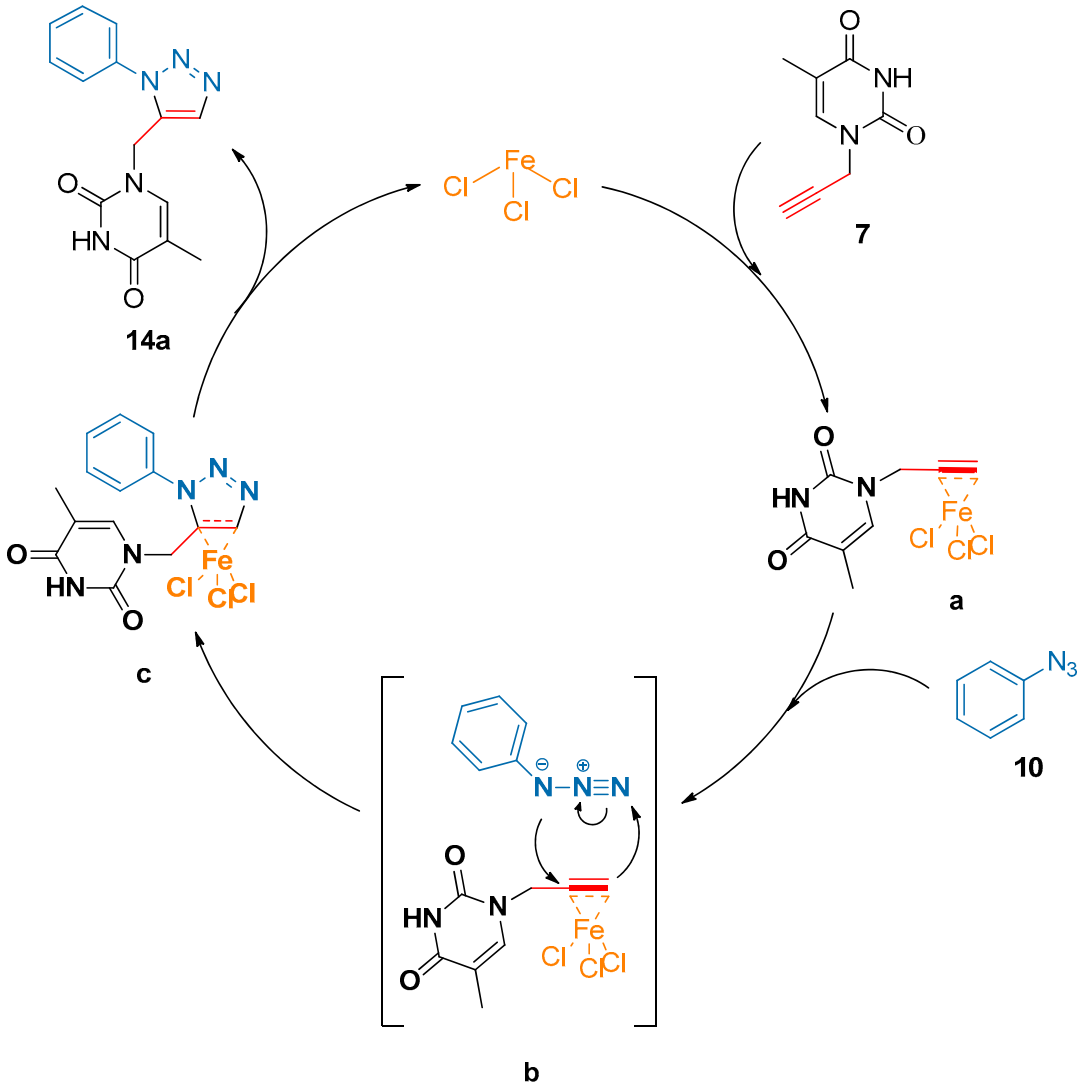

Scheme 4. Proposed catalytic cycle for the regioselective iron(III)-catalyzed azide-alkyne 1,3-dipolar cycloaddition reaction.

Binding interactions mostly involve hydrogen bonds with the protein backbone or with charged residues, which are in general very much favored from the energetic point of view and capable of dictating the local structure [47].

2.3. Pharmacokinetics and ADMET Study

The drug-likeness of the newly synthesized hybrids was further evaluated. The analysis of absorption, distribution, metabolism, and excretion (ADME) was determined in silico by using the online database ADMETlab 2.0 [48]. As reported in Table 3, all hybrids expressed good ADME properties. They showed good water solubility and no violation of the Lipinsky rules of 5 [49]. Although the Caco-2 permeability was not excellent in

some cases, effective intestinal absorption was found for all compounds, not only with the ADMETlab 2.0 software but also using the Brain Or IntestinaL EstimateD permeation method (BOILED-Egg) that evaluates the accessibility of compounds to the gastrointestinal (GI) tract and blood–brain barrier [50] (Figure 3). The boiled egg model revealed that all molecules had satisfactory GI absorption and no sufficient permeability across the blood–brain barrier (BBB), thus indicating good safety for the Central Nervous System (CNS). Moreover, all compounds had a good clearance rate (excretion rate) from the body. The encouraging results reported in Table 3 suggest that these compounds could be eligible as drug candidates, confirming the use of **20a** and **21a** as potential lead compounds for a new class of active pharmaceutical ingredients.

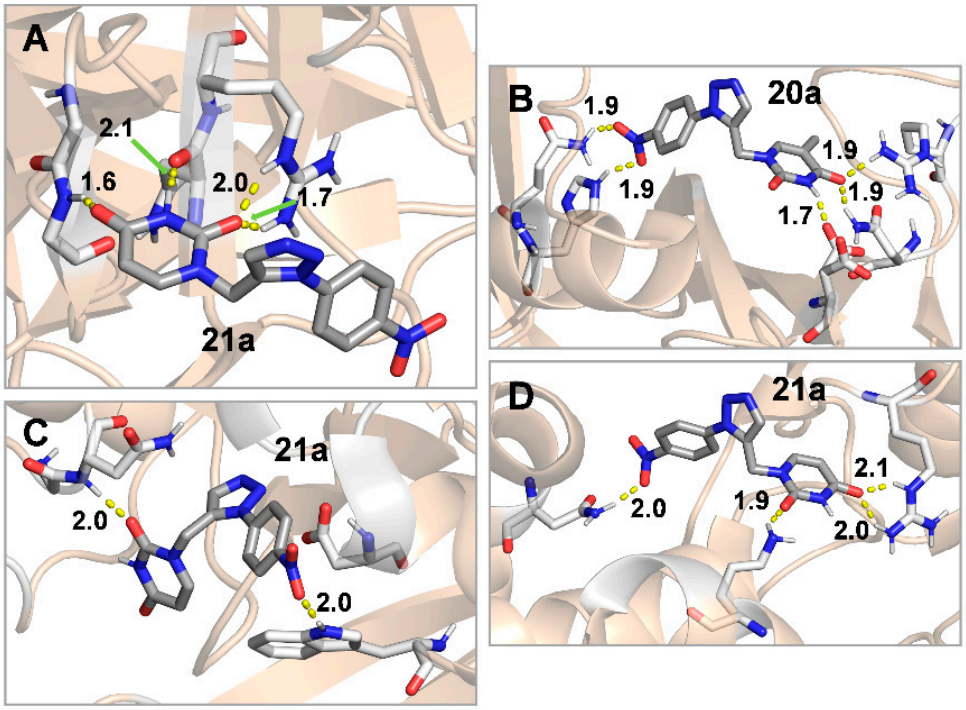

Receptor	Best scores												
	Ligand	**14a**	**15a**	**16a**	**17a**	**18a**	**19a**	**20a**	**21a**	**22a**	**23a**	**24a**	**25a**
SET Domain Bifurcated Protein 1	31.0	28.6	28.5	28.3	28.3	27.9	28.5	25.4	25.4	24.9	28.8	26.9	27.5
Human Norovirus Capsid Protein	21.3	20.3	19.3	19.4	19.6	21.0	18.3	21.6	21.7	20.5	20.6	20.3	20.0
Eosinophil-derived Neurotoxin	16.7	23.7	22.2	21.5	23.7	23.1	22.8	26.8	26.1	25.4	24.1	22.4	22.3
p38 Mitogen-Activated Protein Kinase	28.6	28.5	26.2	27.0	24.7	24.5	22.5	24.7	23.6	23.1	24.7	23.9	23.2
Metallo-β-lactamase	34.5	35.3	34.3	32.6	34.8	34.0	32.8	36.6	36.7	35.2	33.9	35.3	34.0
Human Protein Kinase CK2	26.4	23.0	20.6	19.8	23.4	20.8	19.4	21.0	23.1	21.5	22.2	22.1	20.8
SARS-CoV-2 NSP13 Helicase	22.1	21.7	21.2	18.9	18.3	18.4	18.1	21.3	22.3	21.1	19.6	21.7	18.1

Figure 2. Best docking poses of compounds **14a**–**25a** vs. co-crystalized ligands on selected protein receptors: (**A**) Compound **21a** bound to human norovirus capsid protein (PDB 6GY9). (**B**) Compound **20a** bound to eosinophil-derived neurotoxin (PDB 5E13). (**C**) Compound **21a** bound to metallo-β-lactamase (PDB 7OVE). (**D**) Compound **21a** bound to SARS-CoV-2 NSP13 helicase (PDB 7NNG). Ligands and binding residues are shown as sticks. Non-polar hydrogens have been omitted for clarity. In the table, the docking scores of compounds **14a**–**25a** and literature ligands were compared. The green color refers to scores higher than the literature ligands. The orange color refers to scores lower than the literature ligands. For those cases in which the docking score was higher than literature ligands the receptors are reported in bold.

Table 3. Pharmacokinetic properties as predicted in silico by the software ADMETlab 2.0.

ADMET	Parameters	14a	15a	16a	17a	18a	19a	20a	21a	22a	23a	24a	25a
Physio-Chemical properties	MW	283.29	269.26	287.25	297.31	283.29	301.28	328.28	314.26	332.25	313.31	299.28	317.28
	Log P [a]	0.39	0.044	0.174	0.691	0.368	0.5	0.672	0.286	0.449	0.269	−0.037	0.098
	Log S [b]	−2.011	−1.92	−1.97	−2.055	−2.057	−1.98	−2.968	−2.766	−2.845	−2.278	−2.242	−2.208
Medicinal chemistry	Lipinsky Violation [c]	No	No	No	No	No	No	No	No	No	No	No	No
	SAscore [d]	2.456	2.475	2.536	2.468	2.485	2.544	2.613	2.628	2.684	2.471	2.485	2.545
Absorption	Caco-2 permeability [e]	−5.142	−5.444	−5.129	−5.218	−5.573	−5.216	−5.132	−5.409	−5.139	−5.099	−5.287	−5.03
	Pgp-substrate [f]	0.003	0.001	0.001	0.002	0.001	0.001	0.005	0.001	0.001	0.006	0.002	0.002
	HIA [g]	0.02	0.071	0.021	0.017	0.065	0.15	0.016	0.027	0.023	0.056	0.236	0.053
Distribution	BBB permeability [h]	0.566	0.691	0.721	0.187	0.323	0.188	0.36	0.386	0.232	0.372	0.679	0.59
	Plasma Protein Binding [i]	59.29%	42.51%	49.03%	66.16%	49.75%	58.27%	75.29%	61.81%	68.17%	70.45%	58.58%	60.93%
Metabolism	CYP2D6 substrate [l]	0.106	0.102	0.088	0.118	0.111	0.101	0.117	0.114	0.097	0.156	0.152	0.123
	CYP3A4 substrate [l]	0.403	0.272	0.256	0.354	0.257	0.235	0.24	0.175	0.153	0.457	0.286	0.284
Excretion	Clearance [m]	7.411	6.579	8.095	8.509	7.408	9.215	7.473	6.571	8.108	7.412	6.665	8.128

[a] Log of the octanol/water partition coefficient. Optimal: 0–3. [b] Log of the aqueous solubility. Optimal: −4–0.5 log mol/L. [c] MW ≤ 500; logP ≤ 5; Hacc ≤ 10; Hdon ≤ 5. [d] The synthetic accessibility score is designed to estimate ease of synthesis of drug-like molecules. SAscore ≥ 6, difficult to synthesize; SAscore < 6, easy to synthesize. [e] Optimal: higher than −5.15 Log unit. [f] The output value is the probability of being the Pgp-substrate. [g] Human Intestinal Absorption. Category 1: HIA+(HIA < 30%); Category 0: HIA−(HIA < 30%); The output value is the probability of being HIA+. [h] Blood–Brain Barrier Penetration. Category 1: BBB+; Category 0: BBB−; The output value is the probability of being BBB+. [i] Optimal: <90%. Drugs with high protein binding may have a low therapeutic index. [l] The output value is the probability of being the substrate. [m] High: > 15 mL/min/kg; moderate: 5–15 mL/min/kg; low: <5 mL/min/kg.

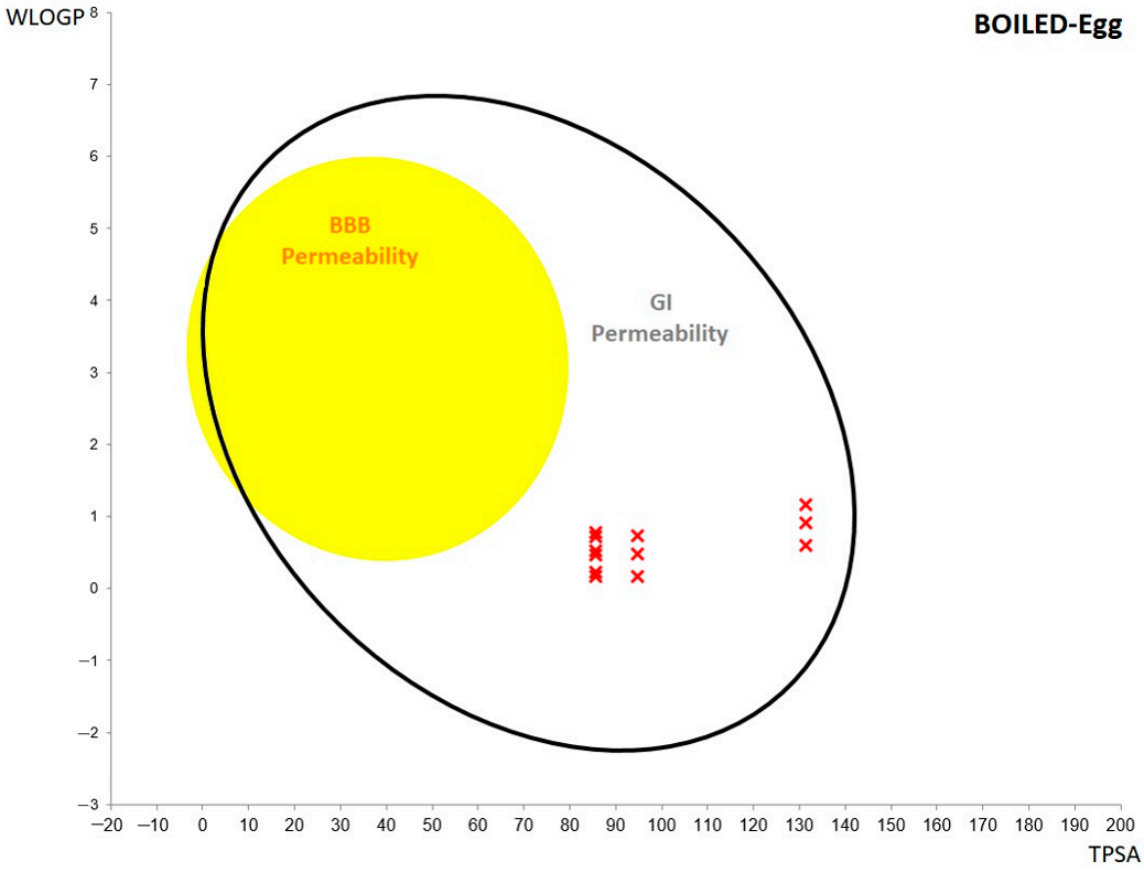

Figure 3. The BOILED-egg model of 1,5-disubstituted 1,2,3-triazole derivatives of pyrimidine nucleobases (**14a**–**25a**). BBB and GI permeability are indicated in yellow and colorless regions, respectively.

3. Materials and Methods

3.1. General Procedure for Nucleobase Propargylation **7–9**

In a three-necked round-bottomed flask, equipped with a bubble condenser and magnetic stir bar, the opportune nucleobase **1–3** (39.6 mmol, 1 eq) in dry hexamethyldisilazane (HMDS, 139 mmol, 3.5 eq) was suspended under nitrogen atmosphere. Subsequently, trimethylsilyl chloride (8.71 mmol, 0.22 eq) and $(NH_4)_2SO_4$ (1.98 mmol, 0.05 eq) were added, and the mixture was stirred at 145 °C for 2 h. After completion, the solution was cooled to room temperature, and the HMDS was evaporated under vacuum. Then, the obtained silylated nucleobase **4–6** was dissolved in dry acetonitrile (150 mL) without any further purification. Propargyl bromide (39.6 mmol, 1 eq) was added dropwise at 80 °C for 30 min, and the reaction was stirred under reflux for 12 h. After cooling to room temperature, acetonitrile was removed under vacuum, and the crude was purified by silica flash chromatography (eluent mixture $CHCl_3/CH_3OH$ 8:2) to give a solid product **7–9**. For characterization data, see Supplementary Materials.

3.2. General Procedure for Nucleobase-Containing 1,5-Disubstituted 1,2,3-Triazoles **14a–25a**

In a 50 mL two-necked round-bottomed flask equipped with a bubble condenser and magnetic stir bar, propargyl nucleobase **7–9** (1.52 mmol, 1 eq) was dissolved in DMF (8 mL). Subsequently, $FeCl_3$ (0.304 mmol, 0.2 eq) and opportune azide **10–13** (3.05 mmol, 2 eq) were added, and the mixture was stirred at 120 °C for 8 h. DMF was removed under vacuum by generating an azeotrope with toluene, and the obtained crude solid was purified on a flash silica gel column (eluent mixture: $CHCl_3$/acetone/CH_3OH 8:1:1 $v/v/v$) to obtain the desired solid product **14a–25a**. The configuration of regioisomers was determined by spectroscopic data reported in Supplementary Materials. Furthermore, to calculate the regioisomeric ratio, the C6H proton on the nucleobases was chosen for both regioisomers (see Supplementary Materials).

3.3. Docking Studies

For each receptor, the docking cavity was centered on the binding site of the crystallographic ligand and allowed to extend in a spherical surrounding volume with a radius of 15 Å. In cases where a metal ion was present at the binding site, the docking cavity was centered on it, and metal parameters were set to maintain the same coordination number as that in the crystallographic structure. In the absence of metals, the XYZ coordinates that defined the center of the cavity were obtained from the position of the co-crystalized ligand, choosing an atom that was reasonably at the center of the ligand. The number of genetic algorithm runs was set to 20 for each analyzed ligand. Protein structures were prepared using UCSF Chimera [51], by reverting selenomethionine to methionine, eliminating alternate locations of side chains, adding hydrogen atoms, assigning appropriate protein atom types, and removing the co-crystalized ligand and solvent molecules. Crystallographic ligands were docked after adding hydrogen atoms with UCSF Chimera and without optimizing their geometries. Conversely, the geometries of the screened ligands **14a–25a** were optimized quantum mechanically. Geometry optimizations and frequency calculations for stationary point characterization were carried out with Gaussian16 [52] using the M06-2X hybrid functional [53], the 6-31G(d,p) basis set, and ultrafine integration grids. Bulk solvent effects in water were considered implicitly through the IEF-PCM polarizable continuum model [54]. As for the potential receptors, 26 targets were initially selected from the Protein Data Bank (Figure S1). The main selection criterion was the presence of a triazole (i.e., 1,2,3- and 1,2,4-triazoles) scaffold or structurally similar heterocycles (i.e., imidazoles, thiazoles) in the crystallographic structure of the ligand–receptor complex. Docking simulations were performed, keeping the coordinates of the protein fixed while allowing flexibilization of the ligands around their rotatable bonds.

3.4. Prediction of Pharmacokinetic Properties

The absorption, distribution, metabolism, and excretion (ADME) analysis and assessment of Lipinski parameters were carried out using the free software "ADMETlab 2.0" supported by the Xiangya School of Pharmaceutical Sciences, Central South University ADMETlab 2.0 (2021) https://admetmesh.scbdd.com (accessed on 12 September 2022) [48]. The main properties considered were physical and chemical properties such as molecular weight, oil/water partition coefficient, and water solubility. Medicinal chemistry parameters were evaluated: the synthetic accessibility score (designed to estimate the ease of synthesis of drug-like molecules) and the violation of Lipinsky's rules. Absorption was studied mainly considering the permeability after oral administration (Caco-2 cell permeability) and human intestinal absorption (HIA). Among the distribution parameters, Plasma Protein Binding and blood brain–barrier (BBB) penetration were selected. CYP2D6 and CYP3A4 were selected as key enzymes in the metabolism of the compounds. Furthermore, clearance was evaluated as an excretion parameter. Finally, the Brain Or IntestinaL EstimateD permeation method (BOILED-Egg) was used to clarify the main distribution tissue for compounds **14a**–**25a [50]**.

4. Conclusions

We have developed a new synthetic approach towards the highly regioselective synthesis of 1,5-disubstituted 1,2,3-triazole derivatives containing pyrimidine nucleobases. *N*1-propargyl nucleobases were first prepared in excellent yields through an alternative route that led only to the *N*1-monoalkylated derivatives. These alkyne compounds were characterized and used in a 1,3-dipolar cycloaddition reaction to obtain the 1,2,3 triazole heterocycles. The 1,5-disubstituted-1,2,3-triazol moiety was obtained in a regioselective way by using $FeCl_3$ as an inexpensive and non-toxic catalyst. It was demonstrated that this procedure worked well for different aryl and benzyl azides. Although some differences were found with aryl azides bearing strong electron-withdrawing and electron-donating groups, reaction yields ranged from good to excellent in all cases. Finally, compounds **20a** and **21a** exhibited the best docking scores against four of the selected protein targets, suggesting potential biologic activity for these scaffolds. In addition, ADMET analysis was also performed using an in silico online database, which predicted that all hybrids might have qualified pharmacokinetic parameters and Lipinski's rule of five properties to claim their intestinal absorption and good clearance rate.

Supplementary Materials: The following supporting information can be downloaded at https://www.mdpi.com/article/10.3390/molecules27238467/s1, Characterization spectra of the *N*-propargyl nucleobases **7**–**9** (^{1}H NMR–^{13}C NMR–HRMS); Characterization spectra of nucleobase-containing disubstituted 1,2,3-triazoles **14a, 14b, 15a**–**25a** (^{1}H NMR–^{13}C NMR–COSY NMR–HRMS); Characterization spectra of derivative **21a** (HMBC and HSQC NMR); Figure S1. Workflow describing the approach used to validate the docking protocol and select the target receptors (first series) and to evaluate the binding capacity of compounds **14a**–**25a** to them.

Author Contributions: Conceptualization, V.A., P.C. and M.A.T.; methodology, V.A., P.C. and M.A.T.; software, P.C., M.A.T. and F.P.; validation, G.J.-O. and L.M.; formal analysis, G.F.; investigation, V.A., F.O., M.A.T. and A.J.; resources, A.D.N.; data curation, F.P. and A.J.; writing—original draft preparation, P.C. and V.A.; writing—review and editing, L.M., G.J.-O. and A.D.N.; visualization, P.C. and F.O.; supervision, L.M. and A.D.N.; funding acquisition, P.C., L.M. and A.D.N. All authors have read and agreed to the published version of the manuscript.

Funding: This research was funded by the University of Calabria and Calabria Region (PAC CALABRIA 2014–2020-Asse Prioritario 12, Azione B 10.5.12 CUP: H28D19000040006). This research was also funded by Agencia Estatal de Investigación (Spain) for projects 099592-B-C22 (to G.J.-O.) and the Severo Ochoa Excellence Accreditation (SEV-2016-0644 to CIC bioGUNE). F. P. thanks the Ministerio de Economía y Competitividad for a Juan de la Cierva Incorporación (IJC2020-045506-I) fellowship.

Institutional Review Board Statement: Not applicable.

Informed Consent Statement: Not applicable.

Data Availability Statement: Not applicable.

Conflicts of Interest: The authors declare no conflict of interest.

Sample Availability: Samples of the compounds are available from the authors.

References

1. Toda, M.; Beer, K.D.; Kuivila, F.M.; Chiller, T.M.; Jackson, B.R. Trends in Agricultural Triazole Fungicide Use in the United States, 1992–2016 and Possible Implications for Antifungal-Resistant Fungi in Human Disease. *Environ. Health Perspect.* **2021**, *129*, 1–12. [CrossRef] [PubMed]
2. Hameed, A.; Farooq, T. *Advances in Triazole Chemistry*; Farooq, T., Ed.; Elsevier: Amsterdam, The Nederlands, 2021; pp. 169–185.
3. Wang, X.; Zhang, X.; Ding, S. 1,2,3-Triazole-based sequence-defined oligomers and polymers. *Polym. Chem.* **2021**, *12*, 2668–2688. [CrossRef]
4. Rodrigues, L.D.; Sunil, D.S.; Chaithra, D.; Bhagavath, P. 1,2,3/1,2,4-Triazole containing liquid crystalline materials: An up-to-date review of their synthetic design and mesomorphic behaviour. *J. Mol. Liq.* **2020**, *297*, 111909. [CrossRef]
5. Brunel, D.; Dumur, F. Recent advances in organic dyes and fluorophores comprising a 1,2,3-triazole moiety. *New J. Chem.* **2020**, *44*, 3546–3561. [CrossRef]
6. Lauko, J.; Kouwer, P.H.J.; Rowan, A.E. 1*H*-1,2,3-Triazole: From Structure to Function and Catalysis. *J. Heterocycl. Chem.* **2017**, *54*, 1677–1699. [CrossRef]
7. Scattergood, P.A.; Sinopoli, A.; Elliott, P.I.P. Synthesis, structural analysis, and photophysical properties of bi-1,2,3-triazoles. *Coord. Chem. Rev.* **2017**, *350*, 136–154. [CrossRef]
8. Xu, Z.; Zhao, S.-J.; Liu, Y. 1,2,3-Triazole-containing hybrids as potential anticancer agents: Current developments, action mechanisms and structure-activity relationships. *Eur. J. Med. Chem.* **2019**, *183*, 111700. [CrossRef]
9. Czyrski, A.; Resztak, M.; Świderski, P.; Brylak, J.; Główka, F.K. The overview on the pharmacokinetic and pharmacodynamic interactions of triazoles. *Pharmaceutics* **2021**, *13*, 1961. [CrossRef]
10. Aggarwal, R.; Sumran, G. An insight on medicinal attributes of 1,2,4-triazoles. *Eur. J. Med. Chem.* **2020**, *183*, 112652. [CrossRef]
11. Bozorova, K.; Zhao, J.; Aisa, H.A. 1,2,3-Triazole-containing hybrids as leads in medicinal chemistry: A recent overview. *Bioorg. Med. Chem.* **2019**, *27*, 3511–3531. [CrossRef]
12. Tornøe, C.W.; Christensen, C.; Meldal, M. Peptidotriazoles on Solid Phase: [1,2,3]-Triazoles by Regiospecific Copper(I)-Catalyzed 1,3-Dipolar Cycloadditions of Terminal Alkynes to Azides. *J. Org. Chem.* **2002**, *67*, 3057–3064. [CrossRef] [PubMed]
13. Rostovtsev, V.V.; Green, L.G.; Fokin, V.V.; Sharpless, K.B. A Stepwise Huisgen Cycloaddition Process: Copper(I)-Catalyzed Regioselective "Ligation" of Azides and Terminal Alkynes. *Angew. Chem. Int. Ed.* **2002**, *41*, 2596–2599. [CrossRef]
14. Zhang, L.; Chen, X.; Xue, P.; Sun, H.H.Y.; Williams, I.D.; Sharpless, K.B.; Fokin, V.V.; Jia, G. Ruthenium-catalyzed cycloaddition of alkynes and organic azides. *J. Am. Chem. Soc.* **2005**, *127*, 15998–15999. [CrossRef] [PubMed]
15. Neto, J.S.S.; Zeni, G. A decade of advances in the reaction of nitrogen sources and alkynes for the synthesis of triazoles. *Coord. Chem. Rev.* **2020**, *409*, 213217. [CrossRef]
16. De Nino, A.; Maiuolo, L.; Costanzo, P.; Algieri, V.; Jiritano, A.; Olivito, F.; Tallarida, M.A. Recent Progress in Catalytic Synthesis of 1,2,3-Triazoles. *Catalysts* **2021**, *11*, 1120. [CrossRef]
17. Shelton, J.; Lu, X.; Hollenbaugh, J.A.; Cho, J.C.; Amblard, F.; Schinazi, R.F. Metabolism, Biochemical Actions, and Chemical Synthesis of Anticancer Nucleosides, Nucleotides, and Base Analogs. *Chem. Rev.* **2016**, *116*, 14379–14455. [CrossRef]
18. Geraghty, R.J.; Aliota, M.T.; Bonnac, L.F. Broad-spectrum antiviral strategies and nucleoside analogues. *Viruses* **2021**, *13*, 667. [CrossRef]
19. Choi, J.-S.; Berdis, A.J. Visualizing Nucleic Acid Metabolism Using Non-natural Nucleosides and Nucleotide Analogs. *Biochim. Biophys. Acta-Proteins Proteom.* **2016**, *1864*, 165–176. [CrossRef]
20. Lin, X.; Liang, C.; Zou, L.; Yin, Y.; Wang, J.; Chen, D.; Lan, W. Advance of structural modification of nucleosides scaffold. *Eur. J. Med. Chem.* **2021**, *214*, 113233. [CrossRef]
21. Efthymiou, T.; Gong, W.; Desaulniers, J.-P. Chemical Architecture and Applications of Nucleic Acid Derivatives Containing 1,2,3-Triazole Functionalities Synthesized via Click Chemistry. *Molecules* **2012**, *17*, 12665–12703. [CrossRef]
22. Sabat, N.; Migianu-Griffoni, E.; Tudela, T.; Lecouvey, M.; Kellouche, S.; Carreiras, F.; Gallier, F.; Uziel, J.; Lubin-Germain, N. Synthesis and antitumor activities investigation of a C-nucleoside analogue of Ribavirin. *Eur. J. Med. Chem.* **2020**, *188*, 112009. [CrossRef] [PubMed]
23. Elayadi, H.; Smietana, M.; Pannecouque, C.; Leyssen, P.; Neyts, J.; Vasseur, J.J.; Lazrek, H.B. Straightforward synthesis of triazoloacyclonucleotide phosphonates as potential HCV inhibitors. *Bioorg. Med. Chem. Lett.* **2010**, *20*, 7365–7368. [CrossRef] [PubMed]
24. Chittepu, P.; Sirivolu, V.R.; Seela, F. Nucleosides and oligonucleotides containing 1,2,3-triazole residues with nucleobase tethers: Synthesis via the azide-alkyne 'Click' reaction. *Bioorg. Med. Chem.* **2008**, *16*, 8427–8439. [CrossRef] [PubMed]
25. Sirivolu, V.R.; Vernekar, S.K.V.; Ilina, T.; Myshakina, N.S.; Parniak, M.A.; Wang, Z. Clicking 3′-Azidothymidine into Novel Potent Inhibitors of Human Immunodeficiency Virus. *J. Med. Chem.* **2013**, *56*, 8765–8780. [CrossRef] [PubMed]

26. González-Olvera, R.; Espinoza-Vázquez, A.; Negrón-Silva, G.E.; Palomar-Pardavé, M.E.; Romero-Romo, M.A.; Santillan, R. Multicomponent Click Synthesis of New 1,2,3-Triazole Derivatives of Pyrimidine Nucleobases: Promising Acidic Corrosion Inhibitors for Steel. *Molecules* **2013**, *18*, 15064–15079. [CrossRef]
27. Elayadi, H.; Smietana, M.; Vasseur, J.J.; Balzarini, J.; Lazrek, H.B. Synthesis of 1,2,3-Triazolyl Nucleoside Analogs as Potential Anti-Influenza A (H3N2 Subtype) Virus Agents. *Arch. Pharm. Chem. Life Sci.* **2014**, *347*, 134–141. [CrossRef]
28. Bortolini, O.; De Nino, A.; Garofalo, A.; Maiuolo, L.; Russo, B.; Procopio, A. Erbium triflate in ionic liquids: A recyclable system of improving selectivity in Diels-Alder reactions. *Appl. Catal. A Gen.* **2010**, *372*, 124–129. [CrossRef]
29. Procopio, A.; Dalpozzo, R.; De Nino, A.; Nardi, M.; Russo, B.; Tagarelli, A. $Er(OTf)_3$ as New Efficient Catalyst for the Stereoselective Synthesis of C-Pseudoglycals. *Synthesis* **2006**, *2*, 0332–0338. [CrossRef]
30. De Nino, A.; Algieri, V.; Tallarida, M.A.; Costanzo, P.; Pedrón, M.; Tejero, T.; Merino, P.; Maiuolo, L. Regioselective Synthesis of 1,4,5-Trisubstituted-1,2,3-Triazoles from Aryl Azides and Enaminones. *Eur. J. Org. Chem.* **2019**, *4*, 5725–5731. [CrossRef]
31. Maiuolo, L.; Algieri, V.; Russo, B.; Tallarida, M.A.; Nardi, M.; Di Gioia, M.L.; Merchant, Z.; Merino, P.; Delso, I.; De Nino, A. Synthesis, Biological and In Silico Evaluation of Pure Nucleobase-Containing Spiro (Indane-Isoxazolidine) Derivatives as Potential Inhibitors of MDM2–p53 Interaction. *Molecules* **2019**, *24*, 2909. [CrossRef]
32. Maiuolo, L.; Algieri, V.; Olivito, F.; De Nino, A. Recent Developments on 1,3-Dipolar Cycloaddition Reactions by Catalysis in Green Solvents. *Catalysts* **2020**, *10*, 65. [CrossRef]
33. Bauer, I.; Knölker, H.J. Iron Catalysis in Organic Synthesis. *Chem. Rev.* **2015**, *115*, 3170–3387. [CrossRef] [PubMed]
34. Peters, H.L.; Jochmans, D.; de Wilde, A.H.; Posthuma, C.C.; Snijder, E.J.; Neyts, J.; Seley-Radtke, K.L. Design, synthesis and evaluation of a series of acyclic fleximer nucleoside analogues with anti-coronavirus activity. *Bioorg. Med. Chem. Lett.* **2015**, *25*, 2923–2926. [CrossRef] [PubMed]
35. Rocha, D.H.A.; Machado, C.M.; Sousa, V.; Sousa, C.F.V.; Silva, V.L.M.; Silva, A.M.S.; Borges, J.; Mano, J.F. Customizable and Regioselective One-Pot N−H Functionalization of DNA Nucleobases to Create a Library of Nucleobase Derivatives for Biomedical Applications. *Eur. J. Org. Chem.* **2021**, *31*, 4423–4433. [CrossRef]
36. Kramer, R.A.; Bleicher, K.H.; Wennemers, H. Design and synthesis of nucleoproline amino acids for the straightforward preparation of chiral and conformationally constrained nucleopeptides. *Helv. Chim. Acta* **2012**, *95*, 2621–2634. [CrossRef]
37. Legros, V.; Hamon, F.; Violeau, B.; Turpin, F.; Djedaini-Pilard, F.; Desiré, J.; Len, C. Toward the Supramolecular Cyclodextrin Dimers Using Nucleobase Pairs. *Synthesis* **2011**, *2*, 0235–0242.
38. Thakur, R.K.; Mishra, A.; Ramakrishna, K.K.G.; Mahar, R.; Shukla, S.K.; Srivastava, A.K.; Tripathi, R.P. Synthesis of novel pyrimidine nucleoside analogues owning multiple bases/sugars and their glycosidase inhibitory activity. *Tetrahedron* **2014**, *70*, 8462–8473. [CrossRef]
39. De Nino, A.; Merino, P.; Algieri, V.; Nardi, M.; Di Gioia, M.L.; Russo, B.; Tallarida, M.A.; Maiuolo, L. Synthesis of 1,5-Functionalized 1,2,3-Triazoles Using Ionic Liquid/Iron(III) Chloride as an Efficient and Reusable Homogeneous Catalyst. *Catalysts* **2018**, *8*, 364. [CrossRef]
40. De Nino, A.; Maiuolo, L.; Merino, P.; Nardi, M.; Procopio, A.; Roca-López, D.; Russo, B.; Algieri, V. Efficient Organocatalyst Supported on a Simple Ionic Liquid as a Recoverable System for the Asymmetric Diels-Alder Reaction in the Presence of Water. *ChemCatChem* **2015**, *7*, 830–835. [CrossRef]
41. Jones, G.; Willett, P.; Glen, R.C.; Leach, A.R.; Taylor, R. Development and validation of a genetic algorithm for flexible docking. *J. Mol. Biol.* **1997**, *267*, 727–748. [CrossRef]
42. Verdonk, M.L.; Cole, J.C.; Hartshorn, M.J.; Murray, C.W.; Taylor, R.D. Improved protein-ligand docking using GOLD. *Proteins* **2003**, *52*, 609–623. [CrossRef] [PubMed]
43. Tan, M.; Hegde, R.S.; Jiang, X. The P domain of norovirus capsid protein forms dimer and binds to histo-blood group antigen receptors. *J. Virol.* **2004**, *78*, 6233–6242. [CrossRef] [PubMed]
44. Rosenberg, H.F. Eosinophil-derived Neurotoxin / RNase 2: Connecting the past, the present and the future. *Curr. Pharm. Biotechnol.* **2008**, *9*, 135–140. [CrossRef] [PubMed]
45. Palzkill, T. Metallo-β-lactamase structure and function. *Ann. N. Y. Acad. Sci.* **2012**, *1277*, 91–104. [CrossRef]
46. Newman, J.A.; Douangamath, A.; Yadzani, S.; Yosaatmadja, Y.; Aimon, A.; Brandão-Neto, J.; Dunnett, L.; Gorrie-stone, T.; Skyner, R.; Fearon, D.; et al. Structure, mechanism and crystallographic fragment screening of the SARS-CoV-2 NSP13 helicase. *Nat. Commun.* **2021**, *12*, 4848–4858. [CrossRef] [PubMed]
47. Calandra, P.; Mandanici, A.; Liveri, V.T. Self-assembly in surfactant-based mixtures driven by acid-base reactions: Bis(2-ethylhexyl) phosphoric acid-n-octylamine systems. *RSC Adv.* **2013**, *3*, 5148–5155. [CrossRef]
48. Xiong, G.; Wu, Z.; Yi, J.; Fu, L.; Yang, Z.; Hsieh, C.; Yin, M.; Zeng, X.; Wu, C.; Lu, A.; et al. ADMETlab 2.0: An Integrated Online Platform for Accurate and Comprehensive Predictions of ADMET Properties. *Nucleic Acids Res.* **2021**, *49*, W5–W14. Available online: https://admetmesh.scbdd.com/ (accessed on 12 September 2022). [CrossRef]
49. Lipinski, C.A.; Lombardo, F.; Dominy, B.W.; Feeney, P.J. Experimental and computational approaches to estimate solubility and permeability in drug discovery and devlopment settings. *Adv. Drug. Deliv. Rev.* **2001**, *46*, 3–26. [CrossRef]
50. Daina, A.; Zoete, V. A BOILED-Egg to predict gastrointestinal absorption and brain penetration of small molecules. *ChemMedChem* **2016**, *11*, 1117–1121. [CrossRef]
51. Pettersen, E.F.; Goddard, T.D.; Huang, C.C.; Couch, G.S.; Greenblatt, D.M.; Meng, E.C.; Ferrin, T.E. UCSF Chimera—A Visualization System for Exploratory Research and Analysis. *J. Comput. Chem.* **2004**, *25*, 1605–1612. [CrossRef]

52. Frisch, M.J.; Trucks, G.W.; Schlegel, H.B.; Scuseria, G.E.; Robb, M.A.; Cheeseman, J.R.; Scalmani, G.; Barone, V.; Mennucci, B.; Petersson, G.A.; et al. *Gaussian 16, Revision C.01*; Gaussian, Inc.: Wallingford, CT, USA, 2016.
53. Zhao, Y.; Truhlar, D.G. The M06 suite of density functionals for main group thermochemistry, thermochemical kinetics, noncovalent interactions, excited states, and transition elements: Two new functionals and systematic testing of four M06-class functionals and 12 other functionals. *Theor. Chem. Acc.* **2008**, *120*, 215–241.
54. Scalmani, G.; Frisch, M.J. Continuous surface charge polarizable continuum models of solvation. I. General formalism. *J. Chem. Phys.* **2010**, *132*, 114110. [CrossRef] [PubMed]

molecules

MDPI

Article

Energetic [1,2,5]oxadiazolo [2,3-*a*]pyrimidin-8-ium Perchlorates: Synthesis and Characterization

Kirill V. Strizhenko [1], Anastasia D. Smirnova [1,2], Sergei A. Filatov [2], Valery P. Sinditskii [1,2], Adam I. Stash [3], Kyrill Yu. Suponitsky [3], Konstantin A. Monogarov [4], Vitaly G. Kiselev [5] and Aleksei B. Sheremetev [1,*]

1 Zelinsky Institute of Organic Chemistry, Russian Academy of Sciences, 119991 Moscow, Russia
2 Mendeleev University of Chemical Technology, 125047 Moscow, Russia
3 Nesmeyanov Institute of Organoelement Compounds, Russian Academy of Sciences, 119334 Moscow, Russia
4 Semenov Federal Research Center for Chemical Physics, Russian Academy of Sciences, 119991 Moscow, Russia
5 Institute of Chemical Kinetics and Combustion, Russian Academy of Sciences, Siberian Branch, 630090 Novosibirsk, Russia
* Correspondence: sab@ioc.ac.ru

Abstract: A convenient method to access the above perchlorates has been developed, based on the cyclocondensation of 3-aminofurazans with 1,3-diketones in the presence of $HClO_4$. All compounds were fully characterized by multinuclear NMR spectroscopy and X-ray crystal structure determinations. Initial safety testing (impact and friction sensitivity) and thermal stability measurements (DSC/DTA) were also carried out. Energetic performance was calculated by using the PILEM code based on calculated enthalpies of formation and experimental densities at r.t. These salts exhibit excellent burn rates and combustion behavior and are promising ingredients for energetic materials.

Keywords: aminofurazans; fused furazans; perchlorates; energetic compound; synthesis; X-ray analysis; impact sensitivity; thermal decomposition; combustion; burning rate

Citation: Strizhenko, K.V.; Smirnova, A.D.; Filatov, S.A.; Sinditskii, V.P.; Stash, A.I.; Suponitsky, K.Y.; Monogarov, K.A.; Kiselev, V.G.; Sheremetev, A.B. Energetic [1,2,5]oxadiazolo [2,3-*a*]pyrimidin-8-ium Perchlorates: Synthesis and Characterization. *Molecules* **2022**, *27*, 8443. https://doi.org/10.3390/molecules27238443

Academic Editor: Gilbert Kirsch

Received: 7 November 2022
Accepted: 25 November 2022
Published: 2 December 2022

Publisher's Note: MDPI stays neutral with regard to jurisdictional claims in published maps and institutional affiliations.

1. Introduction

Most energetic materials are a mixture of substances, among which an oxidizer, fuel, binder and various corrective additives can be specified. The most widely used oxidizer is ammonium perchlorate, NH_4ClO_4 [1–4]. In the early stages of research, compositions based on NH_4ClO_4 included powdered metals as fuel. However, in recent years, there has been a tendency to partially or even completely replace metallic fuels in energetic materials with high-nitrogen compounds characterized by high positive enthalpies of formation.

Energetic salts with nitrogen-rich organic cations and/or anions (typically azole-based ions) are a major area for the development of high-energy materials, since salts have a high density and positive enthalpy of formation, are often thermally stable, and are not volatile [5–7]. Designing energetic salts by combining various cations and anions to achieve a specific purpose is a simple but powerful methodology. Most of these salts, however, have a strongly negative oxygen balance and, with a lack of oxidizer, form toxic or undesirable solid decomposition products [8].

When using energetic salts in combination with solid inorganic oxidizers—for example, with NH_4ClO_4—additional problems are observed. A metathesis reaction between NH_4ClO_4 and energetic azole-based salts leads to the formation of new salts where the anions have been swapped. As a result, the properties of this composition could change unpredictably [9]. To overcome this disadvantage, a variety of energetic organic salts may be limited by the use of perchlorates.

The characteristics of the energetic salts are dictated by the physical and chemical features of both ions in their composition. In this light, the importance of synthesizing organic salts of perchloric acid with various cations and the study of their properties

becomes important. It is important to note that, unlike nitrates, perchlorates have a significant effect on the transformation of organic compounds [10–12], which favors the completeness of the combustion of the latter.

Due to its inherent density, positive enthalpy of formation, thermal stability, and the presence of an active oxygen atom, the 1,2,5-oxadiazole (furazan) ring is an attractive building block for the development of new energetic compounds [13–17]. Significant progress has been achieved in the development of furazan-based salts, some types of which are depicted in Figure 1. Typically, the furazan moiety is located in the anionic part of the energetic salt, as in salts of nitramines **1** [18–23], perchlorylamines **2** [24], dinitromethyl **3** [25–32], tetrazolyl **4** [33–37], pyrazolo [3,4-*c*]furazanates **5** [38–40], and [1,2,3]triazolo [4,5-*c*][1,2,5]oxadiazoles **6** [41]. Cations involving the furazan ring are very rare; in the previously described salts (**7 [42]** and **8 [20]**), the positive charge is located in the side chain.

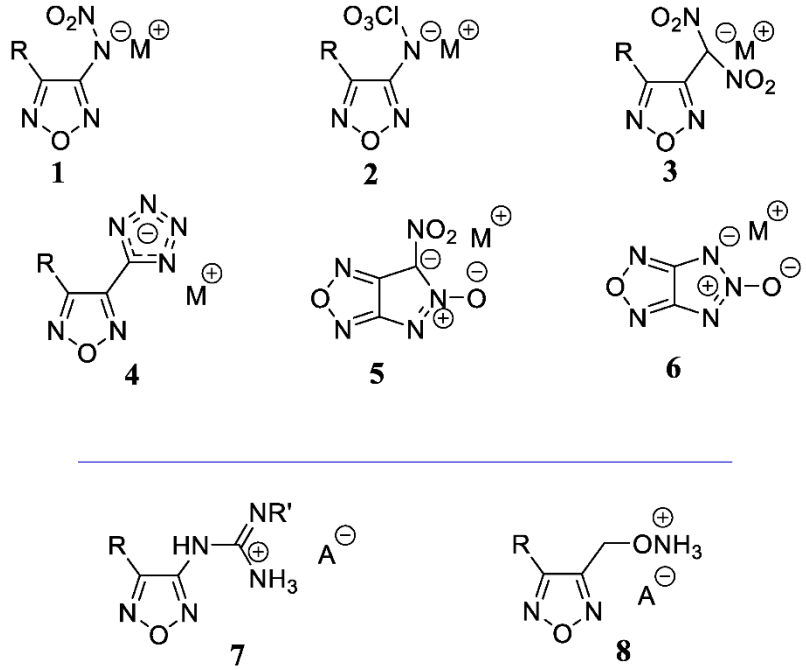

Figure 1. Known energetic furazan-based salts.

There is no literature precedence for energetic salts incorporating a furazan-based backbone with a positive charge on the nitrogen atom of this ring.

Although a few 2-methyl-1,2,5-oxadiazolium [43] and 1,2,5-oxadiazolo [2,3-*a*]-pyrimidi nium perchlorates [44,45] were synthesized, only partial physical and spectral properties were available, but the sensitivity, thermal stability, combustion features, and explosive performance were not reported. However, these early studies have demonstrated that monocyclic salts are less accessible and more reactive.

In light of the above, we report here a new, straightforward method for the synthesis of energetic 1,2,5-oxadiazolo [2,3-*a*]-pyrimidinium perchlorates, and their full characterization, including energetic properties. The only known pathway for the synthesis of 1,2,5-oxadiazolo [2,3-*a*]-pyrimidinium perchlorates is based on the reaction of 3-amino-4-R-furazans **9** with 1,3-dicarbonyl compounds [44]. However, an investigation of the scope and limitations of functionalized reactants has not been previously reported. Although a range of alkyl and aryl-substituted oxadiazolo [2,3-*a*]-pyrimidinium perchlorates have been prepared by this approach, there have been no examples bearing explosophoric groups [46] so far.

2. Results

2.1. Synthesis

Readily available 3-amino-4-methylfurazan (**9a**) [47] became our model precursor of choice. There is a literature report [44] on the synthesis of 1,2,5-oxadiazolo [2,3-*a*]-pyrimidinium perchlorate **10a** from compound **9a** and pentane-2,4-dione in a mixture of AcOH and $HClO_4$, but no synthetic details are given. In our hands, such a procedure turned out to be somewhat unpredictable; the yield of the final 1,2,5-oxadiazolo [2,3-*a*]-pyrimidinium perchlorate **10a** was relatively low (only 23% vs. 73% reported earlier).

After several experiments, we found that replacing AcOH in the reaction mixture with Ac_2O improved the conversion significantly and gave a 44% yield of the product **10a** (Scheme 1). A change in dehydrating agent from Ac_2O to $(CF_3CO)_2O$ allowed us to increase the yield up to 87%. It has been suggested that the solubility of the product **10** in the reaction mixture is the most important in this process. $(CF_3CO)_2O$ is completely unnecessary as a reagent, and the much cheaper and easier-to-handle trifluoroacetic acid was employed instead. Gratifyingly, treatment of amine **9a** with pentane-2,4-dione in a mixture of 58% $HClO_4$ and CF_3CO_2H at room temperature gave the cyclocondensation product **10a** in 3 h. Thus, without any complicated workup, the desired product was isolated in 71% yield and >99% purity through simple filtration and washing.

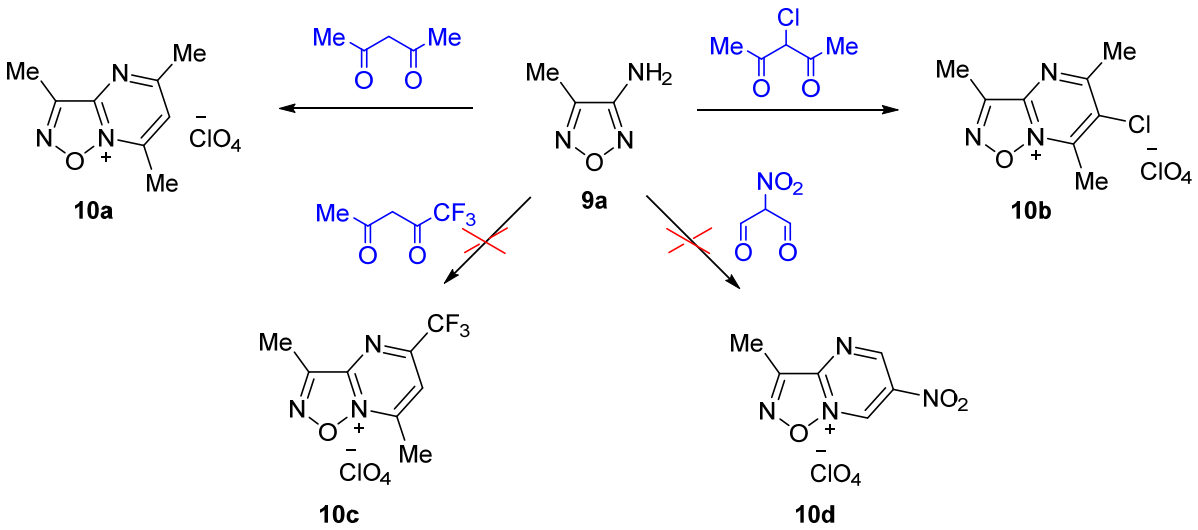

Scheme 1. Reaction of 3-amino-4-methylfurazan (**9a**) with 1,3-dicarbonyl compounds.

With the optimized conditions developed, we explored the scope of the method with a variety of 1,3-dicarbonyl compounds and aminofurazans bearing explosophoric groups. A 1,3-dicarbonyl compound with one halogen, namely 3-chloropentane-2,4-dione, furnished the desired product **10b** in a good yield (85%). The use of 1,3-dicarbonyl compounds possessing strongly electron-withdrawing substituents, e.g., trifluoromethyl or nitro groups (Scheme 1), failed to give the corresponding bicycles **10c** and **10d**.

Scheme 2 shows the results of applying our optimized cyclocondensation conditions to a range of aminofurazans. Aminofurazans bearing a functionalized methyl group, 3-amino-4-chloromethylfurazan (**9b**) [48] and 3-amino-4-azidomethylfurazan (**9c**) [48], were equally effective as the model compound **9a**, with excellent yields (ca. 95%) being obtained for pentane-2,4-dione in the $HClO_4/CF_3CO_2H$ system. Moreover, 3-amino-4-azidofurazan (**9d**) [49,50] was a good substrate for the reaction and gave the target product **9e** in 71% yield. Synthesis of 1,2,5-oxadiazolo [2,3-*a*]-pyrimidinium perchlorate failed in cases where the starting furazan had a very strong electron-withdrawing substituent: reactions with 3-amino-4-nitrofurazan **9e** [51] or with 3-amino-4-*tert*butylazoxyfurazan **9f [52]** did not give the desired salts **10h** and **10i**. Only recovery of the starting materials from the reaction mixture was achieved.

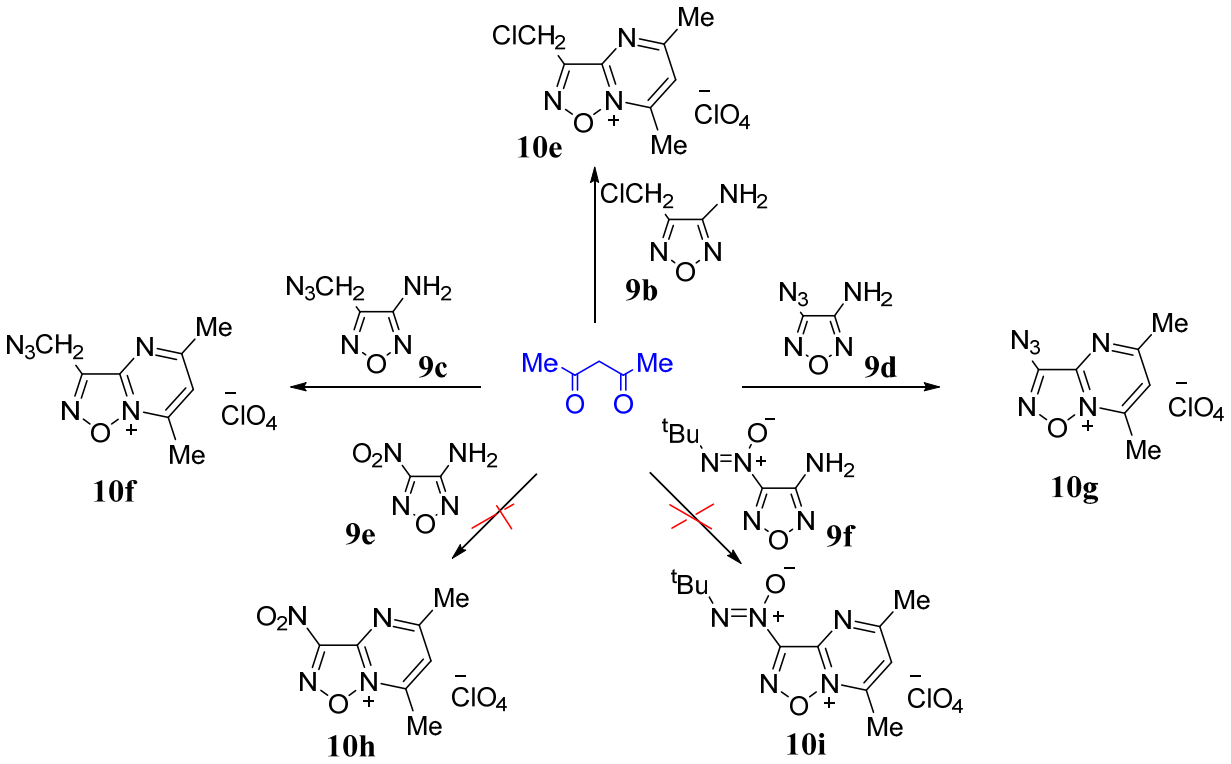

Scheme 2. Reaction of pentane-2,4-dione with aminofurazans.

With the exception of compound **10a**, all perchlorates prepared in this way are new, and the structures of the products have been confirmed by elemental analyses, IR, and ^{1}H, ^{13}C, ^{15}N, and ^{35}Cl NMR spectroscopy. The ^{1}H, ^{13}C and ^{15}N chemical shift assignments were determined by using ^{1}H selective NOE, ^{1}H-^{13}C HSQC, ^{1}H-^{13}C HMBC, and ^{1}H-^{15}N HMBC experiments. In the ^{35}Cl NMR spectrum, the characteristic chlorine signal of the perchlorate anion appeared at 1012 ppm, which is close to the reported values of similar compounds [53]. For clarity, the compound of this study, together with relevant NMR parameters, is depicted in Figure 2.

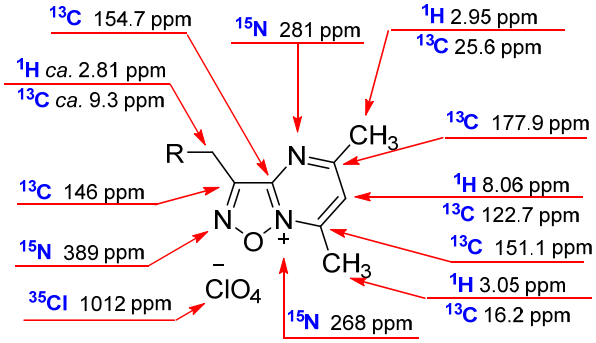

Figure 2. Typical ^{1}H, ^{13}C, ^{15}N, and ^{35}Cl NMR shifts of 1,2,5-oxadiazolo [2,3-*a*]-pyrimidinium perchlorates.

2.2. X-ray Analysis

The X-ray crystal structures of perchlorates **10a**, **10f**, and **10g**, differing only by the substituent at the 1,2,5-oxadiazole ring, are shown in Figures 3 and 4. Both symmetrically independent molecules of methyl compound **10a** adopt a planar structure. Azido groups in three symmetrically independent molecules of **10g** are rotated ca. 17.6°–26.7° out of the plane of the bicyclic backbone. For compound **10f**, the CH_2N_3 substituent deviates even more significantly from the plane of the heterocycle (the C2–C1–C8–N4 torsion angle is equal to 59.7(2)°).

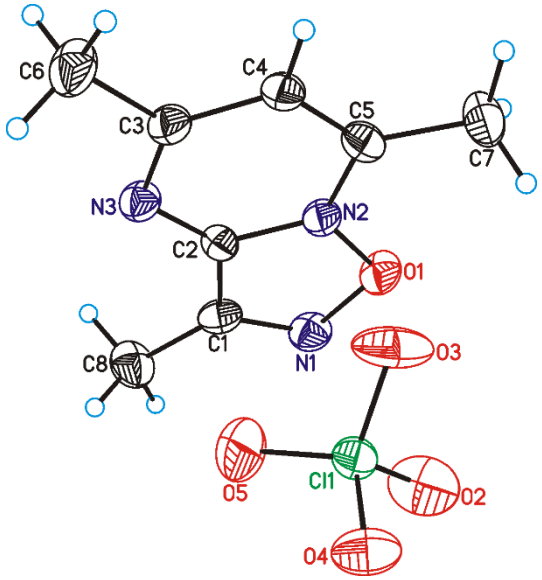

Figure 3. General view of Me compounds **10a** showing atomic numbering. Thermal ellipsoids are given at 50% probability level. The first symmetrically independent molecule is shown.

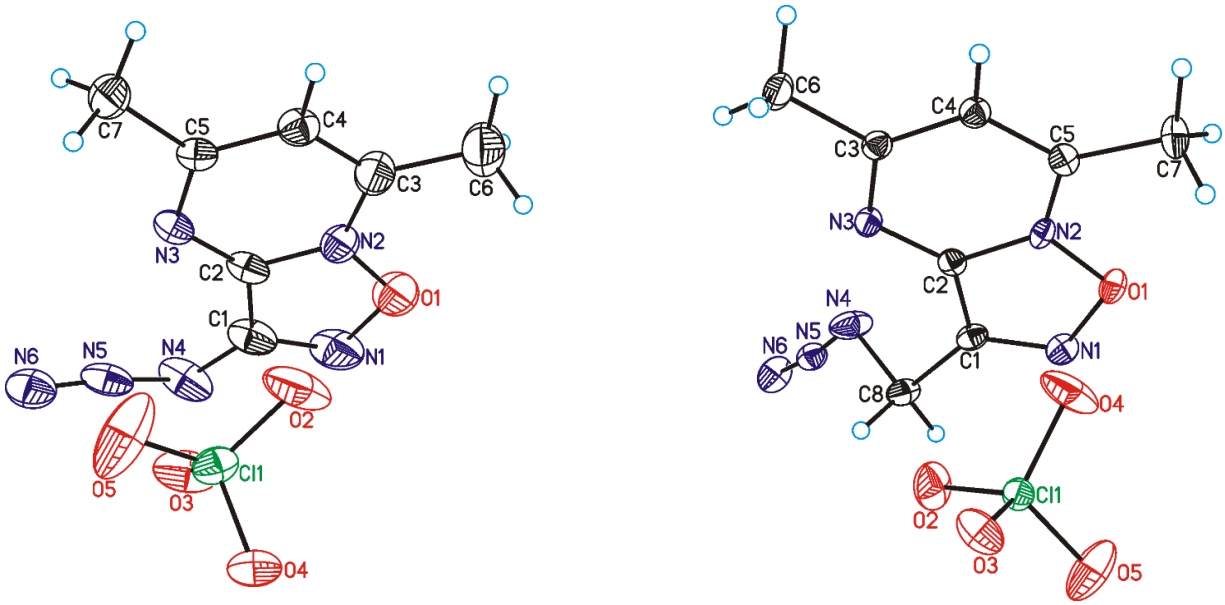

(**a**) (**b**)

Figure 4. General view of azido compounds **10g** (**a**) and **10f** (**b**) showing atomic numbering. Thermal ellipsoids are given at 50% probability level. For **10g**, the first symmetrically independent molecule is shown.

The N–O bond lengths in the 1,2,5-oxadiazole ring, which are usually the most sensitive to the influence of substituents [54–56], are distributed so that the O1–N2 bond is significantly shorter than the other one in all three compounds. The difference in these bonds Δ(NO) (for **10a** and **10g**, the average value over symmetrically independent molecules is used) increases in the order of the decreasing electron-withdrawing effect of the substituent at the C1 atom (the Δ(NO) is 0.022, 0.026, 0.035 Å for compounds **10g**, **10f**, and **10a**, respectively).

For all three compounds, the molecules in the crystal are linked together by O . . . π, C–H . . . O(N), and van-der-Waals interactions. As expected, most of them are observed between anions and cations, as depicted in Figures 5–7. In the cases of azido compounds

(Figures 6 and 7), each anion (except for one in **10g**, Figure 6) is linked to four cations by means of O . . . π and C–H . . . O interactions, and the interaction patterns are quite similar for both compounds. In the case of Me derivatives (Figure 5), each anion is surrounded by three counterions. In all three structures, the cation . . . cation interactions are caused by van-der-Waals forces and weak C–H . . . N hydrogen bonds, while no anion . . . anion contacts are observed.

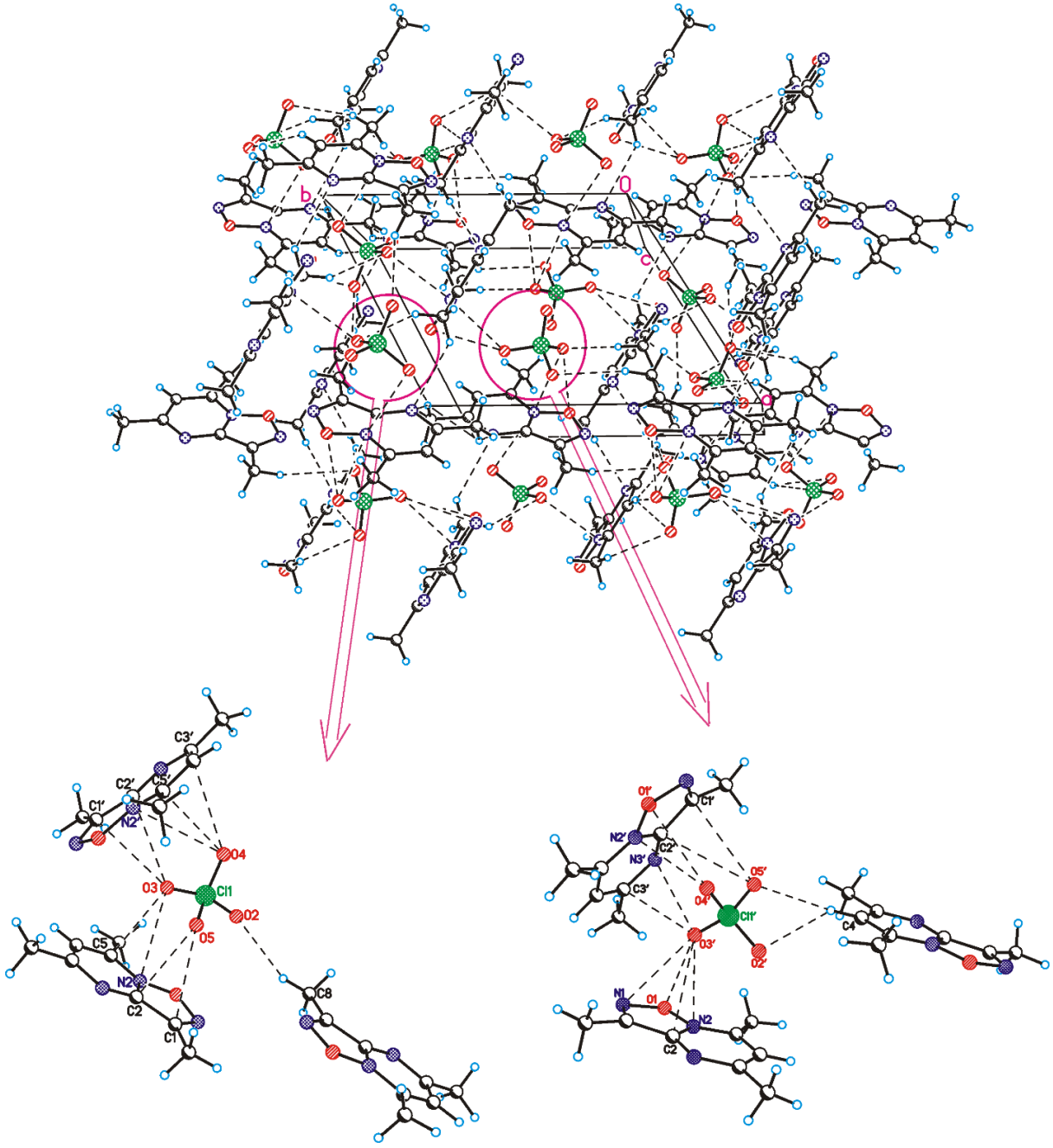

Figure 5. Crystal packing fragment of compound **10a**. C–H . . . N cation . . . cation and C–H . . . O and O . . . π anion . . . cation interactions are shown by dashed lines. Detailed view of anion . . . cation interactions is provided at the bottom. Minor part of the disorder is omitted for clarity.

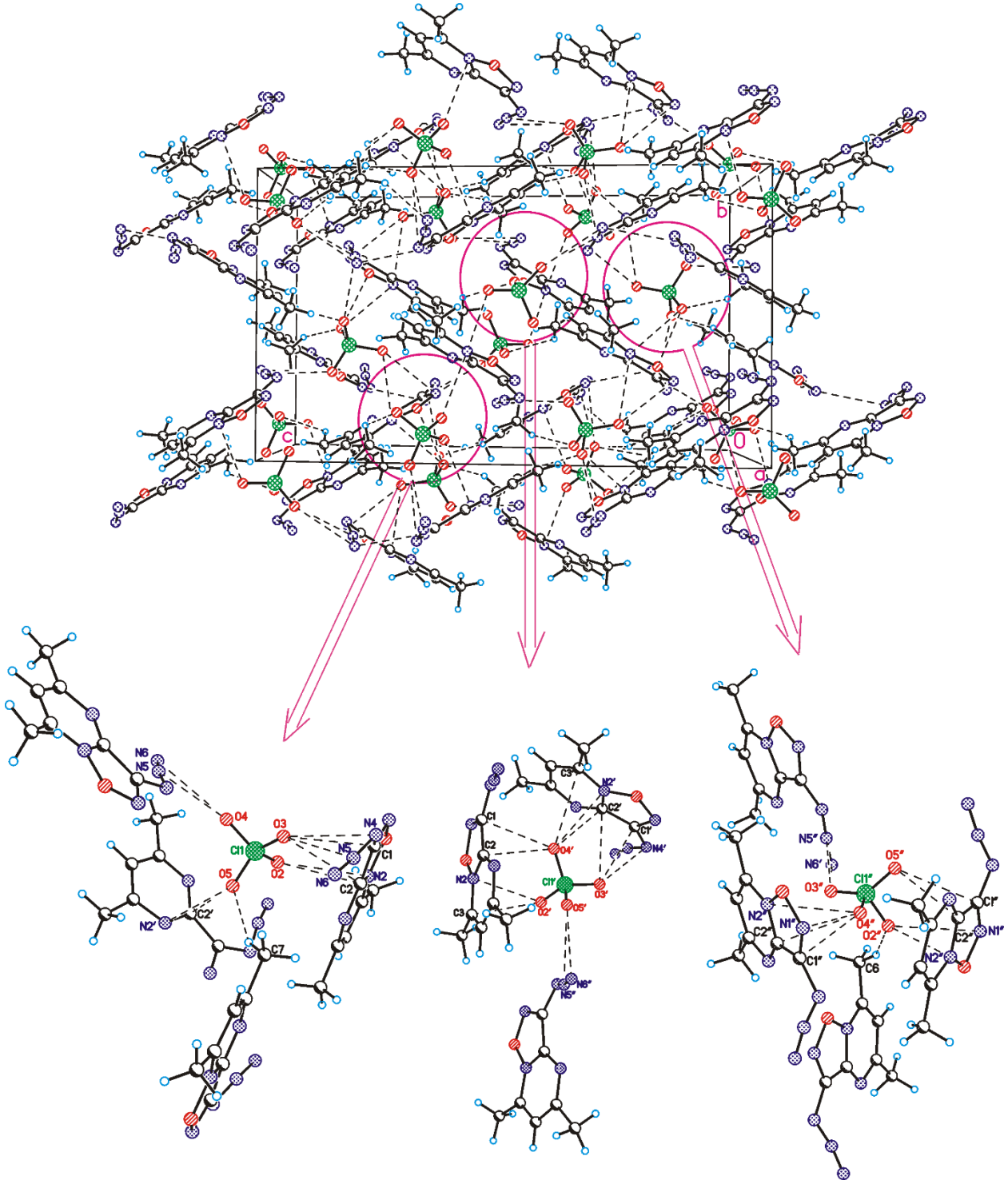

Figure 6. Crystal packing fragment of compound **10g**. C–H . . . N cation–cation and C–H . . . O and O . . . π anion . . . cation interactions are shown by dashed lines. Detailed view of anion . . . cation interactions is provided at the bottom. Minor part of the disorder is omitted for clarity.

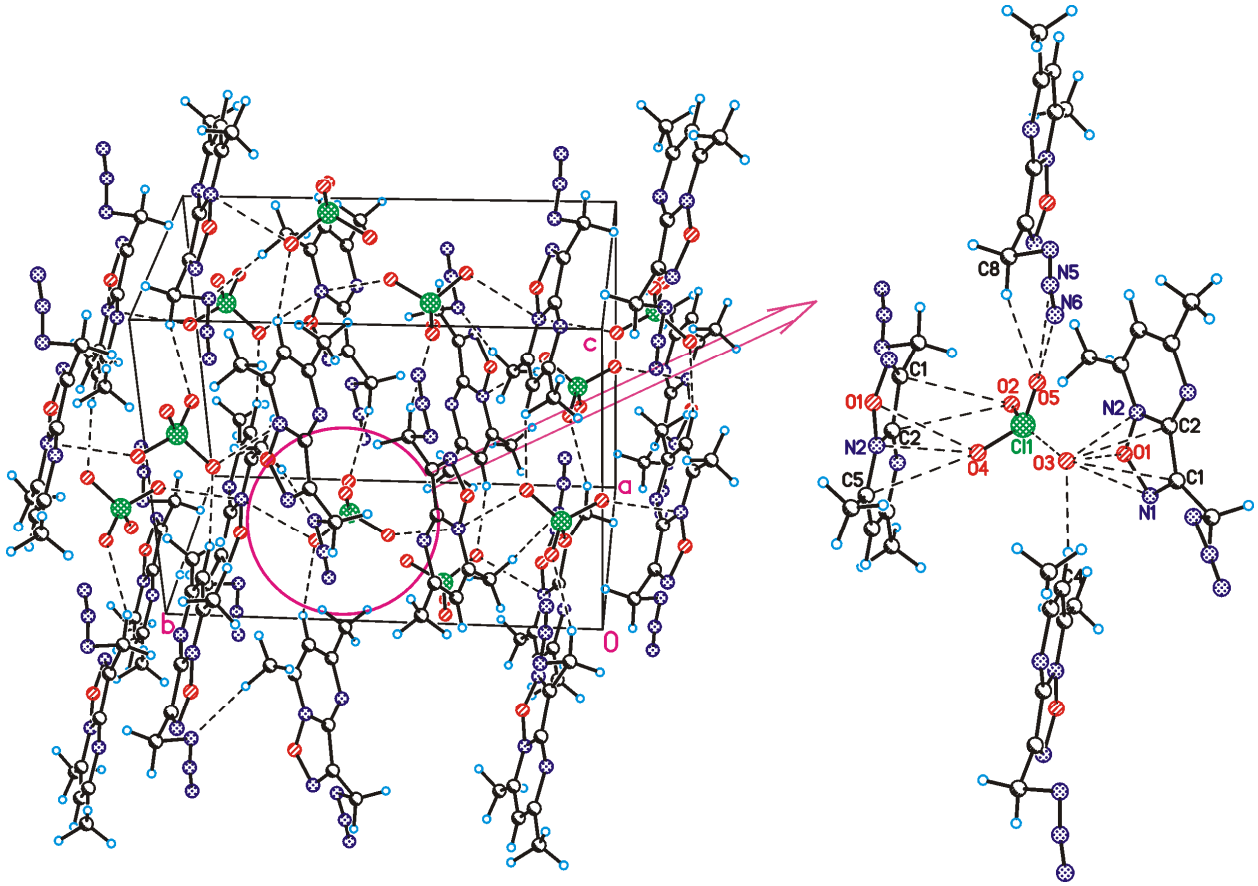

Figure 7. Crystal packing fragment of compound **10f**. C–H ... N cation ... cation and C–H ... O and O ... π anion ... cation interactions are shown by dashed lines. Detailed view of anion–cation interactions is provided on the right side.

As expected, the density of Me compound **10a** (1.549 g cm^{-3} at 100 K) is lower than that of its azido analogues. However, unexpectedly, the density of the azido derivative **10g** turned out to be lower than that of the azidomethyl compound **10f** (1.611 vs. 1.649 g cm^{-3} at 100 K). Probably due to the significant disorder in the structure **10f**, disordered fragments occupy a larger volume, which leads to a decrease in density.

2.3. Initial Safety Testing

For initial safety testing, the impact (IS) and friction (FS) sensitivities of perchlorates **10a**, **10e**–**10g** were measured. The sensitivity measurements were carried out using common BAM techniques and compared to tetrazene, which is considered as the benchmark primary metal-free explosive (Table 1). Compound **10a** bearing the methyl group at 1,2,5-oxadiazole ring and compound **10e** with the chloromethyl group showed similar impact and friction sensitivities. A change in the position of the chlorine atom—namely, its transfer from the methyl group to the pyrimidine ring, as in compound **10c**—slightly reduces the sensitivity to friction and increases the thermal stability. Unexpectedly, when the chloromethyl group was replaced with an azidomethyl group, as in compound **10f**, the sensitivity decreased to 2.6 J. The friction sensitivity of compound **10a** is two times lower than that of the chlorine derivative **10e**, and two times higher than that of azidomethyl compound **10f**. The primary differential scanning calorimetric (DSC, 5 °C min^{-1}) tests are also presented in Table 1.

Table 1. Explosive sensitivity for compounds of this study in comparison with tetrazene.

Compound	Formula	IS, [a] J	FS, [b] N	DSC, [c] °C
10a	$C_8H_{10}Cl_1N_3O_5$ (263.63)	2.0 ± 0.4	32 ± 6	212
10b	$C_8H_9Cl_2N_3O_5$ (298.08)	2.1 ± 0.8	36 ± 8	177
10e	$C_8H_9Cl_2N_3O_5$ (298.08)	2 ± 1	60 ± 30	207
10f	$C_8H_9Cl_1N_6O_5$ (304.65)	2.6 ± 1.1	16 ± 8	142
10g	$C_7H_7Cl_1N_6O_5$ (290.62)	1.0 ± 0.3	5.9 ± 0.8	136
tetrazene	$C_2H_8N_{10}O_1$ (188.15)	3 ± 2	<5	127

[a] Impact sensitivity (STANAG 4489). [b] Friction sensitivity (STANAG 4487). [c] Onset decomposition temperature (DSC, 5 °C min^{-1}).

All perchlorates in this study are more thermally stable than tetrazene, slightly exceeding it in impact sensitivity, but less sensitive to friction. Compound **10g** with the azido group at the 1,2,5-oxadiazole ring is the most impact- and friction-sensitive in this series of salts.

2.4. Thermal Analysis

Since the azide compounds **10f** and **10g** are the most energetic, we continued to characterize them and the model compound **10a** from the point of view of their decomposition under heating. The thermal stabilities of the compounds were determined by DSC and thermogravimetric analysis (TGA) measurements scanning at 10 °C min^{-1}. The model compound **10a** decomposes without melting, and the maximum heat release was observed at 218–219 °C, which is comparable to that of common RDX. However, decomposition proceeds very intensively; an acceptable DSC curve can only be obtained on a sample less than 0.2 mg. In TGA measurements, the weight loss occurring at this temperature is approximately 19%, which is close to MeCN release (15.6%), as previously observed for 1,2,5-oxadiazoles [48,57–62]. Further weight loss is observed after 280 °C, which characterizes the second stage of decomposition (see Supplementary Materials, Figure S1).

Decomposition of the model compound **10a** under isothermal conditions was performed using a Bourdon glass compensation pressure gauge [63] in the temperature range of 160–180 °C. The ratio of the weight of the sample to the volume of the reaction vessel (m/V) was ~1×10^{-3} g cm^3. The destruction of **10a** under this condition proceeds with an acceleration in time, which, at temperatures above 160 °C, turns into a degenerate thermal explosion (Supplementary Materials, Figure S4). During decomposition, only 60–95 cm^3 g or 0.7–1.11 moles of colorless gaseous products were released from a mole of the initial **10a**, most of which condenses during cooling. After stopping the process, a dark brown powder remains at the bottom of the vessel. An absorption band of the ClO_4^- (1100 cm^{-1}) anion was observed in the IR spectrum of the residue.

A probable mechanism of the initial destruction stage of salt **10a** is proposed in Scheme 3. This is consistent with the typical decomposition mechanism of 1,2,5-oxadiazoles previously observed for various compounds of this heterocycle [57,58,60,62]. The breaking of the two bonds of the 1,2,5-oxadiazole ring (indicated in the Scheme 3) gives the nitrile product **A** as a result of the typical ring disintegration process. Rapid intermolecular cyclization of the resulting reactive monocyclic intermediate **B** leads to a tricyclic intermediate **C**, capable of further transformations.

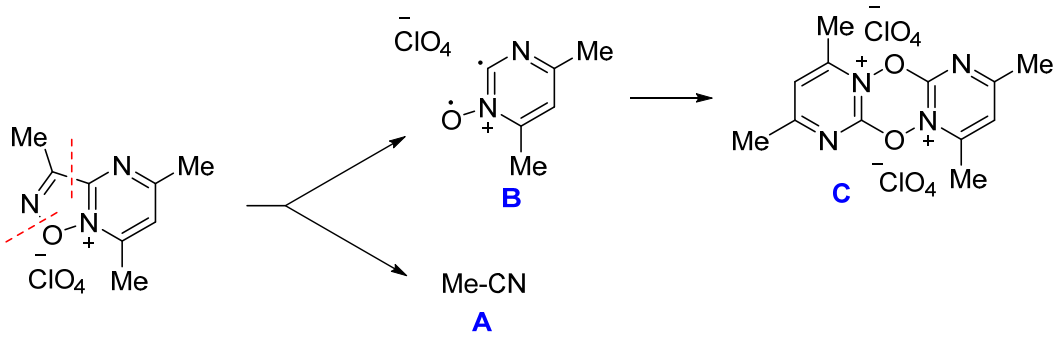

Scheme 3. The proposed first stage of decomposition of salt **10a**.

X-ray diffraction analysis of **10a** shows that the O1–N2 bond is significantly shorter than the other O1–N1 bond of the 1,2,5-oxadiazole ring, which explains the breaking of the latter. The IR spectrum of the final residue includes bands corresponding to C=N bonds (1640, 1590, 1430 cm^{-1}), as well as a strong absorption band of the ClO_4^- anion (1100 cm^{-1}).

The main heat effect is achieved due to the formation of C–O bonds during the formation of tricyclic compound **C**. The formation of two new C–O bonds, even without taking into account the change in the enthalpy part, makes it possible to estimate the heat effect at 746 J g^{-1}, which is in good agreement with the DSC data (1164 J g^{-1}).

Compound **10f** bearing the CH_2N_3 group at the 1,2,5-oxadiazole ring melts at 142 °C (enthalpy of melting L_m > 23 J g^{-1}), and, immediately after this, the exothermic stage of decomposition begins (Supplementary Materials, Figure S3). Decomposition of **10f** proceeds in two stages. At the first, occurring at 143–180 °C with a maximum at 159 °C (1438 J g^{-1}), the weight reduction was 27.6%, which corresponds to a loss of N_3CH_2CN (26.9%), as a result of the breaking of two bonds in the 1,2,5-oxadiazole ring, similar to what was observed for **10a** (Scheme 3). With such isothermal decomposition of **10f**, the gas release is 120 cm^3 g^{-1} or 1.66 mol per mol of the compound (see Supplementary Materials, Figure S6). It is obvious that, in this case, there is also a decomposition of the azide group.

Compound **10g** bearing an electron-withdrawing azide group at the 1,2,5-oxadiazole ring is slightly less thermally stable. When heated using a 10 °C min^{-1} ramp rate, it decomposes in the range of 140–164 °C (maximum heat release of 150 °C). Total energy of the decomposition was 2061 J g^{-1}. Weight loss at this stage reaches 54%, which indicates a deeper decomposition process than is shown in Scheme 3. On the DSC curve, there is another area with weaker heat release at 325 °C, where the weight loss is 21% (see SI, Figure S2).

The decomposition of all compounds of this study under isothermal conditions proceeds with an acceleration in time, and, after completion, a dark brown powder remains at the bottom of the vessel. Here, decomposition was carried out at temperatures below the onset decomposition temperature registered in the DSC. The observed acceleration is associated with the submelting of samples. The analysis of such gas release curves makes it possible to simultaneously determine two decomposition constants, (*i*) in the solid phase (k_s) and (*ii*) in the liquid phase (k_{liq}). The obtained data are summarized in Table 2 and Figure S7 (see Supplementary Materials). The activation energies of decomposition in the solid phase are relatively low (145–164 kJ mol^{-1}) and, within the measurement error (±10 kJ mol^{-1}), practically do not change during the transition to the liquid phase (152–157 kJ mol^{-1}). In general, there are two trends in the data in Table 2. The first is that the decomposition in the liquid phase is much faster than in the solid phase. The second trend is that the rate decomposition constants of the perchlorates of this study, both in the solid phase and in the melt phase, and the Hammett constants of the substituent at the 1,2,5-oxadiazole ring, increase synchronously. A good correlation between the rate of thermal decomposition and the Hammett constant indicates a unified mechanism of the initial stage of destruction of these compounds.

Table 2. Parameters of the Arrhenius equation for perchlorates and benchmark tetrazene.

Sampl	Substituent	σ_I [a]	State	T, °C	logA [b]	E_a, [c] kJ mol^{-1}	k_{150C}, [d] s^{-1} × 10^4
10a	CH_3	−0.07	Solid	160–180	14.5	164	0.015
10f	N_3CH_2	0.11	Solid	110–120	14.3	157	0.084
10g	N_3	0.33	Solid	80–105	15.0	145	12
Tetrazene [e]			Solid	115–125	18.7	163	372
10a	CH_3	−0.07	Liquid	170–180	18.7 [f]	183 [f]	1.1
10f	N_3CH_2	0.11	Liquid	110–130	17.6	157	163
10g	N_3	0.33	Liquid	90–110	18.8	152	530

[a] Hammett constant [64]. [b] The Arrhenius preexponential factor. [c] Activation energy. [d] Rate constant at 150 °C. [e] Data from non-isothermal conditions [65]. [f] Estimated values for two points.

Since the decomposition of compounds proceeds with acceleration, the data obtained under non-isothermal conditions (see Supplementary Materials, Table S1) give the formal kinetics of the total process. Previously, the decomposition of tetrazene was described only under non-isothermal conditions [65]. Comparison of the decomposition kinetics under the same conditions (see Supplementary Materials, Figure S7) reveals that the perchlorates of this study are superior to tetrazene in thermal stability. The decomposition rate constant of tetrazene at 150 °C is several orders of magnitude higher than that of the studied perchlorates (Table 2).

2.5. Combustion

The combustion behaviors of the perchlorates were studied on pressed charges in polyurethane tubes (4 mm inner diameter and ca. 8 mm length). However, at elevated pressures, combustion in the tubes turns into an explosion. For example, the compound **10g** could be burned only at a pressure below 3 MPa. For compound **10f**, a clear result was obtained only when using charges in the form of thin (~1 mm) plates pressed to a high density. The use of such charges avoids the penetration of hot gases into the pores and prevents the transition of layer-by-layer combustion in convective ones. As a result, compound **10f** was able to burn even at high pressures (Figure 8 and Table 3).

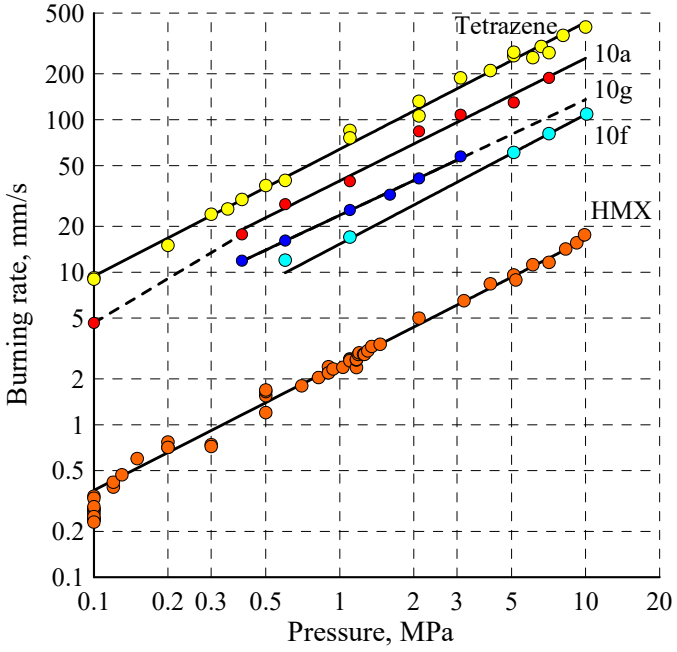

Figure 8. Comparison of burning rates at different pressures for **10a**, **10f**, and **10g** with tetrazene and HMX. Dotted line is extrapolation.

Table 3. The combustion parameters of perchlorates and benchmark compounds.

Compound	Δp, [a] MPa	Burning Rate $r_b = Ap^n$		r_{b10}, [d] mm s^{-1}
		A [b]	n [c]	
10a	0.1–0.4	42.7	0.96	
	0.4–10.0	39.7	0.80	250
10g	0.1–0.4	14.4	0.21	
	0.4–10.0	23.6	0.76	139
10f	5.1–10.0	15.3	0.85	109
Tetrazene	0.1–10.0	64.0	0.83	435
HMX	0.1–10.0	2.47	0.82	16

[a] Pressure range. [b] Empirical coefficient. [c] Pressure exponent in the burning rate law. [d] Calculated burning rate at 10 MPa.

As can be seen from Figure 8, the burning rates of compounds **10** are significantly higher than HMX (1,3,5,7-tetranitro-1,3,5,7-tetraazacyclooctane) [66] and comparable to the burning rates of tetrazene [67].

Remarkably, the burning rates of the perchlorates of this study increase in the following order: **10f** < **10g** < **10a**. However, a similar trend is observed in terms of increasing stability; that is, the decomposition rate of these perchlorates decreases. This result demonstrates a drastic difference from the usual correlations, when an increase in thermal stability leads to a decrease in the burning rate. It can be assumed that the thermolysis of perchlorates, which proceeds with the formation of gaseous products, is a process that determines the temperature of their surfaces during combustion. In this case, the more stable the perchlorate, the higher the temperature of its surface during combustion. If the burning rate is determined by reactions in the condensed phase, which is typical for compounds with low thermal stability [68], the surface temperature at which the leading combustion reaction takes place will be a more significant factor than the decomposition rate.

2.6. Explosive Performance

To evaluate the performance of these newly synthesized compounds, the enthalpies of formation were calculated (see Supplementary Materials) and are summarized in Table 4. Even for the model compound **10a** bearing three ballast methyl groups, the enthalpy of formation is positive and there is +0.56 kJ g^{-1}, which is twice as high as that of benchmark 1,3,5-trinitro-1,3,5-triazinane (RDX; +0.32 kJ g^{-1}). As expected, the introduction of an azide group into one methyl group, and, moreover, the replacement of the methyl group with an azide group, significantly increases the enthalpy of formation, which exceeds the value for tetrazene [69]. This is clearly seen in Table 4. It is obvious that the further replacement of the remaining methyl groups with explosophoric substituents will make it possible to design more effective target products.

Table 4. Explosive performance for compounds of this study in comparison with tetrazene.

Compound	Formula Mw	d^{20}, [a] g cm^{-3}	α [b]	$\Delta_f H^0$, [c] kJ mol^{-1} (kJ g^{-1})	D, [d] m s^{-1}	$P_{C\text{-}J}$, [e] GPa
10a	$C_8H_{10}Cl_1N_3O_5$ (263.63)	1.502	0.262	+147.1 (+0.56)	6400	19
10f	$C_8H_9Cl_1N_6O_5$ (304.65)	1.599	0.268	+552.8 (+1.81)	7000	25
10g	$C_7H_7Cl_1N_6O_5$ (290.62)	1.562	0.314	+557.2 (+1.92)	7000	24
Tetrazene	$C_2H_8N_{10}O_1$ (188.15)	1.635	0.125	+156 [69] (+0.83)	7600	20

[a] Density at room temperature. [b] Oxygen coefficient. For a compound with the molecular formula of $C_xH_yHal_vN_wO_z$, $\alpha = (z + v/2)/(2x + y/2)$. A compound with a > 1 is an oxidizer. [c] Calculated enthalpy of the formation for solid state. [d] Detonation velocity at maximal density. [e] Detonation pressure.

With the crystal density and enthalpy of formation data in hand, the explosive performance of perchlorates was demonstrated with the refined empirical methods implemented in the PILEM code [70]. Since the salts in Table 4 are more than two times poorer in oxygen than RDX (α = 0.667), their detonation velocities are lower than those of RDX (D = 8850 m s^{-1}), close to that of trinitrotoluene (TNT, D = 6663 m s^{-1}), and slightly lower than that of tetrazene.

The results presented in Tables 2 and 4 show that compounds **10f** and **10g** bearing CH_2N_3 and N_3 groups, respectively, have similar performance with respect to detonation velocity and detonation pressure, whereas **10f** is less sensitive to impact and friction. This feature can be used for the further tuning of the [1,2,5]oxadiazolo [2,3-*a*]pyrimidin-8-ium backbone.

3. Materials and Methods

Caution: Although we have encountered no difficulties during preparation and handling of these products, they are potentially explosive energetic materials. Manipulations must be carried out by using appropriate standard safety precautions.

Most of the reagents and starting materials were purchased from commercial sources and used without additional purification. The starting 3-amino-4-methylfurazan (**9a**) [47], 3-amino-4-chloromethylfurazan (**9b**) [48], 3-amino-4-azidomethylfurazan (**9c**) [48], 3-amino-4-azidofurazan (**9d**) [49,50], 3-amino-4-nitrofurazan **9e** [51], and 3-amino-4-*tert*butylazoxyfurazan **9f** [52] were synthesized by using previously reported procedures.

IR spectra were recorded on a BrukerALPHA instrument in KBr pellets. The ^{1}H and ^{13}C, ^{14}N spectra were recorded on a Bruker AM-300 instrument (300.13, 75.47, and 21.69 MHz, respectively) at 299 K. The chemical shifts of ^{1}H and ^{13}C nuclei were reported relative to TMS (^{1}H and ^{13}C, 0.00 ppm). ^{1}H–^{15}N HMBC experiments were run to measure the ^{15}N chemical shifts (^{15}N, relative to liquid NH_3, 0.00 ppm). Elemental analysis was performed on a PerkinElmer 2400 Series II instrument. Analytical TLC was performed using commercially pre-coated silica gel plates (Kieselgel 60 F_{254}), and visualization was effected with short-wavelength UV light.

Thermal stability was studied by differential scanning calorimetry (DSC) using a Mettler Toledo DSC 822e module. The sample (1–2 mg) was weighed in an aluminum crucible (40 μL), sealed under air with a press, and then pierced with a needle to leave two holes with a diameter of ca. 1 mm. The decomposition of a sample was carried out in a nitrogen atmosphere at a purge rate of 50 μL min^{-1}. The temperature of the onset of intense decomposition (T_{onset}) was taken as the temperature determining thermal stability. The samples were subjected to thermostating in the measuring cell at a temperature of 25 °C for 30 min before the start of measurements.

Impact and friction sensitivities were measured with a BAM-type apparatus in a series of experiments according to STANAG procedures [71,72].

The burning rate was determined in a constant-pressure device (Crawford bomb) with a volume of 2 L in a nitrogen atmosphere. The combustion process of the sample was recorded using a pressure strain gauge, which transmitted the signal to a digital oscilloscope. The start and end times of combustion were determined from oscillograms. The burning rate was calculated by dividing the sample height by the burning time and was related to the mean integral pressure during the experiment. The error in determining the burning rate did not exceed 3%.

Single-Crystal X-ray Diffraction Study. The single crystals of perchlorates **10a**, **10f**, and **10g** were grown by crystallization from hot AcOH solution. Single-crystal X-ray diffraction experiments were carried out using a SMART APEX2 CCD diffractometer (λ(Mo-Kα) = 0.71073 Å, graphite monochromator, ω-scans) at 100 K. Collected data were processed by the SAINT and SADABS programs incorporated into the APEX2 program package [73]. The structures were solved by the direct methods and refined by the full-matrix least-squares procedure against F^2 in anisotropic approximation. The refinement was carried out with the SHELXTL program [74]. The CCDC numbers (2210557 for **10a**, 2210558

for **10f**, and 2210559 for **10g**) contain the supplementary crystallographic data for this paper. These data can be obtained free of charge via www.ccdc.cam.ac.uk/data_request/cif, accessed on 1 November 2022.

Crystallographic data for compound **10a**: $C_7H_7N_6O^+ClO_4^-$ are monoclinic, space group $P2_1/c$: a = 15.1208(6) Å, b = 11.7428(5) Å, c = 20.4811(8) Å, β = 98.7126(13)°, V = 3594.7(3) Å^3, Z = 12, M = 290.64, d_{cryst} = 1.611 g·cm^{-3}. $wR2$ = 0.2394 calculated on F^2_{hkl} for all 7199 independent reflections with $2\theta < 52.5°$ (*GOF* = 1.004, R = 0.0680 calculated on F_{hkl} for 5235 reflections with $I > 2\sigma(I)$).

Crystallographic data for compound **10f**: $C_8H_9N_6O^+ClO_4^-$ are monoclinic, space group $P2_1/n$: a = 8.1920(3) Å, b = 13.8353(5) Å, c = 10.8329(4) Å, β = 91.751(2)°, V = 1227.21(8) Å^3, Z = 4, M = 304.66, d_{cryst} = 1.649 g·cm^{-3}. $wR2$ = 0.0805 calculated on F^2_{hkl} for all 2703 independent reflections with $2\theta < 54.2°$ (*GOF* = 1.050, R = 0.0297 calculated on F_{hkl} for 2300 reflections with $I > 2\sigma(I)$).

Crystallographic data for compound **10g**: $C_8H_{10}N_3O^+ClO_4^-$ are triclinic, space group P-1: a = 11.2823(6) Å, b = 11.4350(6) Å, c = 11.6297(6) Å, α = 98.260(3)°, β = 118.986(2)°, γ = 110.895(2)°, V = 1130.45(11) Å^3, Z = 4, M = 263.64, d_{cryst} = 1.549 g·cm^{-3}. $wR2$ = 0.1358 calculated on F^2_{hkl} for all 4613 independent reflections with $2\theta < 52.8°$ (*GOF* = 1.105, R = 0.0522 calculated on F_{hkl} for 3871 reflections with $I > 2\sigma(I)$).

3,5,7-Trimethyl-[1,2,5]oxadiazolo [2,3-*a*]pyrimidin-8-ium perchlorate (**10a**). A mixture of 58% $HClO_4$ (0.97 g, 5.6 mmol), CF_3CO_2H (3.5 mL), and 3-amino-4-methylfurazan (0.5 g, 5.0 mmol) was stirred for 5 min at rt, and pentane-2,4-dione (0.56 g, 5.6 mmol) was added. The mixture was stirred for 3 h at rt and then diluted with Et_2O (20 mL). The precipitate was isolated by filtration, washed with EtOH (3 × 5 mL) and Et_2O (2 × 5 mL), and dried under vacuum to give salt **10a** (80%) as a white solid: mp 213–214 °C dec [lit. [44] mp 195–197 °C (dec)]; IR (KBr) ν 3092, 2934, 1629, 1575, 1563, 1442, 1401, 1377, 1363, 1269, 1205, 1094 cm^{-1}; ^{1}H NMR (CD_3CN) δ 2.84 (s, 3H), 2.95 (s, 3H), 3.05 (s, 3H), 8.06 (s, 1H); ^{13}C NMR (CD_3CN) δ 9.3, 16.2, 25.6, 122.7, 146.2, 151.1, 154.7, 177.9; ^{15}N NMR (CD_3CN) δ 268.8, 281.0, 389.2; ^{35}Cl NMR (CD_3CN) δ 1012.1. Anal. Calcd for $C_8H_{10}ClN_3O_5$ (263.63): C, 36.45; H, 3.82; N, 15.94. Found: C, 36.40; H, 3.79; N, 15.91.

6-Chloro-3,5,7-trimethyl-[1,2,5]oxadiazolo [2,3-*a*]pyrimidin-8-ium perchlorate (**10b**). Following the same procedure outlined above, 3-chloropentane-2,4-dione gave the desired product **10b** (85%) as a white solid: mp 180–181 °C dec; IR (KBr) ν 3026, 2934, 1605, 1552, 1395, 1266, 1095 cm^{-1}; ^{1}H NMR (CD_3CN) δ 2.63 (s, 3H), 3.02 (s, 3H), 3.14 (s, 3H); ^{13}C NMR (CD_3CN) δ 8.9, 15.2, 25.1, 132.1, 143.4, 149.3, 154.5, 175.1. Anal. Calcd for $C_8H_9Cl_2N_3O_5$ (298.08): C, 32.24; H, 3.04; N, 14.10. Found: C, 32.29; H, 3.07; N, 14.05.

3-Chloromethyl-5,7-dimethyl-[1,2,5]oxadiazolo [2,3-*a*]pyrimidin-8-ium perchlorate (**10e**). Following the same procedure outlined above, the reaction of 3-amino-4-chloromethy lfurazan (**9b**) with pentane-2,4-dione gave the desired product **10e** (96%) as a white solid: mp 195–196 °C dec; IR (KBr) ν 3076, 3023, 2932, 1626, 1572, 1441, 1396, 1377, 1262, 1202, 1093, 779, 738, 625 cm^{-1}; ^{1}H NMR (CD_3CN) δ 2.98 (s, 3H), 3.02 (s, 3H), 3.08 (s, 3H), 5.21 (s, 2H), 8.12 (s, 1H); ^{13}C NMR (CD_3CN) δ 15.3, 24.8, 31.8, 122.4, 143.7, 150.6, 153.0, 177.7. Anal. Calcd for $C_8H_9Cl_2N_3O_5$ (298.08): C, 32.24; H, 3.04; N, 14.10. Found: C, 32.21; H, 3.02; N, 14.06.

3-Azidomethyl-5,7-dimethyl-[1,2,5]oxadiazolo [2,3-*a*]pyrimidin-8-ium perchlorate (**10f**). Following the same procedure, the reaction of 3-amino-4-azidomethylfurazan (**9c**) with pentane-2,4-dione gave the desired product **10e** (94%) as a white solid: mp 195–196 °C dec; IR (KBr) ν 3081, 2934, 2215, 2125, 1624, 1573, 1442, 1424, 1333, 1282, 1264, 1195, 1093 cm^{-1}; ^{1}H NMR (CD_3CN) δ 2.93 (s, 3H), 3.05 (s, 3H), 3.08 (s, 3H), 5.04 (s, 2H), 8.08 (s, 1H); ^{13}C NMR (CD_3CN) δ 14.5, 23.9, 42.2, 121.4, 143.3, 149.7, 151.7, 176.7. Anal. Calcd for $C_8H_9ClN_6O_5$ (304.65): C, 31.54; H, 2.98; N, 27.59. Found: C, 31.60; H, 3.03; N, 27.56.

3-Azido-5,7-dimethyl-[1,2,5]oxadiazolo [2,3-*a*]pyrimidin-8-ium perchlorate (**10g**). Following the same procedure, the reaction of 3-amino-4-azidofurazan (**9d**) with pentane-2,4-dione gave the desired product **10g** (71%) as a white solid: mp 140–141 °C dec; IR (KBr) ν 3082, 2930, 2157, 1625, 1543, 1443, 1412, 1306, 1266, 1177, 1091 cm^{-1}; ^{1}H NMR (CD_3CN)

δ 2.96 (s, 3H), 3.05 (s, 3H), 8.13 (s, 1H); ^{13}C NMR (CD_3CN) δ 15.9, 25.6, 123.5, 140.8, 152.0, 153.0, 178.2. Anal. Calcd for $C_7H_7ClN_6O_5$ (290.62): C, 28.93; H, 2.43; N, 28.92. Found: C, 29.00; H, 2.47; N, 28.86.

4. Conclusions

A new group of furazan-based energetic materials, [1,2,5]oxadiazolo [2,3-*a*]pyrimidin-8-ium perchlorates bearing explosophoric groups, have been synthesized for the first time. The synthetic protocol does not require complex procedures, relying on the simple mixing of available reagents and the usual filtering of the desired product. All compounds were fully characterized by multinuclear NMR spectroscopy and X-ray crystal structure determinations. Initial safety testing (impact and friction sensitivity) and thermal stability measurements (DTA) were also carried out. These salts demonstrate an excellent burn rate and combustion behavior. Considering the simplicity of preparation and the inherent combination of properties, the [1,2,5]oxadiazolo [2,3-*a*]pyrimidin-8-ium backbone may be used as an effective building block in the creation of new energetic materials for various purposes.

Supplementary Materials: The following supporting information can be downloaded at: https://www.mdpi.com/article/10.3390/molecules27238443/s1. Figures of thermograms for decomposition in non-isothermal conditions, curves of decomposition in isothermal conditions, estimation of standard (solid-state) enthalpies of formation, and copies of NMR spectra are available in supplementary information. Figure S1. Figure S2. TGA and DSC curves of compound **10g** at a heating rate 10 °C min^{-1}. Figure S3. TGA and DSC curves of compound **10f** at a heating rate 10 °C min^{-1}. Table S1. Results of DSC study for compounds of this study. Figure S4. Gas release curves of compound **10a** at different temperatures. Points are experiment, lines are fittings. Figure S5. Gas release curves of compound **10f** at different temperatures. Points are experiment, lines are fittings. Figure S6. Figure S7. Comparison of decomposition kinetic data for compounds **10a**, **10f**, **10g** and tetrazene obtained in non isothermal (DSC, triangles) and isothermal (Manometry, points) conditions. Figure S8. Effect of Hammett constants of substituent constants at the 1,2,5-oxadiazole ring on the decomposition rate in liquid and solid state. Temperature is 150 °C. Figure S9. The Born-Haber thermodynamic cycle employed for the estimation of the formation enthalpy of the crystalline salts **10a**, **10f**, and **10g**. Table S2. The Thermochemical Properties of compounds **10a**, **10f**, and **10g**. Points are experiment, lines are fittings. Refs. [75–89] are cited in the Supplementary Materials.

Author Contributions: Conceptualization, V.P.S. and A.B.S.; methodology, K.V.S. and A.B.S.; investigation, K.V.S., A.D.S., S.A.F., A.I.S., K.Y.S., K.A.M. and V.G.K.; writing—original draft, V.P.S., K.V.S. and K.Y.S.; writing—review and editing, V.P.S. and A.B.S.; project administration, A.B.S.; funding acquisition, A.B.S. All authors have read and agreed to the published version of the manuscript.

Funding: This research was supported by the Russian Science Foundation (grant no. 20-13-00289).

Institutional Review Board Statement: Not applicable.

Informed Consent Statement: Not applicable.

Data Availability Statement: CCDC 2210557, 2210558 and 2210559 contain the supplementary crystallographic data for this paper. The data can be obtained free of charge from The Cambridge Crystallographic Data Centre via https://www.ccdc.cam.ac.uk/structures.

Acknowledgments: The authors thank the Department of Structural Studies of the Zelinsky Institute of Organic Chemistry for X-ray analyses of compound **10g**. Single-crystal X-ray study of compounds **10a** and **10f** and crystal structure analysis were supported by the Ministry of Science and Higher Education of the Russian Federation (Contract/Agreement No. 075-00697-22-00).

Conflicts of Interest: The authors declare no conflict of interest. The funders had no role in the design of the study; in the collection, analyses, or interpretation of data; in the writing of the manuscript, or in the decision to publish the results.

Sample Availability: Since all the compounds in this study are potentially dangerous, the authors do not assume responsibility for providing these samples. On the other hand, a description of the preparation of all compounds can be found in the manuscript and in the Supplementary Materials.

References

1. Rogov, N.G.; Ischenko, M.A. *Solid Composite Propellants: Components, Requirements, Properties*; SPSTU: St. Petersburg, Russia, 2005. (In Russian)
2. Madyakin, F.P. *Components and Combustion Products of Pyrotechnic Compositions*; KSTU: Kazan, Russia, 2006. (In Russian)
3. Singh, H.; Shekhar, H. *Solid Rocket Propellants: Science and Technology Challenges*; Royal Society of Chemistry: London, UK, 2017.
4. Zhang, L.; Lin, Q.-Q.; Cheng, B.; Wang, P.; Lu, M.; Lin, Q.-H. Effect of hexanitroethane (HNE) and hydrazinium nitroformate (HNF) on energy characteristics of composite solid propellants. *FirePhysChem* **2021**, *1*, 116–122. [CrossRef]
5. Gao, H.; Shreeve, J.M. Azole-Based Energetic Salts. *Chem. Rev.* **2011**, *111*, 7377–7436. [CrossRef] [PubMed]
6. Zhang, Q.; Shreeve, J.M. Energetic Ionic Liquids as Explosives and Propellant Fuels: A New Journey of Ionic Liquid Chemistry. *Chem. Rev.* **2014**, *114*, 10527–10574. [CrossRef]
7. Sebastiao, E.; Cook, C.; Hub, A.; Murugesu, M. Recent developments in the field of energetic ionic liquids. *J. Mater. Chem. A* **2014**, *2*, 8153–8173. [CrossRef]
8. Chingin, K.; Perry, R.H.; Chambreau, S.D.; Vaghjiani, G.L.; Zare, R.N. Generation of melamine polymer condensates upon hypergolic ignition of dicyanamide ionic liquids. *Angew. Chem. Int. Ed.* **2011**, *50*, 8634–8637. [CrossRef] [PubMed]
9. Sheremetev, A.B. Zelinsky Institute of Organic Chemistry, Russian Academy of Sciences, Moscow, Russia. 2001; Unpublished work.
10. Dorofeenko, G.N.; Krivun, S.V.; Dulenko, V.I.; Zhdanov, Y.A. Perchloric acid and its compounds in organic synthesis. *Russ. Chem. Rev.* **1965**, *34*, 88–104, [Translation of *Usp. Khim.* **1965**, *34*, 219–252]. [CrossRef]
11. Deshpande, S.S.; Kumar, A. Activation of Organic Reactions by Perchlorates. *Adv. Org. Synth.* **2005**, *1*, 215–232. [CrossRef]
12. Dalpozzo, R.; Bartoli, G.; Sambri, L.; Melchiorre, P. Perchloric Acid and Its Salts: Very Powerful Catalysts in Organic Chemistry. *Chem. Rev.* **2010**, *110*, 3501–3551. [CrossRef] [PubMed]
13. Sheremetev, A.B.; Makhova, N.N.; Friedrichsen, W. Monocyclic Furazans and Furoxans. *Adv. Heterocycl. Chem.* **2001**, *78*, 65–188. [CrossRef]
14. Fershtat, L.L.; Makhova, N.N. 1,2,5-Oxadiazole-Based High-Energy-Density Materials: Synthesis and Performance. *ChemPlusChem* **2020**, *85*, 13–42. [CrossRef]
15. Zhang, J.; Zhou, J.; Bi, F.; Wang, B. Energetic materials based on poly furazan and furoxan structures. *Chin. Chem. Lett.* **2020**, *31*, 2375–2394. [CrossRef]
16. Li, Y.; Yuan, J.M.; Zhao, W.; Qu, Y.; Xing, X.W.; Meng, J.W.; Liu, Y.C. Application and Development of 3,4-Bis(3-nitrofurazan-4-yl)furoxan (DNTF). *Russ. J. Gen. Chem.* **2021**, *91*, 445–455. [CrossRef]
17. Tang, J.; Yang, H.; Cui, Y.; Cheng, G. Nitrogen-rich tricyclic-based energetic materials. *Mater. Chem. Front.* **2021**, *5*, 7108–7118. [CrossRef]
18. Willer, R.L.; Day, R.S.; Park, D.J. Composition of Salts of 3-Nitramino-4-Nitrofurazan for Propellants. U.S. Patent 5,460,669, 28 June 1995.
19. Williams, G.K.; Brill, T.B. Thermal decomposition of energetic materials 72: Unusual behavior of substituted furazan compounds upon flash pyrolysis. *Combust. Flame* **1998**, *114*, 569–576. [CrossRef]
20. Sheremetev, A.B.; Yudin, I.L.; Aleksandrova, N.S.; Aronova, S.M.; Kryazhevskikh, I.A.; Lempert, D.B. Hydroxylammonium salts of furazan family. *Int. Annu. Conf. ICT* **2003**, *34*, 101/1–101/10.
21. Blomquist, H.R. (Nitramino)Nitrofurazan-Based Monopropellant Smokeless Gas Generating Compositions, Especially for Airbags. U.S. Patent 6,513,834, 29 August 2003.
22. Wang, B.; Xiong, H.; Cheng, G.; Yang, H. Incorporating Energetic Moieties into Four Oxadiazole Ring Systems for the Generation of High-Performance Energetic Materials. *ChemPlusChem* **2018**, *83*, 439–447. [CrossRef]
23. Ma, J.; Chinnam, A.K.; Cheng, G.; Yang, H.; Zhang, J.; Shreeve, J.M. 1,3,4-Oxadiazole Bridges: A Strategy to Improve Energetics at the Molecular Level. *Angew. Chem. Int. Ed.* **2021**, *60*, 5497–5504. [CrossRef] [PubMed]
24. Sheremetev, A.B. (Perchlorylamino)furazans and its salts: New high-energy-density materials with high sensitivity. *Mendeleev Commun.* **2020**, *30*, 490–493. [CrossRef]
25. Li, H.; Zhao, F.; Wang, B.; Zhai, L.; Lai, W.; Liu, N. A new family of energetic salts based on oxybridged bis(dinitromethyl)furazan: Syntheses, characterization and properties. *RSC Adv.* **2015**, *5*, 21422–21429. [CrossRef]
26. Zhai, L.; Fan, X.; Wang, B.; Bi, F.; Liab, Y.; Zhua, Y. A green high-initiation-power primary explosive: Synthesis, 3D structure and energetic properties of dipotassium 3,4-bis(3-dinitromethylfurazan-4-oxy)furazan. *RSC Adv.* **2015**, *5*, 57833–57841. [CrossRef]
27. Tang, Y.; Gao, H.; Imler, G.H.; Parrish, D.A.; Shreeve, J.M. Energetic dinitromethyl group functionalized azofurazan and its azofurazanates. *RSC Adv.* **2016**, *6*, 91477–91482. [CrossRef]
28. Huang, H.; Li, Y.; Yang, J.; Pan, R.; Lin, X. Materials with good energetic properties resulting from the smart combination of nitramino and dinitromethyl group with furazan. *New J. Chem.* **2017**, *41*, 7697–7704. [CrossRef]
29. Ma, Q.; Gu, H.; Huang, J.; Liu, D.; Li, J.; Fan, G. Synthesis and Characterization of New Melt-cast Energetic Salts: Dipotassium and Diaminoguanidinium N,N′-Dinitro-N,N′-Bis(3-dinitromethyl-furazanate-4-yl)methylenediamine. *Propellants Explos. Pyrotech.* **2018**, *43*, 90–95. [CrossRef]
30. Guo, T.; Wang, Z.; Tang, W.; Wang, W.; Bi, F.; Wang, B.; Zhou, Z.; Meng, Z.; Ge, Z. A good balance between the energy density and sensitivity from assembly of bis(dinitromethyl) and bis(fluorodinitromethyl) with a single furazan ring. *J. Anal. Appl. Pyrolysis* **2018**, *134*, 218–230. [CrossRef]

31. Yu, Q.; Chinnam, A.K.; Yin, P.; Imler, G.H.; Parrish, D.A.; Shreeve, J.M. Finding furoxan rings. *J. Mater. Chem. A* **2020**, *8*, 5859–5864. [CrossRef]
32. Zhou, Y.; Gao, H.; Shreeve, J.M. Dinitromethyl groups enliven energetic salts. *Energ. Mater. Front.* **2020**, *1*, 2–15. [CrossRef]
33. Wang, B.; Zhang, G.; Huo, H.; Fan, Y.; Fan, X. Synthesis, characterization and thermal properties of energetic compounds derived from 3-amino-4-(tetrazol-5-yl)furazan. *Chin. J. Chem.* **2011**, *29*, 919–924. [CrossRef]
34. Ilyushin, M.A.; Shugaley, I.V.; Tselinskii, I.V.; Garabadzhiu, A.V. Environmental Problems and Their Solutions of Using Energy-Rich Substances for Initiating Devices. *Russ. J. Gen. Chem.* **2013**, *83*, 2624–2632. [CrossRef]
35. Ilyushin, M.A.; Tselinsky, I.V.; Shugalei, I.V. Environmentally Friendly Energetic Materials for Initiation Devices. *Cent. Eur. J. Energ. Mater.* **2012**, *9*, 293–327.
36. Stepanov, A.I.; Sannikov, V.S.; Dashko, D.V.; Roslyakov, A.G.; Astrat'yev, A.A.; Stepanova, E.V.; Aliev, Z.G.; Goncharov, T.K.; Aldoshin, S.M. Synthesis and properties of 3-azido-4-(2H-tetrazol-5-yl)furazan. *Chem. Heterocycl. Compd.* **2017**, *53*, 779–785. [CrossRef]
37. Dong, Z.; An, D.; Yang, R.; Ye, Z. Insensitive and Thermostable Energetic Materials Based on 3-Ureido-4-tetrazole-furazan: Synthesis, Characterization, and Properties. *Z. Anorg. Allg. Chem.* **2019**, *645*, 1285–1290. [CrossRef]
38. Yu, Q.; Yang, H.; Ju, X.; Lu, C.; Lin, Q.; Zhang, J.; Cheng, G. 1D Energetic Metal-Organic Framework: Sodium 6-Nitro-5-oxidopyrazolo [3,4-*c*][1,2,5]oxadiazol-4-ide with Good Thermal Stability. *ChemistrySelect* **2017**, *2*, 4673–4677. [CrossRef]
39. Tang, Y.; He, C.; Shreeve, J.M. A furazan-fused pyrazole N-oxide via unusual cyclization. *J. Mater. Chem. A* **2017**, *5*, 4314–4319. [CrossRef]
40. Hermann, T.S.; Klapotke, T.M.; Krumm, B. Formation and Characterization of Heavy Alkali and Silver Salts of the 4-Nitro-pyrazolo-(3,4-*c*)-furazan-5-N-oxide Anion. *Propellants Explos. Pyrotech.* **2018**, *43*, 54–61. [CrossRef]
41. Voronin, A.A.; Fedyanin, I.V.; Churakov, A.M.; Pivkina, A.N.; Muravyev, N.V.; Strelenko, Y.A.; Klenov, M.S.; Lempert, D.B.; Tartakovsky, V.A. 4*H*-[1,2,3]Triazolo [4,5-*c*][1,2,5]oxadiazole 5-oxide and Its Salts: Promising Multipurpose Energetic Materials. *ACS Appl. Energy Mater.* **2020**, *3*, 9401–9407. [CrossRef]
42. Sheremetev, A.B.; Yudin, I.L.; Aleksandrova, N.S. High nitrogen furazan derivatives for gas generetors. In Proceedings of the Twenty-Third International Pyrotechnics Seminar, Tsukuba, Japan, 30 September 1997; pp. 377–388.
43. Davis, M.; Deady, L.W.; Homfeld, E. Rates of N-methylation of 2-Methybenzotriazole, 2,1,3-Benzoxadiazole, 2,1,3-Benzothia(or Selena)diazole, 1,2,5-Oxadiazole and 1,2,5-Thiadiazole. *Aust. J. Chem.* **1974**, *27*, 1917–1921. [CrossRef]
44. Bachkovsky, I.P.; Mikhailovsky, A.P.; Chuiguk, V.A. 1,2,5-Oxadiazolo [2,3-*a*]-pyrimidinium salts. *Ukr. Khim. Zh.* **1980**, *46*, 637–639.
45. Struchkov, Y.T.; Batsanov, A.S.; Chuiguk, V.A.; Batog, L.V.; Kulikov, A.S.; Pivina, T.S.; Strelenko, Y.A. 5,7-Dimethyl-3-phenylfurazano- and -furoxano [5,4-*a*]pyrimidinium perchlorates: A new type of condensed system. *Chem. Heterocycl. Comp.* **1992**, *24*, 193–197, [Translation of *Khim. Geterotsikl. Soedin.* **1992**, *2*, 233–238]. [CrossRef]
46. Zhou, J.; Zhang, J.; Wang, B.; Qiu, L.; Sheremetev, A.B. Recent Synthetic Efforts towards High Energy Density Materials: How to Design High-Performance Energetic Structures? *FirePhysChem* **2022**, *2*, 83–139. [CrossRef]
47. Sheremetev, A.B.; Shamshina, Y.L.; Dmitriev, D.E. Synthesis of 3-alkyl-4-aminofurazans. *Russ. Chem. Bull.* **2005**, *54*, 1032–1037, [Translation of *Izv. Akad. Nauk. Ser. Khim.* **2005**, *4*, 1007–1012]. [CrossRef]
48. Sheremetev, A.B.; Mel'nikova, S.F.; Kokareva, E.S.; Nekrutenko, R.E.; Strizhenko, K.V.; Suponitsky, K.Y.; Pham, T.D.; Pivkina, A.N.; Sinditskii, V.P. Nitroxy- and azidomethyl azofurazans as advanced energetic materials. *Def. Technol.* **2022**, *18*, 1369–1381. [CrossRef]
49. Tselinskii, I.V.; Mel'nikova, S.F.; Vergizov, S.N. Azidofurazans in the synthesis of condensed systems. *Zhurnal Org. Khimii* **1981**, *17*, 1123–1124.
50. Rakitin, O.A.; Zalesova, O.A.; Kulikov, A.S.; Makhova, N.N.; Godovikova, T.I.; Khmel'nitskii, L.I. Synthesis and reactivity of furazanyl- and furoxanyldiazonium salts. *Russ. Chem. Bull.* **1993**, *42*, 1865–1870, [Translation of *Izv. Akad. Nauk. Ser. Khim.* **1993**, *11*, 1949–1955]. [CrossRef]
51. Novikova, T.S.; Melnikova, T.M.; Kharitonova, O.V.; Kulagina, V.O.; Aleksandrova, N.S.; Sheremetev, A.B.; Pivina, T.S.; Khmelnitskii, L.I.; Novikov, S.S. An Effective Method for the Oxidation of Aminofurazans to Nitrofurazans. *Mendeleev Commun.* **1994**, *4*, 138–140. [CrossRef]
52. Apasov, E.T.; Sheremetev, A.B.; Dzhetigenov, B.A.; Kalinin, A.V.; Tartakovsky, V.A. Reaction of Silylated Aminonitrofurazan with N-Magnesium Amine Derivatives. *Bull. Russ. Acad. Sci. Div. Chem. Sci.* **1992**, *41*, 1500–1501. [CrossRef]
53. Skibsted, J.; Jakobsen, H.J. ^{35}Cl and ^{37}Cl Magic-Angle Spinning NMR Spectroscopy in the Characterization of Inorganic Perchlorates. *Inorg. Chem.* **1999**, *38*, 1806–1813. [CrossRef] [PubMed]
54. Suponitsky, K.Y.; Lyssenko, K.A.; Antipin, M.Y.; Aleksandrova, N.S.; Sheremetev, A.B.; Novikova, T.S. 4,4-Bis(nitramin)azofurazane and its Salts. Study of Molecular and Crystal Structure Based on X-ray and Quantum Chemical Data. *Russ. Chem. Bull.* **2009**, *58*, 2129–2136. [CrossRef]
55. Suponitsky, K.Y.; Lyssenko, K.A.; Ananyev, I.V.; Kozeev, A.M.; Sheremetev, A.B. Role of Weak Intermolecular Interactions in the Crystal Structure of Tetrakis-furazano [3,4-*c*:3′,4′-*g*:3″,4″-*k*:3‴,4‴-*o*][1,2,5,6,9,10,13,14]octaazacyclohexadecine and Its Solvates. *Cryst. Growth Des.* **2014**, *14*, 4439–4449. [CrossRef]
56. Suponitsky, K.Y.; Smol'yakov, A.F.; Ananyev, I.V.; Khakhalev, A.V.; Gidaspov, A.A.; Sheremetev, A.B. 3,4-Dinitrofurazan: Structural Nonequivalence of Ortho-Nitro Groups as a Key Feature of the Crystal Structure and Density. *ChemistrySelect* **2020**, *5*, 14543–14548. [CrossRef]

57. Manelis, G.B.; Nazin, G.M.; Rubtsov, Y.I.; Strunin, V.A. *Thermal Decomposition and Combustion of Explosives and Propellants*; CRC Press: London, UK, 2003. [CrossRef]
58. Sinditskii, V.P.; Burzhava, A.V.; Sheremetev, A.B.; Aleksandrova, N.S. Thermal and combustion properties of 3,4-Bis(3-nitrofurazan-4-yl)furoxan (DNTF). *Propellants Explos. Pyrotech.* **2012**, *37*, 575–580. [CrossRef]
59. Sinditskii, V.P.; Burzhava, A.V.; Egorshev, V.Y.; Sheremetev, A.B.; Zelenov, V.P. Combustion of Furazanotetrazine Dioxide. *Combust. Explos. Shock. Waves* **2013**, *49*, 117–120, [Translation of *Fiz. Goren. Vzriv.* **2013**, *49*, 134–137]. [CrossRef]
60. Sinditskii, V.P.; Burzhava, A.V.; Chernyi, A.N.; Shmelev, D.S.; Apalkova, V.N.; Palysaeva, N.V.; Sheremetev, A.B. A comparative study of two difurazanyl ethers. *J. Therm. Anal. Calorim.* **2016**, *123*, 1431–1438. [CrossRef]
61. Sinditskii, V.P.; Smirnova, A.D.; Serushkin, V.V.; Aleksandrova, N.S.; Sheremetev, A.B. Furazan-fused azacyclic nitramines: Influence of structural features on the combustion and the thermolysis. *ChemistrySelect* **2020**, *5*, 13868–13877. [CrossRef]
62. Sinditskii, V.P.; Burzhava, A.V.; Sheremetev, A.B. Macrocyclic tetra(azo-) and tetra(azoxyfurazan)s: Comparative study of decomposition and combustion with linear analogs. *Energetic Mater. Front.* **2021**, *2*, 87–95. [CrossRef]
63. Sinditskii, V.P.; Smirnova, A.D.; Serushkin, V.V.; Yudin, N.V.; Vatsadze, I.A.; Dalinger, I.L.; Kiselev, V.G.; Sheremetev, A.B. Nitroderivatives of N-pyrazolyltetrazoles: Thermal decomposition and combustion. *Thermochim. Acta* **2021**, *698*, 178876. [CrossRef]
64. Vereschagin, A.N. *Inductive Effect. Constants of Substituents for Correlation Analysis*; Nauka: Moscow, Russia, 1988.
65. Whelan, D.J.; Spear, R.J.; Read, R.W. The thermal decomposition of some primary explosives as studied by differential scanning calorimetry. *Thermochim. Acta* **1984**, *80*, 149–163. [CrossRef]
66. Sinditskii, V.P.; Egorshev, V.Y.; Berezin, M.V.; Serushkin, V.V. Mechanism of HMX combustion in a wide range of pressures. *Combust. Explos. Shock. Waves* **2009**, *45*, 461–477. [CrossRef]
67. Fogelzang, A.E.; Egorshev, V.Y.; Pimenov, A.Y.; Sinditskii, V.P.; Saklanty, A.R.; Svetlov, B.S. Investigation of the Steady-State Burning of Primary Explosives at High Pressures. *Dokl. Akad. Nauk SSSR* **1985**, *285*, 1449–1452.
68. Sinditskii, V.P.; Egorshev, V.Y.; Serushkin, V.V.; Levshenkov, A.I.; Berezin, M.V.; Filatov, S.A. Combustion of energetic materials governed by reactions in the condensed phase. *Inter. J. Ener. Mat. Chem. Prop.* **2010**, *9*, 147–192. [CrossRef]
69. Kolesov, V.I.; Kapranov, K.O.; Tkacheva, A.V.; Kulagin, I.A. Explosive Characteristics of Tetrazene and MTX-1. *Combust. Explos. Shock Waves.* **2021**, *57*, 350–355. [CrossRef]
70. Muravyev, N.V.; Wozniak, D.R.; Piercey, D.G. Progress and performance of energetic materials: Open dataset, tool, and implications for synthesis. *J. Mater. Chem. A* **2022**, *10*, 11054–11073. [CrossRef]
71. *STANAG 4489*; Explosives, Impact Sensitivity Tests. NATO: Brussels, Belgium, 1999.
72. *STANAG 4487*; Explosives, Friction Sensitivity Tests. NATO: Brussels, Belgium, 2002.
73. Bruker AXS Inc. *APEX2 and SAINT*; Bruker AXS Inc.: Madison, WI, USA, 2014.
74. Sheldrick, G.M. Crystal structure refinement with SHELXL. *Acta Cryst. C* **2015**, *71*, 3–8. [CrossRef] [PubMed]
75. Kissinger, H.E. Reaction kinetics in differential thermal analysis. *Anal. Chem.* **1957**, *29*, 1702–1706. [CrossRef]
76. Jenkins, H.D.B.; Roobottom, H.K.; Passmore, J.; Glasser, L. Relationships among Ionic Lattice Energies, Molecular (Formula Unit) Volumes, and Thermochemical Radii. *Inorg. Chem.* **1999**, *38*, 3609–3620. [CrossRef]
77. Jenkins, H.D.B.; Tudela, D.; Glasser, L. Lattice Potential Energy Estimation for Complex Ionic Salts from Density Measurements. *Inorg. Chem.* **2002**, *41*, 2364–2367. [CrossRef]
78. Curtiss, L.A.; Raghavachari, K.; Redfern, P.C.; Pople, J.A. Assessment of Gaussian-2 and density functional theories for the computation of enthalpies of formation. *J. Chem. Phys.* **1997**, *106*, 1063. [CrossRef]
79. Frisch, M.J.; Trucks, G.W.; Schlegel, H.B.; Scuseria, G.E.; Robb, M.A.; Cheeseman, J.R.; Scalmani, G.; Barone, V.; Petersson, G.A.; Nakatsuji, H.; et al. *Gaussian 09, Revision D.01*; Gaussian, Inc.: Wallingford, CT, USA, 2016.
80. Werner, H.-J.; Knowles, P.J.; Knizia, G.; Manby, F.R.; Schutz, M.; Celani, P.; Korona, T.; Lindh, R.; Mitrushenkov, A.; Rauhut, G.; et al. MOLPRO, Version 2010.1. *Users Man. Version*. 2010. Available online: https://www.molpro.net/pipermail/molpro-user/2010-September/003868.html (accessed on 1 November 2022).
81. Karton, A.; Martin, J.M.L. Explicitly correlated Wn theory: W1-F12 and W2-F12. *J. Chem. Phys.* **2012**, *136*, 124114. [CrossRef]
82. Kesharwani, M.K.; Brauer, B.; Martin, J.M.L. Frequency and Zero-Point Vibrational Energy Scale Factors for Double-Hybrid Density Functionals (and Other Selected Methods): Can Anharmonic Force Fields Be Avoided? *J. Phys. Chem. A* **2015**, *119*, 1701–1714. [CrossRef]
83. Karton, A.; Schreiner, P.R.; Martin, J.M.L. Heats of formation of platonic hydrocarbon cages by means of high-level thermochemical procedures. *J. Comput. Chem.* **2016**, *37*, 49–58. [CrossRef]
84. Kiselev, V.G.; Goldsmith, C.F. Accurate Prediction of Bond Dissociation Energies and Barrier Heights for High-Energy Caged Nitro and Nitroamino Compounds Using a Coupled Cluster Theory. *J. Phys. Chem. A* **2019**, *123*, 4883–4890. [CrossRef] [PubMed]
85. Kiselev, V.G.; Goldsmith, C.F. Accurate Thermochemistry of Novel Energetic Fused Tricyclic 1,2,3,4-Tetrazine Nitro Derivatives from Local Coupled Cluster Methods. *J. Phys. Chem. A* **2019**, *123*, 9818–9827. [CrossRef] [PubMed]
86. Gorn, M.V.; Gritsan, N.P.; Goldsmith, C.F.; Kiselev, V.G. Thermal Stability of Bis-Tetrazole and Bis-Triazole Derivatives with Long Catenated Nitrogen Chains: Quantitative Insights from High-Level Quantum Chemical Calculations. *J. Phys. Chem. A* **2020**, *124*, 7665–7677. [CrossRef] [PubMed]

87. Muravyev, N.V.; Monogarov, K.A.; Melnikov, I.N.; Pivkina, A.N.; Kiselev, V.G. Learning to Fly: Thermochemistry of Energetic Materials by Modified Thermogravimetric Analysis and Highly Accurate Quantum Chemical Calculations. *Phys. Chem. Chem. Phys.* **2021**, *23*, 15522–15542. [CrossRef] [PubMed]
88. Lee, T.J.; Taylor, P.R. A diagnostic for determining the quality of single-reference electron correlation methods. *Int. J. Quantum Chem.* **1989**, *36*, 199–207. [CrossRef]
89. Chase, M.W., Jr. *NIST-JANAF Thermochemical Tables*; American Chemical Society: Washington, DC, USA, 1998; Volume 9.

molecules

MDPI

Article

First Synthesis of 3-Glycopyranosyl-1,2,4-Triazines and Some Cycloadditions Thereof

Éva Bokor *, Attila Ferenczi, Mahir Hashimov, Éva Juhász-Tóth, Zsófia Götz, Alshimaa Ibrahim Zaki and László Somsák *

Department of Organic Chemistry, University of Debrecen, P.O. Box 400, H-4002 Debrecen, Hungary
* Correspondence: bokor.eva@science.unideb.hu (É.B.); somsak.laszlo@science.unideb.hu (L.S.); Tel.: +36-525-129-00 (ext. 22474) (É.B.); +36-525-129-00 (ext. 22348) (L.S.)

Abstract: *C*-glycopyranosyl derivatives of six-membered heterocycles are scarcely represented in the chemical literature and the title 3-glycopyranosyl-1,2,4-triazines are completely unknown. In this paper, the first synthesis of this compound class is accomplished by the cyclocondensation of *C*-glycosyl formamidrazones and 1,2-dicarbonyl derivatives. In addition, the synthesis of *C*-glycopyranosyl 1,2,4-triazin-5(4*H*)-ones was also carried out by the transformation of the above formamidrazones with α-keto-carboxylic esters. Inverse electron demand Diels–Alder reactions of 3-glycopyranosyl-1,2,4-triazines with a bicyclononyne derivative yielded the corresponding annulated 2-glycopyranosyl pyridines.

Keywords: *C*-glycosyl compound; 1,2,4-triazine; amidrazone; IEDDA; pyridine

Citation: Bokor, É.; Ferenczi, A.; Hashimov, M.; Juhász-Tóth, É.; Götz, Z.; Zaki, A.I.; Somsák, L. First Synthesis of 3-Glycopyranosyl-1,2,4-Triazines and Some Cycloadditions Thereof. *Molecules* **2022**, *27*, 7801. https://doi.org/10.3390/molecules27227801

Academic Editors: Alexey M. Starosotnikov, Maxim A. Bastrakov and Igor L. Dalinger

Received: 28 October 2022
Accepted: 9 November 2022
Published: 12 November 2022

1. Introduction

Triazines in general and 1,2,4-triazines in particular are a significant class of six-membered heterocyclic compounds that are constituents of many bioactive molecules, among them marketed drugs [1–3].

C-glycosyl compounds are one of the most intensively explored types of glycomimetics, compounds that resemble natural glycans in their chemical structure or/and biological activity [4]. While *C*-glycosyl derivatives of five-membered heterocycles are widely known and also studied for their biological effects, those of six-membered heterocycles are barely represented in the literature [5]. Recognising this deficiency, we have started a program to synthesise mostly unknown *C*-glycosylated six-membered heterocycles. Thus far, we have published the syntheses of 2-glycopyranosyl pyrimidines [6–8] and 3-glycopyranosyl 1,2,4,5-tetrazines [9].

C-glycosyl 1,2,4-triazines are represented in the literature, to the best of our knowledge, by five compounds altogether: an *O*-perbenzoylated 6-(β-D-arabinofuranosyl)-3-amino-1,2,4-triazine, obtained from the corresponding *C*-glycosyl formaldehyde in a multistep one-pot transformation [10]; *O*-perbenzylated 5-(α- and β-D-ribofuranosyl)-3,6-bis(trifluoromethyl)-1,2,4-triazines [11] and their 2-deoxy-ribofuranosyl counterparts [12], prepared by cycloadditions of the corresponding *C*-glycosyl formimidates and 3,6-bis (trifluoromethyl)-1,2,4,5-tetrazine.

In this work, the synthesis of 3-glycopyranosyl-1,2,4-triazines is reported, which compound class is completely unknown in the chemical literature. In addition, some transformations of these triazines in inverse electron demand Diels–Alder (IEDDA) reactions are also described.

2. Results and Discussion

For the construction of 3-substituted 1,2,4-triazines, the cyclocondensation of carboxamidrazones with 1,2-dicarbonyl derivatives is one of the most common methods [1,13,14].

Thus, for the synthesis of 3-(β-D-glucopyranosyl)-1,2,4-triazines, such transformations were envisaged starting from *O*-perbenzoylated *C*-β-D-glucopyranosyl formamidrazone **1** [15], prepared earlier in our laboratory to get *C*-glucosyl 1,2,4-triazoles [15] and -triazolones [16]. The ring-closures of **1** with α-keto aldehydes in dry EtOH under heating (Table 1, *i*) provided a set of 5-alkyl- and -aryl-substituted 1,2,4-triazines **2b-f** (Entries 2–4,7,8) in high yields. The cyclisations of **1** with glyoxal and benzil were also carried out, resulting in unsubstituted and 5,6-diphenyl-1,2,4-triazines **2a** and **2g**, respectively, in good yields (Entries 1 and 9).

Table 1. Synthesis of 3-(β-D-glucopyranosyl)-1,2,4-triazines.

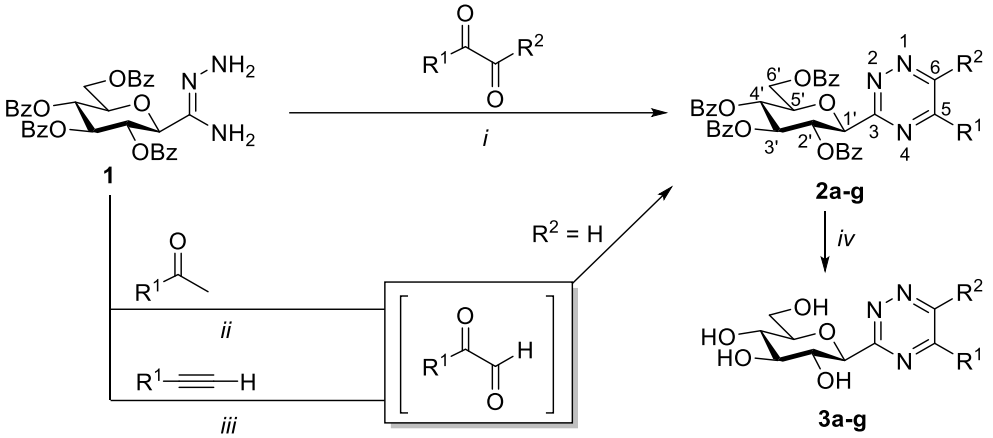

(*i*) dry EtOH, reflux; (*ii*) SeO_2, DMSO, 110 °C; (*iii*) NIS, cat. TsOH, DMSO, 110 °C; (*iv*) NaOMe/MeOH, r.t.

				Conditions and Yields (%)			
Entry		**R^1**	**R^2**		**2**		**3**
1	**a**	H	H	*i*	90	*iv*	63
2	**b**	CH_3	H	*i*	84	*iv*	58
3	**c**	$(CH_3)_3$	H	*i*	83	*iv*	88
4				*i*	83		
5	**d**	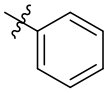	H	*ii*	50	*iv*	72
6				*iii*	60		
7	**e**	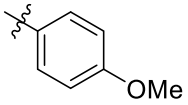	H	*i*	97	*iv*	73
8	**f**	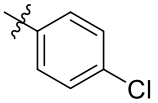	H	*i*	90	*iv*	72
9	**g**	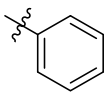	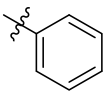	*i*	53	*iv*	84

To test the potential applicability of other starting reagents, the use of methyl ketones or alkynes for the in situ generation of 1,2-dioxo compounds under oxidative conditions [17] was also tried. Thus, one-pot reactions involving the oxidation of acetophenone or phenylacetylene to phenylglyoxal by SeO_2 or NIS, followed by ring-closure with amidrazone **1**, were carried out (Table 1, *ii* and *iii*) to result in the expected 5-phenyl-1,2,4-triazine **2d** in good yields (Table 1, Entries 5 and 6). A comparison of the yields obtained in the direct (*i*) and one-pot reactions (*ii* and *iii*) showed, however, the superior effectiveness of the former procedure (Entry 4 vs. Entries 5 and 6).

In addition, *O*-debenzoylation of the newly synthesised 3-glycosyl 1,2,4-triazines was also performed under Zemplén conditions to give the unprotected derivatives **3a-g** in good yields (Table 1).

In order to extend the scope of the 3-glycopyranosyl-1,2,4-triazines, the synthesis of peracylated glucosamine derivatives was also investigated. *C*-(2-deoxy-2-phthalimido-3,4,6-tri-*O*-acetyl-β-D-glucopyranosyl)formamidrazone (**5**) was prepared first as a precursor by the reaction of the corresponding iminoester **4** [18] with hydrazine hydrate (Table 2). Heating of **5** with 1,2-dicarbonyl derivatives in EtOH furnished the expected heterocycles **6a–e** in moderate to good yields (Table 2).

Table 2. Synthesis of 3-(2′-deoxy-2′-phthalimido-3′,4′,6′-tri-*O*-acetyl-β-D-glucopyranosyl)-1,2,4-triazines.

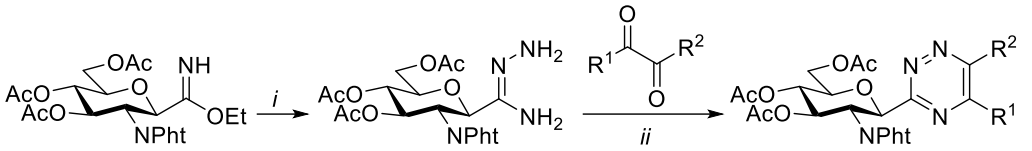

(*i*) $NH_2NH_2 \cdot H_2O$, EtOH, r.t.; (*ii*) dry EtOH, reflux

	R^1	R^2	Yield of 6 (%)
a	H	H	58
b	CH_3	H	62
c	$(CH_3)_3$	H	67
d	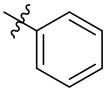	H	73
e	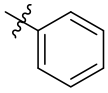	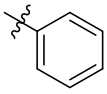	65

The regioselectivity in the formation of **2b–f** and **6b–d** is based on the reactivity pattern of the functional groups involved in the two-step cyclocondensation process. Thus, the condensation between the aldehyde group of higher electrophilicity in the corresponding 1,2-dioxo compound and the hydrazine part of higher nucleophilicity in the amidrazone, as the first step, can be followed by an intramolecular cyclisation of the resulting hydrazone, involving the remaining keto group and the amide-type NH_2, which leads to 3,5-disubstituted 1,2,4-triazines [13,14].

The position of the R^1 substituent in **2b–f** and **6b–d** was also corroborated by ^1H NMR. According to the literature data, the H-6 resonance of 5-substituted 1,2,4-triazines appears in the range of 9.0–10.0 ppm (Figure 1, **A**), while the corresponding H-5 signal for the isomeric 6-substituted derivatives is found below 9.0 ppm (**B**) [14]. This characteristic singlet for **2b–f** and **6b–d** appeared above 9.0 ppm in each case, providing evidence for the formation of the 5-substituted regioisomers.

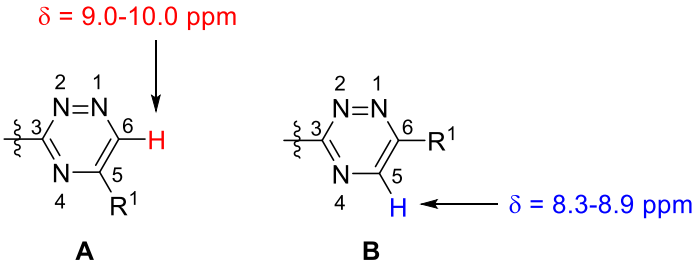

Figure 1. Differentiation of 3,5- and 3,6-disubstituted 1,2,4-triazine isomers by the chemical shift ranges of the H-6/H-5 signals.

C-glycopyranosyl formamidrazones **1** and **5** were also used for the preparation of *C*-glycosyl 1,2,4-triazin-5(4*H*)-ones (Table 3). In the reaction of **1** with ethyl glyoxalate or methyl pyruvate in boiling EtOH, a simple condensation took place, providing the corresponding N^1-alkoxycarbonylalkylidene amidrazones **7a,b** in moderate yields. Carrying out the reaction in boiling toluene triggered the desired intramolecular cyclisation of intermediates **7a,b**, accompanied, however, by a 1,2-elimination of benzoic acid from the sugar moiety, yielding glycal derivatives **8a,b**. Similar concomitant elimination was described earlier in the synthesis of a 3-glycosyl-1*H*-1,2,4-triazol-5(4*H*)-one constructed by the thermal ring-closure of N^1-ethoxycarbonyl-*C*-(2,3,4,6-tetra-*O*-benzoyl-β-D-glucopyranosyl)formamidrazone [16]. Other analogous eliminations were reported during the syntheses of *C*-glycopyranosyl heterocycles (e.g., 1,2,4-oxadiazoles and -thiadiazoles, benzimidazoles, perimidines) from the corresponding *O*-peracylated precursors [5].

Table 3. Synthesis of 3-glycopyranosyl-1,2,4-triazin-5(4*H*)-ones.

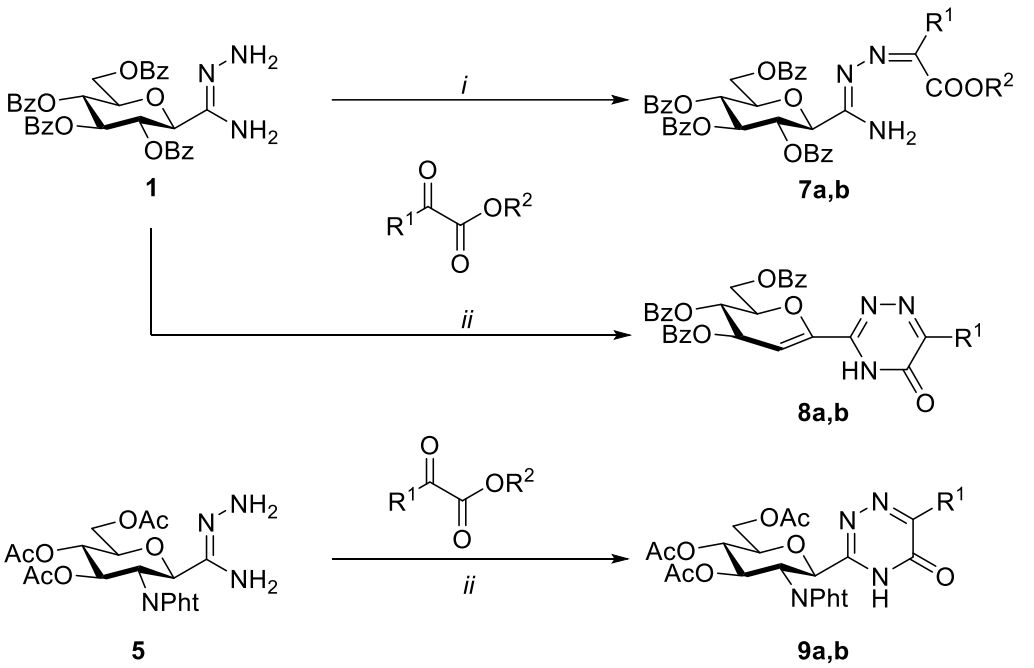

(*i*) dry EtOH, reflux; (*ii*) dry toluene, reflux

Product	R^1	R^2	Yield (%)
7a	H	CH_2CH_3	39
7b	CH_3	CH_3	59
8a	H	-	57
8b	CH_3	-	75
9a	H	-	51
9b	CH_3	-	50

The cyclisations of amidrazone **5** with the same α-keto esters in boiling toluene were also carried out, producing the expected *C*-glucosaminyl heterocycles **9a,b** in acceptable yields (Table 3).

To demonstrate the synthetic utility of the prepared *C*-glycosyl 1,2,4-triazines, some IEDDA reactions with ((1*R*,8*S*,9*r*)-bicyclo[6.1.0]non-4-yn-9-yl)methanol (**10**, BCN) [19] were performed (Table 4). The [4+2] cycloadditions carried out with triazines **2a,b,d** and **3d** were accomplished in CH_2Cl_2 or MeOH at room temperature, producing diastereomeric mixtures of the expected annulated pyridine derivatives **11a,b,d** and **12d** in high yields, respectively.

Table 4. IEDDA reactions of some 3-glucopyranosyl-1,2,4-triazines with a bicyclononyne derivative.

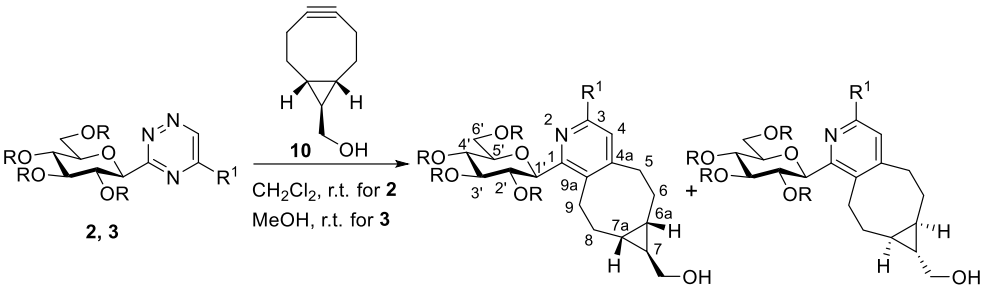

Triazine	R	R^1	Reaction Time	Product	Yield (%)	Diastereomeric Ratio
2a	Bz	H	2 d	**11a**	97	5:4
2b	Bz	CH_3	6 d	**11b**	41	5:4
2d	Bz	Ph	6 d	**11d**	73	5:4
3d	H	Ph	5 d	**12d**	94	1:1

To get further 2-glucopyranosyl pyridines, the transformations of 1,2,4-triazine **2a** with norbornadiene and 1-pyrrolidino-1-cyclopentene were also attempted. The desired heterocycles could not be obtained even at elevated temperatures (e.g., in boiling *m*-xylene) as no significant conversion of the starting material could be observed, while a slow decomposition of the starting material began after a prolonged reaction time (1 day). This may be due to the lack of an electron-withdrawing substituent on the triazine ring, which could activate this heterocycle towards IEDDA reactions.

3. Experimental

3.1. General Methods

Melting points were measured on a Kofler hot stage, and the values are uncorrected. Optical rotations were obtained at ambient temperature using a P-2000 polarimeter (Jasco, Easton, MD, USA). The ^{1}H and ^{13}C NMR spectra of the prepared compounds were recorded with DRX360 (360/90 MHz for ^{1}H/^{13}C) or DRX400 (400/100 MHz for ^{1}H/^{13}C) spectrometers (Bruker, Karlsruhe, Germany). Chemical shifts are referenced to Me_4Si (^{1}H-NMR) or to the residual solvent signals (^{13}C-NMR). For HRMS measurements, a Bruker maXis II (ESI-HRMS) spectrometer was used, and the data were determined in positive ionisation mode. DC Kieselgel 60 F_{254} plates (Sigma-Aldrich, Saint Louis, MO, USA) were used for TLC analysis, and the spots on the plates were visualised under UV light and developed by gentle heating. Column chromatographic purification was performed by using Kieselgel 60 silica gel (Molar Chemicals, Halásztelek, Hungary, particle size 0.063–0.2 mm). Anhydrous EtOH was purchased from VWR Chemicals. Anhydrous $CHCl_3$, toluene and MeOH were obtained by atmospheric distillation from P_4O_{10} ($CHCl_3$ and toluene) or over Mg turnings and iodine (MeOH). *C*-(2,3,4,6-Tetra-*O*-benzoyl-β-D-glucopyranosyl)formamidrazone **1** [15] and ethyl *C*-(2-deoxy-2-phthalimido-3,4,6-tri-*O*-acetyl-β-D-glucopyranosyl)formimidate **4** [18] were synthesised according to our earlier reported methods. ((1*R*,8*S*,9*r*)-Bicyclo [6.1.0]non-4-yn-9-yl)methanol **10** [19] was obtained following a literature procedure.

3.2. General Procedure 1 for the Synthesis of O-Peracylated 3-Glycopyranosyl-1,2,4-triazines **2** *and* **6**

C-glycopyranosyl formamidrazone (**1** or **5**) and the appropriate 1,2-dicarbonyl derivative (1.0–1.2 equiv.) were suspended in anhydrous EtOH (3 mL/100 mg substrate), and the mixture was stirred at reflux temperature until the TLC (1:1 EtOAc-hexane) showed completion of the reaction. The solvent was then evaporated under reduced pressure, and the residue was purified by column chromatography.

3.3. General Procedure 2 for the O-Debenzoylation of Compounds **2** *by the Zemplén Method to obtain 1,2,4-Triazines* ***3***

To a solution of the corresponding *O*-perbenzoylated 3-(β-D-glucopyranosyl)-1,2,4-triazine (**2**) in dry MeOH (5 mL/100 mg substrate), a catalytic amount of NaOMe in dry MeOH (~1M solution) was added. The reaction mixture was allowed to stand at room temperature, and the transformation was judged by TLC (1:1 EtOAc-hexane and 7:3 $CHCl_3$-MeOH). After complete conversion, the reaction mixture was neutralised with a cation exchange resin Amberlyst 15 (H^+ form). The resin was then filtered off, and MeOH was removed under reduced pressure. The resulting crude product was purified by column chromatography.

3.4. General Procedure 3 for the Synthesis of O-Peracylated 3-Glycopyranosyl-1,2,4-triazin-5(4H)-ones ***8*** *and* ***9***

A solution of the *C*-glycopyranosyl formamidrazone (**1** or **5**) and the corresponding α-ketoester (1 equiv.) in anhydrous toluene (3 mL/100 mg substrate) was refluxed, and the transformation was monitored by TLC (2:1 EtOAc-hexane). After completion of the reaction, the solvent was removed in vacuo, and the residue was purified by column chromatography.

3.5. General Procedure 4 for the Preparation of 1-(β-D-Glucopyranosyl)-6,6a,7,7a,8,9-Hexahydro-5H-Cyclopropa[5,6]Cycloocta[1,2-c]Pyridin-7-yl)Methanols ***11*** *and* ***12***

To a solution of the corresponding 3-glucopyranosyl-1,2,4-triazine (**2** or **3**) in CH_2Cl_2 or MeOH (3 mL/100 mg triazine), ((1*R*,8*S*,9*r*)-bicyclo[6.1.0]non-4-yn-9-yl)methanol (**10**, 2 equiv.) was added, and the mixture was stirred at room temperature. When the TLC (1:1 EtOAc-hexane for **11** or 4:1 $CHCl_3$-MeOH for **12**) showed complete disappearance of the triazine, the solvent was removed in vacuo. The residue was purified by column chromatography.

3.6. Synthesis and Characterisation of the New Compounds

3-(2,3,4,6-Tetra-O-benzoyl-β-D-glucopyranosyl)-1,2,4-triazine (**2a**)

Prepared from amidrazone **1** (0.80 g, 1.25 mmol) and an aq. 40 wt.% solution of glyoxal (144 μL, 1.25 mmol) according to general procedure 1. Reaction time: 3 h. Purified by column chromatography (1:2 EtOAc-hexane) to yield 0.75 g (90%) of pale yellow amorphous solids. R_f = 0.48 (1:1 EtOAc-hexane); $[\alpha]_D = -40$ (c 0.20, $CHCl_3$). ^{1}H NMR (360 MHz, $CDCl_3$) δ (ppm): 9.17, 8.70 (2 × 1H, 2 d, *J* = 2.1 Hz in each, H-5, H-6), 8.00, 7.95, 7.85, 7.75 (4 × 2H, 4 d, *J* = 7.92 Hz in each, Ar), 7.53-7.26 (12H, m, Ar), 6.18 (1H, pt, *J* = 9.5, 9.5 Hz, H-2′ or H-3′ or H-4′), 6.08 (1H, pt, *J* = 9.7, 9.6 Hz, H-2′ or H-3′ or H-4′), 5.90 (1H, pt, *J* = 9.5, 9.1 Hz, H-2′ or H-3′ or H-4′), 5.39 (1H, d, *J* = 9.7 Hz, H-1′), 4.69 (1H, dd, *J* = 12.1, < 1 Hz, H-6′a), 4.58 (1H, dd, *J* = 12.1, 5.3 Hz, H-6′b), 4.48-4.44 (1H, m, H-5′); ^{13}C NMR (90 MHz, $CDCl_3$) δ (ppm): 166.1, 165.8, 165.2, 164.8, 164.3 (4 × C=O, C-3), 149.5, 149.4 (C-5, C-6), 133.4, 133.3, 133.2, 133.0, 129.8-129.6, 129.4, 128.7, 128.6, 128.5, 128.4-128.2 (Ar), 80.1, 76.9, 74.1, 71.6, 69.5 (C-1′ − C-5′), 63.4 (C-6′). ESI-HRMS positive mode (m/z): calcd for $C_{37}H_{30}N_3O_9^+$ $[M+H]^+$ 660.1977; $C_{37}H_{29}N_3NaO_9^+$ $[M+Na]^+$ 682.1796. Found: $[M+H]^+$ 660.1972; $[M+Na]^+$ 682.1785.

3-(2,3,4,6-Tetra-O-benzoyl-β-D-glucopyranosyl)-5-methyl-1,2,4-triazine (**2b**)

Prepared from amidrazone **1** (0.10 g, 0.16 mmol) and methyl glyoxal (24 μL, 0.16 mmol) according to general procedure 1. Reaction time: 3 h. Purified by column chromatography (2:3 EtOAc-hexane) to yield 89 mg (84%) of pale yellow amorphous solids. R_f = 0.38 (1:1 EtOAc-hexane); $[\alpha]_D = -12$ (c 0.20, $CHCl_3$). ^{1}H NMR (360 MHz, $CDCl_3$) δ (ppm): 9.03 (1H, s, H-6), 8.01, 7.94, 7.85, 7.75 (4 × 2H, 4 dd, *J* = 7.2, 1.2 Hz in each, Ar), 7.54-7.28 (12H, m, Ar), 6.14 (1H, pt, *J* = 9.5, 9.1 Hz, H-2′ or H-3′ or H-4′), 6.11 (1H, pt, *J* = 9.7, 9.5 Hz, H-2′ or H-3′ or H-4′), 5.90 (1H, pt, *J* = 9.6, 9.6 Hz, H-2′ or H-3′ or H-4′), 5.31 (1H, d, *J* = 9.3 Hz, H-1′), 4.67 (1H, dd, *J* = 12.3, 3.0 Hz, H-6′a), 4.56 (1H, dd, *J* = 12.3, 5.2 Hz, H-6′b), 4.42 (1H, ddd, *J* = 9.7, 5.2, 3.0 Hz, H-5′), 2.56 (3H, s, CH_3); ^{13}C NMR (90 MHz, $CDCl_3$) δ (ppm): 166.1, 165.8, 165.2, 164.7, 163.2 (4 × C=O, C-3), 160.6 (C-5), 149.9 (C-6), 133.4, 133.2, 133.1, 133.0, 129.8-129.7,

129.5, 128.8, 128.7, 128.6, 128.4-128.2 (Ar), 80.1, 76.9, 74.3, 71.4, 69.5 (C-1′ − C-5′), 63.4 (C-6′), 21.8 (CH_3). ESI-HRMS positive mode (m/z): calcd for $C_{38}H_{32}N_3O_9^+$ $[M+H]^+$ 674.2133; $C_{38}H_{31}N_3NaO_9^+$ $[M+Na]^+$ 696.1953. Found: $[M+H]^+$ 674.2134; $[M+Na]^+$ 696.1950.

*3-(2,3,4,6-Tetra-O-benzoyl-β-*D*-glucopyranosyl)-5-tert-butyl-1,2,4-triazine* (**2c**)

Prepared from amidrazone **1** (0.30 g, 0.47 mmol) and 3,3-dimethyl-2-oxobutanal (62 mg, 0.47 mmol) according to general procedure 1. Reaction time: 7 h. Purified by column chromatography (3:7 EtOAc-hexane) to yield 0.28 g (83%) of pale yellow amorphous solids. R_f = 0.26 (3:7 EtOAc-hexane); $[\alpha]_D$ = −11 (c 0.20, $CHCl_3$). ^{1}H NMR (360 MHz, $CDCl_3$) δ (ppm): 9.23 (1H, s, H-6), 8.02, 7.95, 7.86, 7.73 (4 × 2H, 4 dd, *J* = 7.1, 1.2 Hz in each, Ar), 7.54-7.24 (12H, m, Ar), 6.25 (1H, pt, *J* = 9.7, 9.7 Hz, H-2′ or H-3′ or H-4′), 6.13 (1H, pt, *J* = 9.6, 9.5 Hz, H-2′ or H-3′ or H-4′), 5.90 (1H, pt, *J* = 9.7, 9.6 Hz, H-2′ or H-3′ or H-4′), 5.35 (1H, d, *J* = 9.7 Hz, H-1′), 4.69 (1H, dd, *J* = 12.2, 2.9 Hz, H-6′a), 4.53 (1H, dd, *J* = 12.2, 5.0 Hz, H-6′b), 4.44 (1H, ddd, *J* = 9.7, 5.0, 2.9 Hz, H-5′), 1.31 (9H, s, $C(CH_3)_3$); ^{13}C NMR (90 MHz, $CDCl_3$) δ (ppm): 170.0, 166.1, 165.9, 165.2, 164.5 (4 × C=O, C-3), 162.5 (C-5), 146.8 (C-6), 133.4, 133.1, 133.1, 133.0, 130.0-129.5, 129.5, 128.9, 128.8, 128.4-128.2 (Ar), 80.1, 76.9, 74.4, 71.0, 69.5 (C-1′ − C-5′), 63.2 (C-6′), 36.8 ($C(CH_3)_3$), 28.6 ($C(CH_3)_3$). ESI-HRMS positive mode (m/z): calcd for $C_{41}H_{38}N_3O_9^+$ $[M+H]^+$ 716.2603; $C_{41}H_{37}N_3NaO_9^+$ $[M+Na]^+$ 738.2422. Found: $[M+H]^+$ 716.2602; $[M+Na]^+$ 738.2419.

*3-(2,3,4,6-Tetra-O-benzoyl-β-*D*-glucopyranosyl)-5-phenyl-1,2,4-triazine* (**2d**).

Method A: Prepared from amidrazone **1** (1.0 g, 1.57 mmol) and phenyl glyoxal monohydrate (0.29 g, 1.88 mmol) according to general procedure 1. Reaction time: 4 h. Purified by column chromatography (1:2 EtOAc-hexane) to yield 0.95 g (83%) of pale yellow amorphous solids.

Method B: To a solution of acetophenone (19 µL, 0.16 mmol, 1 equiv.) in DMSO (2 mL), SeO_2 (21 mg, 0.19 mmol, 1.2 equiv.) was added. The mixture was heated at 110 °C until the TLC (1:9 EtOAc-hexane) showed the complete transformation of acetophenone (4 h). Formamidrazine **1** (0.10 g, 0.16 mmol) was then added to the mixture, and the heating was continued. When the TLC (1:1 EtOAc-hexane) showed the completion of the reaction (2 h), the mixture was diluted with EtOAc (50 mL) and extracted with water (20 mL). The separated aqueous phase was washed two times with EtOAc (2 × 50 mL). The combined organic phase was dried over $MgSO_4$, filtered and the solvent was removed under reduced pressure. The residue was purified by column chromatography (1:2 EtOAc-hexane). Yield: 57 mg (50%).

Method C: A solution of phenylacetylene (35 µL, 0.32 mmol, 2 equiv.), NIS (43 mg, 0.19 mmol, 1.2 equiv.) and TsOH (3.4 mg, 0.02 mmol, 0.1 equiv.) in DMSO (2 mL) was heated at 110 °C until the TLC (1:9 EtOAc-hexane) indicated the complete conversion of phenylacetylene (4 h). Formamidrazine **1** (0.10 g, 0.16 mmol) was then added to the mixture, and the heating was continued. After completion of the reaction monitored by TLC (2 h), the same steps as described in method **B** were carried out. Yield: 66 mg (60%). R_f = 0.55 (1:1 EtOAc-hexane); $[\alpha]_D$ = −68 (c 0.20, $CHCl_3$). ^{1}H NMR (360 MHz, $CDCl_3$) δ (ppm): 9.58 (1H, s, H-6), 8.17, 8.02, 7.96, 7.87, 7.75 (5 × 2H, 5 d, *J* = 7.2 Hz in each, Ar), 7.59-7.21 (15H, m, Ar), 6.33, 6.18, 5.94 (3 × 1H, 3 pt, *J* = 9.7, 9.7 Hz in each, H-2′, H-3′, H-4′), 5.43 (1H, d, *J* = 9.7 Hz, H-1′), 4.72 (1H, dd, *J* = 12.2, 2.8 Hz, H-6′a), 4.55 (1H, dd, *J* = 12.2, 5.1 Hz, H-6′b), 4.49 (1H, ddd, *J* = 9.7, 5.1, 2.8 Hz, H-5′); ^{13}C NMR (90 MHz, $CDCl_3$) δ (ppm): 166.1, 165.8, 165.2, 164.7, 163.4 (4 × C=O, C-3), 156.0 (C-5), 145.9 (C-6), 133.4, 133.1, 133.0, 132.8, 132.7, 129.8–129.3, 128.8, 128.7, 128.6, 128.5, 128.4–127.9 (Ar), 80.1, 76.9, 74.4, 71.1, 69.5 (C-1′ − C-5′), 63.2 (C-6′). ESI-HRMS positive mode (m/z): calcd for $C_{43}H_{33}N_3NaO_9^+$ $[M+Na]^+$ 758.2109. Found: 758.2107.

*3-(2,3,4,6-Tetra-O-benzoyl-β-*D*-glucopyranosyl)-5-(p-methoxyphenyl)-1,2,4-triazine* (**2e**)

Prepared from amidrazone **1** (0.10 g, 0.16 mmol) and *p*-methoxyphenyl glyoxal monohydrate (0.034 g, 0.19 mmol) according to general procedure 1. Reaction time: 4 h. Purification by column chromatography (1:2 EtOAc-hexane), followed by the crystallisation of the resulting syrup from a mixture of Et_2O (3 mL) and hexane (2 mL), which gave 116 mg (97%) pale yellow crystals. R_f = 0.45 (1:1 EtOAc-hexane); mp = 150–151 °C; $[\alpha]_D$ = −98 (c 0.53,

$CHCl_3$). ^{1}H NMR (400 MHz, $CDCl_3$) δ (ppm): 9.50 (1H, s, H-6), 8.17 (2H, d, *J* = 8.9 Hz, Ar), 8.02, 7.96, 7.87, 7.74 (4 × 2H, 4 dd, *J* = 7.3, 1.2 Hz in each, Ar), 7.54–7.23 (12H, m, Ar), 7.01 (2H, d, *J* = 8.9 Hz, Ar), 6.33, 6.15, 5.92 (3 × 1H, 3 pt, *J* = 9.7, 9.7 Hz in each, H-2′, H-3′, H-4′), 5.37 (1H, d, *J* = 9.7 Hz, H-1′), 4.70 (1H, dd, *J* = 12.3, 2.7 Hz, H-6′a), 4.54 (1H, dd, *J* = 12.3, 5.1 Hz, H-6′b), 4.46 (1H, ddd, *J* = 9.7, 5.1, 2.7 Hz, H-5′), 3.89 (3H, s, OCH_3); ^{13}C NMR (90 MHz, $CDCl_3$) δ (ppm): 166.1, 165.9, 165.2, 164.8, 163.6, 163.1 (4 × C=O, C-3, Ar-C_q), 155.5 (C-5), 145.3 (C-6), 133.4, 133.1, 133.0, 129.8–129.6, 128.9, 128.8, 128.8, 128.4–128.2 (Ar), 125.0 (Ar-C_q), 114.8 (Ar-CH), 80.1, 76.9, 74.5, 70.9, 69.5 (C-1′ − C-5′), 63.3 (C-6′), 55.5 (OCH_3). ESI-HRMS positive mode (m/z): calcd for $C_{44}H_{36}N_3O_{10}^+$ $[M+H]^+$ 766.2395; $C_{44}H_{35}N_3NaO_{10}^+$ $[M+Na]^+$ 788.2215. Found: $[M+H]^+$ 766.2390; $[M+Na]^+$ 788.2208.

*3-(2,3,4,6-Tetra-O-benzoyl-β-*D*-glucopyranosyl)-5-(p-chlorophenyl)-1,2,4-triazine* (**2f**)

Prepared from amidrazone **1** (0.10 g, 0.16 mmol) and *p*-chlorophenyl glyoxal monohydrate (0.035 g, 0.19 mmol) according to general procedure 1. Reaction time: 4 h. Purification by column chromatography (1:2 EtOAc-hexane) gave 109 mg (90%) of pale yellow amorphous solids. R_f = 0.60 (1:1 EtOAc-hexane); $[\alpha]_D$ = −82 (c 0.50, $CHCl_3$). ^{1}H NMR (400 MHz, $CDCl_3$) δ (ppm): 9.57 (1H, s, H-6), 8.13 (2H, d, *J* = 8.4 Hz, Ar), 8.02, 7.96, 7.86, 7.74 (4 × 2H, 4 d, *J* = 7.5 Hz in each, Ar), 7.56-7.24 (14H, m, Ar), 6.28, 6.16, 5.92 (3 × 1H, 3 pt, *J* = 9.6, 9.6 Hz in each, H-2′, H-3′, H-4′), 5.39 (1H, d, *J* = 9.6 Hz, H-1′), 4.72 (1H, dd, *J* = 12.2, 2.1 Hz, H-6′a), 4.54 (1H, dd, *J* = 12.2, 4.9 Hz, H-6′b), 4.47 (1H, ddd, *J* = 9.6, 4.9, 2.1 Hz, H-5′); ^{13}C NMR (90 MHz, $CDCl_3$) δ (ppm): 166.1, 165.9, 165.2, 164.8, 163.5 (4 × C=O, C-3), 154.9 (C-5), 145.6 (C-6), 139.4 (Ar-C_q), 133.5, 133.3, 133.2, 133.1 (Ar), 131.3 (Ar-C_q), 129.9-128.3 (Ar), 80.1, 77.0, 74.4, 71.1, 69.5 (C-1′ − C-5′), 63.2 (C-6′). ESI-HRMS positive mode (m/z): calcd for $C_{43}H_{33}ClN_3O_9^+$ $[M+H]^+$ 770.1900; $C_{43}H_{32}ClN_3NaO_9^+$ $[M+Na]^+$ 792.1719. Found: $[M+H]^+$ 770.1900; $[M+Na]^+$ 792.1718.

*3-(2,3,4,6-Tetra-O-benzoyl-β-*D*-glucopyranosyl)-5,6-diphenyl-1,2,4-triazine* (**2g**)

Prepared from amidrazone **1** (1.0 g, 1.57 mmol) and benzil (0.33 g, 1.57 mmol) according to general procedure 1. Reaction time: 7 h. Purified by column chromatography (1:1 EtOAc-hexane) to yield 0.67 g (53%) of pale yellow solids. R_f = 0.71 (3:7 EtOAc-hexane); mp = 175–179 °C; $[\alpha]_D$ = −26 (c 0.20, $CHCl_3$); ^{1}H NMR (360 MHz, $CDCl_3$) δ (ppm): 8.02, 7.95, 7.87, 7.76 (4 × 2H, 4 d, *J* = 7.4 Hz in each, Ar), 7.55–7.24 (22H, m, Ar), 6.36 (1H, pt, *J* = 9.7, 9.7 Hz, H-2′ or H-3′ or H-4′), 6.15 (1H, pt, *J* = 9.6, 9.5 Hz, H-2′ or H-3′ or H-4′), 5.91 (1H, pt, *J* = 9.7, 9.7 Hz, H-2′ or H-3′ or H-4′), 5.45 (1H, d, *J* = 9.7 Hz, H-1′), 4.69 (1H, dd, *J* = 12.3, 2.6 Hz, H-6′a), 4.54 (1H, dd, *J* = 12.3, 5.1 Hz, H-6′b), 4.48 (1H, ddd, *J* = 9.5, 5.1, 2.6 Hz, H-5′); ^{13}C NMR (90 MHz, $CDCl_3$) δ (ppm): 166.1, 165.9, 165.2, 164.7 (4 × C=O), 161.2, 157.3, 156.5 (C-3, C-5, C-6), 135.0–128.2 (Ar), 79.9, 77.0, 74.6, 71.1, 69.5 (C-1′ − C-5′), 63.3 (C-6′). ESI-HRMS positive mode (m/z): calcd for $C_{49}H_{38}N_3O_9^+$ $[M+H]^+$ 812.2603. Found: 812.2602.

*3-(β-*D*-Glucopyranosyl)-1,2,4-triazine* (**3a**)

Prepared from triazine **2a** (0.25 g, 0.38 mmol) according to general procedure 2. Reaction time: 3 h. Purified by column chromatography (4:1 $CHCl_3$-MeOH) to yield 58 mg (63%) of pale yellow amorphous solids. R_f = 0.32 (7:3 $CHCl_3$-MeOH); $[\alpha]_D$ = −138 (c 0.22, DMSO). ^{1}H NMR (360 MHz, CD_3OD) δ (ppm): 9.30, 8.84 (2 × 1H, 2 d, *J* = 2.5 Hz in each, H-5, H-6), 4.61 (1H, d, *J* = 9.7 Hz, H-1′), 3.84 (1H, pt, *J* = 9.5, 9.1 Hz, H-2′ or H-3′ or H-4′), 3.83 (1H, dd, *J* = 12.1, 2.0 Hz, H-6′a), 3.68 (1H, dd, *J* = 12.1, 5.0 Hz, H-6′b), 3.56 (1H, pt, *J* = 9.1, 8.9 Hz, H-2′ or H-3′ or H-4′), 3.48-3.46 (2H, m, H-2′ or H-3′ or H-4′, H-5′); ^{13}C NMR (90 MHz, CD_3OD) δ (ppm): 167.6 (C-3), 151.7, 150.9 (C-5, C-6), 83.1, 82.8, 79.4, 74.3, 71.4 (C-1′ − C-5′), 62.8 (C-6′). ESI-HRMS positive mode (m/z): calcd for $C_9H_{14}N_3O_5^+$ $[M+H]^+$ 244.0928; $C_9H_{13}N_3NaO_5^+$ $[M+Na]^+$ 266.0747. Found: $[M+H]^+$ 244.0930; $[M+Na]^+$ 266.0746.

*3-(β-*D*-Glucopyranosyl)-5-methyl-1,2,4-triazine* (**3b**)

Prepared from triazine **2b** (0.20 g, 0.3 mmol) according to general procedure 2. Reaction time: 5 h. Purified by column chromatography (4:1 $CHCl_3$-MeOH) to yield 44 mg (58%) pale yellow syrup. R_f = 0.30 (4:1 $CHCl_3$-MeOH); $[\alpha]_D$ = +57 (c 0.20, MeOH). ^{1}H NMR (360 MHz, CD_3OD) δ (ppm): 9.26 (1H, s, H-6), 4.58 (1H, d, *J* = 9.7 Hz, H-1′), 3.88 (1H, dd, *J* = 11.9, 2.2 Hz, H-6′a), 3.87 (1H, pt, *J* = 9.4, 9.2 Hz, H-2′ or H-3′ or H-4′), 3.72 (1H, dd,

J = 11.9, 3.3 Hz, H-6′b), 3.61-3.50 (3H, m, H-2′ and/or H-3′ and/or H-4′, H-5′), 2.63 (3H, s, CH_3); ^{13}C NMR (90 MHz, CD_3OD) δ (ppm): 166.5, 163.0 (C-3, C-5), 151.2 (C-6), 83.0, 82.8, 79.4, 74.3, 71.4 (C-1′ − C-5′), 62.9 (C-6′), 21.9 (CH_3). ESI-HRMS positive mode (m/z): calcd for $C_{10}H_{15}N_3NaO_5^+$ $[M+Na]^+$ 280.0904. Found: 280.0903.

3-(β-D-Glucopyranosyl)-5-tert-butyl-1,2,4-triazine (**3c**)

Prepared from triazine **2c** (0.20 g, 0.28 mmol) according to general procedure 2. Reaction time: 5 h. Purified by column chromatography (9:1 $CHCl_3$-MeOH) to yield 73 mg (88%) of pale yellow solids. R_f = 0.46 (4:1 $CHCl_3$-MeOH); mp = 196–200 °C; $[\alpha]_D$ = +17 (c 0.20, MeOH). ^{1}H NMR (360 MHz, CD_3OD) δ (ppm): 9.46 (1H, s, H-6), 4.59 (1H, d, *J* = 9.7 Hz, H-1′), 3.98 (1H, pt, *J* = 9.4, 9.2 Hz, H-2′ or H-3′ or H-4′), 3.90 (1H, dd, *J* = 12.0, 1.5 Hz, H-6′a), 3.70 (1H, dd, *J* = 12.0, 5.0 Hz, H-6′b), 3.59 (1H, pt, *J* = 9.0, 8.9 Hz, H-2′ or H-3′ or H-4′), 3.54–3.46 (2H, m, H-2′ or H-3′ or H-4′, H-5′), 1.43 (9H, s, $C(CH_3)_3$); ^{13}C NMR (90 MHz, CD_3OD) δ (ppm): 172.0, 166.2 (C-3, C-5), 148.1 (C-6), 83.4, 82.9, 79.5, 74.2, 71.7 (C-1′ − C-5′), 63.0 (C-6′), 38.0 ($C(CH_3)_3$), 29.1 ($C(CH_3)_3$). ESI-HRMS positive mode (m/z): calcd for $C_{13}H_{22}N_3O_5^+$ $[M+H]^+$ 300.1554; $C_{13}H_{21}N_3NaO_5^+$ $[M+Na]^+$ 322.1373. Found: $[M+H]^+$ 300.1550; $[M+Na]^+$ 322.1369.

3-(β-D-Glucopyranosyl)-5-phenyl-1,2,4-triazine (**3d**)

Prepared from triazine **2d** (0.20 g, 0.27 mmol) according to general procedure 2. Reaction time: 4 h. Purified by column chromatography (9:1 $CHCl_3$-MeOH) to yield 62 mg (72%) of pale yellow solids. R_f = 0.43 (4:1 $CHCl_3$-MeOH); mp = 236–240 °C; $[\alpha]_D$ = +44 (c 0.20, DMSO). ^{1}H NMR (360 MHz, DMSO-d_6) δ (ppm): 10.06 (1H, s, H-6), 8.36 (2H, d, *J* = 8.3 Hz, Ar), 7.71–7.62 (3H, m, Ar), 5.11–5.02, 5.57–4.55 (4H, OH), 4.52 (1H, d, *J* = 9.9 Hz, H-1′), 3.98–3.92, 3.75–3.71, 3.48–3.37, 3.27–3.20 (6H, m, H-2′, H-3′, H-4′, H-5′, H-6′a,b); ^{13}C NMR (90 MHz, DMSO-d_6) δ (ppm): 165.2 (C-3), 154.8 (C-5), 146.1 (C-6), 133.0, 132.6, 129.3 (2), 127.8 (2) (Ar), 82.1, 82.0, 77.9, 72.0, 70.4 (C-1′ − C-5′), 61.2 (C-6′). ESI-HRMS positive mode (m/z): calcd for $C_{15}H_{18}N_3O_5^+$ $[M+H]^+$ 320.1241; $C_{15}H_{17}N_3NaO_5^+$ $[M+Na]^+$ 342.1060. Found: $[M+H]^+$ 320.1239; $[M+Na]^+$ 342.1054.

3-(β-D-Glucopyranosyl)-5-(p-methoxyphenyl)-1,2,4-triazine (**3e**)

Prepared from triazine **2e** (96 mg, 0.13 mmol) according to general procedure 2. Reaction time: 2 h. Purified by column chromatography (8:1 $CHCl_3$-MeOH) to yield 32 mg (73%) of pale yellow amorphous solids. R_f = 0.50 (7:3 $CHCl_3$-MeOH); $[\alpha]_D$ = +24 (c 0.49, DMSO). ^{1}H NMR (400 MHz, CD_3OD) δ (ppm): 9.75 (1H, s, H-6), 8.33, 7.12 (2 × 2H, 2 d, *J* = 8.8 Hz in each, Ar), 4.62 (1H, d, *J* = 9.7 Hz, H-1′), 4.02 (1H, pt, *J* = 9.3, 9.2 Hz, H-2′ or H-3′ or H-4′), 3.92-3.90 (4H, m, H-6′a, OCH_3), 3.74 (1H, dd, *J* = 11.5, 2.9 Hz, H-6′b), 3.62 (1H, pt, *J* = 9.0, 9.0 Hz, H-2′ or H-3′ or H-4′), 3.55-3.53 (2H, m, H-2′ or H-3′ or H-4′, H-5′); ^{13}C NMR (90 MHz, CD_3OD) δ (ppm): 166.8, 165.4 (C-3, Ar-C_q), 157.4 (C-5), 146.5 (C-6), 131.1 (2), 126.6, 116.0 (2) (Ar), 83.4, 82.9, 79.5, 74.3, 71.6 (C-1′ − C-5′), 62.9 (C-6′), 56.2 (OCH_3). ESI-HRMS positive mode (m/z): calcd for $C_{16}H_{20}N_3O_6^+$ $[M+H]^+$ 350.1347; $C_{16}H_{19}N_3NaO_6^+$ $[M+Na]^+$ 372.1166. Found: $[M+H]^+$ 350.1340; $[M+Na]^+$ 372.1159.

3-(β-D-Glucopyranosyl)-5-(p-chlorophenyl)-1,2,4-triazine (**3f**)

Prepared from triazine **2f** (79 mg, 0.10 mmol) according to general procedure 2. Reaction time: 2 h. Purified by column chromatography (8:1 $CHCl_3$-MeOH) to yield 26 mg (72%) of pale yellow amorphous solids. R_f = 0.47 (7:3 $CHCl_3$-MeOH); $[\alpha]_D$ = +30 (c 0.53, DMSO). ^{1}H NMR (400 MHz, CD_3OD) δ (ppm): 9.87 (1H, s, H-6), 8.36, 7.62 (2 × 2H, 2 d, *J* = 8.6 Hz in each, Ar), 4.67 (1H, d, *J* = 9.7 Hz, H-1′), 4.02 (1H, pt, *J* = 9.3, 9.3 Hz, H-2′ or H-3′ or H-4′), 3.90 (1H, dd, *J* = 12.3, < 1 Hz, H-6′a), 3.73 (1H, dd, *J* = 12.3, 4.9 Hz, H-6′b), 3.62 (1H, pt, *J* = 9.0, 9.0 Hz, H-2′ or H-3′ or H-4′), 3.54-3.53 (2H, m, H-2′ or H-3′ or H-4′, H-5′); ^{13}C NMR (90 MHz, CD_3OD) δ (ppm): ^{13}C NMR (90 MHz, CD_3OD) δ (ppm): 167.0 (C-3), 156.8 (C-5), 147.0 (C-6), 140.4, 133.3, 130.8 (4) (Ar), 83.4, 82.9, 79.5, 74.3, 71.6 (C-1′ − C-5′), 62.9 (C-6′). ESI-HRMS positive mode (m/z): calcd for $C_{15}H_{17}ClN_3O_5^+$ $[M+H]^+$ 354.0851; $C_{15}H_{16}ClN_3NaO_5^+$ $[M+Na]^+$ 376.0671. Found: $[M+H]^+$ 354.0851; $[M+Na]^+$ 376.0668.

3-(β-D-Glucopyranosyl)-5,6-diphenyl-1,2,4-triazine (**3g**)

Prepared from triazine **2g** (0.15 g, 0.18 mmol) according to general procedure 2. Reaction time: 4 h. Purified by column chromatography (9:1 $CHCl_3$-MeOH) to yield 61 mg

(84%) pale yellow oil. R_f = 0.32 (9:1 $CHCl_3$-MeOH); $[\alpha]_D$ = +42 (c 0.44, MeOH). ^{1}H NMR (360 MHz, CD_3OD) δ (ppm): 7.60-7.34 (10H, m, Ar), 4.75 (1H, d, *J* = 9.7 Hz, H-1′), 4.05 (1H, pt, *J* = 9.5, 9.1 Hz, H-2′ or H-3′ or H-4′), 3.92 (1H, dd, *J* = 12.3, < 1 Hz, H-6′a), 3.75 (1H, dd, *J* = 12.3, 4.5 Hz, H-6′b), 3.65 (1H, pt, *J* = 9.1, 9.0 Hz, H-2′ or H-3′ or H-4′), 3.57-3.55 (2H, m, H-2′ or H-3′ or H-4′, H-5′); ^{13}C NMR (90 MHz, CD_3OD) δ (ppm): ^{13}C NMR (90 MHz, CD_3OD) δ (ppm): 165.0 (C-3), 158.8, 158.7 (C-5, C-6), 136.8, 136.7, 132.0, 131.2 (2), 131.0, 130.7 (2), 129.8 (2), 129.6 (2) (Ar), 83.0, 82.9, 79.5, 74.3, 71.5 (C-1′ − C-5′), 62.9 (C-6′). ESI-HRMS positive mode (m/z): calcd for $C_{21}H_{22}N_3O_5^+$ $[M+H]^+$ 396.1554; $C_{21}H_{21}N_3NaO_5^+$ $[M+Na]^+$ 418.1373. Found: $[M+H]^+$ 396.1555; $[M+Na]^+$ 418.1371.

*C-(2-Deoxy-2-phthalimido-3,4,6-tri-O-acetyl-β-*D*-glucopyranosyl)formamidrazone* (**5**)

Ethyl *C*-(2-deoxy-2-phthalimido-3,4,6-tri-*O*-acetyl-β-D-glucopyranosyl)formimidate (**4**, 1.56 g, 3.17 mmol) was dissolved in anhydrous EtOH (30 mL), and hydrazine monohydrate (154 μL, 3.17 mmol) was added. The reaction mixture was stirred at room temperature, and the transformation of **4** was monitored by TLC (3:2 EtOAc-hexane). After the completion of the reaction (4.5 h), the precipitated product was filtered off and washed with EtOH to give 0.77 g of white solids. The mother liquor was evaporated under reduced pressure to give an oil, which was triturated with diethyl ether to give an additional 0.55 g of white solids. The combined yield of the product: 1.31 g (87%). R_f = 0.32 (3:2 EtOAc-hexane); $[\alpha]_D$ = −13 (c 0.49, MeOH). ^{1}H NMR (360 MHz, $CDCl_3$) δ (ppm): 7.86-7.74 (4H, m, Ar), 5.98 (1H, pt, *J* = 9.8, 9.7 Hz, H-2 or H-3 or H-4), 5.19 (1H, pt, *J* = 9.7, 9.6 Hz, H-2 or H-3 or H-4), 4.81 (1H, d, *J* = 9.9 Hz, H-1), 4.58 (2H, br s, NH_2), 4.50 (1H, pt, *J* = 9.9, 9.6 Hz, H-2 or H-3 or H-4), 4.35 (1H, dd, *J* = 12.3, 4.6 Hz, H-6a), 4.17 (1H, dd, *J* = 12.5, 2.4 Hz, H-6b), 3.98 (1H, ddd, *J* = 9.9, 4.6, 2.4 Hz H-5′), 3.61-3.27 (2H, br signal, NH_2), 2.11, 2.05, 1.88 (3 × 3H, 3 s, CH_3); ^{13}C NMR (90 MHz, $CDCl_3$) δ (ppm): 170.6, 169.9, 169.5 (CH_3-*C*=O), 167.8, 167.4 (Phth-*C*=O), 148.2 (C=N), 134.2, 134.0, 131.6, 131.0, 123.7, 123.3 (Ar), 75.6, 74.2, 70.9, 68.8 (C-1, C-3 − C-5), 62.1 (C-6), 52.7 (C-2), 20.7, 20.5, 20.4 (3 × CH_3). ESI-HRMS positive mode (m/z): calcd for $C_{21}H_{25}N_4O_9^+$ $[M+H]^+$ 477.1616. Found: 477.1613.

*3-(2′-Deoxy-2′-phthalimido-3′,4′,6′-tri-O-acetyl-β-*D*-glucopyranosyl)-1,2,4-triazine* (**6a**)

Prepared from amidrazone **5** (0.10 g, 0.21 mmol) and an aq. 40 wt.% solution of glyoxal (23.8 μL, 0.21 mmol) according to general procedure 1. Purified by column chromatography (1:1 EtOAc-hexane) to yield 58 mg (58%) of pale yellow syrup. R_f = 0.36 (3:2 EtOAc-hexane); $[\alpha]_D$ = −52 (c 0.23, $CHCl_3$). ^{1}H NMR (360 MHz, $CDCl_3$) δ (ppm): 9.16, 8.67 (2 × 1H, 2 d, *J* = 2.4 Hz in each, H-5, H-6), 7.80-7.69 (4H, m, Ar), 6.09 (1H, dd, *J* = 10.3, 9.2 Hz, H-2′ or H-3′ or H-4′), 5.96 (1H, d, *J* = 10.5 Hz, H-1′), 5.36 (1H, dd, *J* = 9.9, 9.3 Hz, H-2′ or H-3′ or H-4′), 5.00 (1H, pt, *J* = 10.5, 10.5 Hz, H-2′ or H-3′ or H-4′), 4.38 (1H, dd, *J* = 12.4, 5.1 Hz, H-6′a), 4.23 (1H, dd, *J* = 12.5, 2.0 Hz, H-6′b), 4.17 (1H, ddd, *J* = 10.3, 5.1, 2.0 Hz, H-5′), 2.10, 2.08, 1.88 (3 × 3H, 3 s, CH_3); ^{13}C NMR (90 MHz, $CDCl_3$) δ (ppm): 170.6, 170.1, 169.4 (CH_3-*C*=O), 167.6, 166.9 (Phth-*C*=O), 164.4 (C-3), 149.4 (2) (C-5, C-6), 134.3, 131.3, 130.8, 123.6 (Ar), 76.8, 76.5, 71.3, 68.8 (C-1′, C-3′ − C-5′), 62.2 (C-6′), 53.2 (C-2′), 20.7, 20.6, 20.4 (3 × CH_3).). ESI-HRMS positive mode (m/z): calcd for $C_{23}H_{23}N_4O_9^+$ $[M+H]^+$ 499.1460; $C_{23}H_{22}N_4NaO_9^+$ $[M+Na]^+$ 521.1279. Found: $[M+H]^+$ 499.1455; $[M+Na]^+$ 521.1279.

*3-(2′-Deoxy-2′-phthalimido-3′,4′,6′-tri-O-acetyl-β-*D*-glucopyranosyl)-5-methyl-1,2,4-triazine* (**6b**)

Prepared from amidrazone **5** (0.10 g, 0.21 mmol) and an aq. 40 wt.% solution of methylglyoxal (32 μL, 0.21 mmol) according to general procedure 1. Purified by column chromatography (2:1 EtOAc-hexane) to yield 67 mg (62%) of pale yellow syrup. R_f = 0.41 (2:1 EtOAc-hexane); $[\alpha]_D$ = −16 (c 0.25, $CHCl_3$). ^{1}H NMR (360 MHz, $CDCl_3$) δ (ppm): 9.00 (1H, s, H-6), 7.86-7.69 (4H, m, Ar), 6.07 (1H, dd, *J* = 10.3, 9.3 Hz, H-2′ or H-3′ or H-4′), 5.88 (1H, d, *J* = 10.5 Hz, H-1′), 5.37 (1H, pt, *J* = 9.9, 9.4 Hz, H-2′ or H-3′ or H-4′), 5.05 (1H, pt, *J* = 10.5, 10.5 Hz, H-2′ or H-3′ or H-4′), 4.38 (1H, dd, *J* = 12.5, 5.0 Hz, H-6′a), 4.23 (1H, dd, *J* = 12.5, 2.1 Hz, H-6′b), 4.15 (1H, ddd, *J* = 10.2, 5.0, 2.1 Hz, H-5′), 2.52 (3H, s, CH_3), 2.10, 2.08, 1.88 (3 × 3H, 3 s, CH_3); ^{13}C NMR (90 MHz, $CDCl_3$) δ (ppm): 170.7, 170.2, 169.5 (CH_3-*C*=O), 167.8, 166.4 (Phth-*C*=O), 163.2. 160.5 (C-3, C-5), 149.9 (C-6), 134.2, 131.4, 131.0, 123.6 (Ar), 76.8, 76.5, 71.4, 68.8 (C-1′, C-3′ − C-5′), 62.2 (C-6′), 53.0 (C-2′), 21.7, 20.7, 20.6,

20.4 (4 × CH_3). ESI-HRMS positive mode (m/z): calcd for $C_{24}H_{25}N_4O_9^+$ $[M+H]^+$ 513.1616; $C_{24}H_{24}N_4NaO_9^+$ $[M+Na]^+$ 535.1435. Found: $[M+H]^+$ 513.1612; $[M+Na]^+$ 535.1429.

*3-(2′-Deoxy-2′-phthalimido-3′,4′,6′-tri-O-acetyl-β-*D*-glucopyranosyl)-5-tert-butyl-1,2,4-triazine* (**6c**)

Prepared from amidrazone **5** (0.10 g, 0.21 mmol) and 3,3-dimethyl-2-oxobutanal (0.028 g, 0.21 mmol) according to general procedure 1. Purified by column chromatography (4:5 EtOAc-hexane) to yield 78 mg (67%) of white syrup. R_f = 0.51 (4:5 EtOAc-hexane); $[\alpha]_D$ = +14 (c 0.28, $CHCl_3$). ^{1}H NMR (360 MHz, $CDCl_3$) δ (ppm): 9.21 (1H, s, H-6), 7.81-7.68 (4H, m, Ar), 6.05 (1H, pt, *J* = 10.3, 9.3 Hz, H-2′ or H-3′ or H-4′), 5.93 (1H, d, *J* = 10.5 Hz, H-1′), 5.37 (1H, pt, *J* = 10.0, 9.3 Hz, H-2′ or H-3′ or H-4′), 5.11 (1H, pt, *J* = 10.5, 10.5 Hz, H-2′ or H-3′ or H-4′), 4.35 (1H, dd, *J* = 12.4, 4.9 Hz, H-6′a), 4.25 (1H, dd, *J* = 12.4, 1.8 Hz, H-6′b), 4.15 (1H, ddd, *J* = 10.0, 4.9, 1.8 Hz, H-5′), 2.10, 2.08, 1.88 (3 × 3H, 3 s, CH_3), 1.28 (9H, s, $C(CH_3)_3$); ^{13}C NMR (90 MHz, $CDCl_3$) δ (ppm): 170.6, 170.1, 169.7, 169.5 (3 × CH_3-*C*=O, C-5), 167.5, 166.5 (2 × Phth-*C*=O), 162.6 (C-3), 146.8 (C-6), 134.2, 131.4, 130.9, 123.4 (Ar), 76.9, 76.5, 71.5, 68.9 (C-1′, C-3′ − C-5′), 62.2 (C-6′), 52.9 (C-2′), 36.7 (*C*$(CH_3)_3$), 28.5 (C(*C*$H_3)_3$), 20.7, 20.6, 20.4 (3 × CH_3). ESI-HRMS positive mode (m/z): calcd for $C_{27}H_{31}N_4O_9^+$ $[M+H]^+$ 555.2086; $C_{27}H_{30}N_4NaO_9^+$ $[M+Na]^+$ 577.1905. Found: $[M+H]^+$ 555.2088; $[M+Na]^+$ 577.1904.

*3-(2′-Deoxy-2′-phthalimido-3′,4′,6′-tri-O-acetyl-β-*D*-glucopyranosyl)-5-phenyl-1,2,4-triazine* (**6d**)

Prepared from amidrazone **5** (0.10 g, 0.21 mmol) and phenylglyoxal monohydrate (0.032 g, 0.21 mmol) according to general procedure 1. Purified by column chromatography (1:1 EtOAc-hexane) to yield 88 mg (73%) of yellow syrup. R_f = 0.41 (3:2 EtOAc-hexane); $[\alpha]_D$ = −86 (c 0.22, $CHCl_3$). ^{1}H NMR (360 MHz, $CDCl_3$) δ (ppm): 9.57 (1H, s, H-6), 8.17–7.52 (9H, m, Ar), 6.10 (1H, pt, *J* = 9.8, 9.7 Hz, H-2′ or H-3′ or H-4′), 6.01 (1H, d, *J* = 10.5 Hz, H-1′), 5.40 (1H, pt, *J* = 9.7, 9.5 Hz, H-2′ or H-3′ or H-4′), 5.24 (1H, pt, *J* = 10.5, 10.5 Hz, H-2′ or H-3′ or H-4′), 4.38 (1H, dd, *J* = 12.3, 4.8 Hz, H-6′a), 4.26-4.17 (2H, m, H-5′, H-6′b), 2.09, 1.90 (9H, 2 s, CH_3). ^{13}C NMR (90 MHz, $CDCl_3$) δ (ppm): 170.7, 170.2, 169.5 (CH_3-*C*=O), 167.8, 167.7 (Phth-*C*=O), 163.4, 155.8 (C-3, C-5), 145.9 (C-6), 134.2, 132.8, 132.6, 129.3, 127.8, 123.5 (Ar), 76.9, 76.6, 71.6, 68.8 (C-1′, C-3′ − C-5′), 62.2 (C-6′), 52.8 (C-2′), 20.7, 20.6, 20.4 (3 × CH_3). ESI-HRMS positive mode (m/z): calcd for $C_{29}H_{27}N_4O_9^+$ $[M+H]^+$ 575.1773; $C_{29}H_{26}N_4NaO_9^+$ $[M+Na]^+$ 597.1592. Found: $[M+H]^+$ 575.1777; $[M+Na]^+$ 597.1593.

*3-(2′-Deoxy-2′-phthalimido-3′,4′,6′-tri-O-acetyl-β-*D*-glucopyranosyl)-5,6-diphenyl-1,2,4-triazine* (**6e**)

Prepared from amidrazone **5** (0.10 g, 0.21 mmol) and benzil (0.042 g, 0.21 mmol) according to general procedure 1. Purified by column chromatography (4:5 EtOAc-hexane) to yield 84 mg (65%) of pale yellow syrup. R_f = 0.51 (4:5 EtOAc-hexane); $[\alpha]_D$ = −60 (c 0.20, $CHCl_3$). ^{1}H NMR (360 MHz, $CDCl_3$) δ (ppm): 7.81-7.27 (14H, m, Ar), 6.10 (1H, dd, *J* = 10.3, 9.3 Hz, H-2′ or H-3′ or H-4′), 6.05 (1H, d, *J* = 10.6 Hz, H-1′), 5.40 (1H, pt, *J* = 10.0, 9.3 Hz, H-2′ or H-3′ or H-4′), 5.30 (1H, pt, *J* = 10.5, 10.5 Hz, H-2′ or H-3′ or H-4′), 4.39 (1H, dd, *J* = 12.6, 5.1 Hz, H-6′a), 4.25 (1H, dd, *J* = 12.6, < 1 Hz, H-6′a), 4.21-4.19 (1H, m, H-5′), 2.08, 1.90 (9H, 2 s, CH_3). ^{13}C NMR (90 MHz, $CDCl_3$) δ (ppm): 170.6, 170.1, 169.4 (CH_3-*C*=O), 167.8, 166.8 (Phth-*C*=O), 161.1, 157.1, 156.2 (C-3, C-5, C-6), 134.8-123.4 (Ar), 76.6, 76.5, 71.6, 68.8 (C-1′, C-3′ − C-5′), 62.2 (C-6′), 52.7 (C-2′), 20.7, 20.6, 20.4 (3 × CH_3). ESI-HRMS positive mode (m/z): calcd for $C_{35}H_{31}N_4O_9^+$ $[M+H]^+$ 651.2086; $C_{35}H_{30}N_4NaO_9^+$ $[M+Na]^+$ 673.1905. Found: $[M+H]^+$ 651.2085; $[M+Na]^+$ 673.1902.

*N^1-Ethoxycarbonylmethylidene-C-(2′,3′,4′,6′-tetra-O-benzoyl-β-*D*-glucopyranosyl)formamidrazone* (**7a**)

A solution of amidrazone **1** (0.10 g, 0.16 mmol) and ethyl glyoxalate (31 μL, 0.16 mmol, an 50% solution in toluene) was boiled in dry EtOH (3 mL) until the TLC (1:1 and 7:3 EtOAc-hexane) showed the complete conversion of **1**. After the completion of the reaction (1 h), the solvent was removed under reduced pressure. After column chromatographic purification (2:3 EtOAc-hexane), 44 mg (39%) of the title compound was obtained as a pale yellow syrup. R_f = 0.53 (1:1 EtOAc-hexane); $[\alpha]_D$ = +23 (c 0.27, $CHCl_3$). ^{1}H NMR (360 MHz, $CDCl_3$) δ (ppm): 8.06-7.83, 7.59-7.26, 7.07 (21H, m, Ar, C*H*=N), 6.02 (1H, pt, *J* = 9.6, 9.6 Hz, H-2′ or H-3′ or H-4′), 5.76 (1H, pt, *J* = 9.8, 9.7 Hz, H-2′ or H-3′ or H-4′), 5.67 (1H, pt, *J* = 9.7, 9.7 Hz, H-2′ or H-3′ or H-4′), 4.69 (1H, dd, *J* = 12.4, 2.7 Hz, H-6′a), 4.54 (1H, dd, *J* = 12.4, 5.2 Hz, H-6′b), 4.51 (1H, d, *J* = 9.7 Hz, H-1′), 4.35-4.25 (1H, m, H-5′), 4.23 (2H, q, *J* = 7.1 Hz, CH_2), 1.28 (3H, t, *J* = 7.1 Hz, CH_3); ^{13}C NMR (90 MHz, $CDCl_3$) δ (ppm): 166.2, 165.6, 165.3,

165.2, 163.7, 160.9 (5 × C=O, C=N), 146.1 (CH=N), 133.6, 133.3, 133.2, 129.9-128.3 (Ar), 76.4, 76.3, 73.4, 70.5, 69.1 (C-1′ − C-5′), 62.8, 61.2 (C-6′, CH_2), 14.1 (CH_3).

N^1-Methoxycarbonylethylidene-C-(2′,3′,4′,6′-tetra-O-benzoyl-β-D-glucopyranosyl)formamidrazone (**7b**)

A solution of amidrazone **1** (0.10 g, 0.16 mmol) and methyl pyruvate (14 μL, 0.16 mmol) was boiled in dry EtOH (3 mL) until the TLC (1:1 and 7:3 EtOAc-hexane) showed the complete conversion of **1**. After the completion of the reaction (1.5 h), the solvent was removed under reduced pressure. After column chromatographic purification (2:3 EtOAc-hexane), 67 mg (59%) of the title compound was obtained as a pale yellow syrup. R_f = 0.53 (1:1 EtOAc-hexane). ^{1}H NMR (360 MHz, $CDCl_3$) δ (ppm): 8.05-7.83, 7.58-7.25, 7.07 (20H, m, Ar), 6.03 (1H, pt, *J* = 9.6, 9.6 Hz, H-2′ or H-3′ or H-4′), 5.94-5.83 (2H, broad signal, NH), 5.75 (1H, pt, *J* = 9.8, 9.7 Hz, H-2′ or H-3′ or H-4′), 5.73 (1H, pt, *J* = 9.6, 9.6 Hz, H-2′ or H-3′ or H-4′), 4.68 (1H, dd, *J* = 12.3, < 1 Hz, H-6′a), 4.55 (1H, dd, *J* = 12.4, 5.4 Hz, H-6′b), 4.55 (1H, d, *J* = 9.7 Hz, H-1′), 4.27 (1H, ddd, *J* = 9.7, 5.4, 2.3 Hz, H-5′), 3.75 (3H, s, OCH_3), 1.60 (3H, s, CH_3); ^{13}C NMR (90 MHz, $CDCl_3$) δ (ppm): 166.1, 165.7, 165.6, 165.2, 165.0 (5 × C=O), 158.3, 153.7 (2 × C=N), 133.6, 133.5, 133.4, 133.2, 129.8-128.3 (Ar), 76.8, 76.4, 73.6, 70.5, 69.2 (C-1′ − C-5′), 62.9 (C-6′), 52.3 (OCH_3), 13.0 (CH_3).

3-(3′,4′,6′-Tri-O-benzoyl-2′-deoxy-D-arabino-hex-1′-enopyranosyl)-1,2,4-triazin-5(4H)-one (**8a**)

Prepared from amidrazone **1** (0.10 g, 0.16 mmol) and ethyl glyoxalate (31 μL, 0.16 mmol, an 50% solution in toluene) according to general procedure 3. Reaction time: 3 d. Purified by column chromatography (7:3 EtOAc-hexane) to yield 50 mg (57%) of pale yellow amorphous solids. R_f = 0.24 (7:3 EtOAc-hexane); $[\alpha]_D$ = −44 (c 0.26, $CHCl_3$). ^{1}H NMR (400 MHz, $CDCl_3$) δ (ppm): 14.05 (1H, br s, NH), 7.97-7.93, 7.67-7.64, 7.53-7.49 (16H, m, Ar, H-6), 6.60 (1H, d, *J* = 3.5 Hz, H-2′), 6.00 (1H, dd, *J* = 5.6, 3.5 Hz, H-3′), 5.87 (1H, pt, *J* = 7.6, 5.6 Hz, H-4′), 5.15 (1H, ddd, *J* = 7.6, 4.6, 3.3 Hz, H-5′), 4.82 (1H, dd, *J* = 12.4, 4.6 Hz, H-6′a), 4.74 (1H, dd, *J* = 12.4, 3.3 Hz, H-6′b); ^{13}C NMR (90 MHz, $CDCl_3$) δ (ppm): 165.3, 164.9, 164.2 (3 × C=O), 161.8, 152.6, 144.6 (C-3, C-5, C-6), 145.4 (C-1′), 133.8, 133.6, 133.4, 129.3-128.6 (Ar), 104.0 (C-2′), 74.8, 67.8, 66.8 (C-3′ − C-5′), 61.2 (C-6′). ESI-HRMS positive mode (m/z): calcd for $C_{30}H_{23}N_3NaO_8^+$ $[M+Na]^+$ 576.1377. Found: 576.1377.

3-(3′,4′,6′-Tri-O-benzoyl-2′-deoxy-D-arabino-hex-1′-enopyranosyl)-6-methyl-1,2,4-triazin-5(4H)-one (**8b**)

Prepared from amidrazone **1** (0.10 g, 0.16 mmol) and methyl pyruvate (14 μL, 0.16 mmol) according to general procedure 3. Reaction time: 6 h. Purified by column chromatography (7:3 EtOAc-hexane) to yield 67 mg (75%) of pale yellow amorphous solids. R_f = 0.42 (7:3 EtOAc-hexane); $[\alpha]_D$ = −29 (c 0.23, $CHCl_3$). ^{1}H NMR (400 MHz, $CDCl_3$) δ (ppm): 13.82 (1H, br s, NH), 7.96-7.95, 7.68-7.64, 7.53-7.49 (15H, m, Ar), 6.37 (1H, broad signal, H-2′), 5.98 (1H, broad signal, H-3′), 5.87 (1H, pt, *J* = 7.0, 6.0 Hz, H-4′), 5.14 (1H, broad signal, H-5′), 4.82 (1H, dd, *J* = 12.3, 4.6 Hz, H-6′a), 4.73 (1H, dd, *J* = 12.3, 2.5 Hz, H-6′b), 2.18 (3H, s, CH_3); ^{13}C NMR (90 MHz, DMSO-d_6) δ (ppm): 165.2, 164.9, 164.4 (3 × C=O), 162.3, 153.2, 152.4 (C-3, C-5, C-6), 145.4 (C-1′), 133.7, 133.6, 133.3, 129.3-128.6 (Ar), 103.5 (C-2′), 74.7, 67.7, 66.8 (C-3′ − C-5′), 61.2 (C-6′), 17.1 (CH_3). ESI-HRMS positive mode (m/z): calcd for $C_{31}H_{26}N_3O_8^+$ $[M+H]^+$ 568.1714; $C_{31}H_{25}N_3NaO_8^+$ $[M+Na]^+$ 590.1534. Found: $[M+H]^+$ 568.1711; $[M+Na]^+$ 590.1531.

3-(2′-Deoxy-2′-phthalimido-3′,4′,6′-tri-O-acetyl-β-D-glucopyranosyl)-1,2,4-triazin-5(4H)-one (**9a**)

Prepared from amidrazone **5** (0.10 g, 0.21 mmol) and ethyl glyoxylate (43 μL, 0.21 mmol) according to general procedure 3. Reaction time: 2 d. Purified by column chromatography (3:2 EtOAc-hexane) to yield 55 mg (51%) of pale yellow syrup. R_f = 0.25 (5:2 EtOAc-hexane); $[\alpha]_D$ = +17 (c 0.21, $CHCl_3$). ^{1}H NMR (360 MHz, $CDCl_3$) δ (ppm): 11.73 (1H, s, NH), 7.90–7.72 (5H, m, Ar, H-6), 6.07 (1H, pt, *J* = 9.8, 9.8 Hz, H-2′ or H-3′ or H-4′), 5.35 (1H, d, *J* = 9.4 Hz, H-1′), 5.23 (1H, pt, *J* = 9.8, 9.6 Hz, H-2′ or H-3′ or H-4′), 4.54 (1H, pt, *J* = 10.5, 10.5 Hz, H-2′ or H-3′ or H-4′), 4.40 (1H, dd, *J* = 12.6, 5.3 Hz, H-6′a), 4.26 (1H, dd, *J* = 12.6, 1.7 Hz, H-6′b), 4.12 (1H, ddd, *J* = 10.0, 5.3, 1.7 Hz, H-5′), 2.13, 2.09, 1.90 (3 × 3H, 3 s, CH_3); ^{13}C NMR (90 MHz, $CDCl_3$) δ (ppm): 171.1, 169.8, 169.6 (CH_3-C=O), 167.8 (2 × Phth-C=O), 161.2, 159.2 (C-3, C-5), 144.3 (C-6), 134.5, 131.3, 123.9 (Ar), 76.2, 71.4, 70.5, 68.5 (C-1′, C-3′ − C-5′), 62.1 (C-6′), 52.5 (C-2′), 20.8, 20.6, 20.4 (3 × CH_3). ESI-HRMS positive mode (m/z): calcd for $C_{23}H_{23}N_4O_{10}^+$ $[M+H]^+$ 515.1409; $C_{23}H_{22}N_4NaO_{10}^+$ $[M+Na]^+$ 537.1228. Found: $[M+H]^+$ 515.1409; $[M+Na]^+$ 537.1226.

3-(2′-Deoxy-2′-phthalimido-3′,4′,6′-tri-O-acetyl-β-D-glucopyranosyl)-6-methyl-1,2,4-triazin-5(4H)-one (**9b**)

Prepared from amidrazone **5** (0.10 g, 0.21 mmol) and methyl pyruvate (23 μL, 0.21 mmol) according to general procedure 3. Reaction time: 2 d. Purified by column chromatography (3:2 EtOAc-hexane) to yield 56 mg (50%) of pale yellow syrup. R_f = 0.25 (5:2 EtOAc-hexane); $[\alpha]_D$ = +45 (c 0.21, $CHCl_3$). ^{1}H NMR (360 MHz, $CDCl_3$) δ (ppm): 11.39 (1H, s, NH), 7.86–7.72 (4H, m, Ar), 6.06 (1H, pt, *J* = 9.8, 9.6 Hz, H-2′ or H-3′ or H-4′), 5.31 (1H, d, *J* = 10.5 Hz, H-1′), 5.23 (1H, pt, *J* = 9.8, 9.5 Hz, H-2′ or H-3′ or H-4′), 4.54 (1H, pt, *J* = 10.5, 9.8 Hz, H-2′ or H-3′ or H-4′), 4.39 (1H, dd, *J* = 12.1, 5.0 Hz, H-6′a), 4.27 (1H, dd, *J* = 12.3, < 1 Hz, H-6′b), 4.16-4-07 (1H, m, H-5′), 2.20 (3H, s, CH_3), 2.14, 2.09, 1.89 (3 × 3H, 3 s, CH_3); ^{13}C NMR (90 MHz, $CDCl_3$) δ (ppm): 171.0, 169.9, 169.6 (CH_3-C=O), 167.9, 167.7 (2 × Phth-*C*=O), 161.9, 158.8, 153.8 (C-3, C-5, C-6), 134.4 (2), 131.4, 131.3, 123.8 (2) (Ar), 76.1, 71.3, 70.5, 68.5 (C-1′, C-3′ − C-5′), 62.1 (C-6′), 52.6 (C-2′), 20.8, 20.6, 20.4 (3 × CH_3), 17.4 (CH_3). ESI-HRMS positive mode (m/z): calcd for $C_{24}H_{25}N_4O_{10}^+$ $[M+H]^+$ 529.1565; $C_{24}H_{24}N_4NaO_{10}^+$ $[M+Na]^+$ 551.1385. Found: $[M+H]^+$ 529.1569; $[M+Na]^+$ 551.1386.

((6aS,7R,7aR)-1-(2′,3′,4′,6′-Tetra-O-benzoyl-β-D-glucopyranosyl)-6,6a,7,7a,8,9-hexahydro-5H-cyclopropa[5,6]cyclookta[1,2-c]pyridin-7-yl)methanol and ((6aR,7S,7aS)-1-(2′,3′,4′,6′-tetra-O-benzoyl-β-D-glucopyranosyl)-6,6a,7,7a,8,9-hexahydro-5H-cyclopropa[5,6]cyclookta[1,2-c]pyridin-7-yl)methanol (**11a**)

Prepared from triazine **2a** (0.10 g, 0.15 mmol) and ((1*R*,8*S*,9*r*)-bicyclo[6.1.0]non-4-yn-9-yl)methanol (**10**, 46 mg, 0.30 mmol) in CH_2Cl_2 according to general procedure 4. Reaction time: 2 d. Purified by column chromatography (1:1 EtOAc-hexane) to give 115 mg (97%) of colourless syrup. Diastereomeric ratio: 5:4. R_f = 0.15 (1:1 EtOAc-hexane). ^{1}H NMR (360 MHz, $CDCl_3$) δ (ppm): 8.29, 8.26 (2 × 1H, 2 d, *J* = 4.8 Hz in each, 2 × H-3), 8.02–7.21 (2 × 20H, m, Ar), 6.94, 6.92 (2 × 1H, 2 d, *J* = 4.8 Hz in each, 2 × H-4), 6.44 (2H, pt, *J* = 9.6, 9.5 Hz, 2 × (H-2′ or H-3′ or H-4′)), 6.11 (2H, pt, *J* = 9.5, 9.5 Hz, 2 × (H-2′ or H-3′ or H-4′)), 5.88, 5.87 (2 × 1H, 2 pt, *J* = 9.7, 9.6 Hz in each, 2 × (H-2′ or H-3′ or H-4′)), 5.27, 5.25 (2 × 1H, 2 d, *J* = 9.7 Hz in each, 2 × H-1′), 4.81, 4.71 (2 × 1H, 2 dd, *J* = 12.2, 2.1 Hz in each, 2 × H-6′a), 4.51, 4.46 (2 × 1H, 2 dd, *J* = 12.2, 5.1 Hz in each, 2 × H-6′b), 4.44–4.37 (2 × 1H, m, 2 × H-5′), 3.36–3.31, 3.18–2.87, 2.75–2.45, 2.38–2.33, 1.47–1.26, 0.66–0.52, 0.36–0.20 (2 × 14H, m, aliphatics, OH); ^{13}C NMR (90 MHz, $CDCl_3$) δ (ppm): 166.2, 166.1, 166.0, 165.9, 165.2, 165.2, 164.5, 164.4 (2 × 4 × C=O), 152.4, 152.3, 151.2, 151.1 (2 × C-1, 2 × C-4a), 146.4 (2 × C-3), 137.6, 137.4 (2 × C-9a), 133.3-132.7, 130.0-128.0 (Ar), 125.9, 125.8 (2 × C-4), 79.0, 78.3, 76.8, 76.8, 75.1, 75.1, 71.3, 71.2, 69.9, 69.8 (2 × (C-1′ − C-5′)), 66.1, 66.1 (2 × C-6′), 63.5, 63.2 (2 × CH_2OH), 33.3, 33.2, 30.0, 29.7, 29.2, 28.5, 28.3, 28.0, 25.8, 25.4, 21.4, 20.8, 20.4, 19.9 (2 × (C-5, C-6, C-6a, C-7, C-7a, C-8, C-9)). ESI-HRMS positive mode (m/z): calcd for $C_{47}H_{44}NO_{10}^+$ $[M+H]^+$: 782.2960; $C_{47}H_{43}NNaO_{10}^+$ $[M+Na]^+$: 804.2779. Found: $[M+H]^+$: 782.2959; $[M+Na]^+$: 804.2779.

((6aS,7R,7aR)-3-Methyl-1-(2′,3′,4′,6′-tetra-O-benzoyl-β-D-glucopyranosyl)-6,6a,7,7a,8,9-hexahydro-5H-cyclopropa[5,6]cyclookta[1,2-c]pyridin-7-yl)methanol and ((6aR,7S,7aS)-3-methyl-1-(2′,3′,4′,6′-tetra-O-benzoyl-β-D-glucopyranosyl)-6,6a,7,7a,8,9-hexahydro-5H-cyclopropa[5,6]cyclookta[1,2-c]pyridin-7-yl)methanol (**11b**)

Prepared from triazine **2a** (0.05 g, 0.074 mmol) and ((1*R*,8*S*,9*r*)-bicyclo[6.1.0]non-4-yn-9-yl)methanol (**10**, 22 mg, 0.148 mmol) in CH_2Cl_2 according to general procedure 4. Reaction time: 6 d. Purified by column chromatography (4:5 EtOAc-hexane) to give 24 mg (41%) of colourless amorphous solids. Diastereomeric ratio: 5:4. R_f = 0.28 (1:1 EtOAc-hexane). ^{1}H NMR (360 MHz, $CDCl_3$) δ (ppm): 8.05-7.23 (2 × 20H, m, Ar), 6.77, 6.76 (2 × 1H, 2 s, 2 × H-4), 6.47, 6.43 (2 × 1H, 2 pt, *J* = 9.7, 9.6 Hz in each, 2 × (H-2′ or H-3′ or H-4′)), 6.07 (2H, pt, *J* = 9.6, 9.6 Hz, 2 × (H-2′ or H-3′ or H-4′)), 5.86, 5.84 (2 × 1H, 2 pt, *J* = 9.7, 9.6 Hz in each, 2 × (H-2′ or H-3′ or H-4′)), 5.17, 5.16 (2 × 1H, 2 d, *J* = 9.7 Hz in each, 2 × H-1′), 4.88, 4.70 (2 × 1H, 2 dd, *J* = 12.1, 2.8 Hz in each, 2 × H-6′a), 4.49 (1H, dd, *J* = 12.1, 5.3 Hz, H-6′b), 4.42-4.33 (3H, m, H-6′b, 2 × H-5′), 3.50-2.32 (m, aliphatics), 2.30, 2.26 (2 × 3H, 2 s, 2 × CH_3), 1.40-0.31 (m, aliphatics, OH); ^{13}C NMR (90 MHz, $CDCl_3$) δ (ppm): 166.3, 166.2, 166.1, 166.0, 165.3, 165.3, 164.7, 164.6 (2 × 4 × C=O), 154.8, 154.6, 152.4, 152.3, 150.4, 150.3 (2 × C-1, 2 × C-4a, 2 × C-3), 134.4, 134.3 (2 × C-9a), 133.3-132.6, 130.1-128.0 (Ar), 125.4, 125.3 (2 × C-4), 79.6, 78.8, 76.9, 76.9, 75.3, 75.2, 71.1, 70.8, 70.0, 69.8 (2 × (C-1′ − C-5′)),

66.3, 65.7 (2 × C-6′), 63.6, 63.0 (2 × CH_2OH), 33.1, 33.0, 30.0, 29.9, 28.8, 28.2, 28.1, 26.8, 25.5, 25.3, 23.5, 23.4, 21.6, 20.8, 20.6, 20.4 (2 × (C-5, C-6, C-6a, C-7, C-7a, C-8, C-9), 2 × CH_3). ESI-HRMS positive mode (m/z): calcd for $C_{48}H_{45}NNaO_{10}^+$ $[M+Na]^+$: 818.2936. Found: 818.2935.

((6aS,7R,7aR)-3-Phenyl-1-(2′,3′,4′,6′-tetra-O-benzoyl-β-D-glucopyranosyl)-6,6a,7,7a,8,9-hexahydro-5H-cyclopropa[5,6]cyclookta[1,2-c]pyridin-7-yl)methanol and ((6aR,7S,7aS)-3-phenyl-1-(2′,3′,4′,6′-tetra-O-benzoyl-β-D-glucopyranosyl)-6,6a,7,7a,8,9-hexahydro-5H-cyclopropa[5,6]cyclookta[1,2-c]pyridin-7-yl)methanol (**11d**)

Prepared from triazine **2d** (0.05 g, 0.068 mmol) and ((1*R*,8*S*,9*r*)-bicyclo[6.1.0]non-4-yn-9-yl)methanol (**10**, 20 mg, 0.136 mmol) in CH_2Cl_2 according to general procedure 4. Reaction time: 6 d. Purified by column chromatography (1:1 EtOAc-hexane) to give 43 mg (73%) of colourless amorphous solids. Diastereomeric ratio: 5:4. R_f = 0.28 (1:1 EtOAc-hexane). ^{1}H NMR (360 MHz, $CDCl_3$) δ (ppm): 8.04-7.15 (2 × 26H, m, Ar, 2 × H-4), 6.69, 6.65 (2 × 1H, 2 pt, *J* = 9.7, 9.7 Hz in each, 2 × (H-2′ or H-3′ or H-4′)), 6.12 (2H, pt, *J* = 9.6, 9.5 Hz, 2 × (H-2′ or H-3′ or H-4′)), 5.89, 5.86 (2 × 1H, 2 pt, *J* = 9.8, 9.6 Hz in each, 2 × (H-2′ or H-3′ or H-4′)), 5.31, 5.29 (2 × 1H, 2 d, *J* = 9.8 Hz in each, 2 × H-1′), 4.90, 4.67 (2 × 1H, 2 dd, *J* = 12.1, 2.9 Hz in each, 2 × H-6′a), 4.50 (1H, dd, *J* = 12.1, 5.3 Hz, H-6′b), 4.42–4.36 (3 × 1H, m, H-6′b, 2 × H-5′), 3.43–3.38, 3.20–2.52, 2.46–2.34, 1.52–1.36, 0.74–0.34 (2 × 13H, m, aliphatics); ^{13}C NMR (90 MHz, $CDCl_3$) δ (ppm): 166.3, 166.3, 166.2, 166.1, 165.3, 165.2, 164.8, 164.6 (2 × 4 × C=O), 154.0, 153.6, 153.0, 153.0, 150.9, 150.8 (2 × C-1, 2 × C-3, 2 × C-4a), 138.9, 138.7, 136.4, 136.1 (2 × C-9a, 2 × Ar-C_q), 133.4-132.5, 129.9-126.8 (Ar), 122.6, 122.3 (2 × C-4), 79.0, 78.4, 76.9, 76.9, 75.6, 75.4, 70.8, 70.5, 69.9, 69.6 (2 × (C-1′ − C-5′)), 66.2, 66.2 (2 × C-6′), 63.7, 62.9 (2 × CH_2OH), 33.5, 30.0, 29.9, 29.1, 28.8, 28.2, 28.0, 25.6, 25.4, 20.5, 20.5, 20.4, 20.3 (2 × (C-5, C-6, C-6a, C-7, C-7a, C-8, C-9)). ESI-HRMS positive mode (m/z): calcd for $C_{53}H_{48}NO_{10}^+$ $[M+H]^+$: 858.3273; $C_{53}H_{47}NNaO_{10}^+$ $[M+Na]^+$: 880.3092. Found: $[M+H]^+$: 858.3272; $[M+Na]^+$: 880.3093.

((6aS,7R,7aR)-1-(β-D-glucopyranosyl)-3-phenyl-6,6a,7,7a,8,9-hexahydro-5H-cyclopropa[5,6]cyclookta[1,2-c]pyridin-7-yl)methanol and ((6aR,7S,7aS)-1-(β-D-glucopyranosyl)-3-phenyl-6,6a,7,7a,8,9-hexahydro-5H-cyclopropa[5,6]cyclookta[1,2-c]pyridin-7-yl)methanol (**12d**)

Prepared from triazine **3d** (20 mg, 0.063 mmol) and ((1*R*,8*S*,9*r*)-bicyclo[6.1.0]non-4-yn-9-yl)methanol (**10**, 19 mg, 0.126 mmol) in MeOH according to general procedure 4. Reaction time: 5 d. Purified by column chromatography (8:1 $CHCl_3$-MeOH) to give 26 mg (94%) of pale yellow amorphous solids. Diastereomeric ratio: 1:1. R_f = 0.21 (8:1 $CHCl_3$-MeOH). ^{1}H NMR (360 MHz, CD_3OD) δ (ppm): 8.02–8.01 (2 × 2H, Ph), 7.58 (2H, s, 2 × H-4), 7.47–7.36 (2 × 3H, m, Ph), 4.65, 4.63 (2 × 1H, 2 d, *J* = 9.3 Hz in each, H-1′), 4.34, 4.33 (2 × 1H, 2 pt, *J* = 9.1, 9.1 Hz in each, 2 × (H-2′ or H-3′ or H-4′)), 3.87–3.51 (2 × 4H, m, 2 × (H-2′ and/or H-3′ and/or H-4′, H-6′a, H6′b), 4.46–3.30 (2H, m, 2 × H-5′), 3.30–3.22, 3.14–3.05, 2.99–2.89, 2.65–2.44, 1.51–1.39, 0.72-0.61 (2 × 13H, m, aliphatics); ^{13}C NMR (90 MHz, CD_3OD) δ (ppm): 155.5, 155.3, 155.3, 155.2, 155.2, 155.1 (2 × C-1, 2 × C-3, 2 × C-4a), 140.8, 140.7, 138.5, 138.5 (2 × C-9a, 2 × Ph-C_q), 129.8, 129.7, 129.6, 129.6, 128.0 (Ph), 123.3, 123.2 (2 × C-4), 82.4, 82.4, 79.7, 79.7, 79.6, 73.8, 73.7, 71.6, 71.5 (2 × (C-1′ − C-5′)), 66.6, 66.5 (2 × C-6′), 62.9, 62.8 (2 × CH_2OH), 35.0, 34.8, 31.1, 31.0, 30.3, 30.1, 29.9, 29.8, 26.6, 26.5, 23.0, 22.9, 22.6, 22.5 (2 × (C-5, C-6, C-6a, C-7, C-7a, C-8, C-9)). ESI-HRMS positive mode (m/z): calcd for $C_{25}H_{31}NNaO_6^+$ $[M+Na]^+$: 464.2044. Found: 464.2042 (Supplementary Materials).

4. Conclusions

The reactions of *C*-glycopyranosyl formamidrazones with 1,2-dielectrophiles (α-keto-aldehydes and esters as well as 1,2-diketones) represent a simple method for the synthesis of hitherto unknown 3-glycopyranosyl-1,2,4-triazines and -1,2,4-triazin-5(4*H*)-ones. The *C*-glycosyl 1,2,4-triazines can be transformed into the corresponding 2-glycopyranosyl pyridines in strain-promoted inverse electron demand Diels–Alder reactions. These new compounds may be interesting for yet unknown applications to be explored in the future.

Supplementary Materials: The following supporting information can be downloaded at: https://www.mdpi.com/article/10.3390/molecules27227801/s1, Copies of the ^{1}H and ^{13}C NMR spectra of the synthesised compounds.

Author Contributions: É.B. conceived the research, coordinated the synthetic studies, raised funding, and wrote and edited the paper. A.F., M.H., É.J-T., Z.G. and A.I.Z. performed the experiments and prepared the compounds. L.S. wrote the paper and participated in the editing of the manuscript. All authors have read and agreed to the published version of the manuscript.

Funding: This research was funded by the National Research, Development and Innovation Office of Hungary, grant number FK125067.

Institutional Review Board Statement: Not applicable.

Informed Consent Statement: Not applicable.

Data Availability Statement: Not applicable.

Acknowledgments: We thank György Attila Kiss for his technical assistance.

Conflicts of Interest: The authors declare no conflict of interest.

References

1. Zhang, F.-G.; Chen, Z.; Tang, X.; Ma, J.-A. Triazines: Syntheses and Inverse Electron-demand Diels–Alder Reactions. *Chem. Rev.* **2021**, *121*, 14555–14593. [CrossRef] [PubMed]
2. Mondal, J.; Sivaramakrishna, A. Functionalized Triazines and Tetrazines: Synthesis and Applications. *Top. Curr. Chem.* **2022**, *380*, 34. [CrossRef] [PubMed]
3. Kumar, R.; Sirohi, T.S.; Singh, H.; Yadav, R.; Roy, R.K.; Chaudhary, A.; Pandeya, S.N. 1,2,4-Triazine Analogs as Novel Class of Therapeutic Agents. *Mini-Rev. Med. Chem.* **2014**, *14*, 168–207. [CrossRef] [PubMed]
4. Bokor, É. *N*- and *C*-Glycopyranosyl heterocycles as glycogen phosphorylase inhibitors. In *Recent Trends in Carbohydrate Chemistry—Synthesis, Structure and Function of Carbohydrates*; Rauter, A.P., Christensen, B.E., Somsák, L., Kosma, P., Adamo, R., Eds.; Elsevier: Amsterdam, The Netherlands, 2020; Volume 1, pp. 253–300.
5. Bokor, É.; Kun, S.; Goyard, D.; Tóth, M.; Praly, J.-P.; Vidal, S.; Somsák, L. *C*-Glycopyranosyl arenes and hetarenes: Synthetic methods and bioactivity focused on antidiabetic potential. *Chem. Rev.* **2017**, *117*, 1687–1764. [CrossRef] [PubMed]
6. Szennyes, E.; Bokor, É.; Langer, P.; Gyémánt, G.; Docsa, T.; Sipos, Á.; Somsák, L. The first general synthesis of 2-*C*-(β-D-glycopyranosyl)pyrimidines and their evaluation as inhibitors of some glycoenzymes. *New J. Chem.* **2018**, *42*, 17439–17446. [CrossRef]
7. Szennyes, E.; Gyémánt, G.; Somsák, L.; Bokor, É. Synthesis of new series of 2-*C*-(β-D-glucopyranosyl)pyrimidines and their evaluation as inhibitors of some glycoenzymes. *Molecules* **2020**, *25*, 701. [CrossRef] [PubMed]
8. Sipos, Á.; Szennyes, E.; Hajnal, N.É.; Kun, S.; Szabó, K.E.; Uray, K.; Somsák, L.; Docsa, T.; Bokor, É. Dual-Target Compounds against Type 2 Diabetes Mellitus: Proof of Concept for Sodium Dependent Glucose Transporter (SGLT) and Glycogen Phosphorylase (GP) Inhibitors. *Pharmaceuticals* **2021**, *14*, 364. [CrossRef] [PubMed]
9. Bokor, É.; Kecskés, T.D.; Gombás, F.; Fehér, A.; Kardos, E.; Dabian, A.; Vonza, Z.; Szennyes, E.; Somsák, L. First synthesis of *C*-glucopyranosyl 1,2,4,5-tetrazines and their transformation into *C*-glucopyranosyl pyridazines. *New J. Chem.* **2022**; *accepted for publication*. [CrossRef]
10. Ricciardi, F.; Joullie, M.M. Synthetic *C*-Nucleosides. *Synth. Commun.* **1986**, *16*, 35–42. [CrossRef]
11. Richter, M.; Seitz, G. Synthesis of the First 1,2,4-Triazine *C*-Nucleoside and its Transformation to novel Pyridine *C*-Nucleosides by Inverse [4+2]-Cycloaddition Reactions. *Arch. Pharm.* **1995**, *328*, 175–180. [CrossRef]
12. Seitz, G.; Lachmann, J. Synthesis of novel pyridine-, pyrindine- and isoquinoline-substituted α- and β-*C*-nucleosides of 2-deoxy-D-ribose. *Z. Naturforsch. B* **1999**, *54*, 549–558. [CrossRef]
13. Neunhoeffer, H. 1,2,4-Triazines and their Benzo Derivatives. In *Comprehensive Heterocyclic Chemistry*; Katritzky, A.R., Rees, C.V., Eds.; Pergamon: Oxford, UK, 1984; Volume 3, pp. 385–456.
14. Neunhoeffer, H. 1,2,4-Triazines. In *Methoden der Organischen Chemie (Houben-Weyl)*, 4th ed.; Schaumann, E., Ed.; Georg Thieme Verlag KG: Stuttgart, Germany, 1998; Volume E9c, pp. 582–666.
15. Bokor, É.; Fekete, A.; Varga, G.; Szőcs, B.; Czifrák, K.; Komáromi, I.; Somsák, L. *C*-(β-D-Glucopyranosyl)formamidrazones, formic acid hydrazides and their transformations into 3-(β-D-glucopyranosyl)-5-substituted-1,2,4-triazoles: A synthetic and computational study. *Tetrahedron* **2013**, *69*, 10391–10404. [CrossRef]
16. Bokor, É.; Széles, Z.; Docsa, T.; Gergely, P.; Somsák, L. *C*-Glucopyranosyl-1,2,4-triazol-5-ones: Synthesis and inhibition of glycogen phosphorylase. *Carbohydr. Res.* **2016**, *429*, 128–134. [CrossRef] [PubMed]
17. Tang, D.; Wang, J.; Wu, P.; Guo, X.; Li, J.H.; Yang, S.; Chen, B.H. Synthesis of 1,2,4-triazine derivatives *via* [4+2] domino annulation reactions in one pot. *RSC Adv.* **2016**, *6*, 12514–12518. [CrossRef]

18. Bokor, É.; Kyriakis, E.; Solovou, T.G.A.; Koppány, C.; Kantsadi, A.L.; Szabó, K.E.; Szakács, A.; Stravodimos, G.A.; Docsa, T.; Skamnaki, V.T.; et al. Nanomolar inhibitors of glycogen phosphorylase based on β-D-glucosaminyl heterocycles: A combined synthetic, enzyme kinetic and protein crystallography study. *J. Med. Chem.* **2017**, *60*, 9251–9262. [CrossRef] [PubMed]
19. Dommerholt, J.; Schmidt, S.; Temming, R.; Hendriks, L.J.A.; Rutjes, F.; van Hest, J.C.M.; Lefeber, D.J.; Friedl, P.; van Delft, F.L. Readily Accessible Bicyclononynes for Bioorthogonal Labeling and Three-Dimensional Imaging of Living Cells. *Angew. Chem. Int. Edit.* **2010**, *49*, 9422–9425. [CrossRef] [PubMed]

molecules

MDPI

Article

Mechanochemical Approach towards Multi-Functionalized 1,2,3-Triazoles and Anti-Seizure Drug Rufinamide Analogs Using Copper Beads

Dhananjay Bhattacherjee [1], Igor S. Kovalev [1], Dmitry S. Kopchuk [1,2], Matiur Rahman [1], Sougata Santra [1,*], Grigory V. Zyryanov [1,2], Pralay Das [3,4], Rituraj Purohit [4,5], Vladimir L. Rusinov [1,2] and Oleg N. Chupakhin [1,2]

1 Department of Organic and Biomolecular Chemistry, Ural Federal University, 19 Mira Street, 620002 Yekaterinburg, Russia
2 I. Ya. Postovsky Institute of Organic Synthesis, Ural Branch of the Russian Academy of Sciences, 22 S. Kovalevskoi Street, 620219 Yekaterinburg, Russia
3 Chemical Technology Division, CSIR-Institute of Himalayan Bioresource Technology (CSIR-IHBT), Palampur 176061, India
4 Academy of Scientific and Innovative Research (AcSIR), Ghaziabad 201002, India
5 Structural Bioinformatics Lab, CSIR-Institute of Himalayan Bioresource Technology (CSIR-IHBT), Palampur 176061, India
* Correspondence: sougatasantra85@gmail.com

Abstract: Highly regiospecific, copper-salt-free and neat conditions have been demonstrated for the 1,3-dipolar azide-alkyne cycloaddition (AAC) reactions under mechanochemical conditions. A group of structurally challenging alkynes and heterocyclic derivatives was efficiently implemented to achieve highly functionalized 1,4-disubstituted-1,2,3-triazoles in good to excellent yield by using the Cu beads without generation of unwanted byproducts. Furthermore, the high-speed ball milling (HSBM) strategy has also been extended to the synthesis of the commercially available pharmaceutical agent, Rufinamide, an antiepileptic drug (AED) and its analogues. The same strategy was also applied for the synthesis of the Cl-derivative of Rufinamide. Analysis of the single crystal XRD data of the triazole was also performed for the final structural confirmation. The Cu beads are easily recoverable from the reaction mixture and used for the further reactions without any special treatment.

Keywords: click chemistry; mechanochemical synthesis; 1,2,3-triazole; cycloaddition reaction; Rufinamide synthesis; solvent-free

Citation: Bhattacherjee, D.; Kovalev, I.S.; Kopchuk, D.S.; Rahman, M.; Santra, S.; Zyryanov, G.V.; Das, P.; Purohit, R.; Rusinov, V.L.; Chupakhin, O.N. Mechanochemical Approach towards Multi-Functionalized 1,2,3-Triazoles and Anti-Seizure Drug Rufinamide Analogs Using Copper Beads. *Molecules* **2022**, *27*, 7784. https://doi.org/10.3390/molecules27227784

Academic Editors: Alexey M. Starosotnikov, Maxim A. Bastrakov and Igor L. Dalinger

Received: 9 October 2022
Accepted: 7 November 2022
Published: 11 November 2022

1. Introduction

The 1,2,3-triazole moiety represents one of the versatile classes of heterocycles because of their widespread applications as pharmaceutical agents, agrochemicals, biochemicals and polymers [1–14]. The seminal work on "click chemistry" by Huisgen, followed by the further independent development by Meldal et al. and Sharpless-Fokin has encouraged extensive research on the 1,2,3-triazole molecule [15–17]. Over the last two decades, a plethora of reports have been documented for the 1,3-dipolar azide-alkyne cycloaddition (AAC) reaction and mostly involves Cu catalysis [18–27]. The assessment transition metal catalysis for the synthesis of heterocycles is common practice in modern research. Hence, several other transition metals, such as Pd, Ru, Zn, Ag, Ni, Au, etc., have also been efficiently manifested for the AAC reaction [28–43]. Among the 12 principles of green chemistry, the use of non-toxic and/or volatile organic solvents, minimal generation of organic wastes, atom economic synthesis and the use of environmentally benign chemicals have introduced an upsurging interest in contemporary organic synthesis. This field is also emerging with the use of various nonconventional energy sources, such as microwave, ultrasound, mechanical mixing, electrochemical methods and visible-light-driven organic transformations [44]. Complementing solution-based synthesis, the mechanochemical operations

provide an environmentally benign alternative to negate the demand for bulk organic solvents, thereby finding an application in a plethora of organic transformations [45–51]. In a broader sense, the application of mechanical energies such as compression, shearing or friction under solvent-free conditions have been promising techniques for the utilization of mechanoresponsive materials to access active pharmaceutical ingredients (API) and thereby making a strong impact for pharmaceutical industries [52]. This technique also provides a cleaner source of energy for organic transformations. In 2011, the planetary ball mill was used by Schubert et al. for a solvent-free AAC reaction using catalytic amounts of $Cu(OAc)_2$ and sodium ascorbate [53]. Later on, several reports for the solvent-free synthesis of 1,2,3-triazoles were completed in which a homogeneous Cu catalyst or stoichiometric amount of Cu powder were used [54–56]. To enhance the catalyst regeneration in these reactions, the immobilization of copper on the heterogenous matrix has been employed. In 2013, Ranu et al. efficiently demonstrated Cu/Al_2O_3 as catalyst for the AAC reaction under ball milling without using any solvent and additive [57] (Scheme 1a). Recently, Amini et al. showed the catalytic activity of immobilised Cu NPs on WO3 surface for the AAC reaction under solvent-free conditions [58]. For the first time, the Mack laboratory introduced the use of Cu-vial and 3/16" Cu ball in an efficient AAC reaction under 16 h milling in solvent-free conditions [59] (Scheme 1b).

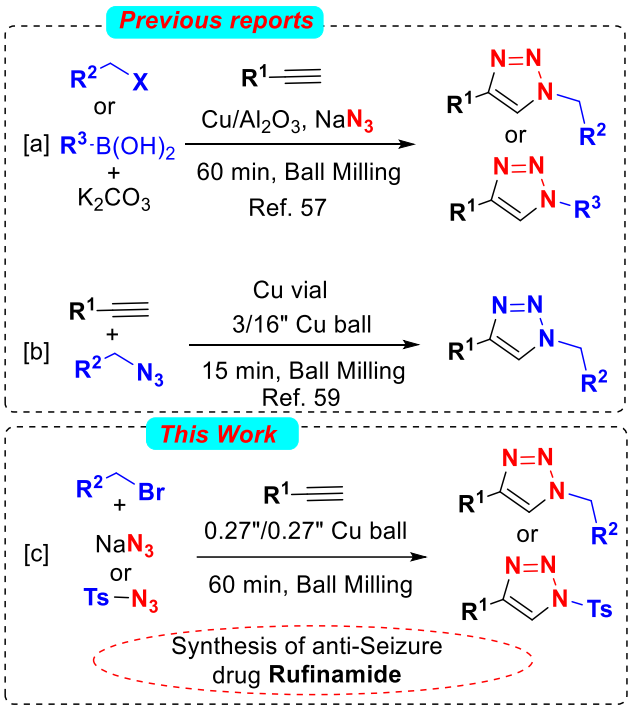

Scheme 1. Mechanochemical strategies of CuAAC reaction. (**a**) Previous approach of AAC reaction using Cu/Al_2O_3 as catalyst under ball milling; (**b**) Previous approach using Cu-vial and 3/16" Cu ball under ball milling; (**c**) The present approach under ball milling conditions.

In their strategy, three component reactions such as phenylacetylene, benzyl bromide and sodium azide, on grinding for 16h, afforded the desired 1-benzyl-4-phenyltriazole in quantitative yield under the one-step, one-vial multicomponent CuAAC reaction.

Epilepsy is a chronic neurological disorder in the brain that affects people of all ages worldwide. Rufinamide (brand name Banzel [60] or Inovelon [61], developed by Novartis and manufactured by Eisai) has been already reported as a sodium channel blocker and an antiepileptic drug (AED) with a broad spectrum of efficacy. It is an FDA-approved orphan drug used for the adjunctive treatment of seizures associated with Lennox–Gastaut syndrome (LGS). The common strategies for the synthesis of Rufinamide involve 1,3-dipolar cycloaddition reaction using 2-chloroacrylonitrile, propiolic acid and esters or (E)-methyl 3-

methoxyacrylate [62–67]. Recent synthetic developments involve flow microreactor systems via multistep synthesis in a compartmentalized continuous flow integrated with in-line separation techniques [68–71]. We envisioned that mechanochemical conditions could be useful for the synthesis of Rufinamide and its analogs via [2+3] CuAAC reaction and, to the best of our knowledge, this approach is still uncommon in the literature. Herein we wish to report a mechanochemical strategy of 1,3-dipolar Huisgen cycloaddition of various azides, generated in situ, with a dipolarophile (alkyne) to construct structurally important 1,2,3-triazoles as well as Rufinamide and its analogs by using Cu beads (Scheme 1c).

2. Results and Discussion

At the commencement of our investigation, we chose 4-ethylnyl toluene (**1a**) and 2-bromo-1-(*m*-tolyl)ethan-1-one (**2a**) as bench stable substrates to react in the presence of inorganic azide. Different mechanochemical parameters of the reaction such as time, rpm limit, equivalency, and number of copper balls were optimized in order to obtain the desired 1,2,3-triazoles in the highest yield. The results of the optimization of the mechanochemical reaction conditions are reported below (Table 1). Thus, we have observed that **1a** (50 mg, 0.431 mmol), **2a** (183.6 mg, 0.862 mmol) and NaN_3 (56 mg, 0.862 mmol) satisfactorily afforded **3a** in 86% of yield under neat reaction conditions for 3h of mechanochemical grinding with 5-Cu beads at 500 rpm (Table 1, Entry 4). Intriguingly, the overall yield of the triazoles also depends on the number of Cu beads in the reaction (Figure 1).

Table 1. Mechanochemical optimization of reaction parameters [1].

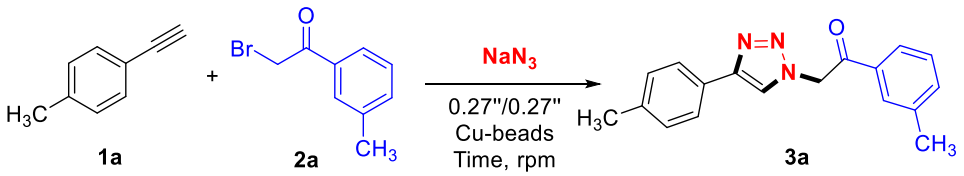

Entry	Equiv. of Azide	RPM	Time (h)	Conversion (%)	Selectivity (%)	Yields (%) [2]
1	1.2	300	1	68	35	24
2	1.2	400	2	80	70	56
3	1.2	500	3	88	89	79
4	2.0	500	3	98	88	86
5	2.0	500	4	98	88	86
6	2.0	400	3	82	78	64
7	2.4	500	3	98	88	86

[1] Reaction conditions: **1a** (0.431 mmol), **2a** (0.862 mmol), sodium azide (0.862 mmol), 5-Cu beads, 500 rpm; [2] yields refer after chromatographic purification.

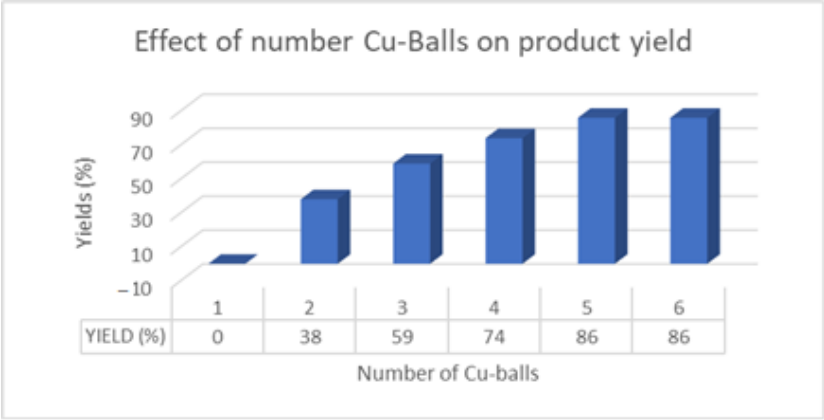

Figure 1. Effect of cylindrical Cu beads (0.27/0.27″) on the product yield.

These conditions were useful for the further assessment of the various alkynes and benzoylmethyl bromides. We did not observe much electronic control of different alkynes as well as benzoylmethyl bromides over the reaction yield for the three component reactions, and products **3b**–**d** were obtained in 63–73% yield. In all the cases we isolated unreacted starting alkynes in small quantities. In the case of biphenyl acetylene, the observed yield of the product **3e** was 42% and the conversion of the starting material was poor. The poor yield may be attributed to the three-component reaction in the presence of unactivated copper beads, as well as the low reactivity of sterically and electronically unfavorable alkyne species. Changing the equivalency or the grinding time did not improve the yield of the desired product significantly. To our delight, an excellent yield of **3e** was found by changing the reaction technique. The same reaction was carried out in a stepwise fashion, in which the benzoylmethyl bromide derivatives were first converted into corresponding azido derivatives (see Supplementary Materials) and then employed under optimized mechanochemical conditions. Then, we introduced structurally interesting and highly sterically hindered alkynes for the anticipated CuAAC reaction. Under the conditions of three-component coupling, we again encountered low-to-moderate yield for the compounds **3f**–**k** (Figure 2). However, the stepwise fashion of the mechanochemical reaction gave excellent yield of the products **3f**–**k** (Figure 2). In all these reactions, benzoylmethyl bromide derivatives had no marked effect on the yield of the final 1,2,3-triazole derivatives (Figure 2). It is noteworthy that the mechanochemical synthesis of 1,2,3-triazole lead to the formation of only 1,4- regioisomers and formation of 1,2-isomers were not observed. Owing to the inherent biological activity of the sulphonamides, we have targeted triazole based sulphonamides molecules under mechanochemical conditions (Figure 3). We encountered the low yield of products in the case of three-component mechanochemical coupling of alkynes, sodium azides and tosylchlorides. Therefore, the tosylazides (**4a**) were prepared using the reported conditions (see Supplementary Materials) and then employed in the 1,3-dipolar cycloaddition. In all cases, good-to-excellent yield of the triazole-based sulphonamides **5a**–**e** were observed. Interestingly, only the formation of 1,4-regioisomer was observed to have excellent selectivity.

Finally, to confirm the structure of the obtained products, single-crystal XRD experiments were carried out for the 1,2,3-triazole **3b,** and the obtained single-crystal XRD structure is presented below (Figure 4).

To demonstrate the synthetic utility of the present reaction, we successfully prepared Rufinamide (compound **7f**), a commercially available antiepileptic drug (AED) and its Cl-analogue (compound **6f**) in good overall yields (Scheme 2). The Cl-analogue of Rufinamide was prepared by starting from easily available 2,6-dichloro benzaldehyde precursor followed by the synthesis of 2,6-dichlorobenzyl azides (see Supplementary Materials). Without any tedious purification of these organic azides, we treated with propiolic esters under optimised mechanochemical grinding using copper beads. The ethyl ester of the propiolic acid under our optimised mechanochemical conditions gave the formation of the desired 1,4-isomer only compared to the methyl ester derivative of propiolic acid derivatives. To our delight, we observed the formation of yellow crude after the reaction which contained only 1,4-regioisomer (**6e**) as a major product and gave 67% yield after purification. We have also observed that the mechanochemical conditions gave better results in the case of two-component reactions, i.e., alkyne and organic azide, rather than three. The triazlic esters (**6e**) can be easily converted into the amide derivatives using treatment with ammonia water in methanol. A similar experimental procedure was followed for the synthesis of the commercially available drug Rufinamide **7f** in 79% of overall yield with greater selectivity (Scheme 2).

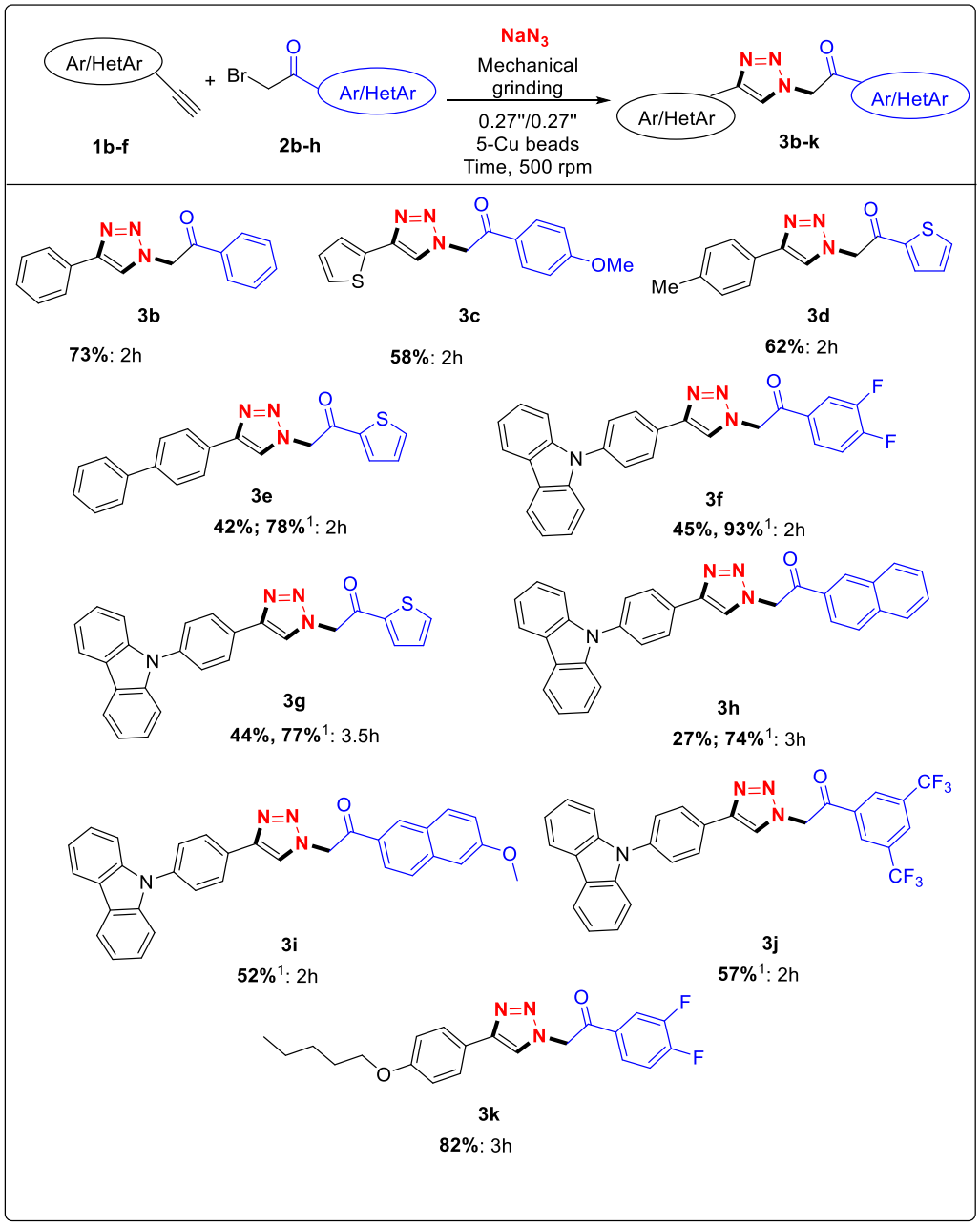

Figure 2. Scope of various alkynes and benzoylmethyl bromides in mechanochemical CuAAC reaction. Reaction conditions: Ar/HetAr alkynes **1b–f** (1 equiv.), benzoylmethyl bromides **2b–h** (1.2 equiv.), sodium azide (1.2 equiv.), 5-Cu beads, 500 rpm; [1] stepwise route.

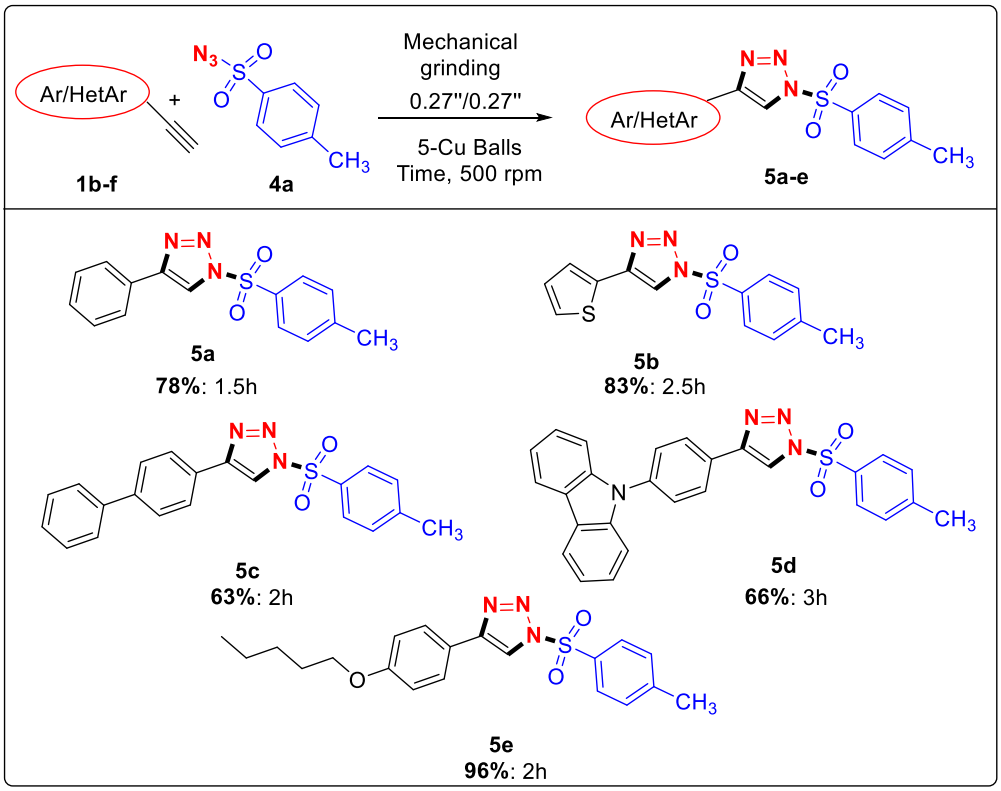

Figure 3. Scope of various alkynes in CuAAC with tosyl azides under mechanochemical conditions. Reaction conditions: Ar/HetAr alkynes **1b–f** (1 equiv.), tosyl azide **4a** (1.2 equiv.), 5-Cu beads, 500 rpm.

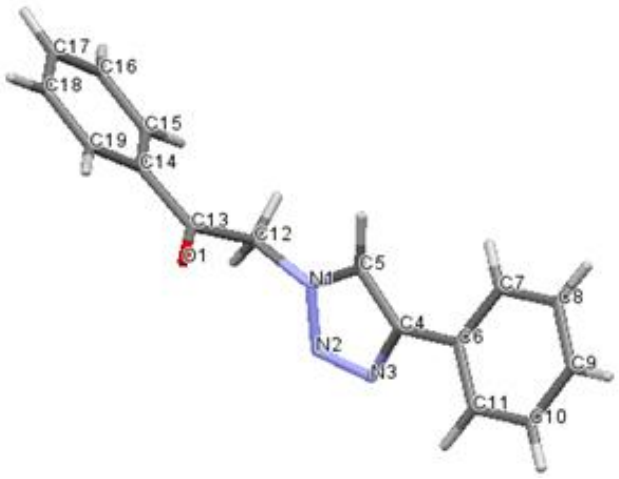

Figure 4. Single crystal XRD structure of **3b**. CCDC number for the compound **3b** is 2123952.

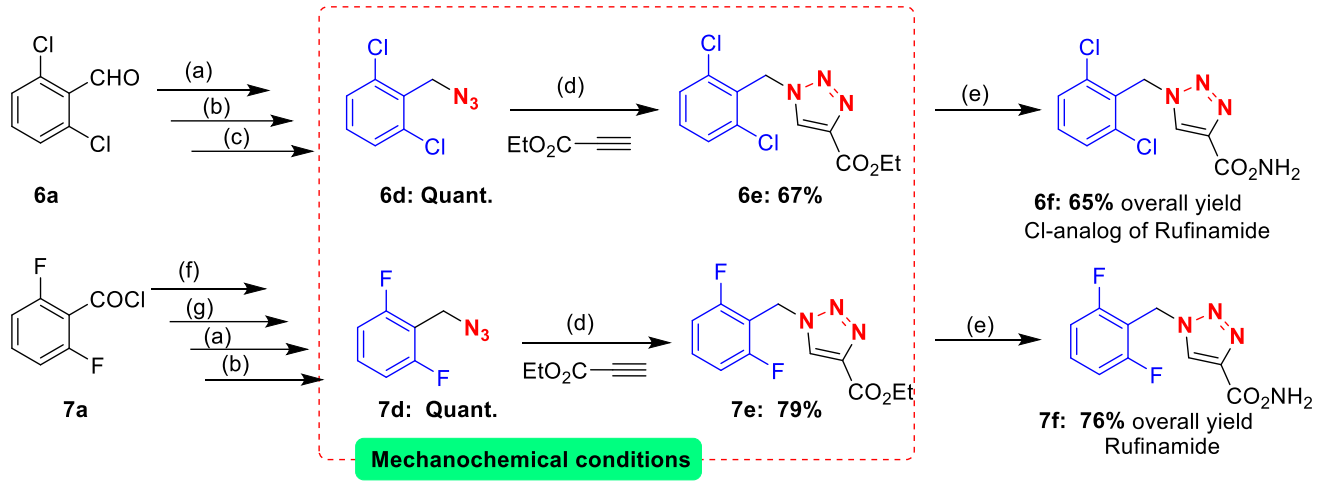

Reaction conditions: (a) $NaBH_4$ (2.5 equiv.) in CH_3OH for 2 h at rt; (b) PBr_3 (1.1 equiv.) in DCM at 0°C for 12 h; (c) NaN_3 (4 equiv.) in acetone/water for 6 h at rt; (d) Alkyne (0.8 equiv.), Azide (1.0 equiv.), Mechanical grinding: 0.27"/0.27" 5-Cu beads, 500 rpm, 2 h; (e) NH_4OH in CH_3OH under reflux; (f) NEt_3 (1 equiv.) in ethanol at 60 °C for 2h; (g) $LiAlH_4$ in dry THF at 60 °C for 2 h.

Scheme 2. Total synthesis of anti-seizure drug Rufinamide and analogues.

Plausible Catalytic Pathway

From the previous discussions, we have observed the in situ generation of stable and isolable organic azides (**IIA**) as the key intermediate, followed by 1,2,3-triazole formation. In some cases, we also performed reactions between the alkynes and organic azides to enhance the overall yield. Based on the previous literature reports [72–76] and the above experimental findings, a plausible reaction mechanism is suggested as shown in Figure 5. The proposed catalytic cycle for the CuAAC of alkynes with the azides consists of an initial copper acetylide formation to afford intermediate **I**. We surmised that, in the catalytic cycle, NaN_3 can change the valence state of Cu during the reaction and that this might be responsible for the observed activity [77,78]. The Cu(I) species reacts with an alkyne to create a copper acetylide. On the other hand, benzoylmethyl bromides react with sodium azides to form benzoylmethyl azides, **IIA**, which are one of the key intermediates in the catalytic cycle. The 1,3-dipolar cyclization of the resulting dinuclear copper intermediate (**III** and **IV**) and benzoylmethyl azides **IIA**, followed by protonation, provided the formation of target 1,2,3-triazole **VI** and the regeneration of the Cu catalyst. The generation of intermediate **III** and **IV** is supported by reference [73]. It worth mentioning that Cu-beads are recyclable, and after sonication with acetone the Cu-beads can be returned to the reaction without losing both the grinding performance and the catalytic activity.

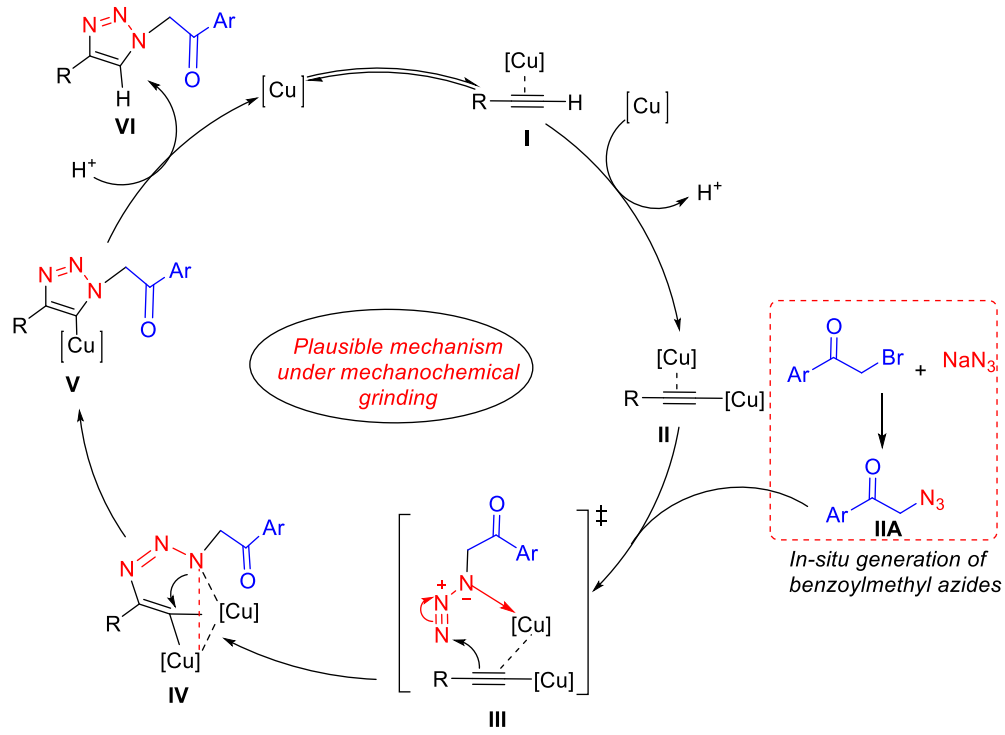

Figure 5. Plausible reaction pathway of the Huisgen cycloaddtion.

3. Conclusions

In summary, we have developed a regiospecific, environmentally benign mechanochemical grinding for a 1,3-dipolar Huisgen cycloaddition reaction between terminal alkynes and azides using Cu-beads. Highly functionalized 1,2,3-triazoles were prepared selectively in good-to-excellent yield using an easy workup technique and without generation of unwanted waste. This energy- and cost-effective process has also been extended for the synthesis of Rufinamide, a commercially available antiepileptic drug (AED) and its Cl-analog. The crystallographic data of the triazole molecule also established structural confirmation. Furthermore, the in silico studies of the prepared molecules are still under investigation and the results will be published in due course. Finally, this research may encourage the synthetic community to develop active pharmaceutical ingredients using greener energy sources and impact the pharmaceutical industries.

4. Experimental Section

General experimental procedure for the mechanochemical cycloaddition reaction: PM100 stainless steel grinding bowl with an internal volume of 25 mL, containing 0.27/0.27-inch cylindrical copper beads (5 beads) was charged with alkynes (1 equivalent), equimolar quantities of benzoylmethylbromide (2 equiv. unless otherwise mentioned) and sodium azide (2 equiv. otherwise mentioned). The grinding bowl was then equipped with a stainless steel bowl cap and placed in the mechanical ball milling instrument. The reaction mixture within the grinding bowl was allowed to rotate for 3 h (unless otherwise mentioned) at the speed of 500 rpm. The progress of the reaction was monitored by the TLC and the reaction mixture was extracted with dichloromethane. The crude was concentrated under reduced pressure and the product was isolated using silica gel (230–400) column chromatography under hexane/ethylacetate gradient.

Supplementary Materials: The following are available online at https://www.mdpi.com/article/10.3390/molecules27227784/s1, Figure S1: GC-MS of azidation of tosylchloride, Figure S2: Synthesis of 2,6-dichlorobenzyl azide from its aldehyde precursor, Figure S3: Reduction of 2,6-difluorobenzoyl chloride to 2,6-difluorobenzyl azide, Figure S4: Spectral data (^{1}H, ^{13}C, GC-MS) for synthesized compounds, Figure S5: ORTEP diagram of compound **3b [79]**.

Author Contributions: Conceptualization, D.B., S.S. and G.V.Z.; methodology, D.B., I.S.K., D.S.K., M.R. and R.P.; software, I.S.K., D.S.K., P.D. and R.P.; validation, S.S., G.V.Z., P.D., V.L.R. and O.N.C.; formal analysis, D.B., P.D. and R.P.; investigation, D.B. and S.S.; resources, S.S. and G.V.Z.; data curation, D.B., M.R., P.D. and R.P.; writing—original draft preparation, D.B. and S.S.; writing—review and editing, S.S. and G.V.Z.; visualization, S.S., P.D., V.L.R. and O.N.C.; supervision, S.S., G.V.Z. and O.N.C.; project administration, S.S. and G.V.Z.; funding acquisition, S.S. and G.V.Z. All authors have read and agreed to the published version of the manuscript.

Funding: This research was funded by the Ministry of Science and Higher Education of the Russian Federation (ref. # 075-15-2022-1118 dated 29 June 2022).

Institutional Review Board Statement: Not applicable.

Informed Consent Statement: Not applicable.

Data Availability Statement: Data are contained within the article or Supplementary Material.

Conflicts of Interest: The authors declare no conflict of interest.

References

1. Whiting, M.; Muldoon, J.; Lin, Y.-C.; Silverman, S.M.; Lindstrom, W.; Olson, A.J.; Kolb, H.C.; Finn, M.G.; Sharpless, K.B.; Elder, J.H.; et al. Inhibitors of HIV-1 Protease by Using In Situ Click Chemistry. *Angew. Chem. Int. Ed.* **2006**, *45*, 1435–1439. [CrossRef] [PubMed]
2. Kolb, H.C.; Sharpless, K.B. The growing impact of click chemistry on drug discovery. *Drug Discov. Today* **2003**, *8*, 1128–1137. [CrossRef]
3. Giffin, M.J.; Heaslet, H.; Brik, A.; Lin, Y.C.; Cauvi, G.; Wong, C.-H.; McRee, D.E.; Elder, J.H.; Stout, C.D.; Torbett, B.E. A Copper(I)-Catalyzed 1,2,3-Triazole Azide−Alkyne Click Compound Is a Potent Inhibitor of a Multidrug-Resistant HIV-1 Protease Variant. *J. Med. Chem.* **2008**, *51*, 6263–6270. [CrossRef]
4. Fann, W.-Q.; Katritzky, A.R. *Comprehensive Heterocyclic Chemistry*, 2nd ed.; Katritzky, A.R., Rees, C.W., Scriven, E.F.V., Eds.; Elsevier Science: Oxford, UK, 1996; Volume 4, p. 1.
5. Xiong, X.; Tang, Z.; Sun, Z.; Meng, X.; Song, S.; Quan, Z. Supported copper (I) catalyst from fish bone waste: An efficient, green and reusable catalyst for the click reaction toward *N*-substituted 1,2,3-triazoles. *Appl. Organomet. Chem.* **2018**, *32*, e3946. [CrossRef]
6. Yadav, P.; Lal, K.; Kumar, A.; Guru, S.K.; Jaglan, S.; Bhushan, S. Green synthesis and anticancer potential of chalcone linked-1,2,3-triazoles. *Eur. J. Med. Chem.* **2017**, *126*, 944–953. [CrossRef]
7. Joy, M.N.; Bodke, Y.D.; Telkar, S.; Bakulev, V.A. Synthesis of Coumarins Linked With 1,2,3-Triazoles under Microwave Irradiation and Evaluation of their Antimicrobial and Antioxidant Activity. *J. Mex. Chem. Soc.* **2020**, *64*, 53–73. [CrossRef]
8. Joy, M.N.; Beliaev, N.; Beryozkina, T.V.; Bakulev, V.A. Design and the synthesis of 1-heteroaryl-1,2,3-triazoles connected to coumarins via ether linker. *J. Heterocycl. Chem.* **2020**, *57*, 3173–3185. [CrossRef]
9. Brockunier, L.L.; Parmee, E.R.; Ok, H.O.; Candelore, M.R.; Cascieri, M.A.; Colwell, L.F., Jr.; Deng, L.; Feeney, W.P.; Forrest, M.J.; Hom, G.J. Human β_3-adrenergic receptor agonists containing 1,2,3-triazole-substituted benzenesulfonamides. *Bioorganic Med. Chem. Lett.* **2000**, *10*, 2111–2114. [CrossRef]
10. Dheer, D.; Singh, V.; Shankar, R. Medicinal attributes of 1,2,3-triazoles: Current developments. *Bioorganic Chem.* **2017**, *71*, 30–54. [CrossRef]
11. Ryu, E.-H.; Zhao, Y. Efficient Synthesis of Water-Soluble Calixarenes Using Click Chemistry. *Org. Lett.* **2005**, *7*, 1035–1037. [CrossRef]
12. Such, G.K.; Quinn, J.F.; Quinn, A.; Tjipto, E.; Caruso, F. Assembly of Ultrathin Polymer Multilayer Films by Click Chemistry. *J. Am. Chem. Soc.* **2006**, *128*, 9318–9319. [CrossRef] [PubMed]
13. Lober, S.; Rodriguez-Loaiza, P.; Gmeiner, P. Click Linker: Efficient and High-Yielding Synthesis of a New Family of SPOS Resins by 1,3-Dipolar Cycloaddition. *Org. Lett.* **2003**, *5*, 1753–1755. [CrossRef] [PubMed]
14. Lutz, J.-F. 1,3-Dipolar cycloadditions of azides and alkynes: A universal ligation tool in polymer and materials science. *Angew. Chem. Int. Ed.* **2007**, *46*, 1018–1025. [CrossRef] [PubMed]
15. Huisgen, R. 1,3-Dipolar Cycloadditions. *Proc. Chem. Soc.* **1961**, 357–396. [CrossRef]
16. Tornoe, C.W.; Christensen, C.; Meldal, M. Peptidotriazoles on Solid Phase: [1,2,3]-Triazoles by Regiospecific Copper(I)-Catalyzed 1,3-Dipolar Cycloadditions of Terminal Alkynes to Azides. *J. Org. Chem.* **2002**, *67*, 3057–3064. [CrossRef] [PubMed]

17. Rostovtsev, V.V.; Green, L.G.; Fokin, V.V.; Sharpless, K.B. A Stepwise Huisgen Cycloaddition Process: Copper(I)-Catalyzed Regioselective "Ligation" of Azides and Terminal Alkynes. *Angew. Chem. Int. Ed.* **2002**, *41*, 2596–2599. [CrossRef]
18. Meldal, M.; Tornøe, C.W. Cu-Catalyzed Azide−Alkyne Cycloaddition. *Chem. Rev.* **2008**, *108*, 2952–3015. [CrossRef]
19. Tiwari, V.K.; Mishra, B.B.; Mishra, K.B.; Mishra, N.; Singh, A.S.; Chen, X. Cu-Catalyzed Click Reaction in Carbohydrate Chemistry. *Chem. Rev.* **2016**, *116*, 3086–3240. [CrossRef]
20. Joy, M.N.; Beliaev, N.; Beryozkina, T.V.; Bakulev, V.A. A facile access for the synthesis of 1-hetero(aryl)-1,2,3-triazoles linked to equol under mild conditions. *Synth. Commun.* **2020**, *50*, 3086–3092. [CrossRef]
21. Zhu, L.; Brassard, C.J.; Zhang, X.; Guha, P.M.; Clark, R.J. On the Mechanism of Copper(I)-Catalyzed Azide-alkyne Cycloaddition. *Chem. Rec.* **2016**, *16*, 1501–1517. [CrossRef]
22. Sarkar, A.; Santra, S.; Kundu, S.K.; Hajra, A.; Zyryanov, G.V.; Chupakhin, O.N.; Charushin, V.N.; Majee, A. A decade update on solvent and catalyst-free neat organic reactions: A step forward towards sustainability. *Green Chem.* **2016**, *18*, 4475–4525. [CrossRef]
23. Leonardi, M.; Villacampa, M.; Menéndez, J.C. Multicomponent mechanochemical synthesis. *Chem. Sci.* **2018**, *9*, 2042–2064. [CrossRef] [PubMed]
24. Haldón, E.; Nicasio, M.C.; Pérez, P.J. Copper-catalysed azide-alkyne cycloadditions (CuAAC): An update. *Org. Biomol. Chem.* **2015**, *13*, 9528–9550. [CrossRef]
25. Sokolova, N.V.; Nenajdenko, V.G. Recent advances in the Cu(i)-catalyzed azide-alkyne cycloaddition: Focus on functionally substituted azides and alkynes. *RSC Adv.* **2013**, *3*, 16212–16242. [CrossRef]
26. Berg, R.; Straub, B.F. Advancements in the mechanistic understanding of the copper-catalyzed azide-alkyne cycloaddition. *Beilstein J. Org. Chem.* **2013**, *9*, 2715–2750. [CrossRef] [PubMed]
27. Saini, P.; Sonika; Singh, G.; Kaur, G.; Singh, J.; Singh, H. Robust and Versatile Cu(I) metal frameworks as potential catalysts for azide-alkyne cycloaddition reactions: Review. *Mol. Catal.* **2021**, *504*, 111432. [CrossRef]
28. Shil, A.K.; Kumar, S.; Sharma, S.; Chaudhary, A.; Das, P. Polystyrene resin supported palladium(0) (Pd@PR) nanocomposite mediated regioselective synthesis of 4-aryl-1-alkyl/(2-haloalkyl)-1H-1,2,3-triazoles and their N-vinyl triazole derivatives from terminal alkynes. *RSC Adv.* **2015**, *5*, 11506–11514. [CrossRef]
29. Johansson, J.R.; Beke-Somfai, T.; Said Stålsmeden, A.; Kann, N. Ruthenium-Catalyzed Azide Alkyne Cycloaddition Reaction: Scope, Mechanism, and Applications. *Chem. Rev.* **2016**, *116*, 14726–14768. [CrossRef]
30. Meng, X.; Xu, X.; Gao, T.; Chen, B. Zn/C-Catalyzed Cycloaddition of Azides and Aryl Alkynes. *Eur. J. Org. Chem.* **2010**, *2010*, 5409–5414. [CrossRef]
31. Paplal, B.; Nagaraju, S.; Sridhar, B.; Kashinath, D. Regioselective Synthesis of Functionalized 1,2,3-triazoles via Oxidative [3+2]-cycloaddition Using Zn(OAc)2-^{t}BuOOH or ZnO Nanoparticle as Catalyst System in Aqueous Medium. *Catal. Commun.* **2017**, *9*, 115–120. [CrossRef]
32. Morozova, M.A.; Yusubov, M.S.; Kratochvil, B.; Eigner, V.; Bondarev, A.A.; Yoshimura, A.; Saito, A.; Zhdankin, V.V.; Trusova, M.E.; Postnikov, P.S. Regioselective $Zn(OAc)_2$-catalyzed Azide-Alkyne Cycloaddition in Water: The Green Click-chemistry. *Org. Chem. Front.* **2017**, *4*, 978–985. [CrossRef]
33. Sultana, J.; Sarma, D. Ag-catalyzed azide-alkyne cycloaddition: Copper free approaches for synthesis of 1,4-disubstituted 1,2,3-triazoles. *Catal. Rev.* **2020**, *62*, 96–117. [CrossRef]
34. McNulty, J.; Keskar, K.; Vemula, R. The First Well-Defined Silver(I)-Complex- Catalyzed Cycloaddition of Azides onto Terminal Alkynes at Room Temperature. *Chem. Eur. J.* **2011**, *17*, 14727–14730. [CrossRef] [PubMed]
35. McNulty, J.; Keskar, K. Discovery of a Robust and Efficient Homogeneous Silver(I) Catalyst for the Cycloaddition of Azides onto Terminal Alkynes. *Eur. J. Org. Chem.* **2012**, *2012*, 5462–5470. [CrossRef]
36. Ortega-Arizmendi, A.I.; Aldeco-Perez, E.; Cuevas-Yanez, E. Alkyne-Azide Cycloaddition Catalyzed by Silver Chloride and "Abnormal" Silver N-Heterocyclic Carbene Complex. *Sci. World J.* **2013**, *2013*, 186537. [CrossRef] [PubMed]
37. Salam, N.; Sinha, A.; Roy, A.S.; Mondal, P.; Jana, N.R.; Islam, S.M. Synthesis of Silver–Graphene Nanocomposite and Its Catalytic Application for the One-pot Three component Coupling Reaction and One-pot Synthesis of 1,4-disubstituted 1,2,3-triazoles in Water. *RSC Adv.* **2014**, *4*, 10001–10012. [CrossRef]
38. Basu, P.; Bhanja, P.; Salam, N.; Dey, T.K.; Bhumik, A.; Das, D.; Islam, S.M. Silver Nanoparticles Supported over Al_2O_3@Fe_2O_3 Core-shell Nanoparticles as an Efficient Catalyst for One-pot Synthesis of 1,2,3-triazoles and Acylation of Benzyl Alcohol. *Mol. Catal.* **2017**, *439*, 31–40. [CrossRef]
39. Ferretti, A.M.; Ponti, A.; Molteni, G. Silver(I) Oxide Nanoparticles as a Catalyst in the Azide-Alkyne Cycloaddition. *Tetrahedron Lett.* **2015**, *56*, 5727–5730. [CrossRef]
40. Ali, A.A.; Chetia, M.; Saikia, B.; Saikia, P.J.; Sarma, D. $AgN(CN)_2$/DIPEA/H_2O-EG: A Highly Efficient Catalytic System for Synthesis of 1,4-disubstituted-1,2,3 Triazoles at Room Temperature. *Tetrahedron Lett.* **2015**, *56*, 5892–5895. [CrossRef]
41. Rao, H.S.P.; Chakibanda, G. Raney Ni Catalyzed Azide-alkyne Cycloaddition Reaction. *RSC Adv.* **2014**, *4*, 46040–46048. [CrossRef]
42. Arado, O.D.; Monig, H.; Wagner, H.; Franke, J.-H.; Langewisch, G.; Held, P.A.; Studer, A.; Fuchs, H. On-surface Azide-alkyne Cycloaddition on Au(111). *ACS Nano* **2013**, *7*, 8509–8515. [CrossRef] [PubMed]
43. Boominathan, M.; Pugazhenthiran, N.; Nagaraj, M.; Muthusubramanian, S.; Murugesan, S.; Bhuvanesh, N. Nanoporous Titania-Supported Gold Nanoparticle-Catalyzed Green Synthesis of 1,2,3-triazoles in Aqueous Medium. *ACS Sustain. Chem. Eng.* **2013**, *1*, 1405–1411. [CrossRef]

44. Margetić, D.; Štrukil, V. *Mechanochemical Organic Synthesis*; Elsevier: Boston, MA, USA, 2016; pp. 351–360.
45. Kubota, K.; Ito, H. Mechanochemical Cross-Coupling Reactions. *Trends Chem.* **2020**, *2*, 1066–1081. [CrossRef]
46. Do, J.-L.; Friscic, T. Mechanochemistry: A Force of Synthesis. *ACS Cent. Sci.* **2017**, *3*, 13–19. [CrossRef] [PubMed]
47. Andersen, J.; Mack, J. Mechanochemistry and organic synthesis: From mystical to practical. *Green Chem.* **2018**, *20*, 1435–1443. [CrossRef]
48. Howard, J.L.; Cao, Q.; Browne, D.L. Mechanochemistry as an emerging tool for molecular synthesis: What can it offer? *Chem. Sci.* **2018**, *9*, 3080–3094. [CrossRef]
49. Bolm, C.; Hernández, J.G. Mechanochemistry of gaseous reactants. *Angew. Chem. Int. Ed.* **2019**, *58*, 3285–3299. [CrossRef]
50. Hernández, J.G.; Bolm, C. Altering Product Selectivity by Mechanochemistry. *J. Org. Chem.* **2017**, *82*, 4007–4019. [CrossRef]
51. Stolle, A.; Szuppa, T.; Leonhardt, S.E.S.; Ondruschka, B. Ball milling in organic synthesis: Solutions and challenges. *Chem. Soc. Rev.* **2011**, *40*, 2317–2329. [CrossRef]
52. Baig, R.B.N.; Varma, R.S. Alternative energy input: Mechanochemical, microwave and ultrasound-assisted organic synthesis. *Chem. Soc. Rev.* **2012**, *41*, 1559–1584. [CrossRef]
53. Thorwirth, R.; Stolle, A.; Ondruschka, B.; Wild, A.; Schubert, U.S. Fast, ligand- and solvent-free copper-catalyzed click reactions in a ball mill. *Chem. Commun.* **2011**, *47*, 4370–4372. [CrossRef] [PubMed]
54. Sahu, A.; Agrawal, R.K.; Pandey, R.K. Synthesis and systemic toxicity assessment of quinine-triazole scaffold with antiprotozoal potency. *Bioorganic Chem.* **2019**, *88*, 102939. [CrossRef] [PubMed]
55. Tireli, M.; Maračić, S.; Lukin, S.; Kulcsár, M.J.; Žilić, D.; Cetina, M.; Halasz, I.; Raić-Malić, S.; Užarević, K. Solvent-free copper-catalyzed click chemistry for the synthesis of *N*-heterocyclic hybrids based on quinoline and 1,2,3-triazole. *Beilstein J. Org. Chem.* **2017**, *13*, 2352–2363. [CrossRef]
56. Rinaldi, L.; Martina, K.; Baricco, F.; Rotolo, L.; Cravotto, G. Solvent-Free Copper-Catalyzed Azide-Alkyne Cycloaddition under Mechanochemical Activation. *Molecules* **2015**, *20*, 2837–2849. [CrossRef] [PubMed]
57. Mukherjee, N.; Ahammed, S.; Bhadra, S.; Ranu, B.C. Solvent-free one-pot synthesis of 1,2,3-triazole derivatives by the 'Click' reaction of alkyl halides or aryl boronic acids, sodium azide and terminal alkynes over a Cu/Al_2O_3 surface under ball-milling. *Green Chem.* **2013**, *15*, 389–397. [CrossRef]
58. Amini, M.; Hajipour, E.; Akbari, A.; Chae, K.H. Immobilization of copper nanoparticles on WO_3 with enhanced catalytic activity for the synthesis of 1,2,3-triazoles. *Appl. Organomet. Chem.* **2020**, *34*, e5959. [CrossRef]
59. Cook, T.L.; Walker, J.A.; Mack, J. Scratching the catalytic surface of mechanochemistry: A multicomponent CuAAC reaction using a copper reaction vial. *Green Chem.* **2013**, *15*, 617–619. [CrossRef]
60. Available online: https://www.webmd.com/drugs/2/drug-151652/banzel-oral/details (accessed on 6 November 2022).
61. Available online: https://www.ema.europa.eu/en/medicines/human/EPAR/inovelon (accessed on 6 November 2022).
62. Portmann, R.; Novartis, A.G. Process for preparing 1-substituted 4-cyano-1,2,3-triazoles. U.S. Patent 6,156,907, 5 December 2000.
63. Attolino, E.; Colombo, L.; Mormino, I.; Allegrini, P. Method for the preparation of rufinamide. US Patent 2010/0234616 A1, 16 September 2010.
64. Attolino, E.; Colombo, L.; Mormino, I.; Allegrini, P. Method for the preparation of rufinamide. US Patent 8,198,459 B2, 12 June 2012.
65. De Leon Martin, A.A.; Bellmunt, J.B.; Clotet, J.H.; Carandell, L.S.; Pasecual, G.F.; Bertran, J.C.; Barjoan, P.D. Process for preparing rufinamide intermediate. US Patent 2013/0045998 A1, 21 February 2013.
66. Kankan, R.N.; Rao, D.R.; Birari, D.R. Process for the preparation of rufinamide. WO Patent 2010/043849, 22 April 2010.
67. Mudd, W.H.; Stevens, E.P. An efficient synthesis of rufinamide, an antiepileptic drug. *Tetrahedron Lett.* **2010**, *51*, 3229. [CrossRef]
68. Padmaja, R.D.; Chanda, K. A Short Review on Synthetic Advances towards the Synthesis of Rufinamide, an Antiepileptic Drug. *Org. Process Res. Dev.* **2018**, *22*, 457–466. [CrossRef]
69. Borukhova, S.; Noël, T.; Metten, B.; de Vos, E.; Hessel, V. From alcohol to 1,2,3-triazole via a multi-step continuous-flow synthesis of a rufinamide precursor. *Green Chem.* **2016**, *18*, 4947. [CrossRef]
70. Zhang, P.; Russell, M.G.; Jamison, T.F. Continuous Flow Total Synthesis of Rufinamide. *Org. Process Res. Dev.* **2014**, *18*, 1567–1570. [CrossRef]
71. Jiao, J.; Nie, W.; Yu, T.; Yang, F.; Zhang, Q.; Aihemaiti, F.; Yang, T.; Liu, X.; Wang, J.; Li, P. Multi-Step Continuous-Flow Organic Synthesis: Opportunities and Challenges. *Chem. Eur. J.* **2021**, *27*, 4817–4838. [CrossRef] [PubMed]
72. Hein, J.E.; Fokin, V.V. Copper-catalyzed azide-alkynecycloaddition (CuAAC) and beyond: New reactivity of copper(I) acetylides. *Chem. Soc. Rev.* **2010**, *39*, 1302–1315. [CrossRef] [PubMed]
73. Worrell, B.T.; Malik, J.A.; Fokin, V.V. Direct Evidence of a Dinuclear Copper Intermediate in Cu(I)-Catalyzed Azide-Alkyne Cycloadditions. *Science* **2013**, *340*, 457–460. [CrossRef]
74. Zhou, H.; Jian, W.; Qian, B.; Ye, C.; Li, D.; Zhou, J.; Bao, H. Copper-Catalyzed Ligand-Free Diazidation of Olefins with $TMSN_3$ in CH_3CN or in H_2O. *Org. Lett.* **2017**, *19*, 6120–6123. [CrossRef]
75. Yuan, Y.-A.; Lu, D.-F.; Chen, Y.-R.; Xu, H. Iron-Catalyzed Direct Diazidation for a Broad Range of Olefins. *Angew. Chem. Int. Ed.* **2016**, *55*, 534–538. [CrossRef]
76. Yamada, Y.M.A.; Sarkar, S.M.; Uozumi, Y. Amphiphilic Self-Assembled Polymeric Copper Catalyst to Parts per Million Levels: Click Chemistry. *J. Am. Chem. Soc.* **2012**, *134*, 9285–9290. [CrossRef]

77. Mohammed, S.; Padala, A.K.; Dar, B.A.; Singh, B.; Sreedhar, B.; Vishwakarma, R.A.; Bharate, S.B. Recyclable clay supported Cu (II) catalyzed tandem one-pot synthesis of 1-aryl-1,2,3-triazoles. *Tetrahedron* **2012**, *68*, 8156–8162. [CrossRef]
78. Kuang, G.-C.; Michaels, H.A.; Simmons, J.T.; Clark, R.J.; Zhu, L. Chelation-Assisted, Copper(II)-Acetate-Accelerated Azide−Alkyne Cycloaddition. *J. Org. Chem.* **2010**, *75*, 6540–6548. [CrossRef]
79. Curphey, T.J. Preparation of p-Toluenesulfonyl Azide. A Cautionary Note. *Org. Prep. Proced. Int.* **1981**, *13*, 112–115. [CrossRef]

molecules

MDPI

Article

Electrochemically Induced Synthesis of Imidazoles from Vinyl Azides and Benzyl Amines

Vera A. Vil', Sergei S. Grishin and Alexander O. Terent'ev *

N. D. Zelinsky Institute of Organic Chemistry, Russian Academy of Sciences, 47 Leninsky Prospect, Moscow 119991, Russia

* Correspondence: terentev@ioc.ac.ru

Abstract: An electrochemically induced synthesis of imidazoles from vinyl azides and benzyl amines was developed. A wide range of imidazoles were obtained, with yields of 30 to 64%. The discovered transformation is a multistep process whose main steps include the generation of electrophilic iodine species, 2*H*-azirine formation from the vinyl azide, followed by its reactions with benzyl amine and with imine generated from benzyl amine. The cyclization and aromatization of the obtained intermediate lead to the target imidazole. The synthesis proceeds under constant current conditions in an undivided cell. Despite possible cathodic reduction of various unsaturated intermediates with C=N bonds, the efficient electrochemically induced synthesis of imidazoles was carried out.

Keywords: electrochemistry; imidazoles; vinyl azides

Citation: Vil', V.A.; Grishin, S.S.; Terent'ev, A.O. Electrochemically Induced Synthesis of Imidazoles from Vinyl Azides and Benzyl Amines. *Molecules* **2022**, *27*, 7721. https://doi.org/10.3390/molecules27227721

Academic Editors: Alexey M. Starosotnikov, Maxim A. Bastrakov and Igor L. Dalinger

Received: 24 October 2022
Accepted: 7 November 2022
Published: 9 November 2022

1. Introduction

The imidazole family of N-heterocycles is widely found in natural products and pharmaceutical compounds [1–5]. Additionally, imidazoles are used in organic chemistry and material design [6,7]. As a result, various methods have been developed to synthesize 1,2,4-trisubstituted-(1*H*)-imidazoles [8–10]. Substituted imidazoles were obtained from aryl ketones and benzylamines using N-heterocyclic carbene (NHC)/$BF_3{\cdot}Et_2O$/*tert*-butyl hydroperoxide (TBHP) [11], CuI/$BF_3{\cdot}Et_2O/O_2$ [12], I_2/HCl/O_2 [13], and $NaIO_4$/2,2,6,6-tetramethylpiperidin-1-yl)oxyl (TEMPO) [14] systems (Scheme 1a). The electrochemical cyclization of aryl ketones [15,16] with benzyl amines into 1,2,4-trisubstituted-(1*H*)-imidazoles was also reported (Scheme 1a). Approaches to 1,2,4-trisubstituted imidazoles via cyclization of enamides [17] and enamines [18] with benzyl amines were developed. However, there are some problems associated with these strategies, due to necessity of stoichiometric chemical reagents or heavy metal residues. Therefore, metal-free and stoichiometric-oxidant-free multicomponent strategies for the synthesis of imidazoles are highly desirable.

Vinyl azides have versatile reactivity: they can be nucleophiles, electrophiles, 1,3-dipoles, or radical acceptors [19,20]. Due to their ability to eliminate N_2 during transformation, vinyl azides are convenient precursors in organic synthesis [21–23]. It is becoming increasingly popular to use vinyl azides as substrates for the preparation of N-heterocyclic compounds [24]. Oxidative cyclization of vinyl azides and benzyl amines into substituted imidazoles using I_2/TBHP was reported (Scheme 1b) [25].

Nowadays, electro-organic synthesis is considered to be among the areas of organic chemistry with the most active development [26–33]. Currently, much attention is devoted to electrochemical synthesis of heterocyclic structures [34–40], which have always been essential scaffolds in organic chemistry. However, there are only a few examples of the electrochemically induced formation of the C−N bond for the synthesis of heterocyclic compounds such as imidazoles [15,41–43].

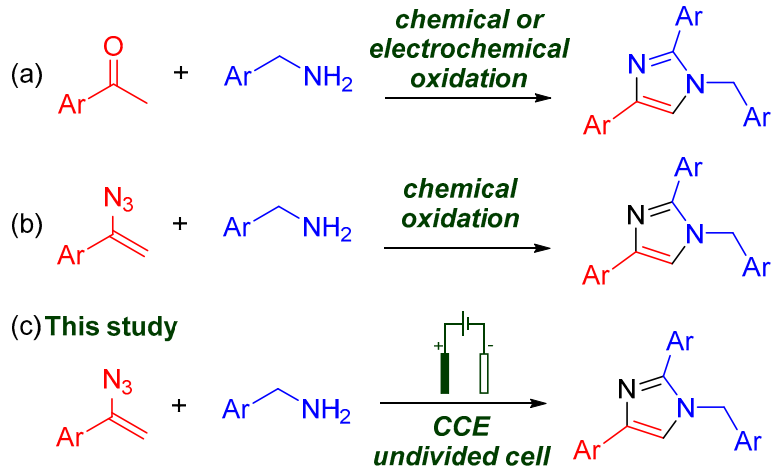

Scheme 1. (**a**,**b**) Known methods for the synthesis of 1,2,4-trisubstituted imidazoles. (**c**) The presented herein method for imidazole synthesis.

The electrolysis can be performed in an undivided or divided cell under controlled potential (CPE) or constant current conditions (CCE). Constant current (CCE) conditions benefit from the high current density, shorter process time, and technically convenient reaction setup. Using an undivided cell is more practical, but at the same time, undesirable processes connected to the counter-electrode action at reaction intermediates must be avoided.

As far as we know, the electrochemical method for the synthesis of substituted imidazoles using vinyl azides has not been disclosed yet. Inspired by the synthetic application of vinyl azides and our experience in the organic electrosynthesis [44], herein, we report an electrochemical approach to imidazoles from vinyl azides and benzyl amines (Scheme 1c).

2. Results and Discussion

We began testing our hypotheses using (1-azidovinyl)benzene **1a** and benzyl amine **2a** as the model substrates in N,N-dimethylformamide (DMF) with tetrabutylammonium iodide (TBAI) as the electrolyte under electrolysis at 30 mA (j = 10 mA/cm^2) with 4.0 F/mol electricity passed, as shown in Table 1. To our delight, the expected 1-benzyl-2,4-diphenyl-1*H*-imidazole (**3a**) was isolated, with a yield of 24% from the crude mixture (entry 1, Table 1). We then investigated other reaction parameters. The detailed optimization of the imidazole electrosynthesis is presented in SI (Table S1).

Screening of electrolytes indicated that KI (37%, entry 2) was superior to TBAI and $LiClO_4$, which gave lower yields (entries 1 and 3, 24% and 22%, respectively). The yield of **3a** has not risen with an increase in benzyl amine amount to 4.0 eq. (entry 4). The addition of *p*-TsOH·H_2O improved the **3a** yield up to 48% (entry 5). The product (**3a**) was isolated, with a yield of 39% with the applied current density 20 mA/cm^2 (entry 6). The yield increased as the amount of electricity passed achieved 6.0 F/mol (entry 7). When the electric current was absent, traces of the product formed (entry 8). Several acids were later screened. When H_2SO_4 or CH_3SO_3H were employed, the expected product (**3a**) was not detected (entries 9, 10); the replacement of *p*-TsOH·H_2O with Amberlyst-15 dramatically lowered the yield (entry 11). To compare the influence of the cathode materials, the reaction was carried out with glassy carbon, stainless steel, and nickel cathodes (entries 12–14). Nickel cathode was almost as effective as platinum (48%, entries 7 and 14), the others were less. Product **3a** was obtained with a yield of 36% when a graphite plate was employed as anode (entry 15), and even lower yield was observed with platinum plate as anode (entry 16). Similar efficiency was obtained when dimethyl sulfoxide (DMSO) (34%, entry 17) was used as a solvent. However, the yield of product **3a** decreased to 18% when the reaction was performed in PhCl (entry 18). The reduction in the temperature to 70 °C led to the best **3a** yield (61%, entry 19). A further reduction in the temperature to 50 °C significantly drops

the yield of the cyclization product, suggesting that the temperature also plays a crucial role in the electrochemical cyclization (entry 20). Under optimal conditions (yield **3a** 61%, entry 19), a complete conversion of **1a** was observed, with no evidence of byproducts that could be isolated.

Table 1. Optimization of imidazole electrosynthesis [1].

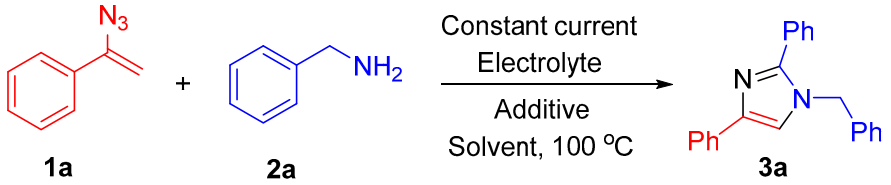

Entry	Cathode/Anode	Electrolyte (eq)	Additive (eq.)	Solvent	Current Density, mA/cm^2	Electricity Passed per 1a, F/mol	Yield 3a, %
1	Pt/GC	TBAI (1.0)	-	DMF	10.0	4.0	24
2	Pt/GC	KI (1.0)	-	DMF	10.0	4.0	37
3	Pt/GC	$LiClO_4$ (1.0)	-	DMF	10.0	4.0	22
4 [2]	Pt/GC	KI (1.0)	-	DMF	10.0	4.0	33
5	Pt/GC	KI (1.0)	*p*-TsOH·H_2O (2.0)	DMF	10.0	4.0	48
6	Pt/GC	KI (1.0)	*p*-TsOH·H_2O (2.0)	DMF	20.0	4.0	39
7	Pt/GC	KI (1.0)	*p*-TsOH·H_2O (2.0)	DMF	20.0	6.0	55
8	Pt/GC	KI (1.0)	*p*-TsOH·H_2O (2.0)	DMF	-	-	7
9	Pt/GC	KI (1.0)	H_2SO_4 (2.0)	DMF	20.0	6.0	-
10	Pt/GC	KI (1.0)	CH_3SO_3H (2.0)	DMF	20.0	6.0	-
11	Pt/GC	KI (1.0)	Amberlyst-15 (2.0)	DMF	20.0	6.0	46
12	GC/GC	KI (1.0)	*p*-TsOH·H_2O (2.0)	DMF	20.0	6.0	15
13	SS/GC	KI (1.0)	*p*-TsOH·H_2O (2.0)	DMF	20.0	6.0	34
14	Ni/GC	KI (1.0)	*p*-TsOH·H_2O (2.0)	DMF	20.0	6.0	48
15	Pt/C	KI (1.0)	*p*-TsOH·H_2O (2.0)	DMF	20.0	6.0	36
16	Pt/Pt	KI (1.0)	*p*-TsOH·H_2O (2.0)	DMF	20.0	6.0	22
17	Pt/GC	KI (1.0)	*p*-TsOH·H_2O (2.0)	DMSO	20.0	6.0	34
18	Pt/GC	KI (1.0)	*p*-TsOH·H_2O (2.0) n-Bu_4NClO_4 (1.0)	PhCl	20.0	6.0	18
19 [3]	Pt/GC	KI (1.0)	*p*-TsOH·H_2O (2.0)	DMF	20.0	6.0	61
20 [4]	Pt/GC	KI (1.0)	*p*-TsOH·H_2O (2.0)	DMF	20.0	6.0	31

[1] General reaction conditions: undivided cell, glassy carbon plate anode/platinum plate cathode (3 cm^2), constant current, **1a** (1.0 mmol, 145.2 mg), **2a** (2.0 mmol, 214.4 mg), solvent (10.0 mL), 100 °C, and air atmosphere. [2] **3a** (4.0 mmol, 428.8 mg). [3] 70 °C. [4] 50 °C.

With the best conditions in hand (Table 1, entry 19), we next turned our attention to the scope of various vinyl azides **1** as depicted in Scheme 2. Substituted (1-azidovinyl)benzenes **1** were subjected to transformation under the reaction conditions. All (1-azidovinyl)benzenes **1** containing electron-donating (e.g., CH_3, *t*-Bu, and OCH_3) as well as electron-withdrawing groups (e.g., F, Br, and Cl) worked well, affording the desired products **3a**–**3i** with yields of 34–64%. (1-Azidovinyl)benzene **1j** with the other azido-group gave the desired product **3j** with a yield of 30%. The aliphatic vinyl azide **1k** did not provide the cyclization product, and the possible reason is insufficient stabilization of the imine-enamine intermediates due to the lack of a conjugated bond system.

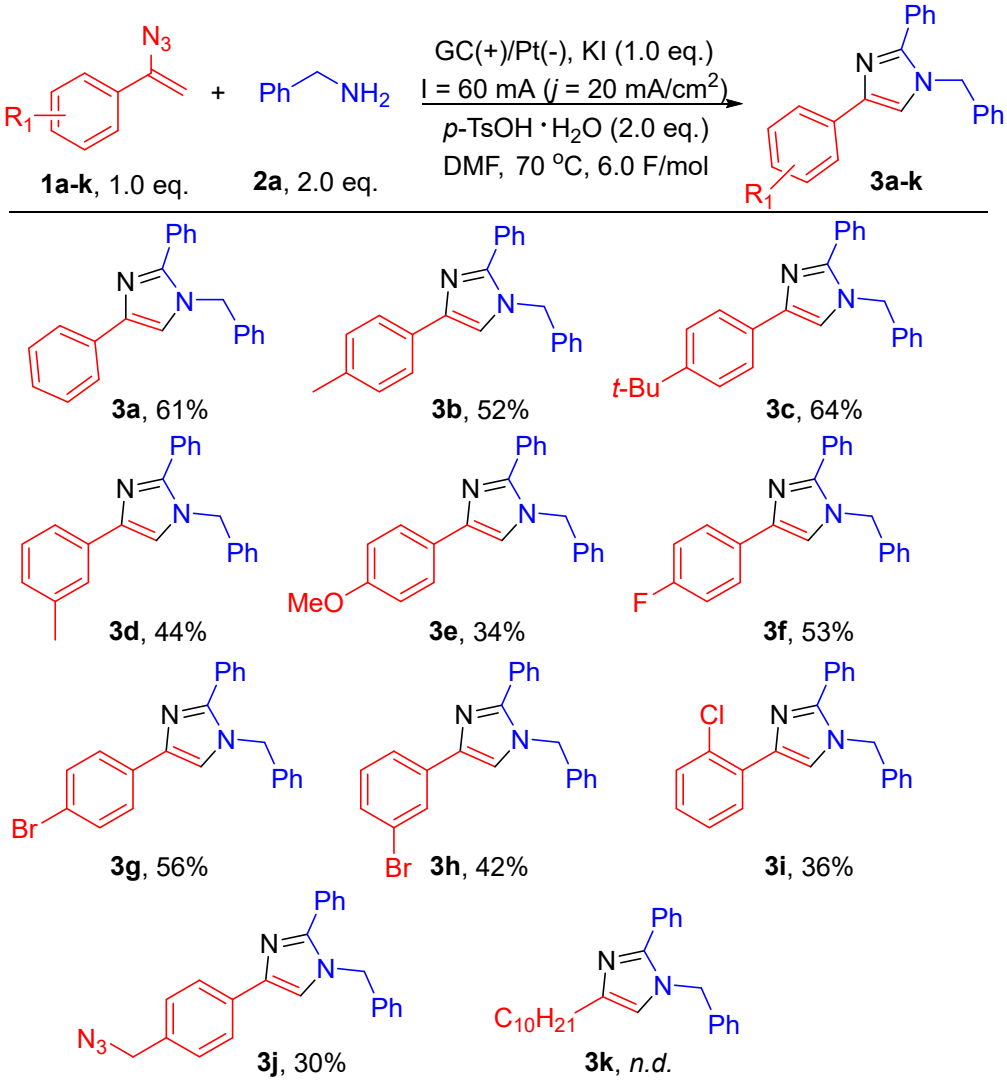

Scheme 2. The scope of vinyl azides **1**.

Subsequently, representative amines **2** with electron-donating and electron-withdrawing groups were evaluated (Scheme 3). The various benzyl amines **2** were suitable for this transformation, giving the desired products **3l**–**p**, with yields of 35–55%. 2-(Aminomethyl)furan and 3-(aminomethyl)pyridine afforded the corresponding products **3q** and **3r** with yields of 38% and 30%, respectively. The application of 1-aminohexane did not lead to the cyclization product.

In order to determine the reaction mechanism, we conducted a series of control experiments (Scheme 4). Firstly, **1a** and **2a** were placed with iodine (4.0 eq.) as the oxidant, so the target product **3a** was not observed, and acetophenone was isolated in a 20% yield (Scheme 4a). This result demonstrated the unique reactivity of the electrochemical system, which is far more complex than the iodine generation. Moreover, ω-iodoacetophenone **4** and acetophenone **5**, instead of **1a**, were investigated under electrochemical conditions (Scheme 4b,c). The reaction of ω-iodoacetophenone **4** with benzyl amine **2a** did not lead to the desired imidazole **3a**, unlike the reaction of acetophenone **5** with benzyl amine **2a**. The imidazole **3a** was synthesized from acetophenone, **5** with a low yield of 14% under optimal conditions (Scheme 4c). These results implied that the iodination of α-carbon in the vinyl substrate might not be the required reaction step. The substrate **2a** was employed to react with 3-phenyl-2*H*-azirine **6**; the product **3a** was obtained with a yield of 35%, thus 3-phenyl-2*H*-azirine **6** might be the intermediate in electrochemically induced synthesis of substituted imidazoles (Scheme 4d).

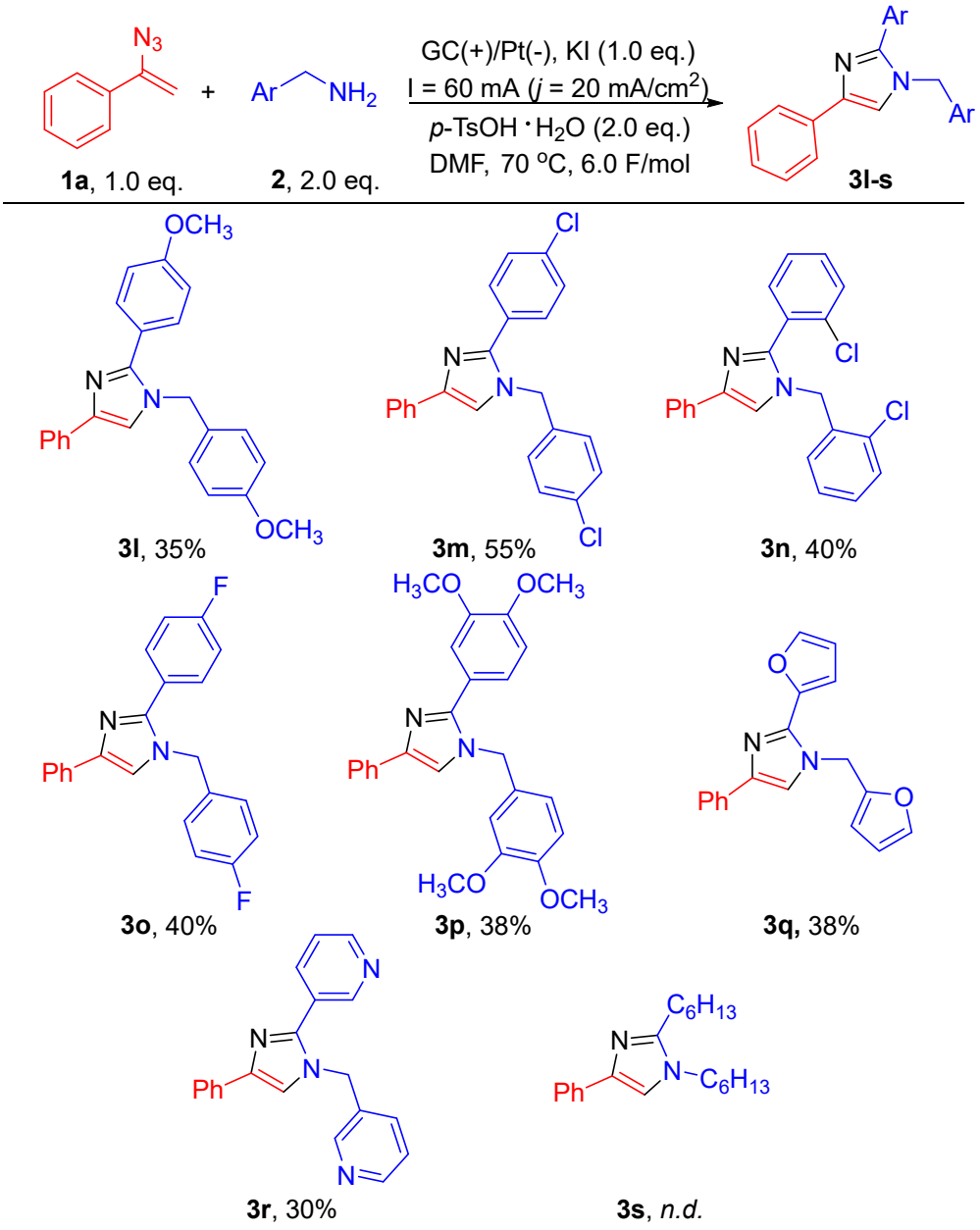

Scheme 3. The scope of benzyl amines **2**.

To understand the influence of the cathodic processes and *p*-TsOH on the yield of **3a**, we performed comparative electrochemical experiments in undivided and divided electrochemical cells (Scheme 5). There is no significant difference in **3a** yield between an undivided and divided electrochemical cells in the presence of *p*-TsOH. Without acid the reaction in the divided cell resulted in higher yields than in the undivided one. So, in the undivided cell, an acid is likely reduced on the cathode, preventing cathodic side processes.

Cyclic voltammetry (CV) was used to study the redox potentials of the substrates (Figure 1). The mixture of DMF and *p*-TsOH·H_2O did not show considerable reactivity in anodic oxidation under the potential below 1.4 V (curve a). The KI demonstrated two reversible anodic waves at 0.4 and 0.9 V in the presence of the acid, which is in accordance with the triiodide (I_3^-) and iodine (I_2) formation (curve b) [45]. The CV of vinyl azide **1a** and *p*-TsOH·H_2O exhibited a broad and reversible wave above 1.0 V (curve c). The mixture of benzyl amine **2a** and *p*-TsOH·H_2O turned out to be electrochemically inert under the potential below 1.5 V (curve d). The addition of KI to the mixture of benzyl amine **2a** and *p*-TsOH·H_2O led to decreased oxidation and reduction peaks of KI (curves b, d, e). The

mixture vinyl azide **1a**, benzyl amine **2a**, KI, and *p*-TsOH·H_2O (curves e, f) demonstrated increased oxidation peaks, which may indicate the oxidation of the reaction products from vinyl azide **1a** with electrochemically generated intermediates from benzyl amine **2a**, KI, and *p*-TsOH·H_2O.

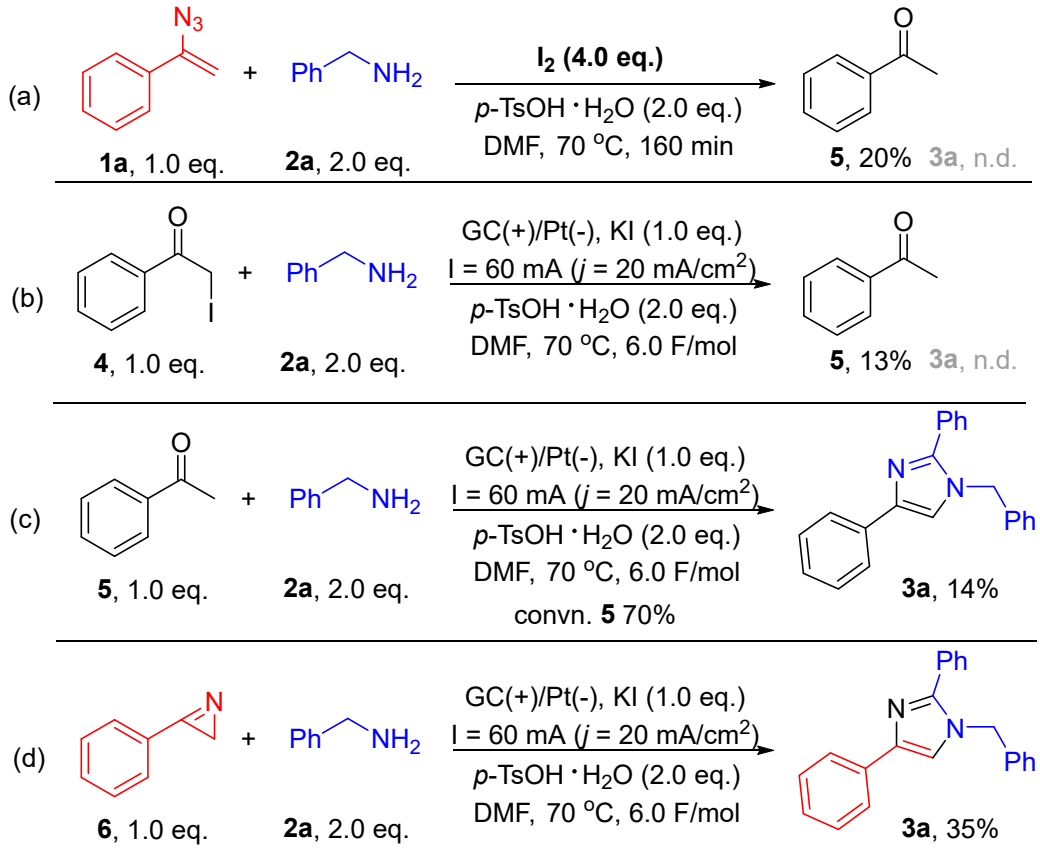

Scheme 4. Control experiments. (**a**) The use of iodine as the oxidant. (**b**,**c**) The electrolysis of benzyl amine with ω-iodoacetophenone **4** and acetophenone **5**. (**d**) The electrolysis of benzyl amine with 3-phenyl-2*H*-azirine **6**.

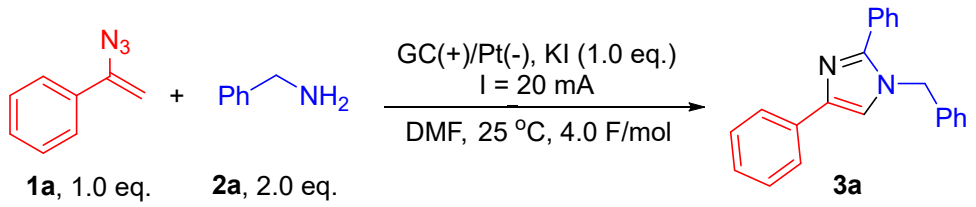

divided cell *(anodic compartment)*	
without acid	22%
p-TsOH · H_2O (2.0 eq.)	16%
undivided cell	
without acid	12%
p-TsOH · H_2O (2.0 eq.)	18%

Scheme 5. Comparing the divided and undivided electrochemical cells.

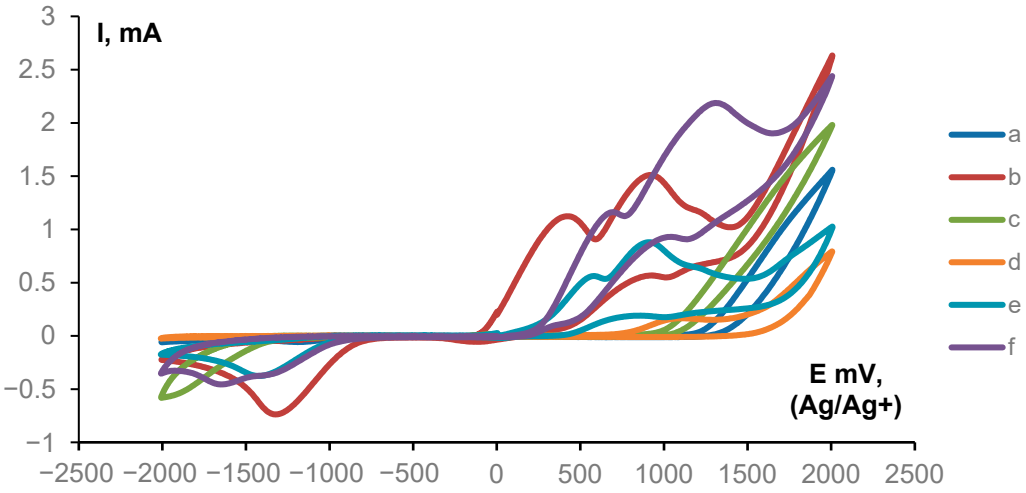

Figure 1. CV curves for the corresponding solutions on a working glassy-carbon electrode (d = 3 mm) under a scan rate of 0.1 V/s at 20 °C. (a) A 0.2 M solution of *p*-TsOH·H_2O in 0.1 M *n*-Bu_4NBF_4 solution in DMF; (b) a 0.1 M solution of KI in a 0.2 M solution of *p*-TsOH·H_2O in 0.1 M *n*-Bu_4NBF_4 solution in DMF; (c) mixture of vinyl azide **1a** and *p*-TsOH·H_2O in 0.1 M *n*-Bu_4NBF_4 solution in DMF; (d) mixture of amine **2a** and *p*-TsOH·H_2O in 0.1 M *n*-Bu_4NBF_4 solution in DMF; (e) mixture of amine **2a** and *p*-TsOH·H_2O in a 0.1 M solution of KI in 0.1 M *n*-Bu_4NBF_4 solution in DMF; (f) mixture of vinyl azide **1a**, amine **2a** and *p*-TsOH·H_2O in a 0.1 M solution of KI in 0.1 M *n*-Bu_4NBF_4 solution in DMF.

Based on our experimental results and previous works [17,25,46], a plausible reaction mechanism for electrochemical transformation of vinyl azides and benzyl amines into imidazoles was proposed in Scheme 6. First, molecular iodine is generated via the anodic oxidation of I^- [15,16,22]. Generated I_2 can further react with the I^- to result in I_3^- formation or with traces of water from the solvent, as well as OH^- generated on the cathode, to give electrophilic iodine species [47,48]. Then, molecular iodine oxidizes **2a** to form imine **8**. The vinyl azide **1a** is converted to 2*H*-azirine **6** by thermal decomposition. A nucleophilic attack of starting benzyl amine **2a** to 2*H*-azirine **6** leads to intermediate **7** [25]. Subsequently, **7** reacts with imine **8** to provide intermediate **9**, which has imine-enamine tautomerism with intermediate **10** under optimized conditions. Due to this tautomerism, two routes are possible. The route I includes the oxidation of **10** into intermediate **11**, further cyclization into intermediate **12**, and ammonia elimination providing the target imidazole **3a**. According to route II, intermediate **9** cyclizes into imidazolidine **13**, which eliminates NH_3 with the formation of intermediate **14**. The oxidation of **14** results in imidazole **3a**.

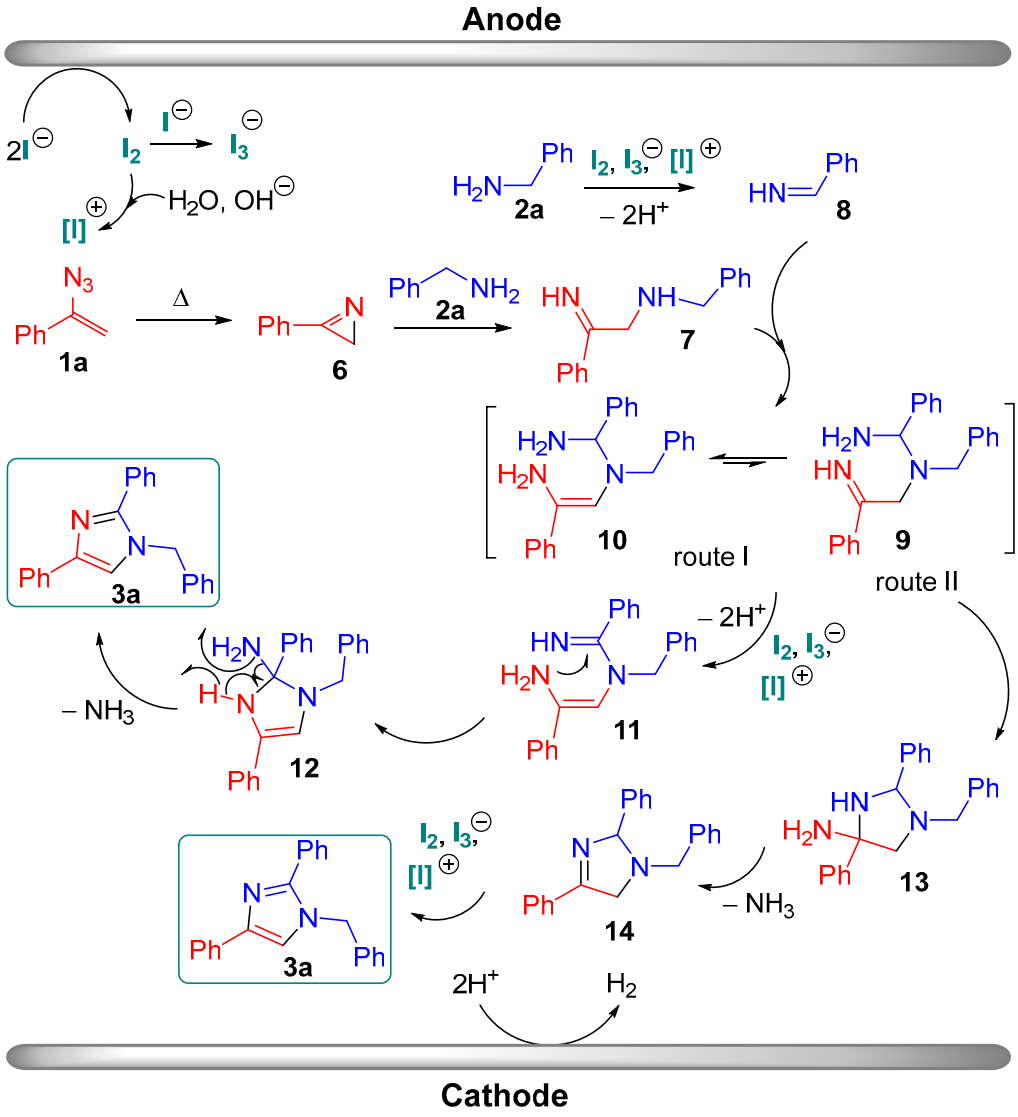

Scheme 6. The proposed reaction mechanism.

3. Materials and Methods

3.1. General Materials and Methods

^{1}H and ^{13}C NMR spectra were recorded on Bruker AVANCE II 300 spectrometer (300.13 and 75.48 MHz, respectively) in $CDCl_3$. Chemical shifts were reported in parts per million (ppm), and the residual solvent peak was used as an internal reference: ^{1}H ($CDCl_3$ δ = 7.25 ppm), ^{13}C ($CDCl_3$ δ = 77.00 ppm). Multiplicity was indicated as follows: s (singlet), d (doublet), t (triplet), q (quartet), sept (septet), m (multiplet).

High-resolution mass spectra (HR-MS) were measured on a Bruker micrOTOF II instrument using electrospray ionization (ESI). The measurements were performed in a positive ion mode (interface capillary voltage—4500 V); mass range from m/z 50 to m/z 3000 Da; external calibration with Electrospray Calibrant Solution (Fluka). A syringe injection was used for all acetonitrile solutions (flow rate 3 µL/min). Nitrogen was applied as a dry gas; interface temperature was set at 180 °C.

FT-IR spectra were recorded on Bruker Alpha instrument.

The TLC analysis was carried out on standard silica gel chromatography plates (DC-Fertigfolien ALUGRAM^{R} Xtra SIL G/UV$_{254}$). Column chromatography was performed using silica gel (0.040–0.060 mm, 60 A).

DMF, *p*-TsOH°H_2O, TBAI, KI, NH_4I, NH_4Br, $LiClO_4$, H_2SO_4, CH_3SO_3H, Amberlyst-15, and chlorobenzene were purchased from commercial sources and were used as is. All solvents were distilled before use using standard procedures.

3.2. Synthesis of Starting Compounds

(1-Azidovinyl)benzene (**1a**), 1-(1-azidovinyl)-4-methylbenzene (**1b**), 1-(1-azidovinyl)-4-tertbutylbenzene (**1c**), 1-(1-azidovinyl)-3-methylbenzene (**1d**), 1-(1-azidovinyl)-4-methoxylbenzene (**1e**), 1-(1-azidovinyl)-4-fluorobenzene (**1f**), 1-(1-azidovinyl)-4-bromobenzene (**1g**), 1-(1-azidovinyl)-3-bromobenzene (**1h**), and 1-(1-azidovinyl)-2-chlorobenzene (**1i**) were synthesized according to the literature through the bromination of corresponding styrenes followed by the reaction of dibromides with NaN_3 [49]. 1-(Azidomethyl)-4-(1-azidovinyl)benzene (**1j**) was synthesized according the same procedure from 1-(chloromethyl)-4-vinylbenzene as a result of simultaneous azidation of formed dibromide and nucleophilic substitution of chlorine atom [49]. 2-Azidododec-1-ene was synthesized according to the literature through the reaction between styrenes and I_2/NaN_3 system followed by dehydroiodination with *t*-BuOK [50].

Amines **2** were obtained from commercial suppliers and used without further purification.

3.3. Electrochemical Cell

For the electrosynthesis glassy carbon and platinum plates from Russian commercial suppliers were used as electrodes (glassy carbon: СУ-2000: ТУ 1916-027-27208846-01; platinum grade: AISI 304). The reactions were performed in a common chemical tube. Undivided electrochemical cell equipped with glassy carbon plate anode and platinum plate cathode with reaction mixture during electrolysis under constant current conditions. The detailed electrochemical equipment was presented in our previous study [44].

Before all electrochemical reactions, the electrodes were placed into a 5 M solution of KOH and this mixture was electrolyzed for 10 min at j = 200 mA/cm^2. After that, the polarity of electrodes was changed and the mixture was electrolyzed under these conditions again. After electrolysis, the electrodes were washed with running water and then with acetone. All these procedures help to clean the electrodes from the impurities from the previous electrolysis.

3.4. General Experimental Procedure for Schemes 2 and 3

An undivided cell was equipped with a glassy carbon anode (3 cm^2) and a platinum plate cathode (3 cm^2) and connected to a DC regulated power supply. The solution of **1a** (1.0 mmol, 1.0 eq.), **2a** (2.0 mmol, 2.0 eq.), *p*-TsOH°H_2O (2.0 mmol, 380.0 mg, 2.0 eq.), and KI (1.0 mmol, 166.0 mg, 1.0 eq.) in 10 mL of DMF was electrolyzed using constant current conditions at 70 °C under magnetic stirring for 160 min with I = 60 mA (j = 20 mA/cm^2). After that, the reaction mixture was diluted with H_2O (30 ml) and washed with mixture of PE and ethyl acetate (1:1) (2 × 30 mL). The combined organic layer was washed with a 0.3 M solution of $Na_2S_2O_3$ (2 × 10 mL), water (2 × 10 mL), dried over Na_2SO_4 and concentrated under reduced pressure using a rotary evaporator (15–20 mmHg), (bath temperature, ca. 30–40 °C). Product **3** was isolated by chromatography on SiO_2.

3.4.1. 1-Benzyl-2,4-diphenyl-1*H*-imidazole (**3a**)

Yellow solid. Yield 61% (189.7 mg, 0.61 mmol, PE/EtOAc = from 15:1 to 2:1 as eluent), mp = 123–124 °C (lit. [25] mp = 123–124 °C). R_f = 0.36 (PE:EtOAc = 5:1). ^{1}H NMR (300.13 MHz, $CDCl_3$, δ): 7.88 (d, J = 7.4 Hz, 2H), 7.68–7.58 (m, 2H), 7.51–7.43 (m, 3H), 7.43–7.35 (m, 5H), 7.33–7.27 (m, 2H), 7.23–7.13 (m, 2H), 5.26 (s, 2H). ^{13}C{^{1}H} NMR (75.48 MHz, $CDCl_3$, δ): 148.7, 141.6, 136.9, 134.2, 130.5, 129.1, 128.7, 128.6, 128.0, 126.9, 126.7, 125.0, 116.9, 50.5. HRMS (ESI-TOF) m/z [M + H]$^+$. Calcd for $[C_{22}H_{19}N_2]^+$: 311.1543. Found: 311.1543. IR (KBr): 3469, 3034, 1651, 1474, 1446, 1398, 772, 736, 697 cm^{-1}. The compound was previously described in [25].

3.4.2. 1-Benzyl-2-phenyl-4-(p-tolyl)-1*H*-imidazole (**3b**)

Yellow solid. Yield 52% (168.5 mg, 0.52 mmol, PE/EtOAc = from 15:1 to 2:1 as eluent), mp = 140–142 °C (lit. [25] mp = 138–140 °C). R_f = 0.37 (PE:EtOAc = 5:1). ^{1}H NMR (300.13 MHz, $CDCl_3$, δ): 7.75 (d, *J* = 8.0 Hz, 2H), 7.68–7.58 (m, 2H), 7.47–7.38 (m, 3H), 7.37–7.28 (m, 3H), 7.24–7.10 (m, 5H), 5.21 (s, 2H), 2.36 (s, 3H). ^{13}C{^{1}H} NMR (75.48 MHz, $CDCl_3$, δ): 148.5, 141.6, 137.0, 136.6, 131.2, 130.5, 129.3, 129.2, 129.1, 128.7, 128.1, 126.8, 125.0, 116.5, 50.6, 21.3. HRMS (ESI-TOF) *m*/*z* [M + H]$^+$. Calcd for $[C_{23}H_{21}N_2]^+$: 325.1699. Found: 325.1696. IR (KBr): 3542, 3498, 3468, 3438, 3066, 3029, 2957, 2924, 2855, 1729, 1644, 1646, 1273, 1178, 822, 763, 731, 698 cm^{-1}. The compound was previously described in [25].

3.4.3. 1-Benzyl-4-(4-(*tert*-butyl)phenyl)-2-phenyl-1*H*-imidazole (**3c**)

Yellow liquid. Yield 64% (234.6 mg, 0.64 mmol, PE/EtOAc = from 15:1 to 2:1 as eluent). R_f = 0.25 (PE:EtOAc = 5:1). ^{1}H NMR (300.13 MHz, $CDCl_3$, δ): 7.80 (d, *J* = 8.3 Hz, 2H), 7.68–7.58 (m, 2H), 7.46–7.37 (m, 5H), 7.37–7.29 (m, 3H), 7.23 (s, 1H), 7.13 (d, *J* = 6.6 Hz, 2H), 5.22 (s, 2H), 1.36 (s, 9H). ^{13}C{^{1}H} NMR (75.48 MHz, $CDCl_3$, δ): 149.9, 148.5, 141.7, 137.1, 131.3, 130.6, 129.2, 129.1, 129.0, 128.7, 128.0, 126.7, 125.5, 124.8, 116.6, 50.6, 34.6, 31.5. HRMS (ESI-TOF) *m*/*z* [M + H]$^+$. Calcd for $[C_{26}H_{27}N_2]^+$: 367.2169. Found: 367.2165. IR (KBr): 3465, 3444, 3142, 3116, 3064, 3029, 2957, 2866, 1604, 1495, 1470, 1451, 1415, 1365, 1202, 836, 773, 730, 699, 522 cm^{-1}. The compound was previously described in [25].

3.4.4. 1-Benzyl-2-phenyl-4-(m-tolyl)-1*H*-imidazole (**3d**)

Yellow solid. Yield 44% (142.7 mg, 0.44 mmol, PE/EtOAc = from 15:1 to 2:1 as eluent), mp = 124–126 °C (lit. [15] mp = 125–126 °C). R_f = 0.23 (PE:EtOAc = 5:1). ^{1}H NMR (300.13 MHz, $CDCl_3$, δ): 7.78 (s, 1H), 7.69–7.59 (m, 3H), 7.47–7.38 (m, 3H), 7.39–7.27 (m, 4H), 7.24 (s, 1H), 7.17–7.07 (m, 3H), 5.18 (s, 2H), 2.41 (s, 3H). ^{13}C{^{1}H} NMR (75.48 MHz, $CDCl_3$, δ): 148.5, 141.5, 138.1, 136.9, 133.9, 130.4, 128.98, 128.95, 128.6, 128.4, 127.9, 127.6, 126.6, 125.6, 122.0, 116.9, 50.4, 21.5. HRMS (ESI-TOF) *m*/*z* [M + H]$^+$. Calcd for $[C_{23}H_{21}N_2]^+$: 325.1699. Found: 325.1695. IR (KBr): 3471, 3134, 3030, 2952, 2918, 1604, 1449, 1402, 1359, 753, 696 cm^{-1}. The compound was previously described in [15].

3.4.5. 1-Benzyl-4-(4-methoxyphenyl)-2-phenyl-1*H*-imidazole (**3e**)

Yellow liquid. Yield 34% (115.6 mg, 0.34 mmol, PE/EtOAc = from 10:1 to 2:1 as eluent). R_f = 0.13 (PE:EtOAc = 5:1). ^{1}H NMR (300.13 MHz, $CDCl_3$, δ): 7.78 (d, *J* = 8.6 Hz, 2H), 7.67–7.57 (m, 2H), 7.47–7.39 (m, 3 H), 7.38–7.30 (m, 3H), 7.19–7.10 (m, 3H), 6.92 (d, *J* = 8.6 Hz, 2H), 5.21 (s, 2H), 3.82 (s, 3H). ^{13}C{^{1}H} NMR (75.48 MHz, $CDCl_3$, δ): 159.0, 148.4, 141.3, 136.9, 130.2, 129.21, 129.15, 128.8, 128.1, 126.8, 126.7, 126.4, 115.9, 114.1, 55.4, 50.7. HRMS (ESI-TOF) *m*/*z* [M + H]$^+$. Calcd for $[C_{23}H_{21}N_2O]^+$: 341.1648. Found: 341.1649. IR (KBr): 3446, 3427, 3126, 3103, 3060, 3030, 2959, 2835, 1612, 1559, 1497, 1453, 1248, 1172, 1024, 833, 765, 698, 526 cm^{-1}. The compound was previously described in [15].

3.4.6. 1-Benzyl-4-(4-fluorophenyl)-2-phenyl-1*H*-imidazole (**3f**)

Yellow solid. Yield 53% (174.0 mg, 0.53 mmol, PE/EtOAc = from 10:1 to 2:1 as eluent), mp = 105–107 °C (lit. [25] mp = 106–107 °C). R_f = 0.67 (PE:EtOAc = 2:1). ^{1}H NMR (300.13 MHz, $CDCl_3$, δ): 7.87–7.75 (m, 2H), 7.66–7.57 (m, 2H), 7.46–7.39 (m, 3H), 7.38–7.31 (m, 3H), 7.19 (s, 1H), 7.17–7.10 (m, 2H), 7.09–7.00 (m, 2H), 5.20 (s, 2H). ^{13}C{^{1}H} NMR (75.48 MHz, $CDCl_3$, δ): 162.0 (d, *J* = 245.4 Hz), 148.7, 140.7, 136.8, 130.4 (d, *J* = 2.8 Hz), 129.12, 129.07, 129.0, 128.7, 128.1, 126.7, 126.60 (d, *J* = 7.9 Hz), 116.5, 115.4 (d, *J* = 21.5 Hz), 50.55. HRMS (ESI-TOF) *m*/*z* [M + H]$^+$. Calcd for $[C_{22}H_{18}FN_2]^+$: 329.1449. Found: 329.1443. IR (KBr): 3458, 3059, 3032, 2357, 1644, 1495, 1348, 1218, 1156, 840, 761, 731, 695, 583, 519 cm^{-1}. The compound was previously described in [25].

3.4.7. 1-Benzyl-4-(4-bromophenyl)-2-phenyl-1*H*-imidazole (**3g**)

Yellow solid. Yield 56% (218.0 mg, 0.56 mmol, PE/EtOAc = from 10:1 to 2:1 as eluent), mp = 166–167 °C (lit. [25] mp = 164–166 °C). R_f = 0.71 (PE:EtOAc = 2:1). ^{1}H NMR

(300.13 MHz, $CDCl_3$, δ): 7.72 (d, *J* = 8.4 Hz, 2H), 7.66–7.57 (m, 2H), 7.48 (d, *J* = 8.4 Hz, 2H), 7.46–7.40 (m, 3H), 7.39–7.30 (m, 3H), 7.22 (s, 1H), 7.17–7.08 (m, 2H), 5.19 (s, 2H). $^{13}C\{^1H\}$ NMR (75.48 MHz, $CDCl_3$, δ): 148.8, 140.4, 136.7, 133.1, 131.6, 130.2, 129.2, 129.1, 129.0, 128.7, 128.1, 126.8, 126.6, 120.5, 117.1, 50.6. HRMS (ESI-TOF) *m*/*z* $[M + H]^+$. Calcd for $[C_{22}H_{18}BrN_2]^+$: 389.0648, 391.0628. Found: 389.0645, 391.0628. IR (KBr): 3472, 3129, 3059, 3025, 2977, 2952, 1599, 1550, 1478, 1413, 1188, 1070, 946, 830, 767, 701, 506 cm^{-1}. The compound was previously described in [25].

3.4.8. 1-Benzyl-4-(3-bromophenyl)-2-phenyl-1*H*-imidazole (**3h**)

Yellow solid. Yield 42% (163.5 mg, 0.42 mmol, PE/EtOAc = from 10:1 to 2:1 as eluent), mp = 104–106 °C. R_f = 0.69 (PE:EtOAc = 2:1). ^1H NMR (300.13 MHz, $CDCl_3$, δ): 8.02 (s, 1H), 7.75 (d, *J* = 7.7 Hz, 1H), 7.66–7.56 (m, 2 H), 7.48–7.39 (m, 3H), 7.38–7.29 (m, 4H), 7.25–7.17 (m, 2H), 7.17–7.09 (m, 2H), 5.21 (s, 2H). $^{13}C\{^1H\}$ NMR (75.48 MHz, $CDCl_3$, δ): 148.9, 140.2, 136.7, 136.3, 130.3, 130.2, 129.7, 129.3, 129.2, 129.1, 128.8, 128.2, 128.0, 126.8, 123.5, 122.9, 117.5, 50.7. HRMS (ESI-TOF) *m*/*z* $[M + H]^+$. Calcd for $[C_{22}H_{18}BrN_2]^+$: 389.0648. Found: 389.0645. IR (KBr): 3477, 3129, 3062, 3031, 2951, 1600, 1566, 1468, 1450, 1205, 1072, 956, 872, 735, 697, 461 cm^{-1}.

3.4.9. 1-Benzyl-4-(2-chlorophenyl)-2-phenyl-1*H*-imidazole (**3i**)

Yellow liquid. Yield 36% (124.2 mg, 0.36 mmol, PE/EtOAc = from 15:1 from 2:1 as eluent). R_f = 0.31 (PE:EtOAc = 5:1). ^1H NMR (300.13 MHz, $CDCl_3$, δ): 8.35 (dd, *J* = 7.9, 1.6 Hz, 1H), 7.77 (s, 1H), 7.67–7.58 (m, 2H), 7.46–7.39 (m, 4H), 7.38–7.30 (m, 4H), 7.22–7.10 (m, 3H), 5.26 (s, 2H). $^{13}C\{^1H\}$ NMR (75.48 MHz, $CDCl_3$, δ): 147.8, 137.6, 136.9, 132.5, 130.9, 130.4, 130.2, 129.8, 129.12, 129.07, 128.7, 128.0, 127.5, 126.9, 126.6, 121.7, 50.6. HRMS (ESI-TOF) *m*/*z* $[M + H]^+$. Calcd for $[C_{22}H_{18}ClN_2]^+$: 345.1153. Found: 345.1149. IR (KBr): 3449, 3147, 3057, 3031, 1473, 1451, 1426, 1351, 1182, 1047, 764, 736, 700, 560 cm^{-1}. The compound was previously described in [25].

3.4.10. 4-(4-(Azidomethyl)phenyl)-1-benzyl-2-phenyl-1*H*-imidazole (**3j**)

Yellow liquid. Yield 30% (109.6 mg, 0.30 mmol, PE/EtOAc = from 15:1 to 2:1 as eluent). R_f = 0.55 (PE:EtOAc = 2:1). ^1H NMR (300.13 MHz, $CDCl_3$, δ): 7.86 (d, *J* = 8.2 Hz, 2H), 7.66–7.56 (m, 2H), 7.48–7.39 (m, 3H), 7.38–7.28 (m, 5H), 7.26 (s, 1H), 7.18–7.08 (m, 2H), 5.20 (s, 2H), 4.32 (s, 2H). $^{13}C\{^1H\}$ NMR (75.48 MHz, $CDCl_3$, δ): 148.8, 141.0, 136.8, 134.2, 133.7, 130.4, 129.14, 129.07, 128.7, 128.6, 128.1, 126.8, 125.4, 117.2, 54.8, 50.6. HRMS (ESI-TOF) *m*/*z* $[M + H]^+$. Calcd for $[C_{23}H_{20}N_5]^+$: 366.1713. Found: 366.1712. IR (KBr): 3108, 3063, 3031, 2929, 2875, 2098, 1613, 1498, 1471, 1452, 1422, 1355, 1249, 1181, 1075, 1021, 948, 848, 771, 732, 699 cm^{-1}.

3.4.11. 1-(4-Methoxybenzyl)-2-(4-methoxyphenyl)-4-phenyl-1*H*-imidazole (**3l**)

Yellow liquid. Yield 35% (129.7 mg, 0.35 mmol, PE/EtOAc = 5:1 as eluent). R_f = 0.38 (PE:EtOAc = 2:1). ^1H NMR (300.13 MHz, $CDCl_3$, δ): 7.80 (d, *J* = 7.3 Hz, 2H), 7.57–7.47 (m, 2H), 7.33 (t, *J* = 7.6 Hz, 2H), 7.24–7.14 (m, 2H), 7.04 (d, *J* = 8.6 Hz, 2H), 6.96–6.89 (m, 2H), 6.88–6.78 (m, 2H), 5.09 (s, 2H), 3.81 (s, 3H), 3.77 (s, 1H). $^{13}C\{^1H\}$ NMR (75.48 MHz, $CDCl_3$, δ): 160.3, 159.4, 148.5, 141.3, 134.3, 130.5, 129.0, 128.6, 128.2, 126.8, 125.0, 123.2, 116.5, 114.5, 114.1, 55.44, 55.42, 50.1. HRMS (ESI-TOF) *m*/*z* $[M + H]^+$. Calcd for $[C_{24}H_{23}N_2O_2]^+$: 371.1754. Found: 371.1751. IR (KBr): 3130, 3060, 3033, 3002, 2957, 2935, 2834, 1611, 1514, 1485, 1457, 1295, 1253, 1177, 1029, 838, 735, 697, 611, 518 cm^{-1}. The compound was previously described in [25].

3.4.12. 1-(4-Chlorobenzyl)-2-(4-chlorophenyl)-4-phenyl-1*H*-imidazole (**3m**)

Yellow liquid. Yield 55% (208.6 mg, 0.55 mmol, PE/EtOAc = from 15:1 to 2:1 as eluent). R_f = 0.29 (PE:EtOAc = 5:1). ^1H NMR (300.13 MHz, $CDCl_3$, δ): 7.80 (d, *J* = 7.5 Hz, 2H), 7.54–7.44 (m, 2H), 7.42–7.35 (m, 4H), 7.34–7.27 (m, 2H), 7.26–7.18 (m, 2H), 7.01 (d, *J* = 8.3 Hz, 2H), 5.12 (s, 2H). $^{13}C\{^1H\}$ NMR (75.48 MHz, $CDCl_3$, δ): 147.4, 142.0, 135.3, 135.1, 134.1,

133.8, 130.2, 129.4, 129.0, 128.8, 128.7, 128.0, 127.2, 125.0, 117.1, 50.0. HRMS (ESI-TOF) m/z $[M + H]^+$. Calcd for $[C_{22}H_{17}Cl_2N_2]^+$: 379.0763. Found: 379.0760. IR (KBr): 3130, 3062, 3032, 2931, 1896, 1606, 1489, 1450, 1411, 1180, 1092, 1014, 947, 910, 837, 732. 696, 488 cm^{-1}. The compound was previously described in [25].

3.4.13. 1-(2-Chlorobenzyl)-2-(2-chlorophenyl)-4-phenyl-1*H*-imidazole (**3n**)

Yellow solid. Yield 40% (151.7 mg, 0.40 mmol, PE/EtOAc = from 15:1 to 2:1 as eluent), mp = 134–136 °C (lit. [15] mp = 135–136 °C). R_f = 0.22 (PE:EtOAc = 5:1). ^1H NMR (300.13 MHz, $CDCl_3$, δ): 7.81 (d, *J* = 7.4 Hz, 2H), 7.51–7.42 (m, 2H), 7.40–7.27 (m, 5H), 7.25–7.11 (m, 4H), 6.97–6.87 (m, 1H), 5.08 (s, 2H). $^{13}C\{^1H\}$ NMR (75.48 MHz, $CDCl_3$, δ): 145.9, 141.5, 134.7, 133.9, 133.8, 133.1, 132.8, 131.1, 129.9, 129.7, 129.5, 129.3, 128.6, 127.3, 127.0, 126.9, 124.9, 115.9, 48.2. HRMS (ESI-TOF) m/z $[M + H]^+$. Calcd for $[C_{22}H_{17}Cl_2N_2]^+$: 379.0763. Found: 379.0761. IR (KBr): 3138, 3057, 2937, 2854, 1604, 1446, 1405, 1382, 1336, 1192, 1028, 948, 915, 753, 697, 506 cm^{-1}. The compound was previously described in [15].

3.4.14. 1-(4-Fluorobenzyl)-2-(4-fluorophenyl)-4-phenyl-1*H*-imidazole (**3o**)

Yellow liquid. Yield 40% (138.6 mg, 0.40 mmol, PE/EtOAc = from 10:1 to 2:1 as eluent). R_f = 0.62 (PE:EtOAc = 2:1). ^1H NMR (300.13 MHz, $CDCl_3$, δ): 7.87–7.77 (m, 2H), 7.60–7.49 (m, 2H), 7.36 (t, *J* = 7.6 Hz, 2H), 7.28–7.22 (m, 1H), 7.21 (s, 1H), 7.16–7.09 (m, 1H), 7.09–6.97 (m, 5H), 5.12 (s, 2H). $^{13}C\{^1H\}$ NMR (75.48 MHz, $CDCl_3$, δ): 164.5 (d, *J* = 247.0 Hz), 161.24 (d, *J* = 245.2Hz), 147.6, 141.7, 133.9, 132.4 (d, *J* = 3.3 Hz), 131.0 (d, *J* = 8.4 Hz), 128.7, 128.5 (d, *J* = 8.2 Hz), 127.1, 126.6 (d, *J* = 3.7 Hz), 125.0, 116.8, 116.1 (d, *J* = 19.4 Hz), 115.8 (d, *J* = 19.7 Hz), 49.9. ^{19}F NMR (282 MHz, $CDCl_3$) δ -112.31, -114.50. HRMS (ESI-TOF) m/z $[M + H]^+$: Calcd for $[C_{22}H_{17}F_2N_2]^+$: 347.1354. Found: 347.1354. IR (KBr): 3129, 3065, 3038, 2932, 1607, 1511, 1485, 1451, 1419, 1226, 1159, 1097, 1015, 947, 910, 843, 733, 697, 607, 505 cm^{-1}. The compound was previously described in [15].

3.4.15. 1-(3,4-Dimethoxybenzyl)-2-(3,4-dimethoxyphenyl)-4-phenyl-1*H*-imidazole (**3p**)

Yellow solid. Yield 38% (163.6 mg, 0.38 mmol, PE/EtOAc = 3:1 as eluent), mp = 181–183 °C (lit. [25] mp = 182–184 °C). R_f = 0.15 (PE:EtOAc = 2:1). ^1H NMR (300.13 MHz, $CDCl_3$, δ): 7.84 (d, *J* = 7.4 Hz, 2H), 7.36 (t, *J* = 7.4 Hz, 2 H), 7.28–7.17 (m, 3H), 7.13 (d, *J* = 8.6 Hz, 1H), 6.94–6.79 (m, 2H), 6.74–6.66 (m, 1H), 6.63 (s, 1H), 5.16 (s, 2H), 3.90 (s, 3H), 3.87 (s, 3H), 3.82 (s, 3H), 3.80 (s, 3H). $^{13}C\{^1H\}$ NMR (75.48 MHz, $CDCl_3$, δ): 149.9, 149.5, 149.1, 148.9, 148.4, 141.1, 133.9, 129.4, 128.6, 126.9, 125.0, 123.0, 121.6, 119.1, 116.7, 112.5, 111.6, 111.1, 109.9, 56.0, 55.9, 50.4. HRMS (ESI-TOF) m/z $[M + H]^+$. Calcd for $[C_{26}H_{27}N_2O_4]^+$: 431.1965. Found: 431.1969. IR (KBr): 3453, 3130, 3099, 3012, 2959,2936,2835, 1606, 1515, 1442, 1320, 1261, 1244, 1141, 1025, 812, 765, 723, 696 cm^{-1}. The compound was previously described in [25].

3.4.16. 2-(Furan-2-yl)-1-(furan-2-ylmethyl)-4-phenyl-1*H*-imidazole (**3q**)

Yellow liquid. Yield 38% (110.3 mg, 0.38 mmol, PE/EtOAc = from 10:1 to 2:1 as eluent). R_f = 0.55 (PE:EtOAc = 2:1). ^1H NMR (300.13 MHz, $CDCl_3$, δ): 7.81 (d, *J* = 7.4 Hz, 2H), 7.58–7.51 (m, 1H), 7.40–7.30 (m, 3H), 7.25–7.20 (m, 2H), 6.96 (d, *J* = 3.4 Hz, 1H), 6.58–6.49 (m, 1H), 6.36–6.31 (m, 1H), 6.31–6.26 (m, 1H), 5.36 (s, 2H). $^{13}C\{^1H\}$ NMR (75.48 MHz, $CDCl_3$, δ): 149.3, 145.4, 143.1, 142.9, 141.7, 139.1, 133.7, 128.6, 127.0, 125.1, 116.7, 111.7, 110.7, 110.4, 109.1, 44.0. HRMS (ESI-TOF) m/z $[M + H]^+$. Calcd for $[C_{18}H_{15}N_2O_2]^+$: 291.1128. Found: 291.1125. IR (KBr): 3124, 3061, 3032, 2928, 2853, 1678, 1606, 1482, 1446, 1343, 1222, 1185, 1149, 1073, 1011, 948, 909, 885, 816, 736, 696, 596, 504 cm^{-1}. The compound was previously described in [15].

3.4.17. 3-(4-Phenyl-1-(Pyridin-3-Ylmethyl)-1*H*-Imidazol-2-yl)Pyridine (**3r**)

Yellow liquid. Yield 30% (93.7 mg, 0.30 mmol, PE/EtOAc = 1:1 as eluent). R_f = 0.10 (PE:EtOAc = 1:1). ^1H NMR (300.13 MHz, $CDCl_3$, δ): 8.80 (s, 1H), 8.61 (d, *J* = 4.7, 1H), 8.52 (d, *J* = 4.7, 1H), 8.40 (s, 1H), 7.88 (d, *J* = 7.8 Hz, 1H), 7.78 (d, *J* = 7.9 Hz, 2H), 7.40–7.29 (m, 4H),

7.29–7.19 (m, 3H), 5.20 (s, 2H). $^{13}C\{^1H\}$ NMR (75.48 MHz, $CDCl_3$, δ): 150.1, 149.7, 149.3, 148.2, 145.4, 142.6, 136.4, 134.3, 133.4, 131.9, 128.7, 127.3, 126.5, 125.0, 124.0, 123.6, 117.3, 48.4. HRMS (ESI-TOF) m/z [M + H]$^+$. Calcd for $[C_{20}H_{17}N_4]^+$: 313.1448. Found: 313.1440. IR (KBr): 3386, 3127, 3059, 3035, 2934, 2219, 1606, 1575, 1481, 1450, 1426, 1193, 1090, 1027, 912, 816, 731, 644, 507 cm^{-1}.

4. Conclusions

In summary, we have disclosed the electrochemical synthesis of imidazoles from vinyl azides and benzyl amines in moderate to high yields. Application of an electric current makes it possible to conduct the reaction without application of unrecoverable chemical oxidants. The process was carried out under constant current conditions in an experimentally simple undivided electrochemical cell equipped with a platinum cathode and a glassy carbon anode. Potassium iodide served as both a supporting electrolyte and a redox catalyst. With the use of cyclic voltammetry and control experiments, a possible reaction pathway was proposed. Presumably, during the reaction, 2*H*-azirine is generated from the vinyl azide followed by its reaction with benzyl amine and the corresponding imine. The cyclization and aromatization of the obtained intermediate lead to the target imidazole.

Supplementary Materials: The following supporting information can be downloaded at: https://www.mdpi.com/article/10.3390/molecules27227721/s1, Figure S1: CV curves; Table S1: Detailed optimization of imidazole electrosynthesis, characterization data of synthesized compounds, NMR spectra, HRMS, and IR spectra.

Author Contributions: Conceptualization, V.A.V. and A.O.T.; methodology, S.S.G.; writing—original draft preparation, V.A.V. and S.S.G.; writing—review and editing, V.A.V. and A.O.T. All authors have read and agreed to the published version of the manuscript.

Funding: This research received no external funding.

Institutional Review Board Statement: Not applicable.

Informed Consent Statement: Not applicable.

Data Availability Statement: The data presented in this study are available in insert article or Supplementary Materials here.

Conflicts of Interest: The authors declare no conflict of interest.

Sample Availability: Samples of the compounds **3** are available from the authors.

References

1. Sharma, P.; LaRosa, C.; Antwi, J.; Govindarajan, R.; Werbovetz, K.A. Imidazoles as Potential Anticancer Agents: An Update on Recent Studies. *Molecules* **2021**, *26*, 4213. [CrossRef]
2. Fan, Y.-L.; Jin, X.-H.; Huang, Z.-P.; Yu, H.-F.; Zeng, Z.-G.; Gao, T.; Feng, L.-S. Recent advances of imidazole-containing derivatives as anti-tubercular agents. *Eur. J. Med. Chem.* **2018**, *150*, 347–365. [CrossRef] [PubMed]
3. Siwach, A.; Verma, P.K. Synthesis and therapeutic potential of imidazole containing compounds. *BMC Chem.* **2021**, *15*, 12. [CrossRef]
4. Beltran-Hortelano, I.; Alcolea, V.; Font, M.; Pérez-Silanes, S. The role of imidazole and benzimidazole heterocycles in Chagas disease: A review. *Eur. J. Med. Chem.* **2020**, *206*, 112692. [CrossRef] [PubMed]
5. Jin, Z. Muscarine, imidazole, oxazole and thiazole alkaloids. *Nat. Prod. Rep.* **2009**, *26*, 382–445. [CrossRef] [PubMed]
6. Ouakki, M.; Galai, M.; Cherkaoui, M. Imidazole derivatives as efficient and potential class of corrosion inhibitors for metals and alloys in aqueous electrolytes: A review. *J. Mol. Liq.* **2022**, *345*, 117815. [CrossRef]
7. Chen, W.-C.; Zhu, Z.-L.; Lee, C.-S. Organic Light-Emitting Diodes Based on Imidazole Semiconductors. *Adv. Opt. Mater.* **2018**, *6*, 1800258. [CrossRef]
8. Rossi, R.; Angelici, G.; Casotti, G.; Manzini, C.; Lessi, M. Catalytic Synthesis of 1,2,4,5-Tetrasubstituted 1H-Imidazole Derivatives: State of the Art. *Adv. Synth. Catal.* **2019**, *361*, 2737–2803. [CrossRef]
9. Daraji, D.G.; Prajapati, N.P.; Patel, H.D. Synthesis and Applications of 2-Substituted Imidazole and Its Derivatives: A Review. *J. Heterocycl. Chem.* **2019**, *56*, 2299–2317. [CrossRef]
10. Shabalin, D.A.; Camp, J.E. Recent advances in the synthesis of imidazoles. *Org. Biomol. Chem.* **2020**, *18*, 3950–3964. [CrossRef]

11. Alanthadka, A.; Elango, S.D.; Thangavel, P.; Subbiah, N.; Vellaisamy, S.; Chockalingam, U.M. Construction of substituted imidazoles from aryl methyl ketones and benzylamines via N-heterocyclic carbene-catalysis. *Catal. Commun.* **2019**, *125*, 26–31. [CrossRef]
12. Cai, Z.-J.; Wang, S.-Y.; Ji, S.-J. CuI/BF3·Et2O Cocatalyzed Aerobic Dehydrogenative Reactions of Ketones with Benzylamines: Facile Synthesis of Substituted Imidazoles. *Org. Lett.* **2012**, *14*, 6068–6071. [CrossRef] [PubMed]
13. Huang, H.; Ji, X.; Wu, W.; Jiang, H. Practical Synthesis of Polysubstituted Imidazoles via Iodine- Catalyzed Aerobic Oxidative Cyclization of Aryl Ketones and Benzylamines. *Adv. Synth. Catal.* **2013**, *355*, 170–180. [CrossRef]
14. Geng, F.; Wu, S.; Gan, X.; Hou, W.; Dong, J.; Zhou, Y. TEMPO mediated oxidative annulation of aryl methyl ketones with amines/ammonium acetate for imidazole synthesis. *Org. Biomol. Chem.* **2022**, *20*, 5416–5422. [CrossRef] [PubMed]
15. Yang, Z.; Zhang, J.; Hu, L.; Li, A.; Li, L.; Liu, K.; Yang, T.; Zhou, C. Electrochemical HI-mediated Intermolecular C–N Bond Formation to Synthesize Imidazoles from Aryl Ketones and Benzylamines. *J. Org. Chem.* **2020**, *85*, 5952–5958. [CrossRef] [PubMed]
16. Zeng, L.; Li, J.; Gao, J.; Huang, X.; Wang, W.; Zheng, X.; Gu, L.; Li, G.; Zhang, S.; He, Y. An electrochemical oxidative multicomponent cascade annulation of ketones and amines used to produce imidazoles. *Green Chem.* **2020**, *22*, 3416–3420. [CrossRef]
17. Cao, J.; Zhou, X.; Ma, H.; Shi, C.; Huang, G. A facile and efficient method for the synthesis of 1,2,4-trisubstituted imidazoles with enamides and benzylamines. *RSC Adv.* **2016**, *6*, 57232–57235. [CrossRef]
18. Wang, W.; Zhang, S.; Shi, G.; Chen, Z. Electrochemical synthesis of 1,2,4,5-tetrasubstituted imidazoles from enamines and benzylamines. *Org. Biomol. Chem.* **2021**, *19*, 6682–6686. [CrossRef]
19. Fu, J.; Zanoni, G.; Anderson, E.A.; Bi, X. α-Substituted vinyl azides: An emerging functionalized alkene. *Chem. Soc. Rev.* **2017**, *46*, 7208–7228. [CrossRef]
20. Nguyen, T.K.; Titov, G.D.; Khoroshilova, O.V.; Kinzhalov, M.A.; Rostovskii, N.V. Light-induced one-pot synthesis of pyrimidine derivatives from vinyl azides. *Org. Biomol. Chem.* **2020**, *18*, 4971–4982. [CrossRef]
21. Yin, W.; Wang, X. Recent advances in iminyl radical-mediated catalytic cyclizations and ring-opening reactions. *New J. Chem.* **2019**, *43*, 3254–3264. [CrossRef]
22. Mulina, O.M.; Zhironkina, N.V.; Paveliev, S.A.; Demchuk, D.V.; Terent'ev, A.O. Electrochemically Induced Synthesis of Sulfonylated N-Unsubstituted Enamines from Vinyl Azides and Sulfonyl Hydrazides. *Org. Lett.* **2020**, *22*, 1818–1824. [CrossRef] [PubMed]
23. Paveliev, S.A.; Churakov, A.I.; Alimkhanova, L.S.; Segida, O.O.; Nikishin, G.I.; Terent'ev, A.O. Electrochemical Synthesis of O-Phthalimide Oximes from α-Azido Styrenes via Radical Sequence: Generation, Addition and Recombination of Imide-N-Oxyl and Iminyl Radicals with C−O/N−O Bonds Formation. *Adv. Synth. Catal.* **2020**, *362*, 3864–3871. [CrossRef]
24. Nayl, A.A.; Aly, A.A.; Arafa, W.A.A.; Ahmed, I.M.; Abd-Elhamid, A.I.; El-Fakharany, E.M.; Abdelgawad, M.A.; Tawfeek, H.N.; Bräse, S. Azides in the Synthesis of Various Heterocycles. *Molecules* **2022**, *27*, 3716. [CrossRef] [PubMed]
25. Xiang, L.; Niu, Y.; Pang, X.; Yang, X.; Yan, R. I2-catalyzed synthesis of substituted imidazoles from vinyl azides and benzylamines. *Chem. Commun.* **2015**, *51*, 6598–6600. [CrossRef]
26. Yoshida, J.-I.; Kataoka, K.; Horcajada, R.; Nagaki, A. Modern Strategies in Electroorganic Synthesis. *Chem. Rev.* **2008**, *108*, 2265–2299. [CrossRef]
27. Frontana-Uribe, B.A.; Little, R.D.; Ibanez, J.G.; Palma, A.; Vasquez-Medrano, R. Organic electrosynthesis: A promising green methodology in organic chemistry. *Green Chem.* **2010**, *12*, 2099–2119. [CrossRef]
28. Horn, E.J.; Rosen, B.R.; Baran, P.S. Synthetic Organic Electrochemistry: An Enabling and Innately Sustainable Method. *ACS Cent. Sci.* **2016**, *2*, 302–308. [CrossRef]
29. Sperry, J.B.; Wright, D.L. The application of cathodic reductions and anodic oxidations in the synthesis of complex molecules. *Chem. Soc. Rev.* **2006**, *35*, 605–621. [CrossRef]
30. Wiebe, A.; Gieshoff, T.; Möhle, S.; Rodrigo, E.; Zirbes, M.; Waldvogel, S.R. Electrifying Organic Synthesis. *Angew. Chem. Int. Ed.* **2018**, *57*, 5594–5619. [CrossRef]
31. Yan, M.; Kawamata, Y.; Baran, P.S. Synthetic Organic Electrochemical Methods Since 2000: On the Verge of a Renaissance. *Chem. Rev.* **2017**, *117*, 13230–13319. [CrossRef] [PubMed]
32. Waldvogel, S.R.; Janza, B. Renaissance of Electrosynthetic Methods for the Construction of Complex Molecules. *Angew. Chem. Int. Ed.* **2014**, *53*, 7122–7123. [CrossRef] [PubMed]
33. Vil', V.A.; Merkulova, V.M.; Ilovaisky, A.I.; Paveliev, S.A.; Nikishin, G.I.; Terent'ev, A.O. Electrochemical Synthesis of Fluorinated Ketones from Enol Acetates and Sodium Perfluoroalkyl Sulfinates. *Org. Lett.* **2021**, *23*, 5107–5112. [CrossRef] [PubMed]
34. Francke, R. Recent advances in the electrochemical construction of heterocycles. *Beilstein J. Org. Chem.* **2014**, *10*, 2858–2873. [CrossRef]
35. Jiang, Y.; Xu, K.; Zeng, C. Use of Electrochemistry in the Synthesis of Heterocyclic Structures. *Chem. Rev.* **2018**, *118*, 4485–4540. [CrossRef]
36. Sbei, N.; Listratova, A.V.; Titov, A.A.; Voskressensky, L.G. Recent Advances in Electrochemistry for the Synthesis of N-Heterocycles. *Synthesis* **2019**, *51*, 2455–2473. [CrossRef]
37. Liang, S.; Zeng, C.-C. Organic electrochemistry: Anodic construction of heterocyclic structures. *Curr. Opin. Electrochem.* **2020**, *24*, 31–43. [CrossRef]

38. Ye, Z.; Wu, Y.; Chen, N.; Zhang, H.; Zhu, K.; Ding, M.; Liu, M.; Li, Y.; Zhang, F. Enantiospecific electrochemical rearrangement for the synthesis of hindered triazolopyridinone derivatives. *Nat. Commun.* **2020**, *11*, 3628. [CrossRef]
39. Li, Y.; Ye, Z.; Chen, N.; Chen, Z.; Zhang, F. Intramolecular electrochemical dehydrogenative N–N bond formation for the synthesis of 1,2,4-triazolo[1,5-a]pyridines. *Green Chem.* **2019**, *21*, 4035–4039. [CrossRef]
40. Ye, Z.; Zhang, F. Recent Advances in Constructing Nitrogen-Containing Heterocycles via Electrochemical Dehydrogenation. *Chin. J. Chem.* **2019**, *37*, 513–528. [CrossRef]
41. Feng, M.-L.; Li, S.-Q.; He, H.-Z.; Xi, L.-Y.; Chen, S.-Y.; Yu, X.-Q. Electrochemically initiated intermolecular C–N formation/cyclization of ketones with 2-aminopyridines: An efficient method for the synthesis of imidazo[1,2-a]pyridines. *Green Chem.* **2019**, *21*, 1619–1624. [CrossRef]
42. Qian, P.; Yan, Z.; Zhou, Z.; Hu, K.; Wang, J.; Li, Z.; Zha, Z.; Wang, Z. Electrocatalytic Intermolecular C(sp3)–H/N–H Coupling of Methyl N-Heteroaromatics with Amines and Amino Acids: Access to Imidazo-Fused N-Heterocycles. *Org. Lett.* **2018**, *20*, 6359–6363. [CrossRef] [PubMed]
43. Qian, P.; Yan, Z.; Zhou, Z.; Hu, K.; Wang, J.; Li, Z.; Zha, Z.; Wang, Z. Electrocatalytic Tandem Synthesis of 1,3-Disubstituted Imidazo[1,5-a]quinolines via Sequential Dual Oxidative C(sp3)–H Amination in Aqueous Medium. *J. Org. Chem.* **2019**, *84*, 3148–3157. [CrossRef] [PubMed]
44. Vil', V.A.; Grishin, S.S.; Baberkina, E.P.; Alekseenko, A.L.; Glinushkin, A.P.; Kovalenko, A.E.; Terent'ev, A.O. Electrochemical Synthesis of Tetrahydroquinolines from Imines and Cyclic Ethers via Oxidation/Aza-Diels-Alder Cycloaddition. *Adv. Synth. Catal.* **2022**, *364*, 1098–1108. [CrossRef]
45. El-Hallag, I.S. Electrochemical oxidation of iodide at a glassy carbon electrode in methylene chloride at various temperatures. *J. Chilean Chem. Soc.* **2010**, *55*, 67–73. [CrossRef]
46. Sun, J.; Nie, Q.; Fang, X.; He, Z.; Zhang, G.; Li, Y.; Li, Y. Vinyl azide as a synthon for DNA-compatible divergent transformations into N-heterocycles. *Org. Biomol. Chem.* **2022**, *20*, 5045–5049. [CrossRef]
47. Wen, J.; Shi, W.; Zhang, F.; Liu, D.; Tang, S.; Wang, H.; Lin, X.-M.; Lei, A. Electrooxidative Tandem Cyclization of Activated Alkynes with Sulfinic Acids To Access Sulfonated Indenones. *Org. Lett.* **2017**, *19*, 3131–3134. [CrossRef]
48. Liu, K.; Song, C.; Lei, A. Recent advances in iodine mediated electrochemical oxidative cross-coupling. *Org. Biomol. Chem.* **2018**, *16*, 2375–2387. [CrossRef]
49. Dey, R.; Banerjee, P. Lewis Acid Catalyzed Diastereoselective Cycloaddition Reactions of Donor–Acceptor Cyclopropanes and Vinyl Azides: Synthesis of Functionalized Azidocyclopentane and Tetrahydropyridine Derivatives. *Org. Lett.* **2017**, *19*, 304–307. [CrossRef]
50. Andresini, M.; Degannaro, L.; Luisi, R. A sustainable strategy for the straightforward preparation of 2H-azirines and highly functionalized NH-aziridines from vinyl azides using a single solvent flow-batch approach. *Beilstein J. Org. Chem.* **2021**, *17*, 203–209. [CrossRef]

molecules

MDPI

Article

Synthesis, Characterization and DFT Study of a New Family of High-Energy Compounds Based on *s*-Triazine, Carborane and Tetrazoles

Anton V. Makarenkov [1], Sergey S. Kiselev [1], Elena G. Kononova [1], Fedor M. Dolgushin [2], Alexander S. Peregudov [1], Yurii A. Borisov [1] and Valentina A. Ol'shevskaya [1,*]

[1] A.N. Nesmeyanov Institute of Organoelement Compounds, Russian Academy of Sciences, 28, bld. 1 Vavilova Street, 119334 Moscow, Russia
[2] N.S. Kurnakov Institute of General and Inorganic Chemistry, Russian Academy of Sciences, 31 Leninsky Prosp., 119071 Moscow, Russia
* Correspondence: olshevsk@ineos.ac.ru

Abstract: An efficient one-pot synthesis of carborane-containing high-energy compounds was developed via the exploration of carbon–halogen bond functionalization strategies in commercially available 2,4,6-trichloro-1,3,5-triazine. The synthetic pathway first included the substitution of two chlorine atoms in *s*-triazine with 5-R-tetrazoles (R = H, Me, Et) units to form disubstituted tetrazolyl 1,3,5-triazines followed by the sequential substitution of the remaining chlorine atom in 1,3,5-triazine with carborane N- or S-nucleophiles. All new compounds were characterized by IR- and NMR spectroscopy. The structure of four new compounds was confirmed by single crystal X-ray diffraction analysis. The density functional theory method (DFT B3LYP/6-311 + G*) was used to study the geometrical structures, enthalpies of formation (EOFs), energetic properties and highest occupied and lowest unoccupied molecular orbital (HOMO and LUMO) energies and the detonation properties of synthesized compounds. The DFT calculation revealed compounds processing the maximum value of the detonation velocity or the maximum value of the detonation pressure. Theoretical terahertz frequencies for potential high-energy density materials (HEDMs) were computed, which allow the opportunity for the remote detection of these compounds.

Keywords: carborane; tetrazole; HEMDs; DFT; single crystal X-ray diffraction

Citation: Makarenkov, A.V.; Kiselev, S.S.; Kononova, E.G.; Dolgushin, F.M.; Peregudov, A.S.; Borisov, Y.A.; Ol'shevskaya, V.A. Synthesis, Characterization and DFT Study of a New Family of High-Energy Compounds Based on *s*-Triazine, Carborane and Tetrazoles. *Molecules* **2022**, *27*, 7484. https://doi.org/10.3390/molecules27217484

Academic Editors: Alexey M. Starosotnikov, Maxim A. Bastrakov and Igor L. Dalinger

Received: 3 October 2022
Accepted: 28 October 2022
Published: 2 November 2022

1. Introduction

In recent years, extensive efforts have been devoted to the development of high-energy density materials (HEDMs) such as propellants, explosives and pyrotechnics for commercial and military applications. There are many compounds that can be attributed to this category, and the analysis of their energetic characteristics provides information on the relationship between the structure and properties [1–3]. Among them, promising types of high-energy compounds are acyclic compounds, strained, fused and caged compounds, nitrogen heterocyclic compounds [4–6]. Nitrogen-containing heterocycles have traditionally been in the center of focus in the preparation of high-energy compounds due to their large positive heat of formation, high density, insensitivity and the presence of energetic N=N and C=N bonds. Upon decomposition, nitrogen-rich molecules would produce a large quantity of nitrogen gas and large amounts of energy [7–11].

Moreover, energetic materials based on heterocyclic compounds are considered as attractive candidates for a replacement of conventional high-energy materials, such as 2,4,6-trinitrotoluene (TNT), 1,3,5-trimethylene-2,4,6-trinitramine (RDX), and 1,3,5,7-tetranitrotetraaza-cyclooctane (HMX) [12,13]. Earlier works showed that 1,3,5-triazine is an important framework for the construction of numerous energetic compounds, owing to its positive heat of formation, high nitrogen content (53.8%), and thermal stability. Moreover, their nitrogen content can be increased

by substitution with suitable functional groups. Chemically modified 1,3,5-triazine with a variety of nitrogen-containing substituents have been demonstrated to be promising HEDMs [14–16]. The key compound for their preparation is cyanuric chloride, which can be readily functionalized through the conventional S_NAr reactions with various nucleophiles including a variety of energetic moieties [17]. Indeed, the replacement of chlorine atoms in cyanuric chloride by tetrazole moieties offers the possibility of tuning the energetic properties in order to produce nitrogen-rich HEDMs with improved energetic properties [18]. Tetrazole is an important functionality of the most of energetic materials due to 80% nitrogen content, stability, and high enthalpy of formation. The enthalpies of formation of tetrazole in the crystalline and gaseous states are ΔH_f(cr) = 236.1 kJ/mol (56.4 kcal/mol) and ΔH_f(g) = 327.2 kJ/mol (78 kcal/mol), respectively [19,20]. Tetrazoles are also characterized by high potential energy and low sensitivity to friction and shock and are thus used as green energetic materials in propellants, gas generators, explosives and pyrotechnics. Tetrazoles have some advantages compared to classical high-energy materials such as lower toxicity, easier synthesis, being cleaner and environmentally friendly decomposition [21].

Among the variety of HEDMs, boron-containing materials have also drawn particular attention because of boron's high heat of combustion on both a gravimetric (58 kJ/g) and volumetric (136 kJ/cm^3) basis [22–24]. Amorphous boron of more than 99% purity is added to propellant compositions as a fuel additive and burn rate modifier [22]. However, the application of pure boron powder in the solid propellant composition has some disadvantages such as the difficulty in ignition and incomplete combustion in the presence of atmospheric oxygen [25,26]. New types of boron materials for energetic composition were prepared to resolve this problem. It is believed [27] that the use of boron in a composition with aluminum can increase the combustion efficiency of boron due to a synergistic effect of composite systems including Al and B as well as the capping of boron nanoparticles with a polymer can provide a solution to the aforementioned problem. The use of an energetic polymer for that purpose can bring additional heat close to the surface of the nanoparticles and facilitate their ignition [27].

However, nowadays studies in the field of boron HEDMs have been directed towards the preparation of the monomolecular systems featuring high heats of formation and high nitrogen content based on tetraazido-, azole and azolium borate salts [28–30]. Potential candidates for the development of new boron energetic materials with both high energy and low sensitivity are nitrogen-rich carborane systems [31,32], the functionalization strategies of which have been recently described. The *closo*-carboranes ($C_2B_{10}H_{12}$) are boron-rich icosahedral compounds with unique structural and electronic properties, remarkable thermal and chemical stability, spherical geometry, and exceptional hydrophobic character [33]. They are characterized by the existence of three-center two-electron bonds, and can be considered as three-dimensional delocalized aromatic systems [34,35], demonstrating many features with that of benzene. The remarkable thermal and chemical stabilities make them unique candidates for use in several special applications in the fields of materials science [36,37] including HEDMs since they demonstrate a high enthalpy (ΔH_f = 42 kcal/mol) of formation [38]. Previously, it was shown by us that carboranyl-substituted tetrazoles are prospective for their potential applications as HEDMs [31,32]. In this work, aiming to achieve promising energy-rich materials with carborane exploration, the synthetic route for three-component high energy systems containing *s*-triazine, carborane and tetrazoles within one molecule was been developed. Spectroscopic, structural data and DFT calculations for new compounds are reported.

2. Result and Discussion

2.1. Synthesis

Our initial goal was to develop an efficient strategy for the preparation of nitrogen-rich carborane-containing HEDMs. 2,4,6-Trichloro-1,3,5-triazine, i.e., cyanuric chloride (**1**), was suggested as the trifunctional rigid linker for the synthesis of desired compounds since it is a relatively stable nitrogen heteroaromatic system, promising for derivatization with various

nucleophiles during S_NAr reaction capable of forming a variety of highly structured polyfunctionalized intermediates [39]. The synthetic pathway to obtain new *s*-triazine derivatives modified with tetrazoles and carborane cluster is shown in Scheme 1.

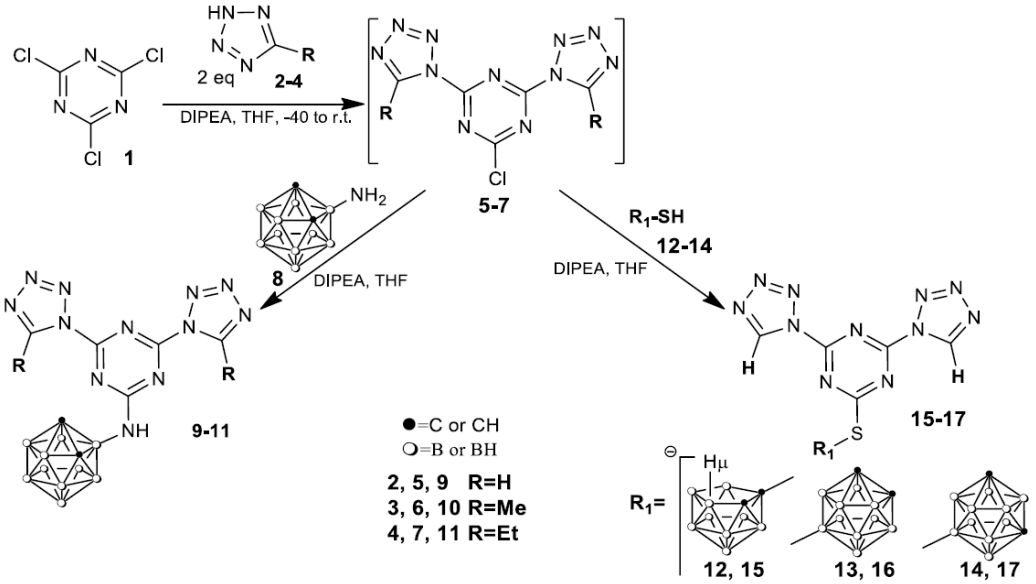

Scheme 1. Reactions of intermediates **5**–**7** with amino- and mercaptocarboranes.

Tetrazoles **2**–**4** were reacted with cyanuric chloride **1** (molar ratio 2:1) at −40 °C to ambient temperature for 2–24 h in THF in the presence of DIPEA as an HCl scavenger demonstrating, by TLC ($CHCl_3$-acetone 10:1), the formation of 2-chloro-4,6-ditetrazolyl-1,3,5-triazines intermediates **5**–**7**. It should be noted that the formation of disubstituted compounds **5**–**7** depends on the structure of tetrazoles **2**–**4** and under similar reaction conditions, a decrease in the reactivity and a significant increase in the reaction time in series **2** (2–3 h) ≥ **3** (6–7 h) ≥ **4** (24 h) were observed. The sequential substitution of the remaining electrophilic site in **5**–**7** with the carborane cluster was carried out by treating the reaction mixture with 3-amino-*o*-carborane **8** [40] and heating at 20–25 °C for 20–24 h to afford the desired compounds **9**–**11** in 59–84% isolated yields as white solids.

At the same time, the reactivity of intermediate **5** towards isomeric mercapto carboranes **12**–**14** in which mercapto group is bound to electron-deficient **12** [41] or electron-donating **13**, **14** carborane groups [42] was studied in order to clarify the effect of the carborane structure on the energetic characteristics of the synthesized compounds. The reaction of **5** with carboranes **12**–**14** readily proceeded in THF in the presence of DIPEA for 3 h at ambient temperature to afford compounds **15**–**17** in 50–79% yields. It was found that the reaction of carborane **12** with **5** is accompanied by the deboronation of a *closo*-carborane cluster to afford anionic *nido*-derivative **15**, obtained as cesium salt.

A similar reaction of phenyltetrazole **18** with cyanuric chloride **1** and aminocarborane **8** led to the formation of a complex mixture of products from which three substances were isolated and characterized by X-ray diffraction analysis (Scheme 2), namely 5-(*o*-carborane-3-yl)amino-2,9-diphenylbis [1,2,4]tri-azolo[1,5-a:1′,5′-c][1,3,5]triazine **19**, 2-(2-benzoylhydrazinyl)-4-(*o*-carborane-3-yl)amino- 6-(5-phenyl-2*H*-tetrazol-2-yl)-1,3,5-triazine **20** and 3,7,11-triphenyltris([1,2,4]triazolo) [4,3-a:4′,3′-c:4′′,3′′-e] [1,3,5]triazine **21**.

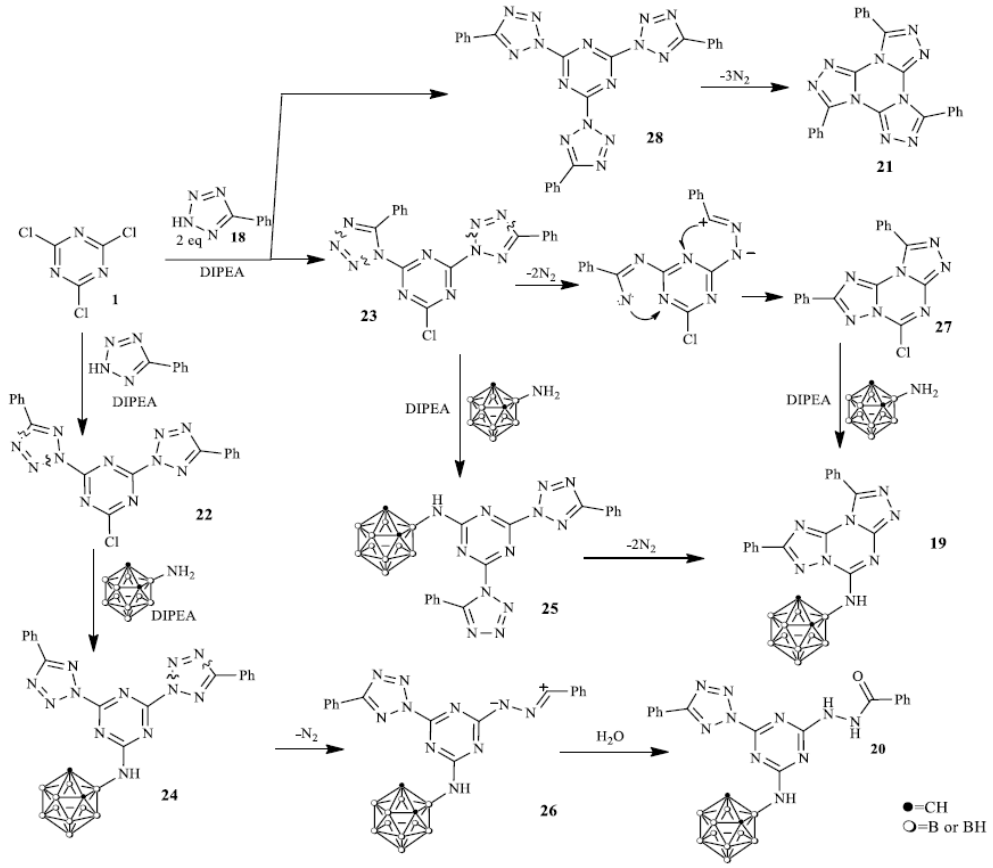

Scheme 2. Reaction of phenyltetrazole **18** with aminocarborane **8**.

A very concise discussion of the key players in this area and their contribution may also be placed here. The reaction of the tetrazole **18** and cyanuric chloride **1** led to the formation of tetrazole N^1- and N^2-substituted [43–46] *s*-triazine regioisomers **22**, **23** and their reaction with carborane **8** resulted in the formation of unstable intermediates **24**, **25**. The evolution of nitrogen in compound **25** afforded fused carborane triazolotriazine **19** according to the known rearrangement [47] while **24** was received via the interaction of the intermediate 1,3-dipole **26** with H_2O [48] used for the reaction treatment. Trimer **21** could be formed via a self-cyclization of the symmetrical tris(tetrazolyl)triazine **28** [47,49,50]. The low thermal stability of intermediates **22**–**25** is in good agreement with the DFT calculations. DFT calculations (Figure 1) for compound **25** showed that this compound can be easily transformed into a stable compound **19** via a successive evolution of nitrogen molecules from two tetrazole rings in **25**. This process can be characterized by a negative value of the enthalpy of the process and a change in the Gibbs free energy (in parentheses) in the form of the following the equation:

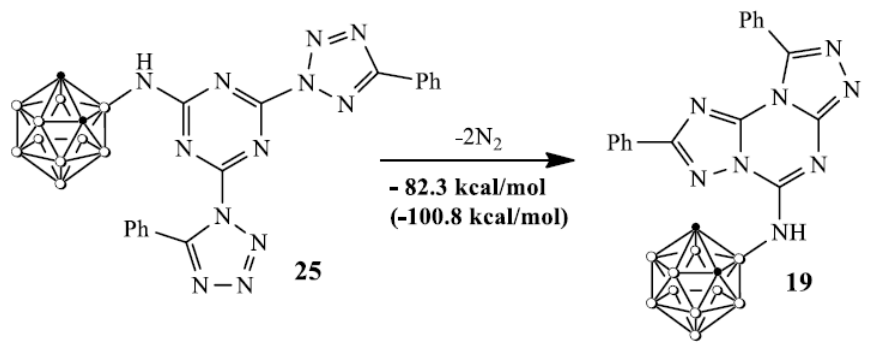

Figure 1. Values of enthalpy and a change in the Gibbs free energy in the process of transformation of **25** into **19**.

Apparently, the ease of the decomposition of complex **25** with the release of two nitrogen molecules is due to the relatively small activation energy of this process. Simple energy estimation confirms this conclusion. The comparison of similar reactions for compounds **9** and **10**, where R = H and Me, showed that the activation energies for R = Ph are approximately 20 kcal lower than for compounds **9** and **10**.

2.2. NMR Spectral Data of Prepared Compounds

All the prepared compounds are stable in air and could be stored for extended periods of time.

In the ^{1}H NMR spectra, tetrazole CH protons in compound **9** (Figure S1) appeared downfield at δ = 10.1 ppm, protons of the tetrazole methyl groups in compound **10** (Figure S9) were observed at δ = 3.0 ppm and protons of the tetrazole ethyl groups in compound **11** (Figure S11) were observed at δ = 3.5 ppm (CH_2) and δ = 1.4 ppm (CH_3), respectively. The protons of B^3-NH amino groups in all synthesized compounds were observed as broad singlets at δ = 9.0–9.1 ppm. The signals of the carborane CH protons in compounds **9**–**11** shifted downfield relatively to the corresponding signals in amine **8** due to the electron-withdrawal effect of the *s*-triazine ring and manifested as broad singlets at δ = 5.3 ppm. The ^{11}B NMR spectra for compounds **9**–**11** are also in good agreement with the structures of the synthesized compounds and are in the range from δ = −4.5 to −14.5 ppm, supporting the *closo*-structure of carborane polyhedron. The signals of the substituted B^3-NH atoms appeared as singlets in the region of δ = −6.0−−6.5 ppm. In ^{1}H NMR spectra, the signals of tetrazole CH protons in *s*-triazines **15**–**17** were observed as singlets at δ = 8.95–10.17 ppm, as in the case of compounds **9**–**11**, which indicates the absence of a significant influence of the carborane electronic properties on the tetrazole ring. The signal of the carborane CH protons for compound **17** (Figure S21) was observed as a broadened singlet at δ = 3.98 ppm, whereas in the case of compounds **15** and **16**, carborane CH protons appeared as two broadened singlets at δ = 3.16, 3.69 ppm for **15** (Figure S17) and at δ = 4.84, 4.90 ppm for **16** (Figure S19). The ^{11}B NMR signals of compounds **16** and **17** are in a range from δ = 1.8 to −14.4 ppm for **16** and from −4.4 to −17.5 ppm for **17** and the signals of substituted boron atoms in position 9 were observed as singlets at δ = 1.8 ppm and −4.4 ppm for compounds **16** (Figure S20) and **17** (Figure S22), respectively. For *nido*-derivative **15** (Figure S17), a characteristic extra hydrogen atom signal was observed in the ^{1}H NMR spectrum at δ = −1.9 ppm in the form of a broadened doublet, and in the ^{11}B NMR spectrum, a characteristic doublet of doublet signal was observed at δ = −34.4 ppm (Figure S18), attributed to the boron atom in position 10 of *nido*-carborane polyhedron.

Nevertheless, it should be noted that special features for compounds **9**–**11** were observed in their NMR spectra. In the NMR spectra of 5-alkyl (**10**, **11**) and 5-H (**9**) carborane-substituted bis(tetrazolyl)-*s*-triazines prepared using 3-amino-*o*-carborane **8**, a splitting of signals related to protons of alkyl groups of substituted tetrazoles **10**, **11** and protons of the CH-group of the unsubstituted tetrazole ring of the compound **9** is observed. Initially, the splitting of the proton signal of tetrazole ring substituents in the ^{1}H NMR spectra was attributed to the formation of a mixture of 4- and 5-isomeric tetrazoles, which was observed for the most spatially hindered phenyl-tetrazole **18** and described in detail in the literature [43–46]; however, in this case, the ratio of the tetrazole ring proton signals should have shifted towards 1,4-tetrazoles in accordance with the increase in the steric effect of the substituent in the starting compounds. However, this was not found in real spectra. In all cases, the signal was divided into two equal multiplets, in which the spin–spin interaction constants correspond to the proton interaction usual for such groups. The most likely explanation of this phenomenon is the hindrance rotation of the 3-amino-*o*-carborane fragment and tetrazoles relative to the central *s*-triazine ring. To confirm this idea, the NMR spectra of compound **9** were recorded in both acetone-D_6 (Figure S1) and acetonitrile-D_3 (Figure S2), since their ability to coordinate with the amino group at the carborane fragment and heterocycles is significantly different. In the less coordinating acetonitrile, an increase in the difference between the signals was found to be almost twice without changing the

ratio of their integrals, which indicates in favor of the hypothesis of a hindrance rotation. This conclusion was also supported by the ^{1}H NMR spectra of compound **9** recorded in acetone at different temperatures (Figure S4). A gradual broadening and fusion of the proton signals of the tetrazole CH groups with an increase in temperature was observed, which is characteristic of the splitting of the proton signal caused by hindrance rotation (Figure 2).

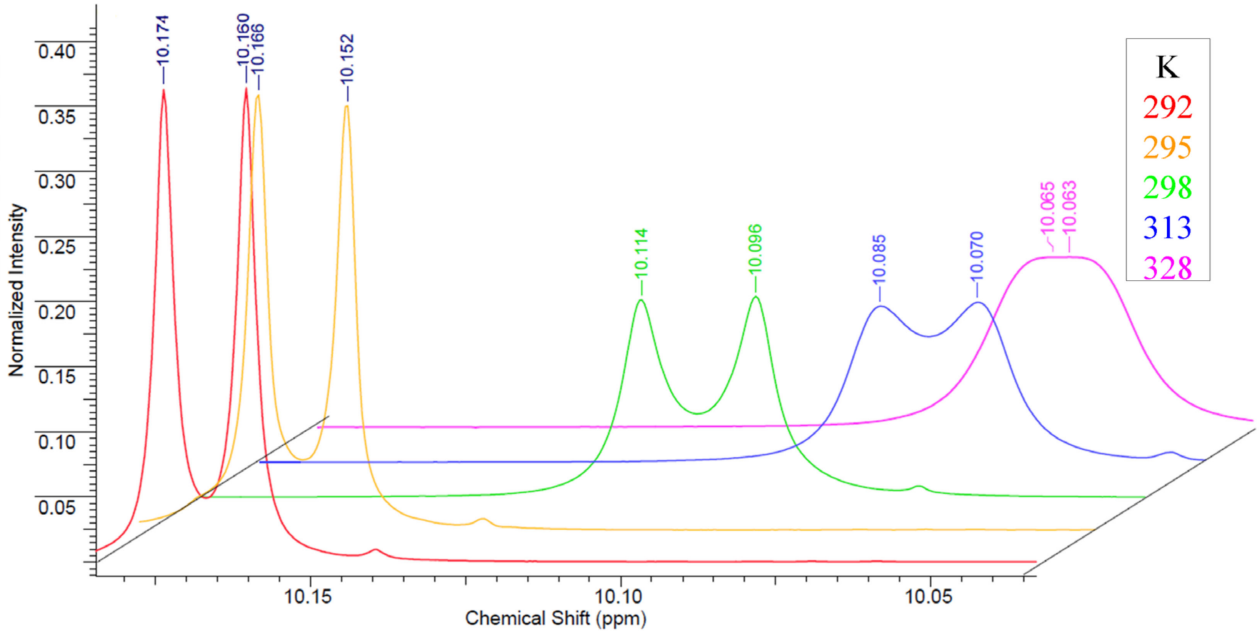

Figure 2. ^{1}H NMR spectra of compound **9** recorded in acetone-D_6 at different temperatures.

The structure of compound **9** was also studied with NOESY(EXSY) NMR spectra (Figure S7). The broad signal of the NH proton reveals a lower intensity (0.4) due to the exchange with H_2O protons. The presence of such an exchange follows from the NOESY(EXSY) NMR spectra (Figure S7). In this spectrum, in addition to antiphase signals related to spatially close CH protons of carborane and tetrazole, in-phase cross peaks of the NH proton (δ = 9.09 ppm) with signals at δ = 3.78 ppm and δ = 2.88 ppm were found. These signals, apparently, correspond to water protons, which has been confirmed by the absence of correlation peaks in the HMQC NMR spectrum (Figure S8). The doubling of the signals in these NMR spectra is due to the different shielding of the indicator signals of compound **9** in the two conformations (see above in the discussion of the results). No such effect was observed in compounds **15**–**17** prepared using mercaptocarboranes.

The structure of compound **9** was also supported by the X-ray diffraction study (Figure 3). This substance crystallizes with one acetone molecule and has a certain degree of disorder in the superposition of the tetrazole CH group and nitrogen atom. Despite the fact that the X-ray data of compound **9** are not completely unambiguous, according to the totality of information based on the NMR spectra and X-ray study and taking into account the data obtained by the X-ray study for **10**, it can be unequivocally stated that the observed splitting of the signal of protons of alkyl groups of substituted tetrazoles **10**, **11** and protons of the CH-group of the unsubstituted tetrazole ring of compound **9** is due to the hindrance rotation of the 3-amino-*o*-carborane fragment and tetrazoles relative to the central *s*-triazine ring.

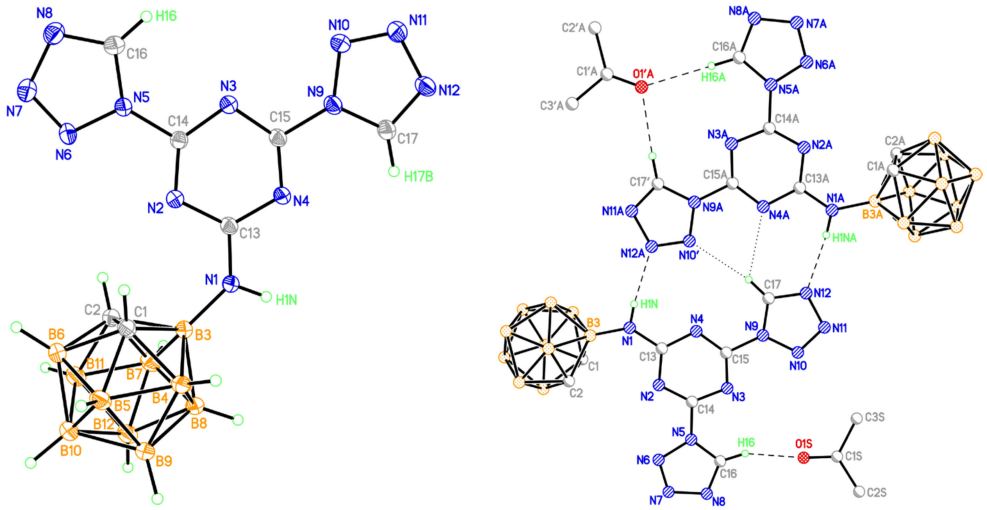

Figure 3. (**a**) Molecular structure of compound **9** (thermal ellipsoids are drawn at the 50% probability level). (**b**) Hydrogen-bonded associate of two conformers of compound **9** (only those hydrogen atoms that are involved in hydrogen bonds are shown).

2.3. X-ray Crystallography

The crystals of compounds **9** and **10** suitable for X-ray diffraction were obtained by the slow evaporation of acetone at room temperature from the solution of the corresponding compound, whereas crystals of **19** and **20** were obtained by the slow evaporation of the solution system chloroform–methanol (10:1) for **19** and dichloromethane-ethyl acetate (8:1) for **20** at room temperature, respectively. The molecular structures of **9**, **10**, **19** and **20** were determined by means of the single crystal X-ray diffraction study (Figures 3–8). Selected data and parameters of X-ray structures for **9**, **10**, **19** and **20** are given in the ESI (Tables S1–S9).

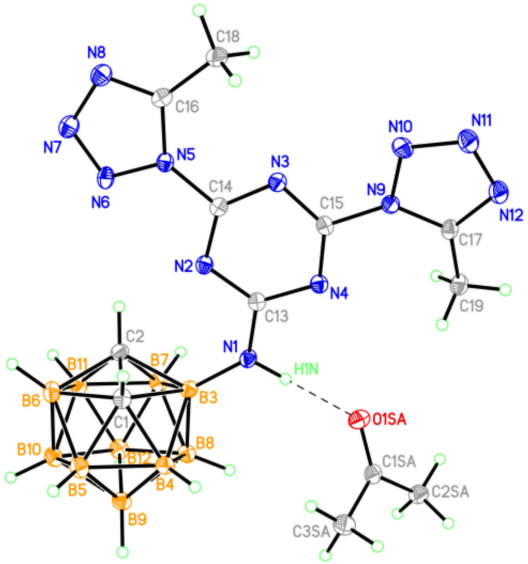

Figure 4. The general view of compound **10** in the crystal (thermal ellipsoids are drawn at the 50% probability level.

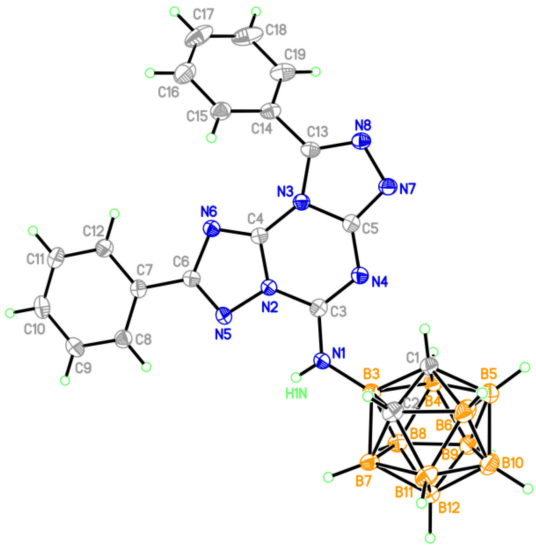

Figure 5. Molecular structure of compound **19** (thermal ellipsoids are drawn at the 50% probability level).

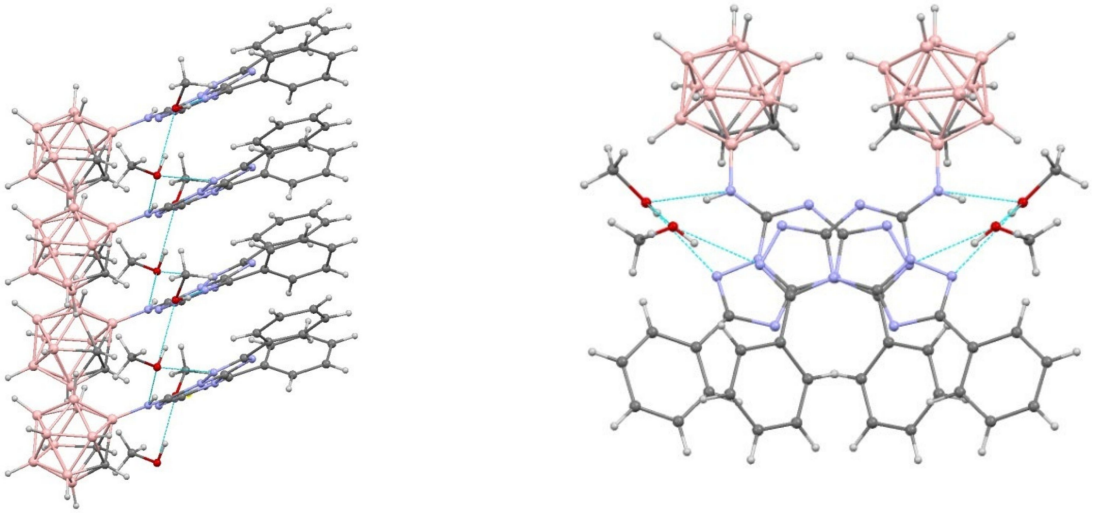

(**a**) (**b**)

Figure 6. A fragment of an H-bonded stack in the crystal structure of 19 in two projections: (**a**) along the *a* axis of the crystal; and (**b**) along the *c* axis of the crystal.

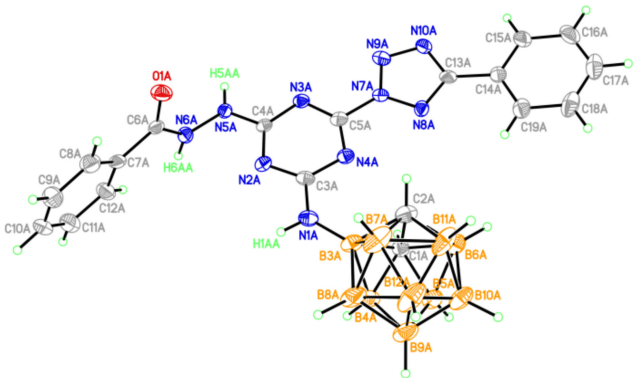

Figure 7. One of two crystallographically independent molecules (A) of compound **20** (thermal ellipsoids are drawn at the 50% probability level).

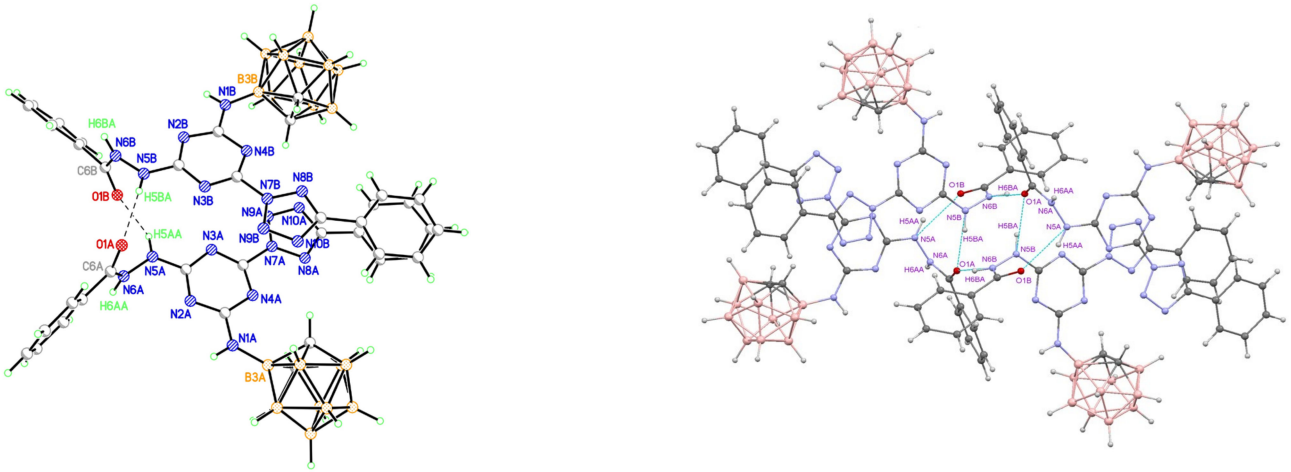

(**a**) (**b**)

Figure 8. (**a**) H-Bonded dimer formed by two crystallographically independent molecules (A and B) of compound **20**; and (**b**) centrosymmetric H-bonded tetramers.

According to the X-ray data, both tetrazole rings in **9** are in the plane of the central *s*-triazine cycle (the dihedral angles between planes of the tetrazole and *s*-triazine units are 3.6 and 7.3°). However, the degree of delocalization in the heterocyclic π-system is low, as evidenced by the noticeable alternation of the lengths of C-N and N-N bonds, especially in five-membered tetrazole rings (Table S1). In the crystal, numerous stacking contacts between the planar heterocyclic systems of adjacent molecules are formed (the interplanar distances are 3.27 and 3.29 Å, the shortest interatomic contacts are C(13)···N(7)$_{-1+x,y,z}$ 3.016(2) Å, C(15)···N(8)$_{-1+x,y,z}$ 3.186(2) Å, C(15)···C(15)$_{-x,1-y,1-z}$ 3.293(2) Å, C(13)···N(10)$_{-x,1-y,1-z}$ 3.209(2) Å). The structure of the carborane polyhedron in **9** (bond lengths are C(1)-C(2) 1.650(2), C-B 1.692(2)-1.718(2), B-B 1.767(2)-1.795(2) Å), as in other studied compounds, corresponds to the standard geometry of the icosahedral *o*-$C_2B_{10}H_{12}$ carborane. The positions of N(10) and C(17) atoms (Figure 3a) are occupied by carbon and nitrogen atoms with equal contribution; this observation implies the presence of two conformers of compound **9** in the crystal. One of the possible hydrogen-bonded associates of two conformers of compound **9** united by two N-H···N hydrogen bonds and C-H···N contacts is presented in Figure 3b.

A solvate acetone molecule is present in the independent part of the unit cell. These solvate molecules are bound to the molecules of compound **9** by either one or two C-H···O hydrogen bonds (Table S6). The H-bonded dimers of **9** form stacks along the [1 1 0] crystallographic direction, which, due to π–π interactions between terminal tetrazole rings (the shortest interatomic contact is N(6)···N(7)$_{1-x,2-y,1-z}$ 3.042(2) Å), are combined into double layers parallel to *ab* plane (Figure S23). The layers are additionally stabilized due to weak C-H···N hydrogen bonds between the carborane fragments and the nitrogen atoms of the tetrazole rings of neighboring molecules (Table S6). Each layer is framed on the outer side by a hydrophobic surface of carborane fragments, and there are no shortened contacts between the layers.

Methyl substituents at the carbon atoms of the five-membered heterocycles in **10** (Figure 4) create steric hindrance to the formation of hydrogen-bonded dimers in the crystal, as observed in structure **9**. In the independent part of the unit cell, there is a solvate acetone molecule, the oxygen atom of which serves as an acceptor of the H-bond with molecule **10** (Table S7).

The methyl substituents lead to a slight violation of the planarity of the heterocyclic system (the dihedral angles between the planes of the tetrazole and *s*-triazine units are 10.3 and 14.6°). Nevertheless, in structure **10**, as in structure **9**, stacking contacts between neighboring molecules are also observed, although with looser stacking (interplanar distances are increased to 3.59 Å). The s-triazine rings in **9** and **10** are flat with an accuracy of 0.02 Å.

In crystal **10**, the supramolecular assembling is close to that observed in **9**. The layered packing with shortened stacking contacts between heterocyclic systems and no specific interactions between layers is observed (Figure S24).

In compound **19** (Figure 5), six and five fused membered rings in the tricyclic fragment have a planar structure (the maximum deviation from the plane of the triazine ring is 0.19 Å for the N8 atom) with phenyl substituents twisted from this plane by 17.3° (at C(6) atom) and 38.6° (at C(13) atom).

Fused heterocycles form compact stacks (Figure 6) extended along the *c* axis of the crystal with interplanar separations of 3.3 Å and shortest interatomic contacts of C(6)···N(8)$_{0.5-x,y,\ -0.5+z}$ 3.122(4) Å and N(6)···C(13)$_{0.5-x,y,\ -0.5+z}$ 3.107(4) Å.

In the independent part of the unit cell of **19**, there are two solvate methanol molecules that additionally stabilize the stack by linking neighboring molecules with a network of H-bonds (Table S8). These stacks are joined in the crystal exclusively due to weak van der Waals interactions, i.e., C-H···C, C-H···O, and H···H. However, in this structure, as in **9** and **10**, layers containing either heterocyclic or carborane fragments of molecules can be distinguished (Figure S25).

In the independent part of the unit cell of **20,** there are two crystallographically independent molecules (A and B) that have the same spatial structure (Figure 7).

In both independent molecules of compound **20**, the tetrazole ring and the phenyl substituent are in the plane of the central *s*-triazine ring (the dihedral angles between planes of these rings range from 2.4 to 11.0°). The benzoylhydrazinyl group is almost orthogonal to the plane of the triazine ring (the C(4)-N(5)-N(6)-C(6) torsion angle is 87.7(4) and 81.8(4)° in A and B, respectively). Similarly to what was observed in structures **9**, **10**, and **19**, in the crystal of **20,** the set of specific intermolecular interactions namely, hydrogen bonds and π–π stacking interactions, were realized. Two independent molecules of compound **20** form centrosymmetric H-bonded tetramers (Figure 8 and Table S9), which are joined in the crystal due to π–π stacking interactions (the interplanar distance is 3.2 Å, the shortest interatomic contacts are C(5A)···C(5A)$_{1-x,1-y,1-z}$ 3.223(7) Å, C(3A)···N(9A)$_{1-x,1-y,1-z}$ 3.235(7) Å, C(5A)···N(9B) 3.222(7) Å). The crystal packing of **20** has a layered structure with alternating heterocyclic and carborane fragments (Figure S26).

Hirshfeld Surface Analysis

Hirshfeld surface (HS) analysis is documented as an authoritative tool to qualitatively assess the nature of intermolecular interactions within crystal structures and thoroughly identify the interactions throughout the surface around the molecules [51–54].

Hirshfeld surface, overall interactions and individual interatomic contacts were computed using the CrystalExplorer17 software [55] for all the compounds studied by X-ray. The obtained data agree well with the X-ray data presented above for molecules **9**, **10**, **19,** and **20** and add a quantification of intermolecular interactions.

Contacts H···H contribute the most to the crystal packing of compound **9**, **10**, **19**, **20**, with a percentage contribution from 45.5% to 60.5%. These are the most crucial and significant interatomic contacts. In addition to the H···H contacts, the N···H and C···H contacts are also crucial in defining the crystal packing. Hirshfeld surface analysis showed that important contributions to the crystal packing of compounds **9** (Figures S27 and S28) and **10** (Figures S29 and S30) are from N···H interactions (29.2% and 28.5%, respectively), while C···H interactions are less essential (less 4%). On the contrary, we found for compounds **19** (Figures S31 and S32) and **20** (Figures S33–S35) that intermolecular C···H contacts (14.4% and ~16%, respectively) make the largest contributions to crystal packing, while N···H contacts (10.5% and ~12%, respectively) are slightly inferior. Additionally, the notable contribution of N···N and C···N contacts (7–10%) which corresponds to π–π interactions between flat heterocycle fragments of the molecules should also be noted in all the structures.

In spite of a notable difference in the values of individual interatomic contacts in pairs **9**, **10** and **19**, **20**, the supramolecular packing of all the compounds studied was

characterized by common features, namely the alternation of hydrophobic fragments formed by the interaction of boron clusters where H···H contacts dominate and fragments with a domination of N···H contacts (H-bonds) where heterocycle fragments are grouped. (Figures S36 and S37).

*2.4. Theoretical Studies of Carborane-Substituted Bis(Tetrazolyl)-s-triazines (***9**–**11**, **15**–**17***)*

2.4.1. Computational Details

The calculations of compounds **9**–**11**, **15**–**17** were performed according to density functional theory (DFT) [56]. The Becke–Lee–Yang–Parr hybrid functional (B3LYP) [57,58] was applied in basis 6-311 + G*. All calculations with a full optimization of the geometry of molecules and calculation of normal oscillation frequencies at 298 K and 1 atm were performed using the GAUSSIAN-09 program [59] under the LINUX operating system. If the imaginary frequencies of normal vibrations appeared, the optimization was repeated. The accuracy of the results of the calculated geometry optimization was supported by the comparison of the computed data with the experimental ones obtained for compounds **9** and **10** by X-ray single crystal analysis.

2.4.2. Geometry and Electronic Structure

The results of the geometry optimization for all prepared compounds are given in Table S10 (Supplementary Materials), while the geometry of molecule **10** is presented below (Figure 9).

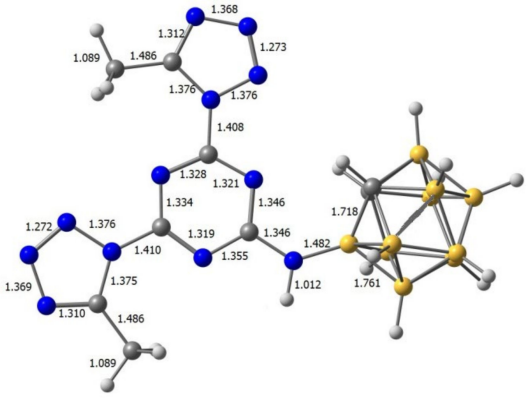

Figure 9. Calculated geometry of compound **10**.

A comparison of the experimental and theoretical interatomic distances of molecule **10** (Table 1) demonstrates that the calculations at the DFT B3LYP/6-311 + G* level can be considered as an adequate one for the geometry optimization of the carborane-substituted bis(tetrazolyl)-*s*-triazines.

Table 1. Comparison of the experimental and theoretical interatomic distances for molecule **10**.

Interatomic Distances	Experiment, Å	Calculations, Å
N=N (tetrazole)	1.281(2)–1.284(2)	1.272
N-N (tetrazole)	1.372(1)–1.380(2)	1.369, 1.376
C=N (tetrazole)	1.312(2)	1.312
C-N (tetrazole)	1.364(2)–1.366(2)	1.375
C-C (tetrazole-alkyl)	1.483(2)	1.486
N-C (triazine)	1.313(2)–1.362(2)	1.346
B-B (carborane)	1.761(2)–1.790(2)	1.761
C-B (carborane)	1.691(2)–1.726(2)	1.718
C-C (carborane)	1.645(2)	1.641

The calculated values of the total energy and entropy of compounds **9–11**, **15–17** (6-311 + G* basis set) in the gas phase based on computed geometries are listed in Table S11.

The thermal stability and impact sensitivity of HEDM are of great importance during their manufacturing, storage and handling. The energy gaps (Δε) between HOMO and LUMO help characterize the chemical reactivity and kinetic stability of molecules [60–63]. It is quite expected that the variation of the nature of substituents, their position and number can change the value of the HOMO–LUMO gap which thus affects the reactivity and stability of the compounds.

In recent works [64,65], the B3LYP functional was successfully used for carborane systems and the accuracy of the applied DFT/B3LYP method was confirmed by calculations in the MRCC3 software package [64].

The calculated values of HOMO and LUMO energies based on the DFT B3LYP/6-311 + G* level for the compounds **9–11** and **15–17** in a gas phase are presented in Table 2 while the plots of HOMO and LUMO iso-surfaces are provided in Figure 10.

Table 2. Computed HOMO and LUMO energies and the frontier molecular orbital energy gap values for compounds **9–11** and **15–17** in gas phase.

Compound	HOMO, eV	LUMO, eV	Δε, eV
9	−8.35	−3.40	4.95
10	−8.20	−3.16	5.15
11	−8.17	−3.12	5.05
15	−8.33	−3.75	4.57
16	−7.46	−2.97	4.49
17	−7.54	−3.05	4.49

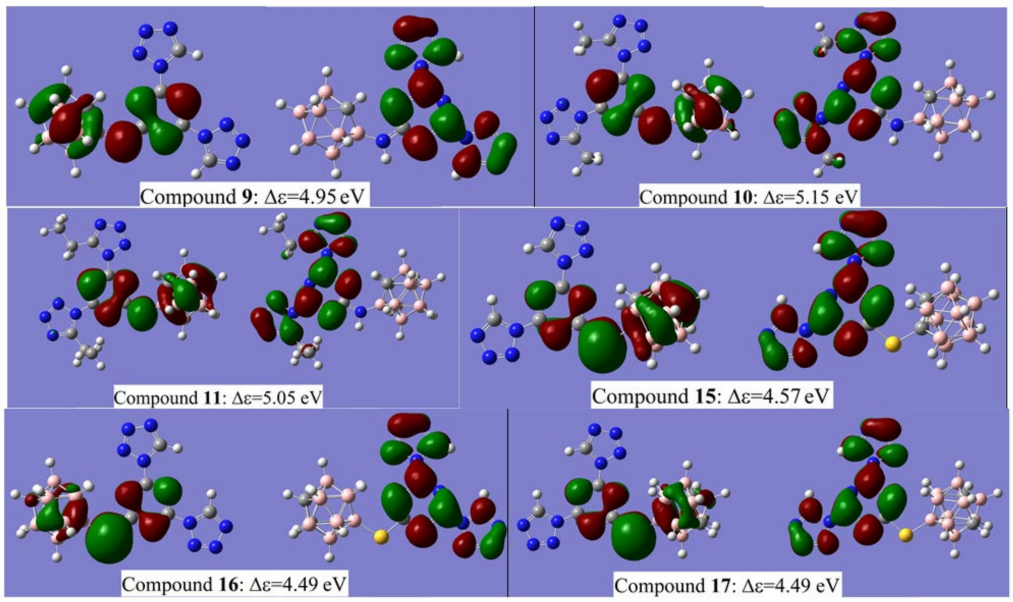

Figure 10. Plots of HOMO (left) and LUMO (right) *iso*-surfaces for compounds **9–11** and **15–17**.

The results of the visualization of HOMO and LUMO *iso*-surfaces demonstrate that for all molecules studied, the HOMO *iso*-surface is mainly localized on carborane and *s*-triazine moieties and either on the -NH- or -S- linker. The LUMO *iso*-surface can be found on tetrazole and *s*-triazine fragments. The substitution of the boron atom of carborane cages elevates both HOMO and LUMO levels, while on carbon atom reduces them. Methyl and ethyl substituents in tetrazole rings attached to *s*-triazine elevate the HOMO energy and reduce LUMO energy. The presence of sulfur linker elevates both HOMO and LUMO energy levels. Due to this complicated influence of the structural units, compounds **9**, **10** and **11** are characterized by the largest computed values of Δε. These are 116, 121 and 119

kcal/mol, respectively. However, magnitudes of Δε found for compounds **15**, **16** and **17** are less (107, 105 and 105 kcal/mol) compared to **9**, **10** and **11**, as these types of energetic materials are still less impact-sensitive than classical diaminotrinitrobenzene (DATB) and trinitroaniline (TNA), whose Δε values are 91 kcal/mol and 90 kcal/mol, respectively [60].

2.4.3. The Evaluation of the Enthalpy of Formation (EOF) of the Carborane-Substituted Bis(Tetrazolyl)-s-triazines in a Gas Phase

EOF is an important parameter for the description of the energetic materials. As there are few experimental data on the EOFs of the high-energy carborane compounds studied in the literature, the application of quantum-chemical calculations becomes essential. The EOF estimation of the compounds requires the knowledge of their total energies and the total energies of the combining elements at the standard conditions.

For the estimation of the EOFs of HEMDs, the method of isodesmic reactions is used [66] and good results can be achieved in the reactions where atomic groups are kept invariable. However, only the precise experimental values for all the model compounds allow you to attain the high accuracy. To overcome the errors caused by the difference in the experimental magnitudes of the EOF of the model compound, it is needed to consider at least several isodesmic reactions with the various components. However, for some compounds under investigation, no experimental data on EOFs even for the possible model compounds were found.

As a result, the EOF values based on DFT B3LYP/6-311 + G* calculations for the molecules in a gas phase were used in the present work. As in the case of graphite and crystalline boron, such computations are inapplicable, and the assumption about the equality of the calculated and experimental EOF values for the gas molecules of 2H-tetrazole and o-carborane was applied [38,67,68]. The total energies with the correction on zero vibrations E_{zpc} were used. These computed parameters are E′(C) = −38.12527664 a.u., E′(B) = −24.867864 a.u., E′(S) = −398.2066 a.e. To confirm the reliability of the data found for carbon, boron and sulfur, the calculations for similar molecules were carried out. The theoretical results compared with the experimental ones are presented in Table S7. The data presented in Table S7 demonstrate that this method of the estimation of EOF gives a deviation of the calculated values from the experimental ones on 4–5%. The plot of the interdependence of our calculated EOF magnitudes and the experimental ones for the test compounds is shown on Figure 11.

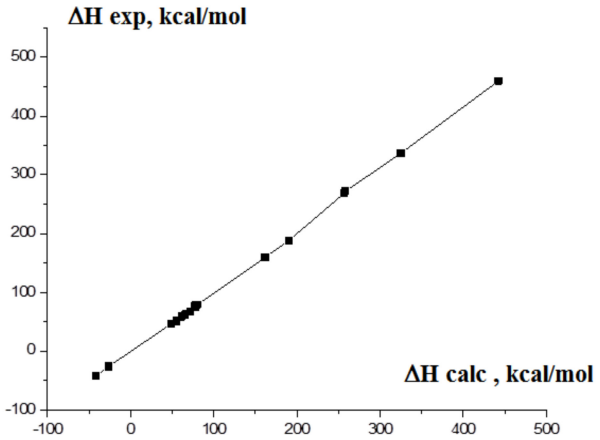

Figure 11. The interdependence of the calculated and experimental EOF values of tested compounds.

Using the values of parameters [32] for the crystalline carbon and boron, the EOF magnitudes of compounds **9**–**11** and **15**–**17** were calculated (see Table 3).

Table 3. Calculated values of EOFs (ΔH_{298}) of compounds **9**–**11** and **15**–**17** (B3LYP 6-311 + G*).

Compound	ΔH_{298}, kcal/mol	Compound	ΔH_{298}, kcal/mol
9	181.90	**2** [a]	198.09
10	165.70	**3** [a]	181.78
11	165.11	**4** [a]	131.44
15	217.07		
16	191.93		
17	176.69		

[a] Magnitudes for **2**–**4** were taken from Yu. A. Borisov et al. [32].

According to the data of Table 3, the lowest EOF values can be found in the case of molecules with an NH-linker which indicates their greater stability among the studied compounds. As for energetic properties, all of them are characterized by rather high EOF magnitudes and can be considered to be promising HEDMs as their EOF values are notably higher than those of trinitrotoluene (TNT) and hexogen (RDX, Research Department Explosive) (79.45 and 59.20 kcal/mol), respectively, calculated in [69].

2.4.4. Predicted Detonation Performances

The detonation velocity and the pressure of detonation are important parameters in the field of explosives engineering. For the computation of the detonation properties of carborane-substituted bis(tetrazolyl)-*s*-triazines, the method given in [70,71] was applied. The detonation velocity (D) and the pressure of detonation (P) are described with Kamlet–Jacobs semi-empirical equations:

$$D = 1.01 \cdot (N \cdot M^{1/2} \cdot Q^{1/2})^{1/2} \cdot (1 + 1.30\ p_0); P = 1.558 \cdot p_0{}^2 \cdot N \cdot M^{1/2} \cdot Q^{1/2}$$

where D is the velocity of detonation (km/s); P—pressure of detonation (kbar); N—a mole number of detonated gas per mole of the explosive material (EM); M—mole mass (g/mol) of the detonated gas; Q—heat of explosion EM (J/g); and p_0—density of EM (g/cm^3).

The computed values of the heat of explosion Q (J/g), the velocity of detonation D (km/s), and the pressure of detonation P (GPa) of molecules **9**–**11** and **15**–**17** in a gaseous phase are given in Table 4.

Table 4. The calculated values of the detonation properties of compounds **9**–**11** and **15**–**17**.

Compound	N_g	M_g, g/mol	Q, J/g	p_0, g/cm^3	D, km/s	P, GPa
9	13	376.24	2022.22	1.25	7.21	50.233
10	15	404.27	1716.54	1.53	7.61	76.286
11	17	432.30	1599.36	1.34	7.43	60.147
15	12	393.20	2311.36	1.36	12.14	54.32
16	12	393.20	2043.67	1.34	11.77	51.08
17	12	393.20	1881.40	1.36	11.53	49.01

Based on the dataset of Tables 3 and 4, all the studied carborane-substituted bis(tetrazolyl)-*s*-triazines can be considered to be promising candidates for HEDMs as the EOFs of all these compounds exceeds the EOF of the known explosive RDX (189.5 kJ/mol or 45.3 kcal/mol) [72,73]. The EOF values for the most energetic compounds **9**, **15** and **16** are 4.0, 4.7 and 3.9 times larger than the same parameters in the case of RDX. Moreover, the computed pressure of the detonation of the compounds **9**, **10**, **11** and **15** exceeds the pressure at the front of the RDX shock wave (approximately 30 GPa [74–76]) by 1.7-fold, 2.5-fold, 2.0-fold and 1.8-fold, respectively.

2.4.5. Calculation of Terahertz Spectra of Compounds **9**–**11** and **15**–**17**

The development of technologies to perform the remote detection of dangerous substances is in very high demand in different fields. Recently, these methods have been complemented by impulse terahertz spectroscopy. Many compounds are characterized by the spectral fingerprints in the terahertz range (usually in the ~0.1–3.0 THz region [77]) which makes terahertz radiation suitable for their identification. Moreover, the transparency of many materials to THz radiation discovers the great possibility for the application of this technique in the security maintenance.

In this section of the paper, the computed frequencies (v; THz) and the corresponding intensities (H; A^4/AMU, AMU—reduced masses) of the terahertz spectra (DFT B3LYP/6-311 + G*) of compounds **9**–**11** and **15**–**17** in the 0.1–3.0 THz range are presented in Table 5.

Table 5. The calculated terahertz spectra of compounds **9**–**11** and **15**–**17**.

№	v; THz	H; A^4/AMU
9	0.6318, 0.8716, 1.2169, 1.4147, 1.4726, 2.1909, 2.5481, 3.0131	0.0013, 7.7105, 0.3268, 2.1826, 0.0605, 0.9840, 4.8842, 0.1518
10	0.4804, 0.5809, 0.7574, 0.8082, 1.371, 2.2101, 2.3605, 3.2013	0.0488, 3.4348, 7.2903, 1.1846, 2.0584, 1.2134, 4.6308, 0.2778
11	0.3168, 0.4199, 0.5698, 0.8613, 1.3083, 1.8885, 2.1009, 2.4997, 2.7895	0.8664, 0.5331, 2.6898, 4.5956, 1.7012, 2.2347, 2.0728, 1.4025, 0.3292
15	0.5478, 0.6870, 1.0455, 1.4581, 1.4918, 2.0758, 2.5671, 2.9889	0.4160, 0.2409, 4.6181, 0.5253, 0.7730, 0.6649, 5.1412, 0.1173
16	0.4267, 0.7548, 0.9538, 1.1091, 1.2381, 2.1343, 2.5848, 2.9406	0.4525, 0.2305, 0.8381, 10.9865, 1.6792, 4.3092, 4.8631, 0.0469
17	0.8451, 0.8923, 0.9935, 1.1842, 1.4842, 2.1501, 2.5904, 3.0237	0.3138, 0.0540, 0.4024, 11.5329, 1.3079, 3.5439, 4.9537, 0.0586

3. Experimental

3.1. Materials and Methods

^{1}H and ^{11}B NMR spectra were recorded on a Bruker Avance-400 spectrometer operating at 400.13 MHz for ^{1}H NMR and 128.28 MHz for ^{11}B NMR and Bruker AvanceTM 500 spectrometer (Bruker BioSpin AG, Zurich, Switzerland) (at 500.13, 125.47 MHz for ^{1}H and ^{13}C, respectively). Chemical shifts (δ) were referenced to the residual solvent peak acetone-D_6, 2.05 ppm, acetonitrile-D_3 1.93 ppm, for ^{1}H, external BF_3 OEt_2 for ^{11}B. IR spectra were recorded on a Bruker FTIR spectrometer Tensor 37 in KBr pellets. Merck silica gel L0.040–0.080 mesh was used for column chromatography. The identities of new compounds were verified by TLC on Silufol plates.

Bruker AvanceTM 500 spectrometer (Germany) (at 500.13, 160.46, and 125.47 MHz for ^{1}H, ^{11}B and ^{13}C, respectively). The ^{1}H chemical shifts were measured relative to the signal of the solvents, acetonitrile-D_3 and acetone-D_6.

3.2. X-ray Crystallography

Single-crystal X-ray diffraction experiments were carried out with a Bruker SMART APEX II diffractometer (graphite monochromated Mo-K_a radiation, λ = 0.71073 Å, ω-scan technique). All structures were solved by the direct methods and refined by the full-matrix least squares technique against F^2 with anisotropic thermal parameters for all non-hydrogen atoms using the SHELXL software, version 2018/3, Bruker AXS Inc., Madison, WI, USA [78]. Figure 3a,b, Figures 4, 5, 7 and 8a were made with an XP program included in SHELXL program package [78]. Figure 6a,b and Figure 8b were made with Mercury (version 4.3.1) [79]. Hirshfeld surfaces and the associated 2D fingerprint plots were calculated using the CrystalExplorer17 software [55]. In structures **9**, **10** and **19**, the hydrogen atoms of the carborane ligands, as well NH and OH groups were located from the Fourier syntheses and isotropically refined without restrictions. The remaining hydrogen atoms in these structures and all hydrogen atoms in structure **20** were placed geometrically and included in the structure factors calculation in the riding motion approximation. In structure **20**, the highly disordered solvate molecules (presumably, methylene chloride) were detected in the residual density. Unfortunately, these solvate molecules could not be successfully modeled even with restraints. The contribution of undefined electron density peaks was treated as diffusion scattering, and it was excluded using the SQUEEZE routine implemented in the PLATON program [80]. Crystal data and the parameters of

the refinements for **9**, **10**, **19** and **20** are listed in Table S5. The crystallographic data for the structures for compounds **9**, **10**, **19** and **20** have been deposited at the Cambridge Crystallographic Data Centre (CCDC) as supplementary publications No. CCDC 2177931, 2177932, 2177933 and 2177934, respectively.

3.3. Method of Calculation

The evaluation of geometry optimization, enthalpies of formation (EOF), energetic properties, stability, the detonation properties and terahertz spectra of selected compounds were estimated based on DFT B3LYP/6-311 + G* [56–58] calculations using GAUSSIAN-09 [59] under LINUX (see Section 2.4.1).

*3.4. General Procedure for the Preparation of 4,6-bis(5-Alkyltetrazol-1-yl)-2-[(o-Carborane-3-yl)Amino]-1,3,5-Triazines (***9**–**11***)*

To a solution of 2,4,6-trichloro-1,3,5-triazine **1** (0.5 g, 2.7 mmol) in dry THF (8 mL), a mixture of DIPEA (1 mL, 0.74 g, 5.7 mmol) and the corresponding tetrazole **2**, **3** or **4** (5.43 mmol) in dry THF (5 mL) was added dropwise at −30 °C–−40 °C within 20 min under an argon atmosphere. Then, the resulting mixture was slowly (2–4 h) warmed to room temperature and stirred until the starting compounds disappeared (TLC control, $CHCl_3$-Acetone 10:1) to form ditetrazolyl-1,3,5-triazines **5**–**7**. After that, a mixture of DIPEA (0.38 g, 2.86 mmol) and 3-amino-*o*-carborane **8** (0.44 g, 2.8 mmol) in THF (5 mL) was slowly added at −10 °C to the corresponding reaction mixture of compounds **5**, **6** or **7** and then stirred at ambient temperature until the carborane **8** disappeared (4 h for **9**, 8h for **10**, and 10 h for **11**, TLC control, toluene). Upon reaction completion, the solvents were evaporated in vacuo, the residue was dissolved in EtOAc (100 mL) and washed with water (3 × 100 mL) and the organic layer was dried over Na_2SO_4. EtOAc was evaporated to dryness and the residue of the prepared compound **9**, **10** or **11** was treated as indicated below.

3.4.1. 2-[(*o*-Carborane-3-yl)amino]-4,6-di(1H-Tetrazol-1-yl)-1,3,5-triazine (**9**)

The residue was treated with Et_2O (20 mL), the precipitate that formed was filtered off and washed with Et_2O–$CHCl_3$ (1: 2, 50 mL) mixture, and dried to yield compound **9** 0.85 g (84%); ^{1}H NMR (acetone-D_6, 400.13 MHz) δ: 10.15 (s, the rotamer 1, 1H, N_4CH), 10.11 (s, the rotamer 2, 1H, N_4CH), 10.13 (s, J = 14 Hz, 2H, N_4CH),] 9.08 (br s, 1H, carborane NH), 5.33 (br s, 2H, carborane CH); ^{13}C NMR (acetone-D_6, 125.77 MHz) δ: 169.73 (s, 1C, **C**-2 1,3,5-triazine), 160.64 and 160.79 (s, 2C, **C** 4,6-position of 1,3,5-triazine *), 143.11 and 143.19 (s, 2C, **C**H-tetrazole *); 57.26 (s, 2C, **C**H-carborane, 29.72 (s, ($\mathbf{C}H_3$)$_2$CO **); ^{11}B NMR (acetone-D_6, 128.28 MHz) δ: −4.4 (d, J = 144 Hz, 2B), −6.2 (s, 1B, B^3), −10.1 (d, J = 149 Hz, 1B), −12.8 (d, J = 170 Hz, 2B), −14.3 (d, J = 172 Hz, 4B);. IR (KBr) ν: 3067 (carborane CH), 2598 (BH), 1614, 1585, 1472, 1451(N=N) cm^{-1}.

* The doubling of the signals in these NMR spectra is due to the different shielding of the indicator signals of compound **9** in the two conformations

** Complex of acetone with compound **9**.

3.4.2. 2-[(*o*-Carborane-3-yl)amino]-4,6-di(5-Methyl-1H-tetrazol-1-yl)-1,3,5-triazine (**10**)

The residue was treated with Et_2O (20 mL), the precipitate that formed was filtered off and washed with Et_2O–$CHCl_3$ (2:1, 50 mL) mixture, and dried to yield compound **10** 0.77 g (70%); ^{1}H NMR (acetone-D_6, 400.13 MHz) δ: 8.99 (br s, 1H, NH), 5.32 (br s, 2H, carborane CH), 3.01 (s, the rotamer 1, 3H, CH_3), 2.96 (s, the rotamer 2, 3H, CH_3); ^{11}B NMR (acetone-D_6, 128.28 MHz), δ: −4.5 (d, J = 147 Hz, 2B), –6.1 (s, 1B, B^3), –10.2 (d, J = 154 Hz, 1B), −12.8 (d, J = 177 Hz, 2B), −14.4 (d, J = 182 Hz, 4B). IR (KBr) ν: 3038 (carborane CH), 2587 (BH), 1609, 1574, 1549 (N=N) cm^{-1}.

3.4.3. 2-[(*o*-Carborane-3-yl)amino]-4,6-di(5-Ethyl-1H-tetrazol-1-yl)-1,3,5-triazine (**11**)

The residue was treated with hexane (20 mL), the precipitate that formed was filtered off and washed with Et_2O (60 mL) and dried to yield compound **11** 0.70 g (59%); ^{1}H NMR

(acetone-D_6, 400.13 MHz) δ: 9.01 (br s, 1H, NH), 5.33 (br s, 2H, carborane CH), 3.48 (q, the rotamer 1, J = 7.3 Hz, 2H, CH_2), 3.43 (q, the rotamer 2, J = 7.3 Hz, 2H, CH_2), 1.45 (t, the rotamer 1, J = 7.3 Hz, 3H, CH_3), 1.42 (t, the rotamer 2, J = 7.3 Hz, 3H, CH_3); ^{11}B NMR (acetone-D_6, 128.28 MHz) δ: −4.5 (d, J = 147 Hz, 2B), −6.0 (s, 1B, B^3), −10.2 (d, J = 147 Hz, 1B), −12.8 (d, J = 170 Hz, 2B), −14.3 (d, J = 172 Hz, 4B). IR (KBr) ν: 3032 (carborane CH), 2588 (BH), 1607, 1577, 1551 (N=N) cm^{-1}.

*3.5. General Procedure for the Preparation of 2-[(Carborane-9-yl)tio]-4,6-di(1H-Tetrazol-1-yl)-1,3,5-triazines (***15**, **16**, **17***)*

To a solution of ditetrazolyl-1,3,5-triazine **5** prepared from triazine **1** (0.5 g, 2.7 mmol) and tetrazole **2** (0.38 g, 5.43 mmol) in dry THF (8 mL) and DIPEA (1 mL, 0.74 g, 5.7 mmol) with stirring for 3 h, a mixture of DIPEA (0.38 g, 2.86 mmol) and 1-mercapto-o-carborane **13** (0.49 g, 2.8 mmol) in THF (5 mL) was slowly added at –10 °C. The reaction mixture was then stirred at ambient temperature for 3 h. THF was evaporated in vacuo, the residue was treated with hexane (20 mL) and the formed precipitate was filtered off and washed with Et_2O (20 mL).

3.5.1. 2-[(Nido-7,8-dicarbaundecaboran-7-yl)tio]-4,6-di(1H-tetrazol-1-yl)-1,3,5-triazinyl] Esium (**15**)

After the general procedure, the solid was washed with $CHCl_3$ (20 mL). After that, the solid was dissolved in H_2O–acetone mixture (10:1) and CsCl (0.67 g, 4 mmol) was added to the obtained solution. The acetone was removed in vacuo, the formed precipitate was filtered off, washed with water and crystallized ($CHCl_3$– acetone 20:1) to yield compound **15** 0.89 g (50%); ^{1}H NMR (acetone-D_6, 400.13 MHz) δ: 8.95 (s, 2H, N_4CH), 3.69 (br s, 1H, carborane CH), 3.16 (br s, 1H, carborane CH); ^{11}B NMR (acetone-D_6, 128.28 MHz) δ: −3.0 (d, J = 145 Hz, 1B), −9.2 (d, J = 144 Hz, 3B), −12.4 (d, J = 175 Hz, 2B), −18.8 (d, J = 149 Hz, 1B) −22.8 (d, J = 123 Hz, 1B), –34.4 (dd, J = 50.0, 123 Hz, 1B); IR (KBr) ν: 3070 (carborane CH), 2578 (BH), 1579, 1467(N=N) cm^{-1}.

3.5.2. 2-[(*o*-Carborane-9-yl)tio]-4,6-di(1H-tetrazol-1-yl)-1,3,5-triazine (**16**)

Yield: 0.77 g (70%); ^{1}H NMR (acetone-D_6, 400.13 MHz) δ: 10.15 (s, 2H, N_4CH), 4.90 (br s, 1H, carborane CH), 4.84 (br s, 1H, carborane CH); ^{11}B NMR (acetone-D_6, 128.28 MHz) δ: 1.8 (s, 1B, B^9), −2.6 (d, J = 149 Hz, 1B), −8.9 (d, J = 153 Hz, 2B), −13.3 (d, J = 156 Hz, 2B), −14.4 (d, J = 154 Hz, 4B); IR (KBr) ν: 3063 (carborane CH), 2613 (BH), 1580, 1465 (N=N) cm^{-1}.

3.5.3. 2-[(*m*-Carborane-9-yl)tio]-4,6-di(1H-tetrazol-1-yl)-1,3,5-triazine (**17**)

Yield: 0.88 g (79%). ^{1}H NMR (acetone-D_6, 400.13 MHz) δ: 10.17 (s, 2H, N_4CH), 3.98 (br s, 2H, carborane CH); ^{11}B NMR (acetone-D_6, 128.28 MHz) δ: −4.4 (s, 1B, B^9), −5.8 (d, J = 170 Hz, 2B), −10.2 (d, J = 151 Hz, 1B), −12.5 (d, J = 139 Hz, 2B), −13.5 (d, J = 153 Hz, 2B), −16.6 (d, J = 177 Hz, 1B), –17.5 (d, J = 150 Hz, 1B). IR (KBr) ν: 3053 (carborane CH), 2624 (BH), 1580, 1466 (N=N) cm^{-1}.

3.6. General Procedure for the Preparation of Compounds **19**–**21**

To a solution of 2,4,6-trichloro-1,3,5-triazine **1** (0.5 g, 2.7 mmol) in dry THF (8 mL), a mixture of DIPEA (1 mL, 0.74 g, 5.7 mmol) and 5-phenyltetrazole (0.78 g, 5.43 mmol) in dry THF (5 mL) was added dropwise at −50 °C within 20 min under an argon atmosphere. Then, the resulting mixture was slowly (18 h) warmed to room temperature and stirred until the starting compounds disappeared (TLC control, $CHCl_3$–acetone 10:1). After that, a mixture of DIPEA (0.38 g, 2.86 mmol) and 3-amino-*o*-carborane **8** (0.44 g, 2.8 mmol) in THF (5 mL) was slowly added at −20 °C to the reaction and then stirred at ambient temperature until carborane **8** disappeared (15 h, TLC control, toluene). Upon the reaction completion, the solvents were evaporated in vacuo, the residue was dissolved in EtOAc (100 mL), washed with water (3 × 100 mL), the organic layer was dried over Na_2SO_4, evaporated to dryness and the residue was treated with hexane (15 mL) and Et_2O (15 mL), the formed

solid was purified by column chromatography on SiO_2 using hexane-EtOAc 5:1 and 1:2 systems as an eluent.

3.6.1. 5-(*o*-Carborane-3-yl)amino-2,9-diphenyl-bis[1,2,4]triazolo[1,5-a:1′,5′-c][1,3,5]triazine (**19**)

Yield: 0.23 g (18%); ^{1}H NMR (acetone-D_6, 400.13 MHz) δ: 9.09 (br s, 1H, NH), 8.25 (m, 4H, Ph), 7.61 (m, 6H, Ph), 5.48 (br s, 2H, carborane CH); ^{11}B NMR (acetone-D_6, 128.28 MHz) δ: −4.5 (d, J = 141 Hz, 2B), −6.0 (s, 1B, B^3), −10.2 (d, J = 161 Hz, 1B), −12.7 (d, J = 161 Hz, 2B), −14.5 (d, J = 158 Hz, 4B); IR (KBr) ν: 3072 (carborane CH), 2560 (BH) cm^{-1}.

3.6.2. 2-(2-Benzoylhydrazinyl)-4-(*o*-carborane-3-yl)amino-6-(5-phenyl-2H-tetrazol-2-yl)-1,3,5-triazine (**20**)

Yield: 0.14 g (10%); ^{1}H NMR (acetone-D_6, 400.13 MHz) δ: 9.39 (m, 1H, NH), 8.28 (m, 2H, Ph), 8.14 (m, 2H, Ph), 8.14 (m, 1H, Ph), 8.02 (m, 1H, Ph), 7.60 (m, 6H, Ph), 5.39 (m, 2H, carborane CH); ^{11}B NMR (Acetone-D_6, 128.28 MHz), δ: −4.9 (d, J = 141 Hz, 3B), −10.3 (d, J = 141 Hz, 1B), −12.9 (d, J = 163 Hz, 2B), −14.9 (d, J = 170 Hz, 4B); IR (KBr) ν: 3072 (carborane CH), 2565 (BH) cm^{-1}.

3.6.3. 3,7,11-Triphenyl[tris([1,2,4]triazolo)[4,3-a:4′,3′-c:4″,3″-e][1,3,5]triazine (**21**) [47,49,50]

Yield: 70 mg (6%); ^{1}H NMR (acetone-D_6, 400.13 MHz) δ: 8.05 (dd, J =1.9, 8.1 Hz, 2H,), 7.65 (m, 3H).

4. Conclusions

Recently, more attention has been focused on the design and synthesis of modern high-energy compounds based on nitrogen heterocycles and other energetic entities having energy characteristics suitable for the potential replacement of the traditional energetic materials.

In this article, a series of new high-energy compounds was successfully synthesized and fully characterized based on the one-stage functionalization of cyanuric chloride with nitrogen-rich 5-R-tetrazoles (R = H, Me, Et) and aminocarborane or mercaptocarboranes, reducing the number of reaction steps and therefore the amount of by-products in the preparation of these compounds. All the components of prepared compounds have been widely used while designing energetic materials. Synthesized compounds have high enthalpies of formation and excellent energetic properties such as heat of combustion and the heat of the explosion which makes these compounds promising alternatives for commonly used energetic compounds. Based on the DFT calculations, it was shown that compound **15** possessed the maximum value of the detonation velocity of all the considered compounds, and compound **10** demonstrated the maximum value of the detonation pressure. Theoretical terahertz frequencies have been calculated for potential high-energy density materials (HEDMs), enabling the remote detection of these compounds.

Supplementary Materials: The following supporting information can be downloaded at: https://www.mdpi.com/article/10.3390/molecules27217484/s1, Figure S1. ^{1}H NMR spectra of compound **9** in CD_3CN; Figure S2. ^{1}H NMR spectra of compound **9** in acetone-D_6; Figure S3. ^{1}H NMR spectra (500.13 MHz) of **9** in acetone-D_6; Figure S4. ^{1}H NMR spectra of **9** in acetone-D_6 at various temperatures; Figure S5. ^{13}C NMR spectra (125.76 MHz) of compound **9** in acetone-D_6; Figure S6. ^{11}B{^{1}H} and ^{11}B NMR spectra of compound **9** in acetone-D_6; Figure S7. NOESY spectra of compound **9**; Figure S8. HMBC spectra of compound **9**; Figure S9. ^{1}H NMR spectra of compound **10** in acetone-D_6. Signals at δ = 1.02 ppm and δ = 3.39 ppm attributed to the protons of EtOAc; Figure S10. ^{11}B{^{1}H} and ^{11}B NMR spectra of compound **10** in acetone-D_6; Figure S11. ^{1}H NMR of compound **11** in acetone-D_6; Figure S12. ^{11}B{^{1}H} and ^{11}B NMR spectra of compound **11** in acetone-D_6; FigureS13. ^{1}H NMR spectra of compound **19** in acetone-D_6; Figure S14. ^{11}B{^{1}H} and ^{11}B NMR spectra of compound **19** in acetone-D_6; Figure S15. ^{1}H NMR spectra of **20** in acetone-D_6; Figure S16. ^{11}B{^{1}H} and ^{11}B NMR spectra of compound **20** in acetone-D_6; Figure S17. ^{1}H NMR spectra of compound **15** in acetone-D_6; Figure S18. ^{11}B{^{1}H} and ^{11}B NMR spectra of compound **15** in acetone-D_6; Figure S19. ^{1}H NMR spectra of compound **16** in acetone-D_6; Figure S20. ^{11}B{^{1}H} and ^{11}B NMR spectra of compound **16** in acetone-D_6; Figure S21. ^{1}H NMR spectra of compound **17** in acetone-D_6; Figure S22. ^{11}B{^{1}H} and ^{11}B

NMR spectra of compound **17** in acetone-D_6; Table S1. X-ray data for compound **9**; Table S2. X-ray data for compound **10**; Table S3. X-ray data for compound **19**, Table S4. X-ray data for compound **20**; Table S5. Crystal data, data collection and structure refinement parameters for **9**, **10**, **19** and **20**; Figure S23. The fragment of double layer in the crystal of **9** (projection along the *b* axis); the shortened intermolecular contacts are shown with dotted lines. Table S6. Hydrogen bonds observed in the crystal of compound **9**; Table S7. Hydrogen bonds observed in the crystal of compound **10**; Figure S24. Fragment of crystal packing in **10** (projection along the *b* axis); Table S8. Hydrogen bonds observed in the crystal of compound **19**; Figure S25. Fragment of crystal packing in **19** (projection along the *c* axis); Table S9. Hydrogen bonds observed in the crystal of compound **20**; Figure S26. Fragment of crystal packing of **20** (projection along the *b* axis); Figure S27. Hirshfeld surfaces (a) and full fingerprint plots (b) of compound **9**; Figure S28. Individual interatomic contacts of compound **9** with percentage contribution in the crystal packing greater than 4.5%; Figure S29. Hirshfeld surfaces (a) and full fingerprint plots (b) of compound **10**; Figure S30. Individual interatomic contacts of compound **10** with a percentage contribution in the crystal packing greater than 4.5%; FigureS31. Hirshfeld surfaces (a) and full fingerprint plots (b) of compound **19**; Figure S32. Individual interatomic contacts of compound **19** with a percentage contribution in the crystal packing greater than 4.5%; Figure S33. Hirshfeld surfaces of compound **20**; Figure S34. Full fingerprint plots of compound **20**; Figure S35. Individual interatomic contacts of compound **20** (for two crystallographically independent molecules A and B) with a percentage contribution in the crystal packing greater than 4.5%; Figure S36. The supramolecular assembling of compound **9**. Hirshfeld surfaces mapped over d_{norm}, generated from intermolecular H···H contacts. Figure S37. Supramolecular assembling of compound **9**. Hirshfeld surfaces mapped over d_{norm}, generated from intermolecular N···H contacts or interactions; Table S10. Geometry structure of studied compounds; Table S11. The calculated values of total energy and entropy of compounds **9**–**11**, **15**–**17**, **19** and **25** (6-311 + G* basis set) in the gas phase; Table S12. Comparison of calculated and experimental EOF values of test molecules (kcal/mol).

Author Contributions: Conceptualization, A.V.M. and V.A.O.; methodology, A.V.M., S.S.K. and Y.A.B.; investigation, A.V.M., S.S.K., E.G.K., F.M.D., A.S.P., Y.A.B. and V.A.O.; writing—original draft preparation, A.V.M. and V.A.O.; writing—review and editing, V.A.O.; visualization, A.V.M., S.S.K., F.M.D. and Y.A.B.; supervision, V.A.O.; project administration, V.A.O. All authors have read and agreed to the published version of the manuscript.

Funding: This research received no external funding.

Institutional Review Board Statement: Not applicable.

Informed Consent Statement: Not applicable.

Data Availability Statement: CCDC 2177931, 2177932, 2177933 and 2177934 contain the supplementary crystallographic data for this paper. The data can be obtained free of charge from The Cambridge Crystallographic Data Centre via https://www.ccdc.cam.ac.uk/structures.

Acknowledgments: This work was supported by the Ministry of Science and Higher Education of the Russian Federation (Agreement No 075-00697-22-00) and was performed employing the equipment of Center for molecular composition studies of INEOS RAS. The single-crystal X-ray diffraction analysis was performed using the equipment of the JRC PMR IGIC RAS.

Conflicts of Interest: The authors declare no conflict of interest.

Sample Availability: Samples of the compounds are available from the authors.

References

1. Keshavarz, M.H.; Klapötke, T.M. *The Properties of Energetic Materials*; Walter de Gruyter GmbH: Berlin, Germany; Boston, MA, USA, 2018.
2. Damse, R.S.; Ghosh, M.; Naik, N.H.; Sikder, A.K. Thermoanalytical Screening of Nitrogen-Rich Compounds for Ballistic Requirements of Gun Propellant. *J. Propul. Power* **2009**, *25*, 249–256. [CrossRef]
3. Keshavarz, M. Prediction of densities of acyclic and cyclic nitramines, nitrate esters and nitroaliphatic compounds for evaluation of their detonation performance. *J. Hazard. Mater.* **2007**, *143*, 437–442. [CrossRef] [PubMed]
4. Agrawal, J.P. *High Energy Materials: Propellants, Explosives and Pyrotechnics*; WILEY-VCH Verlag GmbH & Co. KGaA: Weinheim, Germany, 2010.

5. Wang, R.; Guo, Y.; Zeng, Z.; Twamley, B.; Shreeve, J.M. Furazan-Functionalized Tetrazolate-Based Salts: A New Family of Insensitive Energetic Materials. *Chem. Eur. J.* **2009**, *15*, 2625–2634. [CrossRef] [PubMed]
6. O'Sullivan, O.T.; Zdilla, M.J. Properties and Promise of Catenated Nitrogen Systems As High-Energy-Density Materials. *Chem. Rev.* **2020**, *120*, 5682–5744. [CrossRef]
7. Chavez, D.E.; Hiskey, M.A. 1,2,4,5-tetrazine based energetic materials. *J. Energetic Mater.* **1999**, *17*, 357–377. [CrossRef]
8. Tao, G.-H.; Guo, Y.; Joo, Y.-H.; Twamley, B.; Shreeve, J.M. Energetic nitrogen-rich salts and ionic liquids: 5-aminotetrazole (AT) as a weak acid. *J. Mater. Chem.* **2008**, *18*, 5524–5530. [CrossRef]
9. Dippold, A.A.; Klapötke, T.M. Synthesis and Characterization of 5-(1,2,4-Triazol-3-yl)tetrazoles with Various Energetic Functionalities. *Chem. Asian J.* **2013**, *8*, 1463–1471. [CrossRef]
10. Thottempudi, V.; Zhang, J.; He, C.; Shreeve, J.M. Azo substituted 1,2,4-oxadiazoles as insensitive energetic materials. *RSC Adv.* **2014**, *4*, 50361–50364. [CrossRef]
11. Hafner, K.; Klapötke, T.M.; Schmid, P.C.; Stierstorfer, J. Synthesis and Characterization of the Asymmetric 1,2-Dihydroxy-5,5′-bitetrazole and Selected Nitrogen Rich Derivatives. *Eur. J. Inorg. Chem.* **2015**, *17*, 2794–2803. [CrossRef]
12. Gao, H.; Shreeve, J.M. Azole-based energetic salts. *Chem. Rev.* **2011**, *111*, 7377–7436. [CrossRef]
13. Zhang, Q.; Shreeve, J.M. Energetic Ionic Liquids as Explosives and Propellant Fuels: A New Journey of Ionic Liquid Chemistry. *Chem. Rev.* **2014**, *114*, 10527–10574. [CrossRef]
14. Frem, D. Theoretical Studies on Energetic Properties of s-Triazine Substituted Aminofurazan and Aminofuroxan Derivatives—High Performance Energetic Material Systems. *Combust. Explos. Shock Waves* **2014**, *50*, 441–446. [CrossRef]
15. Shastin, A.V.; Godovikova, T.I.; Korsunskii, B.L. Nitro derivatives of 1,3,5-triazine: Synthesis and properties. *Russ. Chem. Rev.* **2003**, *72*, 279–287. [CrossRef]
16. Gidaspov, A.A.; Bakharev, V.V.; Suponitsky, K.Y.; Nikitin, V.G.; Sheremetev, A.B. High-density insensitive energetic materials: 2,4,6-tris(2-fluoro-2,2-dinitroethoxy)-1,3,5-triazine. *RSC Adv.* **2016**, *6*, 104325–104329. [CrossRef]
17. Patel, R.B.; Malhotra, A. (Eds.) *Triazines: Synthesis, Applications and Toxicity*; Nova Science Publishers: New York, NY, USA, 2012; 209p.
18. Rao, M.H.; Ghule, V.D.; Muralidharan, K. 2,4,6-tris[bis(1H-tetrazol-5-yl)amino]-1,3,5-triazine as a nitrogen-rich material. *J. Chem. Sci.* **2017**, *129*, 657–661. [CrossRef]
19. McEwan, W.S.; Rigg, M.W. The heats of combustion of compounds containing the tetrazole Ring. *J. Am. Chem. Soc.* **1951**, *73*, 4725–4727. [CrossRef]
20. Ivashkevich, O.A.; Gaponik, P.N.; Koren, A.O.; Bubel, O.N.; Fronchek, E.V. Comparative semiempirical calculations of tetrazole derivatives. *Int. J. Quantum Chem.* **1992**, *43*, 813–826. [CrossRef]
21. Ghule, V.D.; Radhakrishnan, S.; Jadhav, P.M. Computational studies on tetrazole derivatives as potential high energy materials. *Struct. Chem.* **2011**, *22*, 775–782. [CrossRef]
22. Jose, R.; Lima, P.; Dubois, C.; Mader, O.; Stowe, R.; Ringuette, S. Boron nanoparticle-rich fuels for gas generators and propellants. *Int. J. Energetic Mater. Chem. Propul.* **2010**, *9*, 437–446. [CrossRef]
23. Akhavan, J. *Chemistry of Explosives*, 2nd ed.; The Royal Society of Chemistry: Cambridge, UK, 2004.
24. Macri, B.J. Boron-Fuel-Rich Propellant Compositions. U.S. Patent 3986909, 24 March 1976.
25. Koch, E.-C.; Klapçtke, T.M. Boron-Based High Explosives. *Propellants Explos. Pyrotech.* **2012**, *37*, 335–344. [CrossRef]
26. Liu, T.-K.; Shyuf, I.-M.; Hsia, Y.-S. Effect of Fluorinated Graphite on Combustion of Boron and Boron-Based Fuel-Rich Propellants. *J. Propul. Power* **1996**, *12*, 26–34. [CrossRef]
27. Glotov, O.G.; Surodina, G.S. Combustion of Aluminum and Boron Agglomerates Free Falling in Air. I. Experimental Approach. *Combust. Explos. Shock Waves* **2019**, *55*, 335–344. [CrossRef]
28. Fraenk, W.; Habereder, T.; Hammerl, A.; Klapötke, T.M.; Krumm, B.; Mayer, P.; Nöth, H.; Warchhold, M. Highly Energetic Tetraazidoborate Anion and Boron Triazide Adducts. *Inorg. Chem.* **2001**, *40*, 1334–1340. [CrossRef]
29. Glück, J.; Klapötke, T.M.; Rusan, M.; Stierstorfer, J. Green colorants based on energetic azole borates. *Chem. Eur. J.* **2014**, *20*, 15947–15960. [CrossRef]
30. Yin, P.; Zhang, Q.; Shreeve, J.M. Dancing with Energetic Nitrogen Atoms: Versatile N-Functionalization Strategies for N-Heterocyclic Frameworks in High Energy Density Materials. *Acc. Chem. Res.* **2016**, *49*, 4–16. [CrossRef] [PubMed]
31. Ol'shevskaya, V.A.; Makarenkov, A.V.; Kononova, E.G.; Peregudov, A.S.; Lyssenko, K.A.; Kalinin, V.N. An efficient synthesis of carboranyl tetrazoles via alkylation of 5-R-1H-tetrazoles with allylcarboranes. *Polyhedron* **2016**, *115*, 128–136. [CrossRef]
32. Borisov, Y.A.; Makarenkov, A.V.; Kiselev, S.S.; Kononova, E.G.; Ponomaryov, A.B.; Budnik, M.I.; Ol'shevskaya, V.A. Prediction of energetic properties of carboranyl tetrazoles based on DFT study. *Mater. Chem. Phys.* **2020**, *240*, 122209. [CrossRef]
33. Hey-Hawkins, E.; Teixidor, C.V. *Boron-Based Compounds: Potential and Emerging Applications in Medicine*; John Wiley & Sons Ltd.: Hoboken, NJ, USA, 2018.
34. King, R.B. Three-Dimensional Aromaticity in Polyhedral Boranes and Related Molecules. *Chem. Rev.* **2001**, *101*, 1119–1152. [CrossRef] [PubMed]
35. Aihara, J. Three-dimensional aromaticity of polyhedral boranes. *J. Am. Chem. Soc.* **1978**, *100*, 3339–3342. [CrossRef]
36. Dash, B.P.; Satapathy, R.; Maguire, J.A.; Hosmane, N.S. Polyhedral boron clusters in materials science. *New J. Chem.* **2011**, *35*, 1955–1972. [CrossRef]
37. Hosmane, N.S. *Boron Science New Technologies and Applications*; CRC Press, Taylor & Francis Group: Boca Raton, FL, USA, 2012.

38. Zakharkin, L.I. Some recent advances in the chemistry of dicarba-*closo*-dodecaboranes. *Pure Appl. Chem.* **1972**, *29*, 513–526. [CrossRef]
39. Blotny, G. Recent applications of 2,4,6-trichloro-1,3,5-triazine and its derivatives in organic synthesis. *Tetrahedron* **2006**, *62*, 9507–9522. [CrossRef]
40. Zakharkin, L.I.; Kalinin, V.N.; Gedymin, V.V. Synthesis and some reactions of 3-amino-*o*-carboranes. *J. Organometal. Chem.* **1969**, *16*, 371–379. [CrossRef]
41. Zakharkin, L.I.; Kalinin, V.N.; Snyakin, A.P.; Kvasov, B.A. Effect of solvents on the electronic properties of 1-*o*-, 3-*o*- and 1-*m*-carboranyl groups. *J. Organometal. Chem.* **1969**, *18*, 19–26. [CrossRef]
42. Zakharkin, L.I.; Kovredov, A.I.; Ol'shevskaya, V.A. Synthesis of 9-(fluorophenyl)-*o*-, 9-(fluorophenyl)-*m*-, and 2-(fluorophenyl)-*p*-carboranes and determination of electronic effects of 9-*o*-, 9-*m*-, and 2-*p*-carboranyl groups. *Russ Chem. Bull.* **1981**, *30*, 1775–1777. [CrossRef]
43. Bhatt, U. Five-Membered Heterocycles with Four Heteroatoms: Tetrazoles. In *Modern Heterocyclic Chemistry*; Wiley-VCH Verlag GmbH & Co. KGaA: Hoboken, NJ, USA, 2011; pp. 1401–1430. [CrossRef]
44. Wittenberger, S.J. Recent Developments in Tetrazole Chemistry. A Review. *Org. Prep. Proced. Int.* **1994**, *26*, 499–531. [CrossRef]
45. Benson, F.R. The Chemistry of the Tetrazoles. *Chem. Rev.* **1947**, *41*, 1–61. [CrossRef]
46. Neochoritis, C.G.; Zhao, T.; Dömling, A. Tetrazoles via Multicomponent Reactions. *Chem. Rev.* **2019**, *119*, 1970–2042. [CrossRef]
47. Tartakovsky, V.A.; Frumkin, A.E.; Churakov, A.M.; Strelenko, Y.A. New approaches to synthesis of tris[1,2,4]triazolo[1,3,5]triazines. *Russ. Chem. Bull. Int. Ed.* **2005**, *54*, 719–725. [CrossRef]
48. Zhao, S.; Dai, J.; Hu, M.; Liu, C.; Meng, R.; Liu, X.; Wang, C. Photo-induced Coupling Reaction of Tetrazoles and Carboxylic Acids in Aqueous Solution: Application in the Protein Labelling. *Chem. Commun.* **2016**, *52*, 4702–4705. [CrossRef]
49. Huisgen, R.; Sturm, H.V.; Seidel, M.; Ringöffnungen der Azole, V. Weitere Reaktionen der Tetrazole mit elektrophilen Agenzien. *Chem. Ber.* **1961**, *94*, 1555–1562. [CrossRef]
50. Detert, H. Tristriazolotriazines: Luminescent Discotic Liquid Crystals. *Eur. J. Org. Chem.* **2018**, *33*, 4501–4507. [CrossRef]
51. Anitha, K.; Sivakumar, S.; Arulraj, R.; Rajkumar, K.; Kaur, M.; Jasinski, J.P. Synthesis, crystal structure, DFT calculations and Hirshfeld surface analysis of 3-butyl-2,6-bis- (4-fluoro-phen-yl)piperidin-4-one. *Acta Crystallogr. E Crystallogr. Commun.* **2020**, *76*, 651–655. [CrossRef] [PubMed]
52. McKinnon, J.J.; Spackman, M.A.; Mitchell, A.S. Novel tools for visualizing and exploring intermolecular interactions in molecular crystals. *Acta Crystallogr. B.* **2004**, *60*, 627–668. [CrossRef] [PubMed]
53. McKinnon, J.J.; Jayatilaka, D.; Spackman, M.A. Towards quantitative analysis of intermolecular interactions with Hirshfeld surfaces. *Chem. Commun.* **2007**, *37*, 3814–3816. [CrossRef]
54. Haroon, M.; Akhtar, T.; Yousuf, M.; Tahir, M.N.; Rasheed, L.; Zahra, S.S.; Haq, I.U.; Ashfaq, M. Synthesis, crystal structure, Hirshfeld surface investigation and comparative DFT studies of ethyl 2-[2-(2-nitrobenzylidene)hydrazinyl]thiazole- 4-carboxylate. *BMC Chem.* **2022**, *16*, 18. [CrossRef]
55. Turner, M.J.; McKinnon, J.J.; Wolff, S.K.; Grimwood, D.J.; Spackman, P.R.; Jayatilaka, D.; Spackman, M.A. *CrystalExplorer17*; University of Western Australia: Crawley, Australia, 2017.
56. Parr, R.G.; Yang, Y. *Density-Functional Theory of Atoms and Molecules*; Oxford University Press: Oxford, UK, 1989.
57. Becke, A.D. Density-functional exchange-energy approximation with correct asymptotic behavior. *Phys. Rev. A* **1988**, *38*, 3098–3100. [CrossRef]
58. Lee, C.; Yang, W.; Parr, R.G. Development of the Colle-Salvetti correlation-energy formula into a functional of the electron density. *Phys. Rev. B* **1988**, *37*, 785–789. [CrossRef]
59. Frisch, M.J.; Trucks, G.W.; Schlegel, H.B.; Scuseria, G.E.; Robb, M.A.; Cheeseman, J.R.; Scalmani, G.; Barone, V.; Mennucci, B.; Petersson, G.A.; et al. *Gaussian 09W, Version 7*; Gaussian, Inc.: Wallingford, CT, USA, 2009.
60. Salem, L. *Electrons in Chemical Reactions: First Principles*; Wiley-Interscience Publication, John Willey&Sons: New York, NY, USA; Chichester, UK; Brisbane, Australia; Toronto, ON, Canada; Singapore, 1982.
61. Huang, Y.; Rong, C.; Zhang, R.; Liu, S. Evaluating frontier orbital energy and HOMO/LUMO gap with descriptors from density functional reactivity theory. *J. Mol. Model.* **2017**, *23*, 3. [CrossRef]
62. Pereira, D.H.; La Porta, F.A.; Santiago, R.T.; Garcia, D.R.; Ramalho, T.C. New Perspectives on the Role of Frontier Molecular Orbitals in the Study of Chemical Reactivity: A Review. *Braz. Chem. Soc.* **2016**, *8*, 425–453. [CrossRef]
63. Yu, J.; Su, N.Q.; Yang, W. Describing Chemical Reactivity with Frontier Molecular Orbitalets. *JACS Au* **2022**, *2*, 1383–1394. [CrossRef]
64. Buzsáki, D.; Kovács, M.B.; Hümpfner, E.; Harcsa-Pinterb, Z.; Kelemen, Z. Conjugation between 3D and 2D aromaticity: Does it really exist? The case of carborane-fused heterocycles. *Chem. Sci.* **2022**, *13*, 11388–11393. [CrossRef]
65. Poater, J.; Viñas, C.; Solà, M.; Teixidor, F. 3D and 2D aromatic units behave like oil and water in the case of benzocarborane derivatives. *Nat. Commun.* **2022**, *13*, 3844. [CrossRef]
66. Dorofeeva, O.V.; Ryzhova, O.N.; Suntsova, M.A. Accurate Prediction of Enthalpies of Formation of Organic Azides by Combining G4 Theory Calculations with an Isodesmic Reaction Scheme. *J. Phys. Chem. A* **2013**, *117*, 6835–6845. [CrossRef]
67. Naylor, R.D.; Kirby, S.P.; Pedley, J.B. *Thermochemical Data of Organic Compounds*; Chapman and Hall: London, UK; New York, NY, USA, 1986.

68. Pepekin, V.I.; Metyushin, Y.N.; Kalinin, V.N.; Lebedev, Y.A.; Zakharkin, L.I.; Apin, A.Y. Thermochemistry of *ortho*- and *meta*-carboranes ($B_{10}H_{10}C_2H_2$). *Russ. Chem. Bull.* **1971**, *20*, 212–216. [CrossRef]
69. Xi, H.-W.; Goh, H.W.; Xu, J.Z.; Foo Lee, P.P.; Lim, K.H. Theoretical design and exploration of novel high energy density materials based on silicon. *J. Energetic Mat.* **2018**, *36*, 291–301. [CrossRef]
70. Ewi, T.; Zhu, W.; Zhang, J.; Xiao, H. DFT study on energetic tetrazolo-[1,5-b]-1,2,4,5-tetrazine and 1,2,4-triazolo-[4,3-b]- 1,2,4,5-tetrazine derivatives. *J. Hazard. Mater.* **2010**, *179*, 581–590. [CrossRef]
71. Kamlet, M.J.; Jacobs, E.J. Chemistry of Detonations. I. A Simple Method for Calculating Detonation Properties of C–H–N–O Explosives. *J. Chem. Phys.* **1968**, *48*, 23–35. [CrossRef]
72. Manaa, M.R.; Fried, L.E.; Kuo, I.-F.W. Determination of enthalpies of formation of energetic molecules with composite quantum chemical methods. *Chem. Phys. Lett.* **2016**, *648*, 31–35. [CrossRef]
73. Osmont, A.; Catoire, L.; Gökalp, I.R.; Yang, V. Ab initio quantum chemical predictions of enthalpies of formation, heat capacities, and entropies of gas-phase energetic compounds. *Combust. Flame* **2007**, *151*, 262–273. [CrossRef]
74. Guo, D.; Zybin, S.V.; An, Q.; Goddard, W.A., III; Huang, F. Prediction of the Chapman–Jouguet chemical equilibrium state in a detonation wave from first principles based reactive molecular dynamics. *Phys. Chem. Chem. Phys.* **2016**, *18*, 2015–2022. [CrossRef] [PubMed]
75. Zhou, Z.Q.; Nie, J.X.; Ou, Z.C.; Qin, J.F.; Jiao, Q.J. Effects of the aluminum content on the shock wave pressure and the acceleration ability of RDX-based aluminized explosives. *J. Appl. Phys.* **2014**, *116*, 144906–144908. [CrossRef]
76. Kanel, G.I.; Razorenov, S.V.; Fortov, V.E. *Shock-Wave Phenomena and the Properties of Condensed Matter*; Springer: New York, NY, USA, 2004.
77. Davies, A.G.; Burnett, A.D.; Fan, W.; Linfield, E.H.; Cunningham, J.E. Terahertz spectroscopy of explosives and drugs. *Mater. Today* **2008**, *11*, 18–26. [CrossRef]
78. Sheldrick, G.M. Crystal structure refinement with SHELXL. *Acta Cryst.* **2015**, *C71*, 3–8. [CrossRef]
79. Macrae, C.F.; Sovago, I.; Cottrell, S.J.; Galek, P.T.A.; McCabe, P.; Pidcock, E.; Platings, M.; Shields, G.P.; Stevens, J.S.; Towler, M.; et al. Mercury 4.0: From visualization to analysis, design and prediction. *J. Appl. Cryst.* **2020**, *53*, 226–235. [CrossRef]
80. Spek, A.L. PLATON SQUEEZE: A tool for the calculation of the disordered solvent contribution to the calculated structure factors. *Acta Cryst.* **2015**, *C71*, 9–18. [CrossRef]

molecules

MDPI

Article

Substitutional Diversity-Oriented Synthesis and In Vitro Anticancer Activity of Framework-Integrated Estradiol-Benzisoxazole Chimeras

Ferenc Kovács [1], Dóra Izabella Adamecz [2], Ferenc István Nagy [2], Benedek Papp [2], Mónika Kiricsi [2] and Éva Frank [1,*]

[1] Department of Organic Chemistry, University of Szeged, Dóm tér 8, H-6720 Szeged, Hungary
[2] Department of Biochemistry and Molecular Biology, Doctoral School of Biology, University of Szeged, Közép fasor 52, H-6726 Szeged, Hungary
* Correspondence: frank@chem.u-szeged.hu; Tel.: +36-62-544-275

Abstract: Hybridization of steroids and other pharmacophores often modifies the bioactivity of the parent compounds, improving selectivity and side effect profile. In this study, estradiol and 3′-(un)substituted benzisoxazole moieties were combined into novel molecules by structural integration of their aromatic rings. Simple estrogen starting materials, such as estrone, estradiol and estradiol-3-methylether were used for the multistep transformations. Some of the heterocyclic derivatives were prepared from the estrane precursor by a formylation or Friedel–Crafts acylation—oximation—cyclization sequence, whereas others were obtained by a functional group interconversion strategy. The antiproliferative activities of the synthesized compounds were assessed on various human cervical, breast and prostate cancer cell lines (HeLa, MCF-7, PC3, DU-145) and non-cancerous MRC-5 fibroblast cells. Based on the primary cytotoxicity screens, the most effective cancer-selective compounds were selected, their IC_{50} values were determined and their apoptosis-inducing potential was evaluated by quantitative real-time PCR. Pharmacological studies revealed a strong structure–function relationship, where derivatives with a hydroxyl group on C-17 exhibited stronger anticancer activity compared to the 17-acetylated counterparts. The present study concludes that novel estradiol-benzisoxazole hybrids exert remarkable cancer cell-specific antiproliferative activity and trigger apoptosis in cancer cells.

Keywords: estradiol; benzisoxazole; hybrid; cancer selectivity; apoptosis induction

Citation: Kovács, F.; Adamecz, D.I.; Nagy, F.I.; Papp, B.; Kiricsi, M.; Frank, É. Substitutional Diversity-Oriented Synthesis and In Vitro Anticancer Activity of Framework-Integrated Estradiol-Benzisoxazole Chimeras. *Molecules* **2022**, *27*, 7456. https://doi.org/10.3390/molecules27217456

Academic Editors: Alexey M. Starosotnikov, Maxim A. Bastrakov and Igor L. Dalinger

Received: 6 October 2022
Accepted: 24 October 2022
Published: 2 November 2022

1. Introduction

Naturally occurring and synthetic benzisoxazoles [1], particularly their 3-substituted representatives [2], are important pharmacophores and serve as valuable tools for drug design and discovery, having a high number of positive hits in biological screens. Because of their versatile properties and potential as selective ligands for a variety of macromolecular targets, these bicyclic aromatic ring systems constitute the essential structural motif in a wide range of pharmacologically active compounds, including a number of potential anticancer agents (Figure 1) [3–9]. Furthermore, the benzisoxazole scaffold is often used as a bioisosteric replacement for the benzoyl group of biologically active molecules [10].

Chemical modification of natural steroids with different heterocycles provides a way to alter the function of the parent compound, and several derivatives have been demonstrated to be effective in the prevention and treatment of many types of cancers [11]. Although there are no examples in the literature for the synthesis of steroidal benzisoxazoles, the incorporation of the five-membered isoxazole ring into a sterane backbone in either a connected [12–14] or a condensed manner [15] led to some effective antiproliferative agents (**I**–**VIII**, Figure 1). Nevertheless, the phenolic A-ring of estrogens offers the possibility to synthesize aromatic ring-integrated benzisoxazole hybrids and this modification may have beneficial outcomes in several aspects. First, molecular hybridization of steroids with other

potentially active compounds often modulates bioactivity and improves the selectivity and side effect profile of the individual compounds [16,17]. In addition, derivatization of estrogens at the C2–C3 position by the introduction of a fused heteroring while simultaneously eliminating the phenolic OH group makes it likely that the novel derivative will not be able to bind to the estrogen receptor, and will therefore be free of undesired hormonal effects [18]. Even estradiol (E2) derivatives substituted at C-2 with different functional groups, such as 2-methoxyestradiol (2-ME2) and its structural analogues [19], in which the phenolic OH group required for estrogen receptor binding is intact, do not have hormonal effects due to steric and electronic factors induced by the C-2 group [20]. Modification of the OH group, which plays a key role as an H-donor in hormone receptor binding [20], together with the C-2 functionalization through a heteroring formation, can clearly reduce the interaction with the target protein. At the same time, the 3-OH group of 2-ME2 analogs can be held responsible for their rapid metabolic degradation [21], so the incorporation of the oxygen into a heteroring can increase pharmacokinetic stability as well. Although the sterane backbone can be favorable promoting cell membrane penetration and thus the delivery to the site of action, the heteroatoms of the incorporated isoxazole moiety may be involved in H-bonding interactions to the target macromolecule other than a hormone receptor. However, it is important to note that sterane-based structures may have a very complex mode of action in the human body [22], e.g., at least five different aspects of the anticancer mechanism of action of 2-ME2 have been elucidated so far [21].

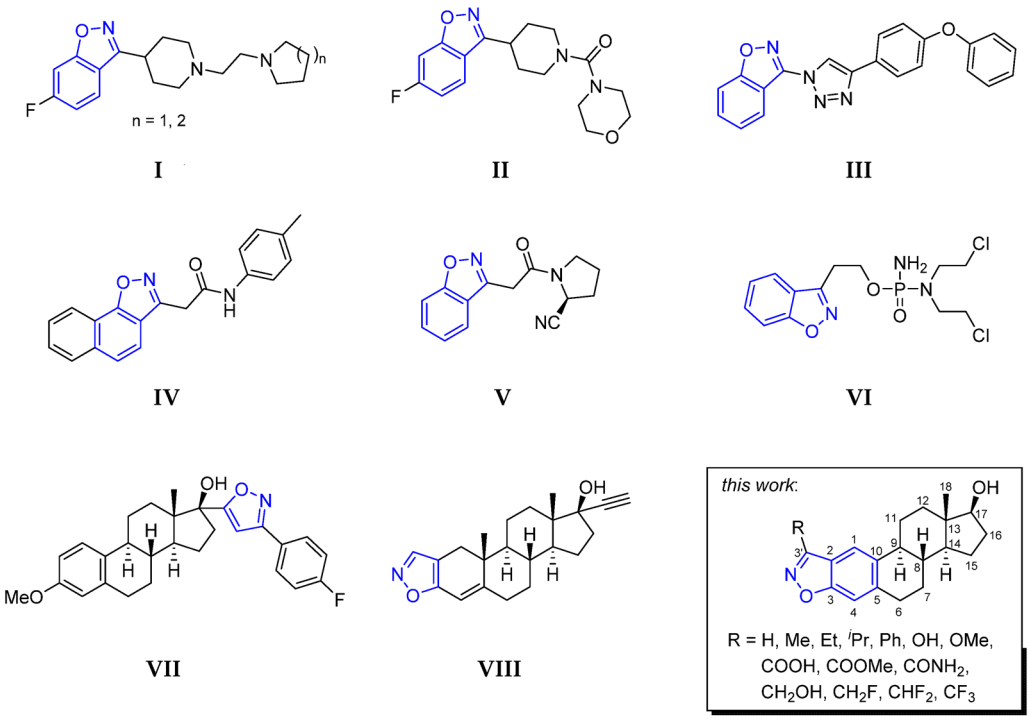

Figure 1. Benzisoxazoles (**I**–**VI**) [3–8] and steroidal isoxazoles (**VII**,**VIII**) [13,15] with anticancer activity and the proposed E2-benzisoxazole hybrids.

As a continuation of our ongoing research for designing steroidal A-ring integrated chimeras with anticancer activity [18,23–26], a benzisoxazole scaffold containing different substituents at the C-3′ position of the heteroring was hybridized with the aromatic ring of E2. According to a comprehensive analysis of the chemical structure of marketed anticancer agents, the most abundant functional groups of these drugs are OH, COOH, COOR, NH_2 and F; moreover, 43.4% of them contain both aromatic and non-aromatic rings as part of their structure [27]. These structural features were taken into account in designing the synthesis of novel compounds that show diversity in the substitution pattern of the *N*,*O*-heterocyclic ring. Virtual screening of the pharmacokinetic parameters using ChemAxon's Chemicalize

software [28] showed that almost all the molecules designed to be produced meet the drug-like criteria defined by Lipinski and Veber [29,30] (Supplementary Material p50).

Various protocols for the synthesis of 3-substituted benzisoxazoles have been reported so far [31]. Among others, catalytic cyclizations of 2-hydroxyaryl aldoximes and ketoximes [32] leading to the N–O bond formation through intramolecular Mitsunobu reaction [33] or by conversion of the hydroxyl group of the oximes to good, leaving groups followed by base-catalyzed ring-closure, are well-known procedures [3,34]. However, due to the necessity of a strong base or high temperature, these methods often involve the formation of other products; e.g., Beckmann rearrangement of the oxime and subsequent cyclization can lead to isomeric benzoxazoles. A new route using 2,3-dichloro-5,6-dicyano-1,4-benzoquinone (DDQ)/PPh_3 at room temperature (RT) was reported to overcome these disadvantages [34]. Since the phenolic substructure is present in estrogens, the 2-hydroxyaryl aldehyde or ketone precursors of oximes can be obtained by regioselective formylation or Friedel–Crafts acylation. Although some drawbacks of these approaches could be found, such as the need for 3–4 reaction steps from E2 to benzisoxazoles, we tried to optimize each step in order to achieve high conversions without the formation of undesirable byproducts.

The newly synthesized benzisoxazole derivatives were evaluated for their in vitro antiproliferative activities on DU-145 and PC3 (both prostate cancer), HeLa (cervical cancer) and MCF-7 (breast cancer) cell lines. For comparison, the cytotoxicity of the compounds was tested on MRC-5 non-cancerous lung fibroblast cells. According to the results of the initial screening, the most potent anticancer agents were selected, their IC_{50} values were determined and their apoptosis-inducing potential was examined by reverse transcription quantitative polymerase chain reaction (RT-qPCR) measurements.

2. Results and Discussion

2.1. Syntheses

Based on the literature background, the synthesis of estradiol-A-ring-integrated unsubstituted benzoisoxazole and those containing diverse functional groups at C-3′ position of the heteroring were designed (Figure 1). For the multistep transformations estrone (E1), estradiol (E2) and estradiol-3-methylether (E2Me) were used as starting materials. Some of the reactions (if R = H, Me, Et, ^{i}Pr, Ph, COOMe, CF_3, OH, OMe) were initiated by regioselective formylation or Friedel–Crafts acylation at the C-2 position of the corresponding estrane precursor (**1** or E2). The following oxime formation and activation of the oxime-OH offered the possibility of cyclization with the phenolic OH group to isoxazole under appropriate conditions. In other cases (if R = COOH, $CONH_2$, CH_2OH, CH_2F, CHF_2), a common 3′-methylcarboxylated benzisoxazole intermediate served as a precursor for additional functional group interconversion (FGI).

After a nearly quantitative oximation [35] of 2-formyl-E2 (**2a**), obtained by regioselective Cashiragi *ortho*-formylation of E2 [36], DDQ/PPh_3-induced ring-closure of the 2-hydroxyaryl aldoxime moiety in **3a** [34] proceeded rapidly to result in an unsubstituted A-ring-condensed isoxazole derivative (**4a**) in high yield (Scheme 1). During the 3-step sequence, only formylation reduced the efficiency, leading to a ca. 60% yield of 2-formyl-E2 (**2a**). The residual E2 and the minor 4-formyl isomer with similar polarity to that of **2a** were removed by column chromatography and subsequent recrystallization. For the similar synthesis of the 3′-methyl- (**4b**), 3′-ethyl (**4c**), 3′-isopropyl (**4d**) and 3′-phenyl-substituted steroidal benzisoxazoles (**4e**), estradiol-3-methylether-17-acetate (**1**) was used as starting material in order to protect the reactive OH groups of E2 during Friedel–Crafts acylation reactions. Regioselective $AlCl_3$-induced electrophilic substitution on C-2 with acetyl chloride (AcCl) [23], propionyl chloride, isobutyryl chloride or benzoyl chloride (BzCl) with simultaneous deprotection of 3-OH by the excess Lewis acid, and the following alkaline deprotection of 17-OH led to acylated E2 derivatives **2b**–**e** in good yields. Compound **2g** obtained by the similar conversion of **1** with methyl chlorooxoacetate was not subjected to alkaline treatment due to its diester character but was used for the next reaction step. Analo-

gous CF_3-substituted isoxazole **2f** could not be synthesized from **1**, since only trifluoroacetic anhydride (TFAA) instead of the more reactive acyl chloride was available as a reagent for the electrophile generation and in this case, the 3-OMe group of **1** did not activate the *ortho* position of the aromatic ring enough for an electrophilic attack. Thus, Friedel–Crafts acylation from E2 was performed under controlled conditions. Low temperature and 6 equiv. of $AlCl_3$ were required for high yield of the desired product (**2f**). Although the formation of an unidentified apolar by-product (probably as a result of Wagner-Meerwein rearrangement) was observed with increasing temperature, only *O*-acylation of E2 occurred by using less (2 equiv.) Lewis acid. The structures of the 2-substituted derivatives were determined by ^1H and ^{13}C NMR spectroscopy (Supplementary Material, p2–49). The regioselective entry of the formyl or acyl substituents into C-2 position was supported by the two singlet signals for C-1 and C-4 in the ^1H NMR spectra of **2a–g**. In all cases, the carbonyl-C of the formyl or acyl group as well as the other carbon peaks, if relevant, of the introduced moiety were also observed in the ^{13}C NMR (J-mod) spectra.

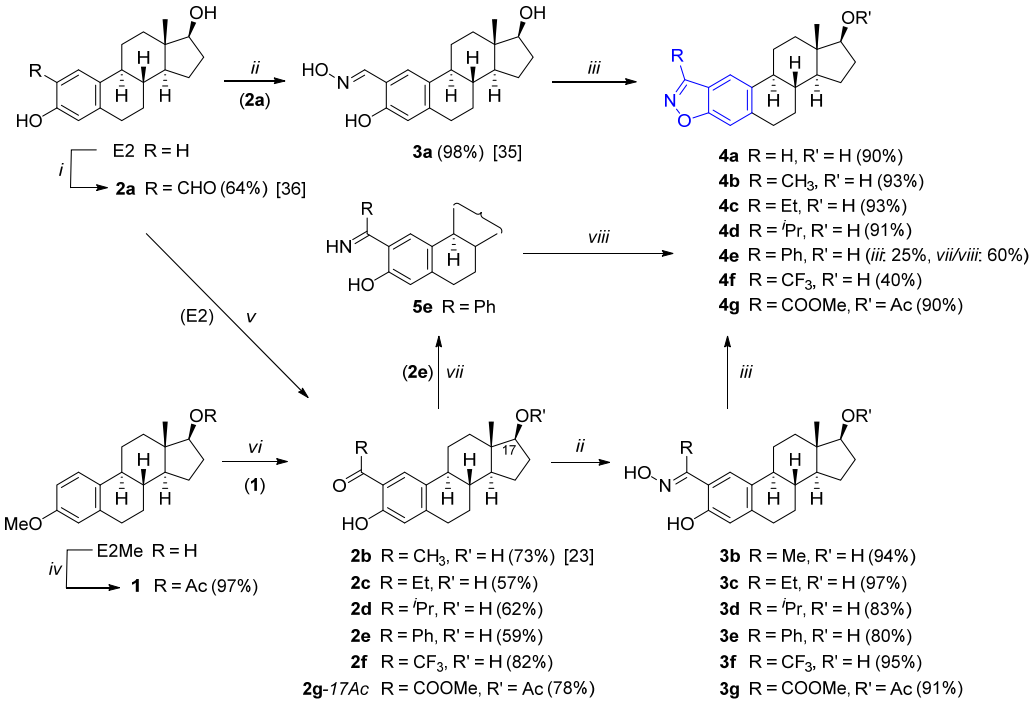

Scheme 1. Synthesis of A-ring-condensed isoxazoles from E2 and E2Me. *Reagents and conditions*: (i) EtMgBr, THF, $(CH_2O)_n$, hexamethylphosphoramide (HMPA), benzene, 80 °C, 20 h; KOH, MeOH, RT, 1 h; (ii) $NH_2OH{\cdot}HCl$, NaOAc or pyridine, EtOH, RT (for **3a** and **3g**) or reflux (for **3b–f**), 2–24 h; (iii) DDQ, PPh_3, DCM, RT, 10 min (for **4a**, **4f** and **4g**), with the addition of Et_3N (for **4b–e**); (iv) Ac_2O, cat. H_2SO_4, sonication, RT, 5 min; (v) TFAA (for **2f**), $AlCl_3$, DCM, 0 °C, 4 h; (vi) AcCl (for **2b**), EtC(O)Cl (for **2c**), ^{i}PrC(O)Cl (for **2d**), BzCl (for **2e**), $Cl(CO)_2OMe$ (for **2g**), $AlCl_3$, DCM, 0 °C to RT, 4 h, followed by alkaline deacetylation with NaOH in MeOH/DCM (1:9) (for **2b–f**); (vii) NH_3/MeOH (6M), RT, 2 h; (viii) NCS, K_2CO_3, THF, RT, overnight.

Next, condensation reactions of ketones **2b–g** were carried out with hydroxylamine to afford the corresponding oximes as a single isomer (**3b**, **3c** and **3g**) [37] or mixtures of *E* and *Z* forms (**3d–f**) [38] (Scheme 1). Subsequent DDQ/PPh_3-initiated cyclization of the oximes in dichloromethane (DCM) under mild conditions afforded the desired E2-benzisoxazole hybrids (**4b–g**). It is worth mentioning that lower yields (25% and 40%) were obtained for **4e** and **4f**. Because of stereoelectronic reasons, only one of the oxime isomers was able to cyclize to isoxazole with the bulky adduct formed from DDQ and PPh_3 [34], whereas the other remained unchanged during the reaction, as confirmed by thin-layer chromatography (TLC) monitoring. Additionally, the presence of the Ph group in **3e** activated the compound

towards Beckmann rearrangement, leading to the formation of 2-phenylbenzoxazole as the main product. In order to enhance the yield, an alternative route was carried out for the transformation of **2e**, involving an imine formation (**5e**) with ammonia and the following chlorination/dehydrohalocyclization by *N*-chlorosuccinimide (NCS)/K_2CO_3 [39]. In this case, steric factors do not impede the cyclization to **4e**, and a higher yield (60%) was obtained (Scheme 1). Unfortunately, this latter method did not work for the conversion of the trifluoromethyl derivative **2f**.

For the synthesis of two additional heterocyclic derivatives (**4h** and **4i**), E1 was used as a starting material (Scheme 2). After regioselective Friedel–Crafts acylation with TFAA and a subsequent haloform reaction of **6a** [40], an E2-salicylic acid domain-integrated hybrid (**6b**) was produced. This compound was next converted to a hydroxamic acid derivative of E2 (**7**) by a three-step sequence involving C-17 ketone reduction, methylester formation of the acid moiety [41] and the final nucleophilic acyl substitution with NH_2OH [42]. Mitsunobu-triggered heterocyclization in anhydrous THF at RT [43] afforded 3′-hydroxybenzisoxazole **4h** in 89% yield, whereas its *O*-methylation furnished **4i** in 82% yield (Scheme 2).

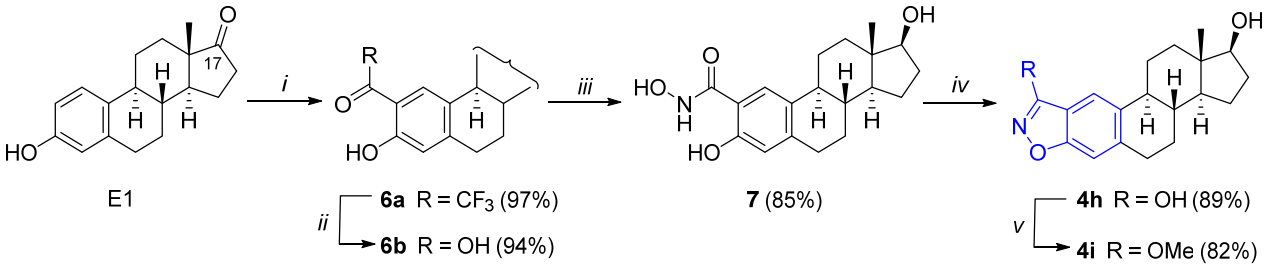

Scheme 2. Synthesis of A-ring-condensed isoxazoles from E1. *Reagents and conditions*: (i) TFAA, $AlCl_3$, DCM, 0 °C to RT, 4.5 h, (ii) KOH, EtOH/H_2O, reflux, 4 h; (iii) three steps: $NaBH_4$/EtOH, RT, 30 min (**6c**, R = OH, 17β-OH at C-17); MeI, Na_2CO_3, DMF, 50 °C, 2 h (**6d**, R = OMe, 17β-OH at C-17); NH_2OH (50 wt. % aq. solution), KOH, MeOH/dioxane, RT, 30 min; (iv) diisopropyl azodicarboxylate (DIAD), PPh_3, THF, RT, 2 h; (v) MeI, K_2CO_3, DMF, RT, 1 h.

In the following, additional benzisoxazole derivatives were synthesized by FGI of the pre-formed substituted heteroring (Scheme 3). Reduction of the previously obtained 17-*O*-protected 3′-methyl ester (**4g**) with $NaBH_4$ in MeOH gave **4j**. Deacetylation of 17-OH led to **4k**, whereas conversion of **4j** with diethylaminosulfur trifluoride (DAST) in DCM and subsequent deprotection afforded the fluoromethylated product **4m** in high yield. On the other hand, **4j** was mildly oxidized with Dess-Martin periodinane (DMP) to **4n**, which was then transformed to **4p** by nucleophilic fluorination followed by deacetylation of **4o**. Interestingly, treatment of **4n** with LiOH or NaOH initiated not only deacetylation but also formic acid elimination accompanied by heteroring opening to give 2-cyano-E2 (**8**). The same product (**8**) was also obtained from **4a** by Kemp elimination [33] or from **4q** by decarboxylation under the influence of heat and/or basic medium. Otherwise, the latter product (**4q**) was prepared by alkaline hydrolysis of the two ester functionalities in **4g** at RT. Starting from **4q**, two additional derivatives (**4r** and **4s**) were also synthesized by FGI. The preparation of the 3′-amino-benzisoxazole-E2 hybrid (**4t**) proved to be the most difficult challenge. Since the DDQ/PPh_3-induced cyclization of amidoxime **9** obtained from **8** failed and 2-amino-oxazole **10** was formed instead of the desired isoxazole **4t** by Tiemann rearrangement, the Curtius rearrangement of the acyl azide available from **4q** with diphenylphosphorylazide (DPPA) in refluxing toluene was tried to carry out. Nevertheless, unfortunately, this reaction did not lead to success either. The reaction did not proceed even to the formation of the azide, so the preparation of the amino-substituted derivative (**4t**) was discarded.

Structural determination of the novel steroidal A-ring-fused isoxazoles (**4a**–**s**) was accomplished using ^{1}H NMR, ^{13}C NMR (J-mod) and MS measurements. The fact of the cyclization was confirmed by the disappearance of the proton signal of the phenolic OH

group in the proton spectra, and in the case of the 3′-substituted derivatives (**4b**–**s**) by the negative peak of the three hydrogen-free, sp^2-hybridized carbon atoms (C-2, C-3, and C-3′). For the unsubstituted isoxazole **4a**, the peak of 3′-H was detected at 8.60 ppm, whereas C-3′ was observed as a positive signal at 146.2 ppm. The measured molecular masses were in good agreement with those calculated from the structures.

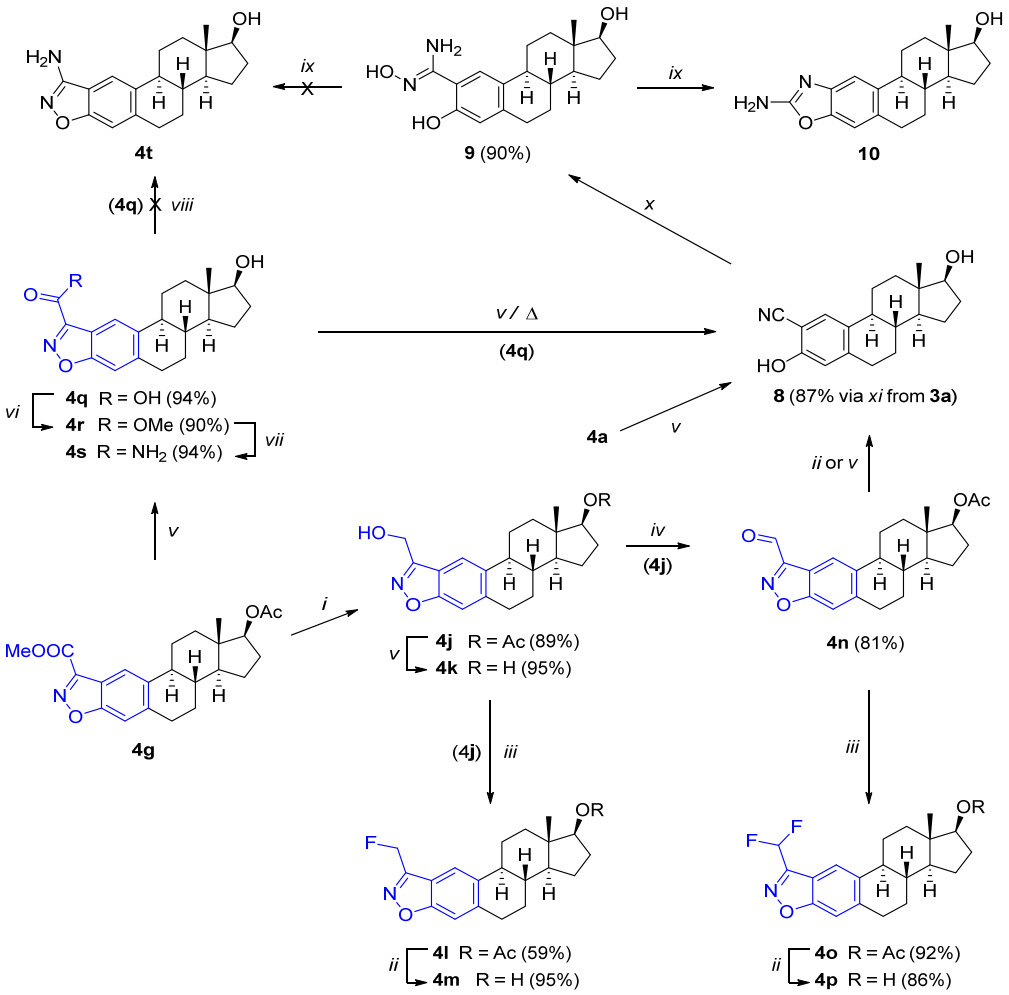

Scheme 3. Synthesis of A-ring-condensed 3′-substituted isoxazoles by FGI. *Reagents and conditions*: (i) $NaBH_4$, MeOH, RT, 1 h; (ii) LiOH, THF/H_2O, RT, 2–24 h; (iii) DAST, DCM, RT, 1–2 h; (iv) DMP, DCM, RT, 2 h; (v) NaOH, MeOH/DCM, RT, 1–20 h; (vi) MeOH, H_2SO_4, reflux, 36 h; (vii) NH_3/MeOH (6M), RT, 4 h. (viii) DPPA, toluene, reflux, overnight; (ix) DDQ, PPh_3, with or without the addition of Et_3N, DCM, RT, 1 h; (x) NH_2OH (50 wt. % aq. solution), Na_2CO_3, EtOH, reflux, overnight; (xi) DIAD, PPh_3, ACN, 1 h.

2.2. Pharmacological Studies

With the newly synthesized estradiol-A-ring-integrated benzisoxazole derivatives in our hand, we set off to investigate their in vitro anticancer activity. First, all compounds were solubilized in cell culture grade dimethyl sulfoxide (DMSO) at a final concentration of either 2.5, 5 or 10 mM, respectively, depending on the solubility. Then, each compound was subjected to a preliminary toxicity screen on prostate cancer (DU-145, PC3), cervical cancer (HeLa) and MCF-7 breast cancer cell lines. The non-cancerous MRC-5 cells were also incorporated into the tests to determine the cancer-selective antiproliferative effect of the synthesized molecules. Cells of each cell line were incubated for 72 h with the compounds applied at 2.5 µM concentration, then MTT cell viability assays were carried out. The results of the viability screen (Supplementary Material p51) are shown as a heatmap (Figure 2).

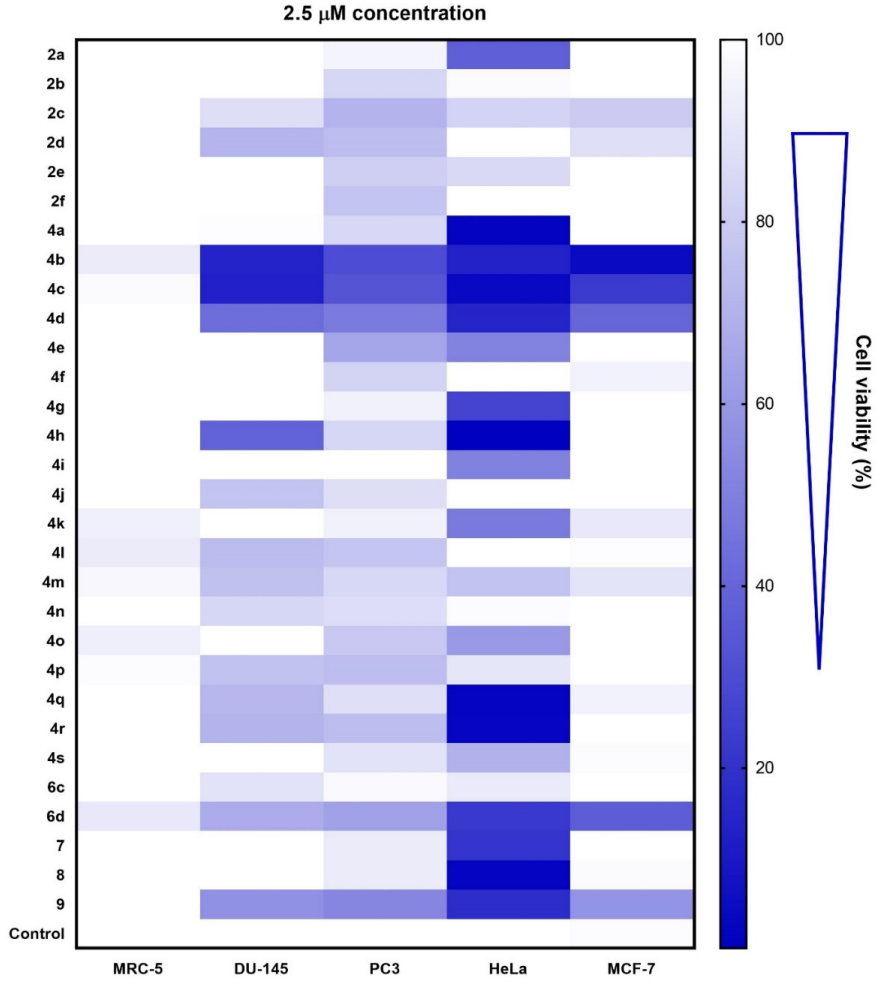

Figure 2. Representative heatmap of the primary cytotoxic performance of estradiol derivatives on cancerous DU-145, PC3, HeLa and MCF-7 cell lines as well as on non-cancerous human fibroblasts (MRC-5) (compound concentration = 2.5 μM; incubation time = 72 h). Control represents the viability of untreated cells.

The cytotoxicity screen resulted in a great number of positive hits, whereas the estradiol derivatives exhibited strong antiproliferative activity on cancer cells, in particular, HeLa cells were highly sensitive to the treatments. Furthermore, most compounds presented outstanding cancer cell-selective performance by showing remarkable activity on cancerous cell lines, but no or negligible effect on non-cancerous fibroblasts. To validate these findings, we selected the three most promising derivatives, namely **4b**, **4c** and **4d** (3′-methyl, 3′-ethyl, and 3′-isopropyl substituted steroidal benzisoxazoles), and examined their anticancer efficiency more thoroughly. We assessed the minimal inhibitory concentration (IC_{50}) of the compounds by treating DU-145, HeLa, MCF-7 and MRC-5 cells with either **4b**, **4c** or **4d** in 1, 2, 3, 4, 5, 6, 8 and 10 μM concentrations for 72 h and for the viability data, dose-response curves were fitted (Supplementary Material, p52–53) and IC_{50} values were calculated accordingly (Table 1). For comparison, the IC_{50} values of cisplatin on the same cell lines are also included [24].

These results agreed with the primary cytotoxicity screen (Figure 2), as the obtained IC_{50} concentrations verified that the tested compounds were selectively effective and very potent on every cancer cell line involved in the examination. The IC_{50} values of the molecules were at least one but sometimes even two magnitudes higher on non-cancerous MRC-5 cells than on malignant cells. Interestingly, each estradiol-benzisoxazole hybrid was more effective on the three cancer cell lines than the classic chemotherapy drug cisplatin. In fact, cisplatin affected the viability of non-cancerous fibroblasts similarly

to steroids; nevertheless, it exhibited significantly weaker antiproliferative capacity on cancer cells than the steroidal chimeras. In summary, potent and tumour cell-selective compounds were found on breast, cervical and prostate cancer cell lines among these E2-benzisoxazole hybrids with 3′-methyl (**4b**), 3′-ethyl (**4c**) and 3′-isopropyl (**4d**) substitution, i.e., this alkyl substitution of the heterocycle proved to be favourable in terms of biological effect and selectivity.

Table 1. IC_{50} values (μM ± SD) of the selected compounds and cisplatin determined on various cancer cell lines and on non-cancerous MRC-5 cells.

Cell Lines	IC_{50} Values (μM ± SD)			
	4b	**4c**	**4d**	**Cisplatin**
MRC-5	27.08 ± 4.06	18.39 ± 2.02	32.36 ± 3.23	32 ± 1.2
DU-145	1.09 ± 0.05	0.56 ± 0.06	2.87 ± 0.2	118 ± 1.1
HeLa	0.46 ± 0.03	0.28 ± 0.03	1.1 ± 0.08	>330
MCF-7	0.34 ± 0.02	0.25 ± 0.03	1.2 ± 0.1	296 ± 1.1

Cisplatin values according to our publication [24].

Lastly, to delineate the possible mechanism of cytotoxicity induced by these novel steroidal heterocycles, we evaluated the apoptosis-inducing potential of the selected three compounds. Most cancer cells try to evade apoptosis and avoid undergoing this form of programmed cell death, which is often the reason behind the ineffectiveness of chemotherapy. Thus, examination of the apoptosis-triggering capacity of newly synthesized anticancer agents is imperative. For this, DU-145, HeLa, and MCF-7 cells were treated with either **4b**, **4c** or **4d** in different concentrations for 72 h. After treatments, total RNA was isolated, reverse transcribed into cDNA and the relative expression levels of some key apoptotic marker genes (BAX, Casp-3, p21, p53) were measured by real-time qPCR (Figure 3). Since MCF-7 cells are known to be deficient in functional caspase-3 due to a deletion in exon 3 of the gene [44], we did not examine the relative transcript levels of this gene in MCF-7 breast cancer cells.

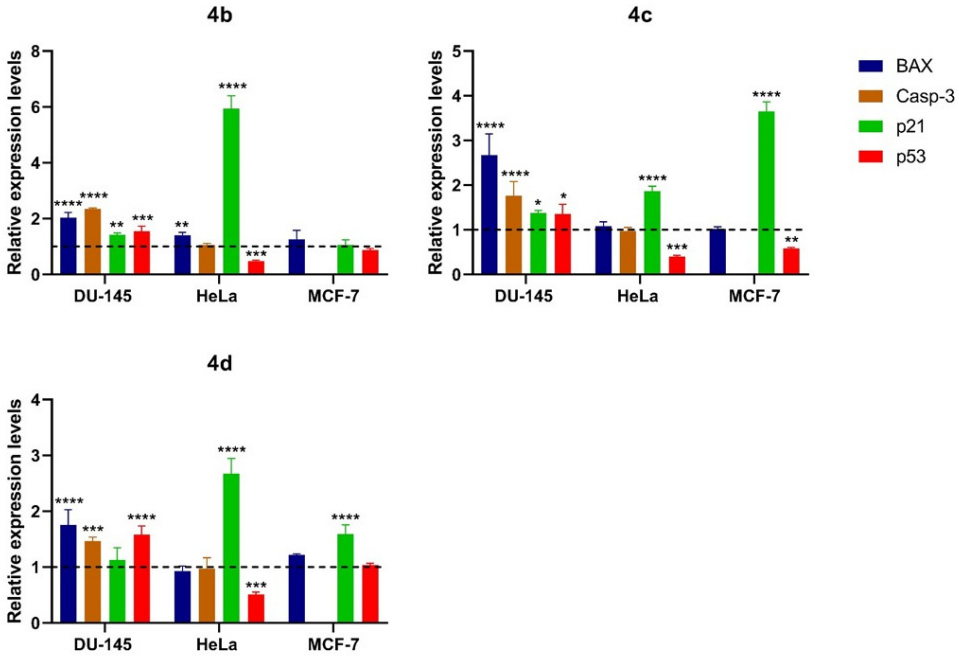

Figure 3. The relative mRNA levels of pro-apoptotic markers BAX, Casp-3, p21, p53 in DU-145, HeLa and MCF-7 cells treated with **4b** (DU-145: 2 μM HeLa: 1 μM, MCF-7 1 μM), **4c** (DU-145: 1 μM HeLa: 1 μM, MCF-7 1 μM) and **4d** (DU-145: 4 μM HeLa: 2 μM, MCF-7 2 μM). Fisher's LSD test, *: $p < 0.05$, **: $p < 0.01$, ***: $p < 0.001$, ****: $p < 0.0001$.

In accordance with the cytotoxicity data, we found that exposure of cancer cells to any of the three E2-benzisoxazole hybrids induced significant alterations in the expression profile of the examined pro-apoptotic genes (Figure 3). The most sensitive marker was p21 since massive upregulation of p21 expression was observable on each cancer cell line following treatments. Of the three cancerous cell types, DU-145 cells were the most affected, as increased transcript levels of every pro-apoptotic marker, i.e., p21, BAX, Casp-3 as well as p53 were also visible in the case of DU-145 cells.

3. Materials and Methods

3.1. General

Chemicals, reagents and solvents were purchased from commercial suppliers (Sigma-Aldrich and Alfa Aesar) and used without further purification. Amylene-stabilized dichloromethane was used for the Friedel–Crafts acylations, cyclizations and the Dess–Martin oxidation as solvent. Melting points (Mps) were determined on an SRS Optimelt digital apparatus and are uncorrected. The transformations were monitored by TLC using 0.25 mm thick Kieselgel-G plates (Si 254 F, Merck). The compound spots were detected by spraying with 5% phosphomolybdic acid in 50% aqueous phosphoric acid. Purifications by column chromatograpy (CC) were carried out on silica gel 60, 40–63 μm (Merck) using flash mode. Elementary analysis data were obtained with a PerkinElmer CHN analyzer model 2400. NMR spectra were recorded with a Bruker DRX 500 instrument at RT in $CDCl_3$ or DMSO-d_6 using residual solvent signals as an internal reference. Chemical shifts are reported in ppm (δ scale) and coupling constants (J) are given in Hz. Multiplicities of the ^{1}H signals are indicated as a singlet (s), a broad singlet (bs), a doublet (d), a doublet of doublets (dd), a doublet of triplets (dt), a triplet (t), a triplet of doublets (td), a quartet (q) or a multiplet (m). ^{13}C NMR spectra are ^{1}H-decoupled and the J-MOD pulse sequence was used for multiplicity editing. In this spin-echo type experiment, the signal intensity is modulated by the different coupling constants J of carbons depending on the number of attached protons. Both protonated and unprotonated carbons can be detected (CH_3 and CH carbons appear as positive signals, whereas CH_2 and C carbons appear as negative signals). The purified derivatives were dissolved in high purity acetonitrile and introduced with an Agilent 1290 Infinity II liquid chromatography pump to an Agilent 6470 tandem mass spectrometer equipped an electrospray ionization chamber. Flow rate was 0.5 mL·min^{-1} and contained 0.1% formic acid or 0.1% ammonium hydroxide to help facilitate ionization. The instrument operated in MS1 scan mode with 135 V fragmentor voltage, and the spectra were recorded from 300 to 500 m/z, which were corrected with the background.

3.2. Chemistry

3.2.1. 3-Methoxyestra-1,3,5(10)-triene-17β-acetate (**1**)

E2Me (2.86 g, 10.0 mmol) was suspended in Ac_2O (10 mL), and after adding a catalytic amount of H_2SO_4 (1 drop), the mixture was sonicated for 5 min. The resulting homogenous solution was poured into ice-cold water (100 mL), and the precipitate was filtered off, washed with water and dried. The crude product was purified by CC (EtOAc/hexane = 5:95). Recrystallized from MeOH/H_2O. Yield (**1**): 3.12 g (95%, white crystals); Mp: 100–102 °C; Anal. Calcd. for $C_{21}H_{28}O_3$ (328.45) C 76.79; H 8.59. Found C 76.48; H 8.77. ^{1}H NMR (500 MHz, $CDCl_3$): δ 0.83 (3H, s, 18-CH_3), 1.23–1.64 (7H, overlapping m), 1.70–1.80 (1H, m), 1.89 (2H, m), 2.06 (3H, s, Ac-CH_3), 2.16–2.27 (2H, m), 2.25–2.33 (1H, m), 2.79–2.93 (2H, m), 3.78 (3H, s), 4.69 (1H, dd, J 7.8, 9.2, 17-αH), 6.63 (1H, d, J 2.8, 4-H), 6.71 (1H, dd, J 2.8, 8.6, 2-H), 7.20 (1H, dd, J 1.1, 8.6, 1-H); ^{13}C NMR (125 MHz, $CDCl_3$) δ 12.2 (18-CH_3), 21.3 (Ac-CH_3), 23.4 (CH_2), 26.4 (CH_2), 27.4 (CH_2), 27.7 (CH_2), 29.9 (CH_2), 37.1 (CH_2), 38.7 (8-CH), 43.1 (13-C), 44.0 (9-CH), 50.0 (14-CH), 55.3 (3-MeO), 82.9 (17-CH), 111.6 (2-CH), 114.0 (4-CH), 126.5 (1-CH), 132.7 (10-C), 138.0 (5-C), 157.6 (3-C), 171.4 (Ac-C=O); ESI-MS m/z 329.2 $[M + H]^+$, 329.2 calcd. for $[C_{21}H_{29}O_3]^+$.

3.2.2. General Procedure for the Synthesis of Compounds **2c**–**e** and **2g-17Ac**

Step 1. To a solution of **1** (328 mg, 1.0 mmol) in DCM (10 mL), $AlCl_3$ (800 mg, 6 equiv.) and acyl chloride (1.5 equiv.) were added at 0 °C. After 30 min, the ice bath was removed, the reaction mixture was allowed to warm to RT and stirred for another 4 h. The mixture was poured into diluted HCl (1 M, 20 mL), stirred for 10 min and extracted with EtOAc (3 × 20 mL). The combined organic phase was washed with water (30 mL) and brine (30 mL), dried over anhydrous Na_2SO_4 and then concentrated in vacuo. The crude product was purified by CC to afford the 17-Ac derivatives of **2c**–**e** or **2g**.

Step 2. Subsequent deacetylation was perfomed (for **2c**-17Ac, **2d**-17Ac and **2d**-17Ac) by the addition of NaOH (3 equiv.) in MeOH/DCM = 1:9 (0.1 M) under stirring at RT for 1 h. After evaporating off the solvents under reduced pressure, HCl (1 M, 10 mL) was added to the residue and extracted with EtOAc (3 × 10 mL). The combined organic phase was washed with water (10 mL) and brine (10 mL), dried over anhydrous Na_2SO_4 and concentrated in vacuo.

2-Propionylestra-1,3,5(10)-triene-3-ol-17β-acetate (**2c**-17Ac) and 2-propionylestra-1,3,5(10)-triene-3,17β-diol (**2c**): According to Section 3.2.2, propionyl chloride (130 µL, 138 mg) was used for Step 1. Eluent (CC): EtOAc/hexane = 10:90. Recrystallized from MeOH. Yield (**2c**-17Ac): 240 mg (65%, white needles); Mp: 169–171 °C; Anal. Calcd. for $C_{23}H_{30}O_4$ (370.49) C 74.56; H 8.16. Found C 74.43; H 8.37. ^{1}H NMR (500 MHz, $CDCl_3$): δ 0.84 (3H, s, 18-CH_3), 1.23 (3H, t, *J* 7.3, CH_3 of propionyl), 1.26–1.48 (5H, overlapping m), 1.45–1.55 (1H, m), 1.52–1.62 (1H, m), 1.70–1.79 (1H, m), 1.85–1.95 (2H, m), 2.07 (3H, s, Ac-CH_3), 2.14–2.26 (2H, m), 2.26–2.34 (1H, m), 2.78–2.92 (2H, m), 2.96–3.05 (2H, m, CH_2 of propionyl), 4.70 (1H, t, *J* 8.5, 17-αH), 6.69 (1H, s, 4-H), 7.63 (1H, s, 1-H), 12.12 (1H, s, 3-OH); ^{13}C NMR (125 MHz, $CDCl_3$) δ 8.5 (CH_3 of propionyl), 12.2 (18-CH_3), 21.3 (Ac-CH_3), 23.4 (CH_2), 26.4 (CH_2), 27.0 (CH_2), 27.7 (CH_2), 30.0 (CH_2), 31.5 (CH_2), 36.9 (CH_2), 38.5 (8-CH), 43.0 (13-C), 43.6 (9-CH), 50.0 (14-CH), 82.7 (17-CH), 117.5 (2-C), 117.8 (4-CH), 126.5 (1-CH), 131.4 (C), 146.9 (C), 160.2 (3-C), 171.3 (Ac-C=O), 206.8 (C=O of propionyl); ESI-MS: *m*/*z* 371.2 $[M + H]^+$, 371.2 calcd. for $[C_{23}H_{31}O_4]^+$.

In Step 2, **2c**-17Ac (160 mg, 0.43 mmol) and NaOH (52 mg, 1.30 mmol) were used. The crude product was recrystallized from MeOH. Yield (**2c**): 124 mg (87%, white crystals); Mp: 137–139 °C; Anal. Calcd. for $C_{21}H_{28}O_3$ (328.45) C 76.79; H 8.59. Found C 76.50; H 8.82. ^{1}H NMR (500 MHz, $CDCl_3$): δ 0.80 (3H, s, 18-CH_3), 1.15–1.27 (1H, m), 1.20–1.28 (3H, m, CH_3 of propionyl), 1.27–1.62 (7H, overlapping m), 1.66–1.76 (1H, m), 1.85–1.93 (1H, m), 1.95–2.02 (1H, m), 2.08–2.21 (2H, m), 2.29–2.37 (1H, m), 2.85 (2H, m), 2.93–3.05 (2H, m), 3.74 (1H, q, *J* 7.7, 7.7, 7.7), 6.69 (1H, s, 4-H), 7.65 (1H, s, 1-H), 12.12 (1H, s, 3-OH); ^{13}C NMR (125 MHz, $CDCl_3$) δ 8.6 (CH_3 of propionyl), 11.2 (18-CH_3), 23.3 (CH_2), 26.5 (CH_2), 27.0 (CH_2), 30.0 (CH_2), 30.8 (CH_2), 31.5 (CH_2), 36.7 (CH_2), 38.8 (8-CH), 43.3 (13-C), 43.7 (9-CH), 50.2 (14-CH), 82.0 (17-CH), 117.4 (2-C), 117.8 (4-CH), 126.5 (1-CH), 131.6 (C), 147.0 (C), 160.2 (3-C), 206.8 (C=O); ESI-MS: *m*/*z* 329.2 $[M + H]^+$, 329.2 calcd. for $[C_{21}H_{29}O_3]^+$.

2-Isobutyrylestra-1,3,5(10)-triene-3-ol-17β-acetate (**2d**-17Ac) and 2-isobutyrylestra-1,3,5(10)-triene-3,17β-diol (**2d**): According to Section 3.2.2, isobutyryl chloride (157 µL, 160 mg) was used for Step 1. Eluent (CC): EtOAc/hexane = 10:90. Recrystallized from MeOH. Yield (**2d**-17Ac): 258 mg (67%, yellowish white scales); Mp: 167–169 °C; Anal. Calcd. for $C_{24}H_{32}O_4$ (384.52) C 74.97; H 8.39. Found C 74.72; H 8.61. ^{1}H NMR (500 MHz, $CDCl_3$): δ 0.84 (3H, s, 18-CH_3), 1.24 (6H, dd, *J* 6.4, 6.4, 2 × CH_3 of isobutyryl), 1.26–1.31 (1H, m), 1.28–1.52 (5H, overlapping m), 1.49–1.62 (1H, m), 1.70–1.80 (1H, m), 1.85–1.95 (2H, m), 2.07 (3H, s, Ac-CH_3), 2.15–2.29 (2H, m), 2.26–2.34 (1H, m), 2.79–2.93 (2H, m), 3.59 (1H, m, CH of isobutyryl), 4.70 (1H, t, *J* 8.5, 17-αH), 6.71 (1H, s, 4-H), 7.66 (1H, s, 1-H), 12.29 (1H, s, 3-OH); ^{13}C NMR (125 MHz, $CDCl_3$) δ 12.2 (18-CH_3), 19.5 (one of the CH_3 of isobutyryl), 19.6 (the other CH_3 of isobutyryl), 21.3 (Ac-CH_3), 23.4 (CH_2), 26.4 (CH_2), 27.0 (CH_2), 27.7 (CH_2), 30.0 (CH_2), 34.9 (CH), 36.9 (CH_2), 38.5 (CH), 43.0 (13-C), 43.6 (9-CH), 50.0 (14-CH), 82.7 (17-CH), 116.4 (2-C), 118.0 (4-CH), 126.5 (1-CH), 131.4 (C), 147.0 (C), 160.9 (3-C), 171.3 (Ac-C=O), 210.5 (C=O of isobutyryl); ESI-MS: *m*/*z* 385.2 $[M + H]^+$, 385.2 calcd. for $[C_{24}H_{33}O_4]^+$.

In Step 2, **2d**-17Ac (220 mg, 0.57 mmol) and NaOH (68 mg, 1.70 mmol) were used. Yield (**2d**): 180 mg (92%, white powder); Mp: 130–132 °C; Anal. Calcd. for $C_{22}H_{30}O_3$ (342.48) C 77.16; H 8.83. Found C 76.93; H 8.99. ^{1}H NMR (500 MHz, $CDCl_3$): δ 0.80 (3H, s, 18-CH_3), 1.16–1.27 (1H, m), 1.24 (6H, dd, *J* 6.8, 6.8, 2 × CH_3 of isobutyryl), 1.28–1.60 (7H, overlapping m), 1.67–1.77 (1H, m), 1.85–1.93 (1H, m), 1.95–2.03 (1H, m), 2.08–2.23 (2H, m), 2.29–2.38 (1H, m), 2.79–2.93 (2H, m), 3.60 (1H, m, CH of isobutyryl), 3.75 (1H, t, *J* 8.7, 17-αH), 6.71 (1H, s, 4-H), 7.68 (1H, s, 1-H), 12.29 (1H, s, 3-OH); ^{13}C NMR (125 MHz, $CDCl_3$) δ 11.2 (18-CH_3), 19.5 (one CH_3 of isobutyryl), 19.6 (the other CH_3 of isobutyryl), 23.3 (CH_2), 26.5 (CH_2), 27.0 (CH_2), 30.0 (CH_2), 30.8 (CH_2), 34.9 (CH), 36.7 (CH_2), 38.8 (CH), 43.4 (13-C), 43.7 (9-CH), 50.2 (14-CH), 82.0 (17-CH), 116.4 (2-C), 118.0 (4-CH), 126.5 (1-CH), 131.5 (C), 147.1 (C), 160.9 (3-C), 210.5 (C=O); ESI-MS: *m*/*z* 343.2 $[M + H]^+$, 343.2 calcd. for $[C_{22}H_{31}O_3]^+$.

2-Benzoylestra-1,3,5(10)-triene-3-ol-17β-acetate (**2e**-17Ac) and 2-benzoylestra-1,3,5(10)-triene-3,17β-diol (**2e**): According to Section 3.2.2, benzoyl chloride (174 µL, 211 mg) was used for Step 1. Eluent (CC): Et_2O/hexane = 10:90. Yield (**2e**-17Ac): 272 mg (65%, yellow powder); Mp: 148–150 °C; Anal. Calcd. for $C_{27}H_{30}O_4$ (418.53) C 77.48; H 7.23. Found C 77.40; H 7.57; ^{1}H NMR (500 MHz, $CDCl_3$): δ 0.83 (3H, s, 18-CH_3), 1.18–1.31 (1H, m), 1.28–1.36 (1H, m), 1.33–1.40 (1H, m), 1.37–1.44 (1H, m), 1.41–1.49 (1H, m), 1.50–1.61 (2H, m), 1.70–1.79 (1H, m), 1.79–1.85 (1H, m), 1.86–1.95 (1H, m), 1.98–2.06 (1H, s), 2.04 (3H, s, Ac-CH_3), 2.10–2.27 (2H, m), 2.83–2.98 (2H, m), 4.64–4.71 (1H, m, 17-αH), 6.79 (1H, s, 4-H), 7.48 (1H, s, 4-H), 7.46–7.53 (2H, overlapping m, 3′-H and 5′-H), 7.55–7.62 (1H, m, 4′-H), 7.64–7.70 (2H, m, 2′-H and 6′-H), 11.82 (1H, s, 3-OH); ^{13}C NMR (125 MHz, $CDCl_3$) δ 12.2 (18-CH_3), 21.2 (Ac-CH_3), 23.4 (CH_2), 26.2 (CH_2), 27.0 (CH_2), 27.7 (CH_2), 30.1 (CH_2), 36.9 (CH_2), 38.6 (8-CH), 43.1 (13-C), 43.6 (9-CH), 50.1 (14-CH), 82.7 (17-CH), 117.4 (2-C), 117.8 (4-CH), 128.4 (3′-CH and 5′-CH), 129.3 (2′-CH and 6′-CH), 130.6 (4′-CH), 131.3 (C), 131.9 (1-CH), 138.5 (C), 147.3 (C), 161.2 (3-C), 171.2 (Ac-C=O), 201.3 (Bz-C=O); ESI-MS: *m*/*z* 419.2 $[M + H]^+$, 419.2 calcd. for $[C_{27}H_{31}O_4]^+$.

In Step 2, **2e**-17Ac (230 mg, 0.55 mmol) and NaOH (66 mg, 1.65 mmol) were used. Yield (**2e**): 186 mg (90%, white powder); Mp: 126–128 °C; Anal. Calcd. for $C_{25}H_{28}O_3$ (376.50) C 79.76; H 7.50. Found C 79.56; H 7.84. ^{1}H NMR (500 MHz, $CDCl_3$): δ 0.77 (3H, s, 18-CH_3), 1.12–1.54 (8H, overlapping m), 1.65–1.75 (1H, m), 1.84–1.94 (2H, m), 2.00–2.08 (1H, m), 2.05–2.17 (2H, m), 2.79–2.98 (2H, m), 3.66–3.75 (1H, m, 17-αH), 6.79 (1H, s, 4-H), 7.49 (1H, s, 1-H), 7.48–7.55 (2H, m, 3′-H and 5′-H), 7.55–7.62 (1H, m, 4′-H), 7.64–7.70 (2H, m, 2′-H and 6′-H), 11.85 (1H, s, 3-OH); ^{13}C NMR (125 MHz, $CDCl_3$) δ 11.2 (18-CH_3), 23.2 (CH_2), 26.2 (CH_2), 27.0 (CH_2), 30.2 (CH_2), 30.7 (CH_2), 36.6 (CH_2), 38.8 (8-CH), 43.3 (13-C), 43.7 (9-CH), 50.2 (14-CH), 81.9 (17-CH), 117.3 (2-C), 117.8 (4-CH), 128.5 (2′-CH and 6′-CH), 129.2 (3′-CH and 5′-CH), 130.6 (CH), 131.4 (C), 131.9 (CH), 138.4 (C), 147.4 (C), 161.1 (3-C), 201.4 (C=O); ESI-MS: *m*/*z* 377.2 $[M + H]^+$, 377.2 calcd. for $[C_{25}H_{29}O_3]^+$.

2-(Methyloxoacetyl)-estra-1,3,5(10)-triene-3-ol-17β-acetate (**2g**-17Ac): The synthesis was carried out according to Section 3.2.2, but on a larger scale using E2Me (1.64 g, 5 mmol) and methyl chlorooxoacetate (690 µL, 920 mg) for Step 1. Eluent (CC): EtOAc/hexane = 20:80. Yield (**2g**-17Ac): 1.56 g (78%, yellow crystals); Mp: 134–136 °C; Anal. Calcd. for $C_{23}H_{28}O_6$ (400.47) C 68.98; H 7.05. Found C 68.75; H 7.22. ^{1}H NMR (500 MHz, $CDCl_3$): δ 0.83 (3H, s, 18-CH_3), 1.22–1.61 (7H, overlapping m), 1.70–1.79 (1H, m), 1.86–1.95 (2H, m), 2.06 (3H, s, Ac-CH_3), 2.12–2.28 (3H, m), 2.81–2.97 (2H, m), 3.99 (3H, s, COOC$\underline{H}_3$), 4.65–4.72 (1H, m, 17-αH), 6.75 (1H, s, 4-H), 7.58 (1H, s, 1-H), 10.98 (1H, s, 3-OH); ^{13}C NMR (125 MHz, $CDCl_3$) δ 12.2 (18-CH_3), 21.3 (Ac-CH_3), 23.4 (CH_2), 26.1 (CH_2), 26.8 (CH_2), 27.7 (CH_2), 30.3 (CH_2), 36.7 (CH_2), 38.3 (8-CH), 43.0 (13-C), 43.4 (9-CH), 50.0 (14-CH), 53.1 (COO$\underline{C}H_3$), 82.7 (17-CH), 114.4 (2-C), 117.9 (4-CH), 128.9 (1-CH), 132.7 (C), 150.1 (C), 161.7 (3-C), 163.2 ($\underline{C}OOCH_3$), 171.3 (Ac-C=O), 189.8 (C=O of ketone); ESI-MS: *m*/*z* 399.0 $[M - H]^-$, 399.2 calcd. for $[C_{23}H_{27}O_6]^-$.

2g-17Ac was not deacetylated in Step 2.

3.2.3. 2-Trifluoracetylestra-1,3,5(10)-triene-3,17β-diol (**2f**)

To a solution of E2 (272 mg, 1.0 mmol) in DCM (10 mL), $AlCl_3$ (800 mg, 6 equiv.) and TFAA (1.5 mmol, 1.5 equiv.) were added and the mixture was stirred at 0 °C for 4 h. After completion, it was poured into HCl solution (1 M, 20 mL), stirred for 10 min and extracted with EtOAc (3 × 20 mL). The combined organic phase was washed with water (30 mL) and brine (30 mL), then dried over anhydrous Na_2SO_4 and concentrated in vacuo. The crude product was purified by CC (DCM). Recrystallized from dioxane/H_2O. Yield (**2f**): 302 mg (82%, yellow crystals); Mp: 104–106 °C; Anal. Calcd. for $C_{20}H_{23}F_3O_3$ (368.40) C 65.21; H 6.29. Found C 65.12; H 6.48. ^{1}H NMR (500 MHz, $CDCl_3$): δ 0.79 (3H, s, 18-CH_3), 1.15–1.24 (1H, m), 1.24–1.33 (1H, m), 1.30–1.48 (4H, m), 1.45–1.60 (2H, m), 1.66–1.76 (1H, m), 1.87–1.95 (1H, m), 1.96–2.05 (1H, m), 2.08–2.25 (2H, m), 2.25–2.34 (1H, m), 2.82–2.98 (2H, m), 3.71–3.78 (1H, t, *J* 8.5, 17-αH), 6.79 (1H, s, 4-CH), 7.69 (1H, s, 1-H), 10.86 (1H, s, 3-OH); ^{13}C NMR (125 MHz, $CDCl_3$) δ 11.2 (18-CH_3), 23.2 (CH_2), 26.1 (CH_2), 26.7 (CH_2), 30.4 (CH_2), 30.7 (CH_2), 36.5 (CH_2), 38.5 (8-CH), 43.3 (13-C), 43.6 (9-CH), 50.2 (14-CH), 81.9 (17-CH), 112.2 (2-C), 116.8 (1C, q, *J* 290.2, CF_3), 118.3 (4-CH), 127.2 (1C, q, *J* 3.9, 1-CH), 133.2 (C), 151.1 (C), 162.4 (C), 183.9 (1C, q, *J* 34.8, C=O); ESI-MS: m/z 367.0 $[M-H]^-$, 367.2 calcd. for $[C_{20}H_{22}F_3O_3]^-$.

3.2.4. General Procedure for the Synthesis of Oximes **3a**–**g**

To a solution of 2-substituted estradiol derivative (**2a**–**g**, 1.0 mmol) in EtOH (10 mL), hydroxylamine hydrochloride and a base were added in excess and the mixture was stirred at ambient temperature for a certain period. The solvent was removed under reduced pressure, and the residue was suspended in water (10 mL) and extracted with EtOAc (3 × 10 mL). The combined organic phase was washed with NH_4Cl (1 M, 10 mL), water (10 mL) and brine (10 mL), and then dried over anhydrous Na_2SO_4 and concentrated *in vacuo*. The crude product was purified by CC.

Estra-1,3,5(10)-triene-3,17β-diol-2-carbaldehyde oxime (**3a**): According to Section 3.2.4, 2-formyl-estradiol (**2a**, 300 mg), hydroxylamine hydrochloride (104 mg, 1.5 equiv.) and sodium acetate (164 mg, 2 equiv.) were used. Conditions: RT, 1 h. CC (EtOAc/DCM = 5:95). Yield (**3a**): 309 mg (98%, white powder); Mp > 180 °C (decomp.); Anal. Calcd. for $C_{19}H_{25}NO_3$ (315.41) C 72.35; H 7.99; N 4.44. Found C 72.30; H 8.17; N 4.33. ^{1}H NMR (500 MHz, DMSO-d_6): δ 0.67 (3H, s, 18-CH_3), 1.05–1.44 (7H, overlapping m), 1.53–1.63 (1H, m), 1.74–1.82 (1H, m), 1.82–1.94 (2H, m), 2.03–2.12 (1H, m), 2.20–2.28 (1H, m), 2.71–2.77 (2H, m), 3.53 (1H, td, *J* 8.5, 3.9, 17-αH), 4.41 (1H, d, *J* 4.7, 17-OH), 6.56 (1H, s, 4-H), 7.34 (1H, s, 1-H), 8.27 (1H, s, HC=N), 9.75 (1H, s, NOH), 11.11 (1H, s, 3-OH); ^{13}C NMR (125 MHz, DMSO-d_6): δ 11.1 (18-CH_3), 22.6 (CH_2), 25.9 (CH_2), 26.6 (CH_2), 28.9 (CH_2), 29.8 (CH_2), 36.4 (CH_2), 38.4 (8-CH), 42.7 (13-C), 43.2 (9-CH), 49.5 (14-CH), 79.9 (17-CH), 115.4 (4-CH), 115.5 (2-C), 125.0 (1-CH), 131.3 (10-C), 139.2 (5-C), 148.6 (HC=N), 153.7 (3-C); ESI-MS: m/z 314.0 $[M-H]^-$, 314.2 calcd. for $[C_{19}H_{24}NO_3]^-$.

(Estra-1,3,5(10)-triene-3,17β-diol-2-yl)ethan-1-one oxime (**3b**): According to Section 3.2.4, 2-acetyl-estradiol (**2b**, 314 mg, 1.0 mmol), hydroxylamine hydrochloride (104 mg, 1.5 equiv.) and sodium acetate (164 mg, 2 equiv.) were used. Conditions: reflux, 2 h. CC (EtOAc/DCM = 5:95). Yield: 309 mg (94%, white crystals); Mp: 240–242 °C; Anal. Calcd. for $C_{20}H_{27}NO_3$ ($C_{20}H_{27}NO_3$) C 72.92; H 8.26; N 4.25. Found C 72.86; H 8.58; N 4.03. ^{1}H NMR (500 MHz, $CDCl_3$): δ 0.79 (3H, s, 18-CH_3), 1.15–1.58 (8H, overlapping m), 1.66–1.76 (1H, m), 1.84–1.93 (1H, m), 1.93–2.06 (1H, m), 2.07–2.25 (2H, m), 2.29–2.37 (1H, m), 2.32–2.36 (3H, s, CH_3 of acetoxime), 2.80–2.87 (2H, m), 3.74 (1H, t, *J* 8.5, 17-αH), 6.68 (1H, s, 4-H), 7.32 (1H, s, 1-H), 7.65 (1H, s, NOH), 10.94 (1H, s, 3-OH); ^{13}C NMR (125 MHz, $CDCl_3$) δ 10.9 (CH_3), 11.2 (CH_3), 23.3 (CH_2), 26.6 (CH_2), 27.3 (CH_2), 29.5 (CH_2), 30.8 (CH_2), 36.8 (CH_2), 39.0 (8-CH), 43.4 (13-C), 44.0 (9-CH), 50.2 (14-CH), 82.1 (17-CH), 116.4 (2-C), 117.0 (4-CH), 124.5 (1-CH), 131.2 (10-C), 140.3 (5-C), 155.5 (C), 159.8 (C); ESI-MS: m/z 328.0 $[M-H]^-$, 328.2 calcd. for $[C_{20}H_{26}NO_3]^-$.

(Estra-1,3,5(10)-triene-3,17β-diol-2-yl)propan-1-one oxime (**3c**): According to Section 3.2.4, 2-propanoyl-estradiol (**2c**, 328 mg), hydroxylamine hydrochloride (104 mg, 1.5 equiv.)

and sodium acetate (164 mg, 2 equiv.) were used. Conditions: reflux, overnight. CC (MeOH/DCM = 2:98). Yield (**3c**): 333 mg (97%, white crystals); Mp: 240–242 °C; Anal. Calcd. for $C_{21}H_{29}NO_3$ (343.47) C 73.44; H 8.51; N 4.08. Found C 73.10; H 8.84; N 3.97. ^{1}H NMR (500 MHz, DMSO-d_6): δ 0.67 (3H, s, 18-CH_3), 1.08 (3H, t, *J* 7.5, CH_3 of propionyl oxime), 1.07–1.43 (7H, overlapping m), 1.54–1.63 (1H, m), 1.75–1.82 (1H, m), 1.83–1.94 (2H, m), 2.07–2.16 (1H, m), 2.28–2.35 (1H, m), 2.71–2.86 (4H, overlapping m, 6-H_2 and CH_2 of propionyl oxime), 3.53 (1H, td, *J* 8.5, 4.8, 17-αH), 4.45–4.50 (1H, m, 17-OH), 6.55 (1H, s, 4-H), 7.27 (1H, s, 1-H), 11.27 (1H, s), 11.31 (1H, s); ^{13}C NMR (125 MHz, DMSO-d_6): δ 11.0 (CH_3), 11.2 (CH_3), 17.6 (CH_2), 22.7 (CH_2), 26.0 (CH_2), 26.7 (CH_2), 28.8 (CH_2), 29.9 (CH_2), 36.5 (CH_2), 38.5 (8-CH), 42.8 (13-C), 43.4 (9-CH), 49.5 (14-CH), 80.0 (17-CH), 115.5 (2-C), 116.2 (4-CH), 124.1 (1-CH), 130.6 (C), 138.8 (C), 155.1 (3-C), 162.2 (C=N); ESI-MS: *m*/*z* 344.2 $[M + H]^+$, 344.2 calcd. for $[C_{21}H_{30}NO_3]^+$.

(Estra-1,3,5(10)-triene-3,17β-diol-2-yl)-2-methylpropan-1-one oxime isomers: According to Section 3.2.4, 2-isobutyryl-estradiol (**2d**, 342 mg), hydroxylamine hydrochloride (347 mg, 5 equiv.) and pyridine (1 mL) were used. Conditions: reflux, overnight. CC (MeOH/DCM = 2:98). Yield of the faster eluting isomer (**3d**-*E*): 175 mg (49%, white crystals); Mp: 211–213 °C; Anal. Calcd. for $C_{22}H_{31}NO_3$ (357.49) C 73.92; H 8.74; N 3.92. Found C 73.80; H 9.10; N 3.86. ^{1}H NMR (500 MHz, DMSO-d_6): δ 0.66 (3H, s, 18-CH_3), 1.14 (6H, dd, *J* 6.9, 6.9, 2 × CH_3 of isobutyryl oxime), 1.06–1.25 (2H, m), 1.24 (1H, s), 1.24–1.35 (3H, m), 1.35–1.43 (1H, m), 1.53–1.63 (1H, m), 1.74–1.81 (1H, m), 1.81–1.94 (2H, m), 2.04–2.13 (1H, m), 2.19–2.26 (1H, m), 2.66–2.75 (2H, m), 3.38 (1H, m, CH of isobutyryl oxime), 3.52 (1H, td, *J* 8.5, 4.8, 17-αH), 4.47 (1H, d, *J* 4.8, 17-OH), 6.51 (1H, s, 4-H), 7.03 (1H, s, 1-H), 10.00 (1H, s), 10.85 (1H, s); ^{13}C NMR (125 MHz, DMSO-d_6): δ 11.2 (18-CH_3), 18.7 (2 × CH_3 of isobutyryl oxime), 22.7 (CH_2), 26.1 (CH_2), 26.8 (CH_2), 27.3 (CH of isobutyryl oxime), 28.8 (CH_2), 29.9 (CH_2), 36.5 (CH_2), 38.6 (8-CH), 42.8 (13-C), 43.3 (9-CH), 49.5 (14-CH), 80.0 (17-CH), 115.6 (4-CH), 119.2 (2-C), 126.0 (1-CH), 130.0 (C), 137.6 (C), 153.8 (C), 162.9 (C); ESI-MS: *m*/*z* 358.2 $[M + H]^+$, 358.2 calcd. for $[C_{22}H_{32}NO_3]^+$.

Yield of the slower eluting isomer (**3d**-*Z*): 121 mg (34%, white crystals); Mp: 214–216 °C; Anal. Calcd. for $C_{22}H_{31}NO_3$ (357.49) C 73.92; H 8.74; N 3.92. Found C 73.71; H 9.03; N 3.68. ^{1}H NMR (500 MHz, DMSO-d_6): δ 0.66 (3H, s, 18-CH_3), 1.02 and 1.03 (6H, overlapping d, 2 × CH_3 of isobutyryl oxime), 1.06–1.43 (7H, overlapping m), 1.53–1.63 (1H, m), 1.74–1.93 (3H, m), 2.03–2.12 (1H, m), 2.15–2.22 (1H, m), 2.65–2.76 (3H, m), 3.48–3.56 (1H, m, 17-αH), 4.45–4.49 (1H, d, *J* 4.8, 17-OH), 6.49 (1H, s, 4-H), 6.78 (1H, s, 1-H), 8.74 (1H, bs), 10.26 (1H, bs); ^{13}C NMR (125 MHz, DMSO-d_6): δ 11.2 (18-CH_3), 20.2 (one CH_3 of isobutyryl oxime), 20.2 (the other CH_3 of isobutyryl oxime), 22.7 (CH_2), 26.1 (CH_2), 26.9 (CH_2), 28.9 (CH_2), 29.9 (CH_2), 33.4 (CH of isobutyryl oxime), 36.5 (CH_2), 38.6 (8-CH), 42.8 (13-C), 43.4 (9-CH), 49.5 (14-CH), 80.0 (17-CH), 115.3 (4-CH), 120.0 (2-C), 125.5 (1-CH), 130.0 (C), 136.8 (C), 151.4 (C), 159.7 (C); ESI-MS: *m*/*z* 358.2 $[M + H]^+$, 358.2 calcd. for $[C_{22}H_{32}NO_3]^+$.

(Estra-1,3,5(10)-triene-3,17β-diol-2-yl)(phenyl)methanone oxime isomers (**3e**): According to Section 3.2.4, 2-benzoyl-estradiol (**2e**, 377 mg), hydroxylamine hydrochloride (347 mg, 5 equiv.) and pyridine (1 mL) were used. Conditions: reflux, 48 h. CC (EtOAc/DCM = 2:98 to 5:95). Yield of the faster eluting isomer (**3e**-*E*): Yield: 172 mg (44%, white powder); Mp: 280–282 °C; Anal. Calcd. for $C_{25}H_{29}NO_3$ (391.51) C 76.70; H 7.47; N 3.58. Found C 76.38; H 7.73; N 3.49. ^{1}H NMR (500 MHz, DMSO-d_6): δ 0.61 (3H, s, 18-CH_3), 0.99–1.40 (7H, overlapping m), 1.50–1.60 (1H, m), 1.61–1.71 (2H, m), 1.72–1.80 (1H, m), 1.80–1.91 (1H, m), 1.92–2.01 (1H, m), 2.71–2.77 (2H, m), 3.42–3.50 (1H, td, *J* 8.5, 4.8, 17-αH), 4.41–4.46 (1H, d, *J* 4.9, 17-OH), 6.62 (1H, s), 6.67 (1H, s), 7.25–7.31 (2H, m), 7.42–7.53 (3H, m), 11.00 (1H, s), 11.40 (1H, s); ^{13}C NMR (125 MHz, DMSO-d_6): δ 11.1 (18-CH_3), 22.7 (CH_2), 25.7 (CH_2), 26.6 (CH_2), 28.8 (CH_2), 29.9 (CH_2), 36.2 (CH_2), 38.4 (8-CH), 42.7 (13-C), 43.1 (9-CH), 49.4 (14-CH), 79.9 (17-CH), 116.1 (4-CH), 117.0 (2-C), 126.5 (1-CH), 128.2 (2′-CH and 6′-CH), 128.4 (3′-CH and 5′-CH), 128.6 (4′-CH), 130.4 (C), 132.1 (C), 139.1 (C), 155.0 (C), 159.1 (C); ESI-MS: *m*/*z* 390.1 $[M - H]^-$, 390.2 calcd. for $[C_{25}H_{28}NO_3]^-$.

Yield of the slower eluting isomer (**3e**-*Z*): 141 mg (36%, white powder); Mp: 277–279 °C; Anal. Calcd. for $C_{25}H_{29}NO_3$ (391.51) C 76.70; H 7.47; N 3.58. Found C 76.47; H 7.69; N

3.20. ^{1}H NMR (500 MHz, DMSO-d_6): δ 0.67 (3H, s, 18-CH_3), 1.02–1.43 (7H, overlapping m), 1.54–1.64 (1H, m), 1.75–1.84 (2H, m), 1.83–1.94 (1H, m), 2.06–2.18 (2H, m), 2.74–2.81 (2H, m), 3.51 (1H, td, *J* 8.5, 4.8, 17-αH), 4.46 (1H, d, *J* 4.8, 17-OH), 6.57 (1H, s), 6.83 (1H, s), 7.29–7.33 (3H, m), 7.37–7.42 (2H, m), 8.91 (1H, s), 11.04 (1H, s); ^{13}C NMR (125 MHz, DMSO-d_6): δ 11.2 (18-CH_3), 22.7 (CH_2), 26.1 (CH_2), 26.9 (CH_2), 29.0 (CH_2), 29.9 (CH_2), 36.5 (CH_2), 38.6 (8-CH), 42.8 (13-C), 43.4 (9-CH), 49.5 (14-CH), 80.0 (17-CH), 115.4 (4-CH), 118.6 (2-CH), 126.2 (1-CH), 126.3 (2′-CH and 6′-CH), 128.1 (3′-CH and 5′-CH), 128.3 (4′-CH), 130.3 (C), 136.8 (C), 137.4 (C), 151.9 (C), 153.9 (C); ESI-MS: m/z 390.1 $[M - H]^-$, 390.2 calcd. for $[C_{25}H_{28}NO_3]^-$.

(Estra-1,3,5(10)-triene-3,17β-diol-2-yl)-2,2,2-trifluoroethan-1-one oxime isomers (**3f**): According to Section 3.2.4, 2-trifluoracetyl-estradiol (**2f**, 356 mg), hydroxylamine hydrochloride (695 mg, 10 equiv.) and pyridine (1.5 mL) were used. Conditions: reflux, overnight. CC (EtOAc/hexane = 20:80) yielded an inseparable mixture of *Z*- and *E*-isomers (1:2). Yield (**3f**): 364 mg (95%, white powder); Mp: 180–182 °C; Anal. Calcd. for $C_{20}H_{24}F_3NO_3$ (383.41) C 62.65; H 6.32; N 3.29. Found C 62.60; H 6.57; N 3.04. ^{1}H NMR (500 MHz, DMSO-d_6): δ 0.66 (3H, s, 18-CH_3), 1.05–1.43 (7H, overlapping m), 1.53–1.63 (1H, m), 1.75–1.94 (3H, m), 2.04–2.13 (1H, td, *J* 11.2, 3.9), 2.14–2.25 (1H, m), 2.68–2.81 (2H, dd, *J* 10.0, 5.9), 3.48–3.58 (1H, td, *J* 8.5, 4.7, 17-αH), 4.45–4.49 (1H, d, *J* 4.8, 17-OH), 6.56 and 6.58 (1H, s, 4-H of *E*- and *Z*-isomers), 6.88 and 6.98 (1H, s, 1-H of *E*- and *Z*-isomers), 9.45 and 9.61 (1H, bs and s, 3-OH of *E*- and *Z*-isomers), 12.21 and 12.53 (1H, bs and s, NOH of *E*- and *Z*-isomers); ^{13}C NMR (125 MHz, DMSO-d_6): δ 11.2 (18-CH_3), 22.7 (CH_2), 26.0 (CH_2), 26.7 (CH_2), 29.0 (6-CH_2 of *Z*-isomer), 29.0 (6-CH_2 of *E*-isomer), 29.9 (CH_2), 36.5 (12-CH_2 of *E*-isomer), 36.5 (12-CH_2 of *Z*-isomer) 38.4 (8-CH), 42.8 (13-C), 43.2 (9-CH of *Z*-isomer), 43.3 (9-CH of *E*-isomer), 49.5 (14-CH), 80.0 (17-CH), 112.3 (2-C), 115.1 (1-CH of *Z*-isomer), 115.4 (4-CH of *E*-isomer), 116.0 (2-C), 118.2. (1C, q, *J* 282.2, CF_3 of *Z*-isomer), 121.2 (1C, q, *J* 273.7, CF_3 of *E*-isomer), 125.8 (1-CH of *E*-isomer), 127.4 (1-CH of *Z*-isomer), 130.6 (10-C of *E*-isomer), 130.7 (10-C of *Z*-isomer, 139.5 (5-C of *E*-isomer), 139.8 (5-C of *Z*-isomer), 144.5 (1C, q, *J* 32.1, C=N of *E*-isomer), 145.1 (1C, q, *J* 30.3, C=N of *Z*-isomer), 152.7 (3-C of *E*-isomer), 153.9 (3-C of *Z*-isomer); ESI-MS: m/z 382.0 $[M - H]^-$, 382.2 calcd. for $[C_{20}H_{23}F_3NO_3]^-$.

Methyl-2-(estra-1,3,5(10)-triene-3-hydroxy-17β-acetoxy-2-yl)-2-hydroxyimino acetate (**3g**): According to Section 3.2.4, 2-(methyloxoacetyl)estradiol-17β-acetate (**2g**-*17Ac*, 400 mg), hydroxylamine hydrochloride (104 mg, 1.5 equiv.) and pyridine (1 mL) were used. The synthesis was repeated in duplicate. Conditions: RT, overnight. CC (EtOAc/hexane = 20:80). Yield (**3g**): 378 mg (91%, white powder, as a single isomer); Mp: 188–189 °C. Anal. Calcd. for $C_{23}H_{29}NO_6$ (415.49) C 66.49; H 7.04; N 3.37. Found C 66.35; H 7.42; N 3.24. ^{1}H NMR (500 MHz, DMSO-d_6): δ 0.77 (3H, s, 17-CH_3), 1.22–1.41 (6H, overlapping m), 1.44–1.55 (1H, m), 1.63–1.72 (1H, m), 1.74–1.84 (2H, m), 2.01 (3H, s, Ac-CH_3), 2.04–2.20 (3H, m), 2.71–2.78 (2H, m), 3.77 (3H, s, COOC$\underline{H}_3$), 4.57–4.64 (1H, t, *J* 8.5, 17-αH), 6.56 (1H, s, 4-H), 7.22 (1H, s, 1-H), 9.74 (1H, s, 3-OH), 11.72 (1H, s, NOH); ^{13}C NMR (125 MHz, DMSO-d_6): δ 11.8 (18-CH_3), 20.8 (Ac-CH_3), 22.7 (CH_2), 25.7 (CH_2), 26.5 (CH_2), 27.1 (CH_2), 28.8 (CH_2), 36.3 (CH_2), 37.9 (8-CH), 42.4 (13-C), 42.8 (9-CH), 49.0 (14-CH), 51.8 (COO$\underline{C}H_3$), 81.8 (17-CH), 114.7 (2-C), 116.0 (4-CH), 124.0 (1-CH), 131.1 (10-C), 140.0 (5-C), 149.6 (C=N), 153.3 (3-C), 163.9 ($\underline{C}OOCH_3$), 170.3 (Ac-C=O); ESI-MS: m/z 414.1 $[M - H]^-$, 414.2 calcd. for $[C_{23}H_{28}NO_6]^-$.

3.2.5. General Procedure for the Synthesis of Compounds **4a**–**g**

DDQ (1.5 equiv.) was added slowly to a solution of PPh_3 (1.5 equiv.) in DCM (0.5 M), and stirred for 1 min. This suspension was added to a solution of oxime (**3a**–**g**, 1.0 equiv.) and Et_3N (2.0 equiv.) in DCM (0.2 M), and stirred for 10 min at RT. The solvent was removed under reduced pressure. The residue was dissolved in EtOAc/MeOH, and Celite® was added (~10× weight of the crude sample), which was then concentrated in vacuo and purified by CC.

Isoxazolo[4′,5′:2,3]estra-1,3,5(10)-triene-17β-ol (**4a**): According to Section 3.2.5, **3a** (158 mg, 0.50 mmol) was used for the reaction. Eluent (CC): EtOAc/hexane = 30:70. Yield (**4a**): 134 mg (90%, white powder); Mp: 176–178 °C; Anal. Calcd. for $C_{19}H_{23}NO_2$ (297.40) C 76.74; H 7.80; N 4.71. Found C 76.55; H 7.96; N 4.33. ^{1}H NMR (500 MHz, $CDCl_3$): δ

0.80 (3H, s, 18-CH_3), 1.18–1.57 (7H, overlapping m), 1.58–1.68 (1H, m), 1.70–1.78 (1H, m), 1.89–2.08 (2H, m), 2.09–2.20 (1H, m), 2.27–2.35 (1H, m), 2.35–2.44 (1H, m), 3.00–3.06 (2H, m), 3.76 (1H, t, *J* 8.5, 17-αH), 7.32 (1H, s, 4-H), 7.61 (1H, s, 1-H), 8.60 (1H, d, *J* 1.1, 3′-H); ^{13}C NMR (125 MHz, $CDCl_3$) δ 11.2 (18-CH_3), 23.4 (CH_2), 26.5 (CH_2), 27.0 (CH_2), 30.4 (CH_2), 30.7 (CH_2), 36.7 (CH_2), 38.6 (8-CH), 43.3 (13-C), 44.2 (9-CH), 50.5 (14-CH), 81.9 (17-CH), 108.8 (4-CH), 117.8 (2-CH), 119.7 (1-C), 137.6 (10-C), 141.0 (5-C), 146.2 (3′-CH), 161.1 (3-C); ESI-MS: *m*/*z* 296.0 $[M - H]^-$, 296.2 calcd. for $[C_{19}H_{22}NO_2]^-$.

3′-Methylisoxazolo[4′,5′:2,3]estra-1,3,5(10)-triene-17β-ol (**4b**): According to Section 3.2.5, **3b** (150 mg, 0.46 mmol) was used for the reaction. Eluent (CC): EtOAc/hexane = 30:70. Yield (**4b**): 132 mg (93%, white crystals); Mp: 168–170 °C; Anal. Calcd. for $C_{20}H_{25}NO_2$ (311.42) C 77.14; H 8.09; N 4.50. Found C 77.10; H 8.34; N 4.26. ^{1}H NMR (500 MHz, $CDCl_3$): δ 0.80 (3H, s 18-CH_3), 1.19–1.32 (1H, m), 1.31–1.56 (6H, overlapping m), 1.59–1.79 (2H, m), 1.89–1.99 (1H, m), 2.02 (1H, m), 2.09–2.20 (1H, m), 2.27–2.36 (1H, m), 2.39–2.47 (1H, m), 2.54 (3H, s, 3′-CH_3), 2.99–3.05 (2H, m), 3.72–3.80 (1H, m, 17-αH), 7.24 (1H, s, 4-H), 7.50 (1H, s, 1-H); ^{13}C NMR (125 MHz, $CDCl_3$) δ 10.2 (CH_3), 11.2 (CH_3), 23.4 (CH_2), 26.6 (CH_2), 27.1 (CH_2), 30.4 (CH_2), 30.8 (CH_2), 36.7 (CH_2), 38.7 (8-CH), 43.3 (13-C), 44.2 (9-CH), 50.5 (14-CH), 82.0 (17-CH), 109.0 (4-CH), 116.9 (1-CH), 120.6 (2-C), 136.9 (10-C), 140.5 (5-C), 154.9 (C=N), 161.6 (3-C); ESI-MS: *m*/*z* 312.2 $[M - H]^+$, 312.2 calcd. for $[C_{20}H_{26}NO_2]^+$.

3′-Ethylisoxazolo[4′,5′:2,3]estra-1,3,5(10)-triene-17β-ol (**4c**): According to Section 3.2.5, 3**c** (50 mg, 0.15 mmol) was used for the reaction. Eluent (CC): DCM. Yield (**4c**): 43 mg (93%, white crystals); Mp: 166–168 °C; Anal. Calcd. for $C_{21}H_{27}NO_2$ (325.45) C 77.50; H 8.36; N 4.30. Found C 77.38; H 8.67; N 4.16. ^{1}H NMR (500 MHz, $CDCl_3$): δ 0.82 (3H, s, 18-CH_3), 1.21–1.32 (1H, m), 1.31–1.56 (6H, overlapping m), 1.45 (3H, t, *J* 7.4, 7.4, CH_3 of ethyl), 1.60–1.73 (1H, m), 1.70–1.80 (1H, m), 1.90–1.98 (1H, m), 1.99–2.07 (1H, m), 2.10–2.21 (1H, m), 2.28–2.37 (1H, m), 2.39–2.48 (1H, m), 2.95–3.06 (4H, m), 3.73–3.81 (1H, m, 17-αH), 7.27 (1H, s, 4-CH), 7.54 (1H, s, 1-CH); ^{13}C NMR (125 MHz, $CDCl_3$) δ 11.2 (18-CH_3), 12.4 (CH_3 of ethyl), 19.1 (CH_2), 23.4 (CH_2), 26.6 (CH_2), 27.1 (CH_2), 30.4 (CH_2), 30.8 (CH_2), 36.7 (CH_2), 38.7 (8-CH), 43.4 (13-C), 44.3 (9-CH), 50.5 (14-CH), 82.0 (17-CH), 109.1 (4-CH), 117.0 (1-CH), 119.9 (C), 136.8 (C), 140.4 (C), 159.6 (C), 161.8 (C); ESI-MS: *m*/*z* 326.2 $[M + H]^+$, 326.2 calcd. for $[C_{21}H_{28}NO_2]^+$.

3′-Isopropylisoxazolo[4′,5′:2,3]estra-1,3,5(10)-triene-17β-ol (**4d**): According to Section 3.2.5, **3d** (80 mg, 0.22 mmol, 1:1 mixture of *E* and *Z*-oximes) was used for the reaction. Eluent (CC): EtOAc/hexane = 40:60. Yield (**4d**): 68 mg (91%, white crystals); Mp: 168–169 °C; Anal. Calcd. for $C_{22}H_{29}NO_2$ (339.48) C 77.84; H 8.61; N 4.13. Found C 77.58; H 8.74; N 4.02. ^{1}H NMR (500 MHz, $CDCl_3$): δ 0.81 (3H, s, 18-CH_3), 1.21–1.30 (1H, m), 1.31–1.47 (4H, overlapping m), 1.49 (6H, d, *J* 7.1, 2 × CH_3 of ^{i}Pr), 1.47–1.56 (2H, m), 1.59–1.79 (2H, m), 1.90–1.97 (1H, m), 1.99–2.06 (1H, m), 2.10–2.21 (1H, m), 2.28–2.37 (1H, m), 2.39–2.46 (1H, m), 2.99–3.05 (2H, m), 3.38 (1H, m, CH of ^{i}Pr), 3.73–3.81 (1H, m, 17-αH), 7.27 (1H, s, 4-H), 7.58 (1H, s, 1-H); ^{13}C NMR (125 MHz, $CDCl_3$) δ 11.2 (18-CH_3), 21.3 (one CH_3 of ^{i}Pr), 21.4 (the other CH_3 of ^{i}Pr), 23.4 (CH_2), 26.6 (CH_2), 27.0 (CH of ^{i}Pr), 27.1 (CH_2), 30.4 (CH_2), 30.8 (CH_2), 36.7 (CH_2), 38.7 (8-CH), 43.4 (13-C), 44.3 (9-CH), 50.5 (14-CH), 82.0 (17-CH), 109.2 (4-CH), 117.4 (1-CH), 119.2 (2-C), 136.6 (C), 140.3 (C), 162.0 (C), 163.1 (C); ESI-MS: *m*/*z* 340.2 $[M + H]^+$, 340.2 calcd. for $[C_{22}H_{30}NO_2]^+$.

3′-Phenylisoxazolo[4′,5′:2,3]estra-1,3,5(10)-triene-17β-ol (**4e**): Method A (Scheme 1, iii): According to Section 3.2.5, **3e** (100 mg, 0.26 mmol, 1:1 mixture of *E* and *Z*-oximes) was used for the reaction. Eluent (CC): EtOAc/DCM = 2:98. Yield (**4e**): 24 mg (25%, yellowish white solid); Method B (Scheme 1, vii/viii): **2e** (62 mg, 0.16 mmol) was dissolved in NH_3 (6M in MeOH, 0.5 mL) and stirred for 2 h at RT. The solvent was then removed under reduced pressure, and the residue (**5e**) was redissolved in THF (1 mL). NCS (33 mg, 1.5 equiv.) and K_2CO_3 (69 mg, 3.0 equiv.) were added to the solution, and the resulting suspension was stirred at RT overnight. After evaporating off the solvent, the residue was suspended in water (10 mL) and extracted with EtOAc (3 × 10 mL). The combined organic phase was washed with HCl (1M, 10 mL), water (10 mL) and brine (10 mL), dried over anhydrous Na_2SO_4 and concentrated in vacuo. The crude product was purified by CC (DCM). Yield

(**4e**): 37 mg (60%, as yellowish white solid); Mp: 196–198 °C; Anal. Calcd. for $C_{25}H_{27}NO_2$ (373.50) C 80.40; H 7.29; N 3.75. Found C 80.02; H 7.56; N 3.55. ^{1}H NMR (500 MHz, $CDCl_3$): δ 0.81 (3H, s, 18-CH_3), 1.20–1.53 (7H, overlapping m), 1.61–1.80 (2H, m), 1.86–1.99 (1H, m), 1.99–2.09 (1H, m), 2.09–2.21 (1H, m), 2.31–2.39 (1H, m), 2.40–2.47 (1H, m), 3.03–3.09 (2H, m), 3.74–3.80 (1H, t, *J* 8.5, 17-αH), 7.35 (1H, s, 4-H), 7.47–7.60 (3H, overlapping m, 3″-H, 4″-H and 5″-H), 7.78 (1H, s, 1-H), 7.90–7.97 (2H, m, 2″-H and 6″-H); ^{13}C NMR (125 MHz, $CDCl_3$) δ 11.2 (18-CH_3), 23.4 (CH_2), 26.7 (CH_2), 27.1 (CH_2), 30.4 (CH_2), 30.8 (CH_2), 36.8 (CH_2), 38.8 (8-CH), 43.4 (13-C), 44.4 (9-CH), 50.6 (14-CH), 82.0 (17-CH), 109.3 (4-CH), 117.9 (1-CH), 119.0 (2-C), 128.2 (2″-CH and 6″-CH), 129.2 (3″-CH and 5″-CH), 129.6 (1″-C), 130.2 (4″-CH), 137.7 (C), 140.7 (C), 157.3 (C), 162.8 (C); ESI-MS: *m*/*z* 374.2 $[M + H]^+$, 374.2 calcd. for $[C_{25}H_{28}NO_2]^+$.

3′-Trifluoromethylisoxazolo[4′,5′:2,3]estra-1,3,5(10)-triene-17β-ol (**4f**): According to Section 3.2.5, **3f** (115 mg, 0.30 mmol, mixture of *E* and *Z*-oximes) was used for the reaction. Eluent (CC): EtOAc/hexane = 20:80. Yield (**4f**): 44 mg (40%, white crystals); Mp: 106–108 °C; Anal. Calcd. for $C_{20}H_{22}F_3NO_2$ (365.40) C 65.74; H 6.07; N 3.83. Found C 65.60; H 6.41; N 3.75. ^{1}H NMR (500 MHz, $CDCl_3$): δ 0.81 (3H, s, 18-CH_3), 1.21–1.32 (1H, m), 1.31–1.43 (2H, m), 1.40–1.49 (3H, m), 1.48–1.57 (1H, m), 1.61–1.79 (2H, m), 1.91–1.99 (1H, m), 2.00–2.09 (1H, m), 2.09–2.20 (1H, m), 2.29–2.38 (1H, m), 2.38–2.47 (1H, m), 2.99–3.11 (2H, m), 3.73–3.80 (1H, t, *J* 8.6, 17-αH), 7.39 (1H, s, 4-H), 7.66 (1H, s, 1-H); ^{13}C NMR (125 MHz, $CDCl_3$) δ 11.1 (18-CH_3), 23.4 (CH_2), 26.4 (CH_2), 26.8 (CH_2), 30.4 (CH_2), 30.7 (CH_2), 36.6 (CH_2), 38.4 (8-CH), 43.3 (13-C), 44.2 (9-CH), 50.5 (14-CH), 81.9 (17-CH), 109.4 (4-CH), 115.7 (2-C), 116.8 (1-CH), 120.5 (1C, q, *J* 271.3, CF_3), 139.6 (C), 142.8 (C), 149.8 (1C, q, *J* 38.2, 3′-C), 163.2 (3-C); ESI-MS: *m*/*z* 368.3 $[M+3H]^+$, 366.2 calcd. for $[C_{20}H_{23}F_3NO_2]^+$.

3′-Carboxymethylisoxazolo[4′,5′:2,3]estra-1,3,5(10)-triene-17β-acetate (**4g**): According to Section 3.2.5, **3g** (700 mg, 1.68 mmol) was used for the reaction. Eluent (CC): EtOAc/hexane = 20:80. Yield (**4g**): 601 mg (90%, yellowish white crystals); Mp: 176–178 °C; Anal. Calcd. for $C_{23}H_{27}NO_5$ (397.47) C 69.50; H 6.85; N 3.52. Found C 69.28; H 7.03; N 3.39. ^{1}H NMR (500 MHz, $CDCl_3$): δ 0.85 (3H, s, 18-CH_3), 1.27–1.42 (1H, m), 1.39–1.52 (4H, overlapping m), 1.50–1.71 (2H, m), 1.73–1.83 (1H, m), 1.90–2.00 (2H, m), 2.07 (3H, s, Ac-CH_3), 2.20–2.30 (1H, m), 2.30–2.39 (1H, m), 2.40–2.49 (1H, m), 2.98–3.11 (2H, m), 4.08 (3H, s, COOC$\underline{H}_3$), 4.68–4.75 (1H, m, 17-αH), 7.36 (1H, s, 4-H), 7.99 (1H, s, 1-H); ^{13}C NMR (125 MHz, $CDCl_3$) δ 12.2 (18-CH_3), 21.3 (Ac-CH_3), 23.5 (CH_2), 26.4 (CH_2), 26.9 (CH_2), 27.7 (CH_2), 30.4 (CH_2), 36.8 (CH_2), 38.2 (8-CH), 43.0 (13-C), 44.1 (9-CH), 50.3 (14-CH), 53.0 (COO$\underline{C}H_3$), 82.7 (17-CH), 109.1 (4-CH), 118.2 (2-C), 118.7 (1-CH), 139.2 (C), 141.8 (C), 150.0 (3′-C), 161.0 (3-C), 163.3 ($\underline{C}OOCH_3$), 171.3 (Ac-C=O); ESI-MS: *m*/*z* 398.2 $[M + H]^+$, 398.2 calcd. for $[C_{23}H_{28}NO_5]^+$.

3.2.6. 3-Hydroxy-2-trifluoracetylestra-1,3,5(10)-triene-17-one (**6a**)

To a suspension of E1 (1.08 g, 4.0 mmol) in DCM (30 mL), $AlCl_3$ (3.2 g, 6 equiv.) and TFAA (670 µL, 1.2 equiv.) were added at 0 °C. After 30 min, the ice bath was removed, the reaction was gradually warmed to RT and stirred for 4 h. The reaction was poured into ice-cold HCl (1 M, 100 mL) and stirred for 10 min. The layers were separated and the aqueous phase was extracted with EtOAc (3 × 30 mL). The combined organic phase was washed with aq. $NaHCO_3$ (10 wt. %, 40 mL), water (40 mL) and brine (40 mL), then dried over anhydrous Na_2SO_4 and concentrated in vacuo. The crude product was purified by CC (EtOAc/hexane = 10:90). Yield (**6a**): 1.42 g (97%, yellow crystals); Mp: 179–181 °C; Anal. Calcd. for $C_{20}H_{21}F_3O_3$ (366.38) C 65.57; H 5.78. Found C 65.46; H 5.97. ^{1}H NMR (500 MHz, $CDCl_3$): δ 0.92 (3H, s, 18-CH_3), 1.41–1.69 (6H, overlapping m), 1.96–2.11 (3H, m), 2.11–2.21 (1H, m), 2.21–2.33 (1H, m), 2.34–2.42 (1H, m), 2.48–2.57 (1H, m), 2.87–3.03 (2H, m), 6.82 (1H, s, 4-H), 7.69 (1H, s, 1-H), 10.87 (1H, s, 3-OH); ^{13}C NMR (125 MHz, $CDCl_3$) δ 13.9 (18-CH_3), 21.7 (CH_2), 25.7 (CH_2), 26.1 (CH_2), 30.2 (CH_2), 31.5 (CH_2), 35.9 (CH_2), 38.0 (8-CH), 43.6 (13-C), 48.0 (9-CH), 50.5 (14-CH), 112.3 (2-C), 116.7 (1C, q, *J* 290.0, CF_3), 118.4 (4-CH), 127.3 (1C, q, *J* 3.9, 1-CH), 132.6 (C), 150.7 (C), 162.5 (3-C), 183.9 (1C, q, *J* 35.0, C=O), 220.3 (17-C=O); ESI-MS: *m*/*z* 365.0 $[M - H]^-$, 365.1 calcd. for $[C_{20}H_{20}F_3O_3]^-$.

3.2.7. 3-Hydroxy-17-oxoestra-1,3,5(10)-triene-2-carboxylic Acid (**6b**)

To a solution of **6a** (1.35 g, 3.68 mmol) in EtOH (20 mL), KOH (2.06 g, 10 equiv.) in water (3 mL) was added, and the mixture was kept at reflux temperature for 3 h. Then, it was acidified with HCl (6 M) and the EtOH was removed under reduced pressure. To the residue HCl (1 M, 10 mL) was added and extracted with EtOAc (3 × 10 mL). The combined organic phase was washed with brine (20 mL), dried over anhydrous Na_2SO_4 and concentrated in vacuo. The crude product was purified by CC (EtOAc/DCM = 10:90 with 1% AcOH additive to reduce tailing). Yield (**6b**): 1.09 g (94%, white powder); Mp > 190 °C (decomp.); Anal. Calcd. for $C_{19}H_{22}O_4$ (314.38) C 72.59; H 7.05. Found C 72.62; H 7.24. ^{1}H NMR (500 MHz, DMSO-d_6): δ 0.82 (3H, s, 18-CH_3), 1.29–1.52 (5H, overlapping m), 1.52–1.61 (1H, m), 1.73–1.80 (1H, m), 1.88–1.99 (2H, m), 2.01–2.11 (1H, m), 2.12–2.20 (1H, m), 2.26–2.34 (1H, m), 2.39–2.48 (1H, m), 2.77–2.90 (2H, m), 6.66 (1H, s, 4-H), 7.66 (1H, s, 1-H), 11.08 (1H, bs, 3-OH), 13.54 (1H, bs, COOH); ^{13}C NMR (125 MHz, DMSO-d_6): δ 13.4 (18-CH_3), 21.1 (CH_2), 25.4 (CH_2), 25.6 (CH_2), 29.0 (CH_2), 31.2 (CH_2), 35.3 (CH_2), 37.4 (8-CH), 42.9 (13-C), 47.2 (9-CH), 49.5 (14-CH), 110.4 (2-C), 116.4 (4-CH), 126.5 (1-CH), 130.9 (C), 145.4 (C), 158.8 (3-C), 171.9 (C=O of carboxyl), 219.5 (C=O of ketone); ESI-MS: m/z 313.0 $[M - H]^-$, 313.1 calcd. for $[C_{19}H_{21}O_4]^-$.

3.2.8. Three-Step Synthesis of Compound **7**

Synthesis of 3,17β-dihydroxyestra-1,3,5(10)-triene-2-carboxylic acid (**6c**) by the reduction of **6b**: To a solution of **6b** (1.05 g, 3.34 mmol) in EtOH (30 mL), $NaBH_4$ (631 mg, 5 equiv.) was added in small portions over a 10 min period and stirring was continued for 30 min at RT. The mixture was neutralized with HCl (6 M) and the EtOH was removed under reduced pressure. To the residue HCl (1 M, 10 mL) was added and extracted with EtOAc (3 × 10 mL). The combined organic phase was washed with brine (20 mL), dried over anhydrous Na_2SO_4 and concentrated in vacuo. The crude product was purified by CC (EtOAc/DCM = 20:80 with 1% AcOH additive to reduce tailing). Yield (**6c**): 1.01 g (96%, white powder); Mp > 240 °C (decomp.); Anal. Calcd. for $C_{19}H_{24}O_4$ (316.40) C 72.13; H 7.65. Found C 72.04; H 7.95. ^{1}H NMR (500 MHz, DMSO-d_6): δ 0.65 (3H, s, 18-CH_3), 1.02–1.43 (7H, overlapping m), 1.52–1.62 (1H, m), 1.74–1.81 (1H, m), 1.82–1.93 (2H, m), 2.03–2.12 (1H, m), 2.18–2.26 (1H, m), 2.71–2.86 (2H, m), 3.48–3.55 (1H, t, *J* 8.5, 17-αH), 4.29–4.66 (1H, bs, 17-OH), 6.63 (1H, s, 4-H), 7.65 (1H, s, 1-H), 10.97 (1H, bs, 3-OH), 13.64 (1H, bs, COOH); ^{13}C NMR (125 MHz, DMSO-d_6): δ 11.1 (18-CH_3), 22.7 (CH_2), 25.9 (CH_2), 26.4 (CH_2), 29.1 (CH_2), 29.8 (CH_2), 36.4 (CH_2), 38.2 (8-CH), 42.7 (13-C), 43.0 (9-CH), 49.5 (14-CH), 80.0 (17-CH), 110.3 (2-C), 116.3 (4-CH), 126.5 (1-CH), 131.4 (C), 145.5 (C), 158.7 (3-C), 172.0 (C=O of carboxyl); ESI-MS: m/z 315.0 $[M - H]^-$, 315.2 calcd. for $[C_{19}H_{23}O_4]^-$.

Synthesis of 3,17β-dihydroxyestra-1,3,5(10)-triene-2-carboxylic acid methyl ester (**6d**) by esterification of **6c**: To a solution of **6c** (950 mg, 3.00 mmol) in DMF (10 mL), Na_2CO_3 (382 mg, 1.2 equiv.) and MeI (280 µL, 1.5 equiv.) were added and the mixture was stirred at 50 °C for 2 h. Then, it was repeatedly concentrated under vacuum with the addition of toluene, and then water (10 mL) was added and extracted with EtOAc (3 × 10 mL). The combined organic phase was washed with aq. $NaHCO_3$ (10 wt. %, 2 × 10 mL), water (10 mL) and brine (10 mL), and then dried over anhydrous Na_2SO_4 and concentrated *in vacuo*. The crude product was purified by CC (EtOAc/DCM = 5:95). Yield (**6d**): 912 mg (92%, white crystals); Mp: 154–156 °C; Anal. Calcd. for $C_{20}H_{26}O_4$ (330.42) C 72.70; H 7.93. Found C 72.46; H 8.27. ^{1}H NMR (500 MHz, $CDCl_3$): δ 0.78 (3H, s, 18-CH_3), 1.14–1.24 (1H, m), 1.24–1.58 (7H, overlapping m), 1.64–1.75 (1H, m), 1.84–1.92 (1H, m), 1.93–2.01 (1H, m), 2.09–2.19 (2H, m), 2.31–2.39 (1H, m), 2.82–2.92 (2H, m), 3.70–3.77 (1H, t, *J* 8.5, 17-αH), 3.92 (3H, s, COOC$\underline{H}_3$), 6.70 (1H, s, 4-H), 7.73 (1H, s, 1-H), 10.48 (1H, s, 3-OH); ^{13}C NMR (125 MHz, $CDCl_3$) δ 11.2 (18-CH_3), 23.3 (CH_2), 26.4 (CH_2), 27.0 (CH_2), 30.0 (CH_2), 30.7 (CH_2), 36.7 (CH_2), 38.8 (8-CH), 43.4 (13-C), 43.8 (9-CH), 50.2 (14-CH), 52.2 (COO$\underline{C}H_3$), 82.0 (17-CH), 110.1 (2-C), 117.1 (4-CH), 126.6 (1-CH), 132.0 (C), 146.3 (C), 159.3 (3-C), 170.8 ($\underline{C}OOCH_3$); ESI-MS: m/z 331.2 $[M + H]^+$, 331.2 calcd. for $[C_{20}H_{27}O_4]^+$.

Synthesis of 2-hydroxycarbamoylestra-1,3,5(10)-triene-3,17β-diol (**7**) by hydroxamation of **6d**: To a solution of **6d** (898 mg, 2.72 mmol) in MeOH/THF = 2:1 (27 mL), aq. NH_2OH (50 wt. %, 2.50 mL, 15 equiv.) and KOH (1.15 g, 7.5 equiv.) were added at 0 °C and the mixture was stirred at RT for 30 min. Then, it was poured into ice-cold HCl (2 M, 50 mL), and the precipitate was filtered off and dried. The crude product was used in the next step without further purification. Yield (**7**): 874 mg (97%, pale tan powder); Mp > 200 °C (decomp.); Anal. Calcd. for $C_{19}H_{25}NO_4$ (331.41) C 68.86; H 7.60; N 4.23. Found C 68.98; H 7.87; N 4.04. ^{1}H NMR (500 MHz, DMSO-d_6): δ 0.68 (3H, s, 18-CH_3), 1.04–1.14 (1H, m), 1.12–1.44 (6H, overlapping m), 1.53–1.63 (1H, m), 1.74–1.82 (1H, m), 1.83–1.94 (2H, m), 2.03–2.11 (1H, m, 2.33–2.41 (1H, m), 2.72–2.79 (2H, m), 3.49–3.57 (1H, td, *J* 8.6, 4.7, 17-αH), 4.39–4.44 (1H, d, *J* 4.8, 17-OH), 6.57 (1H, s, 4-H), 7.57 (1H, s, 1-H), 9.14 (1H, s, NOH), 11.35 (1H, s, NH), 12.03 (1H, s, 3-OH); ^{13}C NMR (125 MHz, DMSO-d_6): δ 11.1 (18-CH_3), 22.6 (CH_2), 25.8 (CH_2), 26.4 (CH_2), 28.9 (CH_2), 29.8 (CH_2), 36.3 (CH_2), 38.3 (8-CH), 42.7 (13-C), 43.3 (9-CH), 49.5 (14-CH), 79.9 (17-CH), 111.0 (2-C), 116.4 (4-CH), 123.3 (1-CH), 130.9 (C), 142.6 (C), 157.2 (3-C), 166.7 (C=O); ESI-MS: *m*/*z* 332.2 $[M + H]^+$, 332.2 calcd. for $[C_{19}H_{26}NO_4]^+$.

3.2.9. 3′-Hydroxyisoxazolo[4′,5′:2,3]estra-1,3,5(10)-triene-17β-ol (**4h**)

DIAD (615 µL, 3.12 mmol) was added to a solution of PPh_3 (820 mg, 3.12 mmol) in THF (25 mL), followed by the addition of **7** (828 mg, 2.5 mmol) and the mixture was stirred at RT for 2 h. Then, it was concentrated under reduced pressure and purified by CC (isopropanol/DCM = 2:98 to 5:95). Yield (**4h**): 697 mg (89%, white powder); Mp > 220 °C (decomp.); Anal. Calcd. for $C_{19}H_{23}NO_3$ (313.40) C 72.82; H 7.40; N 4.47. Found C 72.99; H 7.72; N 4.18. ^{1}H NMR (500 MHz, DMSO-d_6): δ 0.67 (3H, s, 18-CH_3), 1.05–1.45 (7H, overlapping m), 1.54–1.64 (1H, m), 1.75–1.83 (1H, m), 1.82–1.94 (2H, m), 2.12–2.28 (2H, m), 2.77–2.83 (2H, m), 3.49–3.56 (1H, t, *J* 8.5, 17-αH), 4.49 (1H, bs, 17-OH), 6.92 (1H, s), 6.94 (1H, s), 11.37 (1H, bs, 3′-OH); ^{13}C NMR (125 MHz, DMSO-d_6): δ 11.2 (18-CH_3), 22.7 (CH_2), 26.2 (CH_2), 26.7 (CH_2), 29.1 (CH_2), 29.9 (CH_2), 36.5 (CH_2), 38.2 (8-CH), 42.7 (13-C), 43.8 (9-CH), 49.6 (14-CH), 80.0 (17-CH), 106.3 (4-CH), 109.1 (1-CH), 128.2 (C), 130.1 (C), 135.7 (C), 141.6 (C), 154.7 (C); ESI-MS: *m*/*z* 314.2 $[M + H]^+$, 314.2 calcd. for $[C_{19}H_{24}NO_3]^+$.

3.2.10. 3′-Methoxyisoxazolo[4′,5′:2,3]estra-1,3,5(10)-triene-17β-ol (**4i**)

To a solution of 4h (157 mg, 0.50 mmol) in DMF (1 mL), K_2CO_3 (207 mg, 3 equiv.) and MeI (47 µL, 1.5 equiv.) were added, and the mixture was stirred at RT for 1 h. Then, it was repeatedly concentrated under reduced pressure with the addition of toluene, and then water (10 mL) was added to the residue and extracted with EtOAc (3 × 10 mL). The combined organic phase was washed with aq. $NaHCO_3$ (10 wt. %, 2 × 10 mL), water (10 mL) and brine (10 mL), and then dried over anhydrous Na_2SO_4 and concentrated in vacuo. The crude product was purified by CC (EtOAc/DCM = 10:90). Yield (4i): 134 mg (82%, white crystals); Mp: 220–222 °C; Anal. Calcd. for $C_{20}H_{25}NO_3$ (327.42) C 73.37; H 7.70; N 4.28. Found C 73.65; H 7.89; N 4.11. ^{1}H NMR (500 MHz, $CDCl_3$): δ 0.80 (3H, s, 18-CH_3), 1.17–1.63 (8H, overlapping m), 1.67–1.77 (1H, m), 1.86–1.94 (1H, m), 1.96–2.03 (1H, m), 2.08–2.19 (1H, m), 2.22–2.38 (2H, m), 2.82–2.96 (2H, m), 3.37 (3H, s, 3′-OMe), 3.75 (1H, t, J 8.5, 17-αH), 6.87 (1H, s, 4-H), 6.90 (1H, s, 1-H); ^{13}C NMR (125 MHz, $CDCl_3$) δ 11.2 (18-CH_3), 23.3 (CH_2), 26.9 (CH_2), 27.2 (CH_2), 28.2 (3′-OMe), 29.8 (CH_2), 30.8 (CH_2), 36.8 (CH_2), 38.7 (8-CH), 43.3 (13-C), 44.5 (9-CH), 50.3 (14-CH), 82.0 (17-CH), 105.1 (4-CH), 110.1 (1-CH), 129.9 (C), 131.5 (C), 136.4 (C), 141.1 (C), 155.3 (C); ESI-MS: m/z 328.2 $[M + H]^+$, 328.2 calcd. for $[C_{20}H_{26}NO_3]^+$.

3.2.11. 3′-Hydroxymethylisoxazolo[4′,5′:2,3]estra-1,3,5(10)-triene-17β-acetate (**4j**)

To a solution of **4g** (397 mg, 1.0 mmol) in EtOH (10 mL), $NaBH_4$ (151 mg, 4 equiv.) was added in small portions and stirred at RT for 1 h. The solution was acidified with HCl (6 M) and EtOH was evaporated. The residue was suspended in water (10 mL), extracted with EtOAc (3 × 10 mL). The combined organic phase was washed with water (10 mL), brine

(10 mL), dried over anhydrous Na_2SO_4 and concentrated in vacuo. The crude product was purified by CC (MeOH/DCM = 2:98). Yield (**4j**): 327 mg (89%, greenish white crystals); Mp: 114–116 °C; Anal. Calcd. for $C_{22}H_{27}NO_4$ (369.46) C 71.52; H 7.37; N 3.79. Found C 71.43; H 7.69; N 3.46. ^{1}H NMR (500 MHz, $CDCl_3$): δ 0.84 (3H, s, 18-CH_3), 1.22–1.68 (7H, overlapping m), 1.72–1.82 (1H, m), 1.89–1.97 (2H, m), 2.07 (3H, s, Ac-CH_3), 2.11–2.18 (1H, t, *J* 6.3, CH_2-OH), 2.18–2.29 (1H, m), 2.29–2.44 (2H, m), 2.96–3.08 (2H, m), 4.67–4.74 (1H, m, 17-αH), 5.06 (2H, d, *J* 6.2, CH_2-OH), 7.28 (1H, s, 4-H), 7.67 (1H, d, *J* 1.4, 1-H); ^{13}C NMR (125 MHz, $CDCl_3$) δ 12.2 (18-CH_3), 21.3 (Ac-CH_3), 23.5 (CH_2), 26.4 (CH_2), 27.0 (CH_2), 27.7 (CH_2), 30.4 (CH_2), 36.9 (CH_2), 38.3 (8-CH), 43.0 (13-C), 44.1 (9-CH), 50.3 (14-CH), 57.1 (CH_2-OH), 82.7 (17-H), 109.0 (4-CH), 117.5 (1-CH), 118.8 (2-C), 137.4 (10-C), 141.0 (5-C), 157.6 (3′-C), 162.3 (3-C), 171.4 (Ac-C=O); ESI-MS: *m*/*z* 370.2 $[M + H]^+$, 370.2 calcd. for $[C_{22}H_{28}NO_4]^+$.

3.2.12. 3′-Hydroxymethylisoxazolo[4′,5′:2,3]estra-1,3,5(10)-triene-17β-ol (**4k**)

To a solution of **4j** (74 mg, 0.20 mmol) in MeOH/DCM = 1:9 (2 mL), NaOH (24 mg, 3 equiv.) was added and the mixture was stirred at RT for 1 h. Then, it was concentrated under reduced pressure and the crude product was purified by CC (MeOH/DCM = 2:98). Yield (**4k**): 62 mg (95%, white crystals); Mp: 218–220 °C; Anal. Calcd. for $C_{20}H_{25}NO_3$ (327.42) C 73.37; H 7.70; N 4.28. Found C 73.20; H 8.08; N 4.09. ^{1}H NMR (500 MHz, DMSO-d_6): δ 0.68 (3H, s, 18-CH_3), 1.12–1.44 (6H, overlapping m), 1.44–1.57 (1H, m), 1.58–1.66 (1H, m), 1.78–1.96 (3H, m), 2.22–2.30 (1H, m), 2.33–2.41 (1H, m), 2.90–3.03 (2H, m), 3.55 (1H, td, *J* 8.5, 4.5, 17-αH), 4.50 (1H, d, *J* 4.7, 17-OH), 4.82 (2H, d, *J* 4.5, CH_2-OH), 5.65–5.71 (1H, m, CH_2-OH), 7.38 (1H, s, 4-H), 7.82 (1H, s, 1-H); ^{13}C NMR (125 MHz, DMSO-d_6): δ 11.1 (18-CH_3), 22.8 (CH_2), 26.1 (CH_2), 26.4 (CH_2), 29.5 (CH_2), 29.9 (CH_2), 36.3 (CH_2), 38.1 (8-CH), 42.7 (13-C), 43.6 (9-CH), 49.8 (14-CH), 54.7 (CH_2-OH), 79.9 (17-CH), 108.2 (4-CH), 118.1 (1-CH), 118.9 (2-C), 136.8 (10-C), 140.5 (5-C), 158.4 (3′-C), 161.0 (3-C); ESI-MS: *m*/*z* 328.2 $[M + H]^+$, 328.2 calcd. for $[C_{20}H_{26}NO_3]^+$.

3.2.13. 3′-Fluoromethylisoxazolo[4′,5′:2,3]estra-1,3,5(10)-triene-17β-acetate (**4l**)

To a solution of **4j** (150 mg, 0.41 mmol) in DCM (2.5 mL), DAST (85 μL, 1.6 equiv.) was added under a nitrogen atmosphere and stirred at RT for 1 h. The reaction was quenched with the addition of aq. $NaHCO_3$ (10 wt. %, 10 mL) and extracted with DCM (3 × 10 mL). The combined organic phase was washed with water (10 mL), brine (10 mL), dried over anhydrous Na_2SO_4 and concentrated in vacuo. The crude product was purified by CC (EtOAc/hexane = 10:90). Yield (**4l**): 89 mg (59%, white crystals); Mp: 141–143 °C; Anal. Calcd. for $C_{22}H_{26}FNO_3$ (371.45) C 71.14; H 7.06; N 3.77. Found C 71.01; H 7.43; N 3.68. ^{1}H NMR (500 MHz, $CDCl_3$): δ 0.85 (3H, s, 18-CH_3), 1.24–1.69 (7H, overlapping m), 1.73–1.83 (1H, m), 1.90–2.00 (2H, m), 2.07 (3H, s, Ac-CH_3), 2.18–2.30 (1H, m), 2.30–2.44 (2H, m), 2.97–3.09 (2H, m), 4.68–4.75 (1H, m, 17-αH), 5.66–5.84 (2H, d, *J* 47.0, CH_2F), 7.32 (1H, s, 4-H), 7.68 (1H, s, 1-H); ^{13}C NMR (125 MHz, $CDCl_3$) δ 12.2 (18-CH_3), 21.3 (Ac-CH_3), 23.5 (CH_2), 26.4 (CH_2), 27.0 (CH_2), 27.7 (CH_2), 30.4 (CH_2), 36.9 (CH_2), 38.3 (8-CH), 43.0 (13-C), 44.1 (9-CH), 50.3 (14-CH), 76.2 (1C, d, *J* 166.7, CH_2F), 82.7 (17-CH), 109.1 (4-CH), 117.4 (1-CH), 118.7 (2-C), 137.9 (C), 141.4 (C), 154.2 (1C, d, *J* 22.9, 3′-C), 162.4 (3-C), 171.4 (Ac-C=O); ESI-MS: *m*/*z* 372.2 $[M + H]^+$, 372.2 calcd. for $[C_{22}H_{27}FNO_3]^+$.

3.2.14. 3′-Fluoromethylisoxazolo[4′,5′:2,3]estra-1,3,5(10)-triene-17β-ol (**4m**)

To a solution of **4l** (62 mg, 0.17 mmol) in THF (1.7 mL), LiOH (1 M, 510 μL, 3 equiv.) was added and the mixture was stirred at RT overnight. Then, it was concentrated under reduced pressure and the crude product was purified by CC (EtOAc/DCM = 5:95). Yield (**4m**): 52 mg (95%, white crystals); Mp: 184–186 °C; Anal. Calcd. for $C_{20}H_{24}FNO_2$ (329.42) C 72.92; H 7.34; N 4.25. Found C 72.98; H 7.46; N 4.03. ^{1}H NMR (500 MHz, $CDCl_3$): δ 0.80 (3H, s, 18-CH_3), 1.18–1.31 (1H, m), 1.31–1.58 (6H, overlapping m), 1.61–1.79 (2H, m), 1.90–1.99 (1H, m), 1.99–2.06 (1H, m), 2.09–2.20 (1H, m), 2.28–2.37 (1H, m), 2.39–2.47 (1H, m), 2.97–3.09 (2H, m), 3.72–3.79 (1H, t, *J* 8.5, 17-αH), 5.69–5.84 (2H, d, *J* 47.0, CH_2F), 7.31 (1H, s, 4-H), 7.69 (1H, s, 1-H); ^{13}C NMR (125 MHz, $CDCl_3$) δ 11.2 (18-CH_3), 23.4 (CH_2), 26.5 (CH_2), 27.0

(CH_2), 30.4 (CH_2), 30.7 (CH_2), 36.7 (CH_2), 38.6 (8-CH), 43.3 (13-C), 44.2 (9-CH), 50.5 (14-CH), 76.2 (1C, d, *J* 166.8, CH_2F) 81.9 (17-CH), 109.1 (4-CH), 117.4 (1-CH), 118.7 (2-C), 138.1 (C), 141.5 (C), 154.2 (1C, d, *J* 22.6, 3′-C), 162.4 (3-C). ESI-MS: *m*/*z* 330.2 $[M + H]^+$, 330.2 calcd. for $[C_{20}H_{25}FNO_2]^+$.

3.2.15. 3′-Formylisoxazolo[4′,5′:2,3]estra-1,3,5(10)-triene-17β-acetate (**4n**)

To a solution of **4j** (148 mg, 0.40 mmol) in DCM (5 mL), Dess–Martin periodinane (255 mg, 1.5 equiv.) was added under a nitrogen atmosphere and the mixture was stirred at RT for 2 h. The reaction was filtered into a separating funnel through cotton wool, and then water was added (10 mL) and extracted with DCM (3 × 10 mL). The combined organic phase was washed with aq. $NaHCO_3$ (10 wt. %, 10 mL), water (10 mL) and brine (10 mL), and then dried over anhydrous Na_2SO_4 and concentrated in vacuo. The crude product was purified by CC (hexane/DCM = 20:80). Yield (**4n**): 119 mg (81%, yellowish white crystals); Mp: 159–160 °C; Anal. Calcd. for $C_{22}H_{25}NO_4$ (367.44) C 71.91; H 6.86; N 3.81. Found C 71.74; H 7.15; N 3.59. ^{1}H NMR (500 MHz, $CDCl_3$): *δ* 0.85 (3H, s, 18-CH_3), 1.24–1.70 (7H, overlapping m), 1.72–1.82 (1H, m), 1.90–2.00 (2H, m), 2.07 (3H, s, Ac-CH_3), 2.19–2.30 (1H, m), 2.30–2.40 (1H, m), 2.40–2.49 (1H, m), 2.98–3.10 (2H, m), 4.67–4.74 (1H, m, 17-αH), 7.39 (1H, s 4-H), 8.05 (1H, s, 1-H), 10.39 (1H, s, CHO); ^{13}C NMR (125 MHz, $CDCl_3$) *δ* 12.2 (18-CH_3), 21.3 (Ac-CH_3), 23.5 (CH_2), 26.3 (CH_2), 26.8 (CH_2), 27.7 (CH_2), 30.4 (CH_2), 36.8 (CH_2), 38.2 (8-CH), 43.0 (13-C), 44.1 (9-CH), 50.3 (14-CH), 82.7 (17-CH), 109.0 (4-CH), 116.3 (2-C), 118.8 (1-CH), 139.8 (C), 142.1 (C), 155.5 (C), 163.4 (C), 171.4 (Ac-C=O), 186.0 (CHO); ESI-MS: *m*/*z* 368.2 $[M + H]^+$, 368.2 calcd. for $[C_{22}H_{26}NO_4]^+$.

3.2.16. 3′-Difluoromethylisoxazolo[4′,5′:2,3]estra-1,3,5(10)-triene-17β-acetate (**4o**)

To a solution of **4n** (62 mg, 0.17 mmol) in DCM (2.0 mL), DAST (90 μL, 4.0 equiv.) was added at 0 °C under a nitrogen atmosphere and stirred at RT for 2 h. The reaction was quenched with the addition of aq. $NaHCO_3$ (10 wt. %, 10 mL) and extracted with DCM (3 × 10 mL). The combined organic phase was washed with water (10 mL), brine (10 mL), dried over anhydrous Na_2SO_4 and concentrated in vacuo. The crude product was purified by CC (EtOAc/hexane = 3:97). Yield (**4o**): 61 mg (92%, white crystals); Mp: 137–139 °C; Anal. Calcd. for $C_{22}H_{25}F_2NO_3$ (389.44) C 67.85; H 6.47; N 3.60. Found C 67.55; H 6.80; N 3.49. ^{1}H NMR (500 MHz, $CDCl_3$): *δ* 0.86 (3H, s, 18-CH_3), 1.27–1.71 (7H, overlapping m), 1.72–1.83 (1 H, m), 1.91–2.00 (2H, m), 2.07 (3H, s, Ac-CH_3), 2.19–2.30 (1H, m), 2.30–2.37 (1H, m), 2.37–2.45 (1H, m), 3.01–3.08 (2H, m), 4.67–4.76 (1H, t, *J* 8.4, 17-αH), 6.83–7.17 (1H, t, *J* 53.5, CHF_2), 7.36 (1H, s, 4-H), 7.74 (1H, s, 1-H); ^{13}C NMR (125 MHz, $CDCl_3$) *δ* 12.2 (18-CH_3), 21.3 (Ac-CH_3), 23.5 (CH_2), 26.3 (CH_2), 26.9 (CH_2), 27.8 (CH_2), 30.4 (CH_2), 36.9 (CH_2), 38.3 (8-CH), 43.0 (13-C), 44.1 (9-CH), 50.4 (14-CH), 82.7 (17-H), 109.2 (4-CH), 110.5 (1C, t, *J* 236.5, CHF_2), 116.1 (2-C), 117.5 (1-CH), 138.8 (C), 142.2 (C), 153.0 (1C, t, *J* 30.6, C=N), 162.9 (3-C), 171.3 (Ac-C=O); ESI-MS: *m*/*z* 390.2 $[M + H]^+$, 390.2 calcd. for $[C_{22}H_{26}F_2NO_3]^+$.

3.2.17. 3′-Difluoromethylisoxazolo[4′,5′:2,3]estra-1,3,5(10)-triene-17β-ol (**4p**)

To a solution of **4o** (47 mg, 0.12 mmol) in THF (1.2 mL), LiOH (1 M, 360 μL, 3 equiv.) was added and the mixture was stirred at RT overnight. Then, it was concentrated under reduced pressure and the crude product was purified by CC (DCM). Yield (**4p**): 36 mg (86%, white crystals); Mp: 148–150 °C; Anal. Calcd. for $C_{20}H_{23}F_2NO_2$ (347.41) C 69.15; H 6.67; N 4.03. Found C 69.10; H 6.84; N 3.88. ^{1}H NMR (500 MHz, $CDCl_3$): *δ* 0.81 (3H, s, 18-CH_3), 1.20–1.57 (7H, overlapping m), 1.62–1.79 (2H, m), 1.90–1.99 (1H, m), 1.99–2.07 (1H, m), 2.09–2.20 (1H, m), 2.28–2.37 (1H, m), 2.39–2.48 (1H, m), 2.98–3.08 (2H, m), 3.73–3.80 (1H, t, *J* 8.5, 17-αH), 6.82–7.14 (1H, t, *J* 53.5, CHF_2), 7.35 (1H, s, 4-CH), 7.75 (1H, s, 1-CH); ^{13}C NMR (125 MHz, $CDCl_3$) *δ* 11.2 (18-CH_3), 23.4 (CH_2), 26.5 (CH_2), 26.9 (CH_2), 30.5 (CH_2), 30.8 (CH_2), 36.7 (CH_2), 38.6 (8-CH), 43.4 (13-C), 44.3 (9-CH), 50.6 (14-CH), 81.9 (17-CH), 109.2 (4-CH), 110.5 (1C, t, *J* 236.5, CHF_2), 116.1 (2-C), 117.5 (1-CH), 138.9 (C), 142.2 (C), 153.0 (1C, t, *J* 30.8, 3′-C), 162.9 (3-C); ESI-MS: *m*/*z* 348.2 $[M + H]^+$, 348.2 calcd. for $[C_{20}H_{24}F_2NO_2]^+$.

3.2.18. 17β-Hydroxy-isoxazolo[4′,5′:2,3]estra-1,3,5(10)-triene-3′-carboxylic Acid (**4q**)

To a solution of **4g** (180 mg, 0.45 mmol) in MeOH/DCM = 1:9 (4.5 mL), NaOH (108 mg, 6 equiv.) was added and the mixture was stirred at RT for 1 h. Then, it was concentrated under reduced pressure, redissolved in MeOH and poured into ice-cold HCl (2M, 20 mL). The precipitate was filtered off and dried under vacuum. Yield (**4q**): 144 mg (94%, white powder); Mp > 150 °C (decomp.); Anal. Calcd. for $C_{20}H_{23}NO_4$ (341.41) C 70.36; H 6.79; N 4.10. Found C 70.53; H 7.01; N 3.84. ^{1}H NMR (500 MHz, DMSO-d_6): δ 0.65 (3H, s, 18-CH_3), 1.03–1.42 (7H, overlapping m), 1.52–1.62 (1H, m), 1.72–1.79 (1H, m), 1.79–1.86 (1H, m), 1.83–1.93 (1H, m), 1.99–2.08 (1H, m), 2.21–2.29 (1H, m), 2.72–2.78 (2H, m), 3.47–3.54 (1H, t, *J* 8.5, 17-αH), 4.49 (1H, bs, 17-OH), 6.66 (1H, s, 4-H), 7.36 (1H, s, 1-H), 10.99 (1H, bs, COOH); ^{13}C NMR (125 MHz, DMSO-d_6): δ 11.2 (18-CH_3), 22.7 (CH_2), 25.7 (CH_2), 26.4 (CH_2), 29.3 (CH_2), 29.8 (CH_2), 36.4 (CH_2), 38.1 (8-CH), 42.7 (13-C), 43.0 (9-CH), 49.4 (14-CH), 80.0 (17-CH), 96.3 (C), 115.9 (4-CH), 117.8 (C), 124.2 (C), 129.5 (1-CH), 131.4 (C), 144.1 (C), 158.4 (C); ESI-MS: *m*/*z* 342.2 $[M + H]^+$, 342.2 calcd. for $[C_{20}H_{24}NO_4]^+$.

3.2.19. 17β-Hydroxy-isoxazolo[4′,5′:2,3]estra-1,3,5(10)-triene-3′-carboxylic Acid Methyl Ester (**4r**)

To a solution of **4q** (100 mg, 0.29 mmol) in MeOH (3 mL), cc. H_2SO_4 (1 drop) was added and kept at reflux temperature for 36 h. Then, it was neutralized with $NaHCO_3$ and concentrated in vacuo. The crude product was purified by CC (EtOAc/DCM = 10:90). Yield (**4r**): 94 mg (90%, white powder); Mp: 201–203 °C; Anal. Calcd. for $C_{21}H_{25}NO_4$ (355.43) C 70.96; H 7.09; N 3.94. Found C 70.73; H 7.34; N 3.65. ^{1}H NMR (500 MHz, $CDCl_3$): δ 0.80 (3H, s, 18-CH_3), 1.21–1.58 (7H, overlapping m), 1.62–1.79 (2H, m), 1.90–1.99 (1H, m), 1.99–2.06 (1H, m), 2.09–2.23 (1H, m), 2.29–2.38 (1H, m), 2.43–2.52 (1H, m), 2.98–3.10 (2H, m), 3.72–3.80 (1H, td, *J* 8.5, 3.3, 17-αH), 4.08 (3H, s, COOC$\underline{H}_3$), 7.36 (1H, s, 4-CH), 7.99 (1H, s, 1-H); ^{13}C NMR (125 MHz, $CDCl_3$) δ 11.2 (18-CH_3), 23.4 (CH_2), 26.5 (CH_2), 26.9 (CH_2), 30.4 (CH_2), 30.7 (CH_2), 36.7 (CH_2), 38.5 (8-CH), 43.3 (13-C), 44.3 (9-CH), 50.5 (14-CH), 53.0 (COO$\underline{C}H_3$), 81.9 (17-CH), 109.1 (4-CH), 118.2 (2-C), 118.7 (1-CH), 139.3 (C), 141.8 (C), 150.0 (C), 161.0 (C), 163.3 ($\underline{C}OOCH_3$); ESI-MS: *m*/*z* 356.2 $[M + H]^+$, 356.2 calcd. for $[C_{21}H_{26}NO_4]^+$.

3.2.20. 17β-Hydroxy-isoxazolo[4′,5′:2,3]estra-1,3,5(10)-triene-3′-carboxamide (**4s**)

To a solution of **4r** (62 mg, 0.17 mmol) in NH_3 (6 M in MeOH, 2 mL), cat. KCN was added and the mixture was stirred at RT for 4 h, and then it was concentrated in vacuo. The crude product was purified by CC (EtOAc/DCM = 50:50). Yield (**4s**): 56 mg (94%, white crystals); Mp: 250–252 °C; Anal. Calcd. for $C_{20}H_{24}N_2O_3$ (340.42) C 70.57; H 7.11; N 8.23. Found C 70.37; H 7.44; N 8.06. ^{1}H NMR (500 MHz, DMSO-d_6): δ 0.67 (3H, s, 18-CH_3), 1.11–1.44 (6H, overlapping m), 1.47–1.66 (2H, m), 1.78–1.95 (3H, m), 2.23–2.38 (2H, m), 2.91–3.05 (2H, m), 3.50–3.58 (1H, td, *J* 8.5, 4.8, 17-αH), 4.48–4.53 (1H, d, *J* 4.8, 17-OH), 7.51 (1H, s, 4-CH), 7.94 (1H, s, 1-H), 7.98 (1H, s, one H of NH_2), 8.29 (1H, s, the other H of NH_2); ^{13}C NMR (125 MHz, DMSO-d_6): δ 11.1 (18-CH_3), 22.8 (CH_2), 26.0 (CH_2), 26.2 (CH_2), 29.5 (CH_2), 29.8 (CH_2), 36.3 (CH_2), 37.9 (8-CH), 42.7 (13-C), 43.4 (9-CH), 49.8 (14-H), 79.9 (17-CH), 108.5 (4-CH), 117.7 (2-C), 118.5 (1-CH), 138.4 (C), 141.3 (C), 151.9 (3′-C), 160.7 (3-C), 161.9 ($CONH_2$); ESI-MS: *m*/*z* 341.2 $[M + H]^+$, 341.2 calcd. for $[C_{20}H_{25}N_2O_3]^+$.

3.2.21. 2-Cyanoestra-1,3,5(10)-triene-3,17β-ol (**8**) by Cyclization Followed by Kemp Elimination from **3a** (Scheme 3, xi)

DIAD (490 μL, 2.50 mmol) was added to a solution of PPh_3 (656 mg, 2.50 mmol) in ACN (10 mL), followed by the addition of **3a** (315 mg, 1.00 mmol). The reaction mixture was stirred at RT for 1 h, and then it was concentrated under reduced presure. The crude product was purified by CC (EtOAc/hexane = 10:90 to 40:60). Yield (**8**): 258 mg (87%, white powder); Mp > 200 °C (decomp.); Anal. Calcd. for $C_{19}H_{23}NO_2$ (297.40) C 76.74; H 7.80; N 4.71. Found C 76.50; H 8.14; N 4.66. ^{1}H NMR (500 MHz, DMSO-d_6): δ 0.65 (3H, s, 18-CH_3), 1.02–1.45 (7H, overlapping m), 1.52–1.62 (1H, m), 1.71–1.93 (3H, m), 1.99–2.10 (1H, m), 2.22–2.30 (1H, m), 2.73–2.80 (2H, m), 3.51 (1 H, t, *J* 8.5, 17-αH), 4.48 (1H, s, 17-OH),

6.67 (1H, s, 4-H), 7.39 (1H, s, 1-H), 10.63 (1H, s, 3-OH); ^{13}C NMR (125 MHz, DMSO-d_6): δ 11.1 (18-CH_3), 22.7 (CH_2), 25.6 (CH_2), 26.3 (CH_2), 29.3 (CH_2), 29.8 (CH_2), 36.3 (CH_2), 38.1 (8-CH), 42.7 (13-C), 42.9 (9-CH), 49.4 (14-CH), 79.9 (17-CH), 96.2 (2-C), 115.7 (4-CH), 117.5 (CN), 129.6 (1-CH), 132.0 (C), 144.2 (C), 157.6 (3-C); ESI-MS: m/z 298.2 $[M + H]^+$, 298.2 calcd. for $[C_{19}H_{24}NO_2]^+$.

3.2.22. Estra-1,3,5(10)-triene-3,17β-diol-2-carboxamidoxime (**9**)

To a solution of 8 (48 mg, 0.16 mmol) in EtOH (2 mL), Na_2CO_3 (34 mg, 2 equiv.) and aq. NH_2OH (50 wt. %, 49 µL, 5 equiv.) were added and the mixture was refluxed overnight. After being concentrated under reduced presure, water (10 mL) was added and extracted with EtOAc (3 × 10 mL). The combined organic phase was washed with water (10 mL) and brine (10 mL), dried over anhydrous Na_2SO_4 and concentrated in vacuo. The crude product was purified by CC (EtOAc/DCM = 20:80). Yield (9): 48 mg (90%, white powder); Mp > 210 °C (decomp.); Anal. Calcd. for $C_{19}H_{26}N_2O_3$ (330.43) C 69.06; H 7.93; N 8.48. Found C 69.13; H 8.15; N 8.29. ^{1}H NMR (500 MHz, DMSO-d_6): δ 0.67 (3H, s, 18-CH_3), 1.07–1.44 (8H, overlapping m), 1.54–1.62 (1H, m), 1.75–1.81 (1H, m), 1.83–1.94 (2H, m), 2.04–2.13 (1H, m), 2.70–2.76 (2H, m), 3.49–3.57 (1H, td, *J* 8.3, 4.7, 17-αH), 4.47 (1H, d, *J* 4.8, 17-OH), 6.28 (2H, s, -NH_2), 6.49 (1H, s, 4-H), 7.47 (1H, s, 1-H), 9.85 (1H, s, -OH), 11.89 (1H, s, -OH); ^{13}C NMR (125 MHz, DMSO-d_6): δ 11.3 (18-CH_3), 22.8 (CH_2), 25.9 (CH_2), 26.7 (CH_2), 28.9 (CH_2), 29.9 (CH_2), 36.5 (CH_2), 38.6 (8-CH), 42.8 (13-C), 43.7 (9-CH), 49.6 (14-CH), 80.0 (17-CH), 112.2 (2-C), 115.9 (4-CH), 122.6 (1-CH), 130.2 (C), 138.7 (C), 153.7 (C), 154.9 (C); ESI-MS: m/z 331.2 $[M + H]^+$, 331.2 calcd. for $[C_{19}H_{27}N_2O_3]^+$.

3.2.23. 2′-Aminooxazolo[4′,5′:2,3]estra-1,3,5(10)-triene-17β-ol (**10**)

DDQ (52 mg, 0.23 mmol) was added slowly to the solution of PPh_3 (59 mg, 0.23 mmol) in DCM (1 mL), and the mixture was stirred for 1 min. This suspension was added to a solution of **9** (50 mg, 0.15 mmol) and Et_3N (45 µL, 0.30 mmol) in DCM (1 mL), and the mixture was stirred at RT for 30 min. After 30 min, another portion of DDQ/PPh_3 was added and stirred until TLC indicated the complete conversion of the starting material. The solvent was removed under vacuum; the residue was dissolved in EtOAc/MeOH, and then Celite® was added (~10 × weight of the crude sample) and the solvent was removed *in vacuo*. The crude product was purified by CC (EtOAc/hexane = 70:30). Yield (**10**): 33 mg (70%, white powder); Mp > 210 °C (decomp.); Anal. Calcd. for $C_{19}H_{24}N_2O_2$ (312.41) C 73.05; H 7.74; N 8.97. Found C 73.26; H 7.98; N 8.75. ^{1}H NMR (500 MHz, DMSO-d_6): δ 0.67 (3H, s, 18-CH_3), 1.08–1.46 (7H, overlapping m), 1.54–1.64 (1H, m), 1.76–1.82 (1H, m), 1.83–1.94 (2H, m), 2.13–2.22 (1H, m), 2.30 (1H, m), 2.76–2.89 (2H, m, 6-H_2), 3.53 (1H, td, *J* 8.5, 4.6, 17-αH), 4.48 (1H, d, *J* 4.8, 17-OH), 6.96 (1H, s, 4-H), 7.08 (1H, s, 1-H), 7.15 (2H, s, NH_2); ^{13}C NMR (125 MHz, DMSO-d_6): δ 11.2 (18-CH_3), 22.8 (CH_2), 26.3 (CH_2), 27.0 (CH_2), 29.3 (CH_2), 29.9 (CH_2), 36.6 (CH_2), 38.5 (8-CH), 42.7 (13-C), 44.1 (9-CH), 49.7 (14-CH), 80.0 (17-CH), 107.8 (4-CH), 111.8 (3-CH), 128.3 (5-C), 135.3 (10-C), 141.6 (2-C), 146.2 (3-C), 162.3 (2′-C); ESI-MS: m/z 313.2 $[M + H]^+$, 313.2 calcd. for $[C_{19}H_{25}N_2O_2]^+$.

3.3. Pharmacology

3.3.1. Cell Culture

All cell lines were obtained from the American Type Culture Collection and maintained in a standard incubator under normal cell culture conditions (37 °C, 5% CO_2, 95% humidity). DU-145, PC3 (both prostate cancer) HeLa (cervical cancer) and MCF-7 (breast cancer) cell lines were maintained in RPMI-1640 medium (Biosera), whereas MRC-5 (non-cancerous fibroblast) cells were cultured in EMEM medium (Biosera). Both RPMI-1640 and EMEM media were supplemented with 10% fetal bovine serum (FBS), 2 mM glutamine and 1% penicillin-streptomycin.

3.3.2. Cell Viability Assay

For the pharmacological studies, each compound was dissolved in cell culture grade DMSO (Sigma) at a final concentration of 2.5, 5 or 10 mM (depending on solubility). For the initial screening, cells were seeded at 3×10^3 cells/well density in 96-well plates and left to adhere overnight. The next day, cells were treated with each of the steroid derivatives at 2.5 μM concentration for 72 h. Control cells received DMSO treatment (solvent of the steroid derivatives). For IC_{50} measurements, cells were seeded in the same way as above. The next day cells were treated with either **4b**, **4c** or **4d** in 1, 2, 3, 4, 5, 6, 8 and 10 μM concentration for 72 h to obtain the dose-response curves. After 72-h treatments in both cases (initial screening, IC_{50} measurements), MTT assays were conducted. For this, treatment media were replaced with fresh media containing 0.5 mg/mL 3-(4,5-dimethylthiazol-2-yl)-2,5-diphenyl tetrazolium bromide (MTT) reagent (Sigma-Aldrich). Cells were incubated with MTT reagent-containing media for 1–3 h, and then the formed formazan crystals were solubilized in DMSO, and the absorbance of the samples was measured at 570 nm with Synergy HTX microplate reader (BIOTEK®). The average viability of the DMSO-treated cells was considered 100%. On the viability data, dose-response curves were fitted (Supplementary Material p52–53), and IC_{50} values were calculated accordingly. The experiments were repeated three times using three biological replicates.

3.3.3. Reverse Transcription Quantitative Polymerase Chain Reaction (RT-qPCR)

For total RNA isolation, cells were seeded in 60 mm dishes at 0.8×10^6 cells/dish density and left to adhere overnight. The next day, cells were treated with either **4b**, **4c** or **4d** in different concentrations for 72 h (**4b** (DU-145: 2 μM HeLa: 1 μM, MCF-7 1 μM), **4c** (DU-145: 1 μM HeLa: 1 μM, MCF-7 1 μM) and **4d** (DU-145: 4 μM HeLa: 2 μM, MCF-7 2 μM)). After the treatments, total RNA was isolated with the RNeasy® Mini Kit (QIAGEN, Hilden, Germany) according to the manufacturer′s recommendation. The concentration and purity of the isolated total RNA were measured with the NanoDrop ND 1000 Spectrophotometer (Thermo Fisher Scientific, Waltham, MA, USA). From each sample, 1 μg RNA was reverse transcribed in a 20 μL reaction with the TaqMan® Reverse Transcription kit (Applied Biosystems, Thermo Fisher Scientific, Waltham, MA, USA) following the manufacturer′s instructions. cDNA was diluted 5X to a final volume of 100 μL. qPCR reactions were performed with PicoReal™ Real-time PCR (Thermo Fisher Scientific, Waltham, MA, USA) using SYBR Green qPCR Master Mix (Thermo Fisher Scientific, Waltham, MA, USA). Reactions were carried out in a 10 μL reaction volume (5 μL SYBR Green, 3 μL RNase-free H_2O, 1 μL cDNA, 1 μL primer-mix). The sequence and final concentration of the used primers are found within the Supplementary Material p54. Relative transcript levels were determined by the ΔΔCt method, using GAPDH as the reference gene. Experiments were repeated twice with three biological replicates.

3.3.4. Statistical Analysis

Data analysis, IC_{50} value calculations, graphical representation of data (heatmap, dose–response curves and qPCR diagrams) and statistical analysis (non-linear regression, two-way ANOVA) were carried out using GraphPad Prism 8.0.1 software. Differences between the control and treated samples were considered statistically significant, if $p < 0.05$.

4. Conclusions

In summary, a compound library containing novel estradiol-benzisoxazole chimeras, differing only in their C-3′ substituent of the heteroring, was created via multistep pathways. The majority of the 19 new heterocyclic compounds were obtained from appropriately synthesized 2-substituted E1 or E2 precursors, and subsequent ring closure involving the 3-OH functionality was performed by high conversion. However, some products were obtained from a 3′-methoxycarbonyl-substituted isoxazole derivative by further modification of its ester group. The steroid products, including all intermediates, were structurally characterized and subjected to in vitro pharmacological studies. The primary screen to test the

antiproliferative activity of the obtained compounds provided numerous positive hits, several derivatives exhibited strong anticancer performance, and most estradiol-benzisoxazole hybrids showed remarkable cancer cell selectivity. The three most promising compounds, the 3′-methyl, 3′-ethyl and 3′-isopropyl substituted steroidal benzisoxazoles showed a high degree of cytotoxicity on all tested cancerous cell lines, whereas treatment of non-cancerous cells with these derivatives resulted in no, or minimal change in cell viability. The minimal inhibitory concentrations (IC_{50}) of the three compounds were determined on cancerous and non-cancerous cell lines. Interestingly, the IC_{50} values of each molecule were one or two magnitudes lower for the cancerous cell lines compared to the values obtained on non-cancerous fibroblasts. The IC_{50} values of the most potent derivatives were compared to that of cisplatin, a clinically available drug, where we found that unlike cisplatin, estradiol-benzisoxazole hybrids show an outstanding cancer cell specificity. Lastly, we found that each of the three compounds exhibit strong apoptosis inducing potential, which could be the underlying cause of their impressive anticancer performance. Based on our findings, estradiol-benzisoxazole hybridization seems to be exceptionally advantageous for securing excellent anticancer activity; therefore, this structural motif should be considered in rational drug design and future synthesis approaches for clinical cancer therapy. The mechanism of action of the most potent steroidal hybrids as well as their hormone receptor binding will be further investigated.

Supplementary Materials: The following supporting information can be downloaded at: https://www.mdpi.com/article/10.3390/molecules27217456/s1, p2–49: ^{1}H NMR and ^{13}C NMR spectra of the synthesized compounds, Table in p50: Predicted pharmacokinetic parameters of synthesized compounds, Table in p51: Mean ± SD values of primary growth inhibitory screen (given as cell viability) used to construct the heatmap, Figure in p52–53: Dose response curves used to evaluate IC_{50} concentrations of the selected compounds and Table in p54: List, sequence and final concentrations of primers used in qRT-PCR.

Author Contributions: Conceptualization, resources, supervision and writing—review and editing, É.F. and M.K.; chemical synthesis and methodology, F.K.; pharmacological studies and methodology, D.I.A., F.I.N. and B.P.; writing— original draft preparation, F.K., F.I.N., M.K. and É.F. All authors have read and agreed to the published version of the manuscript.

Funding: This research received no external funding.

Institutional Review Board Statement: Not applicable.

Informed Consent Statement: Not applicable.

Data Availability Statement: Not applicable.

Acknowledgments: This work was supported by the ÚNKP-21-5-SZTE-592 and ÚNKP-22-3-SZTE-432 New National Excellence Program of the Ministry for Culture and Innovation from the source of the National Research, Development and Innovation Fund, by the János Bolyai Research Scholarship of the Hungarian Academy of Sciences (BO/00878/19/8 for M.K.), and the National Scientists Academy under the sponsorship of the Hungarian Ministry of Innovation and Technology (FEIF/646-4/2021-ITM to F.I.N.).

Conflicts of Interest: The authors declare no conflict of interest.

Sample Availability: Samples of the compounds are not available from the authors.

References

1. Rakesh, K.P.; Shantharam, C.S.; Sridhara, M.B.; Manukumar, H.M.; Qin, H.-L. Benzisoxazole: A Privileged Scaffold for Medicinal Chemistry. *Med. Chem. Commun.* **2017**, *8*, 2023–2039. [CrossRef]
2. Dubrovskiy, A.V.; Jain, P.; Shi, F.; Lushington, G.H.; Santini, C.; Porubsky, P.; Larock, R.C. Solution-Phase Synthesis of a Diverse Library of Benzisoxazoles Utilizing the [3 + 2] Cycloaddition of in Situ-Generated Nitrile Oxides and Arynes. *ACS Comb. Sci.* **2013**, *15*, 193–201. [CrossRef]
3. Rangappa, K.S.; Basappa. New Cholinesterase Inhibitors: Synthesis and Structure-Activity Relationship Studies of 1,2-Benzisoxazole Series and Novel Imidazolyl-d^2-Isoxazolines. *J. Phys. Org. Chem.* **2005**, *18*, 773–778. [CrossRef]

4. Benaka Prasad, S.B.; Vinaya, K.; Ananda Kumar, C.S.; Swarup, S.; Rangappa, K.S. Synthesis of Novel 6-Fluoro-3-(4-Piperidinyl)-1,2-Benzisoxazole Derivatives as Antiproliferative Agents: A Structure–Activity Relationship Study. *Investig. New Drugs* **2009**, *27*, 534–542. [CrossRef] [PubMed]
5. Ashwini, N.; Garg, M.; Mohan, C.D.; Fuchs, J.E.; Rangappa, S.; Anusha, S.; Swaroop, T.R.; Rakesh, K.S.; Kanojia, D.; Madan, V.; et al. Synthesis of 1,2-Benzisoxazole Tethered 1,2,3-Triazoles That Exhibit Anticancer Activity in Acute Myeloid Leukemia Cell Lines by Inhibiting Histone Deacetylases, and Inducing P21 and Tubulin Acetylation. *Bioorg. Med. Chem.* **2015**, *23*, 6157–6165. [CrossRef]
6. Soman, S.S.; Soni, J.N.; Patel, T.B. Synthesis of New Naphthoisoxazole Amide Derivatives and Study of Their Biological Evaluations. *Med. Chem. Res.* **2014**, *23*, 3803–3809. [CrossRef]
7. Karandikar, S.; Soni, R.; Soman, S.S.; Umar, S.; Suresh, B. 1,2-Benzisoxazole-3-Acetamide Derivatives as Dual Agents for DPP-IV Inhibition and Anticancer Activity. *Synth. Commun.* **2018**, *48*, 2877–2887. [CrossRef]
8. Jain, M.; Kwon, C.-H. 1,2-Benzisoxazole Phosphorodiamidates as Novel Anticancer Prodrugs Requiring Bioreductive Activation. *J. Med. Chem.* **2003**, *46*, 5428–5436. [CrossRef]
9. Mohareb, R.M.; El-Sayed, N.N.E.; Abdelaziz, M.A. The Knoevenagel Reactions of Pregnenolone with Cyanomethylene Reagents: Synthesis of Thiophene, Thieno[2,3-b]Pyridine, Thieno[3,2-d]Isoxazole Derivatives of Pregnenolone and Their in Vitro Cytotoxicity towards Tumor and Normal Cell Lines. *Steroids* **2013**, *78*, 1209–1219. [CrossRef]
10. Uto, Y. 1,2-Benzisoxazole Compounds: A Patent Review (2009–2014). *Expert Opin. Ther. Pat.* **2015**, *25*, 643–662. [CrossRef]
11. Tantawy, M.A.; Nafie, M.S.; Elmegeed, G.A.; Ali, I.A.I. Auspicious Role of the Steroidal Heterocyclic Derivatives as a Platform for Anti-Cancer Drugs. *Bioorg. Chem.* **2017**, *73*, 128–146. [CrossRef]
12. Baranovsky, A.V.; Ladyko, A.S.; Shatskaya, V.A.; Scherbakov, A.M. 14β-(Isoxazol-3-Yl)Methylestrane Steroids: Chemoselective Synthesis and Transformations with Heterocyclic Ring Opening. *Russ. J. Org. Chem.* **2019**, *55*, 202–214. [CrossRef]
13. Kovács, D.; Kádár, Z.; Mótyán, G.; Schneider, G.; Wölfling, J.; Zupkó, I.; Frank, É. Synthesis, Characterization and Biological Evaluation of Some Novel 17-Isoxazoles in the Estrone Series. *Steroids* **2012**, *77*, 1075–1085. [CrossRef] [PubMed]
14. Arya, G.C.; Kaur, K.; Jaitak, V. Isoxazole Derivatives as Anticancer Agent: A Review on Synthetic Strategies, Mechanism of Action and SAR Studies. *Eur. J. Med. Chem.* **2021**, *221*, 113511. [CrossRef]
15. Baydoun, E.; Atia-tul-Wahab; Mehmood, H.; Ahmad, M.S.; Malik, R.; Smith, C.; Choudhary, M.I. Microbial Transformation of Danazol with *Cunninghamella blakesleeana* and Anti-Cancer Activity of Danazol and Its Transformed Products. *Steroids* **2016**, *105*, 121–127. [CrossRef]
16. Borah, P.; Chowdhury, P. Steroid Hybrid Systems: New Molecular Entities with Potential Therapeutical Spectrum. *Curr. Drug Ther.* **2017**, *12*, 3–22. [CrossRef]
17. Bansal, R.; Acharya, P.C. Man-Made Cytotoxic Steroids: Exemplary Agents for Cancer Therapy. *Chem. Rev.* **2014**, *114*, 6986–7005. [CrossRef]
18. Kovács, F.; Gopisetty, M.K.; Adamecz, D.I.; Kiricsi, M.; Enyedy, É.A.; Frank, É. Synthesis and Conversion of Primary and Secondary 2-Aminoestradiols into A-Ring-Integrated Benzoxazolone Hybrids and Their in Vitro Anticancer Activity. *RSC Adv.* **2021**, *11*, 13885–13896. [CrossRef]
19. Kumar, B.S.; Raghuvanshi, D.S.; Hasanain, M.; Alam, S.; Sarkar, J.; Mitra, K.; Khan, F.; Negi, A.S. Recent Advances in Chemistry and Pharmacology of 2-Methoxyestradiol: An Anticancer Investigational Drug. *Steroids* **2016**, *110*, 9–34. [CrossRef] [PubMed]
20. Anstead, G.M.; Carlson, K.E.; Katzenellenbogen, J.A. The Estradiol Pharmacophore: Ligand Structure-Estrogen Receptor Binding Affinity Relationships and a Model for the Receptor Binding Site. *Steroids* **1997**, *62*, 268–303. [CrossRef]
21. Minorics, R.; Zupko, I. Steroidal Anticancer Agents: An Overview of Estradiol-Related Compounds. *ACAMC* **2018**, *18*, 652–666. [CrossRef] [PubMed]
22. Dang, X.; Liu, Z.; Zhou, Y.; Chen, P.; Liu, J.; Yao, X.; Lei, B. Steroids-Specific Target Library for Steroids Target Prediction. *Steroids* **2018**, *140*, 83–91. [CrossRef] [PubMed]
23. Molnár, B.; Gopisetty, M.K.; Adamecz, D.I.; Kiricsi, M.; Frank, É. Multistep Synthesis and In Vitro Anticancer Evaluation of 2-Pyrazolyl-Estradiol Derivatives, Pyrazolocoumarin-Estradiol Hybrids and Analogous Compounds. *Molecules* **2020**, *25*, 4039. [CrossRef]
24. Molnár, B.; Gopisetty, M.K.; Nagy, F.I.; Adamecz, D.I.; Kása, Z.; Kiricsi, M.; Frank, É. Efficient Access to Domain-Integrated Estradiol-Flavone Hybrids via the Corresponding Chalcones and Their in Vitro Anticancer Potential. *Steroids* **2022**, *187*, 109099. [CrossRef]
25. Baji, Á.; Gyovai, A.; Wölfling, J.; Minorics, R.; Ocsovszki, I.; Zupkó, I.; Frank, É. Microwave-Assisted One-Pot Synthesis of Steroid–Quinoline Hybrids and an Evaluation of Their Antiproliferative Activities on Gynecological Cancer Cell Lines. *RSC Adv.* **2016**, *6*, 27501–27516. [CrossRef]
26. Kiss, M.A.; Peřina, M.; Bazgier, V.; May, N.V.; Baji, Á.; Jorda, R.; Frank, É. Synthesis of Dihydrotestosterone Derivatives Modified in the A-Ring with (Hetero)Arylidene, Pyrazolo[1,5-a]Pyrimidine and Triazolo[1,5-a]Pyrimidine Moieties and Their Targeting of the Androgen Receptor in Prostate Cancer. *J. Steroid Biochem. Mol. Biol.* **2021**, *211*, 105904. [CrossRef]
27. Mao, F.; Ni, W.; Xu, X.; Wang, H.; Wang, J.; Ji, M.; Li, J. Chemical Structure-Related Drug-Like Criteria of Global Approved Drugs. *Molecules* **2016**, *21*, 75. [CrossRef]
28. ChemAxon. Chemicalize Was Used for the Prediction of Structural Properties and Lipophilicities. Available online: https://chemicalize.com/ (accessed on 1 September 2021).

29. Lipinski, C.A. Lead- and Drug-like Compounds: The Rule-of-Five Revolution. *Drug Discov. Today Technol.* **2004**, *1*, 337–341. [CrossRef]
30. Veber, D.F.; Johnson, S.R.; Cheng, H.-Y.; Smith, B.R.; Ward, K.W.; Kopple, K.D. Molecular Properties That Influence the Oral Bioavailability of Drug Candidates. *J. Med. Chem.* **2002**, *45*, 2615–2623. [CrossRef]
31. Chen, G.; Liu, H.; Li, S.; Tang, Y.; Lu, P.; Xu, K.; Zhang, Y. A Novel PPh_3 Mediated One-Pot Method for Synthesis of 3-Aryl or Alkyl 1,2-Benzisoxazoles. *Org. Lett.* **2017**, *19*, 1792–1795. [CrossRef]
32. Udd, S.; Jokela, R.; Franzén, R.; Tois, J. Copper-Catalyzed Cyclization of Z-Oximes into 3-Methyl-1,2-Benzisoxazoles. *Tetrahedron Lett.* **2010**, *51*, 1030–1033. [CrossRef]
33. Whiting, E.; Lanning, M.E.; Scheenstra, J.A.; Fletcher, S. Chromatography-Free Entry to Substituted Salicylonitriles: Mitsunobu-Triggered Domino Reactions of Salicylaldoximes. *J. Org. Chem.* **2015**, *80*, 1229–1234. [CrossRef]
34. Iranpoor, N.; Firouzabadi, H.; Nowrouzi, N. A Novel Method for the Highly Efficient Synthesis of 1,2-Benzisoxazoles under Neutral Conditions Using the Ph_3P/DDQ System. *Tetrahedron Lett.* **2006**, *47*, 8247–8250. [CrossRef]
35. Hughes, R.A.; Harris, T.; Altmann, E.; McAllister, D.; Vlahos, R.; Robertson, A.; Cushman, M.; Wang, Z.; Stewart, A.G. 2-Methoxyestradiol and Analogs as Novel Antiproliferative Agents: Analysis of Three-Dimensional Quantitative Structure-Activity Relationships for DNA Synthesis Inhibition and Estrogen Receptor Binding. *Mol. Pharmacol.* **2002**, *61*, 1053–1069. [CrossRef]
36. Peters, R.H.; Chao, W.-R.; Sato, B.; Shigeno, K.; Zaveri, N.T.; Tanabe, M. Steroidal Oxathiazine Inhibitors of Estrone Sulfatase. *Steroids* **2003**, *68*, 97–110. [CrossRef]
37. Paterni, I.; Bertini, S.; Granchi, C.; Tuccinardi, T.; Macchia, M.; Martinelli, A.; Caligiuri, I.; Toffoli, G.; Rizzolio, F.; Carlson, K.E.; et al. Highly Selective Salicylketoxime-Based Estrogen Receptor β Agonists Display Antiproliferative Activities in a Glioma Model. *J. Med. Chem.* **2015**, *58*, 1184–1194. [CrossRef]
38. Frank, É.; Mucsi, Z.; Szécsi, M.; Zupkó, I.; Wölfling, J.; Schneider, G. Intramolecular Approach to Some New D-Ring-Fused Steroidal Isoxazolidines by 1,3-Dipolar Cycloaddition: Synthesis, Theoretical and in Vitro Pharmacological Studies. *New J. Chem.* **2010**, *34*, 2671. [CrossRef]
39. Conn, P.J.; Hopkins, C.R.; Lindsley, C.W.; Niswender, C.M.; Engers, D.W.; Panarese, J.; Bollinger, S.; Engers, J. Benzoisoxazole-substituted compounds as MGLUR4 allosteric potentiators, compositions, and methods of treating neurological dysfunction. U.S. Patent No. 9,980,945, 29 May 2018.
40. Tam, T.L.D.; Xu, J. Carboxylic Acid Directed C–H Arylation of Azulene. *Org. Lett.* **2020**, *22*, 5009–5013. [CrossRef]
41. Guo, W.; Li, J.; Fan, N.; Wu, W.; Zhou, P.; Xia, C. A Simple and Effective Method for Chemoselective Esterification of Phenolic Acids. *Synth. Commun.* **2005**, *35*, 145–152. [CrossRef]
42. Lalut, J.; Payan, H.; Davis, A.; Lecoutey, C.; Legay, R.; Sopkova-de Oliveira Santos, J.; Claeysen, S.; Dallemagne, P.; Rochais, C. Rational Design of Novel Benzisoxazole Derivatives with Acetylcholinesterase Inhibitory and Serotoninergic 5-HT4 Receptors Activities for the Treatment of Alzheimer's Disease. *Sci. Rep.* **2020**, *10*, 3014. [CrossRef]
43. Van Eker, D.; Chauhan, J.; Murphy, W.A.; Conlon, I.L.; Fletcher, S. Chromatography-Free, Mitsunobu-Triggered Heterocyclizations of Salicylhydroxamic Acids to 3-Hydroxybenzisoxazoles. *Tetrahedron Lett.* **2016**, *57*, 5301–5303. [CrossRef]
44. Jänicke, R.U. MCF-7 Breast Carcinoma Cells Do Not Express Caspase-3. *Breast Cancer Res. Treat.* **2009**, *117*, 219–221. [CrossRef]

molecules

MDPI

Article

Efficient Synthesis of 4,8-Dibromo Derivative of Strong Electron-Deficient Benzo[1,2-*d*:4,5-*d'*]bis([1,2,3]thiadiazole) and Its S_NAr and Cross-Coupling Reactions

Timofey N. Chmovzh [1,2], Daria A. Alekhina [1], Timofey A. Kudryashev [1,3] and Oleg A. Rakitin [1,*]

[1] N. D. Zelinsky Institute of Organic Chemistry, Russian Academy of Sciences, 119991 Moscow, Russia
[2] Nanotechnology Education and Research Center, South Ural State University, 454080 Chelyabinsk, Russia
[3] Department of Chemistry, Moscow State University, 119899 Moscow, Russia
* Correspondence: orakitin@ioc.ac.ru; Tel.: +7-499-135-5327

Abstract: An efficient synthesis of hydrolytically and thermally stable 4,8-dibromobenzo[1,2-*d*:4,5-*d'*]bis([1,2,3]thiadiazole) by the bromination of its parent heterocycle is reported. The structure of 4,8-dibromobenzo[1,2-*d*:4,5-*d'*]bis([1,2,3]thiadiazole) was confirmed by X-ray analysis. The conditions for the selective aromatic nucleophilic substitution of one bromine atom in this heterocyclic system by nitrogen nucleophiles are found, whereas thiols formed the bis-derivatives only. Suzuki–Miyaura cross-coupling reactions were found to be an effective method for the selective formation of various mono- and di(het)arylated derivatives of strong electron-deficient benzo[1,2-*d*:4,5-*d'*]bis([1,2,3]thiadiazole), and Stille coupling can be employed for the preparation of bis-arylated heterocycles, which can be considered as useful building blocks for the synthesis of DSSCs and OLEDs components.

Keywords: sulfur–nitrogen heterocycles; benzo[1,2-*d*:4,5-*d'*]bis([1,2,3]thiadiazole); aromatic nucleophilic substitution; Suzuki and Stille cross-coupling reactions; X-ray analysis

Citation: Chmovzh, T.N.; Alekhina, D.A.; Kudryashev, T.A.; Rakitin, O.A. Efficient Synthesis of 4,8-Dibromo Derivative of Strong Electron-Deficient Benzo[1,2-*d*:4,5-*d'*]bis([1,2,3]thiadiazole) and Its S_NAr and Cross-Coupling Reactions. *Molecules* **2022**, *27*, 7372. https://doi.org/10.3390/molecules27217372

Academic Editor: Antonio Massa

Received: 14 October 2022
Accepted: 25 October 2022
Published: 30 October 2022

1. Introduction

Organic photovoltaics is a developing technology with a unique set of properties, such as low-cost solution processing with nontoxic materials, the possibility of using small amounts of materials due to ultrathin absorber films, and the ease of varying the most important characteristics of materials [1]. The chromophores, both polymeric and low-molecular weight, used in these devices, consisting of a combination of electron-donating (D) and electron-withdrawing (A) groups linked either directly or, preferably, through a π-conjugated bridges (π), have been extensively studied. The electron-deficient π-conjugated building blocks play an essential role in achieving the most important characteristics, such as light absorption, light emission and charge carrier mobility in materials by reducing the bandgap by promoting intramolecular charge transfer (ICT) [2,3]. The most important property of the acceptor is the electron affinity, which is related to the energy of the lowest unoccupied molecular orbital (LUMO). The choice of acceptor is crucial to achieving high performance in materials such as bulk heterojunction solar cells (BHJ) [4,5], dye-sensitized solar cells (DSSCs) [4,6,7], n-type organic field-effect transistors [8,9], near-infrared absorption and emissions materials [10,11], and electrochromic materials [12,13]. Although many heterocyclic acceptor building blocks are known [14], 2,1,3-benzothiadiazole (BTD) occupies an exceptional place among them [15,16]. Nevertheless, there is a strong demand to create ultra-high electron-deficient building blocks based on it to improve the special characteristics of photovoltaic materials [17,18]. Several attempts have been made. The attachment of strong electron-withdrawing groups (i.e., fluorine) at positions 5 and 6 has produced many different materials derived from 5,6-difluoro-2,1,3-benzothiadiazole [13]. Recently, the synthesis of an ultra-high electron-deficient [1,2,5]thiadiazolo[3,4-*d*]pyridazine system with the formal replacement of carbon atoms in the 5- and/or 6-positions by electronegative atoms

nitrogen has been reported [19]; it has been shown to be an important intermediate for the synthesis of dyes with various possible applications [18,20,21]. A third way to increase the electron-withdrawing strength of the benzothiadiazole ring is heteroannelation at positions 5 and 6 to create an acceptor, such as benzo-[1,2-*c*:4,5-*c*′]bis[1,2,5]thiadiazole (benzo-bis-thiadiazole, BBT), a sulfur–nitrogen heterocycle with the lowest LUMO energy [19]. The synthesis and functionalization of benzo[1,2-*c*:4,5-*c*′]bis[1,2,5]thiadiazole derivatives has been well investigated [22]. On the other hand, the possibilities of its bis(isothiadiazole) isomer, benzo[1,2-*d*:4,5-*d*′]bis([1,2,3]thiadiazole) (isoBTD), have been largely unexplored. Meanwhile, it has been shown that the replacement of the 1,2,5-thiadiazole ring in 2,1,3-benzothiadiazole (BTD) by the 1,2,3-thiadiazole ring leads to benzo[*d*][1,2,3]thiadiazole (isoBTD) compounds with properties similar to those of BTD, but with higher values of E_{LUMO} and the band gap (Eg), which indicates a high electronic conductivity due to the high stability of the molecule in the excited state. The careful selection of components in the design of appropriate compounds with benzo[*d*][1,2,3]thiadiazole as an internal acceptor can lead to promising photovoltaic materials [23]. In this regard, it becomes relevant to study the BBT isomer, benzo[1,2-*d*:4,5-*d*′]bis([1,2,3]thiadiazole) (isoBTD), which differs in the order of atoms in two five-membered heterocyclic rings. Figure 1 shows the boundary orbital energies (E_{HOMO} and E_{LUMO}) for 2,1,3-benzothiadiazole, as well as its derivatives and isomers.

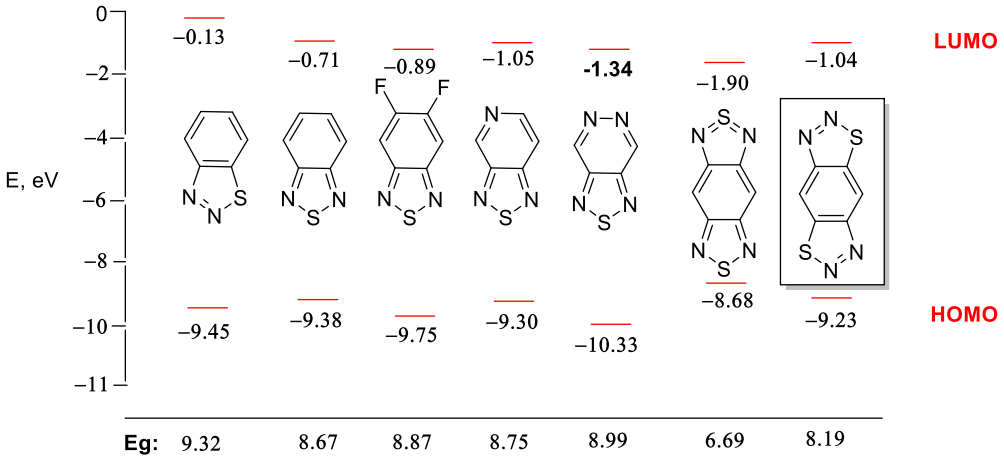

Figure 1. HOMO–LUMO energy levels and energy gap values for electron-deficient heterocycles for 2,1,3-benzothiadiazole, as well as its derivatives and isomers.

The data in Table 1 show that the fusion of a benzothiadiazole with another electron-withdrawing ring is the preferred method for increasing the electron-withdrawing capacity of the heterocyclic system, because it reduces the most important characteristic for photovoltaic materials, the energy band gap (E_g). Nevertheless, E_g for isoBTD compounds is much higher than for BTD derivatives, which determines the stability of the molecule in the exited state, and as a result the high electron conductivity, and requires a careful selection of donor moieties in the dye by designing photovoltaic components.

Dihalogenated (usually dibrominated) derivatives of the electron-deficient heterocycles shown in Figure 1 are most often employed to prepare components of various photovoltaic materials [22,24,25]. 4,8-Dibromobenzo[1,2-*d*:4,5-*d*′]bis([1,2,3]thiadiazole) **1** was described as a minor component of an inseparable mixture of three compounds, with tricycle **2** and its mono-derivative **3** obtained by the nitrosation of 2,5-diaminobenzene-1,4-dithiol dihydrochoride **4** in HBr (Scheme 1) [26]. Neither the yield of compound **1** nor its spectral and analytical data are given in the paper.

Table 1. Bromination of benzo[1,2-*d*:4,5-*d'*]bis([1,2,3]thiadiazole) **2**.

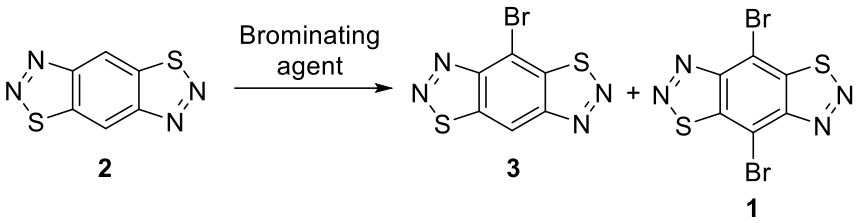

Entry	Brominating Agent	Solvent	Conditions	Yields (%)		
				2	**3**	**1**
1	NBS	AcOH	25 °C, 12 h	85	0	0
2	NBS	$CHCl_3$	25 °C, 24 h	88	0	0
3	NBS	DMF	25 °C, 24 h	82	0	0
4	NBS	$CHCl_3$	61 °C, 12 h	82	0	0
5	NBS	DMF	110 °C, 12 h	78	0	0
6	Br_2	dioxane	25 °C, 12 h	80	0	0
7	HBr	HBr	80 °C, 12 h	70	20	5
8	Br_2	HBr	80 °C, 12 h	10	60	2
9	Br_2	HBr	110 °C, 12 h	0	45	15
10	Br_2	HBr	120 °C, 12 h	0	5	38
11	Br_2	HBr	120 °C, 18 h	0	0	40
12	Br_2	HBr	130 °C, 18 h	0	0	30

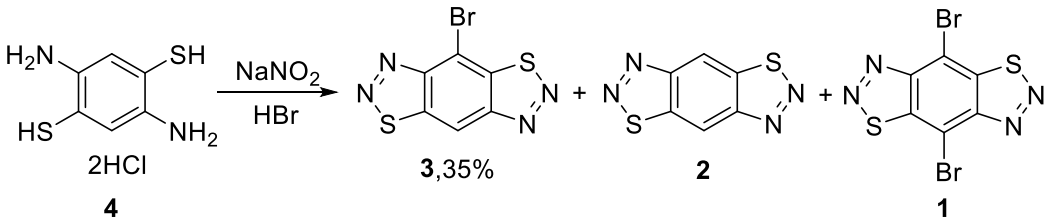

Scheme 1. Nitrosation of 2,5-diaminobenzene-1,4-dithiol dihydrochoride **4**.

Herein, we describe the synthesis of 4,8-dibromobenzo[1,2-*d*:4,5-*d'*]bis([1,2,3]thiadiazole) **1**, its spectral and analytical data, S_NAr and cross-coupling reactions as a basis for the preparation of compounds that are of interest as photovoltaic materials.

2. Results and Discussion

2.1. Synthesis of 4,8-Dibromobenzo[1,2-d:4,5-d']bis([1,2,3]thiadiazole) **1**

Taking into account the failures in the synthesis of compound **1** from 2,5-diaminobenzene-1,4-dithiol dihydrochoride **4**, we decided to synthesize this compound from unsubstituted tricycle **2**, which is easily formed from dithiol **4** in almost quantitative yields upon nitrosation in hydrochloric acid [27]. We recently found that the bromination of tricycle **2** in hydrobromic acid can selectively give 4-bromobenzo[1,2-*d*:4,5-*d'*]bis([1,2,3]thiadiazole) **3** in good yields [28]. In a continuation of this study, the bromination of benzo[1,2-*d*:4,5-*d'*]bis([1,2,3]thiadiazole) **2** was carried out by varying the nature of the brominating agent (NBS and bromine), the solvent, and the reaction temperature. The results are summarized in Table 1.

The use of *N*-bromosuccinimide in a solvent (AcOH, $CHCl_3$, DMF) or molecular bromine (Br_2) in dioxane as brominating agents at room temperature did not lead to mono- **3** and di-bromides **1**; only starting compound **2** was isolated from the reaction mixture (Table 1, entries 1–6), which can be explained by the high electron-withdrawing character of tricycle **2**, which slows down the reaction of electrophilic bromination. Carrying out the reaction in hydrobromic acid with heating in the absence of molecular bromine also led to a low conversion of compound **2**, and 4-bromobenzo[1,2-*d*:4,5-*d'*]bis([1,2,3]thiadiazole) **3** was isolated in a 20% yield, while the yield of 4,8-dibromobenzo[1,2-*d*:4,5-*d'*]bis([1,2,3]thiadiazole)

1 did not exceed 5% (Entry 7). This result is similar to the formation of the mixture of compounds **1**, **2**, and **3,** which was obtained by the nitrosation of 2,5-diaminobenzene-1,4-dithiol dihydrochoride **4** in HBr (Scheme 1). Carrying out the reaction when heated to 80 °C in hydrobromic acid in the presence of molecular bromine made it possible to increase the yield of 4-bromobenzo[1,2-*d*:4,5-*d'*]bis([1,2,3]thiadiazole) **3** to 60%. However, trace amounts of 4,8-dibromobenzo[1,2-*d*:4,5-*d'*]bis([1,2,3]thiadiazole) **1** were detected in the reaction mixture (Entry 8). Increasing both the reaction temperature to 120 °C and the amount of bromine made it possible to increase the yield of the target 4,8-dibromobenzo[1,2-*d*:4,5-*d'*]bis([1,2,3]thiadiazole) **1** up to 38%, while the yield of monobromo derivative **3** was only 5% (Entry 10). The longer heating of the reaction mixture (18 h) led to the target dibromide in a 40% yield (Entry 11). A further increase in the temperature of the reaction medium to 130 °C gave a slight decrease in the yield of the target compound (Entry 12). Thus, we have developed a method for the selective preparation of 4,8-dibromobenzo[1,2-*d*:4,5-*d'*]bis([1,2,3]thiadiazole) **1** in moderate yield. Unfortunately, the reactivity of the parent ultra-high electron-withdrawing heterocycles, such as benzo-[1,2-*c*:4,5-*c'*]bis[1,2,5]thiadiazole (BBT) or benzo[1,2-*d*:4,5-*d'*]bis([1,2,3]thiadiazole) **2,** has not been previously studied. We assume that for such compounds, the reactions of the electrophilic substitution of the hydrogen atom are difficult, and it is necessary to apply the conditions of radical reactions (for example, bromine in hydrobromic acid). The reactivity of the unsubstituted tricycle **2** will be reported in more detail in our next publication.

4,8-Dibromobenzo[1,2-*d*:4,5-*d'*]bis([1,2,3]thiadiazole) **1** is a high-melting yellow solid with mp > 250 °C (Supplementary Materials). It is stable to hydrolysis at room temperature and can be kept in a freezer under argon for a few months without noticeable changes. Its structure was fully proven by NMR, mass and IR spectroscopy, and finally established by single-crystal X-ray diffraction study (Figure 2).

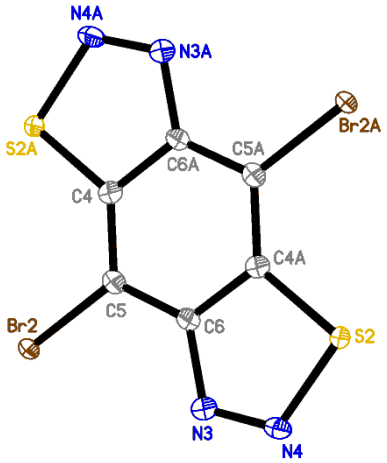

Figure 2. The general view of 4,8-dibromobenzo[1,2-*d*:4,5-*d'*]bis([1,2,3]thiadiazole) **1** in a representation of atoms by thermal ellipsoids (*p* = 50%).

2.2. Aromatic Nucleophilic Substitution of 4,8-Dibromobenzo[1,2-d:4,5-d']bis([1,2,3]thiadiazole) **1**

The nucleophilic substitution in 1,2,5-thiadiazoles and 1,2,3-thiadiazoles fused with benzene or strong electron-withdrawing heterocycles has been poorly investigated. Two examples of nucleophilic substitution with morpholine and piperidine are known for 4,7-dibromobenzo[*c*][1,2,5]thiadiazole **5** [29,30], one reaction with morpholine for 4,7-dibromobenzo[*d*][1,2,3]thiadiazole **6** [31] and two procedures with morpholine and thiophenol for benzo[1,2-*c*:4,5-*c'*]bis[1,2,5]thiadiazole **7** [32]. The formation of mono-substituted derivatives **8,9** in the first two cases and bis-derivative **10** for the more activated tricycle **7** was observed (Scheme 2).

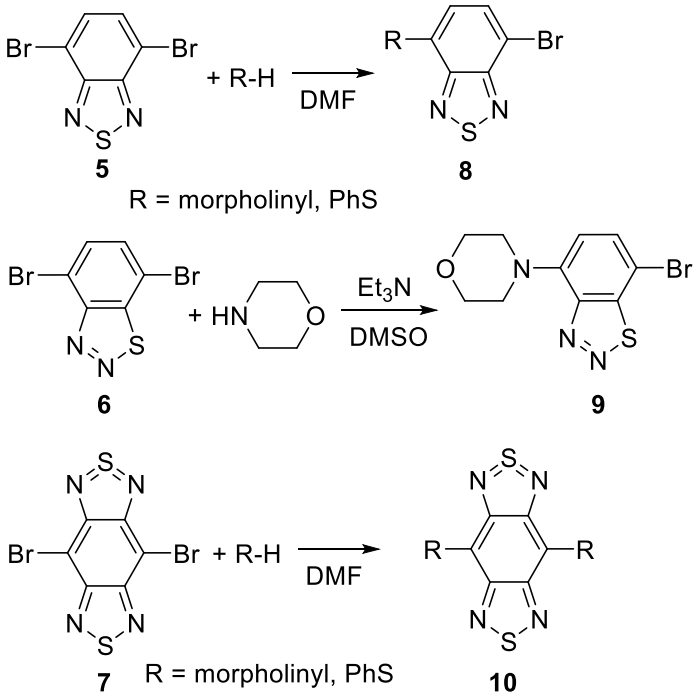

Scheme 2. Nucleophilic substitution in fused 1,2,5-thiadiazoles and 1,2,3-dithiazoles.

Aromatic nucleophilic substitution in 4,7-dibromo[1,2,5]thiadiazolo[3,4-*d*]pyridazine **11** was recently investigated [14], and selective conditions were found for the substitution of one or two bromine atoms by oxygen and nitrogen nucleophiles, whereas thiols formed only bis-derivatives (Scheme 3).

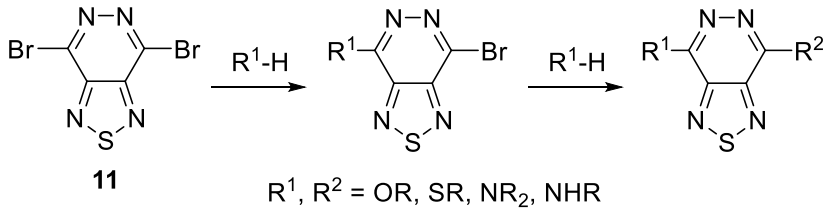

Scheme 3. Nucleophilic substitution in 4,7-dibromo[1,2,5]thiadiazolo[3,4-*d*]pyridazine **11**.

In order to find selective conditions for the formation of mono- and bis-substituted products in 4,8-dibromobenzo[1,2-*d*:4,5-*d*']bis([1,2,3]thiadiazole) **1**, its reactions with nitrogen, sulfur- and oxygen-containing nucleophiles were systematically studied.

The treatment of 4,8-dibromobenzo[1,2-*d*:4,5-*d*']bis([1,2,3]thiadiazole) **1** with morpholine gave mono- and bis-substituted derivatives, depending on the reaction conditions. Carrying out the reaction at room temperature, regardless of the solvent used (DCM, MeCN, DMF) and the amount of morpholine, resulted in the mono-substitution product **12a** in low to moderate yields (Table 2, entries 1–6). Refluxing of the reaction mixture in MeCN for 24 h with two morpholine equivalents gave a mono-substituted product **12a** with the best yield of 78% (Entry 7). Heating in DMF under similar conditions did not improve the yield of **12a** (70%, entry 8). The formation of bis-substituted product **13a** in a moderate yield was achieved by the prolonged heating of dibromide **1**, with an excess of morpholine at 130 °C (Entry 9). Thus, optimal conditions were found for the synthesis of an asymmetric compound **12a** and a disubstituted product **13a**.

Table 2. Nucleophilic substitution of 4,8-dibromobenzo[1,2-*d*:4,5-*d'*]bis([1,2,3]thiadiazole) **1** with morpholine.

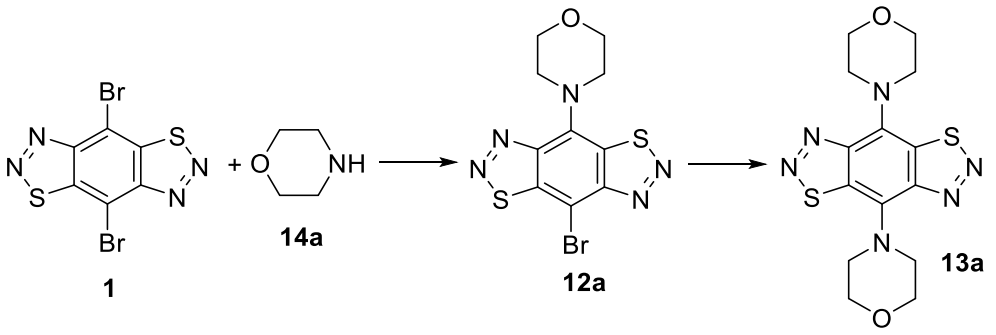

Entry	Morpholine (Eqv.)	Solvent	Temp. (°C)	Time (h)	Yields (%)	
					12a	13a
1	2	DCM	25	6	15	0
2	4	DCM	25	6	16	0
3	2	MeCN	25	8	20	0
4	4	MeCN	25	8	22	0
5	2	DMF	25	8	55	0
6	4	DMF	25	8	57	0
7	2	MeCN	80	18	78	0
8	2	DMF	80	12	70	0
9	6	DMF	130	24	0	40

We applied the conditions found for nucleophilic substitution reactions to other primary and secondary amines. Piperidine **14b** was found to react similarly to morpholine, forming mono-**12b** and bis-**13b** derivatives with moderate yields (Table 3, entries 1 and 2). A somewhat unexpected result was obtained for pyrrolidine **14c**, which was converted into a mono-derivative **12c** both when carrying out the reaction in acetonitrile and when heated at 130 °C in DMF; in the second case, the yield of the mono-product **12c** decreased, apparently due to its partial decomposition at elevated temperatures (Entries 3,4). With the cyclopentaindoline derivative **14d** and aniline **14e**, dibromide **1** reacted when heated to 100–130 °C in DMF with an excess of amine, to form only mono-substitution products **12d**,**e** in moderate yields (Entries 6–9). However, with more basic aliphatic primary amines, such as cyclohexylamine **14f** and *tert*-butylamine **14g**, no nucleophilic aromatic substitution reaction products were isolated, and only the partial decomposition of the starting dibromide **1** occurred when heated to 100–130 °C in DMF (Entries 10–16). When mono-adduct **12a** and cyclohexylamine were heated in DMF at 130 °C, the latter decomposed within 12 h to form a mixture of products, from which it was not possible to isolate identifiable compounds.

It was shown that carbazole and diphenylamine did not react with 4,8-dibromobenzo[1,2-*d*:4,5-*d'*]bis([1,2,3]thiadiazole) **1** under the studied conditions. Our attempts to carry out reactions using sodium salts of these amines (obtained in situ from carbazole or diphenylamine and NaH) were also unsuccessful—dibromide **1** decomposed when reacted with sodium carbazolate or sodium diphenylamide in THF or DMF for 3 h, and heated at a temperature of 60 °C.

Thus, we have successfully developed effective methods for introducing aromatic and aliphatic amines into the 4,8-dibromobenzo[1,2-*d*:4,5-*d'*]bis([1,2,3]thiadiazole) molecule **1** with the selective formation of mono-**12** and bis-**13** substitution products (Supplementary Materials). Nucleophilic aromatic substitution reactions under mild conditions led to the formation of the mono-substitution product **12**. The introduction of a donor fragment into the dibromide molecule leads to a decrease in the reactivity of position 4 or 7 of the benzene ring. Therefore, to replace the second bromine atom, it is necessary to apply severe conditions, namely, to heat the reaction mixture in DMF to 130 °C.

Table 3. The nucleophilic substitution of 4,8-dibromobenzo[1,2-*d*:4,5-*d'*]bis([1,2,3]thiadiazole) **1** with aromatic and aliphatic amines.

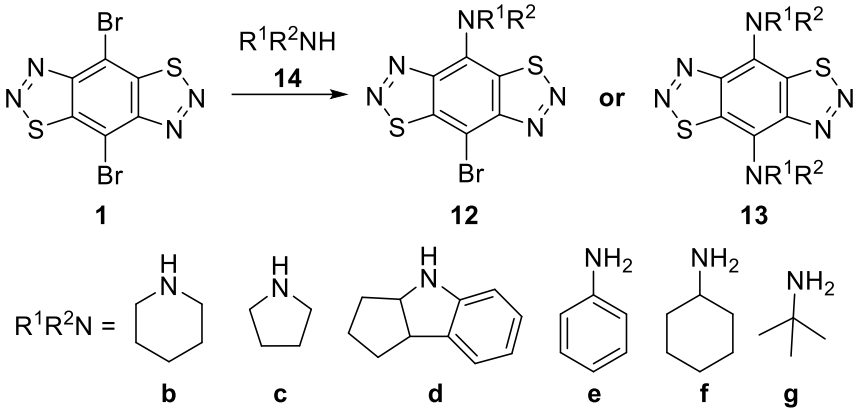

Entry	Amine (Eqv.)	Solvent	Temp. (°C)	Time (h)	Yields (%)	
					12	**13**
1	**14b** (2)	MeCN	80	18	**12b** (70)	0
2	**14b** (6)	DMF	130	24	0	**13b** (50)
3	**14c** (2)	MeCN	80	18	**12c** (72)	0
4	**14c** (6)	DMF	130	24	**12c** (65)	0
5	**14d** (2)	MeCN	80	18	0	0
6	**14d** (2)	DMF	130	18	**12d** (60)	0
7	**14d** (6)	DMF	130	24	**12d** (55)	0
8	**14e** (2)	MeCN	80	18	0	0
9	**14e** (2)	DMF	100	18	**12e** (55)	0
10	**14f** (2)	$CHCl_3$	61	18	0	0
11	**14f** (2)	MeCN	80	18	0	0
12	**14f** (2)	DMF	100	18	0	0
13	**14f** (6)	DMF	130	24	0	0
14	**14g** (2)	$CHCl_3$	61	18	0	0
15	**14g** (2)	MeCN	80	18	0	0
16	**14g** (2)	DMF	100	18	0	0

The reactions of 4,8-dibromobenzo[1,2-*d*:4,5-*d'*]bis([1,2,3]thiadiazole) **1** with such *S*-nucleophiles as thiophenol, hexylthiol, and dodecanethiol were studied. It was shown that when dibromide **1** was treated with thiophenol at room temperature in THF or DMF, the formation of only trace amounts of dimercapto derivative **15a** was observed, even when using less than a two-fold equivalent of thiol (Table 4, entries 1,2). The use of one equivalent of base and thiophenol resulted in a mixture of disubstituted derivative **15a** and starting dibromide **1**, and our attempts to isolate the mono-substituted derivative were unsuccessful. The reaction with two equivalents of sodium thiophenolate led to an increase in the yield of bis(phenylthio) derivative **15a** to 80% (Entry 3). The optimal conditions for the preparation of **15a** were extended to hexanethiol and dodecanothiol, which resulted in the preparation of bis-thiols **15b**,**c** in high yields (Supplementary Materials).

Dibromo derivative **1** proved to be sufficiently resistant to hydrolysis. Our study of the reaction of dibromide with various *O*-nucleophiles, such as alcohols (water, methanol, ethanol, *n*-butanol, *tert*-butanol, phenol) and corresponding alcoholates, showed that 4,8-dibromobenzo[1,2-*d*:4,5-*d'*]bis([1,2,3]thiadiazole) **1** did not react with them in both THF and DMF. The heating of the reaction mixtures also did not lead to the nucleophilic substitution of bromine atoms, and starting compound **1** was isolated in all cases.

Table 4. Reaction of 4,8-dibromobenzo[1,2-*d*:4,5-*d'*]bis([1,2,3]thiadiazole) **1** with *S*-nucleophiles.

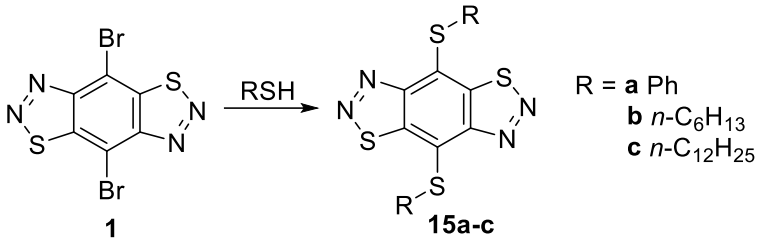

1 **15a-c**

Entry	RSH (Equiv.)	Solvent	Base (Equiv.)	Time (h)	Yield (%)
1	**a** (2)	THF	-	4	**15a** (5) *
2	**a** (2)	DMF	-	1	**15a** (8) *
3	**a** (2)	THF	NaH (2)	6	**15a** (80)
4	**b** (2)	THF	NaH (2)	6	**15b** (78)
5	**c** (2)	THF	NaH (2)	6	**15c** (75)

* Dibromide **1** was isolated in 51–53% yields.

2.3. Cross-Coupling Reactions of 4,8-Dibromobenzo[1,2-d:4,5-d']bis([1,2,3]thiadiazole) **1**

4,8-Dibromobenzo[1,2-*d*:4,5-*d'*]bis([1,2,3]thiadiazole) **1** was investigated in palladium-catalyzed Suzuki–Miyaura and Stille coupling reactions in order to obtain mono- and bis-aryl(hetaryl)thiadiazolopyridazines. The mono-arylation of dibromo derivatives of strong electron-deficient heterocycles is the most challenging task, and requires special attention to achieve the best yields [15,19,25].

2.3.1. Suzuki–Miyaura Coupling

The behavior of 4,8-dibromobenzo[1,2-*d*:4,5-*d'*]bis([1,2,3]thiadiazole) **1** in the palladium-catalyzed Suzuki–Miyaura coupling reactions was investigated in order to find the best conditions for the preparation of mono- and bis-aryl derivatives. In the reaction of dibromo derivative **1** with thiophen-2-yl-pinacolate ester **16a** and boronic acid **17a**, the base, solvent, and reaction temperature were varied. The results of this study are summarized in Table 5. We have shown that the nature of the reagents, solvents, and the temperature of the reaction medium significantly affect the course of chemical transformations. The tetrakis(triphenylphosphine)palladium complex ($Pd(PPh_3)_4$) most widely used in these transformations was employed as a catalyst. It was shown that when the reaction with pinacolate ester **16a** (1 eqv) was carried out at 110 °C in toluene for 24 h, the formation of the mono-coupling product **18a** was observed in 72% yield (Table 6, entry 1). The presence of water to dissolve inorganic salts reduced the yield of product **18a** to 50%, which is apparently associated to side reactions (Entry 2). We have shown that when using 2-thiopheneboronic acid **17a**, the mono-coupling product **18a** was isolated in almost the same yield (70%) as thiophen-2-pinacolate ester **16a** (cf. entries 1, 3). Since the use of 2-thiopheneboronic acid **17a** did not lead to an increase in the yield of the target product **18a**, and also because to the lower stability of 2-thiopheneboronic acids **17**, pinacolate esters of boronic acids **16** were employed in further studies. Carrying out the reaction in xylene at 130 °C with two eqv. of pinacolate ester **16a** resulted in the bis-coupling product **19a** with a 65% yield (Entry 4). The best conditions for the synthesis of mono-**18a** and bis-**19a** products were extended to other pinacolate esters **16b**–**h**. In all cases, mono-coupling products **18b**–**h** and bis-products **19b**–**h** were selectively formed by refluxing the reaction mixtures in toluene with one eqv. **16** (**18b**–**h**) or in xylene with two eqv. **17** (**19b**–**h**) in moderate yields (50–72%) (Entries 5–18).

Table 5. Suzuki–Miyaura cross-coupling of 4,8-dibromobenzo[1,2-*d*:4,5-*d'*]bis([1,2,3]thiadiazole) **1** with pinacolate esters **16a**–**h** and boronic acid **17a**.

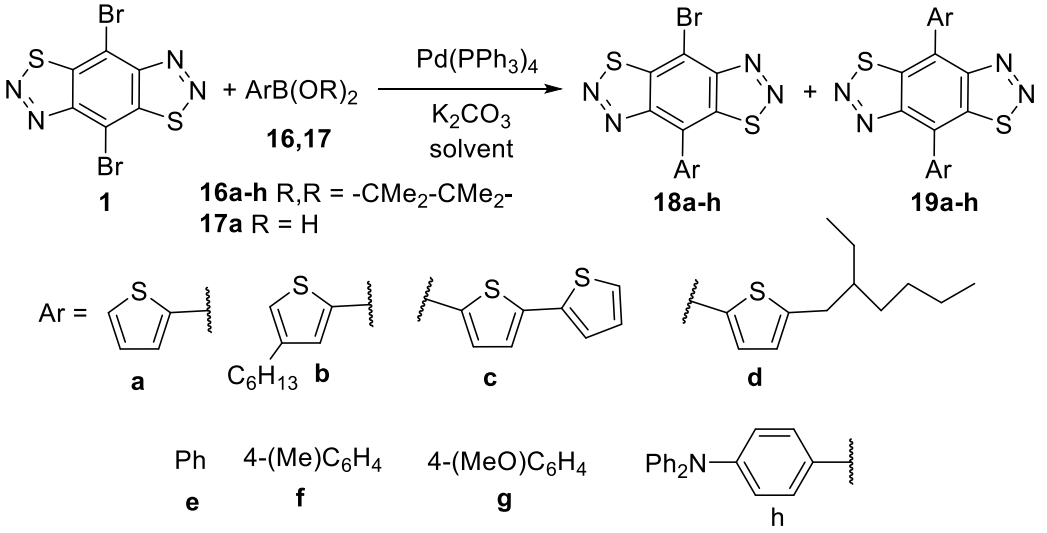

Entry	$B(OR)_2$ (Equiv)	Solvent	Conditions	Yields (%)	
				18	**19**
1	**16a** (1)	toluene	110 °C, 18 h	72	0
2	**16a** (1)	toluene/H_2O	110 °C, 20 h	50	0
3	**17a** (1)	toluene	110 °C, 18 h	70	0
4	**16a** (2)	xylene	130 °C, 24 h	0	65
5	**16b** (1)	toluene	110 °C, 18 h	70	0
6	**16b** (2)	xylene	130 °C, 24 h	0	63
7	**16c** (1)	toluene	110 °C, 18 h	65	0
8	**16c** (2)	xylene	130 °C, 24 h	0	50
9	**16d** (1)	toluene	110 °C, 18 h	68	0
10	**16d** (2)	xylene	130 °C, 24 h	68	0
11	**16e** (1)	toluene	110 °C, 18 h	70	0
12	**16e** (2)	xylene	130 °C, 24 h	0	50
13	**16f** (1)	toluene	110 °C, 18 h	67	0
14	**16f** (2)	xylene	130 °C, 24 h	0	55
15	**16g** (1)	toluene	110 °C, 18 h	60	0
16	**16g** (2)	xylene	130 °C, 24 h	0	65
17	**16h** (1)	toluene	110 °C, 18 h	72	0
18	**16h** (2)	xylene	130 °C, 24 h	0	67

Thus, it was found that the Suzuki reaction between 4,8-dibromobenzo[1,2-*d*:4,5-*d'*]bis([1,2,3]thiadiazole) **1** and pinacolate esters **16** requires the use of anhydrous solvents, and mono-**18** and bis-**19** coupling products can be selectively obtained by changing the reaction temperature (Supplementary Materials).

2.3.2. Stille Coupling

We studied the Stille reaction of 4,8-dibromobenzo[1,2-*d*:4,5-*d'*]bis([1,2,3]thiadiazole) **1** with various aromatic and heteroaromatic stannyl derivatives **20a**–**h** to synthesize both mono- and bis-coupling products. Optimal conditions were developed for the reaction with thienyltributyl stannate **20a** in toluene in the presence of $PdCl_2(PPh_3)_2$ as the most widely used catalyst in these transformations. When refluxing in toluene, the reaction could not be stopped at the stage of the mono-aryl derivative's **18a** formation, even when one equivalent of stannate **20a** was used (Table 6, entry 1). By employing two equivalents of stannate **20a**, the bis-coupling product **19a** was isolated in high yields (Entry 2). Careful temperature control allowed us to find the best conditions for the synthesis of the mono-aryl derivative **18a** by heating the reaction mixture at 60 °C for 16 h, although we could not

avoid the formation of the bis-product in small amounts (Entry 3). An increase in the reaction temperature to 80 °C led to a decrease in the selectivity of the formation of the mono-coupling product **18a**, and a decrease in the reaction to 40 °C led to a decrease in the yield of the product **18a** (Entries 4,5). The conditions found for the formation of bis-**19a** and mono-**18a** adducts (Entries 2,3) were applied to other aryl(hetaryl) stannates **20**. As a result, a series of mono- **18a**–**h** and bis-substitution products **19a**–**h** were isolated in moderate to high yields (Entries 6–19).

Table 6. Stille cross-coupling of 4,8-dibromobenzo[1,2-*d*:4,5-*d'*]bis([1,2,3]thiadiazole) **1** with aryl- and heteroaryl-tributylstannanes **20a**.

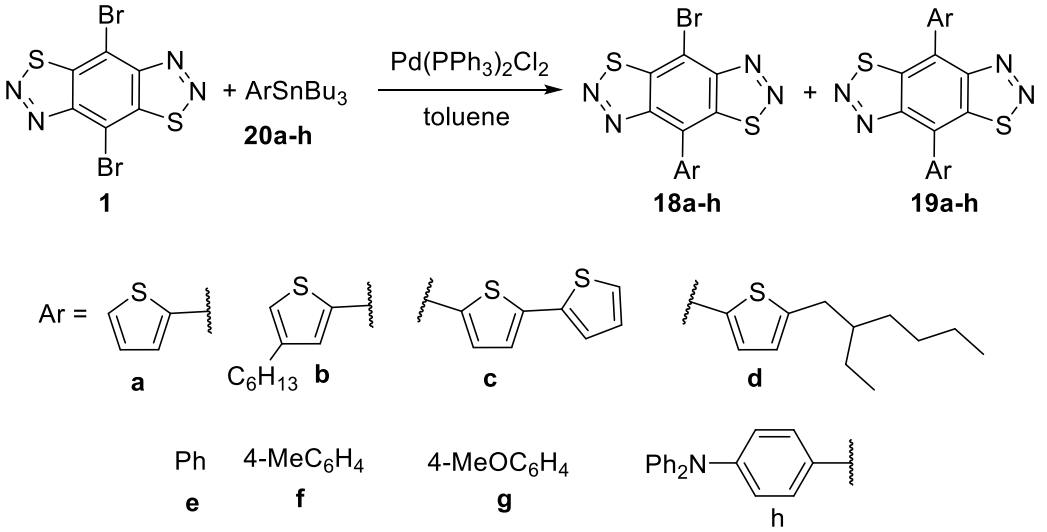

Entry	$ArSnBu_3$ (Equiv.)	Solvent	Temp., °C	Time, h	Yields, %	
					18	**19**
1	**20a** (1)	toluene	110	14	0	35
2	**20a** (2)	toluene	110	14	0	67
3	**20a** (1)	toluene	60	16	70	3
4	**20a** (1)	toluene	80	16	55	15
5	**20a** (1)	toluene	40	16	58	0
6	**20b** (1)	toluene	60	16	73	5
7	**20b** (2)	toluene	110	14	0	64
8	**20c** (1)	toluene	60	16	67	4
9	**20c** (2)	toluene	110	14	0	57
10	**20d** (1)	toluene	60	16	69	6
11	**20d** (2)	toluene	110	14	0	72
12	**20e** (1)	toluene	60	16	68	7
13	**20e** (2)	toluene	110	14	0	65
14	**20f** (1)	toluene	60	16	68	8
15	**20f** (2)	toluene	110	14	0	65
16	**20g** (1)	toluene	60	16	50	3
17	**20g** (2)	toluene	110	14	0	55
18	**20h** (1)	toluene	60	16	64	7
19	**20h** (2)	toluene	110	14	0	69

Thus, we have shown that the Stille reactions, compared with the Suzuki reactions, proceeded faster and with similar yields, but less selectively in the case of the formation of mono-coupling products **18**.

3. Experimental Section

3.1. Materials and Reagents

The chemicals were purchased from commercial sources (Sigma-Aldrich, St. Louis, MO, USA) and used as received. Benzo[1,2-*d*:4,5-*d'*]bis([1,2,3]thiadiazole) **2** [27], 4,4,5,5-tetramethyl-2-(thiophen-2-yl)-1,3,2-dioxaborolane **16a** [33], 2-(4-hexylthiophen-2-yl)-4,4,5,5-tetramethyl-1,3,2-dioxaborolane **16b** [34], 2-([2,2′-bithiophen]-5-yl)-4,4,5,5-tetramethyl-1,3,2-dioxaborolane **16c** [35], (4-(diphenylamino)phenyl)boronic acid **17h** [36], tributyl(4-hexyl-2-thienyl)stannane **20b** [37], [2,2′-bithiophen]-5-yltributylstannane **20c** [38], tributyl(5-(2-ethylhexyl)thiophen-2-yl)stannane **20d** [39], tributyl(*p*-tolyl)stannane **20f** [40], tributyl(4-methoxyphenyl)stannane **20g** [40], and diphenyl-(4-tributylstannanyl-phenyl)-amine **20h** [41] were prepared according to the published methods and characterized by NMR spectra. All synthetic operations were performed under a dry argon atmosphere. The solvents were purified by distillation over the appropriate drying agents.

3.2. Analytical Instruments

The melting points were determined on a Kofler hot-stage apparatus and were uncorrected. ^{1}H and ^{13}C NMR spectra were taken with a Bruker AM-300 machine (Bruker Ltd., Moscow, Russia) with TMS as the standard. *J* values are given in Hz. MS spectra (EI, 70 eV) were obtained with a Finnigan MAT INCOS 50 instrument (Thermo Finnigan LLC, San Jose, CA, USA). High-resolution MS spectra were measured on a Bruker micrOTOF II instrument using electrospray ionization (ESI). IR spectra were measured with a Bruker "Alpha-T" instrument (Bruker, Billerica, MA, USA) in KBr pellets. The HOMO–LUMO energies were calculated using the Gaussian 16 Rev C.01 program M11 DFT functional with a 6–31+g(d) basis.

3.3. X-ray Analysis

X-ray diffraction data were collected at 100 K on a four-circle Rigaku Synergy S diffractometer equipped with a HyPix600HE area-detector (kappa geometry, shutterless ω-scan technique), using graphite mono-chromatized Cu K_α-radiation. The intensity data were integrated and corrected for absorption and decay by the CrysAlisPro program (Austin, TX, USA, accessed on 1 September 2022) [42]. The structure was solved by direct methods using SHELXT and refined on F^2 using SHELXL-2018 [43] in the OLEX2 program [44]. All non-hydrogen atoms were refined with individual anisotropic displacement parameters. All hydrogen atoms were placed in ideal calculated positions and refined as riding atoms with relative isotropic displacement parameters. A rotating group model was applied for methyl groups. The Cambridge Crystallographic Data Centre holds the supplementary crystallographic data for this paper (Table 7), No. CCDC 2210625 (compound **1**). These data can be obtained free of charge via http://www.ccdc.cam.ac.uk/conts/retrieving.html, accessed on 1 September 2022 (or from the CCDC, 12 Union Road, Cambridge CB2 1EZ, UK; Fax: +44-1223-336033; E-mail: deposit@ccdc.cam.ac.uk).

3.4. 4,8-Dibromobenzo[1,2-d:4,5-d']bis([1,2,3]thiadiazole) **1**

Bromine (2.5 mL, 48.55 mmol) was added dropwise to a solution of compound **2** (650 mg, 3.35 mmol) in HBr (18 mL) at 80 °C. The reaction mixture was stirred for 18 h at 120 °C, cooled to room temperature, poured onto ice, washed with $NaHSO_3$, extracted with EtOAc and dried over $MgSO_4$. The solvent was evaporated under reduced pressure. The residue was purified by column chromatography (silica gel Merck 60, CH_2Cl_2) to give the title compound **1**. Yield 471 mg (40%), yellow solid. Eluent—CH_2Cl_2/hexane, 1:2 (*v*/*v*). Mp > 250 °C. (R_f = 0.3, CH_2Cl_2). IR ν_{max} (KBr, cm^{-1}): 2925, 2853, 1300, 1287, 1191, 1160, 1082, 968, 890, 811, 547, 511. ^{13}C NMR (75 MHz, $CDCl_3$): δ 153.3, 143.4, 105.0. HRMS (ESI-MS), *m*/*z*: calcd for $C_6{}^{79}Br_2N_4S_2$ [M + Ag]$^+$, 456.6977, found, 456.6977. MS, *m*/*z* (%): 353 ([M + 1]$^+$, 60), 352 (M$^+$, 80), 351 ([M − 1]$^+$, 58), 296 (100), 217 (62), 173 (70), 149 (85), 136 (68), 92 (86), 68 (75), 44 (10), 28 (5).

Table 7. Crystal data and structural refinement for compound **1**.

	Compound 1
Empirical formula	$C_6Br_2N_4S_2$
Formula weight	352.04
Temperature	100.00(10) K
Wavelength	0.71073 Å
Crystal system	monoclinic
Space group	$P12_1/_{n1}$
Unit cell dimensions	a = 16.1779(4) Å
	b = 3.88730(10) Å
	c = 16.1804(4) Å $\alpha = 90^\circ$ $\beta = 119.312(3)^\circ$ $\gamma = 90^\circ$
Volume	887.28(4) $Å^3$
Z	4
Density (calculated)	2.635 Mg/m^3
Absorption coefficient	9.562 mm^{-1}
F(000)	664
Crystal size	$0.56 \times 0.3 \times 0.2$ mm^3
Theta range for data collection	2.492 to 26.996°
Index ranges	$-20 \leq h \leq 20$, $-4 \leq k \leq 4$, $-20 \leq l \leq 20$
Reflections collected	28,713
Independent reflections	1924 [R(int) = 0.0815]
Completeness to theta = 25.242°	99.9%
Absorption correction	Semi-empirical from equivalents
Max. and min. transmission	1.00000 and 0.12670
Refinement method	Full-matrix least-squares on F^2
Data/restraints/parameters	1924/0/92
Goodness-of-fit on F^2	1.054
Final R indices [I > 2sigma(I)]	R1 = 0.0399, wR2 = 0.1083
R indices (all data)	R1 = 0.0401, wR2 = 0.1086
Extinction coefficient	n/a
Largest diff. peak and hole	2.244 and −0.679 e.Å-3

3.5. General Procedure for the Preparation of Mono-Aminated Products **12a–c**

Amine **14a–c** (0.29 mmol) was added to a solution of 4,8-dibromobenzo[1,2-*d*:4,5-*d'*]bis([1,2,3]thiadiazole) **1** (50 mg, 0.14 mmol) in dry MeCN (10 mL) at room temperature and the mixture was stirred at reflux for 18 h, poured into water (20 mL) and extracted with CH_2Cl_2 (3×35 mL). The combined organic layers were washed with brine, dried over $MgSO_4$, filtered, and concentrated under reduced pressure. The crude product was purified by column chromatography (silica gel Merck 60).

3.5.1. 4-(8-Bromobenzo[1,2-*d*:4,5-*d'*]bis([1,2,3]thiadiazole)-4-yl)morpholine (**12a**)

Orange solid, 39 mg (78%), eluent—CH_2Cl_2/hexane, 2:1 (*v*/*v*). R_f = 0.1 (CH_2Cl_2:hexane, 1:1, (*v*/*v*)). Mp = 150–153 °C. IR ν_{max} (KBr, cm^{-1}): 2960, 2920, 2857, 1640, 1531, 1458, 1432, 1376, 1341, 1313, 1277, 1249, 1187, 1113, 1029, 984, 874, 815, 631, 511. ^{1}H NMR (300 MHz,

$CDCl_3$): δ 4.04–4.01 (m, 4H), 3.99–3.95 (m, 4H). ^{13}C NMR (75 MHz, $CDCl_3$): δ 157.5, 148.4, 145.9, 138.9, 131.2, 94.7, 67.4, 52.3. HRMS (ESI-TOF), m/z: calcd for $C_{10}H_9{}^{79}BrN_5OS_2$ $[M + H]^+$, 357.9426, found, 357.9417. MS (EI, 70 eV), m/z (I, %): 359 ($[M + 1]^+$, 12), 358 ($[M]^+$, 11), 331 (14), 245 (30), 149 (31), 43 (35), 28 (100).

3.5.2. 4-Bromo-8-(piperidin-1-yl)benzo[1,2-*d*:4,5-*d'*]bis([1,2,3]thiadiazole) (**12b**)

Orange solid, 37 mg (75%), eluent—CH_2Cl_2/hexane, 1:1 (v/v). R_f = 0.4 (CH_2Cl_2:hexane, 1:1, (v/v)). Mp = 143–145 °C. IR ν_{max} (KBr, cm^{-1}): 2936, 2846, 1641, 1531, 1442, 1376, 1344, 1315, 1264, 1238, 1188, 1153, 1099, 1019, 979, 890, 865, 847, 817, 603, 539. ^1H NMR (300 MHz, $CDCl_3$): δ 3.97–3.94 (m, 4H), 1.94–1.84 (m, 6H). ^{13}C NMR (75 MHz, $CDCl_3$): δ 157.5, 148.1, 145.9, 140.0, 131.0, 92.57, 53.5, 26.8, 24.4. HRMS (ESI-TOF), m/z: calcd for $C_{11}H_{10}{}^{79}BrN_5S_2$ $[M]^+$, 354.9556, found, 354.9563. MS (EI, 70 eV), m/z (I, %): 357 ($[M + 1]^+$, 5), 356 ($[M]^+$, 4), 329 (27), 317 (24), 212 (80), 105 (78), 77 (45), 55 (40), 41 (100), 28 (78).

3.5.3. 4-Bromo-8-(pyrrolidin-1-yl)benzo[1,2-*d*:4,5-*d'*]bis([1,2,3]thiadiazole) (**12c**)

Orange solid, 36 mg (77%), eluent—CH_2Cl_2/hexane, 1:2 (v/v). R_f = 0.3 (CH_2Cl_2:hexane, 1:1, (v/v)). Mp = 153–155 °C. IR ν_{max} (KBr, cm^{-1}): 2955, 2921, 1854, 1638, 1540, 1447, 1373, 1354, 1323, 1303, 1260, 1236, 1177, 1119, 991, 893, 870, 816, 739, 667, 515. ^1H NMR (300 MHz, $CDCl_3$): δ 4.30 (t, J = 6.5, 4H), 2.23–2.19 (m, 4H). ^{13}C NMR (75 MHz, $CDCl_3$): δ 157.6, 146.6, 144.7, 138.3, 127.1, 87.0, 53.8, 29.8. HRMS (ESI-TOF), m/z: calcd for $C_{10}H_9{}^{79}BrN_5S_2$ $[M + H]^+$, 341.9477, found, 341.9475. MS (EI, 70 eV), m/z (I, %): 344 ($[M + 2]^+$, 3), 343 ($[M + 1]^+$, 50), 342 (M^+, 4), 341 ($[M - 1]^+$, 46), 315 (55), 285 (25), 256 (23), 206 (40), 191 (35), 178 (37), 149 (86), 96 (48), 69 (50), 57 (100), 41 (95), 27 (47), 18 (84).

3.6. General Procedure for the Preparation of Mono-Aminated Products **12d**,**e**

Aniline **14d**, **14e** (27 mg, 0.29 mmol) was added to a solution of 4,8-dibromobenzo[1,2-*d*:4,5-*d'*]bis([1,2,3]thiadiazole) **2** (50 mg, 0.14 mmol) in dry DMF (10 mL), and the mixture was stirred at 100–130 °C for 18 h, poured into water and extracted with CH_2Cl_2 (3 × 35 mL). The combined organic layers were washed with water and brine, dried over $MgSO_4$, filtered, and concentrated under reduced pressure. The crude product was purified by column chromatography (silica gel Merck 60).

3.6.1. 4-Bromo-8-(2,3,3*a*,8*b*-tetrahydrocyclopenta[*b*]indol-4(1*H*)-yl)benzo[1,2-*d*:4,5-*d'*] bis([1,2,3]thiadiazole) (**12d**)

Violet solid, yield 36 mg (60%), eluent—CH_2Cl_2/hexane, 1:2 (v/v)). R_f = 0.4 (CH_2Cl_2/hexane, 1:1 (v/v)). Mp = 178–180 °C. IR ν_{max} (KBr, cm^{-1}): 2957, 2924, 2853, 1597, 1523, 1480, 1444, 1366, 1306, 1259, 1187, 1080, 1023, 968, 881, 813, 749, 695, 535, 523. ^1H NMR (300 MHz, $CDCl_3$): δ 7.32–7.26 (m, 2H), 7.11 (t, J = 7.7, 1H), 6.99 (t, J = 7.4, 1H), 6.36–6.30 (m, 1H), 4.03–3.97 (m, 1H), 2.12–1.94 (m, 2H), 1.74–1.45 (m, 4H). ^{13}C NMR (75 MHz, $CDCl_3$): δ 157.7, 150.5, 145.3, 144.5, 136.4, 126.8, 125.6, 124.5, 124.1, 122.2, 111.0, 97.6, 72.8, 46.8, 35.2, 33.7, 24.8. HRMS (ESI-TOF), m/z: calcd for $C_{17}H_{12}{}^{79}BrN_5S_2$ $[M]^+$, 428.9712, found, 428.9708. MS (EI, 70 eV), m/z (I, %): 432 ($[M + 2]^+$, 4), 431 ($[M + 1]^+$, 39), 430 (M^+, 3), 429 ($[M - 1]^+$, 41), 403 (58), 375 (26), 346 (53), 147 (30), 115 (28), 67 (50), 57 (47), 41 (100), 27 (80).

3.6.2. 8-Bromo-*N*-phenylbenzo[1,2-*d*:4,5-*d'*]bis([1,2,3]thiadiazole)-4-amine (**12e**)

Red solid, yield 50 mg (55%), eluent—CH_2Cl_2/hexane, 1:1 (v/v)). R_f = 0.3 (CH_2Cl_2/hexane, 1:1 (v/v)). Mp = 157–160 °C. IR ν_{max} (KBr, cm^{-1}): 2958, 2924, 2853, 1729, 1548, 1495, 1465, 1450, 1425, 1323, 1287, 1262, 1099, 1078, 1022, 967, 868, 810, 743, 717, 696, 533. ^1H NMR (300 MHz, $CDCl_3$): δ 8.28 (s, 1H), 7.56–7.50 (m, 3H), 7.32 (dd, J = 7.5, 1.5, 2H). ^{13}C NMR (75 MHz, $CDCl_3$): δ 158.3, 144.8, 144.4, 136.6, 134.1, 129.8, 128.2, 127.0, 123.4, 91.3. HRMS (ESI-TOF), m/z: calcd for $C_{12}H_7{}^{79}BrN_5S_2$ $[M + H]^+$, 363.9321, found, 363.9321. MS (EI, 70 eV), m/z (I, %): 364 ($[M]^+$, 4), 363 ($[M - 1]^+$, 3), 337 (20), 228 (40), 184 (45), 149 (20), 125 (35), 77 (98), 51 (100), 28 (23).

3.7. General Procedure for the Preparation of Bis-Aminated Products **13a**,**b**

Amine **14** (0.84 mmol) was added to a solution of 4,8-dibromobenzo[1,2-*d*:4,5-*d'*]bis([1,2,3]thiadiazole) **1** (50 mg, 0.14 mmol) in dry DMF (10 mL) at room temperature and the mixture was stirred at 130 °C for 24 h, poured into water (20 mL) and extracted with CH_2Cl_2 (3 × 35 mL). The combined organic layers were washed with brine, dried over $MgSO_4$, filtered, and concentrated under reduced pressure. The crude product was purified by column chromatography (silica gel Merck 60).

3.7.1. 4,8-Dimorpholinobenzo[1,2-*d*:4,5-*d'*]bis([1,2,3]thiadiazole) (**13a**)

Red solid, 20 mg (40%), eluent—CH_2Cl_2. R_f = 0.1 (CH_2Cl_2). Mp > 250 °C. IR ν_{max} (KBr, cm^{-1}): 2968, 2947, 2918, 2849, 1827, 1637, 1539, 1480, 1442, 1371, 1327, 1298, 1272, 1251, 1108, 1068, 992, 922, 887, 824, 632, 514. ^{1}H NMR (300 MHz, $CDCl_3$): δ 4.01–3.98 (m, 8H), 3.77–3.74 (m, 8H). ^{13}C NMR (75 MHz, $CDCl_3$): δ 153.0, 135.7, 133.2, 67.7, 52.6. HRMS (ESI-TOF), *m*/*z*: calcd for $C_{14}H_{16}N_6O_2S_2$ $[M]^+$, 364.0771, found, 364.0769. MS (EI, 70 eV), *m*/*z* (*I*, %): 364 ($[M]^+$, 12), 192 (20), 45 (21), 28 (100).

3.7.2. 4,8-Di(piperidin-1-yl)benzo[1,2-*d*:4,5-*d'*]bis([1,2,3]thiadiazole) (**13b**)

Red solid, 20 mg (50%), eluent—CH_2Cl_2/hexane, 1:2 (*v*/*v*). R_f = 0.6 (CH_2Cl_2:hexane, 1:1 (*v*/*v*)). Mp = 158–160 °C. IR ν_{max} (KBr, cm^{-1}): 2928, 2847, 2804, 1637, 1479, 1446, 1372, 1327, 1313, 1268, 1241, 1202, 1112, 1072, 1056, 1030, 982, 855, 823, 737, 701, 614, 515. ^{1}H NMR (300 MHz, $CDCl_3$): δ 3.68–3.64 (m, 8H), 1.87–1.73 (m, 12H). ^{13}C NMR (75 MHz, $CDCl_3$): δ 153.0, 135.8, 134.0, 53.7, 27.0, 24.5. HRMS (ESI-TOF), *m*/*z*: calcd for $C_{16}H_{20}N_6S_2$ $[M]^+$, 360.1185, found, 360.1183. MS (EI, 70 eV), *m*/*z* (*I*, %): 360 ($[M]^+$, 20), 303 (21), 275 (14), 247 (19), 219 (22), 192 (15), 96 (35), 55 (40), 41 (100), 29 (20).

3.8. General Procedure for the Reaction of 4,8-Dibromobenzo[1,2-d:4,5-d']Bis([1,2,3]Thiadiazole) **1** *with Thiols*

Sodium hydride (6 mg, 0.28 mmol) was added to a solution of thiol (0.28 mmol) in dry THF (15 mL) at 0 °C with stirring. The reaction mixture was stirred at 0 °C for 30 min, then 4,8-dibromobenzo[1,2-*d*:4,5-*d'*]bis([1,2,3]thiadiazole) **1** (50 mg, 0.14 mmol) was added. The mixture was stirred for 6 h at room temperature. On completion (monitored by TLC), the mixture was poured into water (20 mL) and extracted with CH_2Cl_2 (3 × 5 mL). The combined organic layers were washed with brine, dried over $MgSO_4$, filtered, and concentrated under reduced pressure. The crude product was purified by column chromatography.

3.8.1. 4,8-Bis(phenylthio)benzo[1,2-*d*:4,5-*d'*]bis([1,2,3]thiadiazole) (**15a**)

Orange solid, 45 mg (80%), Mp = 168–172 °C, eluent—CH_2Cl_2/hexane, 1:2 (*v*/*v*). R_f = 0.4 (CH_2Cl_2/hexane, 1:1 (*v*/*v*)). IR ν_{max} (KBr, cm^{-1}): 1574, 1492, 1468, 1438, 1397, 1371, 1310, 1265, 1231, 1155, 1065, 1020, 1000, 907, 815, 748, 688, 566, 500. ^{1}H NMR (300 MHz, $CDCl_3$): δ 7.66–7.58 (m, 4H), 7.54–7.40 (m, 6H). ^{13}C NMR (75 MHz, $CDCl_3$): δ 156.3, 141.4, 135.7, 135.0, 130.2, 130.0, 123.8. HRMS (ESI-TOF), *m*/*z*: calcd for $C_{18}H_{11}N_4S_4$ $[M + H]^+$, 410.9861, found, 410.9849. MS (EI, 70 eV), *m*/*z* (*I*, %): 410 ($[M]^+$, 100), 320 (80), 290 (35), 277 (37), 201 (15), 177 (16), 169 (13), 136 (13), 77 (50), 51 (15).

3.8.2. 4,8-Bis(hexylthio)benzo[1,2-*d*:4,5-*d'*]bis([1,2,3]thiadiazole) (**15b**)

Yellow solid, 46 mg (78%), eluent—CH_2Cl_2/hexane, 1:4 (*v*/*v*). R_f = 0.7 (CH_2Cl_2/hexane, 1:1 (*v*/*v*)). Mp = 78–80 °C. IR ν_{max} (KBr, cm^{-1}): 2957, 2924, 2853, 1637, 1461, 1412, 1375, 1315, 1280, 1239, 1179, 906, 811, 723, 515. ^{1}H NMR (300 MHz, $CDCl_3$): δ 3.62 (t, *J* = 7.4, 4H), 1.66 (p, *J* = 7.3, 4H), 1.48–1.39 (m, 4H), 1.27–1.21 (m, 8H), 0.84 (t, *J* = 7.0, 6H). ^{13}C NMR (75 MHz, $CDCl_3$): δ 155.7, 145.3, 122.5, 36.9, 31.2, 30.0, 28.2, 22.4, 13.9. HRMS (ESI-TOF), *m*/*z*: calcd for $C_{18}H_{27}N_4S_4$ $[M + H]^+$, 427.1113, found, 427.1108. MS (EI, 70 eV), *m*/*z* (*I*, %): 426 ($[M]^+$, 4), 314 (M^+, 3), 215 (4), 136 (5), 101 (7), 55 (25), 43 (100), 29 (95).

3.8.3. 4,8-Bis(dodecylthio)benzo[1,2-*d*:4,5-*d*′]bis([1,2,3]thiadiazole) (**15c**)

Yellow solid, 46 mg (78%), eluent—CH_2Cl_2/hexane, 1:2 (*v*/*v*). R_f = 0.9 (CH_2Cl_2). Mp = 78–80 °C. IR ν_{max} (KBr, cm^{-1}): 2955, 2922, 2851, 1642, 1469, 1414, 1375, 1312, 1262, 1238, 1177, 1084, 1026, 903, 806, 719, 517. ^{1}H NMR (300 MHz, $CDCl_3$): δ 3.62 (t, *J* = 7.3, 4H), 1.65 (p, *J* = 7.3, 4H), 1.47–1.38 (m, 4H), 1.32–1.21 (m, 32H), 0.87 (t, *J* = 6.6, 6H). ^{13}C NMR (75 MHz, $CDCl_3$): δ 155.7, 145.3, 122.5, 36.9, 31.9, 30.0, 29.7, 29.6, 29.58, 29.51, 29.4, 29.0, 28.5, 22.7, 14.1. HRMS (ESI-TOF), *m*/*z*: calcd for $C_{30}H_{50}N_4S_4Ag$ $[M]^+$, 701.1964, found, 701.1954. MS (EI, 70 eV), *m*/*z* (*I*, %): 595 ($[M]^+$, 12), 215 (8), 97 (3), 83 (5), 69 (18), 57 (50), 43 (100), 29 (35).

3.9. General Procedure for the Preparation of Mono-Substituted Products **18** *under Suzuki Coupling Conditions (Procedure A)*

A mixture of 4,8-dibromobenzo[1,2-*d*:4,5-*d*′]bis([1,2,3]thiadiazole) **1** (50 mg, 0.14 mmol), boronic ether **16a**–**h** or its acid **17a** (0.14 mmol), K_2CO_3 (19 mg, 0.14 mmol), and $Pd(PPh_3)_4$ (24 mg, 15% mmol) in dry toluene (8 mL) was degassed by argon and heated at 110 °C in a sealed vial. On completion (monitored by TLC), the mixture was poured into water and extracted with CH_2Cl_2 (3 × 35 mL). The combined organic layers were washed with brine, dried over $MgSO_4$, filtered, and concentrated under reduced pressure. The crude product was purified by column chromatography.

3.10. General Procedure for the Preparation of Bis-Substituted Products **19** *under Suzuki Coupling Conditions (Procedure B)*

A mixture of 4,8-dibromobenzo[1,2-*d*:4,5-*d*′]bis([1,2,3]thiadiazole) **1** (50 mg, 0.14 mmol), boronic ether **16a**–**h** or its acid **17a** (0.28 mmol), K_2CO_3 (38 mg, 0.28 mmol), and $Pd(PPh_3)_4$ (24 mg, 15% mmol) in dry xylene (8 mL) was degassed by argon and heated at 130 °C in a sealed vial. On completion (monitored by TLC), the mixture was poured into water and extracted with CH_2Cl_2 (3 × 35 mL). The combined organic layers were washed with brine, dried over $MgSO_4$, filtered, and concentrated under reduced pressure. The crude product was purified by column chromatography.

3.11. General Procedure for the Preparation of Mono-Substituted Products **18** *under Stille Coupling Conditions (Procedure C)*

$PdCl_2(PPh_3)_2$ (14 mg, 15% mmol) and stannane **20a**–**h** (0.14 mmol) were added to a solution of 4,8-dibromobenzo[1,2-*d*:4,5-*d*′]bis([1,2,3]thiadiazole) **1** (50 mg, 0.14 mmol) in anhydrous toluene (4 mL) The resulting cloudy yellow mixture was stirred and degassed by argon in a sealed vial. The resulting yellow mixture was then stirred at 60 °C for the desired time. On completion (monitored by TLC), the mixture was washed with water and the organic layer was extracted with CH_2Cl_2 (3 × 35 mL), dried over $MgSO_4$ and then concentrated in vacuo. The products were isolated by column chromatography.

3.12. General Procedure for the Preparation of Bis-Substituted Products **19** *under Stille Coupling Conditions (Procedure D)*

$PdCl_2(PPh_3)_2$ (14 mg, 15% mmol) and stannane **20a**–**h** (0.28 mmol) were added to a solution of 4,8-dibromobenzo[1,2-*d*:4,5-*d*′]bis([1,2,3]thiadiazole) **1** (50 mg, 0.14 mmol) in anhydrous toluene (4 mL) The resulting cloudy yellow mixture was stirred and degassed by argon in a sealed vial. The resulting yellow mixture was then stirred at 110 °C for the desired time. On completion (monitored by TLC), the mixture was washed with water and the organic layer was extracted with CH_2Cl_2 (3 × 35 mL), dried over $MgSO_4$ and then concentrated in vacuo. The products were isolated by column chromatography.

3.12.1. 4-Bromo-8-(thiophen-2-yl)benzo[1,2-*d*:4,5-*d*′]bis([1,2,3]thiadiazole) (**18a**)

Yellow solid, 35 mg (72%, procedure A) or 34 mg (70%, procedure C), eluent—CH_2Cl_2:hexane, 1:1 (*v*/*v*).R_f = 0.4 (CH_2Cl_2). Mp = 198–200 °C. IR ν_{max} (KBr, cm^{-1}): 1738, 1641, 1494, 1464, 1413, 1262, 1186, 1081, 1023, 809, 701, 544. ^{1}H NMR (300 MHz, $CDCl_3$): *δ* 8.20 (d, *J* = 3.9, 1H), 7.76 (d, *J* = 5.2, 1H), 7.36 (t, *J* = 4.5, 1H). ^{13}C NMR (75 MHz, $CDCl_3$): *δ* 156.1, 152.2, 139.32, 139.1, 137.0, 131.7, 130.8, 128.8, 122.4, 104.4. HRMS (ESI-TOF), *m*/*z*:

calcd for $C_{10}H_4{}^{79}BrN_4S_3$ $[M + H]^+$, 354.8776, found, 354.8772. MS (EI, 70 eV), m/z (I, %): 356 ($[M + 2]^+$, 2), 355 ($[M + 1]^+$, 31), 354 ($[M]^+$, 35), 353 ($[M - 1]^+$, 6), 328 (100), 298 (10), 247 (40), 219 (35), 175 (42), 151 (75), 117 (13), 93 (32), 69 (20), 45 (22).

3.12.2. 4-Bromo-8-(4-hexylthiophen-2-yl)benzo[1,2-*d*:4,5-*d*′]bis([1,2,3]thiadiazole) (**18b**)

Yellow solid, 43 mg (70%, procedure A) or 44 mg (73%, procedure C), eluent—CH_2Cl_2:hexane, 1:2 (v/v). R_f = 0.6 (CH_2Cl_2:hexane, 1:1). Mp = 67–69 °C. IR ν_{max} (KBr, cm^{-1}): 2954, 2924, 2852, 1642, 1449, 1397, 1371, 1327, 1306, 1263, 1237, 1109, 1089, 892, 812, 727, 581, 537. ^{1}H NMR (300 MHz, $CDCl_3$): δ 8.09 (s, 1H), 7.35 (s, 1H), 2.76 (t, J = 7.7, 2H), 1.73 (p, J = 7.2, 2H), 1.42–1.31 (m, 6H), 0.91 (t, J = 6.9, 3H). ^{13}C NMR (75 MHz, $CDCl_3$): δ 155.9, 152.0, 145.4, 144.7, 138.8, 136.4, 133.3, 125.6, 122.5, 103.8, 31.6, 30.5, 30.4, 28.9, 22.6, 14.1. HRMS (ESI-TOF), m/z: calcd for $C_{16}H_{16}{}^{79}BrN_4S_3$ $[M + H]^+$, 438.9715, found, 438.9730. MS (EI, 70 eV), m/z (I, %): 440 ($[M + 1]^+$, 3), 439 ($[M]^+$, 2), 412 (3), 355 (2), 312 (2), 235 (7), 164 (8), 125 (11), 111 (15), 97 (50), 83 (52), 69 (60), 57 (98), 43 (100), 29 (75).

3.12.3. 4-([2,2′-Bithiophen]-5-yl)-8-bromobenzo[1,2-*d*:4,5-*d*′]bis([1,2,3]thiadiazole) (**18c**)

Red solid, 39 mg (65%, procedure A) or 41 mg (67%, procedure C), eluent—CH_2Cl_2:hexane, 1:1 (v/v). R_f = 0.4 (CH_2Cl_2:hexane, 1:1 (v/v)). Mp = 130–132 °C. IR ν_{max} (KBr, cm^{-1}): 1639, 1445, 1423, 1375, 1308, 1268, 1123, 892, 812, 689, 537. ^{1}H NMR (300 MHz, $CDCl_3$): δ 8.09 (d, J = 4.0, 1H), 7.40–7.34 (m, 3H), 7.14–7.07 (m, 1H). ^{13}C NMR (75 MHz, $CDCl_3$): δ 156.3, 151.9, 144.9, 143.5, 138.4, 136.2, 135.2, 132.6, 128.4, 126.3, 125.4, 125.0, 122.0, 103.9. HRMS (ESI-TOF), m/z: calcd for $C_{14}H_6{}^{79}BrN_4S_4$ $[M + H]^+$, 436.8653, found, 436.8642. MS (EI, 70 eV), m/z (I, %): 439 ($[M + 2]^+$, 5), 438 ($[M]^+$, 43), 437 ($[M]^+$, 4), 436 ($[M - 1]$, 39), 410 (37), 382 (10), 329 (52), 301 (20), 257 (62), 233 (71), 225 (20), 149 (60), 127 (55), 117 (53), 93 (70), 69 (100), 45 (95).

3.12.4. 4-Bromo-8-(5-(2-ethylhexyl)thiophen-2-yl)benzo[1,2-*d*:4,5-*d*′]bis([1,2,3]thiadiazole) (**18d**)

Yellow solid, 44 mg (68%, procedure A) or 45 mg (69%, procedure C), eluent—CH_2Cl_2:hexane, 1:1 (v/v). R_f = 0.6 (CH_2Cl_2). Mp = 57–60 °C. IR ν_{max} (KBr, cm^{-1}): 2955, 2922, 2853, 1639, 1455, 1421, 1376, 1307, 1266, 1213, 1104, 892, 813, 544. ^{1}H NMR (300 MHz, $CDCl_3$): δ 8.06 (d, J = 3.8, 1H), 7.01 (d, J = 3.8, 1H), 2.90 (d, J = 6.8, 2H), 1.77–1.69 (m, 1H), 1.45–1.31 (m, 8H), 0.97–0.89 (m, 6H). ^{13}C NMR (75 MHz, $CDCl_3$): δ 156.0, 151.8, 151.6, 144.7, 138.3, 134.4, 131.8, 126.9, 122.7, 103.1, 41.5, 34.4, 32.4, 29.7, 25.6, 23.0, 14.1, 10.8. HRMS (ESI-TOF), m/z: calcd for $C_{18}H_{20}{}^{79}BrN_4S_3$ $[M + H]^+$, 467.0028, found, 467.0019. MS (EI, 70 eV), m/z (I, %): 470 ($[M + 2]^+$, 1), 469 ($[M + 1]^+$, 2), 468 ($[M]^+$, 11), 467 ($[M - 1]^+$, 2), 466 ($[M - 2]^+$, 9), 440 (6), 369 (3), 341 (5), 326 (4), 232 (5), 188 (10), 105 (30), 83 (35), 71 (60), 57 (100), 43 (95), 29 (15).

3.12.5. 4-Bromo-8-phenylbenzo[1,2-*d*:4,5-*d*′]bis([1,2,3]thiadiazole) (**18e**)

Yellow solid, 34 mg (70%, procedure A) or 32 mg (67%, procedure C), eluent—CH_2Cl_2:hexane, 1:1 (v/v). R_f = 0.4 (CH_2Cl_2). Mp = 163–165 °C. IR ν_{max} (KBr, cm^{-1}): 1725, 1445, 1398, 1371, 1343, 1316, 1275, 1211, 1188, 1155, 1078, 1025, 924, 898, 823, 766, 698, 538. ^{1}H NMR (300 MHz, $CDCl_3$): δ 7.97–7.93 (m, 2H), 7.68–7.61 (m, 3H). ^{13}C NMR (75 MHz, $CDCl_3$): δ 155.8, 153.9, 144.6, 141.6, 136.3, 130.5, 129.5, 129.4, 128.9, 105.3. HRMS (ESI-TOF), m/z: calcd for $C_{12}H_6{}^{79}BrN_4S_2$ $[M + H]^+$, 348.9212, found, 348.9222. MS (EI, 70 eV), m/z (I, %): 350 ($[M+]^+$, 2), 349 ($[M]^+$, 1), 322 (20), 241 (50), 213 (18), 169 (96), 145 (100), 137 (15), 117 (18), 93 (35), 69 (45), 43 (30).

3.12.6. 4-Bromo-8-(*p*-tolyl)benzo[1,2-*d*:4,5-*d*′]bis([1,2,3]thiadiazole) (**18f**)

Yellow solid, 34 mg (67%, procedure A) or 35 mg (68%, procedure C), eluent—CH_2Cl_2:hexane, 1:1 (v/v). R_f = 0.5 (CH_2Cl_2). Mp = 135–137 °C. IR ν_{max} (KBr, cm^{-1}): 2958, 2924, 2854, 1729, 1493, 1461, 1401, 1385, 1283, 1187, 1081, 1023, 969, 894, 812, 723, 491. ^{1}H NMR (300 MHz, $CDCl_3$): δ 7.90 (d, J = 7.9, 2H), 7.46 (d, J = 7.9, 2H), 2.52 (s, 3H). ^{13}C

NMR (75 MHz, $CDCl_3$): δ 155.8, 153.8, 147.2, 144.6, 141.0, 133.4, 130.2, 129.4, 128.1, 104.8, 21.6. HRMS (ESI-TOF), m/z: calcd for $C_{13}H_8{}^{79}BrN_4S_2$ $[M + H]^+$, 362.9368, found, 362.9370. MS (EI, 70 eV), m/z (I, %): 363 ($[M]^+$, 3), 362 ($[M - 1]^+$, 1), 361 ($[M - 2]^+$, 5), 360 ($[M - 3]^+$, 5), 359 ($[M - 4]^+$, 2), 318 (98), 303 (15), 285 (16), 159 (98), 115 (97), 93 (50), 69 (85), 57 (100), 43 (96).

3.12.7. 4-Bromo-8-(4-methoxyphenyl)benzo[1,2-*d*:4,5-*d*′]bis([1,2,3]thiadiazole) (**18g**)

Yellow solid, 32 mg (60%, procedure A) or 26 mg (50%, procedure C), eluent—CH_2Cl_2:hexane, 1:1 (v/v). R_f = 0.2 (CH_2Cl_2). Mp = 125–127 °C. IR ν_{max} (KBr, cm^{-1}): 2957, 2925, 2854, 1641, 1609, 1502, 1460, 1429, 1376, 1301, 1264, 1179, 1081, 1029, 967, 885, 829, 815, 702, 614, 534. ^{1}H NMR (300 MHz, $CDCl_3$): δ 7.92 (d, J = 8.7, 2H), 7.16 (d, J = 8.7, 2H), 3.94 (s, 3H). ^{13}C NMR (75 MHz, $CDCl_3$): δ 161.3, 155.8, 153.8, 144.6, 141.3, 131.1, 128.9, 128.5, 114.9, 104.3, 55.6. HRMS (ESI-TOF), m/z: calcd for $C_{13}H_8{}^{79}BrN_4OS_2$ $[M + H]^+$, 378.9317, found, 378.9314. MS (EI, 70 eV), m/z (I, %): 380 ($[M + 1]^+$, 7), 379 ($[M]^+$, 5), 350 (20), 271 (80), 199 (90), 175 (100), 132 (55), 28 (9).

3.12.8. 4-(8-Bromobenzo[1,2-*d*:4,5-*d*′]bis([1,2,3]thiadiazole)-4-yl)-*N*,*N*-diphenylaniline (**18h**)

Red solid, 52 mg (72%, procedure A) or 46 mg (64%, procedure C), eluent—CH_2Cl_2:hexane, 1:2 (v/v). R_f = 0.5 (CH_2Cl_2:hexane, 1:1 (v/v)). Mp = 165–168 °C. IR ν_{max} (KBr, cm^{-1}): 1588, 1468, 1432, 1331, 1315, 1274, 1193, 1075, 1026, 814, 753, 695, 618, 512. ^{1}H NMR (300 MHz, $CDCl_3$): δ 7.83 (d, J = 8.7, 2H), 7.35 (t, J = 7.7, 4H), 7.24–7.08 (m, 8H). ^{13}C NMR (75 MHz, $CDCl_3$): δ 155.9, 153.7, 150.0, 146.8, 144.7, 141.0, 130.6, 129.7, 129.1, 128.4, 125.9, 124.5, 121.4, 103.8. HRMS (ESI-TOF), m/z: calcd for $C_{24}H_{14}{}^{79}BrN_5S_2$ $[M]^+$, 514.9869, found, 514.9874. MS (EI, 70 eV), m/z (I, %): 519 ($[M + 2]^+$, 5), 518 ($[M + 1]^+$, 10), 517 ($[M]^+$, 75), 516 ($[M - 1]^+$, 11), 515 ($[M - 2]^+$, 70), 489 (8), 459 (6), 408 (50), 380 (35), 336 (100), 312 (65), 167 (12), 149 (15), 77 (20), 51 (11).

3.12.9. 4,8-Di(thiophen-2-yl)benzo[1,2-*d*:4,5-*d*′]bis([1,2,3]thiadiazole) (**19a**)

Red solid, 32 mg (65%, procedure B) or 33 mg (67%, procedure D), eluent—CH_2Cl_2:hexane, 1:2 (v/v). R_f = 0.5 (CH_2Cl_2:hexane, 1:1 (v/v)). Mp > 250 °C. IR ν_{max} (KBr, cm^{-1}): 1637, 1513, 1442, 1412, 1376, 1341, 1315, 1267, 1064, 819, 797, 700, 549. ^{1}H NMR (300 MHz, $CDCl_3$): δ 8.20 (dd, J = 3.8, 1.2, 2H), 7.74 (dd, J = 5.1, 1.2, 2H), 7.37 (dd, J = 5.1, 3.8, 2H). ^{13}C NMR (75 MHz, $CDCl_3$): δ 154.1, 139.6, 137.7, 131.1, 130.2, 128.4, 120.2. HRMS (ESI-TOF), m/z: calcd for $C_{14}H_7N_4S_4$ $[M + H]^+$, 358.9548, found, 358.9544. MS (EI, 70 eV), m/z (I, %): 360 ($[M + 2]^+$, 21), 359 ($[M + 1]^+$, 22), 358 ($[M]^+$, 96), 330 (45), 302 (98), 270 (30), 226 (28), 151 (50), 69 (48), 57 (85), 43 (100), 29 (99), 17 (98).

3.12.10. 4,8-Bis(4-hexylthiophen-2-yl)benzo[1,2-*d*:4,5-*d*′]bis([1,2,3]thiadiazole) (**19b**)

Red solid, 46 mg (63%, procedure B) or 47 mg (57%, procedure D), eluent—CH_2Cl_2:hexane, 1:3 (v/v). R_f = 0.7 (CH_2Cl_2:hexane, 1:1 (v/v)). Mp = 134–136 °C. IR ν_{max} (KBr, cm^{-1}): 2961, 2928, 2851, 1645, 1461, 1180, 1071, 925, 761, 555, 459. ^{1}H NMR (300 MHz, $CDCl_3$): δ 8.09 (d, J = 1.3, 2H), 7.32 (d, J = 1.3, 2H), 2.77 (t, J = 7.7, 4H), 1.75 (p, J = 7.6, 4H), 1.45–1.33 (m, 12H), 0.94–0.89 (m, 6H). ^{13}C NMR (75 MHz, $CDCl_3$): δ 154.0, 145.0, 139.4, 137.4, 132.7, 125.0, 120.8, 31.6, 30.5, 30.4, 29.0, 22.6, 14.1. HRMS (ESI-TOF), m/z: calcd for $C_{26}H_{31}N_4S_4$ $[M + H]^+$, 527.1426, found, 527.1407. MS (EI, 70 eV), m/z (I, %): 528 ($[M + 2]^+$, 37), 527 ($[M + 1]^+$, 50), 526 ($[M]^+$, 98), 479 (11), 455 (40), 441 (93), 427 (30), 413 (42), 329 (25), 235 (40), 165 (98), 120 (70), 105 (99), 69 (96), 55 (99), 29 (100).

3.12.11. 4,8-Di([2,2′-bithiophen]-5-yl)benzo[1,2-*d*:4,5-*d*′]bis([1,2,3]thiadiazole) (**19c**)

Violet solid, 36 mg (50%, procedure B) or 471 mg (57%, procedure D), eluent—CH_2Cl_2:hexane, 1:2 (v/v). R_f = 0.5 (CH_2Cl_2:hexane, 1:1 (v/v)). Mp > 250 °C. IR ν_{max} (KBr, cm^{-1}): 1728, 1632, 1504, 1456, 1373, 1319, 1276, 1225, 1165, 1122, 1093, 1052, 824, 783, 701, 643, 548, 485. ^{1}H NMR (300 MHz, $CDCl_3$): δ 8.07 (d, J = 4.1 Hz, 2H), 7.39 (d, J = 4.1 Hz, 3H), 7.37 (d, J = 5.1 Hz, 2H), 7.12–7.09 (m, 3H). ^{13}C NMR (75 MHz, $CDCl_3$): δ 153.9, 142.7,

138.9, 136.4, 136.2, 131.9, 128.1, 125.8, 125.0, 124.7, 120.3. HRMS (ESI-TOF), *m*/*z*: calcd for $C_{22}H_{11}N_4S_6$ $[M]^+$, 522.9302, found, 522.9299. MS (EI, 70 eV), *m*/*z* (*I*, %): 524 ($[M + 2]^+$, 26), 523 ($[M + 1]^+$, 25), 522 ($[M]^+$, 100), 466 (90), 434 (35), 421 (32), 389 (30), 233 (80), 201 (50), 177 (45), 127 (30), 18 (60).

3.12.12. 4,8-Bis(5-(2-ethylhexyl)thiophen-2-yl)benzo[1,2-*d*:4,5-*d*′]bis([1,2,3]thiadiazole) (**19d**)

Red solid, 55 mg (68%, procedure B) or 58 mg (72%, procedure D), eluent—CH_2Cl_2:hexane, 1:4 (*v*/*v*). R_f = 0.7 (CH_2Cl_2:hexane). Mp = 78–80 °C. IR ν_{max} (KBr, cm^{-1}): 2957, 2924, 2855, 1664, 1376, 1313, 1272, 1245, 1139, 1088, 1013, 871, 816, 782, 703, 642, 545, 508. ^{1}H NMR (300 MHz, $CDCl_3$): δ 8.01 (d, *J* = 3.8, 2H), 7.00 (d, *J* = 3.8, 2H), 2.90 (d, *J* = 6.8, 4H), 1.73 (p, *J* = 5.9, 2H), 1.46–1.30 (m, 16H), 0.94–0.90 (m, 12H). ^{13}C NMR (75 MHz, $CDCl_3$): δ 153.7, 150.5, 138.6, 135.3, 131.1, 126.8, 120.3, 41.5, 34.4, 32.5, 28.9, 25.7, 23.0, 14.2, 10.9. HRMS (ESI-TOF), *m*/*z*: calcd for $C_{30}H_{39}N_4S_4$ $[M + H]^+$, 583.2052, found, 583.2045. MS (EI, 70 eV), *m*/*z* (*I*, %): 584 ($[M + 2]^+$, 4), 583 ($[M + 1]^+$, 6), 582 ($[M]^+$, 27), 525 (2), 497 (3), 483 (6), 427 (8), 343 (6), 328 (7), 252 (4), 177 (12), 164 (8), 121 (6), 57 (100), 41 (97), 29 (60).

3.12.13. 4,8-Diphenylbenzo[1,2-*d*:4,5-*d*′]bis([1,2,3]thiadiazole) (**19e**)

Yellow solid, 24 mg (50%, procedure B) or 31 mg (65%, procedure D), eluent—CH_2Cl_2: hexane, 1:2 (*v*/*v*). R_f = 0.5 (CH_2Cl_2:hexane, 1:1 (*v*/*v*)). Mp > 250 °C. IR ν_{max} (KBr, cm^{-1}): 1572, 1491, 1445, 1374, 1317, 1275, 1210, 1186, 1153, 1077, 1024, 978, 923, 898, 823, 766, 743, 696, 643, 539, 476. ^{1}H NMR (300 MHz, $CDCl_3$): δ 7 8.01 (d, *J* = 7.0, 4H), 7.69–7.58 (m, 6H). ^{13}C NMR (75 MHz, $CDCl_3$): δ 155.3, 141.7, 137.0, 130.0, 129.5, 129.2, 127.9. HRMS (ESI-TOF), *m*/*z*: calcd for $C_{18}H_{11}N_4S_2$ $[M + H]^+$, 347.0420, found, 347.0421. MS (EI, 70 eV), *m*/*z* (*I*, %): 348 ($[M + 2]^+$, 1), 347 ($[M + 1]^+$, 2), 346 ($[M]^+$, 7), 317 (3), 290 (100), 258 (10), 245 (4), 145 (30), 51 (3).

3.12.14. 4,8-Di-*p*-tolylbenzo[1,2-*d*:4,5-*d*′]bis([1,2,3]thiadiazole) (**19f**)

Yellow solid, 28 mg (55%, procedure B) or 34 mg (65%, procedure D), eluent—CH_2Cl_2: hexane, 1:2 (*v*/*v*). R_f = 0.4 (CH_2Cl_2:hexane 1:1 (*v*/*v*)). Mp > 250 °C. IR ν_{max} (KBr, cm^{-1}): 1607, 1446, 1373, 1311, 1277, 1209, 1182, 1119, 1101, 1021, 940, 898, 831, 802, 716, 652, 627, 582, 530, 491. ^{1}H NMR (300 MHz, $CDCl_3$): δ 7.90 (d, *J* = 7.9, 4H), 7.90 (d, *J* = 7.9, 4H), 2.52 (s, 6H). ^{13}C NMR (75 MHz, $CDCl_3$): δ 155.5, 141.7, 140.4, 134.3, 130.0, 129.6, 127.9, 21.6. HRMS (ESI-TOF), *m*/*z*: calcd for $C_{20}H_{15}N_4S_2$ $[M + H]^+$, 375.0733, found, 375.0725. MS (EI, 70 eV), *m*/*z* (*I*, %): 374 ($[M]^+$, 8), 318 (70), 303 (5), 285 (3), 159 (100), 115 (97), 93 (25), 63 (14), 39 (30).

3.12.15. 4,8-Bis(4-methoxyphenyl)benzo[1,2-*d*:4,5-*d*′]bis([1,2,3]thiadiazole) (**19g**)

Orange solid, 32 mg (60%, procedure B) or 26 mg (50%, procedure D), eluent—CH_2Cl_2:hexane, 1:1 (*v*/*v*). R_f = 0.2 (CH_2Cl_2:hexane, 1:1 (*v*/*v*)). Mp > 250 °C. IR ν_{max} (KBr, cm^{-1}): 1605, 1519, 1450, 1371, 1316, 1302, 1282, 1256, 1178, 1026, 816, 718, 546, 515. ^{1}H NMR (300 MHz, $CDCl_3$): δ 7.97 (d, *J* = 8.3, 4H), 7.17 (d, *J* = 8.3, 4H), 3.95 (s, 6H). HRMS (ESI-TOF), *m*/*z*: calcd for $C_{20}H_{15}N_4O_2S_2$ $[M + H]^+$, 407.0631, found, 407.0626. MS (EI, 70 eV), *m*/*z* (*I*, %): 407 ($[M + 1]^+$, 1), 406 ($[M]^+$, 10), 335 (100), 307 (25), 292 (12), 264 (8), 175 (20), 160 (21), 132 (98), 93 (6), 15 (70).

3.12.16. 4,4′-(Benzo[1,2-*d*:4,5-*d*′]bis([1,2,3]thiadiazole)-4,8-diyl)bis(*N*,*N*-diphenylaniline) (**19h**)

Red solid, 63 mg (67%, procedure B) or 65 mg (69%, procedure D), eluent—CH_2Cl_2:hexane, 1:2 (*v*/*v*). R_f = 0.5 (CH_2Cl_2:hexane, 1:1 (*v*/*v*)). Mp > 250 °C. IR ν_{max} (KBr, cm^{-1}): 1587, 1514, 1489, 1444, 1329, 1315, 1277, 1192, 1176, 841, 817, 753, 734, 695, 653, 620, 509. ^{1}H NMR (300 MHz, $CDCl_3$): δ 7.85 (d, *J* = 8.2, 4H), 7.35–7.30 (m, 8H), 7.24–7.08 (m, 16H). ^{13}C NMR (75 MHz, $CDCl_3$): δ 155.4, 149.4, 147.0, 141.2, 130.5, 129.6, 129.5, 127.0, 125.6, 124.0, 121.6. HRMS (ESI-TOF), *m*/*z*: calcd for $C_{42}H_{29}N_6S_2$ $[M + H]^+$, 681.1890, found, 681.1901.

4. Conclusions

4,8-Dibromobenzo[1,2-*d*:4,5-*d'*]bis([1,2,3]thiadiazole) was successfully prepared in a moderate yield by the heating of a parent heterocycle with bromine in hydrobromic acid. Its structure was finally confirmed by single-crystal X-ray diffraction study. Aromatic nucleophilic substitution and palladium-catalyzed cross-coupling reactions were found to be powerful tools for the selective synthesis of various mono- and bis-derivatives. It was found that 4,8-dibromobenzo[1,2-*d*:4,5-*d'*]bis([1,2,3]thiadiazole) is resistant to the action of water, alcohols and corresponding alcoholates; when using aromatic nucleophilic substitution (S_NAr), mono- and bis-aminated derivatives were successfully obtained, while thiols formed only bis-derivatives, and the reaction could not be stopped at the stage of the formation of mono-thiols. The Stille coupling of 4,8-dibromobenzo[1,2-*d*:4,5-*d'*]bis([1,2,3]thiadiazole) is useful for the synthesis of bis-arylated heterocycles, while Suzuki–Miyaura coupling can be successfully employed for the selective formation of various mono- and di-(het)arylated derivatives of benzo[1,2-*d*:4,5-*d'*]bis([1,2,3]thiadiazole). The obtained compounds can represent an effective basis for the design and construction of components of organic light-emitting diodes and solar cells.

Supplementary Materials: The following are available online at https://www.mdpi.com/article/10.3390/molecules27217372/s1, Characterization data including ^1H, ^{13}C NMR and HRMS spectra for compounds **1**, **12**, **13**, **15**, **18**, **19** and quantum chemical calculations data.

Author Contributions: O.A.R. and T.N.C. conceived and designed the study; T.N.C., D.A.A., T.A.K. performed the experiments; T.N.C. analyzed the data. All authors have read and agreed to the published version of the manuscript.

Funding: We gratefully acknowledge financial support from the Russian Science Foundation (Grant no. 22-23-00252).

Institutional Review Board Statement: Not applicable.

Informed Consent Statement: Not applicable.

Data Availability Statement: Not applicable.

Acknowledgments: The authors thank I. S. Golovanov (N.D. Zelinsky Institute of Organic Chemistry) for the DFT calculations of benzo[1,2-*d*:4,5-*d'*]bis([1,2,3]thiadiazole).

Conflicts of Interest: The authors declare no conflict of interest.

Sample Availability: Samples of the compounds **1–3**, **12**, **13**, **15**, **18** and **19** are available from the authors.

References

1. Van der Staaij, F.M.; van Keulen, I.M.; von Hauff, E. Organic Photovoltaics: Where Are We Headed? *Sol. RRL* **2021**, *5*, 2100167. [CrossRef]
2. Yan, J.; Saunders, B.R. Third-generation solar cells: A review and comparison of polymer:fullerene, hybrid polymer and perovskite solar cells. *RSC Adv.* **2014**, *4*, 43286–43314. [CrossRef]
3. Takimiya, K.; Osaka, I.; Nakano, M. π-Building Blocks for Organic Electronics: Revaluation of "Inductive" and "Resonance" Effects of π-Electron Deficient Units. *Chem. Mater.* **2014**, *26*, 587–593. [CrossRef]
4. Duan, C.; Huang, F.; Cao, Y. Recent development of push–pull conjugated polymers for bulk-heterojunction photovoltaics: Rational design and fine tailoring of molecular structures. *J. Mater. Chem.* **2012**, *22*, 10416–10434. [CrossRef]
5. Lee, C.-P.; Li, C.-T.; Ho, K.-C. Use of organic materials in dye-sensitized solar cells. *Mater. Today* **2017**, *20*, 267–282. [CrossRef]
6. Wu, Y.; Zhu, W. Organic sensitizers from D–p–A to D–A–p–A: Effect of the internal electron-withdrawing units on molecular absorption, energy levels and photovoltaic performances. *Chem. Soc. Rev.* **2013**, *42*, 2039–2058. [CrossRef]
7. Knyazeva, E.A.; Rakitin, O.A. Influence of structural factors on the photovoltaic properties of dye-sensitized solar cells. *Russ. Chem. Rev.* **2016**, *85*, 1146–1183. [CrossRef]
8. Zhao, Y.; Guo, Y.; Liu, Y. 25th Anniversary Article: Recent Advances in n-Type and Ambipolar Organic Field-Effect Transistors. *Adv. Mater.* **2013**, *25*, 5372–5391. [CrossRef]
9. Guo, X.; Facchetti, A.; Marks, T.J. Imide- and Amide-Functionalized Polymer Semiconductors. *Chem. Rev.* **2014**, *114*, 8943–9021. [CrossRef]

10. Zhang, Y.; Zou, J.; Cheuh, C.-C.; Yip, H.-L.; Jen, A.K.-Y. Significant Improved Performance of Photovoltaic Cells Made from a Partially Fluorinated Cyclopentadithiophene/Benzothiadiazole Conjugated Polymer. *Macromolecules* **2012**, *45*, 5427–5435. [CrossRef]
11. Stuart, A.C.; Tumbleston, J.R.; Zhou, H.; Li, W.; Liu, S.; Ade, H.; You, W. Fluorine Substituents Reduce Charge Recombination and Drive Structure and Morphology Development in Polymer Solar Cells. *J. Am. Chem. Soc.* **2013**, *135*, 1806–1815. [CrossRef] [PubMed]
12. Parker, T.C.; Patel, D.G.; Moudgil, K.; Barlow, S.; Risko, C.; Brédas, J.-L.; Reynolds, J.R.; Marder, S.R. Heteroannulated acceptors based on benzothiadiazole. *Mater. Horizons* **2015**, *2*, 22–36. [CrossRef]
13. Roncali, J. Molecular Engineering of the Band Gap of π-Conjugated Systems: Facing Technological Applications. *Macromol. Rapid Commun.* **2007**, *28*, 1761–1775. [CrossRef]
14. Chmovzh, T.; Knyazeva, E.; Lyssenko, K.; Popov, V.; Rakitin, O. Safe Synthesis of 4,7-Dibromo[1,2,5]thiadiazolo[3,4-d]pyridazine and Its SNAr Reactions. *Molecules* **2018**, *23*, 2576. [CrossRef]
15. Rakitin, O.A. Fused 1,2,5-thia- and 1,2,5-selenadiazoles: Synthesis and application in materials chemistry. *Tetrahedron Lett.* **2020**, *61*, 152230. [CrossRef]
16. Rakitin, O.A. 1,2,5-Thiadiazoles. In *Comprehensive Heterocyclic Chemistry IV*; Elsevier: Amsterdam, The Netherlands, 2022; pp. 371–406.
17. Zhou, H.; Yang, L.; Price, S.C.; Knight, K.J.; You, W. Enhanced Photovoltaic Performance of Low-Bandgap Polymers with Deep LUMO Levels. *Angew. Chemie Int. Ed.* **2010**, *49*, 7992–7995. [CrossRef]
18. Leventis, A.; Chmovzh, T.N.; Knyazeva, E.A.; Han, Y.; Heeney, M.; Rakitin, O.A.; Bronstein, H. A novel low-bandgap pyridazine thiadiazole-based conjugated polymer with deep molecular orbital levels. *Polym. Chem.* **2020**, *11*, 581–585. [CrossRef]
19. Chmovzh, T.N.; Knyazeva, E.A.; Mikhalchenko, L.V.; Golovanov, I.S.; Amelichev, S.A.; Rakitin, O.A. Synthesis of the 4,7-Dibromo Derivative of Highly Electron-Deficient [1,2,5]Thiadiazolo[3,4-d]pyridazine and Its Cross-Coupling Reactions. *Eur. J. Org. Chem.* **2018**, *2018*, 5668–5677. [CrossRef]
20. Chmovzh, T.N.; Knyazeva, E.A.; Tanaka, E.; Popov, V.V.; Mikhalchenko, L.V.; Robertson, N.; Rakitin, O.A. [1,2,5]Thiadiazolo[3,4-d]Pyridazine as an Internal Acceptor in the D-A-π-A Organic Sensitizers for Dye-Sensitized Solar Cells. *Molecules* **2019**, *24*, 1588. [CrossRef]
21. Korshunov, V.M.; Chmovzh, T.N.; Chkhetiani, G.R.; Taydakov, I.V.; Rakitin, O.A. New D–A–D luminophores of the [1,2,5]thiadiazolo[3,4-d]pyridazine series. *Mendeleev Commun.* **2022**, *32*, 371–373. [CrossRef]
22. Chmovzh, T.N.; Rakitin, O.A. Benzobischalcogenadiazoles: Synthesis and applications (microreview). *Chem. Heterocycl. Compd.* **2022**, *58*, 307–309. [CrossRef]
23. Gudim, N.S.; Knyazeva, E.A.; Mikhalchenko, L.V.; Golovanov, I.S.; Popov, V.V.; Obruchnikova, N.V.; Rakitin, O.A. Benzothiadiazole vs. iso-Benzothiadiazole: Synthesis, Electrochemical and Optical Properties of D–A–D Conjugated Molecules Based on Them. *Molecules* **2021**, *26*, 4931. [CrossRef] [PubMed]
24. Konstantinova, L.S.; Knyazeva, E.A.; Rakitin, O.A. Recent Developments in the Synthesis and Applications of 1,2,5-Thia- and Selenadiazoles. A Review. *Org. Prep. Proced. Int.* **2014**, *46*, 475–544. [CrossRef]
25. Knyazeva, E.A.; Rakitin, O.A. 4,7-Dibromo-substituted 2,1,3-benzothia(selena, oxa)diazoles and [1,2,5]thia(selena)diazolo[3,4-c]pyridines as building blocks in solar cells components (microreview). *Chem. Heterocycl. Compd.* **2017**, *53*, 855–857. [CrossRef]
26. Bianchi, L.; Zhang, X.; Chen, Z.; Chen, P.; Zhou, X.; Tang, Y.; Liu, B.; Guo, X.; Facchetti, A. New Benzo[1,2-d:4,5-d′]bis([1,2,3]thiadiazole) (iso-BBT)-Based Polymers for Application in Transistors and Solar Cells. *Chem. Mater.* **2019**, *31*, 6519–6529. [CrossRef]
27. Facchetti, A.; Chen, Z.; Brown, J.E. Semiconducting Compounds and Related Devices. U.S. Patent 9,708,346, 19 October 2016.
28. Chmovzh, T.N.; Alekhina, D.A.; Kudryashev, T.A.; Rakitin, O.A. 4-Bromobenzo[1,2-d:4,5-d′]bis([1,2,3]thiadiazole). *Molbank* **2022**, *2022*, M1362. [CrossRef]
29. Chen, S.; Li, Y.; Yang, W.; Chen, N.; Liu, H.; Li, Y. Synthesis and Tuning Optical Nonlinear Properties of Molecular Crystals of Benzothiadiazole. *J. Phys. Chem. C* **2010**, *114*, 15109–15115. [CrossRef]
30. Bolisetty, M.N.K.P.; Li, C.-T.; Thomas, K.R.J.; Bodedla, G.B.; Ho, K.-C. Benzothiadiazole-based organic dyes with pyridine anchors for dye-sensitized solar cells: Effect of donor on optical properties. *Tetrahedron* **2015**, *71*, 4203–4212. [CrossRef]
31. Gudim, N.S.; Knyazeva, E.A.; Obruchnikova, N.V.; Rakitin, O.A.; Popov, V.V. 4-(7-Bromobenzo[d][1,2,3]thiadiazol-4-yl)morpholine. *Molbank* **2021**, *2021*, M1202. [CrossRef]
32. Yamashita, Y.; Ono, K.; Tomura, M.; Tanaka, S. Synthesis and Properties of Benzobis(thiadiazole)s with Nonclassical π-Electron Ring Systems. *Tetrahedron* **1997**, *53*, 10169–10178. [CrossRef]
33. Trippé-Allard, G.; Lacroix, J.-C. Synthesis of nitro- and amino-functionalized π-conjugated oligomers incorporating 3,4-ethylenedioxythiophene (EDOT) units. *Tetrahedron* **2013**, *69*, 861–866. [CrossRef]
34. El-Shehawy, A.A.; Abdo, N.I.; El-Barbary, A.A.; Lee, J.-S. A selective and direct synthesis of 2-bromo-4-alkylthiophenes: Convenient and straightforward approaches for the synthesis of head-to-tail (HT) and tail-to-tail (TT) dihexyl-2,2′-bithiophenes. *Tetrahedron Lett.* **2010**, *51*, 4526–4529. [CrossRef]
35. Melucci, M.; Barbarella, G.; Sotgiu, G. Solvent-Free, Microwave-Assisted Synthesis of Thiophene Oligomers via Suzuki Coupling. *J. Org. Chem.* **2002**, *67*, 8877–8884. [CrossRef] [PubMed]

36. Li, Z.H.; Wong, M.S. Synthesis and Functional Properties of End-Dendronized Oligo(9,9-diphenyl)fluorenes. *Org. Lett.* **2006**, *8*, 1499–1502. [CrossRef] [PubMed]
37. Kuo, C.-Y.; Huang, Y.-C.; Hsiow, C.-Y.; Yang, Y.-W.; Huang, C.-I.; Rwei, S.-P.; Wang, H.-L.; Wang, L. Effect of Side-Chain Architecture on the Optical and Crystalline Properties of Two-Dimensional Polythiophenes. *Macromolecules* **2013**, *46*, 5985–5997. [CrossRef]
38. Kitagawa, T.; Matsubara, H.; Okazaki, T.; Komatsu, K. Electrochemistry of the Self-Assembled Monolayers of Dyads Consisting of Tripod-Shaped Trithiol and Bithiophene on Gold. *Molecules* **2014**, *19*, 15298–15313. [CrossRef]
39. Vegiraju, S.; Hsieh, C.-M.; Huang, D.-Y.; Chen, Y.-C.; Priyanka, P.; Ni, J.-S.; Esya, F.A.; Kim, C.; Yau, S.L.; Chen, C.-P.; et al. Synthesis and characterization of solution-processable diketopyrrolopyrrole (DPP) and tetrathienothiophene (TTA)-based small molecules for organic thin film transistors and organic photovoltaic cells. *Dye. Pigment.* **2016**, *133*, 280–291. [CrossRef]
40. Oikawa, A.; Kindaichi, G.; Shimotori, Y.; Okimoto, M.; Hoshi, M. Simple preparation of aryltributylstannanes and its application to one-pot synthesis of diaryl ketones. *Tetrahedron* **2015**, *71*, 1705–1711. [CrossRef]
41. Quinton, C.; Chi, S.-H.; Dumas-Verdes, C.; Audebert, P.; Clavier, G.; Perry, J.W.; Alain-Rizzo, V. Novel s-tetrazine-based dyes with enhanced two-photon absorption cross-section. *J. Mater. Chem. C* **2015**, *3*, 8351–8357. [CrossRef]
42. *CrysAlisPro*, version 1.171.41.106a. User Inspired Software for Single Crystal X-Ray Diffractometers. Rigaku Oxford Diffraction. 2021. Available online: https://www.rigaku.com/products/crystallography/chrysalis(accessed on 1 January 2020).
43. Sheldrick, G.M. SHELXT—Integrated space-group and crystal-structure determination. *Acta Crystallogr. Sect. A Found. Adv.* **2015**, *71*, 3–8. [CrossRef]
44. Sheldrick, G.M. Crystal structure refinement with SHELXL. *Acta Crystallogr. Sect. C Struct. Chem.* **2015**, *71*, 3–8. [CrossRef] [PubMed]

molecules

MDPI

Article

Multifunctional Derivatives of Spiropyrrolidine Tethered Indeno-Quinoxaline Heterocyclic Hybrids as Potent Antimicrobial, Antioxidant and Antidiabetic Agents: Design, Synthesis, In Vitro and In Silico Approaches

Nouha Bouali [1,†], Manel Ben Hammouda [2,†], Iqrar Ahmad [3], Siwar Ghannay [4], Amira Thouri [5], Amal Dbeibia [6], Harun Patel [3], Walid Sabri Hamadou [1], Karim Hosni [7], Mejdi Snoussi [1,8], Mohd Adnan [1], Md Imtaiyaz Hassan [9,*], Emira Noumi [1], Kaïss Aouadi [4,10] and Adel Kadri [11,12]

[1] Department of Biology, College of Science, Hail University, P.O. Box 2440, Hail 2440, Saudi Arabia
[2] Laboratory of Heterocyclic Chemistry Natural Product and Reactivity/CHPNR, Department of Chemistry, Faculty of Science of Monastir, University of Monastir, Monastir 5000, Tunisia
[3] Division of Computer Aided Drug Design, Department of Pharmaceutical Chemistry, R. C. Patel Institute of Pharmaceutical Education and Research, Shirpur 425405, Maharashtra, India
[4] Department of Chemistry, College of Science, Qassim University, Buraidah 51452, Saudi Arabia
[5] Laboratory of Bioresources, Biology Integrative and Valorization, Higher Institute of Biotechnology of Monastir, University of Monastir, Monastir 5000, Tunisia
[6] Laboratory of Analyzes, Treatment and Valorization of Environmental Pollutants and Products, Faculty of Pharmacy of Monastir, University of Monastir, Monastir 5019, Tunisia
[7] Laboratoire des Substances Naturelles, Institute National de Recherche et d'Analyse Physico-Chimique, Biotechpôle de Sidi Thabet, Sidi Thabet 2020, Tunisia
[8] Laboratory of Genetics, Biodiversity and Valorization of Bio-Resources (LR11ES41), Higher Institute of Biotechnology of Monastir, University of Monastir, Avenue Tahar Haddad, BP74, Monastir 5000, Tunisia
[9] Center for Interdisciplinary Research in Basic Sciences, Jamia Millia Islamia, New Delhi 110025, India
[10] Department of Chemistry, Faculty of Science of Monastir, University of Monastir, Avenue of the Environment, Monastir 5019, Tunisia
[11] Department of Chemistry, Faculty of Science and Arts of Baljurashi, Albaha University, Al Bahah P.O. Box 1988, Saudi Arabia
[12] Department of Chemistry, Faculty of Science of Sfax, University of Sfax, B.P. 1171, Sfax 3000, Tunisia
* Correspondence: mihassan@jmi.ac.in
† These authors contributed equally to this work.

Citation: Bouali, N.; Hammouda, M.B.; Ahmad, I.; Ghannay, S.; Thouri, A.; Dbeibia, A.; Patel, H.; Hamadou, W.S.; Hosni, K.; Snoussi, M.; et al. Multifunctional Derivatives of Spiropyrrolidine Tethered Indeno-Quinoxaline Heterocyclic Hybrids as Potent Antimicrobial, Antioxidant and Antidiabetic Agents: Design, Synthesis, In Vitro and In Silico Approaches. *Molecules* **2022**, *27*, 7248. https://doi.org/10.3390/molecules27217248

Academic Editors: Alexey M. Starosotnikov, Maxim A. Bastrakov, Igor L. Dalinger and Fawaz Aldabbagh

Received: 8 September 2022
Accepted: 17 October 2022
Published: 25 October 2022

Abstract: To combat emerging antimicrobial-resistant microbes, there is an urgent need to develop new antimicrobials with better therapeutic profiles. For this, a series of 13 new spiropyrrolidine derivatives were designed, synthesized, characterized and evaluated for their in vitro antimicrobial, antioxidant and antidiabetic potential. Antimicrobial results revealed that the designed compounds displayed good activity against clinical isolated strains, with **5d** being the most potent (MIC 3.95 mM against *Staphylococcus aureus* ATCC 25923) compared to tetracycline (MIC 576.01 mM). The antioxidant activity was assessed by trapping DPPH, ABTS and FRAP assays. The results suggest remarkable antioxidant potential of all synthesized compounds, particularly **5c**, exhibiting the strongest activity with IC_{50} of 3.26 ± 0.32 mM (DPPH), 7.03 ± 0.07 mM (ABTS) and 3.69 ± 0.72 mM (FRAP). Tested for their α-amylase inhibitory effect, the examined analogues display a variable degree of α-amylase activity with IC_{50} ranging between 0.55 ± 0.38 mM and 2.19 ± 0.23 mM compared to acarbose (IC_{50} 1.19 ± 0.02 mM), with the most active compounds being **5d**, followed by **5c** and **5j**, affording IC_{50} of 0.55 ± 0.38 mM, 0.92 ± 0.10 mM, and 0.95 ± 0.14 mM, respectively. Preliminary structure–activity relationships revealed the importance of such substituents in enhancing the activity. Furthermore, the ADME screening test was applied to optimize the physicochemical properties and determine their drug-like characteristics. Binding interactions and stability between ligands and active residues of the investigated enzymes were confirmed through molecular docking and dynamic simulation study. These findings provided guidance for further developing leading new spiropyrrolidine scaffolds with improved dual antimicrobial and antidiabetic activities.

Keywords: spiropyrrolidine derivatives; antimicrobial; antioxidant; antidiabetic; ADME; molecular docking and dynamic simulation

1. Introduction

The emergence of multidrug-resistant bacteria, often called "superbugs", has become a global public health issue according to the World Health Organization (WHO) [1,2]. The WHO has declared antimicrobial resistance to be one of the 10th greatest public health threats facing humanity [2]. The lack of new drug development as well as the misuse and overuse of antimicrobials remains the main factors that have led to the rise and spread of drug-resistant pathogens, which has slowed down the eradication process of infectious diseases [3]. Antibiotic resistance has gradually developed and now affects all pathogenic bacteria. It results from the repeated administration of antibiotics in humans or animals, which creates conditions, called "selection pressure" favoring the acquisition and dissemination of antibiotic-resistant strains [4]. Therefore, antibiotics and other antimicrobial drugs lose their effectiveness and infections become increasingly difficult or even impossible to treat and lead to death [5].

Diabetes mellitus (DM) is a noncommunicable disease (NCDs) that includes a group of metabolic conditions characterized by hyperglycemia and resulting from defects in insulin action, insulin secretion or both [6,7]. Chronic hyperglycemia is associated with considerable morbidity and mortality, especially from cardiovascular and renal failure, with long-term damage and dysfunction of the eyes, kidneys, blood vessels, nerves and heart [8–10]. It is furthermore a common belief that people with diabetes are generally more vulnerable to infectious disease than those without diabetes [11]. α-Amylase attracts more attention due to its potential ability on attacking of α-1,4-glycosidic linkage by hydrolysis and was known as a hydrolyze enzyme containing Ca^{+2} ion in its active pocket. Its main role is to catalyze the conversion of starch into glucose and maltose by involving water molecules [12,13]. Additionally, some medications such as acarbose, voglibose and miglitol, despite their adverse side effects, have been employed as inhibitors of the hydrolyzing ability of the α-amylase enzyme and consequently blocked the absorption of glucose [14].

Quinoxalines, also known as benzo[a]pyrazines, are nitrogen-containing heterocycles scaffolds that have attracted enormous attention in synthetic and medicinal chemistry because of their widespread prevalence in nature. In addition, indeno [1,2-b]quinoxaline, as a privileged core with active pharmacophore and therapeutic value such as anticancer [15], antiproliferative [16] and Jun N-terminal kinase inhibitory effects [17], was used in the elaboration of various spiro-polycyclic frameworks. In this perspective, spiropyrrolidine derivatives play an important role in both medicinal chemistry and drug discovery, owing to their prominent pharmaceutical potency, including antileaucamic, anticonvulsant antiviral and local anesthetic activities [18]. They also exhibited antimicrobial [19], antibacterial [20], antifungal [20], antimalarial [20], anti-inflammatory [21], analgesic [21], antidiabetic [22], antitubercular [23], antiproliferative [24], anticholinesterase [25], anticancer [26], and antimycobacterial [27] properties. Spirotryprostatin, (+)-elacomine, (−)-horsfiline, formosanine, alstonisine and (−)-coerulescine (Figure 1) are among the most relevant spiropyrrolidine analogues.

Moreover, the spirocyclic moieties, especially those with pyrrolidine-embedded spiroatom are pharmacologically very attractive because of their interesting therapeutic activities, such antimicrobial [28], antiproliferative [29] and anti-acetylcholinesterase (AChE) and antibutylcholinesterase (BChE) activities [30]. Motivated by the aforementioned information and in connection to our previous studies in developing antimicrobial [31–42], antioxidant [39–48] and antidiabetic [7,8,10] agents, we herein disclose the design, synthesis and biological evaluation of a series of a novel class of spiropyrrolidine tethered indeno-quinoxaline heterocyclic hybrids. To determine the role of different functionalities in the formation of a ligand–protein complex, an in silico molecular docking study of the

most potent derivatives was performed against *S. aureus* tyrosyl-tRNA synthetase (PDB ID, 1JIJ), human peroxiredoxin 5 (PRDX5) (PDB code: 1HD2) and human pancreatic *α*-amylase (PDB code: 2QV4), followed by an ADMET study.

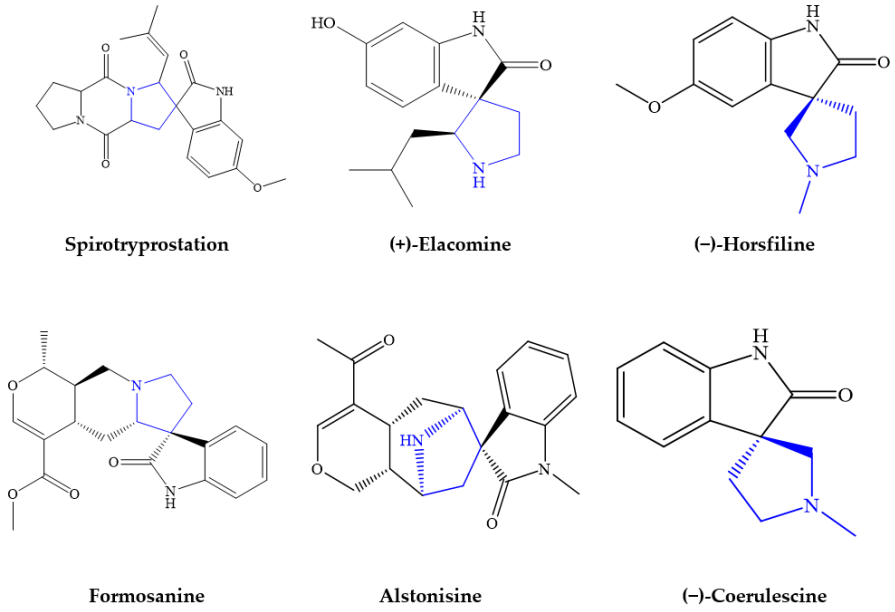

Figure 1. Highly pronounced biological spiropyrrolidine derivatives.

2. Results and Discussion

2.1. Chemistry

As shown in Scheme 1, we have chosen as a model the following four components: ninhydrin 1, o-phenylenediamine 2, sarcosine 3 and (*E*)-3-arylidene-1-methylpyrrolidine-2,5-dione 4a (Ar = C6H5) [49,50]. The reaction was carried out at different temperatures in acetonitrile and methanol. The obtained results show that the regio- and the stereoselectivity of this reaction depend both on the solvent and on the temperature (Table 1). Indeed, this optimization study revealed that the best results were obtained by refluxing the reaction mixture in methanol for 4 h, providing spiro[indenoquinoxaline-pyrrolidines] 5a with an excellent yield (81%) (Table 1, entry 5). Increasing the reaction time has no effect on the reaction yield.

Table 1. Optimization of the reaction conditions [a].

Entry	Solvent	T (°C)	Time (h)	Yield [b] (%)
1	CH_3CN	25	8	-
2	CH_3CN	80	4	35
3	CH_3CN	80	12	43
4	MeOH	25	8	-
5	MeOH	64	4	81
6	MeOH	64	24	81

[a] The reactions were carried out with **1** (0.5 mmol), **2** (0.5 mmol), **3** (0.75mmol) and **4a** (0.5 mmol) in solvent (5 mL). [b] Overall yields after isolation of the products by column chromatography. - No reaction due to insufficient solubility.

After establishing the appropriate reaction conditions (Table 1, entry **5**), we tried to extend the scope of this reaction by using a series of different dipolarophiles, **4a–m**. This was performed in order to examine the influence of the electronic effects exerted by the substituent in positions *o*, *m* and *p* of the aryl group of imides **4** on the result of the reaction (Scheme 2). Both electron donating and electron-withdrawing groups exerted by the substituent at the o, m or *p*-position of the aryl group of imides **4** have a very limited influence on the efficiency of the cycloaddition reaction. For example,

dipolarophiles 4 bearing electron-neutral (H), or electron-withdrawing substituent (e.g., *p*-Cl, *m*-Cl), or electron-donating (e.g., *p*-OMe or *m*-OMe) groups reacted smoothly to give spiro[indenoquinoxaline-pyrrolidines] products **5a–m** in good yields along with excellent diastereoselectivities (Scheme 2).

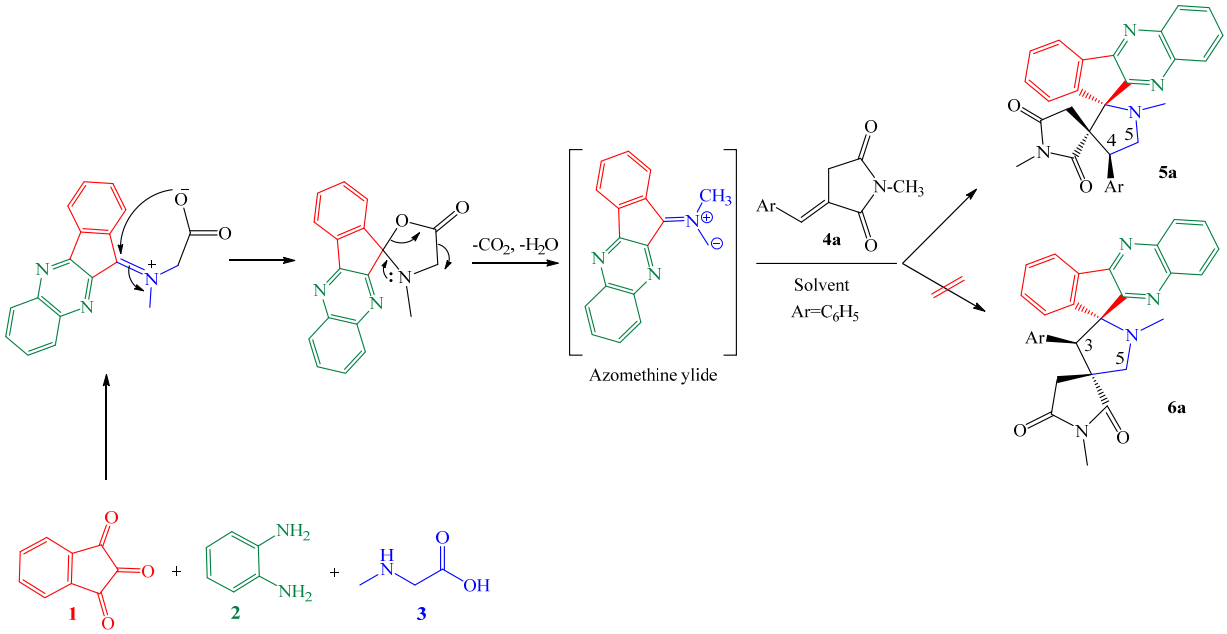

Scheme 1. 1, 3-Dipolar cycloaddition leading spiro[indenoquinoxaline-pyrrolidines] **5a**.

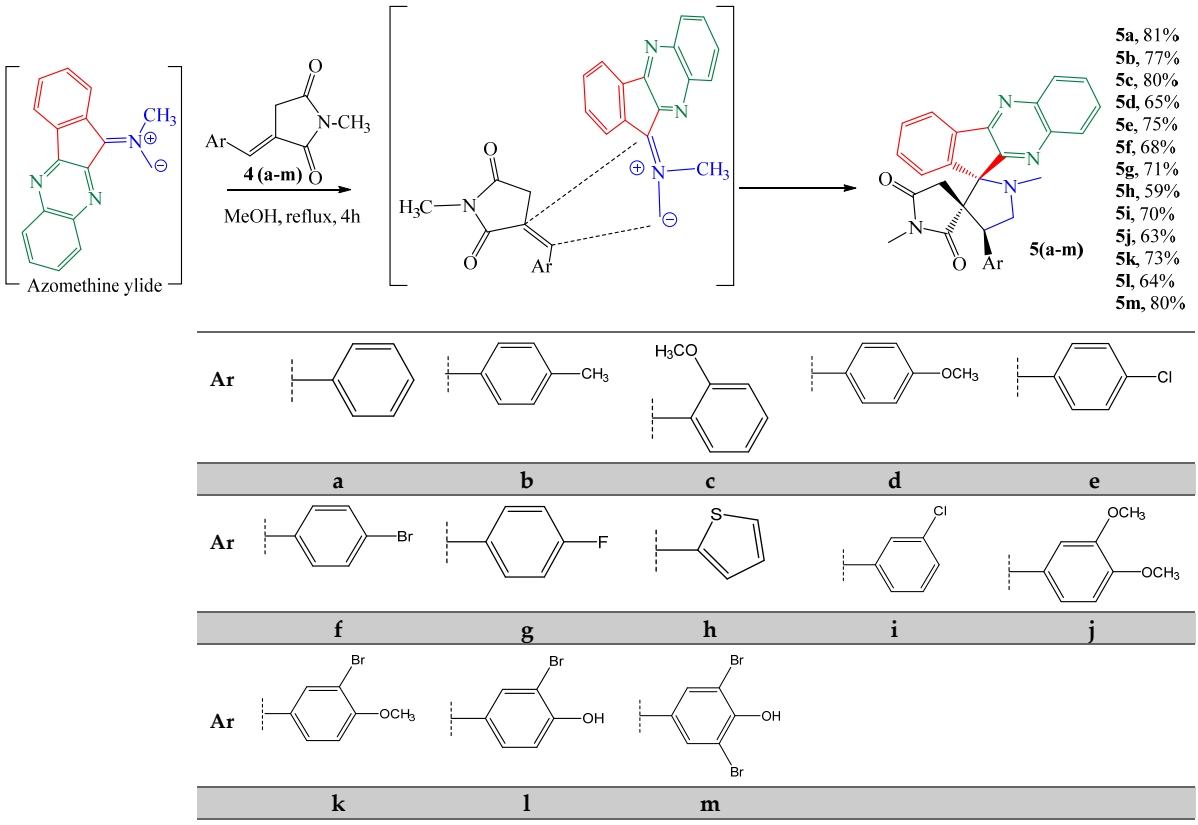

Scheme 2. Substrate scope. All reactions were carried out with **1** (0.5 mmol), **2** (0.5 mmol), **3** (0.75 mmol) and **4a–m** (0.5 mmol) in MeOH (5.0 mL) at reflux for 4 h. Yields of the isolated cycloadducts are given.

The structures and the relative configuration of the isolated spiropyrrolidines **5a–m** were elucidated by analyzing their spectroscopic data (NMR1D and NMR 2D).

2.2. Spectroscopic of the Isomeric Cycloadducts

The specific regioisomer was determined on the basis of the ^{1}H NMR chemical shifts of the H-4 and H-5 protons [51] (Figure 2).

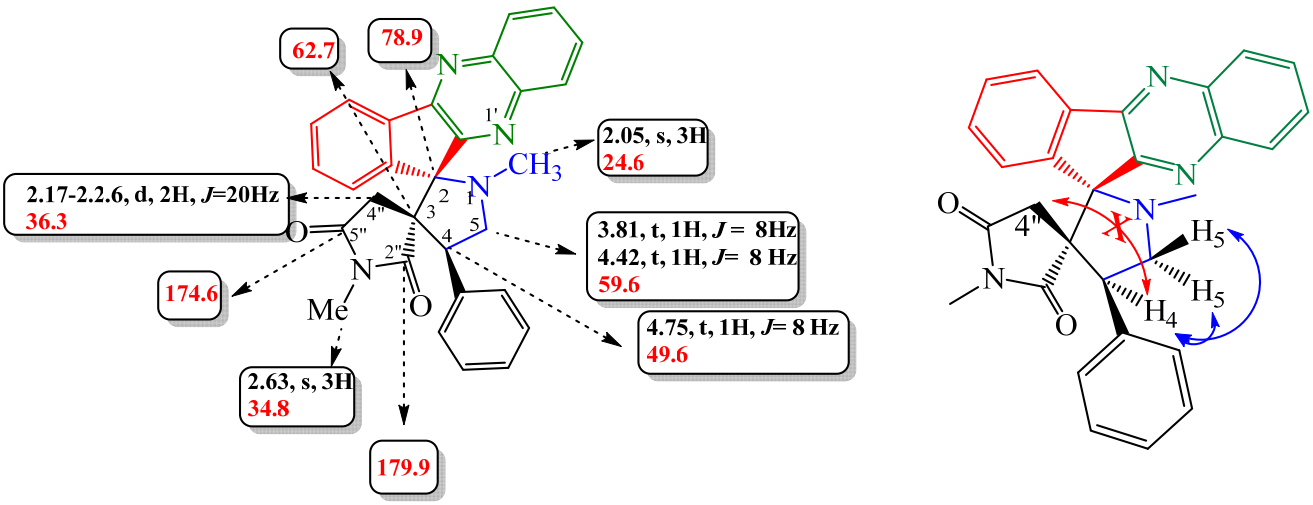

Figure 2. Selected ^{1}H and ^{13}C NMR (red) chemical shifts (ppm) (**left**) and the NOESY correlations (**right**) of **5a**.

The ^{1}H NMR spectrum of **5a** shows the –NCH3 proton of the pyrrolidine ring exhibited a singlet at 2.05 ppm. Two mutually coupled doublets at δ 2.17–2.26 ppm were observed with a 2J coupling of 20 Hz, corresponding to the 4″-CH_2 group. At 2.63 ppm, a three-proton integration singlet attributable to the Me–N protons of the pyrrolidine-2,5-dione ring. The H-4 and 5-CH_2 protons appear as three triplets at 3.81, 4.42 and 4.75 ppm (J = 8 Hz), respectively (Figure 2). The multiplicity of the signals, three triplets, are clearly corroborating the regiochemistry of the cycloaddition reaction. If the hypothetical alternative regioisomer **6a** (Scheme 1) would have been formed, the pyrrolidinyl protons H-3 and 5-CH_2 should give rise to a singlet and two doublet patterns in the ^{1}H NMR spectrum. The aromatic protons found in the region between δ 7.31 and 8.27 ppm appear as a multiplet. The ^{13}C NMR spectrum shows two peaks at δ 62.7 and 78.9 ppm, corresponding to the two spirocarbons C-3 and C-2. The pyrrolizidinyl carbons C-4 and C-5 appear at δ 49.6 and 59.6 ppm, respectively. In addition, the resonances at δ 174.6 ppm and δ 179.9 ppm are due to groups of pyrrolidine-2,5-dione. Experimental 2D NMR methods such as the NOESY, COSY and HMBC were used to further determine the stereo- and regioselectivity of the 1,3-dipolar cycloaddition leading to the **5a–m** cycloadducts. The HMBC spectrum of **5a** (see supplementary materials) indicated the following significant correlation between H4/C4″; H5/C4; H4/C5; H4/C3; CH2/C3 and H5/C3. The NOESY spectrum of compounds **5a** (see supplementary materials) shows correlations between H4/H5 protons; H4/HAr; H5/HAr, H5/N-CH_3 (pyrrolidine) and H4″/H5 protons. Additionally, no correlation was observed between H4 and H4″ protons. The COSY spectrum of **5a** (see supplementary materials) shows correlations between H4/H5 protons. The υ(C=O) absorptions at 1695 cm^{-1} in the IR spectrum of **5a** are due to the carbonyl groups of the imide. All these observations further confirm the stereochemistry proposed in (Figure 2).

It is worth noting that in all cases, the reactions were found to be highly regioselective, leading to the generation of only one regioisomer **5**. No indication for the copresence of isomer **6**, even in smaller amounts, was found (Scheme 1).

2.3. Biological Screening

2.3.1. Antimicrobial Activity vs. Structure Activity Relationship Studies

The antimicrobial screening of the synthesized compounds **5a–m** was investigated using the disc diffusion method towards different pathogenic strains. The results depicted in Table 1 are expressed quantitatively by MIC, MBC, MFC, MBC/MIC and MFC/MIC values. As shown, all compounds displayed potent antibacterial and moderate antifungal activities against the tested strains when compared to the standard drug, tetracycline and amphotericin B, respectively. A structure–activity relationship study confirmed that relocation of same substituent on phenyl ring affects the biological activity of the synthesized derivatives. Among the obtained series, compound **5d**, with a methoxy group attached to the phenyl ring at the *p*-position, displayed the highest antibacterial activity compared to the standard tetracycline against most of the tested bacterial strains. Nevertheless, the presence of the methoxy group at the *o*-position (**5c**) seems to decrease the antimicrobial activity. This decreased was less pronounced in **5j**, having another methoxy group in the *m*-position when compared to **5d**. Replacing the *m*-methoxy group (**5j**) with a bromo group (**5k**) decreased the antibacterial activity, especially against *S. aureus* but did not affect the antifungal potency. Additionally, compounds **5e** with a chloro group and **5g** with a fluoro group attached to the *p*-position of the phenyl ring showed equipotent activity; however, when replaced by the bulky bromo groups at the *p*-position (**5f**), a decrease in the antimicrobial activity was detected, and overall, all the strains may be explained by the bulkiness of this group during its binding mode to the cell of the microbes via the activating the apoptosis processes. Further, compounds **5i** with the chloro group at the *m*-position of the phenyl ring showed reduced antibacterial activity and similar antifungal activity when compared to **5e** (chloro group at *p*-position). Moreover, **5i**, with a hydroxy group at the *p*-position and the bromo group at the *m*-position of the phenyl ring showed weaker activity than **5m** substituted with another bulky bromo group on the second *m*-position.

The analysis of the bactericidal (MBC/MIC $\leq$ 4)/bacteriostatic (MBC/MIC > 4) or fungicidal (MFC/MIC $\leq$ 4)/fungistatic (MFC/MIC > 4) characteristics of our compounds revealed that, except against *S. aureus* for **5c–e**, **5g–h**, and **5j–i**, the remaining compounds exhibited bactericidal and fungicidal characteristics towards all tested strains (Table 2).

2.3.2. Antioxidant Activity vs. Structure Activity Relationship Studies

Free radicals are well-known to play a pivotal role in the pathogenesis of various human diseases causing damage to cells. Thus, it is of utmost importance to protect us against free radicals and save our health. Indeed, to assess their versatile synthetic applicability, the antioxidant potency of our synthesized new compounds was assessed using DPPH, ABTS and FRAP assays and compared to that of Trolox as a standard. The results were expressed by their IC_{50} values, the effective concentration at which 50% of the radicals were scavenged (Table 3).

Table 2. MIC, MBC, MFC, MBC/MIC and MFC/MIC of the synthesized compounds against the tested pathogenic strains.

Entry	MBC (mM), MFC (mM), MBC/MIC and MFC/MIC																	
	Gram-Positive Bacteria						Gram-Negative Bacteria						Fungi					
	S. aureus ATCC 25923			*M. luteus* NCIMB 8166			*E. coli* ATCC 25922			*P. aeruginosa* ATCC 27853			*C. albicans* ATCC 90028			*C. krusei* ATCC 6258		
	MIC	MBC	MBC/MIC	MIC	MBC	MBC/MIC	MIC	MBC	MBC/MIC	MIC	MBC	MBC/MIC	MIC	MFC	MFC/MIC	MIC	MFC	MFC/MIC
5a	135.12	270.24	2	135.12	-	-	270.24	540.49	2	135.12	540.49	4	135.12	135.12	1	67.56	67.56	1
5b	65.57	524.58	8	524.58	-	-	262.29	524.58	2	131.14	524.58	4	131.14	262.29	2	65.57	65.57	1
5c	31.71	507.54	16	126.88	-	-	253.77	507.54	4	253.77	507.54	2	63.44	63.44	1	63.44	63.44	1
5d	3.95	126.88	32	63.44	253.77	4	126.88	507.54	4	126.88	507.54	4	31.71	126.88	4	15.85	15.85	1
5e	15.71	251.51	16	251.51	251.51	1	251.51	503.02	2	125.75	503.02	4	62.87	62.87	1	31.42	31.42	1
5f	115.43	230.86	2	230.86	-	-	230.86	461.73	2	115.43	230.86	2	57.71	57.71	1	57.71	57.71	1
5g	16.25	260.12	16	130.06	-	-	260.12	520.25	2	130.06	260.12	2	65.03	65.03	1	32.50	32.50	1
5h	33.33	533.53	16	133.38	133.38	1	266.76	533.53	2	133.38	266.76	2	66.69	266.76	4	66.69	66.69	1
5i	125.75	503.02	4	251.51	251.51	1	251.51	503.02	2	125.75	503.02	4	125.75	503.02	-	31.42	31.42	1
5j	14.94	478.38	32	239.19	478.38	2	239.19	478.38	2	239.19	478.38	2	119.59	239.19	2	59.79	59.79	1
5k	54.68	437.47	8	218.73	-	-	218.73	437.47	2	218.73	437.47	2	218.73	218.73	1	54.68	54.68	1
5l	28.02	448.47	16	112.11	224.23	2	224.23	448.47	2	112.11	448.47	4	56.05	448.47	8	28.02	28.02	1
5m	24.54	196.43	8	98.21	-	-	196.43	196.43	1	98.21	392.87	4	98.21	98.21	1	49.10	49.10	1
Tetracycline	576.01	288.00	2	576.01	1152.02	2	281.25	288.00	1	576.01	1152.02	2	-	-	-	-	-	-
Amphotericin B		-			-	-		-	-		-	-	5.41	5.41	1	5.41	5.41	1

-: No activity.

Table 3. In vitro antioxidant and antidiabetic activities of the synthesized compounds.

Entry	IC_{50} (mM)			
	DPPH	**ABTS**	**FRAP**	**α-Amylase**
5a	15.36 ± 0.65	49.19 ± 0.46	17.02 ± 0.52	1.19 ± 0.02
5b	33.74 ± 0.004	57.51 ± 0.55	63.26 ± 0.21	2.00 ± 0.30
5c	3.26 ± 0.32	7.03 ± 0.07	3.69 ± 0.72	0.92 ± 0.10
5d	7.44 ± 0.15	9.78 ± 0.30	8.09 ± 0.82	0.55 ± 0.38
5e	6.12 ± 0.01	12.16 ± 0.18	6.54 ± 0.18	1.91 ± 0.37
5f	16.13 ± 0.39	18.12 ± 0.53	7.93 ± 0.44	1.69 ± 0.28
5g	26.03 ± 0.50	7.19 ± 0.11	20.54 ± 0.60	1.94 ± 0.37
5h	19.13 ± 0.23	18.04 ± 0.13	6.32 ± 0.68	1.90 ± 0.054
5i	7.80 ± 0.32	11.39 ± 0.36	5.98 ± 0.52	1.33 ± 0.72
5j	19.20 ± 0.19	11.56 ± 0.05	5.98 ± 0.17	0.95 ± 0.14
5k	123.44 ± 0.45	7.69 ± 0.36	6.03 ± 0.12	2.19 ± 0.23
5l	15.28 ± 0.37	15.19 ± 0.31	3.26 ± 0.45	2.16 ± 0.35
5m	47.29 ± 0.06	14.56 ± 0.26	7.38 ± 0.14	1.40 ± 0.11
Trolox	31.24 ± 3.67	99.88 ± 0.31	41.87 ± 2.07	-
Acarbose	-	-	-	1.19 ± 0.02

Antioxidant compounds donate a hydrogen atom or electrons to DPPH and convert it to a stable molecule, 1,1-diphenyl-picryl hydrazine. Following the DPPH radical scavenging test, compounds **5c** with a methoxy group at the o-position, **5d** with a methoxy group at the m-position, **5e** with a chloro group at the *p*-position and **5i** with a hydroxy group at the *p*-position showed potent antioxidant activity with IC_{50} values of 3.26 ± 0.32 mM, 6.12 ± 0.01 mM, 7.44 ± 0.15 mM and 7.80 ± 0.32 mM, respectively. Interestingly, **5a** with unsubstituted benzene, **5f** with a bromo group at the *m*-position and **5i** with a hydroxy group at the *p*-position and bromo group at the *m*-position of the phenyl ring displayed equipotent DPPH scavenging activity; however, incorporating a methoxy group at the para-position of the phenyl ring (**5b**) reduced the activity two-times, and the remaining compounds **5m** and **5k** displayed the weakest activity, exceeding the standard Trolox. Further, compounds **5e** with a chloro group (IC_{50} = 6.12 ± 0.01), **5f** with a bromo group (IC_{50} = 16.13 ± 0.39) and **5g** with a fluoro group (IC_{50} = 26.03 ± 0.50) attached to the *p*-position of the phenyl ring showed excellent scavenging DPPH effects due to the electron-withdrawing inductive effect of halogens, with **5e** exerting a 5.1-fold better DPPH scavenging activity than the standard, Trolox. Nonetheless, the presence of a chloro group at the *m*-position of the aryl ring decreases the DPPH scavenging activity due to the loss of electron density. Remarkably, **5k**, bearing p-methoxy and *m*-bromo groups, turned out to the less active compound due to the presence of bulky bromine group at the *m*-position.

The antioxidant results related to the capture of ABTS radical revealed that out of the synthesized analogues, **5c**, **5g** and **5k** exhibited the strongest scavenging activity. An enhancement in the activity has been shown when replacing the m-methoxy group (**5j**) with a bromo group (**5k**). On the other hand, compounds 5g, bearing a fluoro group, displayed better ABTS scavenging activity than **5e** with a chloro group and **5f** with the bulky bromo group at the p-aromatic position, which remain about 14, 8 and 6-fold higher than Trolox, respectively.

Based on the FRAP test, our results indicate that, except **5b**, all compounds showed more potent antioxidant activity than the standard, Trolox, with **5c** bearing methoxy group at *o*-position of the phenyl ring has the greatest antioxidant activity, followed by **5i**, **5h** and **5e** exhibiting similar activity, about 6.5-fold higher than Trolox. Although compounds **5e** with a chloro group displayed higher activity than **5g** with a fluoro group attached to the *p*-position of the phenyl ring, when replaced by the bulky bromo groups at the *p*-position (**5f**), the activity remains much higher.

2.3.3. Antidiabetic Activity vs. Structure Activity Relationship Studies

The inhibitory effects of the synthesized analogues against α-amylase have been assessed as a strategy in lowering the postprandial hyperglycemia. The highest inhibitory effect was recorded to compound **5d** (0.55 ± 0.38 mM) with a methoxy group at the *p*-position, followed by **5c** (0.92 ± 0.10 mM) with a methoxy group at the *o*-position and **5j** (0.95 ± 0.14 mM) with two methoxy groups at the *p*- and *m*-positions exceeding that of acarbose (1.19 ± 0.02 mM). The decreased activity from **5d** to **5j**, which differs only by the presence of the m-methoxy group, was related to its electron-withdrawing effect. In addition to that, **5a** displayed similar activity to acarbose and the remaining compounds have shown lower activity. The presence of a methyl group with electron-donating effect also decreased the activity when compared to **5a**. The presence of different halogen groups (**5e**, **5f** and **5g**) in the *p*-position of the phenyl ring does not have a significant influence on the activity. The remaining analogues also displayed potent α-amylase inhibition (Table 3).

Based on the aforementioned SAR analysis, we assume that electron-withdrawing substituents increase the activity by increasing the polarity within/around the molecules, respectively.

2.4. Computational Studies

Druglikeness and Pharmacokinetics

The SwissADME web-based server was employed to predict ADME (absorption, distribution, metabolism, excretion) properties that cover the pharmacokinetic issues and determine whether a drug molecule reaches the target protein in the body and how long it stays in the bloodstream. They also provide a baseline for further in vivo trials and are considered as major steps for drugs targeting the central nervous system (CNS) because the ability of CNS drugs to penetrate the blood–brain barrier is of prime importance in drug metabolism. All compounds meet the Lipinski's rule of five that states that an orally active drug has the number of hydrogen bond acceptors (HBA) $\leq$ 10, hydrogen bond donors (HBD) $\leq$ 5, molecular weight (MW) < 500 Da and Log P (the logarithm of octanol water partition coefficient) $\leq$ 5 and possesses a good bioavailability score of 0.55. They exhibited a lipophilicity given by the consensus Log Po/w in the range of 2.73–3.29. They displayed high GI (gastrointestinal) absorption, with only 5e and 5i were found to be BBB (blood-brain barrier) permeant, and **5c**, **5d** and **5j** were P-gp substrates. Cytochrome P450s, known as an important enzyme system for drug metabolism in the liver with CYP2D6 and CYP3A4, which are the two main subtypes of cytochrome P450, with the latter responsible for the metabolism of about 60% of xenobiotics, including drugs, carcinogens, steroids, and eicosanoids. The predicted results revealed that the selected compound was CYP2D6, but all were found to be CYP3A4 inhibitors. The skin permeability (log Kp) defines the rate of a chemical penetrating across the stratum corneum with a predicted ADME value for the design compounds in the acceptance range to be within (Table 4) the skin permeability (log Kp) for the design compounds to be within the range of −7.95 to 7.30 cm/s

The prediction of Radar plot for oral bioavailability (Table 2) indicated similar bioavailability scores for **5c–d** and **5e,i** and were found within the data range and pink color zone.

The inbuilt BOILED-Egg model allows for intuitive evaluation of passive gastrointestinal absorption and brain penetration in function of the position of the molecules in the WLOGP-versus-TPSA referential, revealed that **5c**, **5d** and **5j**, located in the white region for high probability of passive absorption by the gastrointestinal tract as well as no BBB penetration and P-gp positive; however, **5e** and **5i** in the yellow region are for high BBB penetration and were P-gp negative (Figure 3).

Table 4. ADME properties of potent synthesized compounds.

Entry	5c	5d	5e	5i	5j
Physicochemical Properties/Lipophilicity/Druglikeness					
Molecular weight	492.57	492.57	496.99	496.99	522.59
Num. heavy atoms	37	37	36	36	39
Num. arom. heavy atoms	12	12	12	12	12
Num. rotatable bonds	0.33	0.33	0.31	0.31	0.35
Num. H-bond acceptors	2	2	1	1	3
Num. H-bond donors	6	6	5	5	7
Molar Refractivity	0	0	0	0	0
TPSA	155.61	155.61	154.12	154.12	162.10
Consensus Log Po/w	2.77	2.76	3.21	3.29	2.73
Lipinski's Rule	Yes	Yes	Yes	Yes	Yes
Bioavailability Score	0.55	0.55	0.55	0.55	0.55
Pharmacokinetics					
GI absorption	High	High	High	High	High
BBB permeant	No	No	Yes	Yes	No
P-gp substrate	Yes	Yes	No	No	Yes
CYP1A2 inhibitor	No	No	Yes	Yes	No
CYP2C19 inhibitor	Yes	Yes	Yes	Yes	Yes
CYP2C9 inhibitor	No	No	No	No	No
CYP2D6 inhibitor	No	No	No	No	No
CYP3A4 inhibitor	Yes	Yes	Yes	Yes	Yes
Log Kp (cm/s)	−7.74	−7.74	−7.30	−7.30	−7.95

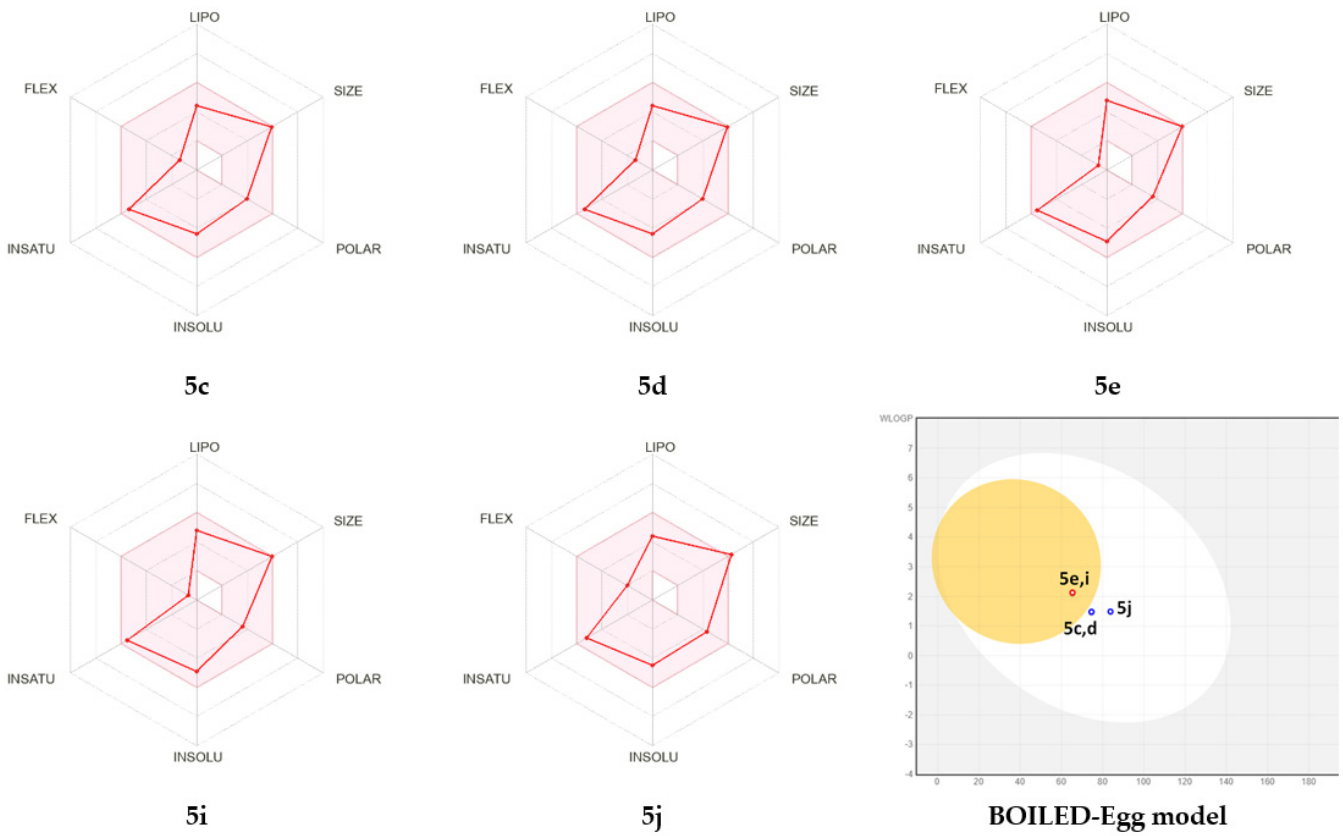

Figure 3. Bioavailability radar and BOILED-Egg model of potent synthesized compounds.

2.5. Molecular Docking and Dynamic Simulation

2.5.1. Molecular Docking

Molecular docking analyses were carried out using the Glide software to better understand the interactions of promising compounds with *S. aureus* tyrosyl-tRNA synthetase, tyrosine kinase and human pancreatic α-amylase enzymes. The protein–ligand interaction is significant in structurally based drug design. In this approach, Glide docking score, emodel, glide energy score, and MMGBSA ΔG Bind are kept as support for the present work (Figure 4).

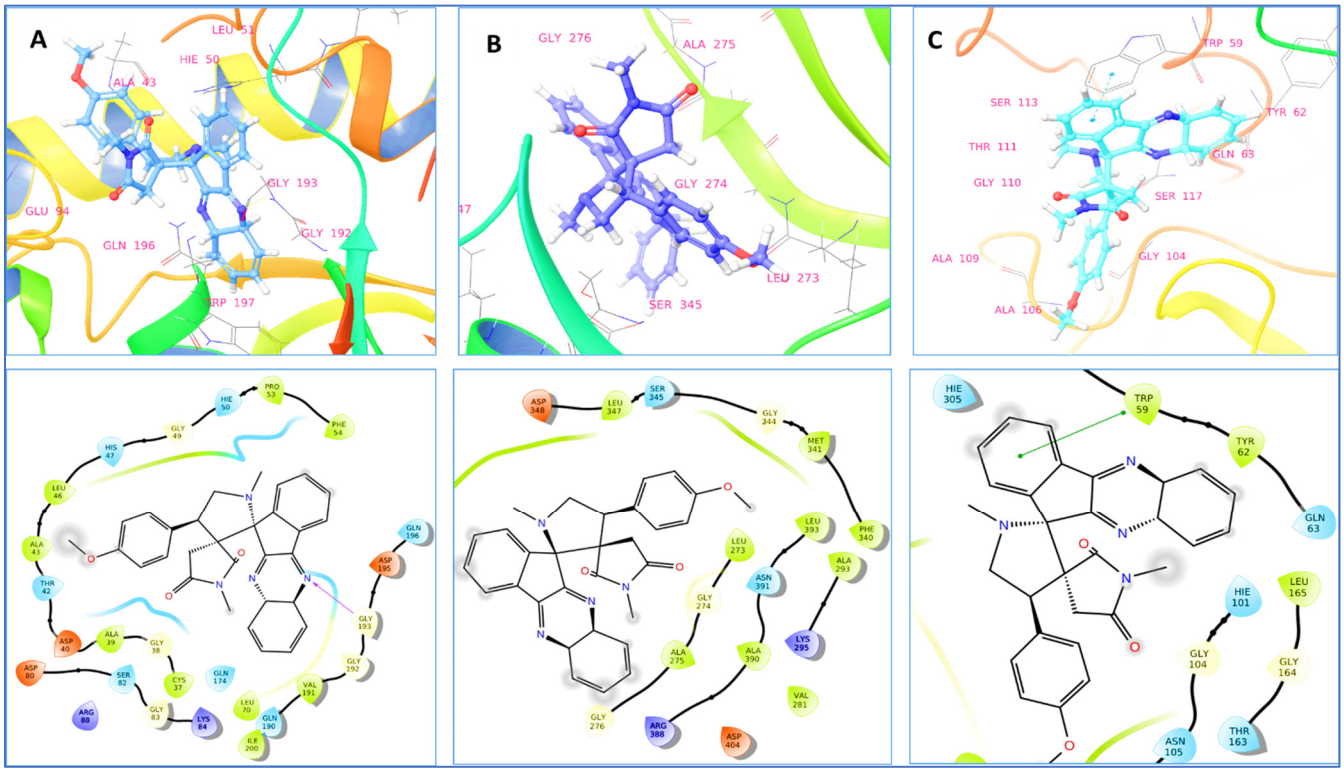

Figure 4. Binding interaction of promising compound **5d** with (**A**) *S. aureus* tyrosyl-tRNA synthetase (PDB ID: 1JIJ); (**B**) Tyrosine kinase (PDB ID: 2HCK). (**C**) Human pancreatic α-amylase (PDB ID: 2QV4).

The minimum Glide energy required for the formation of complex between the ligand and the protein indicates excellent binding affinity. Very low energy indicates that the ligand is buried in the cavity of the receptor. The Glide binding energy of the promising compounds was found to be −27.625 to −46.196 kcal/mol. According to the results of the binding study, compound 5d formed one hydrogen bond with Gly193 of the *S. aureus* tyrosyl-tRNA synthetase target at a 2.70A° bond length. The methoxyphenyl and 1-methylpyrrolidine-2,5-dione portions of compound 5d were shown to have substantial van der Waals contacts with Gly38 (−1.489 kcal/mol), Asp40 (−2.166 kcal/mol), and Ala39 (−2.154 kcal/mol), which demonstrated that the molecule is entrenched within the active site (Table 5).

Complementary van der Waals interactions are shown between the co-crystallized ligand (SB-239629) and this pocket, which are delineated by the residues Ala37, Asp38, Thr40, Ala41, Ser43, Leu44, His48 and Ile101. This implies that compound **5d** could have a tyrosyl-tRNA inhibitory effect on *S. aureus* (Figure 4A). The compound **5d** is the second highest scoring compound in tyrosine kinase protein (2HCK), with a docking score of (−5.732 kcal/mol) and binding free energy of (−53.11 kcal/mol), but it was unable to connect any hydrogen bond contacts with the 2HCK receptor while making close contacts with Leu273, Gly274, Ala275 and Gly276 (Figure 4B). Compound **5d**, on the other hand, also has the best docking score (−6.182 kcal/mol) and binding free energy

score (−59.16 kcal/mol) in human pancreatic α-amylase (2QV4). Compound **5d** in this target protein exhibits π–π interactions with hydrophobic residue Trp59 (Figure 4C). In the cavity of α-amylase, the amino acids Leu165 (−2.603 kcal/mol), Thr163 (−1.233 kcal/mol), Leu162 (−0.504 kcal/mol) and Gln63(−1.591 kcal/mol) stabilize the compound **5d** through non-bonded van der Waals interaction. Through van der Waals interactions with Leu162, Leu165, Tyr151, Ile148 and Ala198, the co-crystallized inhibitor also interacts significantly with a variety of hydrophobic protein residues inside the active site.

Table 5. Glide dock score and binding free energy of promising compounds with targeted proteins.

Compound	Docking Score	Glide Emodel	Glide Energy	Prime Energy	MMGBSA ΔG Bind
		***S. aureus* Tyrosyl-tRNA Synthetase (1JIJ)**			
5d	−6.843	−57.042	−46.196	−12980.2	−43.02
5e	−4.834	−30.317	−27.625	−12967.4	−20.76
5j	−5.529	−56.637	−44.992	−12980.4	−47.93
Reference [a]	−7.973	−98.597	−68.426	13103.87	−63.92
		Tyrosine Kinase (2HCK)			
5e	−5.804	−41.828	−39.753	−17858.1	−58.03
5d	−5.732	−45.891	−37.914	−17853	−53.11
5i	−5.288	−41.24	−36.51	−17847.7	−54.74
5c	−5.022	−32.357	−30.204	−17827.1	−34.18
Reference [a]	−8.551	−67.224	−45.767	−17945.56	−59.30
		Human Pancreatic α-Amylase (2QV4)			
5d	−6.182	−41.759	−35.02	−22748.8	−59.16
5c	−6.172	−36.006	−33.572	−22749.8	−51.25
5j	−6.146	−46.534	−38.443	−22751.3	−56.64
Reference [a]	−8.141	−99.527	−74.699	−22821.47	−76.71

[a] co-crystalized ligand.

2.5.2. Molecular Dynamic Simulations

The molecular dynamics simulation study was conducted to understand the structural stability of the complexes. The root mean square deviations of the Cα atoms from the docked complexes were analyzed to understand the rigidity of the complexes [52,53]. The average values of Cα atoms RMSD for 1JIJ-**5d** complex, 2HCK-**5d** complex and 2QV4-**5d** complex were 2.400 ± 0.46 Å, 2.655 ± 0.39 Å and 1.808 ± 0.17 Å, respectively (Figure 5). The 1JIJ-**5d** complex's RMSD pattern progressed from 2 ns to 78 ns, then displayed a steady state pattern. However, the 2HCK-5d complex had an average RMSD of 2.5 Å until 37 ns, then a rising trend with minor fluctuation until 80 ns, then the RMSD gradually decreased towards the end of the simulation. The consistency pattern of RMSD is seen in the 2QV4-5d complex, indicating more stability among the assessed complexes. All of the complexes had a maximum RMSD that was less than 3.6 Å, indicating that they were relatively stable.

To determine flexibility across the amino acid residues, the docked complexes' root mean square fluctuations (RMSF) were examined [54,55]. With the exception of the loop region and the C-terminal, overall, the amino acids were stable during the simulation window with an RMSF range of between 0.40 Å and 4.50Å. Maximum fluctuation is seen in 1JIJ-**5d** complex with Glu236 and Ser237, with RMSF of 3.763 Å and 4.274 Å, respectively. The 1JIJ amino acids that have made contact with **5d** during the simulation trajectory include: Cys37, Gly38, Ala39, Asp40, Thr42, His47, Gly49, His50, Pro53, Phe54, Asp80, Ser82, Gly83, Lys84, Glu86, Glu87, Arg88, Val89, Tyr170, Val191, Gly193, Ser194, Asp195, Gln196, Asn199, Ile221, Leu223, Gly233, Lys234 and Trp241 (Figure 6A). All these had a lower RMSF than 1.5 Å, which indicates a lower level of flexibility of the complex. Except for the amino acids Phe 424 (3.864 Å), Lys 423 (5.036 Å) and Gly 411(3.447 Å), in the 2HCK-**5d** complex all the interacting residues exhibit a lesser magnitude of RMSF. Leu273, Gly274, Ala275 and Gly276, important residues that share hydrophobic interactions in this protein, displayed RMSFs of 1.92 Å, 2.38 Å, 2.32 Å, 2.36 Å and 2.43A Å, respectively (Figure 6B).

However, only the amino acid Gly351 in the 2QV4-5d complex has an elevated RMSF of 3Å. The rest of the amino acids in this protein have a RMSF below 3 Å, which validates its stability (Figure 6C).

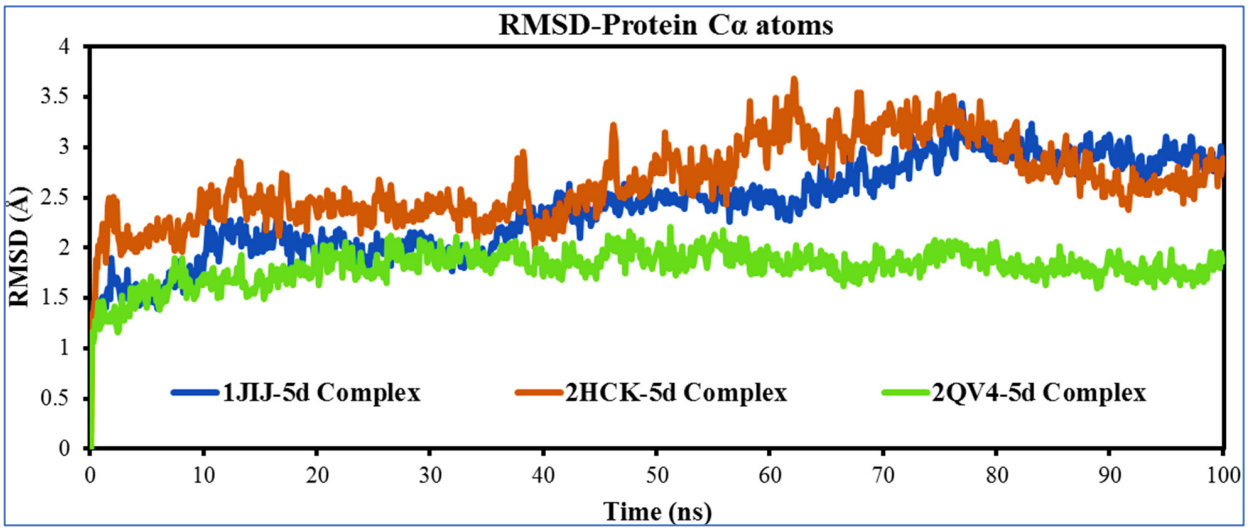

Figure 5. Time dependent RMSD plots of 1JIJ-**5d** complex (Blue), 2HCK-**5d** complex (red), and 2QV4-**5d** complex (green) obtained from 100 ns MD simulation Trajectories.

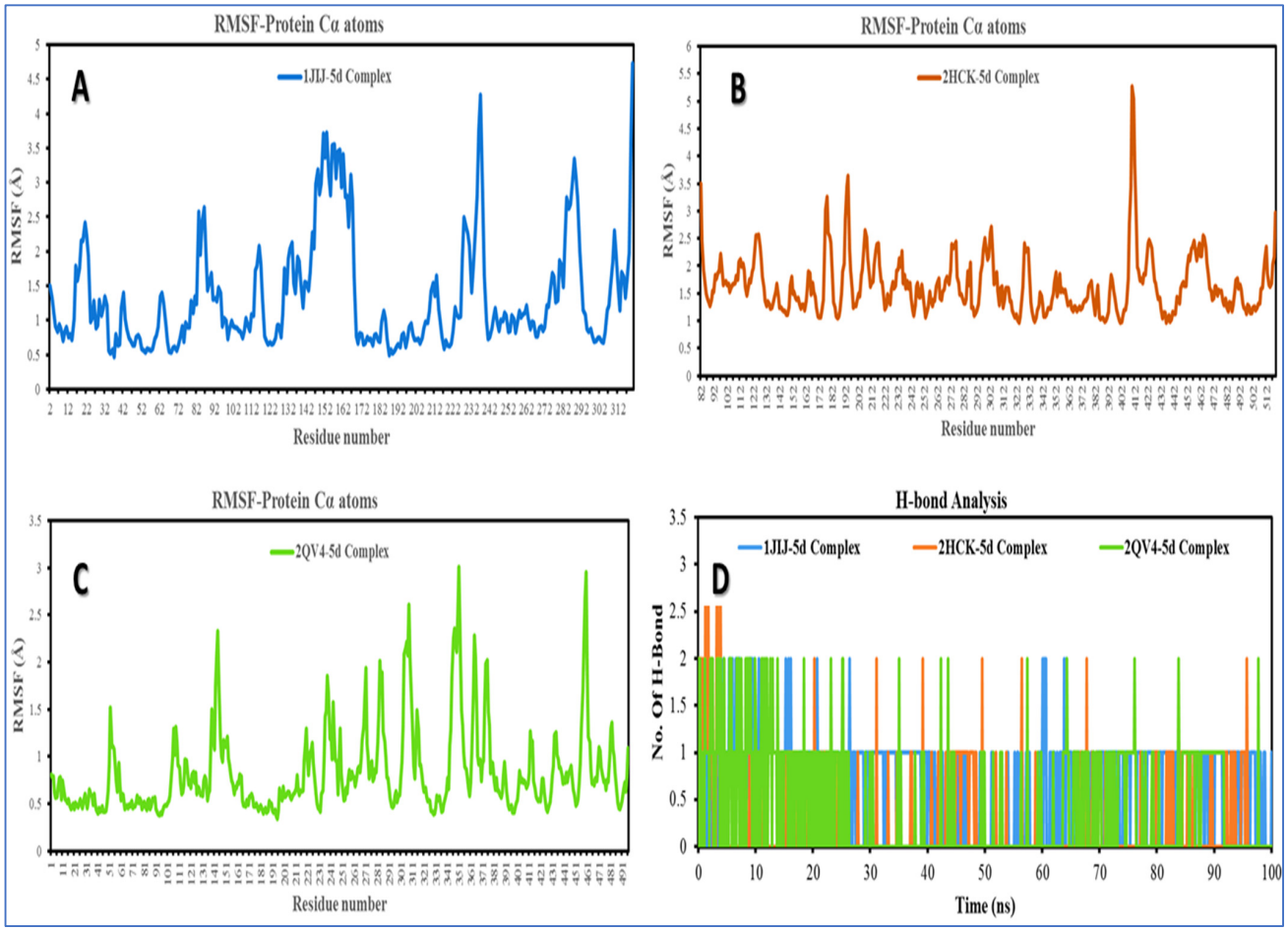

Figure 6. RMSF plot of (**A**). 1JIJ-5d complex (blue), (**B**). 2HCK-5d complex (red), (**C**). 2QV4-5d complex (green) and (**D**). Hydrogen bond analysis of all complexes.

Hydrogen bond formation is important in stabilizing the structure of proteins and ligand–protein complexes since it minimizes the system's energy. The ligand-protein hydrogen bonding patterns were studied in all the complexes and portrayed in graphs in comparison with time. According to hydrogen bonding data, the 2HCK-**5d** complex forms more hydrogen bonds with several critical residues at the binding site, whereas another complex forms hydrogen bonds with one to two residues. In the case of the 2QV4-**5d** complex, a maximum of two hydrogen bonds was formed, while the 1JIJ-**5d** complex, 2HCK-**5d** complex formed one hydrogen bond each (Figure 6D). However, the average number of hydrogen bonds formed with the 1JIJ-**5d** complex, 2HCK-**5d** complex and 2QV4-**5d** was 0.75, 0.20, and 0.34, respectively, which suggests that hydrogen bond formation events happen moderately with the 2HCK-**5d** complex, and it may be stabilized by hydrophobic interaction as well as ionic interaction. Assessing the radius of gyration (RGyr), which may provide information on the system's overall tightness, is another way of determining the root mean square distance of a collection of atoms from their common center of mass [56,57]. On analyzing the RGyr plot, we have interpreted that the RGyr values of the 1JIJ-**5d** complex, 2HCK-**5d** complex and 2QV4-**5d** complex were 4.254 Å, 4.096 Å and 4.248 Å, respectively. The RGyr profiles of the complexes were stable and maintained their integrity throughout the duration of the simulation (Figure 7).

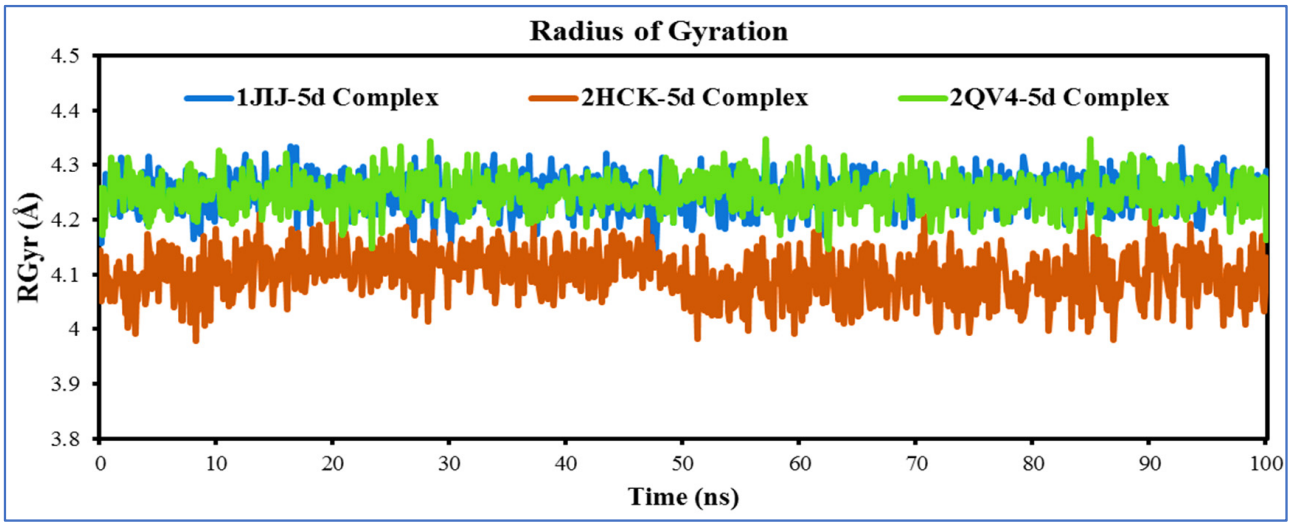

Figure 7. Time dependent radius of gyration (RGyr) plot of 1JIJ-5d complex (blue), 2HCK-5d complex (red) and 2QV4-5d complex (green) obtained from 100 ns MD simulation trajectories.

2.5.3. PCA Analysis

In order to comprehend how proteins, move in response to ligand binding, the PCA of Cα atoms was investigated. By selecting crucial data points that indicate eigenvectors and eigenvalues that reflect the associated protein motion and the direction of motion, PCA analysis may project the high-dimensional protein dynamics into the low-dimensional space [58,59]. The PC1 and PC2 contributions for compound **5d** in a complex with the 1JIJ, 2HCK and 2QV4 systems were 42.81%, 37.14%, 16.73% and 13.06%, 12.51% and 13.24%, respectively. The data indicate that a smaller area of phase space was covered by each of the three drug–protein complexes. When compared to the 1JIJ-**5d** complex and 2HCK-**5d** complex, the 2QV4-**5d** complex in particular lowered the essential dynamics to the lowest level of functional motion. In conclusion, the correlation between the PCA results and the RMSD and RMSF results strengthens the validity of the study (Figure 8).

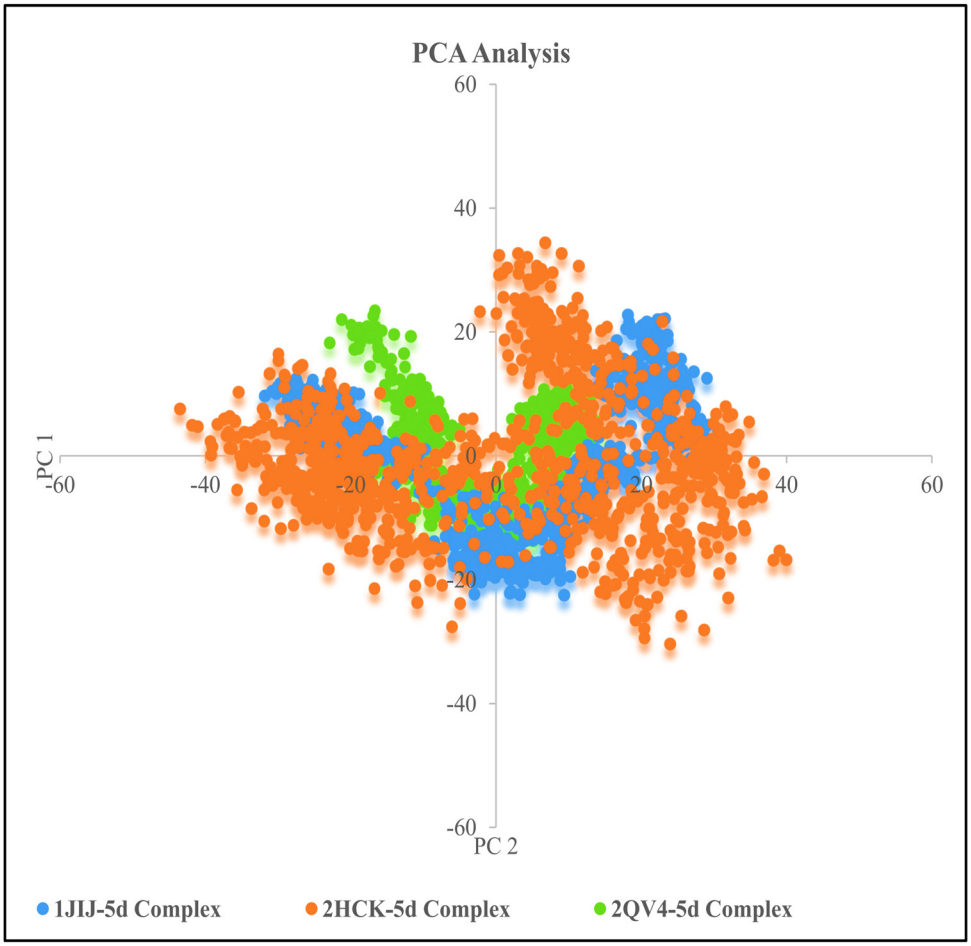

Figure 8. Two-dimensional projection of motion of trajectory of compound **5d** bound with proteins over the PC1 and PC2.

2.5.4. MMGBSA Binding Free Energy Analysis

Any small molecule's binding energy can reflect its affinity for a protein. MM/GBSA is a popular and reliable approach for estimating post-simulation binding free energy because it considers protein flexibility, polarizability, solvability, and entropy, which are frequently overlooked in docking procedures, and it is therefore more accurate than that of most scoring functions in use in molecular docking [59]. To explore the affinity of compound **5d** towards the 1JIJ, 2HCK and 2QV4, the binding free energy was estimated from the trajectory of MD simulation using the MMGBSA approach. The stability of the receptor-ligand complex is considered strong when the computed values of binding free energies are more negative. According to the Table 6 MMGBSA results, compound **5d** forms a stable and strong bond with the 1JIJ, 2HCK, and 2QV4; these complexes are thermodynamically favorable. In particular, binding energies of −34.15 and −45.92 kcal/mol were obtained for the 2HCK-**5d** complex and 2QV4-**5d** complex, respectively, while a much higher value was found for the 1JIJ-**5d** complex (−53.25kcal/mol); hence, the compound 5d order of affinity towards protein was as follows: 2HCK > 2QV4 > 1JIJ. Additionally, Tables S1–S3 (see supplementary materials) includes the results of computations for several additional interactions, including electrostatic energy, van der Waals interactions, nonpolar solvation energy, etc. The binding energy was revealed to be influenced adversely by solvation energy (ΔG Bind Solv GB) and favorably by Coulomb/electrostatic (ΔG Bind Coulomb) van der Waals energy (ΔG Bind VDW).

Table 6. The Prime MMGBSA (ensemble-averaged) binding free energies (kcal/mol) of compound **5d** with targeted proteins during the 100 ns MD simulation.

MMGBSA Components (kcal/mol)	1JIJ-5d Complex	2HCK-5d Complex	2QV4-5d Complex
ΔG Bind	−53.25	−34.15	−45.92
ΔG Bind Coulomb	−9.72	−6.28	−3.55
ΔG Bind H bond	−0.54	−0.19	−0.33
ΔG Bind Lipo	−18.56	−12.93	−20.37
ΔG Bind Solv GB	34.23	19.24	16.57
ΔG Bind VDW	−58.70	−34.61	−37.90

3. Materials and Methods

3.1. General Experimental Methods

^{1}H and ^{13}C NMR were recorded using a Bruker spectrometer (Bruker, Bremen, Germany) operating at 400 and 100 MHz, respectively. The chemical shifts were recorded in ppm relative to tetramethylsilane and with the solvent resonance as the internal standard. Data were reported as follows: chemical shift, multiplicity (brs = broad singlet, s = singlet, d = doublet, dd = doublet of doublets, t = triplet, m = multiplet), coupling constants (Hz), integration. 13C NMR data were collected with complete proton decoupling. Chemical shifts were reported in ppm with respect to TMS with the solvent resonance as internal standard. Elemental analyses were performed on a Perkin Elmer 2400 Series II Elemental CHNS analyzer. Column chromatography was carried out on silica gel (300–400 mesh, Qingdao Marine Chemical Ltd., Qingdao, China). Thin layer chromatography (TLC) was performed on TLC silica gel 60 F254 plates 0.2 mm 200 × 200 nm. The spots were visualized using UV light at 254 nm and 360 nm.

General Procedure for the Preparation of Spiro-Indenoquinoxaline Pyrrolizidines **5a–m**

A mixture of ninhydrin **1** (0.5 mmol) and 1,2-phenylenediamine **2** (0.5 mmol) and sarcosine **3** (0.5 mmol) was stirred for 10 min in 10 mL of methanol followed by the addition of dipolarophile **4** (0.5 mmol). The mixture was then refluxed for 8h until completion of the reaction as evidenced by TLC. The solvent was removed under reduced pressure and the crude product obtained was purified by column chromatography on silica gel using ethylacetate-cyclohexane (3:7 v/v) as eluent to provide the pure product **5a–m**.

5a: Spiro [2,11″]indeno-[1,2b]-quinoxaline-spiro-[3,3′]-N-methylsuccinimide-4-(phenyl) hexahydro-1H-pyrrolidines.

White solid (105 mg, 81%); mp 173–175 °C; IR (FTIR, cm^{-1}): ν = 2970, 2900, 1695, 1405. 1H NMR (400 MHz, CDCl3) δ (ppm): 2.05 (s, 3H, CH3), 2.17–2.26 (m, 2H, H4′), 2.63(s, 3H, CH3), 3.79–3.83 (t, 1H, *J* = 8 Hz, H5), 4.39–4.44 (t, 1H, *J* = 8 Hz, H5), 4.72–4.77 (t, 1H, *J* = 8 Hz, H4), 7.31–8.27 (m, 13H, Ar-H). 13C NMR (100 MHz, CDCl3) δ 24.6, 34.8, 36.3, 49.6, 59.6, 62.7, 78.9, 122.5, 127.4, 127.7, 128.9, 129.2, 129.4, 129.6, 130.1, 130.3, 131.7, 137.9, 138.0, 140.8, 142.2, 144.4, 153.7, 161.2, 174.6, 179.9. Anal. Calcd. For C29H24N4O2: C, 75.62; H, 5.21; N, 12.15. Found. C, 75.63; H, 5.20; N, 12.16.

5b: Spiro [2,11″]indeno-[1,2b]-quinoxaline-spiro-[3,3′]-N-methylsuccinimide-4-(4-methylphenyl)hexahydro-1H-pyrrolidines.

White solid (85 mg, 77%); mp 183–185 °C; IR (FTIR, cm^{-1}): ν = 2968, 2904, 1705, 1393. 1H NMR (400 MHz, CDCl3) δ (ppm): 2.05 (s, 3H, CH3), 2.20–2.24 (m, 2H, H4′), 2.36(s, 3H, CH3), 2.63(s, 3H, CH3), 3.77–3.81 (t, 1H, *J* = 8 Hz, H5), 4.37–4.41 (t, 1H, *J* = 8 Hz, H5), 4.70–4.72 (t, 1H, *J* = 8 Hz, H4), 7.22–8.26 (m, 12H, Ar-H). 13C NMR (100 MHz, CDCl3) δ 21.1, 24.6, 34.8, 36.2, 49.3, 59.5, 62.7, 78.8, 122.5, 127.5, 129.2, 129.4, 129.6, 129.8,129.9, 130.2, 130.3, 131.6, 138.0, 134.2, 134.7, 137.4, 137.9, 140.8, 153.7, 161.2, 174.7, 179.9. Anal. Calcd. For C30H26N4O2: C, 75.92; H, 5.47; N, 11.80. Found. C, 75.94; H, 5.50; N, 11.81.

5c: Spiro [2,11″]indeno-[1,2b]-quinoxaline-spiro-[3,3′]-N-methylsuccinimide-4-(2 methoxyphenyl)hexahydro-1H-pyrrolidines.

White solid (102 mg, 80%); mp 196–198 °C; 1H NMR (400 MHz, CDCl3) δ (ppm): 2.04 (s, 3H, CH3), 2.37–2.45(d, 1H, *J* = 9 Hz, H4′), 2.86 (s, 3H, CH3), 3.63 (s, 3H, OCH3), 3.73–3.77 (t, 1H, *J* = 8 Hz, H5), 4.63–4.67 (t, 1H, *J* = 8 Hz, H5), 4.79–4.84 (t, 1H, *J* = 12 Hz, H4), 6.82–8.19 (m, 12H, Ar-H). 13C NMR (100 MHz, CDCl3) δ 24.7, 35.1, 35.7, 43.1, 55.1, 56.6, 60.6, 78.9, 120.7, 122.3, 126.0, 127.5, 128.5, 129.1, 129.2, 129.5, 130.0, 130.1, 130.4, 132.0, 138.6, 141.0, 141.9, 143.7, 153.3, 162.0, 175.5, 181.1. Anal. Calcd. For C30H26N4O3: C, 73.44; H, 5.30; N, 11.41. Found. C, 73.45; H, 5.31; N, 11.42.

5d: Spiro [2,11″]indeno-[1,2b]-quinoxaline-spiro-[3,3′]-N-methylsuccinimide-4-(4-methoxyphenyl)hexahydro-1H-pyrrolidines.

White solid (69 mg, 65%); mp 179–181 °C; IR (FTIR, cm^{-1}): ν = 2984, 2903, 1692, 1393. 1H NMR (400 MHz, CDCl3) δ (ppm): 2.10 (s, 3H, CH3), 2.35–2.46 (m, 2H, H4′), 2.59(s, 3H, CH3), 3.72–3.84 (t, 2H, *J* = 8 Hz, H5), 3.91 (s, 3H, OCH3), 4.89–4.94(t, 1H, *J* = 8 Hz, H4), 7.34–8.10 (m, 12H, Ar-H). 13C NMR (100 MHz, CDCl3) δ 24.1, 31.7, 34.5, 48.0, 52.5, 55.4, 61.6, 79.3, 122.5, 124.8, 127.2, 128.9, 129.1, 129.5, 130.1, 130.3, 130.7, 131.6, 132.4, 132.5, 132.9, 133.5, 136.8, 140.3, 152.6, 161.0, 174.6, 177.4. Anal. Calcd. For C30H26N4O3: C, 73.44; H, 5.30; N, 11.41. Found. C, 73.45; H, 5.31; N, 11.40.

5e: Spiro [2,11″]indeno-[1,2b]-quinoxaline-spiro-[3,3′]-N-methylsuccinimide-4-(4-chlorophenyl)hexahydro-1H-pyrrolidines.

White solid (80 mg, 75%); mp 182–184 °C; 1H NMR (400 MHz, CDCl3) δ (ppm): 2.11 (s, 3H, CH3), 2.36–2.41 (m, 2H, H4′), 2.59 (s, 3H, CH3), 3.67–3.72(m, 2H, H5), 4.69–4.75 (t, 1H, *J* = 12 Hz, H4), 7.31–8.14 (m, 12H, Ar-H). 13C NMR (100 MHz, CDCl3) δ 24.2, 31.7, 34.5, 48.0, 52.4, 61.6, 79.1, 122.4, 127.0, 128.0, 128.3, 129.0, 129.1, 129.6, 130.1, 131.3, 130.7, 131.6, 132.1, 132.4, 138.8, 142.9, 152.5, 160.9, 174.3, 178.7. Anal. Calcd. For C29H23ClN4O2: C, 70.36; H, 4.64; N, 11.31 Found. C, 70.38; H, 4.65; N, 11.29.

5f: Spiro [2,11″]indeno-[1,2b]-quinoxaline-spiro-[3,3′]-N-methylsuccinimide-4-(4-bromophenyl)hexahydro-1H-pyrrolidines.

White solid (52 mg, 68%); mp 200–202 °C; 1H NMR (400 MHz, CDCl3) δ (ppm): 2.04 (s, 3H, CH3), 2.08–2.11 (m, 2H, H4′), 2.65 (s, 3H, CH3), 3.80–3.84(t, 1H, *J* = 8 Hz, H5), 4.33–4.38 (t, 1H, *J* = 12 Hz, H4), 4.65–4.70(t, 1H, *J* = 12Hz, H4), 7.50–8.24 (m, 12H, Ar-H). 13C NMR (100 MHz, CDCl3) δ 24.7, 34.7, 36.3, 49.0, 59.9, 62.5, 78.9, 122.6, 127.2, 129.3, 129.4, 130.4, 1130.5, 131.3, 131.8, 131.9, 132.1, 132.6, 137.1, 140.7, 142.2, 144.1, 153.7, 161.2, 174.2, 179.9. Anal. Calcd. For C29H23BrN4O2: C, 64.56; H, 4.26; N, 10.38. Found. C, 64.57; H, 4.28; N, 10.39.

5g: Spiro [2,11″]indeno-[1,2b]-quinoxaline-spiro-[3,3′]-N-methylsuccinimide-4-(4-fluorophenyl)hexahydro-1H-pyrrolidines.

White solid (83 mg, 71%); mp 205–207 °C; ^{1}H NMR (400 MHz, CDCl3) δ (ppm): 2.04 (s, 3H, CH3), 2.10–2.38 (m, 2H, H4′), 2.64 (s, 3H, CH3), 3.80–3.84(t, 1H, *J* = 8 Hz, H5), 4.33–4.38 (t, 1H, *J* = 12 Hz, H5), 4.68–4.73 (t, 1H, *J* = 8 Hz, H4), 7.09–8.23 (m, 12H, Ar-H). 13C NMR (100 MHz, CDCl3) δ 24.6, 34.7, 36.3, 48.9, 60.1, 62.6, 78.9, 122.5, 127.3, 129.3, 129.5, 130.4, 131.7, 131.8, 132.0, 132.1, 133.0, 138.0, 140.7, 144.2, 153.7, 161.3, 174.3, 180.0. Anal. Calcd. For C29H23FN4O2: C, 72.78; H, 4.80; N, 11.70. Found. C, 72.77; H, 4.81; N, 11.71.

5h: Spiro [2,11″]indeno-[1,2b]-quinoxaline-spiro-[3,3′]-N-methylsuccinimide-4-(4-thiophenyl)hexahydro-1H-pyrrolidines.

White solid (52 mg, 59%); mp 203–205 °C; ^{1}H NMR (400 MHz, CDCl3) δ (ppm): 2.10 (s, 3H, CH3), 2.33–2.36 (d, 1H, *J* = 12 Hz, H4′), 2.62 (s, 3H, CH3), 3.09–3.14 (d, 1H, *J* = 20, H4′), 3.68–3.74 (m, 2H, H5), 4.69 (t, 1H, *J* = 8 Hz, H4), 7.20–8.27 (m, 12H, Ar-H). 13C NMR (100 MHz, CDCl3) δ 24.2, 31.9, 34.5, 48.8, 52.4, 61.4, 79.2, 122.5, 124.7, 127.1, 128.9, 129.5, 129.7, 130.2, 130.9, 131.6, 132.5, 132.8, 136.8, 138.5, 142.2, 143.1, 152.6, 161.0, 174.5, 178.6. Anal. Calcd. For C27H22N4O2 S: C, 69.50; H, 4.71; N, 12.00. Found. C, 69.49; H, 4.72; N, 12.02.

5i: Spiro [2,11″]indeno-[1,2b]-quinoxaline-spiro-[3,3′]-N-methylsuccinimide-4-(3-chloro-phenyl)hexahydro-1H-pyrrolidines.

White solid (96 mg, 70%); mp 193–195 °C; 1H NMR (300 MHz, CDCl3) δ (ppm): 2.04 (s, 3H, CH3), 2.10–2.12(m, 2H, H4′), 3.82–3.88 (t, 1H, *J* = 9 Hz, H5), 4.34–4.40 (t, 1H, *J* = 9.3 Hz,

H5), 4.63–4.69 (t, 1H, *J* = 8.7 Hz, H4), 7.32–8.38 (m, 12H, Ar-H). 13C NMR (75 MHz, CDCl3) δ 24.6, 31.5, 34.8, 49.1, 52.9, 62.4, 79.7, 122.5, 124.8, 126.3, 126.6, 129.0, 129.6, 130.3, 130.5, 130.8, 131.6, 132.4, 132.5, 134.3, 134.9, 136.8, 141.5, 156.6, 161.2, 174.4, 177.0. Anal. Calcd. For C29H23ClN4O2: C, 70.36; H, 4.64; N, 11.31. Found. C, 70.33; H, 4.68; N, 11.30.

5j: Spiro [2,11″]indeno-[1,2b]-quinoxaline-spiro-[3,3′]-N-methylsuccinimide-4-(3,4-dimethoxyphenyl)hexahydro-1H-pyrrolidines.

White solid (79 mg, 63%); mp 211–213 °C; 1H NMR (400 MHz, CDCl3) δ (ppm): 2.10 (s, 3H, CH3), 2.36–2.38(d, 1H, *J* = 8 Hz, H4′), 2.41 (s, 3H, CH3), 3.66–3.69 (d, 1H, *J* = 12 Hz, H4′), 3.70–3.73 (m, 2H, H5), 4.01 (s, 6H, 2(OCH3)), 4.50–4.54 (t, 1H, *J* = 8 Hz, H4), 6.95–8.22 (m, 11H, Ar-H). 13C NMR (100 MHz, CDCl3) δ 24.2, 31.5, 34.5, 49.9, 52.5, 55.9, 56.0, 61.8, 79.4, 122.3, 126.5, 126.9, 127.2, 128.9, 129.0, 129.1, 129.5, 130.1, 130.2, 130.6, 138.6, 140.5, 141.3, 142.1, 143.2, 148.4, 150.8, 161.1, 174.6, 181.4. Anal. Calcd. For C31H28N4O4: C, 71.51; H, 5.37; N, 10.75. Found. C, 71.51; H, 5.36; N, 11.76.

5k: Spiro [2,11″]indeno-[1,2b]-quinoxaline-spiro-[3,3′]-N-methylsuccinimide-4-(3-bromo-4-methoxyphenyl)hexahydro-1H-pyrrolidines.

White solid (68mg, 73%); mp 209–211 °C; 1H NMR (400 MHz, CDCl3) δ (ppm): 2.10 (s, 3H, CH3), 2.33–2.38 (m, 2H, H4′), 2.59 (s, 3H, CH3), 3.64–3.72 (m, 2H, H5), 4.00 (s, 3H, OCH3), 4.87–4.93 (t, 1H, *J* = 8 Hz, H4), 6.99–8.22 (m, 11H, Ar-H). 13C NMR (100 MHz, CDCl3) δ 24.2, 31.7, 34.5, 49.4, 52.4, 56.3, 61.6, 79.2, 122.3, 127.0, 127.8, 128.9, 129.1, 129.6, 130.1, 130.7, 132.2, 136.6, 138.5, 141.2, 142.2, 143.0, 152.6, 161.0, 174.4, 177.8. Anal. Calcd. For C30H25BrN4O3: C, 63.27; H, 4.39; N, 9.83. Found. C, 63.28; H, 4.41; N, 9.84.

5l: Spiro [2,11″]indeno-[1,2b]-quinoxaline-spiro-[3,3′]-N-methylsuccinimide-4-(3-bromo-4-hydroxy-phenyl)hexahydro-1H-pyrrolidines.

White solid (73 mg, 64%); mp 189–191 °C; 1H NMR (400 MHz, CDCl3) δ (ppm): 2.09 (s, 3H, CH3), 2.16–2.28(m, 2H, H4′), 2.62 (s, 3H, CH3), 3.75–3.81 (t, 1H, *J* = 8 Hz, H5), 4.38–4.43 (t, 1H, *J* = 8 Hz, H5), 4.71–4.75 (t, 1H, *J* = 8 Hz, H4), 7.42–8.29 (m, 11H, Ar-H). 13C NMR (100 MHz, CDCl3) δ 24.6, 34.8, 36.4, 49.1, 59.7, 62.8, 79.0, 122.5, 125.8, 126.1, 127.4, 129.2, 129.4, 129.6, 129.8, 130.3, 131.7, 134.8, 137.9, 140.8, 142.2, 144.5, 150.6, 153.7, 161.3, 174.8, 180.0. Anal. Calcd. For C29H23BrN4O3: C, 62.70; H, 4.14; N, 10.08. Found. C, 62.74; H, 4.15; N, 10.11.

5m: Spiro [2,11″]indeno-[1,2b]-quinoxaline-spiro-[3,3′]-N-methylsuccinimide-4-(3,5-dibromo-4-hydroxyphenyl)hexahydro-1H-pyrrolidines.

White solid (98 mg, 80%); mp 214–216 °C; 1H NMR (400 MHz, CDCl3) δ (ppm): 2.00 (s, 3H, CH3), 2.47–2.51 (m, 2H, H4′), 2.69 (s, 3H, CH3), 3.82–3.87 (t, 1H, *J* = 8 Hz, H5), 4.23–4.28 (t, 1H, *J* = 12 Hz, H5), 4.49–4.55 (t, 1H, *J* = 8 Hz, H4), 7.57–8.45 (m, 10H, Ar-H). 13C NMR (100 MHz, CDCl3) δ 24.7, 34.5, 36.6, 48.3, 61.1, 62.6, 78.8, 122.6, 125.7, 126.8, 129.3, 129.6, 130.5, 130.6, 131.9, 133.2, 134.0, 138.2, 140.7, 142.2, 143.8, 148.9, 153.5, 161.4, 174.1, 180.3. Anal. Calcd. For C29H22 Br2N4O3: C, 54.86; H, 3.46; N, 8.82. Found. C, 54.89; H, 3.47; N, 8.84.

3.2. Pharmacological Study

3.2.1. Antimicrobial Activity

In the present study, the antimicrobial activity of the synthesized compounds was screened by agar disc diffusion method according to the protocol described by Kadri et al. [49], against four bacteria, namely *Staphylococcus aureus* ATCC 25923, *Micrococccus luteus* NCIMB 8166, *Escherichia coli* ATCC 25,922 and *Pseudomonas aeruginosa* ATCC 27853. Moreover, it was tested against two fungal strains, namely *Candida albicans* ATCC 90,028 and *Candida krusei* ATCC 6258. The inoculums of the microorganisms were adjusted to 0.1 at OD600 for bacteria and 0.4 at OD540 for yeasts) and then streaked onto Muller–Hinton (MH) and Sabouraud (SB) agar plates using a sterile cotton mop. Sterile filter discs (diameter 6 mm, Biolife Italy) were placed at the surface of the appropriate agar media and 10 µL of the product dissolved in 10% of solvent was dropped onto each disc. Tetracycline (10 mg/mL; 10 µL/disc) and amphotericin B (10 mg/mL; 10 µL/disc) were used as reference antibiotics. After incubation at 37 °C for 24h, the antibacterial activities

were evaluated by measuring an inhibition zone formed around the disc. Each assay was performed in triplicate.

3.2.2. Antioxidant Activity

DPPH free Radical Scavenging Activity.

DPPH, the stable artificial free radicals, has been widely used for the measurement of free radical scavenging capacity of the compounds in ethanol and aqueous systems [60]. Briefly, 2 mL DPPH solution (0.2 mM, in 95% ethanol) was incubated with 2 mL different concentrations of compounds solution. Then, the reaction mixture was shaken and incubated in the dark for 40 min at room temperature. The absorbance was immediately recorded at 517 nm against ethanol with a spectrophotometer (Metash, model UV-5200, Shanghai Xiwen Biotech. Co., Ltd, Shanghai, China). The DPPH free radical scavenging rate was calculated using the equation:

$$\text{DPPH scavenging activity (\%)} = A_0 - A_1/A_0 \times 100$$

where A_0 was the absorbance of the control reaction (containing all reagents except the tested compound), and A1 was the absorbance of the test reaction (containing all reagents with the tested compound). The percentage of DPPH radical scavenging activity was plotted against the sample concentration to acquire the IC_{50} value, defined as the concentration of sample necessary to cause 50% inhibition. Radical scavenging activity (RSA) was calculated from the IC_{50} value as the equation: $RSA = pIC_{50} = -\lg[IC_{50}]$. The smaller the IC_{50} value, the larger is the RSA value and the higher is the antioxidant activity.

Radical Scavenging Activity ABTS.

The ABTS assay was performed as previously described by Tuberoso et al. [61]. $ABTS^+$ radical was generated by oxidation of ABTS with potassium persulfate. The blue–green ABTS was produced through the reaction between 2 mM ABTS and 70 mM potassium persulfate in water. The mixture was left to stand in the dark for 12 to 16 h before use. The ABTS solution was diluted with methanol to an absorbance of 0.700 ± 0.005 at 734 nm. Then 2 mL of diluted ABTS solution was mixed with 100 µL of samples and absorbance was measured after 1 min incubation at room temperature. A standard curve was obtained by using Trolox as standard solution. The results were expressed as µM Trolox equivalent.

The mixture of 7 mmol/L aqueous ABTS solution with 2.45 mmol/L potassium persulfate solution constitutes a stable $ABTS^+$ stock solution that was allowed to stand in the dark and at room temperature for 12 to 16 h before use. A 1 mL sample of the diluted ABTS solution (adjusted to 0.7 ± 0.02 at 743 nm) was added to 10 µL of each product. The absorbance was determined after 6 min. The percentage inhibition of the $ABTS^{\cdot}$ radical was calculated from the following equation:

$$\text{\% inhibition} = (Abs_{control} - Abs_{test})/Abs_{control} \times 100$$

Abs control: the control absorbance.

Abs test: the absorbance of the test sample after 6 min.

Ferric reducing power assay (FRAP).

The FRAP assay was used to determine the AC of the products by the reduction of Fe(III) and Fe (II). Briefly, Fe(III) was reduced to Fe(II), and Fe(II) was mixed with TPTZ to form a blue complex with strong absorption peak at 593 nm at pH = 3.6 condition. Acetate buffer (pH = 3.6), TPTZ solution (10 mM, in 40 mM hydrochloric acid) and $FeCl_3$ solution (20 mM, in water) were mixed in a ratio of 10:1:1 to prepare FRAP working solution. The products solution (0.5 mL) was mixed with 4.0 mL FRAP working solution, and reacted at 37 °C for 30 min in the dark, and the absorbance at 593 nm was immediately recorded with a spectrophotometer. The result was expressed as the equivalent amount of Trolox per mole of the samples (mol TE/mol) [62].

3.2.3. α-Amylase Inhibitory Assay

The inhibition of α-amylase enzyme assays was performed according to the protocol described by Amamou et al. [63]. Each compound was dissolved in the minimum of DMSO at different concentrations and then diluted in sodium phosphate buffer (0.02 M, pH 6.9, with 0.006 M NaCl). The DMSO level did not exceed 1% in the mixture. After that, 50 µL of each sample solution was added to 50 µL of α-amylase solution (0.5 mg/mL dissolved in the same buffer medium. After pre-incubation for 10 min at 25 °C, 50 µL of the starch solution (1% in buffer solution) was added to the mixture. After incubation at 25 °C for 10 min, the reaction was mixed with 100 µL of 3,5-dinitrosalicylic acid (DNS) solution. At this point, the test tubes were placed in a boiling water bath for 5 min, followed by cooling to room temperature. Next, each solution was diluted with 1 mL of distilled water. Over time, the absorbance was measured at 540 nm by Thermo ScientificTM MultiskanTM GO Microplate Spectrophotometer (Thermo Fisher Scientific Oy, Ratastie, Finland) using a 96-well microplate.

The α-amylase inhibitory activity was determined as follows:

$$\text{Inhibition (\%)} = 100\ [(\text{Abs}_{\text{Control}} - \text{Abs}_{\text{Sample}})/(\text{Abs}_{\text{Control}})]$$

3.3. Computational Study

3.3.1. Molecular Docking

Molecular docking was conducted in order to assess the binding interactions of the promising compounds. Initially, by using the LigPrep module synthesized compounds, their structures were transformed from 2D to low-energy 3D conformers with satisfactory bond lengths and angles. The 3D structures of *S. aureus* tyrosyl-tRNA synthetase, tyrosine kinases, and human pancreatic α-amylase were obtained from the PDB database under the accession codes 1JIJ, 2HCK and 2QV4, respectively. Before docking, all protein crystal structures were prepared using the Protein Preparation wizard tool by Schrodinger to address any structural problems. This process involves changing the bond order, adding hydrogens, looking for disulfide bonds and filling in side chains and loops that are lacking [64,65]. Constrained minimization was additionally applied to the protein structure. In which, heavier atoms in the structure are constrained to reduce torsional stress throughout this reduction phase, while hydrogens are left unconstrained. Using the Schrodinger Receptor Grid Generation tool, a crystalized ligand structure was selected to generate a 3D grid with accurate dimensions to represent the active part of the receptor [66]. The binding free energy of protein–ligand complexes was calculated using Prime of Schrodinger.

3.3.2. Molecular Dynamics (MD) Simulation

Protein–ligand complexes that showed good binding interactions were subjected to MD studies using Desmond for 100 ns [66]. The chloride and sodium ions are added to neutralize the net charge of the system to zero, and the system is submerged in an orthorhombic box (10 Å × 10 Å ×10 Å) filled with SPC water molecules [67,68]. The MD job was performed using an NPT ensemble at a 300 K temperature and 1.01325 bar pressure, which were kept throughout the simulation. To assess the stability of the docked ligands for each system, 1000 trajectories were collected during the simulations and evaluated with different parameters [69]. The conformational ensemble (1000 snapshots collected from 0 to 100 ns) acquired from the MD simulations was subjected to principal component analysis (PCA). By creating a covariance matrix and addressing the atomic movements responsible for the conformational changes, PCA aids in capturing the displacement of Cα atoms. PCA with the trj essential dynamic command was used to investigate protein-ligand confirmations and major global movements following ligand binding. The complete MD simulations were accomplished in the Z2 TWR G4 WKS, Linux (Ubuntu 18.04.3 LTS 64-bit) environment with a CPU Core i7-9700, DDR4-2666 nECC RAM and a NVIDIA Quadro P620/PCIe/SSE2 CUDA core GPU.

3.3.3. ADME Study

Pharmacokinetic properties of the titled compounds were predicted using ADME (absorption, distribution, metabolism and excretion) descriptors by a SwissADME online server (http://www.swissadme.ch/ assessed on 29 July 2022) [70,71].

4. Conclusions

The present report details the design and synthesis of a novel series of spiropyrrolidine tethered indeno-quinoxaline heterocyclic hybrids as potent antimicrobial, antioxidant and antidiabetic agents. The structures of the aforementioned compounds were confirmed using different spectroscopic techniques. These designed compounds were evaluated in vitro for their antimicrobial, antioxidant and antidiabetic potential. The results demonstrated that most of the tested compounds showed potent antibacterial and antifungal activities towards pathogenic strains. Interestingly, these analogues also exhibited remarkable α-amylase inhibitory effects. Molecular docking and molecular dynamics simulation studies revealed that compound 5d in complex with *S. aureus* tyrosyl-tRNA synthetase, Tyrosine kinase, and human pancreatic α-amylase have good docking and molecular dynamics profiles. Some of the studied compounds can be considered promising lead compounds in the design of more potent dual antimicrobials and antidiabetic agents.

Supplementary Materials: The following supporting information can be downloaded at: https://www.mdpi.com/article/10.3390/molecules27217248/s1. Figure S1. ^{1}H NMR ($CDCl_3$) spectrum of Compound (**5a**), Figure S2. ^{13}C NMR ($CDCl_3$) spectrum of Compound (**5a**), Figure S3. ^{1}H NMR ($CDCl_3$) spectrum of Compound (**5b**), Figure S4. ^{13}C NMR ($CDCl_3$) spectrum of Compound (**5b**), Figure S5. ^{1}H NMR ($CDCl_3$) spectrum of Compound (**5c**), Figure S6. ^{13}C NMR ($CDCl_3$) spectrum of Compound (**5c**) Figure S7. ^{1}H NMR ($CDCl_3$) spectrum of Compound (**5d**), Figure S8. ^{13}C NMR ($CDCl_3$) spectrum of Compound (**5d**), Figure S9. ^{1}H NMR ($CDCl_3$) spectrum of Compound (**5e**), Figure S10. ^{13}C NMR ($CDCl_3$) spectrum of Compound (**5e**), Figure S11. ^{1}H NMR ($CDCl_3$) spectrum of Compound (**5f**), Figure S12. ^{13}C NMR ($CDCl_3$) spectrum of Compound (**5f**), Figure S13. ^{1}H NMR ($CDCl_3$) spectrum of Compound (**5g**), Figure S14. ^{13}C NMR ($CDCl_3$) spectrum of Compound (**5g**), Figure S15. ^{1}H NMR ($CDCl_3$) spectrum of Compound (**5h**), Figure S16. ^{13}C NMR ($CDCl_3$) spectrum of Compound (**5h**), Figure S17. ^{1}H NMR ($CDCl_3$) spectrum of Compound (**5i**), Figure S18. ^{13}C NMR ($CDCl_3$) spectrum of Compound (**5i**), Figure S19. ^{1}H NMR ($CDCl_3$) spectrum of Compound (**5j**), Figure S20. ^{13}C NMR ($CDCl_3$) spectrum of Compound (**5j**), Figure S21. ^{1}H NMR ($CDCl_3$) spectrum of Compound (**5k**), Figure S22. ^{13}C NMR ($CDCl_3$) spectrum of Compound (**5k**), Figure S23. ^{1}H NMR ($CDCl_3$) spectrum of Compound (**5l**), Figure S24. ^{13}C NMR ($CDCl_3$) spectrum of Compound (**5l**), Figure S25. ^{1}H NMR ($CDCl_3$) spectrum of compound (**5m**), Figure S26. ^{13}C NMR ($CDCl_3$) spectrum of Compound (**5m**), Figure S27. ^{1}H-^{1}HCOSY ($CDCl_3$) spectrum of Compound (**5a)**, Figure S28. ^{1}H-^{1}H NOESY($CDCl_3$) spectrum of Compound (**5a)**, Figure S29. HMBC ($CDCl_3$) spectrum of Compound (**5a)**, Figure S30. IR Spectra of Compound (**5a**). Table S1: MM-GBSA binding free energies components for the 1JIJ-5d Complex obtained from molecular dynamics trajectories; Table S2: MM-GBSA binding free energies components for the 2HCK-5d Complex obtained from molecular dynamics trajectories; Table S3: MM-GBSA binding free energies components for the 2QV4-5d Complex obtained from molecular dynamics trajectories.

Author Contributions: Conceptualization, A.K., K.A., S.G., N.B., W.S.H., M.B.H., M.A., M.I.H., K.H. and M.S.; methodology, A.K., K.A., S.G., N.B., M.B.H., A.D. and A.T.; software, I.A., H.P. and A.K.; investigation, I.A., H.P., A.K., A.D., A.T., K.A. and S.G.; writing—original draft preparation, K.A., I.A., H.P., S.G. and A.K.; writing—review and editing, A.K., I.A., K.A., S.G. and E.N.; supervision, E.N. and A.K.; project administration, E.N. All authors have read and agreed to the published version of the manuscript.

Funding: This research has been funded by Scientific Research Deanship at University of Ha'il-Saudi Arabia through project number MDR-22 021.

Institutional Review Board Statement: Not applicable.

Informed Consent Statement: Not applicable.

Data Availability Statement: Not applicable.

Conflicts of Interest: The authors declare no conflict of interest.

Sample Availability: Samples of the compounds are available from the authors.

References

1. Lammie, S.L.; Hughes, J.M. Antimicrobial resistance, food safety, and one health: The need for convergence. *Annu. Rev. Food Sci. Technol.* **2016**, *7*, 287–312. [CrossRef] [PubMed]
2. Rana, M.S.; Usman, M.; Salman, M.; Alam, M.M.; Ikram, A.; Umair, M.; Qadir, M. Potential impact of COVID-19 pandemic on escalating antimicrobial resistance in Pakistan. *J. Infect.* **2021**, *83*, 12–13. [CrossRef] [PubMed]
3. Martínez-Álvarez, S.; Sanz, S.; Olarte, C.; Hidalgo-Sanz, R.; Carvalho, I.; Fernández-Fernández, R.; Torres, C. Antimicrobial Resistance in Escherichia coli from the Broiler Farm Environment, with Detection of SHV-12-Producing Isolates. *Antibiotics* **2022**, *11*, 444. [CrossRef] [PubMed]
4. Larsson, D.G.; Flach, C.F. Antibiotic resistance in the environment. *Nat. Rev. Microbiol.* **2022**, *20*, 257–269. [CrossRef] [PubMed]
5. Dhingra, S.; Rahman, N.A.A.; Peile, E.; Rahman, M.; Sartelli, M.; Hassali, M.A.; Haque, M. Microbial resistance movements: An overview of global public health threats posed by antimicrobial resistance, and how best to counter. *Front. Public Health* **2020**, *8*, 535668. [CrossRef]
6. Hajlaoui, H.; Arraouadi, S.; Mighri, H.; Ghannay, S.; Aouadi, K.; Adnan, M.; Kadri, A. HPLC-MS profiling, antioxidant, antimicrobial, antidiabetic, and cytotoxicity activities of Arthrocnemum indicum (Willd.) Moq. extracts. *Plants* **2022**, *11*, 232. [CrossRef]
7. Ghannay, S.; Snoussi, M.; Messaoudi, S.; Kadri, A.; Aouadi, K. Novel enantiopure isoxazolidine and C-alkyl imine oxide derivatives as potential hypoglycemic agents: Design, synthesis, dual inhibitors of α-amylase and α-glucosidase, ADMET and molecular docking study. *Bioorg. Chem.* **2020**, *104*, 104270. [CrossRef]
8. Aouadi, K.; Hajlaoui, H.; Arraouadi, S.; Ghannay, S.; Snoussi, M.; Kadri, A. Phytochemical Profiling, Antimicrobial and α-Glucosidase Inhibitory Potential of Phenolic-Enriched Extracts of the Aerial Parts from Echium humile Desf.: In Vitro Combined with In Silico Approach. *Plants* **2022**, *11*, 1131. [CrossRef]
9. Hajlaoui, H.; Arraouadi, S.; Noumi, E.; Aouadi, K.; Adnan, M.; Khan, M.A.; Kadri, A.; Snoussi, M. Antimicrobial, antioxidant, anti-acetylcholinesterase, antidiabetic, and pharmacokinetic properties of *Carum carvi* L. and *Coriandrum sativum* L. essential oils alone and in combination. *Molecules* **2021**, *26*, 3625. [CrossRef]
10. Kadri, A.; Aouadi, K. In vitro antimicrobial and α-glucosidase inhibitory potential of enantiopure cycloalkylglycine derivatives: Insights into their in silico pharmacokinetic, druglikeness, and medicinal chemistry properties. *J. Appl. Pharm. Sci.* **2020**, *10*, 107–115.
11. Kim, E.J.; Ha, K.H.; Kim, D.J.; Choi, Y.H. Diabetes and the risk of infection: A national cohort study. *Diabetes Metab. J.* **2019**, *43*, 804. [CrossRef] [PubMed]
12. Sundarram, A.; Murthy, T.P.K. α-amylase production and applications: A review. *J. Appl. Environ. Microbiol.* **2014**, *2*, 166–175.
13. Ghabi, A.; Brahmi, J.; Alminderej, F.; Messaoudi, S.; Vidald, S.; Kadri, A.; Aouadi, K. Multifunctional isoxazolidine derivatives as α-amylas e and α-glucosidase inhibitors. *Bioorg. Chem.* **2020**, *98*, 103713. [CrossRef] [PubMed]
14. Dirir, A.M.; Daou, M.; Yousef, A.F.; Yousef, L.F. A review of alpha-glucosidase inhibitors from plants as potential candidates for the treatment of type-2 diabetes. *Phytochem. Rev.* **2022**, *21*, 1049–1079. [CrossRef]
15. Tseng, C.H.; Chen, Y.R.; Tzeng, C.C.; Liu, W.; Chou, C.K.; Chiu, C.C.; Chen, Y.L. Discovery of indeno[1,2-b]quinoxaline derivatives as potential anticancer agents. *Eur. J. Med. Chem.* **2016**, *27*, 258–273. [CrossRef] [PubMed]
16. Tseng, C.-H.; Tzeng, C.-C.; Yang, C.-L.; Lu, P.-J.; Chen, H.-L.; Li, H.-Y.; Chuang, Y.-C.; Yang, C.-N.; Chen, Y.-L. Synthesis and antiproliferative evaluation of certain indeno [1, 2-c] quinoline derivatives. Part 2. *J. Med. Chem.* **2010**, *53*, 6164–6179. [CrossRef]
17. Schepetkin, I.A.; Khlebnikov, A.I.; Potapov, A.S.; Kovrizhina, A.R.; Matveevskaya, V.V.; Belyanin, M.L.; Atochin, D.N.; Zanoza, S.O.; Gaidarzhy, N.M.; Lyakhov, S.A.; et al. Synthesis, biological evaluation, and molecular modeling of 11H-indeno[1,2-b]quinoxalin-11-one derivatives and tryptanthrin-6-oxime as c-Jun N-terminal kinase inhibitors. *Eur. J. Med. Chem.* **2019**, *161*, 179–191. [CrossRef]
18. Almansour, A.I.; Arumugam, N.; Soliman, S.M.; Krishnamoorthy, B.S.; Halet, J.-F.; Priya, R.V.; Suresh, J.; Al-thamili, D.M.; Al-aizari, F.A.; Kumar, R.S. Stereoselective synthesis, structure and DFT studies on fluoro- and nitro- substituted spirooxindole-pyrrolidine heterocyclic hybrids. *J. Mol. Struct.* **2021**, *1237*, 130396. [CrossRef]
19. Bhaskar, G.; Arun, Y.; Balachandran, C.; Saikumar, C.; Perumal, P.T. Synthesis of novel spirooxindole derivatives by one pot multicomponent reaction and their antimicrobial activity. *Eur. J. Med. Chem.* **2012**, *51*, 79–91. [CrossRef]
20. Haddad, S.; Boudriga, S.; Akhaja, T.N.; Raval, J.P.; Porzio, F.; Soldera, A.; Askri, M.; Knorr, M.; Rousselin, Y.; Kubicki, M.M.; et al. A Strategic Approach to the Synthesis of Functionalized Spirooxindole Pyrrolidine Derivatives: In vitro Antibacterial, Antifungal, Antimalarial and Antitubercular studies. *New J. Chem.* **2015**, *39*, 520–528. [CrossRef]
21. Rajanarendar, E.; Ramakrishna, S.; Reddy, K.G.; Nagaraju, D.; Reddy, Y.N. A facile synthesis, anti-inflammatory and analgesic activity of isoxazolyl-2,3-dihydrospiro[benzo[f] isoindole-1,30-indoline]-20,4,9-triones. *Bioorg. Med. Chem. Lett.* **2013**, *23*, 3954–3958. [CrossRef] [PubMed]

22. Toumi, A.; Boudriga, S.; Hamden, K.; Sobeh, M.; Cheurfa, M.; Askri, M.; Knorr, M.; Strohmann, B.C.L. Synthesis, antidiabetic activity and molecular docking study of rhodanine-substitued spirooxindole pyrrolidine derivatives as novel α-amylase inhibitors. *Bioorg. Chem.* **2021**, *106*, 104507. [CrossRef] [PubMed]
23. Hammouda, M.B.; Boudriga, S.; Hamden, K.; Askri, M.; Knorr, M.; Strohmann, C.; Brieger, L.; Krupp, A.; Anouar, E.H.; Snoussi, M.; et al. New Spiropyrrolothiazole Derivatives Bearing an Oxazolone Moiety as Potential Antidiabetic Agent: Design, Synthesis, Crystal Structure, Hirshfeld Surface Analysis, ADME and Molecular Docking Studies. *J. Mol. Struct.* **2022**, *1254*, 132398. [CrossRef]
24. Kathirvelan, D.; Haribabu, J.; Reddy, B.S.R.; Balachandran, C.; Duraipandiyan, V. Facile and diastereoselective synthesis of 3,20-spiropyrrolidine-oxindoles derivatives, their molecular docking and antiproliferative activities. *Bioorg. Med. Chem. Lett.* **2015**, *25*, 389–399. [CrossRef]
25. Arumugam, N.; Almansour, A.I.; Kumar, R.S.; Kotresha, D.; Saiswaroop, R.; Venketesh, S. Dispiropyrrolidinylpiperidone embedded indeno[1,2-b]quinoxaline heterocyclic hybrids: Synthesis, cholinesterase inhibitory activity and their molecular docking simulation. *Bioorg. Med. Chem.* **2019**, *27*, 2621–2628. [CrossRef] [PubMed]
26. Yu, B.; Yu, D.Q.; Liu, H.M. Spirooxindoles: Promising scaffolds for anticancer agents. *Eur. J. Med. Chem.* **2015**, *97*, 673–698. [CrossRef]
27. Rajesh, S.M.; Perumal, S.; Menendez, J.C.; Yogeeswari, P.; Sriram, D. Antimycobacterial activity of spirooxindolo-pyrrolidine, pyrrolizine and pyrrolothiazole hybrids obtained by a three-component regio- and stereoselective 1,3-dipolar cycloaddition. *Med. Chem. Commun.* **2011**, *2*, 626–630. [CrossRef]
28. Asad, M.; Arshad, M.N.; Asiri, A.M.; Khan, S.A.; Rehan, M.; Oves, M. Synthesis, Characterization, Molecular Docking and Antimicrobial Activity of Novel Spiropyrrolidine Derivatives. *Polycycl. Aromat. Compd.* **2021**, *42*, 5385–5397. [CrossRef]
29. Almansour, A.I.; Kumar, R.S.; Beevi, F.; Nasrolahi Shirazi, A.; Osman, H.; Ismail, R.; Ali, M.A. Facile, regio-and diastereoselective synthesis of spiro-pyrrolidine and pyrrolizine derivatives and evaluation of their antiproliferative activities. *Molecules* **2014**, *19*, 10033–10055. [CrossRef]
30. Arumugam, N.; Suresh babu, P.; Angamuthu, G.; Kotresha, D.; Manohar, T.S.; Venketesh, S. Spiropyrrolidine/spiroindolizino [6, 7-b] indole heterocyclic hybrids: Stereoselective synthesis, cholinesterase inhibitory activity and their molecular docking study. *Bioorg. Chem.* **2018**, *79*, 64–71. [CrossRef]
31. Haddaji, F.; Papetti, A.; Noumi, E.; Colombo, R.; Deshpande, S.; Aouadi, K.; Adnan, M.; Kadri, A.; Selmi, B.; Snoussi, M. Bioactivities and in silico study of *Pergularia tomentosa* L. phytochemicals as potent antimicrobial agents targeting type IIA topoisomerase, TyrRS, and Sap1 virulence proteins. *Environ. Sci. Poll. Res.* **2021**, *28*, 25349–25367. [CrossRef] [PubMed]
32. Othman, I.M.M.; Gad-Elkareem, M.A.M.; Anouar, E.H.; Snoussi, M.; Aouadi, K.; Kadri, A. Novel fused pyridine derivatives containing pyrimidine moiety as prospective tyrosyl-tRNA synthetase inhibitors: Design, synthesis, pharmacokinetics and molecular docking studies. *J. Mol. Struct.* **2020**, *1219*, 128651. [CrossRef]
33. Ben Mefteh, F.; Daoud, A.; Bouket, A.C.; Thissera, B.; Kadri, Y.; Cherif-Silini, H.; Eshelli, M.; Alenezi, F.N.; Vallat, A.; Oszako, T.; et al. Date Palm Tree's Root-Derived Endophytes as Fungal Cell Factories for Diverse Bioactive Metabolites. *Int. J. Mol. Sci.* **2018**, *19*, 1986. [CrossRef] [PubMed]
34. Ghannay, S.; Kadri, A.; Aouadi, K. Synthesis, in vitro antimicrobial assessment, and computational investigation of pharmacokinetic and bioactivity properties of novel trifluoromethylated compounds using in silico ADME and toxicity prediction tools. *Monatsh. Chem.* **2020**, *151*, 267–280. [CrossRef]
35. Othman, I.M.M.; Gad-Elkareem, M.A.M.; Anouar, E.H.; Aouadi, K.; Kadri, A.; Snoussi, M. Design, synthesis ADMET and molecular docking of new imidazo[4,5-b]pyridine-5-thione derivatives as potential tyrosyl-tRNA synthetase inhibitors. *Bioorg. Chem.* **2020**, *102*, 104105. [CrossRef]
36. Othman, I.M.M.; Gad-Elkareem, M.A.M.; Radwan, H.A.; Badraoui, R.; Aouadi, K.; Snoussi, M.; Kadri, A. Synthesis, Structure-Activity Relationship and in silico Studies of Novel Pyrazolothiazole and Thiazolopyridine Derivatives as Prospective Antimicrobial and Anticancer Agents. *ChemistrySelect* **2021**, *6*, 7860–7872. [CrossRef]
37. Alminderej, F.; Bakari, S.; Almundarij, T.I.; Snoussi, M.; Aouadi, K.; Kadri, A. Antimicrobial and Wound Healing Potential of a New Chemotype from *Piper cubeba* L. Essential Oil and In Silico Study on *S. aureus* tyrosyl-tRNA Synthetase Protein. *Plants* **2021**, *10*, 205–224. [CrossRef]
38. Othman, I.M.M.; Gad-Elkareem, M.A.M.; Anouar, E.H.; Aouadi, K.; Snoussi, M.; Kadri, A. New substituted pyrazolones and dipyrazolotriazines as promising tyrosyl-tRNA synthetase and peroxiredoxin-5 inhibitors: Design, synthesis, molecular docking and structure-activity relationship (SAR) analysis. *Bioorg. Chem.* **2021**, *109*, 104704. [CrossRef]
39. Mseddi, K.; Alimi, F.; Noumi, E.; Veettil, V.N.; Deshpande, S.; Adnan, M.; Hamdi, A.; Elkahoui, S.; Alghamdi, A.; Kadri, A.; et al. Thymus musilii Velen. as a promising source of potent bioactive compounds with its pharmacological properties: In vitro and in silico analysis. *Arab. J. Chem.* **2020**, *13*, 6782–6801. [CrossRef]
40. Felhi, S.; Hajlaoui, H.; Ncir, M.; Bakari, S.; Ktari, N.; Saoudi, M.; Gharsallah, N.; Kadri, A. Nutritional, phytochemical and antioxidant evaluation and FT-IR analysis of freeze-dried extracts of Ecballium elaterium fruit juice from three localities. *Food Sci. Technol.* **2016**, *36*, 646–655. [CrossRef]
41. Felhi, S.; Saoudi, M.; Daoud, A.; Hajlaoui, H.; Ncir, M.; Chaabane, R.; El Feki, A.; Gharsallah, N.; Kadri, A. Investigation of phytochemical contents, in vitro antioxidant and antibacterial behavior and in vivo anti-inflammatory potential of Ecballium elaterium methanol fruits extract. *Food Sci. Technol.* **2017**, *37*, 558–563. [CrossRef]

42. Bakari, S.; Hajlaoui, H.; Daoud, A.; Mighri, H.; Ross-Garcia, J.M.; Gharsallah, N.; Kadri, A. Phytochemicals, antioxidant and antimicrobial potentials and LC-MS analysis of hydroalcoholic extracts of leaves and flowers of Erodium glaucophyllum collected from Tunisian Sahara. *Food Sci. Biotechnol.* **2018**, *38*, 310–317. [CrossRef]
43. Ghannay, S.; Bakari, S.; Ghabi, A.; Kadri, A.; Msaddek, M.; Aouadi, K. Stereoselective synthesis of enantiopure N-substituted pyrrolidin-2,5-dione derivatives by 1,3-dipolar cycloaddition and assessment of their in vitro antioxidant and antibacterial activities. *Bioorg. Med. Chem. Lett.* **2017**, *27*, 2302–2307. [CrossRef] [PubMed]
44. Ghannay, S.; Bakari, S.; Msaddek, M.; Vidal, S.; Kadri, A.; Aouadi, K. Design, synthesis, molecular properties and in vitro antioxidant and antibacterial potential of novel enantiopure isoxazolidine derivatives. *Arab. J. Chem.* **2020**, *13*, 2121–2131. [CrossRef]
45. Noumi, E.; Snoussi, M.; Anouar, E.H.; Alreshidi, M.; Veettil, V.N.; Elkahoui, S.; Adnan, M.; Patel, M.; Kadri, A.; Aouadi, K.; et al. HR-LCMS-Based Metabolite Profiling, Antioxidant, and Anticancer Properties of *Teucrium polium* L. Methanolic Extract: Computational and In Vitro Study. *Antioxidants* **2020**, *9*, 1089. [CrossRef]
46. Alminderej, F.; Bakari, S.; Almundarij, T.I.; Snoussi, M.; Aouadi, K.; Kadri, A. Antioxidant Activities of a New Chemotype of Piper cubeba L. Fruit Essential Oil (Methyleugenol/Eugenol): In Silico Molecular Docking and ADMET Studies. *Plants* **2020**, *9*, 1534. [CrossRef] [PubMed]
47. Brahmi, J.; Ghannay, S.; Bakari, S.; Kadri, A.; Aouadi, K.; Msaddek, M.; Vidal, S. Unprecedented stereoselective synthesis of 3-methylisoxazolidine-5-aryl-1,2,4-oxadiazoles via 1,3-dipolar cycloaddition and study of their in vitro antioxidant activity. *Synth. Commun.* **2016**, *46*, 2037–2044. [CrossRef]
48. Badraoui, R.; Rebai, T.; Elkahoui, S.; Alreshidi, M.; Veettil, V.N.; Noumi, E.; Al-Motair, K.A.; Aouadi, K.; Kadri, A.; De Feo, V.; et al. *Allium subhirsutum* L. as a Potential Source of Antioxidant and Anticancer Bioactive Molecules: HR-LCMS Phytochemical Profiling, In Vitro and In Vivo Pharmacological Study. *Antioxidants* **2020**, *9*, 1003. [CrossRef] [PubMed]
49. Kutyashev, I.B.; Barkov, A.Y.; Zimnitskiy, N.S.; Korotaev, V.Y.; Sosnovskikh, V.Y. Different behavior of azomethine ylides derived from 11 H-indeno [1, 2-b] quinoxalin-11-one and proline/sarcosine in reactions with 3-nitro-2 H-chromenes. *Chem. Heterocycl.* **2019**, *55*, 861–874. [CrossRef]
50. Zimnitskiy, N.S.; Barkov, A.Y.; Ulitko, M.V.; Kutyashev, I.B.; Korotaev, V.Y.; Sosnovskikh, V.Y. An expedient synthesis of novel spiro [indenoquinoxaline-pyrrolizidine]-pyrazole conjugates with anticancer activity from 1, 5-diarylpent-4-ene-1, 3-diones through the 1, 3-dipolar cycloaddition/ cyclocondensation sequence. *New J. Chem.* **2020**, *44*, 16185–16199. [CrossRef]
51. Rajesh, S.M.; Bala, B.D.; Perumal, S. Multi-component, 1, 3-dipolar cycloaddition reactions for the chemo-, regio-and stereoselective synthesis of novel hybrid spiroheterocycles in ionic liquid. *Tetrahedron. Lett.* **2012**, *53*, 5367–5371. [CrossRef]
52. Ayipo, Y.O.; Ahmad, I.; Najib, Y.S.; Sheu, S.K.; Patel, H.; Mordi, M.N. Molecular modelling and structure-activity relationship of a natural derivative of o-hydroxybenzoate as a potent inhibitor of dual NSP3 and NSP12 of SARS-CoV-2: In silico study. *J. Biomol. Struct. Dyn.* **2022**. *ahead of print*. [CrossRef]
53. Abdelgawad, M.A.; Oh, J.M.; Parambi, D.G.T.; Kumar, S.; Musa, A.; Ghoneim, M.M.; Nayl, A.A.; El-Ghorab, A.H.; Ahmad, I.; Patel, H.; et al. Development of bromo- and fluoro-based α, β-unsaturated ketones as highly potent MAO-B inhibitors for the treatment of Parkinson's disease. *J. Mol. Struct.* **2022**, *1266*, 133545. [CrossRef]
54. Ghosh, S.; Das, S.; Ahmad, I.; Patel, H. In silico validation of anti-viral drugs obtained from marine sources as a potential target against SARS-CoV-2 Mpro. *J. Indian Chem. Soc.* **2021**, *98*, 100272. [CrossRef]
55. Farhan, M.M.; Guma, M.A.; Rabeea, M.A.; Ahmad, I.; Patel, H. Synthesizes, Characterization, Molecular docking and in vitro Bioactivity study of new compounds containing Triple Beta Lactam Rings. *J. Mol. Struct.* **2022**, *1269*, 133781. [CrossRef]
56. Ahmad, I.; Akand, S.R.; Shaikh, M. Synthesis, molecular modelling study of the methaqualone analogues as anti-convulsant agent with improved cognition activity and minimized neurotoxicity. *J. Mol. Struct.* **2022**, *1251*, 131972. [CrossRef]
57. Osmaniye, D.; Karaca, Ş.; Kurban, B.; Baysal, M.; Ahmad, I.; Patel, H.; Özkay, Y.; Asım Kaplancıklı, Z. Design, synthesis, molecular docking and molecular dynamics studies of novel triazolothiadiazine derivatives containing furan or thiophene rings as anticancer agents. *Bioorg. Chem.* **2022**, *122*, 105709. [CrossRef]
58. Girase, R.; Ahmad, I.; Pawara, R.; Patel, H. Optimizing cardio, hepato and phospholipidosis toxicity of the Bedaquiline by chemoinformatics and molecular modelling approach. SAR and QSAR in environmental research, 1–21. *Advance* **2022**. *online publication*. [CrossRef]
59. Ahmad, I.; Pawara, R.H.; Girase, R.T.; Pathan, A.Y.; Jagatap, V.R.; Desai, N.; Ayipo, Y.O.; Surana, S.J.; Patel, H. Synthesis, Molecular Modeling Study, and Quantum-Chemical-Based Investigations of Isoindoline-1, 3-diones as Antimycobacterial Agents. *ACS Omega* **2022**, *7*, 21820–21844. [CrossRef]
60. Piang-Siong, W.; de Caro, P.; Marvilliers, A.; Chasseray, X.; Payet, B.; Shum Cheong Sing, A.; Illien, B. Contribution of trans-aconitic acid to DPPH scavenging ability in different media. *Food Chem.* **2017**, *214*, 447–452. [CrossRef]
61. Tuberoso, C.I.G.; Boban, M.; Bifulco, E.; Budimir, D.; Pirisi, F.M. Antioxidant capacity and vasodilatory properties of Mediterranean food: The case of Cannonau wine, myrtle berries liqueur and strawberry-tree honey. *Food Chem.* **2013**, *140*, 686–691. [CrossRef] [PubMed]
62. Rodriguez-Bonilla, P.; Gandia-Herrero, F.; Matencio, A.; Garcia-Carmona, F.; Lopez-Nicolas, J.M. Comparative study of the antioxidant capacity of four stilbenes using ORAC, ABTS+, and FRAP techniques. *Food Anal. Method* **2017**, *10*, 2994–3000. [CrossRef]

63. Amamou, S.; Lazreg, H.; Hafsa, J.; Majdoub, H.; Rihouey, C.; Le Cerf, D.; Achour, L. Effect of extraction condition on the antioxidant, antiglycation and α-amylase inhibitory activities of *Opuntia* macrorhiza fruit peels polysaccharides. *LWT* **2020**, *127*, 109411. [CrossRef]
64. Patel, H.; Ansari, A.; Pawara, R.; Ansari, I.; Jadhav, H.; Surana, S. Design and synthesis of novel 2,4-disubstituted aminopyrimidines: Reversible non-covalent T790M EGFR inhibitors. *J. Recept. Signal Transduct. Res.* **2018**, *38*, 393–412. [CrossRef]
65. Patel, H.; Ahmad, I.; Jadhav, H.; Pawara, R.; Lokwani, D.; Surana, S. Investigating the Impact of Different Acrylamide (Electrophilic Warhead) on Osimertinib's Pharmacological Spectrum by Molecular Mechanic and Quantum Mechanic Approach. *Comb. Chem. High Throughput Screen.* **2021**, *25*, 149–166. [CrossRef]
66. Shaw, D.E. Research, Schrödinger Release (2021-1). Desmond Molecular Dynamics System. Maestro-Desmond Interoperability Tools. Available online: https://www.schrodinger.com/products/desmond (accessed on 7 September 2022).
67. Chaudhari, B.; Patel, H.; Thakar, S.; Ahmad, I.; Bansode, D. Optimizing the Sunitinib for cardio-toxicity and thyro-toxicity by scaffold hopping approach. *Silico Pharmacol.* **2022**, *10*, 10. [CrossRef]
68. Ayipo, Y.O.; Alananzeh, W.A.; Ahmad, I.; Patel, H.; Mordi, M.N. Structural modelling and in silico pharmacology of β-carboline alkaloids as potent 5-HT1A receptor antagonists and reuptake inhibitors. *J. Biomol. Struct. Dyn.* **2022**, 1–17. [CrossRef] [PubMed]
69. Bharadwaj, K.K.; Ahmad, I.; Pati, S.; Ghosh, A.; Sarkar, T.; Rabha, B.; Patel, H.; Baishya, D.; Edinur, H.A.; Abdul Kari, Z.; et al. Potent Bioactive Compounds from Seaweed Waste to Combat Cancer Through Bioinformatics Investigation. *Front. Nutr.* **2022**, *9*, 889276. [CrossRef]
70. Snoussi, M.; Redissi, A.; Mosbah, A.; De Feo, V.; Adnan, M.; Aouadi, K.; Alreshidi, M.; Patel, M.; Kadri, A.; Noumi, E. Emetine, a potent alkaloid for the treatment of SARS-CoV-2 targeting papain-like protease and non-structural proteins: Pharmacokinetics, molecular docking and dynamic studies. *J. Biomol. Struct. Dyn* **2021**. *ahead of print*. [CrossRef]
71. Aouadi, K.; Hajlaoui, H.; Arraouadi, S.; Ghannay, S.; Snoussi, M.; Kadri, A. HPLC/MS Phytochemical Profiling with Antioxidant Activities of *Echium humile* Desf. Extracts: ADMET Prediction and Computational Study Targeting Human Peroxiredoxin 5Receptor. *Agronomy* **2021**, *11*, 2165. [CrossRef]

molecules

MDPI

Article

MnO_2-Mediated Oxidative Cyclization of "Formal" Schiff's Bases: Easy Access to Diverse Naphthofuro-Annulated Triazines

Ramil F. Fatykhov [1], Igor A. Khalymbadzha [1,2], Ainur D. Sharapov [1], Anastasia P. Potapova [1], Nataliya N. Mochulskaya [1], Anton N. Tsmokalyuk [1], Alexandra V. Ivoilova [1], Polina N. Mozharovskaia [1], Sougata Santra [1,*] and Oleg N. Chupakhin [1,2]

[1] Department of Organic and Biomolecular Chemistry, Chemical Engineering Institute, Ural Federal University, 19 Mira Str., 620002 Ekaterinburg, Russia
[2] Postovsky Institute of Organic Synthesis, Ural Branch of the Russian Academy of Sciences, 22 S. Kovalevskaya Str., 620990 Ekaterinburg, Russia
* Correspondence: sougatasantra85@gmail.com

Abstract: A different type of MnO_2-induced oxidative cyclization of dihydrotriazines has been developed. These dihydrotriazines are considered as a "formal" Schiff's base. This method provided easy access to naphthofuro-fused triazine via the C-C/C-O oxidative coupling reaction. The reaction sequence comprised the nucleophilic addition of 2-naphthol or phenol to 1,2,4-triazine, followed by oxidative cyclization. The scope and limitations of this novel coupling reaction have been investigated. Further application of the synthesized compound has been demonstrated by synthesizing carbazole-substituted benzofuro-fused triazines. The scalability of the reaction was demonstrated at a 40 mmol load. The mechanistic study strongly suggests that this reaction proceeds through the formation of an O-coordinated manganese complex.

Keywords: oxidative cyclization; manganese(IV) oxide; 1,2,4-triazine; phenols; cross-coupling

Citation: Fatykhov, R.F.; Khalymbadzha, I.A.; Sharapov, A.D.; Potapova, A.P.; Mochulskaya, N.N.; Tsmokalyuk, A.N.; Ivoilova, A.V.; Mozharovskaia, P.N.; Santra, S.; Chupakhin, O.N. MnO_2-Mediated Oxidative Cyclization of "Formal" Schiff's Bases: Easy Access to Diverse Naphthofuro-Annulated Triazines. *Molecules* **2022**, *27*, 7105. https://doi.org/10.3390/molecules27207105

Academic Editors: Alexey M. Starosotnikov, Maxim A. Bastrakov and Igor L. Dalinger

Received: 2 October 2022
Accepted: 13 October 2022
Published: 21 October 2022

Publisher's Note: MDPI stays neutral with regard to jurisdictional claims in published maps and institutional affiliations.

1. Introduction

In organic synthesis, C−H functionalization in the presence of transition metal catalysts has become one of the fundamental methods, and has had a massive impact on synthetic organic chemistry, medicinal chemistry, and material science [1–8]. In this context, cross dehydrogenative coupling (CDC) reactions have gained much interest in the last decade [9–15] among all types of C-H functionalization/activation reactions. This type of coupling reaction allows the construction of a C-C bond or C-X bond directly from C-H-containing substrates in the presence of an oxidant via the formal removal of a H_2 molecule. In addition, these methods avoid the prefunctionalization of starting materials, which makes the synthetic routes straightforward and more efficient. For CDC reactions, various transition metals such as Pd, Cu, Ag, Rh, and Ru have been extensively studied due to their high efficiency. However, the exploration of manganese catalysis in CDC reactions is in high demand due to its low price, ready availability, sustainability, nontoxicity, and environmentally friendly properties [16]. Simple manganese salts were sensibly employed in the CDC reaction due to their ability to undergo the reaction in a radical way.

Benzofuro-fused N-heterocycles are considered as common structural motifs in biologically active compounds, drug candidates and fluorescence materials (Figure 1). For example, benzofuro [2,3-*b*]pyridine, in particular Elbfluorene **I**, and its derivatives are important cyclin-dependent kinase inhibitors [17–20], the benzofuro [3,2-*d*]pyrimidine derivative Amuvatinib **II** is a multitarget tyrosine kinase inhibitor [21–24], and benzofuro[2,3-*b*]pyrazine **III** was designed as a deep-blue fluorescent emitter [25].

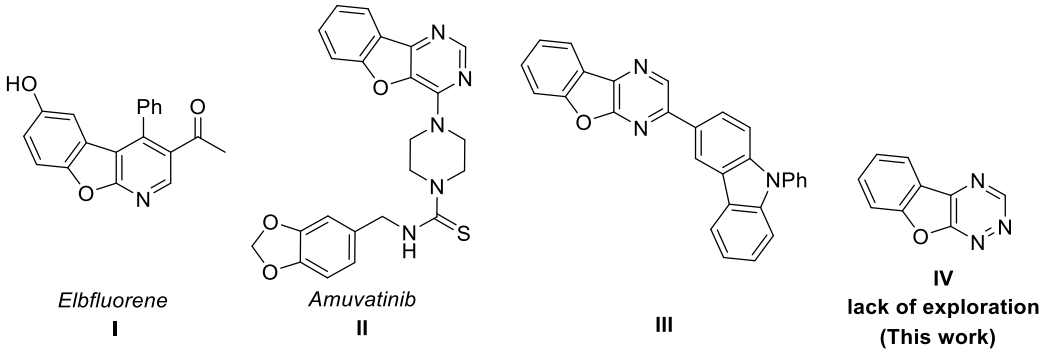

Figure 1. Representative benzofuro-fused N-heterocycles.

Considering the importance of this moiety, several methods have been developed for developing benzofuro-fused N-heterocycles such as pyridine, pyrimidine and pyrazine derivatives. The first synthetic approach comprises the annulation of the heterocyclic ring to a benzofuran core (Scheme 1a) [26–34]. Alternatively, other approaches include the intramolecular cyclization (C-C bond formation) of arylhetaryl ethers [35–40] (Scheme 1b) or the intramolecular cyclization (C-O bond formation) of 2-hetaryl-substituted phenol derivatives [41–47] (Scheme 1c), as well as the intermolecular tandem C-C/C-O cross-coupling reaction of prefunctionalized substrate [48–50] to form a furan ring fused between the benzene and mono/diazine ring. However, these approaches usually require multistep synthesis, harsh reaction conditions, and the use of transition metal catalysts or special reagents and conditions.

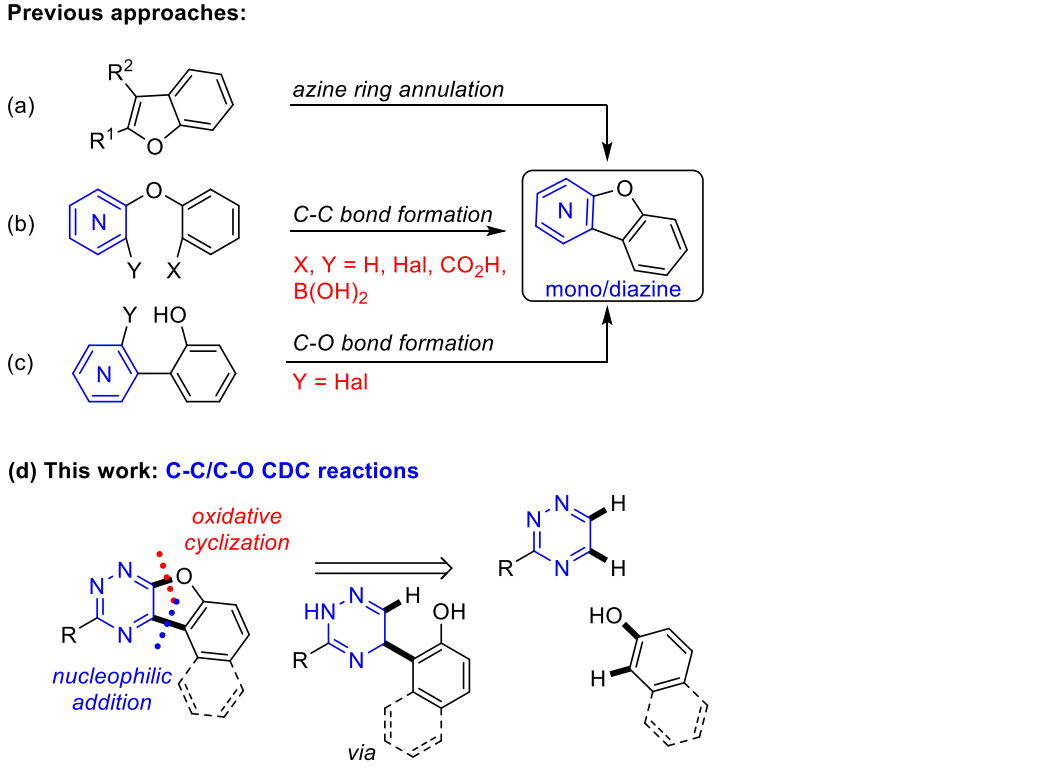

Scheme 1. Approaches to Benzofuro-fused N-heterocycles. (**a**–**c**): Known approaches; (**d**) Approach of this work.

On the other hand, it is worth mentioning that information about the synthetic and applied data of benzofuro-fused triazines is lacking in the literature. To date, only a few studies have investigated the synthesis of benzofurotriazine derivatives. In 1988, Eid et al. reported the synthesis of naphthofuro[2,3-*e*][1,2,4]triazine in a 33% overall yield via the

annulation of the triazine core to naphthofuran-1,2-dione [51]. The reaction was carried out in four steps. Later, Seitz and Richter reported that the intramolecular [4+2]-cycloaddition of 2-(tetrazinyloxy)benzonitrile led to the formation of benzofuro[3,2-*e*][1,2,4]triazine derivatives [52]. Neunhoeffer et al. synthesized benzofuro[2,3-e][1,2,4]triazine at 26% yield using the tandem S_N^H-S_N^{ipso} reaction of resorcinol and 1,2,4-triazine with a good leaving group [53]. Unfortunately, these methods represent the only examples of benzofurotriazine derivatives, and provide poor yields of the desired products. At the same time, 1,2,4-triazines represent readily accessible and cheap building blocks for the construction of pyridine [54–62], pyrimidine [63,64] or pyrazine [59,65,66] cores via the sequence of Diels-Alder/*retro*-Diels-Alder reactions.

In a continuation of our research on CDC reactions in triazines [54,67] and diazines [68], herein, we are pleased to report an unusual synthesis of benzofuro-fused 1,2,4-triazines via the sequence of C-C/C-O CDC reactions of 1,2,4-triazines with 2-naphthols or phenols (Scheme 1d). The reaction proceeded through the formation of 1,4-dihydrotriazine, followed by oxidative cyclization.

2. Results and Discussion

Based on retrosynthetic analysis of benzofurotriazine (Scheme 1d), we assume that 5,6-unsubstituted triazine and α-unsubstituted phenol are the best building blocks for the construction of the desired molecule through a sequence of C-C/C-O cross-coupling reactions. Earlier, our [67,69,70] and other [70,71] research groups demonstrated that 5,6-unsubstituted 1,2,4-triazines may be used in a two-step CDC reaction with various aromatic C-nucleophiles via the formation of 1,4-dihydrotriazine derivatives as intermediates, followed by aromatization to bi(het)aryl products. As mentioned above, the prefunctionalized azine is required for C-O cross-coupling reaction [53]. On the other hand, it is well known that the phenolic Schiff's bases readily undergoes intramolecular oxidative cyclization in the presence of various oxidizing agents, in particular, hypervalent iodine compounds [72–75], lead(IV) acetate [76–78], or manganese salts such as $Mn(OAc)_3{\cdot}2H_2O$ [78,79] and MnO_2 [80]. We hypothesized that 1,4-dihydrotriazines containing 2-hydroxyaryl moiety can be considered as a "formal" phenolic Schiff's base (Scheme 2).

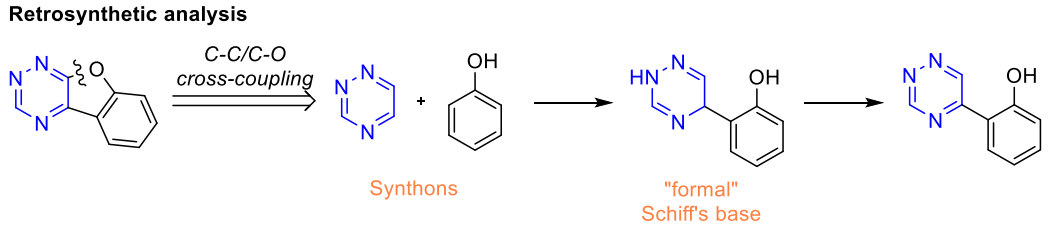

Scheme 2. Retrosynthetic analyses of benzofurotriazine scaffold.

Based on this hypothesis, we have focused our attention on the oxidative cyclization of dihydrotriazines easily obtainable from triazine and naphthol. For example, the reaction of readily available 3-methylthio-1,2,4-triazine **1a** and naphthol **2a** yields dihydrotriazine **3aa** (Scheme 3), which was used for the initial screening of the optimal conditions. Using standard oxidizing agent, such as phenyliodonine(III) diacetate, phenyliodonine(III) bis(trifluoroacetate) or $Pb(OAc)_4$, for the oxidative cyclization of the phenolic Schiff's base, only a complex mixture was isolated from the reaction. Surprisingly, when using MnO_2 for the oxidation of the "formal" Schiff's base **3aa,** the desired oxidative coupling product naphthofurotriazine **4aa** was formed in one step. At the same time, the side product **5aa** was also observed in the reaction (Scheme 3). After comprehensive screening (Please see Supporting Information for details, Section S6), we found that the vigorous stirring (1500 rpm) of **3aa** in $CHCl_3$ at 50 °C in the presence of 3 equiv. of γ-MnO_2 [81] provided the naphthofurotriazine **4aa** in an almost quantitative yield after 3 h (Table 1, entry 1). Besides γ-MnO_2, other manganese salts such as $Mn(OAc)_3{\cdot}2H_2O$, $Mn(OAc)_2.4H_2O$ and $MnCl_2$, $Mn(acac)_2$ were not so effective for this reaction, or provided **4aa** in very poor

yields (Table 1, entries 3-6), except MnO_2 impregnated with nitric acid [82], which afforded **4aa** in a good yield (Table 1, entry 2). One may assume that $Mn(OAc)_3$ has low oxidative potential in organic media [83] compared to MnO_2. Other alternative oxidants such as Ag_2O, DTBP and DDQ led to low yields (Table 1, entries 7-9), and *p*-chloranil exclusively provided compound **5aa** in a high yield (Table 1, entry 10). The use of other solvents such as 1,1,1,3,3,3-hexafluoro-2-propanol (HFIP), EtOH, DCE or benzene clearly gave worse results (Table 1, entries 11-14). By increasing the temperature, the yield of **4aa** was decreased (Table 1, entry 15). In contrast, lower conversion was observed at room temperature (Table 1, entry 16). Carrying out the reaction in the presence of a decreased amount of MnO_2 (Table 1, entry 17) had negative effects on the efficiency of the reaction. In contrast, using 5 equiv. of MnO_2 increased the yield of the side product **5aa** (Table 1, entry 18). At the same time, all attempts were unsuccessful to cyclize **5aa** to **4aa**.

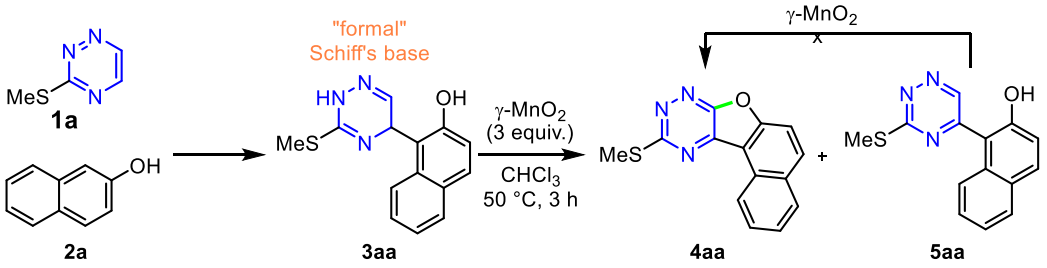

Scheme 3. Synthesis and oxidation of dihydrotriazine **3aa**.

Table 1. Optimization of the reaction conditions [1].

Entry	Conditions	4aa (%) [b]	5aa (%) [b]
1	Using 3 equiv. of γ-MnO_2	>99	trace
2	HNO_3@γ-MnO_2 instead of γ-MnO_2	75	trace
3	$Mn(OAc)_2.4H_2O$ instead of γ-MnO_2	-	-
4	$MnCl_2$ instead of γ-MnO_2	-	-
5	$Mn(acac)_2$ instead of γ-MnO_2	-	-
6	$Mn(OAc)_3.2H_2O$ instead of γ-MnO_2	29	5
7	Ag_2O instead of γ-MnO_2	60	-
8	DTBP instead of γ-MnO_2	35	15
9	DDQ instead of γ-MnO_2	39	43
10	*p*-Chloranil instead of γ-MnO_2	-	89
11	HFIP instead of $CHCl_3$	89	trace
12	EtOH instead of $CHCl_3$	66	trace
13	DCE instead of $CHCl_3$	85	trace
14	Benzene instead of $CHCl_3$	90	trace
15	Performed at 60 °C	94	4
16	Performed at 25 °C	91	3
17	Using 2 equiv. of γ-MnO_2	85	3
18	Using 5 equiv. of γ-MnO_2	90	6

[1] Conditions: **3aa** (0.2 mmol), solvent (4 mL), 3 h. [b] ^1H NMR yield using 1,3,5-trimethoxybenzene as an internal standard.

In order to study the applicability of the proposed oxidative coupling reaction, we synthesized a series of starting dihydrotriazines **3**. It was observed that our earlier proposed method [54] of the nucleophilic addition of 5,7-dimethoxycoumarins to 1,2,4-triazines with some modifications allowed us to prepare a series of compounds **3** using a variety of 3-S-substituted 1,2,4-triazines **1** and 2-naphthols **2** (Scheme 4). In all cases, the reaction proceeded with high regioselectivity to give compounds **3** in good to high yields. When methoxy- or hydroxy-substituted 2-naphthols **2b-e** were involved in the reaction with 1,2,4-triazine, the best yields were achieved in the presence of $BF_3{\cdot}OEt_2$ under refluxed conditions in methanol.

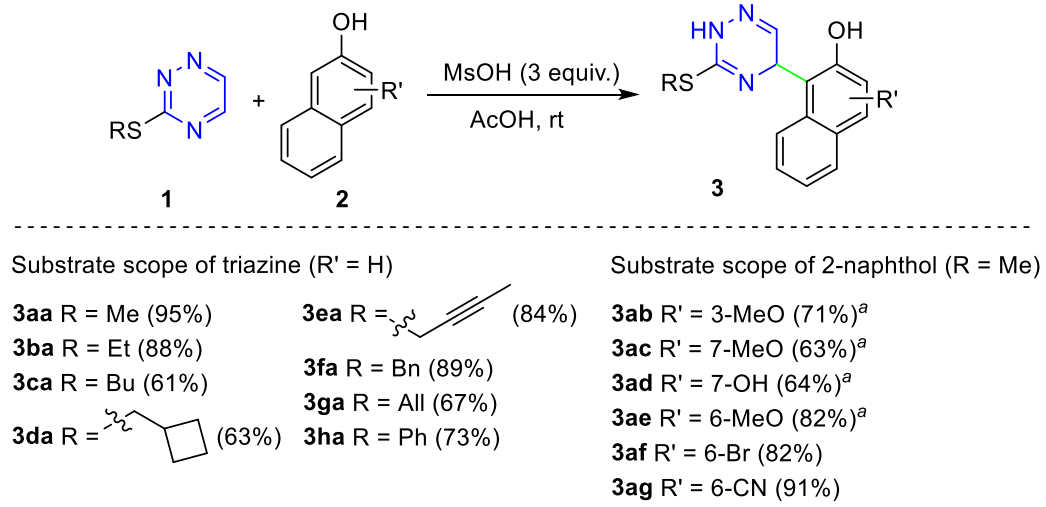

Scheme 4. Substrate scope for the synthesis of compounds **3**. Reaction conditions*:* **1** (1 mmol), **2** (1 mmol), MsOH (3 mmol) in AcOH (4 mL). [a] **1** (1 mmol), **2** (1 mmol), $BF_3{\cdot}OEt_2$ (8 mmol) in methanol 4 mL under reflux.

With the optimized reaction conditions and a set of dihydrotriazines **3** in hand, we then examined the applicability and scope of this MnO_2-induced oxidative cyclization reaction of dihydrotriazines **3**. At first, the scope of the reaction was studied with respect to different S-substituents in the dihydrotriazine core, and the results are summarized in Scheme 5. The naphthofuro-fused triazine **4aa** was isolated in a 95% yield under optimal reaction conditions after recrystallization from MeCN. Other 3-alkylthio-substituted triazine derivatives **3ba-3da** and **3fa** also underwent oxidative cyclization, producing only the desired cyclic product **4** in good to high yields. Moreover, 3-(but-2-yn-1-yl)- and 3-allylthio derivatives **3ea** and **3ga** smoothly transformed to **4ea** and **4ga** in 70% and 78% yields, respectively. However, in the case of phenylthio-substituted derivative **3ha,** a 5:1 mixture of **4ha** and **5ha** was isolated. Next, an investigation of this coupling reaction on 3-methylthiotriazine adducts **3ab-3ag** showed that the naphthyl ring substituted with various functional groups at different positions afforded the corresponding products with good to excellent yields. For example, bromo-, hydroxy-, methoxy- and cyano-substituted adducts **3ab-3ag** underwent oxidative cyclization with high regioselectivity to give only naphthofuro[3,2-*e*]triazine derivatives **4** in up to 91% yields (Scheme 5).

Encouraged by these results, we then investigated the oxidative cyclization reaction of triazine not bearing S-substituents (Scheme 6). In particular, 3-phenyl and 3-(4-methoxyphenyl) (PMP) derivatives **3ia** and **3ja** prepared under standard conditions (MsOH, AcOH) underwent MnO_2-induced oxidative cyclization to afford cyclic products **4ia** and **4ja,** respectively, as minor products with up to 28% yield. In contrast, 3-methyltriazine **1k** smoothly reacted with 2-naphthol **2a** in AcOH without the addition of MsOH, leading to the corresponding adduct **3la**, which was oxidized in the presence of MnO_2 to generate the desired **4la** as a major product in a 48% overall yield. Similar to triazine **1k**, 3-benzyltriazine **1l** was also involved in the same cascade reaction to give the mixture of **4ka** and **5ka** in a ratio of 1:1. In addition, we were pleased to find that the oxidative cyclization of **3ma** bearing the *N*-morpholinyl group in a triazine core produced the respective oxidative product **4ma** in a 75% yield. Actually, the adduct **3ma** was synthesized in situ by the interaction between triazine **1m** and 2-naphthol **2a** in the presence of $BF_3{\cdot}OEt_2$ under reflux in methanol.

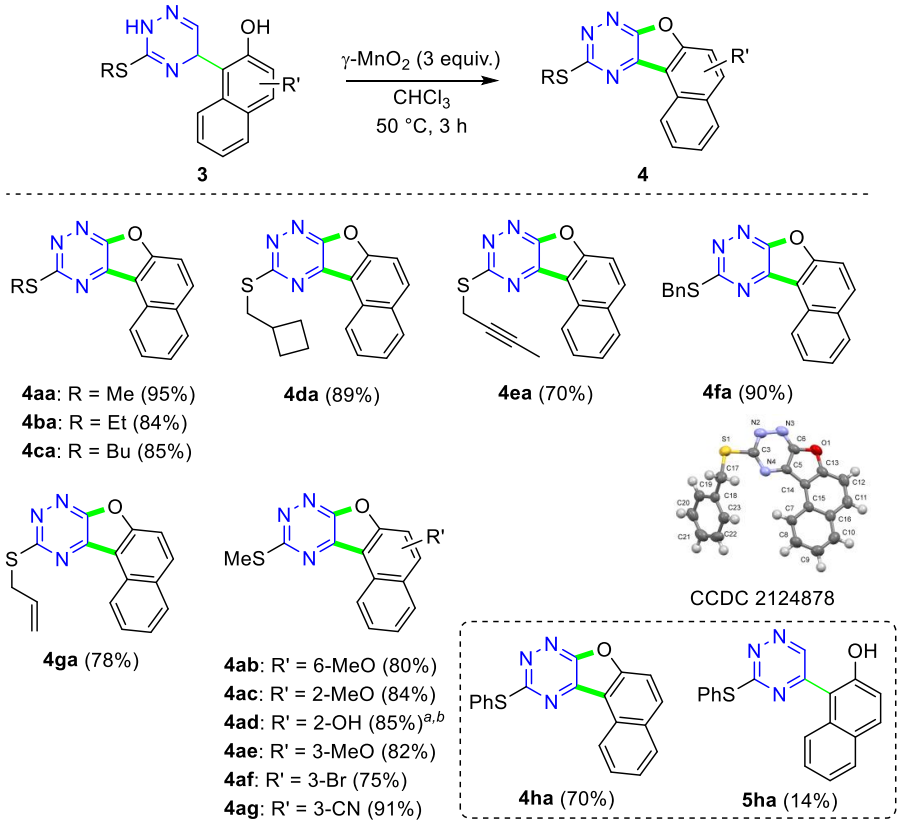

Scheme 5. Substrate scope for the synthesis of benzofuro-fused 1,2,4-triazines 4. Reaction conditions: **3** (0.2 mmol), γ-MnO_2 (0.6 mmol) in $CHCl_3$ (3 mL), 50 °C, 3 h. [a] Two-step yield; [b] $CHCl_3$:EtOH (v/v = 4:1, 3 mL).

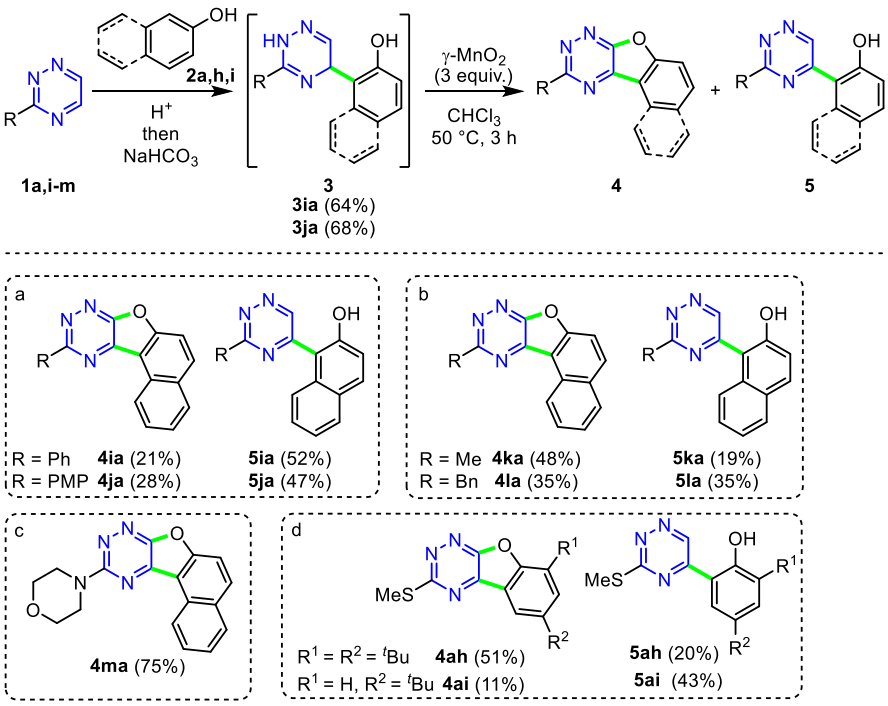

Scheme 6. Addition/oxidative cyclization sequence of triazine with naphthol and phenol. Reaction conditions: **1** (1 mmol), **2** (1 mmol), (**a**) MsOH (3 mmol), AcOH (5 mL), rt; (**b**) AcOH (5 mL), rt; (**c**) $BF_3{\cdot}OEt_2$ (3 mmol), MeOH (5 mL), reflux; (**d**) TFA (4 mL), rt.

Further, we explored the reactivity of *p*-substituted phenols in these sequence reactions. Unfortunately, all attempts to prepare the starting materials (**3**) under standard conditions (MsOH, AcOH, rt) failed, and only starting materials **1** and **2** were isolated from the reactions. However, we found that the use of trifluoroacetic acid (TFA) as the activator and medium at room temperature could allow the formation of unstable compounds **3ah** and **3ai** by the nucleophilic addition of phenol to the triazine core. These two compounds (**3ah** and **3ai**) underwent the oxidative cyclization reaction, giving benzofuro[3,2-*e*]triazine **4** in lower to moderate yields. At the same time, biaryl by-products **5ah** and **5ai** were also isolated.

For further assessing the synthetic utility of the method, we performed the addition and coupling reaction sequence again at the gram scale. Thus, under slightly optimized conditions, we synthesized compound **4ad** from triazine **1a** and naphthol **2d** at 40 mmol loading in an 85% yield via two steps (Scheme 4).

The thiomethyl group is a versatile moiety for coupling reactions. In triazines, the thiomethyl group may be easily substituted with aryl boronic acids [84,85] or trialkyl(aryl)stannanes [86] using Liebeskind–Srogl coupling [87]. To demonstrate the synthetic potential of benzofuro-annulated triazines, we performed the substitution of the thiomethyl group with an aryl substituent. The reaction of triazine **4aa** with 4-carbazolylphenylboronic acid **6** provided the corresponding coupling product **7** in a 73% yield (Scheme 7a).

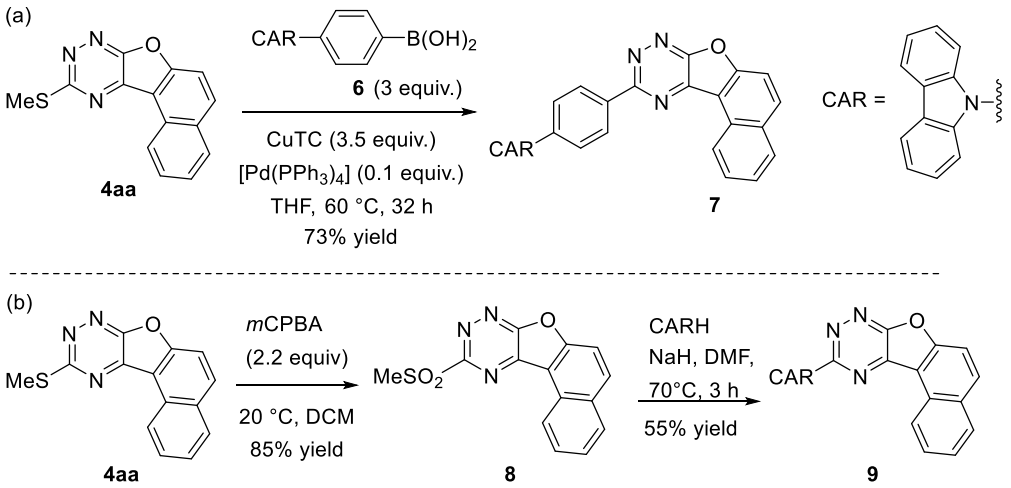

Scheme 7. Further application of the synthesized compound. (**a**) Suzuki coupling; (**b**) Replacement of good leaving group.

Furthermore, a thiomethyl group can easily be oxidized with *m*CPBA to afford the methylsulfonyl group, which can be substituted with various nucleophiles [88–90]. Treatment of the synthesized compound **4aa** with *m*CPBA gave the corresponding sulfonyl derivative **8** at an 85% yield. After that, we successfully synthesized carbazole-substituted naphthofuro-fused 1,2,4-triazine **9** via the subsequent replacement of the sulfonyl group in **8** with carbazole in the presence of sodium hydride (Scheme 7b). It is worth mentioning that these types of carbazole-substituted triazine derivatives have potential uses in biological fields [91,92] and OLED applications [93].

To gain some mechanistic insights into this oxidative cyclization, we first carried out several control experiments. When (2,2,6,6-tetramethylpiperidin-1-yl)oxyl (TEMPO) or butylated hydroxytoluene (BHT) was added to the oxidative cyclization of **3aa** under the standard reaction conditions (Scheme 8a), the desired product **4aa** was obtained in a yield up 81%, suggesting that radicals may not be involved in the catalytic cycle, in contrast to the earlier published cyclization of the Schiff's base in the presence of Mn salt [78,79]. The slight decrease in yield is probably due to the deactivation of manganese oxide under the reducing action of TEMPO and BHT. In addition, a high yield of **4aa** was achieved, even

when performing the reaction under a N_2 atmosphere, demonstrating that aerobic oxygen is not the oxidizing agent in this transformation (Scheme 8a).

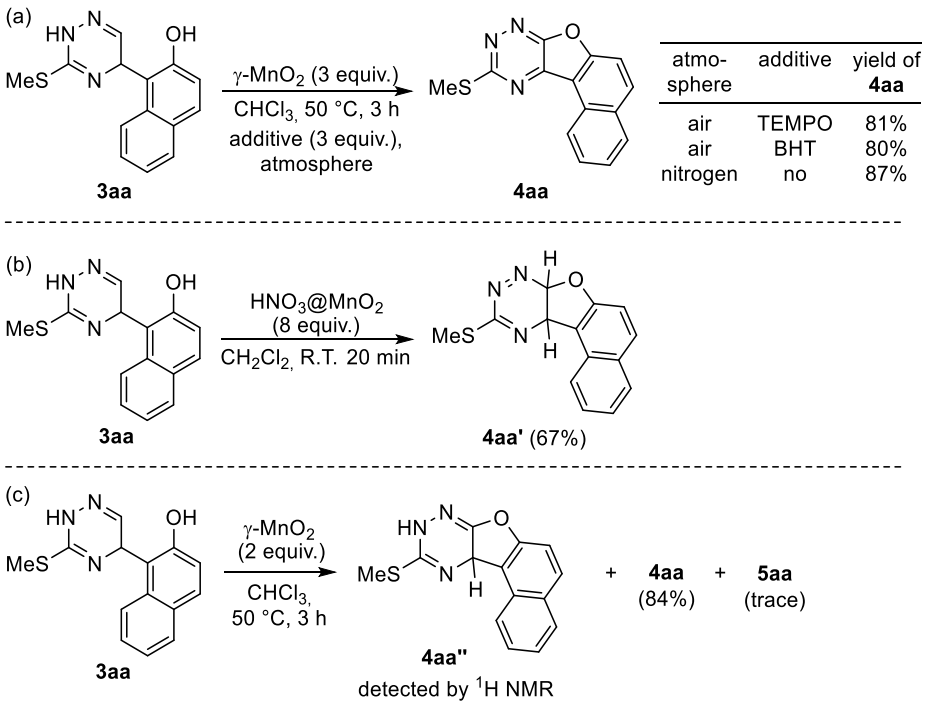

Scheme 8. Control experiments for mechanistic investigation. (**a**) Oxidation in an inert and oxygen atmosphere; (**b**) Using MnO_2 impregnated with HNO_3; (**c**) Isolation of intermediates.

Subsequently, in order to get some information about possible reaction intermediates, we carried out the oxidative cyclization of **3aa** under various conditions. After several trials, we managed to isolate one of the possible intermediates, **4aa′**, in the presence of MnO_2 impregnated with nitric acid [82] in CH_2Cl_2 at room temperature (Scheme 8b). The structure of the intermediate **4aa′** was supported by NMR and HRMS data. The ^{1}H NMR spectrum comprises two dihydrotriazine proton doublets at 5.69 and 5.66 ppm with an SSCC (spin–spin coupling constant) of 10.8 Hz. Another intermediate **4aa′′** was detected by ^{1}H NMR analysis (Please see Supporting Information for details, Section S6) in the crystallized reaction mixture when the reaction was carried out in the presence of a twofold excess of MnO_2 (Scheme 8c). We ascribed the structure of dihydrotriazine to this compound since a single proton resonance at the sp^3 carbon is observed in the ^{1}H NMR spectrum.

After summarizing these preliminary mechanistic studies, a plausible reaction mechanism of the oxidative cyclization has been postulated (Scheme 9). The reaction may proceed through two different pathways: path a and path b. In path a, the reaction starts with the formation of an O-coordinated complex **A**, which agrees well with the oxidation of alcohol to aldehyde in the presence of MnO_2 [94]. Then, complex **A** undergoes intramolecular nucleophilic addition to generate an intermediate **4aa′** with the elimination of Mn(II) species detected by an EPR experiment (Please see Supporting Information for details, Section S6). Then, the quick tautomerization of **4aa′** leads to the intermediate **4aa′′**, which is aromatized with the second equivalent of MnO_2, as well as with 1,4-dihydropyridine [95–98] or 1,4-dihydrotriazine [71,99], to give the final product **4aa**. On the other hand, if we consider path b, at the first step, MnO_2 may coordinate with the nitrogen atom of the triazine core, leading to *N*-coordinated complex **B**, which is also aromatized with the formation of biaryl product **5aa**. Thus, the formation of the final product depends on the position of the initial coordination of the manganese dioxide, through which the reaction can proceed through the regular aromatization of dihydrotriazine (path A) or through the path of oxidative cyclization (path A).

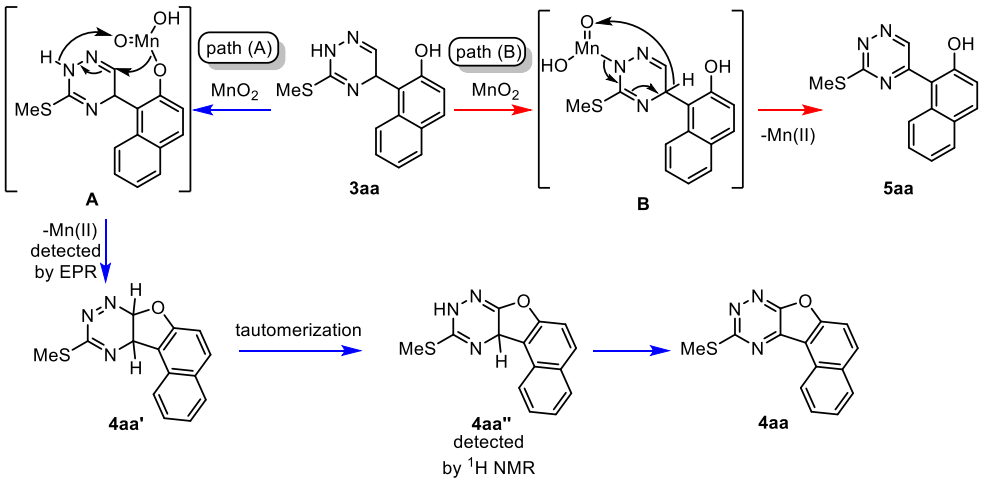

Scheme 9. Proposed pathways of oxidation of dihydrotriazines. (**A**) Oxidative cyclization; (**B**) Regular aromatization.

In order to rationalize the regioselectivity of pathways of the products' formation (**4** vs. **5**) we have performed a series of DFT calculations of the electron density of HOMO and HOMO-1 in the compounds **3aa**, **3fa**, **3ha** and **3ia** (Figure 2). The results show that the electron density on the oxygen atom of the hydroxyl group is comparable with the one on the nitrogen of the triazine core in compounds **3aa** and **3ha**. However, the larger energy gap between HOMO and HOMO-1 of **3aa** compared with the energy gap in **3ha** increased the regioselectivity of the formation of O-coordinated manganese ester. In the case of compound **3ia**, the localization of the orbitals on the triazine N2 nitrogen (HOMO-1) was higher than those on the phenol oxygen (HOMO). So, the reaction proceeds partially via the aromatization of dihydrotriazine, rather than through oxidative cyclization. As follows from Figure 2, the important role of the alkylthio group is that it reduces the electron density at the nitrogen atom of dihydrotriazine, which leads to a reaction at the phenolic oxygen atom. Therefore, these results suggest that MnO_2 may coordinate with either oxygen or nitrogen atoms, depending on the delocalization of the electron density of HOMO and HOMO-1 on the corresponding oxygen or nitrogen atom, and the energy gap between these orbitals.

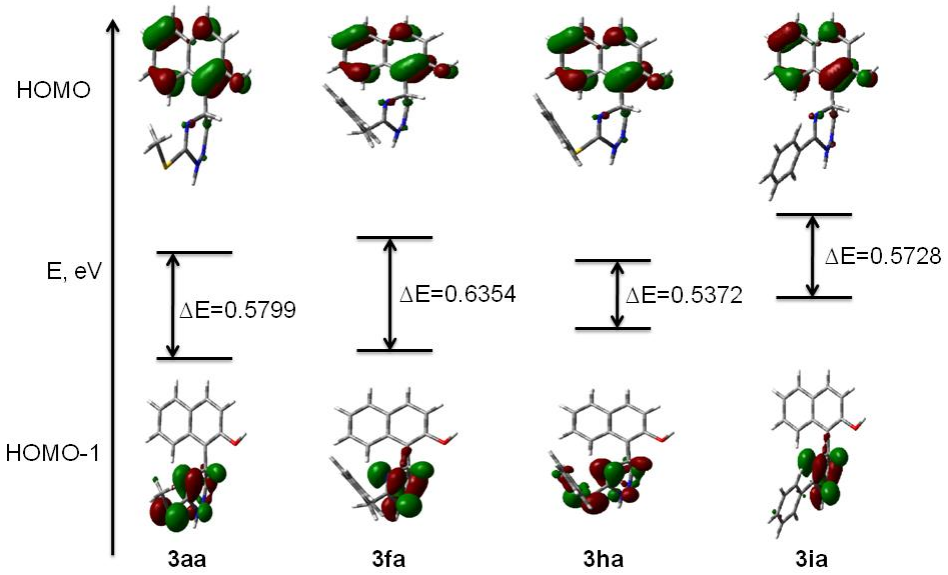

Figure 2. Localizations of electron density on nitrogen and oxygen atoms for compounds **3aa**, **3fa**, **3ha**, and **3ia**.

3. Materials and Methods

General Information: All commercially available chemicals were used without further purifications. ^{1}H NMR (400 MHz) and ^{13}C NMR (101 MHz) spectra were registered on a Bruker DRX-400 Avance spectrometer with DMSO-d_6 or $CDCl_3$ as the solvent at ambient temperature. Chemical shifts are reported in ppm, and coupling constants are given in Hz. Data for ^{1}H NMR are recorded as follows: chemical shift (ppm), multiplicity (s, singlet; d, doublet; t, triplet; q, quartet; quin, quintet; sex, sextet; m, multiplet; br s, broad signal), integration and coupling constant (Hz). High-resolution mass spectra were recorded on an Agilent UHPLC/MS Accurate-Mass Q-TOF 1290/6545. EPR spectra were obtained using a Bruker Elexsys E500 CW-EPR spectrometer (modulation amplitude was set as 0.3 mT). The simulation of the EPR spectra was performed using the package EasySpin 5.2 software [100]. Molecular geometry optimization and the calculation of energies of molecules were carried out in the gas phase using the B3LYP DFT functional [101] with a 6-311 + G (d, p) basis set [102] according to [103] in Gaussian09 [104]. The plots of electron densities of molecular orbitals were obtained using the GaussView 6.0 software [105]. X-ray analysis for compound **5fa** was executed on an Xcalibur 3 diffractometer (MoKα radiation, graphite monochromator, 295(2) K, φ- and ω-scanning with a step of 1°). Thin-layer chromatography (TLC) was performed on a silica gel-coated glass slide (Merck, Silica gel G for TLC). Column chromatography was carried out on silica gel (60 Å, 0.035−0.070 mm). Images of ^{1}H and ^{13}C NMR spectra are provided on pages S26–S81 of the Supplementary Materials.

*3.1. Synthesis of S-substituted 3-thio-1,2,4-triazines **1a-f***

S-substituted 3-thio-1,2,4-triazines **1a-f** were prepared from the corresponding salt of S-substituted isothiosemicarbazide (2 mmol) and glyoxal solution according to the following procedure [106].

A solution of 40% glyoxal (8 mmol, 1160 mg) and $NaHCO_3$ (5 mmol, 420 mg) in ice water (40 mL) was added to a solution of S-substituted isothiosemicarbazide hydrogen iodide (2 mmol) dissolved in ice water (40 mL). The reaction mixture was stirred for 15 min; during that time, the evolution of gas (CO_2) was observed. The reaction mixture was left in the fridge overnight and the aqueous solution was extracted with chloroform. The combined organic layer was washed with 10% oxalic acid, dried over anhydrous Na_2SO_4, filtered, and concentrated in vacuo to obtain oil or a solid triazine compound.

3.1.1. Synthesis of 3-(phenylthio)-1,2,4-triazine **1h**

Compound **1h** was prepared via the oxidation of **1a** with *m*CPBA using a modified procedure [107] followed by the treatment of compound **1a′** with thiophenol.

*m*CPBA (11.6 g, 77%, 52 mmol) and anhydrous Na_2SO_4 (4.0 g) were successively added to DCM (60 mL); the mixture was stirred for 15 min and then filtered and the filter cake was washed with 10 mL of DCM to obtain a clear dichloromethane solution of *m*CPBA. A dichloromethane solution of 3-methylthio-1,2,4-triazine **1a** (3.0 g, 23.6 mmol) was added to this dichloromethane solution of *m*CPBA at −10 °C with stirring. The reaction mixture was allowed to heat to ambient temperature and then stirred for an additional 3 h. Dichloromethane was evaporated under reduced pressure to obtain a dry mixture of 3-(methylsulfonyl)-1,2,4-triazine **1a′** and *m*-chlorobenzoic acid. The mixture was dissolved in pyridine (40 mL) and thiophenol (5.3 mL, 5.72 g, 52 mmol) was added after. After 24 h the mixture was evaporated in vacuo, and the residue was treated with a mixture of dichloromethane and aqueous $NaHCO_3$. The organic layer was evaporated, yielding pure compound **1h**.

3.1.2. Synthesis of 3-phenyl- and 3-(4-methoxyphenyl)-1,2,4-triazines **1i** and **1j**

Compounds **1i** and **1j** were prepared according to the published procedure [108]. The spectroscopic data for compound **1i** are in agreement with the literature [109].

3.1.3. Synthesis of 3-methyl- and 3-benzyl-1,2,4-triazine **1k** and **1l**

Compounds **1k** and **1l** were prepared according to the known procedure [110]. The spectroscopic data of compounds **1k** are in agreement with the published data [110].

3.1.4. Synthesis of 4-(1,2,4-triazin-3-yl)morpholine **1m**

Compound **1m** was prepared according to the published procedure [111].

*3.2. General Procedure for the Synthesis of Dihydrotriazines **3***

3.2.1. Method A

To a stirred solution of triazine **1a-j** (1 mmol, 1 equiv.) and 2-naphthol **2a,f,g** (1 mmol, 1 equiv.) in acetic acid (4 mL), we added a methanesulfonic acid (195 µL, 3 mmol, 3 equiv.). The resulting mixture was stirred at room temperature for 1-5 h. The progress of the reaction was monitored using TLC. After the completion of the reaction, the reaction mixture was diluted with water (20 mL), neutralized with aq. $NaHCO_3$ solution and extracted with AcOEt (3 × 10 mL). The combined organic phase was dried over anhydrous Na_2SO_4, filtered, and concentrated under reduced pressure. The residue was purified by silica gel chromatography or recrystallization from the corresponding solvent to afford product **3**.

3.2.2. Method B

To a stirred solution of triazine **1a** (1 mmol, 1 equiv.) and 2-naphthol **2b-e** (1 mmol, 1 equiv.) in methanol (4 mL) we added $BF_3{\cdot}OEt_2$ (985 µL, 8 mmol, 8 equiv.) and the resulting mixture was refluxed for 5 h. After cooling the methanol was evaporated under reduced pressure, and the residue was dissolved in AcOEt (10 mL) and washed with 5% aq. $NaHCO_3$ solution (50 mL). The organic layer was dried over anhydrous Na_2SO_4, filtered, and evaporated under reduced pressure. The crude product was recrystallized from MeCN to obtain the product **3ab-3ae**.

*3.3. General Procedure for the Synthesis of Naphthofuro-Fused Triazines **4***

To a stirred solution of **3** (0.2 mmol, 1 equiv.) in $CHCl_3$ (3 mL), MnO_2 (52 mg, 0.6 mmol, 3 equiv.) was added in one portion. The resulting mixture was stirred at 50 °C for 3 h. The completion of the reaction was monitored by TLC. The reaction mixture was then cooled to room temperature; the MnO_2 was filtered and the filter cake was washed with $CHCl_3$ (3 × 10 mL). The combined organic phase was concentrated under reduced pressure. The residue was purified by chromatography on silica gel or recrystallization to afford the pure product **4**.

3.3.1. 10-(Methylthio)naphtho[1′,2′:4,5]furo[3,2-*e*][1,2,4]triazine **4aa**

Pale yellow needles after recrystallization from MeCN. Yield 51 mg, 95%; m.p. 185–187 °C. ^{1}H NMR ($CDCl_3$): 8.78–8.66 (m, 1H, H-1), 8.20–8.06 (m, 1H, H-5), 7.97–7.86 (m, 1H, H-4), 7.76–7.52 (m, 3H, H-2, H-3, H-6), 2.79 (s, 3H, SCH_3); ^{13}C NMR ($CDCl_3$): 169.8, 160.0, 158.6, 143.7, 137.0, 130.5, 129.6, 129.2, 128.7, 126.7, 124.7, 112.7, 112.6, 14.8. Anal. Calcd. For $C_{14}H_9N_3OS$: C, 62.91; H, 3.39; N, 15.72%; found: C, 62.96; H, 3.47; N, 15.79%.

3.3.2. 10-(Ethylthio)naphtho[1′,2′:4,5]furo[3,2-*e*][1,2,4]triazine **4ba**

Pale yellow needles after recrystallization from MeCN. Yield 47 mg, 84%; m.p. 141–143 °C. ^{1}H NMR ($CDCl_3$): 8.97–8.88 (m, 1H, H-1), 8.28–8.21 (m, 1H, H-5), 8.06–7.99 (m, 1H, H-4), 7.87–7.75 (m, 2H, H-2, H-6), 7.70–7.62 (m, 1H, H-3), 3.44 (q, 2H, J = 7.3 Hz, SCH_2), 1.56 (t, 3H, J = 7.3 Hz, CH_3); ^{13}C NMR ($CDCl_3$): 169.6, 160.1, 158.7, 143.9, 137.0, 130.6, 129.6, 129.3, 128.9, 126.8, 124.8, 112.9, 112.7, 26.1, 14.4. Anal. Calcd. For $C_{15}H_{11}N_3OS$: C, 64.04; H, 3.94; N, 14.94%; found: C, 64.12; H, 3.99; N, 14.85%.

3.3.3. 10-(Butylthio)naphtho[1′,2′:4,5]furo[3,2-*e*][1,2,4]triazine **4ca**

Pale yellow needles after recrystallization from MeCN. Yield 53 mg, 85%; m.p. 121–123 °C. ^{1}H NMR ($CDCl_3$): 8.83–8.75 (m, 1H, H-1), 8.20–8.12 (m, 1H, H-5), 7.99–7.92 (m, 1H, H-4),

7.79–7.55 (m, 3H, H-2, H-3, H-6), 3.45–3.33 (m, 2H, SCH_2), 1.96–1.83 (m, 2H, SCH_2CH_2), 1.68–1.53 (m, 2H, $SCH_2CH_2C\underline{H_2}$), 1.08–0.97 (m, 3H, CH_3); ^{13}C NMR ($CDCl_3$): 169.8, 160.1, 158.7, 143.9, 137.1, 130.6, 129.6, 129.4, 128.9, 126.8, 124.9, 113.0, 112.8, 31.4, 31.3, 22.3, 13.9. Anal. Calcd. For $C_{17}H_{15}N_3OS$: C, 66.00; H, 4.89; N, 13.58%; found: C, 66.09; H, 4.82; N, 13.50%.

3.3.4. 10-((Cyclobutylmethyl)thio)naphtho[1′,2′:4,5]furo[3,2-*e*][1,2,4]triazine **4da**

Yellow needles after recrystallization from MeCN. Yield 57 mg, 89%; m.p. 154–156 °C. ^{1}H NMR ($CDCl_3$): 8.81–8.76 (m, 1H, H-1), 8.17 (d, 1H, *J* = 9.0 Hz, H-5), 7.98–7.93 (m, 1H, H-4), 7.78–7.72 (m, 1H, H-2), 7.70 (d, 1H, *J* = 9.0 Hz, H-6), 7.63–7.57 (m, 1H, H-3), 3.53–3.44 (m, 2H, SCH_2), 2.90–2.80 (m, 1H, CH-1′), 2.29–2.18 (m, 2H, CH_2-3′), 1.98–1.83 (m, 4H, CH_2-2′, CH_2-4′); ^{13}C NMR ($CDCl_3$): 169.7, 160.0, 158.7, 143.8, 137.0, 130.6, 129.6, 129.3, 128.8, 126.7, 124.8, 112.8, 112.7, 37.9, 34.7, 28.0, 18.2. Anal. Calcd. For $C_{18}H_{15}N_3OS$: C, 67.27; H, 4.70; N, 13.07%; found: C, 67.35; H, 4.78; N, 13.12%.

3.3.5. 10-(But-2-yn-1-ylthio)naphtho[1′,2′:4,5]furo[3,2-*e*][1,2,4]triazine **4ea**

Brown powder after purification by chromatography on silica gel using *n*-hexane-ethyl acetate (10:1). Yield 45 mg, 70%; m.p. 163–165 °C. ^{1}H NMR ($CDCl_3$): 8.88–8.83 (m, 1H, H-1), 8.22 (d, 1H, *J* = 9.0 Hz, H-5), 8.02–7.97 (m, 1H, H-4), 7.82–7.77 (m, 1H, H-2), 7.74 (d, 1H, *J* = 9.0 Hz, H-6), 7.67–7.61 (m, 1H, H-3), 4.15 (q, 2H, *J* = 2.5 Hz, SCH_2), 1.84 (t, 3H, *J* = 2.5 Hz, CH_3); ^{13}C NMR ($CDCl_3$): 168.4, 160.1, 158.8, 143.9, 137.3, 130.6, 129.8, 129.8, 128.9, 126.9, 124.9, 112.9, 112.7, 79.5, 73.7, 21.0, 3.9. Anal. Calcd. For $C_{17}H_{11}N_3OS$: C, 66.87; H, 3.63; N, 13.76%; found: C, 66.80; H, 3.60; N, 13.86%.

3.3.6. 10-(Benzylthio)naphtho[1′,2′:4,5]furo[3,2-*e*][1,2,4]triazine **4fa**

Yellow needles after recrystallization from MeCN. Yield 63 mg, 90%; m.p. 161–163 °C. ^{1}H NMR ($CDCl_3$): 8.82–8.73 (m, 1H, H-1), 8.17 (d, 1H, *J* = 9.1 Hz, H-5), 7.97–7.93 (m, 1H, H-4), 7.78–7.72 (m, 1H, H-3), 7.70 (d, 1H, *J* = 9.1 Hz, H-6), 7.26–7.56 (m, 3H, H-2, Ph), 7.38–7.32 (m, 2H, Ph), 7.30–7.25 (m, 1H, Ph), 4.66 (m, 1H, SCH_2); ^{13}C NMR ($CDCl_3$): 169.0, 160.2, 158.8, 143.9, 137.2, 137.1, 130.6, 129.7, 129.4, 129.4, 128.9, 128.7, 127.6, 126.8, 124.9, 112.9, 112.7, 36.1. Anal. Calcd. For $C_{20}H_{13}N_3OS$: C, 69.95; H, 3.82; N, 12.24%; found: C, 69.85; H, 3.76; N, 12.20%.

3.3.7. 10-(Allylthio)naphtho[1′,2′:4,5]furo[3,2-*e*][1,2,4]triazine **4ga**

Pale yellow powder after recrystallization from MeCN. Yield 46 mg, 78%; m.p. 126–128 °C. ^{1}H NMR ($CDCl_3$): 8.83–8.74 (m, 1H, H-1), 8.17 (d, 1H, *J* = 9.1 Hz, H-5), 7.99–7.93 (m, 1H, H-4), 7.78–7.72 (m, 1H, H-3), 7.70 (d, 1H, *J* = 9.1 Hz, H-6), 7.64–7.57 (m, 1H, H-2), 6.13 (ddt, 1H, ^3J = 6.9 Hz, ^3J(cis) = 10.0 Hz, ^3J(trans) = 17.0 Hz, CH-2′), 5.47 (dd, 1H, ^3J(trans) = 16.9 Hz, *J* = 1.2 Hz, CH-3a′), 5.22 (d, 1H, ^3J(cis) = 10.0 Hz, CH-3b′), 4.06 (d, 2H, ^3J = 6.9 Hz, SCH_2); ^{13}C NMR ($CDCl_3$): 168.9, 160.1, 158.7, 143.8, 137.1, 133.1, 130.6, 129.7, 129.3, 128.8, 126.8, 124.8, 118.7, 112.9, 112.7, 34.5. Anal. Calcd. For $C_{16}H_9N_3OS$: C, 65.97; H, 3.11; N, 14.42%; found: C, 65.90; H, 3.18; N, 14.50%.

A mixture of **4ha** and **5ha** was separated by silica gel chromatography using *n*-hexane-ethyl acetate (17:1) to isolate **4ha** and *n*-hexane-ethyl acetate (10:1) to give **5ha**.

3.3.8. 10-(Phenylthio)naphtho[1′,2′:4,5]furo[3,2-*e*][1,2,4]triazine **4ha**

Yellow powder. Yield 46 mg, 70%; m.p. 196–198 °C. ^{1}H NMR ($CDCl_3$): 8.58–8.53 (m, 1H, H-1), 8.22–8.17 (m, 1H, H-5), 8.00–7.95 (m, 1H, H-4), 7.83–7.77 (m, 2H, Ph), 7.75–7.67 (m, 2H, H-3, H-6), 7.64–7.58 (m, 1H, H-2), 7.56–7.50 (m, 3H, Ph); ^{13}C NMR ($CDCl_3$): 170.0, 160.3, 158.8, 144.0, 137.2, 135.8, 130.6, 129.7, 129.6, 129.5, 129.3, 129.2, 128.8, 126.8, 124.8, 113.0, 112.7. Anal. Calcd. For $C_{19}H_{11}N_3OS$: C, 69.29; H, 3.37; N, 12.76%; found: C, 69.20; H, 3.45; N, 12.70%.

3.3.9. 1-(3-(Phenylthio)-1,2,4-triazin-5-yl)naphthalen-2-ol **5ha**

Yellow powder. Yield 9 mg, 14%; m.p. 149–151 °C. ^{1}H NMR ($CDCl_3$): 11.01 (s, 1H, OH), 9.51 (s, 1H, H-6′), 8.09–8.03 (m, 1H, H-8), 7.84 (d, 1H, *J* = 9.0 Hz, H-4), 7.82–7.76 (m, 1H, H-5), 7.75–7.67 (m, 2H, Ph), 7.59–7.51 (m, 4H, Ph, H-7), 7.44–7.37 (m, 1H, H-6), 7.07 (d, 1H, *J* = 9.0 Hz, H-3); ^{13}C NMR ($CDCl_3$): 172.3, 160.8, 155.7, 146.2, 136.2, 136.0, 130.8 (2C), 130.3, 129.5, 129.2, 128.7, 126.9, 124.7, 123.2, 119.7, 108.9. Anal. Calcd. For $C_{19}H_{13}N_3OS$: C, 68.86; H, 3.95; N, 12.68%; found: C, 68.77; H, 3.90; N, 12.60%.

A mixture of **4ia** and **5ia** was separated by chromatography using *n*-hexane-ethyl acetate (15:1) to give **4ia** and *n*-hexane-ethyl acetate (8:1) to give **5ia**.

3.3.10. 10-Phenylnaphtho[1′,2′:4,5]furo[3,2-*e*][1,2,4]triazine **4ia**

Pale yellow solid. Yield 12 mg, 21%, m.p. 189–191 °C. Rf = 0.54 (ethyl acetate:hexane, 1:1). ^{1}H NMR ($CDCl_3$): 9.09–8.99 (m, 1H, H-1), 8.75–8.64 (m, 2H, Ph), 8.24–8.14 (m, 1H, H-5), 8.03–7.94 (m, 1H, H-4), 7.86–7.73 (m, 2H, H-2, H-6), 7.66–7.52 (m, 4H, H-3, Ph); ^{13}C NMR ($CDCl_3$): 161.5, 160.8, 158.5, 143.9, 136.7, 135.7, 131.2, 130.7, 129.6, 129.3, 129.1, 129.0, 128.5, 126.7, 124.9, 113.7, 112.8. Anal. Calcd. For $C_{19}H_{11}N_3O$: C, 76.76; H, 3.73; N, 14.13%; found: C, 76.83; H, 3.70; N, 14.19%.

3.3.11. 1-(3-Phenyl-1,2,4-triazin-5-yl)naphthalen-2-ol **5ia**

Yellow solid. Yield 31 mg, 52%, m.p. 204–206 °C. Rf = 0.39 (ethyl acetate:hexane, 1:1). ^{1}H NMR (DMSO-d_6): 12.45–12.16 (br s, 1H, OH), 9.77 (s, 1H, H-6′), 8.56–8.47 (m, 2H, Ph), 8.21–8.11 (m, 1H, H-8), 7.95 (d, 1H, *J* = 9.0 Hz, H-4), 7.90–7.83 (m, 1H, H-5), 7.67–7.55 (m, 4H, H-6, Ph), 7.49–7.42 (m, 1H, H-7), 7.28 (d, 1H, *J* = 9.0 Hz, H-3); ^{13}C NMR (DMSO-d_6): 161.3, 160.3, 155.9, 148.3, 135.8, 134.2, 132.4, 131.0, 129.6, 129.3 (2C), 128.7, 128.4, 124.7, 123.1, 119.6, 109.4. Anal. Calcd. For $C_{19}H_{13}N_3O$: C, 76.24; H, 4.38; N, 14.04%; found: C, 76.32; H, 4.45; N, 14.12%.

A mixture of **4ja** and **5ja** was separated by silica gel chromatography using *n*-hexane-ethyl acetate (17:1) to isolate **4ja** and *n*-hexane-ethyl acetate (7:1) to give **5ja**.

3.3.12. 10-(4-Methoxyphenyl)naphtho[1′,2′:4,5]furo[3,2-*e*][1,2,4]triazine **4ja**

Pale yellow solid. Yield 18 mg, 28%; m.p. 205–207 °C. Rf = 0.53 (ethyl acetate:hexane, 1:1). ^{1}H NMR ($CDCl_3$): 9.05–8.99 (m, 1H, H-1), 8,64 (d, 2H, *J* = 8.8 Hz, Ph), 8.19 (d, 1H, *J* = 9.0 Hz, H-5), 8.02–7.94 (m, 1H, H-4), 7.85–7.78 (m, 1H, H-3), 7.76 (d, 1H, *J* = 9.0 Hz, H-6), 7.66–7.58 (m, 1H, H-2), 7.08 (d, 2H, *J* = 8.8 Hz, Ph), 3.93 (s, 3H, OCH_3); ^{13}C NMR ($CDCl_3$): 162.3, 161.4, 160.6, 158.4, 143.9, 136.5, 130.7, 130.1, 129.5, 129.3, 129.1, 128.3, 126.7, 124.9, 114.3, 113.7, 112.8, 55.6. Anal. Calcd. For $C_{20}H_{13}N_3O_2$: C, 73.38; H, 4.00; N, 12.84%; found: C, 73.30; H, 3.92; N, 12.94%.

3.3.13. 1-(3-(4-Methoxyphenyl)-1,2,4-triazin-5-yl)naphthalen-2-ol **5ja**

Yellow solid. Yield 31 mg, 47%; m.p. 178–180 °C. Rf = 0.41 (ethyl acetate:hexane, 1:1). ^{1}H NMR (DMSO-d_6): 12.33–12.08 (br s, 1H, OH), 9.59 (s, 1H, H-6′), 8.38 (d, 2H, *J* = 8.7 Hz, Ph), 8.09–8.01 (m, 1H, H-8), 7.87–7.81 (m, 1H, H-4), 7.80–7.72 (m, 1H, H-5), 7.54–7.45 (m, 1H, H-7 or H-6), 7.39–7.30 (m, 1H, H-6 or H-7), 7.22–7.13 (m, 1H, H-3), 7.03–6.95 (d, 2H, *J* = 8.7 Hz, Ph), 3.83 (s, 3H, OCH_3); ^{13}C NMR (DMSO-d_6): 162.5, 156.8, 154.1, 151.0, 135.1, 132.6, 132.2, 131.6, 129.1, 128.4, 128.0, 127.8, 127.6, 123.4, 123.1, 118.1, 113.9, 55.7. Anal. Calcd. For $C_{20}H_{15}N_3O_2$: C, 72.94; H, 4.59; N, 12.76%; found: C, 72.83; H, 4.65; N, 12.70%.

3.3.14. 6-Methoxy-10-(methylthio)naphtho[1′,2′:4,5]furo[3,2-*e*][1,2,4]triazine **4ab**

Yellow powder after recrystallization from MeCN. Yield 48 mg, 80%; m.p. 183–185 °C. ^{1}H NMR ($CDCl_3$): 8.55–8.51 (m, 1H, H-4 or H-1), 7.71–7.66 (m, 1H, H-1 or H-4), 7.55–7.50 (m, 1H, H-3 or H-2), 7.79–7.50 (m, 1H, H-2 or H-3), 7.32 (s, 1H, H-5), 4.13 (s, 3H, OCH_3), 2.78 (s, 3H, SCH_3); ^{13}C NMR ($CDCl_3$): 169.9, 159.9, 149.9, 145.0, 143.3, 131.2, 127.6, 126.9, 126.8, 124.3, 123.6, 114.1, 113.3, 56.5, 14.8. Anal. Calcd. For $C_{15}H_{11}N_3O_2S$: C, 60.59; H, 3.73; N, 14.13%; found: C, 60.67; H, 3.65; N, 14.04%.

3.3.15. 2-Methoxy-10-(methylthio)naphtho[1′,2′:4,5]furo[3,2-*e*][1,2,4]triazine **4ac**

Yellow powder after recrystallization from MeCN. Yield 50 mg, 84%; m.p. 219–221 °C. ^{1}H NMR ($CDCl_3$): 8.22–8.19 (m, 1H, H-1), 8.14–8.10 (m, 1H, H-4), 7.88 (d, 1H, *J* = 8.9 Hz, H-4), 7.57 (d, 1H, *J* = 8.9 Hz, H-3), 7.27–7.22 (m, 1H, H-3), 4.06 (s, 3H, OCH_3), 2.81 (s, 3H, SCH_3); ^{13}C NMR ($CDCl_3$): 169.6, 161.0, 160.2, 159.4, 144.1, 136.8, 131.0, 125.7, 118.8, 112.0, 109.8, 104.2, 96.3, 55.8, 14.8. Anal. Calcd. For $C_{15}H_{11}N_3O_2S$: C, 60.59; H, 3.73; N, 14.13%; found: C, 60.50; H, 3.66; N, 14.10%.

3.3.16. 10-(Methylthio)naphtho[1′,2′:4,5]furo[3,2-*e*][1,2,4]triazin-2-ol **4ad**

According to the general procedure, in the mixture of $CHCl_3$:EtOH (4:1) as solvent, **4ad** was obtained as yellow powder after recrystallization from EtOH. Yield 38 mg, 68%; m.p. 282–284 °C. ^{1}H NMR (DMSO-d_6): 10.61 (s, 1H, OH), 8.30 (d, 1H, *J* = 8.9 Hz, H-6), 8.03–7.97 (m, 2H, H-1, H-4), 7.70 (d, 1H, *J* = 8.9 Hz, H-4), 7.57 (d, 1H, *J* = 8.9 Hz, H-3), 7.19–7.14 (m, 1H, H-3), 2.76 (s, 3H, SCH_3); ^{13}C NMR (DMSO-d_6): 168.0, 159.9, 159.1, 159.1, 144.0, 137.4, 131.6, 130.2, 124.4, 118.4, 110.5, 108.9, 106.5, 14.1. Anal. Calcd. For $C_{14}H_9N_3O_2S$: C, 59.35; H, 3.20; N, 14.83%; found: C, 59.25; H, 3.15; N, 14.75%.

3.3.17. 3-Methoxy-10-(methylthio)naphtho[1′,2′:4,5]furo[3,2-*e*][1,2,4]triazine **4ae**

Yellow powder after recrystallization from MeCN. Yield 49 mg, 82%; m.p. 214–216 °C. ^{1}H NMR ($CDCl_3$): 8.83 (d, 1H, *J* = 8.9 Hz, H-1), 8.13 (d, 1H, *J* = 9.0 Hz, H-5), 7.74 (d, 1H, *J* = 9.0 Hz, H-6), 7.47 (dd, 1H, *J* = 8.9 Hz, *J* = 2.5 Hz, H-2), 7.33 (d, 1H, *J* = 2.5 Hz, H-4), 3.98 (s, 3H, OCH_3), 2.83 (s, 3H, SCH_3); ^{13}C NMR ($CDCl_3$): 169.7, 160.2, 158.3, 157.6, 143.9, 135.9, 132.2, 126.3, 123.8, 121.7, 113.1 (2C), 108.2, 55.6, 14.9. Anal. Calcd. For $C_{15}H_{11}N_3O_2S$: C, 60.59; H, 3.73; N, 14.13%; found: C, 60.65; H, 3.82; N, 14.10%.

3.3.18. 3-Bromo-10-(methylthio)naphtho[1′,2′:4,5]furo[3,2-*e*][1,2,4]triazine **4af**

Yellow powder after recrystallization from toluene. Yield 53 mg, 75%; m.p. 244–246 °C. ^{1}H NMR ($CDCl_3$): 8.86 (d, 1H, *J* = 8.7 Hz, H-1), 8.23 (d, 1H, *J* = 1.8 Hz, H-4), 8.19 (d, 1H, *J* = 9.1 Hz, H-5), 7.92 (dd, 1H, *J* = 8.7 Hz, *J* = 1.8 Hz, H-2), 7.85 (d, 1H, *J* = 9.1 Hz, H-6), 2.85 (s, 3H, SCH_3); ^{13}C NMR ($CDCl_3$): 170.2 160.3, 158.7, 143.6, 136.0, 133.0, 132.0, 131.5, 127.5, 126.6, 120.8, 114.1, 113.2, 14.9. Anal. Calcd. For $C_{14}H_8BrN_3OS$: C, 48.57; H, 2.33; N, 12.14%; found: C, 48.50; H, 2.26; N, 12.06%.

3.3.19. 10-(Methylthio)naphtho[1′,2′:4,5]furo[3,2-*e*][1,2,4]triazine-3-carbonitrile **4ag**

Yellow solid after recrystallization from MeCN. Yield 54 mg, 91%; m.p. 283–285 °C. ^{1}H NMR ($CDCl_3$): 9.09 (d, 1H, *J* = 8.5 Hz, H-1), 8.44 (d, 1H, *J* = 1.5 Hz, H-4) 8.33 (d, 1H, *J* = 9.1 Hz, H-5), 7.99 (dd, 1H, *J* = 8.5 Hz, *J* = 1.5 Hz, H-2), 7.96 (d, 1H, *J* = 9.1 Hz, H-6), 2.85 (s, 3H, SCH_3); ^{13}C NMR ($CDCl_3$): 170.7, 160.4, 159.8, 143.3, 136.8, 134.9, 130.9, 130.6, 129.9, 126.3, 118.6, 115.1, 113.4, 110.7, 14.9. Anal. Calcd. For $C_{15}H_8N_4OS$: C, 61.63; H, 2.76; N, 19.17%; found: C, 61.72; H, 2.86; N, 19.22%.

3.3.20. Synthesis of 10-alkyl naphtho[1′,2′:4,5]furo[3,2-*e*][1,2,4]triazines **4ka** and **4la**

To a stirred solution of corresponding triazine **1k** or **1l** (1 mmol, 1 equiv.) in acetic acid (4 mL), 2-naphthol **2a** (144 mg, 1 mmol, 1 equiv.) was added. Then the mixture was stirred at room temperature for 5 h, concentrated under reduced pressure, dissolved in $CHCl_3$ (10 mL) and washed with saturated aq. $NaHCO_3$ solution (10 mL). The organic layer was dried over anhydrous Na_2SO_4 and filtered. To the organic phase, MnO_2 (261 mg, 3.0 mmol, 3 equiv.) was added in one portion and the mixture was stirred at 50 °C for 3 h. The reaction mixture was then cooled to room temperature. MnO_2 was filtered and washed with $CHCl_3$ (3 × 10 mL). The combined organic phase was concentrated under reduced pressure to give a mixture of **4** and **5**, which was separated by chromatography on silica gel using a mixture of *n*-hexane-ethyl acetate as the eluent.

A mixture of **4ka** and **5ka** was separated by chromatography on silica gel using *n*-hexane-ethyl acetate (25:1) to isolate **4ka** and *n*-hexane-ethyl acetate (8:1) to give **5ka**.

3.3.21. 10-Methylnaphtho[1′,2′:4,5]furo[3,2-*e*][1,2,4]triazine **4ka**

Yellow solid. Yield 113 mg, 48%; m.p. 190–192 °C. Rf = 0.46 (ethyl acetate:hexane, 1:1). ^{1}H NMR ($CDCl_3$): 8.98–8.92 (m, 1H, H-1), 8.24–8.17 (m, 1H, H-5), 8.04–7.98 (m, 1H, H-4), 7.84–7.72 (m, 2H, H-2, H-6), 7.68–7.59 (m, 1H, H-3), 3.08 (s, 3H, CH_3); ^{13}C NMR ($CDCl_3$): 164.4, 160.6, 158.4, 144.0, 136.7, 130.7, 129.5, 129.3, 129.0, 126.7, 124.9, 113.4, 112.8, 23.9. Anal. Calcd. For $C_{14}H_9N_3O$: C, 71.48; H, 3.86; N, 17.86%; found: C, 71.39; H, 3.93; N, 17.92%.

3.3.22. 1-(3-Methyl-1,2,4-triazin-5-yl)naphthalen-2-ol **5ka**

Pale yellow solid. Yield 45 mg, 19%; m.p. 168–170 °C. Rf = 0.25 (ethyl acetate:hexane 1:1). ^{1}H NMR (DMSO-d_6): 10.46 (s, 1H, OH), 9.44 (s, 1H, H-6′), 8.01–7.96 (m, 1H, H-4), 7.92–7.85 (m, 1H, H-8 or H-5), 7.73–7.67 (m, 1H, H-5 or H-8), 7.45–7.29 (m, 3H, H-3, H-6, H-7), 2.85 (s, 3H, CH_3); ^{13}C NMR (DMSO-d_6): 166.2, 156.4, 153.8, 150.2, 132.3, 132.1, 128.3, 127.9, 127.4, 123.3, 123.2, 118.1, 113.8, 23.6. Anal. Calcd. For $C_{14}H_{11}N_3O$: C, 70.87; H, 4.67; N, 17.71%; found: C, 70.77; H, 4.72; N, 17.80%.

A mixture of **4la** and **5la** was separated by chromatography on silica gel using *n*-hexane-ethyl acetate (17:1) to give **4la,** and *n*-hexane-ethyl acetate (10:1) to give **5la**.

3.3.23. 10-Benzylnaphtho[1′,2′:4,5]furo[3,2-*e*][1,2,4]triazine **4la**

Pale yellow solid. Yield 109 mg, 35%; m.p. 226–228 °C. Rf = 0.57 (ethyl acetate:hexane, 1:1). ^{1}H NMR (DMSO-d_6): 8.89–8.82 (m, 1H, H-1), 8.49 (d, 1H, *J* = 9.0 Hz H-5), 8.25–8.20 (m, 1H, H-4), 8.06 (d, 1H, *J* = 9.0 Hz H-6), 7.93–7.87 (m, 1H, H-3 or H-2), 7.74–7.69 (m, 1H, H-2 or H-3), 7.49–7.44 (m, 2H, Ph), 7.37–7.32 (m, 2H, Ph), 7.27–7.22 (m, 1H, Ph), 4.62 (s, 2H, CH_2); ^{13}C NMR (DMSO-d_6): 165.0, 160.2, 158.0, 143.9, 138.1, 137.0, 130.2, 129.5 (2C), 129.0 (2C), 128.3 (2C), 128.1, 126.4 (2C), 123.7, 112.9, 112.5, 42.7. Anal. Calcd. For $C_{20}H_{13}N_3O$: C, 77.16; H, 4.21; N, 13.50%; found: C, 77.25; H, 4.30; N, 13.57%.

3.3.24. 1-(3-Methyl-1,2,4-triazin-5-yl)naphthalen-2-ol **5la**

Pale yellow solid. Yield 110 mg, 35%; m.p. 155–157 °C. Rf = 0.34 (ethyl acetate:hexane, 1:1). ^{1}H NMR (DMSO-d_6): 10.55 (s, 1H, OH), 9.49 (s, 1H, H-6′), 8.01–7.94 (m, 1H, H-4), 7.90–7.84 (m, 1H, H-8 or H-5), 7.63–7.55 (m, 1H, H-5 or H-8), 7.43–7.22 (m, 8H, H-3, H-6, H-7, Ph), 4.47 (s, 2H, CH_2); ^{13}C NMR (DMSO-d_6): 167.9, 156.7, 154.0, 150.6, 137.7, 132.6, 132.0, 129.2, 128.5, 128.3, 128.0, 127.3, 126.6, 123.4, 123.1, 118.0, 113.5, 43.0. Anal. Calcd. For $C_{20}H_{15}N_3O$: C, 76.66; H, 4.83; N, 13.41%; found: C, 76.75; H, 4.74; N, 13.48%.

3.3.25. 10-Morpholinonaphtho[1′,2′:4,5]furo[3,2-*e*][1,2,4]triazine **4ma**

To a stirred solution of 4-(1,2,4-triazin-3-yl)morpholine **1m** (1 mmol, 1 equiv.) and 2-naphthol **2a** (1 mmol, 1 equiv.) in methanol (4 mL) $BF_3{\cdot}OEt_2$ (370 μL, 3 mmol, 3 equiv.) was added dropwise, and the resulting mixture was refluxed for 3 h. After cooling to room temperature the methanol was evaporated under reduced pressure, and the residue was dissolved in $CHCl_3$ (10 mL) and washed with aq. $NaHCO_3$. Then, the organic layer was dried over Na_2SO_4 and filtered. To the resulting solution MnO_2 (261 mg, 3 mmol, 3 equiv.) was added in one portion and the mixture was stirred at 50 °C for 3 h. The reaction mixture was cooled to room temperature. MnO_2 was filtered and washed with $CHCl_3$ (3 × 10 mL). The combined organic phase was concentrated under reduced pressure, and the residue was crystallized from MeCN to afford pure **4ma**. Yellow powder. Yield 225 mg, 75%; m.p. 230–232 °C. ^{1}H NMR ($CDCl_3$): 8.87–8.82 (m, 1H, H-1), 8.19 (d, 1H, *J* = 9.1 Hz, H-5), 8.02–7.96 (m, 1H, H-4), 7.80–7.73 (m, 1H, H-3), 7.70 (d, 1H, *J* = 9.1 Hz, H-6), 7.65–7.58 (m, 1H, H-2), 4.07–4.00 (m, 4H, morpholine), 3.95–3.88 (m, 4H, morpholine); ^{13}C NMR ($CDCl_3$): 161.1, 158.9, 157.7, 144.2, 136.0, 130.5, 129.3, 129.3, 129.2, 126.3, 124.6, 113.5, 113.0, 67.0, 45.1. Anal. Calcd. For $C_{17}H_{14}N_4O_2$: C, 66.66; H, 4.61; N, 18.29%; found: C, 66.75; H, 4.54; N, 18.36%.

3.3.26. Synthesis of Benzofuro-Fused Triazines **4ah** and **4ai**

To a solution of triazine **1a** (127 mg, 1 mmol) in TFA (4 mL), a corresponding phenol **2h** or **2i** (1 mmol) was added, and the resulting mixture was stirred at room temperature

for 24 h. The completion of the reaction was monitored by TLC. Then, the reaction mixture was concentrated under reduced pressure. The residue was dissolved in $CHCl_3$ (10 mL) and washed with 5% aq. $NaHCO_3$. The organic layer was dried over Na_2SO_4 and filtered. MnO_2 (52 mg, 0.6 mmol, 3 equiv.) was added to the resulting solution in one portion and the mixture was stirred at 50 °C for 3 h, cooled to room temperature, and MnO_2 was filtered and the filter cake washed with $CHCl_3$ (3 × 10 mL). The combined organic phase was concentrated under reduced pressure. The residue was purified by silica gel chromatography to afford the pure product, using *n*-hexane-ethyl acetate (80:1) to afford **4ah** or **4ai** and *n*-hexane-ethyl acetate (40:1) to give **5ah** or **5ai**.

3.3.27. 6,8-Di-tert-butyl-3-(methylthio)benzofuro[3,2-*e*][1,2,4]triazine **4ah**

Yellow powder. Yield 167 mg, 51%; m.p. 105–107 °C. Rf = 0.67 (ethyl acetate:hexane, 1:1). ^{1}H NMR ($CDCl_3$): 8.08 (d, 1H, *J* = 1.8 Hz H-5), 7.78 (d, 1H, *J* = 1.8 Hz, H-7), 2.79 (s, 3H, SCH_3), 1.57 (s, 9H, $C(CH_3)_3$), 1.41 (s, 9H, $C(CH_3)_3$); ^{13}C NMR ($CDCl_3$): 169.1, 160.7, 155.8, 148.6, 144.2, 136.1, 130.3, 118.8, 118.0, 35.4, 35.0, 31.7, 29.8, 14.8. Anal. Calcd. For $C_{18}H_{23}N_3OS$: C, 65.62; H, 7.04; N, 12.75%; found: C, 65.72; H, 7.10; N, 12.82%.

3.3.28. 2,4-Di-tert-butyl-6-(3-(methylthio)-1,2,4-triazin-5-yl)phenol **5ah**

Pale yellow powder. Yield 67 mg, 20%; m.p. 113–115 °C. Rf = 0.64 (ethyl acetate:hexane, 1:1). ^{1}H NMR ($CDCl_3$): 12.73 (s, 1H, OH), 9.50 (s, 1H, H-6′), 7.69 (d, 1H, *J* = 2.3 Hz, H-5), 7.57 (d, 1H, *J* = 2.3 Hz, H-3), 2.75 (s, 3H, SCH_3), 1.46 (s, 9H, $C(CH_3)_3$), 1.35 (s, 9H, $C(CH_3)_3$); ^{13}C NMR ($CDCl_3$): 170.1, 160.0, 156.0, 141.8, 141.6, 139.0, 130.9, 121.2, 113.0, 35.5, 34.6, 31.5, 29.5, 14.1. Anal. Calcd. For $C_{18}H_{25}N_3OS$: C, 65.22; H, 7.60; N, 12.68%; found: C, 65.31; H, 7.51; N, 12.74%.

3.3.29. 6-(tert-Butyl)-3-(methylthio)benzofuro[3,2-*e*][1,2,4]triazine **4ai**

Yellow powder. Yield 30 mg, 11%; m.p. 136–138 °C. Rf = 0.64 (ethyl acetate:hexane, 1:1). ^{1}H NMR ($CDCl_3$): 8.23 (d, 1H, *J* = 1.8 Hz, H-5), 7.88 (dd, 1H, *J* = 1.8 Hz, *J* = 8.9 Hz, H-7), 7.61 (d, 1H, *J* = 8.9 Hz, H-8), 2.78 (s, 3H, SCH_3), 1.42 (s, 9H, $C(CH_3)_3$); ^{13}C NMR ($CDCl_3$): 169.3, 161.0, 157.2, 149.0, 144.1, 133.5, 120.6, 118.5, 112.8, 35.3, 31.6, 14.8. Anal. Calcd. For $C_{14}H_{15}N_3OS$: C, 61.52; H, 5.53; N, 15.37%; found: C, 61.59; H, 5.44; N, 15.30%.

3.3.30. 4-(tert-Butyl)-2-(3-(methylthio)-1,2,4-triazin-5-yl)phenol **5ai**

Yellow powder. Yield 120 mg, 43%; m.p. 123–125 °C. Rf = 0.59 (ethyl acetate:hexane, 1:1). ^{1}H NMR ($CDCl_3$): 11.97 (s, 1H, OH), 9.49 (s, 1H, H-6′), 7.80 (d, 1H, *J* = 2.0 Hz, H-3), 7.53 (dd, 1H, *J* = 2.0 Hz, *J* = 8.8 Hz, H-5), 6.99 (d, 1H, *J* = 8.8 Hz, H-8), 2.71 (s, 3H, SCH_3), 1.34 (s, 9H, $C(CH_3)_3$); ^{13}C NMR ($CDCl_3$): 170.6, 160.3, 155.3, 142.9, 141.2, 133.5, 123.2, 119.1, 113.2, 34.4, 31.4, 14.0. Anal. Calcd. For $C_{14}H_{17}N_3OS$: C, 61.06; H, 6.22; N, 15.26%; found: C, 61.13; H, 6.29; N, 15.16%.

3.3.31. 40 mmol Scaled Synthesis of **3ad**

To a stirred solution of triazine **1a** (5.10 g, 40 mmol, 1 equiv.) and 2,7-dihydroxynaphthalene **2d** (6.40 g, 40 mmol, 1 equiv.) in methanol (40 mL), $BF_3.OEt_2$ (40 mL, 320 mmol, 8 equiv.) was added dropwise and the resulting mixture was refluxed for 8 h. After cooling the methanol was evaporated under reduced pressure, and then the residue was treated with AcOEt (30 mL) and stirred for 15 min. The precipitate formed was filtered and washed with AcOEt (10 mL). The precipitate was suspended in AcOEt and the resulting mixture was washed with aq. $NaHCO_3$ solution. The organic layer was dried over anhydrous Na_2SO_4, filtered, and evaporated under reduced pressure to give **3ad**. The **3ad** was dissolved in a mixture of $CHCl_3$:EtOH (4:1, 300 mL). To the resulting solution, MnO_2 (10.44 g, 120 mmol, 3 equiv.) was added in one portion. The resulting mixture was stirred at 50 °C for 6 h. The completion of the reaction was monitored by TLC. The reaction mixture was then cooled to room temperature, and the MnO_2 was filtered and washed with $CHCl_3$ (3 × 50 mL).

The combined organic phase was concentrated under reduced pressure. The residue was recrystallized in EtOH to give pure **4ad** (9.62 g, 85% in two steps).

*3.4. Further Modifications of Compound **4aa***

3.4.1. 10-(4-(Carbazol-9-yl)phenyl)naphtho[1′,2′:4,5]furo[3,2-*e*][1,2,4]triazine 7

To a solution of 10-(methylthio)naphtho[1′,2′:4,5]furo[3,2-*e*][1,2,4]triazine **4aa** (100 mg, 1 equiv.) in dry THF (5 mL), we added CuTC (249 mg, 3.5 equiv), $Pd[PPh_3]_4$ (43 mg, 10 mol%) and (4-(9*H*-carbazol-9-yl)phenyl)boronic acid (322 mg, 3 equiv.). Then, the reaction mixture was stirred at reflux for 32 h. The progress of the reaction was monitored by TLC. After completion, the solvent was evaporated under reduced pressure and the residue was purified by flash chromatography using *n*-hexane-ethyl acetate (10:1→5:1) to give a pure product **7** as yellow powder. Yield 126 mg, 73%; m.p. 280–282 °C. ^{1}H NMR ($CDCl_3$): 9.22–9.18 (m, 1H, H-1), 9.01–8.97 (m, 2H, H-2′′), 8.34–8.29 (m, 1H, H-5), 8.20–8.16 (m, 2H, H-1′), 8.11–8.08 (m, 1H, H-4), 7.94–7.82 (m 4H, H-2, H-6, H-3′′), 7.74–7.70 (m, 1H, H-3), 7.60-7.57 (m, 2H, H-4′), 7.48–7.43 (m, 2H, H-3′ or H-2′), 7.36-7.31 (m, 2H, H-2′ or H-3′); ^{13}C NMR ($CDCl_3$): 161.1, 161.0, 158.8, 144.3, 140.7, 140.5, 137.1, 134.5, 130.9, 130.2, 129.8, 129.6, 129.2, 127.2, 126.9, 126.3, 125.1, 123.8, 120.6, 120.5, 113.8, 112.9, 110.1. Anal. Calcd. For $C_{31}H_{18}N_4O$: C, 80.50; H, 3.92; N, 12.11%; found: C, 80.31; H, 4.07; N, 11.96%.

3.4.2. 10-(Methylsulfonyl)naphtho[1′,2′:4,5]furo[3,2-*e*][1,2,4]triazine **8**

*m*CPBA (427 mg, ≤77%, 2.2 equiv.) was dissolved in dry DCM (5 mL), Na_2SO_4 (2.0 g) was added to the resulting solution and the mixture was stirred for 10 min. Na_2SO_4 was filtered and washed with DCM (3 × 5 mL). The obtained solution of *m*CPBA was added dropwise to a solution of **4aa** (133 mg, 0.5 mmol) in DCM (4 mL) at 0 °C. Then the reaction mixture was stirred at room temperature for 12 h. The progress of the reaction was monitored by TLC. After completion of the reaction, the mixture was quenched with an aqueous solution of $NaHCO_3$, washed with water and dried over Na_2SO_4, and the solvent was evaporated under reduced pressure. The residue was purified by flash chromatography using *n*-hexane-chloroform (2:1) as eluent to give pure **8** as **a** yellow powder. Yield 127 mg, 85%; m.p. 248–251 °C. ^{1}H NMR ($CDCl_3$): 9.07–9.04 (m, 1H, H-1), 8.43–8.39 (m, 1H, H-5), 8.11–8.08 (m, 1H, H-4), 7.93–7.88 (m, 2H, H-2, H-6), 7.76–7.72 (m, 1H, H-3), 7.65–7.58 (m, 1H, H-2), 3.66 (s, 2H, SO_2CH_3); ^{13}C NMR ($CDCl_3$): 163.8, 161.6, 160.4, 145.3, 139.5, 131.0, 130.7, 129.7, 128.7, 127.8, 125.5, 113.0, 112.6, 40.6. Anal. Calcd. For $C_{14}H_9N_3O_3S$: C, 56.18; H, 3.03; N, 14.04%; found: C, 56.05; H, 3.20; N, 13.96%.

3.4.3. 10-(Carbazol-9-yl)naphtho[1′,2′:4,5]furo[3,2-*e*][1,2,4]triazine **9**

To a solution of carbazole (106 mg, 1.9 equiv.) in dry DMF (3 mL), we added NaH (60% suspension in mineral oil, 19 mg, 1.4 equiv.) and the mixture was stirred for 10 min. Then methylsulfonyl derivative **8** (100 mg, 0.33 mmol) was added to the resulting solution and the mixture was heated at 70 °C for 12 h. After completion of the reaction, the mixture was diluted with water (15 mL), and the forming precipitate was filtered and washed with water and ethanol and purified by flash chromatography using n-hexane:chloroform (2:1) as the eluent to give pure **9** as a yellow powder. Yield 71 mg, 55%; m.p. 250–253 °C. ^{1}H NMR (HMPA d-18): 9.02–8.98 (m, 1H, H-1), 8.95-8.90 (d, *J* = 9.1 Hz, 1H, H-5), 8.85–8.78 (m, 2H, H-1′), 8.58–8.54 (m, 1H, H-4), 8.51–8.46 (m, 2H, H-4′), 8.42 (d, *J* = 9.1 Hz, 1H, H-6), 8.15–8.09 (m, 1H, H-3 and H-2), 7.89–7.82 (m, 1H, H-2 and H-3), 7.68–7.61 (m, 2H, H-3′ or H-2′), 7.50–7.43 (m, 2H, H-2′ or H-3′); ^{13}C NMR (HMPAd-18): 160.2, 159.8, 157.9, 144.5, 139.4, 139.3, 131.5, 130.9, 130.6, 128.9, 127.3, 127.1, 126.0, 124.0, 122.9, 121.0, 115.1, 113.8, 113.2. Anal. Calcd. For $C_{25}H_{14}N_4O$: C, 77.71; H, 3.65; N, 14.50%; found: C, 77.90; H, 2.81; N, 14.29%.

4. Conclusions

In summary, we have developed an unusual MnO_2-induced oxidative cyclization in adducts of phenols and triazines. This method provides easy two-step access to benzofuro-

fused triazine via the nucleophilic addition of the 2-naphthol to 1,2,4-triazine, followed by oxidative cyclization. The scope and limitations of this novel reaction have been investigated. Further application of the synthesized compound has been demonstrated by synthesizing carbazole-substituted benzofuro-fused triazines. The mechanistic study has revealed that the process proceeds through the formation of an O-coordinated Mn complex. We believe that the present methodology will open a new door to synthesizing important building blocks of α-sulfonylamino ketones.

Supplementary Materials: The supporting information can be downloaded at: https://www.mdpi.com/article/10.3390/molecules27207105/s1. Synthesis of the starting 1,2,4-triazines, **3**, **4**, **4aa** derivatives; Preliminary mechanistic studies; DFT calculations; ^{1}H and ^{13}C NMR spectra for compounds **1**,**3–5**,**7–9**, **4aa′**.

Author Contributions: Conceptualization, I.A.K., S.S. and O.N.C.; methodology, R.F.F., A.D.S. and A.P.P., N.N.M., A.V.I. and P.N.M.; software, A.N.T.; validation, I.A.K. and S.S.; formal analysis, R.F.F., I.A.K. and S.S.; investigation, R.F.F., A.D.S., A.P.P., N.N.M., A.V.I. and P.N.M.; resources, R.F.F. and I.A.K.; data curation, R.F.F., I.A.K. and S.S.; writing—original draft preparation, R.F.F., I.A.K. and S.S.; writing—review and editing, S.S.; visualization, I.A.K. and S.S.; supervision, O.N.C.; project administration, R.F.F., I.A.K. and S.S.; funding acquisition, R.F.F. and I.A.K. All authors have read and agreed to the published version of the manuscript.

Funding: This research was funded by the Russian Scientific Foundation (Grant #21-13-00304, synthesis of compounds **4**) and the Council on Grants of the President of the Russian Federation (Ref. #NSh- 1223.2022.1.3, synthesis of the starting compounds **1** and DFT studies).

Institutional Review Board Statement: Not applicable.

Informed Consent Statement: Not applicable.

Data Availability Statement: Data are contained within the article or Supplementary Materials.

Conflicts of Interest: The authors declare no conflict of interest.

Sample Availability: Samples of the all compounds are available from the authors.

References

1. Engle, K.M.; Mei, T.-S.; Wasa, M.; Yu, J.-Q. Weak coordination as a powerful means for developing broadly useful C–H functionalization reactions. *Acc. Chem. Res.* **2012**, *45*, 788–802. [CrossRef] [PubMed]
2. Kuhl, N.; Hopkinson, M.N.; Wencel-Delord, J.; Glorius, F. Beyond Directing Groups: Transition-Metal-Catalyzed C-H Activation of Simple Arenes. *Angew. Chem. Int. Ed.* **2012**, *51*, 10236–10254. [CrossRef] [PubMed]
3. Neufeldt, S.R.; Sanford, M.S. Controlling site selectivity in palladium-catalyzed C–H bond functionalization. *Acc. Chem. Res.* **2012**, *45*, 936–946. [CrossRef] [PubMed]
4. Sun, C.-L.; Li, B.-J.; Shi, Z.-J. Direct C−H transformation via iron catalysis. *Chem. Rev.* **2011**, *111*, 1293–1314. [CrossRef] [PubMed]
5. Yamaguchi, J.; Yamaguchi, A.D.; Itami, K. C-H Bond Functionalization: Emerging Synthetic Tools for Natural Products and Pharmaceuticals. *Angew. Chem. Int. Ed.* **2012**, *51*, 8960–9009. [CrossRef]
6. Rit, R.K.; Yadav, M.R.; Ghosh, K.; Sahoo, A.K. Reusable directing groups [8-aminoquinoline, picolinamide, sulfoximine] in C(sp^3)–H bond activation: Present and future. *Tetrahedron* **2015**, *71*, 4450–4459. [CrossRef]
7. Bag, S.; Patra, T.; Modak, A.; Deb, A.; Maity, S.; Dutta, U.; Dey, A.; Kancherla, R.; Maji, A.; Hazra, A.; et al. Remote *para*-C–H Functionalization of Arenes by a D-Shaped Biphenyl Template-Based Assembly. *J. Am. Chem. Soc.* **2015**, *137*, 11888–11891. [CrossRef]
8. Yoshikai, N. Cobalt-Catalyzed C-C Bond-Forming Reactions via Chelation-Assisted CH Activation. *Yuki Gosei Kagaku Kyokaishi* **2014**, *72*, 1198–1206. [CrossRef]
9. Phillips, A.M.F.; Guedes da Silva, M.F.C.; Pombeiro, A.J.L. New Trends in Enantioselective Cross-Dehydrogenative Coupling. *Catalysts* **2020**, *10*, 529. [CrossRef]
10. Bosque, I.; Chinchilla, R.; Gonzalez-Gomez, J.C.; Guijarro, D.; Alonso, F. Cross-dehydrogenative coupling involving benzylic and allylic C–H bonds. *Org. Chem. Front.* **2020**, *7*, 1717–1742. [CrossRef]
11. Zhang, J.; Liu, L.; Chen, T.; Han, L. Cross-Dehydrogenative Alkynylation: A Powerful Tool for the Synthesis of Internal Alkynes. *ChemSusChem* **2020**, *13*, 4776–4794. [CrossRef] [PubMed]
12. Moriyama, K. Recent advances in oxidative C–C coupling reaction of amides with carbon nucleophiles. *Tetrahedron Lett.* **2017**, *58*, 4655–4662. [CrossRef]

13. Li, C.-J. Cross-dehydrogenative coupling (CDC): Exploring C−C bond formations beyond functional group transformations. *Acc. Chem. Res.* **2009**, *42*, 335–344. [CrossRef] [PubMed]
14. Tian, T.; Li, Z.; Li, C.-J. Cross-dehydrogenative coupling: A sustainable reaction for C–C bond formations. *Green Chem.* **2021**, *23*, 6789–6862. [CrossRef]
15. Huang, C.-Y.; Kang, H.; Li, J.; Li, C.-J. En route to intermolecular cross-dehydrogenative coupling reactions. *J. Org. Chem.* **2019**, *84*, 12705–12721. [CrossRef]
16. Rohit, K.R.; Radhika, S.; Saranya, S.; Anilkumar, G. Manganese-Catalysed Dehydrogenative Coupling—An Overview. *Adv. Synth. Catal.* **2020**, *362*, 1602–1650. [CrossRef]
17. Voigt, B.; Meijer, L.; Lozach, O.; Schächtele, C.; Totzke, F.; Hilgeroth, A. Novel CDK inhibition profiles of structurally varied 1-aza-9-oxafluorenes. *Bioorg. Med. Chem. Lett.* **2005**, *15*, 823–825. [CrossRef]
18. Tell, V.; Mahmoud, K.A.; Wichapong, K.; Schächtele, C.; Totzke, F.; Sippl, W.; Hilgeroth, A. Novel aspects in structure–activity relationships of profiled 1-aza-9-oxafluorenes as inhibitors of Alzheimer's disease-relevant kinases cdk1, cdk5 and gsk3β. *MedChemComm* **2012**, *3*, 1413–1418. [CrossRef]
19. Tell, V.; Holzer, M.; Herrmann, L.; Mahmoud, K.A.; Schächtele, C.; Totzke, F.; Hilgeroth, A. Multitargeted drug development: Discovery and profiling of dihydroxy substituted 1-aza-9-oxafluorenes as lead compounds targeting Alzheimer disease relevant kinases. *Bioorg. Med. Chem. Lett.* **2012**, *22*, 6914–6918. [CrossRef]
20. Schade, N.; Koch, P.; Ansideri, F.; Krystof, V.; Holzer, M.; Hilgeroth, A. Evaluation of Novel Substituted Furopyridines as Inhibitors of Protein Kinases Related to Tau Pathology in Alzheimer's Disease. *Med. Chem.* **2021**, *17*, 844–855. [CrossRef]
21. Marciano, R.; David, H.B.; Akabayov, B.; Rotblat, B. The Amuvatinib Derivative, N-(2H-1,3-Benzodioxol-5-yl)-4-{thieno [3,2-d]pyrimidin-4-yl}piperazine-1-carboxamide, Inhibits Mitochondria and Kills Tumor Cells under Glucose Starvation. *Int. J. Mol. Sci.* **2020**, *21*, 1041. [CrossRef] [PubMed]
22. Salem, M.S.H.; Abdel Aziz, Y.M.; Elgawish, M.S.; Said, M.M.; Abouzid, K.A.M. Design, synthesis, biological evaluation and molecular modeling study of new thieno [2,3-d]pyrimidines with anti-proliferative activity on pancreatic cancer cell lines. *Bioorg. Chem.* **2020**, *94*, 103472. [CrossRef] [PubMed]
23. Phillip, C.J.; Zaman, S.; Shentu, S.; Balakrishnan, K.; Zhang, J.; Baladandayuthapani, V.; Taverna, P.; Redkar, S.; Wang, M.; Stellrecht, C.M.; et al. Targeting MET kinase with the small-molecule inhibitor amuvatinib induces cytotoxicity in primary myeloma cells and cell lines. *J. Hematol. Oncol.* **2013**, *6*, 92. [CrossRef] [PubMed]
24. Cui, J.J. Targeting receptor tyrosine kinase MET in cancer: Small molecule inhibitors and clinical progress. *J. Med. Chem.* **2014**, *57*, 4427–4453. [CrossRef]
25. Huang, C.-C.; Xue, M.-M.; Wu, F.-P.; Yuan, Y.; Liao, L.-S.; Fung, M.-K. Deep-blue and hybrid-white organic light emitting diodes based on a twisting carbazole-benzofuro [2,3-*b*] pyrazine fluorescent emitter. *Molecules* **2019**, *24*, 353. [CrossRef] [PubMed]
26. Salman, G.A.; Nisa, R.U.; Iaroshenko, V.O.; Iqbal, J.; Ayub, K.; Langer, P. Pyrrole versus quinoline formation in the palladium catalyzed reaction of 2-alkynyl-3-bromothiophenes and 2-alkynyl-3-bromofurans with anilines. A combined experimental and computational study. *Org. Biomol. Chem.* **2012**, *10*, 9464–9473. [CrossRef] [PubMed]
27. Loidreau, Y.; Marchand, P.; Dubouilh-Benard, C.; Nourrisson, M.-R.; Duflos, M.; Loaëc, N.; Meijer, L.; Besson, T. Synthesis and biological evaluation of N-aryl-7-methoxybenzo[*b*]furo [3,2-*d*]pyrimidin-4-amines and their N-arylbenzo[b]thieno [3,2-d]pyrimidin-4-amine analogues as dual inhibitors of CLK1 and DYRK1A kinases. *Eur. J. Med. Chem.* **2013**, *59*, 283–295. [CrossRef]
28. Rao, Y.; Li, Z.; Yin, G. Clean and efficient assembly of functionalized benzofuro [2,3-*c*] pyridines via metal-free one-pot domino reactions. *Green Chem.* **2014**, *16*, 2213–2218. [CrossRef]
29. Brikci-Nigassa, N.M.; Bentabed-Ababsa, G.; Erb, W.; Chevallier, F.; Picot, L.; Vitek, L.; Fleury, A.; Thiéry, V.; Souab, M.; Robert, T.; et al. 2-Aminophenones, a common precursor to N-aryl isatins and acridines endowed with bioactivities. *Tetrahedron* **2018**, *74*, 1785–1801. [CrossRef]
30. Yonekura, K.; Shinoda, M.; Yonekura, Y.; Tsuchimoto, T. Indium-Catalyzed Annulation of o-Acylanilines with Alkoxyheteroarenes: Synthesis of Heteroaryl[b]quinolines and Subsequent Transformation to Cryptolepine Derivatives. *Molecules* **2018**, *23*, 838. [CrossRef]
31. Yu, Z.; Zhang, Y.; Tang, J.; Zhang, L.; Liu, Q.; Li, Q.; Gao, G.; You, J. Ir-Catalyzed Cascade C–H Fusion of Aldoxime Ethers and Heteroarenes: Scope and Mechanisms. *ACS Catal.* **2020**, *10*, 203–209. [CrossRef]
32. Bouarfa, S.; Bentabed-Ababsa, G.; Erb, W.; Picot, L.; Thiéry, V.; Roisnel, T.; Dorcet, V.; Mongin, F. Iodothiophenes and Related Compounds as Coupling Partners in Copper-Mediated N-Arylation of Anilines. *Synthesis* **2021**, *53*, 1271–1284. [CrossRef]
33. Rong, B.; Xu, G.; Yan, H.; Zhang, S.; Wu, Q.; Zhu, N.; Fang, Z.; Duan, J.; Guo, K. Synthesis of benzofuro-and benzothieno [2,3-*c*]pyridines via copper-catalyzed [4+2] annulation of ketoxime acetates with acetoacetanilide. *Org. Chem. Front.* **2021**, *8*, 2939–2943. [CrossRef]
34. Sadeghzadeh, P.; Pordel, M.; Davoodnia, A. Synthesis of 3*H*-[1]Benzofuro [2,3-*b*]imidazo [4,5-*f*]quinolines as New Fluorescent Heterocyclic Systems for Dye-Sensitized Solar Cells. *Russ. J. Org. Chem.* **2021**, *57*, 440–447. [CrossRef]
35. Yue, W.S.; Li, J.J. A concise synthesis of all four possible benzo [4,5]furopyridines via palladium-mediated reactions. *Org. Lett.* **2002**, *4*, 2201–2203. [CrossRef]
36. Sun, W.; Wang, M.; Zhang, Y.; Wang, L. Synthesis of Benzofuro [3,2-*b*]pyridines via Palladium-Catalyzed Dual C–H Activation of 3-Phenoxypyridine 1-Oxides. *Org. Lett.* **2015**, *17*, 426–429. [CrossRef] [PubMed]

37. Shanahan, R.M.; Hickey, A.; Reen, F.J.; O'Gara, F.; McGlacken, G.P. Synthesis of Benzofuroquinolines via Phosphine-Free Direct Arylation of 4-Phenoxyquinolines in Air. *Eur. J. Org. Chem.* **2018**, *2018*, 6140–6149. [CrossRef]
38. Shanahan, R.M.; Hickey, A.; Bateman, L.M.; Light, M.E.; McGlacken, G.P. One-Pot Cross-Coupling/C–H Functionalization Reactions: Quinoline as a Substrate and Ligand through N–Pd Interaction. *J. Org. Chem.* **2020**, *85*, 2585–2596. [CrossRef]
39. Rathod, P.K.; Jonnalagadda, S.; Panaganti, L. A simple and efficient synthesis of benzofuroquinolines via the decarboxylative cross-coupling. *Tetrahedron Lett.* **2021**, *66*, 152808. [CrossRef]
40. Nakamura, S.; Tohnai, N.; Nishii, Y.; Hinoue, T.; Miura, M. Effect of Substitution Pattern of *tert*-Butyl Groups in a Bisbenzofuropyrazine Core π-System on Optical Properties: Unique Mechanochromic Fluorescence Behavior. *ChemPhotoChem* **2019**, *3*, 46–53. [CrossRef]
41. Singh, R.; Bhatia, H.; Prakash, P.; Debroye, E.; Dey, S.; Dehaen, W. Tandem Nenitzescu reaction/nucleophilic aromatic substitution to form novel pyrido fused indole frameworks. *Eur. J. Org. Chem.* **2021**, *2021*, 4865–4875. [CrossRef]
42. Qi, X.; Xiang, H.; He, Q.; Yang, C. Synthesis of multisubstituted 2-aminopyrroles/pyridines via chemoselective Michael addition/intramolecular cyclization reaction. *Org. Lett.* **2014**, *16*, 4186–4189. [CrossRef] [PubMed]
43. Miliutina, M.; Janke, J.; Hassan, S.; Zaib, S.; Iqbal, J.; Lecka, J.; Sévigny, J.; Villinger, A.; Friedrich, A.; Lochbrunner, S.; et al. A domino reaction of 3-chlorochromones with aminoheterocycles. Synthesis of pyrazolopyridines and benzofuropyridines and their optical and ecto-5′-nucleotidase inhibitory effects. *Org. Biomol. Chem.* **2018**, *16*, 717–732. [CrossRef] [PubMed]
44. Ma, Z.; Jing, C.; Hang, D.; Fan, H.; Duan, L.; Fang, S.; Yan, L. Synthesis, characterization, and photoelectric properties of iridium(III) complexes containing an N hetero-dibenzofuran C^N ligand. *RSC Adv.* **2021**, *11*, 11004–11010. [CrossRef] [PubMed]
45. Liu, J.; Fitzgerald, A.E.; Mani, N.S. Facile assembly of fused benzo [4,5]furo heterocycles. *J. Org. Chem.* **2008**, *73*, 2951–2954. [CrossRef] [PubMed]
46. Cramp, S.; Dyke, H.J.; Higgs, C.; Clark, D.E.; Gill, M.; Savy, P.; Jennings, N.; Price, S.; Lockey, P.M.; Norman, D.; et al. Identification and hit-to-lead exploration of a novel series of histamine H4 receptor inverse agonists. *Bioorg. Med. Chem. Lett.* **2010**, *20*, 2516–2519. [CrossRef] [PubMed]
47. Chen, J.-L.; Steglich, W. Synthesis of some benzofuronaphthyridines and benzofuronaphthyridine derivatives. *J. Heterocycl. Chem.* **1993**, *30*, 909–912. [CrossRef]
48. Xiao, X.; Lai, M.; Song, Z.; Geng, M.; Ding, J.; Xie, H.; Zhang, A. Design, synthesis and pharmacological evaluation of bicyclic and tetracyclic pyridopyrimidinone analogues as new KRASG12C inhibitors. *Eur. J. Med. Chem.* **2021**, *213*, 113082. [CrossRef]
49. Ondachi, P.W.; Comins, D.L. Synthesis of Fused-Ring Nicotine Derivatives from (*S*)-Nicotine. *J. Org. Chem.* **2010**, *75*, 1706–1716. [CrossRef]
50. Kumar, K.S.; Adepu, R.; Kapavarapu, R.; Rambabu, D.; Krishna, G.R.; Reddy, C.M.; Priya, K.K.; Parsa, K.V.L.; Pal, M. $AlCl_3$ induced C-arylation/cyclization in a single pot: A new route to benzofuran fused N-heterocycles of pharmacological interest. *Tetrahedron Lett.* **2012**, *53*, 1134–1138. [CrossRef]
51. Eid, M.M.; Kadry, A.M.; Hassan, R.A. Synthesis and reactions of some 6-(2-hydroxy-1-naphthyl)-1,2,4-triazines. *J. Heterocycl. Chem.* **1988**, *25*, 1117–1118. [CrossRef]
52. Seitz, G.; Richter, J. Donorsubstituierte Benzonitrile als Seitenkettendienophile bei der intramolekularen [4+2]-Cycloaddition mit inversem Elektronenbedarf. *Chem. Ber.* **1989**, *122*, 2177–2181. [CrossRef]
53. Chupakhin, O.N.; Rusinov, G.L.; Beresnev, D.G.; Charushin, V.N.; Neunhoeffer, H. A simple one pot synthesis of condensed 1,2,4-triazines by using the tandem a_N-S_N^{ipso} and S_N^H-S_N^{ipsa} reactions. *J. Heterocycl. Chem.* **2001**, *38*, 901–907. [CrossRef]
54. Fatykhov, R.F.; Savchuk, M.I.; Starnovskaya, E.S.; Bobkina, M.V.; Kopchuk, D.S.; Nosova, E.V.; Zyryanov, G.V.; Khalymbadzha, I.A.; Chupakhin, O.N.; Charushin, V.N.; et al. Nucleophilic substitution of hydrogen–the Boger reaction sequence as an approach towards 8-(pyridin-2-yl) coumarins. *Mendeleev Commun.* **2019**, *29*, 299–300. [CrossRef]
55. Savchuk, M.I.; Kopchuk, D.S.; Taniya, O.S.; Nikonov, I.L.; Egorov, I.N.; Santra, S.; Zyryanov, G.V.; Chupakhin, O.N.; Charushin, V.N. 5-Aryl-6-arylthio-2, 2′-bipyridine and 6-Arylthio-2, 5-diarylpyridine Fluorophores: Pot, Atom, Step Economic (PASE) Synthesis and Photophysical Studies. *J. Fluoresc.* **2021**, *31*, 1099–1111. [CrossRef]
56. Raw, S.A.; Taylor, R.J.K. Highly substituted pyridines via tethered imine–enamine (TIE) methodology. *Chem. Commun.* **2004**, 508–509. [CrossRef]
57. Papadopoulou, M.V.; Taylor, E.C. Intramolecular Diels-Alder reactions of 1,2,4-triazines. Synthesis of 3-alkylpyridines via Raney nickel desulfurization of thieno [2,3-*b*] pyridines. *Tetrahedron* **2021**, *89*, 132158. [CrossRef]
58. Moseev, T.D.; Nikiforov, E.A.; Varaksin, M.V.; Starnovskaya, E.S.; Savchuk, M.I.; Nikonov, I.L.; Kopchuk, D.S.; Zyryanov, G.V.; Chupakhin, O.N.; Charushin, V.N. Novel Pentafluorophenyl-and Alkoxyphenyl-Appended 2, 2′-Bipyridine Push–Pull Fluorophores: A Convenient Synthesis and Photophysical Studies. *Synthesis* **2021**, *53*, 3597–3607. [CrossRef]
59. Lipińska, T.; Branowska, D.; Rykowski, A. 1,2,4-triazines in organic synthesis. 8. Intramolecular diels-alder reaction of 5-acyl-1, 2, 4-triazineoxime ethers. New route of synthesis of alkylhetarylketones. *Chem. Heterocycl. Compd.* **1999**, *35*, 334–342. [CrossRef]
60. Krinochkin, A.P.; Kopchuk, D.S.; Kim, G.A.; Shevyrin, V.A.; Santra, S.; Rahman, M.; Taniya, O.S.; Zyryanov, G.V.; Rusinov, V.L.; Chupakhin, O.N. Water-soluble luminescent lanthanide complexes based on C6-DTTA-appended 5-aryl-2, 2′-bipyridines. *Polyhedron* **2020**, *181*, 114473. [CrossRef]
61. Fernández, S.Y.; Raw, S.A.; Taylor, R.J.K. Improved methodologies for the preparation of highly substituted pyridines. *J. Org. Chem.* **2005**, *70*, 10086–10095. [CrossRef] [PubMed]

62. Chen, Z.; Ren, N.; Ma, X.; Nie, J.; Zhang, F.-G.; Ma, J.-A. Silver-Catalyzed [3 + 3] Dipolar Cycloaddition of Trifluorodiazoethane and Glycine Imines: Access to Highly Functionalized Trifluoromethyl-Substituted Triazines and Pyridines. *ACS Catal.* **2019**, *9*, 4600–4608. [CrossRef]
63. Yamanaka, H.; Sagi, M.; Wada, K.; Konno, S. Studies on as-triazine derivatives. XV, Intramolecular reverse-electron demand Diels-Alter reaction of 1,2,4-triazine derivatives. *Heterocycles* **1990**, *30*, 1009–1021. [CrossRef]
64. Taylor, E.C.; Pont, J.L. Intramolecular Diels-Alder reactions of 1,2,4-triazines. Synthesis of condensed pyrimidines. *J. Org. Chem.* **1987**, *52*, 4287–4292. [CrossRef]
65. Taylor, E.C.; Pont, J.L.; Warner, J.C. Heterodienophilic intramolecular Diels-Alder reactions of 1,2,4-triazines: Synthesis of novel polycyclic condensed pyrazines and lumazines. *Tetrahedron* **1987**, *43*, 5159–5168. [CrossRef]
66. Taylor, E.C.; French, L.G. Intramolecular Diels-Alder reactions of 1,2,4-triazines. Routes to condensed pyrazines via cycloaddition of nitrile dienophiles. *J. Org. Chem.* **1989**, *54*, 1245–1249. [CrossRef]
67. Khalymbadzha, I.A.; Chupakhin, O.N.; Fatykhov, R.F.; Charushin, V.N.; Schepochkin, A.V.; Kartsev, V.G. Transition-metal-free cross-dehydrogenative coupling of triazines with 5,7-dihydroxycoumarins. *Synlett* **2016**, *27*, 2606–2610. [CrossRef]
68. Khalymbadzha, I.A.; Fatykhov, R.F.; Chupakhin, O.N.; Charushin, V.N.; Tseitler, T.A.; Sharapov, A.D.; Inytina, A.K.; Kartsev, V.G. Transition-Metal-Free C–C Coupling of 5, 7-Dihydroxybenzopyrones with Quinoxalones and Pteridinones. *Synthesis* **2018**, *50*, 2423–2431. [CrossRef]
69. Utepova, I.A.; Nemytov, A.I.; Ishkhanian, V.A.; Chupakhin, O.N.; Charushin, V.N. Metal-free C–H/C–H coupling of 1,3-diazines and 1,2,4-triazines with 2-naphthols facilitated by Brønsted acids. *Tetrahedron* **2020**, *76*, 131391. [CrossRef]
70. Fatykhov, R.; Khalymbadzha, I.; Chupakhin, O. Cross-Dehydrogenative Coupling Reactions between Phenols and Hetarenes: Modern Trends in Cross-Coupling Chemistry of Phenols. *Adv. Synth. Catal.* **2022**, *364*, 1052–1068. [CrossRef]
71. Alphonse, F.-A.; Suzenet, F.; Keromnes, A.; Lebret, B.; Guillaumet, G. A general approach to selective functionalization of 1, 2, 4-triazines using organometallics in palladium-catalyzed cross-coupling and addition reactions. *Synthesis* **2004**, *2004*, 2893–2899. [CrossRef]
72. Costa, S.P.G.; Oliveira, E.; Lodeiro, C.; Raposo, M.M.M. Heteroaromatic alanine derivatives bearing (oligo) thiophene units: Synthesis and photophysical properties. *Tetrahedron Lett.* **2008**, *49*, 5258–5261. [CrossRef]
73. Verma, V.; Singh, K.; Kumar, D.; Klapötke, T.M.; Stierstorfer, J.; Narasimhan, B.; Qazi, A.K.; Hamid, A.; Jaglan, S. Synthesis, antimicrobial and cytotoxicity study of 1,3-disubstituted-1*H*-naphtho [1,2-*e*][1,3]oxazines. *Eur. J. Med. Chem.* **2012**, *56*, 195–202. [CrossRef]
74. Koleda, O.; Broese, T.; Noetzel, J.; Roemelt, M.; Suna, E.; Francke, R. Synthesis of benzoxazoles using electrochemically generated hypervalent iodine. *J. Org. Chem.* **2017**, *82*, 11669–11681. [CrossRef]
75. Babbs, A.; Berg, A.; Chatzopoulou, M.; Davies, K.E.; Davies, S.G.; Edwards, B.; Elsey, D.J.; Emer, E.; Guiraud, S.; Harriman, S.; et al. 2-Arylbenzo[d]oxazole Phosphinate Esters as Second-Generation Modulators of Utrophin for the Treatment of Duchenne Muscular Dystrophy. *J. Med. Chem.* **2020**, *63*, 7880–7891. [CrossRef]
76. Ravinaik, B.; Ramachandran, D.; Rao, M.V.B. Synthesis and anticancer evaluation of amide derivatives of 1, 3, 4-oxadiazole linked with benzoxazole. *Russ. J. Gen. Chem.* **2019**, *89*, 1003–1008. [CrossRef]
77. Ferreira, R.C.M.; Raposo, M.M.M.; Costa, S.P.G. Heterocyclic amino acids as fluorescent reporters for transition metals: Synthesis and evaluation of novel furyl-benzoxazol-5-yl-l-alanines. *N. J. Chem.* **2018**, *42*, 3483–3492. [CrossRef]
78. Varma, R.S.; Kumar, D. Manganese triacetate oxidation of phenolic schiffs bases: Synthesis of 2-arylbenzoxazoles. *J. Heterocycl. Chem.* **1998**, *35*, 1539–1540. [CrossRef]
79. Ozokan, K.G.; Gumus, M.K.; Kaban, S. Synthesis of hetaryl-substituted benzoxazoles via oxidative cyclization of phenolic schiff's bases. *J. Heterocycl. Chem.* **2008**, *45*, 1831–1834. [CrossRef]
80. Bougrin, K.; Loupy, A.; Soufiaoui, M. Trois nouvelles voies de synthèse des dérivés 1,3-azoliques sous micro-ondes. *Tetrahedron* **1998**, *54*, 8055–8064. [CrossRef]
81. Vereshchagin, L.I.; Gainulina, S.R.; Podskrebysheva, S.A.; Gaivoroskii, L.A.; Okhapkina, L.L.; Vorob'eva, V.G.; Latyshev, V.P. Reactivity of Manganese Oxides in the Oxidation of Alcohols. *J. Org. Chem. USSR* **1972**, *8*, 1143–1147.
82. Cassis, R.; Valderrama, J.A. Studies on Quinones. XI. Synthesis of Quinones from Hydroquinones by Using Manganese Dioxide and Acid-Impregnated Manganese Dioxide. *Synth. Commun.* **1983**, *13*, 347–356. [CrossRef]
83. Yamaguchi, K.S.; Sawyer, D.T. The Redox Chemistry of Manganese(III) and -(IV) Complexes. *Israel J. Chem.* **1985**, *25*, 164–176. [CrossRef]
84. Moir, M.; Lane, S.; Montgomery, A.P.; Hibbs, D.; Connor, M.; Kassiou, M. The discovery of a potent and selective pyrazolo-[2,3-*e*]-[1,2,4]-triazine cannabinoid type 2 receptor agonist. *Eur. J. Med. Chem.* **2021**, *210*, 113087. [CrossRef]
85. Zhu, Z.; Glinkerman, C.M.; Boger, D.L. Selective N1/N4 1,4-Cycloaddition of 1,2,4,5-Tetrazines Enabled by Solvent Hydrogen Bonding. *J. Am. Chem. Soc.* **2020**, *142*, 20778–20787. [CrossRef] [PubMed]
86. Branowska, D.; Olender, E.; Świętochowska, M.; Karczmarzyk, Z.; Wysocki, W.; Cichosz, I.; Woźna, A.; Urbańczyk-Lipkowska, Z.; Kalicki, P.; Gil, M. Synthesis and optical properties of some 3,4-(ethylenedioxythiophen-2-yl)-1,2,4-triazine derivatives. *Tetrahedron* **2017**, *73*, 411–417. [CrossRef]
87. Fatykhov, R.F.; Chupakhin, O.N.; Rusinov, V.L.; Khalymbadzha, I.A. Copper catalysis for triazines. In *Copper in N-Heterocyclic Chemistry*; Srivastava, A., Ed.; Elsevier: Amsterdam, The Netherlands, 2021; pp. 161–220. [CrossRef]

88. Finlay, M.R.V.; Anderton, M.; Bailey, A.; Boyd, S.; Brookfield, J.; Cairnduff, C.; Charles, M.; Cheasty, A.; Critchlow, S.E.; Culshaw, J.; et al. Discovery of a Thiadiazole–Pyridazine-Based Allosteric Glutaminase 1 Inhibitor Series That Demonstrates Oral Bioavailability and Activity in Tumor Xenograft Models. *J. Med. Chem.* **2019**, *62*, 14, 6540–6560. [CrossRef]
89. Sahin, Z.; Biltekin, S.N.; Ozansoy, M.; Hemiş, B.; Ozansoy, M.B.; Yurttaş, L.; Berk, B.; Demirayak, Ş. Synthesis and in vitro antitumor activities of novel thioamide substituted piperazinyl-1,2,4-triazines. *J. Heterocycl. Chem.* **2022**, *59*, 1333–1340. [CrossRef]
90. Bielawska, A.; Bielawski, K.; Czarnomysy, R.; Gornowicz, A.; Mojzych, M.; Szymanowska, A. The anticancer action of a novel 1,2,4-triazine sulfonamide derivative in colon cancer cells. *Molecules* **2021**, *26*, 2045. [CrossRef]
91. Bashir, M.; Bano, A.; Ijaz, A.S.; Chaudhary, B.A. Recent Developments and Biological Activities of N-Substituted Carbazole Derivatives: A Review. *Molecules* **2015**, *20*, 13496–13517. [CrossRef]
92. Majid, A.; Ashid, M.; Nasir, H.; Joshi, A. A Convenient Synthesis and Reactions of some Substituted 1,2,4-Triazine, and Their Derivatives with Carbazole, Sulfonamide and Trityl Chloride Moiety of Biological Interest. *Eur. J. Mol. Clin. Med.* **2020**, *7*, 994–1002.
93. Zassowski, P.; Ledwon, P.; Kurowska, A.; Herman, A.P.; Lapkowski, M.; Cherpak, V.; Hotra, Z.; Turyk, P.; Ivaniuk, K.; Stakhira, P.; et al. 1,3,5-Triazine and carbazole derivatives for OLED applications. *Dyes Pigment.* **2018**, *149*, 804–811. [CrossRef]
94. Fatiadi, A.J. Active manganese dioxide oxidation in organic chemistry-part I. *Synthesis* **1976**, *1976*, 65–104. [CrossRef]
95. Miri, R.; Firuzi, O.; Peymani, P.; Zamani, M.; Mehdipour, A.R.; Heydari, Z.; Farahani, M.M.; Shafiee, A. Synthesis, Cytotoxicity, and QSAR Study of New Aza-cyclopenta[*b*]fluorene-1,9-dione Derivatives. *Chem. Biol. Drug Des.* **2012**, *79*, 68–75. [CrossRef] [PubMed]
96. Bagley, M.C.; Lubinu, M.C. Microwave-assisted oxidative aromatization of Hantzsch 1, 4-dihydropyridines using manganese dioxide. *Synthesis* **2006**, *2006*, 1283–1288. [CrossRef]
97. Sengoku, T.; Murata, Y.; Suzuki, C.; Takahashi, M.; Yoda, H. Synthesis of new chiral lactam-fused pyridine derivatives. *RSC Adv.* **2015**, *5*, 73562–73565. [CrossRef]
98. Quinonero, O.; Jean, M.; Vanthuyne, N.; Roussel, C.; Bonne, D.; Constantieux, T.; Bressy, C.; Bugaut, X.; Rodriguez, J. Combining organocatalysis with central-to-axial chirality conversion: Atroposelective hantzsch-type synthesis of 4-arylpyridines. *Angew. Chem. Int. Ed.* **2016**, *55*, 1401–1405. [CrossRef]
99. Shabunina, O.V.; Starnovskaya, E.S.; Shaitz, Y.K.; Kopchuk, D.S.; Sadieva, L.K.; Kim, G.A.; Taniya, O.S.; Nikonov, I.L.; Santra, S.; Zyryanov, G.V.; et al. Asymmetrically substituted 5,5′′-diaryl-2,2′:6′,2′′-terpyridines as efficient fluorescence "turn-on" probes for Zn^{2+} in food/cosmetic samples and human urine. *J. Photochem. Photobiol. Chem.* **2021**, *408*, 113101. [CrossRef]
100. Stoll, S.; Schweiger, A. EasySpin, a comprehensive software package for spectral simulation and analysis in EPR. *J. Magn. Reson.* **2006**, *178*, 42–55. [CrossRef]
101. Becke, A.D. Density-functional thermochemistry. III. The role of exact exchange. *J. Chem. Phys.* **1993**, *98*, 5648–5652. [CrossRef]
102. Krishnan, R.; Binkley, J.S.; Seeger, R.; Pople, J.A. Self-consistent molecular orbital methods. XX. A basis set for correlated wave functions. *J. Chem. Phys.* **1980**, *72*, 650–654. [CrossRef]
103. McLean, A.D.; Chandler, G.S. Contracted Gaussian basis sets for molecular calculations. I. Second row atoms, Z=11–18. *J. Chem. Phys.* **1980**, *72*, 5639–5648. [CrossRef]
104. Frisch, M.J.; Trucks, G.W.; Schlegel, H.B.; Scuseria, G.E.; Robb, M.A.; Cheeseman, J.R.; Scalmani, G.; Barone, V.; Petersson, G.A.; Nakatsuji, H.; et al. *Gaussian 09*; Revision D.01; Gaussian, Inc.: Wallingford, CT, USA, 2016.
105. Dennington, R.; Keith, T.; Millam, J. *GaussView*; Version 6; Semichem Inc.: Shawnee Mission, KS, USA, 2019.
106. Ban, K.; Duffy, S.; Khakham, Y.; Avery, V.M.; Hughes, A.; Montagnat, O.; Katneni, K.; Ryan, E.; Baell, J.B. 3-Alkylthio-1,2,4-triazine dimers with potent antimalarial activity. *Bioorg. Med. Chem. Lett.* **2010**, *20*, 6024–6029. [CrossRef] [PubMed]
107. Taylor, E.C.; Macor, J.E.; Pont, J.L. Intramolecular diels-alder reactions of 1, 2, 4-triazines.: A general synthesis of furo [2,3-*b*]pyridines, 2,3-dihydropyrano [2,3-*b*]pyridines, and pyrrolo [2,3-*b*]pyridines. *Tetrahedron* **1987**, *43*, 5145–5158. [CrossRef]
108. Von Neunhoeffer, H.; Hennig, H.; Frühauf, H.-W.; Mutterer, M. Zur synthese von 1,2,4-triazinen. *Tetrahedron Lett.* **1969**, *10*, 3147–3150. [CrossRef]
109. Shkurko, O.P.; Gogin, L.L.; Baram, S.G.; Mamaev, V.P. Electronic spectra of asym-triazinyl groups. *Chem. Heterocycl. Compd.* **1987**, *23*, 216–221. [CrossRef]
110. Courcot, B.; Tran, D.N.; Fraisse, B.; Bonhomme, F.; Marsura, A.; Ghermani, N.E. Electronic Properties of 3,3′-Dimethyl-5,5′-bis(1,2,4-triazine): Towards Design of Supramolecular Arrangements of N-Heterocyclic Cu^{I} Complexes. *Chem. Eur. J.* **2007**, *13*, 3414–3423. [CrossRef]
111. Alekseev, S.G.; Charushin, V.N.; Chupakhin, O.N.; Shorshnev, S.V.; Chernyshev, A.I.; Klyuev, N.A. Reactions of azinium cations. 6. $N_{(1)}$-alkyl-1,2,4-triazinium salts. Reactions with indoles—The first case of the double addition of nucleophiles to a triazine ring. *Chem. Heterocycl. Compd.* **1986**, *22*, 1242–1249. [CrossRef]

MDPI AG
Grosspeteranlage 5
4052 Basel
Switzerland
Tel.: +41 61 683 77 34

Molecules Editorial Office
E-mail: molecules@mdpi.com
www.mdpi.com/journal/molecules

Academic Open
Access Publishing

mdpi.com

ISBN 978-3-7258-2080-1